Get Full Access and More at ExpertConsult.com

Jon A. Jacobson

FUNDAMENTALS OF Musculoskeletal Ultrasound

Edition 2

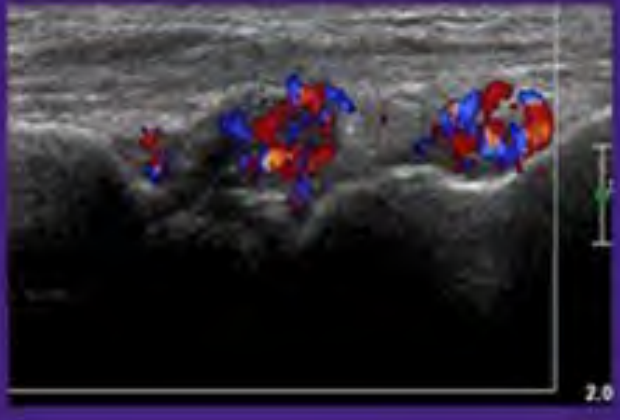

ELSEVIER
SAUNDERS

FUNDAMENTALS OF MUSCULOSKELETAL ULTRASOUND

FUNDAMENTALS OF MUSCULOSKELETAL ULTRASOUND

SECOND EDITION

Jon A. Jacobson, MD
Professor of Radiology
University Of Michigan
Ann Arbor, Michigan

ELSEVIER
SAUNDERS

ELSEVIER
SAUNDERS

1600 John F. Kennedy Blvd.
Ste 1800
Philadelphia, PA 19103-2899

FUNDAMENTALS OF MUSCULOSKELETAL ULTRASOUND, SECOND EDITION
ISBN: 978-1-4557-3818-2

Copyright © 2013, 2007 by Saunders, an imprint of Elsevier Inc.
All rights reserved. No part of this publication may be reproduced or transmitted in any form or by any means, electronic or mechanical, including photocopying, recording, or any information storage and retrieval system, without permission in writing from the publisher. Details on how to seek permission, further information about the Publisher's permissions policies and our arrangements with organizations such as the Copyright Clearance Center and the Copyright Licensing Agency, can be found at our website: www.elsevier.com/permissions.

This book and the individual contributions contained in it are protected under copyright by the Publisher (other than as may be noted herein).

Notices

Knowledge and best practice in this field are constantly changing. As new research and experience broaden our understanding, changes in research methods, professional practices, or medical treatment may become necessary. Practitioners and researchers must always rely on their own experience and knowledge in evaluating and using any information, methods, compounds, or experiments described herein. In using such information or methods they should be mindful of their own safety and the safety of others, including parties for whom they have a professional responsibility. With respect to any drug or pharmaceutical products identified, readers are advised to check the most current information provided (i) on procedures featured or (ii) by the manufacturer of each product to be administered, to verify the recommended dose or formula, the method and duration of administration, and contraindications. It is the responsibility of practitioners, relying on their own experience and knowledge of their patients, to make diagnoses, to determine dosages and the best treatment for each individual patient, and to take all appropriate safety precautions. To the fullest extent of the law, neither the Publisher nor the authors, contributors, or editors, assume any liability for any injury and/or damage to persons or property as a matter of products liability, negligence or otherwise, or from any use or operation of any methods, products, instructions, or ideas contained in the material herein.

Library of Congress Control Number:
Library of Congress Cataloging-in-Publication Data
Jacobson, Jon A. (Jon Arthur)
Fundamentals of musculoskeletal ultrasound / Jon A. Jacobson.—2nd ed.
p. ; cm.
Includes bibliographical references and index.
ISBN 978-1-4557-3818-2 (pbk.)
I. Title.
[DNLM: 1. Musculoskeletal Diseases—Ultrasonography. 2. Musculoskeletal System—Ultrasonography. 3. Ultrasonography—methods. WE 141]
616.7′07543—dc23
2012025676

Senior Content Strategist: Don Scholz
Content Development Specialist: Andrea Vosburgh
Publishing Services Manager: Hemamalini Rajendrababu
Project Manager: Saravanan Thavamani
Design Manager: Steven Stave
Illustrations Manager: Mike Carcel
Marketing Manager: Abigail Swartz

Printed in the United States of America

Last digit is the print number: 9 8 7 6 5 4 3

Working together to grow
libraries in developing countries
www.elsevier.com | www.bookaid.org | www.sabre.org
ELSEVIER BOOK AID International Sabre Foundation

This book is dedicated to my wife Karen and my daughters, Erica and Marie, for their patience and support.

To my parents, Ken and Dorothy, who taught me the value of hard work.

To my residents, fellows, and technologists, who are a joy to teach.

And to my mentors, Marnix van Holsbeeck and Donald Resnick, who continue to amaze me with their knowledge and dedication.

Jon A. Jacobson, MD

Preface

It is my pleasure to present the second edition of the textbook, *Fundamentals of Musculoskeletal Ultrasound*. While constructing this edition, I was amazed at how the field of musculoskeletal ultrasound has advanced in such a short time interval from the construction of the first edition. The goal of this edition is not simply to update the content but also to inform the reader about such advances in the field. The following is a short summary of the items that are new to this updated edition.

The organization of the textbook is similar to the prior version, focused on specific joints after a brief introduction and chapter on basic pathology concepts. Given the increased role of ultrasound in imaging-guided procedures, a new chapter has been added that reviews interventional musculoskeletal ultrasound. Because ultrasound has also emerged as an important tool in the evaluation of inflammatory arthritis and peripheral nerves, content related to these two topics was increased throughout all chapters. References have also been updated and about 40% of the images are new. In addition, color images are now integrated throughout the textbook.

An exciting addition to this textbook is the availability of online material via www.ExpertConsult.com. This has allowed an increase in the number of images and content for each chapter. Consequently, Chapters 1 (Introduction) and 2 (Basic Pathology Concepts) have become Web-only chapters to allow for the expansion of other chapters and the addition of the new interventional chapter in the hard-copy version of the textbook. The use of the Web for material has also allowed the addition of over 200 ultrasound imaging cine clips, which has significant educational benefit as they simulate real-time scanning. Lastly, a complete electronic version of this textbook will be available online at www.expertconsult.com.

It has been exciting to see the popularity and number of clinical applications of musculoskeletal ultrasound increase over such a short time period. With knowledge of anatomy and pathology as seen with ultrasound and proper scanning technique, musculoskeletal ultrasound can play a significant role in the evaluation of the musculoskeletal system.

Jon Jacobson, MD

Acknowledgments

I would like to thank Philips for their support: normal ultrasound images were acquired on an iU22 ultrasound system.

Cine Clip Video Contents

1 Introduction
Video 1-1. Anterior thigh ultrasound: linear transducer
Video 1-2. Anterior thigh ultrasound: curvilinear transducer
Video 1-3. Anisotropy: supraspinatus
Video 1-4. Anisotropy: subscapularis
Video 1-5. Anisotropy: long head of biceps brachii tendon
Video 1-6. Anisotropy: long head of biceps brachii tendon

2 Basic Pathology Concepts
Video 2-1. Extensor pollicis longus: screw impingement
Video 2-2. Infection: isoechoic abscess
Video 2-3. Infection: isoechoic abscess
Video 2-4. Infection: soft tissue gas
Video 2-5. Rheumatoid arthritis: hyperemia and transducer pressure
Video 2-6. Soft tissue gas
Video 2-7. Lipoma: compressibility
Video 2-8. Lipoma: correlation with physical examination findings
Video 2-9. Schwannoma: hyperemia
Video 2-10. Lymph node: hyperplastic (groin)
Video 2-11. Osteochondroma and bursa
Video 2-12. Metastasis: acromion (renal cell carcinoma)

3 Shoulder Ultrasound
Video 3-1. Biceps brachii tendon long head (short axis): normal
Video 3-2. Biceps brachii tendon long head (short axis): anisotropy
Video 3-3. Biceps brachii tendon long head (long axis): normal
Video 3-4. Biceps brachii tendon long head (long axis): anisotropy
Video 3-5. Biceps brachii tendon long head (long axis): normal
Video 3-6. Subscapularis (long axis): normal
Video 3-7. Subscapularis (short axis): normal
Video 3-8. Supraspinatus (long axis): normal
Video 3-9. Supraspinatus (long axis): anisotropy
Video 3-10. Supraspinatus-infraspinatus tendon junction
Video 3-11. Supraspinatus (short axis): normal
Video 3-12. Supraspinatus-infraspinatus tendon junction
Video 3-13. Infraspinatus (long axis): normal
Video 3-14. Suprascapular vein
Video 3-15. Supraspinatus tendon tear: partial, articular
Video 3-16. Supraspinatus tendon tear: partial, bursal
Video 3-17. Supraspinatus tendon tear: full-thickness
Video 3-18. Supraspinatus tear, rotator interval injury, and biceps subluxation
Video 3-19. Supraspinatus tendon tear: focal, full-thickness
Video 3-20. Joint effusion: posterior glenohumeral joint recess
Video 3-21. Joint effusion and subacromial-subdeltoid bursal fluid
Video 3-22. Subacromial-subdeltoid bursal distention
Video 3-23. Supraspinatus tendon tear: cartilage interface sign
Video 3-24. Subscapularis tendon: complete tear
Video 3-25. Calcific tendinosis: shadowing
Video 3-26. Calcific tendinosis: linear
Video 3-27. Calcific tendinosis: amorphous
Video 3-28. Calcific tendinosis: impingement

Video 3-29. Subacromial impingement (at acromion)
Video 3-30. Subacromial impingement (anterior to acromion)
Video 3-31. Subacromial-subdeltoid bursal tissue snapping
Video 3-32. Subacromial-subdeltoid impingement: bone
Video 3-33. Adhesive capsulitis
Video 3-34. Biceps brachii tenosynovitis
Video 3-35. Deltoid fascia shadowing simulating biceps brachii tendon pathology
Video 3-36. Transient biceps brachii tendon dislocation
Video 3-37. Biceps brachii tendon relocation
Video 3-38. Calcific bursitis
Video 3-39. Osteoarthritis
Video 3-40. Intra-articular hemorrhage
Video 3-41. Subscapularis recess
Video 3-42. Posterior labral tear
Video 3-43. Posterior labral tear and paralabral cyst
Video 3-44. Greater tuberosity fracture
Video 3-45. Acromioclavicular joint injury
Video 3-46. Elastofibroma
Video 3-47. Slipping rib syndrome

4 Elbow Ultrasound
Video 4-1. Biceps brachii tendon (medial approach): normal
Video 4-2. Biceps brachii tendon (lateral approach): normal
Video 4-3. Olecranon bursal distention: trauma
Video 4-4. Olecranon bursitis: gout
Video 4-5. Biceps brachii tendon: nonretracted full-thickness tear
Video 4-6. Biceps brachii tendon: partial-thickness tear
Video 4-7. Biceps brachii tendon: post-repair
Video 4-8. Bicipitoradial bursal distention
Video 4-9. Triceps brachii tendon: partial tear
Video 4-10. Ulnar collateral ligament, anterior band: partial-thickness tear
Video 4-11. Ulnar collateral ligament, anterior band: full-thickness tear
Video 4-12. Radial collateral ligament full-thickness tear
Video 4-13. Radial head subluxation
Video 4-14. Snapping elbow
Video 4-15. Ulnar nerve dislocation
Video 4-16. Snapping triceps syndrome
Video 4-17. Snapping triceps syndrome
Video 4-18. Anconeus epitrochlearis: subluxation
Video 4-19. Radial nerve, deep branch: neurofibroma

5 Wrist and Hand Ultrasound
Video 5-1. Median nerve
Video 5-2. Median nerve
Video 5-3. Median nerve
Video 5-4. Extensor pollicis longus
Video 5-5. Adductor pollicis aponeurosis of the thumb
Video 5-6. Radiocarpal joint recess distention: dorsal
Video 5-7. Dorsal wrist recess synovitis (rheumatoid arthritis)
Video 5-8. Distal radioulnar joint recess synovitis (lupus)
Video 5-9. Metacarpophalangeal joint synovitis (rheumatoid arthritis)
Video 5-10. Gouty tophus
Video 5-11. Tenosynovitis: second extensor wrist compartment
Video 5-12. Tenosynovitis: second extensor wrist compartment
Video 5-13. Tenosynovitis: flexor tendon (gout)
Video 5-14. De Quervain tenosynovitis
Video 5-15. De Quervain tenosynovitis
Video 5-16. Screw impingement: extensor pollicis longus
Video 5-17. Dislocation: extensor carpi ulnaris tendon
Video 5-18. Thumb pulley injury and trigger finger
Video 5-19. Extensor digitorum brevis manus
Video 5-20. Carpal tunnel syndrome
Video 5-21. Bifid median nerve and carpal tunnel syndrome

Video 5-22. Radial nerve entrapment in scar tissue
Video 5-23. Stener lesion
Video 5-24. Stener lesion
Video 5-25. Adductor pollicis aponeurosis tear
Video 5-26. Psoriatic arthritis
Video 5-27. Dorsal ganglion cyst
Video 5-28. Dorsal ganglion cyst
Video 5-29. Volar ganglion cyst
Video 5-30. Giant cell tumor of tendon sheath
Video 5-31. Glomus tumor

6 Hip and Thigh Ultrasound
Video 6-1. Rectus femoris, direct head: normal
Video 6-2. Rectus femoris, indirect head: normal
Video 6-3. Lateral femoral cutaneous nerve (right): normal
Video 6-4. Sacroiliac joint: normal
Video 6-5. Piriformis (right): normal
Video 6-6. Piriformis (left): normal
Video 6-7. Anterior thigh: normal
Video 6-8. Anterior thigh: normal
Video 6-9. Septic hip aspiration
Video 6-10. Bulging hip capsule from internal rotation
Video 6-11. Femoroacetabular impingement
Video 6-12. Femoroacetabular impingement
Video 6-13. Trochanteric bursitis: systemic lupus erythematosus
Video 6-14. Abscess
Video 6-15. Hemophilia
Video 6-16. Snapping hip: iliopsoas
Video 6-17. Snapping hip: iliopsoas
Video 6-18. Snapping hip: gluteus maximus
Video 6-19. Snapping hip: iliotibial tract
Video 6-20. Common peroneal nerve: partial transection and neuroma formation
Video 6-21. Lymph node: hyperplasia
Video 6-22. Hernia: spigelian
Video 6-23. Hernia: indirect inguinal
Video 6-24. Hernia: indirect inguinal
Video 6-25. Hernia: indirect inguinal
Video 6-26. Hernia: indirect inguinal
Video 6-27. Hernia: direct inguinal
Video 6-28. Hernia: direct inguinal
Video 6-29. Hernia: femoral
Video 6-30. Hernia: femoral
Video 6-31. Mesh
Video 6-32. Hernia: recurrent
Video 6-33. Lipoma of spermatic cord

7 Knee Ultrasound
Video 7-1. Baker cyst: anisotropy pitfall
Video 7-2. Joint effusion: lateral recess
Video 7-3. Patellar clunk syndrome
Video 7-4. Meniscal displacement
Video 7-5. Gout
Video 7-6. Quadriceps tendon tear: full-thickness
Video 7-7. Gout: patellar tendon
Video 7-8. Gout: popliteus tendon
Video 7-9. Common peroneal nerve entrapment
Video 7-10. Popliteal vein thrombosis

8 Ankle, Foot, and Lower Leg Ultrasound
Video 8-1. Anterior talofibular ligament: normal
Video 8-2. Synovial hypertrophy: rheumatoid arthritis
Video 8-3. Synovial hypertrophy and effusion: rheumatoid arthritis and infection
Video 8-4. Adventitious bursa: rheumatoid arthritis
Video 8-5. Gout: tophus and erosion
Video 8-6. Gout: tophus
Video 8-7. Sinus tarsi bursa of Gruberi
Video 8-8. Flexor hallucis longus impingement
Video 8-9. Longitudinal split tear: peroneus brevis
Video 8-10. Superior peroneal retinaculum injury (type 1) and peroneus longus tendon subluxation
Video 8-11. Peroneal tendon subluxation and tear
Video 8-12. Peroneal tendon subluxation and tear

Video 8-13. Intra-sheath peroneal tendon subluxation

Video 8-14. Intra-sheath peroneal tendon subluxation

Video 8-15. Intra-sheath peroneal tendon subluxation and tear

Video 8-16. Tendon impingement

Video 8-17. Muscle hernia: anterior tibialis

Video 8-18. Muscle hernia: anterior tibialis

Video 8-19. Muscle hernia: anterior tibialis

Video 8-20. Achilles: tendinosis

Video 8-21. Achilles: tendinosis

Video 8-22. Achilles: partial-thickness tear

Video 8-23. Achilles: full-thickness tear

Video 8-24. Achilles: full-thickness tear

Video 8-25. Achilles: full-thickness tear

Video 8-26. Achilles: healing full-thickness tear

Video 8-27. Achilles: repaired

Video 8-28. Plantar fibromatosis

Video 8-29. Morton neuroma

Video 8-30. Morton neuroma

Video 8-31. Morton neuroma: Mulder maneuver

Video 8-32. Tarsal tunnel syndrome from ganglion cyst

Video 8-33. Superficial peroneal nerve neuroma and muscle hernia

9 Interventional Techniques

Video 9-1. In-plane needle guidance approach

Video 9-2. Out-of-plane needle guidance approach

Video 9-3. Indirect localization of target using paperclip

Video 9-4. Needle visualization: jiggle technique

Video 9-5. Needle anisotropy

Video 9-6. Needle oblique to sound beam

Video 9-7. Glenohumeral joint: synovial biopsy

Video 9-8. Acromioclavicular joint: aspiration

Video 9-9. Elbow joint: aspiration (gout)

Video 9-10. Midcarpal joint: aspiration (pseudogout)

Video 9-11. Hip joint: aspiration (infection)

Video 9-12. Knee joint: aspiration (pseudogout)

Video 9-13. Tibiofibular joint: injection

Video 9-14. Ankle joint: synovial biopsy (pigmented villonodular synovitis)

Video 9-15. Metatarsophalangeal joint: aspiration

Video 9-16. Subacromial-subdeltoid bursa: injection

Video 9-17. Subacromial-subdeltoid bursa: injection

Video 9-18. Subacromial-subdeltoid bursa: injection

Video 9-19. Subacromial-subdeltoid bursa: aspiration

Video 9-20. Baker cyst: aspiration

Video 9-21. Baker cyst: injection

Video 9-22. Biceps brachii long head tendon sheath: injection

Video 9-23. De Quervain tenosynovitis: injection

Video 9-24. Iliopsoas: peritendon injection

Video 9-25. Iliopsoas: peritendon injection

Video 9-26. Iliopsoas: peritendon injection

Video 9-27. Calcific tendinosis lavage and aspiration

Video 9-28. Calcific tendinosis lavage and aspiration

Video 9-29. Calcific tendinosis lavage and aspiration

Video 9-30. Calcific tendinosis lavage and aspiration

Video 9-31. Calcific tendinosis lavage and aspiration

Video 9-32. Fenestration: common extensor tendon of elbow

Video 9-33. Fenestration: gluteus medius tendon

Video 9-34. Fenestration: patellar tendon

Video 9-35. Fenestration: Achilles tendon

Video 9-36. Platelet-rich plasma injection: adductor longus

Video 9-37. Platelet-rich plasma injection: patellar tendon

Video 9-38. Ganglion aspiration: knee

Video 9-39. Paralabral cyst aspiration: shoulder

Video 9-40. Biopsy: thigh mass (high-grade sarcoma)

Video 9-41. Biopsy: lymph node (lymphoma)

CHAPTER 1

Introduction

CHAPTER OUTLINE

EQUIPMENT CONSIDERATIONS AND IMAGE FORMATION
SCANNING TECHNIQUE
IMAGE APPEARANCE
SONOGRAPHIC APPEARANCES OF NORMAL STRUCTURES
SONOGRAPHIC ARTIFACTS
MISCELLANEOUS ULTRASOUND TECHNIQUES
COLOR AND POWER DOPPLER
DYNAMIC IMAGING

Additional videos for this topic are available online at www.expertconsult.com.

The full text of this chapter can be accessed online at www.expertconsult.com.

EQUIPMENT CONSIDERATIONS AND IMAGE FORMATION

One of the primary physical components of an ultrasound machine is the transducer, which is connected by a cable to the other components, including the image screen or monitor and the computer processing unit. The transducer is placed on the skin surface and determines the imaging plane and structures that are imaged. Ultrasound is a unique imaging method in that sound waves are used rather than ionizing radiation for image production. An essential principle of ultrasound imaging relates to the piezoelectric effect of the ultrasound transducer crystal, which allows electrical signal to be changed to ultrasonic energy and vice versa. An ultrasound machine sends the electrical signal to the transducer, which results in the production of sound waves. The transducer is coupled to the soft tissues with acoustic transmission gel, which allows transmission of the sound waves into the soft tissues. These sound waves interact with soft tissue interfaces, some of which reflect back toward the skin surface and the transducer, where they are converted to an electrical current used to produce the ultrasound image. At soft tissue interfaces between tissues that have significant differences in impedance, there is sound wave reflection, which produces a bright echo. A sound wave that is perpendicular to the surface of an object being imaged will be reflected more than if it is not perpendicular. In addition to reflection, sound waves can be absorbed and refracted by the soft tissue interfaces. The absorption of a sound wave is enhanced with increasing frequency of the transducer and greater tissue viscosity.[1]

An important consideration in ultrasound imaging is the frequency of the transducer because this determines image quality. A transducer is designated by the range of sound wave frequencies it can produce, described in megahertz (MHz). The higher the frequency, the higher the resolution of the image; however, this is at the expense of sound beam penetration as a result of sound wave absorption.[1] In contrast, a low-frequency transducer optimally assesses deeper structures, but it has relatively lower resolution. Transducers may also be designated as linear or curvilinear (Fig. 1-1). With a linear transducer, the sound wave is propagated in a linear fashion parallel to the transducer surface (Video 1-1). This is optimum in evaluation of the musculoskeletal system to assess linear structures, such as tendons, to avoid artifact. A curvilinear transducer may be used, although less commonly in evaluation of deeper structures because this increases the field of view (Video 1-2), or it may provide guidance of a needle for biopsy or aspiration. A small footprint linear probe is very important for imaging the hand, ankle, and foot given the contours of these body parts that allow only limited contact with the probe surface (see Fig. 1-1C). A small footprint transducer with an offset is helpful when performing procedures on the distal extremities.

The physical size, power, resolution, and cost of ultrasound units vary, and these factors are all related. For example, an ultrasound machine that is approximately 3 × 3 × 4 feet high will likely be very powerful, have many imaging applications,

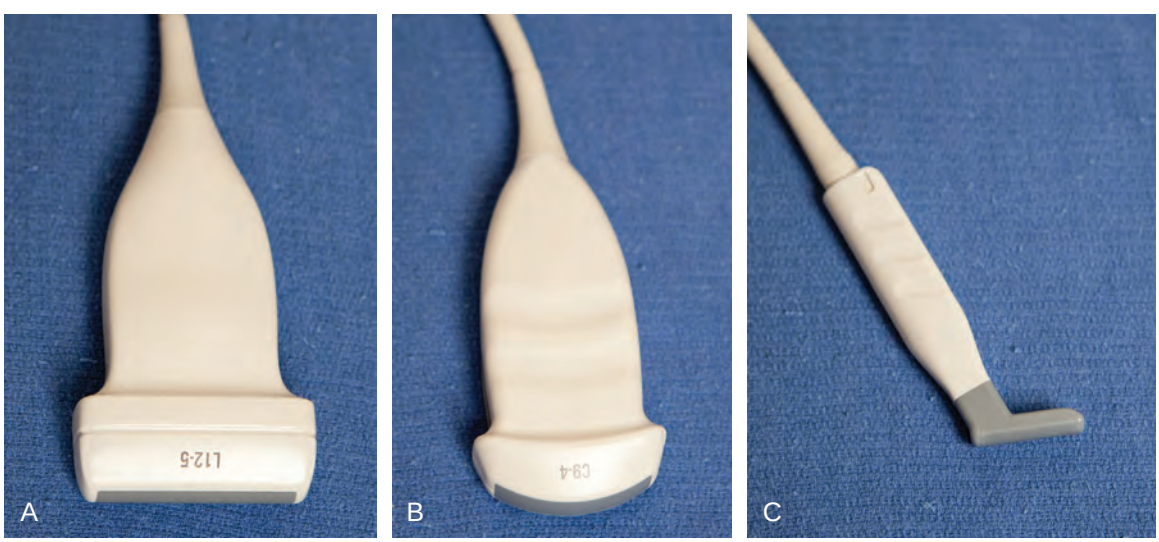

FIGURE 1-1 ■ Transducers. Photographs show linear 12-5 MHz **(A)**, curvilinear 9-4 MHz **(B)**, and compact linear 15-7 MHz **(C)** transducers.

and be able to support multiple transducers, including high-frequency transducers that result in exquisite high-resolution images. Smaller, portable machines are also available, some of which are smaller than a notebook computer. Although these machines cost less than the larger units, there may be tradeoffs related to image resolution and applications. Ultrasound units as small as a handheld electronic device have been introduced, although transducer options remain limited at this time. As technology advances, these differences have been minimized as the portable ultrasound machines have become more powerful and the larger units have become smaller. It is therefore essential in the selection of a proper ultrasound unit to consider how an ultrasound machine will be used, the size of the structures that need to be imaged, the need for machine portability, and the capabilities of the ultrasound machine.

SCANNING TECHNIQUE

To produce an ultrasound image, the transducer is held on the surface of the skin to image the underlying structures. Ample acoustic transmission gel should be used to enable the sound beam to be transmitted from the transducer to the soft tissues and to allow the returning echoes to be converted to the ultrasound image. I prefer a layer of thick transmission gel over a more cumbersome gel standoff pad. Gel that is more like liquid consistency is also less ideal because the gel tends not to stay localized at the imaging site. The transducer should be held between the thumb and fingers of the examiner's dominant hand, with the end of the transducer near the ulnar aspect of the hand (Fig. 1-2A). It is very important during imaging to stabilize or anchor the transducer on the patient with either the small finger or the heel of the imaging hand (see Fig. 1-2B). This technique is essential to maintain proper pressure of the transducer on the skin, to avoid involuntary movement of the transducer, and to allow fine adjustments in transducer positioning. Remember that the sound beam emitted from the transducer is focused relative to the short end of the transducer, and side-to-side movement of the transducer should only be a millimeter at a time.

Various terms describe manual movements of the transducer during scanning. The term *heel-toe* is used when the transducer is rocked or angled along the long axis of the transducer (Fig. 1-3A). The term *toggle* is used when the transducer is angled from side to side (see Fig. 1-3B). With both the heel-toe and toggle maneuvers, the transducer is not moved from its location, but rather the transducer is angled. The term *translate* is used when the transducer is moved to a new location while maintaining a perpendicular angle with the skin surface. The term *sweep* is used when the transducer is slid from side to side while maintaining a stable hand position, similar to sweeping a broom.

With regard to ergonomics, proper ultrasound scanning technique can help minimize fatigue and work-related injuries. Anchoring of the transducer to the patient by making contact between the scanning hand and the patient as described earlier decreases muscle fatigue of the examining arm. In addition, making sure that the scanning hand is lower than the ipsilateral shoulder with the elbow close to the body also decreases fatigue of the shoulder. If the examiner uses a chair, one at the appropriate height, preferably with wheels and with some type of back support,

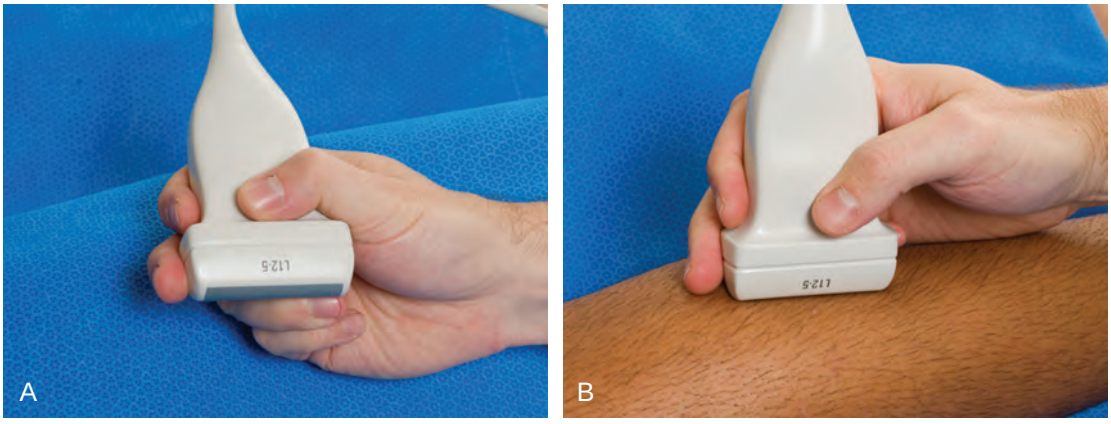

FIGURE 1-2 ■ Transducer positioning. A and **B,** Photographs show that the transducer is stabilized with simultaneous contact of the transducer, the skin surface, and the examiner's hand.

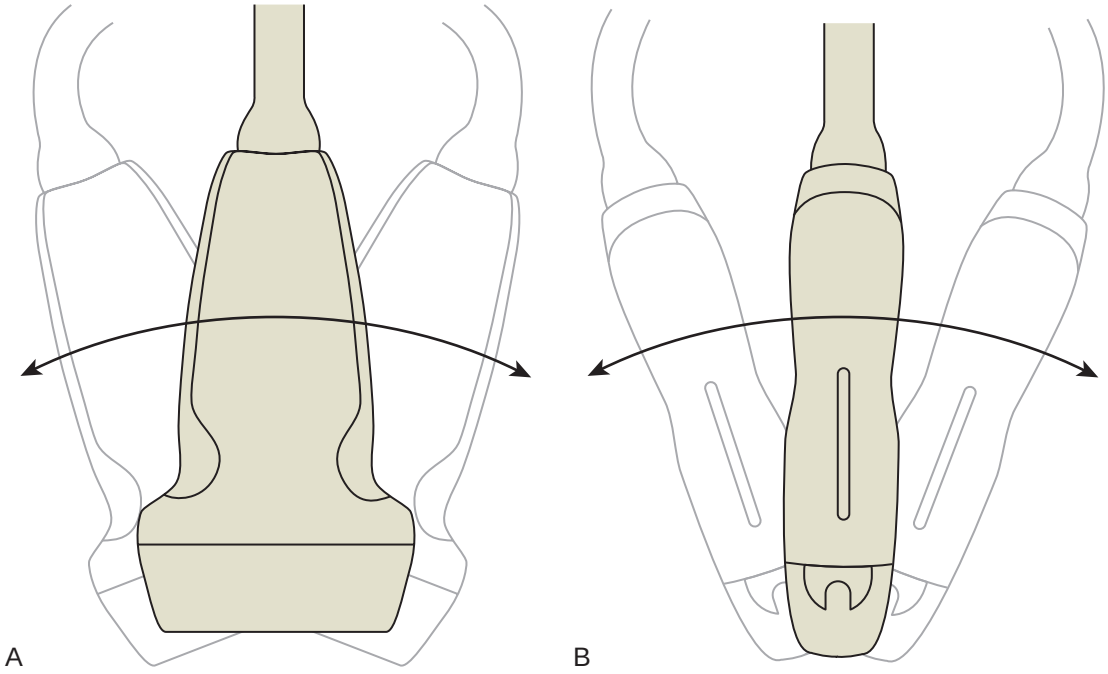

FIGURE 1-3 ■ Transducer movements. A, Heel-toe maneuver. **B,** Toggle maneuver. (Modified from an illustration by Carolyn Nowak, Ann Arbor, Mich; http://www.carolyncnowak.com/medtech.html.)

will improve comfort and maneuverability. Last, the ultrasound monitor should be near the patient's area being scanned so that visualization of both the patient and the monitor can occur while minimizing turning of the head or spine.

There are three basic steps when performing musculoskeletal ultrasound, and these steps are also similar to obtaining an adequate image with magnetic resonance imaging (MRI). The first step is to image the structure of interest in long axis and short axis (if applicable), which depends on knowledge of anatomy. Identification of bone landmarks is important for orientation. The second step is to eliminate artifacts, more specifically anisotropy (see later discussion) when considering ultrasound. When imaging a structure over bone, the cortex will appear hyperechoic and well defined when the sound beam is perpendicular, which indicates that the tissues over that segment of bone are free of anisotropy. The last step is characterization of pathology. Note the use of bone in two of the previous steps to understand anatomy and the proper imaging plane and to indicate that the sound beam is directed correctly to eliminate anisotropy.

IMAGE APPEARANCE

Once the transducer is placed on the patient's skin with intervening gel, a rectangular image (when using a linear transducer) appears on the monitor. The top of the image represents the superficial soft tissues that are in contact with the transducer, and the deeper structures appear toward the lower aspect of the image (Fig. 1-4). To understand the resulting ultrasound image, consider the sound beam as a plane or slice that extends down from the transducer along its long axis. It is this plane that is portrayed on the image. The left and right sides of the image can represent either end of the transducer, and this can usually be switched by using the left-to-right invert button on the ultrasound machine or by simply rotating the transducer 180 degrees. When imaging a structure in long axis, it is

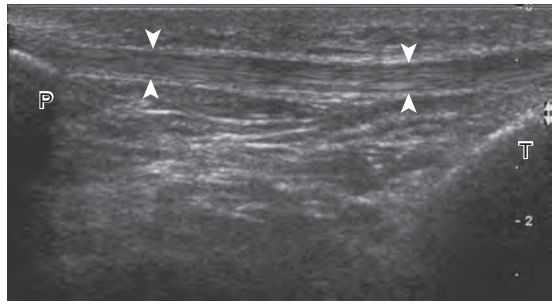

FIGURE 1-4 ■ Normal patellar tendon. Ultrasound image of patellar tendon in long axis *(arrowheads)* shows hyperechoic fibrillar echotexture. P, patella; T, tibia.

common to have the proximal aspect on the left side of the image and the distal aspect on the right.

Image optimization is essential to maximize resolution and clarity. The first step is to select the proper transducer and frequency. Higher-frequency transducers (10 MHz or greater) optimally evaluate superficial structures, whereas lower-frequency transducers are used for deep structures. Linear transducers are typically used, unless the area of interest is deep, such as the hip region, where a curvilinear transducer may be chosen. After the proper transducer is selected and placed on the patient, the next step is to adjust the depth of the sound beam; this is accomplished by a button or dial on the ultrasound machine. The depth of the sound beam is adjusted until the structure of interest is visible and centered in the image (Fig. 1-5A and B). The next step in optimization with many ultrasound machines is to adjust the focal zones of the ultrasound beam, if present on the ultrasound machine. This feature is typically displayed on the side of the image as a number of cursors or other symbols. It is optimum to reduce the number of focal zones to span the area of interest because increased focal zones will decrease the frame rate that produces a windshield-wiper effect. It is also important to move the depth of the focal zones to the depth where the structure is to be imaged to optimize resolution (see Fig. 1-5C). Some ultrasound machines have a broad focal zone that

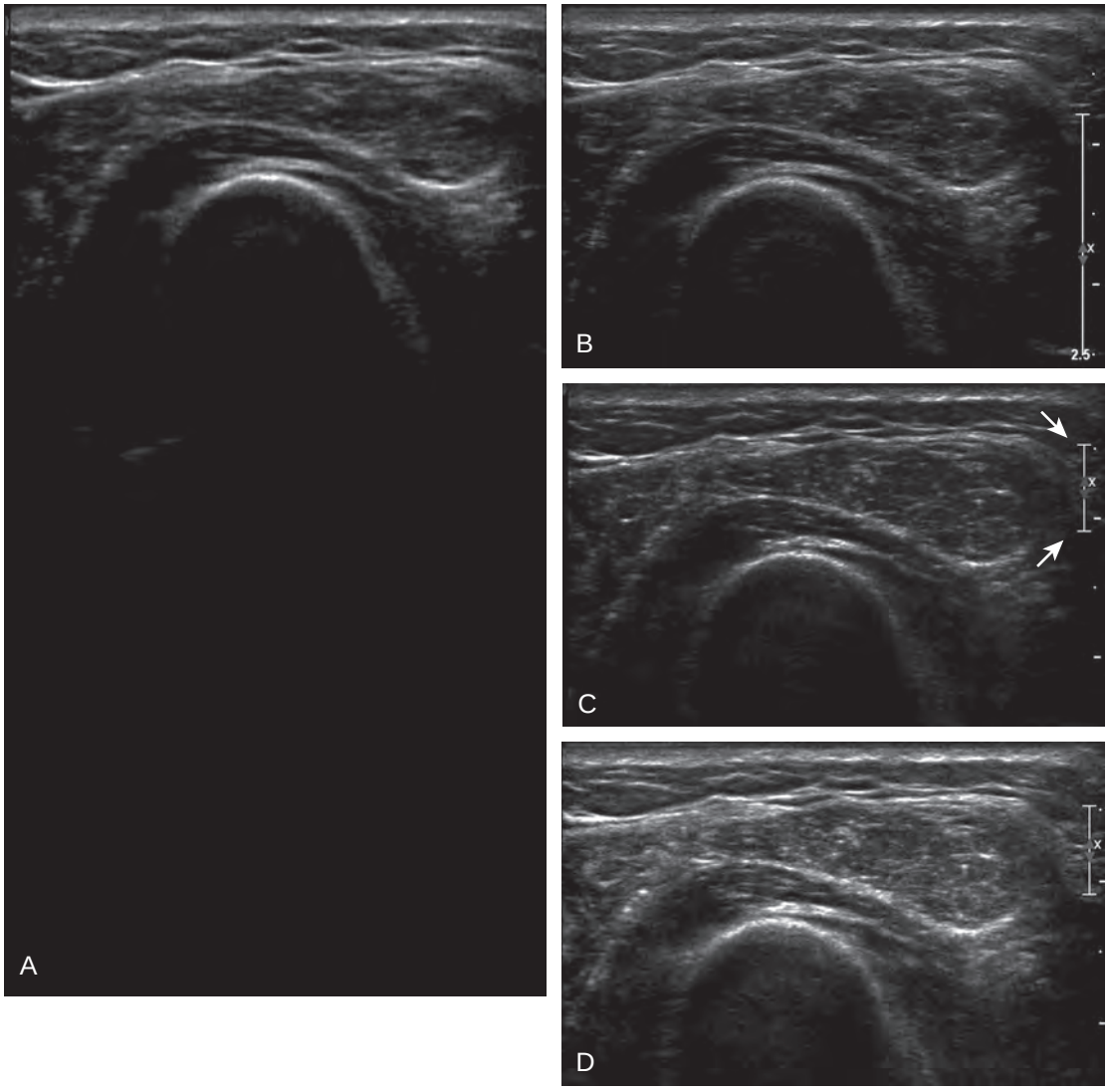

FIGURE 1-5 ■ Optimizing the ultrasound image. A, Ultrasound image of forearm musculature shows improper depth, focal zone, and gain. **B,** Depth is corrected as area of interest is centered in image. **C,** Focal zone width is decreased and centered at area of interest *(arrows)*. **D,** Gain is increased.

may not have to be moved. Finally, the overall gain can be adjusted by a knob on the ultrasound machine to increase or decrease the overall brightness of the echoes, which is in part determined by the ambient light in the examination room (see Fig. 1-5D). The gain should ideally be set where one can appreciate the ultrasound characteristics of normal soft tissues (as described later).

The ultrasound image is produced when the sound beam interacts with the tissues beneath the transducer and this information returns to the transducer. At an interface between tissues where there is a large difference in impedance, the sound beam is strongly reflected, and this produces a very bright echo on the image, which is described as *hyperechoic*. Examples include interfaces between bone and soft tissues, where the area beneath the interface is completely black from shadowing because no echoes extend beyond the interface. An area on the image that has no echo and is black is termed *anechoic*, whereas an area with a weak or low echo is termed *hypoechoic*. If a structure is of equal echogenicity to the adjacent soft tissues, it may be described as *isoechoic*.

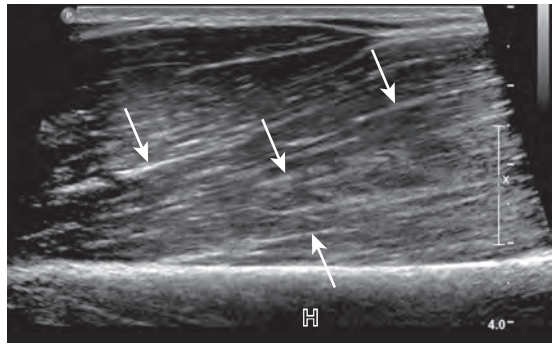

FIGURE 1-6 ■ Muscle. Ultrasound image of brachialis and biceps brachii muscles in long axis shows hypoechoic muscle and hyperechoic fibroadipose septa *(arrows)*. H, humerus.

SONOGRAPHIC APPEARANCES OF NORMAL STRUCTURES

Normal musculoskeletal structures have characteristic appearances on ultrasound imaging.[2] Normal tendons appear hyperechoic with a fiber-like or fibrillar echotexture (see Fig. 1-4).[3] At close inspection, the linear fibrillar echoes within a tendon represent the endotendineum septa, which contain connective tissue, elastic fibers, nerve endings, blood, and lymph vessels.[3] Continuous tendon fibers are best appreciated when they are imaged long axis to the tendon. On such a long axis image, by convention the proximal aspect is on the left side of the image, with the distal aspect on the right. Normal muscle tissue appears relatively hypoechoic (Fig. 1-6). At closer inspection, the hypoechoic muscle tissue is separated by fine hyperechoic fibroadipose septa or perimysium, which surrounds the hypoechoic muscle bundles. The surface of bone or calcification is typically very hyperechoic, with posterior acoustic shadowing and possibly posterior reverberation if the surface of the bone is smooth and flat (see Fig. 1-6). The hyaline cartilage covering the articular surface of bone is hypoechoic and uniform (Fig. 1-7A and B), whereas the fibrocartilage, such as the labrum of the hip and shoulder, and the knee menisci are hyperechoic (see Fig. 1-7B). Ligaments have a hyperechoic, striated

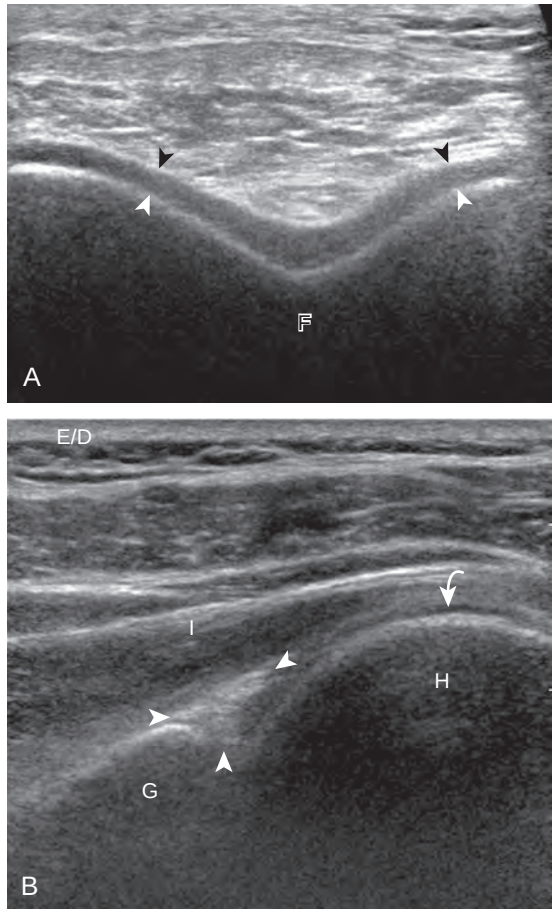

FIGURE 1-7 ■ Cartilage. A, Ultrasound image transverse over the distal anterior femur shows hypoechoic hyaline cartilage *(arrowheads)*. F, femur. **B,** Ultrasound image of infraspinatus in long axis (I) shows a hyperechoic fibrocartilage glenoid labrum *(arrowheads)* and hypoechoic hyaline cartilage *(curved arrow)*. Note hyperechoic epidermis and dermis (E/D), and adjacent deeper hypoechoic hypodermis with hyperechoic septa G, glenoid; H, humerus.

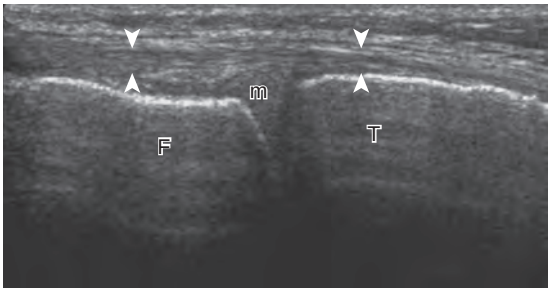

FIGURE 1-8 ■ Tibial collateral ligament. Ultrasound image of tibial collateral ligament of the knee in long axis shows compact fibrillar echotexture *(arrowheads).* F, femur; m, meniscus; T, tibia.

appearance that is more compact compared with tendons (Fig. 1-8). In addition, ligaments are also identified in that they connect two osseous structures. Often normal ligaments may appear relatively hypoechoic when surrounded by hyperechoic subcutaneous fat; however, a compact linear hyperechoic ligament can be appreciated when imaged in long axis perpendicular to the ultrasound beam.

Normal peripheral nerves have a fascicular appearance in which the individual nerve fascicles are hypoechoic, surrounded by hyperechoic connective tissue epineurium (Fig. 1-9).[4] Hyperechoic fat is typically seen around larger peripheral nerves. In short axis, peripheral nerves display a honeycomb or speckled appearance, which allows their identification. Because peripheral nerves have a relatively mixed hyperechoic and hypoechoic echotexture, their appearance changes relative to the adjacent tissues. For example, the median nerve in the forearm, when surrounded by hypoechoic muscle, appears relatively hyperechoic; in contrast, more distally in the carpal tunnel, when it is surrounded by hyperechoic tendon, the median nerve appears relatively hypoechoic (see Fig. 5-3B in Chapter 5). The epidermis and dermis collectively appear hyperechoic, whereas the hypodermis shows hypoechoic fat and hyperechoic fibrous septa (see Fig. 1-7).

SONOGRAPHIC ARTIFACTS

One must be familiar with several artifacts common to musculoskeletal ultrasound. One such artifact is anisotropy.[5] When a tendon is imaged perpendicular to the ultrasound beam, the characteristic hyperechoic fibrillar appearance is displayed. However, when the ultrasound beam is angled as little as 5 degrees relative to the long axis of such a structure, the normal hyperechoic appearance is lost; the tendon becomes more hypoechoic with increased angle (Figs. 1-10 to 1-13). This variation of ultrasound interaction with fibrillar tissues is called *anisotropy*, and it involves tendons and ligaments and, to a lesser extent, muscle. Because abnormal tendons and ligaments may also appear hypoechoic, it is important to focus on that segment of tendon or ligament that is perpendicular to the ultrasound beam, to exclude anisotropy. With a curved structure, such as the distal aspect of the supraspinatus tendon, the transducer is continually moved or angled to exclude anisotropy as the cause of a hypoechoic tendon segment (see Fig. 1-11) (Video 1-3). Anisotropy is noted both in long axis and short axis of ligaments and tendons (Video 1-4), but it occurs when the sound beam is angled relative to the long axis of a structure (see Fig. 1-12). Therefore, to correct for anisotropy, the transducer is angled along the long axis of the imaged tendon or ligament; when imaging a tendon in long axis, the transducer is angled as a heel-toe maneuver (see Fig. 1-3A and Video 1-5),

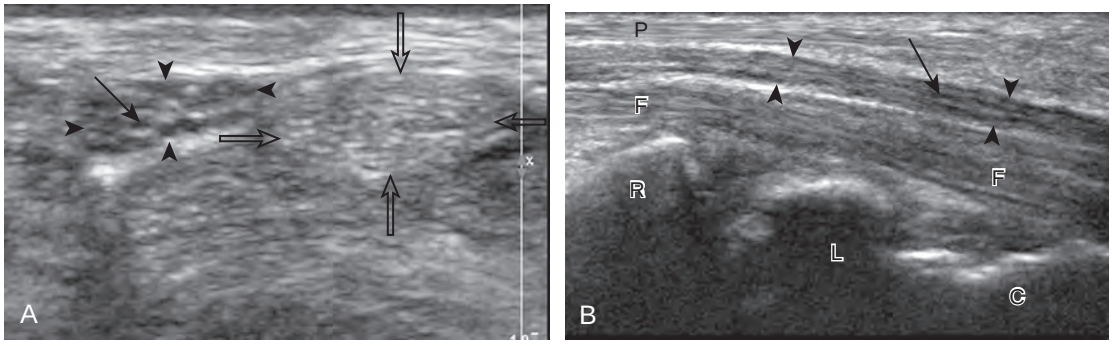

FIGURE 1-9 ■ Median nerve. A, Ultrasound image of median nerve in short axis *(arrowheads)* shows individual hypoechoic nerve fascicles *(arrow)* and the adjacent hyperechoic flexor carpi radialis tendon *(open arrows).* **B,** Ultrasound image of median nerve in long axis *(arrowheads)* shows hypoechoic nerve fascicles *(arrow).* Note the adjacent fibrillar flexor digitorum (F) and palmaris longus (P) tendons. C, capitate; L, lunate; R, radius.

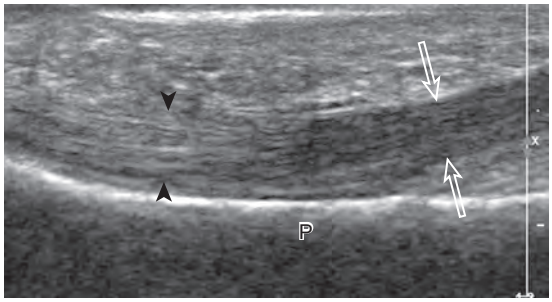

FIGURE 1-10 ■ Anisotropy. Ultrasound image of flexor tendons of the finger in long axis shows normal tendon hyperechogenicity *(arrowheads)* becoming more hypoechoic as the tendon becomes oblique relative to the sound beam *(open arrows).* P, proximal phalanx.

whereas in short axis, the transducer is toggled (see Fig. 1-3B and Video 1-6). Anisotropy can be used to one's advantage in identification of a hyperechoic tendon or ligament in close proximity to hyperechoic soft tissues, such as in the ankle and wrist. When imaging a tendon in short axis, toggling the transducer will cause the tendon to become hypoechoic, thus allowing its distinction from the adjacent hyperechoic fat that does not demonstrate anisotropy (see Fig. 1-12). Once the tendon is identified, it is important to eliminate anisotropy to exclude pathology. Anisotropy is also helpful in identification of some ligaments, such as in the ankle, because they are often adjacent to hyperechoic fat (see Fig. 1-13). In addition, hyperechoic tendon calcifications can be made more conspicuous when they are surrounded by hypoechoic tendon from anisotropy with angulation of the transducer (see Fig. 3-62 in Chapter 3). When performing an interventional procedure, it is anisotropy that causes the needle to become less conspicuous when the needle is not perpendicular to the sound beam (see Fig. 9-7 in Chapter 9).

Another important artifact is *shadowing*. This occurs when the ultrasound beam is reflected, absorbed, or refracted.[6] The resulting image

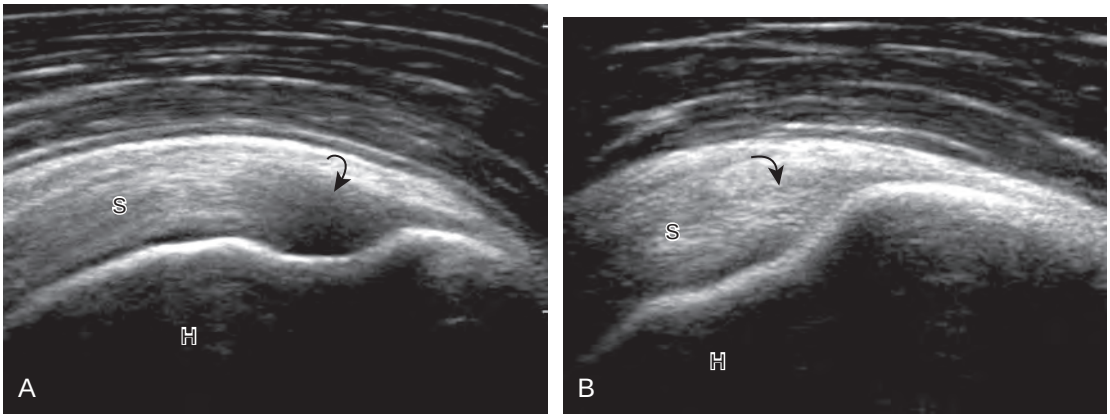

FIGURE 1-11 ■ Anisotropy. Ultrasound images of distal supraspinatus tendon in long axis (S) shows an area of hypoechoic anisotropy *(curved arrow)* **(A),** where the tendon fibers become oblique to the sound beam, which is eliminated **(B)** when the transducer is repositioned so that the tendon fibers are perpendicular to the sound beam. H, humerus.

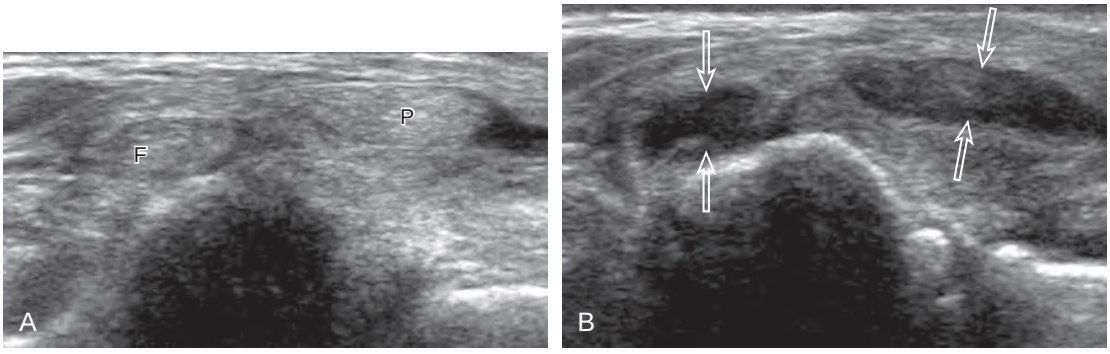

FIGURE 1-12 ■ Anisotropy. Ultrasound images of tibialis posterior (P) and flexor digitorum longus (F) tendons in short axis at the ankle show normal tendon hyperechogenicity **(A)** and hypoechoic anisotropy *(open arrows)* **(B),** when angling or toggling the transducer along the long axis of the tendons, thus aiding in identification of tendons relative to surrounding hyperechoic fat.

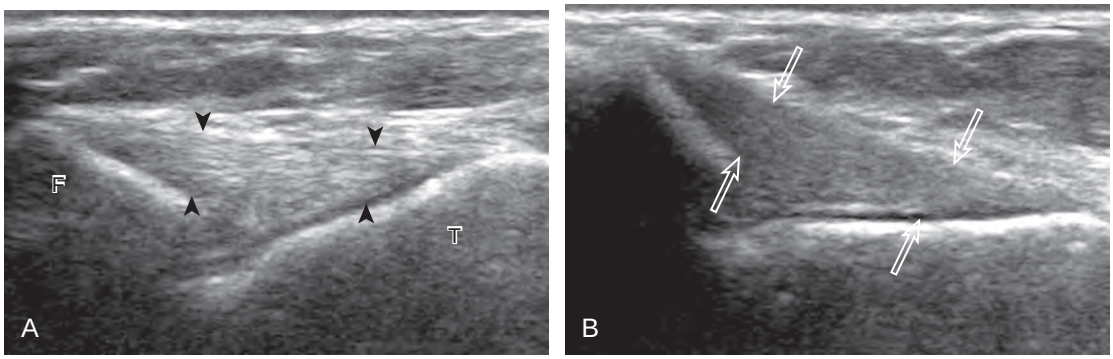

FIGURE 1-13 ■ Anisotropy. Ultrasound images of anterior talofibular ligament in long axis *(arrowheads)* in the ankle show normal ligament hyperechogenicity **(A)** and hypoechoic anisotropy *(open arrows)* **(B),** when angling the transducer along the long axis of the ligament, thus aiding in identification of ligament relative to surrounding hyperechoic fat. F, fibula; T, talus.

shows an anechoic area that extends deep from the involved interface. Examples of structures that produce shadowing include interfaces with bone or calcification (Fig. 1-14), some foreign bodies (see Chapter 2), and gas. An object with a small radius of curvature or a rough surface will display a clean shadow, whereas an object with a large radius of curvature and a smooth surface will display a dirty shadow (resulting from superimposed reverberation echoes).[7] Refractile shadowing may also occur at the edge of some structures, such as a foreign body or the end of a torn Achilles or patellar tendon (Fig. 1-15).[8]

Another type of artifact is *posterior acoustic enhancement* or *increased through-transmission*. This occurs during imaging of fluid (Figs. 1-16 and 1-17) and solid soft tissue tumors, such as peripheral nerve sheath tumors (see Fig. 2-59 in Chapter 2) and giant cell tumors of tendon sheath (Fig. 1-18).[9] In these situations, the sound beam is relatively less attenuated compared with the

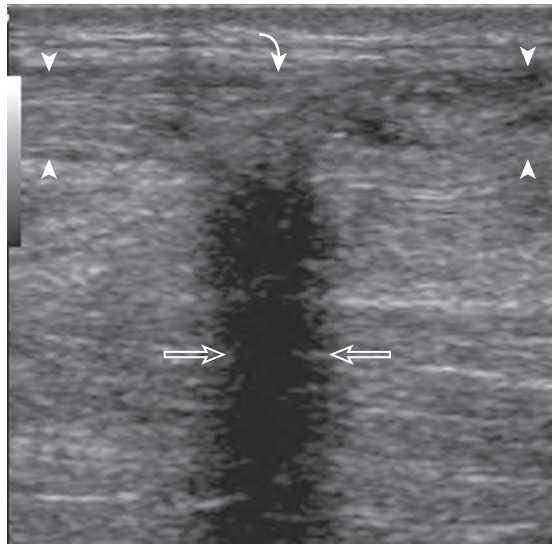

FIGURE 1-15 ■ Refractile shadowing. Ultrasound image of Achilles tendon in long axis *(arrowheads)* shows shadowing *(open arrows)* at the site of a full-thickness tear *(curved arrow).*

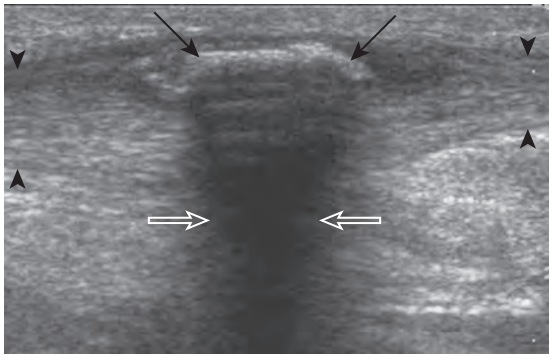

FIGURE 1-14 ■ Shadowing. Ultrasound image of Achilles tendon in long axis *(arrowheads)* shows hyperechoic ossification *(arrows)* with posterior acoustic shadowing *(open arrows).*

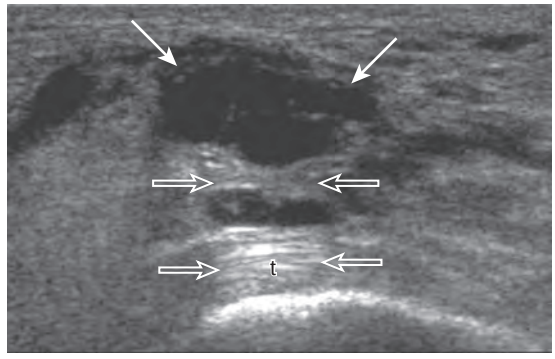

FIGURE 1-16 ■ Increased through-transmission. Ultrasound image of a ganglion cyst *(arrows)* in the ankle shows increased through-transmission *(open arrows).* t, Flexor hallucis longus tendon.

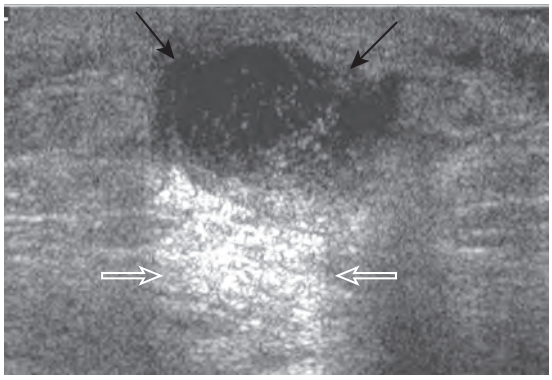

FIGURE 1-17 ■ Increased through-transmission. Ultrasound image of a soft tissue abscess *(arrows)* in the shoulder shows increased through-transmission *(open arrows).*

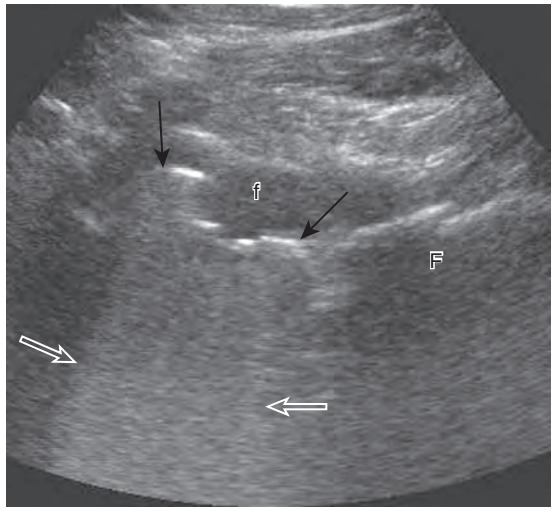

FIGURE 1-19 ■ Ring-down artifact. Ultrasound image in long axis to the femoral component of a total hip arthroplasty shows the hyperechoic metal surface of the arthroplasty *(arrows)* and posterior ring-down artifact *(open arrows).* Note the overlying joint fluid (f) and adjacent native femur (F).

adjacent tissues; therefore, the deeper soft tissues will appear relatively hyperechoic compared with the adjacent soft tissues.[6]

Another artifact with musculoskeletal implications is *posterior reverberation*. This occurs when the surface of an object is smooth and flat, such as a metal object or the surface of bone. In this situation, the sound beam reflects back and forth between the smooth surface and the transducer and produces a series of linear reflective echoes that extend deep to the structure.[6] If the series of reflective echoes is more continuous deep to the structure, the term *ring-down artifact* is used, as may be seen with metal surfaces (Fig. 1-19). Ultrasound is ideal in evaluation of structures immediately overlying metal hardware because this reverberation artifact occurs deep to the hardware without obscuring the superficial soft tissues. Related to posterior reverberation is the comet-tail artifact, such as that seen with soft tissue gas (Fig. 1-20), which appears as a short segment of posterior bright echoes that narrows further from the source of the artifact.

One additional artifact to consider is *beam-width artifact*. This is essentially analogous to volume averaging and occurs if the ultrasound beam is too wide relative to the object being imaged. An example is imaging of a small calcification in which the relatively large beam width may eliminate shadowing. This effect can be reduced by adjusting the focal zone to the level of the object of interest.[6]

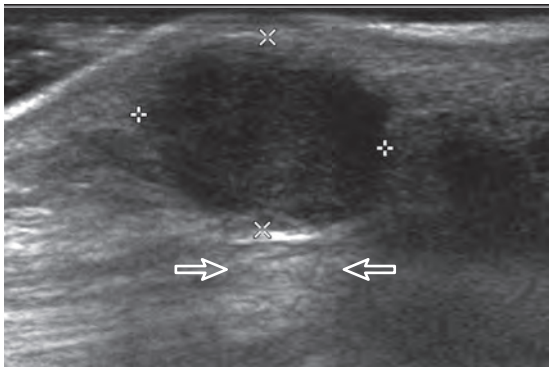

FIGURE 1-18 ■ Increased through-transmission. Ultrasound image of a giant cell tumor of the tendon sheath *(between × and + cursors)* shows increased through-transmission *(open arrows).*

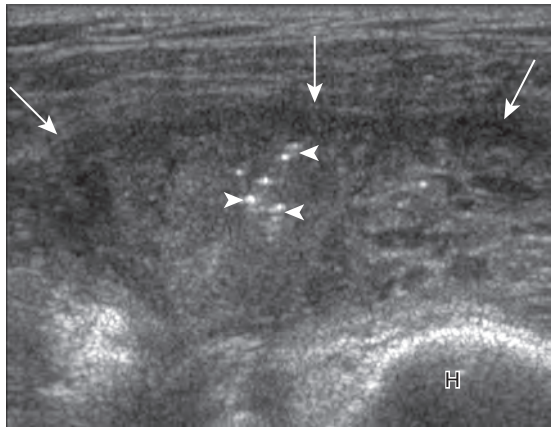

FIGURE 1-20 ■ Comet-tail artifact. Ultrasound over an infected subacromial-subdeltoid bursa *(arrows)* shows hyperechoic foci of gas with comet-tail artifact *(arrowheads).* H, greater tuberosity of the humerus.

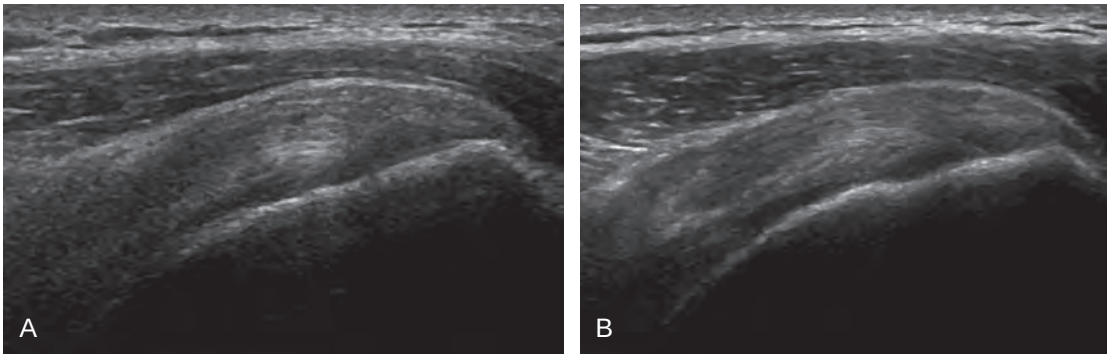

FIGURE 1-21 ■ Spatial compounding. Ultrasound images of the supraspinatus tendon *(arrowheads)* without **(A)** and with **(B)** spatial compounding shows softening of the image in **B.**

MISCELLANEOUS ULTRASOUND TECHNIQUES

Several ultrasound techniques or applications available with some ultrasound machines can enhance scanning and diagnostic capabilities. One such method is *spatial compound sonography*.[10] Unlike conventional ultrasound, sound beams with spatial compound sonography are produced at several different angles, with information combined to form a single ultrasound image. This improves tissue plane definition, but it has a smoothing effect, and motion blur is more likely because frames are compounded (Fig. 1-21). One must be aware that the use of spatial compounding may reduce the artifact produced by a foreign body, which may decrease its conspicuity (see Fig. 2-52 in Chapter 2).

Another ultrasound technique is *tissue harmonic imaging*. Unlike conventional ultrasound, which receives only the fundamental or transmitted frequency to produce the image, with tissue harmonic imaging, harmonic frequencies produced during ultrasound beam propagation through tissues are used to produce the image. This technique assists in evaluation of deep structures and also improves joint and tendon surface visibility.[11] The technique may more clearly delineate the edge of a soft tissue mass (Fig. 1-22) or a fluid-filled tendon tear (Fig. 1-23).

One helpful technique available on some ultrasound machines is *extended field of view*. With this technique, an ultrasound image is produced by combining image information obtained during real-time scanning. This allows imaging of an entire muscle from origin to insertion; it is helpful in measuring large abnormalities (e.g., tumor or tendon tear) and in displaying and communicating ultrasound findings (Figs. 1-24 and 1-25).[12] An alternative to extended field of view imaging that is available on some ultrasound equipment is

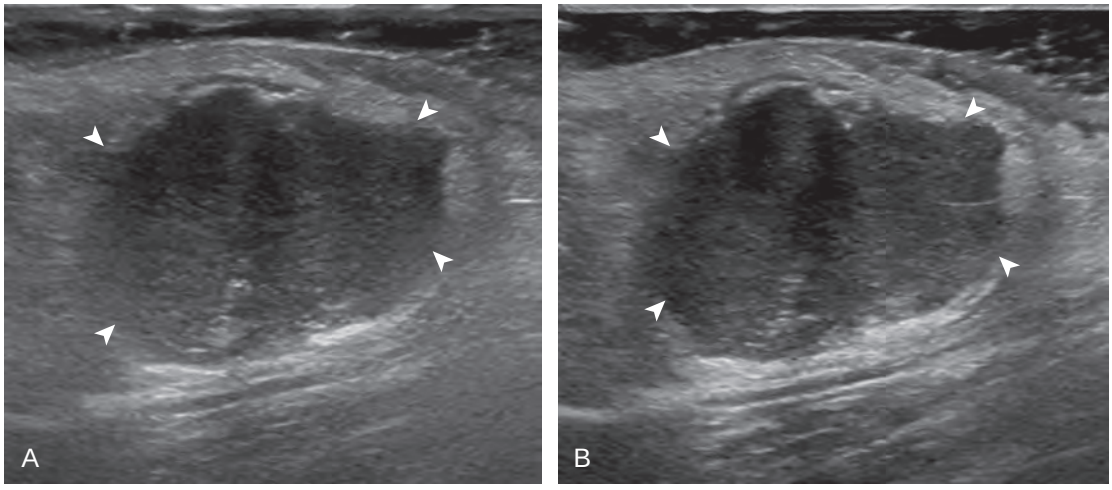

FIGURE 1-22 ■ Tissue harmonic imaging. Ultrasound images of a recurrent giant cell tumor *(arrowheads)* without **(A)** and with **(B)** tissue harmonic imaging shows increased definition of the mass borders in **B.** Note posterior increased through-transmission.

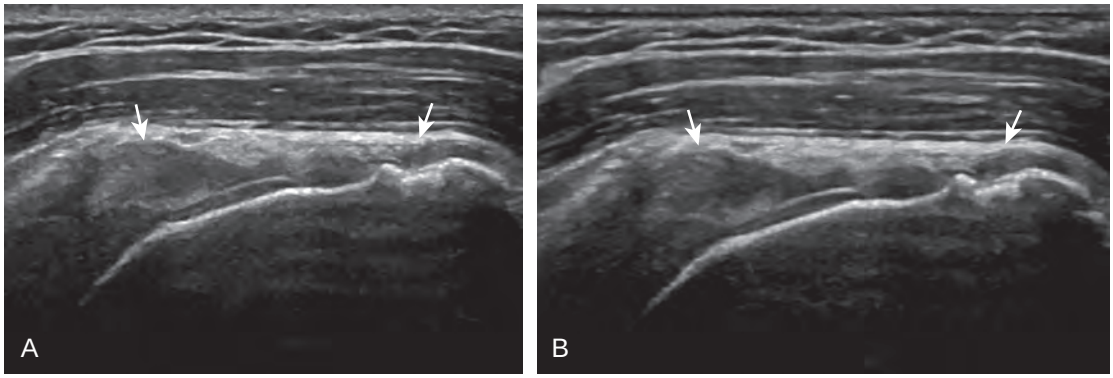

FIGURE 1-23 ■ Tissue harmonic imaging. Ultrasound images of full-thickness supraspinatus tendon tear in long axis *(arrows)* without **(A)** and with **(B)** tissue harmonic imaging shows clearer distinction of retracted tendon stump *(left arrow)* because intervening fluid is more hypoechoic.

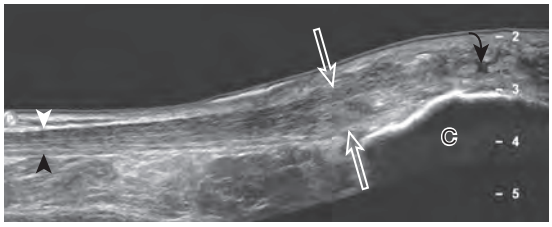

FIGURE 1-24 ■ Extended field of view. Ultrasound image of the Achilles tendon in long axis shows hypoechoic and swollen tendinosis *(open arrows)* and retro-Achilles bursitis *(curved arrow).* Note the normal Achilles thickness proximally *(arrowheads).* C, calcaneus.

the split-screen function, which essentially joins two images on the display screen that doubles the field of view.

A number of ultrasound techniques are relatively new, and their practical musculoskeletal applications are still being defined. One such technique is *three-dimensional ultrasound*, which acquires data as a volume (either mechanically or freehand) and thus enables reconstruction at any imaging plane (Fig. 1-26). This technique has been used to characterize rotator cuff tears and to quantify a volume of tissue such as tumor or synovial proliferation.[13,14] An additional technique is *fusion imaging*, in which real-time ultrasound imaging can be superimposed on computed tomography (CT) or MRI; this has been used to assist with needle guidance for sacroiliac joint injections.[15] One last technique is *ultrasound elastography*, which is used to assess the elastic properties of tissue. With this technique, compression of tissue produces strain or displacement within the tissue. Displacement is less when tissue is hard; it is displayed as blue on the ultrasound image, whereas soft tissue is displayed as red (Fig. 1-27). With regard to musculoskeletal applications, normal tendons appear as blue, whereas areas of tendinopathy, such as of the Achilles tendon or common extensor tendon of the elbow, appear as red.[14,16-19] A future direction is the quantitative measurement of tissue elasticity using *shear-wave ultrasound elastography*.[20]

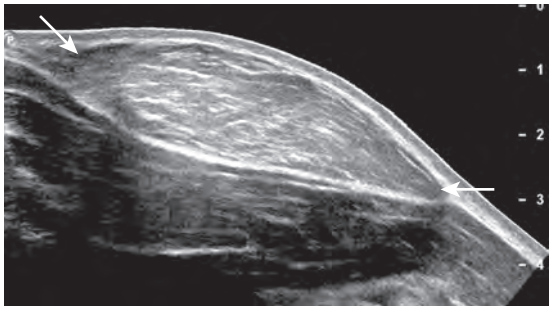

FIGURE 1-25 ■ Extended field of view. Ultrasound image shows full extent of a lipoma *(between arrows).*

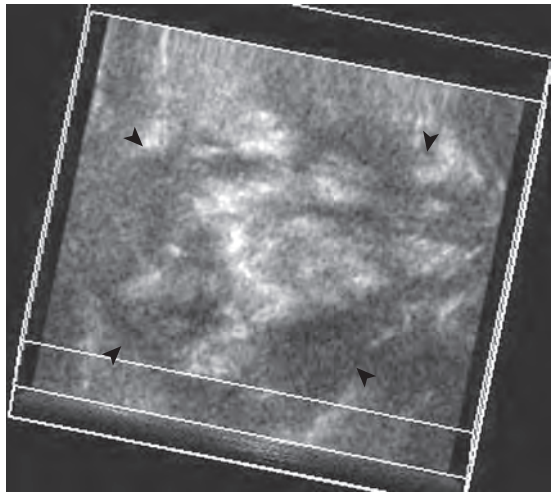

FIGURE 1-26 ■ Three-dimensional imaging. Ultrasound image reconstructed in the coronal plane shows a heterogeneous thigh sarcoma *(arrowheads).*

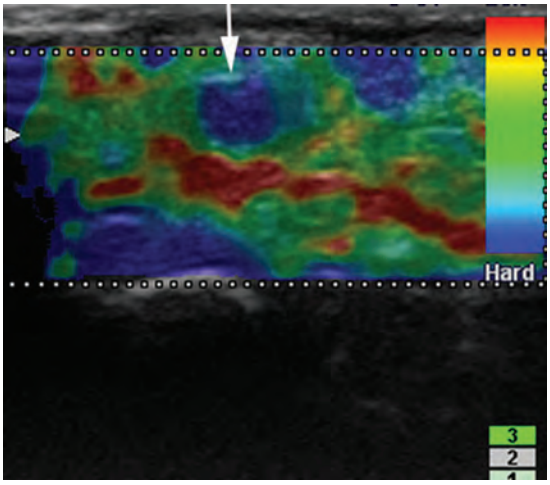

FIGURE 1-27 ■ Ultrasound elastography: foreign body granuloma. Ultrasound images of common extensor tendon elbow show suture granuloma *(blue mass-like area below white arrow).* Note that hard tissues are displayed in blue and soft tissues in red. (Courtesy of Y. Morag, Ann Arbor, Mich.)

COLOR AND POWER DOPPLER

Most ultrasound machines have the option of color and power Doppler imaging, with possible spectral waveform analysis. Ultrasound uses the *Doppler effect*, in which the sound frequency of an object changes as the object travels toward or away from a point of reference, to obtain information about blood flow. *Color flow imaging* shows colored blood flow superimposed on a gray-scale image, in which two colors such as red and blue represent flow toward and away from the transducer, respectively (Fig. 1-28).[21] *Pulsed-wave or duplex Doppler ultrasound* displays an ultrasound image and waveform (Fig. 1-29). There are important considerations to optimize the Doppler ultrasound. Reducing the width of the field of view and increasing the frame rate are helpful. To correct for aliasing (when the Doppler shift frequency of blood is greater than the detected frequency, which causes an error in frequency measurement), one can increase the pulse repetition frequency, lower the ultrasound frequency, or increase the angle between the sound beam and the flow direction toward perpendicular. *Power Doppler* is another method of color Doppler ultrasound that is more sensitive to blood flow (it shows small vessels and slow flow rates) compared with conventional color Doppler, and it assigns a color to blood flow regardless of direction (Fig. 1-30). Power Doppler is extremely sensitive to movement of the transducer, which produces a flash artifact. It is important to adjust the color gain optimally for Doppler imaging to avoid artifact if the setting is too sensitive and for false-negative flow if sensitivity is too low. To optimize power Doppler imaging, set the color background (without the gray-scale displayed) so that the lowest level of color nearly uniformly is present, with only minimal presence of the next highest color level.[22]

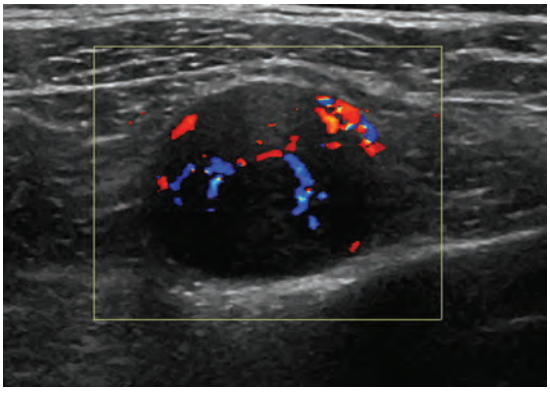

FIGURE 1-28 ■ Color Doppler: schwannoma. Color Doppler ultrasound image shows increased blood flow in hypoechoic peripheral nerve sheath tumor.

Increased blood flow on color or power Doppler imaging may occur with greater perfusion, inflammation, and neovascularity. In imaging soft tissues, color and power Doppler imaging are used to confirm that an anechoic tubular structure is a blood vessel and to confirm blood flow. When a mass is identified, increased blood flow may suggest neovascularity, possibly from malignancy (Fig. 1-31).[23] Although the finding is nonspecific, a tumor without flow is more likely to be benign, and malignant tumors usually demonstrate increased flow and irregular vessels.[24] With regard to superficial lymph nodes, either no flow or hilar flow is more common with benign lymph node enlargement, and spotted, peripheral, or mixed patterns of flow are more common with malignant lymph node enlargement (see Chapter 2).[25] Color or power Doppler imaging is also helpful in the differentiation between complex fluid and a mass or synovitis; the former typically has no internal flow, and the latter may show increased flow.[26] After treatment for inflammatory arthritis, color and power Doppler imaging can show interval decrease in flow, which would indicate a positive response.[27] It is also important to use color Doppler imaging during a biopsy to ensure that major vessels are avoided.

DYNAMIC IMAGING

One significant advantage of ultrasound over other static imaging methods, such as radiography, CT, and conventional MRI, is the *dynamic*

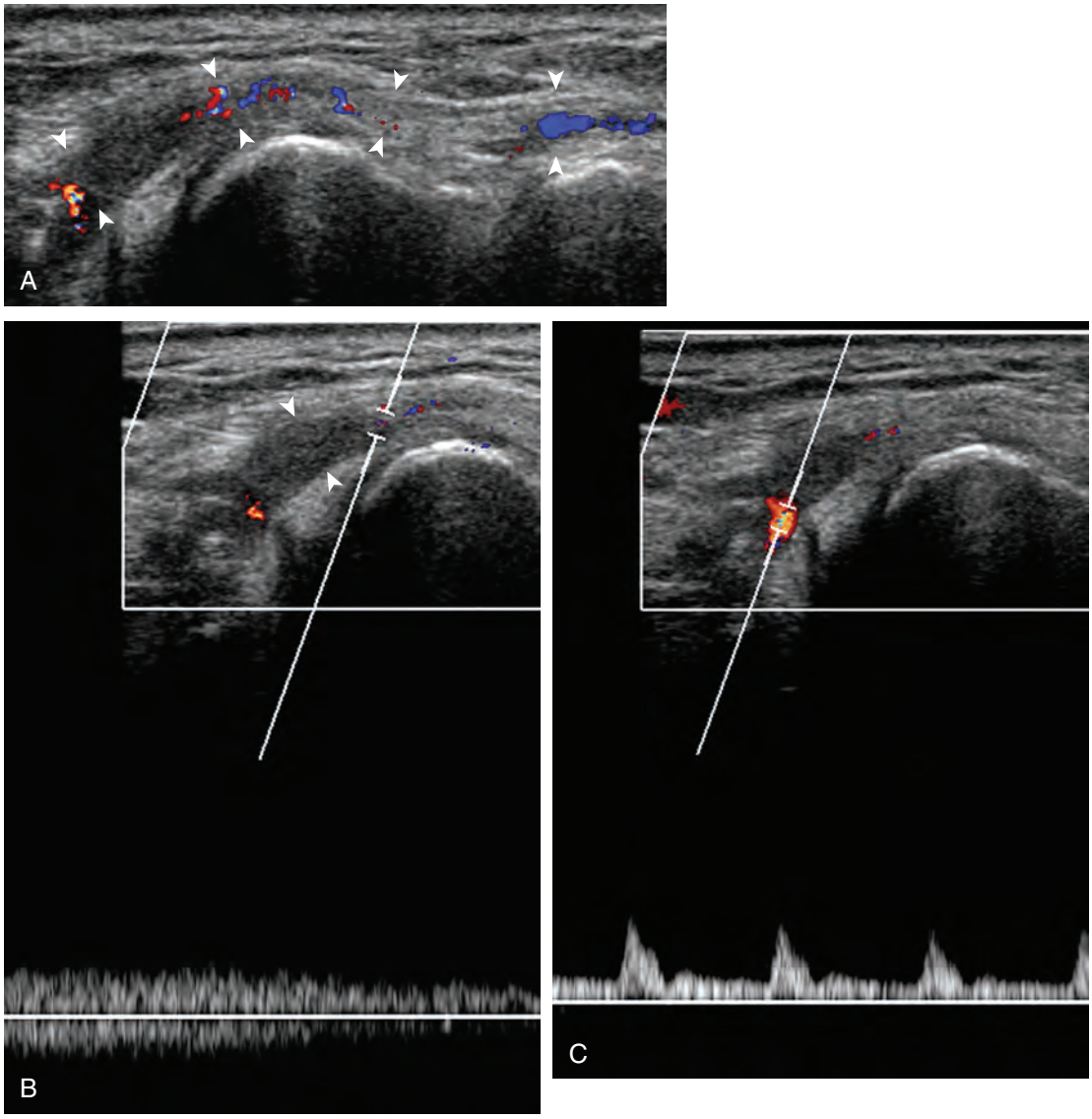

FIGURE 1-29 ■ Color Doppler: Radial artery thrombosis. A, Color Doppler ultrasound image in long axis to the radial artery *(arrowheads)* at the wrist shows hypoechoic thrombus and diminished blood flow. **B,** Pulsed-wave Doppler shows the loss of normal arterial flow at the site of thrombus **(B)** and distal reconstitution from the deep palmar arch **(C)**.

capability. On a basic level, ultrasound evaluation can be directly guided by a patient's history, symptoms, and findings at physical examination. In fact, regardless of the protocol followed for imaging a joint, it is essential that ultrasound is focused during one aspect of the examination over any area of point tenderness or focal symptoms.[28] Once ultrasound examination is begun, the patient can directly give feedback with regard to pain or other symptoms with transducer pressure over an ultrasound abnormality. When a patient has a palpable abnormality, direct palpation under ultrasound visualization will ensure that the imaged abnormality corresponds to the palpable abnormality. Graded compression also provides additional information about soft tissue masses; lipomas are often soft and pliable (see Video 2-7).

In the setting of a rotator cuff tear, compression can help demonstrate the volume loss associated with a full-thickness tear (see Video 3-19). With regard to peripheral nerves, transducer pressure over a nerve at the site of entrapment can reproduce symptoms and help to guide the examination. Transducer pressure over a stump neuroma is also important to determine which neuroma is causing symptoms. If during examination there is question of a complex fluid

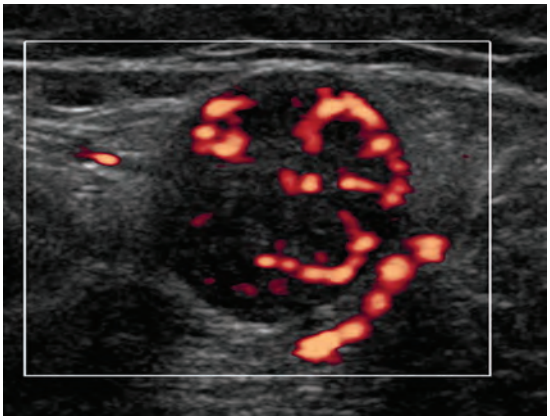

FIGURE 1-30 ■ Power Doppler: schwannoma. Power Doppler ultrasound image shows increased blood flow in hypoechoic peripheral nerve sheath tumor.

collection, variable transducer pressure can demonstrate swirling of internal debris and displacement, which indicates a fluid component (see Videos 6-13 and 6-14). In contrast, synovial proliferation would show only minimal compression without internal movement of echoes, with possible additional findings of flow on color and power Doppler imaging (see Video 8-3).

Dynamic imaging is also important in evaluation of complete full-thickness muscle, tendon, or ligament tear. When a full-thickness muscle or tendon tear is suspected, the muscle-tendon unit may be actively contracted or passively moved during imaging in long axis (see Videos 7-6 and 8-23). Demonstration of muscle or tendon stumps that move away from each other during this dynamic maneuver at the site of the tear indicates full-thickness extent. With regard to ligament tear, a joint can be stressed while imaging in long axis to the ligament to evaluate for ligament disruption and abnormal joint space widening. One example of this is applying valgus stress to the elbow when evaluating for ulnar collateral ligament tear (see Videos 4-10 and 4-11).

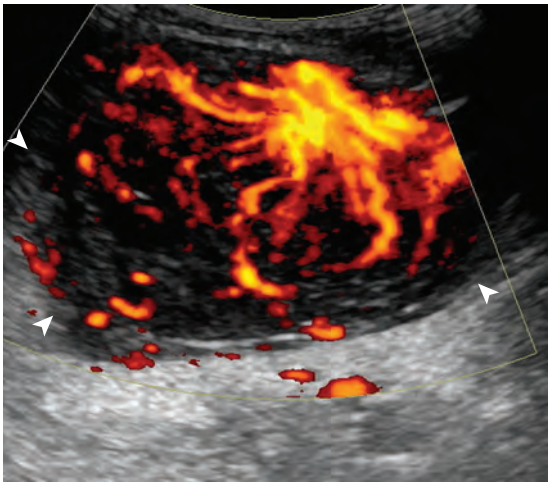

FIGURE 1-31 ■ Power Doppler: B-cell lymphoma. Power Doppler ultrasound image shows increased blood flow in hypoechoic lymphoma *(arrowheads)*. Note posterior increased through-transmission.

One last application of dynamic imaging is in evaluation of an abnormality that is present only when an extremity is moved or positioned in a particular manner. Examples of this include evaluation of the long head of biceps brachii tendon for subluxation or dislocation with shoulder external rotation (see Video 3-36), the ulnar nerve (see Video 4-15) and snapping triceps syndrome with elbow flexion (see Video 4-16), the peroneal tendon with dorsiflexion and eversion of the ankle (see Videos 8-10 through 8-12), and snapping hip syndrome (see Videos 6-16 through 6-19). Muscle contraction is also important for the diagnosis of muscle hernia (see Videos 8-17 through 8-19). Dynamic imaging of a patient during Valsalva maneuver is an important component in evaluation for inguinal region hernia (see Videos 6-22 through 6-32). In addition to the foregoing examples, if the patient has any complaints that occur with a specific movement or position, the ultrasound transducer can be placed over the abnormal area, and the patient can be asked to recreate the symptom.

REFERENCES

1. Curry TSDJ, Murry RC: *Christensen's physics of diagnostic radiology*, ed 4, Philadelphia, 1990, Lea and Febiger.
2. Erickson SJ: High-resolution imaging of the musculoskeletal system. *Radiology* 205:593–618, 1997.
3. Martinoli C, Derchi LE, Pastorino C, et al: Analysis of echotexture of tendons with US. *Radiology* 186:839–843, 1993.
4. Silvestri E, Martinoli C, Derchi LE, et al: Echotexture of peripheral nerves: correlation between US and histologic findings and criteria to differentiate tendons. *Radiology* 197:291–296, 1995.
5. Crass JR, van de Vegte GL, Harkavy LA: Tendon echogenicity: ex vivo study. *Radiology* 167:499–501, 1988.
6. Scanlan KA: Sonographic artifacts and their origins. *AJR Am J Roentgenol* 156:1267–1272, 1991.
7. Rubin JM, Adler RS, Bude RO, et al: Clean and dirty shadowing at US: a reappraisal. *Radiology* 181:231–236, 1991.
8. Hartgerink P, Fessell DP, Jacobson JA, et al: Full- versus partial-thickness Achilles tendon tears: sonographic accuracy and characterization in 26 cases with surgical correlation. *Radiology* 220:406–412, 2001.
9. Reynolds DL, Jr, Jacobson JA, Inampudi P, et al: Sonographic characteristics of peripheral nerve sheath tumors. *AJR Am J Roentgenol* 182:741–744, 2004.
10. Lin DC, Nazarian LN, O'Kane PL, et al: Advantages of real-time spatial compound sonography of the musculoskeletal system versus conventional sonography. *AJR Am J Roentgenol* 179:1629–1631, 2002.
11. Strobel K, Zanetti M, Nagy L, et al: Suspected rotator cuff lesions: tissue harmonic imaging versus conventional US of the shoulder. *Radiology* 230:243–249, 2004.

12. Lin EC, Middleton WD, Teefey SA: Extended field of view sonography in musculoskeletal imaging. *J Ultrasound Med* 18:147–152, 1999.
13. Kang CH, Kim SS, Kim JH, et al: Supraspinatus tendon tears: comparison of 3D US and MR arthrography with surgical correlation. *Skeletal Radiol* 38:1063–1069, 2009.
14. Klauser AS, Peetrons P: Developments in musculoskeletal ultrasound and clinical applications. *Skeletal Radiol* 2009, Sep 3 [Epub ahead of print].
15. Klauser AS, De Zordo T, Feuchtner GM, et al: Fusion of real-time US with CT images to guide sacroiliac joint injection in vitro and in vivo. *Radiology* 256:547–553, 2010.
16. De Zordo T, Chhem R, Smekal V, et al: Real-time sonoelastography: findings in patients with symptomatic Achilles tendons and comparison to healthy volunteers. *Ultraschall Med* 31:394–400, 2010.
17. De Zordo T, Fink C, Feuchtner GM, et al: Real-time sonoelastography findings in healthy Achilles tendons. *AJR Am J Roentgenol* 193:W134–138, 2009.
18. De Zordo T, Lill SR, Fink C, et al: Real-time sonoelastography of lateral epicondylitis: comparison of findings between patients and healthy volunteers. *AJR Am J Roentgenol* 193:180–185, 2009.
19. Klauser AS, Faschingbauer R, Jaschke WR: Is sonoelastography of value in assessing tendons? *Semin Musculoskelet Radiol* 14:323–333, 2010.
20. Arda K, Ciledag N, Aktas E, et al: Quantitative assessment of normal soft-tissue elasticity using shear-wave ultrasound elastography. *AJR Am J Roentgenol* 197:532–536, 2011.
21. Boote EJ: AAPM/RSNA physics tutorial for residents: topics in US: Doppler US techniques: concepts of blood flow detection and flow dynamics. *Radiographics* 23:1315–1327, 2003.
22. Bude RO, Rubin JM: Power Doppler sonography. *Radiology* 200:21–23, 1996.
23. Bodner G, Schocke MF, Rachbauer F, et al: Differentiation of malignant and benign musculoskeletal tumors: combined color and power Doppler US and spectral wave analysis. *Radiology* 223:410–416, 2002.
24. Belli P, Costantini M, Mirk P, et al: Role of color Doppler sonography in the assessment of musculoskeletal soft tissue masses. *J Ultrasound Med* 19:823–830, 2000.
25. Wu CH, Shih JC, Chang YL, et al: Two-dimensional and three-dimensional power Doppler sonographic classification of vascular patterns in cervical lymphadenopathies. *J Ultrasound Med* 17:459–464, 1998.
26. Breidahl WH, Stafford Johnson DB, Newman JS, et al: Power Doppler sonography in tenosynovitis: significance of the peritendinous hypoechoic rim. *J Ultrasound Med* 17:103–107, 1998.
27. Ribbens C, Andre B, Marcelis S, et al. Rheumatoid hand joint synovitis: gray-scale and power Doppler US quantifications following anti-tumor necrosis factor-alpha treatment: pilot study. *Radiology* 229:562–569, 2003.
28. Jamadar DA, Jacobson JA, Caoili EM, et al. Musculoskeletal sonography technique: focused versus comprehensive evaluation. *AJR Am J Roentgenol* 190:5–9, 2008.

CHAPTER 2

Basic Pathology Concepts

CHAPTER OUTLINE

MUSCLE AND TENDON INJURY

BONE INJURY

INFECTION

ARTHRITIS
Rheumatoid Arthritis
Psoriatic Arthritis
Gout
Osteoarthritis

MYOSITIS AND DIABETIC MUSCLE INFARCTION

SOFT TISSUE FOREIGN BODIES

PERIPHERAL NERVE ENTRAPMENT

SOFT TISSUE MASSES
Lipoma
Peripheral Nerve Sheath Tumors
Vascular Anomalies
Ganglion Cysts
Lymph Nodes
Malignant Soft Tissue Tumors

BONE MASSES

Additional videos for this topic are available online at www.expertconsult.com.

The full text of this chapter can be accessed online at www.expertconsult.com.

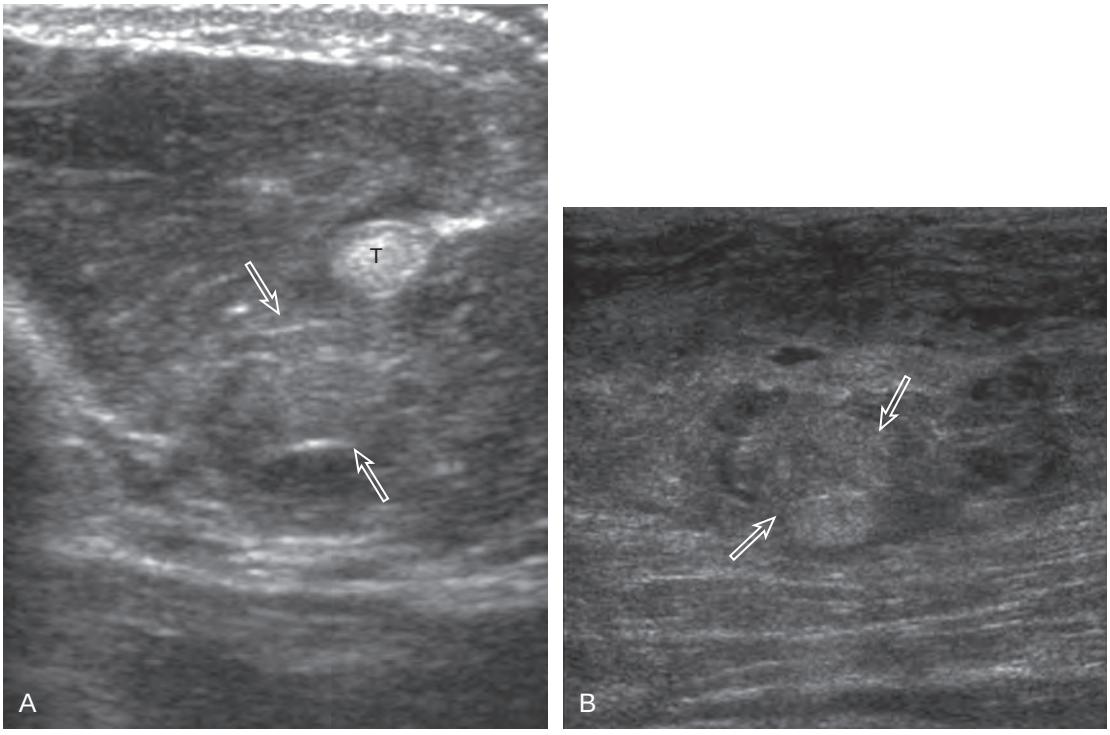

FIGURE 2-1 ■ **Acute muscle injury.** Ultrasound images of **(A)** the thenar musculature and **(B)** the tibialis anterior muscle show areas of hyperechoic hemorrhage *(open arrows)*. T, tendon.

MUSCLE AND TENDON INJURY

Muscle and tendon injuries may be categorized as acute and chronic. Acute injuries tend to take the form of direct impact injury, stretch injury during contraction (strain), or penetrating injury. Acute muscle injury can be clinically categorized as grade 1 (no appreciable fiber disruption), grade 2 (partial tear or moderate fiber disruption with compromised strength), and grade 3 (complete fiber disruption).[1] At sonography, muscle contusion and hemorrhage acutely appear hyperechoic (Fig. 2-1).[2,3] Excessive and intense muscle activity may produce diffuse muscle hyperechogenicity if imaged acutely from transient muscle edema (Fig. 2-2).[4] Partial fiber disruption indicates partial-thickness tear, whereas complete fiber disruption indicates full-thickness tear. One hallmark of full-thickness tear is muscle or tendon retraction, which is made more obvious with passive movement or active muscle contraction. Hemorrhage will later appear more hypoechoic (Fig. 2-3), although a heterogeneous appearance with mixed echogenicity is common (Fig. 2-4). As

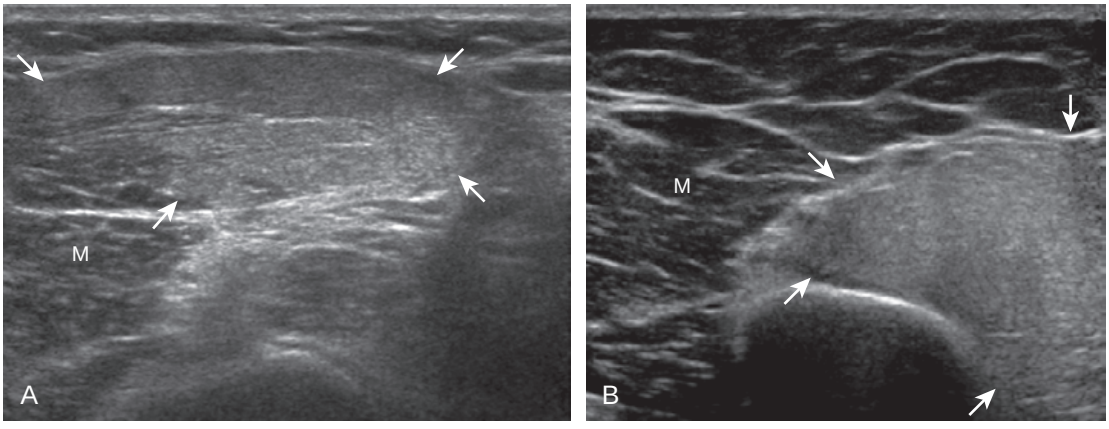

FIGURE 2-2 ■ **Acute muscle edema.** Ultrasound images of **(A)** brachioradialis and **(B)** brachialis muscle in short axis from two different patients show diffuse hyperechoic muscle edema *(arrows)* compared with normal muscle (M).

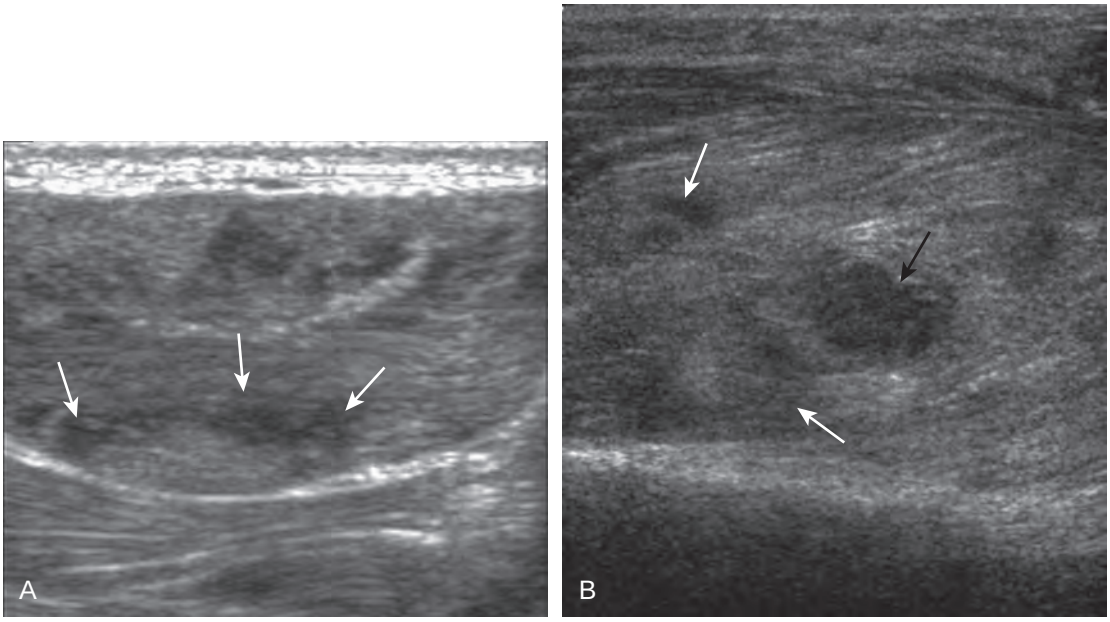

FIGURE 2-3 ■ Subacute muscle injury. Ultrasound images of **(A)** the thenar musculature and **(B)** the tibialis anterior muscle show heterogeneous areas of hypoechoic hemorrhage *(arrows)*.

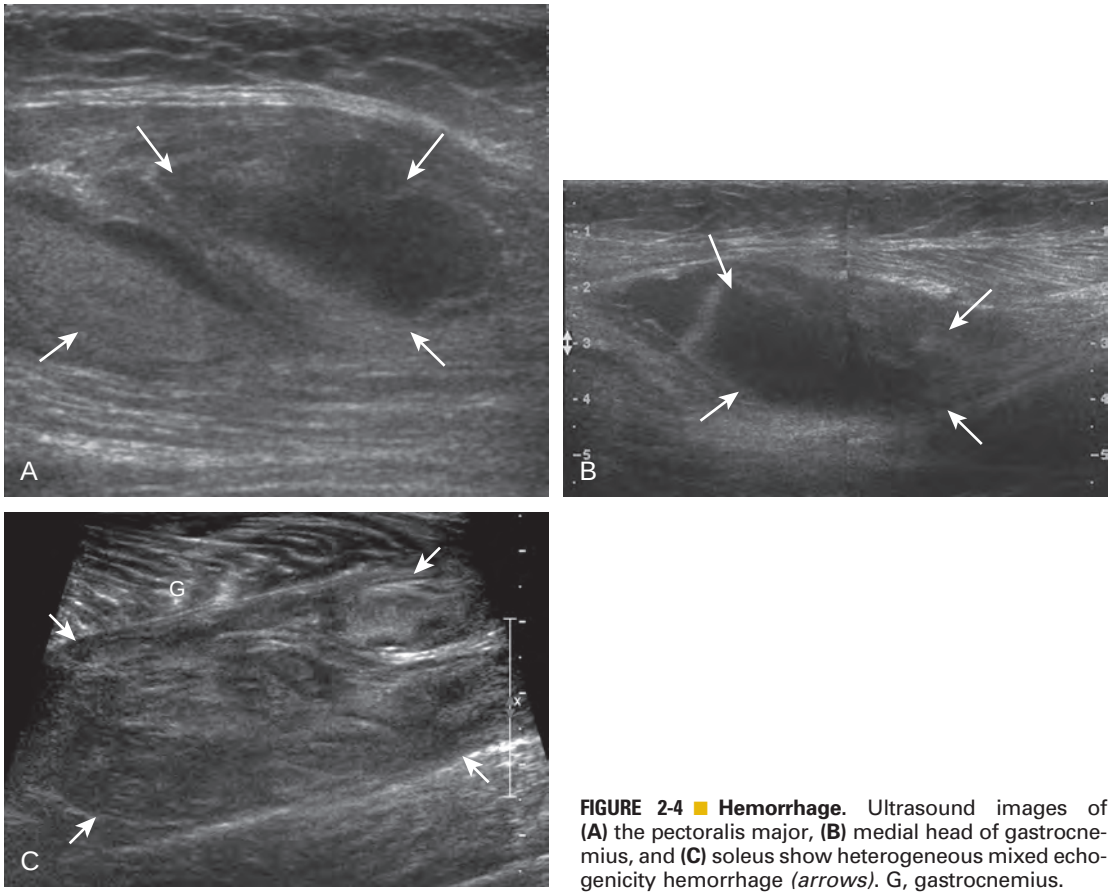

FIGURE 2-4 ■ Hemorrhage. Ultrasound images of **(A)** the pectoralis major, **(B)** medial head of gastrocnemius, and **(C)** soleus show heterogeneous mixed echogenicity hemorrhage *(arrows)*. G, gastrocnemius.

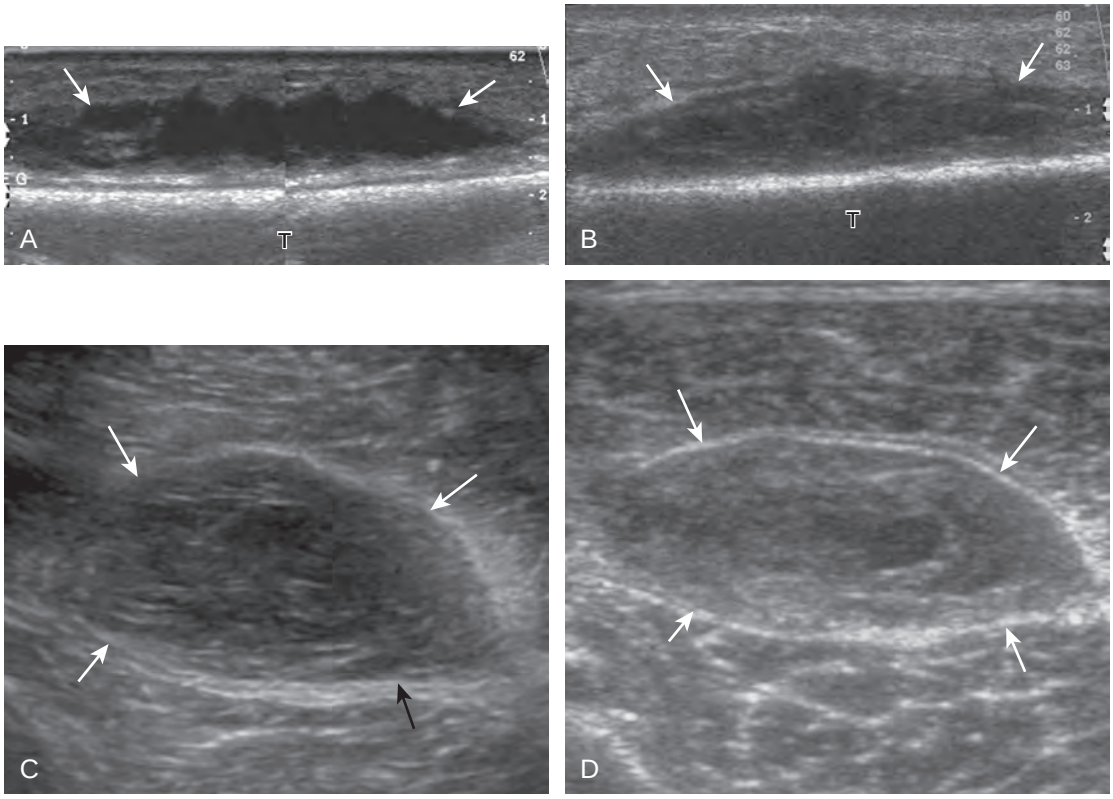

FIGURE 2-5 ■ Organizing hematoma. Ultrasound images (**A** and **B**) anterior to the tibia and (**C** and **D**) within the calf show interval decrease in size of hematoma *(arrows)* (**A** to **B**, **C** to **D**) with increased echogenicity at the periphery. T, tibia.

soft tissue hemorrhage resorbs, a hematoma will become smaller and more echogenic, beginning at the periphery (Fig. 2-5). A residual anechoic fluid collection or seroma may remain (Fig. 2-6). Hemorrhage located between the subcutaneous fat and the adjacent hip musculature can occur with trauma as a degloving-type injury, called the *Morel-Lavallée lesion* (Fig. 2-7).[5] Residual scar formation appears hyperechoic (Fig. 2-8). Heterotopic ossification may remain and is hyperechoic with posterior acoustic shadowing (Fig. 2-9). An area of damaged muscle may ossify, termed *myositis ossificans* (Fig. 2-10), and ultrasound can show early mineralization before visualization on radiography.[6] Often, computed tomography (CT) is needed to demonstrate the

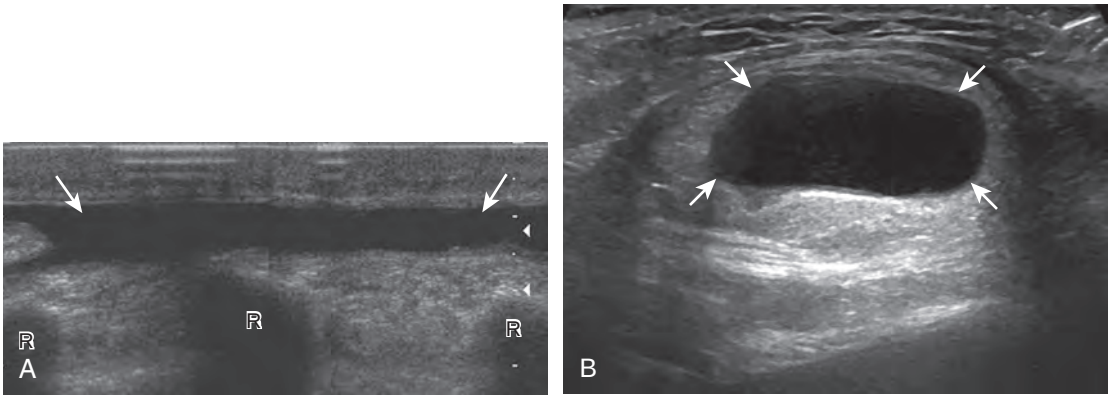

FIGURE 2-6 ■ Seroma. Ultrasound images (**A** and **B**) from two different patients show anechoic fluid collection *(arrows)* at site of prior hemorrhage. R, ribs in **A**.

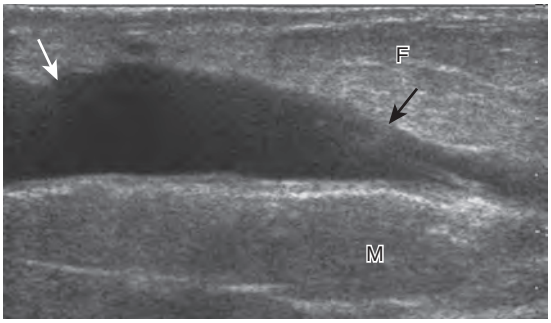

FIGURE 2-7 ■ Morel-Lavallée lesion. Ultrasound image shows anechoic fluid *(arrows)* at the site of prior hemorrhage between subcutaneous fat (F) and musculature (M).

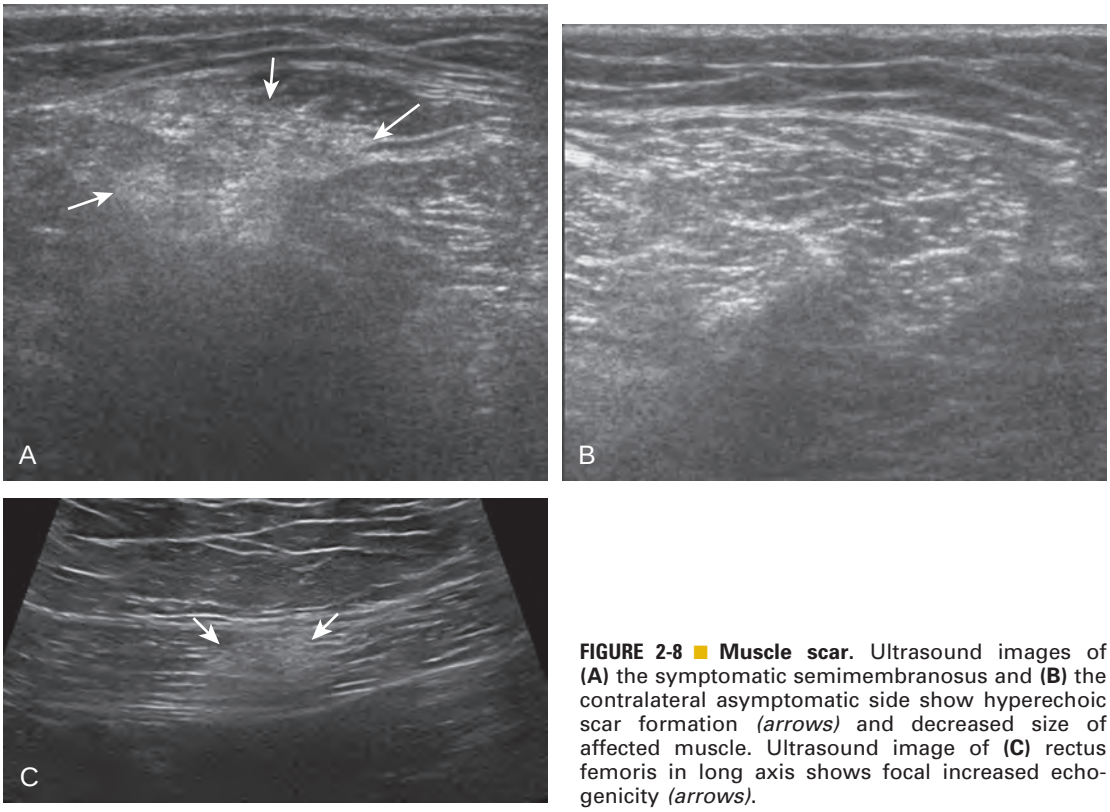

FIGURE 2-8 ■ Muscle scar. Ultrasound images of **(A)** the symptomatic semimembranosus and **(B)** the contralateral asymptomatic side show hyperechoic scar formation *(arrows)* and decreased size of affected muscle. Ultrasound image of **(C)** rectus femoris in long axis shows focal increased echogenicity *(arrows)*.

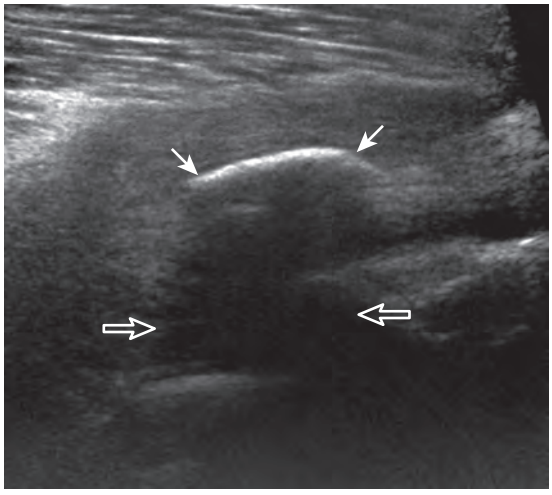

FIGURE 2-9 ■ Heterotopic ossification. Ultrasound image shows hyperechoic surface of heterotopic ossification *(arrows)* with posterior acoustic shadowing *(open arrows)*.

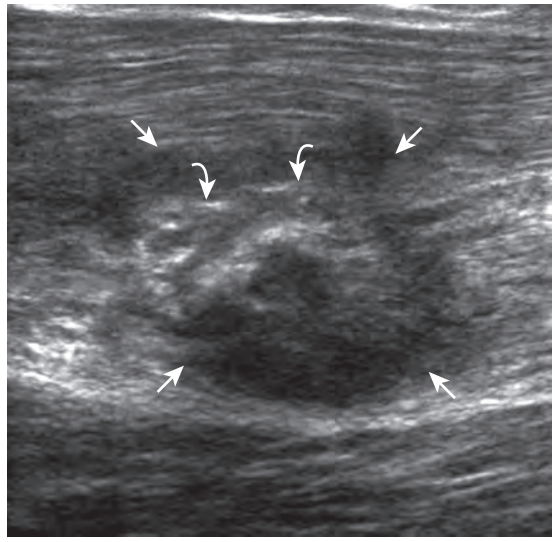

FIGURE 2-10 ■ Myositis ossificans. Ultrasound image shows hypoechoic hemorrhage *(arrows)* with echogenic mineralization *(curved arrows)*.

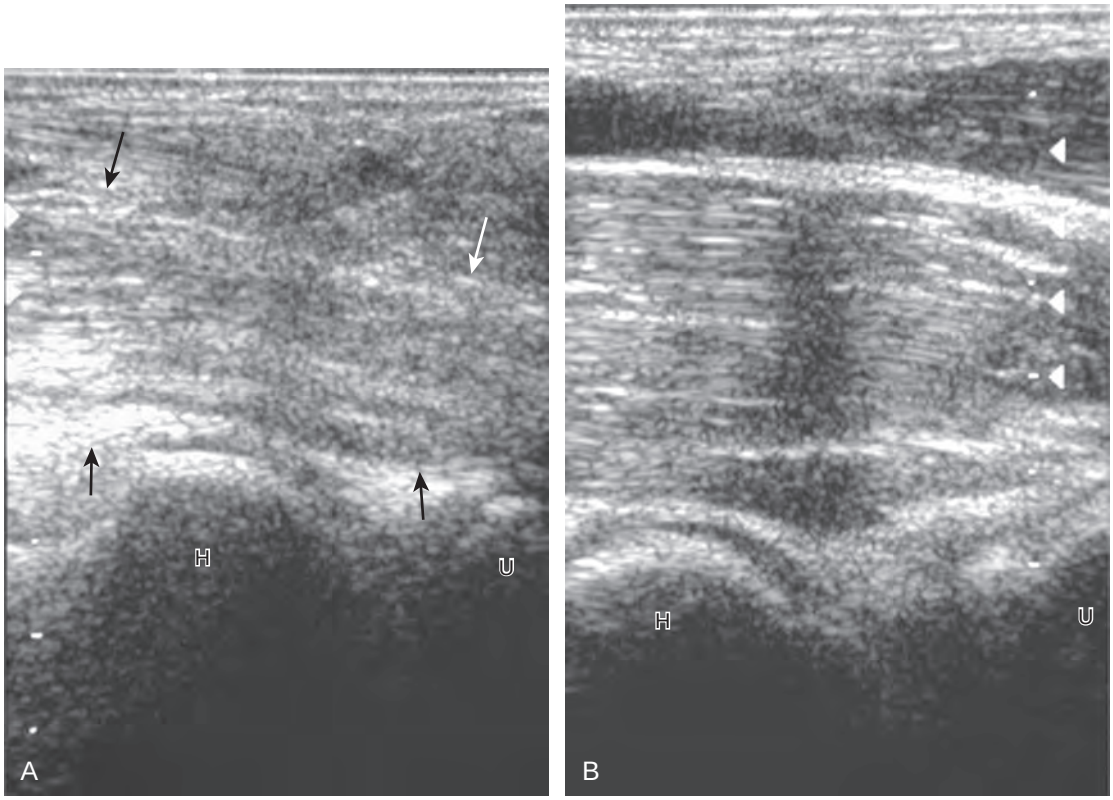

FIGURE 2-11 ■ Muscle atrophy. Ultrasound images of **(A)** the symptomatic brachialis muscle and **(B)** the contralateral asymptomatic side show decreased size and increased echogenicity of the affected muscle *(arrows)*. H, humerus; U, ulna.

peripheral rim of mineralization characteristic of myositis ossificans, given shadowing seen on ultrasound. Prior trauma to muscle or its nerve supply can result in muscle atrophy, which causes increased echogenicity and decreased size of the muscle (Fig. 2-11).

With direct impact injury, the belly of a muscle is typically involved with hematoma and variable fiber disruption (Fig. 2-12). In contrast, stretching of a contracting muscle typically results in injury at the musculotendinous junction and is more common with muscles that span two joints, such as the hamstring muscles of the thigh (Fig. 2-13) and the medial head of the gastrocnemius (Fig. 2-14). It is important to consider the architecture of the muscle imaged in evaluation for

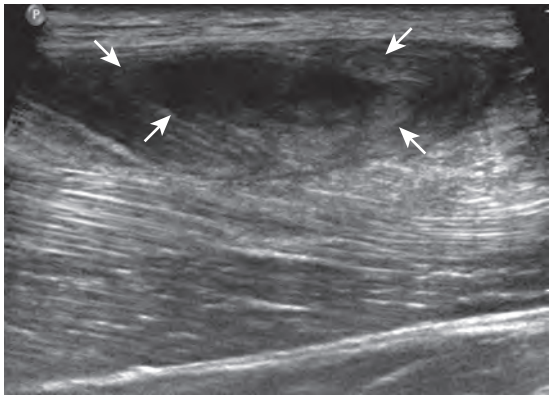

FIGURE 2-12 ■ Muscle contusion and hematoma. Ultrasound image of triceps brachii tendon in long axis shows heterogeneous but predominantly hypoechoic intramuscular hematoma *(arrows)* with partial muscle fiber disruption.

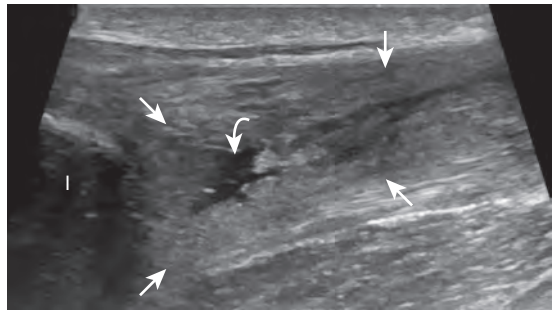

FIGURE 2-13 ■ Proximal semimembranosus injury. Ultrasound image of semimembranosus tendon origin in long axis shows abnormal heterogeneous hypoechoic swelling of the tendon *(arrows)* with anechoic interstitial tears *(curved arrow)*. I, ischium.

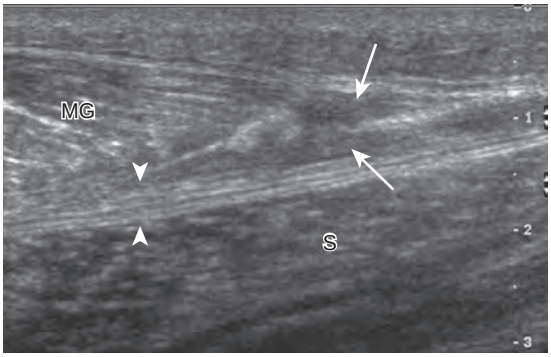

FIGURE 2-14 ■ Medial head of gastrocnemius tear. Ultrasound image of distal medial head of gastrocnemius in long axis shows hypoechoic disruption at the musculotendinous junction *(arrows)*. Note intact plantaris tendon *(arrowheads)*. MG, medial head of gastrocnemius; S, soleus.

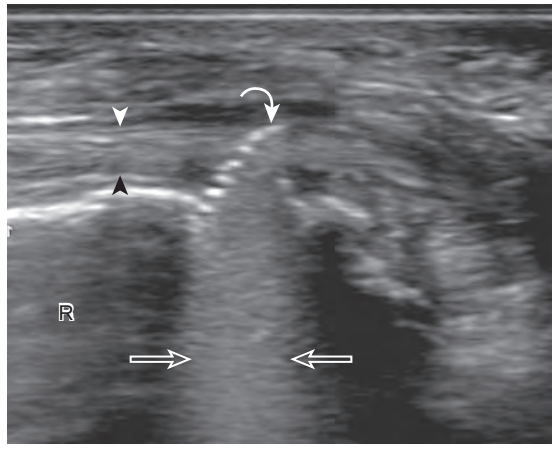

FIGURE 2-15 ■ Screw impingement of extensor carpi radialis tendon. Ultrasound image of extensor carpi radialis tendon in long axis *(arrowheads)* shows a metal screw with reverberation artifact *(open arrows)*, with the tip protruding into the tendon *(curved arrow)*. Note associated tenosynovitis. R, radius.

myotendinous injury. For example, a muscle with a unipennate architecture (e.g., the medial head of the gastrocnemius) shows injury at the myotendinous junction located at its periphery (see Fig. 2-14).[7] A muscle with circumpennate or bipennate architecture (e.g., the indirect head of the rectus femoris) may show injury at its distal musculotendinous junction or within the muscle belly as a central aponeurosis tear (see Fig. 6-59A in Chapter 6).[8] Musculotendinous injury also demonstrates variable echogenicity from hemorrhage and fluid, depending on the age of the injury and the degree of fiber disruption. Passive joint movement or active muscle contraction can demonstrate retraction at the site of the injury that indicates full-thickness tear. Particularly in children, these types of acute tendon injuries may be associated with bone fragment avulsion at the tendon attachments, which appear hyperechoic with possible shadowing.

With penetrating injury or laceration, acute muscle and tendon injury may occur at any site (see Fig. 7-47 in Chapter 7). The obvious physical examination findings usually guide the ultrasound evaluation. Muscle and tendon injuries are again classified as partial-thickness or full-thickness tears. Dynamic imaging is helpful in this distinction because it makes retraction related to full-thickness tears more conspicuous. Gas introduced during the penetrating injury can make evaluation extremely difficult; air appears hyperechoic with heterogeneous posterior shadowing. It is also important to recognize adjacent soft tissue or osseous injuries outside the muscle because lacerations may cause peripheral nerve injury as well (see Fig. 6-80B in Chapter 6).

Chronic muscle and tendon injuries are usually the result of overuse, with tendon degeneration and possible tear. It has been shown that such involved tendons show eosinophilic, fibrillar, and mucoid degeneration but do not contain acute inflammatory cells; therefore, the term *tendinosis* is used rather than *tendinitis*.[9-11] At sonography, tendinosis appears as hypoechoic swelling of the involved tendon, but without tendon fiber disruption (see later chapters). Several tendons may commonly show increased blood flow on color or power Doppler imaging in the setting of tendinosis, such as the patellar tendon, Achilles tendon, and common extensor tendon of the elbow. This increase in blood flow is not due to inflammation but rather represents neovascularity. Tendinosis may progress to partial-thickness and full-thickness tendon tear. Chronic muscle and tendon injuries that result in tear can be associated with atrophy of the muscle, which appears hyperechoic and decreased in size. After surgery, misplaced hardware or screw-tip penetration beyond the bone cortex may cause excessive wear of an adjacent tendon (Fig. 2-15). Ultrasound is helpful in this diagnosis because artifact from metal hardware does not obscure overlying soft tissues. In addition, dynamic imaging with joint movement or muscle contraction can determine whether a tendon is in contact with metal hardware with specific positions (Video 2-1).

BONE INJURY

The normal osseous surfaces are smooth and echogenic with posterior shadowing and possibly reverberation when imaged perpendicular to the

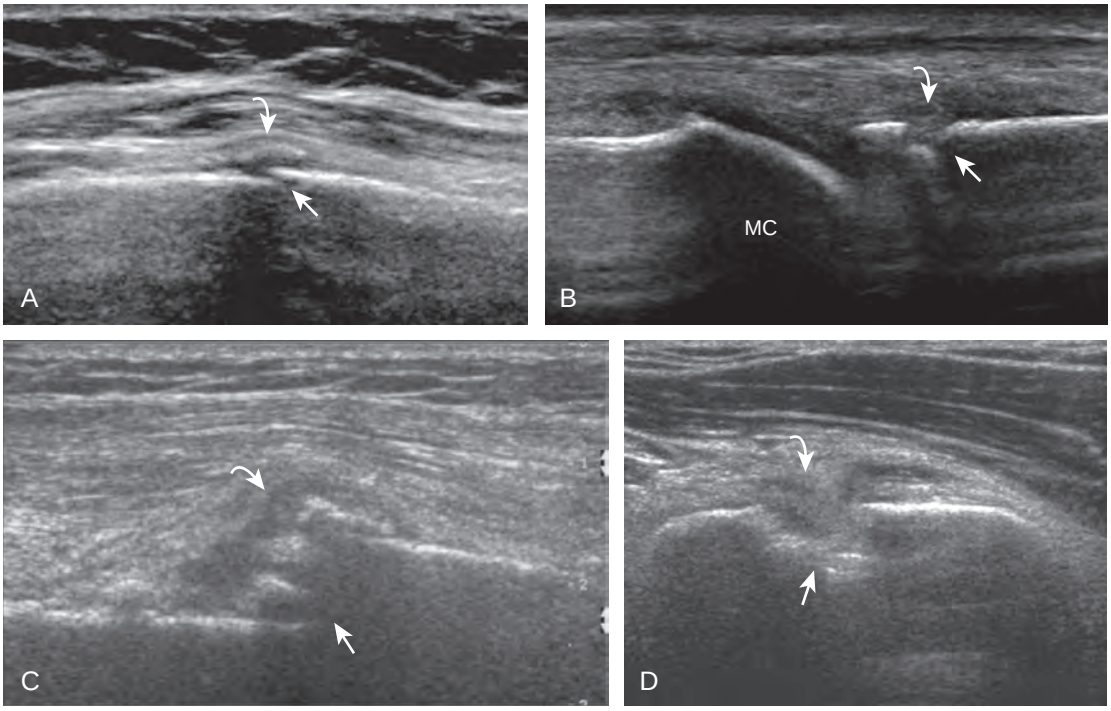

FIGURE 2-16 ■ Fractures. Ultrasound images from four different patients show fractures as cortical discontinuity and step-off deformity *(arrow)* with variable hemorrhage *(curved arrow)* involving **(A)** ribs, **(B)** proximal phalanx, **(C)** humerus, and **(D)** coracoid process. MC, metacarpal head.

sound beam. The hallmark of an acute fracture is discontinuity of the bone cortex with possible step-off deformity (Fig. 2-16).[12] Adjacent mixed echogenicity hemorrhage may also be present. A stress fracture, for example involving a metatarsal, may initially appear as a focal hypoechoic area adjacent to bone, which may progress to fracture step-off deformity or hyperechoic callus formation (see Fig. 8-146 in Chapter 8).[13] This is typically associated with point tenderness induced by pressure from the transducer. A patient also commonly indicates focal pain in the area. It is important at the completion of any ultrasound examination to ask the patient about such focal symptoms because they are often clues to underlying pathology that may not be otherwise evaluated.

Other types of bone injuries involve avulsion at tendon and ligament attachments. In these situations, a small fragment of bone with variable shadowing is seen attached to the involved tendon or ligament (see Fig. 8-143 in Chapter 8). Asymmetrical widening and irregularity of an open growth plate with point tenderness can indicate a physeal injury (Fig. 2-17).[14] It is important to differentiate the findings of bone injury at ultrasound from bone irregularity resulting from osteophytes. This differentiation is possible because osteophytes occur at margins of synovial joints usually without point tenderness, whereas a fracture shows a cortical step-off deformity. Correlation with radiography may also be considered to assist with this differentiation.

In many situations in which a fracture is identified at ultrasound, the fracture is unsuspected. The indication for the examination is often to evaluate a soft tissue or joint abnormality after a

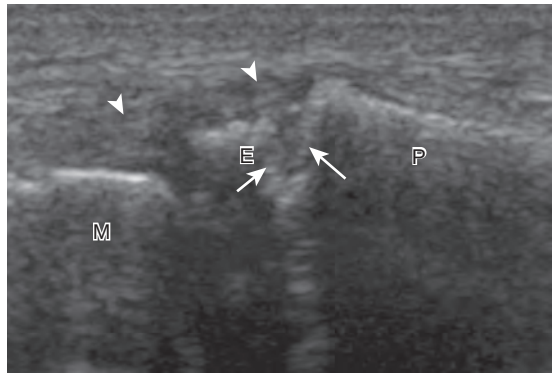

FIGURE 2-17 ■ Growth plate injury. Ultrasound image of first metacarpophalangeal joint in long axis shows bone irregularity, widening, and offset at the physeal plate *(arrows)*. E, epiphysis; M, metacarpal; P, proximal phalanx. Note the collateral ligament *(arrowheads)*.

"negative" radiograph. This is not uncommon in the foot and ankle, where multiple overlapping osseous structures may make radiographic diagnosis of fracture difficult. The other situation is the greater tuberosity fracture of the proximal humerus, which can be overlooked at radiography because of suboptimal patient positioning or suboptimal radiographic technique (see Fig. 3-103 in Chapter 3).[15] It has been shown that ultrasound is more effective than radiography in the diagnosis of rib fracture (see Fig. 2-16A).[16,17] As a fracture begins to heal, early hypoechoic callus becomes hyperechoic hard callus, which can eventually bridge the fracture gap or step-off deformity.[12] This can also be applied to limb-lengthening procedures, in which ultrasound can detect new bone before radiography. Ultrasound has also been shown to be effective in diagnosis of tibial fracture nonunion with static interlocked nail placement; ultrasound can detect healing before radiography, whereas visualization of the hyperechoic nail indicates no overlying callus formation (Fig. 2-18).[12] Another advantage of ultrasound is in the evaluation of nonossified structures, such as the distal humeral epiphyses in children and the anterior costocartilage.[18,19]

INFECTION

The imaging appearances of soft tissue infection are largely predicted by the route of infection spread. For example, in adults, infection commonly occurs through a puncture wound or skin ulcer. This produces infection of the soft tissues or cellulitis, which may have several appearances (Fig. 2-19). Acutely, cellulitis appears as hyperechoic and thickened subcutaneous tissue.[20,21]

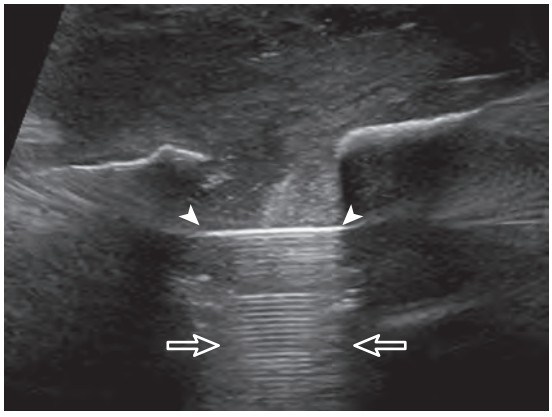

FIGURE 2-18 ■ Fracture nonunion. Ultrasound image shows hyperechoic intramedullary nail *(arrowheads)* with posterior reverberation artifact indicating incomplete healing of the tibial fracture *(open arrows)*.

Later, hypoechoic or anechoic branching channels are visualized, with distortion of the soft tissues and possibly increased flow on color or power Doppler imaging.[20] Such branching channels can coalesce as purulent fluid and can progress to frank abscess, where ultrasound-guided aspiration may be of benefit.[20] However, ultrasound-guided aspiration may be less effective in the setting of methicillin-resistant *Staphylococcus aureus* infection.[22] When evaluating for cellulitis, the findings of anechoic perifascial fluid and gas (appearing as hyperechoic foci with comet-tail artifact or dirty shadowing) at the deep fascia can indicate necrotizing fasciitis.[23] The differential diagnosis for ultrasound findings of hyperechoic subcutaneous fat, as seen with acute cellulitis, includes fat necrosis (Fig. 2-20); however, the latter condition is usually more focal, may be multiple, and is without physical examination findings of infection.[24]

The ultrasound appearance of abscess is variable but predominantly appears as well-defined hypoechoic heterogeneous fluid collection with posterior through-transmission and hyperemia on color or power Doppler imaging (Fig. 2-21).[25] A thick hyperechoic and hyperemic wall may also be seen, as may soft tissue gas.[26] Uncommonly, an abscess may be isoechoic or hyperechoic relative to the adjacent soft tissues (see Fig. 2-21D). In this situation, in which it may be difficult to identify an abscess, increased through-transmission and swirling of echoes within the abscess with transducer pressure are helpful features to indicate the presence of a fluid component (Videos 2-2 and 2-3).[27] Increasing the depth and field of view around a possible abscess often causes the increased through-transmission to become more conspicuous relative to the surrounding tissues.

Some infections occur after surgery and may be located immediately adjacent to metal hardware (see Fig. 2-21E). Ultrasound is ideal for evaluation in this situation because the reverberation artifact from the hardware occurs deep to the metal and does not obscure the overlying soft tissues.[28] Soft tissue infection may also involve a bursa, which can produce complex fluid and synovitis, and possibly gas, which appears hyperechoic with comet-tail artifact (Fig. 2-22) (Video 2-4). Unlike a nonspecific abscess, a bursal fluid collection tends to be more defined and, more importantly, occurs in an area of a known bursa. If an area of soft tissue infection is identified adjacent to bone, then osteomyelitis should be considered (Fig. 2-23). In the presence of cortical irregularity resulting from erosions or destruction, osteomyelitis is likely, although confirmation with magnetic resonance imaging (MRI) is

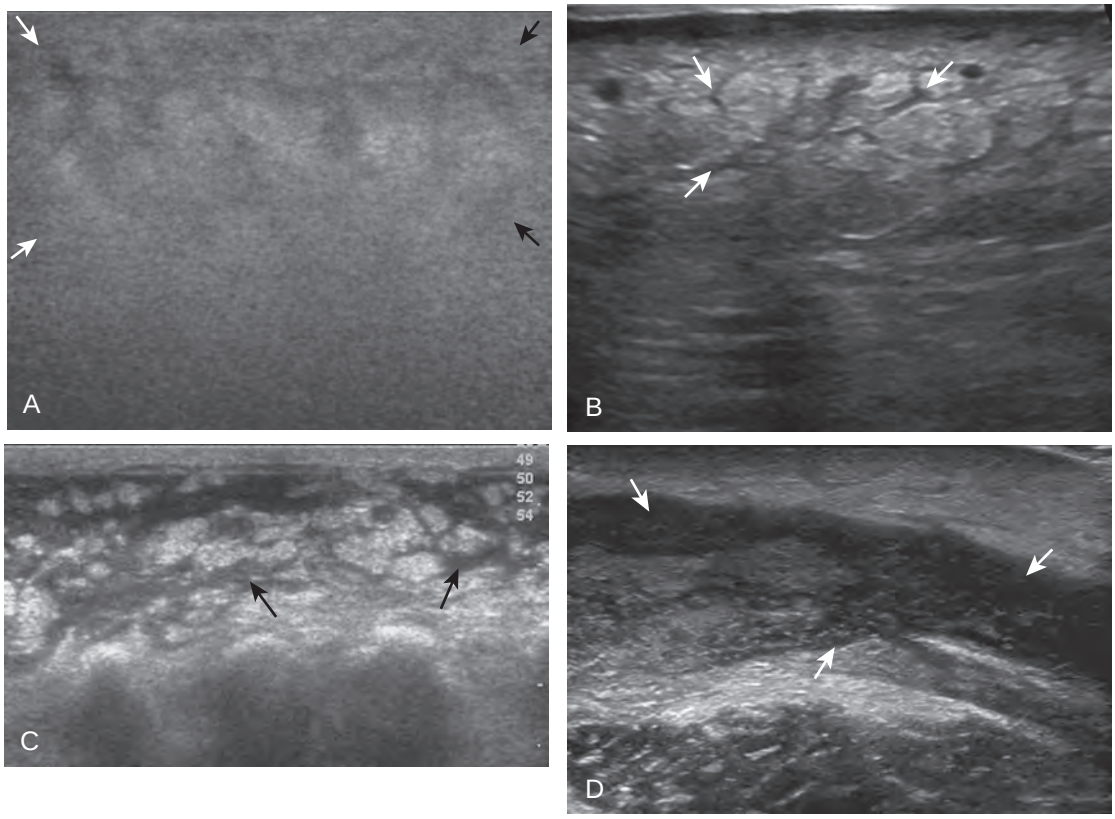

FIGURE 2-19 ■ Cellulitis: progressive findings. Ultrasound images from four different patients show **(A)** diffuse increased echogenicity *(arrows)* with sound beam attenuation, **(B)** increased echogenicity with intervening hypoechoic channels *(arrows)*, **(C)** confluent hypoechoic fluid channels *(arrows)*, and **(D)** hypoechoic infected fluid collection *(arrows)*.

often needed to assess the extent of infection fully.

Another route of infection is hematogenous, which may manifest as a muscle abscess, as septic arthritis, or as osteomyelitis. This mode of infection is more common in children, intravenous drug abusers, or patients with sepsis. In the correct clinical scenario, septic arthritis is suspected when there is fluid distention of a joint recess, which may range from anechoic to hyperechoic, with possible hypoechoic or isoechoic synovial hypertrophy (see later). The

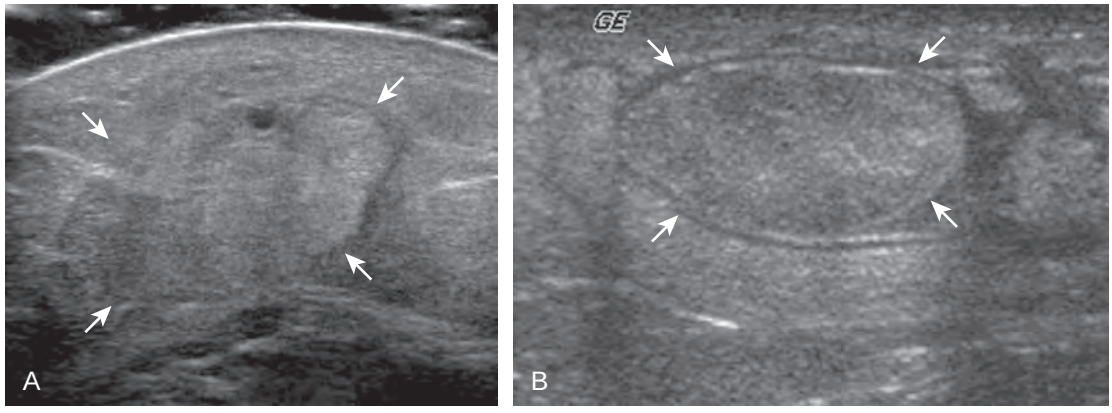

FIGURE 2-20 ■ Fat necrosis. Ultrasound images from two different patients show **(A)** hyperechoic subcutaneous area *(arrows)* and **(B)** focal hyperechoic nodule *(arrows)* representing fat necrosis. (From Walsh M, Jacobson JA, Kim SM, et al: Sonography of fat necrosis involving the extremity and torso with magnetic resonance imaging and histologic correlation. *J Ultrasound Med* 27:1751–1757, 2008. Reproduced with permission from the American Institute of Ultrasound in Medicine.)

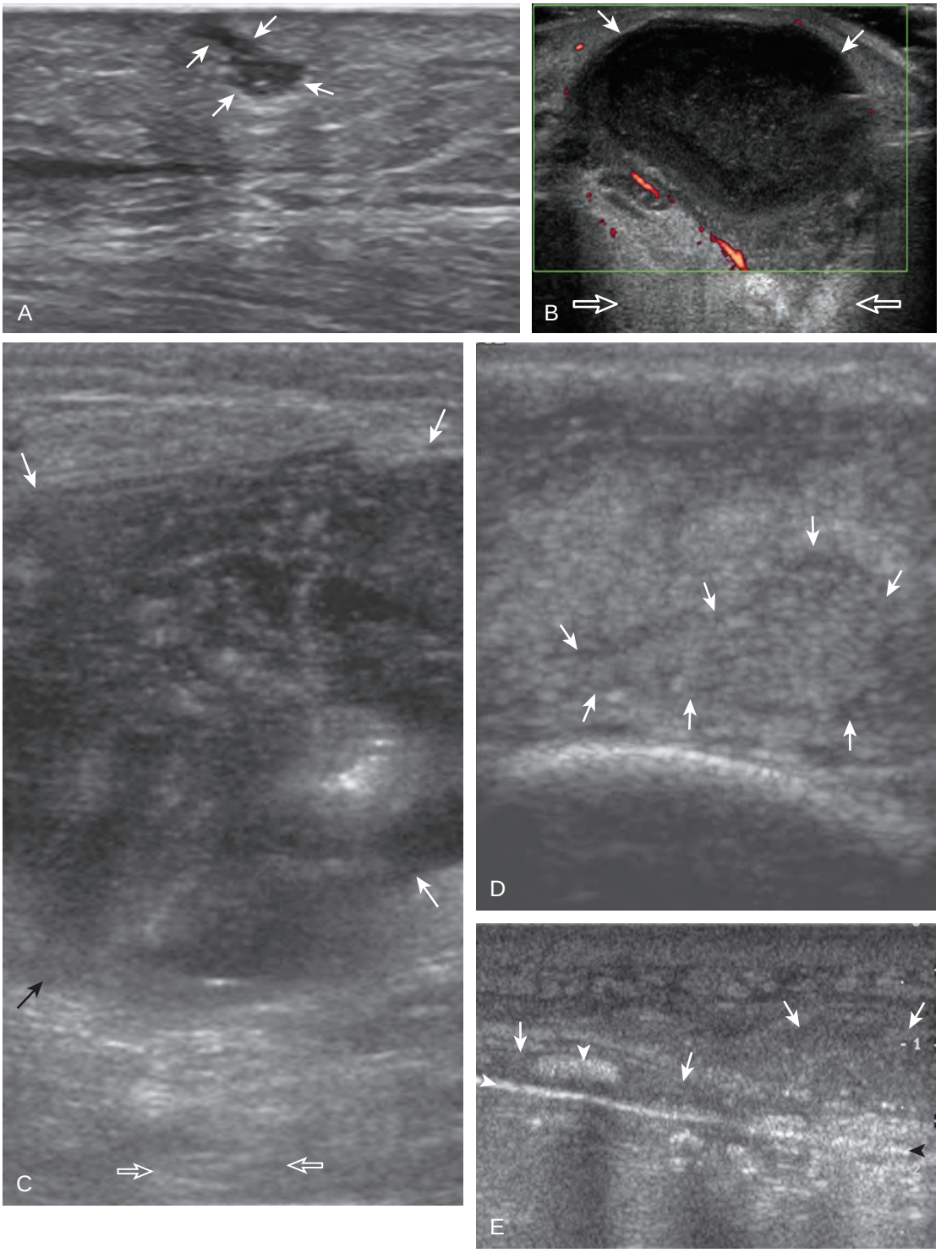

FIGURE 2-21 ■ **Abscess.** Ultrasound images from five different patients show **(A)** small hypoechoic abscess *(arrows)* (methicillin-resistant *Staphylococcus aureus*) with surrounding cellulitis, **(B)** predominantly hypoechoic but heterogeneous abscess *(arrows)*, **(C)** heterogeneous abscess *(arrows)*, and **(D)** isoechoic abscess *(arrows)*. Note increased through-transmission *(open arrows)* in **B** and **C** and gas *(arrowhead)* in **C**. **E,** Ultrasound image shows isoechoic abscess *(arrows)* adjacent to metal side plate and screws *(arrowheads)*.

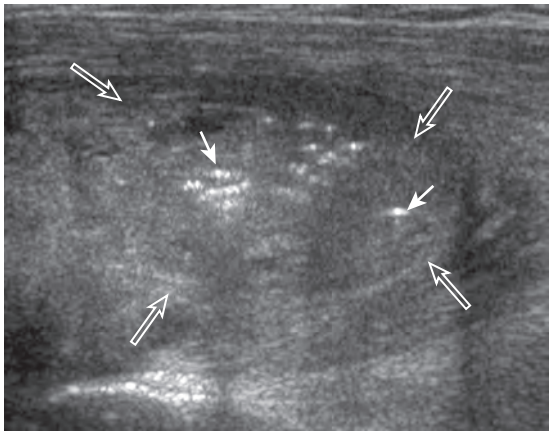

FIGURE 2-22 ■ Septic bursitis with gas. Ultrasound image shows hyperechoic foci of gas *(arrows)* with comet-tail artifacts within a mixed hypoechoic and isoechoic septic subacromial-subdeltoid bursitis *(open arrows)*.

echogenicity of fluid or the presence of flow on color or power Doppler imaging cannot predict the presence of infection, and therefore ultrasound-guided percutaneous fluid aspiration should be considered. When distention of a joint recess is not anechoic, the possibility of complex fluid versus synovial hypertrophy must be considered. To help in this distinction, compressibility of the recess, redistribution of the contents with joint positions, and lack of internal flow on color Doppler imaging suggest complex fluid rather than synovial hypertrophy. When synovial hypertrophy related to a septic joint is present, discontinuity or irregularity of the adjacent bone cortex suggests erosions and possible osteomyelitis (Fig. 2-24). Joint inflammation and synovitis from infection are indistinguishable from other inflammatory conditions, such as rheumatoid arthritis. In children, hematogenous spread of infection

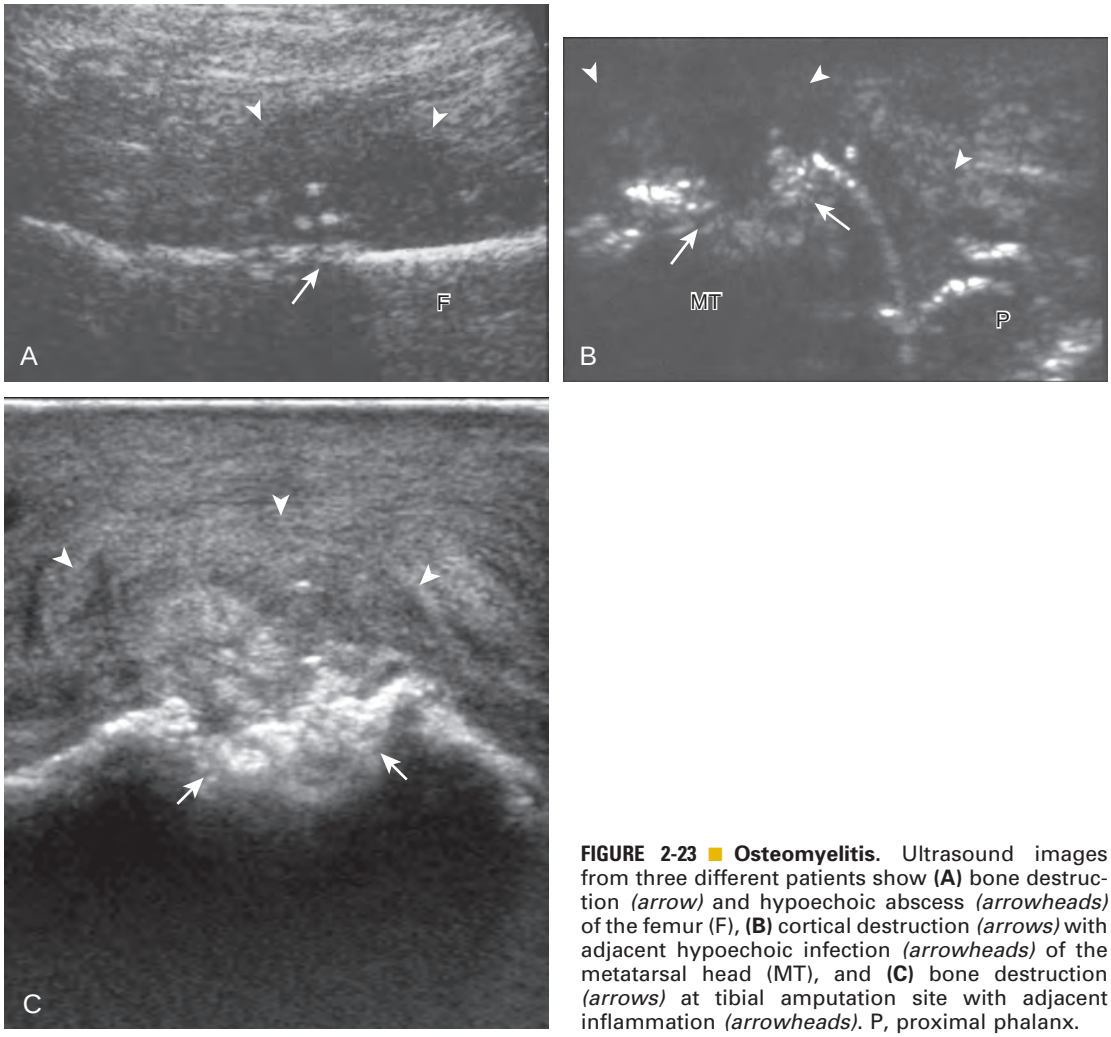

FIGURE 2-23 ■ Osteomyelitis. Ultrasound images from three different patients show **(A)** bone destruction *(arrow)* and hypoechoic abscess *(arrowheads)* of the femur (F), **(B)** cortical destruction *(arrows)* with adjacent hypoechoic infection *(arrowheads)* of the metatarsal head (MT), and **(C)** bone destruction *(arrows)* at tibial amputation site with adjacent inflammation *(arrowheads)*. P, proximal phalanx.

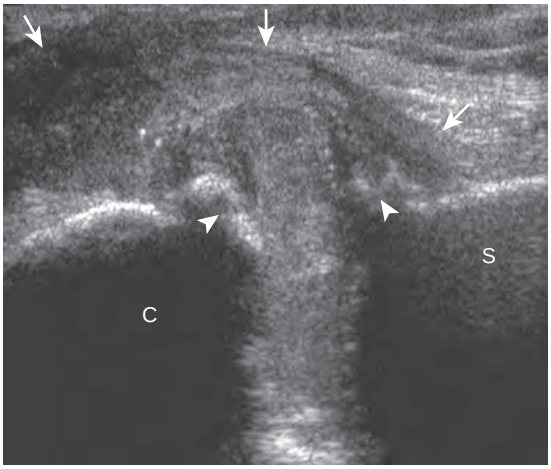

FIGURE 2-24 ■ Septic sternoclavicular joint. Ultrasound image shows heterogeneous distention of the sternoclavicular joint capsule *(arrows)*. Note erosions *(arrowheads)* of the sternum (S) and clavicle (C). (From Johnson M, Jacobson JA, Fessell DP, et al: The sternoclavicular joint: can imaging differentiate infection from degenerative change? *Skeletal Radiol* 39:551–558, 2010.)

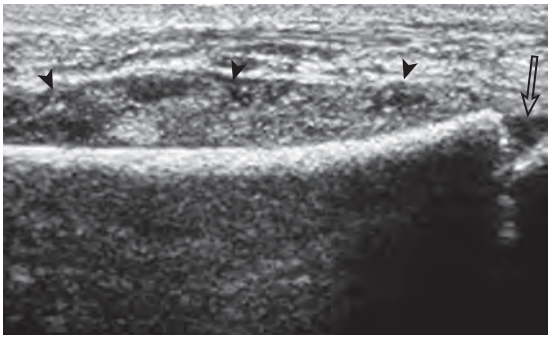

FIGURE 2-25 ■ Subperiosteal abscess. Ultrasound image shows isoechoic subperiosteal abscess *(arrowheads)* (*open arrow*, physis). (Courtesy of P. Strouse, MD, Ann Arbor, Mich.)

may also directly infect the bone. In this situation, a subperiosteal abscess may be identified because the periosteum is loosely adherent in children when compared with adults (Fig. 2-25).

ARTHRITIS

The foregoing descriptions relate to infection of soft tissues and bone. However, inflammation may have noninfective causes. Other inflammatory conditions, such as rheumatoid arthritis, can produce joint findings (effusion, synovial hypertrophy, and erosions), which can resemble infection.[29] Often, the distribution of the abnormalities and the clinical history assist with the differential diagnosis. Infection more commonly causes abnormalities at one site, and this diagnosis must be excluded before considering single-site involvement of a systemic inflammatory arthritis. The following represents general concepts of some inflammatory conditions with additional examples and text found in later chapters.

Rheumatoid Arthritis

The characteristic features of rheumatoid arthritis include synovial hypertrophy and erosions. Ultrasound can be used from early diagnosis to assessment of response to therapy and can guide injections or aspirations. Synovial hypertrophy appears as hypoechoic (Fig. 2-26) or, less commonly, isoechoic (Fig. 2-27) or hyperechoic relative to subdermal fat, poorly compressible tissue within a joint or a joint recess.[30] Synovial hypertrophy may also involve other synovial spaces, such as a bursa or tendon sheath (Fig. 2-28). Flow may be seen on color or power Doppler imaging, depending on the inflammatory activity of the synovitis. When assessing for hyperemia of

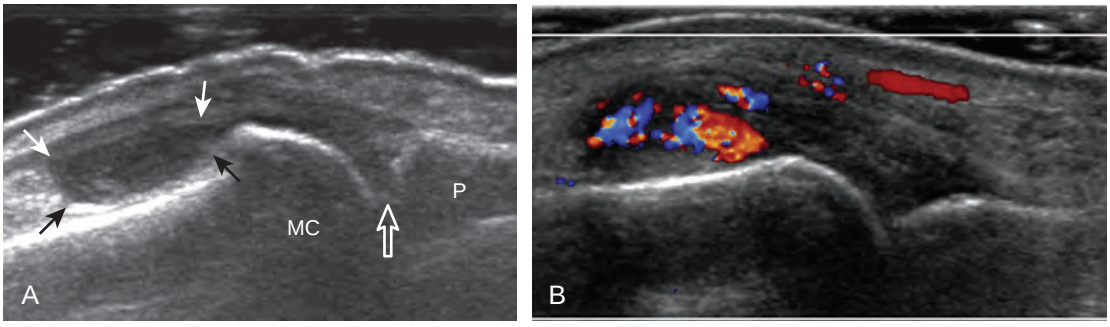

FIGURE 2-26 ■ Rheumatoid arthritis: hypoechoic synovial hypertrophy. Ultrasound images in the sagittal plane show hypoechoic synovial hypertrophy *(arrows)* and hyperemia distending the dorsal **(A)** second and **(B)** third metacarpophalangeal joint recesses, which extend from the metacarpophalangeal joint articulation *(open arrow)*. MC, metacarpal head; P, proximal phalanx.

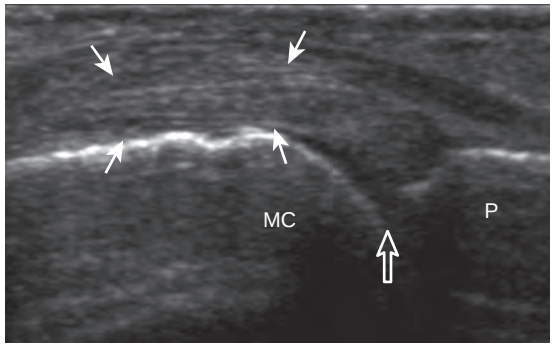

FIGURE 2-27 ■ Rheumatoid arthritis: isoechoic synovial hypertrophy. Ultrasound image in the sagittal plane shows isoechoic synovial hypertrophy *(arrows)* distending the dorsal second metacarpophalangeal joint recess, which extends from the metacarpophalangeal joint articulation *(open arrow)*. MC, metacarpal head; P, proximal phalanx.

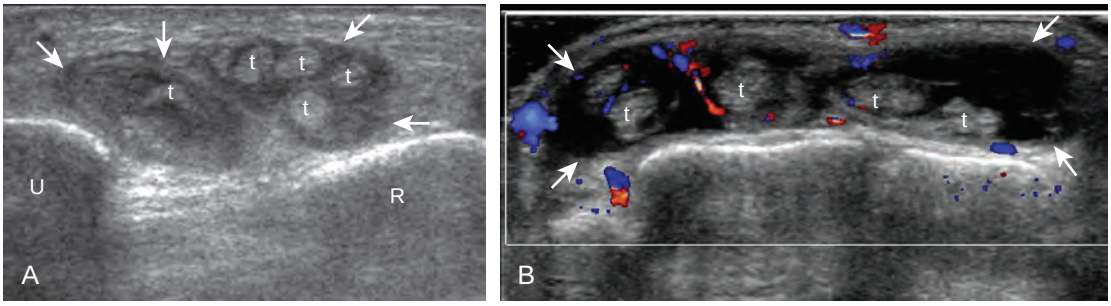

FIGURE 2-28 ■ Rheumatoid arthritis: tenosynovitis. Ultrasound images in short axis to the extensor tendons of the wrist in two different patients show **(A)** hypoechoic synovial hypertrophy *(arrows)* and **(B)** anechoic fluid *(arrows)* and hyperemia. t, tendons; R, radius; U, ulna.

synovial hypertrophy, it is important to minimize transducer pressure to avoid occluding or dampening flow (Fig. 2-29) (Video 2-5). Joint synovial hypertrophy may be seen in the dorsal recesses of the wrist, the volar and dorsal recesses of the metacarpophalangeal and interphalangeal joints of the hand, and the metatarsophalangeal joints of the feet. [31,32] Erosions appear as discontinuity of the bone cortex seen in two orthogonal planes (Fig. 2-30). Such erosions begin in the marginal regions of a joint, where the bone cortex is not covered with hyaline cartilage and is directly exposed to joint inflammation. Ultrasound is sensitive to bone cortex abnormalities but is not specific for erosions, with a reported false-positive rate of 29% for diagnosis of erosions.[33] The

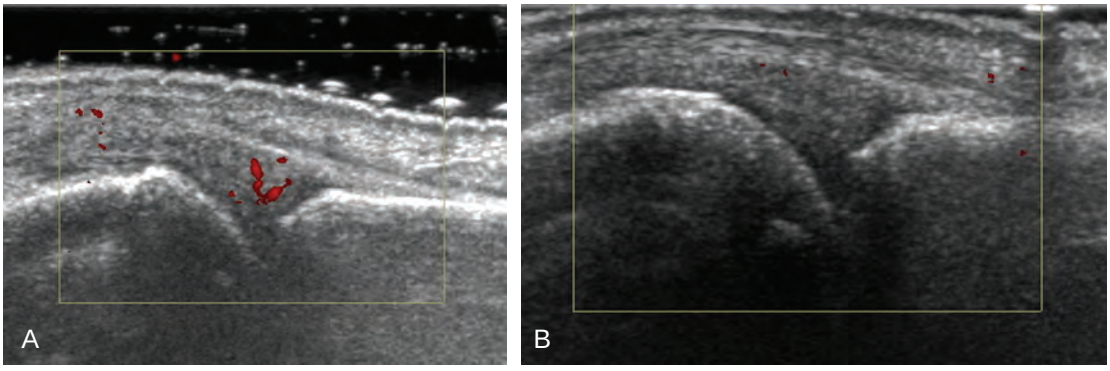

FIGURE 2-29 ■ Hyperemia: effects of compression (rheumatoid arthritis). Ultrasound images in the sagittal plane of the third metacarpophalangeal joint dorsal recess **(A)** without and **(B)** with minimal transducer pressure show hyperemia of isoechoic synovial hypertrophy that is obliterated with transducer pressure. Note intervening thick gel layer between the transducer and skin surface in **A**.

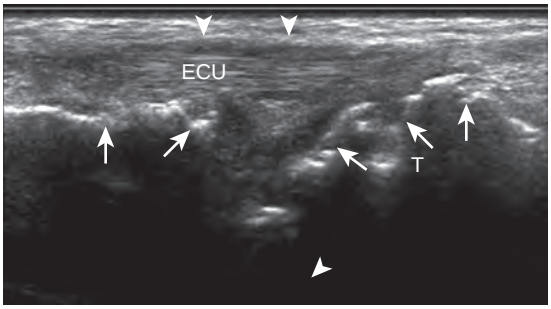

FIGURE 2-30 ■ Rheumatoid arthritis: erosions. Ultrasound image over the lateral wrist in the coronal plane shows erosions *(arrows)* and extensor carpi ulnaris (ECU) tenosynovitis *(arrowheads)*. T, triquetrum.

finding of synovial hypertrophy directly over a cortical irregularity also increases the likelihood that an erosion is present. Correlation with radiographic and clinical findings remains important, in addition to the distribution of imaging findings. For example, rheumatoid arthritis commonly involves the metacarpophalangeal joints of the hands (especially the second), the metatarsophalangeal joints of the feet (usually at least the fifth), and the wrist joints. A rheumatoid nodule typically appears as a hypoechoic nodule at ultrasound (Fig. 2-31).[34]

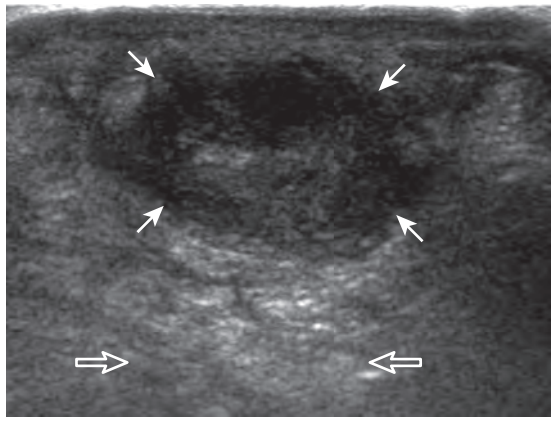

FIGURE 2-31 ■ Rheumatoid nodule. Ultrasound image shows hypoechoic rheumatoid nodule *(arrows)*. Note posterior increased through-transmission *(open arrows)*.

Psoriatic Arthritis

Psoriatic arthritis also involves synovial articulations, which can cause joint effusion, synovial hypertrophy, and erosions (Fig. 2-32A). One distinguishing feature of psoriatic arthritis, similar to other seronegative spondyloarthropathies, is the presence of bone proliferation at tendon and

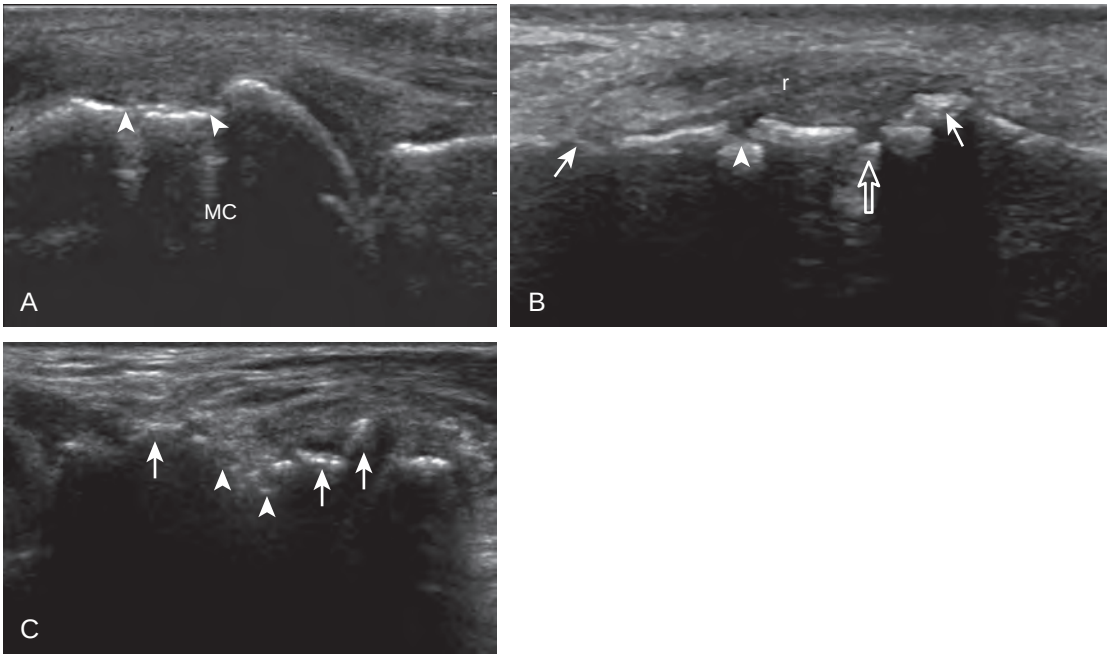

FIGURE 2-32 ■ Psoriatic arthritis. Ultrasound image shows **(A)** metacarpal head (MC) erosion *(arrowheads)*, **(B)** radial collateral ligament (r) of a proximal interphalangeal joint *(open arrow)* with areas of bone proliferation at the ligament attachments *(arrows)* and an erosion *(arrowhead)* with adjacent hypoechoic soft tissue swelling, and **(C)** dorsal wrist in the transverse plane with diffuse areas of bone proliferation *(arrows)*, erosions *(arrowheads)*, and overlying hypoechoic soft tissue swelling.

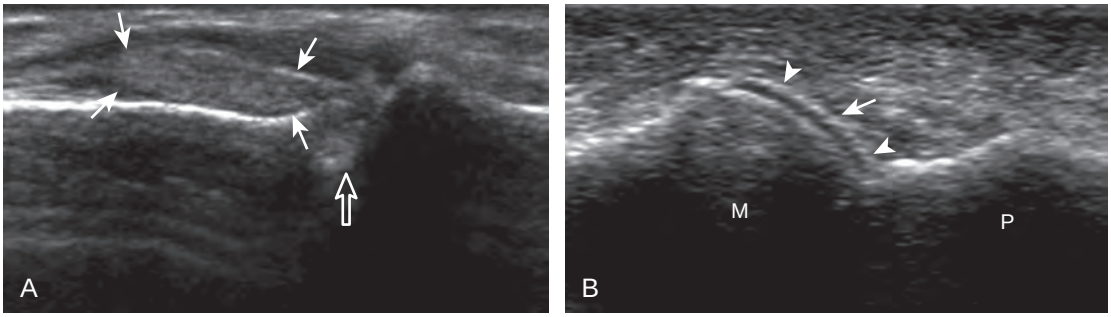

FIGURE 2-33 ■ Gout. Ultrasound images show **(A)** hyperechoic joint effusion *(arrows)* distending dorsal recess of the first metatarsophalangeal joint *(open arrow)*, **(B)** urate crystal deposition on the hyaline cartilage *(arrowheads)* (double contour sign). M, metatarsal head; P, proximal phalanx. (**B,** Courtesy of Ralf Thiele, MD, Rochester, NY.)

ligament attachments (see Fig. 2-32B and C).[35] It is therefore important to assess such sites during evaluation for psoriatic arthritis, such as the collateral ligaments of the digits. Because bone proliferation of psoriatic arthritis may at times appear similar to other forms of bone proliferation, such as osteophytes with osteoarthritis, it is critical to correlate with radiography to assist in this distinction. The presence of hyperemia, often seen in psoriatic arthritis, is another feature. Similarly, it is important to differentiate a degenerative enthesophyte from true inflammatory enthesopathy at a tendon attachment, the latter showing hyperemia and adjacent tendon abnormality with ultrasound and indistinct margins on radiography. The soft tissues over a joint or tendon may also show abnormal swelling and hyperemia.[36]

Gout

The ultrasound findings of gout include joint effusion (with possible visualization of crystals), erosions, and tophi.[37] Joint distention may range from anechoic to heterogeneous, especially in the presence of crystals, tophi, and synovial hypertrophy (Fig. 2-33A). In addition, crystal deposition on the surface of the cartilage (urate icing) will appear hyperechoic, also called the *double contour sign* (see Fig. 2-32B). This finding is differentiated from the normal hyperechoic cartilage interface in that the latter is only seen when the sound beam is perpendicular to the cartilage surface and is uniform. The double contour sign is also different from chondrocalcinosis, in which reflective echoes are located within the cartilage rather than on the surface, as seen with calcium pyrophosphate deposition disease.[38] Monosodium urate tophi characteristically appear as an amorphous but fairly well-defined echogenic area surrounded by a hypoechoic inflammatory halo (Fig. 2-34). A tophus may be associated with adjacent cortical erosion, especially at the medial aspect of the distal first metatarsal (Fig. 2-35). Tendon sheath involvement is also possible (Fig. 2-36). Other common sites for tophi include the olecranon region at the elbow (see Fig. 4-31 in Chapter 4), the patellar tendon (see Fig. 7-54 in Chapter 7), and the popliteus tendon (see Fig. 7-55 in Chapter 7) at the knee.

Osteoarthritis

The hallmark of osteoarthritis is cartilage loss and osteophyte formation, typically in

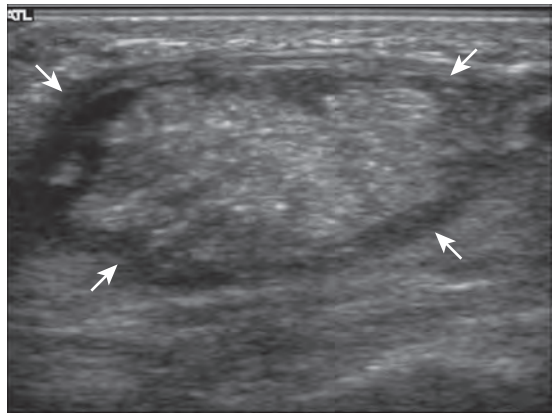

FIGURE 2-34 ■ Gout: tophus. Ultrasound image shows hyperechoic soft tissue tophus with hypoechoic rim *(arrows)*.

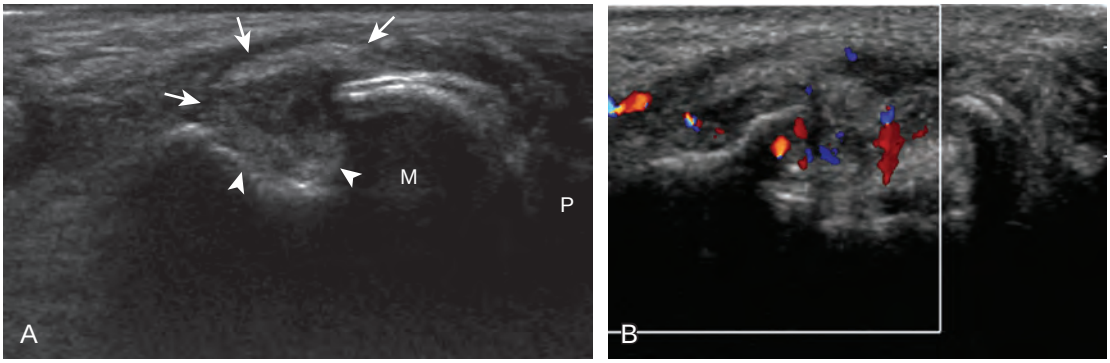

FIGURE 2-35 ■ Gout: tophus and erosion. Ultrasound images in axial plane over medial distal first metatarsal show (**A** and **B**) cortical erosion *(arrowheads)* and adjacent echogenic tophus *(arrows)* with increased flow on color Doppler imaging. M, metatarsal; P, proximal phalanx.

a predictable distribution related primarily to wear-and-tear of a joint. Synovial hypertrophy is often secondary and relatively mild without hyperemia compared with other conditions, such as rheumatoid arthritis.[39] Ultrasound can detect change of osteoarthritis, especially in peripheral joints where image resolution is optimum.[40] Osteophytes appear as a well-defined bone excrescence at a margin of an involved joint. Joint effusion may also be present. Common sites of involvement include the first metatarsophalangeal joint (Fig. 2-37), the interphalangeal and first carpometacarpal joints of the hand and wrist (Fig. 2-38), and the acromioclavicular joint.[41] First metatarsophalangeal joint fluid and acromioclavicular joint involvement are commonly asymptomatic with preclinical osteoarthritis. Synovial hypertrophy may also be seen as hypoechoic, minimally compressible tissue distending a joint recess, although such minimal findings are also commonly seen in asymptomatic joints such as the interphalangeal joints of the hand.[41] In addition, increased flow on color or power Doppler imaging is uncommon, and the presence of synovial hypertrophy does not necessarily correlate with patient symptoms.[39]

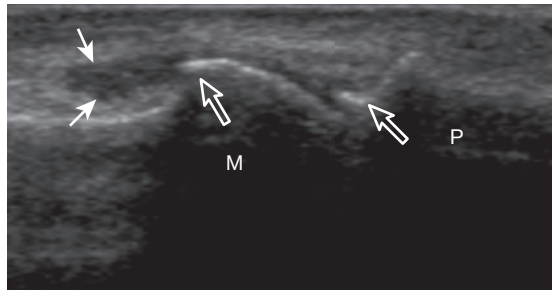

FIGURE 2-37 ■ Osteoarthritis: first metatarsophalangeal joint. Ultrasound image over first metatarsophalangeal joint shows nonspecific mild synovial hypertrophy *(arrows)* and osteophytes *(open arrows)*. M, metatarsal; P, proximal phalanx.

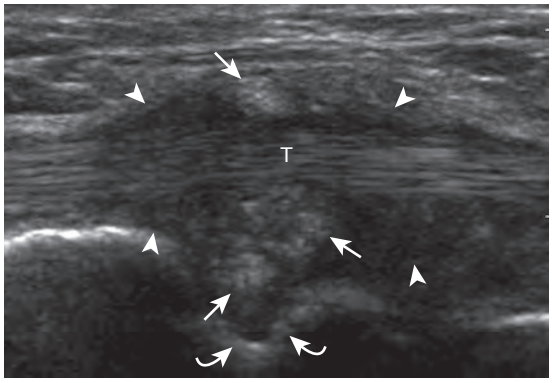

FIGURE 2-36 ■ Gout: tophus and tenosynovitis. Ultrasound image shows hyperechoic tophus *(arrows)* surrounding ankle tendon (T) causing osseous erosion *(curved arrows)* and surrounding hypoechoic tenosynovitis *(arrowheads)*.

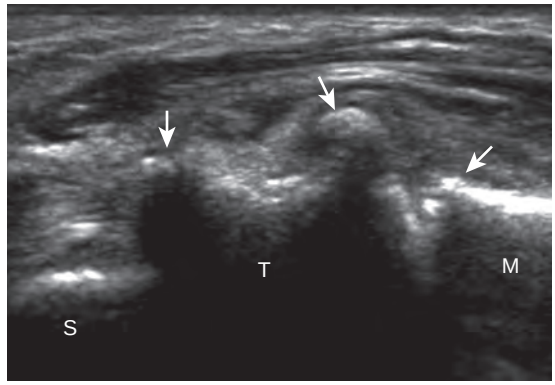

FIGURE 2-38 ■ Osteoarthritis: trapezium. Ultrasound image over thumb base shows trapezium (T) osteophytes *(arrows)* at articulations with scaphoid (S) and first metacarpal (M).

MYOSITIS AND DIABETIC MUSCLE INFARCTION

Inflammatory myositis, such as polymyositis, appears hyperechoic with possible increased flow on color or power Doppler imaging (Fig. 2-39).[4] In later stages, increased muscle echogenicity and diminished volume are characteristic of muscle atrophy. Sarcoidosis may also involve muscle, where the nodular type of sarcoidosis produces hypoechoic masses or nodules.[42]

In the evaluation of inflammation or infection around the thigh or calf, one condition in the differential diagnosis is *diabetic muscle infarction*. In this condition, the involved thigh musculature is hypoechoic and swollen, although the hyperechoic fibroadipose septum or epimysium are still identified throughout, a feature that helps to exclude soft tissue abscess (Fig. 2-40).[43] Subfascial fluid may also be seen. Diabetic muscle infarction most commonly involves the thigh or calf musculature, it may be bilateral, and it occurs in patients with longstanding diabetes.

SOFT TISSUE FOREIGN BODIES

Another cause of soft tissue infection is a soft tissue foreign body. At sonography, all foreign bodies are initially hyperechoic (Fig. 2-41), although organic or plant material may become less echogenic over time.[44] The surface of the foreign body is more echogenic and conspicuous when the sound beam is perpendicular to the surface of the foreign body (Fig. 2-42). It is therefore important not only to image directly over the entry site, but also to interrogate the involved soft tissues from various angles in order to have the sound beam perpendicular to the surface of the foreign body. It is often helpful to use a thick layer of gel to float the transducer above the skin surface so as not to overlook any superficial foreign bodies and to optimize the sound beam angulation (see Fig. 2-42D).

Conspicuity of a soft tissue foreign body is additionally enhanced by the soft tissue reaction around the foreign body and the foreign body artifact if present.[45] A hypoechoic halo with possible hyperemia may be present, and it represents hemorrhage, granulation tissue, and abscess. This produces a halo appearance as the hypoechoic reaction surrounds the hyperechoic foreign body (Fig. 2-43). Some foreign bodies, such as metal, may have little if any foreign body response (Fig. 2-44).

Foreign body artifact depends on the surface attributes of the foreign body more than on its internal composition.[44] For example, a foreign body with a smooth and flat surface, such as glass,

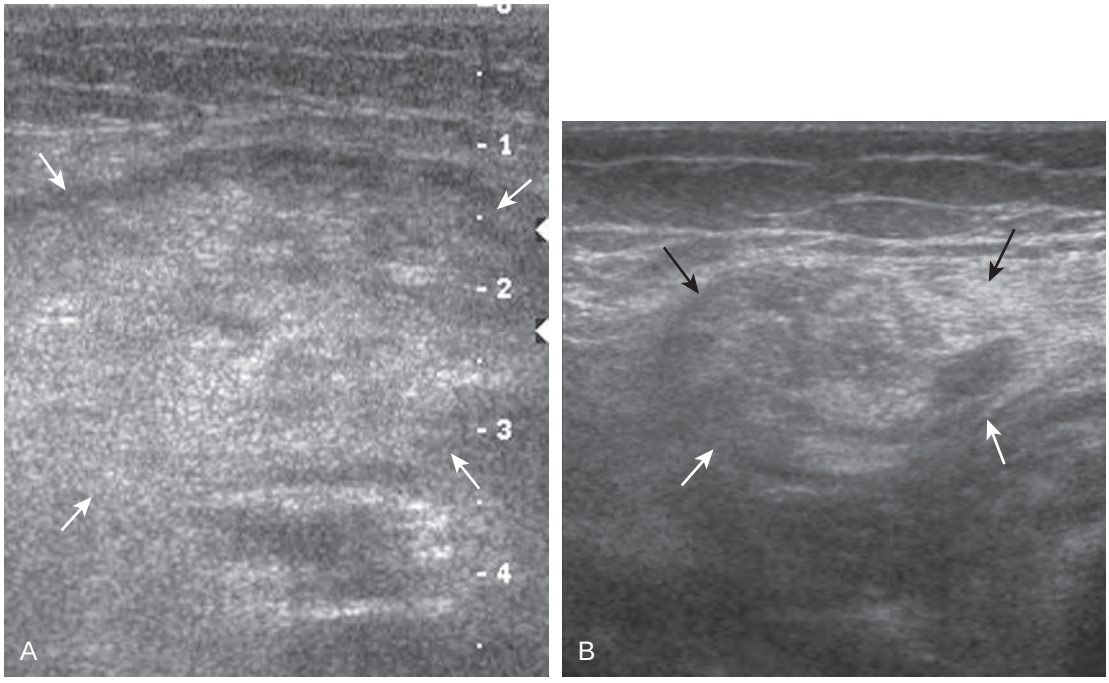

FIGURE 2-39 ■ Myositis. Ultrasound images show **(A)** increased echogenicity and size of the sartorius *(arrows)* representing inflammatory myositis and **(B)** increased echogenicity of the rectus femoris *(arrows)* representing postchemotherapy and radiation recall myositis.

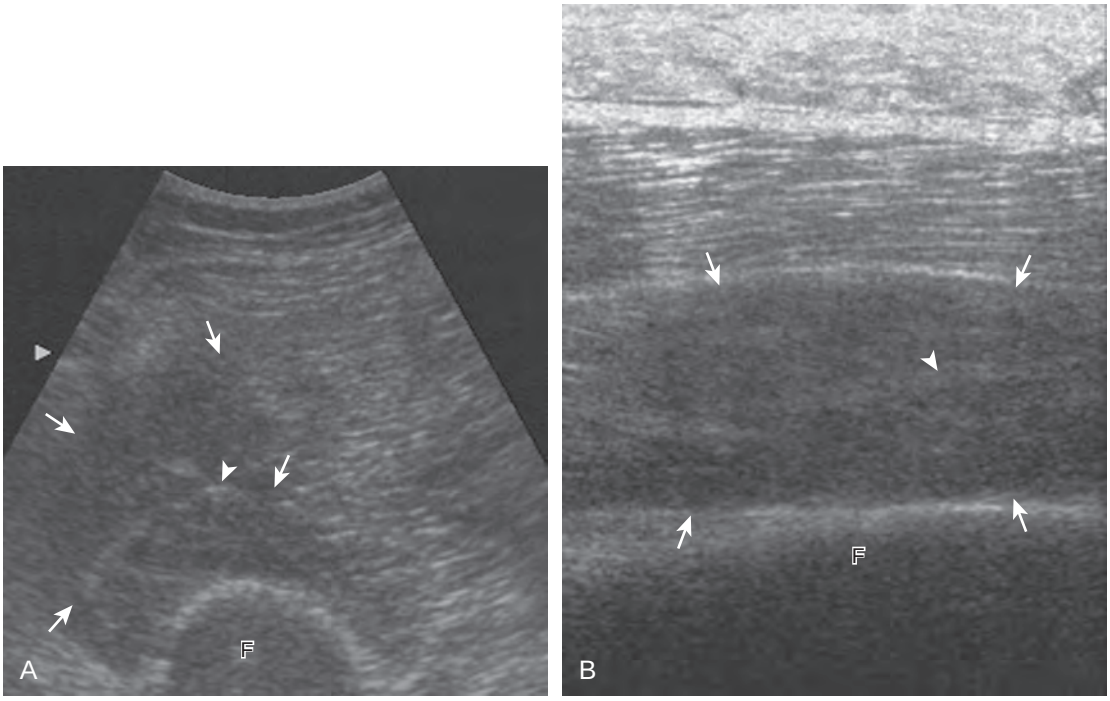

FIGURE 2-40 ■ Diabetic muscle infarction. Ultrasound images in **(A)** short axis and **(B)** long axis to the rectus femoris show hypoechoic swelling of the vastus intermedius muscle *(arrows)*. Note visible hyperechoic fibroadipose septa or epimysium *(arrowheads)*. F, femur.

produces posterior reverberation artifact (Fig. 2-45). A foreign body with an irregular surface and small radius of curvature usually shows posterior shadowing (Fig. 2-46). Many foreign bodies show both shadowing and reverberation artifact (see Figs. 2-41 and 2-44). It is important that the field of view around the foreign body include soft tissues deep to the foreign body to help the viewer recognize any posterior artifact.

Although ultrasound can accurately identify and localize all soft tissue foreign bodies, it is most important in evaluation of foreign bodies that are not radiopaque on radiography, such as those composed of wood or plastic (Fig. 2-47).[44] All glass is opaque on radiographs if it is large enough to be resolved, if it is projected off any adjacent osseous structures, and if it is imaged with proper radiographic technique.[44] One potential pitfall in sonography of soft tissue of foreign bodies is the presence of soft tissue gas, usually the result of prior attempted removal or, less likely, infection, which in itself may simulate a foreign body and alter the sonographic characteristics of a foreign body (Fig. 2-48) (Video 2-6).[46]

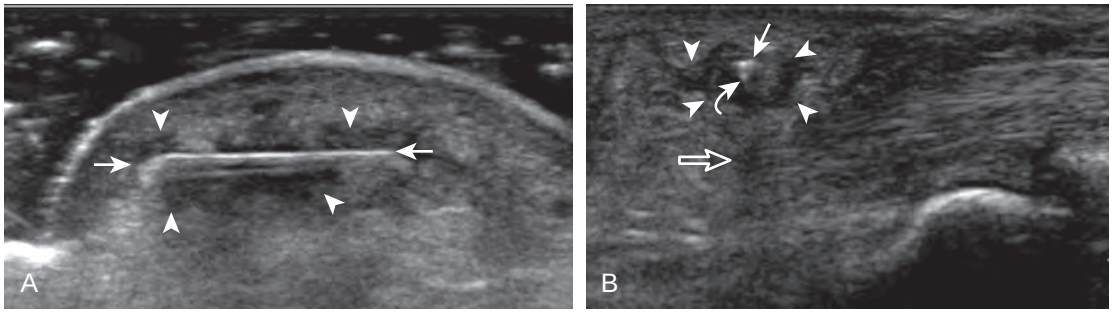

FIGURE 2-41 ■ Wooden foreign body. Ultrasound images in **(A)** long axis and **(B)** short axis to a hyperechoic wooden foreign body *(arrows)* show hypoechoic halo *(arrowheads)* with mild shadowing *(open arrow)* and posterior reverberation *(curved arrow)* artifact.

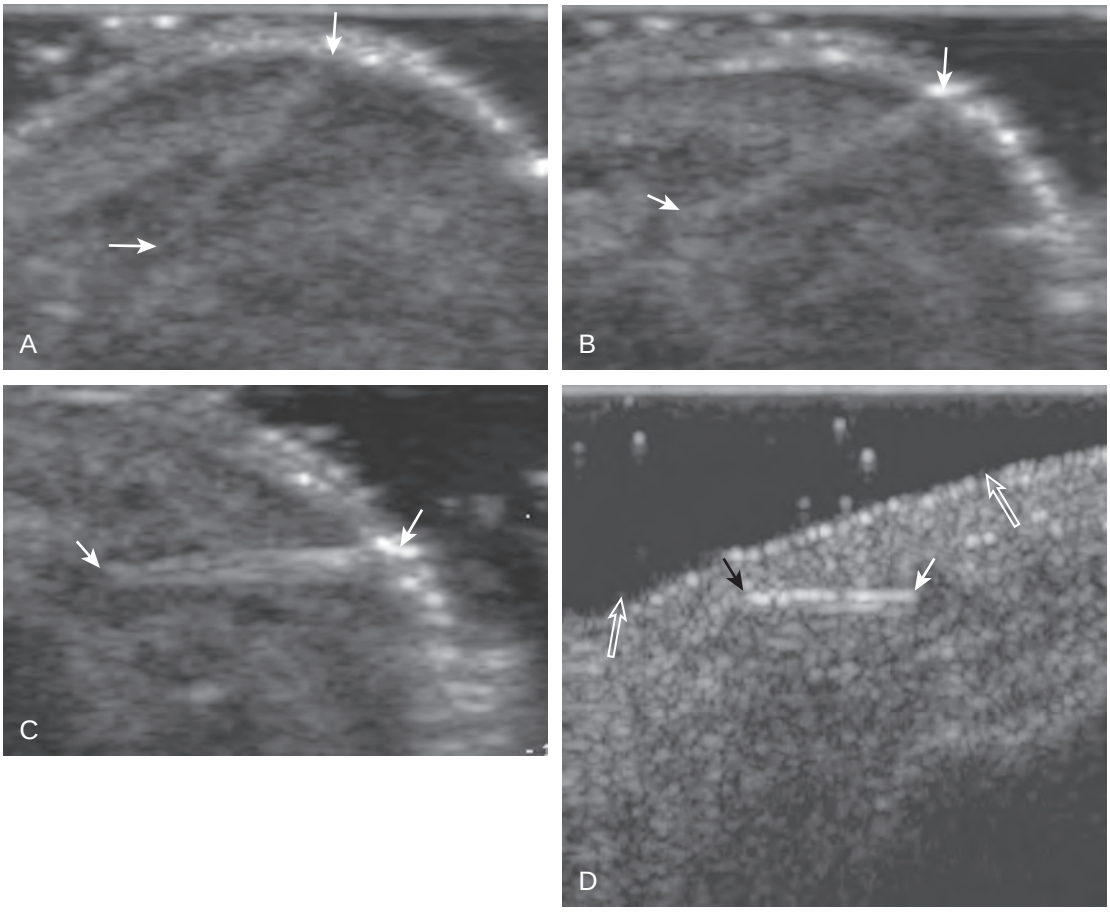

FIGURE 2-42 ■ Wooden foreign body. A to **C,** Ultrasound images show hyperechoic wooden splinter *(arrows)*, which becomes more echogenic and conspicuous when imaged perpendicular to the sound beam. **D,** Ultrasound image shows thick layer of gel *(open arrows)* used to allow the wooden foreign body *(arrows)* to be imaged perpendicular to the sound beam.

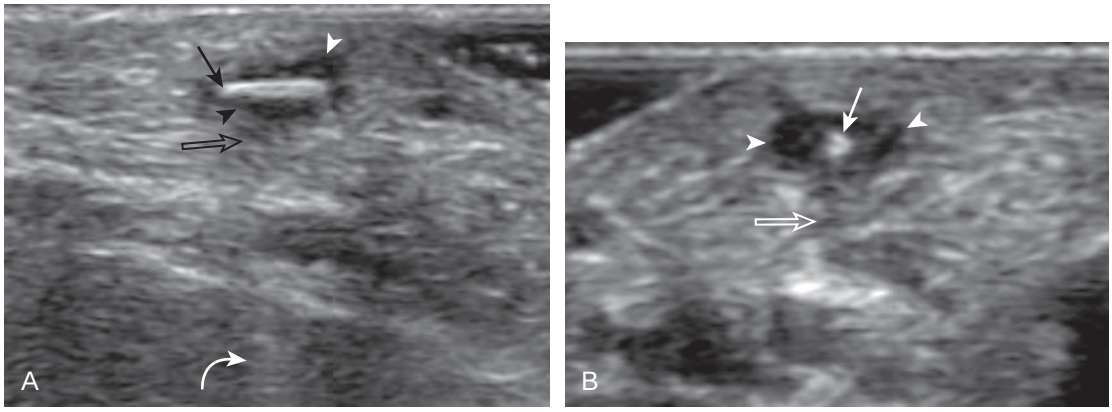

FIGURE 2-43 ■ Wooden foreign body. Ultrasound images in **(A)** long axis and **(B)** short axis to a hyperechoic rose thorn *(arrow)* show hypoechoic halo *(arrowheads)* with mild shadowing *(open arrow)* and posterior reverberation *(curved arrow)* artifact.

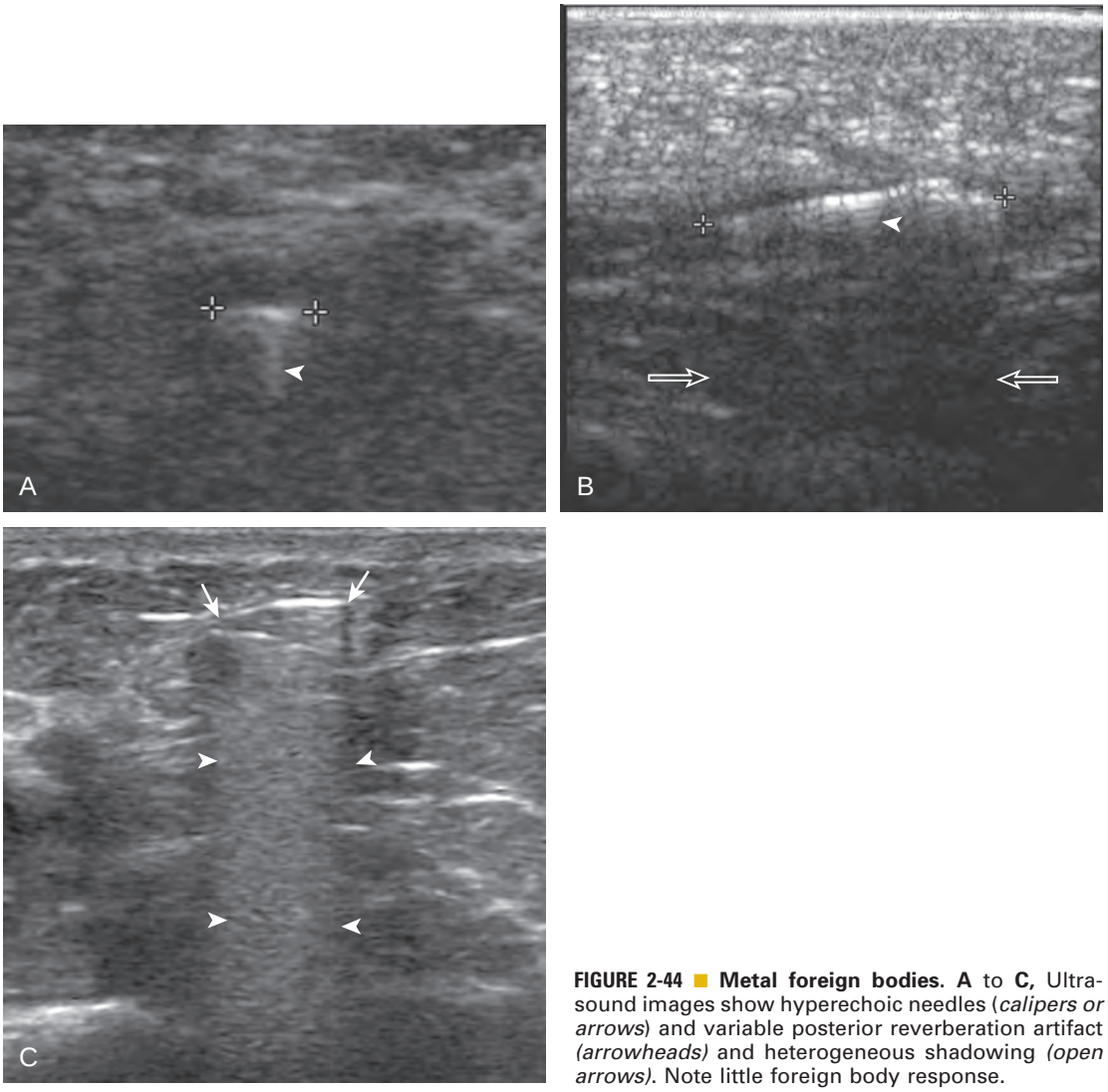

FIGURE 2-44 ■ Metal foreign bodies. A to **C,** Ultrasound images show hyperechoic needles (*calipers or arrows*) and variable posterior reverberation artifact *(arrowheads)* and heterogeneous shadowing *(open arrows)*. Note little foreign body response.

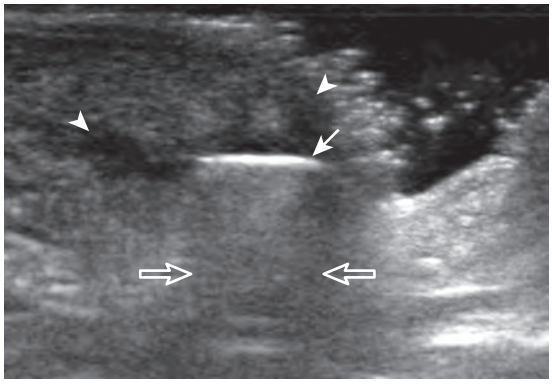

FIGURE 2-45 ■ Glass foreign body. Ultrasound image shows hyperechoic glass foreign body *(arrow)*, adjacent hypoechoic inflammation *(arrowheads)*, and central posterior reverberation artifact and peripheral shadowing *(open arrows)*.

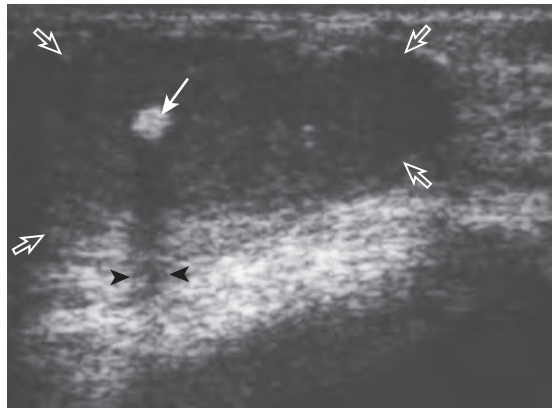

FIGURE 2-46 ■ Wooden foreign body. Ultrasound image shows a hyperechoic wooden splinter *(arrow)* with posterior acoustic shadowing *(arrowheads)* and a surrounding hypoechoic abscess *(open arrows)*. Note increased through-transmission deep to the abscess.

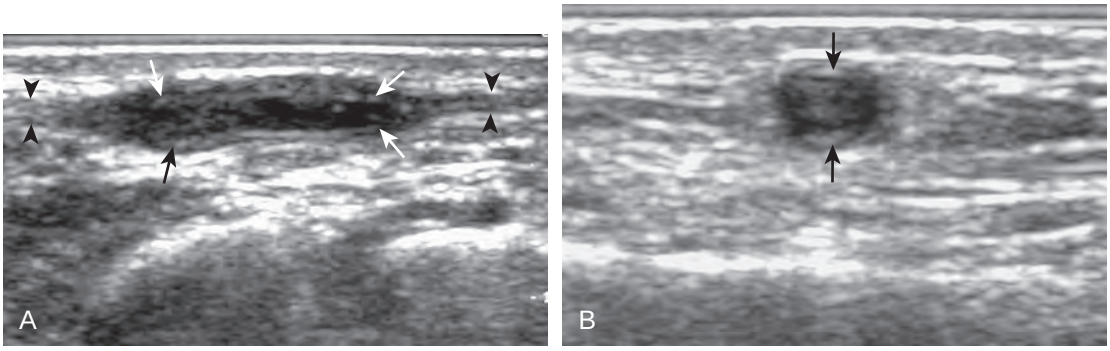

FIGURE 2-47 ■ Plastic catheter foreign body. Ultrasound images in **(A)** long axis and **(B)** short axis to a superficial foot vein show the hyperechoic walls *(arrows)* of the plastic catheter within the collapsed vein *(arrowheads)*. (From Fessell DP, Jamadar DA, Jacobson JA, et al: Sonography of dorsal ankle and foot abnormalities. *AJR Am J Roentgenol* 181:1571–1573, 2003.)

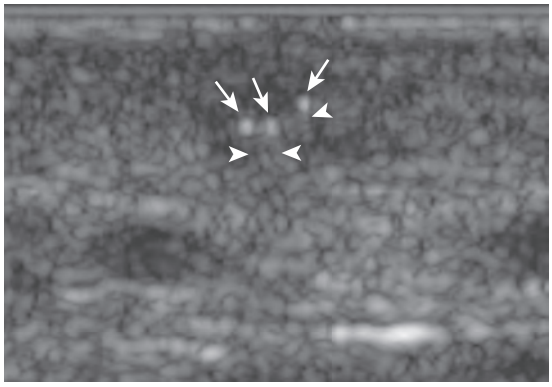

FIGURE 2-48 ■ Soft tissue gas. Ultrasound image shows hyperechoic gas foci *(arrows)* with comet-tail artifacts *(arrowheads)*. No foreign body was present.

Ultrasound can also assess for related complications, such as adjacent tenosynovitis (Fig. 2-49), periostitis (Fig. 2-50), and abscess (Fig. 2-51).[45] Ultrasound can aid removal by accurately marking the skin surface over the foreign body before removal, by guiding a localization wire, or by directly guiding percutaneous removal.[47,48] A chronic foreign body reaction may simulate a soft tissue mass. The use of spatial compound sonography may smooth out the image and affects the appearance of the foreign body and associated artifacts (Fig. 2-52).

PERIPHERAL NERVE ENTRAPMENT

There are specific anatomic sites where a peripheral nerve may be entrapped, typically when a nerve traverses a confined space as a result of osseous, ligamentous, or fibrous constraints.[49-51] Examples in the upper extremity include the median nerve in the carpal tunnel (carpal tunnel syndrome) (see Fig. 5-61 in Chapter 5), the ulnar nerve in the Guyon canal (ulnar canal syndrome) (see Fig. 5-70 in Chapter 5), the ulnar nerve in the cubital tunnel of the elbow (cubital tunnel syndrome) (see Fig. 4-54 in Chapter 4), and the deep branch of the radial nerve at the level of the

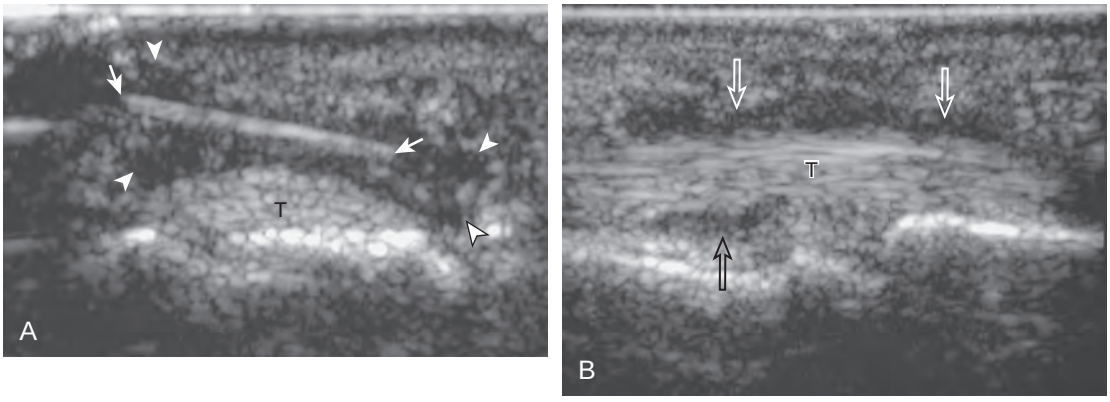

FIGURE 2-49 ■ Foreign body: septic tenosynovitis. Ultrasound images (**A** and **B**) show a hyperechoic wooden splinter *(arrows)* with a hypoechoic halo *(arrowheads)* and more proximal septic tenosynovitis *(open arrows)*. T, flexor digitorum profundus tendon.

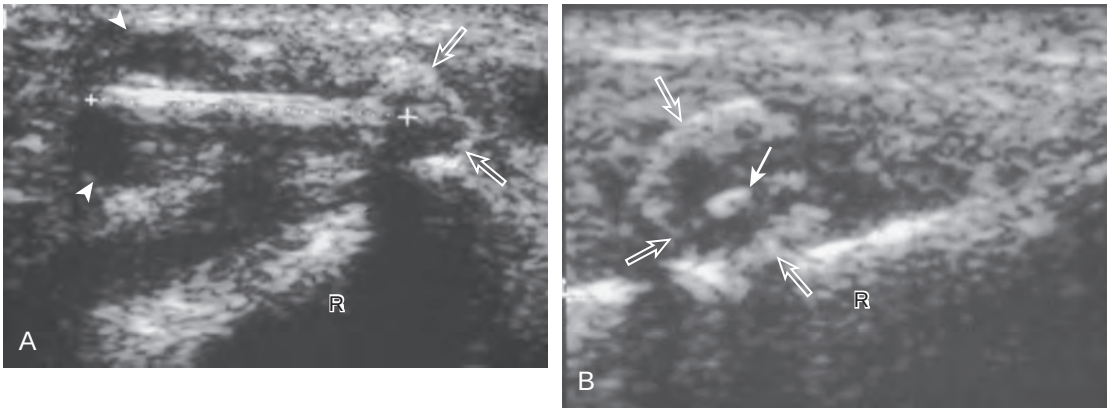

FIGURE 2-50 ■ Foreign body: periostitis. Ultrasound images (**A** and **B**) show a hyperechoic wooden splinter *(calipers and arrow)* with a hypoechoic halo *(arrowheads)* and hyperechoic periostitis *(open arrows)*. R, radius.

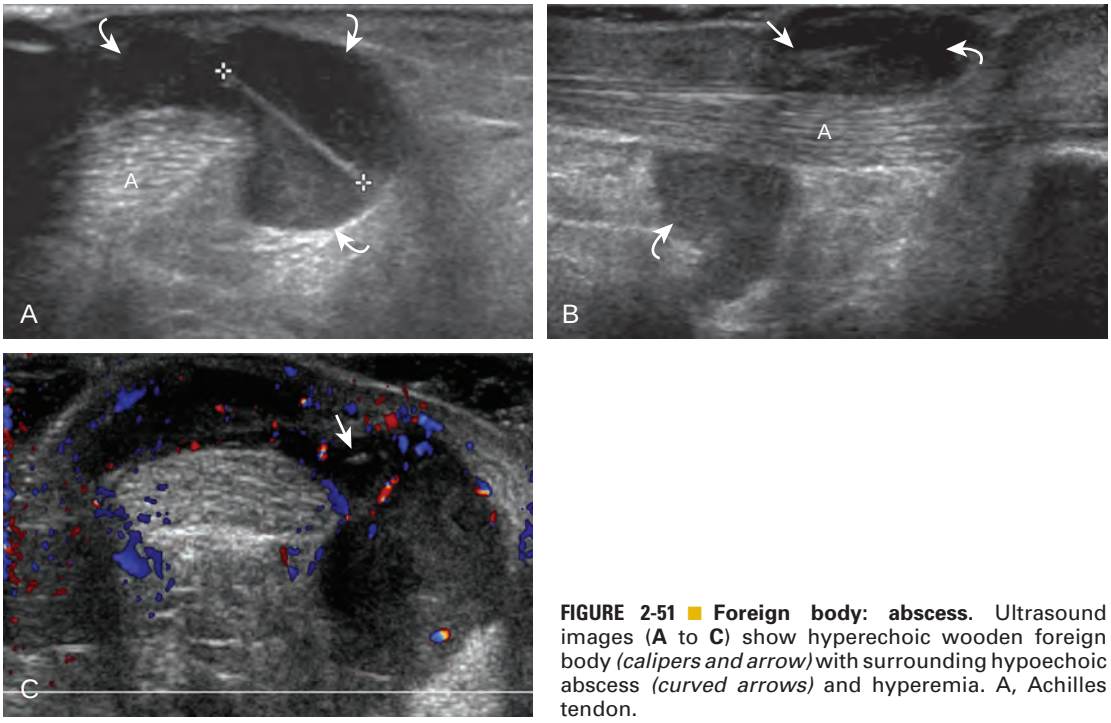

FIGURE 2-51 ■ Foreign body: abscess. Ultrasound images (**A** to **C**) show hyperechoic wooden foreign body *(calipers and arrow)* with surrounding hypoechoic abscess *(curved arrows)* and hyperemia. A, Achilles tendon.

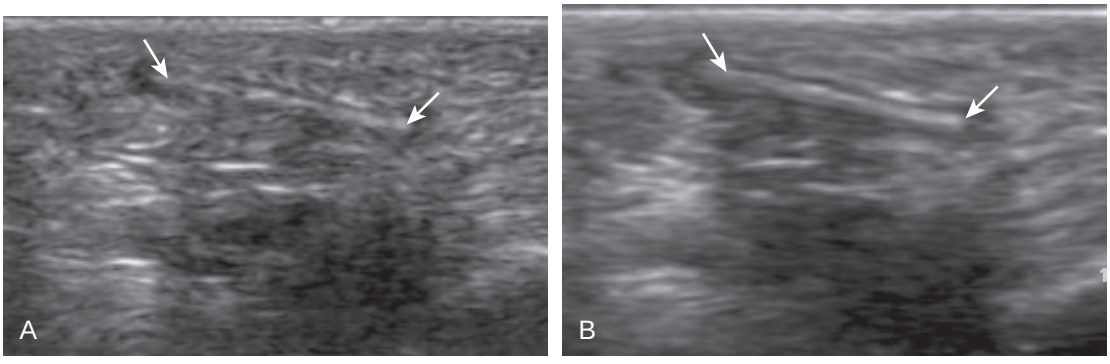

FIGURE 2-52 ■ Spatial compound sonography. Ultrasound images **(A)** without and **(B)** with spatial compounding show the hyperechoic wooden foreign body *(arrows)* and mild hypoechoic halo.

supinator muscle (posterior interosseous nerve or supinator syndrome) (see Fig. 4-66 in Chapter 4). Examples in the lower extremity include the tibial nerve at the ankle (tarsal tunnel syndrome) (see Fig. 8-153 in Chapter 8) and the common plantar digital nerve in the distal foot (Morton neuroma) (see Fig. 8-152 in Chapter 8). Common sonographic features of each of these conditions are hypoechoic swelling of the involved nerve at the entrapment site and possible compression distally. Many times, transducer pressure on the nerve elicits symptoms. Evaluation for denervation and muscle atrophy is also a clue to peripheral nerve entrapment and chronicity, where ultrasound shows increased echogenicity of the involved muscle. Knowledge of peripheral nerve anatomy and of sites prone to nerve compression is vital for an accurate diagnosis.

SOFT TISSUE MASSES

Although the etiology of some soft tissue tumors may be suggested based on anatomic location, physical examination findings, and the patient's history and age, many masses remain nonspecific by ultrasound. The primary roles of ultrasound in this situation are to differentiate cyst versus solid mass and to guide biopsy for definitive histologic diagnosis. Ultrasound does play an important role in the assessment of benign subcutaneous masses by improving diagnostic accuracy.[52] In the following chapters, soft tissue masses that are specific or common to each anatomic region are discussed. Some masses occur throughout the body and have similar sonographic features regardless, and several of these are discussed here.

Lipoma

Soft tissue lipomas can occur anywhere in the body and may be multiple, although many lipomas involve the shoulder region, upper extremity, trunk, and back. Soft tissue lipomas may be located within the subcutaneous fat, within muscle, or within tissue planes. When present in the subcutaneous tissues, the findings of a homogeneous, oval, isoechoic to minimally hyperechoic mass, with little or no flow on color or power Doppler imaging, that is soft and pliable with transducer pressure are compatible with lipoma (Fig. 2-53) (Video 2-7). When a lipoma is located in an intramuscular location, the appearance is somewhat nonspecific but often is relatively hyperechoic (Fig. 2-54).[53] Because an

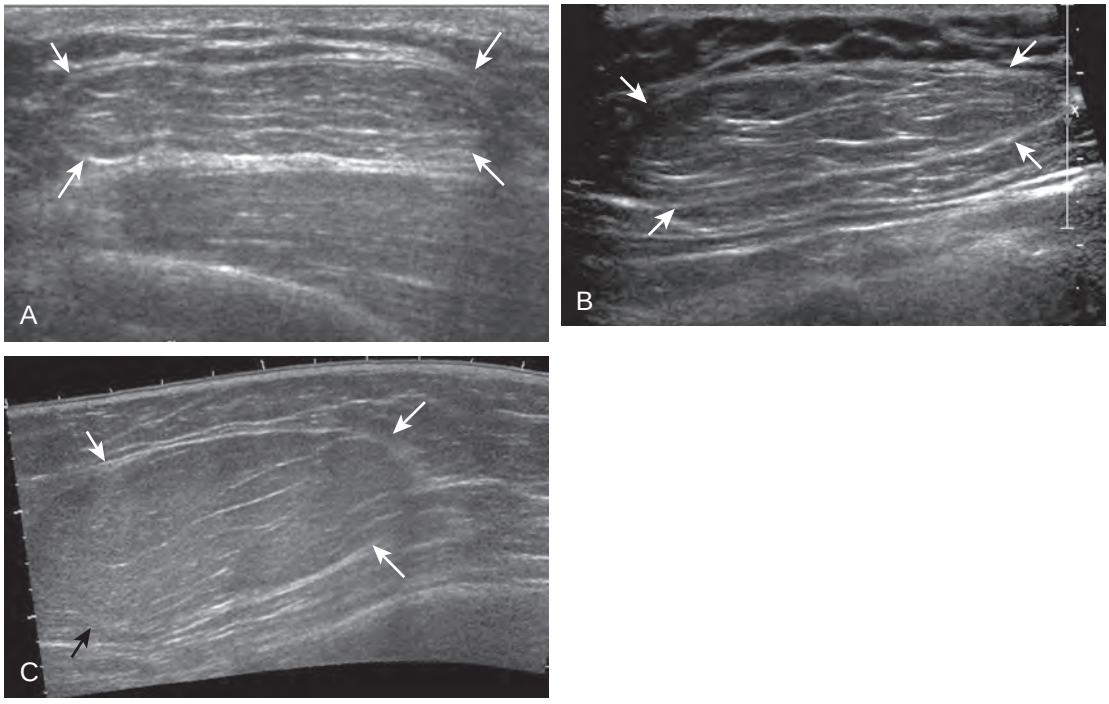

FIGURE 2-53 ■ Subcutaneous lipomas. Ultrasound images from three different patients show well-defined oval isoechoic to minimally hyperechoic subcutaneous lipomas *(arrows)*.

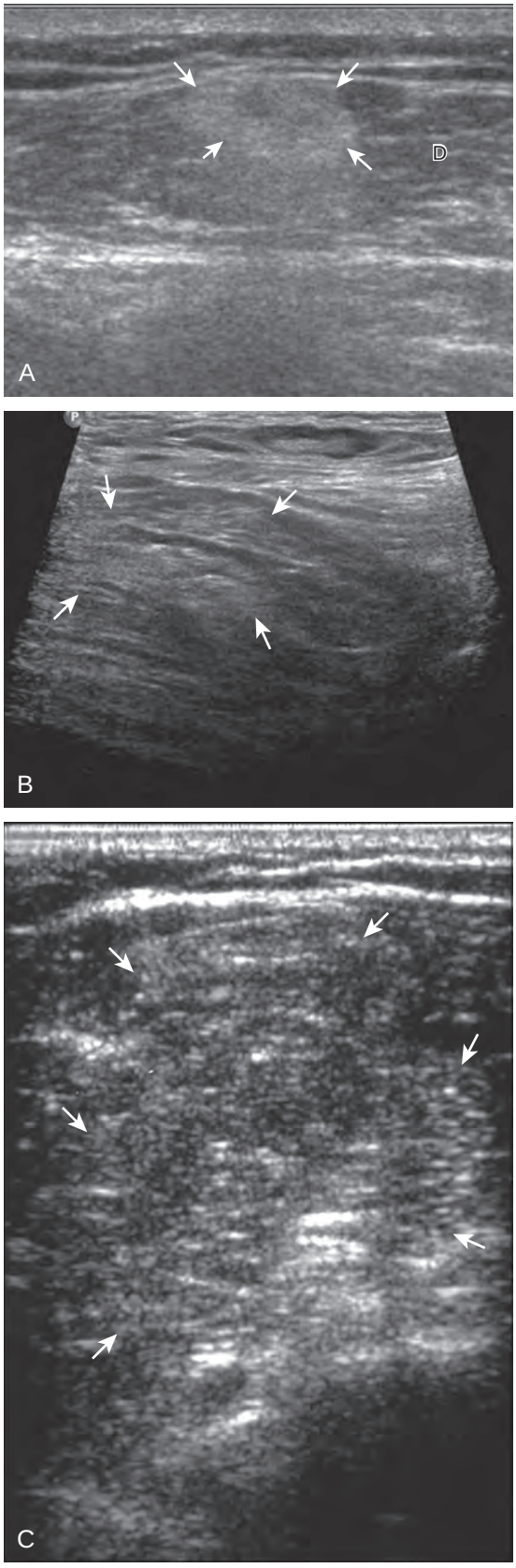

FIGURE 2-54 ■ Intramuscular lipomas. Ultrasound images from three different patients show hyperechoic intramuscular lipomas *(arrows)*. D, deltoid muscle.

intramuscular lipoma and its margins are more difficult to define and a lipomatous tumor is more likely to be malignant when in a deep compared with a superficial location, MRI is typically indicated to confirm a suspected intramuscular lipoma.

The variable echogenicity of a lipoma is related to the amount of fat and connective tissue in the tumor as well as to the surrounding tissue echogenicity. For example, a homogeneous fatty mass is hypoechoic; as the amount of fibrous tissue within the lipoma increases, the lipoma will appear more hyperechoic owing to the reflective soft tissue interfaces (Fig. 2-55).[53] In addition, a lipoma that is isoechoic to the surrounding subcutaneous fat appears relatively hyperechoic when it is located in muscle. Subcutaneous lipomas that are isoechoic to the surrounding tissues may not be immediately apparent on ultrasound. It is important to correlate directly with physical examination findings, with direct palpation of the mass under ultrasound visualization (Video 2-8), or by placing an opened paperclip or other similar marker over the edge of the palpable mass and then scanning the region.[47]

The sensitivity and specificity of ultrasound in the diagnosis of a subcutaneous lipoma are 88% and 99%, respectively.[52] In the correct clinical setting, sonography may determine that a soft tissue mass is compatible with a lipoma; however, a mass that is enlarging or a painful mass requires MRI or histologic evaluation for confirmation. A low-grade well-differentiated liposarcoma has a variable appearance but is often hyperechoic, related to the amount of soft tissue stranding or nodules within the predominantly fatty tumor (Fig. 2-56). A high-grade or poorly differentiated liposarcoma is heterogeneous but predominantly hypoechoic, similar to other sarcomas (see later section in this chapter). Any fatty mass that is not isolated to the subcutaneous tissue should undergo MRI for confirmation.

If a small hyperechoic mass is seen in the subcutaneous tissues, additional diagnoses should be considered. With this appearance, one possibility would be an angiolipoma, which is considered a vascular variant of a lipoma or hamartoma; it is multiple and painful in about 50% of patients (Fig. 2-57). Subcutaneous fat necrosis (as part of panniculitis or after trauma) has a variable appearance but may look like a focal hyperechoic mass or nodule (see Fig. 2-20B).[24] Dermatofibrosarcoma protuberans may appear as either a hypoechoic (discussed later in Malignant Soft Tissue Tumors) or hyperechoic subcutaneous mass; the latter appearance is different from a lipoma, given a wide base contact with the skin with possible ill-defined borders and hyperemia.[54]

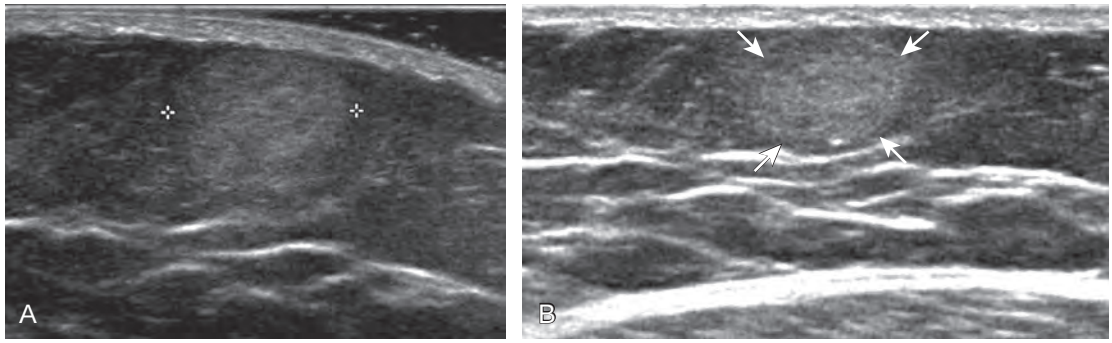

FIGURE 2-55 ■ Lipomas: echogenic. Ultrasound images from two different patients show hyperechoic subcutaneous lipomas *(between cursors and arrows)*.

Peripheral Nerve Sheath Tumors

A solid soft tissue mass that is in continuity with a peripheral nerve is diagnostic for a peripheral nerve sheath tumor. Ultrasound is often used to demonstrate peripheral nerve continuity given its high resolution. At ultrasound, a peripheral nerve sheath tumor is hypoechoic with a low level of homogeneous internal echoes, round or oval, and appears well defined (Fig. 2-58). Increased through-transmission is usually seen deep to the mass, which may cause the hypoechoic mass to be mistaken for a complex cyst; however, the presence of flow on color or power Doppler imaging confirms the solid nature of the mass (Fig. 2-59) (Video 2-9).[55] Transducer pressure over a peripheral nerve sheath tumor usually elicits symptoms.

A solitary peripheral nerve sheath tumor that is eccentric to the peripheral nerve is characteristic of a schwannoma (or neurilemmoma) (see Fig. 8-154 in Chapter 8), whereas neurofibromas tend to be central relative to the nerve, although differentiation between the two is often not possible with ultrasound.[56] A target appearance has also been described in neurofibromas, which appears as an echogenic fibrous center surrounded by a hypoechoic myxoid periphery, reported as a possible indicator of a benign peripheral nerve sheath tumor (Fig. 2-60A).[57] Neurofibromas may have three different forms: localized (see Fig. 2-60A), plexiform, and diffuse.[58] Plexiform neurofibroma is described as a "bag of worms" appearance (see Fig. 2-60B), whereas the diffuse form appears as diffuse echogenic subcutaneous tissues with hypoechoic tubules (see Fig. 2-60C), most commonly involving the head and neck region. Peripheral nerve sheath tumors may have internal cystic areas (Fig. 2-61) and calcification (such as in a longstanding or ancient schwannoma). Ultrasound cannot accurately differentiate benign from malignant peripheral nerve sheath tumors; the latter often appear similar to other soft tissue malignancies (Fig. 2-62).

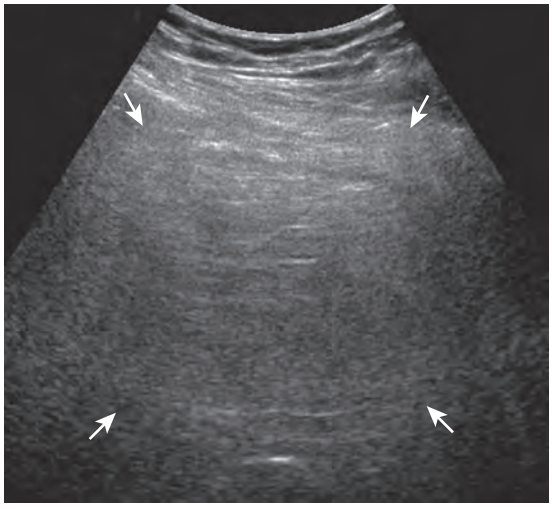

FIGURE 2-56 ■ Liposarcoma (well differentiated, low grade). Ultrasound image shows large hyperechoic mass *(arrows)*.

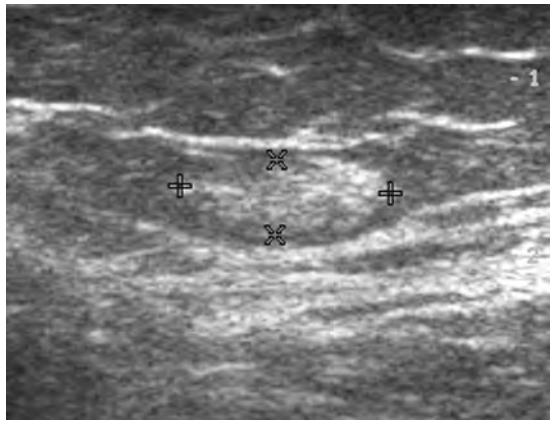

FIGURE 2-57 ■ Angiolipoma. Ultrasound image shows a hyperechoic angiolipoma (*calipers*).

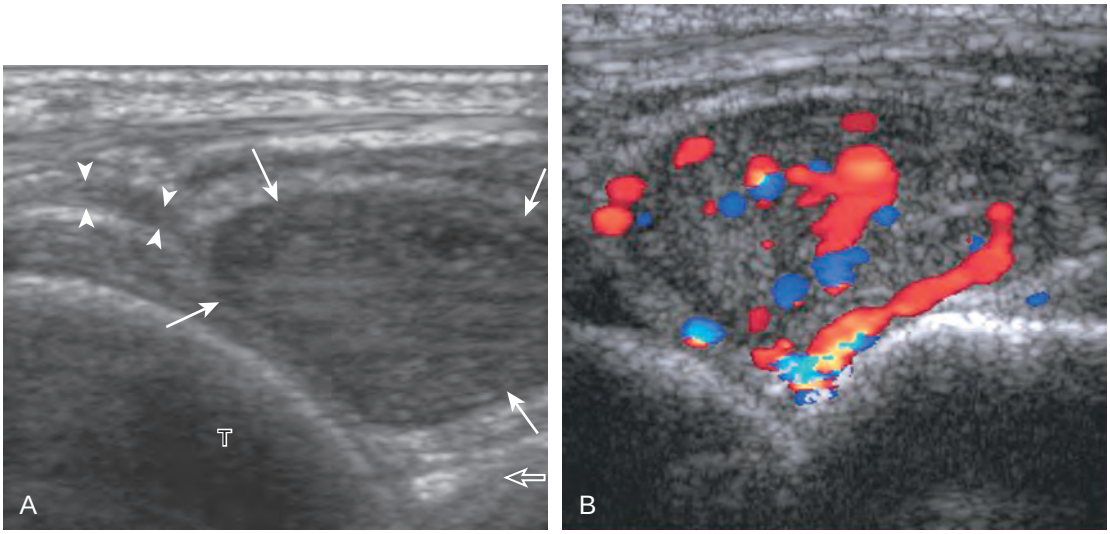

FIGURE 2-58 ■ Schwannoma. Ultrasound images show (**A** and **B**) a hypoechoic schwannoma *(arrows)* with homogeneous diffuse internal echoes. Note flow on color Doppler imaging, continuity with a branch of the deep peroneal nerve *(arrowheads)*, and increased through-transmission *(open arrow)*. T, talus.

Vascular Anomalies

Based on clinical and histologic findings, soft tissue vascular anomalies can be categorized into vascular tumors and vascular malformations.[59,60] A common childhood vascular tumor is an infantile hemangioma, which undergoes spontaneous involution in most cases. Vascular malformations are subcategorized as low flow (capillary, venous, lymphatic, or a combination of each) and high flow (arteriovenous fistula and arteriovenous malformation).[59] Although this is one described classification system, focal and well-defined intramuscular vascular lesions commonly presenting in an adult may also be called *hemangiomas*, subdivided by their dominant vascularity.[61]

At ultrasound, an infantile hemangioma is characterized by a mixed hyperechoic and hypoechoic mass with few or no visible vessels but with increased flow on color or power Doppler imaging.[59] Intramuscular vascular malformations have a heterogeneous appearance, with a variable echogenicity, ranging from hypoechoic to isoechoic to hyperechoic, which often infiltrates the involved soft tissue (Figs. 2-63 and 2-64).[59,62] Anechoic or hypoechoic channels that demonstrate flow on color or power Doppler imaging are typical, although flow may be very slow and difficult to identify without augmenting flow with manual compression. The hyperechoic areas represent the interfaces with the vascular structures, associated fatty tissue, and

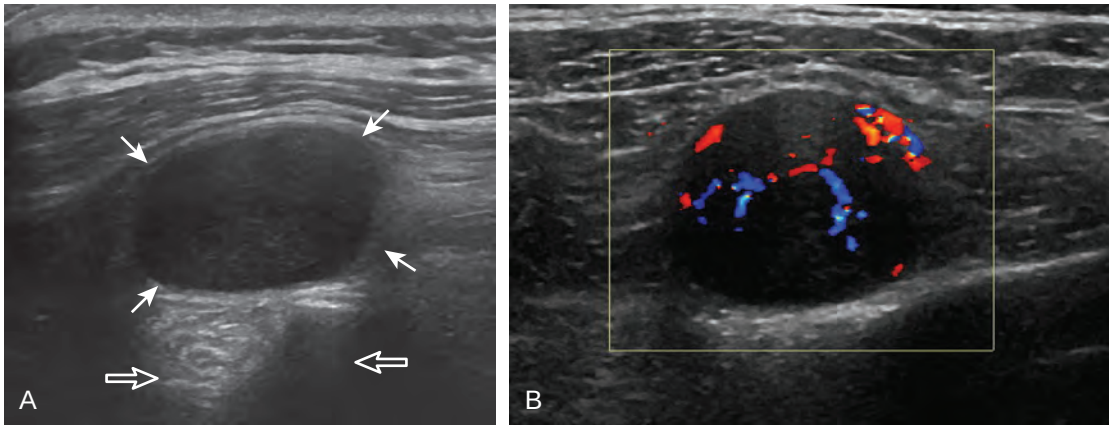

FIGURE 2-59 ■ Schwannoma: pseudocyst appearance. A, Ultrasound image shows a hypoechoic schwannoma *(arrows)* with posterior increased through-transmission *(open arrows)* that may simulate a cyst. **B,** Note flow on color Doppler imaging that indicates that the abnormality is a solid mass and not a cyst.

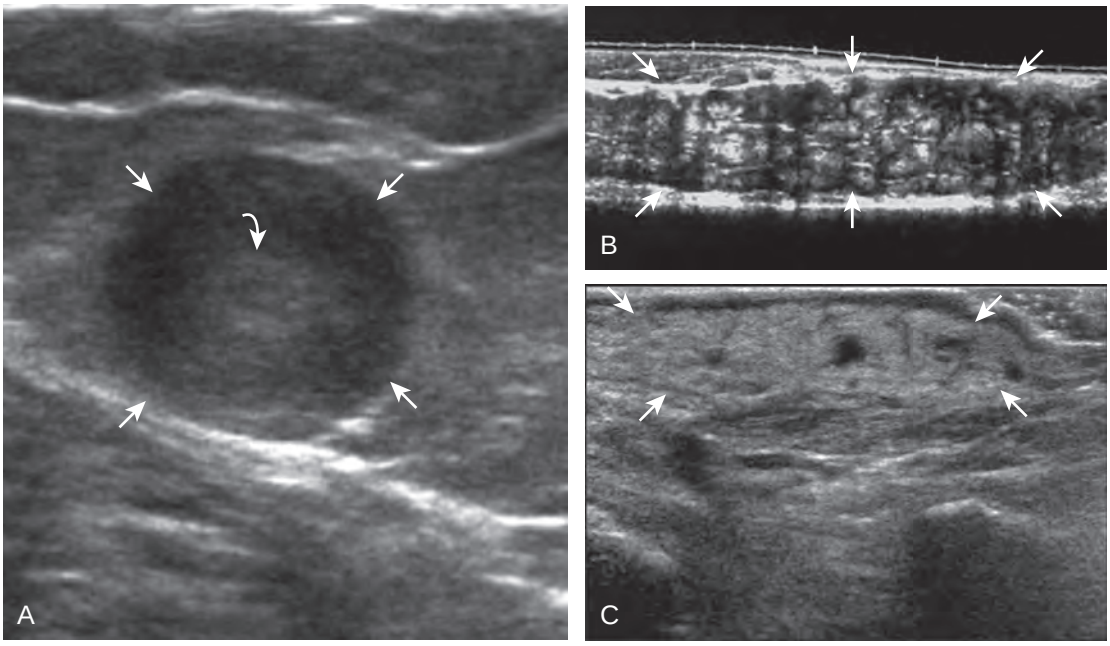

FIGURE 2-60 ■ Forms of neurofibromas. Ultrasound images from three different patients show **(A)** solitary neurofibroma appearing hypoechoic *(arrows)* with hyperechoic center *(curved arrow)* creating a target appearance, **(B)** plexiform neurofibroma *(arrows)*, and **(C)** diffuse subcutaneous neurofibroma *(arrows)*.

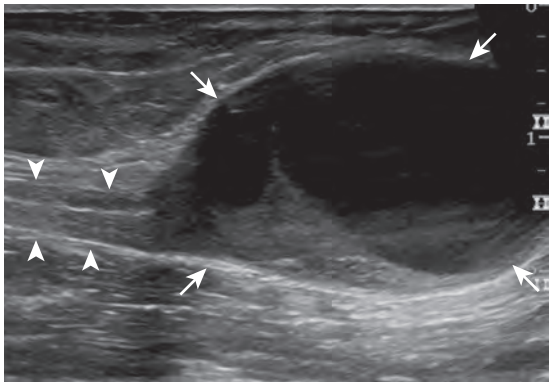

FIGURE 2-61 ■ Schwannoma: cystic. Ultrasound image shows peripheral nerve continuity *(arrowheads)* with a predominantly cystic schwannoma *(arrows)*. Note increased through-transmission.

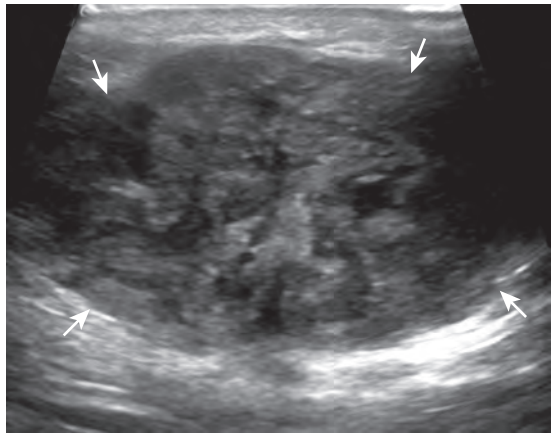

FIGURE 2-62 ■ Malignant peripheral nerve sheath tumor. Ultrasound image shows heterogeneous but predominantly hypoechoic mass *(arrows)* with increased through-transmission.

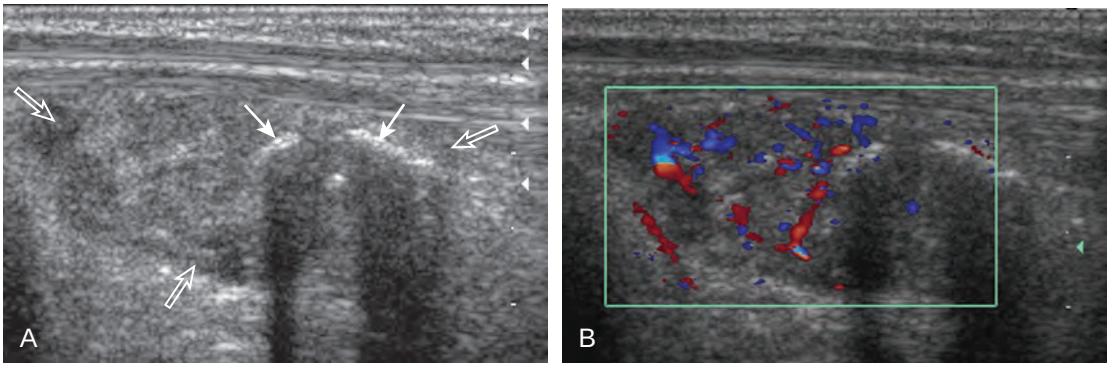

FIGURE 2-63 ■ Vascular malformation (intramuscular). A and **B,** Ultrasound images show a heterogeneous hypoechoic and isoechoic vascular malformation *(open arrows)* with hyperemia and hyperechoic and shadowing calcifications *(arrow)*.

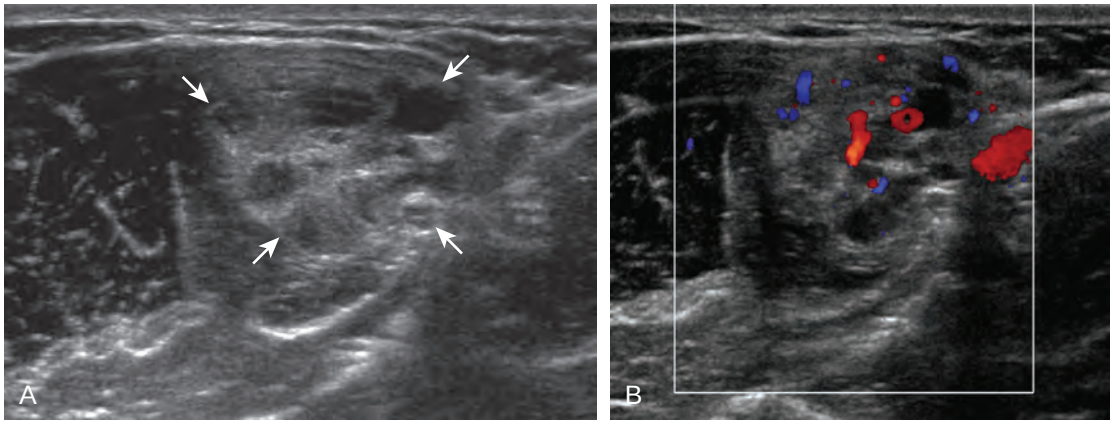

FIGURE 2-64 ■ Vascular malformation (intramuscular). A and **B,** Ultrasound images show a heterogeneous hypoechoic and isoechoic vascular malformation *(arrows)* with hyperemia.

adjacent soft tissues. Focal hyperechoic and shadowing phleboliths, which represent dystrophic calcification in an organizing thrombus, may also be seen. When evaluating a vascular anomaly with ultrasound, the presence of an area of abnormal vascular channels without an associated soft tissue mass suggests the diagnosis of a vascular malformation, such as an arteriovenous malformation having the appearance of a tangle of vessels (Fig. 2-65).[59,63] Both infantile hemangiomas and arteriovenous malformations tend to have a greater vessel density than other vascular malformations.[63] It is important to distinguish the foregoing features of vascular anomalies from more nonspecific neovascularity and possible dystrophic calcification of a malignant soft tissue neoplasm. Demonstration of the characteristic features of phleboliths on radiography is helpful; however, percutaneous biopsy may be required.

Ganglion Cysts

Ganglion cysts have several appearances at ultrasound. The most common appearance is that of a hypoechoic or anechoic, multilocular or multilobular, noncompressible cyst that may look complex.[64,65] Smaller ganglion cysts are more likely hypoechoic and may show only limited increased through-transmission.[65] The multilocular appearance of a cyst is specific to both ganglion cysts and fibrocartilage cysts (parameniscal and paralabral); the location of the multilocular cyst assists in this diagnosis. If in contact with fibrocartilage, then parameniscal or paralabral cyst is likely. If located superficial to the scapholunate ligament (Fig. 2-66), near the radial artery at the wrist (a very common site) (Fig. 2-67), at the sinus tarsi of the ankle (see Fig. 8-159 in Chapter 8), or within the Hoffa infrapatellar fat

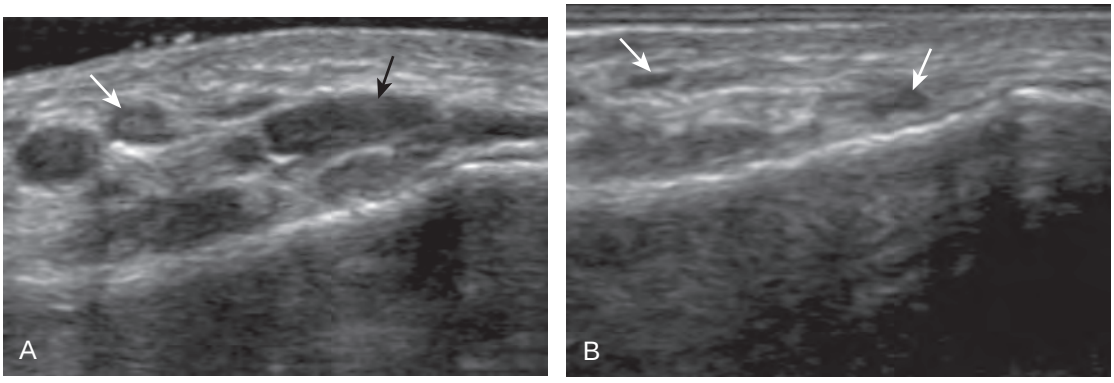

FIGURE 2-65 ■ Arteriovenous malformations. A and **B,** Ultrasound images show compressible anechoic channels *(arrows)* without a soft tissue mass representing an arteriovenous vascular malformation.

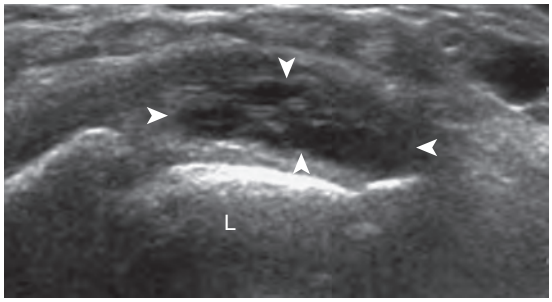

FIGURE 2-66 ■ Ganglion cyst: dorsal wrist. Ultrasound image shows ganglion cyst *(arrowheads)* as hypoechoic and multilobular. L, lunate.

pad or at the gastrocnemius tendon origin at the knee (see Figs. 7-73 and 7-74 in Chapter 7), ganglion cyst is likely. The other appearance of a ganglion cyst is one of a more unilocular fluid collection, which can be associated with wrist, hand, ankle, and foot tendons.[64] Unlike a bursal fluid collection, such unilocular ganglion cysts are usually not compressible and not in a location of an expected bursa. Aspiration should only be attempted with a larger diameter needle (such as a 16- or 18-gauge needle), given the high viscosity of the gel-like fluid.

Lymph Nodes

A normal lymph node will appear oval, with a central hyperechoic hilum and a variable-thickness hypoechoic peripheral cortex rim (Fig. 2-68A).[66] The central echogenicity is not from fat but rather interfaces with sinuses and lymphatic cords.[66] The peripheral hypoechoic cortex will be of variable thickness but should be uniform. Flow on color or power Doppler imaging, if present, should have a hilar pattern. With age and after repeated inflammation, the outer cortex of the node will thin, whereas the central aspect becomes more hyperechoic but may decrease or increase in size. A hyperplastic lymph node will be enlarged but maintain the essential sonographic features of a lymph node as described earlier (see Fig. 2-68B) (Video 2-10). When a lymph node is malignant (primary or metastatic), the echogenic hilum will narrow and could disappear, whereas the outer hypoechoic cortex will enlarge, and the lymph node will lose its oval shape and become round (see Fig. 2-68C). Flow on color or power Doppler imaging will become heterogeneous, mixed, and peripheral (see Fig. 2-68D) Although size criteria are used throughout the body to determine when a lymph node has enlarged, it is critical not to rely solely on size criteria but rather to evaluate the sonographic characteristics for early malignancy, taking into account patient history (see Fig. 2-68E). Increased posterior through-transmission is usually present with abnormal lymph nodes.

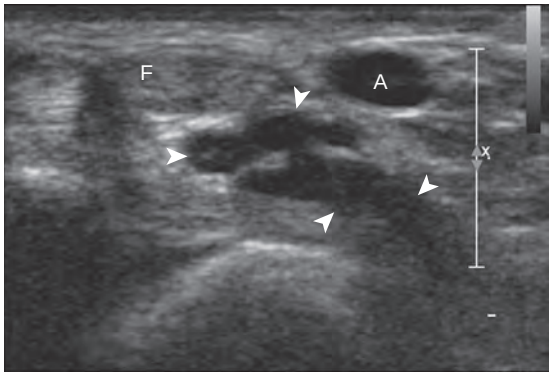

FIGURE 2-67 ■ Ganglion cyst: volar wrist. Ultrasound image in short axis to the radial artery (A) shows an anechoic septated ganglion cyst *(arrowheads)*. F, flexor carpi radialis tendon.

Malignant Soft Tissue Tumors

The precise diagnosis of a malignant soft tissue tumor typically cannot be made with ultrasound; however, a large soft tissue mass that does not originate from a joint or synovial space (bursa or tendon sheath) and that is hypoechoic with hypervascularity suggests a possible malignant origin, although biopsy is required for confirmation. Soft tissue sarcomas are predominantly hypoechoic (Fig. 2-69), with possible heterogeneous hyperechoic and hypervascular regions and anechoic necrotic regions as they enlarge, especially when high grade. Increased posterior through-transmission is usually present, as with most solid soft tissue masses. An important teaching point is that a mass that originates within a joint or synovial space is related to a synovial process (proliferation or inflammation) and rarely malignancy; synovial sarcoma is similar to other sarcomas and appears as a hypoechoic mass near but outside of a joint (see Fig. 2-69C). Granulocytic or myeloid sarcoma (also called *chloroma*), as a complication of myelogenous leukemia, may also appear as a hypoechoic mass (Fig. 2-70).[67] Lymphoma also presents as a hypoechoic mass with increased through-transmission or an infiltrating hypoechoic mass (Fig. 2-71).[68] A soft tissue tumor that is calcified or ossified will require further evaluation with MRI or CT because shadowing may obscure much of the mass (Fig. 2-72).

Common diagnoses can be suggested based on the patient's age and the location of the tumor, but percutaneous biopsy with use of ultrasound guidance is usually needed.[69] With ultrasound

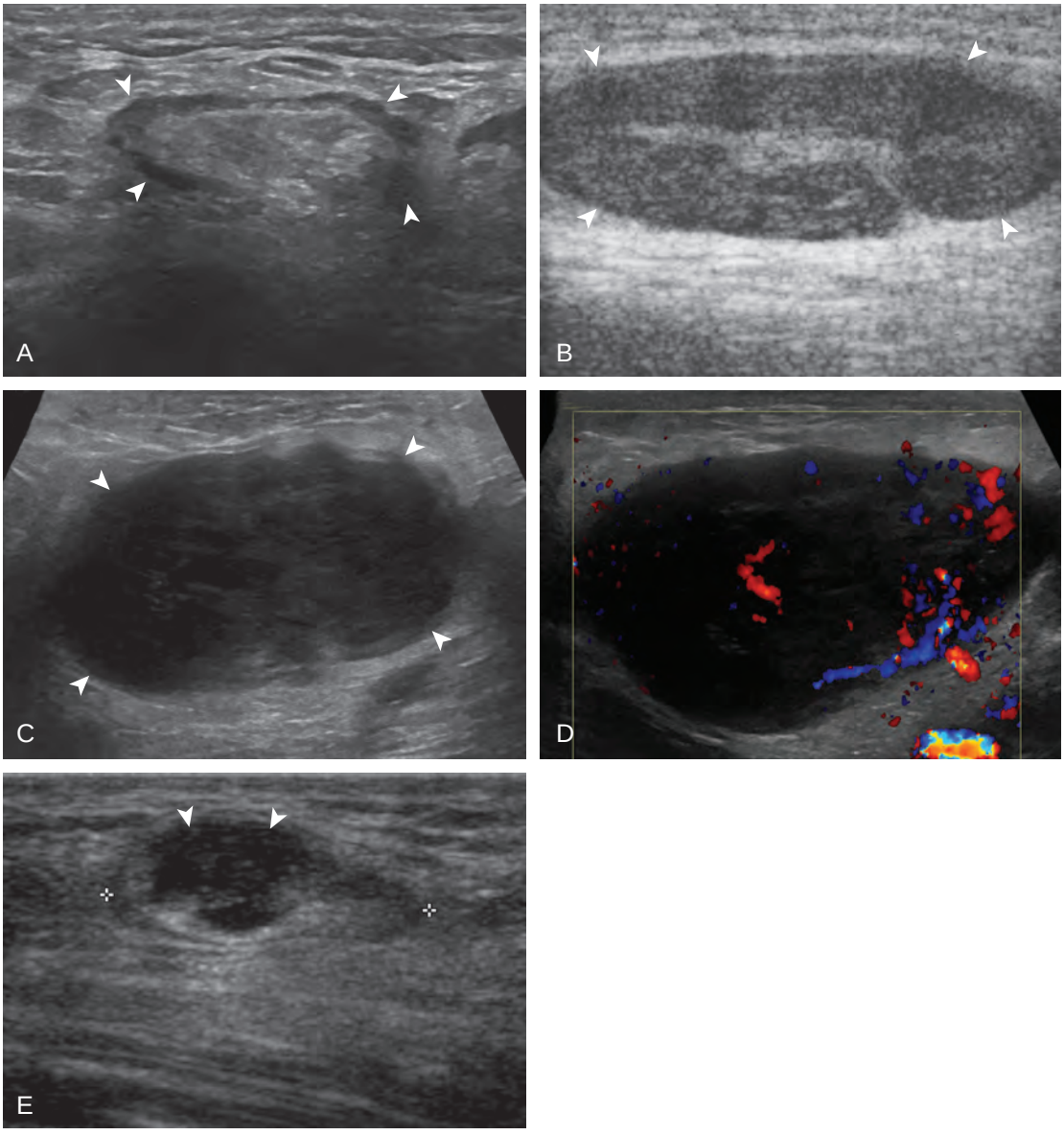

FIGURE 2-68 ■ Ultrasound images show **(A)** normal lymph node *(arrowheads)* (groin), **(B)** hyperplastic lymph node *(arrowheads)* (groin), **(C** and **D)** malignant lymph node *(arrowheads)* (lymphoma), and **(E)** focal lymph node metastasis *(arrowheads)* (angiosarcoma) (*cursors* denote lymph node borders). Note increased through-transmission with abnormal lymph nodes.

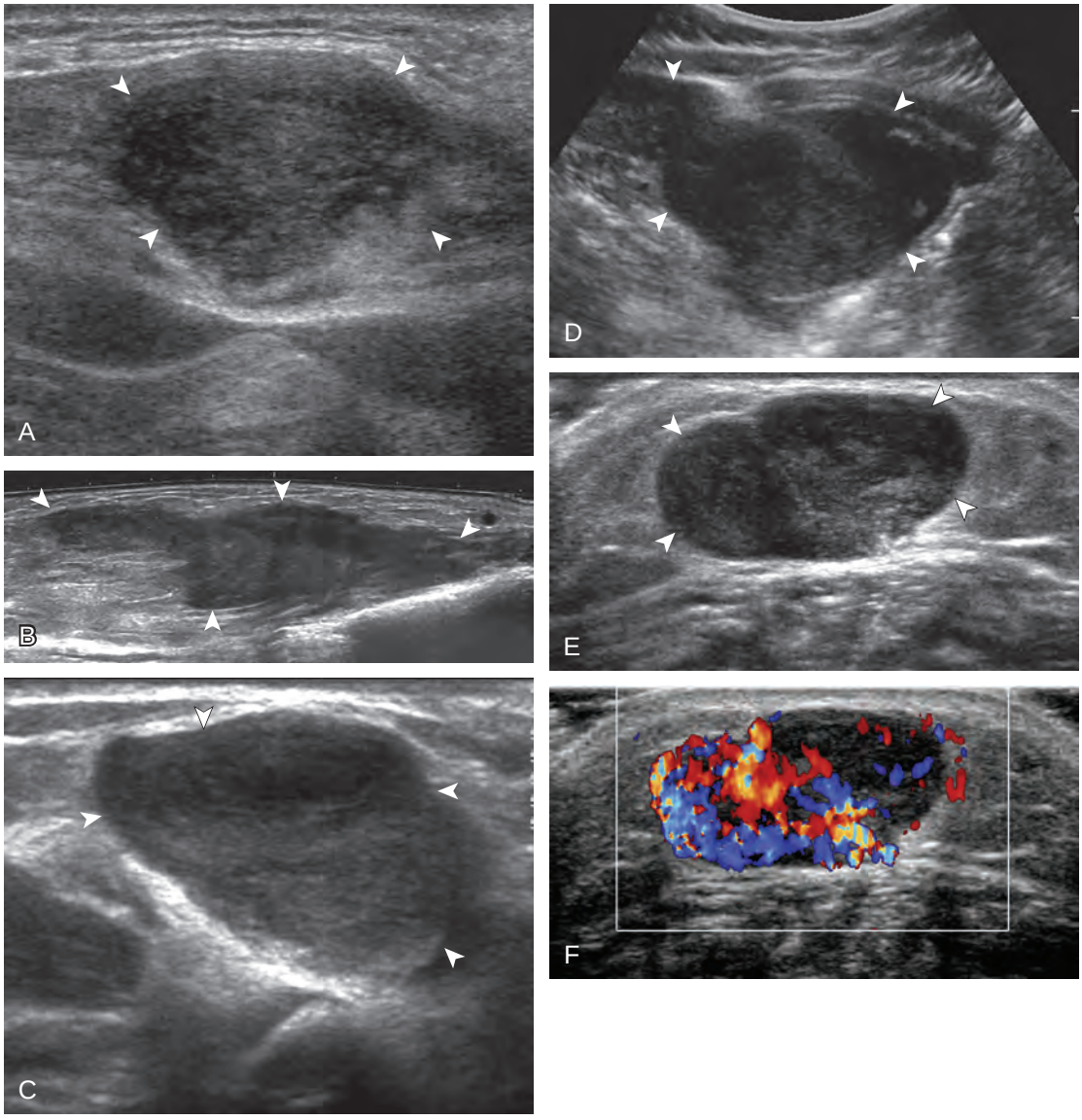

FIGURE 2-69 ■ Soft tissue sarcoma. Ultrasound images show *(arrowheads)* **(A)** undifferentiated pleomorphic sarcoma, **(B)** high-grade leiomyosarcoma, **(C)** synovial sarcoma, **(D)** Ewing sarcoma, and **(E** and **F)** dermatofibrosarcoma protuberans. Note increased through-transmission.

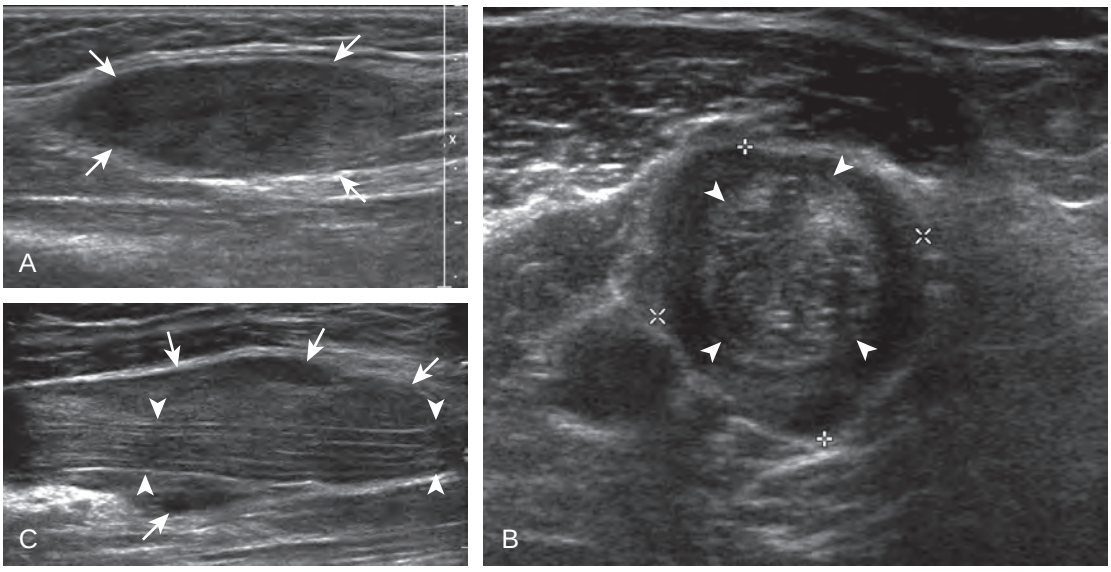

FIGURE 2-70 ■ Granulocytic or myeloid sarcoma (chloroma). Ultrasound images from two different patients show **(A)** soft tissue chloroma *(arrows)* and **(B** and **C)** chloroma *(cursors and arrowheads)* surrounding median nerve *(arrows)* proximal to the elbow.

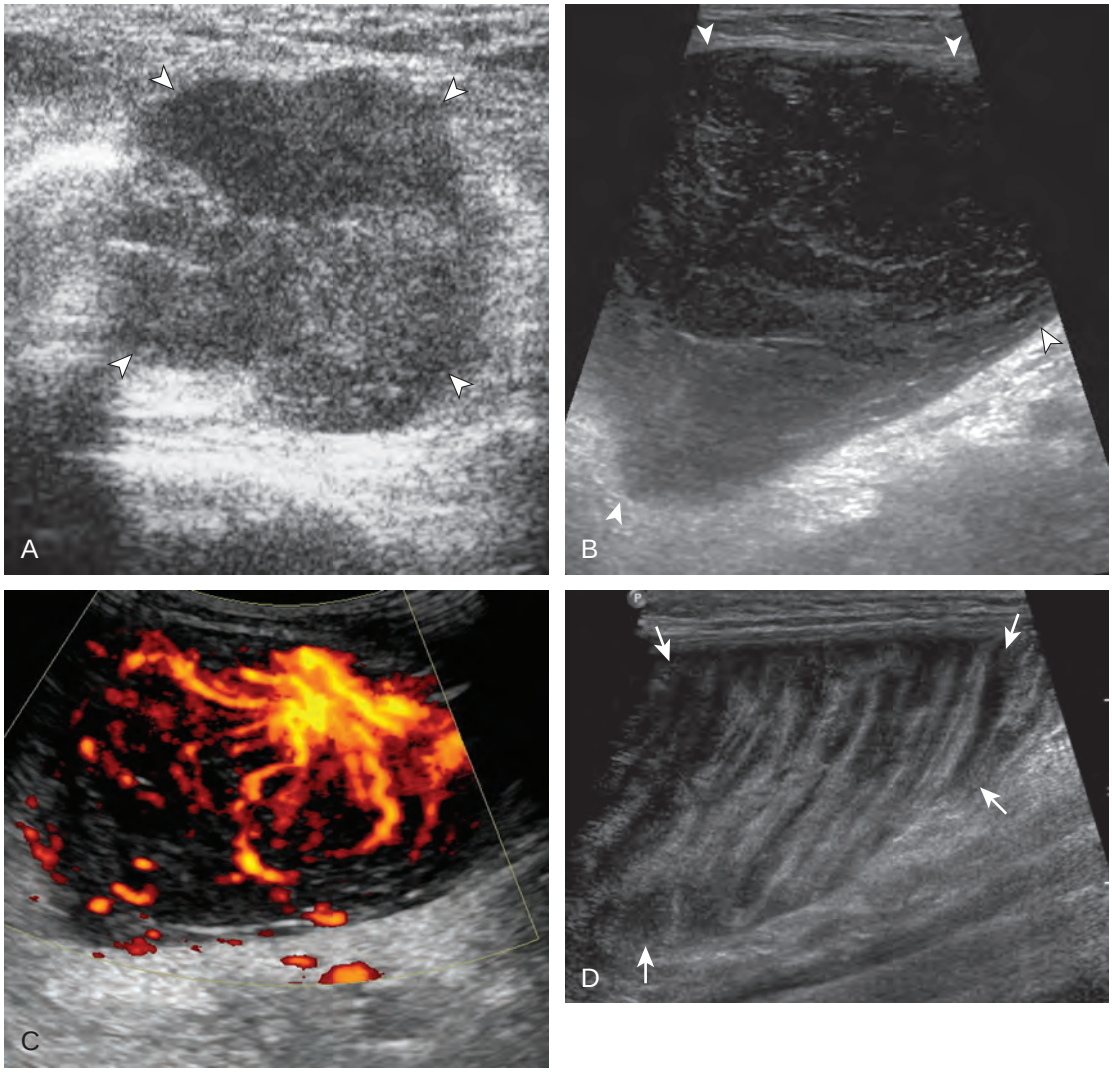

FIGURE 2-71 ■ Lymphoma. Ultrasound images from four different patients show **(A** and **B)** hypoechoic lymphoma *(arrowheads)* with increased through-transmission, **(C)** irregular hypervascularity with power Doppler within hypoechoic lymphoma, and **(D)** infiltrating intramuscular lymphoma *(arrows)*.

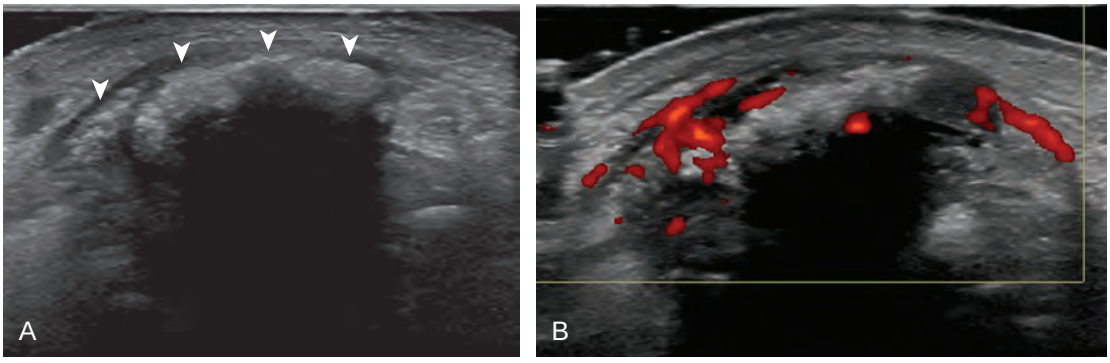

FIGURE 2-72 ■ Soft tissue chondroma. A and **B,** Ultrasound images show hyperechoic surface of the mineralized chondromas *(arrowheads)* with significant shadowing, which obscures the soft tissue mass. Note hyperemia in **B**.

guidance, a needle can be accurately placed into the soft tissue component of the tumor, while avoiding the necrotic center and adjacent neurovascular structures and thus increasing diagnostic yield. Soft tissue metastases are commonly hypoechoic with possible hypervascularity (Fig. 2-73).[70] Ultrasound is also effective in evaluation for recurrence of soft tissue malignancy after treatment (Fig. 2-74).[71] With melanoma, ultrasound can detect soft tissue recurrence or metastasis before findings at clinical examination (see Fig. 2-74A).[72] It has been shown that ultrasound is as effective as MRI in evaluation for soft tissue sarcoma recurrence after treatment (see Fig. 2-74B and C).[73]

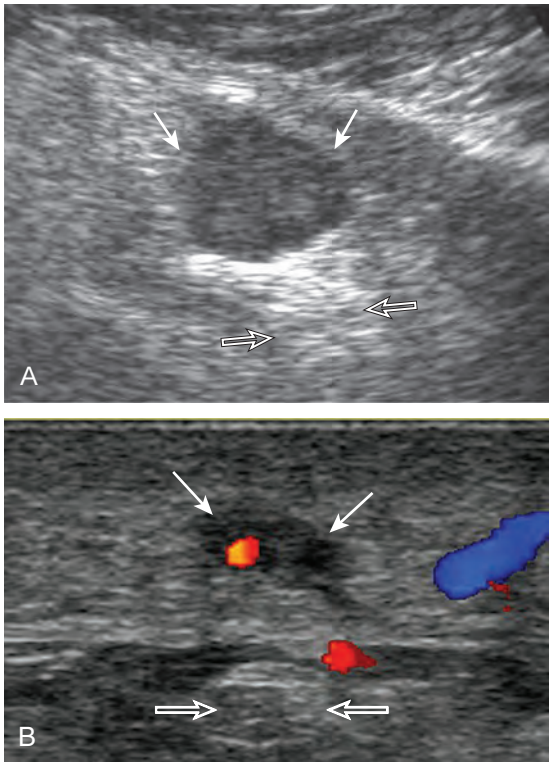

FIGURE 2-73 ■ Soft tissue metastases. Ultrasound images show *(arrows)* **(A)** hypoechoic metastatic lung cancer and **(B)** epithelioid sarcoma. Note increased through-transmission *(open arrows)*.

BONE MASSES

In evaluation for bone involvement from a soft tissue tumor, or a primary benign or malignant osseous tumor, radiography is an important initial imaging method. Ultrasound is limited with regard to osseous abnormalities when compared with MRI; however, a bone process that creates cortical irregularity, destruction, or periosteal reaction may be identified at ultrasound. When using ultrasound to evaluate soft tissue, it is always important to consider the osseous structures as the primary pathologic process. Ultrasound evaluation of an extremity should include the deeper structures such as the underlying osseous structures. Correlation with radiography is always essential, and further evaluation with MRI should always be a consideration.

One primary benign bone abnormality that may be visible at ultrasound is an osteochondroma (or exostosis) (Fig. 2-75) (Video 2-11), which appears as a well-demarcated osseous excrescence that typically points away from the adjacent joint. Correlation with radiography is essential to identify both cortical and medullary continuity with the underlying bone to ensure the correct diagnosis. Ultrasound can also identify complications related to an enchondroma, such as fracture, bursa formation (Fig. 2-76), pseudoaneurysm, and malignant degeneration to chondrosarcoma. Other benign bone lesions that may be visible at ultrasound include aneurysmal bone cysts (Fig. 2-77).

When there is destruction of the bone cortex, an aggressive process is present, and considerations include both primary and secondary bone

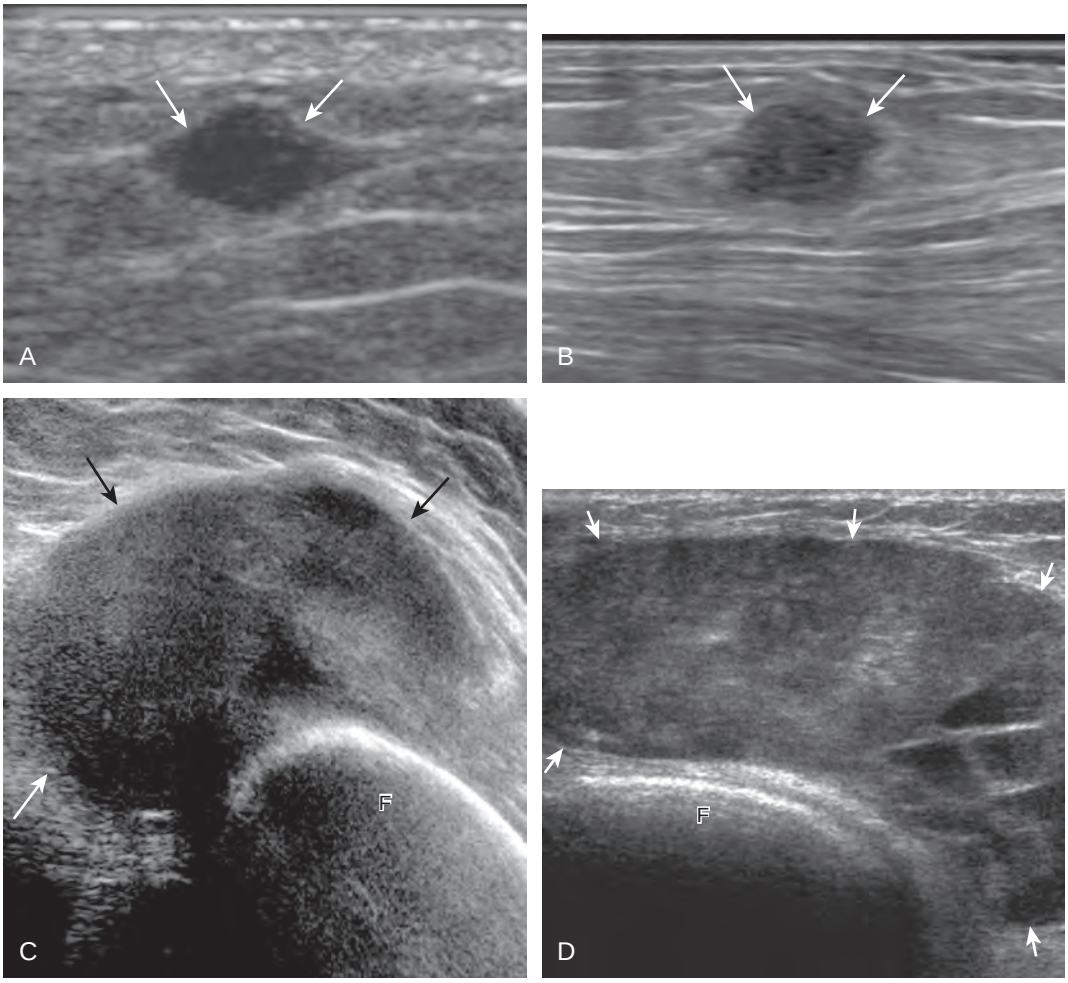

FIGURE 2-74 ■ Soft tissue recurrence. Ultrasound images show *(arrows)* predominantly hypoechoic recurrent **(A)** melanoma, **(B)** sarcoma, **(C)** lymphoma, and **(D)** sarcoma. Note increased heterogeneity with larger tumor size. F, femur.

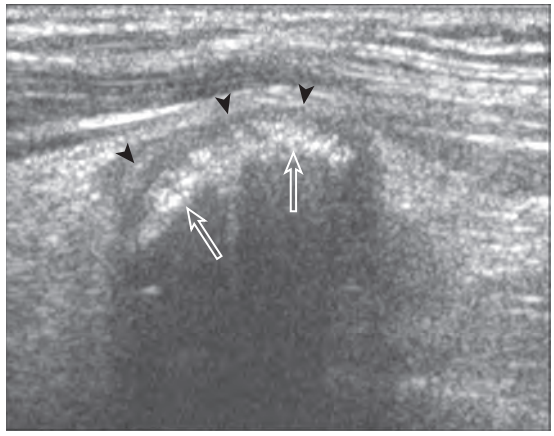

FIGURE 2-75 ■ Osteochondroma (exostosis). Ultrasound image shows a hyperechoic ossified surface *(open arrows)* and an overlying hypoechoic cartilage cap *(arrowheads)* of osteochondroma.

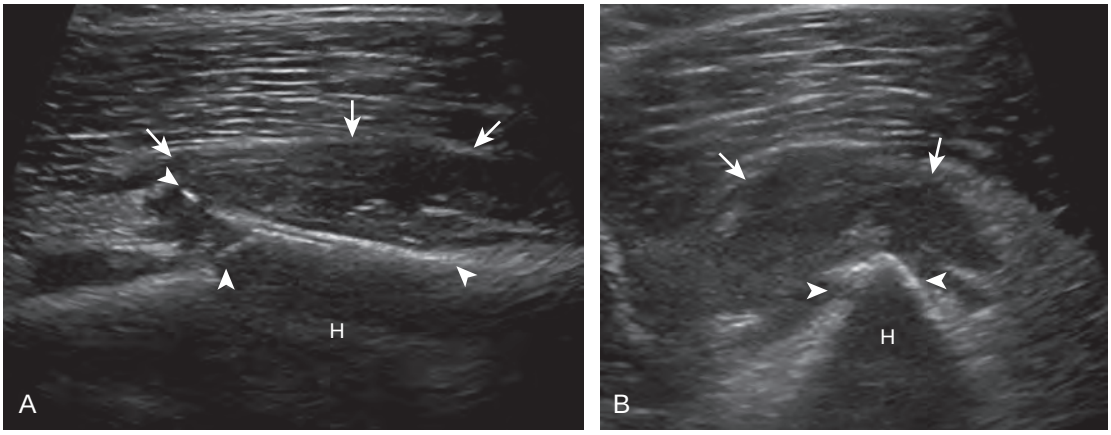

FIGURE 2-76 ■ Osteochondroma (exostosis): bursa formation. Ultrasound images in **(A)** short axis and **(B)** long axis to humerus (H) show osteochondroma *(arrowheads)* and overlying complex hypoechoic bursa *(arrows)*.

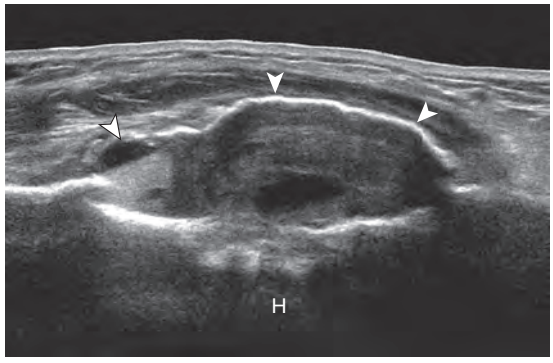

FIGURE 2-77 ■ Aneurysmal bone cyst. Ultrasound images show expansile nature of aneurysmal bone cyst *(arrowheads)*. H, humerus.

malignancy. Correlation with patient age, history, radiography, and distribution of pathology can suggest primary versus secondary processes. Considerations for primary bone tumor include osteosarcoma (Fig. 2-78), malignant fibrous histiocytoma (Fig. 2-79), chondrosarcoma, lymphoma, and Ewing sarcoma (Fig. 2-80). Osseous metastasis may also produce bone destruction (Fig. 2-81) (Video 2-12).[74] A cortically based destructive process suggests lung cancer metastasis (see Fig. 2-81B), whereas an expansile hyperemic process could indicate a vascular metastasis, such as from renal cell or thyroid carcinoma.

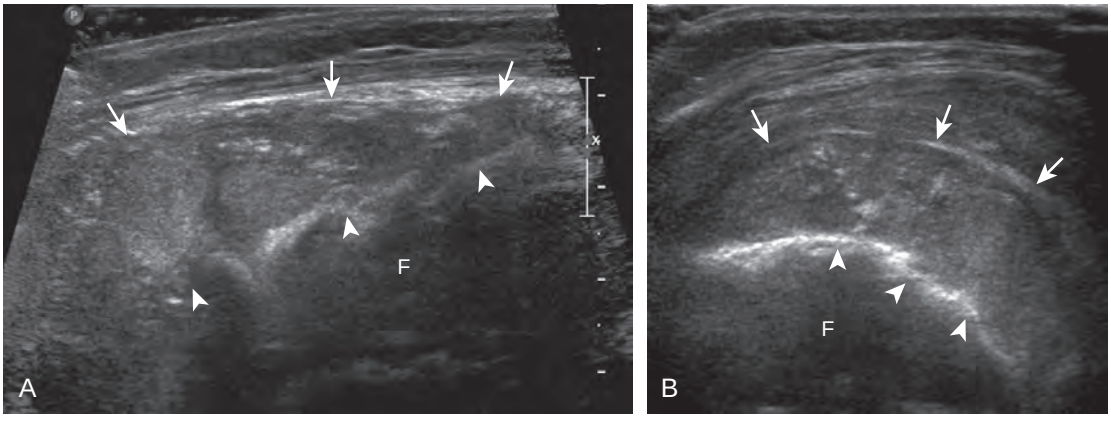

FIGURE 2-78 ■ Osteosarcoma. Ultrasound images in **(A)** long axis and **(B)** short axis to femur show soft tissue mass *(arrows)* extending from femur (F). Note significant cortical irregularity of the femur *(arrowheads)*.

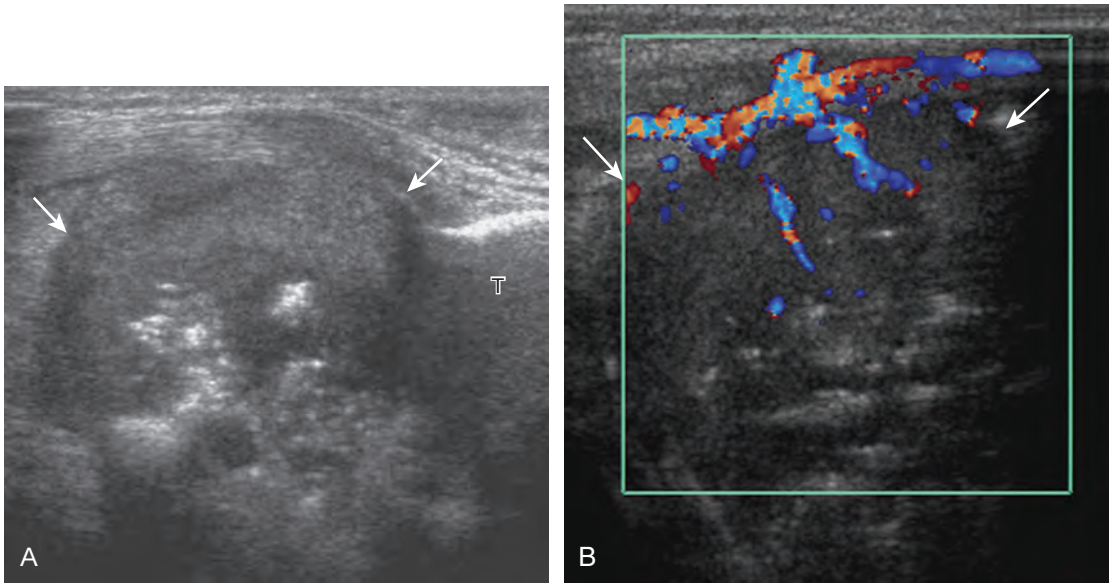

FIGURE 2-79 ■ Malignant fibrous histiocytoma of bone. Ultrasound images show **(A** and **B)** a mixed-echogenicity malignant fibrous histiocytoma *(arrows)* of the tibia (T) that destroys bone.

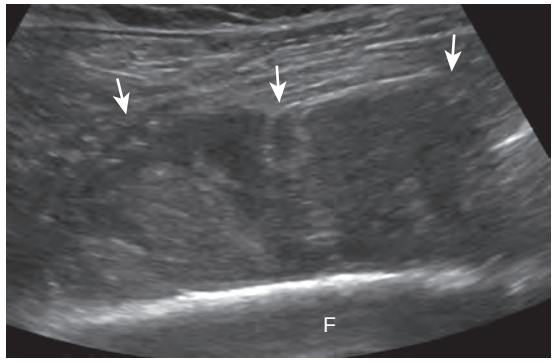

FIGURE 2-80 ■ Ewing sarcoma. Ultrasound image shows hypoechoic soft tissue Ewing sarcoma *(arrows)* originating from the fibula (F). Note absence of gross cortical destruction.

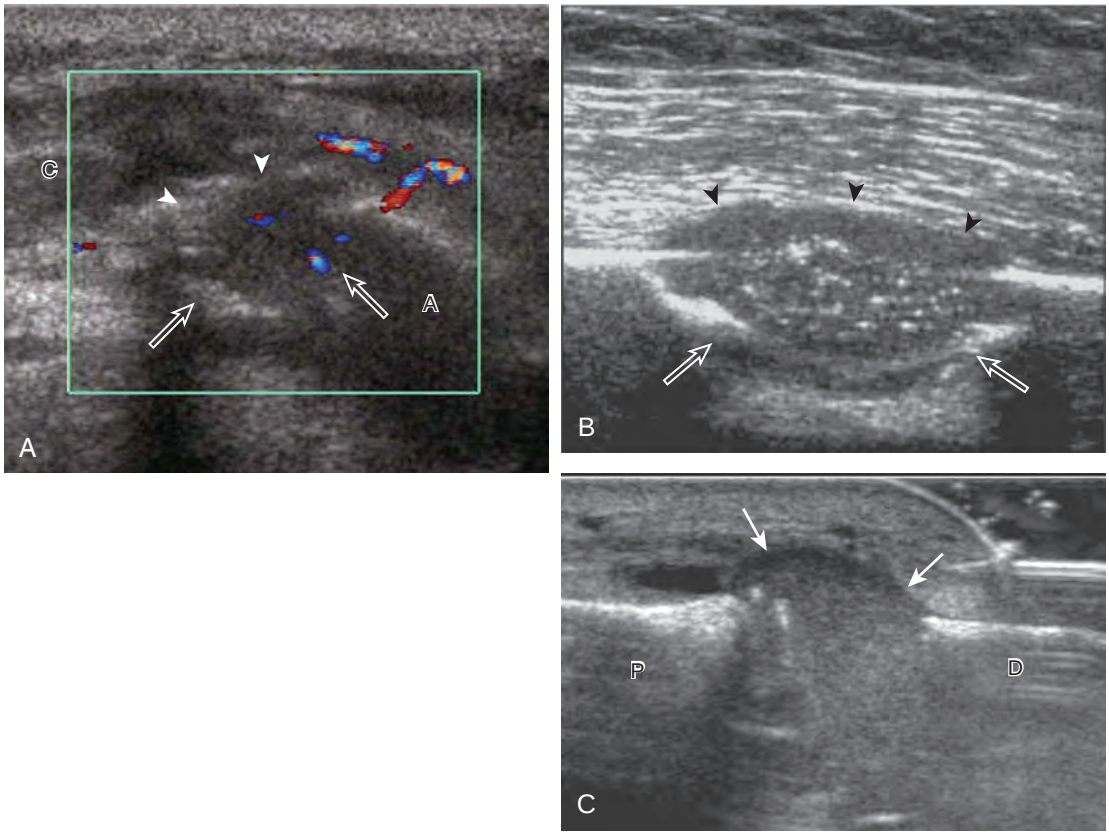

FIGURE 2-81 ■ Osseous metastases. Ultrasound images show **(A)** bone destruction *(open arrows)* with hyperemic soft tissue mass *(arrowheads)* representing a renal cell carcinoma metastasis, **(B)** bone destruction *(open arrows)* centered at the humeral cortex with a soft tissue mass *(arrowheads)* characteristic of a lung cancer metastasis (termed a *cookie-bite lesion*), and **(C)** a lung cancer metastasis *(arrows)* to the distal phalanx of the first toe. A, acromion; C, clavicle; D, distal phalanx; P, proximal phalanx.

REFERENCES

1. Speer KP, Lohnes J, Garrett WE Jr: Radiographic imaging of muscle strain injury. *Am J Sports Med* 21:89–95; discussion 6, 1993.
2. Blankenbaker DG, Tuite MJ: Temporal changes of muscle injury. *Semin Musculoskelet Radiol* 14:176–193, 2010.
3. Lee JC, Healy J: Sonography of lower limb muscle injury. *AJR Am J Roentgenol* 182:341–351, 2004.
4. Adler RS, Garofalo G: Ultrasound in the evaluation of the inflammatory myopathies. *Curr Rheumatol Rep* 11:302–308, 2009.
5. Neal C, Jacobson JA, Brandon C, et al: Sonography of Morel-Lavallée lesions. *J Ultrasound Med* 27:1077–1081, 2008.
6. Tyler P, Saifuddin A: The imaging of myositis ossificans. *Semin Musculoskelet Radiol* 14:201–216, 2010.
7. Peetrons P: Ultrasound of muscles. *Eur Radiol* 12:35–43, 2002.
8. Bianchi S, Martinoli C, Waser NP, et al: Central aponeurosis tears of the rectus femoris: sonographic findings. *Skeletal Radiol* 31:581–586, 2002.
9. Khan KM, Bonar F, Desmond PM, et al: Patellar tendinosis (jumper's knee): findings at histopathologic examination, US, and MR imaging. Victorian Institute of Sport Tendon Study Group. *Radiology* 200:821–827, 1996.
10. Kjellin I, Ho CP, Cervilla V, et al: Alterations in the supraspinatus tendon at MR imaging: correlation with histopathologic findings in cadavers. *Radiology* 181:837–841, 1991.
11. Potter HG, Hannafin JA, Morwessel RM, et al: Lateral epicondylitis: correlation of MR imaging, surgical, and histopathologic findings. *Radiology* 196:43–46, 1995.
12. Craig JG, Jacobson JA, Moed BR: Ultrasound of fracture and bone healing. *Radiol Clin North Am* 37:737–751, ix, 1999.
13. Drakonaki EE, Garbi A: Metatarsal stress fracture diagnosed with high-resolution sonography. *J Ultrasound Med* 29:473–476, 2010.
14. Farley FA, Kuhns L, Jacobson JA, et al: Ultrasound examination of ankle injuries in children. *J Pediatr Orthop* 21:604–607, 2001.
15. Patten RM, Mack LA, Wang KY, et al: Nondisplaced fractures of the greater tuberosity of the humerus: sonographic detection. *Radiology* 182:201–204, 1992.
16. Griffith JF, Rainer TH, Ching AS, et al: Sonography compared with radiography in revealing acute rib fracture. *AJR Am J Roentgenol* 173:1603–1609, 1999.
17. Turk F, Kurt AB, Saglam S: Evaluation by ultrasound of traumatic rib fractures missed by radiography. *Emerg Radiol* 17:473–477, 2010.
18. Malghem J, Vande Berg B, Lecouvet F, et al: Costal cartilage fractures as revealed on CT and sonography. *AJR Am J Roentgenol* 176:429–432, 2001.
19. Ziv N, Litwin A, Katz K, et al: Definitive diagnosis of fracture-separation of the distal humeral epiphysis in

neonates by ultrasonography. *Pediatr Radiol* 26:493–496, 1996.
20. Chao HC, Lin SJ, Huang YC, et al: Sonographic evaluation of cellulitis in children. *J Ultrasound Med* 19:743–749, 2000.
21. Huang MN, Chang YC, Wu CH, et al: The prognostic values of soft tissue sonography for adult cellulitis without pus or abscess formation. *Intern Med J* 39:841–844, 2009.
22. Gaspari RJ, Resop D, Mendoza M, et al: A randomized controlled trial of incision and drainage versus ultrasonographically guided needle aspiration for skin abscesses and the effect of methicillin-resistant *Staphylococcus aureus*. *Ann Emerg Med* 57:483–491, e1, 2011.
23. Wronski M, Slodkowski M, Cebulski W, et al: Necrotizing fasciitis: early sonographic diagnosis. *J Clin Ultrasound* 39:236–239, 2011.
24. Walsh M, Jacobson JA, Kim SM, et al: Sonography of fat necrosis involving the extremity and torso with magnetic resonance imaging and histologic correlation. *J Ultrasound Med* 27:1751–1757, 2008.
25. Bureau NJ, Chhem RK, Cardinal E: Musculoskeletal infections: US manifestations. *Radiographics* 19:1585–1592, 1999.
26. Turecki MB, Taljanovic MS, Stubbs AY, et al: Imaging of musculoskeletal soft tissue infections. *Skeletal Radiol* 39:957–971, 2010.
27. Loyer EM, DuBrow RA, David CL, et al: Imaging of superficial soft-tissue infections: sonographic findings in cases of cellulitis and abscess. *AJR Am J Roentgenol* 166:149–152, 1996.
28. Weiss DB, Jacobson JA, Karunakar MA: The use of ultrasound in evaluating orthopaedic trauma patients. *J Am Acad Orthop Surg* 13:525–533, 2005.
29. Lund PJ, Heikal A, Maricic MJ, et al: Ultrasonographic imaging of the hand and wrist in rheumatoid arthritis. *Skeletal Radiol* 24:591–596, 1995.
30. Wakefield RJ, Balint PV, Szkudlarek M, et al: Musculoskeletal ultrasound including definitions for ultrasonographic pathology. *J Rheumatol* 32:2485–2487, 2005.
31. Backhaus M, Burmester GR, Gerber T, et al: Guidelines for musculoskeletal ultrasound in rheumatology. *Ann Rheum Dis* 60:641–649, 2001.
32. Vlad V, Berghea F, Libianu S, et al: Ultrasound in rheumatoid arthritis—volar versus dorsal synovitis evaluation and scoring. *BMC Musculoskelet Disord* 12:124, 2011.
33. Finzel S, Ohrndorf S, Englbrecht M, et al: A detailed comparative study of high-resolution ultrasound and micro-computed tomography for detection of arthritic bone erosions. *Arthritis Rheum* 63:1231–1236, 2011.
34. Nalbant S, Corominas H, Hsu B, et al: Ultrasonography for assessment of subcutaneous nodules. *J Rheumatol* 30:1191–1195, 2003.
35. Gutierrez M, Filippucci E, De Angelis R, et al: A sonographic spectrum of psoriatic arthritis: "the five targets." *Clin Rheumatol* 29:133–142, 2010.
36. Gutierrez M, Filippucci E, Salaffi F, et al: Differential diagnosis between rheumatoid arthritis and psoriatic arthritis: the value of ultrasound findings at metacarpophalangeal joints level. *Ann Rheum Dis* 70:1111–1114, 2011.
37. Thiele RG: Role of ultrasound and other advanced imaging in the diagnosis and management of gout. *Curr Rheumatol Rep* 13:146–153, 2011.
38. Filippucci E, Riveros MG, Georgescu D, et al: Hyaline cartilage involvement in patients with gout and calcium pyrophosphate deposition disease: an ultrasound study. *Osteoarthritis Cartilage* 17:178–181, 2009.
39. Hayashi D, Roemer FW, Katur A, et al: Imaging of synovitis in osteoarthritis: current status and outlook. *Semin Arthritis Rheum* 41:116–130, 2011.
40. Keen HI, Conaghan PG: Ultrasonography in osteoarthritis. *Radiol Clin North Am* 47:581–594, 2009.
41. Arrestier S, Rosenberg C, Etchepare F, et al: Ultrasound features of nonstructural lesions of the proximal and distal interphalangeal joints of the hands in patients with finger osteoarthritis. *Joint Bone Spine* 78:65–69, 2011.
42. Tohme-Noun C, Le Breton C, Sobotka A, et al: Imaging findings in three cases of the nodular type of muscular sarcoidosis. *AJR Am J Roentgenol* 183:995–999, 2004.
43. Delaney-Sathy LO, Fessell DP, Jacobson JA, et al: Sonography of diabetic muscle infarction with MR imaging, CT, and pathologic correlation. *AJR Am J Roentgenol* 174:165–169, 2000.
44. Horton LK, Jacobson JA, Powell A, et al: Sonography and radiography of soft-tissue foreign bodies. *AJR Am J Roentgenol* 176:1155–1159, 2001.
45. Boyse TD, Fessell DP, Jacobson JA, et al: US of soft-tissue foreign bodies and associated complications with surgical correlation. *Radiographics* 21:1251–1256, 2001.
46. Lyon M, Brannam L, Johnson D, et al: Detection of soft tissue foreign bodies in the presence of soft tissue gas. *J Ultrasound Med* 23:677–681, 2004.
47. Creel SA, Girish G, Jamadar DA, et al: Sonographic surface localization of subcutaneous foreign bodies and masses. *J Clin Ultrasound* 37:158–160, 2009.
48. Shiels WE 2nd, Babcock DS, Wilson JL, et al: Localization and guided removal of soft-tissue foreign bodies with sonography. *AJR Am J Roentgenol* 155:1277–1281, 1990.
49. Jacobson JA, Fessell DP, Lobo Lda G, et al: Entrapment neuropathies I: upper limb (carpal tunnel excluded). *Semin Musculoskelet Radiol* 14:473–486, 2010.
50. Klauser AS, Faschingbauer R, Bauer T, et al: Entrapment neuropathies II: carpal tunnel syndrome. *Semin Musculoskelet Radiol* 14:487–500, 2010.
51. Martinoli C, Bianchi S, Gandolfo N, et al: US of nerve entrapments in osteofibrous tunnels of the upper and lower limbs. *Radiographics* 20:S199–S213; discussion S-7, 2000.
52. Kuwano Y, Ishizaki K, Watanabe R, et al: Efficacy of diagnostic ultrasonography of lipomas, epidermal cysts, and ganglions. *Arch Dermatol* 145:761–764, 2009.
53. Inampudi P, Jacobson JA, Fessell DP, et al: Soft-tissue lipomas: accuracy of sonography in diagnosis with pathologic correlation. *Radiology* 233:763–767, 2004.
54. Shin YR, Kim JY, Sung MS, et al: Sonographic findings of dermatofibrosarcoma protuberans with pathologic correlation. *J Ultrasound Med* 27:269–274, 2008.
55. Reynolds DL Jr, Jacobson JA, Inampudi P, et al: Sonographic characteristics of peripheral nerve sheath tumors. *AJR Am J Roentgenol* 182:741–744, 2004.
56. Tsai WC, Chiou HJ, Chou YH, et al: Differentiation between schwannomas and neurofibromas in the extremities and superficial body: the role of high-resolution and color Doppler ultrasonography. *J Ultrasound Med* 27:161–166; quiz 8–9, 2008.
57. Lin J, Jacobson JA, Hayes CW: Sonographic target sign in neurofibromas. *J Ultrasound Med* 18:513–517, 1999.
58. Chen W, Jia JW, Wang JR: Soft tissue diffuse neurofibromas: sonographic findings. *J Ultrasound Med* 26:513–518, 2007.
59. Dubois J, Alison M: Vascular anomalies: what a radiologist needs to know. *Pediatr Radiol* 40:895–905, 2010.
60. Hein KD, Mulliken JB, Kozakewich HP, et al: Venous malformations of skeletal muscle. *Plast Reconstr Surg* 110:1625–1635, 2002.
61. Kransdorf MJ, Murphey MD, Fanburg-Smith JC: Classification of benign vascular lesions: history, current nomenclature, and suggestions for imagers. *AJR Am J Roentgenol* 197:8–11, 2011.

62. Derchi LE, Balconi G, De Flaviis L, et al: Sonographic appearances of hemangiomas of skeletal muscle. *J Ultrasound Med* 8:263–267, 1989.
63. Paltiel HJ, Burrows PE, Kozakewich HP, et al: Soft-tissue vascular anomalies: utility of US for diagnosis. *Radiology* 214:747–754, 2000.
64. Teefey SA, Dahiya N, Middleton WD, et al: Ganglia of the hand and wrist: a sonographic analysis. *AJR Am J Roentgenol* 191:716–720, 2008.
65. Wang G, Jacobson JA, Feng FY, et al: Sonography of wrist ganglion cysts: variable and noncystic appearances. *J Ultrasound Med* 26:1323–1328; quiz 30–31, 2007.
66. Esen G. Ultrasound of superficial lymph nodes. *Eur J Radiol* 58:345–359, 2006.
67. Pui MH, Fletcher BD, Langston JW: Granulocytic sarcoma in childhood leukemia: imaging features. *Radiology* 190:698–702, 1994.
68. ter Braak BP, Guit GL, Bloem JL: Case 111: Soft-tissue lymphoma. *Radiology* 243:293–296, 2007.
69. Kransdorf MJ: Malignant soft-tissue tumors in a large referral population: distribution of diagnoses by age, sex, and location. *AJR Am J Roentgenol* 164:129–134, 1995.
70. Giovagnorio F, Valentini C, Paonessa A: High-resolution and color Doppler sonography in the evaluation of skin metastases. *J Ultrasound Med* 22:1017–1022; quiz 23–25, 2003.
71. Arya S, Nagarkatti DG, Dudhat SB, et al: Soft tissue sarcomas: ultrasonographic evaluation of local recurrences. *Clin Radiol* 55:193–197, 2000.
72. Fornage BD, Lorigan JG: Sonographic detection and fine-needle aspiration biopsy of nonpalpable recurrent or metastatic melanoma in subcutaneous tissues. *J Ultrasound Med* 8:421–424, 1989.
73. Choi H, Varma DG, Fornage BD, et al: Soft-tissue sarcoma: MR imaging vs sonography for detection of local recurrence after surgery. *AJR Am J Roentgenol* 157:353–358, 1991.
74. Cho KH, Lee YH, Lee SM, et al: Sonography of bone and bone-related diseases of the extremities. *J Clin Ultrasound* 32:511–521, 2004.

CHAPTER 3

Shoulder Ultrasound

CHAPTER OUTLINE

ULTRASOUND EXAMINATION TECHNIQUE
General Comments
Position No. 1: Long Head of Biceps Brachii Tendon
Position No. 2: Subscapularis and Biceps Tendon Dislocation
Position No. 3: Supraspinatus and Infraspinatus
Position No. 4: Acromioclavicular Joint, Subacromial-Subdeltoid Bursa, and Dynamic Evaluation
Position No. 5: Infraspinatus, Teres Minor, and Posterior Glenoid Labrum

ROTATOR CUFF ABNORMALITIES
Supraspinatus Tears and Tendinosis
General Comments
Partial-Thickness Tear
Full-Thickness Tear
Tendinosis
Indirect Signs of Supraspinatus Tendon Tear
Infraspinatus Tears and Tendinosis
Subscapularis Tears and Tendinosis
Rotator Cuff Atrophy
Postoperative Shoulder
Calcific Tendinosis
Impingement Syndrome
Adhesive Capsulitis

PITFALLS IN ROTATOR CUFF ULTRASOUND
Errors in Scanning Technique
Improper Positioning of the Shoulder
Incomplete Evaluation of the Supraspinatus Tendon
Imaging of the Rotator Cuff Too Distally
Misinterpretation of Normal Structures
Misinterpretation of the Rotator Interval
Misinterpretation of the Musculotendinous Junction
Misinterpretation of the Supraspinatus-Infraspinatus Junction
Misinterpretation of Pathology
Subacromial-Subdeltoid Bursa Simulating Tendon
Rim-Rent Tear Versus Intrasubstance Tear
Tendinosis Versus Tendon Tear

BICEPS TENDON
Joint Effusion and Tenosynovitis
Tendon Tear and Tendinosis
Subluxation and Dislocation

SUBACROMIAL-SUBDELTOID BURSA

GLENOHUMERAL JOINT AND RECESSES

GLENOID LABRUM AND PARALABRAL CYST

GREATER TUBEROSITY

PECTORALIS MAJOR

ACROMIOCLAVICULAR JOINT

STERNOCLAVICULAR JOINT

MISCELLANEOUS DISORDERS

Additional videos for this topic are available online at www.expertconsult.com.

The rotator cuff is composed of four tendons (Fig. 3-1). Anteriorly, the subscapularis with its tendons converges onto the lesser tuberosity. Superiorly, the supraspinatus inserts on the superior aspect of the greater tuberosity; its footprint or attachment averages 2.25 cm anterior to posterior, which covers the superior facet and the anterior portion of the middle facet of the greater tuberosity (Fig. 3-2).[1,2] Posterior to the scapula and inferior to the scapular spine, the infraspinatus tendon inserts on the middle facet of the greater tuberosity, and the smaller and more inferior teres minor tendon inserts on the inferior facet of the greater tuberosity. Between the lesser and greater tuberosities anteriorly is the bicipital groove, which contains the long head

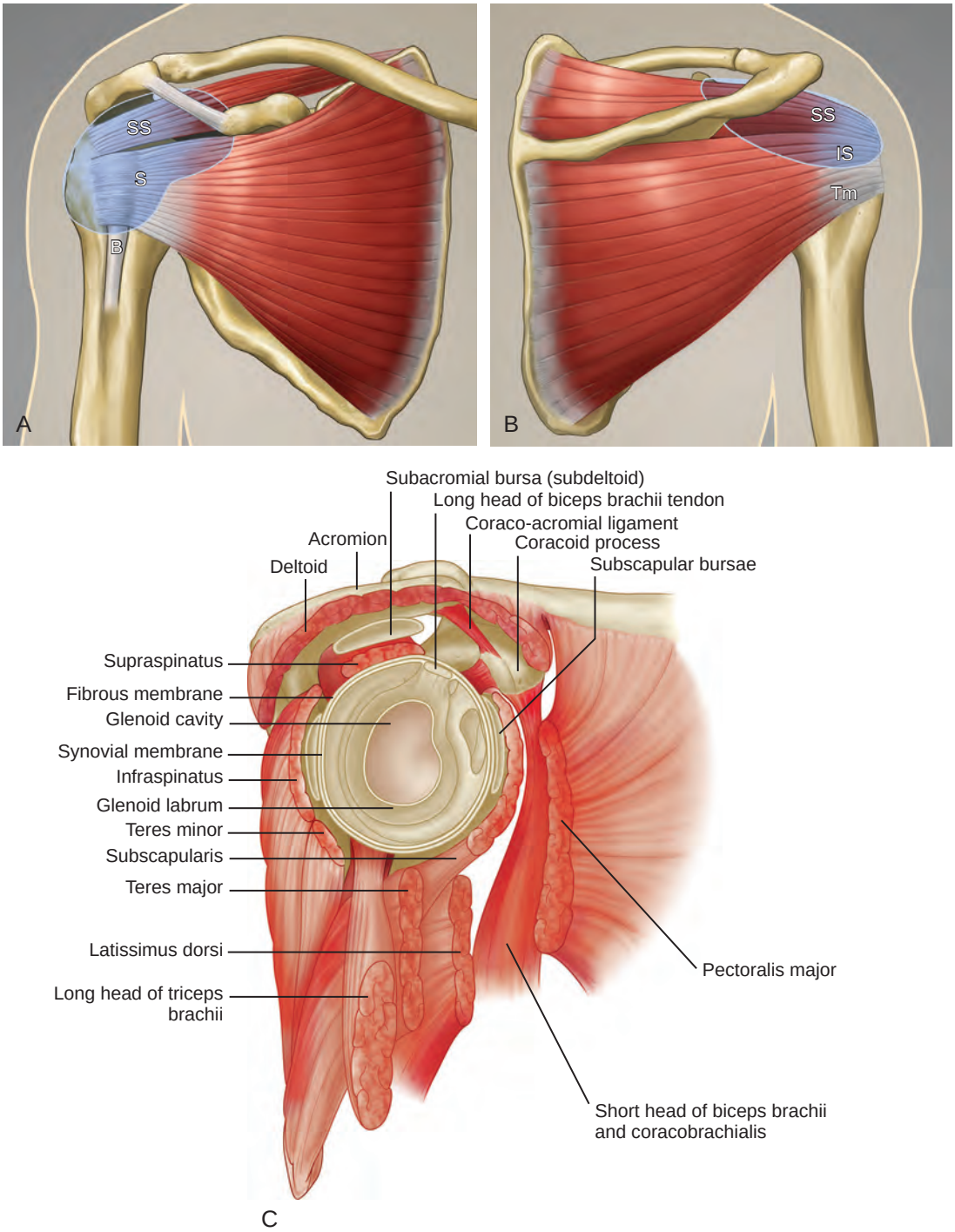

FIGURE 3-1 ■ **Shoulder anatomy. A,** Anterior and **(B)** posterior views of shoulder show supraspinatus (SS), infraspinatus (IS), subscapularis (S), teres minor (Tm), long head of biceps brachii (B), and subacromial-subdeltoid bursa (light blue). **C,** Lateral view of right glenohumeral joint and surrounding muscles with humerus removed. (**A** and **B,** Image courtesy of Carolyn Nowak, Ann Arbor, Michigan. **C,** From Drake R, Vogl W, Mitchell A: *Gray's anatomy for students,* Philadelphia, 2005, Churchill-Livingstone.)

of the biceps brachii tendon; although not a part of the rotator cuff, its proximal intra-articular portion courses through a space between the supraspinatus and subscapularis tendons, called the *rotator interval*. At this location, the intra-articular portion of the biceps tendon is stabilized by the biceps reflection pulley made up of the superior glenohumeral ligament and the coracohumeral ligament, which are essentially thickened reflections of the joint capsule. The

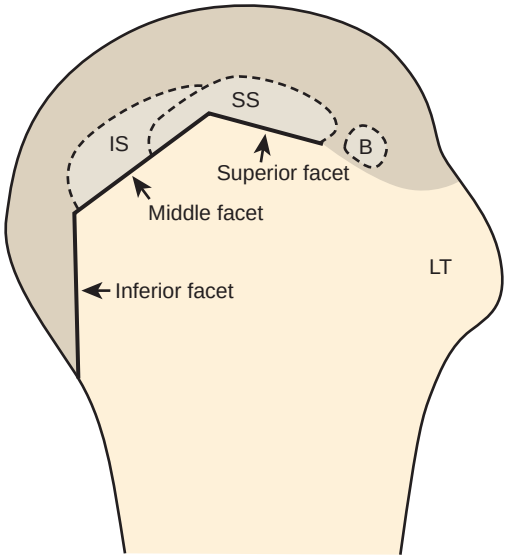

FIGURE 3-2 ■ Greater tuberosity facets. Illustration of lateral humerus shows superior, middle, and inferior facets (B, long head of biceps brachii; IS, infraspinatus; LT, lesser tuberosity; SS, supraspinatus). (Image courtesy of Carolyn Nowak, Ann Arbor, Michigan.)

glenohumeral joint normally communicates with the biceps brachii long head tendon sheath. Several joint recesses also exist and include the axillary recess, which extends inferiorly, and the subscapular recess, which extends medially through the rotator interval to be located inferior to the coracoid process at the superior aspect of the subscapularis tendon in an inverted U shape. The subacromial-subdeltoid bursa is located between the rotator cuff and the overlying deltoid muscle and acromion (see Fig. 3-1). The glenoid labrum represents a rim of fibrocartilage at the periphery of the glenoid.

ULTRASOUND EXAMINATION TECHNIQUE

Table 3-1 is a shoulder ultrasound examination checklist. Examples of diagnostic shoulder ultrasound reports are available online at www.expertconsult.com (see eBox 3-1 and 3-2).

General Comments

For ultrasound examination of the shoulder, the patient sits on a stool with low back support but without wheels, and the sonographer sits on a stool with wheels to allow easy maneuvering. For examination of the patient's left shoulder, the patient faces the ultrasound machine, with the sonographer sitting somewhat between the patient and ultrasound machine if the sonographer is right-handed (Fig. 3-3A, online). For examination of the patient's right shoulder, the patient turns toward the left and faces the sonographer (see Fig. 3-3B, online). The transducer frequency for the shoulder is generally at least 10 MHz, although one may need to use a lower frequency in evaluation of the deeper structures such as the posterior glenoid labrum or if the patient has a large body habitus. It is important to follow a sequence of steps to ensure a complete and thorough evaluation.[3] Although a targeted approach is often used in other peripheral joints, this is not recommended with the shoulder because pain is often diffuse or referred. It is recommended, however, that every sonographic evaluation be followed by targeted evaluation over any area with point tenderness or focal symptoms.

TABLE 3-1 **Shoulder Ultrasound Examination Checklist**

Step	Structures/Pathologic Features of Interest
1	Biceps brachii long head
2	Subscapularis, biceps tendon dislocation
3	Supraspinatus, infraspinatus
4	Acromioclavicular joint, subacromial-subdeltoid bursa, dynamic evaluation
5	Posterior glenohumeral joint, labrum, teres minor, infraspinatus

Position No. 1: Long Head of Biceps Brachii Tendon

The patient places the hand palm up in supination on his or her leg (Fig. 3-4A). This position rotates the bicipital groove anteriorly, an important bone landmark. The transducer is placed in the transverse plane on the patient, and the long head of the biceps brachii tendon is seen within the bicipital groove in short axis (see Fig. 3-4) (Video 3-1). Because the distal biceps tendon courses deep, tendon obliquity to the transducer sound beam commonly creates anisotropy and an artifactual hypoechoic appearance of the normal tendon (see Fig. 3-4C). This is corrected by toggling the transducer inferiorly to aim the sound beam superiorly (Video 3-2). A hyperechoic and well-defined humeral cortex in the floor of the bicipital groove indicates that the sound beam is perpendicular to the overlying biceps tendon. The biceps brachii tendon is evaluated in short axis from proximal to distal. It is important to

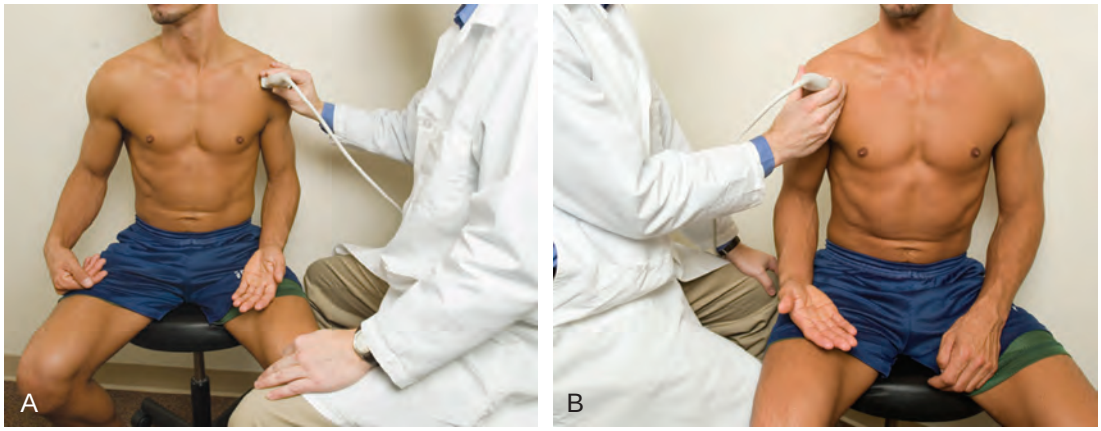

FIGURE 3-3 ■ **A** and **B,** Shoulder ultrasound examination: patient positioning.

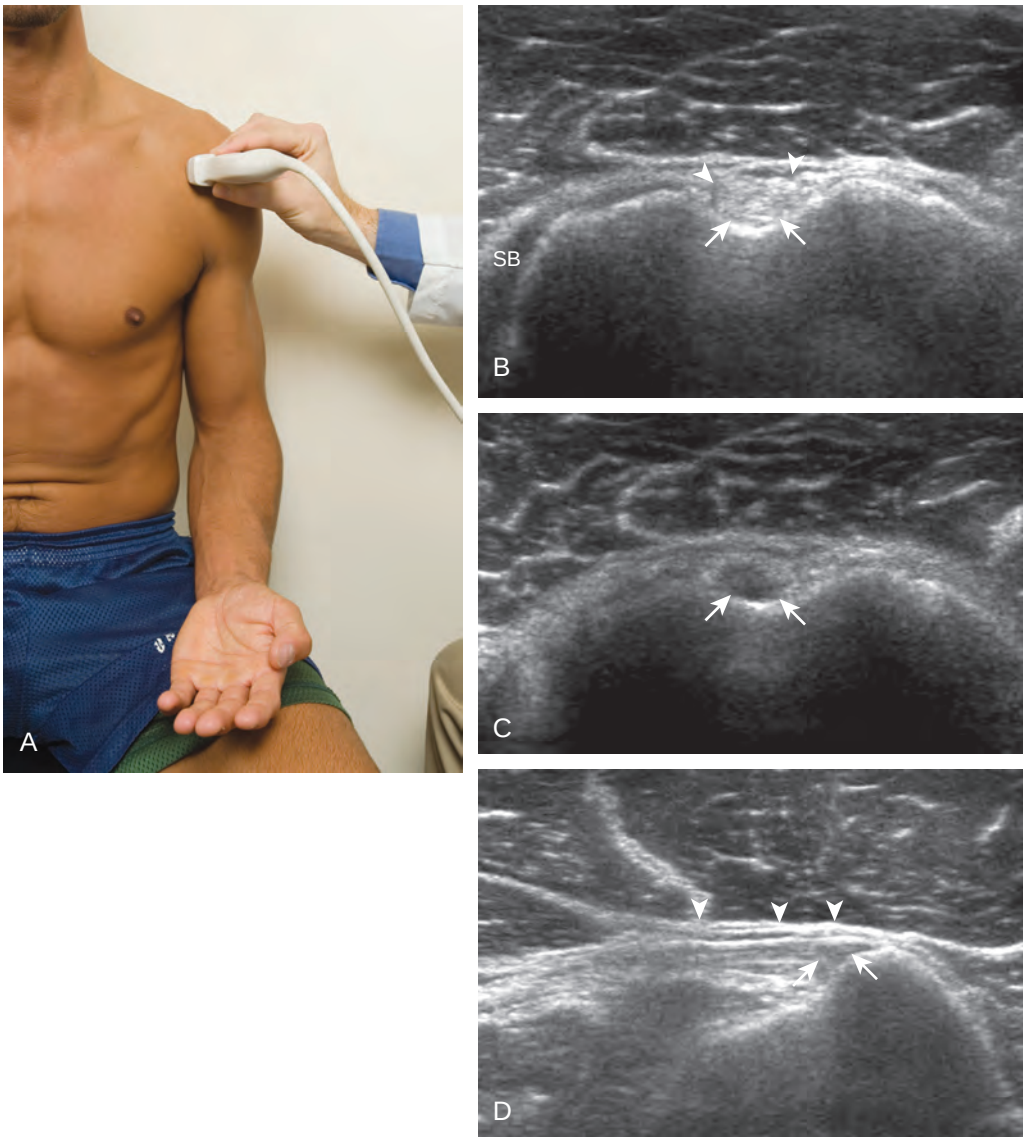

FIGURE 3-4 ■ Biceps brachii long head tendon evaluation: short axis. A, Transverse imaging over the bicipital groove shows **(B)** the hyperechoic biceps brachii long head tendon *(arrows)* within the bicipital groove. Note transverse humeral ligament *(arrowheads)* and subscapularis tendon (SB) (medial is left side of image). **C,** Toggling the transducer creates anisotropy *(arrows)*. **D,** Distal image shows biceps tendon *(arrows)* and overlying pectoralis major tendon *(arrowheads)*.

evaluate the most proximal aspect where the biceps tendon courses over the humeral head because this is a common site for tendon pathology.[4] Evaluation is also continued inferiorly to the level of the pectoralis tendon (see Fig. 3-4D) to assess the pectoralis and biceps because complete biceps brachii long head tendon tears may retract to this level. The transducer is then turned 90 degrees to visualize the tendon in long axis from the humeral head to the pectoralis tendon (Fig. 3-5A) (Video 3-3). Asymmetrical pressure on the distal aspect of the transducer (or heel-toe maneuver) is typically needed to bring the biceps tendon fibers perpendicular to the transducer sound beam to eliminate anisotropy (see Fig. 3-5B and C) (Video 3-4). An additional method to visualize the biceps tendon in long axis is to identify the characteristic pyramid shape of the lesser tuberosity (see Fig. 3-5D); movement of the transducer laterally from this point will visualize the bicipital groove and biceps long head tendon (Video 3-5).

FIGURE 3-5 ■ Biceps brachii long head tendon evaluation: long axis A, Sagittal imaging over the bicipital groove shows **(B)** the biceps tendon *(arrows)* and anisotropy *(open arrow)*. **C,** Anisotropy is corrected when the transducer is positioned perpendicular to the tendon (distal is right side of image). **D,** Note the pyramid shape of the lesser tuberosity (T) medial to the bicipital groove in the sagittal plane. D, deltoid muscle.

Position No. 2: Subscapularis and Biceps Tendon Dislocation

The transducer is placed in the transverse plane, as before, to visualize the bicipital groove and to center the field of view over the lesser tuberosity (see Fig. 3-4A). In this neutral position, although the subscapularis tendon can be seen in long axis, there is significant anisotropy (Fig. 3-6A). Ask the patient to rotate the shoulder externally (see Fig. 3-6B), and this will bring the subscapularis tendon fibers into view perpendicular to the transducer sound beam and will eliminate anisotropy (see Fig. 3-6C) (Video 3-6). It is important to move the transducer superiorly and inferiorly over the lesser tuberosity to ensure complete evaluation of the subscapularis tendon. The transducer should also be moved laterally over the bicipital groove to evaluate for potential biceps brachii tendon subluxation or dislocation, which may be present only in external rotation (see Biceps Tendon, Subluxation and

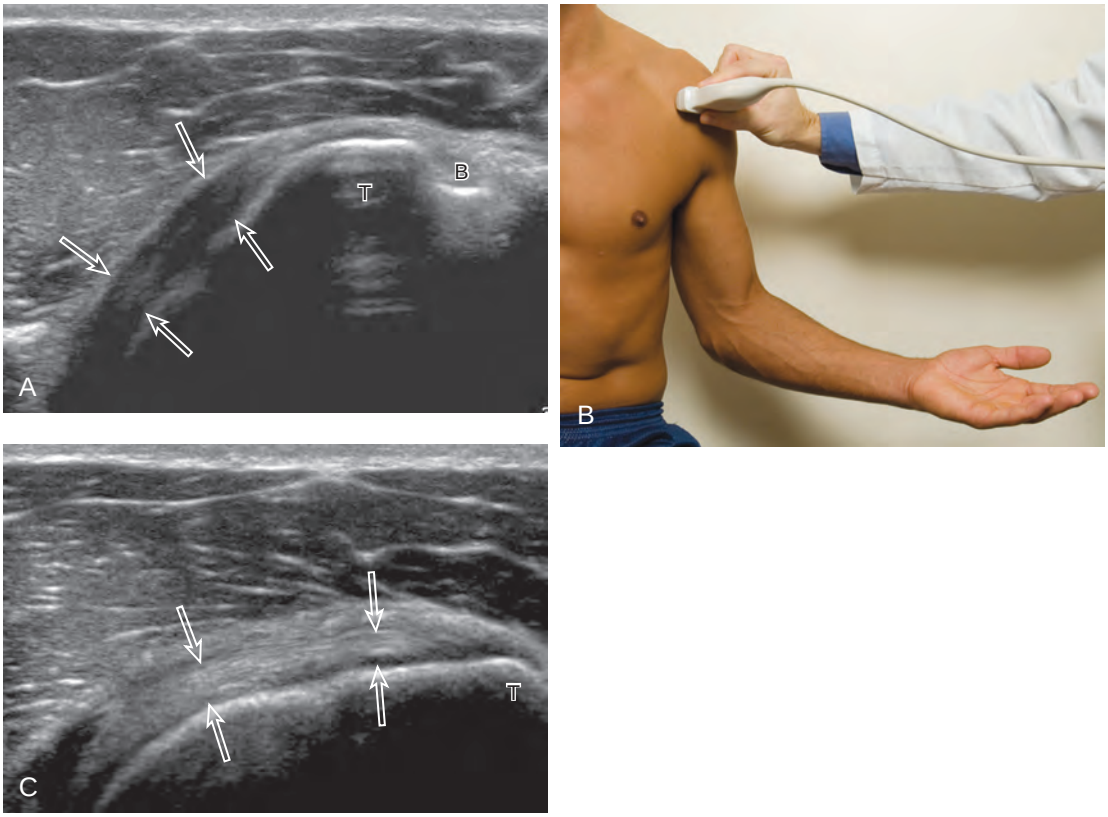

FIGURE 3-6 ■ Subscapularis tendon evaluation: long axis. A, Transverse imaging over the lesser tuberosity (T) shows the subscapularis tendon *(open arrows)* hypoechoic from anisotropy (medial is left side of image). **B,** Imaging with external rotation optimally shows **(C)** the normal hyperechoic subscapularis tendon *(open arrows)*. B, biceps brachii long head tendon.

Dislocation).[5] Center the transducer over the distal subscapularis tendon again, rotate the transducer 90 degrees, and assess the subscapularis tendon in short axis (Fig. 3-7A and B). In this view, it is common to see hypoechoic striations of muscle or interfaces between the several tendon bundles, especially when spatial compound sonography is not used (see Fig. 3-7C) (Video 3-7).

Position No. 3: Supraspinatus and Infraspinatus

The goal when imaging the supraspinatus is to evaluate the tendon in long and short axis. This will avoid numerous diagnostic pitfalls and is an indicator that the operator has a thorough understanding of anatomy and shoulder ultrasound technique. The key to obtaining such images is to understand the anatomy of the greater tuberosity and the effects of various shoulder positioning. If one wanted to assess the supraspinatus tendon in long axis with the shoulder in neutral position, the transducer would be placed in the coronal place over the greater tuberosity; however, in this position, much of the tendon is hidden beneath the acromion, which could hide more proximal cuff tears (Fig. 3-8). One way to correct this is to ask the patient to place the back of his or her ipsilateral hand in the lower lumbar region and to keep the elbow close to the body (called the *Crass position*) (Fig. 3-9).[6] In this position, the humerus is rotated internally such that the greater tuberosity is located anteriorly on the patient. By placing the transducer in the sagittal plane on the patient over the greater tuberosity, a long axis view of the supraspinatus tendon is demonstrated. Rotating the transducer 90 degrees (or transverse on the patient) will produce a short axis image of the supraspinatus. The Crass position is helpful when one is first learning shoulder ultrasound technique in that a long and short axis views are easily obtained; however, the significant disadvantages of this position include limited view of the rotator interval (see later) and, often, significant patient discomfort. Because of this, the *modified Crass position* is used (I primarily use

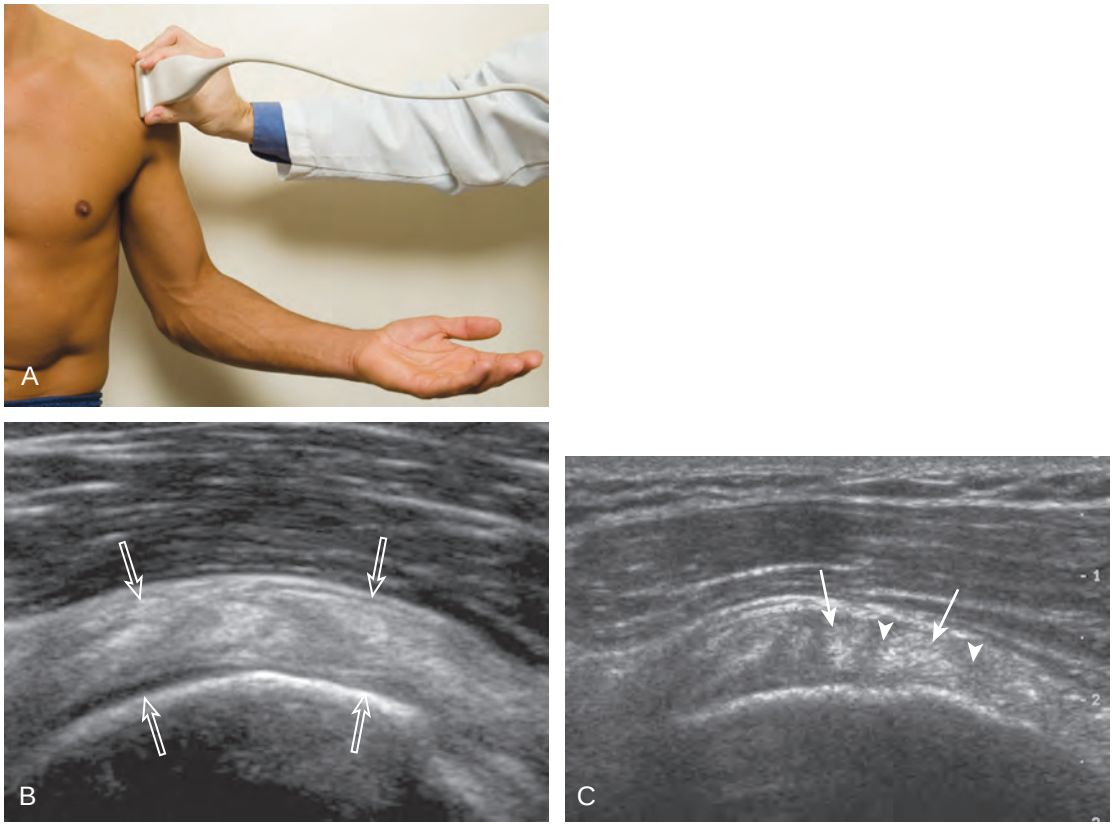

FIGURE 3-7 ■ Subscapularis tendon evaluation: short axis. A, Sagittal imaging over lesser tuberosity shows **(B)** the normal hyperechoic appearance *(open arrows)* (cephalad is left side of image). **C,** Note heterogeneity resulting from visualization of individual hyperechoic tendon bundles *(arrows)* with adjacent hypoechoic muscle *(arrowheads)* when spatial compound imaging is not used.

the modified Crass position and uncommonly the Crass position for problem solving) (Fig. 3-10).[7] To obtain the modified Crass position, the patient is asked to place his or her hand on the ipsilateral hip area. The elbow should be pointed posteriorly to ensure some degree of shoulder external rotation compared with the Crass position; otherwise, the rotator interval may not be visible. The greater tuberosity is now located between the locations in the neutral and Crass positions; therefore, to obtain a long axis view of the supraspinatus tendon, the transducer is placed over the greater tuberosity and pointed superior and oblique toward the patient's ear. Usually, the axis of the transducer is parallel to the proximal biceps tendon and humeral shaft regardless of each position when imaging the supraspinatus in long axis. The transducer is then turned 90 degrees to evaluate the supraspinatus tendon in short axis.

Regardless of patient positioning in the Crass or modified Crass position, supraspinatus evaluation begins with evaluation in long axis because this important view allows visualization of the three surfaces of the supraspinatus tendon. In long axis, the normal supraspinatus will appear hyperechoic and fibrillar, with a convex superior margin (Fig. 3-11) (Video 3-8). The thin hypoechoic layer over the curved humeral head represents the hyaline articular cartilage. At times, a thin hypoechoic layer over the greater tuberosity, which represents the fibrocartilage transition zone between the tendon and bone at the enthesis, may be seen and should not be confused with hyaline articular cartilage over the rounded humeral head. One must be aware that the distal fibers of the tendon curve downward at the greater tuberosity near the articular surface, and the transducer orientation should be adjusted using the heel-toe maneuver to eliminate anisotropy (Fig. 3-12A and B) (Video 3-9). A hyperechoic and well-defined humeral head cortex indicates that the sound beam is perpendicular to the bone and overlying tendon. The footprint of the supraspinatus tendon inserts over approximately 2.25 cm of the greater tuberosity shelf, so the transducer should be moved anterior and posterior over the greater tuberosity (or medial and lateral on the patient in the modified

FIGURE 3-8 ■ Supraspinatus evaluation: neutral position. A, The supraspinatus tendon *(arrow)* inserts laterally on the greater tuberosity. **B,** An anteroposterior shoulder radiograph illustrates that much of the supraspinatus tendon *(arrow)* is hidden beneath the acromion (A). **C,** Ultrasound image long axis to supraspinatus only shows distal supraspinatus *(arrowheads)*. T, greater tuberosity.

Crass position), to ensure complete evaluation.[2] It is important to continue scanning anteriorly along the greater tuberosity until the intra-articular portion of the biceps tendon is seen because this would indicate that the full anterior extent of the supraspinatus was evaluated, a location where supraspinatus tendon tears commonly occur.[8,9] Including a long axis image of the intra-articular portion of the long head biceps brachii tendon will document that the most anterior aspect of the supraspinatus was evaluated (see Fig. 3-11B). As the transducer is moved posteriorly over the middle facet of the greater tuberosity, the infraspinatus is also evaluated (see Fig. 3-11C). At the middle facet, the angle between the greater tuberosity and the articular surface of the humeral head flattens, and alternating hypoechoic linear areas representing anisotropy of the infraspinatus tendon fibers can be seen over the supraspinatus tendon (Video 3-10). Minimal thinning of the cuff over this region may be seen.[10] In addition, the rotator cable may be seen as a distinct hyperechoic structure (see Fig. 3-15).

After assessment of the supraspinatus in long axis, the transducer is turned 90 degrees to evaluate the tendon in short axis (Fig. 3-13) (Video 3-11). First, beginning over the proximal aspect of the supraspinatus, the humeral head should be seen as a round echogenic line with overlying hypoechoic hyaline cartilage (see

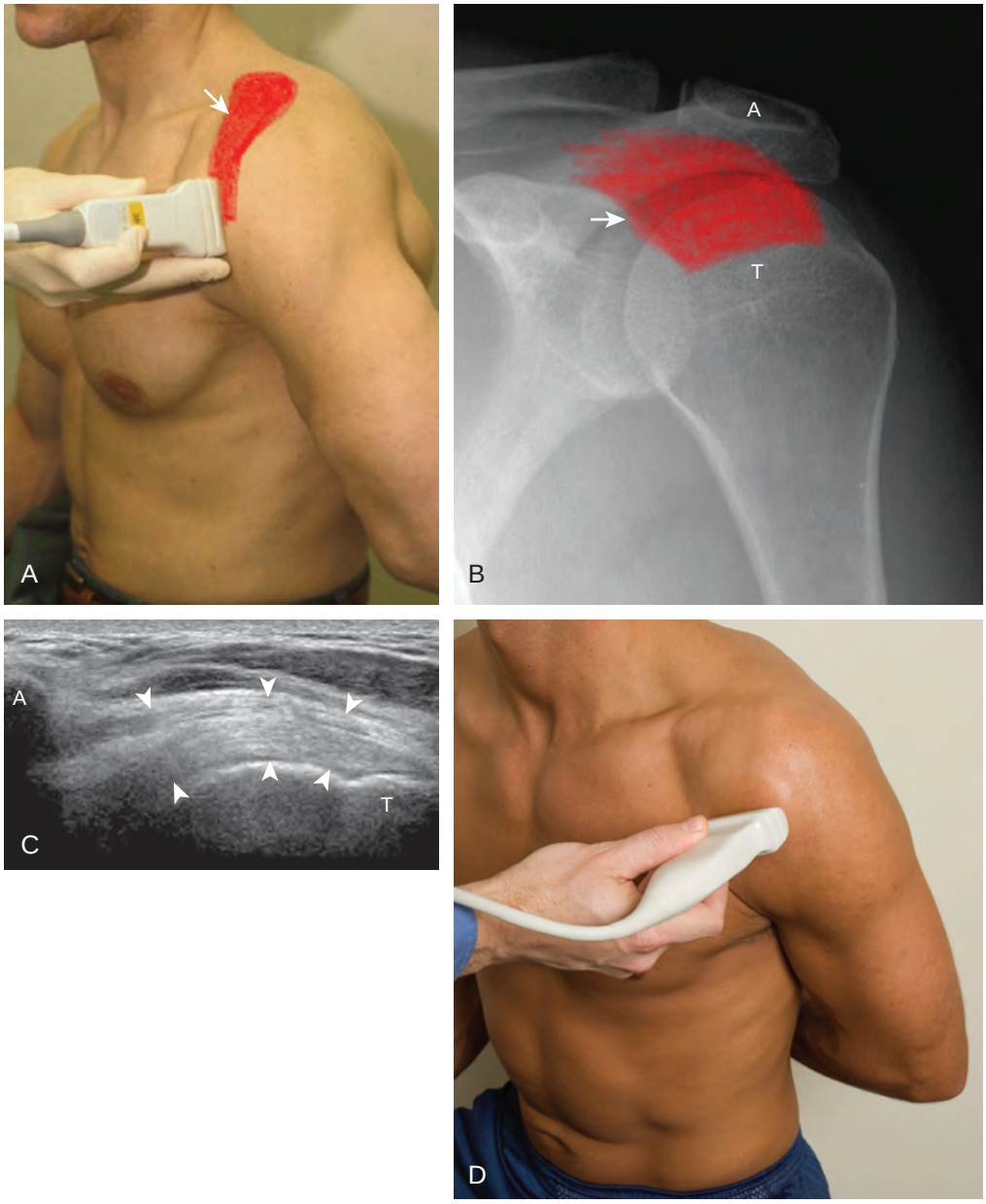

FIGURE 3-9 ■ Supraspinatus evaluation: Crass position. A, B, The greater tuberosity (T) rotates anteriorly with the distal supraspinatus tendon *(arrow)* now visible, which was previously hidden beneath the acromion (A). The transducer is placed anteriorly in the sagittal plane on the body (A) for a long axis view and improved visualization of the supraspinatus *(arrowheads)* **(C)**. The transducer is placed transverse **(D)** for a short axis image of the supraspinatus. A, acromion; T, greater tuberosity.

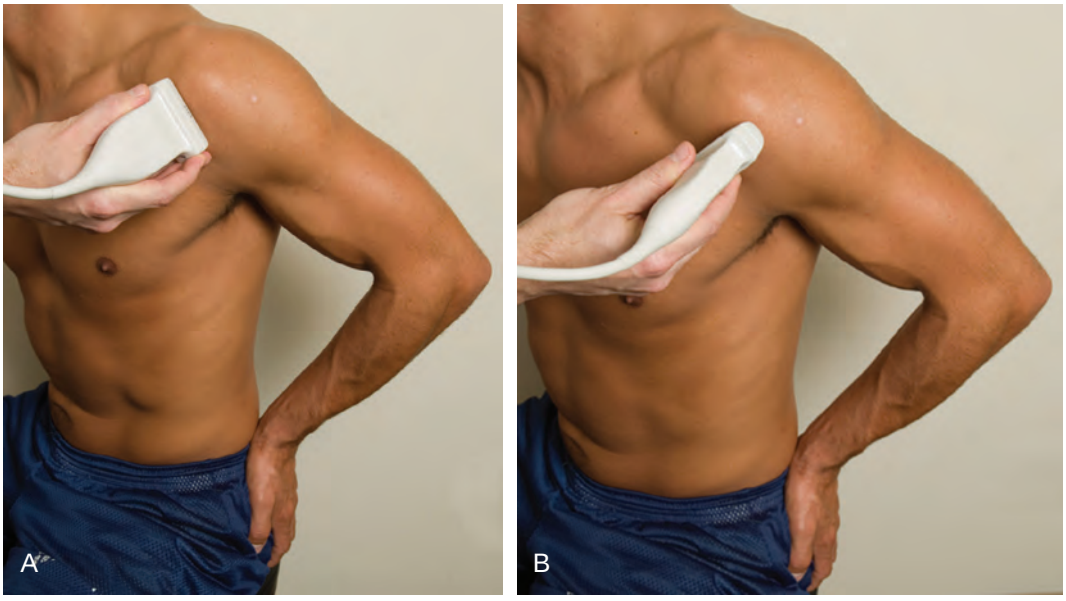

FIGURE 3-10 ■ Supraspinatus evaluation: modified Crass position. The supraspinatus is evaluated in the long axis **(A)** and the short axis **(B)**, with the patient's hand placed near the ipsilateral hip and the elbow directed posteriorly.

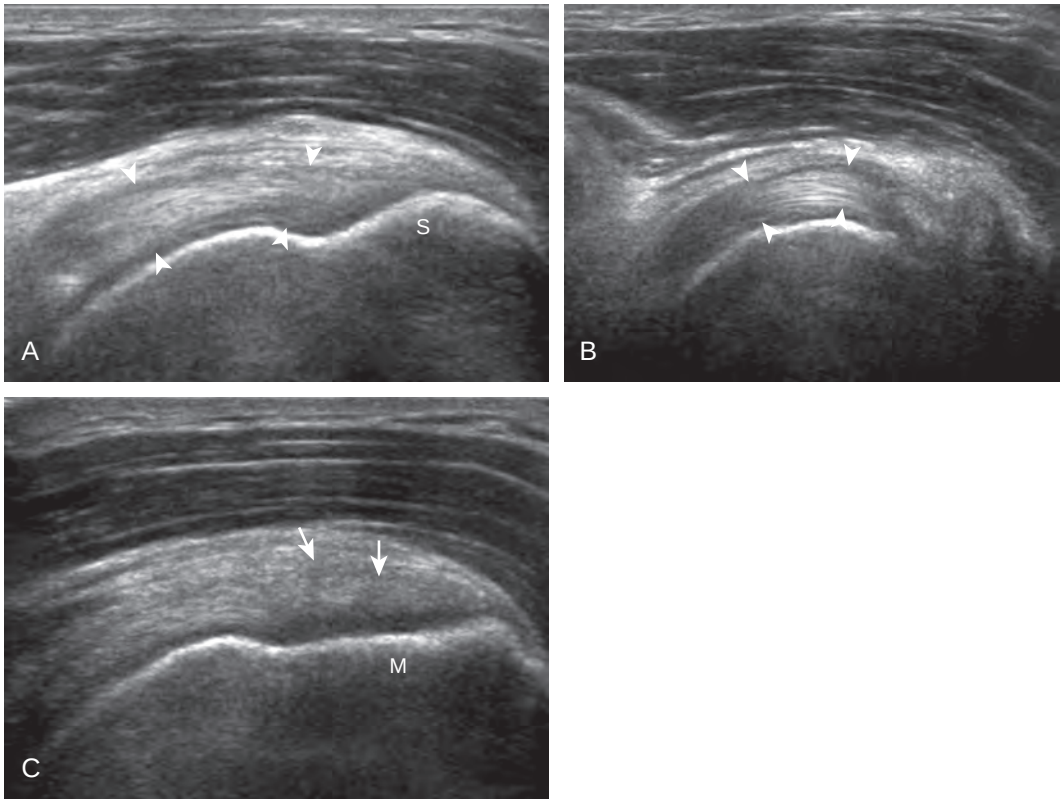

FIGURE 3-11 ■ Supraspinatus: long axis. A, The normal supraspinatus is hyperechoic and fibrillar with a convex superior margin *(arrowheads)*, shown at the level of the superior facet (S). **B,** Transducer positioning in the same plane but anterior to (A) over the rotator interval shows the long head of biceps brachii tendon *(arrowheads)*. **C,** Transducer positioning in the same plane but posterior to (A) over the middle facet (M) shows hypoechoic bands from the overlying infraspinatus *(arrows)*.

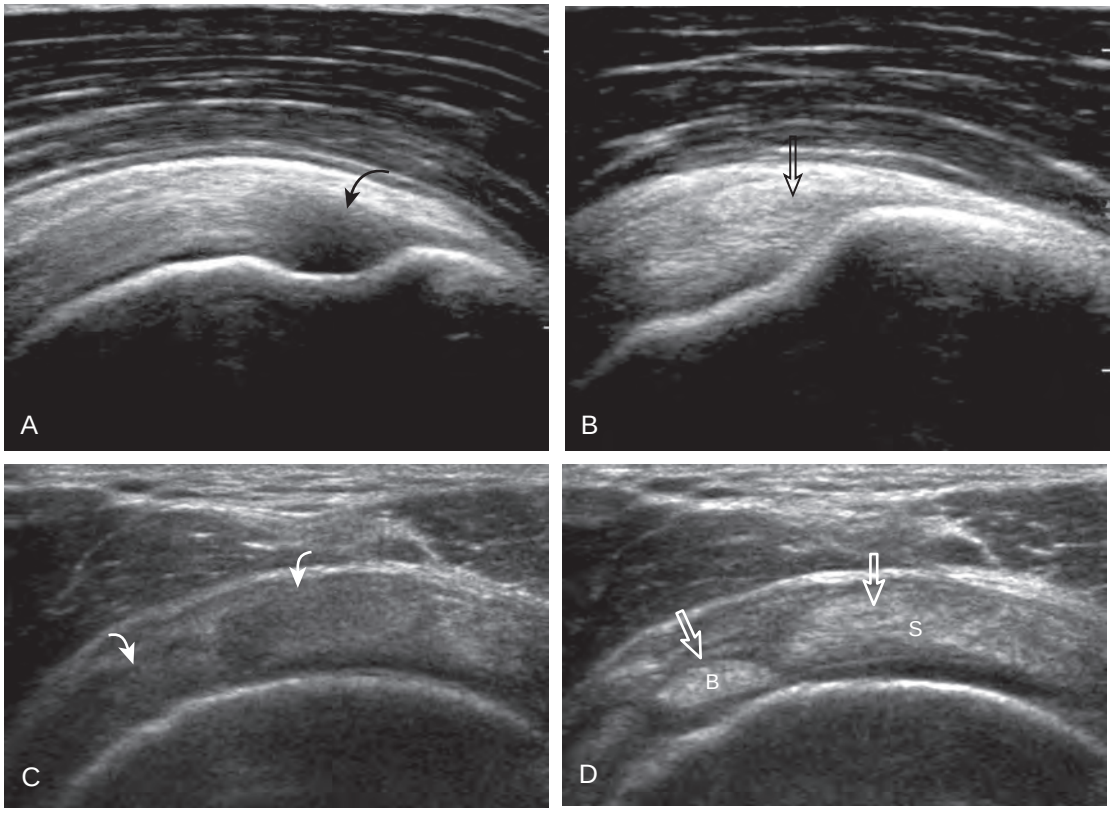

FIGURE 3-12 ■ Supraspinatus tendon: anisotropy. Ultrasound images long axis to the supraspinatus show **(A)** artifactual hypoechogenicity *(curved arrow)* where the distal tendon fibers curve downward to the greater tuberosity, oblique to the sound beam. With the transducer repositioned **(B),** the distal tendon fibers appear hyperechoic *(open arrow)* when they are perpendicular to the sound beam. In short axis **(C),** tendon anisotropy (*curved arrows*) is eliminated with toggling of the transducer to show **(D)** hyperechoic *(open arrows)* supraspinatus (S), biceps brachii (B), and bone cortex.

Fig. 3-13A). The transducer should be toggled until the bone cortex and overlying tendon are hyperechoic and well defined to eliminate anisotropy (see Fig. 3-12C and D). At this level, the rotator cuff should be of fairly uniform thickness, similar to a tire on a wheel, measuring on average 6 ± 1.1 mm.[11] This appearance indicates that the transducer is in the true short axis plane relative to the supraspinatus tendon and not in an oblique plane. The transducer is then moved distally relative to the supraspinatus tendon. As the hyaline cartilage disappears from view, the round humeral head surface will be replaced with the angulated surface of the greater tuberosity facets. At this point, the tendon uniformly becomes thinner, an indication that the transducer position is now beyond the articular surface. The facets of the greater tuberosity from anterior to posterior appear as three flat surfaces: the superior, middle, and inferior facets.[1] The supraspinatus tendon inserts on the superior facet and the superior half of the middle facet, the infraspinatus inserts on the middle facet (overlapping the supraspinatus tendon superficially), and the teres minor inserts on the inferior facet.[1] At this point, both the distal supraspinatus and infraspinatus are assessed. Similar to long axis imaging, alternating hypoechoic lines are seen over the middle facet, which represent anisotropy of the infraspinatus tendon fibers over the supraspinatus (Video 3-12). As the transducer is moved more distally, the greater tuberosity becomes somewhat square, and the rotator cuff thins even more and eventually disappears as the transducer moves beyond the greater tuberosity and beyond the rotator cuff (see Fig. 3-13C and D). Similar to evaluation of the supraspinatus tendon in long axis, it is critical that the intra-articular portion of the biceps tendon (the rotator interval) is identified to indicate that the most anterior aspect of the supraspinatus tendon is evaluated. This is one of the advantages of the modified Crass position because this important landmark is well visualized. In addition, the

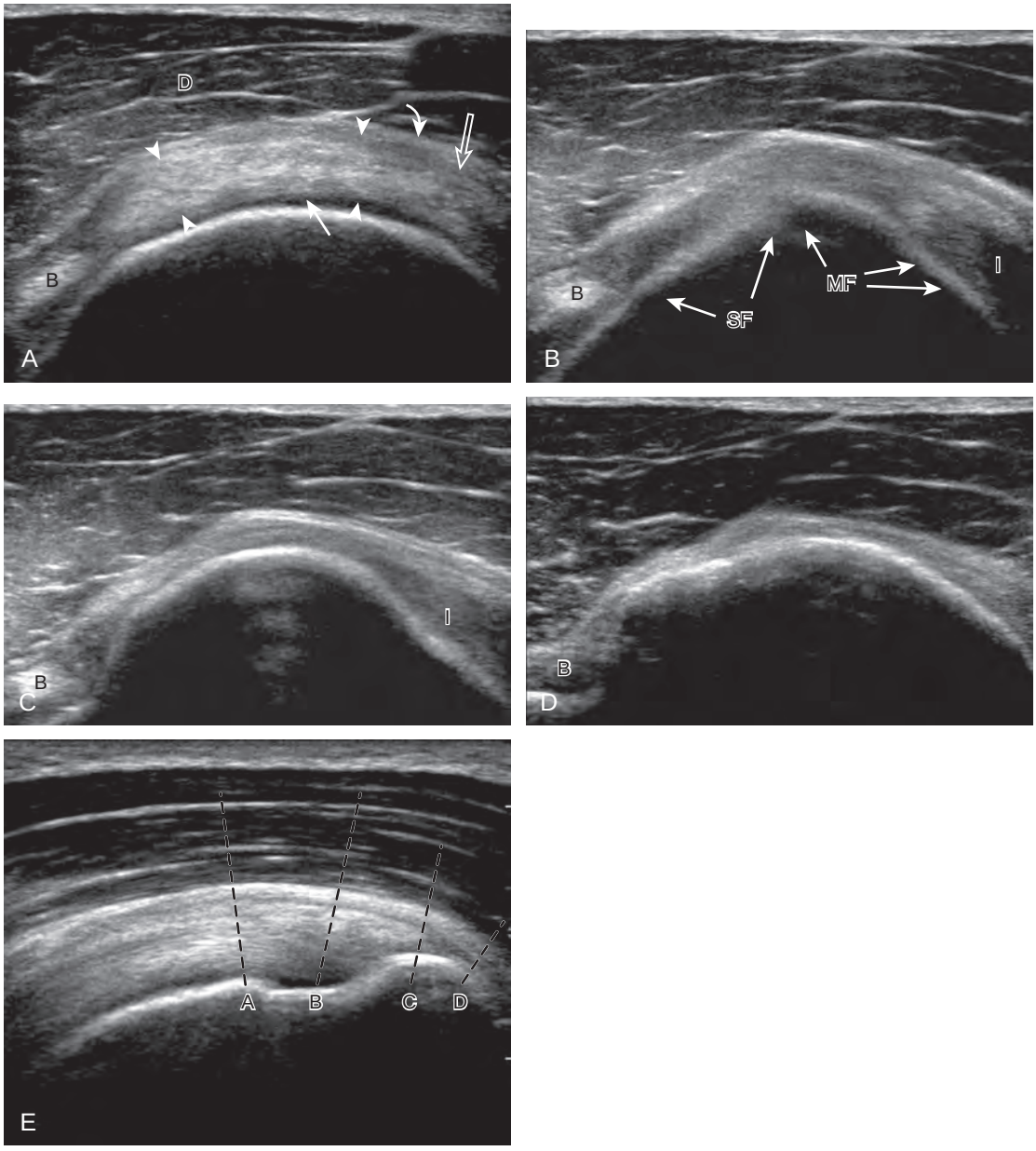

FIGURE 3-13 ■ **Supraspinatus tendon: short axis. A,** The normal supraspinatus *(arrowheads)* over the humeral head is of uniform thickness and hyperechoic. Note the intra-articular portion of the biceps brachii tendon (B) in the rotator interval, supraspinatus-infraspinatus junction *(open arrow)*, hyaline articular cartilage *(arrow)*, collapsed subacromial-subdeltoid bursa *(curved arrow)*, and deltoid muscle (D) (left side of image is anterior on the greater tuberosity). Sequential short axis images of the supraspinatus tendon show **(B** to **D)** gradual thinning of the tendon beyond the hyaline cartilage and absence of the supraspinatus beyond the greater tuberosity. Note the superior facet (SF) and the middle facet (MF) of the greater tuberosity. **E,** Long axis image of the supraspinatus tendon is used as a reference for images A to D. B, biceps tendon; I, infraspinatus tendon.

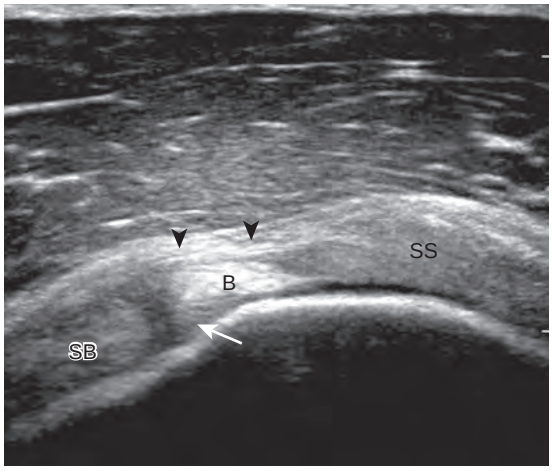

FIGURE 3-14 ■ Rotator interval. Ultrasound image of the intra-articular portion of the biceps brachii long head in short axis (B) at rotator interval shows the coracohumeral ligament and joint capsule *(arrowheads)* and the superior glenohumeral ligament *(arrow)*. SB, subscapularis tendon; SS, supraspinatus tendon.

biceps reflection pulley is identified with the superior glenohumeral ligament seen at the subscapularis aspect of the biceps tendon adjacent to the humerus, and the coracohumeral ligament is identified over the biceps tendon as it courses lateral to merge with the supraspinatus tendon (Fig. 3-14).[12]

Another structure of the rotator cuff is the rotator cable, which may be identified by its characteristic shape and position (Fig. 3-15).[13] The rotator cable has a U shape, with each limb attaching to the greater tuberosity. The curved aspect of the U is visualized with its fibers perpendicular to the supraspinatus at the articular surface. The rotator cable is more prominent in some individuals (termed *cable dominant*) and outlines an area of the rotator cuff within the U, termed the *rotator crescent*.

Position No. 4: Acromioclavicular Joint, Subacromial-Subdeltoid Bursa, and Dynamic Evaluation

The acromioclavicular joint can be located with palpation of the clavicle and placement of the transducer in the coronal-oblique plane over the distal clavicle (Fig. 3-16) or by moving the transducer superiorly in the transverse plane from the bicipital groove region. The acromioclavicular joint is identified by the bone landmarks and hypoechoic joint space, although a hyperechoic fibrocartilage disk may be seen.[14] If the acromioclavicular joint is widened, the patient can place his or her hand on the opposite shoulder to assess for acromioclavicular joint widening or, conversely, narrowing, which may be associated with pain.[15] The transducer is then moved laterally in the coronal place over the proximal humerus beyond the greater tuberosity to assess for fluid within the dependent portion of the subacromial-subdeltoid bursa (see Fig. 3-16C).

To dynamically assess for subacromial impingement, the transducer is positioned in the coronal or coronal-oblique plane to visualize the lateral border of the acromion and the adjacent greater tuberosity (Fig. 3-17). The examiner assesses the supraspinatus tendon and subacromial-subdeltoid bursa dynamically first by passively abducting the arm (with or without elbow flexion). This allows the examiner to slow or stop the patient's movement if the bone landmarks are not visualized to allow repositioning of the transducer and also trains the patient to abduct the arm at a particular speed. The movement is then repeated actively (see Fig. 3-17C and D). Subsequent pooling of fluid in the subacromial-subdeltoid bursa indicates subacromial impingement, although more advanced cases can show additional upward movement of the humeral head.[16,17] The finding of incomplete sliding of the supraspinatus beneath

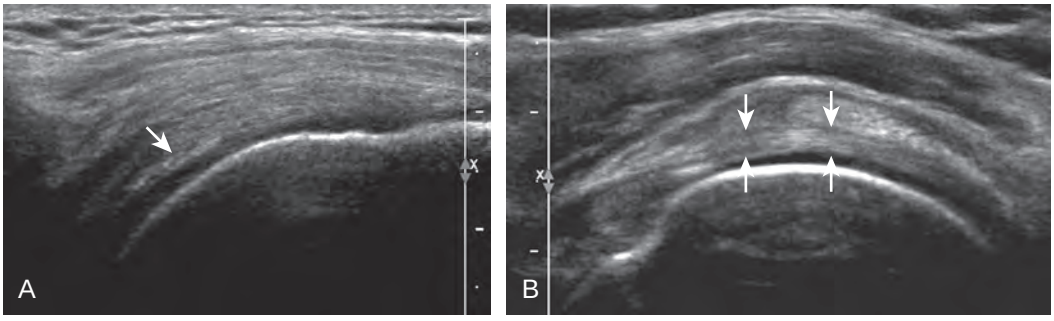

FIGURE 3-15 ■ Rotator cable. Ultrasound images **(A)** long axis and **(B)** short axis to supraspinatus show the hyperechoic and fibrillar rotator cable *(arrows)*. (Courtesy of Y. Morag, MD, Ann Arbor, Mich.)

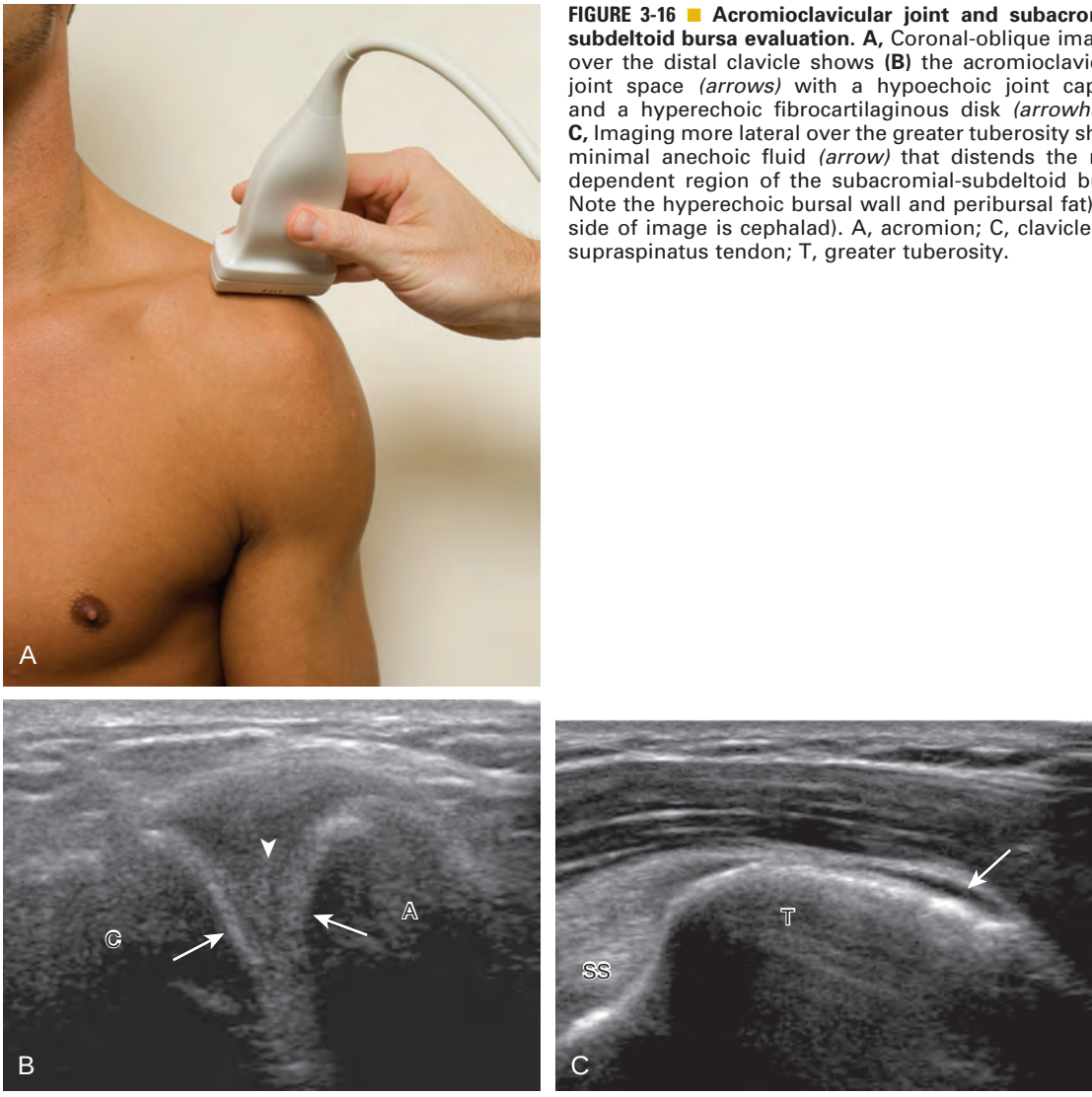

FIGURE 3-16 ■ Acromioclavicular joint and subacromial-subdeltoid bursa evaluation. A, Coronal-oblique imaging over the distal clavicle shows **(B)** the acromioclavicular joint space *(arrows)* with a hypoechoic joint capsule and a hyperechoic fibrocartilaginous disk *(arrowhead)*. **C,** Imaging more lateral over the greater tuberosity shows minimal anechoic fluid *(arrow)* that distends the most dependent region of the subacromial-subdeltoid bursa. Note the hyperechoic bursal wall and peribursal fat) (left side of image is cephalad). A, acromion; C, clavicle; SS, supraspinatus tendon; T, greater tuberosity.

the acromion during this dynamic maneuver indicates adhesive capsulitis.[18] When assessing for subacromial impingement, the transducer should also be moved anterior to the acromion to assess the region of the coracoacromial ligament for abnormal distention of the subacromial-subdeltoid bursa as well.

Position No. 5: Infraspinatus, Teres Minor, and Posterior Glenoid Labrum

The patient rotates on the stool to permit visualization of the posterior structures of the shoulder; initially, the patient keeps his or her hand palm up on the thigh. Place the transducer in the oblique axial plane angled superiorly toward the humeral head parallel and just inferior to the scapular spine (Fig. 3-18). Position the transducer to visualize the well-defined central tendon of the infraspinatus tendon within the infraspinatus muscle at the musculotendinous junction posterior to the glenoid to ensure an imaging plane that is long axis to the infraspinatus (see Fig. 3-18B). The infraspinatus tendon can then be followed distally to its insertion on the middle facet at the posterior aspect of the greater tuberosity. Evaluation of the distal infraspinatus tendon supplements earlier evaluation from the modified Crass position (see Figs. 3-11 and 3-13). If the infraspinatus tendon is not visible because of shadowing beneath the acromion (which is not common), then the patient can place the hand on

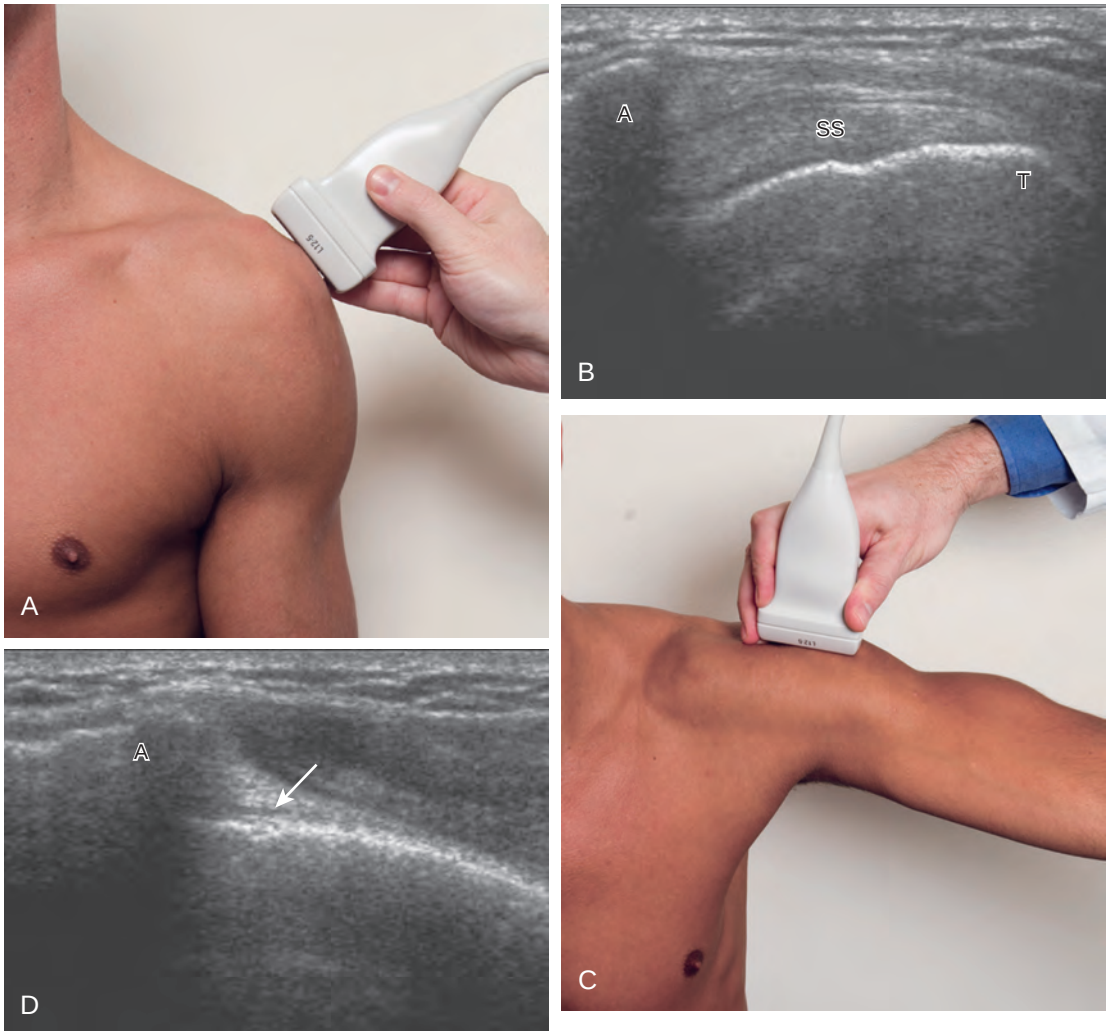

FIGURE 3-17 ■ Dynamic evaluation for subacromial impingement and adhesive capsulitis. A, The transducer is positioned between the greater tuberosity and acromion **(B),** the patient raises the arm **(C)** during visualization with ultrasound. **D,** Normally, the supraspinatus (SS) glides beneath the acromion (A). The subacromial-subdeltoid bursa *(arrow)* remains collapsed without pooling of fluid at the acromion tip. T, greater tuberosity.

the opposite shoulder to improve visualization; this maneuver is less ideal because the infraspinatus tendon, seen linear and perpendicular to the sound beam in neutral shoulder position, becomes curved, introducing anisotropy. The transducer can then be moved inferiorly to visualize the smaller teres minor, with its tendon more superficial over the muscle compared with the infraspinatus tendon (see Fig. 3-18C). The transducer is then turned 90 degrees to evaluate the infraspinatus and teres minor in short axis (Fig. 3-19). An alternate approach in identification of the infraspinatus and teres minor is to palpate the scapular spine, place the transducer sagittal on the patient over the scapular spine, and then move the transducer inferiorly. The first structure identified inferior to the scapular spine is the infraspinatus. Once the infraspinatus and teres minor are identified, the transducer is turned long axis to the infraspinatus tendon to evaluate the hyperechoic triangle-shaped posterior glenoid labrum (see Fig. 3-18B). It is important to slide the transducer medially from the glenohumeral joint to assess the spinoglenoid notch, a site where paralabral cysts may be found. The patient can actively internally and externally rotate the shoulder to assess the infraspinatus tendon and posterior glenoid labrum dynamically (Video 3-13). This maneuver is also important in the evaluation for posterior glenohumeral joint recess fluid, which also facilitates evaluation of potential paralabral tears (see Glenoid Labrum and Paralabral Cyst).

FIGURE 3-18 ■ Infraspinatus (long axis), teres minor (long axis), and posterior labrum evaluation. A, Imaging over the posterior shoulder shows **(B)** the infraspinatus muscle *(open arrows)* and tendon *(curved arrow)*. Note posterior glenoid labrum *(arrowheads)*, spinoglenoid notch *(arrow)*, humeral head (H), glenoid (G), and deltoid muscle (D) (right side of image is distal). **C,** Just inferior to the infraspinatus, the thinner and more superficial hyperechoic teres minor tendon can be seen *(curved arrows)*.

In shoulder external rotation, the suprascapular vein may dilate, and this can simulate a paralabral cyst (see Glenoid Labrum and Paralabral Cyst) (Video 3-14).

To complete the posterior shoulder examination, the transducer is turned 90 degrees and moved medial to assess the infraspinatus and teres minor in short axis globally at the musculotendinous junctions for atrophy or fatty degeneration; the infraspinatus muscle should be nearly twice the size of the teres minor over the scapular body, with normal muscle appearing relatively hypoechoic compared with hyperechoic tendon (see Fig. 3-19B). At this site, a ridge is often seen in the scapula, which forms a concave surface beneath each muscle and aids in their identification. The transducer can be moved superiorly to similarly assess for atrophy of the supraspinatus muscle. An extended field of view image may be considered (if available on the ultrasound machine) (see Fig. 3-19E).[19]

ROTATOR CUFF ABNORMALITIES

Supraspinatus Tears and Tendinosis

General Comments

Most rotator cuff tears involve the supraspinatus tendon, although they may extend posterior to involve the infraspinatus and anterior to involve the biceps reflection pulley and subscapularis tendons.[8] The anterior aspect of the distal supraspinatus is a common site of tear, often near the rotator interval, although a more posterior location near the supraspinatus-infraspinatus junction has been described with degenerative cuff

FIGURE 3-19 ■ Infraspinatus (short axis) and teres minor (short axis). A, Imaging over posterior shoulder shows progressive transition (**B** to **D**) from hypoechoic muscle to hyperechoic tendon of the infraspinatus *(open arrows)* and teres minor *(arrowheads)* (left side of image is superior). Extended field of view image **(E)** shows supraspinatus *(curved arrows)*, infraspinatus *(open arrows)*, and teres minor *(arrowheads)*.

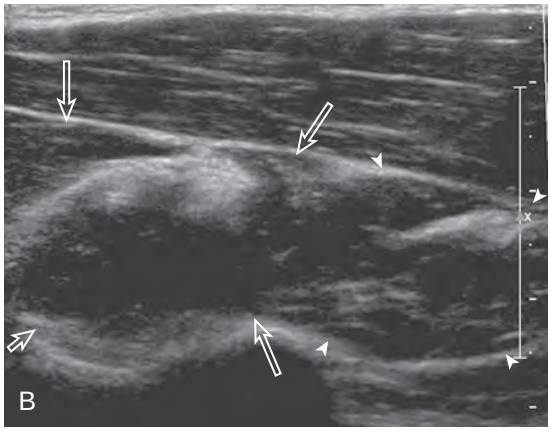

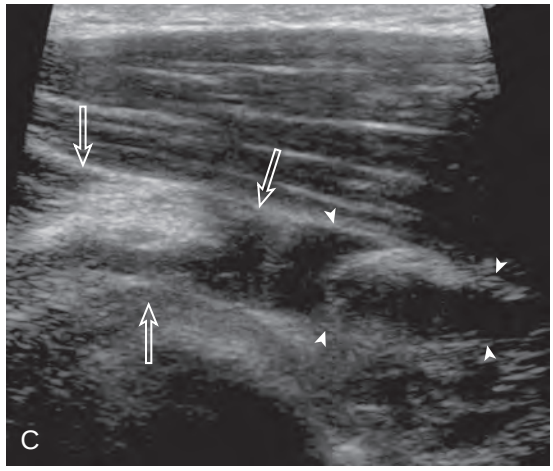

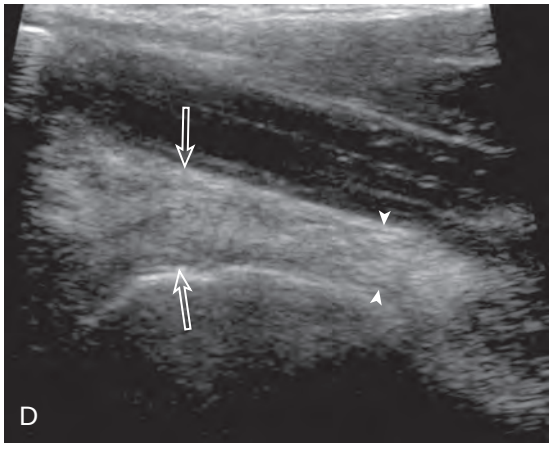

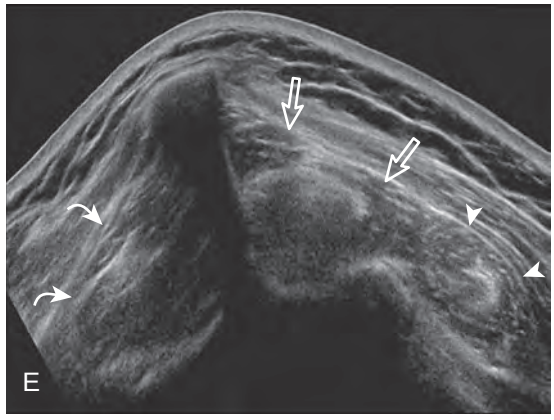

tears.[20] Most tendon tears are the result of chronic attrition and possible superimposed injury, and they typically occur after the age of 40 years. Such chronic supraspinatus tears occur distally and are associated with cortical irregularity of the greater tuberosity, an important indirect sign of supraspinatus tendon tear.[21,22] Acute tears may occur more proximally and may or may not have associated cortical irregularity, depending on the age of the patient and the state of the underlying rotator cuff. Accurate localization of a tendon tear is essential to classify the tear properly (Fig. 3-20). For example, partial-thickness tears could involve either the articular or bursal surface of the tendon. A tear that is localized within the tendon or that extends only to the greater tuberosity surface (or footprint) of the supraspinatus attachment is called an interstitial or intrasubstance tear because it would not be visible at arthroscopy or bursoscopy.[2,8] A tear that extends from articular to bursal surfaces is a full-thickness tear. Correct description and nomenclature are also essential. A full-thickness tear may be focal or incomplete, whereas a full-thickness tear that involves the entire width of a tendon can be termed a *complete* or *full-width* full-thickness tear. Initial evaluation in long axis of the supraspinatus is ideal in that the three surfaces of the rotator cuff (articular, bursal, greater tuberosity) are visible and easily identified.[23] Most tears are anechoic or hypoechoic. As a supraspinatus tendon tear becomes larger, tendon retraction and volume loss of the tendon occur, with loss of the normal superior convex shape. Ultrasound and magnetic resonance imaging (MRI) have comparable accuracies in detection and measurement of rotator cuff tears.[24] A meta-analysis of 65 articles has also shown that ultrasound and MRI are comparable in sensitivity and specificity for the diagnosis of rotator cuff tear.[25]

Partial-Thickness Tear

Partial-thickness supraspinatus tendon tears are characterized by a well-defined hypoechoic or anechoic abnormality that disrupts the tendon

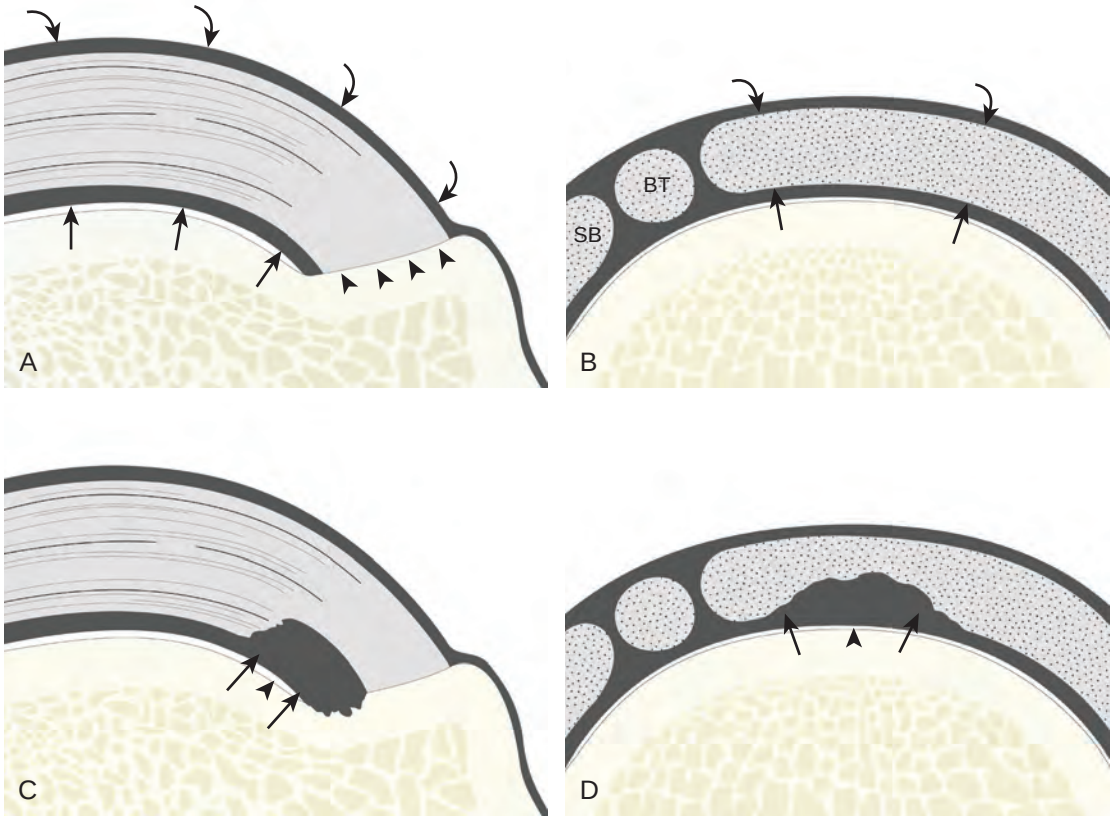

FIGURE 3-20 ■ Supraspinatus tendon tears. Illustrations in long axis **(A)** and short axis **(B)** to the supraspinatus tendon show the articular *(arrows)*, bursal *(curved arrows)*, and greater tuberosity *(arrowheads)* surfaces of the supraspinatus tendon. **C** and **D,** Articular-side partial-thickness tears (black) contact the articular surface *(arrows)* and hyaline cartilage *(arrowhead)*.

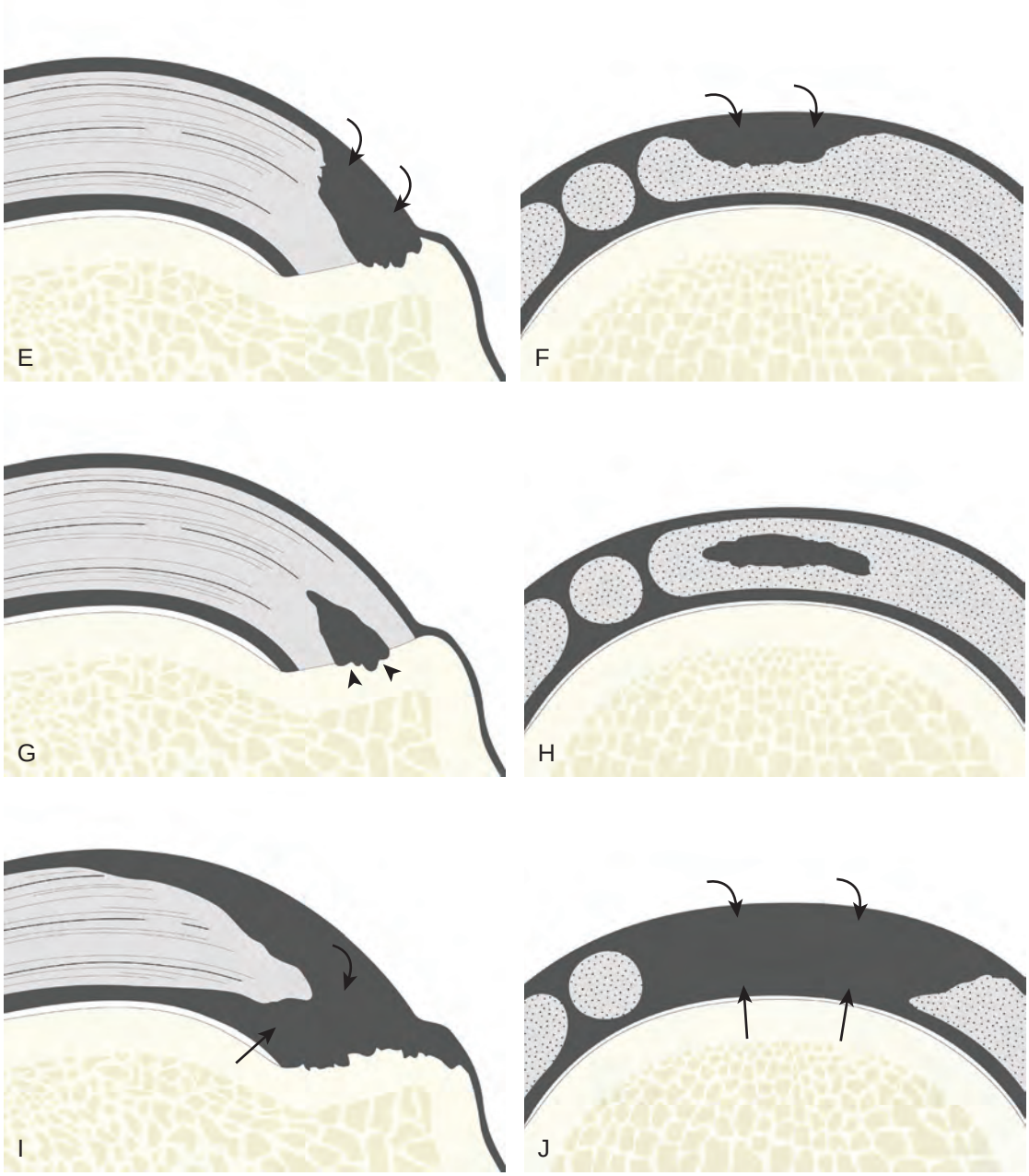

FIGURE 3-20, cont'd ■ **E** and **F,** bursal-side partial-thickness tears (black) contact the bursal surface *(curved arrows)*. **G** and **H,** Intrasubstance tears (black) reside within the tendon not in contact with the articular or bursal surface, although isolated greater tuberosity contact within the tendon may be seen *(arrowheads)*. **I** and **J,** Full-thickness tears extend from articular *(arrows)* to bursal *(curved arrows)* surfaces. Note that all types of tears may contact the greater tuberosity, associated with bone irregularity. BT, biceps tendon; SB, subscapularis tendon.

fibers.[21,26] Such tears may be articular-side or bursal-side partial-thickness tears determined by which surface of the tendon is involved. An intrasubstance or interstitial tear may also be considered a form of partial-thickness tear, but one that does not extend to the articular or bursal surface.

Articular-side partial-thickness tears most commonly involve the supraspinatus anteriorly and distally at the greater tuberosity and are seen with increased frequency in patients younger than 40 years.[8,9] A mixed hyperechoic-hypoechoic appearance may be present, which represents

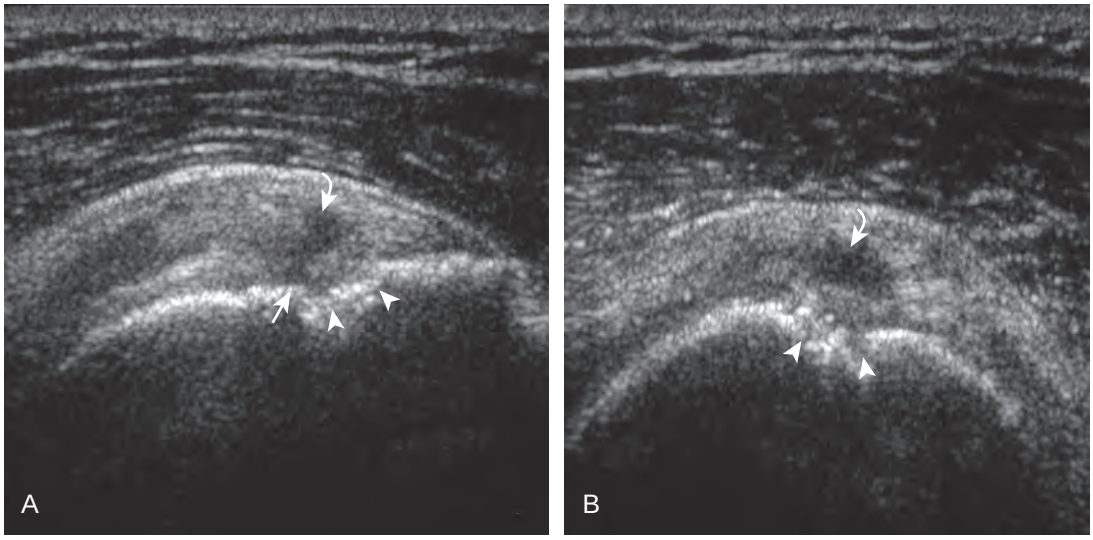

FIGURE 3-21 ■ Supraspinatus tear: articular, partial-thickness. Ultrasound images of supraspinatus tendon in long axis **(A)** and short axis **(B)** show well-defined anechoic disruption of the tendon fibers *(curved arrow)*, which surrounds the hyperechoic tendon stump distally and creates a mixed hyperechoic-hypoechoic appearance. Note contact with the articular surface *(arrow)*, cortical irregularity of the greater tuberosity *(arrowheads)*, and lack of volume loss.

hypoechoic fluid that surrounds the hyperechoic torn tendon stump (Figs. 3-21, 3-22, and 3-23).[26] Cortical irregularity of the greater tuberosity immediately adjacent to the tendon tear is common, related to the chronic cuff attrition at the site of the tear.[21,22] An acute tear of a previously normal cuff or a proximal tear (see Fig. 3-23) does not demonstrate cortical irregularity and more likely appears anechoic from fluid, although these types of tears are less common. With an articular-side partial-thickness tear, the superior surface of the tendon remains convex because global tendon volume loss is usually absent. Articular surface extension of a tear is suggested when the tear is in direct contact with the hypoechoic hyaline cartilage. The hyperechoic interface between the tendon tear and the hyaline cartilage may be accentuated in this situation (called the *cartilage interface sign*).[27] The terms *rim-rent tear* and *PASTA* (partial articular-sided supraspinatus tendon avulsion) *lesion* are used specifically to describe a far-distal articular-side partial-thickness tear, immediately adjacent to the greater tuberosity surface (Video 3-15).[8,9]

A bursal-side partial-thickness supraspinatus tendon tear is also hypoechoic or anechoic, but it

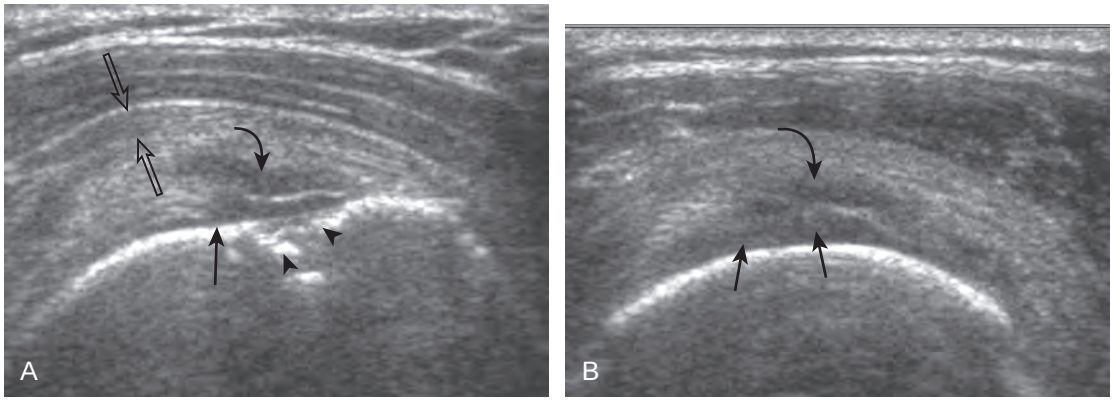

FIGURE 3-22 ■ Supraspinatus tear: articular, partial-thickness (rim-rent). Ultrasound images of supraspinatus tendon in long axis **(A)** and short axis **(B)** show well-defined hypoechoic disruption of the tendon fibers *(curved arrow)* with a mixed hyperechoic-hypoechoic appearance distally. Note contact with the hypoechoic hyaline cartilage at the articular surface *(arrows)*, cortical irregularity of the greater tuberosity *(arrowheads)*, and lack of volume loss. The subacromial-subdeltoid bursa is thickened and isoechoic to tendon *(open arrows)*.

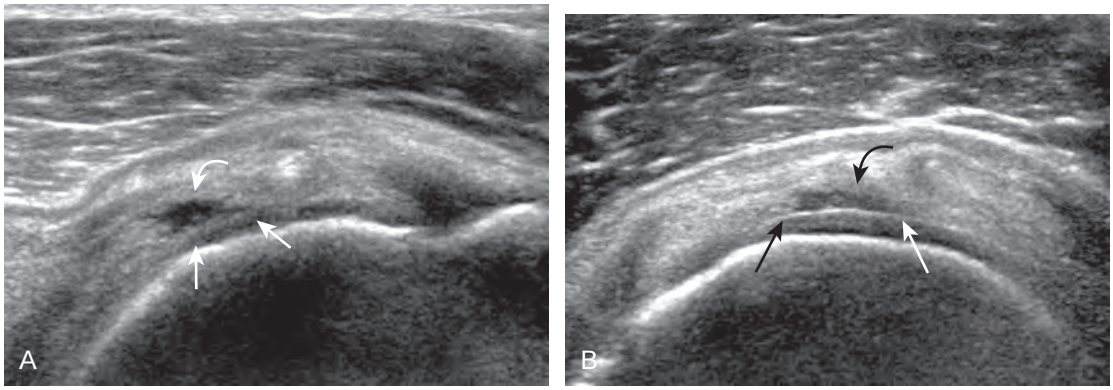

FIGURE 3-23 ■ Supraspinatus tear: articular, partial-thickness. Ultrasound images of supraspinatus tendon in long axis **(A)** and short axis **(B)** show well-defined anechoic disruption of the proximal tendon fibers *(curved arrow)* with articular extension as cartilage interface sign *(arrows)* (hypoechoic area at greater tuberosity is anisotropy).

is localized to the bursal surface (Figs. 3-24, 3-25, 3-26, and 3-27).[21] Tear extension from the bursal surface to the greater tuberosity surface (or tendon footprint), without extension to the articular surface, is still considered a bursal-side partial-thickness tear. Because of the superficial location of the tear, tendon thinning and volume loss of the cuff are usually present. This situation results in loss of the normal superior convexity of the supraspinatus tendon surface, with dipping of the deltoid muscle and subacromial-subdeltoid bursa into the torn tendon gap. Similar to other supraspinatus tendon tears, greater tuberosity cortical irregularity is typically present because the tear extends from the bursal surface to the greater tuberosity surface. If adjacent subacromial-subdeltoid bursal synovial hypertrophy is present, hypoechoic or isoechoic synovial tissue may fill the torn tendon gap, making the tear and tendon thinning less conspicuous (see Fig. 3-27) (Video 3-16).

A tendon tear that does not contact the articular or bursal side of the supraspinatus is termed an *intrasubstance* or *interstitial tear*.[8,9] Such tears may be anechoic or hypoechoic, located within the tendon substance or in contact with the greater tuberosity surface (Fig. 3-28). Cortical irregularity is often seen in the latter situation. Volume loss of the tendon is absent. Extensive intrasubstance tears may either represent or be precursors of a more extensive delamination tear. The presence of a well-defined anechoic cyst within the rotator cuff is usually associated with a supraspinatus articular-side tear (Fig. 3-29).[28]

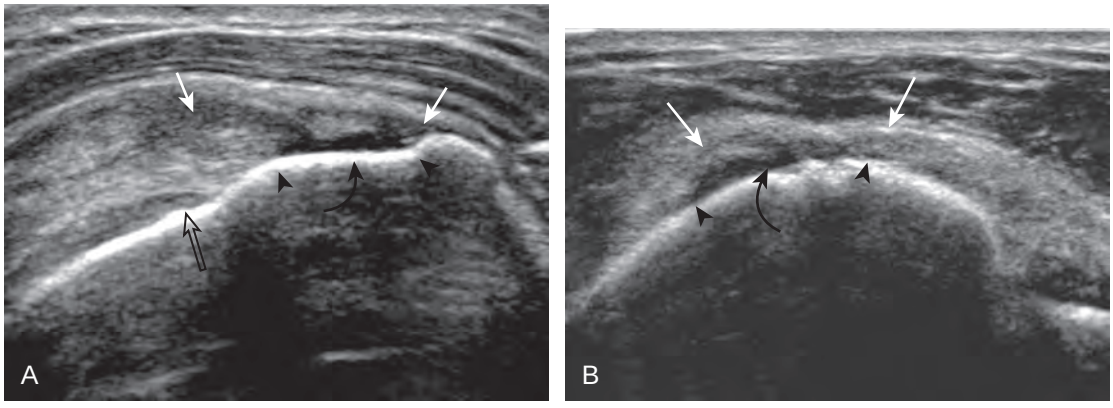

FIGURE 3-24 ■ Supraspinatus tear: bursal, partial-thickness. Ultrasound images of supraspinatus tendon in long axis **(A)** and short axis **(B)** show absence of the bursal aspect of the supraspinatus tendon and replacement with anechoic fluid *(curved arrow)*. Note the bursal extent *(between arrows)* and the greater tuberosity extent *(between arrowheads)* of tear, the absence of contact with the hyaline cartilage *(open arrow)*, and loss of the normal superior convexity. Greater tuberosity cortical irregularity is present in **B.**

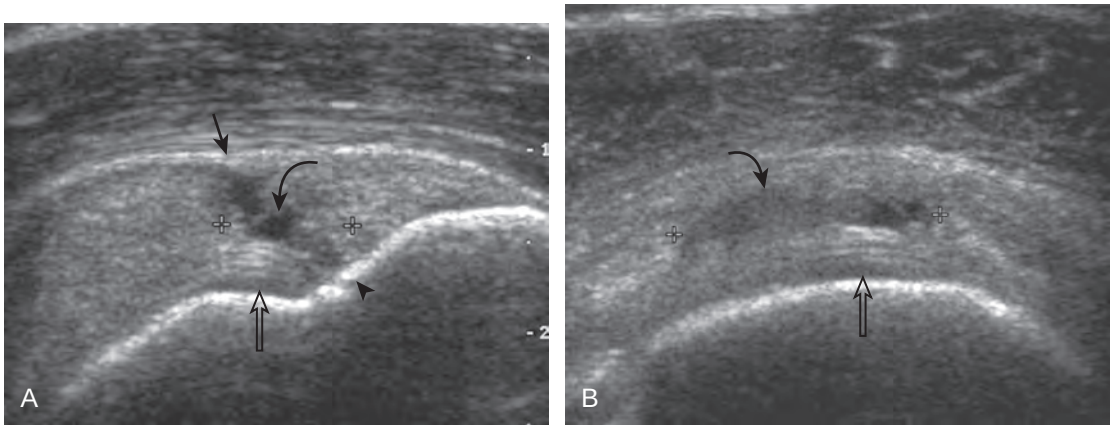

FIGURE 3-25 ■ Supraspinatus tear: bursal, partial-thickness. Ultrasound images of supraspinatus tendon in long axis **(A)** and short axis **(B)** show well-defined hypoechoic disruption of the tendon fibers *(curved arrow, between cursors)*, which extends from the bursal surface *(arrow)* to the greater tuberosity *(arrowhead)*. There is no contact with the hypoechoic hyaline cartilage at the articular surface *(open arrows)*, and this excludes a full-thickness tear.

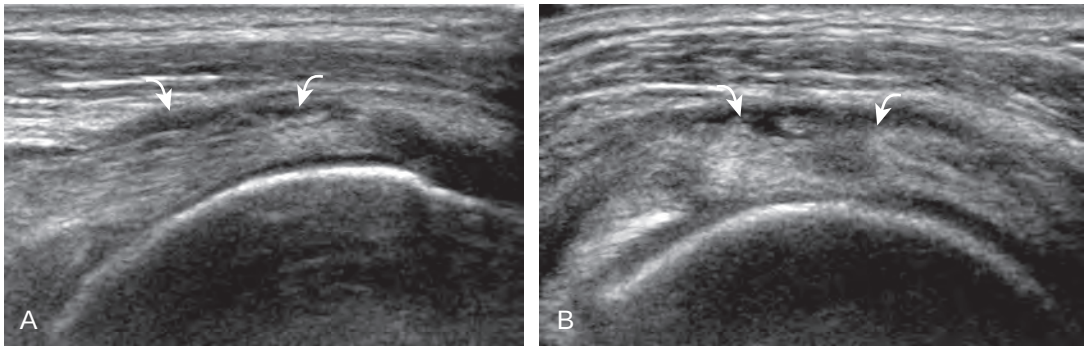

FIGURE 3-26 ■ Supraspinatus tear: bursal, partial-thickness. Ultrasound images of supraspinatus tendon in long axis **(A)** and short axis **(B)** show well-defined hypoechoic disruption of the most superficial tendon fibers *(curved arrows)*.

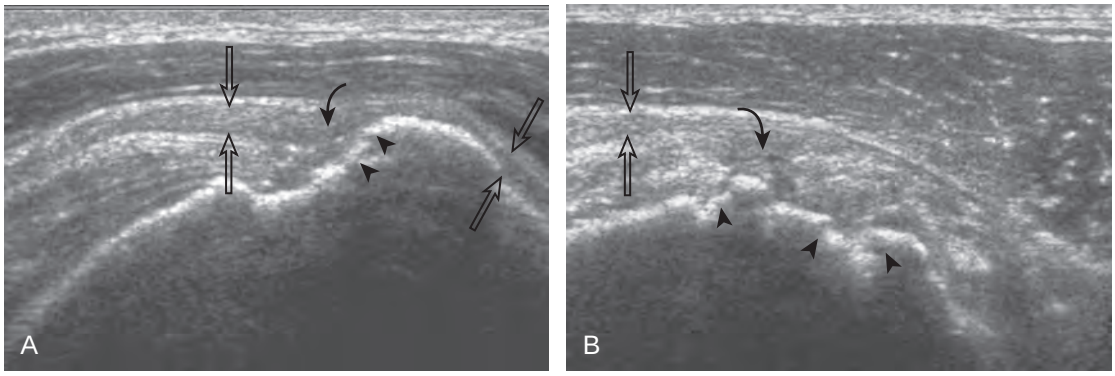

FIGURE 3-27 ■ Supraspinatus tear: bursal, partial-thickness. Ultrasound images of supraspinatus tendon in long axis **(A)** and short axis **(B)** show thinning of the tendon from loss of bursal-side fibers *(curved arrow)*, torn from the greater tuberosity *(arrowheads)*. Note the thickened isoechoic subacromial-subdeltoid bursa *(open arrows)*, which fills the tendon tear and extends beyond the greater tuberosity. The presence of intact articular fibers excludes full-thickness tear.

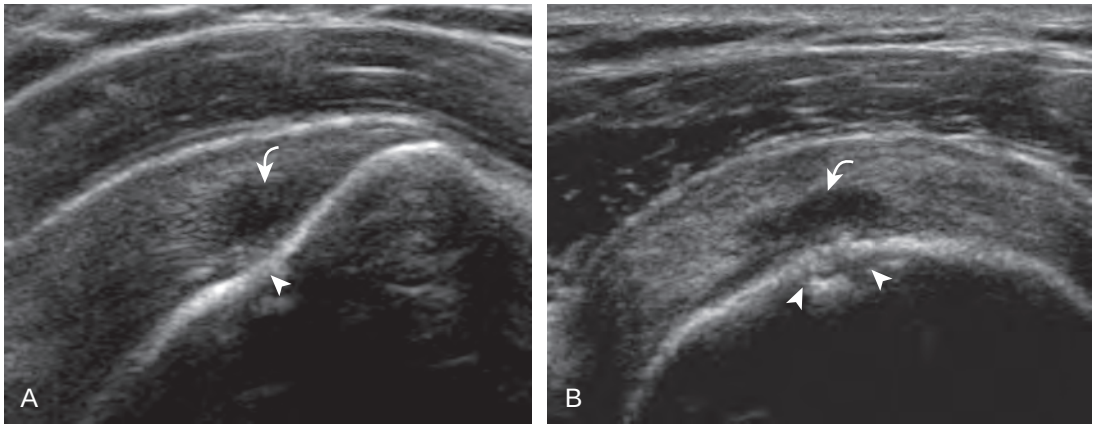

FIGURE 3-28 ■ Intrasubstance tear. Ultrasound images of supraspinatus in long axis **(A)** and short axis **(B)** show focal hypoechoic defect *(curved arrow)* only contacting the greater tuberosity surface with cortical irregularity *(arrowheads)*.

Full-Thickness Tear

A full-thickness supraspinatus tendon tear is characterized by a well-defined hypoechoic or anechoic abnormality that disrupts the hyperechoic tendon fibers and extends from the articular to bursal surfaces of the tendon (Figs. 3-30 through 3-38).[21,24] Anterior and distal location is common, although degenerative supraspinatus tears may be isolated more posterior at the supraspinatus-infraspinatus junction.[8,20] Associated cortical irregularity of the adjacent greater tuberosity surface is usually present at a supraspinatus tear in patients older than 40 years. Identification of a hyperechoic interface between the hypoechoic hyaline cartilage and anechoic or hypoechoic tendon tear (cartilage interface sign) assists in the identification of the articular extent.[27] This finding is only seen when the sound beam is perpendicular to the hyaline cartilage; the heel-toe maneuver when imaging the tendon in long axis and toggling the transducer while in short axis is helpful (see Chapter 1). Small full-thickness tears may not be associated with volume loss of the tendon, especially if filled with fluid. Narrow longitudinal tears are best visualized with the tendon in short axis (see Fig. 3-31). As a tear becomes larger, flattening or concavity of the superior supraspinatus tendon surface with volume loss is typical (Video 3-17). Acute tears may occur more proximally, and more commonly they are anechoic and are filled with fluid (see Fig. 3-34).[29] An acute tear in a patient younger than 40 years or a proximal tear does not demonstrate cortical irregularity, although these types of tears are less common. It is important to describe the location of the tendon tear, the dimensions of the tear in long axis and short axis, and extension to other adjacent tendons. A full-thickness tear that is focal may be termed an *incomplete full-thickness tear*, whereas a tear that involves the entire width of a tendon may be termed a *complete* or *full-width full-thickness tear*. Chronic tears may be associated with extensive remodeling of the greater tuberosity, and the distal torn tendon may be tapered without adjacent fluid but possibly with isoechoic or hyperechoic synovial hypertrophy (see Fig. 3-38). With regard to tear extension to other tendons, a supraspinatus tear that extends posterior to the rotator interval beyond 2.5 cm involves the infraspinatus tendon.[2] In addition, imaging the cuff in short axis over the greater tuberosity facets assists in this determination because a tear that extends over the posterior aspect of the middle facet indicates infraspinatus involvement as well. A supraspinatus tendon tear may also extend anteriorly through

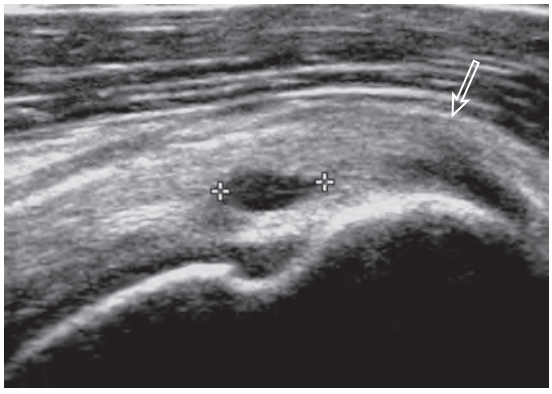

FIGURE 3-29 ■ Intrasubstance cyst. Ultrasound image of supraspinatus tendon in long axis shows an intrasubstance cyst *(between cursors)*. A rotator cuff tear was present (not shown) and connected this cyst to the articular surface (*open arrow*, subacromial-subdeltoid bursal thickening).

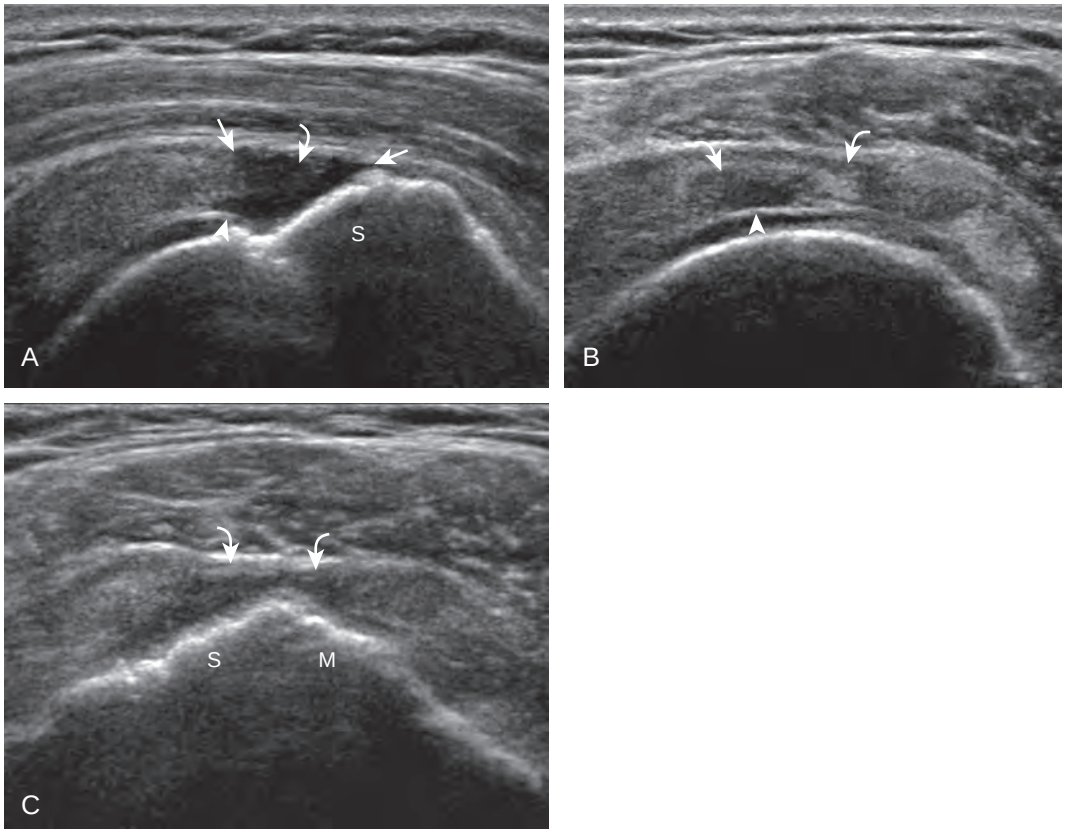

FIGURE 3-30 ■ Supraspinatus tear: full-thickness, focal, acute. Ultrasound images of supraspinatus in long axis **(A)** and short axis **(B** and **C)** show anechoic focal full-thickness tear *(curved arrows)*. Note broader bursal extent *(arrows)* and more focal articular extent with cartilage interface sign *(arrowheads)* as well as cortical irregularity. M, middle facet of greater tuberosity; S, superior facet.

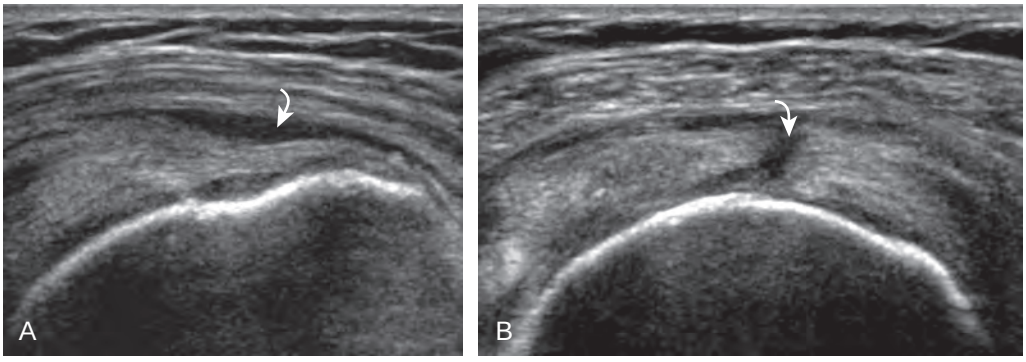

FIGURE 3-31 ■ Supraspinatus tear: full-thickness, focal, acute. Ultrasound images of supraspinatus in long axis **(A)** and short axis **(B)** show anechoic focal full-thickness longitudinal tear *(curved arrow)* best seen in short axis. Note difficulty in visualizing the tear in long axis given longitudinal orientation and narrow width.

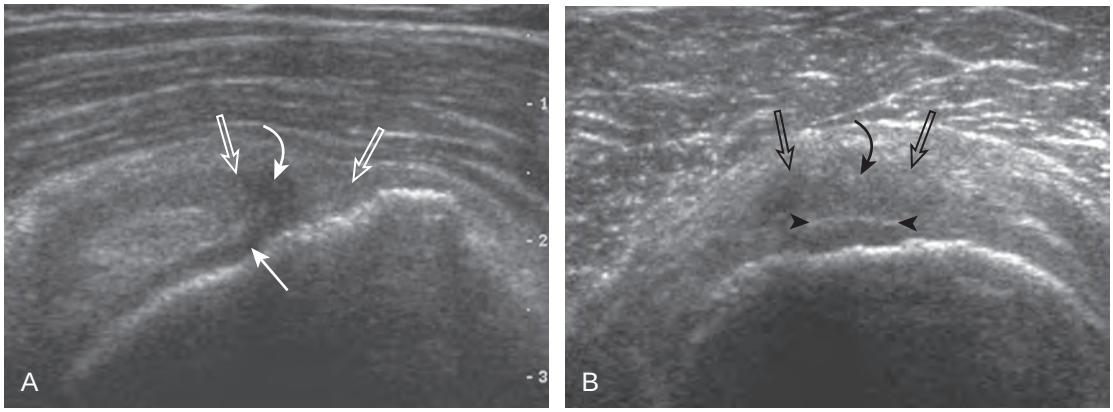

FIGURE 3-32 ■ Supraspinatus tear: full-thickness, focal. Ultrasound images of supraspinatus in long axis **(A)** and short axis **(B)** show hypoechoic disruption of the tendon fibers *(curved arrow)*, which extends from bursal *(open arrows)* to articular *(arrow)* surfaces. Note volume loss of the tendon distally, irregularity of the greater tuberosity, and a cartilage-interfaced sign *(arrowheads)* indicating articular extension.

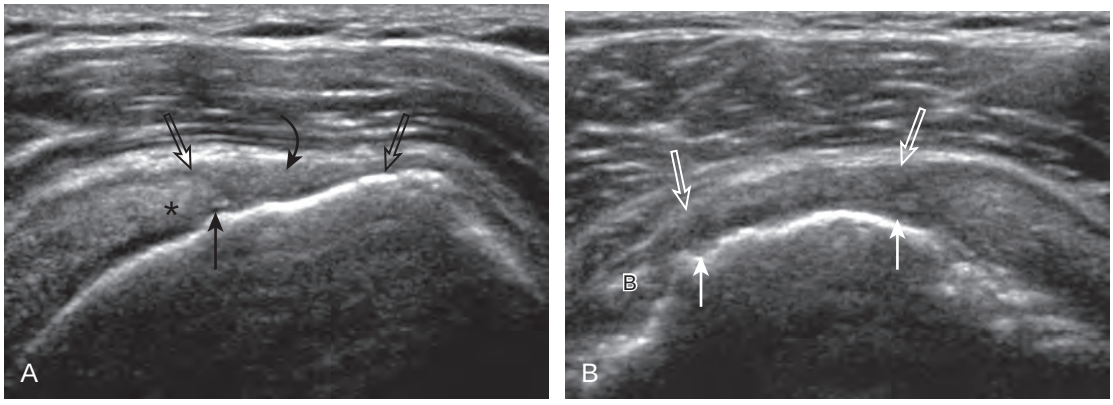

FIGURE 3-33 ■ Supraspinatus tear: full-thickness, near-complete, chronic. Ultrasound images of supraspinatus in long axis **(A)** and short axis **(B)** show a distal tear filled with isoechoic synovitis *(curved arrow)*. Note tendon retraction *(asterisk)*, bursal extent *(open arrows)*, and articular extent *(arrows)* with loss of normal superior convexity (B, intra-articular aspect of biceps tendon).

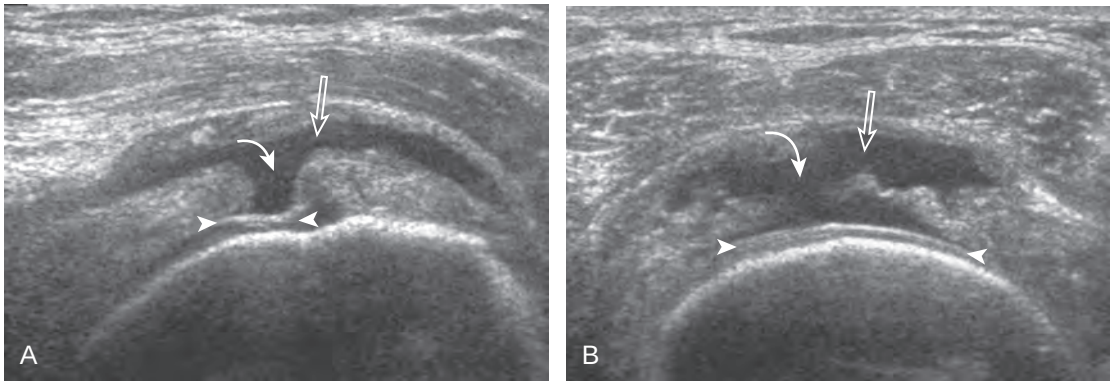

FIGURE 3-34 ■ Supraspinatus tear: full-thickness, complete, acute. Ultrasound images of supraspinatus in long axis **(A)** and short axis **(B)** show fluid-filled anechoic disruption of the tendon fibers *(curved arrows)*, which extends from the subacromial-subdeltoid bursa *(open arrows)* to the articular surface *(arrowheads)*. Note the cartilage interface sign *(arrowheads)*, which shows the articular extent of tear.

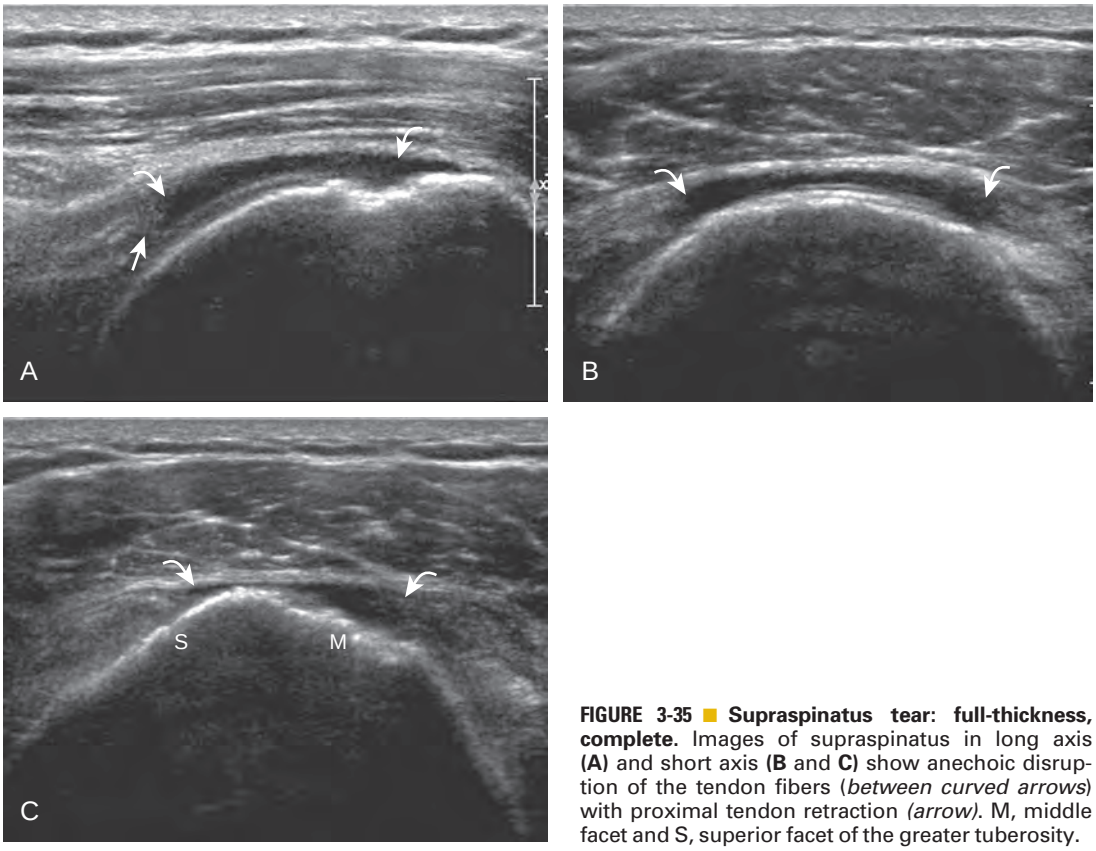

FIGURE 3-35 ■ Supraspinatus tear: full-thickness, complete. Images of supraspinatus in long axis **(A)** and short axis **(B** and **C)** show anechoic disruption of the tendon fibers (*between curved arrows*) with proximal tendon retraction *(arrow)*. M, middle facet and S, superior facet of the greater tuberosity.

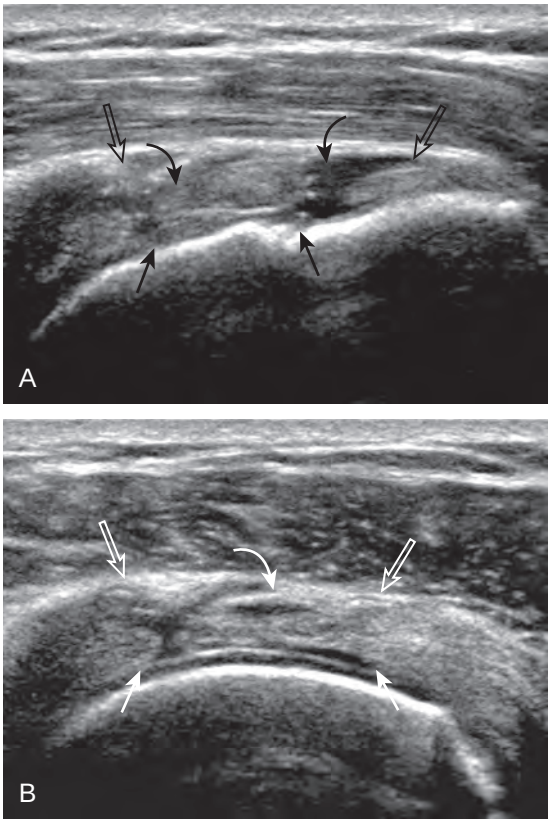

FIGURE 3-36 ■ Supraspinatus tear: full-thickness, complete. Ultrasound images of supraspinatus in long axis **(A)** and short axis **(B)** show anechoic and isoechoic heterogeneous disruption of the tendon fibers *(curved arrows)*. Note the bursal extent *(open arrows)*, articular extent with cartilage interface sign *(arrows)*, and loss of normal superior convexity.

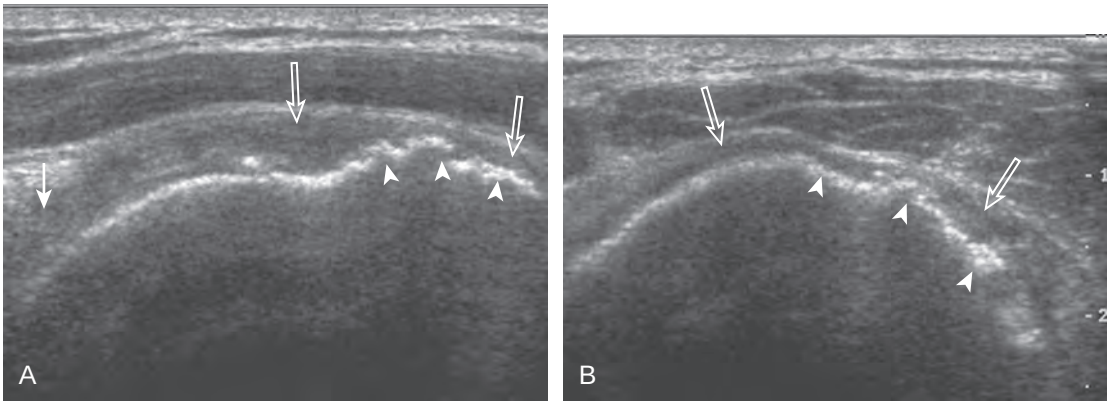

FIGURE 3-37 ■ Supraspinatus tear: full-thickness, complete, chronic. Ultrasound images of supraspinatus in long axis **(A)** and short axis **(B)** show a torn and retracted supraspinatus tendon tear, with the tendon void filled with hypoechoic synovium, hemorrhage, and scar tissue, in continuity with the subacromial-subdeltoid bursa *(open arrows)*. There is significant volume loss of the tendon substance as the torn tendon stump is retracted *(arrow)*. Note significant irregularity and remodeling of the greater tuberosity *(arrowheads)*. On the short axis image **(B)**, the anteroposterior extent greater than 2.5 cm indicates involvement of the infraspinatus tendon.

the rotator interval to involve the cephalad fibers of the subscapularis tendon (see Subscapularis Tears and Tendinosis). A bicep reflection pulley tear and long head of biceps brachii tendon subluxation or dislocation may also occur in this situation (Fig. 3-39) (Video 3-18).[12] It is also important to assess for supraspinatus and infraspinatus atrophy in the setting of a rotator cuff tear because this finding is associated with poor surgical outcome after repair (see Rotator Cuff Atrophy).[30]

Tendinosis

The term *tendinosis* (or *tendinopathy*) is used rather than tendinitis because there are no active inflammatory cells in this condition. This represents a degenerative process with eosinophilic, fibrillar, and mucoid degeneration and possible chondroid metaplasia.[31,32] At ultrasound, focal tendinosis is characterized by a heterogeneous, somewhat ill-defined, hypoechoic area in the tendon without a tendon defect (Fig. 3-40).[21,33] It is important to distinguish this abnormality from anisotropy because both may appear hypoechoic (see Fig. 3-12). Unlike tendon tear, tendinosis is usually less defined, it may be associated with tendon swelling, and it is usually not associated with adjacent cortical irregularity of the greater tuberosity. Diffuse tendinosis may cause the entire tendon to appear hypoechoic, equal in echogenicity to adjacent muscle (Fig. 3-41). Unlike a massive tendon tear, a normal convex superior surface of the supraspinatus is seen.

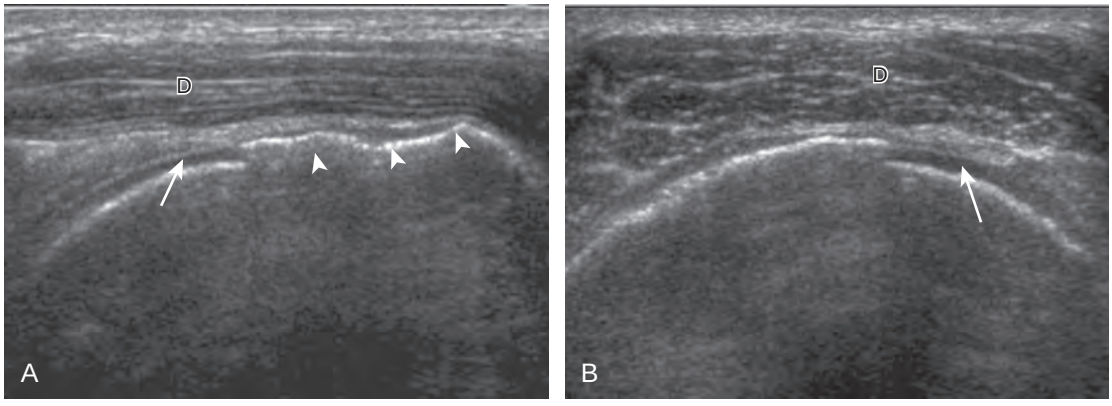

FIGURE 3-38 ■ Supraspinatus tear: full-thickness, complete, chronic. Ultrasound images of supraspinatus in long axis **(A)** and short axis **(B)** show absence of the supraspinatus tendon because it is retracted proximally beneath the acromion. A thin hyperechoic layer represents the collapsed subacromial-subdeltoid bursa, which lies between the deltoid muscle (D) and the hypoechoic hyaline cartilage *(arrow)*. Note significant remodeling of the greater tuberosity *(arrowheads)*.

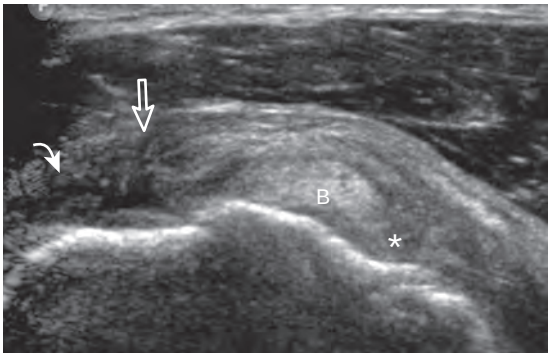

FIGURE 3-39 ■ Biceps reflection pulley tear and subluxation. Ultrasound image in short axis to proximal biceps brachii tendon shows tear of the anterior supraspinatus *(curved arrow)* and coracohumeral ligament *(open arrow)* with lateral subluxation of the biceps tendon (B) from its normal location *(asterisk)*.

Indirect Signs of Supraspinatus Tendon Tear

Tendon Thinning. Thinning or volume loss of the supraspinatus tendon and flattening or superior concavity of the superior supraspinatus tendon surface typically indicate tendon fiber loss. This condition can be seen with full-thickness tendon tears, especially moderate size or larger (see Figs. 3-33 and 3-38), and bursal-sided partial-thickness supraspinatus tendon tears (see Figs. 3-26 and 3-27). The presence of tendon thinning helps to exclude tendinosis because this latter condition, in contrast, shows normal tendon thickness or swelling (see Figs. 3-40 and 3-41) (Video 3-19).

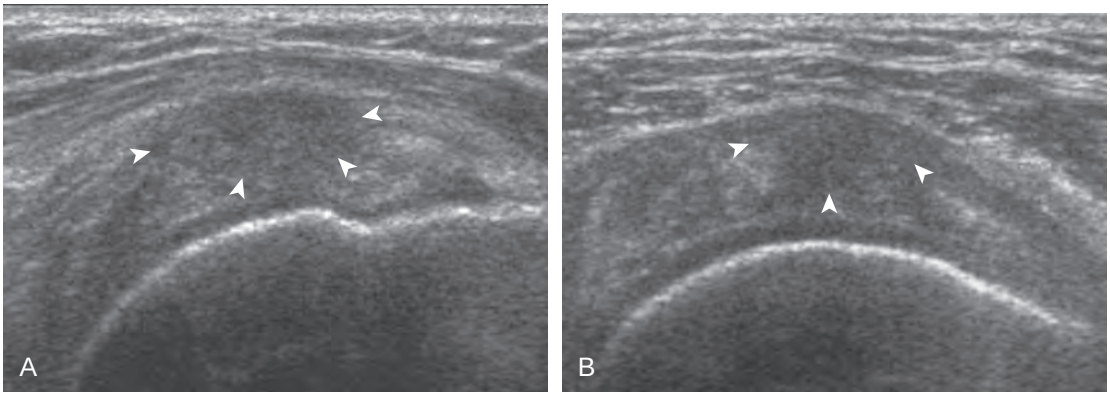

FIGURE 3-40 ■ Supraspinatus tendinosis: focal. Ultrasound images of supraspinatus in long axis **(A)** and short axis **(B)** show focal, ill-defined hypoechogenicity *(arrowheads)* with mild tendon swelling.

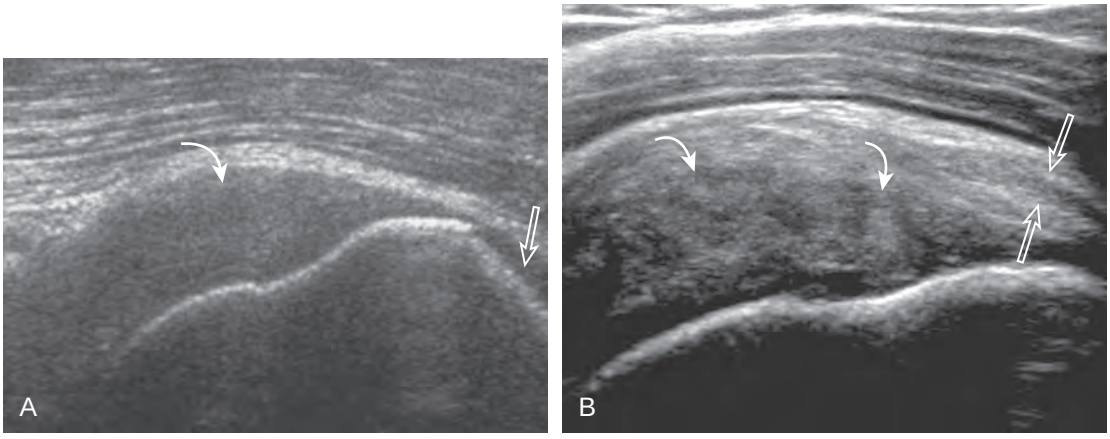

FIGURE 3-41 ■ Supraspinatus tendinosis: diffuse. A and **B,** Ultrasound images of supraspinatus tendon in long axis in two separate patients show diffuse and marked hypoechogenicity throughout the tendon *(curved arrows)* with loss of the normal fibrillar pattern. Note tendon swelling, smooth greater tuberosity, and subacromial-subdeltoid bursal thickening *(open arrows)*.

Cortical Irregularity. When there is cortical irregularity of the greater tuberosity immediately adjacent to a defined hypoechoic or anechoic tendon abnormality of the supraspinatus, this increases the likelihood that the tendon abnormality represents a tear (see Figs. 3-21 and 3-22).[21,22] This finding is most helpful in the differentiation between tendon tear and tendinosis because both may appear as a hypoechoic tendon abnormality. With tendinosis, the hyperechoic greater tuberosity surface is typically smooth, as in the normal state (see Fig. 3-41). Cortical irregularity is common with chronic attrition tears of the supraspinatus, and it may be absent with an acute tendon tear in a younger individual or with proximal tears (see Fig. 3-34). The significance of greater tuberosity cortical irregularity is specific to the attachment of the supraspinatus tendon. Cortical irregularity of the posterior aspect of the greater tuberosity involving the bare area (an area of intra-articular cortex without hyaline cartilage) beneath the infraspinatus tendon is a common finding, possibly a normal variant, and is usually without significance.[34] However, if cortical irregularity at this site is extensive, this too can be associated with articular surface partial-thickness infraspinatus tendon tear and posterior labral tear in the setting of posterosuperior impingement syndrome.[35] Finally, cortical irregularity of the lesser tuberosity of the subscapularis tendon insertion is also a common finding and is of little clinical significance in the absence of an adjacent tendon abnormality.

Joint Effusion and Bursal Fluid. Investigators have shown that the findings of both glenohumeral joint effusion and subacromial-subdeltoid fluid suggest rotator cuff tear with a positive predictive value of 95%.[36] To diagnose joint effusion, the long head of the biceps brachii tendon is evaluated in the bicipital groove for anechoic fluid (Fig. 3-42). The long head of the biceps brachii tendon sheath normally communicates with the glenohumeral joint, so increased joint fluid will collect in this dependent extension of the joint. A tiny sliver of fluid at one side of the biceps tendon is often seen normally, but fluid greater than this is considered abnormal, especially if it is seen circumferential to the biceps tendon. With regard to the posterior glenohumeral joint recess, small effusions may only be visible with the shoulder in external rotation (Video 3-20). With larger joint effusions, fluid in the posterior shoulder joint recess can be seen even in neutral position deep to the infraspinatus tendon (Fig. 3-43). Subacromial-subdeltoid bursal fluid is diagnosed when the hyperechoic walls of the bursa are separated by more than 1 or 2 mm of anechoic fluid.[37] Both joint fluid surrounding the biceps brachii long head tendon and distention of the subacromial-subdeltoid bursa may be seen over the anterior shoulder (Fig. 3-44) (Video 3-21). Bursal fluid may also collect dependently, so it is important to evaluate the most inferior aspect of the bursa to visualize small quantities of fluid (see Fig. 3-16C) (Video 3-22). Although simple joint and bursal fluid is commonly anechoic, complex fluid may appear hypoechoic or even isoechoic to adjacent muscle tissue.

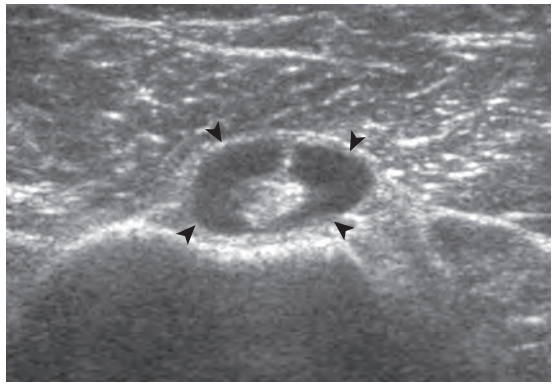

FIGURE 3-42 ■ Joint effusion: biceps tendon sheath communication. Ultrasound image of biceps brachii long head tendon in short axis at bicipital groove shows anechoic joint fluid *(arrowheads)*, which distends the tendon sheath.

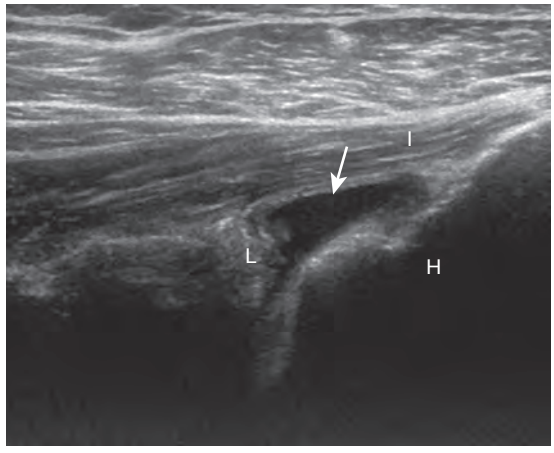

FIGURE 3-43 ■ Joint effusion: posterior glenohumeral recess. Ultrasound image of posterior shoulder and infraspinatus (I) in long axis shows anechoic joint fluid *(arrow)* between the posterior labrum (L) and the humeral head (H).

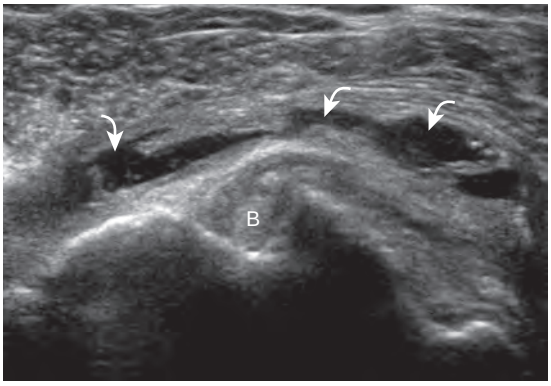

FIGURE 3-44 ■ Subacromial-subdeltoid fluid. Ultrasound image in short axis to the biceps brachii tendon shows a distention of the subacromial-subdeltoid bursa *(curved arrows)* filled with anechoic fluid and heterogeneous synovial hypertrophy. B, biceps brachii long head tendon.

Cartilage Interface Sign. Normally, the surface of the hypoechoic hyaline cartilage that covers the humeral head is hyperechoic when the sound beam is perpendicular to the cartilage and underlying bone cortex. When an adjacent tendon is abnormally hypoechoic, or especially if there is adjacent anechoic fluid, this hyperechoic interface becomes more pronounced and is termed the *cartilage interface sign*.[27] The presence of this sign is helpful in that it indicates a tendon abnormality does extend to the articular surface (see Fig. 3-23) (Video 3-23). This sign may be seen with a hypoechoic tendon abnormality, but it is most striking in the presence of an anechoic fluid-filled tendon tear (see Fig. 3-30).

Infraspinatus Tears and Tendinosis

Similar to the supraspinatus tendon, tears of the infraspinatus tendon may be partial-thickness tears (extending only to the articular or bursal surface, or intrasubstance and not in contact with either the articular or bursal surface) or full-thickness tears (that extend from the bursal to the articular surface) (Fig. 3-45). Tendon tears can appear hypoechoic or anechoic with possible tendon thinning, whereas tendinosis is typically hypoechoic with tendon swelling (Fig. 3-46). Partial-thickness articular-side tears of the infraspinatus have been described in the setting of internal or posterosuperior impingement syndrome.[35] This syndrome relates to impingement between the posterior aspect of the humerus and glenoid when the shoulder is externally rotated and abducted to 90 degrees, thus causing posterosuperior labral tear, marked cortical irregularity of the posterior aspect of the greater tuberosity, and partial-thickness articular infraspinatus tendon tear. Unlike the cortical irregularity of the superior aspect of the greater tuberosity associated with supraspinatus tendon tears, some degree of cortical irregularity of the posterior aspect of the greater tuberosity in the bare area devoid of cartilage is considered a variation of normal.[34] When this irregularity is marked and associated with infraspinatus and adjacent labral disorders, posterosuperior impingement syndrome should be considered. Full-thickness tears of the infraspinatus tendon usually represent posterior extension of a supraspinatus tendon tear and are uncommonly isolated. An infraspinatus tear is present when a supraspinatus tear extends greater

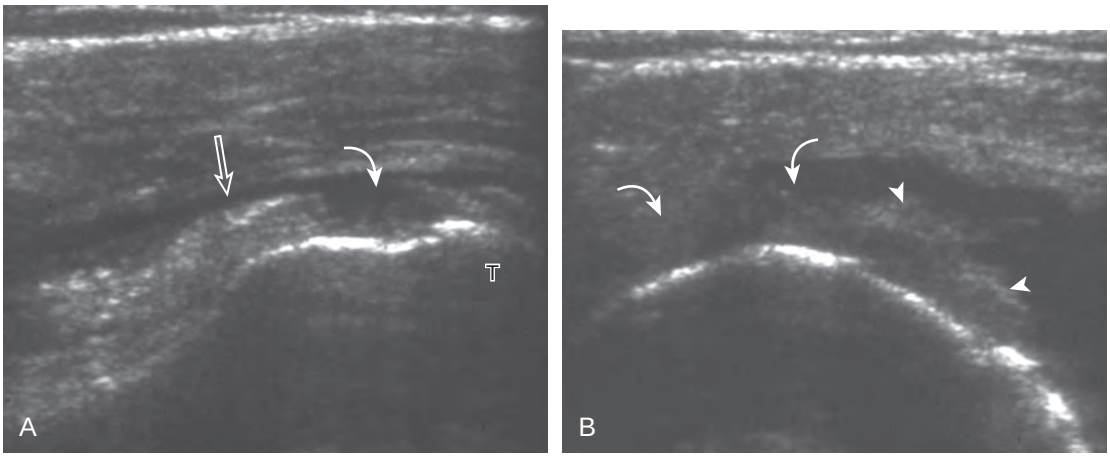

FIGURE 3-45 ■ Infraspinatus tear: full-thickness. Ultrasound images of infraspinatus tendon in long axis **(A)** and short axis **(B)** show disruption of the tendon fibers *(curved arrows)* with fluid-filled subacromial-subdeltoid bursa *(open arrow)* (left side of image is proximal relative to tendon). Note the intact teres minor tendon *(arrowheads)* (left side of image is cephalad in **B**). T, greater tuberosity.

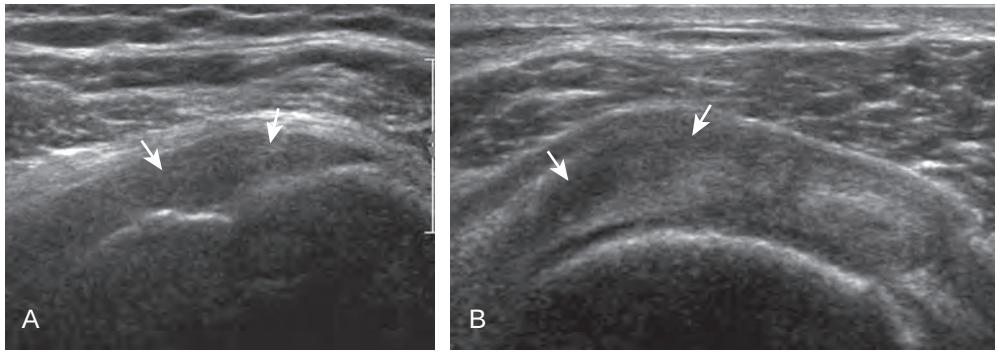

FIGURE 3-46 ■ Infraspinatus: tendinosis. Ultrasound images long axis **(A)** and short axis **(B)** to infraspinatus shows diffuse hypoechoic swelling *(arrows)*.

than 2.5 cm posterior to the intra-articular portion of the long head of the biceps brachii tendon or if the tear is visible over the posterior aspect of the greater tuberosity middle facet (see Fig. 3-37B). When the entire width of the infraspinatus tendon is torn and retracted, this represents a complete full-thickness tear.

Subscapularis Tears and Tendinosis

Similar to infraspinatus tendon tears, isolated tears of the subscapularis tendon are uncommon.[38,39] Isolated full-thickness, complete, or full-width tears appear as complete tendon discontinuity, usually at the lesser tuberosity attachment (Fig. 3-47). Significant tendon retraction is common, and this becomes more obvious with the shoulder positioned in external rotation (Video 3-24). If a fragment of bone is avulsed, this will appear as hyperechoic and shadowing, attached to the subscapularis tendon (Fig. 3-48). The biceps brachii long head tendon may be dislocated into the glenohumeral joint with full-thickness subscapularis tendon tear. More commonly, subscapularis tears are isolated to the cephalad aspect in association with an anterior supraspinatus tendon (Fig. 3-49).[39] A subscapularis tear that extends from the bursal to articular surface that is isolated to the superior aspect would still be described as a focal or incomplete full-thickness tear. In this setting, the long head of the biceps brachii tendon may be dislocated over the lesser tuberosity or into the substance of the subscapularis tendon at the site of the tear (see Biceps Tendon, Subluxation and Dislocation). Tendinosis may also involve the subscapularis, which appears as heterogeneous abnormal hypoechogenicity and possible tendon swelling (Fig. 3-50).

Rotator Cuff Atrophy

In the setting of a rotator cuff tear, the supraspinatus and infraspinatus may undergo fatty

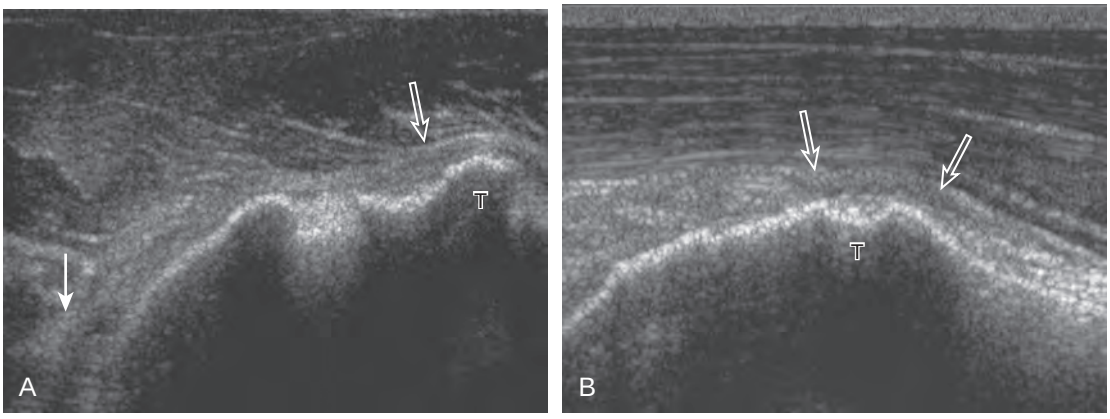

FIGURE 3-47 ■ Subscapularis tear: full-thickness, complete. Ultrasound images of subscapularis tendon in long axis **(A)** and short axis **(B)** show absence of the tendon *(open arrows)* at the lesser tuberosity (T) with proximal retraction *(arrow)* (left side of image is proximal in **A** and cephalad in **B**).

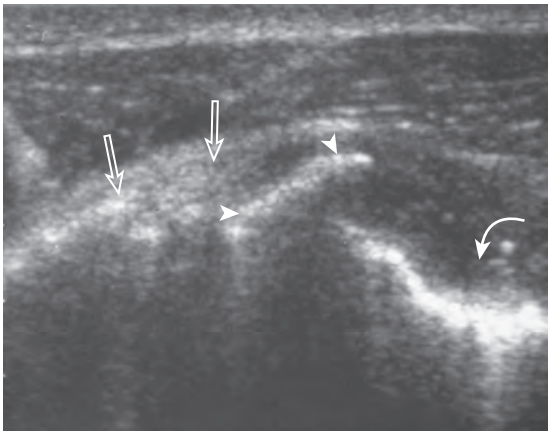

FIGURE 3-48 ■ Subscapularis tendon avulsion. Ultrasound image of subscapularis tendon in long axis shows the avulsed and displaced lesser tuberosity fragment *(arrowheads)*. Note the subscapularis tendon *(open arrows)* attached to bone fragment and the fracture donor site of the proximal humerus *(curved arrow)* (left side of image is proximal relative to the subscapularis).

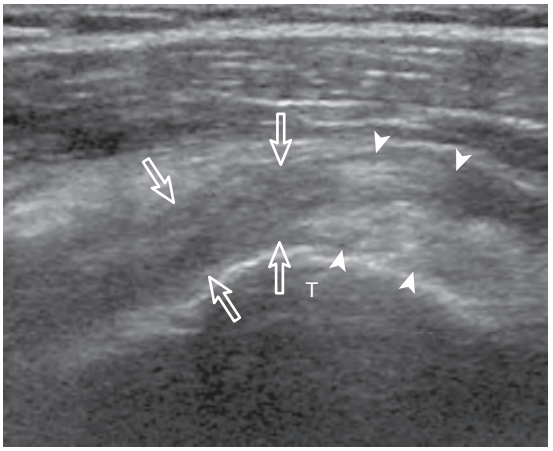

FIGURE 3-49 ■ Subscapularis tear: full-thickness, incomplete or focal. Ultrasound image of subscapularis tendon in short axis shows the absence of the cephalad portion of the tendon *(open arrows)*. Note the intact caudal fibers *(arrowheads)* at the lesser tuberosity (T) (left side of image is cephalad).

degeneration or infiltration and possible atrophy.[40] This is important information because the presence of both fatty infiltration and muscle atrophy is a negative prognostic factor when considering rotator cuff repair.[41] The degree of rotator cuff atrophy relates to size (and therefore retraction and likely chronicity) and location (most are anterior) of the rotator cuff tear.[20,41] Isolated or more pronounced atrophy of the infraspinatus muscle is also possible, even if the large or chronic rotator cuff tear is limited to the supraspinatus, possibly because of compromised suprascapular nerve from altered biomechanics.[30] The subscapularis and teres minor are usually unaffected. Paralabral cyst formation from a labral tear is another potential cause of both supraspinatus and infraspinatus muscle denervation when located in the suprascapular notch, or isolated to the infraspinatus when located in the spinoglenoid notch.

At ultrasound, fatty degeneration or infiltration and muscle atrophy will appear as increased echogenicity of the muscle and resultant poor differentiation between the tendon and muscle.[30] The hyperechoic tendon may appear relatively enlarged with ill-defined borders in the setting of fatty infiltration, best appreciated at the musculotendinous junction in short axis. Fatty atrophy will also result in decreased muscle bulk.[40] Imaging of the involved muscle in short axis is especially helpful in identifying decreased muscle size. One landmark when imaging the infraspinatus for atrophy is the posterior scapular cortex at the level of the musculotendinous junction, where a ridge is typically seen separating the minimal

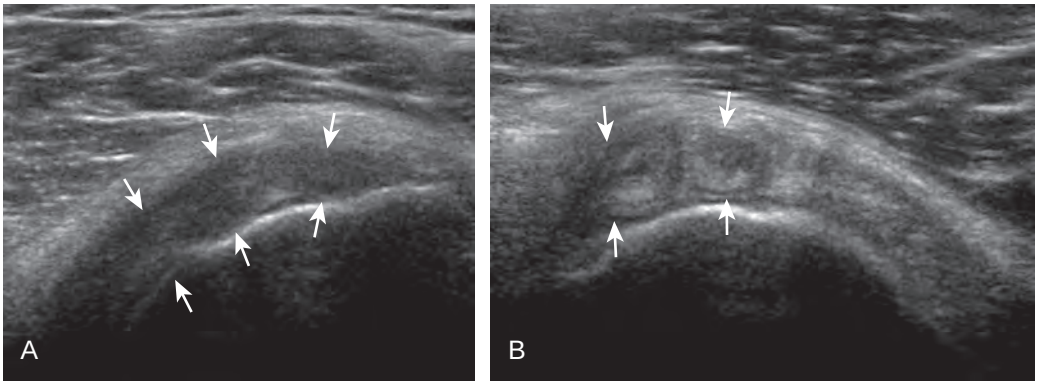

FIGURE 3-50 ■ Subscapularis tear: tendinosis. Ultrasound images of subscapularis tendon in long axis **(A)** and short axis **(B)** show hypoechoic swelling of the cephalad portion of the subscapularis tendon *(arrows)*.

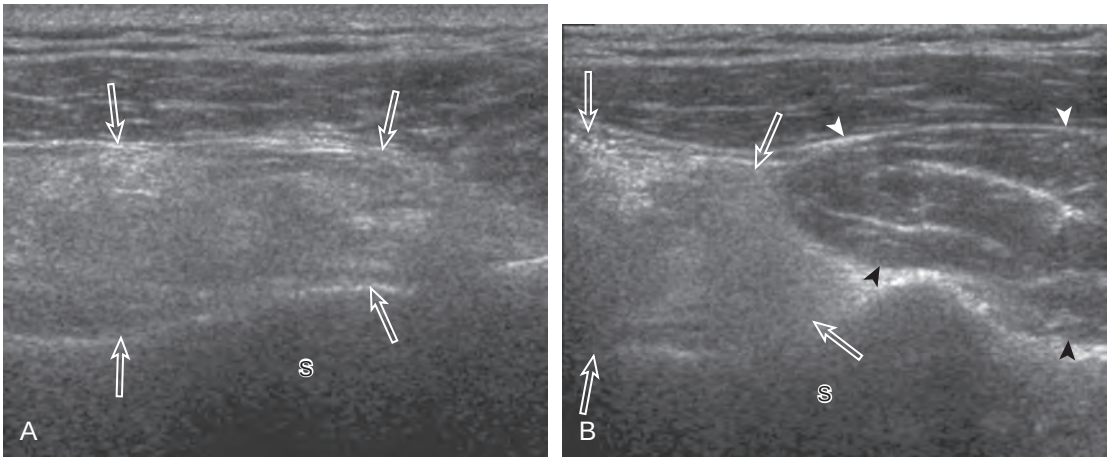

FIGURE 3-51 ■ Infraspinatus atrophy. Ultrasound images of infraspinatus in long axis **(A)** and short axis **(B)** show decreased size and increased echogenicity of the infraspinatus muscle *(open arrows)*, which becomes more apparent when compared with the teres minor *(arrowheads)*. S, scapula.

concavities of the scapula, which help to define the infraspinatus and adjacent teres minor muscles. This site is useful in that the infraspinatus muscle is usually about twice the area compared with the adjacent teres minor. In addition, the echogenicity of the infraspinatus muscle can be compared with the teres minor, which is routinely normal even in the setting of a rotator cuff tear. Infraspinatus atrophy is diagnosed when the muscle echogenicity is greater than the teres minor and the size is less than twice the area (Fig. 3-51). The supraspinatus should also be assessed for atrophy by moving the transducer superiorly from the infraspinatus between the clavicle and scapular spine.[40] Extended field of view imaging may be helpful to demonstrate both supraspinatus and infraspinatus muscle atrophy compared with the teres minor on one image (Fig. 3-52).[19] Muscle echogenicity should not be compared with the overlying deltoid because this muscle is commonly echogenic in older individuals.

Teres minor atrophy may be seen in up to 3% of shoulders, which will appear as increased echogenicity and possible decreased muscle size compared with the infraspinatus.[42] This finding is often asymptomatic and may be due to the presence of a fibrous band or variation in teres minor innervation that predisposes to nerve compression.[42-44] Uncommonly, teres minor atrophy may relate to quadrilateral space syndrome. The quadrilateral space is defined by the borders of the humerus, the long head of the triceps muscle, and the teres minor and teres

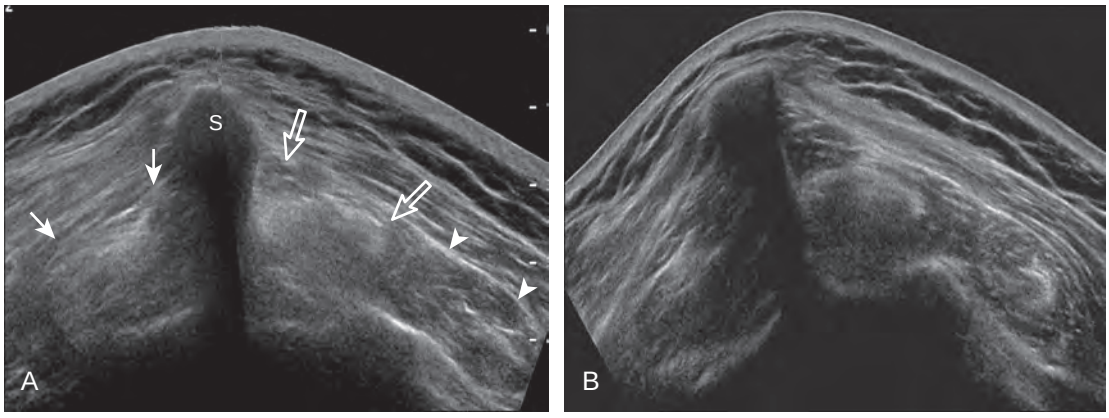

FIGURE 3-52 ■ Infraspinatus and supraspinatus fatty infiltration. Extended field of view ultrasound image **(A)** shows increased echogenicity of the supraspinatus *(arrows)* and infraspinatus *(open arrows)*, especially surrounding the tendons, compared with teres minor *(arrowheads)* and contralateral side **(B)**. S, scapular spine.

major tendons. The axillary nerve and posterior circumflex humeral artery and veins traverse this space, and compression of these structures by fibrous bands, adjacent paralabral cyst, or mass may result in quadrilateral space syndrome.[45] At sonography, the teres minor or deltoid muscle, or both, may appear hyperechoic and small as a result of atrophy (Fig. 3-53).[46] To diagnose subtle abnormalities in size and echogenicity, it is helpful to make comparisons with the contralateral side or to compare the teres minor with the adjacent infraspinatus at the level of the muscle belly because normally the infraspinatus is about twice the size of the teres minor at this level.

Postoperative Shoulder

Evaluation of the rotator cuff after surgery can be challenging; however, ultrasound has been shown to be effective in the evaluation of the postoperative cuff with 89% accuracy.[47] One must be familiar with the types of rotator cuff repairs and aware of the appearances of the repaired and intact rotator cuff. For repair of a rotator cuff tear, a low-grade partial-thickness tear is commonly débrided, whereas a high-grade partial-thickness tear is converted to a full-thickness tear and repaired. Transosseous suture or suture anchors may be used, with the latter being single, multiple, single row, or double row.[48] After rotator cuff repair, the tendon may appear thin and heterogeneous, whereas at other times, the tendon may be thickened and heterogeneously hypoechoic (Figs. 3-54, 3-55, and 3-56).[49-51] The general trend is for the repaired cuff to become more homogenous and hyperechoic over time, with a normal-appearing cuff present by 9 to 12 months. Hyperechoic suture material and suture anchors may be seen, as may the implantation trough, which appears as an angulated contour defect at the greater tuberosity (see Fig. 3-56A). Because suture may cause shadowing of the underlying tendon that may simulate a tendon defect, imaging the cuff in short axis is helpful to show that the anechoic area is narrow and corresponds to the area directly under a suture, which is unlike a rotator cuff defect. If the repaired tendon is attached by suture passing through drill holes in the greater tuberosity, then suture may be seen at the lateral aspect of the greater tuberosity as well. A hyperechoic focus attached to bone with reverberation can be seen with a metallic suture anchor. The area of the subacromial-subdeltoid bursa is commonly hypoechoic and thickened, and many times this bursa has been débrided or resected. Bone irregularity of the acromion could indicate changes related to acromioplasty.

To diagnose recurrent rotator cuff tear after repair, the most important finding is visualization of a tendon defect (Figs. 3-57 and 3-58).[49-51] Compressibility of the anechoic or hypoechoic tendon abnormality helps to differentiate tear from postoperative changes. Most recurrent rotator cuff tears are large or become large, with at least moderate retraction. Identification of retracted suture that is not continuous with the implantation site is additional evidence for a recurrent tear. Another feature of a recurrent cuff is visible suture without surrounding rotator cuff tendon (see Fig. 3-58C and D). Be aware that the many tendon defects are asymptomatic, although larger defects tend to have symptoms. An equivocal ultrasound finding, especially within the first 6 to 9 months, should be reimaged after several weeks or months because such findings may improve over time, whereas a true tear often enlarges.

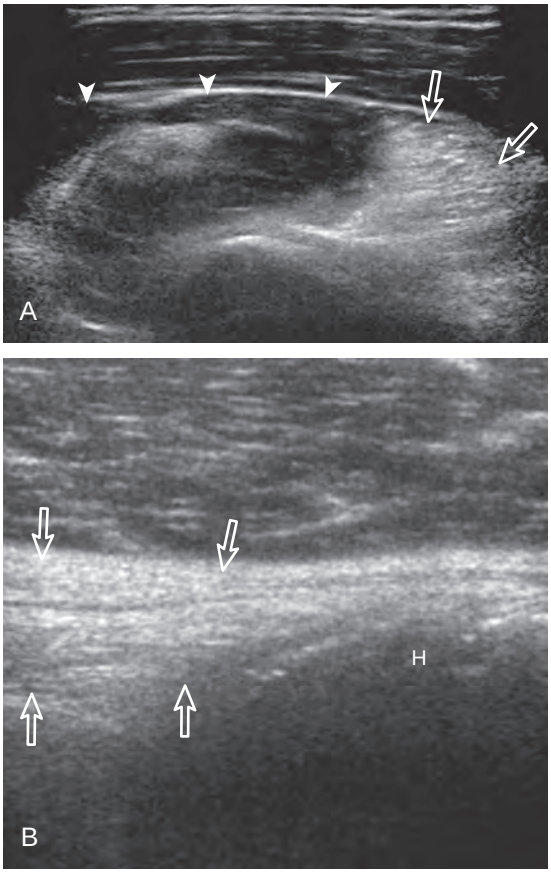

FIGURE 3-53 ■ Teres minor atrophy. Ultrasound images of teres minor in short axis **(A)** and long axis **(B)** show increased echogenicity and decreased size *(open arrows)*. Note the normal appearance of the infraspinatus *(arrowheads)*. H, humerus.

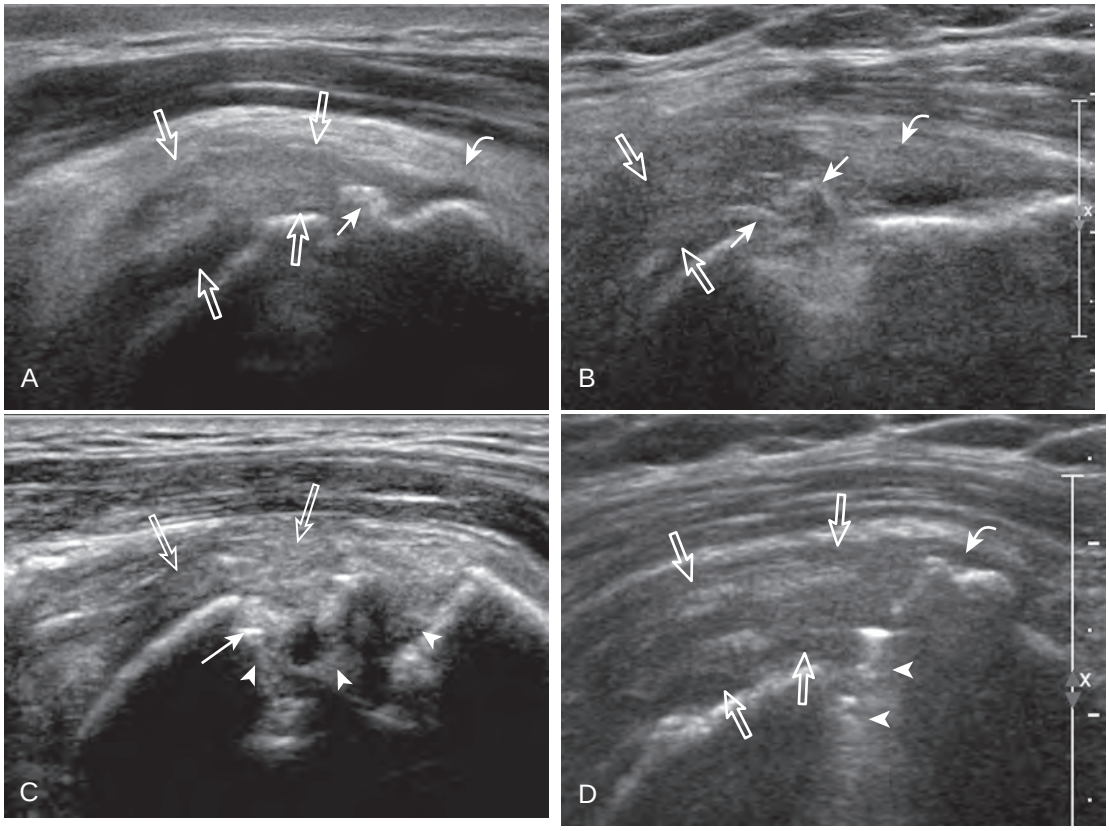

FIGURE 3-54 ■ Postoperative rotator cuff: no recurrent tear. Ultrasound images **(A** to **D)** of supraspinatus tendon in long axis from four patients show variable appearance of repaired and intact supraspinatus tendon *(open arrows)*. Note suture material *(arrows)*, implantation trough *(arrowheads)*, and soft tissue thickening at the site of subacromial-subdeltoid bursa resection *(curved arrow)*. Echogenic metal suture anchor with reverberation artifact is seen in (D) *(arrowheads)*.

Shoulder arthroplasty or joint replacement involves resection of the humeral head, placement of a metal component, and possibly resection and replacement of the glenoid surface.[48] With a conventional shoulder arthroplasty, the greater tuberosity is not resected, so the rotator cuff can be seen with ultrasound attaching normally to the humerus using routine bone landmarks. This is unlike a reverse total shoulder arthroplasty, used when there is an underlying rotator cuff tear before surgery and the tuberosities are resected. At ultrasound, the metal humeral

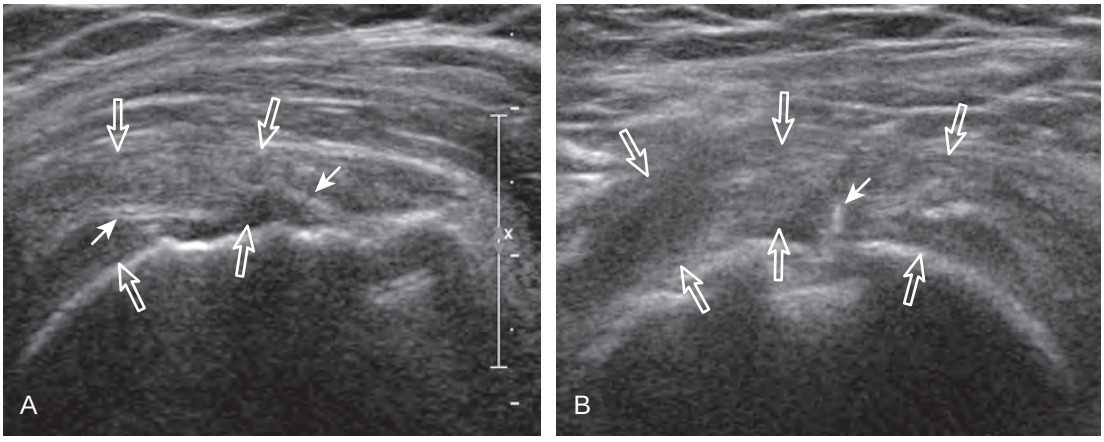

FIGURE 3-55 ■ Postoperative rotator cuff: no recurrent tear. Ultrasound images of supraspinatus tendon in long axis **(A)** and short axis **(B)** show a heterogeneous and appearance *(open arrows)* and a hyperechoic suture *(arrow)*.

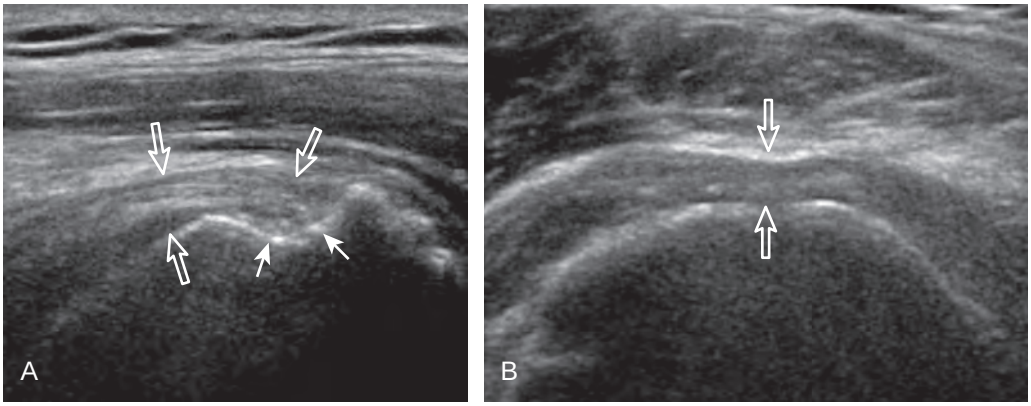

FIGURE 3-56 ■ Postoperative rotator cuff: no recurrent tear. Ultrasound images of supraspinatus tendon in long axis **(A)** and short axis **(B)** show tendon thinning with superior concavity *(open arrows)* and implantation trough *(arrows)*.

component appears hyperechoic and smooth, with reverberation artifact, in the expected location of the humeral head (Fig. 3-59).[52,53] The normal rotator cuff should be identified over the humeral surface attaching to the tuberosities, and therefore tendon discontinuity or nonvisualization similar to the native shoulder is consistent with rotator cuff tear (Fig. 3-60). Ultrasound is ideal in evaluation of the rotator cuff after shoulder arthroplasty because artifact from the joint replacement occurs deep to the components, and the overlying rotator cuff region is easily visualized.

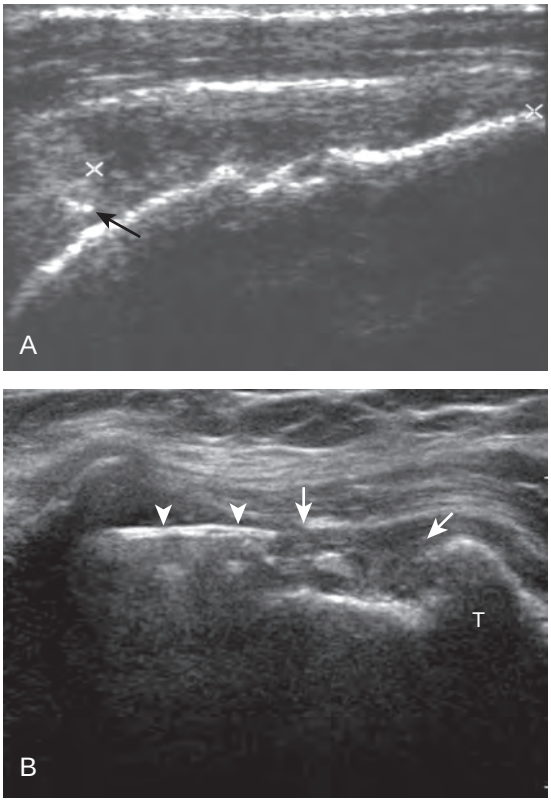

FIGURE 3-57 ■ Postoperative rotator cuff: recurrent tear. Ultrasound image of supraspinatus tendon (long axis) **(A)** shows a large tendon defect *(between cursors)*. Note the hyperechoic suture within the retracted proximal stump *(arrow)*. Ultrasound image of supraspinatus (long axis) in a second patient **(B)** shows a recurrent tear *(arrows)* with displaced suture anchor *(arrowheads)*. T, greater tuberosity.

Calcific Tendinosis

Calcific deposits occur in the rotator cuff primarily as calcium hydroxyapatite deposition, possibly from decreased oxygen tension and fibrocartilaginous metaplasia.[54] The underlying rotator cuff is typically intact. While the supraspinatus is most commonly involved, other rotator cuff tendon involvement is not unusual. The calcific deposits most commonly are hyperechoic with posterior acoustic shadowing (Video 3-25), although appearances may vary (Fig. 3-61). Small calcifications may be linear along the axis of the tendon fibers (see Fig. 3-61A and B) (Video 3-26), whereas others have an amorphous appearance or are globular with minimal or no shadowing (see Fig. 3-61C, D, and E). Cortical erosions and osseous involvement may also be present (see Fig. 3-61F).[55] In approximately 7% of cases, tendon calcification shadowing is absent, and radiographs may be normal if calcifications are in the form of a thick fluid or slurry.[56] When calcific deposit echogenicity is isoechoic to tendon without shadowing, the amorphous echotexture during real-time scanning can be identified, and this replaces the normal fibrillar tendon appearance (Video 3-27). An additional method to help in this distinction is the use of anisotropy. With angulation of the transducer so that the sound beam is not perpendicular to the tendon fibers, the adjacent tendon will appear artifactually hypoechoic

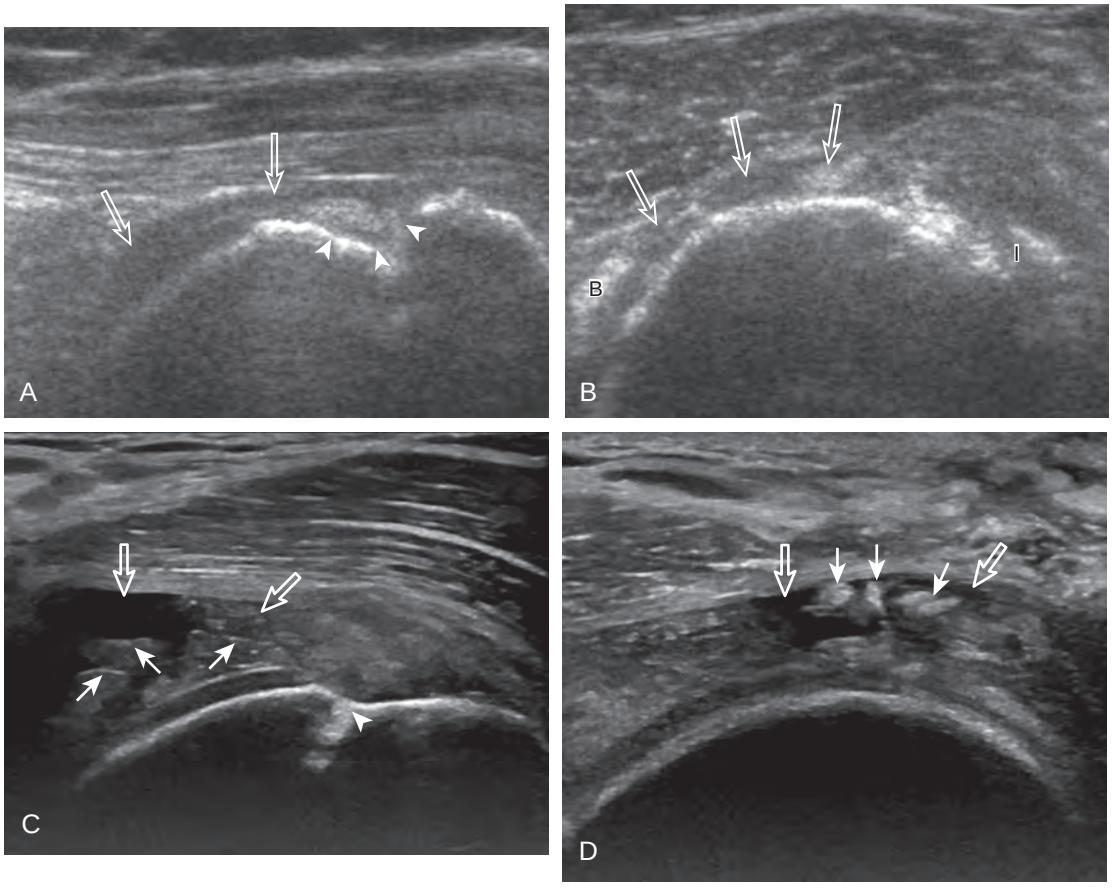

FIGURE 3-58 ■ Postoperative rotator cuff: recurrent tear. Ultrasound images of supraspinatus in long axis **(A)** and short axis **(B)** show absence of the anterior portion of the supraspinatus *(open arrows)*. Note the tendon stump in the implantation trough *(arrowheads)*. Ultrasound images of supraspinatus in long axis **(C)** and short axis **(D)** in a second patient show a proximal tendon tear *(open arrows)* with exposed suture *(arrows)*. Note suture anchor *(arrowhead)*. B, biceps; I, infraspinatus.

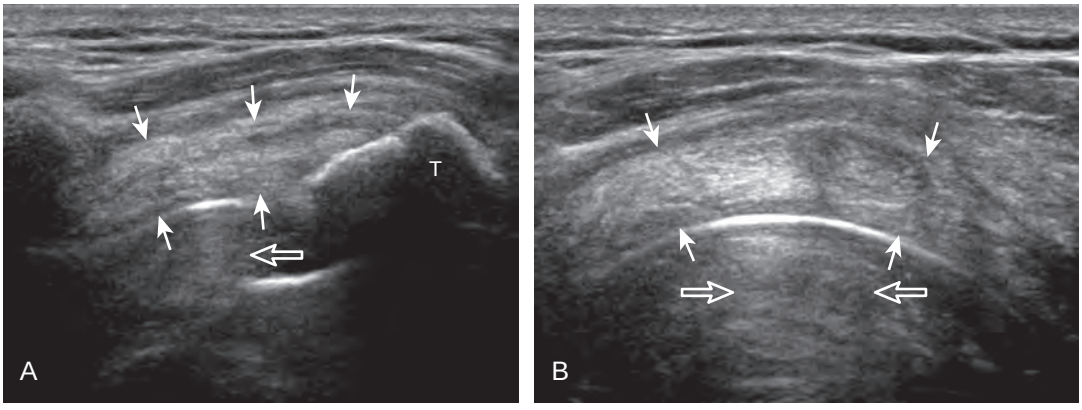

FIGURE 3-59 ■ Rotator cuff after shoulder arthroplasty. Ultrasound images of supraspinatus in long axis **(A)** and short axis **(B)** show intact rotator cuff *(arrows)* at the greater tuberosity (T). Note posterior reverberation artifact *(open arrow)* deep to the arthroplasty. (From Jacobson JA, Miller B, Bedi A, Morag Y: Imaging of the postoperative shoulder. *Semin Musculoskelet Radiol* 15:320-339, 2011.)

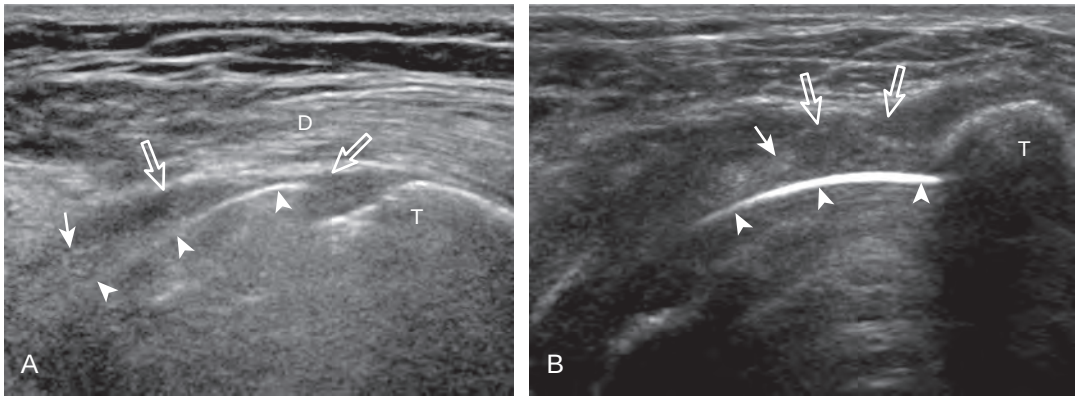

FIGURE 3-60 ■ Rotator cuff tear after shoulder arthroplasty. Ultrasound images of the supraspinatus in long axis in two patients **(A** and **B)** show absence of the tendon *(open arrows)* over the humeral head component of the shoulder arthroplasty *(arrowheads)* and the retracted tendon stump *(arrows)*. The humeral head is high riding and in contact with the deltoid muscle (D). Note posterior reverberation artifact deep to the arthroplasty T, greater tuberosity.

(Fig. 3-62) (see Video 3-27). This does not significantly change the appearance of the calcifications; therefore, the hyperechoic calcific deposits become more conspicuous when they are surrounded by the hypoechoic tendon. Calcifications may be multiple in one or many tendons. In addition, large calcifications may contact the acromion during arm elevation as a form of impingement (Video 3-28).

Calcifications that are amorphous without shadowing are associated with acute symptoms, whereas well-defined calcifications with shadowing are associated with subacute or chronic symptoms.[57] Larger calcifications associated with an abnormal subacromial-subdeltoid bursa are also more likely symptomatic.[58] Increased flow on color and power Doppler imaging around the calcifications may be evident, a finding that correlates with patients' symptoms and a higher likelihood of the resorptive phase (Fig. 3-63).[57] Calcifications may be identified at the bursal edge of the involved tendon with possible extension into the subacromial-subdeltoid bursa (see Subacromial-Subdeltoid Bursa). Ultrasound-guided percutaneous lavage and aspiration of the calcifications have been shown to be effective and improve symptoms, although clinical outcome at 5 and 10 years may be similar regardless of treatment (see Chapter 9).[54]

Impingement Syndrome

Of the rotator cuff tendons, the supraspinatus is prone to impingement. This is because the supraspinatus passes through a confined space between the scapula and the coracoacromial arch, which consists of the acromion, the distal clavicle, the acromioclavicular joint, the coracoid process, and the coracoacromial ligament. The subacromial-subdeltoid bursa also traverses this space over the supraspinatus tendon. Any abnormality that decreases the size of this space, such as an inferior acromioclavicular osteophyte or subacromial enthesophyte, can predispose to tendon impingement. The effect on the supraspinatus tendon is that of tendinosis and possible tear, whereas the overlying subacromial-subdeltoid bursa may be thickened with fluid or synovial hypertrophy. Sonography can suggest the diagnosis of early subacromial impingement when the gradual pooling of subacromial-subdeltoid bursal fluid at the acromion tip during active arm elevation is present (Fig. 3-64) (Video 3-29).[17] This sign is most important when other causes of bursal fluid are excluded, such as primary inflammatory bursitis. For diagnosis of subacromial impingement, the shoulder is dynamically assessed with the transducer in the coronal-oblique plane showing the bone landmarks of the acromion and the greater tuberosity (see Fig. 3-17). Sliding the transducer anterior to the acromion may show bursal thickening beneath or adjacent to the coracoacromial ligament not visible at the level of the acromion because of shadowing (see Fig. 3-64C) (Video 3-30). A subacromial enthesophyte spur may also be seen at the acromion attachment of the coracoacromial ligament, which points anterior and medial from the acromion toward the coracoid process (Fig. 3-65). In addition to pooling of fluid, other findings of subacromial impingement include gradual distention of the subacromial-subdeltoid bursa with synovial tissue or snapping of a thickened bursa (Video 3-31). Another finding described with subacromial impingement is superior bulging of the coracoacromial ligament when imaging the supraspinatus

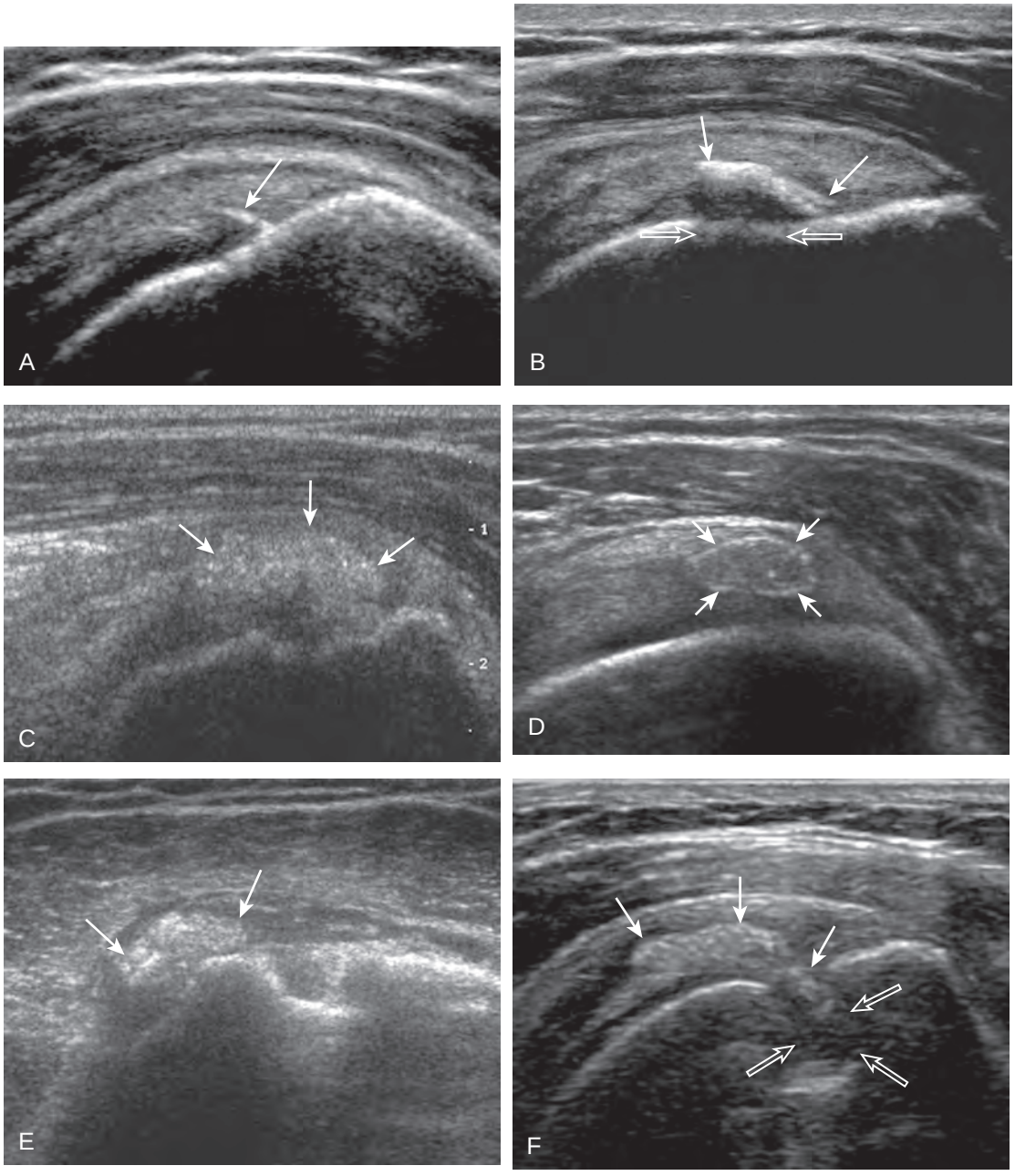

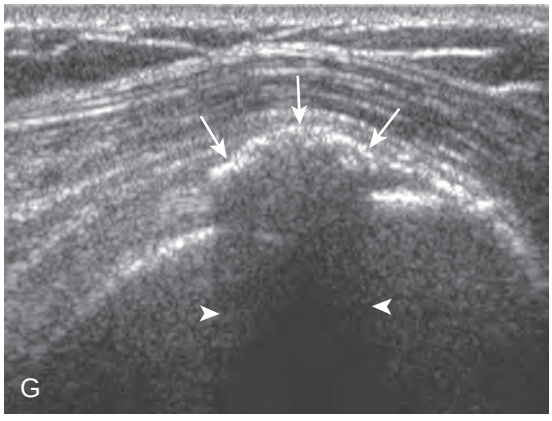

FIGURE 3-61 ■ Calcific tendinosis: variable appearances. Ultrasound images in seven patients show the following: **A,** a well-defined linear calcific deposit *(arrow)* along the supraspinatus tendon fibers; **B,** a slightly larger linear calcific deposit *(arrows)* in the supraspinatus with some shadowing *(open arrows)*; **C,** an amorphous heterogeneous nearly isoechoic calcific deposit *(arrows)* with minimal shadowing that replaces the normal fibrillar tendon architecture; **D,** a globular calcific deposit with internal fluid consistency *(arrows)*; **E,** a globular calcific deposit *(arrows)* in the subscapularis; **F,** a calcific deposit *(arrows)* that extends into the greater tuberosity *(open arrows)* with erosion; and **G,** a well-defined hyperechoic supraspinatus calcific deposit *(arrows)* with posterior acoustic shadowing *(arrowheads)*.

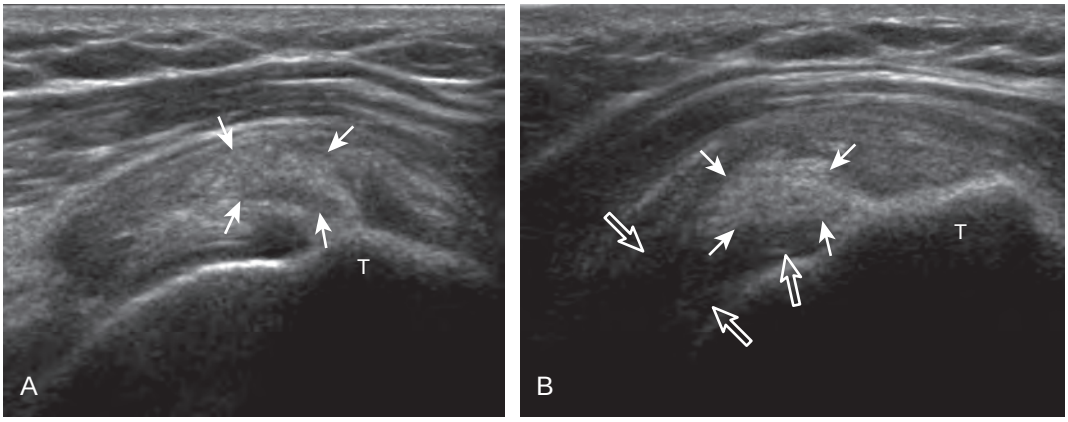

FIGURE 3-62 ■ Calcific tendinosis: anisotropy. Ultrasound image of supraspinatus tendon in long axis **(A)** shows an ill-defined hyperechoic calcific deposit *(arrows)*. Note improved conspicuity of the calcific deposit **(B)** as the surrounding supraspinatus tendon is hypoechoic as a result of anisotropy *(open arrows)* after directing the ultrasound beam obliquely (heel-toe maneuver). T, greater tuberosity.

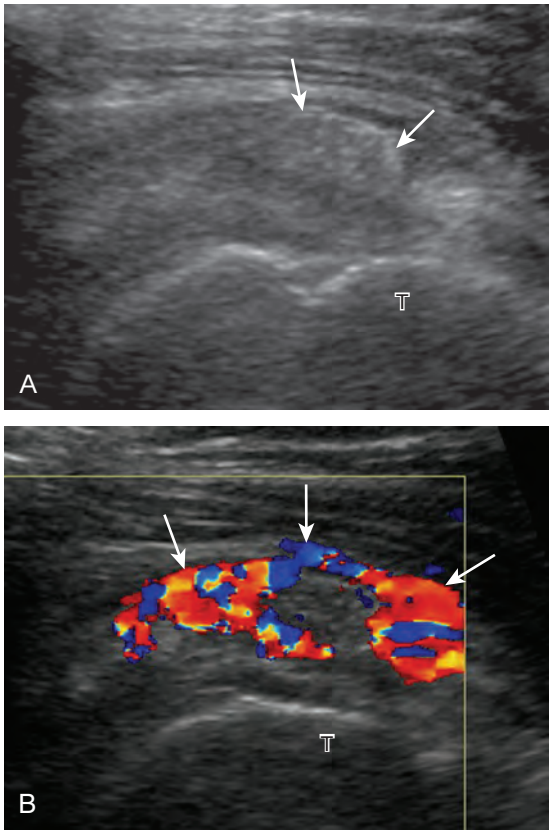

FIGURE 3-63 ■ Calcific tendinosis: hyperemia. Ultrasound images of supraspinatus in long axis (gray-scale in **A,** color Doppler in **B**) shows amorphous hyperechoic calcific deposits within the supraspinatus tendon and the adjacent subacromial-subdeltoid bursa *(arrows)* with adjacent increased blood flow. T, greater tuberosity.

in short axis.[59] Later stages of subacromial impingement include abnormal upward migration of the humeral head.[16] Bone impingement may occur between the acromion and the greater tuberosity, usually in the setting of a rotator cuff tear (Video 3-32). The presence of an os acromiale has also been associated with symptoms of cuff impingement (Fig. 3-66).

Another form of rotator cuff impingement involves the subscapularis tendon and overlying subacromial-subdeltoid bursa between the coracoid process and lesser tuberosity of the proximal humerus. Ultrasound findings in this condition include decreased distance between the coracoid process and the lesser tuberosity (5.9 to 9.6 mm) compared with the asymptomatic side (7.8 to 17.5 mm) with the ipsilateral hand placed on the opposite shoulder.[60] An additional finding is abnormal distention of the anterior aspect of the subacromial-subdeltoid bursa in the region of the subscapularis tendon and coracoid, which further distends with extension and internal rotation, correlating with anteromedial pain.[61]

Adhesive Capsulitis

Adhesive capsulitis or frozen shoulder is characterized by shoulder pain and limitation of motion.[62] Although often of unclear etiology, this condition is associated with diabetes mellitus, trauma, and immobilization.[62] At sonography, adhesive capsulitis can be initially suggested when the patient has limited external shoulder rotation while evaluating the subscapularis. Adhesive capsulitis is also suggested when there is continuous limitation of the sliding movement of the supraspinatus tendon beneath the acromion with active

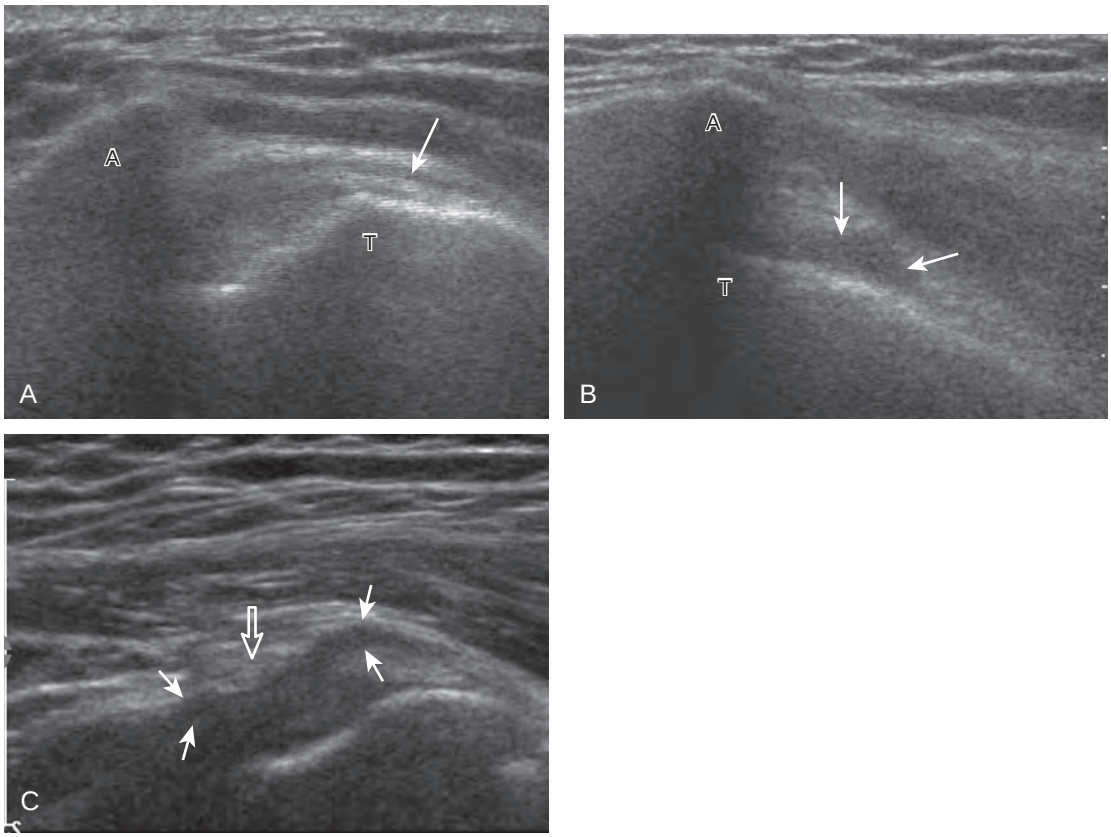

FIGURE 3-64 ■ Impingement syndrome (subacromial). Ultrasound images of supraspinatus in long axis with arm in neutral position **(A)** and abduction **(B)** show gradual distention of the subacromial-subdeltoid bursa with anechoic fluid *(arrows)*. Ultrasound image of supraspinatus in long axis **(C)** anterior to the acromion in a different patient shows hypoechoic distention of the subacromial-subdeltoid bursa *(arrows)* with pooling on either side of the coracoacromial ligament *(open arrow)*. A, acromion; T, greater tuberosity.

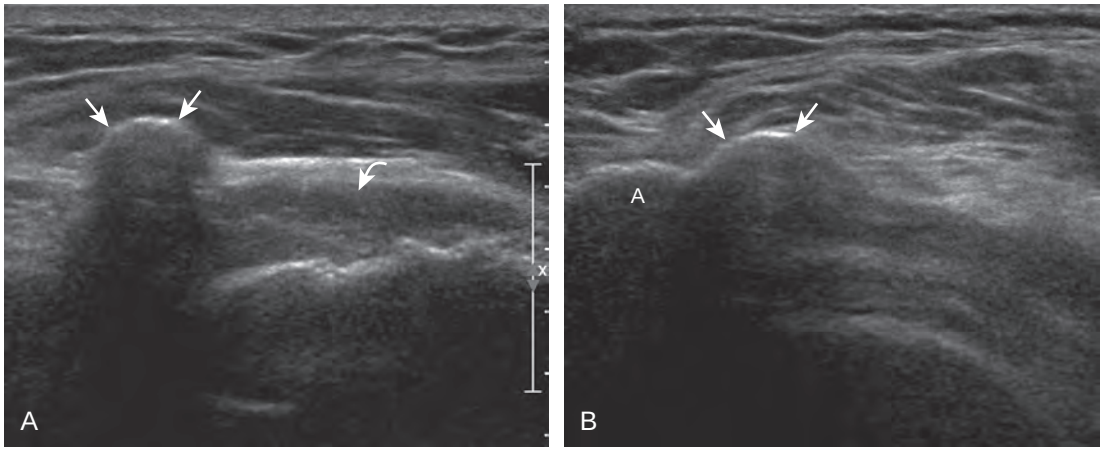

FIGURE 3-65 ■ Impingement: subacromial enthesophyte spur. Ultrasound images of supraspinatus in long axis **(A)** and short axis **(B)** show a large echogenic and shadowing subacromial enthesophyte spur *(arrows)* projecting anterior to the acromion (A) with adjacent supraspinatus tendinosis and tear *(curved arrow)*.

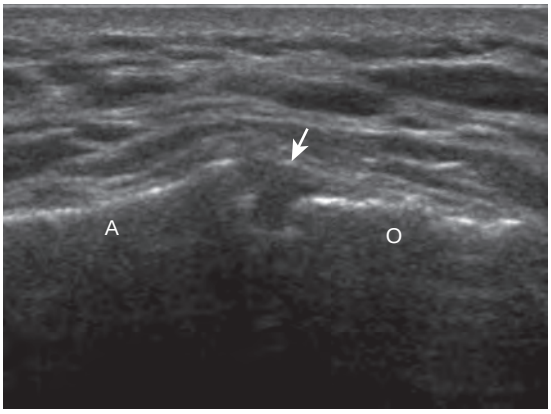

FIGURE 3-66 ■ **Os acromiale.** Ultrasound image over the acromion in the sagittal plane shows a hypoechoic cleft *(arrow)* between the acromion (A) and adjacent anterior acromion ossification center (O).

arm elevation (Fig. 3-67) (Video 3-33).[18] Abnormal hypoechogenicity and hyperemia in the rotator interval, as well as thickening of the coracohumeral ligament, are other described findings with adhesive capsulitis.[63,64]

PITFALLS IN ROTATOR CUFF ULTRASOUND

Errors in Scanning Technique

Improper Positioning of the Shoulder

With the shoulder in neutral position, much of the supraspinatus is hidden beneath the acromion. Although the distal 1 to 2 cm of the tendon may be seen at its footprint, hyperextension of the shoulder (e.g., the Crass or modified Crass position) is needed to expose the supraspinatus tendon for evaluation (Fig. 3-68). In a supine patient, the supraspinatus may also be visualized by having the patient hyperextend the arm posterior to the shoulder.[65]

Incomplete Evaluation of the Supraspinatus Tendon

Many supraspinatus tendon tears occur anteriorly, often near the rotator interval.[8,9] It is important that the entire extent of the supraspinatus tendon, especially the anterior portion, be completely evaluated. This can be ensured with visualization of the intra-articular portion of the biceps brachii tendon in the rotator interval (Fig. 3-69). When imaging the supraspinatus tendon in long axis, the transducer should be moved anteriorly on the greater tuberosity until the biceps tendon is seen. When imaging the supraspinatus tendon in short axis, the biceps tendon should again be visualized to ensure that the anterior aspect of the supraspinatus tendon is evaluated.

Imaging of the Rotator Cuff Too Distally

This can occur when imaging the supraspinatus tendon in short axis. If the transducer is located too distally over the greater tuberosity beyond the rotator cuff attachment, the image of deltoid muscle lying over the proximal humerus may simulate a massive rotator cuff tear because no cuff is visible (see Fig. 3-13D). This diagnosis is easily excluded by turning the transducer 90 degrees, long axis to the supraspinatus tendon, to indicate the improper transducer location. This is another reason that evaluation of the supraspinatus begins in its long axis.

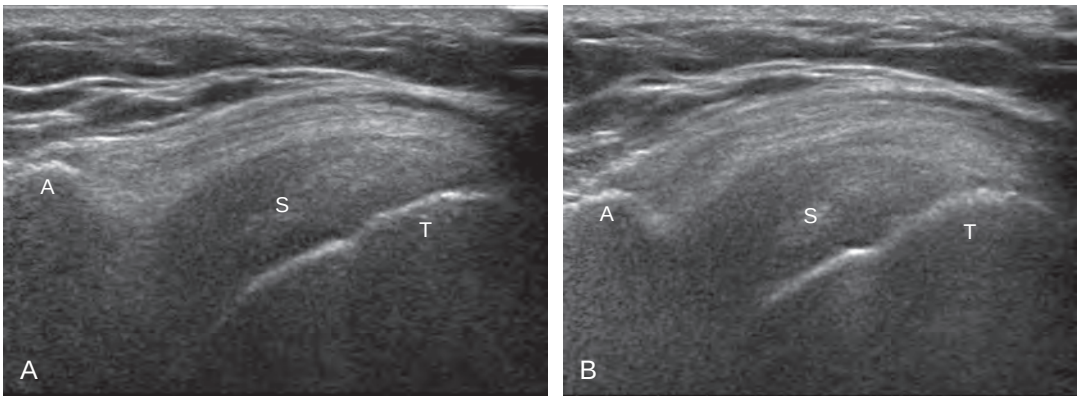

FIGURE 3-67 ■ **Adhesive capsulitis.** Ultrasound images of the supraspinatus tendon in long axis with arm in neutral position **(A)** and elevated to side **(B)** show that the supraspinatus tendon (S) does not slide beneath the acromion (A), with arm elevation. Note the hypoechoic tendinosis of the supraspinatus tendon. T, greater tuberosity.

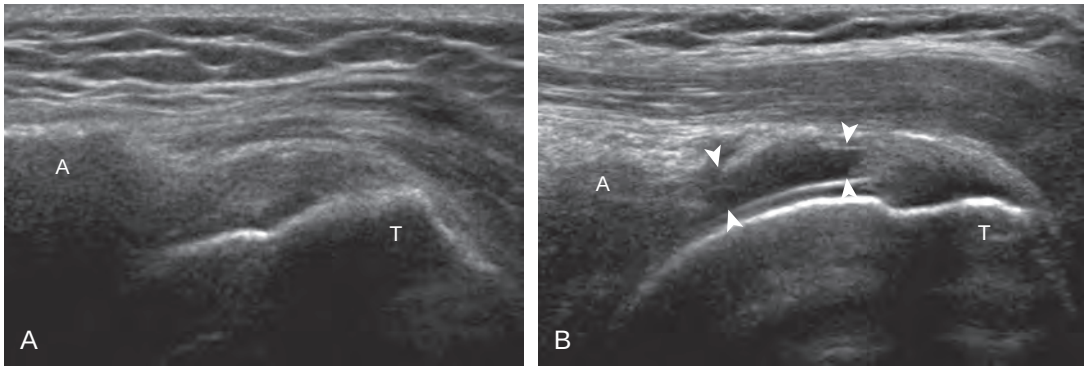

FIGURE 3-68 ■ Supraspinatus tendon in shoulder neutral and hyperextension. Ultrasound images of supraspinatus tendon in long axis with the shoulder in neutral position **(A)** and hyperextension **(B)** show improved visualization of the supraspinatus tear *(arrowheads)* in shoulder hyperextension. A, acromion; T, greater tuberosity.

Misinterpretation of Normal Structures

Misinterpretation of the Rotator Interval

The rotator interval is a space between the superior margin of the subscapularis tendon and the anterior margin of the supraspinatus tendon. Within this interval, the intra-articular portion of the long head of the biceps brachii tendon is located, along with the biceps pulley system of capsular thickening and reflections and the superior glenohumeral and coracohumeral ligaments (see Fig. 3-14).[12] The superior glenohumeral ligament is located at the subscapularis side of the biceps brachii tendon with fibers merging with the coracohumeral ligament, which is located superficial to the biceps tendon. The rotator interval also is the site where the glenohumeral joint communicates with the more medial

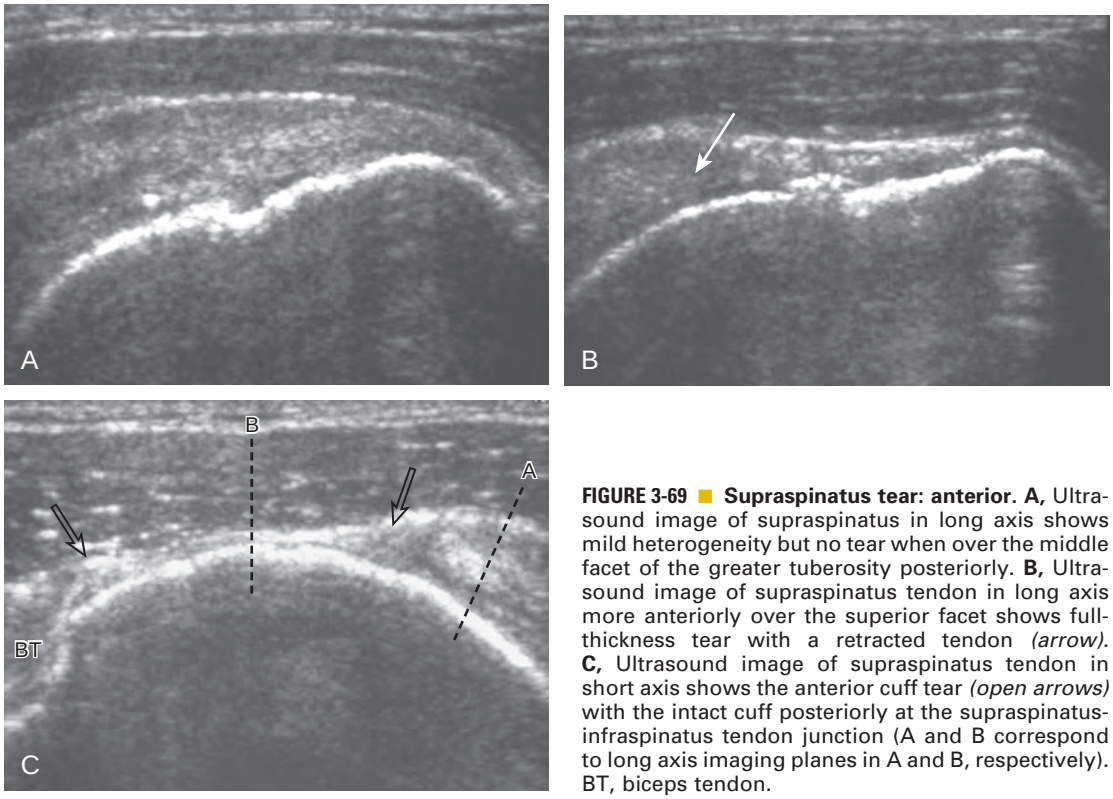

FIGURE 3-69 ■ Supraspinatus tear: anterior. A, Ultrasound image of supraspinatus in long axis shows mild heterogeneity but no tear when over the middle facet of the greater tuberosity posteriorly. **B,** Ultrasound image of supraspinatus tendon in long axis more anteriorly over the superior facet shows full-thickness tear with a retracted tendon *(arrow)*. **C,** Ultrasound image of supraspinatus tendon in short axis shows the anterior cuff tear *(open arrows)* with the intact cuff posteriorly at the supraspinatus-infraspinatus tendon junction (A and B correspond to long axis imaging planes in A and B, respectively). BT, biceps tendon.

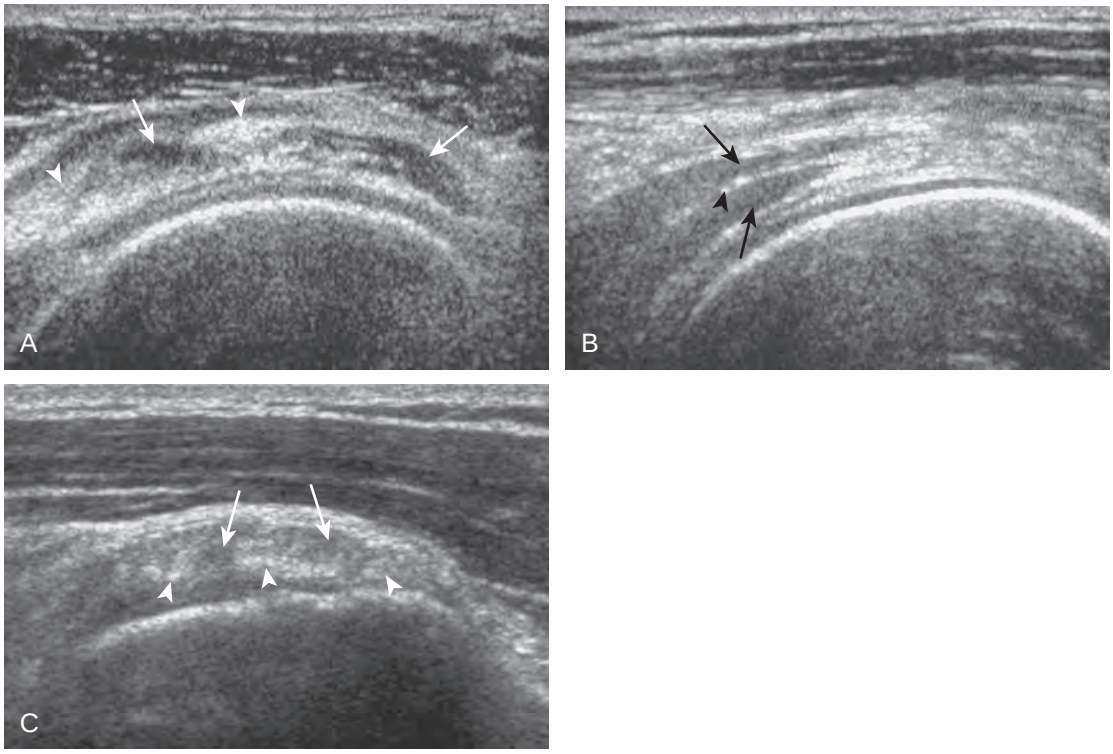

FIGURE 3-70 ■ Musculotendinous junction. Ultrasound images of supraspinatus in short axis **(A)** and long axis **(B)** and ultrasound image of subscapularis tendon in short axis **(C)** show intervening hypoechoic muscle *(arrows)* and hyperechoic tendon *(arrowheads)*.

subscapularis recess. The rotator interval is easily seen when the transducer is transverse to the supraspinatus tendon, although the modified Crass position may be needed to optimize visualization. The biceps tendon appears hyperechoic and is separated from the adjacent supraspinatus by a thin hypoechoic interface, which should not be misinterpreted for tendon tear.[10]

Misinterpretation of the Musculotendinous Junction

The musculotendinous junction represents a transition from hypoechoic muscle to hyerechoic tendon. Because this transition is not uniform, a mixed hyperechoic-hypoechoic appearance may be seen. One example is the proximal aspect of the supraspinatus tendon when one visualizes the oval anterior or central tendon of the supraspinatus and the small and flatter posterior tendon.[66] When imaged in short axis, the intervening hypoechoic areas representing muscle tissue should not be misinterpreted as tendon disease, such as tendinosis (Fig. 3-70A and B). This pitfall is easily avoided by imaging the tendon in long axis, where the tapering appearance of the hypoechoic muscle tissue can be appreciated. A similar effect also involves the subscapularis, where both hypoechoic muscle and hyperechoic tendon are seen (see Fig. 3-70C). This appearance is most obvious in short axis, where several hyperechoic tendon bundles can be seen within hypoechoic muscle. With use of transducers with spatial compound imaging, this normal heterogeneous appearance becomes less conspicuous (see Fig. 3-7B).

Misinterpretation of the Supraspinatus-Infraspinatus Junction

Distally, the fibers of the supraspinatus and infraspinatus converge to form a common cuff of tendon. Over the anterior portion of the middle greater tuberosity facet, infraspinatus tendon fibers overlap supraspinatus tendon fibers.[1] At ultrasound, this produces a series of uniform linear hypoechoic bands superficial to the posterior aspect of the supraspinatus. These bands appear hypoechoic as a result of infraspinatus anisotropy when imaging the supraspinatus in long or short axis (Fig. 3-71). This striped appearance is more conspicuous during real-time

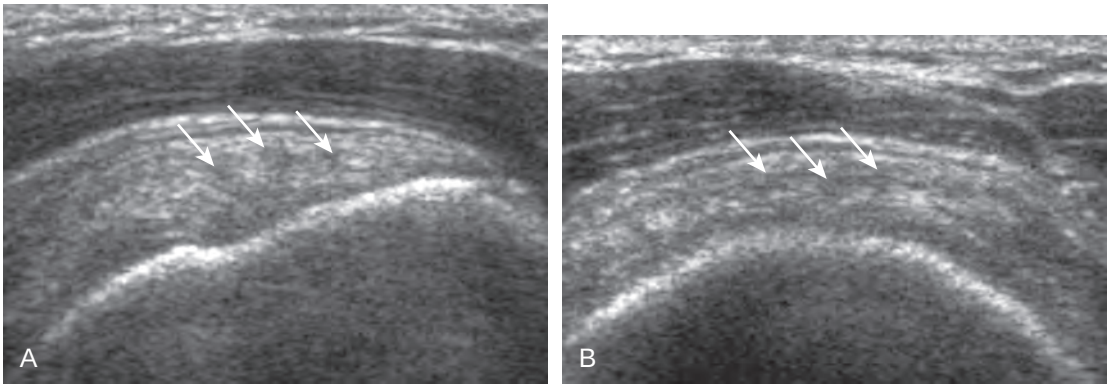

FIGURE 3-71 ■ Supraspinatus-infraspinatus tendon junction. Ultrasound images of supraspinatus tendon in long axis **(A)** and short axis **(B)** show linear, regularly spaced hypoechoic areas *(arrows)* representing anisotropy of infraspinatus tendon fibers that overlap the supraspinatus.

scanning because the fairly equally spaced hypoechoic oblique lines uniformly move through the tendon (see Video 3-8). These hypoechoic areas should not be misinterpreted for tendon pathology. This characteristic appearance can be used to locate the supraspinatus-infraspinatus junction, which is important in the localization of a rotator cuff tear and determination of tear extent. Another finding to assist in identification of the supraspinatus-infraspinatus tendon junction is visualization of slight cuff thinning on transverse imaging at this site. Finally, one can measure 2.5 cm posterior from the biceps brachii tendon at transverse imaging of the supraspinatus because this point indicates the posterior margin of the supraspinatus tendon.[2] The bulk of the infraspinatus tendon is located posterior to this point, although there is overlap of the infraspinatus tendon superficial to the supraspinatus tendon over the middle greater tuberosity facet (see Fig. 3-2).[1]

Misinterpretation of Pathology

Subacromial-Subdeltoid Bursa Simulating Tendon

Although the abnormal subacromial-subdeltoid bursa is often distended with anechoic or hypoechoic fluid, the bursa may contain complex fluid or synovial hypertrophy. In these latter conditions, the echogenicity within the bursa may be isoechoic or even hyperechoic to adjacent muscle, and it may be nearly equal in echogenicity to

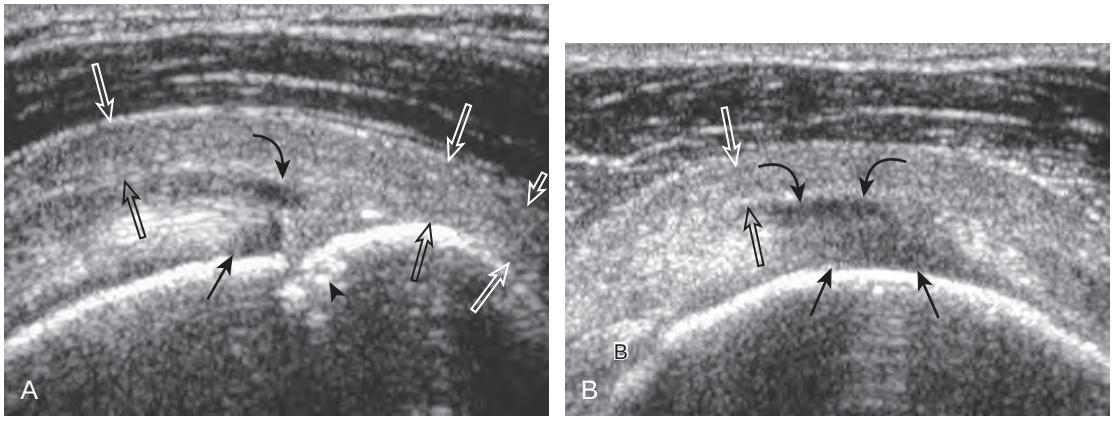

FIGURE 3-72 ■ Full-thickness supraspinatus tear with bursal thickening. Ultrasound images of supraspinatus in long axis **(A)** and short axis **(B)** show a well-defined hypoechoic defect, which extends from the bursal surface *(curved arrows)* to the articular surface *(arrows)*, with bone irregularity of the greater tuberosity *(arrowhead)*. Note diffuse thickening of the subacromial-subdeltoid bursa *(open arrows)*, which extends beyond the greater tuberosity. B, biceps tendon.

tendon (Fig. 3-72). In the presence of a bursal-side partial-thickness tear (see Fig. 3-27) or a full-thickness tendon tear (see Fig. 3-37), the subacromial-subdeltoid bursa may lie within the torn tendon gap. When the bursa is hyperechoic and similar in echogenicity to tendon, it is important not to mistake the bursal contents for intact tendon fibers. The thickened bursa can be differentiated from tendon by the lack of fibrillar architecture and identification of the bursal tissue that extends beyond the greater tuberosity, unlike the rotator cuff. A similar situation may occur in the setting of a massive cuff tear, in which the thin hyperechoic wall of the subacromial-subdeltoid bursa may simulate intact fibers (Fig. 3-73). Because the bursal wall extends beyond the greater tuberosity distal to the rotator cuff tendon attachment to bone, this too excludes tendon fibers as the cause.

Rim-Rent Tear Versus Intrasubstance Tear

A rim-rent tear is an articular-side partial-thickness supraspinatus tendon tear that involves the most distal aspect of the tendon at the greater tuberosity insertion (see Fig. 3-21).[8,9] When a well-defined hypoechoic or anechoic tendon abnormality is at this location, it is important to determine whether the abnormal echogenicity is in contact with the articular surface (representing a rim-rent tear) or is only the greater tuberosity surface within the supraspinatus tendon (an intrasubstance tear) (see Fig. 3-28). In the latter situation, an intrasubstance tear is not seen at arthroscopy or bursoscopy. Therefore, it is critical to determine whether intra-articular extension is seen, which appears as contact between the tendon tear and the hypoechoic hyaline cartilage with a possible cartilage interface sign (Fig. 3-74).

TABLE 3-2 Ultrasound Features of Tendon Tear and Tendinosis

Tear	Tendinosis
Anechoic	Hypoechoic
Well defined	Ill defined
Homogeneous	Heterogeneous
Thin	Swollen
Bone irregularity*	Smooth cortex*

*Specific to greater tuberosity attachment of supraspinatus in patients older than 40 years.

Tendinosis Versus Tendon Tear

Because tendinosis and tendon tear may both appear hypoechoic, one must rely on other sonographic findings to help with this distinction (Table 3-2).[21] If a tendon abnormality is hypoechoic, ill defined, and heterogeneous, then tendinosis is suggested (see Fig. 3-40). In contrast, if a tendon abnormality is more anechoic and well defined, then tendon tear is suggested (see Fig. 3-30). In addition, tendon swelling suggests tendinosis, whereas tendon thinning suggests either bursal-side partial-thickness tear or full-thickness tear. The most important sign that assists in the differentiation between supraspinatus tear and tendinosis in patients older than 40 years is cortical irregularity of the greater tuberosity. A supraspinatus tendon abnormality immediately adjacent to cortical irregularity of the greater tuberosity likely represents a tear. This association is not necessarily found with other

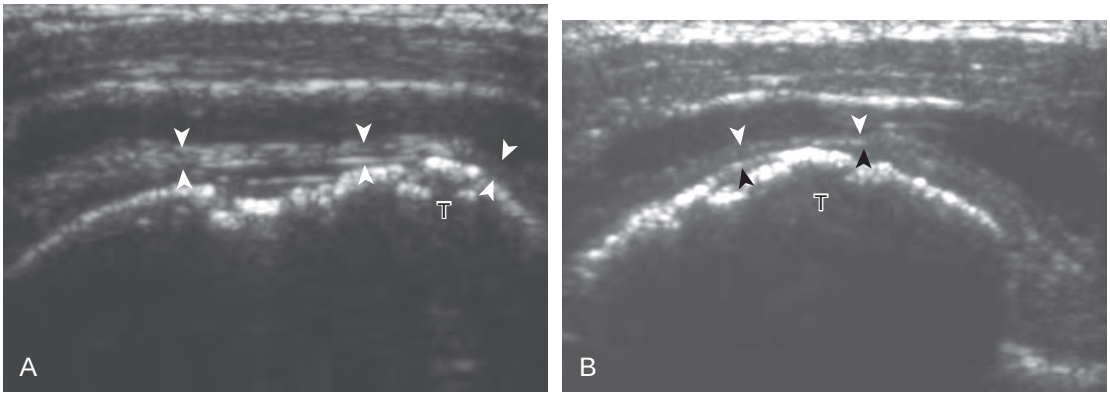

FIGURE 3-73 ■ Massive supraspinatus tear. Ultrasound images of supraspinatus in long axis **(A)** and short axis **(B)** show complete absence of the supraspinatus tendon. Note the hyperechoic linear subacromial-subdeltoid bursal wall *(arrowheads)*, which extends beyond the greater tuberosity (T) and therefore does not represent rotator cuff tendon fibers.

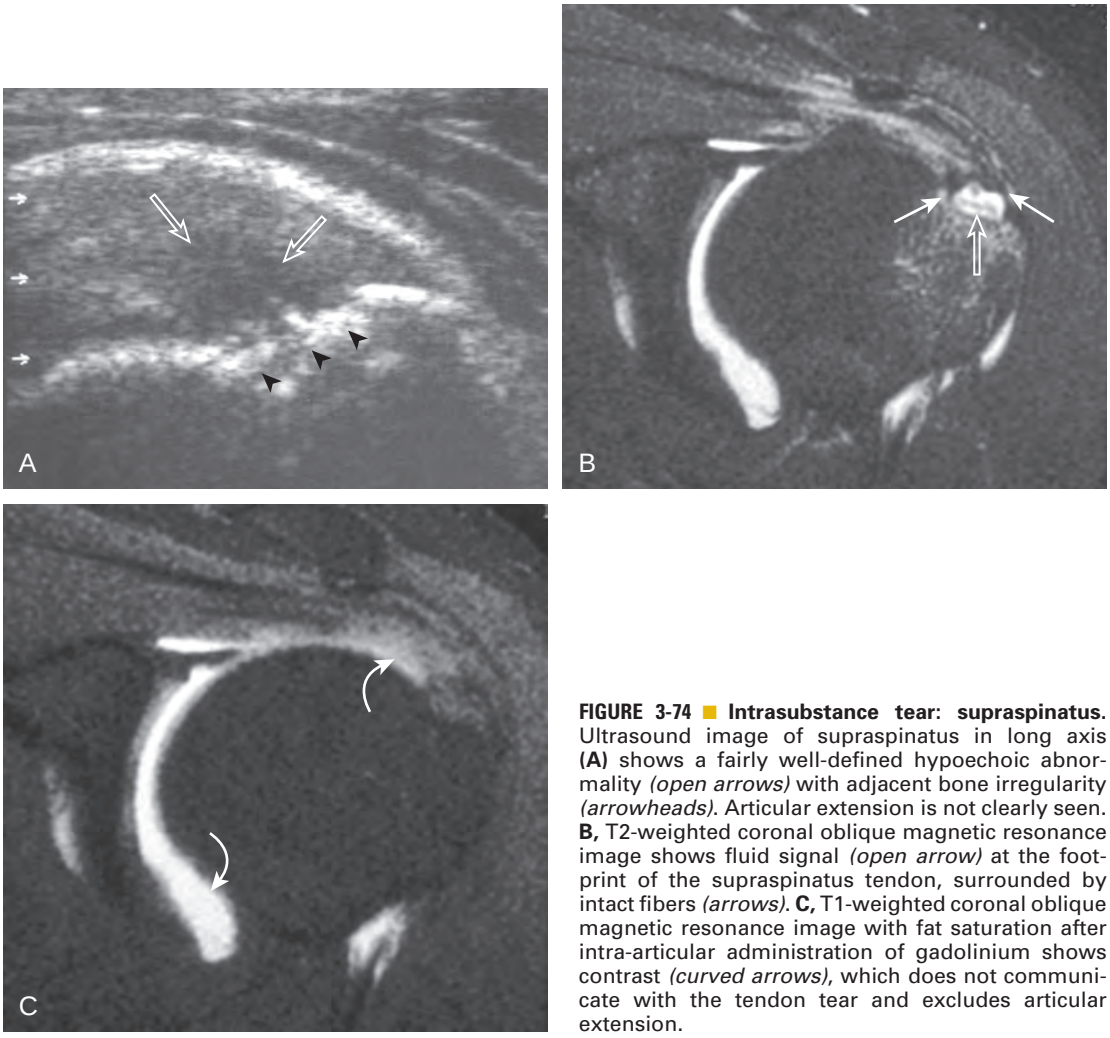

FIGURE 3-74 ■ Intrasubstance tear: supraspinatus. Ultrasound image of supraspinatus in long axis **(A)** shows a fairly well-defined hypoechoic abnormality *(open arrows)* with adjacent bone irregularity *(arrowheads)*. Articular extension is not clearly seen. **B,** T2-weighted coronal oblique magnetic resonance image shows fluid signal *(open arrow)* at the footprint of the supraspinatus tendon, surrounded by intact fibers *(arrows)*. **C,** T1-weighted coronal oblique magnetic resonance image with fat saturation after intra-articular administration of gadolinium shows contrast *(curved arrows)*, which does not communicate with the tendon tear and excludes articular extension.

aspects of the rotator cuff. For example, cortical irregularity often is seen in the lesser tuberosity without adjacent subscapularis tendon abnormality. In addition, some degree of cortical irregularity of the posterior humerus beneath the infraspinatus (termed the *bare area* because it is devoid of cartilage) is considered a variation of normal.[34] However, extensive irregularity in this region, coexisting with posterior labrum tear and partial-thickness infraspinatus tendon tear, indicates posterosuperior impingement syndrome.[67]

BICEPS TENDON

Joint Effusion and Tenosynovitis

Because the tendon sheath of the long head of the biceps brachii tendon normally communicates with the glenohumeral joint, increased joint fluid can be found in this tendon sheath adjacent to the long head of the biceps brachii tendon at the level of the bicipital groove (Fig. 3-75).[68] More than a small sliver of fluid on one side of the biceps tendon is considered abnormal. Joint effusion, if simple, can be anechoic, whereas complex fluid may be hypoechoic, isoechoic, or hyperechoic relative to muscle, and it may resemble synovial hypertrophy (Fig. 3-76). The findings of flow on color or power Doppler imaging and the lack of internal movement with transducer pressure suggest synovial hypertrophy rather than complex fluid.[69] It is also important to differentiate communicating joint effusion from tenosynovitis. If tendon sheath distention is focal, symptomatic with transducer pressure, with hyperemia, this suggests tenosynovitis (Fig. 3-77). Fluid that remains focal or loculated at the level of the bicipital groove with palpation under ultrasound visualization also suggests tenosynovitis (Video

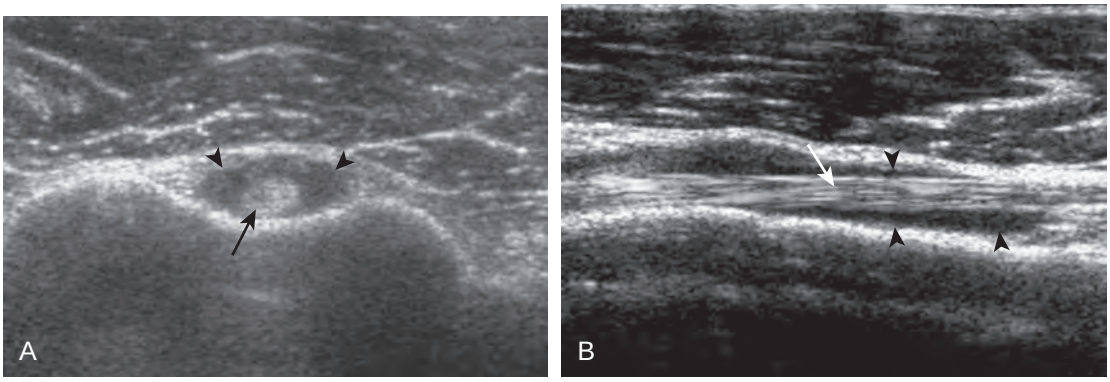

FIGURE 3-75 ■ Joint effusion. Ultrasound images of biceps brachii long head tendon in short axis **(A)** and long axis **(B)** show joint fluid *(arrowheads)*, which surrounds the biceps tendon *(arrows)* (right side of image **A** is medial, distal in **B**).

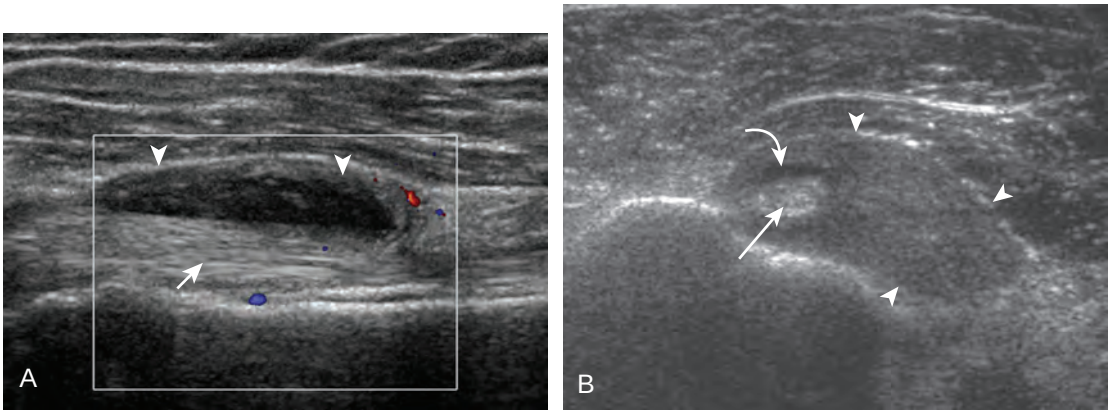

FIGURE 3-76 ■ Complex fluid and synovial hypertrophy. Ultrasound image of the biceps brachii tendon in long axis **(A)** shows hypoechoic complex joint fluid *(arrowheads)* that surrounds the biceps tendon *(arrow)*. Swirling of echoes was seen at real-time imaging, a finding indicating a fluid component. **B,** Ultrasound image of biceps brachii long head tendon in short axis in a different patient shows synovitis *(arrowheads)* that surrounds the biceps tendon *(arrow)*. Note the small anechoic joint effusion *(curved arrow)*.

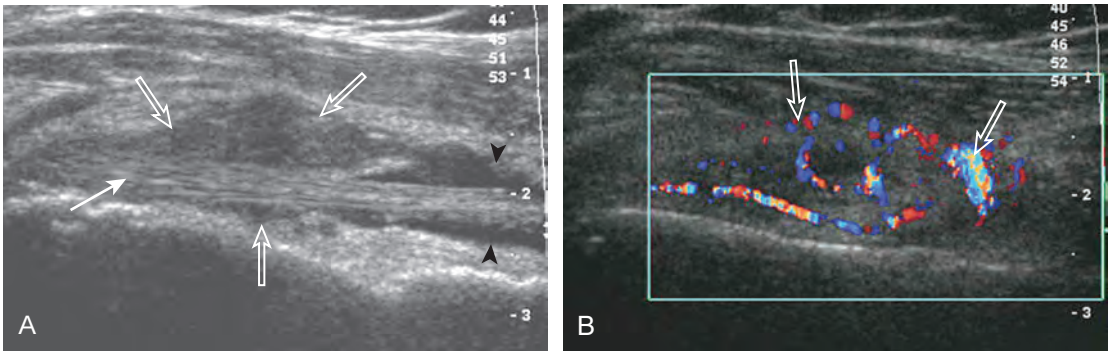

FIGURE 3-77 ■ Biceps tenosynovitis. Gray-scale **(A)** and color Doppler **(B)** ultrasound images long axis to the biceps brachii long head tendon show anechoic joint fluid *(arrowheads)* and hyperemic hypoechoic and isoechoic synovitis *(open arrows)* that surrounds the biceps tendon *(arrow)* (right side of images is distal).

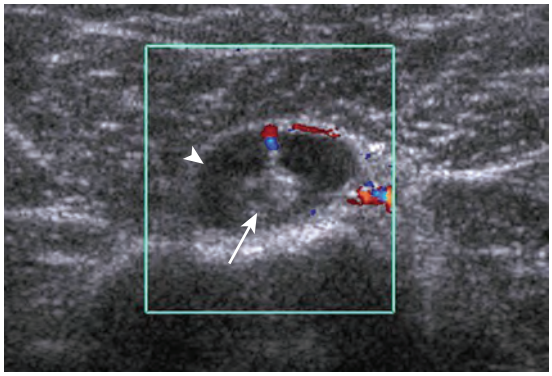

FIGURE 3-78 ■ Joint effusion and normal vascularity. Color Doppler ultrasound image of biceps brachii long head tendon in short axis shows hypoechoic joint fluid *(arrowhead)* that surrounds the biceps tendon *(arrow)*. Note normal vascularity (right side of image is lateral).

3-34). In contrast, a long segment of asymptomatic tendon sheath distention associated with distention of another shoulder joint recess, such as the posterior glenohumeral joint or subscapular recesses, suggests joint effusion. Normal flow seen in a branch of the anterior circumflex humeral artery should not be misinterpreted as abnormal vascularity (Fig. 3-78).[69] It is also important not to mistake distention of the subacromial-subdeltoid bursa for biceps sheath abnormalities because the bursal distention is often seen superficial to the biceps tendon anteriorly (Fig. 3-79; see Fig. 3-44). Intra-articular bodies from the glenohumeral joint are commonly seen within the biceps brachii long head tendon sheath (Fig. 3-80). The finding of joint effusion alone within the long head of the biceps brachii tendon sheath has a positive predictive value of 60% for diagnosis of rotator cuff tear; the additional finding of subacromial-subdeltoid bursal fluid increases the positive predictive value to 95%.[36]

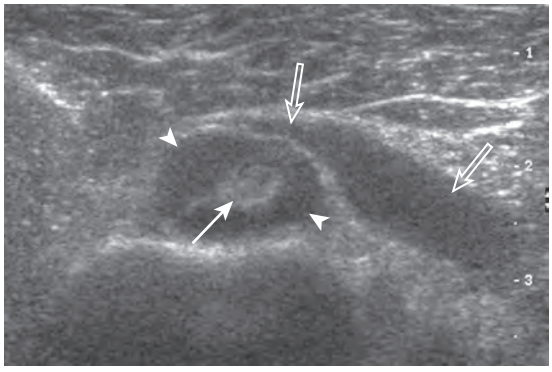

FIGURE 3-79 ■ Subacromial-subdeltoid fluid. Ultrasound image of biceps brachii long head tendon in short axis shows hypoechoic joint fluid *(arrowheads)* that surrounds the biceps tendon *(arrow)*. There is also hypoechoic fluid, which distends the subacromial-subdeltoid bursa *(open arrows)* (right side of image is medial).

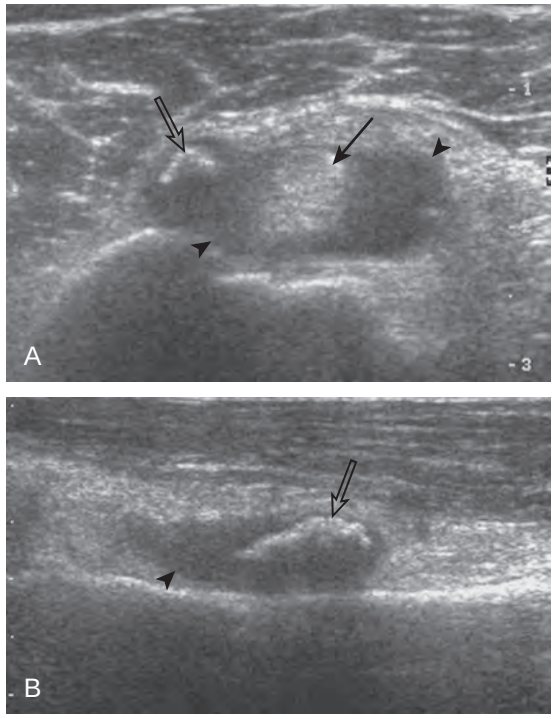

FIGURE 3-80 ■ Intra-articular body. Ultrasound images of biceps brachii long head tendon in short axis **(A)** and long axis **(B)** show joint fluid *(arrowheads)* that surrounds the biceps tendon *(arrow)* with a hyperechoic and partial shadowing ossified intra-articular body *(open arrows)* (right side of image in **A** is medial, distal in **B**).

Tendon Tear and Tendinosis

Tendinosis of the biceps brachii long head tendon appears as hypoechoic enlargement of the tendon, but without tendon fiber disruption (Fig. 3-81). It is important not to misinterpret refraction shadowing from prominent deltoid fascia as abnormality of the biceps brachii tendon (Video 3-35). Pathology of the biceps tendon most commonly occurs within 3.5 cm of the tendon origin, which may be seen proximal to and at the bicipital groove.[4] Assessment of the most proximal biceps is completed with the shoulder in the modified Crass position when the anterior aspect of the supraspinatus tendon and the rotator interval are assessed. When the involved tendon shows additional anechoic clefts or an irregular superficial surface, then superimposed partial-thickness tear is present, especially when the bicipital groove is irregular from osseous spurs (Fig. 3-82).[70] Rarely,

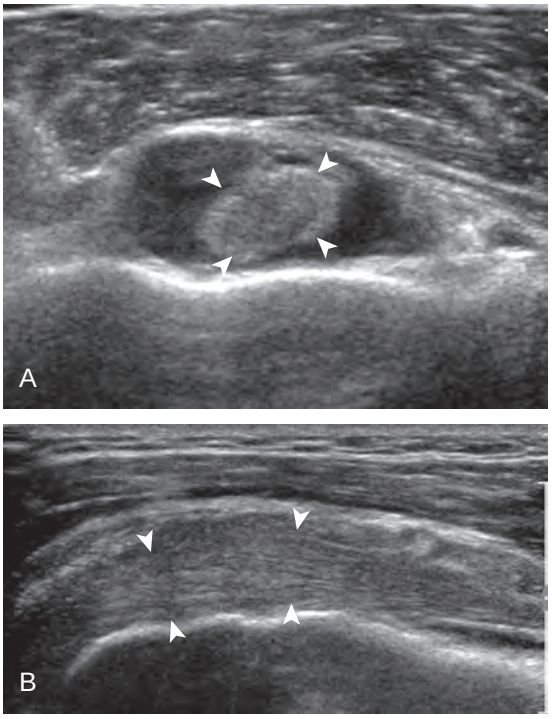

FIGURE 3-81 ■ Biceps brachii tendinosis. Ultrasound images of biceps brachii long head tendon in short axis **(A)** and long axis **(B)** show hypoechoic enlargement of the tendon *(arrowheads)* and fluid distention of tendon sheath (right side of image in **A** is medial, distal in **B**).

an intratendinous ganglion cyst may be seen within the biceps tendon (Fig. 3-83).[71] A full-thickness tear appears as complete fiber disruption and usually results in retraction at the torn tendon stump; therefore, the primary finding is lack of visualization of the long head of biceps tendon or an empty bicipital groove (Fig. 3-84A).[70] There is often isoechoic or hyperechoic synovial hypertrophy or collapsed tendon sheath in the bicipital groove, which should not be misinterpreted as tendon fibers; imaging distally at the pectoralis tendon and proximally in the rotator interval for biceps tendon may be helpful. When there is full-thickness biceps brachii tendon tear, imaging more distally in short axis demonstrates the thickened and retracted distal stump, usually at the pectoralis tendon when chronic, which may or may not be surrounded by hypoechoic or anechoic fluid (see Fig. 3-84B to D). The normal muscle of the short head of the biceps brachii is seen just medially. Refraction shadowing deep to the torn and retracted tendon stump is another indirect sign of full-thickness tear. Often, the proximal aspect of the biceps tear is not seen in the bicipital groove or in the rotator interval because the tear has occurred proximally at the biceps anchor at the glenoid labrum. When the biceps brachii long head tendon is not seen in the bicipital groove, in addition to the possibility of a full-thickness tear, one must also consider the diagnosis of biceps tendon dislocation (see next paragraph). It is also important to inquire about prior surgery because the intra-articular portion of the biceps brachii long head tendon may be surgically transected (termed *tenotomy*) or transected and attached to the humerus (termed *tenodesis*) at the level of the bicipital groove (Fig. 3-85).

Subluxation and Dislocation

When the biceps brachii long head tendon is not normally identified in the bicipital groove, one must consider medial subluxation or dislocation.[5] With subluxation of the long head of the biceps brachii tendon, the tendon is partially out of the bicipital groove and medially displaced so that the medial aspect of the tendon is superficial to the lesser tuberosity (Fig. 3-86). The biceps may

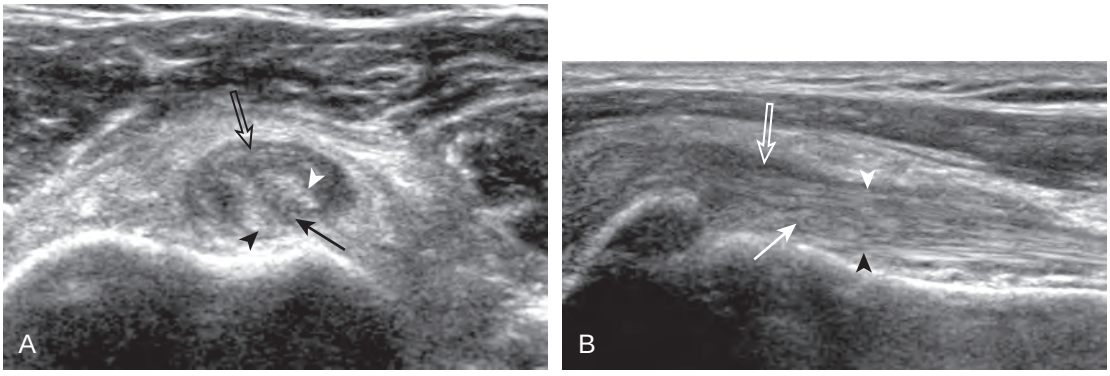

FIGURE 3-82 ■ Biceps brachii tendon: partial-thickness tear. Ultrasound images of biceps brachii tendon in short axis **(A)** and long axis **(B)** show hypoechoic tear *(arrows)* within the biceps tendon *(arrowheads)* with hypoechoic fluid and synovitis *(open arrows)* (right side of image in **A** is medial, distal in **B**).

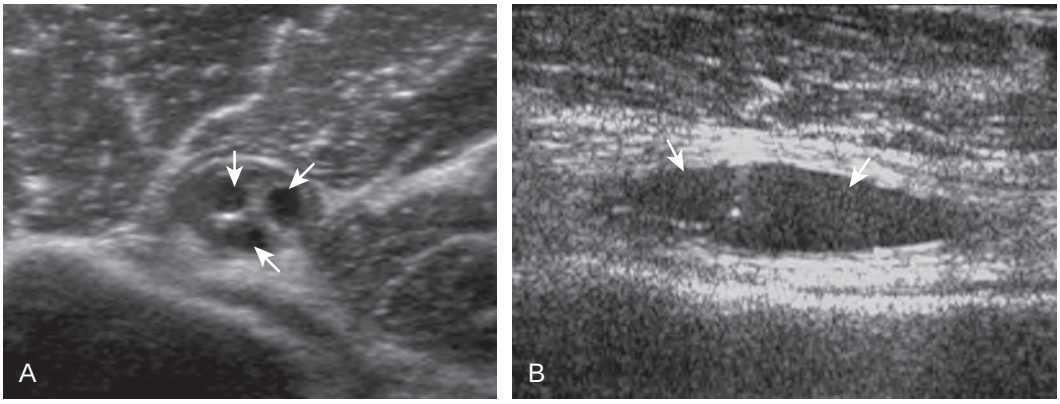

FIGURE 3-83 ■ Biceps brachii tendon: ganglion cyst. Ultrasound images of biceps brachii long head tendon in short axis **(A)** and long axis **(B)** show anechoic cysts *(arrows)* within the biceps tendon.

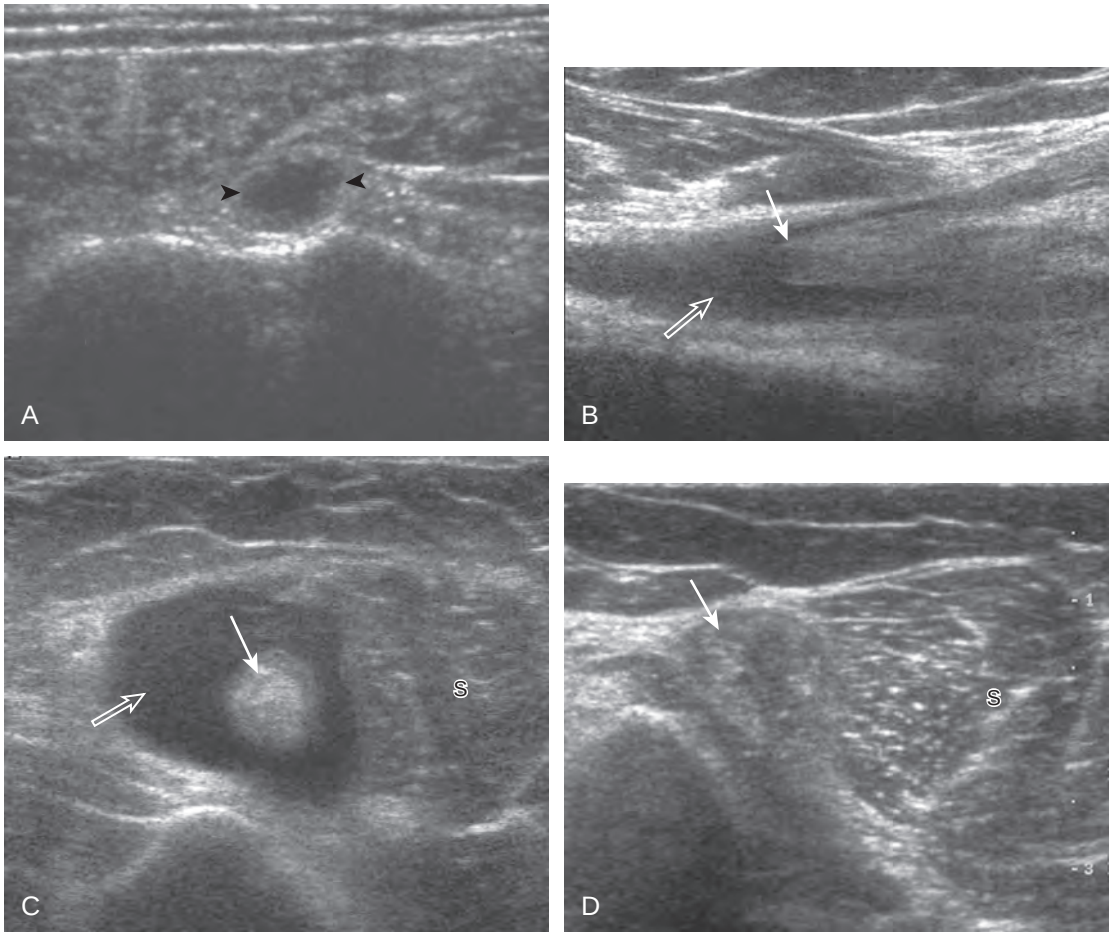

FIGURE 3-84 ■ Biceps brachii tendon: full-thickness tear. Ultrasound image **(A)** transverse over bicipital groove shows anechoic effusion or hemorrhage *(arrowheads)* and no tendon fibers. Ultrasound images of biceps brachii long head tendon more distal in long axis **(B)** and short axis **(C)** show the retracted distal stump *(arrows)* surrounded by hypoechoic fluid *(open arrows)*. Note the normal short head of the biceps brachii (S). Ultrasound image **(D)** short axis to distal biceps in a different patient shows the heterogeneous and inferiorly retracted distal stump *(arrow)* without adjacent fluid (right side of images **A, C,** and **D** is medial, distal in **B**).

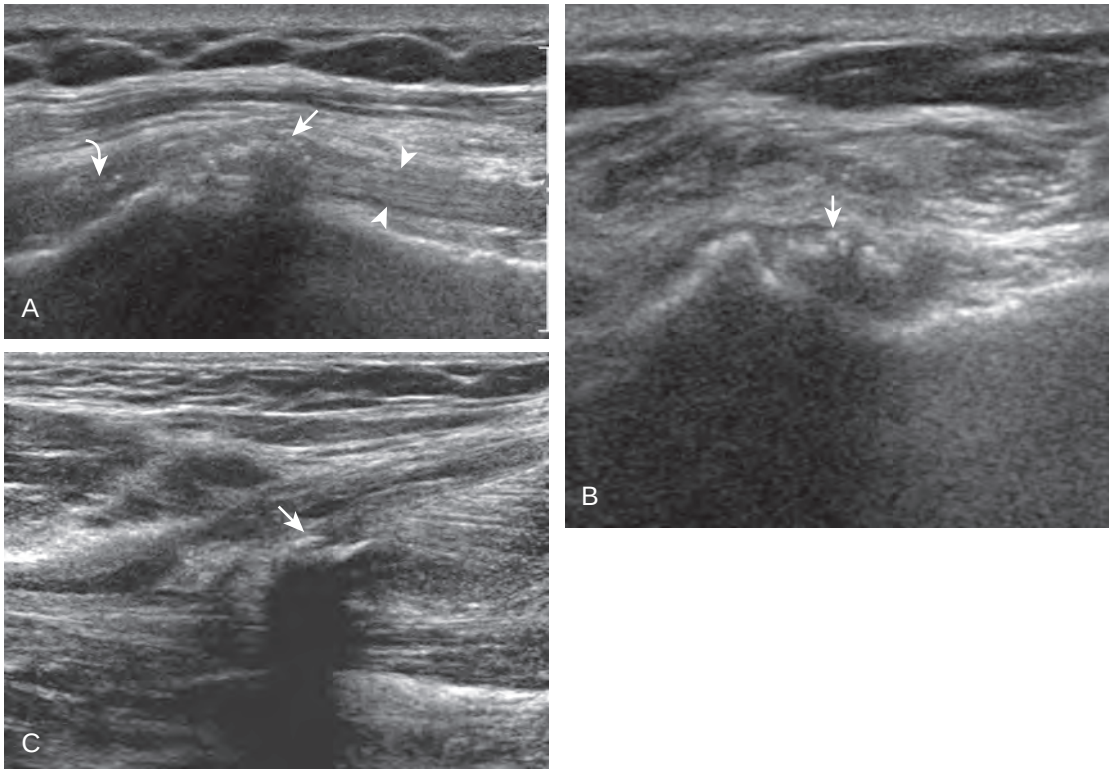

FIGURE 3-85 ■ Biceps brachii tenodesis. Ultrasound images of proximal biceps brachii tendon in long axis **(A)** and short axis **(B)** show tendon *(arrowheads)* attached to the proximal humerus with echogenic suture material *(arrow)*. The biceps tendon is not seen proximally *(curved arrow)* (right side of image is distal). **C,** Ultrasound image of biceps brachii long head (long axis) in a different patient shows a failed tenodesis with echogenic suture and tendon *(arrow)* detached from the humerus and retracted distally.

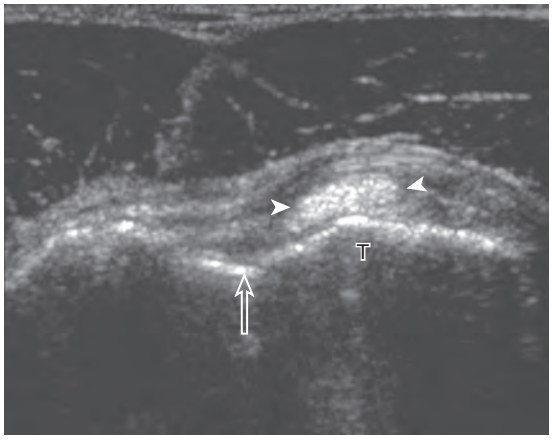

FIGURE 3-86 ■ Biceps brachii tendon subluxation. Ultrasound image of biceps brachii long head tendon in short axis shows subluxation of the biceps tendon *(arrowheads)* medial to the bicipital groove *(open arrow)* and partially superficial to the lesser tuberosity (T) (right side of image is medial).

also dislocate medially and superficially over the lesser tuberosity and subscapularis (Fig. 3-87) (Video 3-36), superficial and medial to the subscapularis (Fig. 3-88), into a subscapularis tendon tear (Fig. 3-89), or through a subscapularis tendon tear into the glenohumeral joint.[12] In these situations, the supporting structures of the biceps tendon at the rotator interval are usually abnormal (see Fig. 3-39) (see Video 3-18). With medial biceps tendon dislocation, the intra-articular location of the biceps brachii long head tendon may be difficult to identify because it may simulate the glenoid labrum or other intra-articular structure; distal imaging in short axis shows the dislocated biceps tendon coursing out of the joint and returning to a normal position lateral to the biceps brachii short head muscle. It is also important to evaluate for abnormal tendon displacement dynamically because abnormal tendon position may only occur with the shoulder in external rotation (Fig. 3-90) (see Video 3-36).[5] The contrary is also true, whereby medial dislocation of the biceps brachii long head tendon

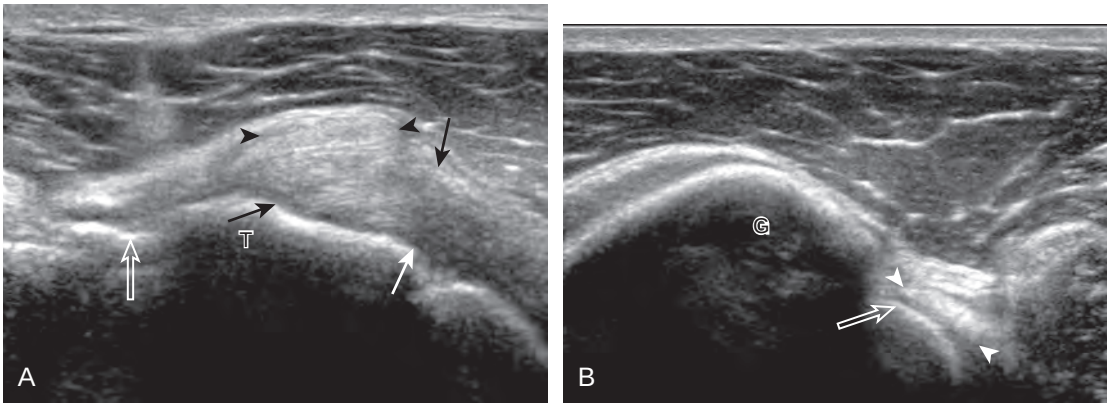

FIGURE 3-87 ■ Biceps brachii tendon dislocation with dynamic relocation. Ultrasound image of biceps brachii long head tendon in short axis **(A)** shows the biceps tendon *(arrowheads)* dislocated superficial to the lesser tuberosity (T) and subscapularis tendon *(arrows)*, which returns to a normal location **(B)** at internal shoulder rotation associated with a painful snap (*open arrows*, bicipital groove; G, greater tuberosity).

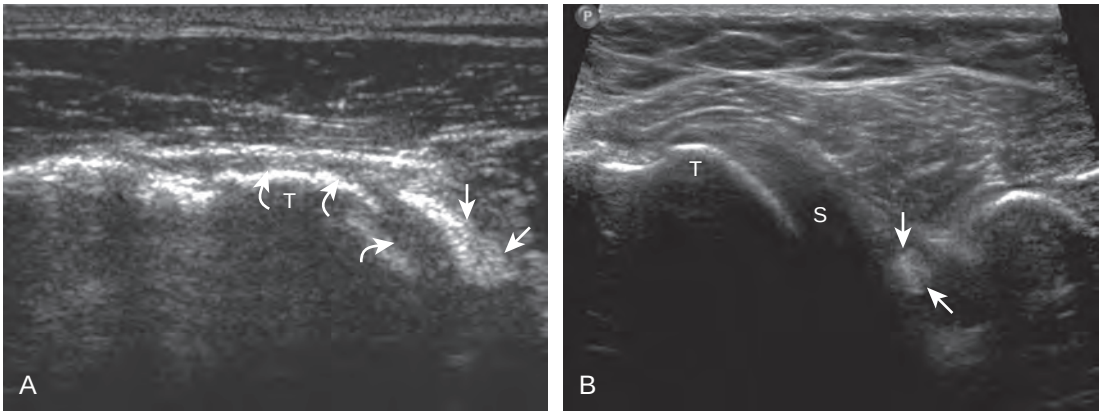

FIGURE 3-88 ■ Biceps brachii tendon dislocation over subscapularis. Ultrasound images of biceps brachii tendon in short axis in two different patients show medial dislocation of biceps *(arrows)*. Note subscapularis tear *(curved arrows)* in **(A)** and normal subscapularis tendon with anisotropy (S) in **(B)** (right side of image is medial). T, lesser tuberosity.

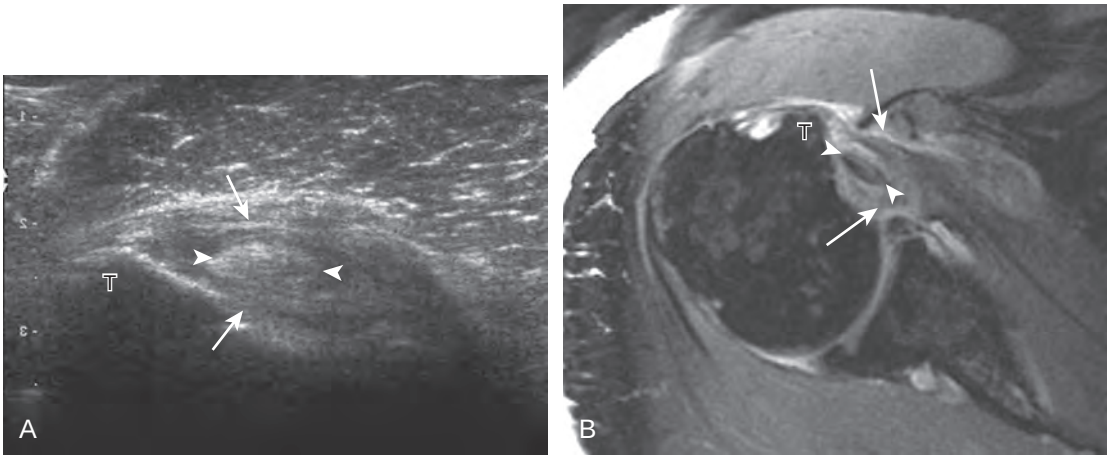

FIGURE 3-89 ■ Biceps brachii tendon dislocation into subscapularis. Ultrasound image **(A)** of biceps brachii tendon in short axis and **(B)** T2-weighted axial magnetic resonance image show medial dislocation of the biceps tendon *(arrowheads)* within the substance of the torn subscapularis tendon *(arrows)* (right side of image A is medial). T, lesser tuberosity.

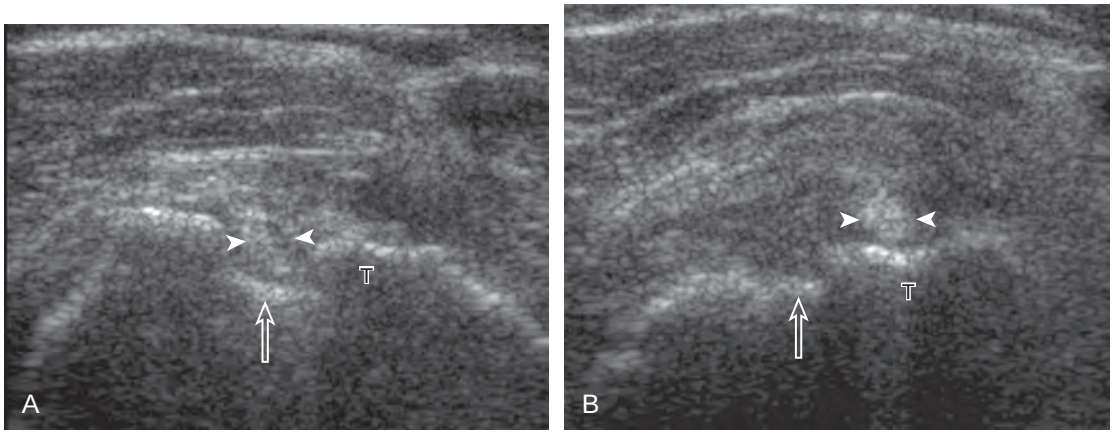

FIGURE 3-90 ■ Transient biceps brachii tendon dislocation. Ultrasound images of biceps brachii tendon in short axis in neutral **(A)** and external rotation **(B)** show medial dislocation of the biceps tendon *(arrowheads)* in **B** (*open arrows*, bicipital groove; right side of images is medial). T, lesser tuberosity.

over the lesser tuberosity in neutral shoulder position may relocate into the bicipital groove, with shoulder internal rotation associated with a painful snap (see Fig. 3-87) (Video 3-37). Subluxation or dislocation of the biceps brachii tendon can be associated with biceps tendon tear (Fig. 3-91).

SUBACROMIAL-SUBDELTOID BURSA

The normal subacromial-subdeltoid bursa is a synovial space, separate from the glenohumeral joint, located between the rotator cuff and the overlying acromion and deltoid muscle (see Fig. 3-1). At ultrasound it appears as a thin, uniform, 1- to 2-mm hypoechoic layer of synovial fluid surrounded by hyperechoic bursal wall and peribursal fat layers.[11,37] Abnormal distention of the subacromial-subdeltoid bursa may appear anechoic or hypoechoic from simple fluid, or it may range from hypoechoic to hyperechoic as a result of complex fluid or synovial hypertrophy (Fig. 3-92). Color or power Doppler imaging may differentiate complex fluid from synovitis because blood flow suggests synovial hypertrophy (Fig. 3-93). The term *bursitis* is often reserved for cases in which inflammation is truly present. Causes of subacromial-subdeltoid bursal distention include impingement, rotator cuff tear, hemorrhage (Fig. 3-94A), and amyloidosis. Inflammatory conditions should also be considered, such as gout (see Fig. 3-94B), rheumatoid arthritis (see Fig. 3-94C), and infection.[37] Identification of hyperechoic foci with ring-down artifact within a complex bursal fluid collection raises concern for gas-producing infection (see Fig. 3-93C). Calcium hydroxyapatite deposition may be located in the bursa (Fig. 3-95) (Video 3-38), or it may extend from the adjacent rotator cuff (see Fig. 3-63). Focal thickening of the subacromial-subdeltoid bursa can indicate chronic impingement; dynamic imaging during active elevation of the arm should be completed to evaluate for impingement of the thickened bursa beneath the acromion, possibly associated with a snapping sensation (see Videos 3-30 and 31). With regard to rotator cuff tears, it has been shown that the presence of subacromial-subdeltoid bursal fluid has a 70% positive predictive value for rotator cuff tear; a combination of joint fluid distention of the long head of the biceps brachii tendon sheath and subacromial-subdeltoid fluid increases the positive predictive

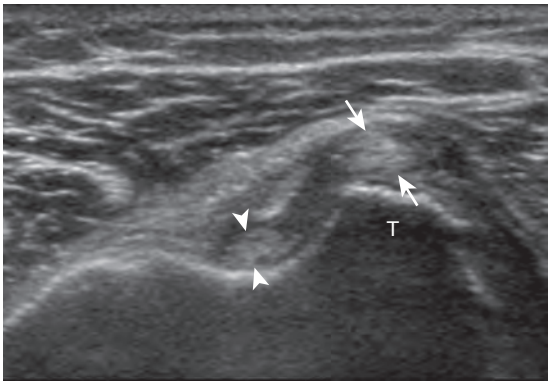

FIGURE 3-91 ■ Biceps brachii tendon split tear and partial dislocation. Ultrasound image of biceps brachii tendon in short axis longitudinal split tear of biceps with part of the tendon dislocated medial *(arrows)* and the other part *(arrowheads)* within the bicipital groove (right side of images is medial). T, lesser tuberosity.

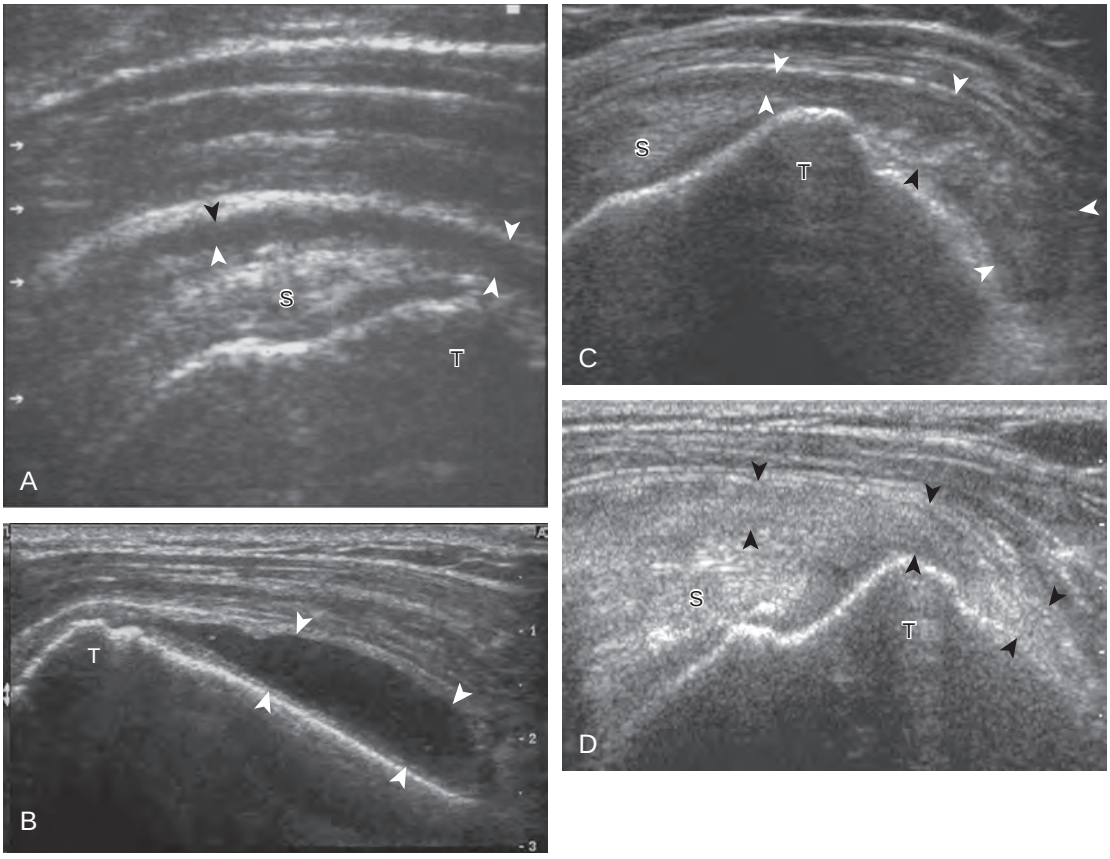

FIGURE 3-92 ■ Subacromial-subdeltoid bursal distention. Ultrasound images long axis to the distal supraspinatus tendon in four different patients show anechoic bursal distention *(arrowheads)* **(A** and **B);** heterogeneous distention from complex fluid, hemorrhage, and synovitis **(C);** and isoechoic/hyperechoic distention from synovial hypertrophy in **(D)**. S, supraspinatus tendon; T, greater tuberosity.

value to 95%.[36] Other causes of subacromial-subdeltoid bursal distention include synovial proliferative disorders, such as pigmented villonodular synovitis and synovial osteochondromatosis.

When the subacromial-subdeltoid bursa is distended, fluid often collects dependently, such as over and beyond the greater tuberosity (see Fig. 3-92B) (see Video 3-22).[37] In this situation, it is important to evaluate this dependent portion of the subacromial-subdeltoid bursa because it may not be readily visualized when evaluation is focused over the rotator cuff at or proximal to the greater tuberosity. Another dependent area of the subacromial-subdeltoid bursa that may become distended is anteriorly over the bicipital groove, often seen in evaluation of the biceps brachii long head tendon (Fig. 3-96). It is important not to mistake this bursal distention for a biceps tendon sheath abnormality (see Video 3-21). More proximal evaluation in the sagittal plane assists in this distinction because bursal disease extends proximally over the rotator cuff, whereas biceps tendon sheath disease either terminates proximally or extends into the joint with the biceps long head tendon. Focal anterior distention of the subacromial-subdeltoid bursa with extension and internal rotation of the shoulder can be associated with symptoms related to coracoid impingement.[61]

GLENOHUMERAL JOINT AND RECESSES

The glenohumeral joint has several recesses that preferentially distend with joint fluid or other joint processes, which include the biceps brachii long head tendon sheath, the posterior glenohumeral joint recess, the subscapularis recess, and the axillary recess. These recesses should be assessed for pathology and also serve as potential sites for joint aspiration or injection. The joint recess where even small amounts of joint fluid

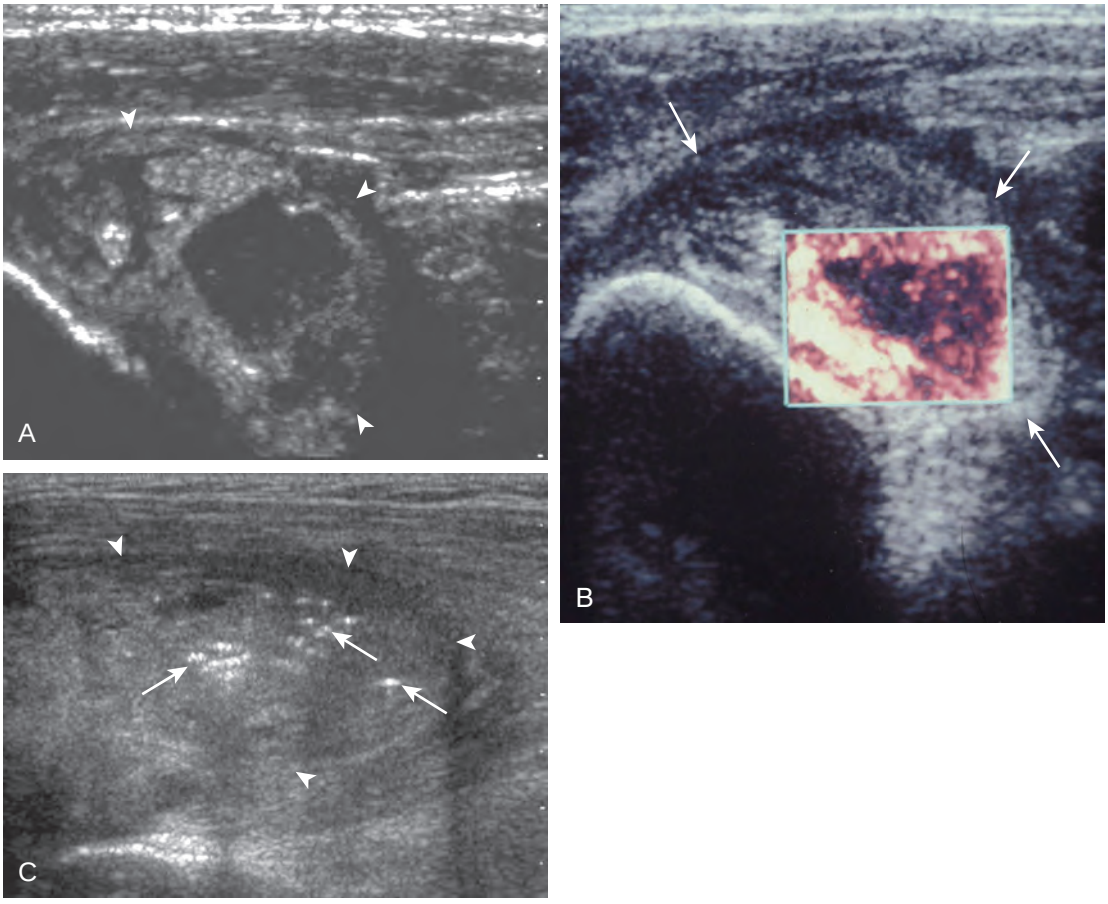

FIGURE 3-93 ■ Septic subacromial-subdeltoid bursitis. Gray-scale **(A)** and power Doppler **(B)** ultrasound images show heterogeneous bursal distention *(arrows* and *arrowheads)* with increased blood flow. **C,** Ultrasound image over the greater tuberosity in a different patient shows heterogeneous distention of the bursa *(arrowheads)* with hyperechoic gas formation *(arrows).*

can be seen is the biceps brachii long head tendon sheath (see Fig. 3-75).[68] As discussed previously, the differential diagnosis for abnormality surrounding the biceps tendon at the bicipital groove includes both localized biceps tenosynovitis (see Fig. 3-77) and a more diffuse joint process related to the glenohumeral joint. Assessing the other joint recess assists in this differential. A pathologic process surrounding the biceps tendon that is out of proportion to findings in other glenohumeral joint recesses suggests a localized process. Another glenohumeral joint recess includes the posterior recess, which is assessed with transducer placement over the infraspinatus tendon, where joint fluid, synovial hypertrophy and intra-articular bodies may be identified (Fig. 3-97) (Videos 3-39 and 3-40). Small amounts of joint fluid may only become visible at this site with the shoulder in external rotation (see Video 3-20).[68] The subscapularis recess also is commonly distended and has a characteristic shape of an inverted "U" over the top of the subscapularis tendon near the coracoid process (Fig. 3-98). This shape distinguishes the subscapularis recess from the uncommon subcoracoid bursa, which is located anterior the subscapularis tendon directly inferior to the coracoid but is not located over the superior edge of the subscapularis tendon and does not communicate with the glenohumeral joint.[72] Another feature of the subscapularis bursa is its change in shape and degree of distention with shoulder movement, increasing with internal rotation and decreasing in external rotation (Video 3-41). The axillary recess is located inferior to the glenohumeral joint imaged from the axilla. In addition to assessing for joint fluid, other joint processes such as intra-articular bodies and synovial hypertrophy can be visible in any of the above described joint recesses. Cortical irregularity involving the articular surface of the humerus could represent osteophytes (see Fig. 3-97A), an osteochondral abnormality, subchondral fracture or collapse from osteonecrosis, a Hill Sachs impaction

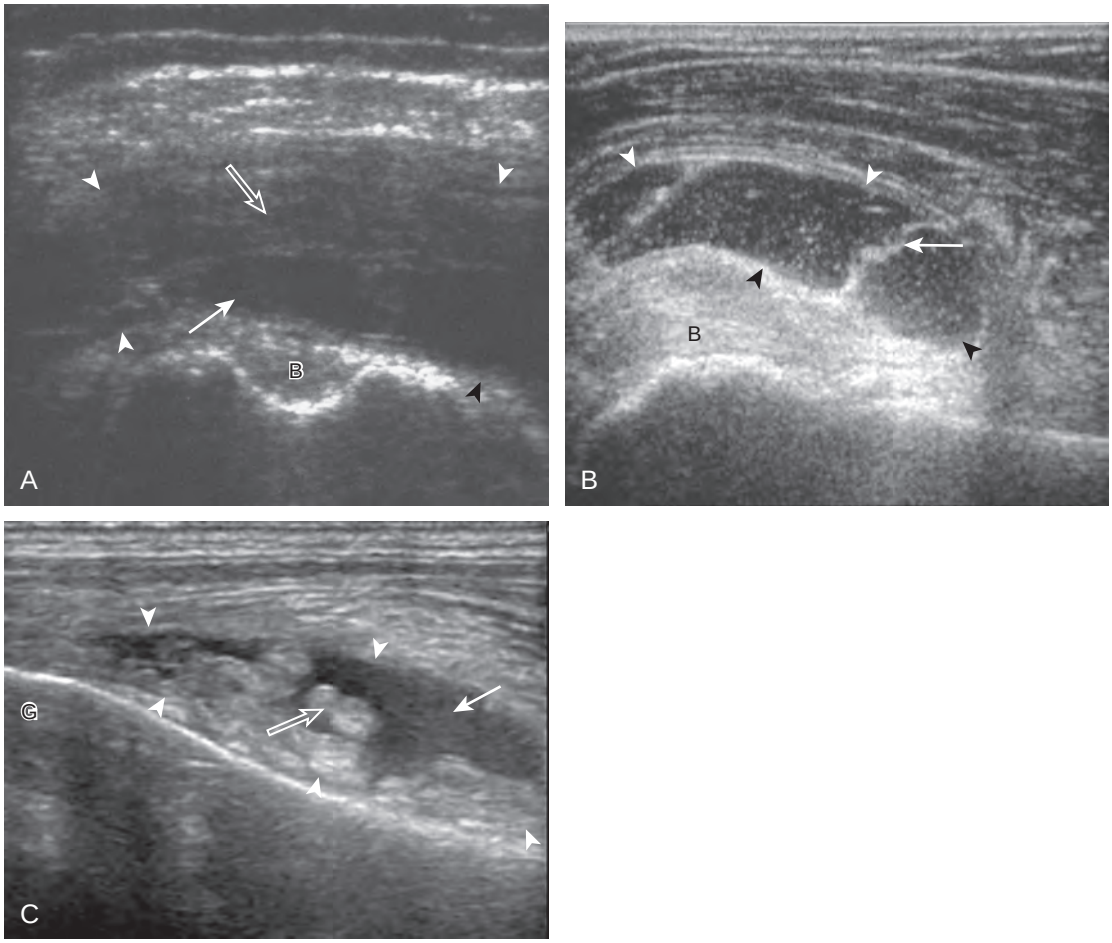

FIGURE 3-94 ■ Subacromial-subdeltoid bursitis. Ultrasound images in three different patients show **(A)** bursal distention *(arrowheads)* appearing as anechoic fluid *(arrow)* and hypoechoic synovitis *(open arrow)* from hemophilia, **(B)** complex fluid and septations *(arrow)* from gout, and **(C)** anechoic fluid *(arrow)* with hyperechoic synovial hypertrophy *(open arrow)* from rheumatoid arthritis. B, biceps tendon; G, greater tuberosity.

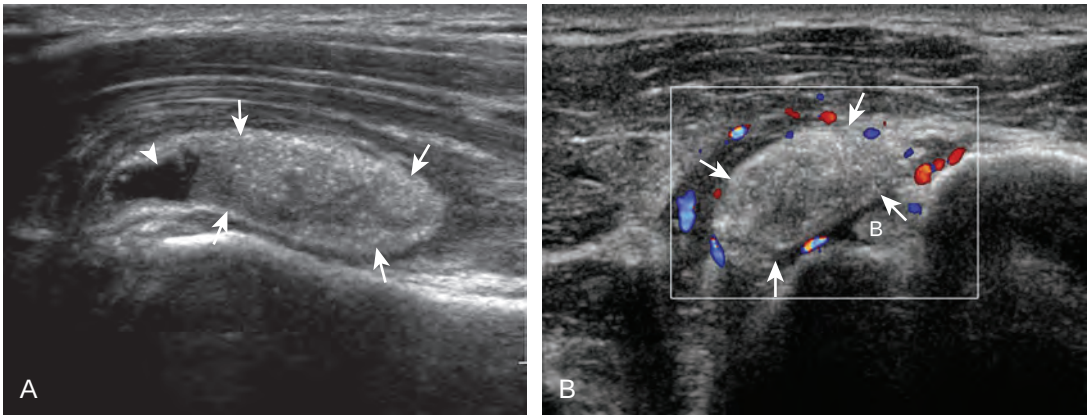

FIGURE 3-95 ■ Calcific bursitis. Ultrasound images **(A, B)** over subacromial-subdeltoid bursa show hyperechoic calcific deposit within bursa *(arrows)*, adjacent anechoic bursal fluid *(arrowhead)*, and (B) surrounding hyperemia. B, biceps brachii long head tendon.

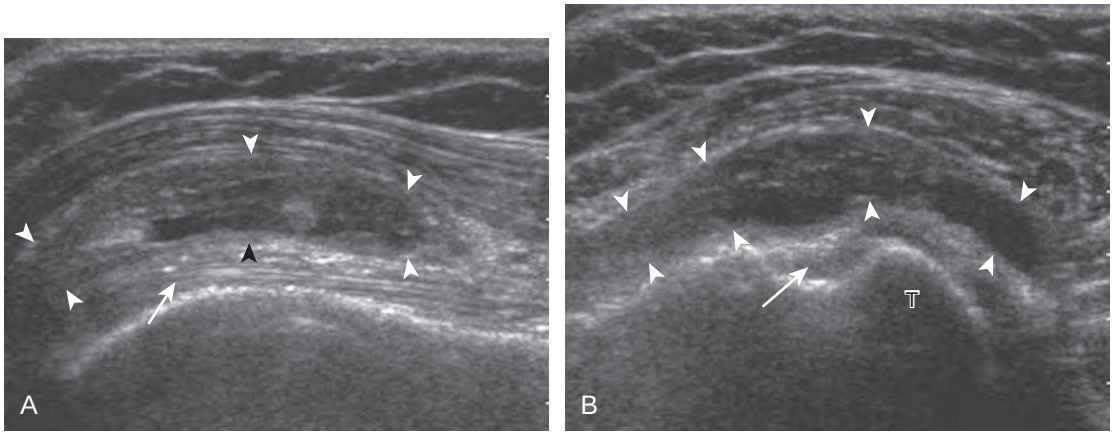

FIGURE 3-96 ■ Subacromial-subdeltoid bursal distention. Ultrasound images in long axis **(A)** and short axis **(B)** to the biceps brachii long head tendon show heterogeneous bursal distention *(arrowheads)* superficial to the biceps tendon *(arrows)* (right side of image in **A** is distal, medial in **B**). T, lesser tuberosity.

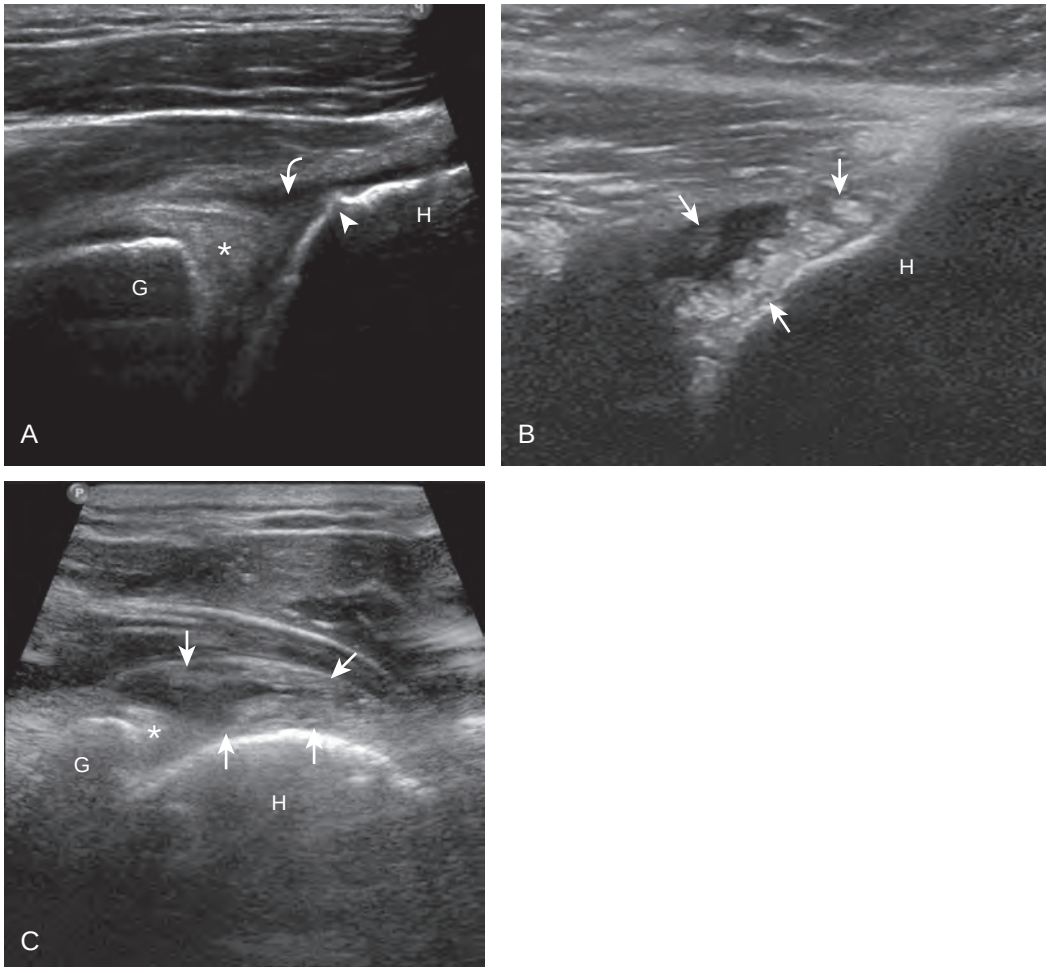

FIGURE 3-97 ■ Posterior glenohumeral joint recess. Ultrasound images in long axis to the infraspinatus tendon in three different patients show **(A)** anechoic fluid *(curved arrow)* with adjacent osteophyte *(arrowhead)*, **(B)** anechoic fluid with echogenic intra-articular hemorrhage *(arrows)*, and **(C)** anechoic fluid with isoechoic synovial hypertrophy *(arrows)* (*asterisk* indicates labrum; right side of images is lateral). H, humeral head; G, glenoid.

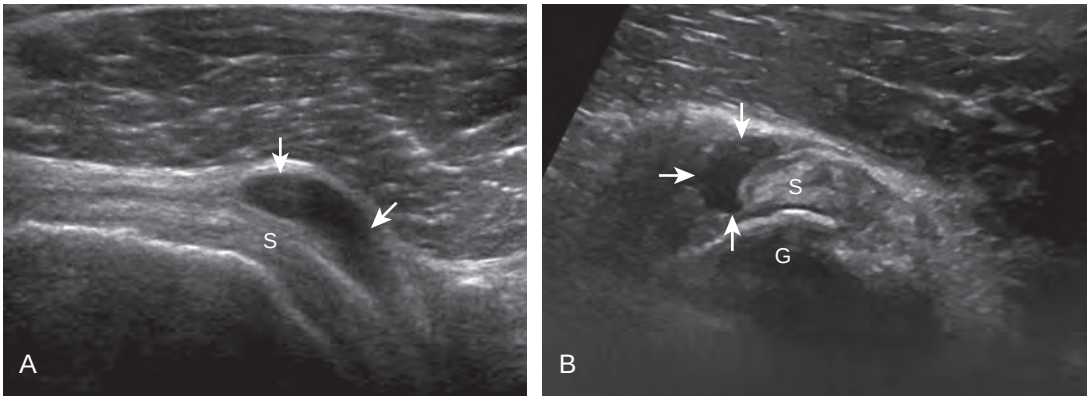

FIGURE 3-98 ■ Subscapularis recess. Ultrasound images of subscapularis in **(A)** long axis and **(B)** short axis show anechoic fluid distention of the subscapularis recess *(arrows)* (right side of image A is medial; right side of image B is inferior). G, glenoid; S, subscapularis tendon.

fracture (Fig. 3-99A), or possibly a true erosion if adjacent synovial hypertrophy (Fig. 3-99B and C). The latter should be differentiated anatomically from cortical irregularity of the greater tuberosity, which is not an inflammatory erosion but rather related to rotator cuff tear (see Figs. 3-21 and 3-22). The adjacent hyaline cartilage and humeral head can also be assessed for layering of monosodium urate crystals (called the double contour sign) in gout.[73]

GLENOID LABRUM AND PARALABRAL CYST

The glenoid labrum is a fibrocartilaginous structure located at the rim of the glenoid, which serves to help stabilize the glenohumeral joint. The normal labrum appears as a hyperechoic, triangular structure attached to the bony glenoid (see Fig. 3-18B).[74] Heterogeneous hypoechogenicity of the labrum indicates degeneration,

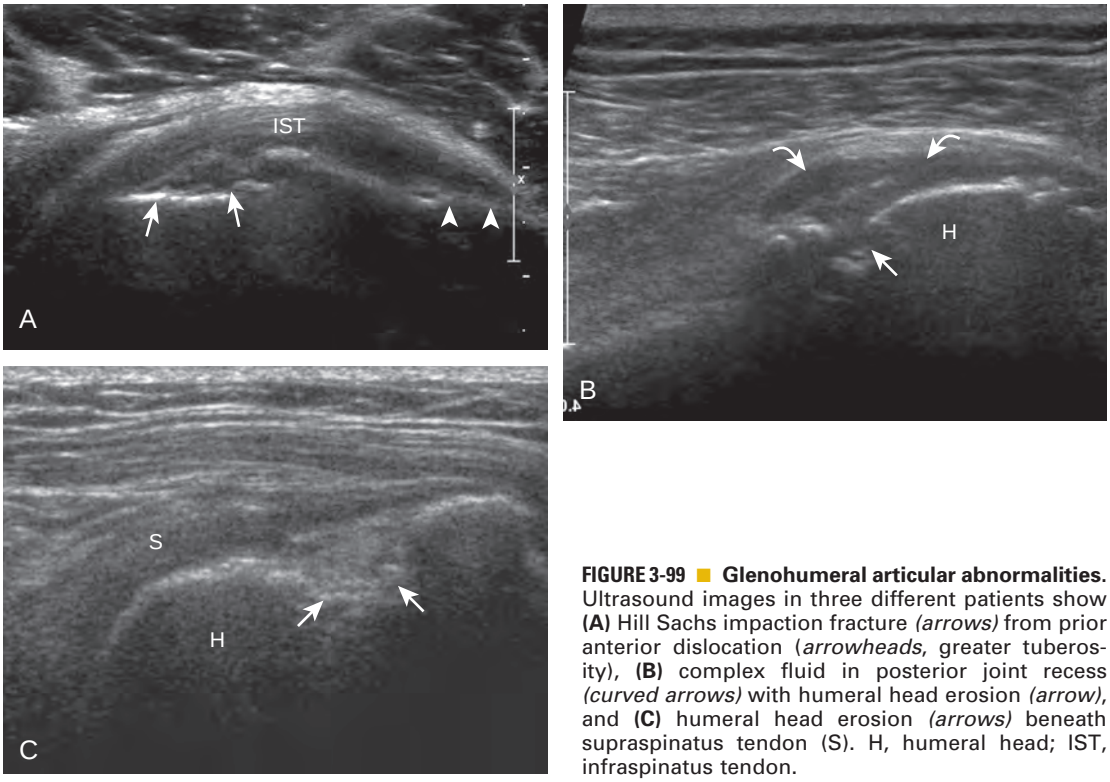

FIGURE 3-99 ■ Glenohumeral articular abnormalities. Ultrasound images in three different patients show **(A)** Hill Sachs impaction fracture *(arrows)* from prior anterior dislocation (*arrowheads*, greater tuberosity), **(B)** complex fluid in posterior joint recess *(curved arrows)* with humeral head erosion *(arrow)*, and **(C)** humeral head erosion *(arrows)* beneath supraspinatus tendon (S). H, humeral head; IST, infraspinatus tendon.

whereas a well-defined hypoechoic or anechoic cleft indicates labral tear (Fig. 3-100) (Video 3-42).[67] Ultrasound is most helpful when the labrum appears normal; an abnormal-appearing labrum at ultrasound should be followed with MRI or preferably magnetic resonance arthrography to define the labral abnormality. One major limitation of ultrasound in evaluation of the labrum is difficultly in visualizing the entire extent of the labrum. The anterior labrum is more difficult to demonstrate compared with the posterior labrum because of the thickness of the overlying soft tissues; evaluation with dynamic imaging may be helpful.[75] Similarly, it is extremely difficult to visualize the superior labrum because of the overlying osseous structures. Nonetheless, routine evaluation of the posterior labrum is easily accomplished during evaluation of the infraspinatus tendon, an area where paralabral cyst formation may occur. It is helpful to evaluate the posterior labrum with the shoulder in external rotation because this position causes joint fluid to locate around the labrum in the posterior glenohumeral joint recess, thereby making a labral tear more conspicuous. The transducer can also be placed over the supraspinatus muscle between the clavicle and scapular spine long axis to the supraspinatus to evaluate for suprascapular notch paralabral cyst.

When a cystic abnormality is seen adjacent to the glenoid labrum, the diagnosis of paralabral cyst should be considered (Fig. 3-101) (Video 3-43).[76] In this setting, an underlying labral tear is usually present. Ultrasound may show the joint fluid extension through the labral tear, which communicates with the paralabral cyst analogous to a parameniscal cyst in the knee. One must be aware that paralabral cysts may extend away from the labrum. This may occur at the suprascapular notch (at the superior margin of the scapula) and at the spinoglenoid notch (between the scapula and base of the scapular spine). It is important to scan medial to the glenoid routinely when imaging the infraspinatus tendon in long axis to evaluate for spinoglenoid notch paralabral cyst. One must not mistake a dilated suprascapular vein transiently present in shoulder-external rotation for a paralabral cyst in the spinoglenoid notch (Fig. 3-102) (see Video 3-14); however, fixed dilation or venous varix may cause suprascapular nerve compression.[77] One potential complication of a posterior paralabral cyst is suprascapular nerve entrapment, which may cause denervation and atrophy of the infraspinatus muscle (when spinoglenoid) or of both supraspinatus and infraspinatus muscles (when suprascapular in location), associated with shoulder pain and weakness (see Fig. 3-52). Although

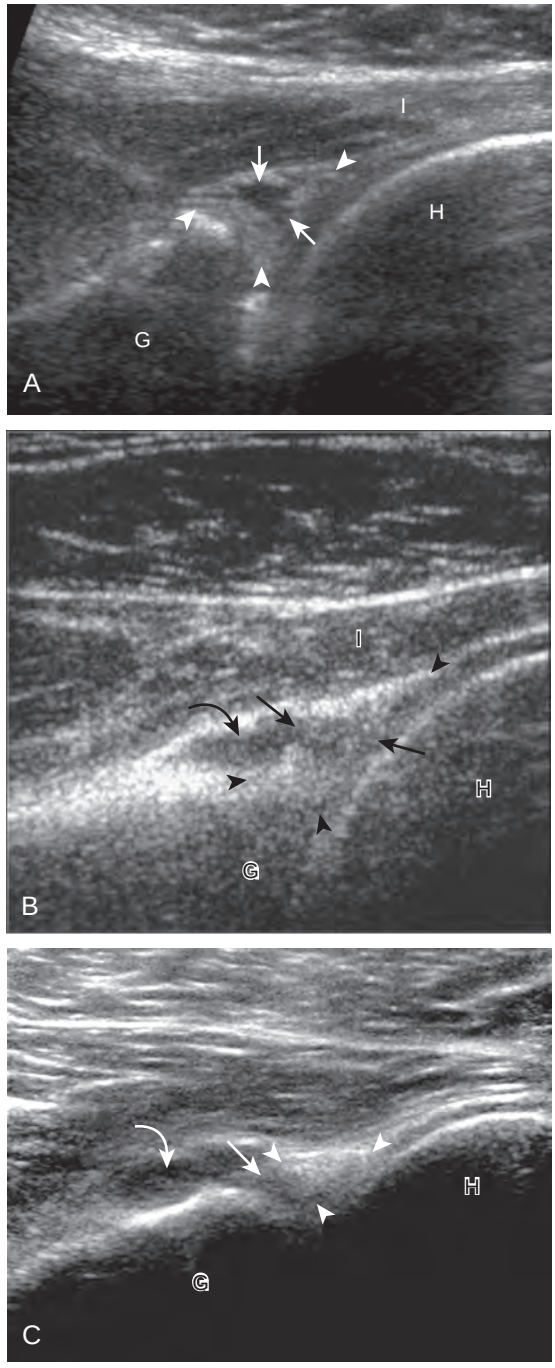

FIGURE 3-100 ■ **Labral tear. A** to **C,** Ultrasound images in long axis to the infraspinatus in three different patients show a hypoechoic cleft *(arrows)* within the posterior labrum *(arrowheads)*. There is an associated paralabral cyst in **(B** and **C)** *(curved arrows)* (right side of image is distal relative to the infraspinatus tendon). G, glenoid; H, humeral head; I, infraspinatus.

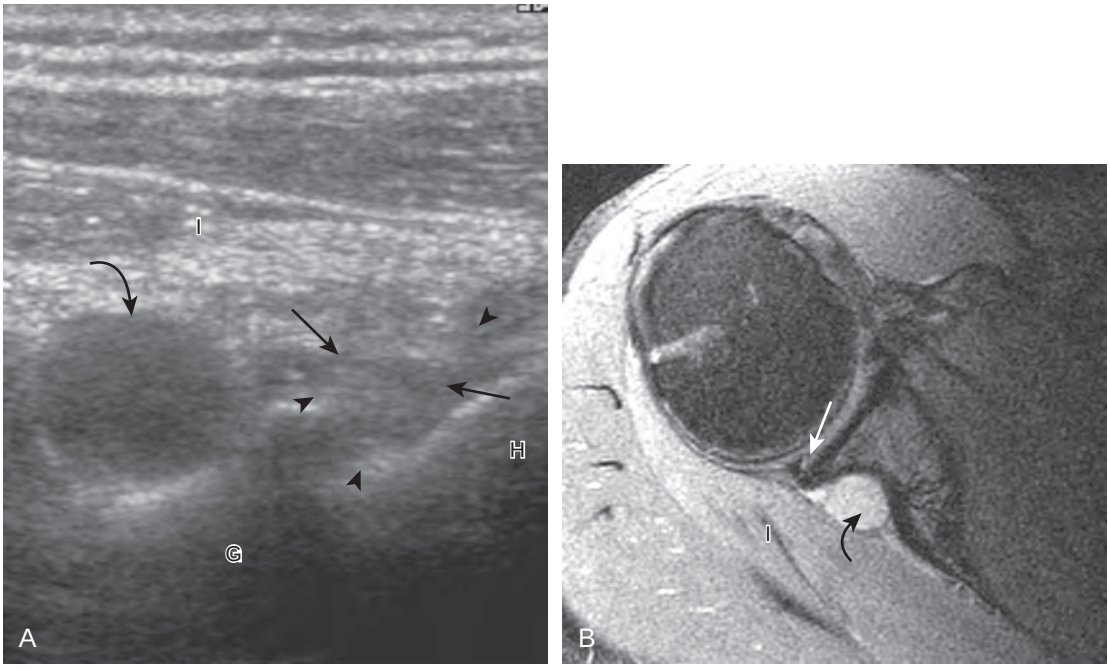

FIGURE 3-101 ■ Paralabral cyst. Ultrasound images in long axis to the infraspinatus **(A)** and T2-weighted axial magnetic resonance image **(B)** show a hypoechoic cleft *(arrows)* within the diffusely hypoechoic posterior labrum *(arrowheads)*. There is an associated spinoglenoid notch paralabral cyst (*curved arrows*). Note atrophy of the infraspinatus (I), appearing small and hyperechoic in A and with increased signal in B. G, glenoid; H, humeral head.

visualization of the normal suprascapular nerve may be difficult, identification of the adjacent suprascapular artery with color or power Doppler imaging assists in its localization. The suprascapular nerve and artery extend inferiorly along the posterior margin of the scapular through the spinoglenoid notch. Ultrasound-guided percutaneous aspiration of a paralabral cyst can be performed (see Chapter 9), although the cyst may recur unless the underlying labral tear is repaired or treated.

GREATER TUBEROSITY

It is not uncommon to identify a greater tuberosity fracture during routine evaluation of the rotator cuff after trauma. This is because a greater tuberosity fracture may be overlooked at radiography, and the patient may then present for ultrasound to evaluate for rotator cuff tear. At sonography, a greater tuberosity fracture appears as a cortical step-off and discontinuity at the junction of the humeral articular surface and greater

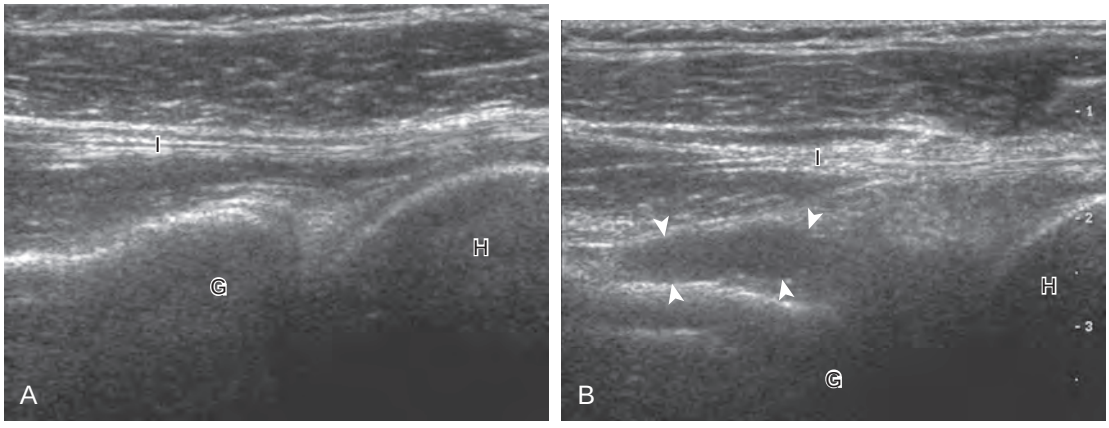

FIGURE 3-102 ■ Transient suprascapular vein dilation. Ultrasound images in long axis to the infraspinatus in neutral **(A)** and external rotation **(B)** show transient dilation of the suprascapular vein *(arrowheads)* (right side of image is distal relative to the infraspinatus). G, glenoid; H, humeral head; I, infraspinatus. No flow was present at power Doppler imaging, which is common given slow flow. Collapse of the suprascapular vein is another differentiating feature from paralabral cyst.

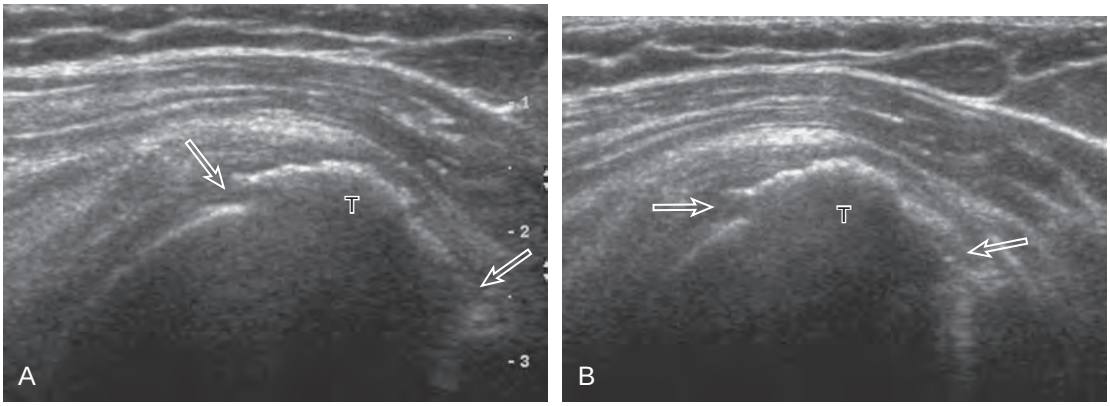

FIGURE 3-103 ■ Greater tuberosity fracture. Ultrasound images in long axis **(A)** and short axis **(B)** to the supraspinatus tendon show cortical discontinuity and step-off deformity *(open arrows)*. T, greater tuberosity.

tuberosity (Fig. 3-103) (Video 3-44).[78] The distal aspect of the fracture is often seen over the lateral aspect of the greater tuberosity or near the humeral metaphysis. It is important not to mistake the step-off deformity of fracture for cortical irregularity of the greater tuberosity related to rotator cuff tear. In the latter situation, focal pitting and cortical irregularity are present at the supraspinatus footprint, whereas fracture is characterized by a long segment cortical step-off and discontinuity at the margins of the greater tuberosity. Often, there is point tenderness directly over the fracture.

PECTORALIS MAJOR

Evaluation of the pectoralis major muscle tendon may not be a part of the routine shoulder examination but rather a focused examination directed by a patient's history or symptoms. The pectoralis muscle consists of two heads, a clavicular head that originates from the medial two thirds of the clavicle, and a sternal head that consists of manubrial and abdominal laminae that originate from the sternum and a portion of the costal cartilage, ribs, and abdominal fascia. As the tendons of the two pectoralis muscular heads extend toward the humerus, they twist 180 degrees so that the clavicular head moves anterior and inferior to the sternal head, which results in the sternal head being superior to the clavicular head at the humerus. The tendon's attachment is 4 to 6 cm in sagittal length just lateral to the bicipital groove of the humeral diaphysis.[79,80]

Evaluation of the pectoralis begins with the biceps brachii long head tendon in short axis over the bicipital groove. The transducer is then moved inferior to the subscapularis tendon attachment, where the pectoralis tendon is identified as it extends over the biceps tendon to attach on the humerus (see Fig. 3-4D). It is important to scan superiorly and inferiorly through the entire 4- to 6-cm tendon attachment to ensure complete evaluation, keeping in mind that the sternal head is superior to the clavicular head. Once the pectoralis major tendon is identified, the transducer can be moved medially to visualize the musculotendinous junction and muscle belly.

Tendon tears appear as hypoechoic or anechoic tendon disruption (Fig. 3-104). Tendon retraction indicates full-thickness tear of at least one of the pectoralis heads. The distinction between musculotendinous junction tear and a more distal tendon tear or bone avulsion is important because the latter requires surgery. Hypoechoic edema with a hyperechoic fracture fragment at the humerus indicates avulsion, whereas nonvisualization of the tendon over the biceps brachii long head tendon indicates a distal tendon tear. A musculotendinous junction abnormality with visible distal tendon is characteristic of a musculotendinous tear. Most pectoralis major tears are partial-thickness tears (one head is torn while the other is intact) located at the musculotendinous junction, most commonly of the sternal head. In this situation, the full-thickness tear of the sternal head may only minimally retract as the clavicular head remains intact. Most full-thickness tears usually involve the distal tendon or the attachment of tendon to the humerus.

ACROMIOCLAVICULAR JOINT

The acromioclavicular joint is routinely evaluated in shoulder sonography. If there is difficulty

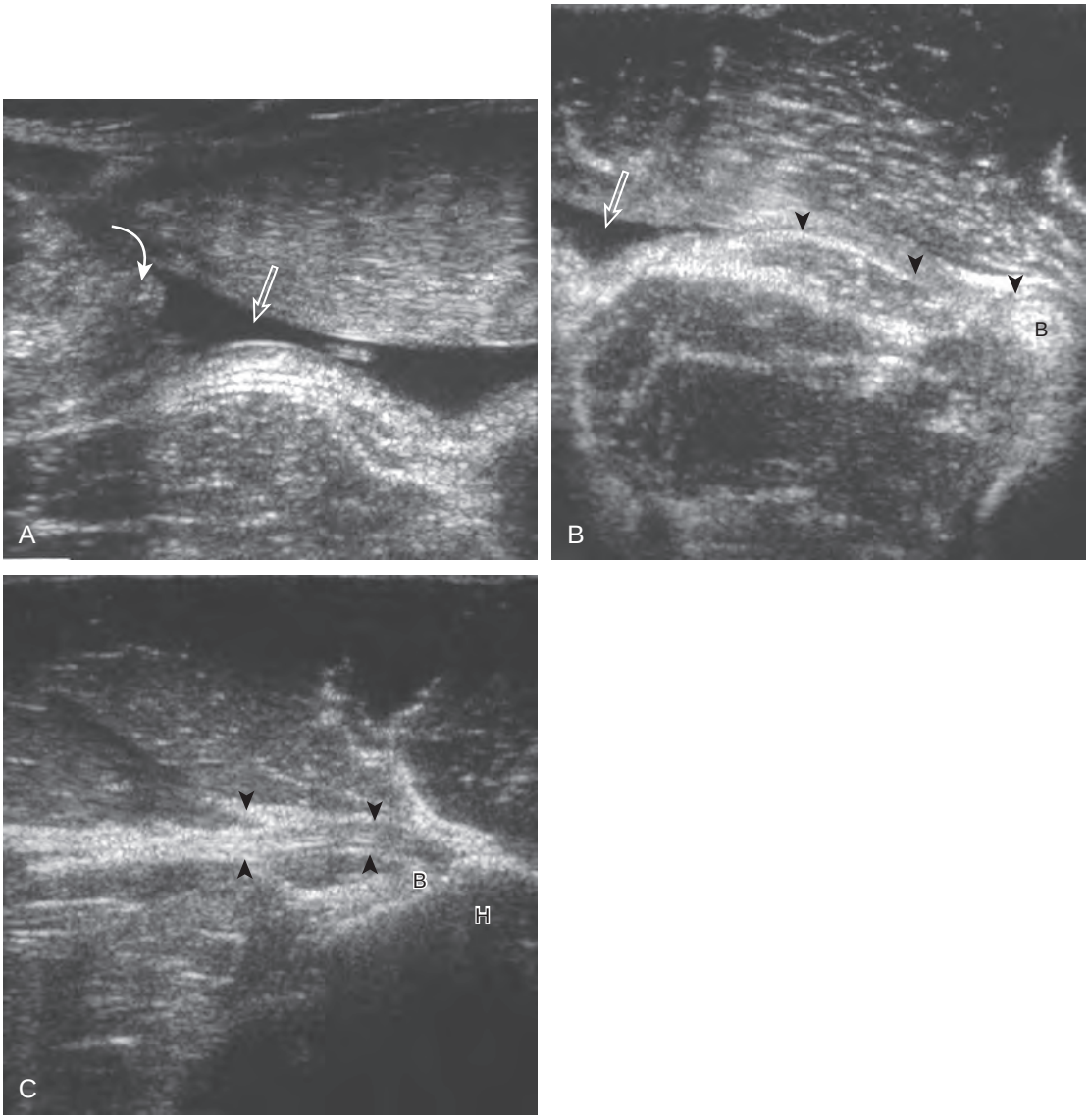

FIGURE 3-104 ■ **Pectoralis major tear.** Ultrasound images in long axis **(A** and **B)** to the pectoralis major show the retracted tear *(curved arrow),* adjacent hemorrhage *(open arrow),* and no visible tendon in its expected location *(arrowheads)* superficial to the biceps tendon (B) (left side of image is proximal relative to the tendon). Ultrasound image long axis **(C)** to the contralateral asymptomatic pectoralis major shows a normal distal tendon *(arrowheads).* H, humerus. (**B** and **C,** From Weaver JS, Jacobson JA, Jamadar DA, et al: Sonographic findings of pectoralis major tears with surgical, clinical, and magnetic resonance imaging correlation in 6 patients. *J Ultrasound Med* 24:28, 2005. Reproduced with permission from the American Institute of Ultrasound in Medicine.)

finding this structure, it can be palpated directly or found by following the clavicle laterally. The acromioclavicular joint can also be found by scanning superiorly from the bicipital groove region in the transverse plane. The normal acromioclavicular joint has smooth cortical margins with less than 3 mm of hypoechoic joint capsule distention.[81] The intra-articular fibrocartilage disk appears hyperechoic but may be difficult to identify. Several pathologic processes involve the acromioclavicular joint.[14] The most common pathologic condition is degenerative osteoarthritis (Fig. 3-105A), seen frequently after the age of 40 years. In this situation, the capsule may be distended, and later there will be bone irregularity, osteophyte formation, and joint space narrowing (often seen with dynamic imaging). The intra-articular fibrocartilage disk is disintegrated in most individuals after the age of 40 years from routine overuse and degenerative change.[82] Cysts

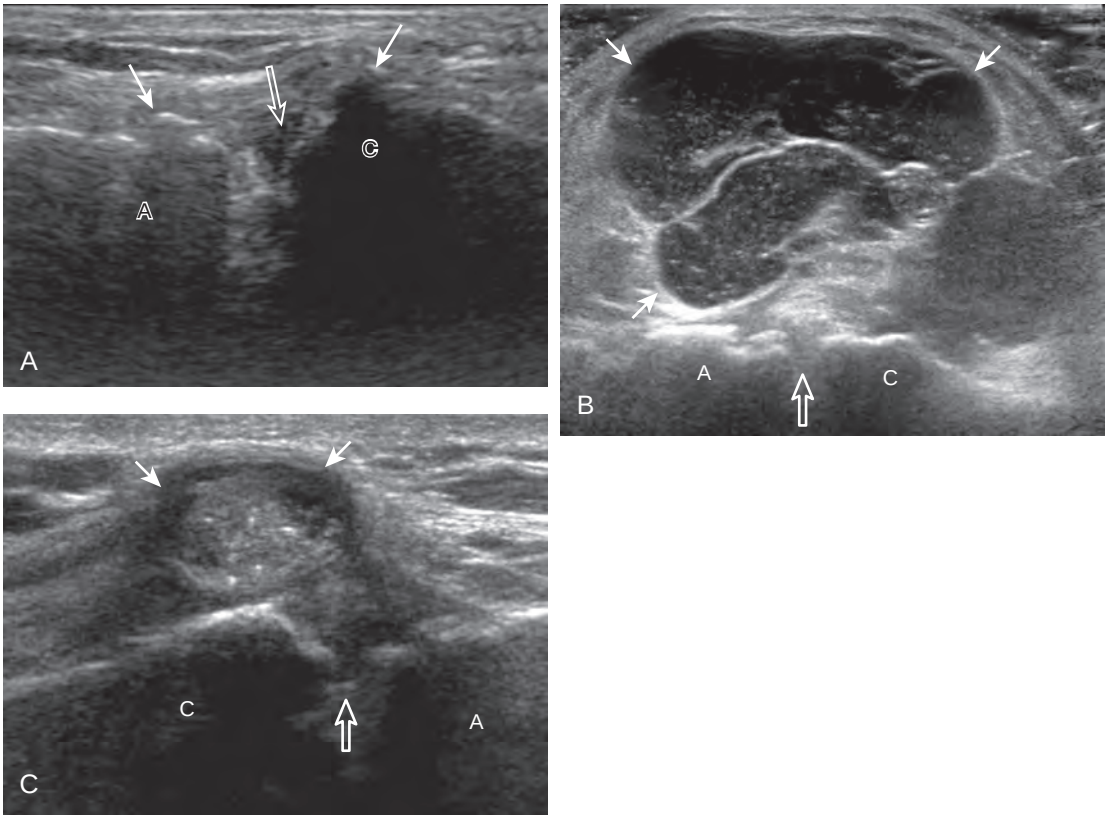

FIGURE 3-105 ■ Acromioclavicular joint osteoarthrosis and cysts. Ultrasound images long axis to the clavicle in three different patients show **(A)** cortical irregularity *(arrows)* from osteophytes and hypoechoic intra-articular fluid *(open arrow)* caused by osteoarthritis, **(B)** a complex cyst *(arrows)* that originates from the acromioclavicular joint *(open arrow)*, and **(C)** synovial fluid *(arrows)* that has extended superiorly through a massive cuff tear and the acromioclavicular joint *(open arrow)* (termed the *geyser sign*). A, acromion; C, clavicle.

may be associated with the acromioclavicular joint, which can produce a mass on physical examination (see Fig. 3-105B). This may be the result of glenohumeral joint fluid that tracks into the acromioclavicular joint in the setting of a chronic and massive supraspinatus tendon tear, called the *geyser sign* (see Fig. 3-105C). If there is widening of the acromioclavicular joint, considerations include trauma and inflammation. In the setting of the acute trauma, one may see widening of the joint, possible elevation of the clavicle, and possible hyperechoic step-off fracture. If symptomatic, it is important to evaluate the acromioclavicular joint dynamically for ligament abnormality (Video 3-45), as described earlier in the section on ultrasound examination techniques (Fig. 3-106).[14,15] With more chronic injury, the acromioclavicular joint may be widened as a result of distal clavicular resorption, termed *post-traumatic osteolysis*, often seen in weight lifters. When widening and cortical irregularity of the distal clavicle and adjacent acromion are associated with fluid or synovial distention of the joint capsule and hyperemia, inflammatory conditions, such as rheumatoid arthritis and infection, should be considered. Infection is more common in intravenous drug abusers and those with septicemia, and ultrasound-guided joint aspiration should be completed to exclude the diagnosis (see Chapter 9) (Fig. 3-107).

STERNOCLAVICULAR JOINT

Ultrasound may be used to evaluate the sternoclavicular joint.[14] A septic joint appears as distention of the joint capsule, with variable-echogenicity fluid and synovitis (Fig. 3-108). Bone erosions, as well as joint space widening or subluxation, may occur. The findings of joint distention greater than 10 mm that extends over both the clavicle and sternum, elevated Westergren red blood cell sedimentation rate, and fever are strong indicators of infection.[83] Ultrasound-guided percutaneous aspiration is recommended if there is any concern for infection. In older women, it is not

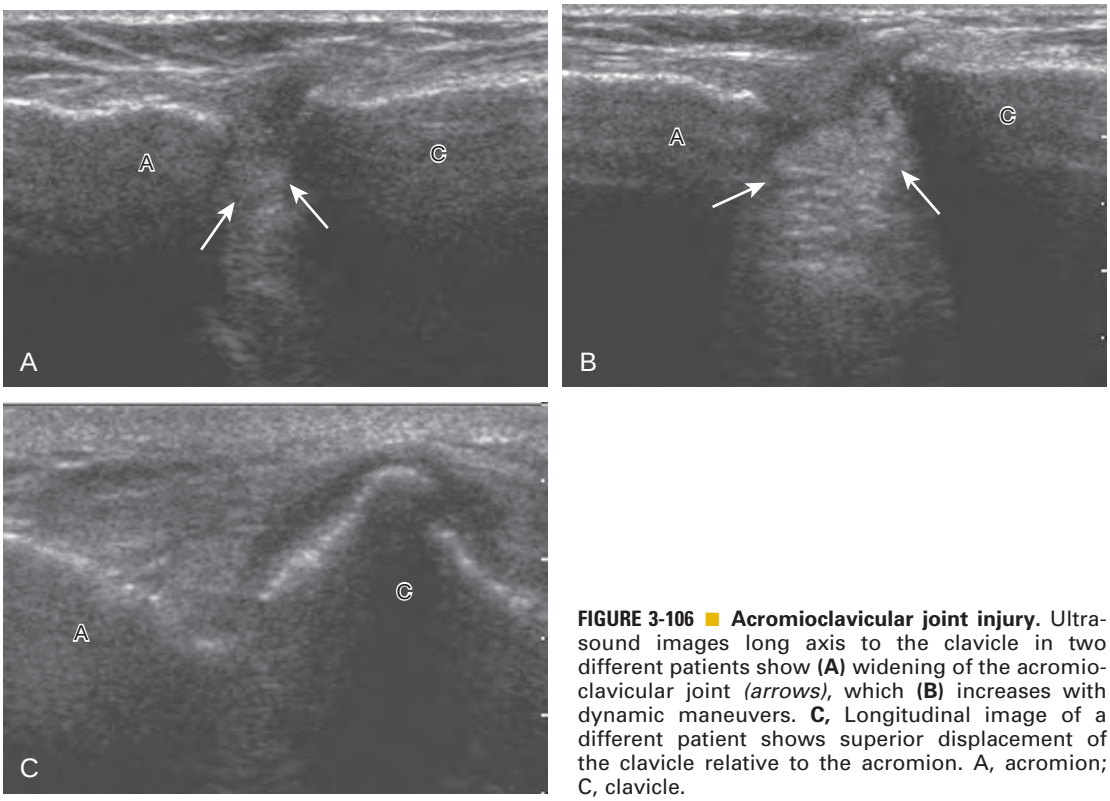

FIGURE 3-106 ■ Acromioclavicular joint injury. Ultrasound images long axis to the clavicle in two different patients show **(A)** widening of the acromioclavicular joint *(arrows)*, which **(B)** increases with dynamic maneuvers. **C,** Longitudinal image of a different patient shows superior displacement of the clavicle relative to the acromion. A, acromion; C, clavicle.

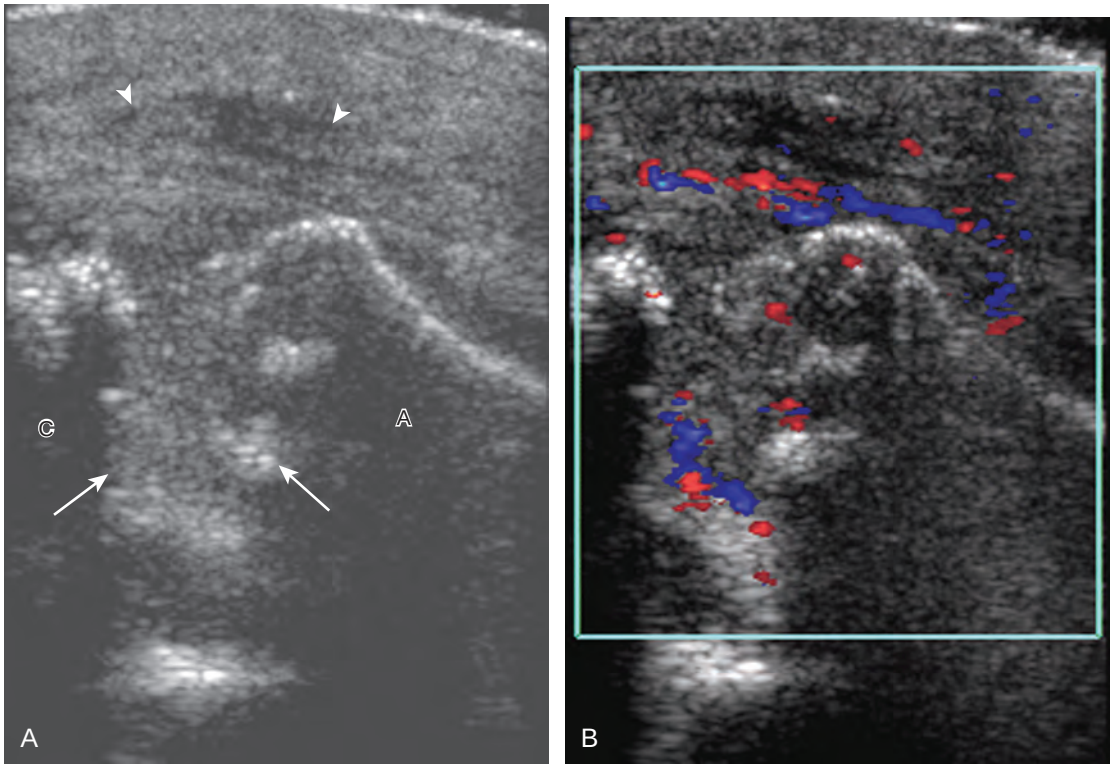

FIGURE 3-107 ■ Acromioclavicular joint infection. Gray-scale **(A)** and color Doppler **(B)** ultrasound images long axis to the clavicle show a widened and irregular acromioclavicular joint *(arrows)* with soft tissue swelling *(arrowheads)* and hyperemia **(B)**. A, acromion; C, clavicle.

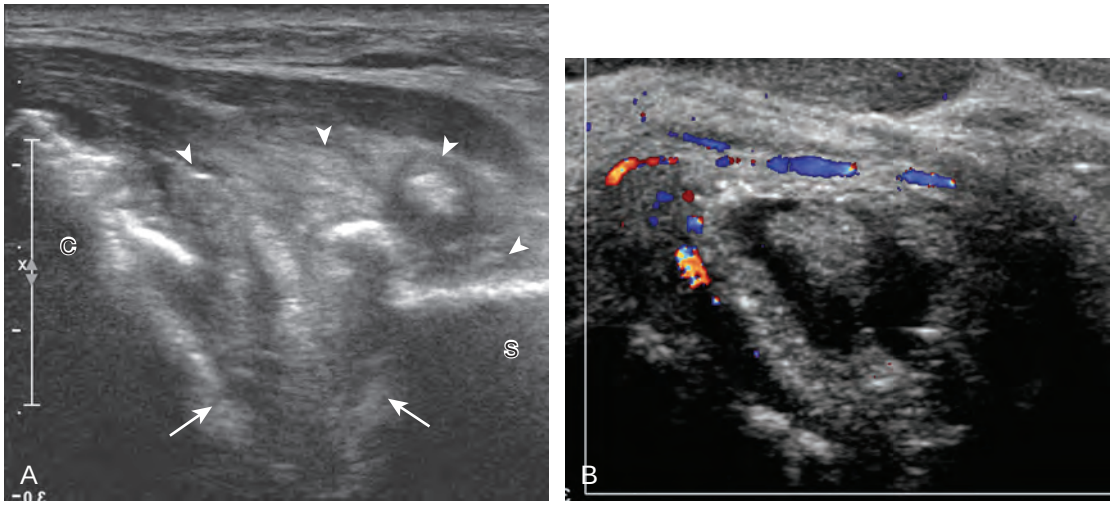

FIGURE 3-108 ■ Sternoclavicular joint infection. Gray-scale **(A)** and color Doppler **(B)** ultrasound images in long axis to the clavicle show a widened and irregular sternoclavicular joint *(arrows)* with soft tissue swelling, fluid, and debris *(arrowheads)* and hyperemia **(B)**. C, clavicle; S, sternum.

uncommon for degenerative changes of a sternoclavicular joint with capsular thickening to present as a soft tissue mass. Ultrasound can also diagnose subluxation or dislocation of the sternoclavicular joint (Fig. 3-109). It is important to include dynamic evaluation because subluxation may be dependent on patient arm positioning. Comparison with the contralateral side is important in diagnosing subtle subluxation. Any suspected posterior subluxation or dislocation should be evaluated with computed tomography to assess for adjacent vascular abnormalities (Fig. 3-110).

MISCELLANEOUS DISORDERS

Other types of shoulder diseases are often identified as examination is directed by the patient's history or symptoms. However, unlike in other peripheral joints, sonographic evaluation of the shoulder should follow a protocol similar to that described earlier because pain from the rotator cuff is often referred to the arm, and symptoms may be misleading. At the completion of the shoulder examination, a focused examination at the site of point tenderness is recommended. This is how disease is identified that may not otherwise be evident during the routine shoulder ultrasound examination.

Lymph node enlargement and other masses can be seen during ultrasound evaluation of the shoulder. A normal axillary lymph node appears oval, with a hypoechoic cortical rim (which decreases in thickness in older age), hyperechoic hilus, and a hilar pattern of vascularity if any. The central hyperechoic area is the result not of fat

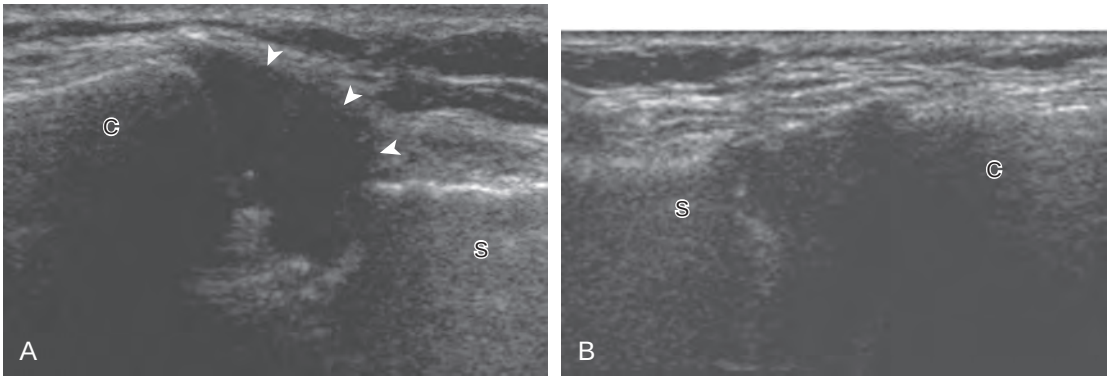

FIGURE 3-109 ■ Sternoclavicular joint dislocation: anterior. Ultrasound image in long axis to the clavicle shows **(A)** anterior dislocation of the clavicular head (C) relative to the sternum (S), with hypoechoic swelling at the sternoclavicular joint *(arrowheads)*. Asymptomatic contralateral sternoclavicular joint **(B)** shows normal alignment.

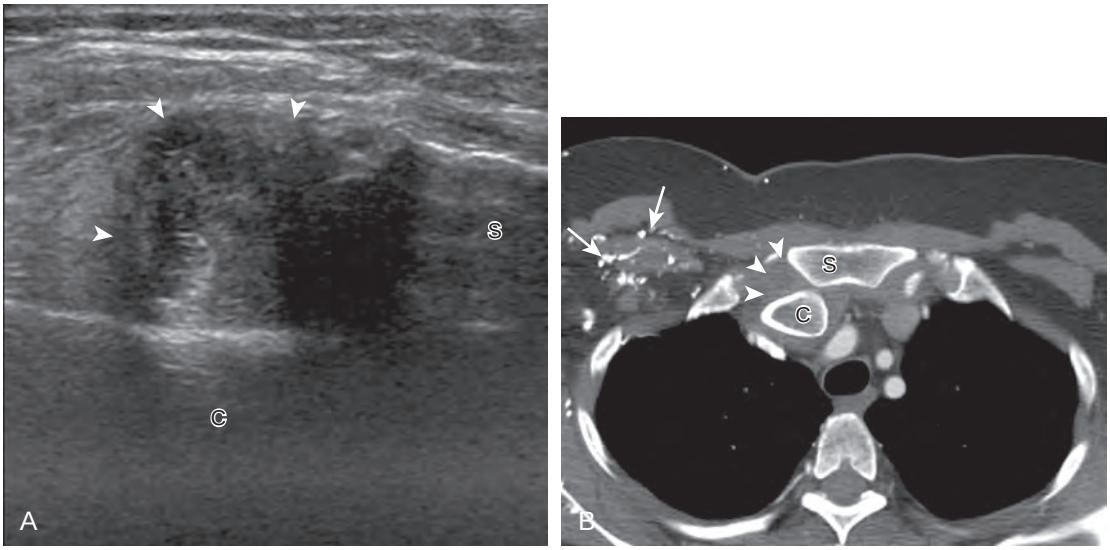

FIGURE 3-110 ■ Sternoclavicular joint dislocation: posterior. Ultrasound image **(A)** long axis to the clavicle and **(B)** contrast-enhanced axial computed tomography image show posterior dislocation of the clavicular head (C) relative to the sternum (S) with hypoechoic swelling at the sternoclavicular joint *(arrowheads)*. Note the chest wall collateral vessels *(arrows)* resulting from right subclavian vein occlusion.

but rather of the reflective interfaces between the sinusoids and fat (Fig. 3-111A). An axillary lymph node that demonstrates eccentric thickening of the cortex, diffuse thickening of the cortex with hilar thinning, absence of the hilum, roundness, or a peripheral vascular pattern on color or power Doppler imaging suggests malignancy.[84] A strict size criterion is not effective because even lymph nodes smaller than 5 mm (largest diameter) have almost 10% risk for malignancy in the setting of breast cancer.[85] Often, ultrasound-guided percutaneous or excisional biopsy is required (see Fig. 3-111B and C; Fig. 3-112). Other soft tissue masses, if not originating from a synovial joint, are often not specific for one diagnosis, and ultrasound-guided percutaneous biopsy is usually required.

The identification of a soft tissue mass at ultrasound is often not specific for one diagnosis, although it limits the differential diagnosis by determining whether a mass is cystic or solid. A heterogeneous fluid collection not representing a bursal fluid collection could represent hematoma or abscess (see Chapter 2). One relatively common mass includes a soft tissue lipoma (see Chapter 2). In the setting of limb amputation, a solid soft tissue mass could represent a neuroma. These masses are often hypoechoic but heterogeneous, and continuity between the mass and a peripheral nerve is essential to the diagnosis (Fig. 3-113). Because neuromas normally develop at a transected peripheral nerve, transducer palpation is important to determine which neuroma is symptomatic, to guide appropriate treatment.

There is one tumor-like abnormality that is specific to the shoulder, which is the elastofibroma.[86] This is not a true tumor, but rather a pseudotumor of fibroelastic tissue, possibly resulting from mechanical friction between the chest wall and the scapula. At ultrasound, elastofibroma appears heterogeneous and hyperechoic, with interspersed curvilinear hypoechoic strands at ultrasound (Fig. 3-114) (Video 3-46). The key to the diagnosis is the location because 99% of these lesions occur at the scapular tip, deep to the serratus anterior and latissimus dorsi muscles. This pseudotumor is most common in older women and may be bilateral in up to 66%.

Patients may also present with a palpable abnormality of the chest wall. One such etiology is a normal variant called the sternalis muscle. This variant occurs in 2% to 11% of the population and is located over the most medial aspect of the pectoralis at the sternum, just lateral to midline and elongated parallel to the rectus abdominis.[87] At ultrasound, the expected location of a sternalis muscle and the sonographic characteristics of normal muscle tissue allow a correct diagnosis (Fig. 3-115, online). A more common cause of a palpable nodule just below the sternum is the xiphoid process. The variable size, ossification, and shape of the xiphoid process can create a palpable mass. At ultrasound, the location, shape, and ultrasound appearance of either bone

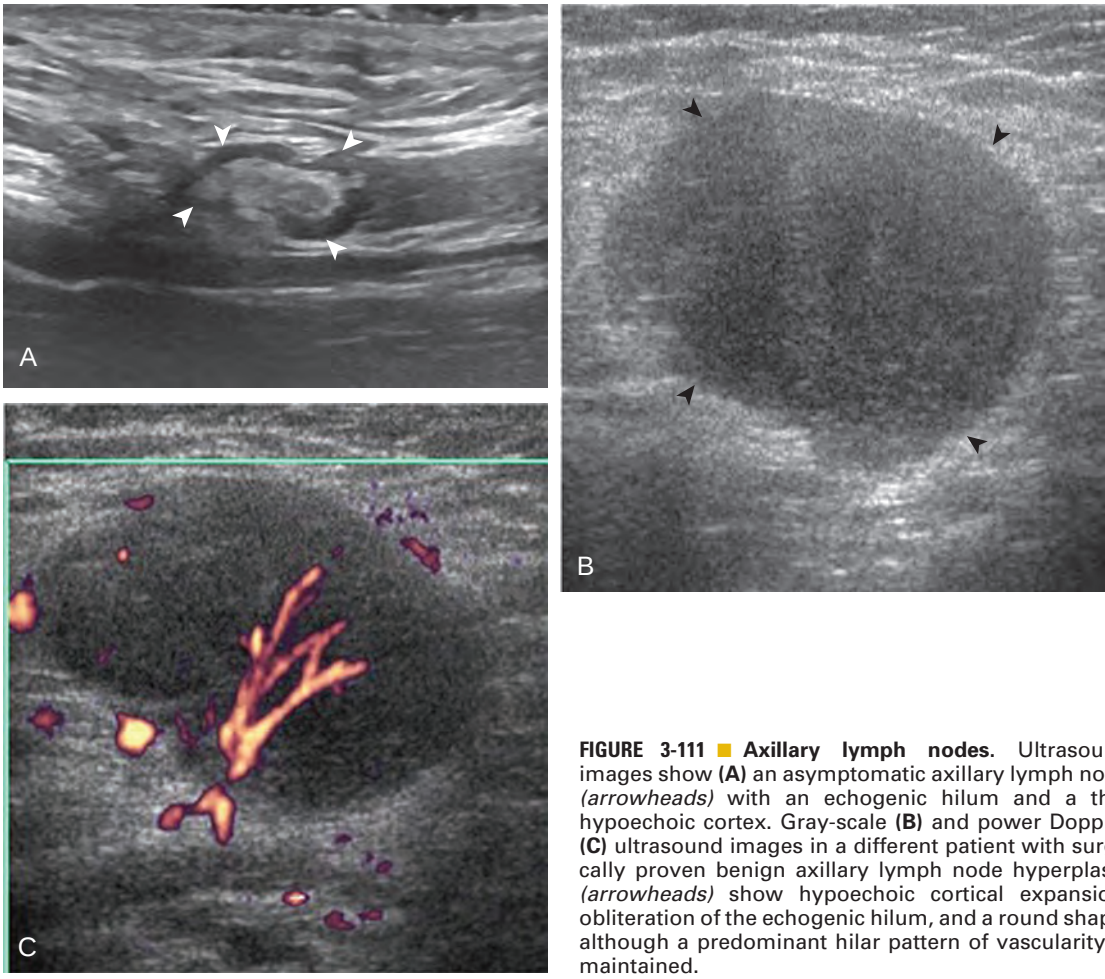

FIGURE 3-111 ■ Axillary lymph nodes. Ultrasound images show **(A)** an asymptomatic axillary lymph node *(arrowheads)* with an echogenic hilum and a thin hypoechoic cortex. Gray-scale **(B)** and power Doppler **(C)** ultrasound images in a different patient with surgically proven benign axillary lymph node hyperplasia *(arrowheads)* show hypoechoic cortical expansion, obliteration of the echogenic hilum, and a round shape, although a predominant hilar pattern of vascularity is maintained.

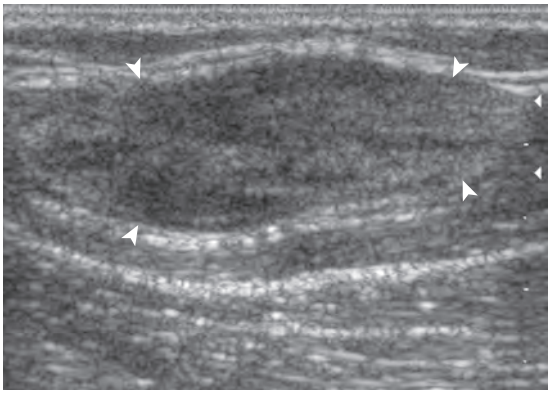

FIGURE 3-112 ■ Lymphoma. Ultrasound image shows an elongated lymph node *(arrowheads)* with cortical expansion and near obliteration of the echogenic hilum.

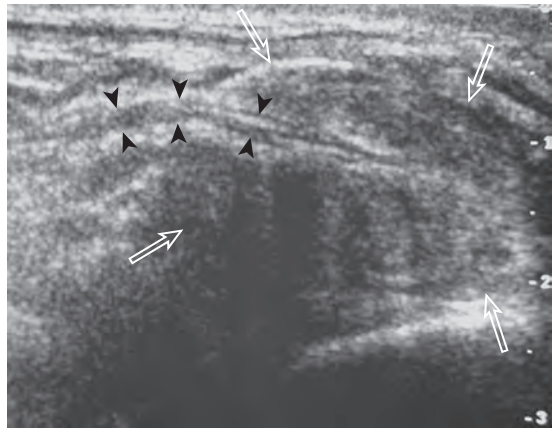

FIGURE 3-113 ■ Amputation neuroma. Ultrasound image shows a round, heterogeneous, but predominantly hypoechoic mass *(open arrows)*, with some posterior shadowing, in continuity with the transected peripheral nerve *(arrowheads)* after forequarter amputation.

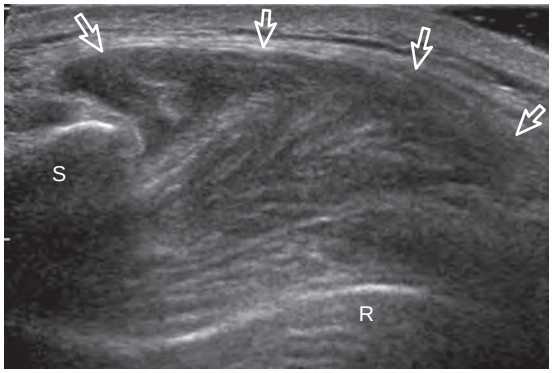

FIGURE 3-114 ■ Elastofibroma. Ultrasound image shows a mixed echogenicity mass *(open arrows)* with internal hypoechoic strands. R, rib; S, scapula.

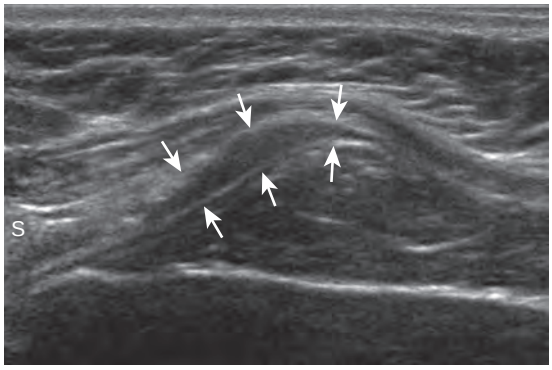

FIGURE 3-116 ■ Xiphoid process. Ultrasound image in the sagittal plane over lower sternum (S) shows a prominent and palpable unossified xiphoid process *(arrows)*.

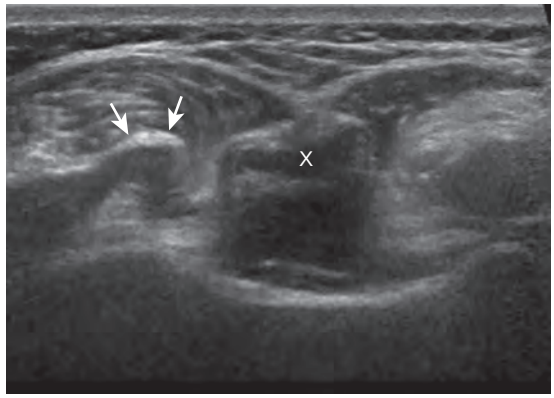

FIGURE 3-117 ■ Slipping rib syndrome. Ultrasound image in the transverse plane over the lower anterior chest wall shows the cartilaginous end of a rib *(arrows)*, which snapped over the xiphoid process (X) dynamically.

or cartilage is characteristic of a xiphoid process (Fig. 3-116). Some individuals present a painful snap associated with the chest wall during activities. The dynamic capabilities of ultrasound are useful to diagnose slipping rib syndrome, in which the abnormal mobility of a lower anterior rib end can cause snapping when it abruptly slips over an adjacent rib or xiphoid process (Fig. 3-117) (Video 3-47).[88]

Online references available at www.expertconsult.com.

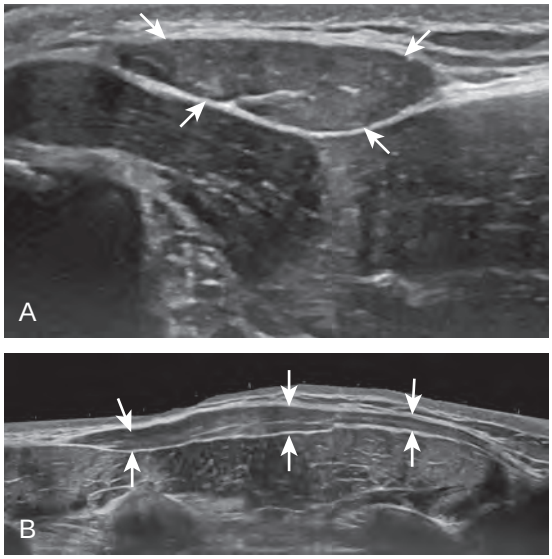

FIGURE 3-115 ■ Sternalis muscle. A and **B,** Ultrasound image in the parasagittal plane over lower anterior chest wall shows the sternalis muscle *(arrows)*.

REFERENCES

1. Minagawa H, Itoi E, Konno N, et al: Humeral attachment of the supraspinatus and infraspinatus tendons: an anatomic study. *Arthroscopy* 14:302–306, 1998.
2. Ruotolo C, Fow JE, Nottage WM: The supraspinatus footprint: an anatomic study of the supraspinatus insertion. *Arthroscopy* 20:246–249, 2004.
3. Jacobson JA: Shoulder US: anatomy, technique, and scanning pitfalls. *Radiology* 260:6–16, 2011.
4. Buck FM, Grehn H, Hilbe M, et al: Degeneration of the long biceps tendon: comparison of MRI with gross anatomy and histology. *AJR Am J Roentgenol* 193:1367–1375, 2009.
5. Farin PU, Jaroma H, Harju A, et al: Medial displacement of the biceps brachii tendon: evaluation with dynamic sonography during maximal external shoulder rotation. *Radiology* 195:845–848, 1995.
6. Crass JR, Craig EV, Feinberg SB: The hyperextended internal rotation view in rotator cuff ultrasonography. *J Clin Ultrasound* 15:416–420, 1987.
7. Ferri M, Finlay K, Popowich T, et al: Sonography of full-thickness supraspinatus tears: comparison of patient positioning technique with surgical correlation. *AJR Am J Roentgenol* 184:180–184, 2005.
8. Schaeffeler C, Mueller D, Kirchhoff C, et al: Tears at the rotator cuff footprint: prevalence and imaging characteristics in 305 MR arthrograms of the shoulder. *Eur Radiol* 21:1477–1484, 2011.
9. Tuite MJ, Turnbull JR, Orwin JF: Anterior versus posterior, and rim-rent rotator cuff tears: prevalence and MR sensitivity. *Skeletal Radiol* 27:237–243, 1998.
10. Middleton WD, Reinus WR, Melson GL, et al: Pitfalls of rotator cuff sonography. *AJR Am J Roentgenol* 146:555–560, 1986.
11. Bretzke CA, Crass JR, Craig EV, et al: Ultrasonography of the rotator cuff: normal and pathologic anatomy. *Invest Radiol* 20:311–315, 1985.
12. Petchprapa CN, Beltran LS, Jazrawi LM, et al: The rotator interval: a review of anatomy, function, and normal and abnormal MRI appearance. *AJR Am J Roentgenol* 195:567–576, 2010.
13. Morag Y, Jacobson JA, Lucas D, et al: US appearance of the rotator cable with histologic correlation: preliminary results. *Radiology* 241:485–491, 2006.
14. Ferri M, Finlay K, Popowich T, et al: Sonographic examination of the acromioclavicular and sternoclavicular joints. *J Clin Ultrasound* 33:345–355, 2005.
15. Peetrons P, Bedard JP: Acromioclavicular joint injury: enhanced technique of examination with dynamic maneuver. *J Clin Ultrasound* 35:262–267, 2007.
16. Bureau NJ, Beauchamp M, Cardinal E, et al: Dynamic sonography evaluation of shoulder impingement syndrome. *AJR Am J Roentgenol* 187:216–220, 2006.
17. Farin PU, Jaroma H, Harju A, et al: Shoulder impingement syndrome: sonographic evaluation. *Radiology* 176:845–849, 1990.
18. Ryu KN, Lee SW, Rhee YG, et al: Adhesive capsulitis of the shoulder joint: usefulness of dynamic sonography. *J Ultrasound Med* 12:445–449, 1993.
19. Kavanagh EC, Koulouris G, Parker L, et al: Does extended-field-of-view sonography improve interrater reliability for the detection of rotator cuff muscle atrophy? *AJR Am J Roentgenol* 190:27–31, 2008.
20. Kim HM, Dahiya N, Teefey SA, et al: Location and initiation of degenerative rotator cuff tears: an analysis of three hundred and sixty shoulders. *J Bone Joint Surg Am* 92:1088–1096, 2010.
21. Jacobson JA, Lancaster S, Prasad A, et al: Full-thickness and partial-thickness supraspinatus tendon tears: value of US signs in diagnosis. *Radiology* 230:234–242, 2004.
22. Wohlwend JR, van Holsbeeck M, Craig J, et al: The association between irregular greater tuberosities and rotator cuff tears: a sonographic study. *AJR Am J Roentgenol* 171:229–233, 1998.
23. Arend CF, da Silva TR: Comparison between exclusively long-axis and multiple-axis sonographic protocols for screening of rotator cuff lesions in symptomatic shoulders. *J Ultrasound Med* 29:1725–1732, 2010.
24. Teefey SA, Rubin DA, Middleton WD, et al: Detection and quantification of rotator cuff tears: comparison of ultrasonographic, magnetic resonance imaging, and arthroscopic findings in seventy-one consecutive cases. *J Bone Joint Surg Am* 86:708–716, 2004.
25. de Jesus JO, Parker L, Frangos AJ, et al: Accuracy of MRI, MR arthrography, and ultrasound in the diagnosis of rotator cuff tears: a meta-analysis. *AJR Am J Roentgenol* 192:1701–1707, 2009.
26. van Holsbeeck MT, Kolowich PA, Eyler WR, et al: US depiction of partial-thickness tear of the rotator cuff. *Radiology* 197:443–446, 1995.
27. van Holsbeeck M, Introcaso JH, Kolowich PA: Sonography of tendons: patterns of disease. *Instr Course Lect* 43:475–481, 1994.
28. Kassarjian A, Torriani M, Ouellette H, et al: Intramuscular rotator cuff cysts: association with tendon tears on MRI and arthroscopy. *AJR Am J Roentgenol* 185:160–165, 2005.
29. Teefey SA, Middleton WD, Bauer GS, et al: Sonographic differences in the appearance of acute and chronic full-thickness rotator cuff tears. *J Ultrasound Med* 19:377–378; quiz 83, 2000.
30. Strobel K, Hodler J, Meyer DC, et al: Fatty atrophy of supraspinatus and infraspinatus muscles: accuracy of US. *Radiology* 237:584–589, 2005.
31. Buck FM, Grehn H, Hilbe M, et al: Magnetic resonance histologic correlation in rotator cuff tendons. *J Magn Reson Imaging* 32:165–172, 2010.
32. Kjellin I, Ho CP, Cervilla V, et al: Alterations in the supraspinatus tendon at MR imaging: correlation with histopathologic findings in cadavers. *Radiology* 181:837–841, 1991.
33. Bachmann GF, Melzer C, Heinrichs CM, et al: Diagnosis of rotator cuff lesions: comparison of US and MRI on 38 joint specimens. *Eur Radiol* 7:192–197, 1997.
34. Jin W, Ryu KN, Park YK, et al: Cystic lesions in the posterosuperior portion of the humeral head on MR arthrography: correlations with gross and histologic findings in cadavers. *AJR Am J Roentgenol* 184:1211–1215, 2005.
35. Tirman PF, Bost FW, Garvin GJ, et al: Posterosuperior glenoid impingement of the shoulder: findings at MR imaging and MR arthrography with arthroscopic correlation. *Radiology* 193:431–436, 1994.
36. Hollister MS, Mack LA, Patten RM, et al: Association of sonographically detected subacromial/subdeltoid bursal effusion and intraarticular fluid with rotator cuff tear. *AJR Am J Roentgenol* 165:605–608, 1995.
37. van Holsbeeck M, Strouse PJ: Sonography of the shoulder: evaluation of the subacromial-subdeltoid bursa. *AJR Am J Roentgenol* 160:561–564, 1993.
38. Farin P, Jaroma H: Sonographic detection of tears of the anterior portion of the rotator cuff (subscapularis tendon tears). *J Ultrasound Med* 15:221–225, 1996.
39. Morag Y, Jamadar DA, Miller B, et al: The subscapularis: anatomy, injury, and imaging. *Skeletal Radiol* 40:255–269, 2011.
40. Khoury V, Cardinal E, Brassard P: Atrophy and fatty infiltration of the supraspinatus muscle: sonography versus MRI. *AJR Am J Roentgenol* 190:1105–1111, 2008.
41. Melis B, DeFranco MJ, Chuinard C, et al: Natural history of fatty infiltration and atrophy of the supraspinatus

muscle in rotator cuff tears. *Clin Orthop Relat Res* 468:1498–1505, 2010.
42. Sofka CM, Lin J, Feinberg J, et al: Teres minor denervation on routine magnetic resonance imaging of the shoulder. *Skeletal Radiol* 33:514–518, 2004.
43. Friend J, Francis S, McCulloch J, et al: Teres minor innervation in the context of isolated muscle atrophy. *Surg Radiol Anat* 32:243–249, 2010.
44. McClelland D, Paxinos A: The anatomy of the quadrilateral space with reference to quadrilateral space syndrome. *J Shoulder Elbow Surg* 17:162–164, 2008.
45. Cothran RL Jr, Helms C: Quadrilateral space syndrome: incidence of imaging findings in a population referred for MRI of the shoulder. *AJR Am J Roentgenol* 184:989–992, 2005.
46. Brestas PS, Tsouroulas M, Nikolakopoulou Z, et al: Ultrasound findings of teres minor denervation in suspected quadrilateral space syndrome. *J Clin Ultrasound* 34:343–347, 2006.
47. Prickett WD, Teefey SA, Galatz LM, et al: Accuracy of ultrasound imaging of the rotator cuff in shoulders that are painful postoperatively. *J Bone Joint Surg Am* 85:1084–1089, 2003.
48. Jacobson JA, Miller B, Bedi A, et al: Imaging of the postoperative shoulder. *Semin Musculoskelet Radiol* 15:320–339, 2011.
49. Fealy S, Adler RS, Drakos MC, et al: Patterns of vascular and anatomical response after rotator cuff repair. *Am J Sports Med* 34:120–127, 2006.
50. Miller BS, Downie BK, Kohen RB, et al: When do rotator cuff repairs fail? Serial ultrasound examination after arthroscopic repair of large and massive rotator cuff tears. *Am J Sports Med* 39:2064–2070, 2011.
51. Nho SJ, Adler RS, Tomlinson DP, et al: Arthroscopic rotator cuff repair: prospective evaluation with sequential ultrasonography. *Am J Sports Med* 37:1938–1945, 2009.
52. Miller TT: Sonography of joint replacements. *Semin Musculoskelet Radiol* 10:79–85, 2006.
53. Sofka CM, Adler RS: Original report. Sonographic evaluation of shoulder arthroplasty. *AJR Am J Roentgenol* 180:1117–1120, 2003.
54. Serafini G, Sconfienza LM, Lacelli F, et al: Rotator cuff calcific tendonitis: short-term and 10-year outcomes after two-needle US guided percutaneous treatment—nonrandomized controlled trial. *Radiology* 252:157–164, 2009.
55. Flemming DJ, Murphey MD, Shekitka KM, et al: Osseous involvement in calcific tendinitis: a retrospective review of 50 cases. *AJR Am J Roentgenol* 181:965–972, 2003.
56. Farin PU: Consistency of rotator-cuff calcifications: observations on plain radiography, sonography, computed tomography, and at needle treatment. *Invest Radiol* 31:300–304, 1996.
57. Chiou HJ, Chou YH, Wu JJ, et al: Evaluation of calcific tendonitis of the rotator cuff: role of color Doppler ultrasonography. *J Ultrasound Med* 21:289–295; quiz 96–97, 2002.
58. Le Goff B, Berthelot JM, Guillot P, et al: Assessment of calcific tendonitis of rotator cuff by ultrasonography: comparison between symptomatic and asymptomatic shoulders. *Joint Bone Spine* 77:258–263, 2010.
59. Wang YC, Wang HK, Chen WS, et al: Dynamic visualization of the coracoacromial ligament by ultrasound. *Ultrasound Med Biol* 35:1242–1248, 2009.
60. Tracy MR, Trella TA, Nazarian LN, et al: Sonography of the coracohumeral interval: a potential technique for diagnosing coracoid impingement. *J Ultrasound Med* 29:337–341, 2010.
61. Stallenberg B, Destate N, Feipel V, et al: Involvement of the anterior portion of the subacromial-subdeltoid bursa in the painful shoulder. *AJR Am J Roentgenol* 187:894–900, 2006.
62. Griesser MJ, Harris JD, Campbell JE, et al: Adhesive capsulitis of the shoulder: a systematic review of the effectiveness of intra-articular corticosteroid injections. *J Bone Joint Surg Am* 93:1727–1733, 2011.
63. Homsi C, Bordalo-Rodrigues M, da Silva JJ, et al: Ultrasound in adhesive capsulitis of the shoulder: is assessment of the coracohumeral ligament a valuable diagnostic tool? *Skeletal Radiol* 35:673–678, 2006.
64. Lee JC, Sykes C, Saifuddin A, et al: Adhesive capsulitis: sonographic changes in the rotator cuff interval with arthroscopic correlation. *Skeletal Radiol* 34:522–527, 2005.
65. Turrin A, Cappello A: Sonographic anatomy of the supraspinatus tendon and adjacent structures. *Skeletal Radiol* 26:89–93, 1997.
66. Seibold CJ, Mallisee TA, Erickson SJ, et al: Rotator cuff: evaluation with US and MR imaging. *Radiographics* 19:685–705, 1999.
67. Tirman PF, Feller JF, Janzen DL, et al: Association of glenoid labral cysts with labral tears and glenohumeral instability: radiologic findings and clinical significance. *Radiology* 190:653–658, 1994.
68. Zubler V, Mamisch-Saupe N, Pfirrmann CW, et al: Detection and quantification of glenohumeral joint effusion: reliability of ultrasound. *Eur Radiol* 21:1858–1864, 2011.
69. Breidahl WH, Stafford Johnson DB, Newman JS, et al: Power Doppler sonography in tenosynovitis: significance of the peritendinous hypoechoic rim. *J Ultrasound Med* 17:103–107, 1998.
70. Skendzel JG, Jacobson JA, Carpenter JE, et al: Long head of biceps brachii tendon evaluation: accuracy of preoperative ultrasound. *AJR Am J Roentgenol* 197:942–948, 2011.
71. Rutten MJ, de Jong MD, van Loon T, et al: Intratendinous ganglion of the long head of the biceps tendon: US and MRI features (2010: 9b). Intratendinous ganglion. *Eur Radiol* 20:2997–3001, 2010.
72. Grainger AJ, Tirman PF, Elliott JM, et al: MR anatomy of the subcoracoid bursa and the association of subcoracoid effusion with tears of the anterior rotator cuff and the rotator interval. *AJR Am J Roentgenol* 174:1377–1380, 2000.
73. Thiele RG, Schlesinger N: Ultrasonography shows disappearance of monosodium urate crystal deposition on hyaline cartilage after sustained normouricemia is achieved. *Rheumatol Int* 30:495–503, 2010.
74. Taljanovic MS, Carlson KL, Kuhn JE, et al: Sonography of the glenoid labrum: a cadaveric study with arthroscopic correlation. *AJR Am J Roentgenol* 174:1717–1722, 2000.
75. Rasmussen OS: Anterior shoulder instability: sonographic evaluation. *J Clin Ultrasound* 32:430–437, 2004.
76. Hashimoto BE, Hayes AS, Ager JD: Sonographic diagnosis and treatment of ganglion cysts causing suprascapular nerve entrapment. *J Ultrasound Med* 13:671–674, 1994.
77. Carroll KW, Helms CA, Otte MT, et al: Enlarged spinoglenoid notch veins causing suprascapular nerve compression. *Skeletal Radiol* 32:72–77, 2003.
78. Patten RM, Mack LA, Wang KY, et al: Nondisplaced fractures of the greater tuberosity of the humerus: sonographic detection. *Radiology* 182:201–204, 1992.
79. Rehman A, Robinson P: Sonographic evaluation of injuries to the pectoralis muscles. *AJR Am J Roentgenol* 184:1205–1211, 2005.
80. Weaver JS, Jacobson JA, Jamadar DA, et al: Sonographic findings of pectoralis major tears with surgical, clinical, and magnetic resonance imaging correlation in 6 patients. *J Ultrasound Med* 24:25–31, 2005.

81. Alasaarela E, Tervonen O, Takalo R, et al: Ultrasound evaluation of the acromioclavicular joint. *J Rheumatol* 24:1959–1963, 1997.
82. Simovitch R, Sanders B, Ozbaydar M, et al: Acromioclavicular joint injuries: diagnosis and management. *J Am Acad Orthop Surg* 17:207–219, 2009.
83. Johnson MC, Jacobson JA, Fessell DP, et al: The sternoclavicular joint: can imaging differentiate infection from degenerative change? *Skeletal Radiol* 39:551–558, 2010.
84. Esen G, Gurses B, Yilmaz MH, et al: Gray scale and power Doppler US in the preoperative evaluation of axillary metastases in breast cancer patients with no palpable lymph nodes. *Eur Radiol* 15:1215–1223, 2005.
85. Obwegeser R, Lorenz K, Hohlagschwandtner M, et al: Axillary lymph nodes in breast cancer: is size related to metastatic involvement? *World J Surg* 24:546–550, 2000.
86. Bianchi S, Martinoli C, Abdelwahab IF, et al: Elastofibroma dorsi: sonographic findings. *AJR Am J Roentgenol* 169:1113–1115, 1997.
87. Nuthakki S, Gross M, Fessell D: Sonography and helical computed tomography of the sternalis muscle. *J Ultrasound Med* 26:247–250, 2007.
88. Meuwly JY, Wicky S, Schnyder P, et al: Slipping rib syndrome: a place for sonography in the diagnosis of a frequently overlooked cause of abdominal or low thoracic pain. *J Ultrasound Med* 21:339–343, 2002.

eBOX 3-1 Sample Diagnostic Shoulder Ultrasound Report

NORMAL

Examination: Ultrasound of the Shoulder
Date of Study: March 11, 2011
Patient Name: Jack White
Registration Number: 8675309
History: Shoulder pain, evaluate for rotator cuff abnormality
Findings: No evidence of joint effusion. The biceps brachii long head tendon is normal without tendinosis, tear, tenosynovitis, or subluxation/dislocation. The supraspinatus, infraspinatus, subscapularis, and teres minor tendons are also normal. No subacromial-subdeltoid bursal abnormality and no sonographic evidence for subacromial impingement with dynamic maneuvers. The posterior labrum is unremarkable. Additional focused evaluation at site of maximal symptoms was unrevealing.
Impression: Unremarkable ultrasound examination of the shoulder. No rotator cuff abnormality.

eBOX 3-2 Sample Diagnostic Shoulder Ultrasound Report

ABNORMAL

Examination: Ultrasound of the Shoulder
Date of Study: March 11, 2011
Patient Name: Jack White
Registration Number: 8675309
History: Shoulder pain, evaluate for rotator cuff abnormality
Findings: There is a focal anechoic tear of the anterior, distal aspect of the supraspinatus tendon measuring 1 cm short axis by 1.5 cm long axis. The anterior margin of the tear is adjacent to the rotator interval. There is no involvement of the subscapularis, infraspinatus, or rotator interval. A moderate amount of infraspinatus and supraspinatus fatty degeneration is present. There is a small joint effusion distending the biceps brachii tendon sheath and moderate distention of the subacromial-subdeltoid bursa. No biceps brachii long head tendon abnormality and no subluxation/dislocation. Mild osteoarthritis of the acromioclavicular joint. Additional focused evaluation at site of maximal symptoms was unrevealing.
Impression: Focal or incomplete full-thickness tear of the supraspinatus tendon with infraspinatus and supraspinatus muscle atrophy.

CHAPTER 4

Elbow Ultrasound

CHAPTER OUTLINE

ELBOW ANATOMY

ULTRASOUND EXAMINATION TECHNIQUE
General Comments
Anterior Evaluation
Medial Evaluation
Lateral Evaluation
Posterior Evaluation

JOINT AND BURSA ABNORMALITIES

TENDON AND MUSCLE ABNORMALITIES
Biceps Brachii
Triceps Brachii
Common Flexor and Extensor Tendons

LIGAMENT ABNORMALITIES

PERIPHERAL NERVE ABNORMALITIES
Ulnar Nerve
Median Nerve
Radial Nerve
Peripheral Nerve Sheath Tumors

EPITROCHLEAR LYMPH NODE

Additional videos for this topic are available online at www.expertconsult.com.

ELBOW ANATOMY

The elbow is a synovial joint composed of three elbow joint articulations: the trochlea and ulna, the capitellum and the radial head, and the proximal ulna and radius (Fig. 4-1). The elbow joint has prominent joint recesses located in the coronoid and radial fossae anteriorly and within the olecranon fossa posteriorly. Within each joint recess exists an intracapsular but extrasynovial fat pad, which becomes displaced with joint distention. The medial elbow joint is stabilized by the ulnar collateral ligament, of which the anterior band that extends anteriorly to the sublime tubercle of the ulna is the most important. Other components of the ulnar collateral ligament include posterior and oblique bands. Laterally, the elbow joint is stabilized by the radial collateral ligament complex, which is composed of the radial collateral ligament, the annular ligament, and a smaller accessory radial collateral ligament. An additional component, the lateral ulnar collateral ligament, extends from the lateral epicondyle to insert on the crista supinator of the proximal ulna.

Anterior to the elbow joint, the brachialis inserts on the ulna, and the biceps brachii tendon inserts on the radial tuberosity. With regard to the biceps brachii, a dual insertion exists where the short head is superficial and inserts more distal relative to the long head on the radial tuberosity.[1] Posteriorly, the triceps brachii inserts on the olecranon process of the proximal ulna, over which is located the olecranon bursa. The lateral and long heads of the triceps brachii represent the most superficial layer of the distal triceps, whereas the deep aspect with a relatively shorter tendon is the medial head.[2] The anconeus is located between the olecranon process and the lateral epicondyle of the humerus. Medially, the common flexor tendon, consisting of the flexor carpi radialis, palmaris longus, flexor carpi ulnaris, and flexor digitorum superficialis, originates on the medial epicondyle of the distal humerus. Laterally, the common extensor tendon, composed of the extensor carpi radialis brevis, extensor digitorum, extensor digiti minimi, and extensor carpi ulnaris, originates at the lateral epicondyle of the

distal humerus. The extensor carpi radialis brevis is the most anteriorly located of the group; the extensor carpi radialis longus originates proximal to the lateral epicondyle on the lateral humeral metaphysis.

The space between the olecranon process of the ulna and the medial epicondyle is bridged by the cubital tunnel retinaculum (or Osborne fascia) and contains the ulnar nerve. Just distal to this, the ulnar nerve enters the true cubital tunnel, between the dual origins of the flexor carpi ulnaris and deep to the arcuate ligament.[3] The median nerve is located medial to the brachial artery and courses distally between the ulnar and humeral heads of the pronator teres. The radial nerve is located at the posterior aspect of the humeral shaft and then courses distally and laterally beneath the brachioradialis, where a deep branch courses between the two heads of the supinator muscle and a superficial branch courses beneath the brachioradialis and into the forearm.

ULTRASOUND EXAMINATION TECHNIQUE

Table 4-1 is an elbow ultrasound examination checklist. Examples of diagnostic elbow ultrasound reports are available online at www.expertconsult.com (see eBox 4-1 and 4-2).

General Comments

Ultrasound examination of the elbow may be completed with the patient sitting and the elbow placed on an examination table, or the patient may lie supine. A high-frequency transducer of at least 10 MHz is typically used because most of the structures are superficial. Evaluation of the elbow may be focused over the area that is clinically symptomatic or that is relevant to the patient's history. Regardless, a complete examination of all areas should always be considered for one to become familiar with normal anatomy and

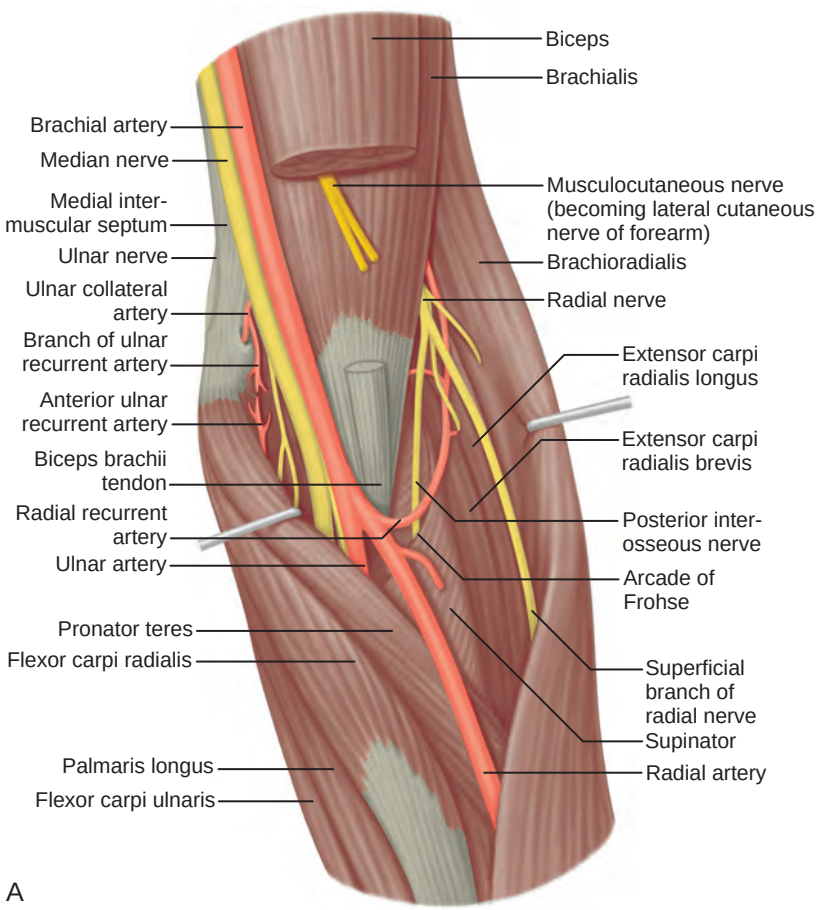

FIGURE 4-1 ■ Elbow anatomy. A, Anterior aspect of the left elbow showing deep structures.

Continued

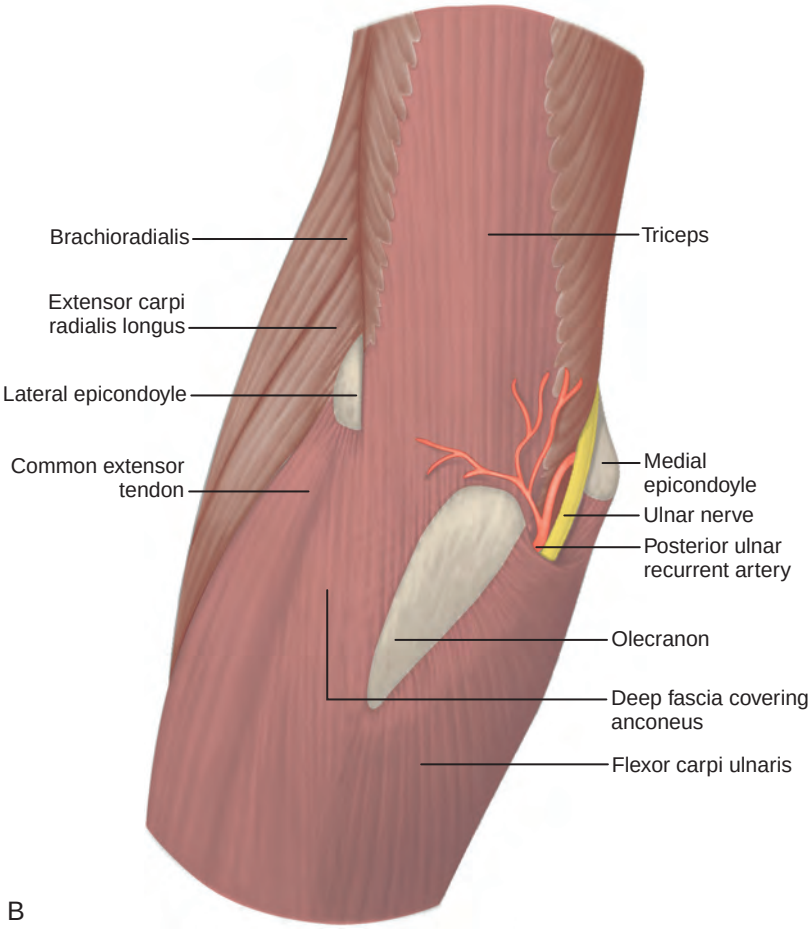

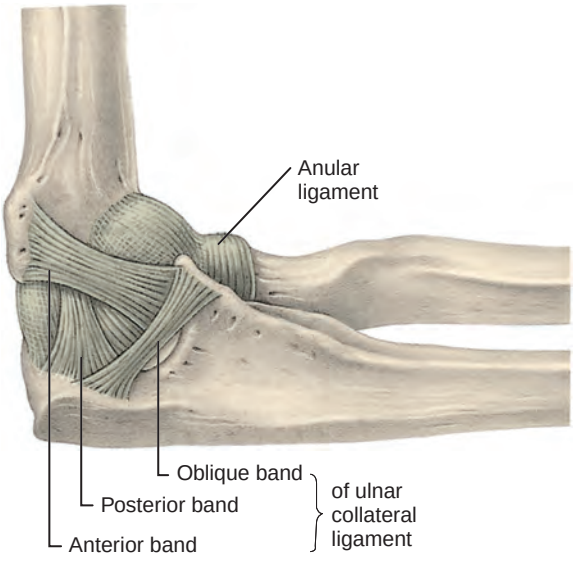

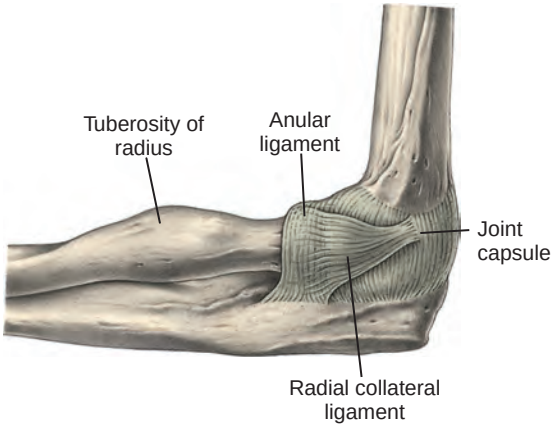

FIGURE 4-1, cont'd ■ **B,** Posterior aspect of the left elbow showing superficial structures. **C,** Medial aspect of the left elbow joint. **D,** Lateral aspect of the left elbow joint. (From Standring S: *Gray's anatomy: the anatomical basis of clinical practice,* ed 39, Edinburgh, 2005, Churchill Livingstone.)

TABLE 4-1 **Elbow Ultrasound Examination Checklist**

Location	Structures of Interest
Anterior	Brachialis Biceps brachii Median nerve Anterior joint recess
Medial	Ulnar collateral ligament Common flexor tendon and pronator teres Ulnar nerve
Lateral	Common extensor tendon Radial collateral ligament complex Radial head and annular recess Capitellum Radial nerve
Posterior	Posterior joint recess Triceps brachii Olecranon bursa

normal variants and to develop quick and efficient sonographic technique.

Anterior Evaluation

The primary structures evaluated from the anterior approach are the brachialis, the distal biceps brachii, the median nerve, and the anterior elbow joint recess. For sonographic evaluation, the elbow is comfortably extended, and the hand is supinated. Evaluation begins with the transducer short axis to the biceps brachii and brachialis just superior to the elbow joint. For orientation, it is helpful to begin at the medial aspect of the anterior elbow and locate the brachial artery, identified by its pulsation and flow on color Doppler imaging (Fig. 4-2). Deep to the brachial artery and in midline is the brachialis muscle, immediately adjacent to the distal humerus. The hypoechoic layer over the hyperechoic cortex is the hyaline articular cartilage. Normal muscle is predominantly hypoechoic with intervening hyperechoic fibroadipose septations. Just lateral to the brachial artery and superficial to the brachialis is the biceps brachii tendon. Immediately medial to the brachial artery is the median nerve, which has a speckled appearance from hypoechoic nerve fascicles and surrounding hyperechoic connective tissue. Medial to the median nerve is the humeral head of the pronator teres muscle. At the far lateral aspect of the anterior elbow is the brachioradialis muscle. In between the brachialis and brachioradialis is an oblique fascial layer, which contains the superficial and deep branches of the radial nerve. More proximal to the elbow joint, the musculocutaneous nerve can be identified between the biceps brachii and brachialis muscles (see Fig. 4-2C).

To evaluate the biceps brachii tendon, the transducer is centered over the biceps tendon and rotated 90 degrees (Fig. 4-3). At this location,

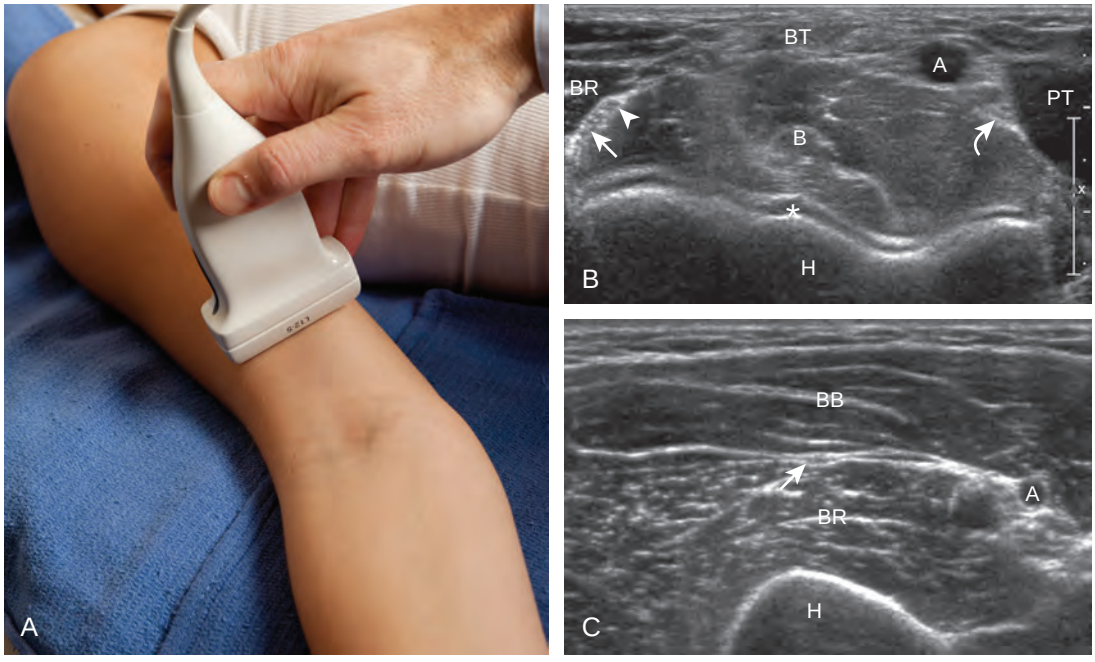

FIGURE 4-2 ■ **Anterior elbow. A,** Transverse imaging over anterior elbow just proximal to elbow joint shows **(B)** brachial artery (A), biceps brachii (BT), brachialis (B), pronator teres (PT), brachioradialis (BR), median nerve *(curved arrow)*, and superficial *(arrowhead)* and deep *(arrow)* branches of radial nerve (*asterisk,* hyaline articular cartilage). **C,** Imaging more proximal to elbow joint shows biceps brachii muscle (BB), brachialis (BR), and musculocutaneous nerve *(arrow)*. H, humerus.

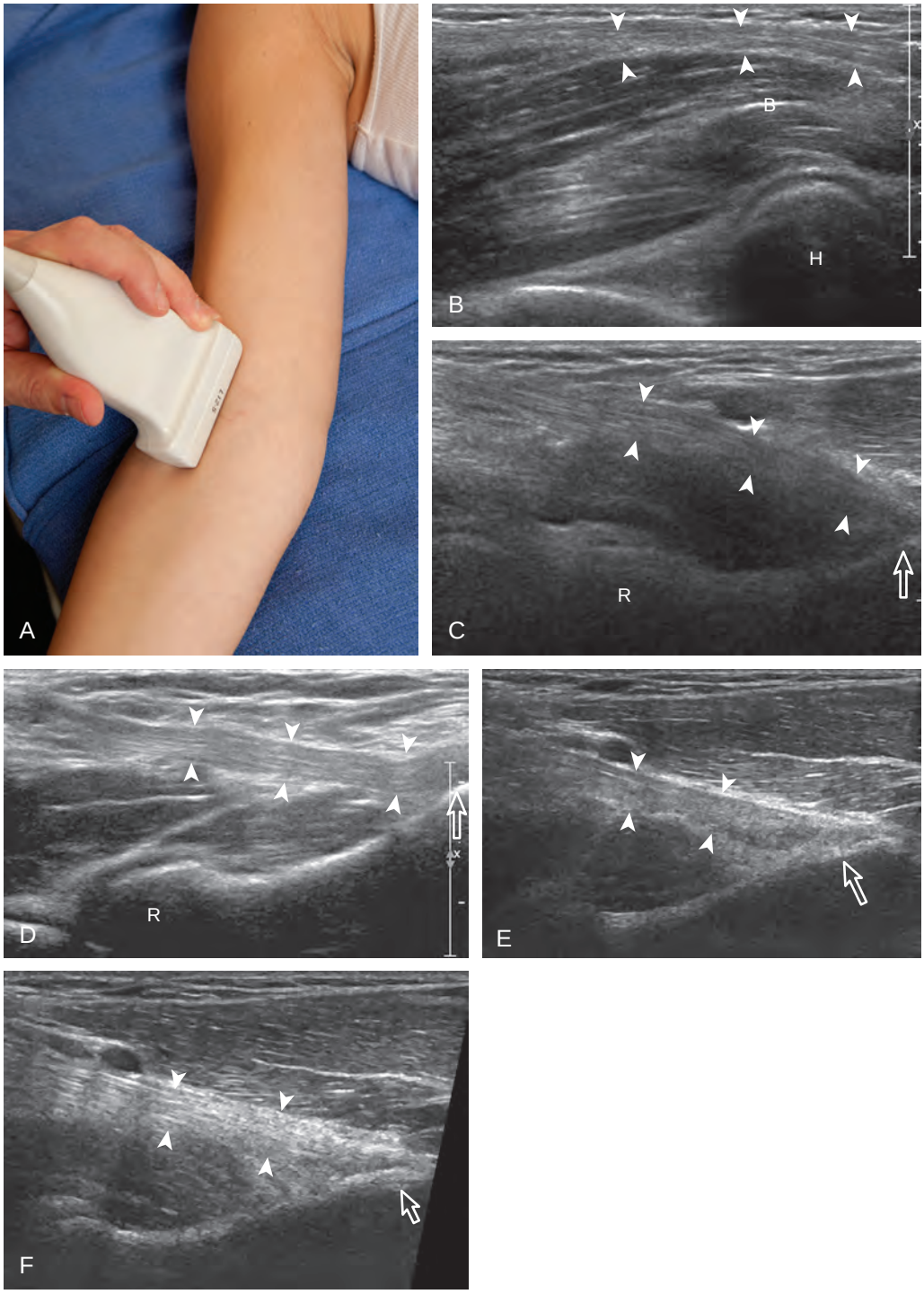

FIGURE 4-3 ■ **Biceps brachii (long axis). A,** Sagittal imaging over the anterior elbow shows **(B)** the biceps brachii tendon in long axis *(arrowheads)* superficial to the brachialis (B). More distal imaging **(C)** shows anisotropy of the distal tendon *(arrowheads)*, which is eliminated when imaging perpendicular to the tendon **(D)** (*open arrow*, radial tuberosity). **E,** The presence of anisotropy *(arrowheads)* may also be reduced with steering of ultrasound beam **(F)**. H, humerus; R, radial head.

the biceps tendon will be hyperechoic and fibrillar with a uniform thickness over the brachialis muscle (see Fig. 4-3B). As the biceps brachii tendon courses deep along the outer contour of the brachialis, the tendon will become hypoechoic from anisotropy (see Fig. 4-3C). Using the heel-toe maneuver, the sound beam is angled superiorly in order to image the tendon perpendicular to eliminate anisotropy (see Fig. 4-3D). Some ultrasound machines will have beam steering, which can assist in reducing anisotropy (see Figs. 4-3E and F). If the distal biceps is difficult to visualize, the elbow position may be changed with additional minimal flexion or extension. The biceps brachii is also evaluated in short axis (Fig. 4-4). The lacertus fibrosis or bicipital aponeurosis can be seen extending from the biceps brachii tendon to the pronator teres and flexor musculature, superficial to the brachial artery and median nerve, by placing the transducer over the anterior elbow angled from the biceps brachii tendon distal and medial (see Fig. 4-4C).

If the distal biceps brachii tendon insertion onto the radial tuberosity in long axis is not clearly seen, a more medial approach should be attempted (Fig. 4-5). With the transducer long axis to the biceps brachii tendon in the sagittal plane on the body, the transducer is moved slightly medial with the beam angled slightly lateral toward the center of the elbow. If the brachial vasculature is visualized, then the transducer needs to be angled laterally. This maneuver is continued, only a millimeter at a time, while adding the heel-toe manuever until the distal tendon is visualized. With the transducer over the medial elbow angled toward the lateral elbow, often the distal biceps brachii tendon can be seen through the medial brachial vasculature as an acoustic window.[4] Distal tendon attachment can also be assessed during supination and pronation dynamically (Video 4-1).

An additional method to evaluate the distal biceps brachii tendon to differentiate a nonretracted full-thickness tear from a partial-thickness tear is from a lateral approach with the elbow flexed.[5] Examination with this technique begins with the transducer in short axis relative to the proximal radius (Fig. 4-6). The radial head is visualized as a curvilinear echogenic structure, and the transducer is moved toward the wrist over the radial neck, where the surrounding supinator muscle can be seen. At this level, the hand can be passively supinated and pronated to visualize movement of the biceps brachii tendon, which is perpendicular to the sound beam (Video 4-2).

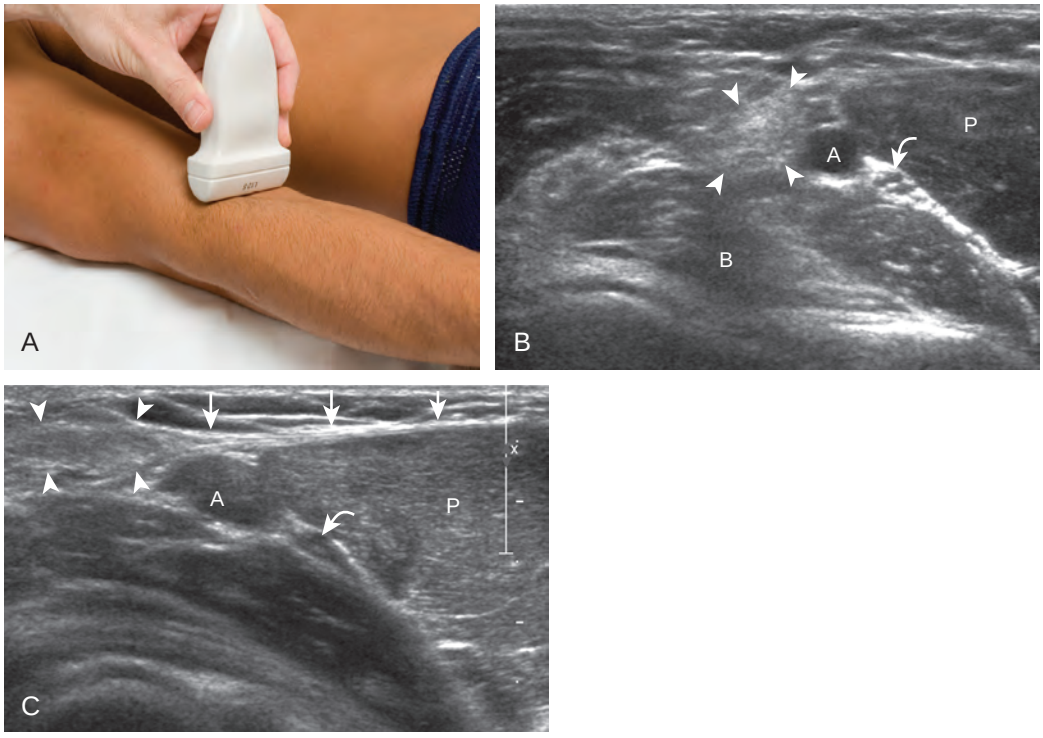

FIGURE 4-4 ■ Biceps brachii (short axis). A, Transverse imaging over anterior elbow shows **(B)** the biceps brachii *(arrowheads)* in short axis (*curved arrow*, median nerve). Note the lacertus fibrosus *(arrows)* in **C,** when the transducer is angled from the biceps tendon toward the medial epicondyle. A, brachial artery; B, brachialis, P, pronator teres.

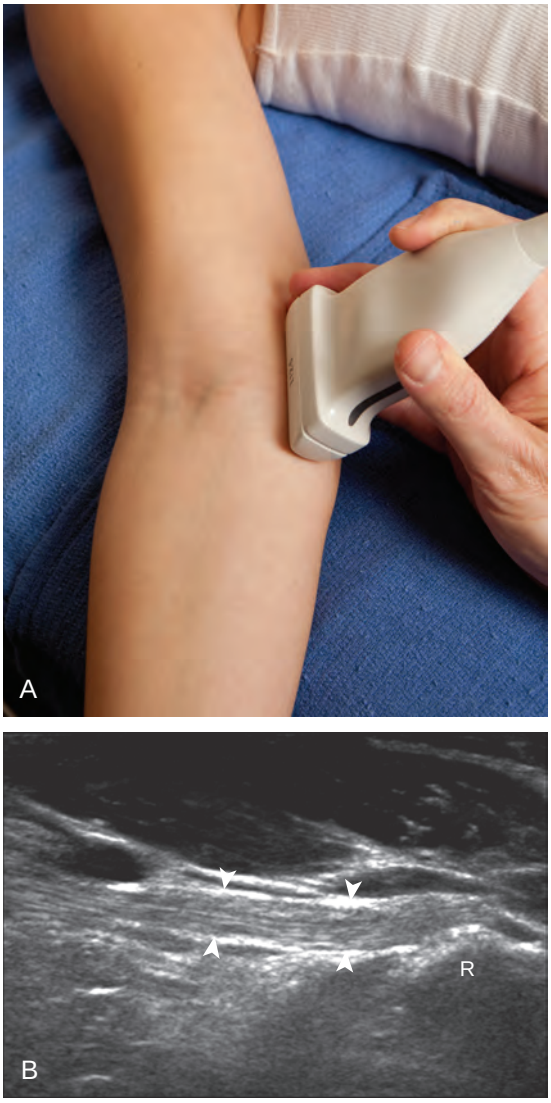

FIGURE 4-5 ■ Biceps brachii: medial approach. A, Coronal-oblique imaging over the medial elbow shows **(B)** the distal biceps brachii tendon *(arrowheads)* and radial tuberosity (R).

There is also one additional method to evaluate the most distal aspect of the biceps brachii tendon (Fig. 4-7), in which the transducer is placed transverse to the radius dorsally between the radius and ulna with the hand in pronation to visualize the radial tuberosity insertion.

To complete the anterior evaluation of the elbow, the transducer is returned to the sagittal plane directly long axis to the brachialis to visualize the anterior recess of the elbow joint (Fig. 4-8A and B). Here, the coronoid fossa and smaller radial fossa are visible as concavities in the distal humerus. Within these fossae, a triangular hyperechoic intracapsular fat pad is normally seen. The hypoechoic hyaline cartilage of the trochlea and capitellum can also be identified. Returning to the original short axis view of the brachial artery, the normal median nerve is again identified in short axis and can be followed distally as it courses between the humeral and ulnar heads of the pronator teres, a potential site of nerve entrapment (see Fig. 4-8C and D). The ulnar head of the pronator teres is located between the median nerve and the ulnar artery.

Medial Evaluation

For medial evaluation, the elbow is slightly flexed to bring the anterior band of the ulnar collateral ligament into the coronal plane. Sonographic evaluation of the medial elbow structures begins by visually identifying or palpating the medial epicondyle of the humerus. The transducer is then placed in long axis to the forearm with the proximal aspect over the medial epicondyle (Fig. 4-9). The characteristic hyperechoic bony contours of the medial epicondyle should be seen. Distal to the medial epicondyle, the humerus has a flattened surface where the humerus articulates with the proximal ulna. In this imaging plane long axis to the forearm, as indicated by the characteristic bone contours, both the common flexor tendon and the anterior band of the ulnar collateral ligament can be identified (see Fig. 4-9B). The origin of the common flexor tendon should be seen at the superficial aspect of the medial epicondyle as hyperechoic and fibrillar, with transition to hypoechoic musculature more distally. In addition, the anterior band of the ulnar collateral ligament is seen attached to the medial epicondyle as hyperechoic and fibrillar, but somewhat more compact than that of tendon. If not perpendicular to the ligament, the anterior band of the ulnar collateral ligament will be hypoechoic from anisotropy, but still fairly uniform in thickness where it extends distally over the joint space to insert on the proximal ulna.[6] The anterior band of the ulnar collateral ligament has a somewhat variable appearance at its proximal attachment to the humerus; it may appear as a uniform band, or it may fan out more proximally, interspersed with hyperechoic fatty tissue.[7] The normal joint recess of the elbow extends proximally between the anterior band of the ulnar collateral ligament and adjacent humerus, but it should not extend medially from this point at the humeral attachment of the ligament or distal over the ulna. The long axis view is the key plane in the imaging of both the common flexor tendon and anterior band of the ulnar collateral ligament, although if a pathologic process is identified, further characterization is completed by

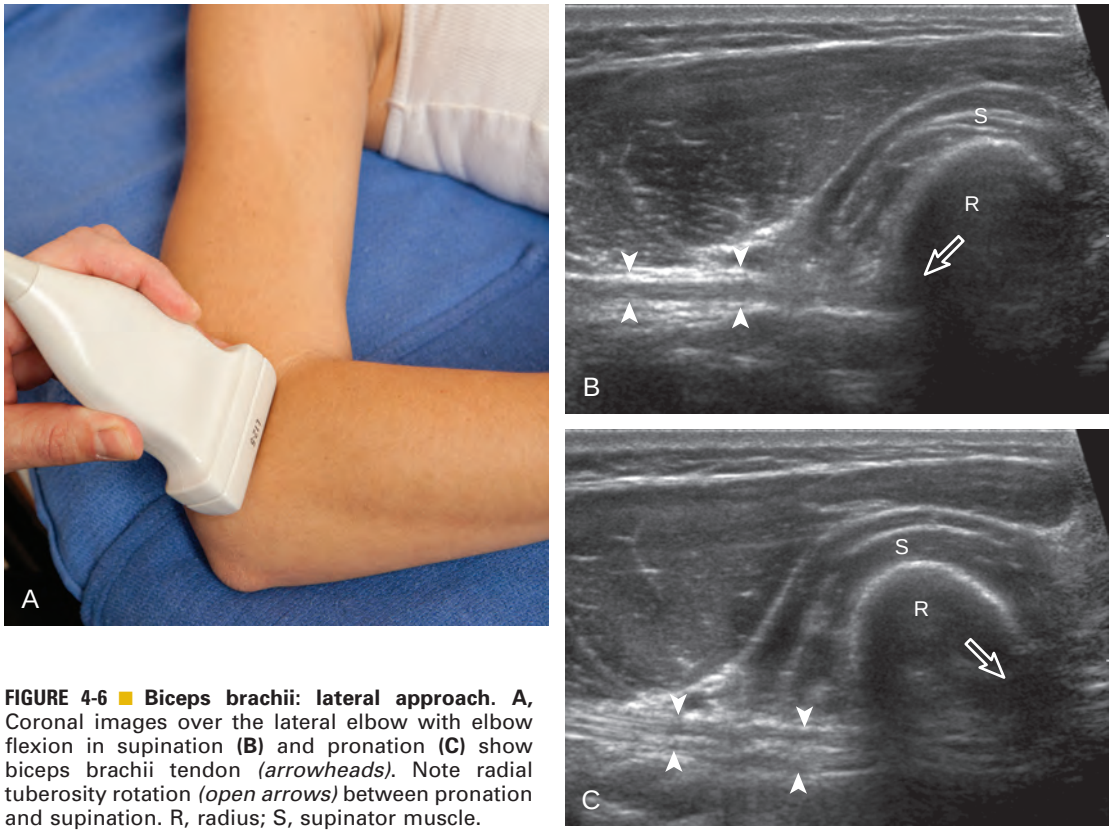

FIGURE 4-6 ■ Biceps brachii: lateral approach. A, Coronal images over the lateral elbow with elbow flexion in supination **(B)** and pronation **(C)** show biceps brachii tendon *(arrowheads)*. Note radial tuberosity rotation *(open arrows)* between pronation and supination. R, radius; S, supinator muscle.

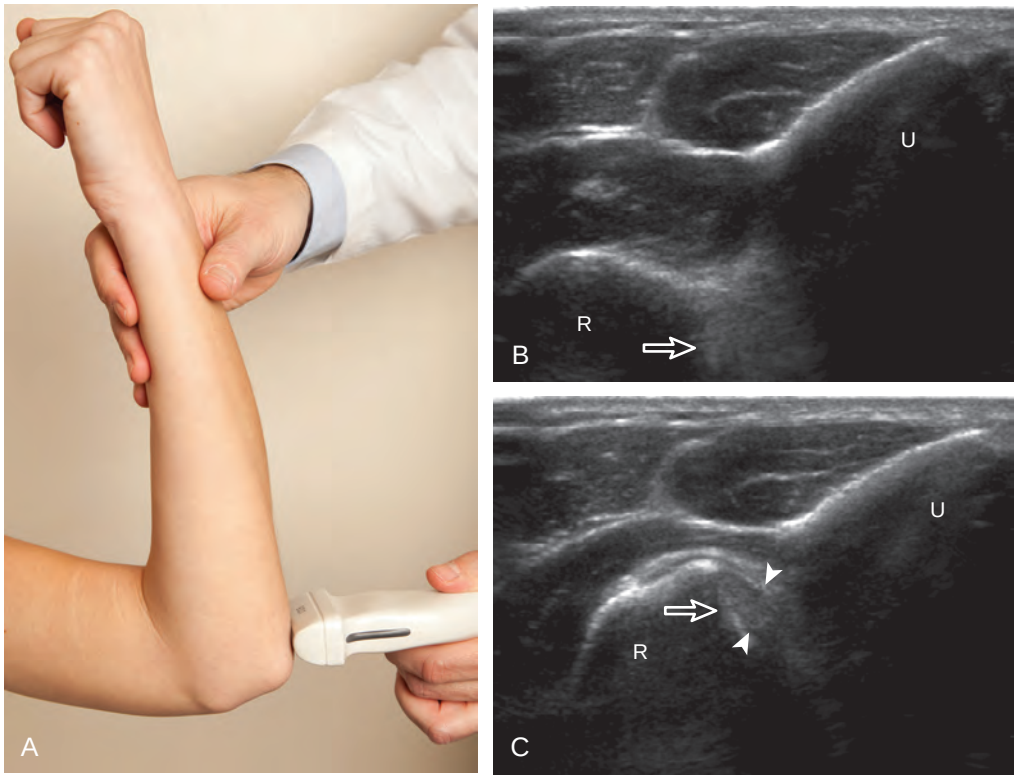

FIGURE 4-7 ■ Biceps brachii tendon: dorsal approach. A, Transverse images over dorsal proximal forearm with arm in flexion and hand in **(B)** supination and **(C)** pronation show distal biceps brachii tendon *(arrowheads)* attachment on radial tuberosity *(open arrows)* only seen in pronation. R, radius; U, ulna.

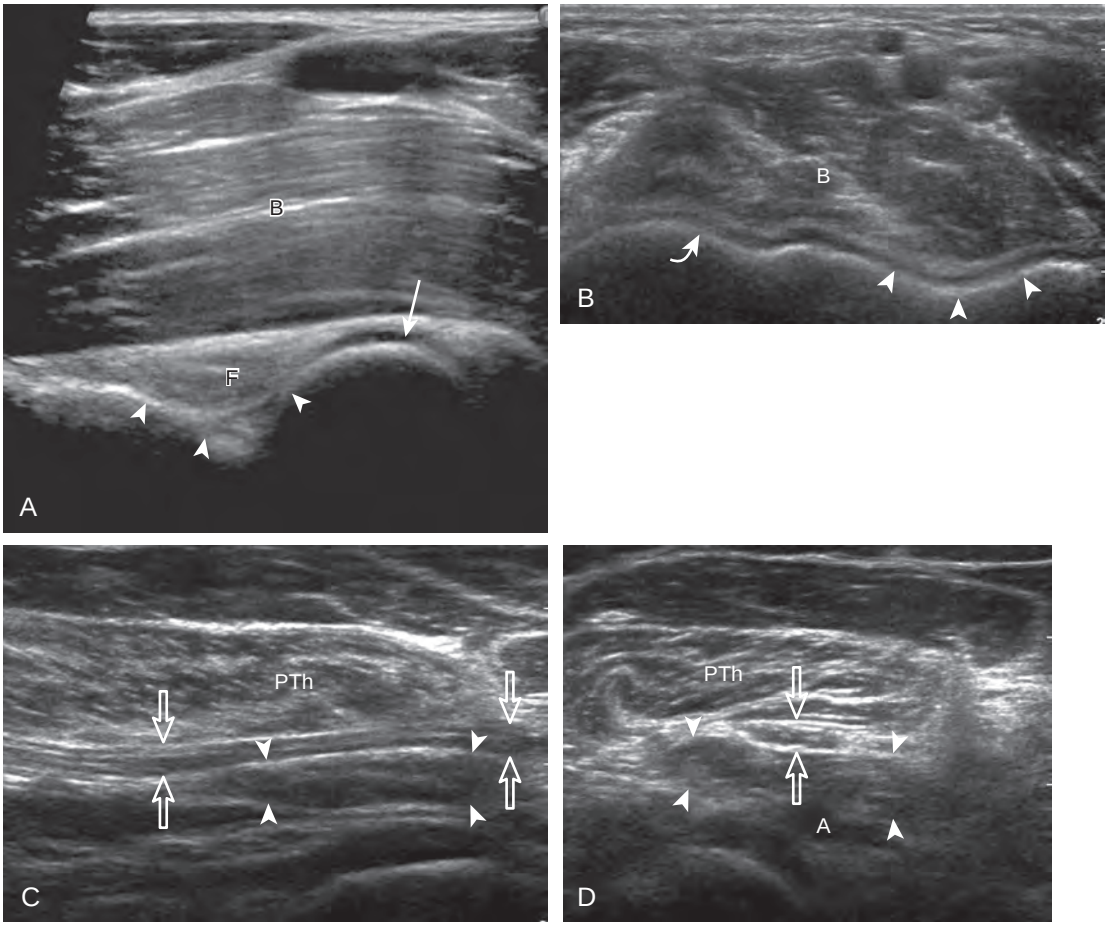

FIGURE 4-8 ■ Anterior elbow joint recesses and median nerve. A, Ultrasound image in long axis to brachialis (B) shows coronoid fossa *(arrowheads)*, anterior elbow fat pad (F), and trochlea hyaline cartilage *(arrow)*. **B,** Ultrasound image short axis to brachialis (B) shows coronoid *(arrowheads)* and radial *(curved arrow)* fossae and hypoechoic hyaline cartilage. Ultrasound images show the median nerve *(open arrows)* in **(C)** long and **(D)** short axis and relationship to the humeral head of the pronator teres (PTh), the ulnar head of pronator teres *(arrowheads)*, and the ulnar artery (A).

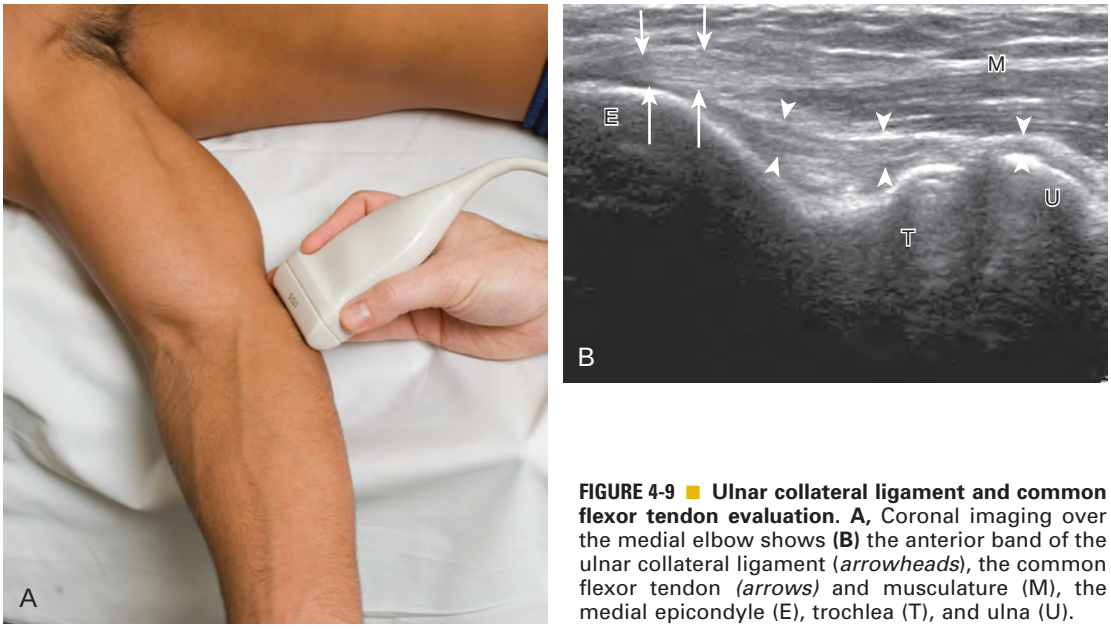

FIGURE 4-9 ■ Ulnar collateral ligament and common flexor tendon evaluation. A, Coronal imaging over the medial elbow shows **(B)** the anterior band of the ulnar collateral ligament (*arrowheads*), the common flexor tendon *(arrows)* and musculature (M), the medial epicondyle (E), trochlea (T), and ulna (U).

imaging in short axis to these structures. In addition, the ulnar collateral ligament and medial joint space can be evaluated with dynamic valgus stress with the elbow in slight flexion to assess for ligamentous injury.[8,9]

After evaluation of the common flexor tendon and anterior band of the ulnar collateral ligament is completed, attention is turned to the cubital tunnel region more posteriorly. To evaluate the cubital tunnel region, the elbow is turned outward so that the bony protuberances of the olecranon process and the medial epicondyle can be visualized and are palpable. Evaluation should begin with the elbow extended; if the elbow is flexed at this point, it is possible that the ulnar nerve may dislocate and be difficult to locate, and identification of an anconeus epitrochlearis becomes difficult as well (see discussion later). The ultrasound transducer is placed in the transverse plane between the olecranon process and the medial epicondyle, and the characteristic hyperechoic and shadowing bone contours of these structures are seen (Fig. 4-10A and B). The ulnar nerve is visible as speckled or honeycomb in appearance from hypoechoic nerve fascicles and hyperechoic connective tissue. However, the ulnar nerve posterior to the medial epicondyle often appears hypoechoic surrounded by hyperechoic fat and may be bilobed or bifid. Superficial to the ulnar nerve, the cubital tunnel retinaculum (or Osborne

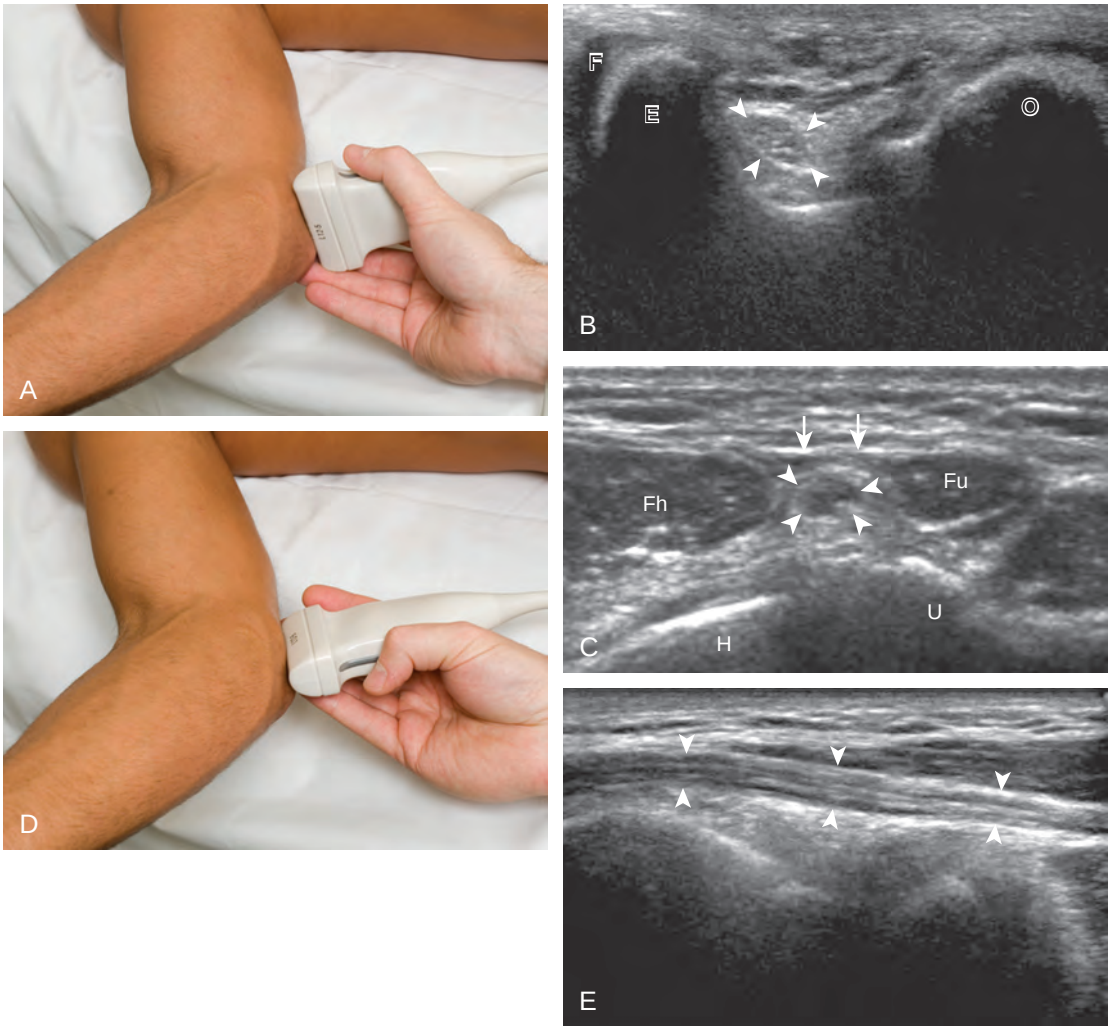

FIGURE 4-10 ■ Ulnar nerve and cubital tunnel evaluation. A, Transverse imaging over the medial elbow between the medial epicondyle and olecranon process shows **(B)** the ulnar nerve *(arrowheads)* posterior to the medial epicondyle (E). Note the common flexor tendon (F) and the olecranon process (O). **C,** Transverse imaging distal to **B** shows the ulnar nerve *(arrowheads)* in the cubital tunnel (*arrows*, arcuate ligament). **D,** Longitudinal imaging shows **(E)** the ulnar nerve *(arrowheads)*. Fh, humeral head of flexor carpi ulnaris; Fu, ulnar head of flexor carpi ulnaris; H, humerus; U, ulna.

fascia) is located and, when present, appears as a thin structure between the olecranon and medial epicondyle. Distally, the ulnar nerve can be followed into the true cubital tunnel between the humeral and ulnar heads of the flexor carpi ulnaris and under the arcuate ligament (see Fig. 4-10C). With rotation of the transducer 90 degrees, the ulnar nerve can be evaluated in long axis (see Fig. 4-10D and E).

It is also important to evaluate the cubital tunnel region dynamically for pathology.[10] With the transducer again placed in the transverse plane between the medial epicondyle and olecranon process and fixed over the medial epicondyle, the patient is asked to actively flex the elbow (Fig. 4-11). During this maneuver, the olecranon process moves out of the imaging plane and is replaced by the hypoechoic triceps brachii muscle. It is often helpful to first perform this maneuver passively so that if the bone contour of the medial epicondyle apex is no longer visualized, the movement can be stopped and the transducer repositioned until the epicondyle is found again and the motion continued. Normally during elbow flexion, the ulnar nerve moves toward the apex of the medial epicondyle but should not translate over the epicondyle anteriorly. Abnormal ulnar nerve translation over the medial epicondyle may be felt as a palpable snap through the transducer, and typically it returns back into normal position as the elbow is extended. It is important not to place too much pressure with the transducer during this dynamic evaluation because this may inhibit the abnormal ulnar nerve translation; intermittent reduction in transducer pressure during the maneuver avoids this pitfall. Ulnar nerve dislocation has been described in up to 20% of asymptomatic individuals, so it is important to correlate with abnormal ulnar nerve morphology and symptoms.[11] It is also essential to differentiate isolated ulnar nerve dislocation from snapping triceps syndrome. In this situation, both the medial head of the triceps muscle and the ulnar nerve dislocate over the medial epicondyle of the humerus in elbow flexion.[7]

Lateral Evaluation

For evaluation of the lateral elbow structures, the arm is rotated inward and slightly flexed. Structures of interest laterally include the common extensor tendon, the radial collateral ligament complex, the radial head and annular recess, and the capitellum. Unlike the medial aspect of the elbow, the lateral epicondyle is not clearly visible to the eye and is more difficult to palpate. Therefore, bone landmarks as seen at sonography are used for orientation. To begin, the transducer is placed in long axis relative to the forearm over the lateral elbow (Fig. 4-12A), and the characteristic hyperechoic shadowing contour of the radial head is readily identified (see Fig. 4-12B). More proximal scanning in this plane reveals the radius articulation with the capitellum, and more proximally, the relatively flattened contour of the lateral epicondyle (see Fig. 4-12C). At this site, the hyperechoic and fibrillar common extensor tendon can be seen originating on the lateral epicondyle. Although the long axis view is optimum in identification of the common extensor tendon, any abnormality should also be characterized in short axis as well. Care should be taken to include evaluation of the most anterior aspect of the common extensor tendon, where tendon abnormalities most commonly occur. Deep to the

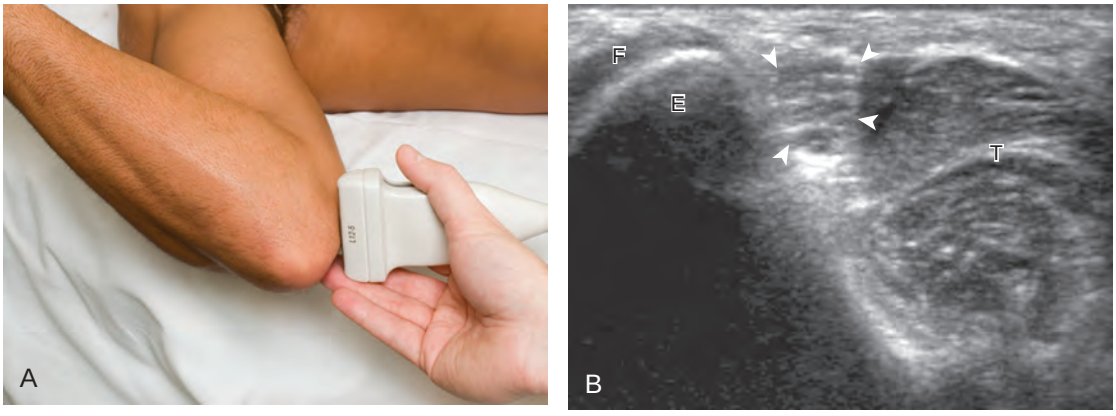

FIGURE 4-11 ■ Ulnar nerve dynamic evaluation. A, Imaging transverse to the humeral shaft at the level of the medial epicondyle in elbow flexion shows **(B)** the ulnar nerve *(arrowheads)* and the triceps (T) posterior to the medial epicondyle (E). F, common flexor tendon.

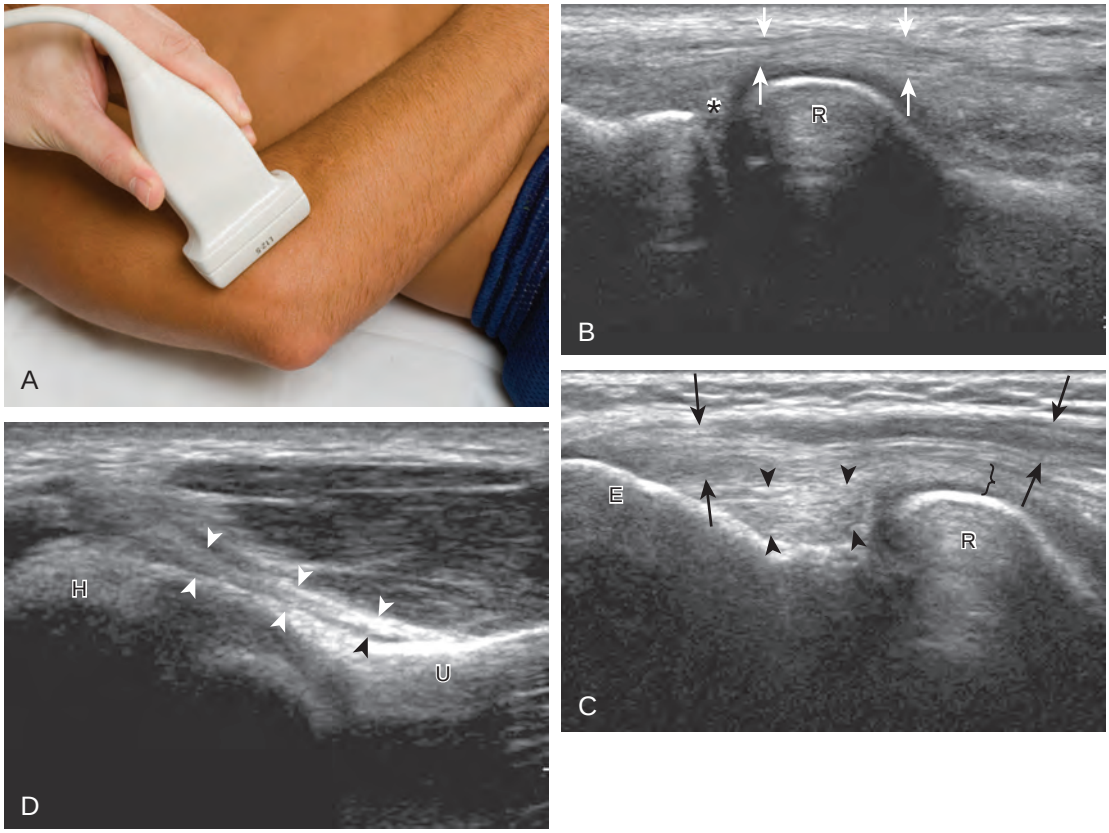

FIGURE 4-12 ■ Common extensor tendon and radial collateral ligament evaluation. A, Lateral imaging in long axis to the forearm over the radial head shows **(B** and **C)** the radial head (R), common extensor tendon *(arrows)*, radial collateral ligament *(arrowheads)*, and annular ligament (*bracket*). Note triangular synovial fold (*asterisk*) in **B**. Transducer placement angled from the lateral epicondyle to the ulna shows **(D)** the lateral ulnar collateral ligament *(arrowheads)* from the humerus (H) to the crista supinator of the ulna (U). E, lateral epicondyle.

common extensor tendon in the long axis plane over the lateral epicondyle is the radial collateral ligament (see Fig. 4-12C).[12] It is often difficult to discern the separation between the proximal common extensor tendon and the adjacent radial collateral ligament; however, if one follows these structures distally, the deeper radial collateral ligament will attach to the annular ligament, seen immediately over the radial head, whereas the more superficial common extensor tendon will continue more superficial and become muscle. If the transducer is placed over the lateral elbow and angled posteriorly from the distal humerus to the ulna, the hyperechoic and fibrillar lateral ulnar collateral ligament can be seen (see Fig. 4-12D).[12,13] At the level of the radial neck, the collapsed annular recess is difficult to discern unless it is abnormally distended (see Fig. 4-20B).

With elbow extension and the transducer anterolateral in the sagittal plane, the thin uniform hypoechoic layer of hyaline cartilage can be seen over the anterior aspect of the capitellum (Fig. 4-13A). At the radiocapitellar joint, a hyperechoic, triangular, meniscus-like synovial reflection or fold, also termed the *posterolateral plica*, extends from the radial collateral ligament and joint capsule into the joint.[14,15] With movement of the transducer posteriorly over the capitellum, the irregular cortex represents a normal appearance void of cartilage and should not be misinterpreted as an osteochondral abnormality.[14] With the elbow in flexion and the transducer posterior in the sagittal plane, the central and posterior aspect of the capitellum hyaline cartilage can also be visualized (Fig. 4-13B).

For evaluation of the radial nerve, one approach is to first find the oblique fascial plane between the brachioradialis and the brachialis anteriorly in the transverse plane, where the deep and superficial branches of the radial nerve are seen as round and hypoechoic (Fig. 4-14A; see Fig. 4-2B). These individual branches can be followed proximally in short axis where they join to form the radial nerve (see Fig. 4-14B and C). Evaluation can continue more proximal to follow the radial nerve as it traverses the intermuscular

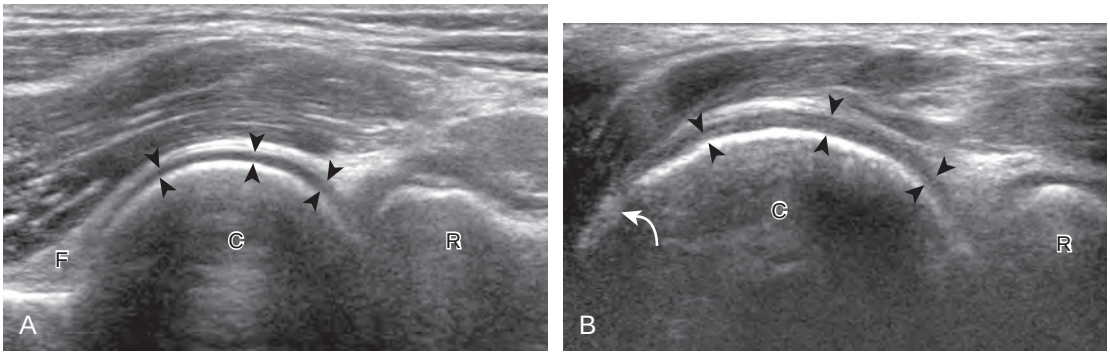

FIGURE 4-13 ■ Capitellum cartilage evaluation. A, Anterior imaging in the sagittal plane over the capitellum (C) shows the hyaline articular cartilage *(arrowheads)*, radial head (R), and anterior fat pad (F) in the radial fossa. Posterior imaging in the sagittal plane with the elbow flexed over the capitellum shows **(B)** the hypoechoic hyaline cartilage *(arrowheads)*. Note the normal bone irregularity *(curved arrow)*.

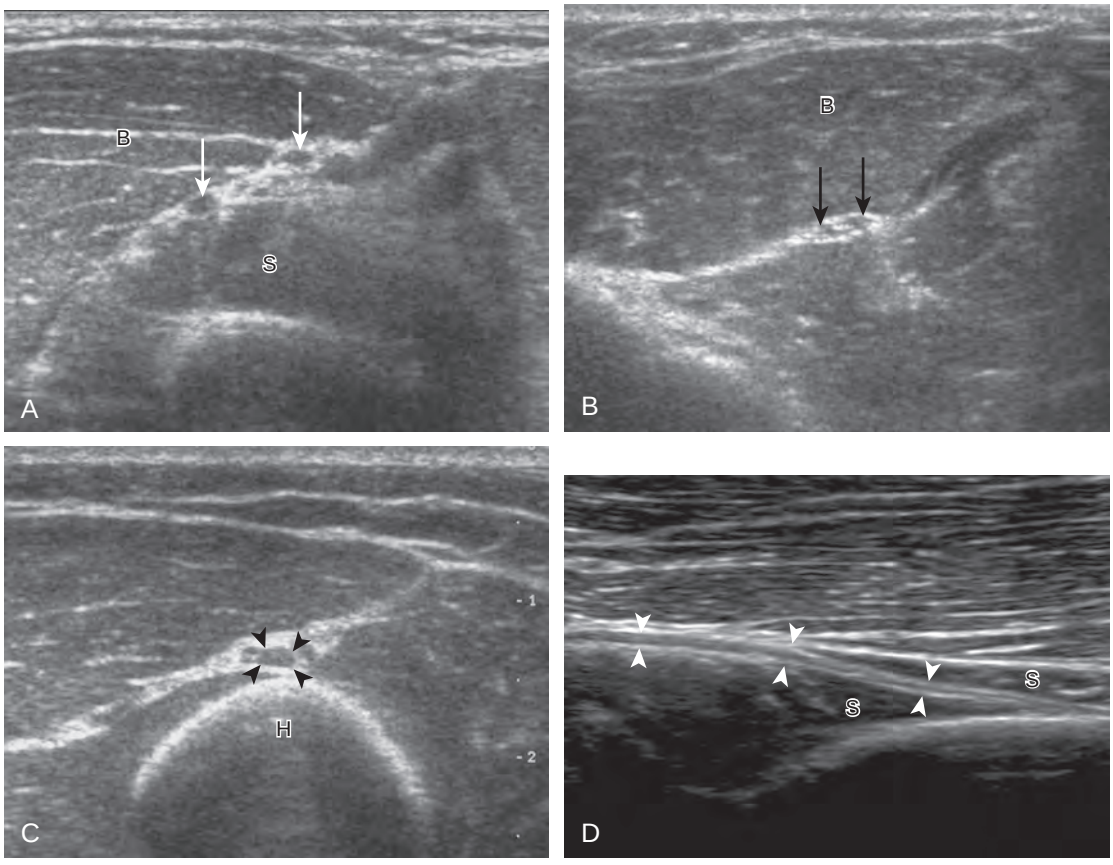

FIGURE 4-14 ■ Radial nerve evaluation. Transverse imaging over anterior elbow (see Fig. 4-2A) shows **(A)** the superficial and deep branches of the radial nerve *(arrows)* deep to the brachioradialis (B). Sequential proximal imaging (**B** and **C**) shows the radial nerve branches *(arrows)* joining to form radial nerve *(arrowheads)* adjacent to the posterior humerus (H). **D,** Sagittal imaging shows the deep branch of the radial nerve *(arrowheads)* in long axis between the two heads of the supinator muscle (S).

fascia and follows the posterior cortex of the humerus. The transducer is turned 90 degrees to evaluate the radial nerve and its branches in long axis as well. Following the radial nerve branches distally, the deep branch is seen entering into the supinator muscle as the posterior interosseous nerve (see Fig. 4-14D). The deep branch of the radial nerve often changes shape as it passes beneath the arcade of Frohse and should not be interpreted as nerve swelling.[16] The superficial branch of the radial nerve may also be followed distally into the forearm.

Posterior Evaluation

To evaluate the posterior structures of the elbow, the patient is asked to flex the elbow to 90 degrees. If the patient is supine, this can be accomplished by asking the patient to place his or her hand across the abdomen. Structures of interest include the posterior joint recess, the triceps brachii, and the soft tissues over the olecranon. By placing the transducer posteriorly in the sagittal plane over the proximal elbow, the characteristic hyperechoic shadowing bone contours of the humerus are identified (Fig. 4-15). As the humeral diaphysis approaches the elbow joint, there is a pronounced concavity, which represents the olecranon fossa. This is also demonstrated in the transverse plane relative to the humerus (Fig. 4-16). This fossa is normally filled with the hyperechoic posterior elbow fat pad and is the site of evaluation for joint fluid, intra-articular bodies, and other joint processes. The hypoechoic trochlear and capitellum hyaline cartilage can also be identified. Superficial to the olecranon recess, the hypoechoic triceps brachii muscle and more distal hyperechoic tendon can be seen inserting onto the olecranon process. Although not discernable in the normal situation, the superficial layer of the triceps brachii represents the confluence of the lateral and long heads, whereas the deeper layer with a very short tendon represents the medial head of the triceps brachii. With elbow extension, the soft tissues superficial to the olecranon process can be evaluated for olecranon bursal fluid. It is important to float the transducer with a thick layer of gel in evaluation for olecranon bursal fluid because minimal transducer pressure may displace small amounts of fluid away from view. Although the sagittal plane is most important in evaluation of the foregoing structures, imaging in the orthogonal transverse plane also shows the above anatomic structures and is important when characterizing pathology.

JOINT AND BURSA ABNORMALITIES

Although a joint effusion may distend the anterior and less commonly the annular joint recesses, the posterior olecranon recess in elbow flexion is the most sensitive location for identification of joint fluid (Fig. 4-17).[17] Imaging in the sagittal plane over the posterior joint recess demonstrates superior and posterior displacement of the hyperechoic fat pad when the joint is distended, similar to findings at radiography. Fat pad displacement, both in the anterior and posterior joint fossae, may result from anechoic simple fluid, although

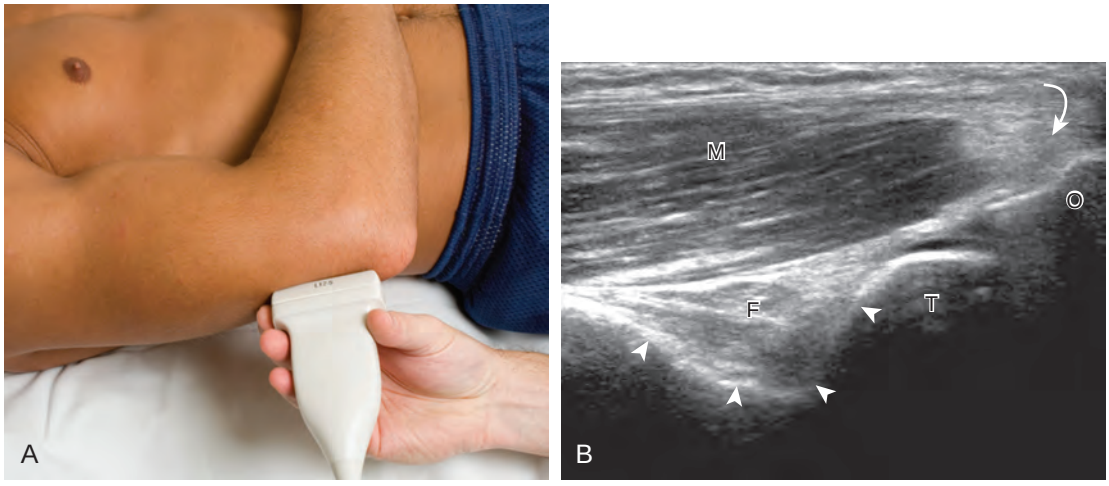

FIGURE 4-15 ■ Posterior joint recess and triceps evaluation (long axis). A, Imaging in the sagittal plane over the elbow flexed shows **(B)** the triceps muscle (M) and tendon *(curved arrow)*, olecranon fossa *(arrowheads)*, and hyperechoic fat pad (F). Note the trochlea (T) with hypoechoic hyaline cartilage and the olecranon (O).

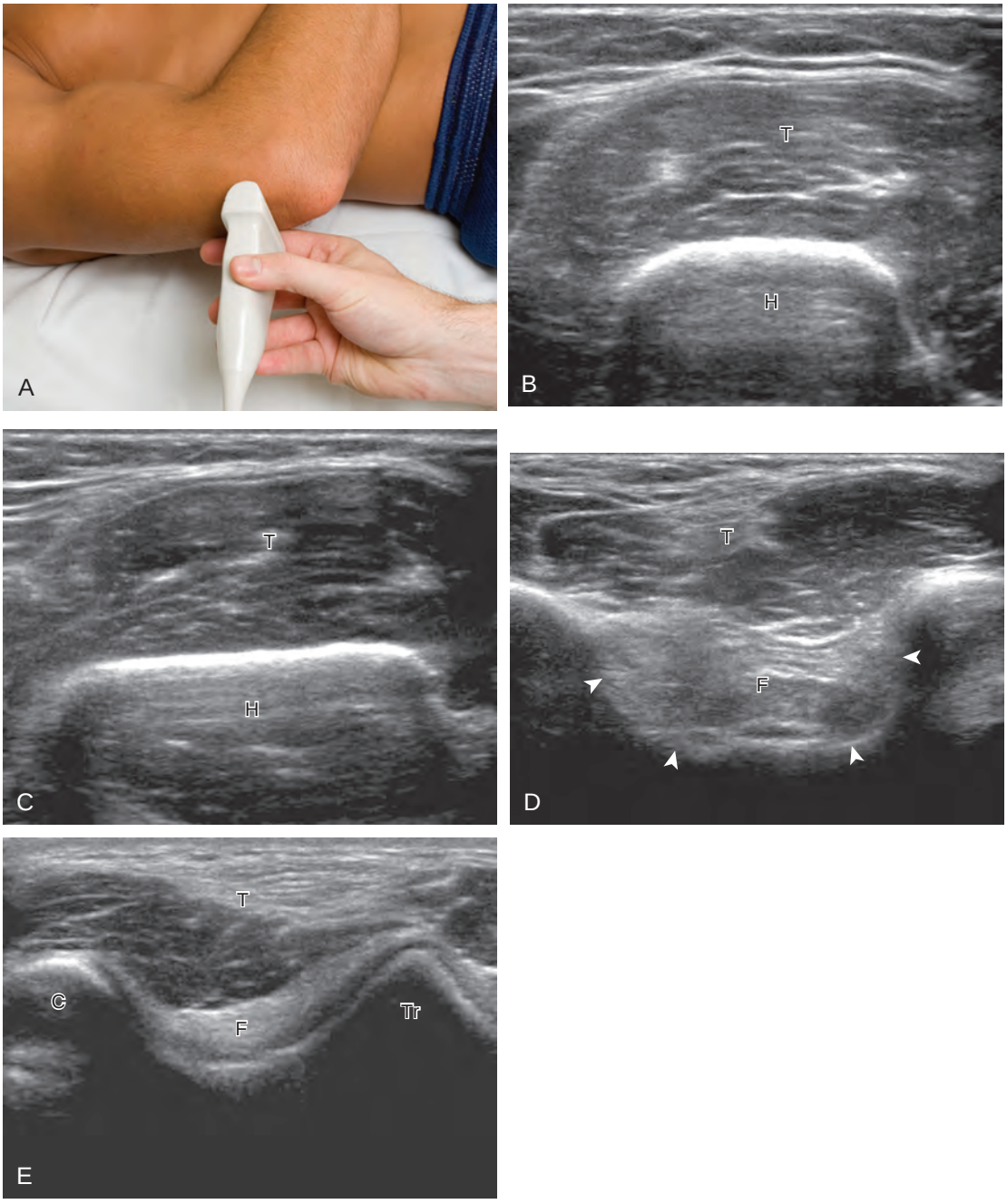

FIGURE 4-16 ■ Posterior joint recess and triceps evaluation (short axis). A, Imaging transverse to the distal humerus shows **(B** to **E)** the triceps muscle (T) and gradual flattening of the humerus surface (H) to form the olecranon fossa *(arrowheads)*. Note the posterior fat pad (F) and the hypoechoic hyaline cartilage of the trochlea (Tr) and capitellum (C).

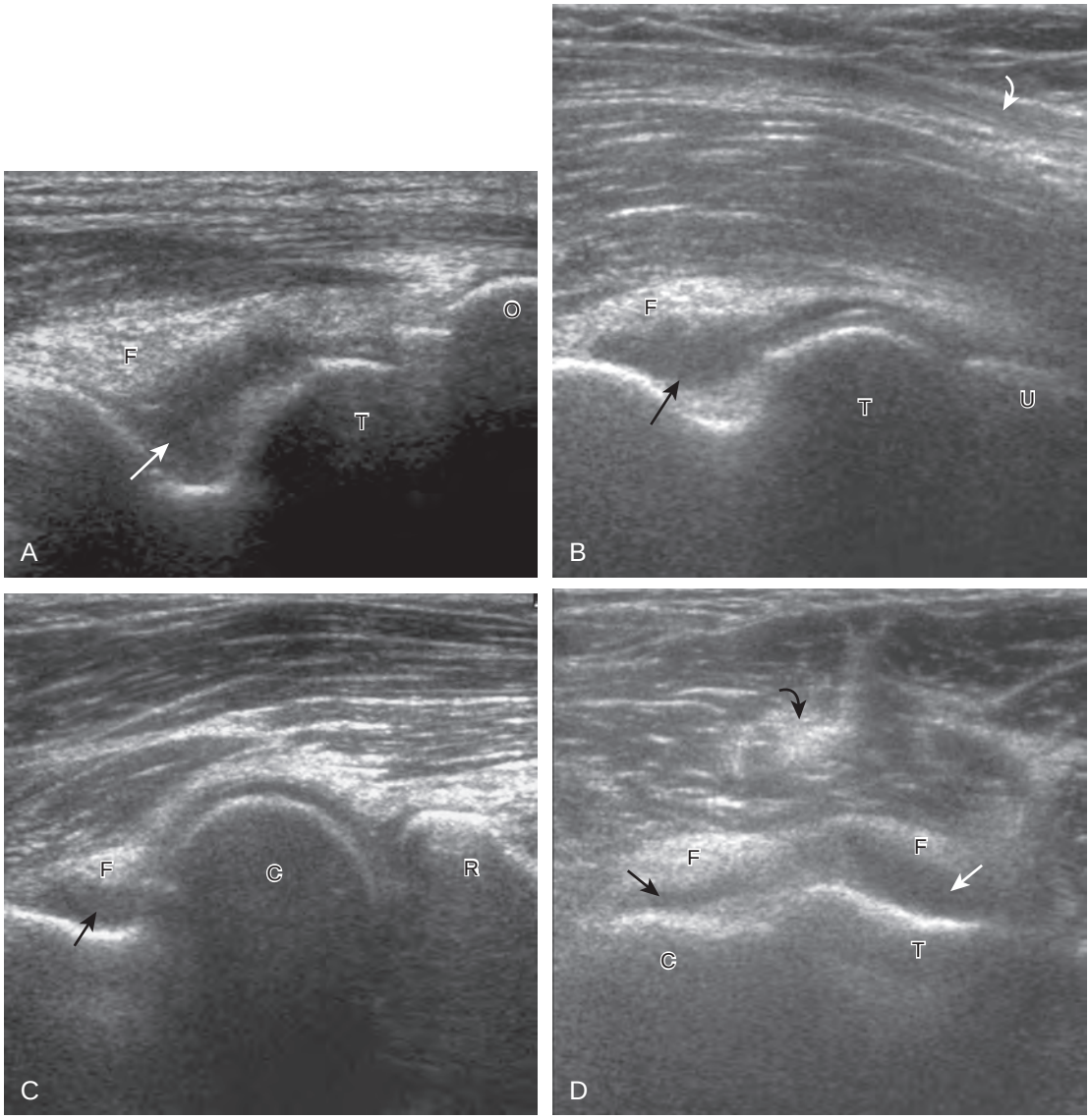

FIGURE 4-17 ■ **Elbow joint effusion. (A)** Sagittal posterior, **(B)** sagittal anterior, **(C)** sagittal anterolateral, and **(D)** transverse anterior ultrasound images show anechoic joint fluid *(arrows)* with displacement of the hyperechoic fat pads (F) within **(A)** the olecranon fossa, **(B** and **D)** the coronoid fossa, and **(C** and **D)** the radial fossa (*curved arrow*, biceps brachii tendon). C, capitellum; R, radial head; O, olecranon; T, trochlea; U, coronoid process of ulna.

complex fluid may vary from hypoechoic to hyperechoic (Fig. 4-18). Heterogeneous joint fluid may be caused by hemorrhage or infection (Fig. 4-19). Synovial hypertrophy, more commonly diffuse, may also distend the joint recesses and may appear hypoechoic (or, less commonly, isoechoic or hyperechoic) relative to the subcutaneous fat. The findings of joint recess compressibility, redistribution or motion of joint recess contents with transducer pressure, and lack of increased blood flow on color or power Doppler imaging suggest complex fluid rather than synovial hypertrophy when their gray-scale appearances are similar. Synovial hypertrophy may be the result of infection (Fig. 4-20), rheumatoid arthritis (Fig. 4-21), and other inflammatory arthritides (Fig. 4-22), or less likely an adjacent bone process, such as intra-articular osteoid osteoma (Fig. 4-23, online).[18] Chronic synovial hypertrophy can result in significant distention of the joint recesses, potentially compressing the ulnar nerve (Fig. 4-24) and radial nerve (Fig. 4-25). In the setting of synovitis, cortical discontinuity and irregularity could

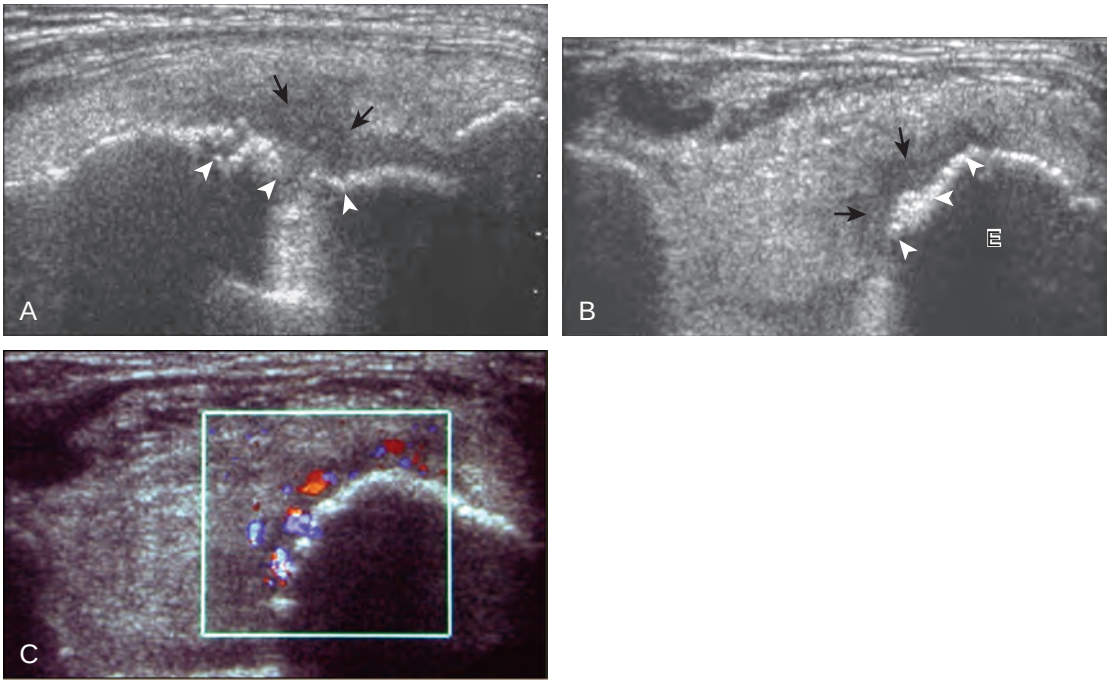

FIGURE 4-23 ■ **Intra-articular osteoid osteoma.** Sagittal **(A)** and transverse **(B)** ultrasound images at the posterior aspect of the medial epicondyle (E) show focal hypoechoic synovial hypertrophy *(arrows)*, cortical irregularity, and bone proliferation *(arrowheads)* at the site of an osteoid osteoma nidus. **C,** Note hyperemia on color Doppler images. (From Ebrahim FS, Jacobson JA, Lin J, et al: Intraarticular osteoid osteoma: sonographic findings in three patients with radiographic, CT, and MR imaging correlation. *AJR Am J Roentgenol* 177:1391–1395, 2001.)

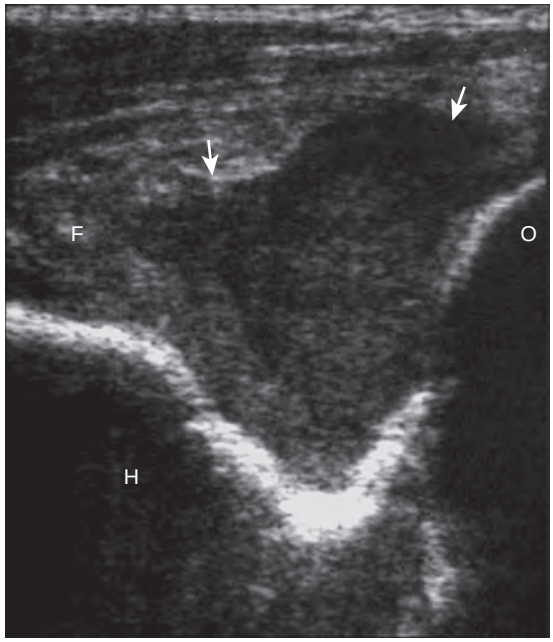

FIGURE 4-18 ■ Septic elbow joint. Sagittal ultrasound image over the posterior elbow shows heterogeneous hypoechoic distention of the posterior joint recess *(arrows)* with displacement of the hyperechoic fat pad (F). H, humerus; O, olecranon.

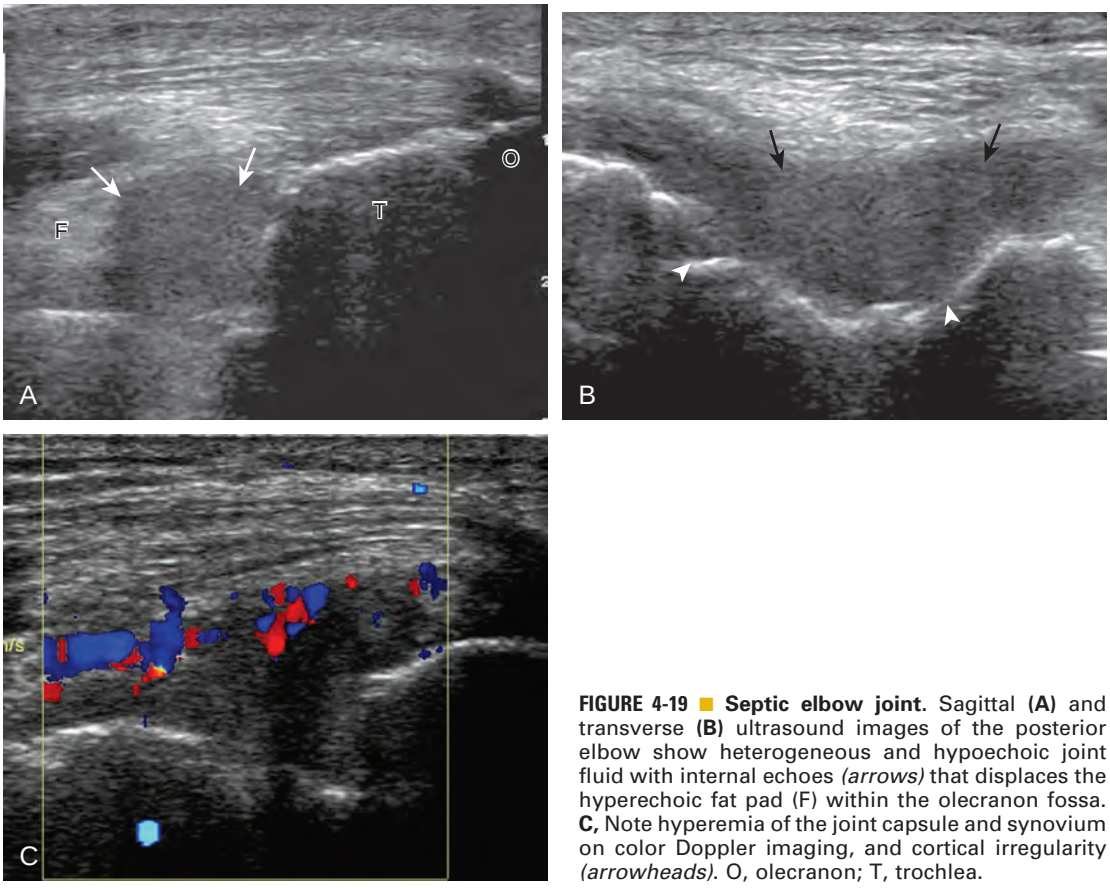

FIGURE 4-19 ■ Septic elbow joint. Sagittal **(A)** and transverse **(B)** ultrasound images of the posterior elbow show heterogeneous and hypoechoic joint fluid with internal echoes *(arrows)* that displaces the hyperechoic fat pad (F) within the olecranon fossa. **C,** Note hyperemia of the joint capsule and synovium on color Doppler imaging, and cortical irregularity *(arrowheads)*. O, olecranon; T, trochlea.

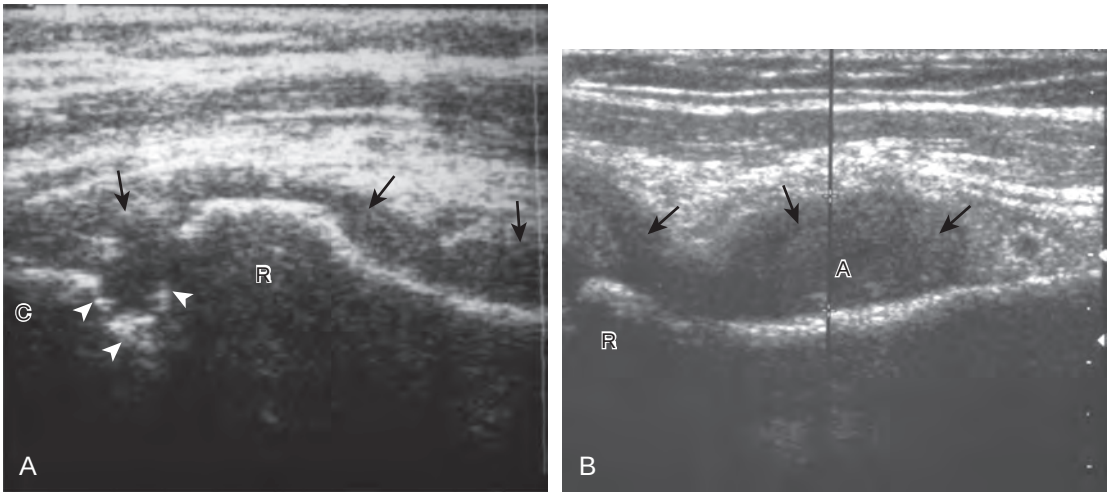

FIGURE 4-20 ■ Elbow joint infection: coccidiomycosis. Coronal ultrasound images **(A)** over and **(B)** distal to the radial head (R) show hypoechoic synovial hypertrophy *(arrows)* that extends from the elbow joint to the annular recess (A). Note subchondral bone erosions *(arrowheads)*. C, capitellum.

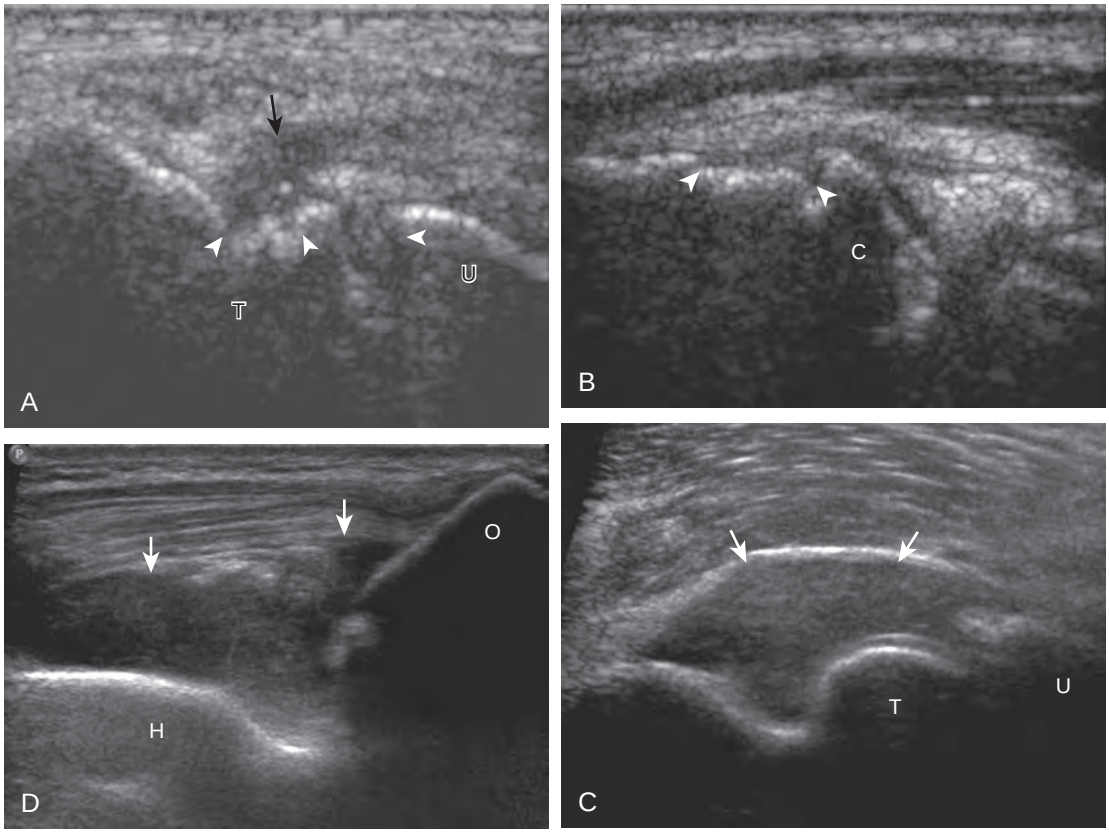

FIGURE 4-21 ■ Rheumatoid arthritis. Ultrasound images **(A)** at the medial elbow and (**B**) posterolateral elbow show hypoechoic synovial hypertrophy *(arrows)*. Note subchondral bone erosions *(arrowheads)* and thinning of the hyaline cartilage of the capitellum (C). Ultrasound images of the anterior **(C)** and posterior **(D)** elbow from a different patient show hypoechoic synovial hypertrophy *(arrows)*. H, humerus; O, olecranon; T, trochlea; U, ulna.

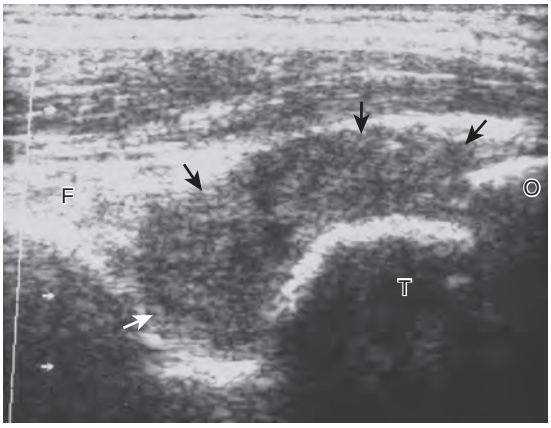

FIGURE 4-22 ■ Seronegative spondyloarthropathy. Sagittal ultrasound image over the posterior elbow shows synovial hypertrophy as hypoechoic to isoechoic *(arrows)*, which distends the posterior elbow recess with fat pad displacement (F). O, olecranon; T, trochlea.

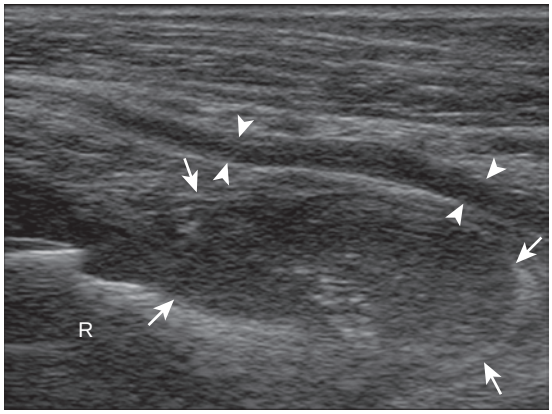

FIGURE 4-25 ■ Radial nerve, deep branch compression: rheumatoid arthritis. Ultrasound image in long axis to deep branch of radial nerve *(arrowheads)* shows compression by annular recess distended with synovial hypertrophy *(arrows)*. R, radius. (Courtesy of V. Flores, MD, Fort Worth, Tex. From Jacobson JA, Fessell DP, Lobo Lda G, et al: Entrapment neuropathies I: upper limb (carpal tunnel excluded). *Semin Musculoskel Radiol* 14:473–486, 2010.)

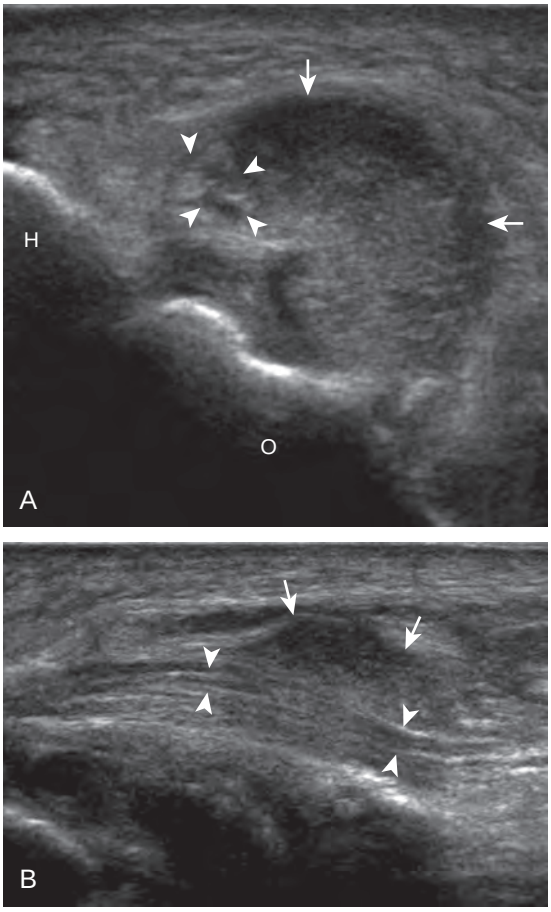

FIGURE 4-24 ■ Ulnar nerve compression: rheumatoid arthritis. Ultrasound images in short axis **(A)** and long axis **(B)** to the ulnar nerve *(arrowheads)* show compression by adjacent hypoechoic to isoechoic synovial hypertrophy *(arrows)*. H, humerus; O, olecranon.

represent bone erosions (see Figs. 4-20 and 4-21). Other synovial proliferative disorders, such as pigmented villonodular synovitis and synovial osteochondromatosis, are also possible, with calcified hyperechoic foci identified within the synovium in the latter condition. Rarely, a soft tissue mass, such as an intra-articular fibroma, may be found (Fig. 4-26, online). In addition to evaluation of the joint recesses for fluid or synovial hypertrophy, it is important to evaluate for intra-articular bodies, which if ossified will be hyperechoic, with possible shadowing. Common sites for intra-articular bodies include the olecranon, coronoid, and annular recesses (Fig. 4-27). Evaluation of the articular hyaline cartilage for an osteochondral abnormality, particularly over the capitellum, is important in this setting because the donor site for the intra-articular body may be identified (Fig. 4-28). In patients with trauma, joint effusion may be hemorrhagic, and the finding of step-off deformity of the radial head or neck indicates fracture (Fig. 4-29).

The olecranon bursa is located superficial to the olecranon process of the ulna and is a common site of pathology. Although the normal and collapsed olecranon bursa is difficult to identify, anechoic or hypoechoic distention makes this structure quite conspicuous. It is important to float the transducer on a layer of thick gel in evaluation for olecranon bursal fluid because minimal transducer pressure may displace bursal fluid from view (Video 4-3). If the bursal distention is hypoechoic, isoechoic, or hyperechoic, considerations include complex fluid, synovial hypertrophy, and other types of synovial

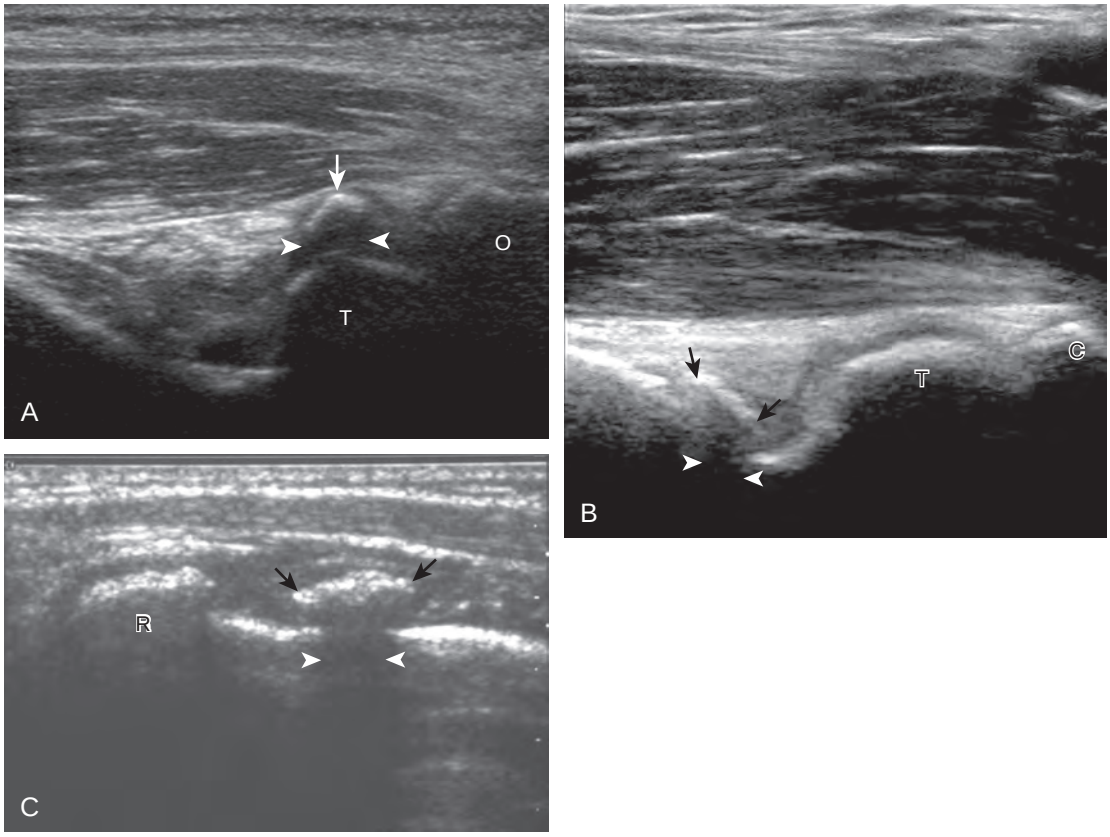

FIGURE 4-27 ■ Intra-articular bodies. A, Sagittal ultrasound images over the olecranon recess posteriorly, **(B)** the coronoid recess anteriorly, and **(C)** the annular recess show hyperechoic *(arrows)* and shadowing *(arrowheads)* ossified intra-articular bodies. C, coronoid process; O, olecranon; R, radial head; T, trochlea.

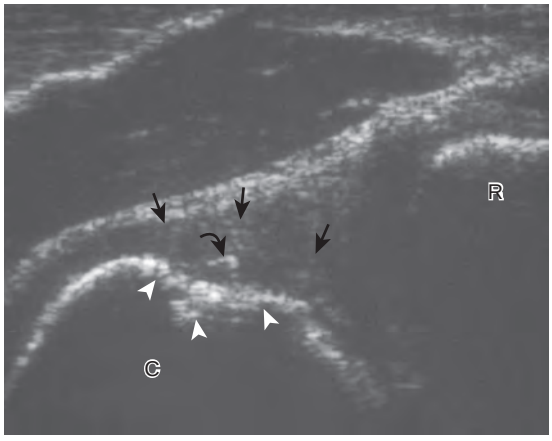

FIGURE 4-28 ■ Osteochondral abnormality of capitellum. Sagittal ultrasound image shows bone irregularity of the capitellum *(arrowheads)*, with thickening and increased echogenicity of the overlying hyaline cartilage *(arrows)*. Note bone fragment *(curved arrow)*. C, capitellum; R, radius.

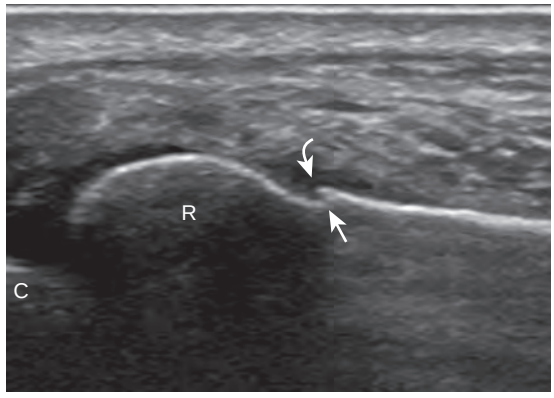

FIGURE 4-29 ■ Radius neck fracture. Sagittal ultrasound image over the radial neck shows step-off deformity *(arrow)*, which represents a radius fracture with adjacent hypoechoic soft tissue hemorrhage *(curved arrow)*. C, capitellum; R, radial head.

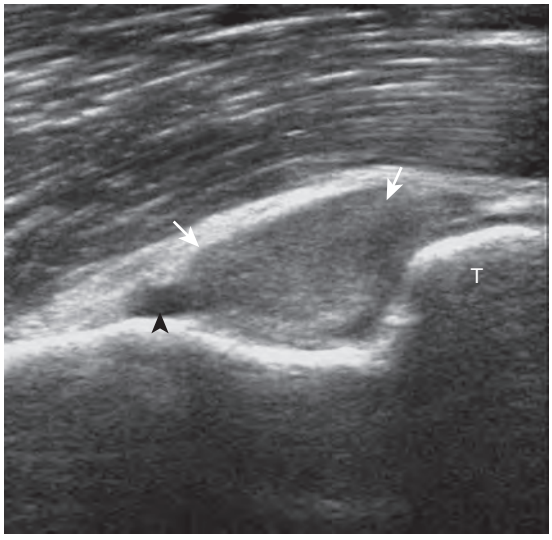

FIGURE 4-26 ■ Intra-articular fibroma. Sagittal image over the anterior elbow shows a well-defined isoechoic to hyperechoic mass *(arrows)* within the anterior joint recess with minimal joint effusion *(arrowhead)*. T, trochlea.

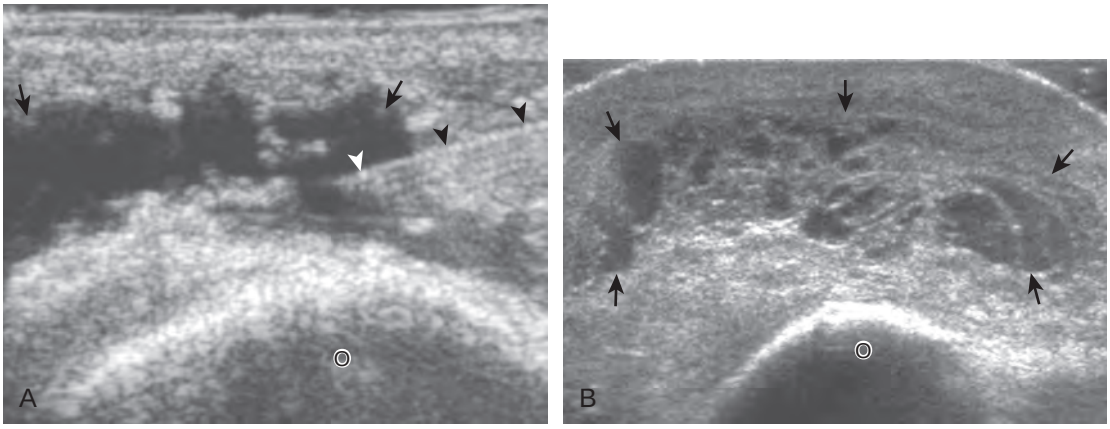

FIGURE 4-30 ■ Olecranon bursitis: trauma. Transverse ultrasound images over the olecranon process (O) from two different patients show **(A)** hypoechoic *(arrows)* and **(B)** heterogeneous distention *(arrows)* of the olecranon bursa from trauma. Note the needle *(arrowheads)* directed into the bursa in **A** under ultrasound guidance.

proliferation. Similar to joint recess distention, the findings of joint recess compressibility, redistribution or motion of bursal contents with transducer pressure, and lack of increased blood flow on color or power Doppler imaging suggest complex fluid over synovial hypertrophy when their gray-scale appearances are similar (Video 4-4). Causes of bursal distention include trauma (Fig. 4-30), gout (Fig. 4-31), rheumatoid arthritis (Fig. 4-32), and infection (Fig. 4-33). The characteristic location and well-defined borders of the olecranon bursa distinguish this from a nonspecific fluid collection or abscess. If there is concern for infection, ultrasound-guided percutaneous aspiration may be considered (see Fig. 4-30A). The presence of cortical irregularity

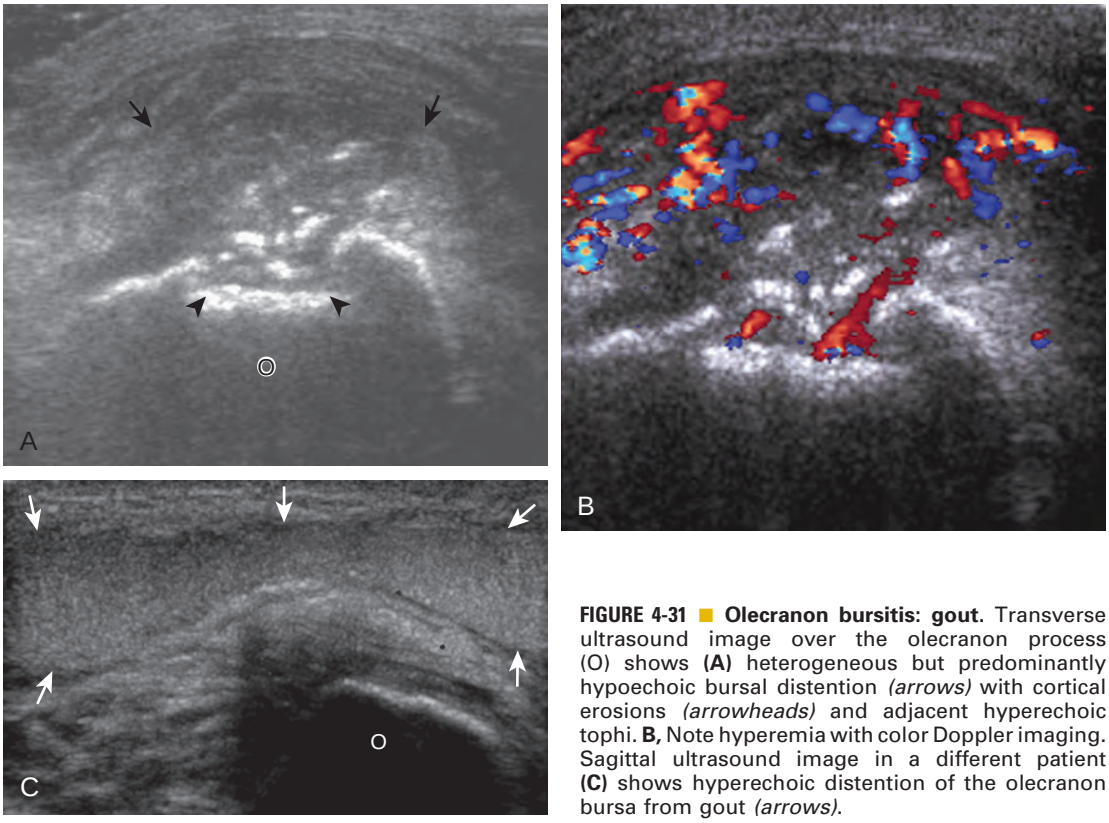

FIGURE 4-31 ■ Olecranon bursitis: gout. Transverse ultrasound image over the olecranon process (O) shows **(A)** heterogeneous but predominantly hypoechoic bursal distention *(arrows)* with cortical erosions *(arrowheads)* and adjacent hyperechoic tophi. **B,** Note hyperemia with color Doppler imaging. Sagittal ultrasound image in a different patient **(C)** shows hyperechoic distention of the olecranon bursa from gout *(arrows)*.

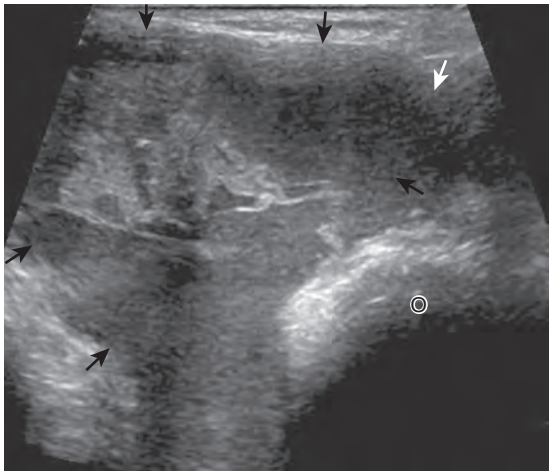

FIGURE 4-32 ■ Olecranon bursitis: rheumatoid arthritis. Transverse ultrasound image over the olecranon process (O) shows heterogeneous but predominantly hypoechoic distention from fluid and synovial hypertrophy *(arrows)*.

could indicate adjacent erosions related to inflammation. Another bursa in the elbow, the bicipitoradial bursa, is described later in the discussion of the biceps brachii tendon.

TENDON AND MUSCLE ABNORMALITIES

Biceps Brachii

Distal biceps brachii tendon tears most commonly occur near the tendon's insertion 1 to 2 cm proximal to the radial tuberosity.[19] Usually secondary to forced extension against active elbow flexion, this injury increases in prevalence with increasing age, typically seen after the age of 40 years. With a full-thickness tear, many injuries are associated with significant retraction of the torn tendon stump, typically visualized several centimeters proximal to the radius directly superficial to the brachialis muscle and at the level of the elbow joint (Fig. 4-34). However, one must be aware that retraction may be minimal or absent when the bicipital aponeurosis (or lacertus fibrosus), which extends from the biceps medially, is intact (Fig. 4-35).[19,20] Like other tendon tears, a full-thickness tear is characterized by anechoic or hypoechoic tendon fiber disruption. The presence of tendon retraction at the tendon tear is a useful finding to indicate a full-thickness tear.

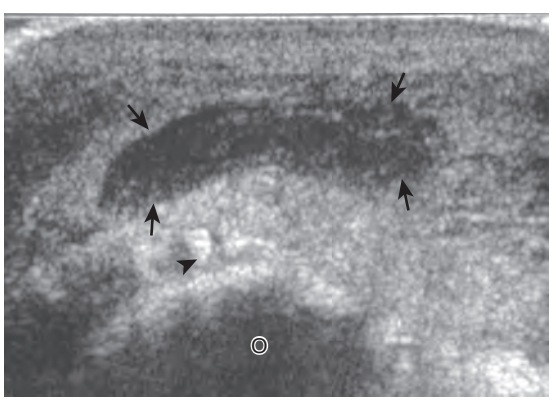

FIGURE 4-33 ■ Olecranon bursitis: infection. Transverse ultrasound image over the olecranon process (O) shows hypoechoic distention *(arrows)* with increased through-transmission enhancement from infected fluid. Note the incidental enthesophyte spurs *(arrowhead)*.

The diagnosis of nonretracted full-thickness tear, partial-thickness tear, and tendinosis of the distal biceps brachii tendon becomes more problematic because of the oblique course of the distal tendon and resulting anisotropy.[20] Tendinosis appears as hypoechoic swelling of the tendon (Fig. 4-36), whereas partial-thickness tears have superimposed hypoechoic or anechoic tendon fiber disruption and tendon thinning (Fig. 4-37). In contrast, the distal biceps brachii tendon should be uniform in thickness even when hypoechoic from anisotropy. Distal partial-thickness tear may only involve one of the two heads.[1] Isolated tear of the superficial short head may be seen, where distal shadowing from the torn and retracted tendon stump may create difficulty in evaluation of the deeper long head (Fig. 4-38). To differentiate a partial-thickness tendon tear from a nonretracted full-thickness tear, lateral evaluation with dynamic imaging is helpful (see Fig. 4-6).[5] In the setting of a full-thickness tear, the visualized proximal tendon segment will show little or no movement when the hand is moved from pronation to neutral (Video 4-5). In contrast, a partial-thickness tear will show movement or translation of the tendon equal to the amount of rotation of the radial tuberosity, indicating that fibers remain attached to the radial tuberosity (Video 4-6). Similar technique is used to evaluate for re-tear after tendon repair (Video 4-7). Dynamic evaluation can be completed using the medial approach as well.[4]

One must also be aware of another pathologic condition at the distal biceps tendon that can cause interpretation difficulties, namely, distention of the bicipitoradial bursa. This normal bursa surrounds the distal biceps brachii tendon as it approaches the radial tuberosity.[21] When the bursa is distended, it may contain anechoic simple fluid, or it may appear as heterogeneous hypoechoic, isoechoic, and hyperechoic complex fluid and synovial hypertrophy with possible flow

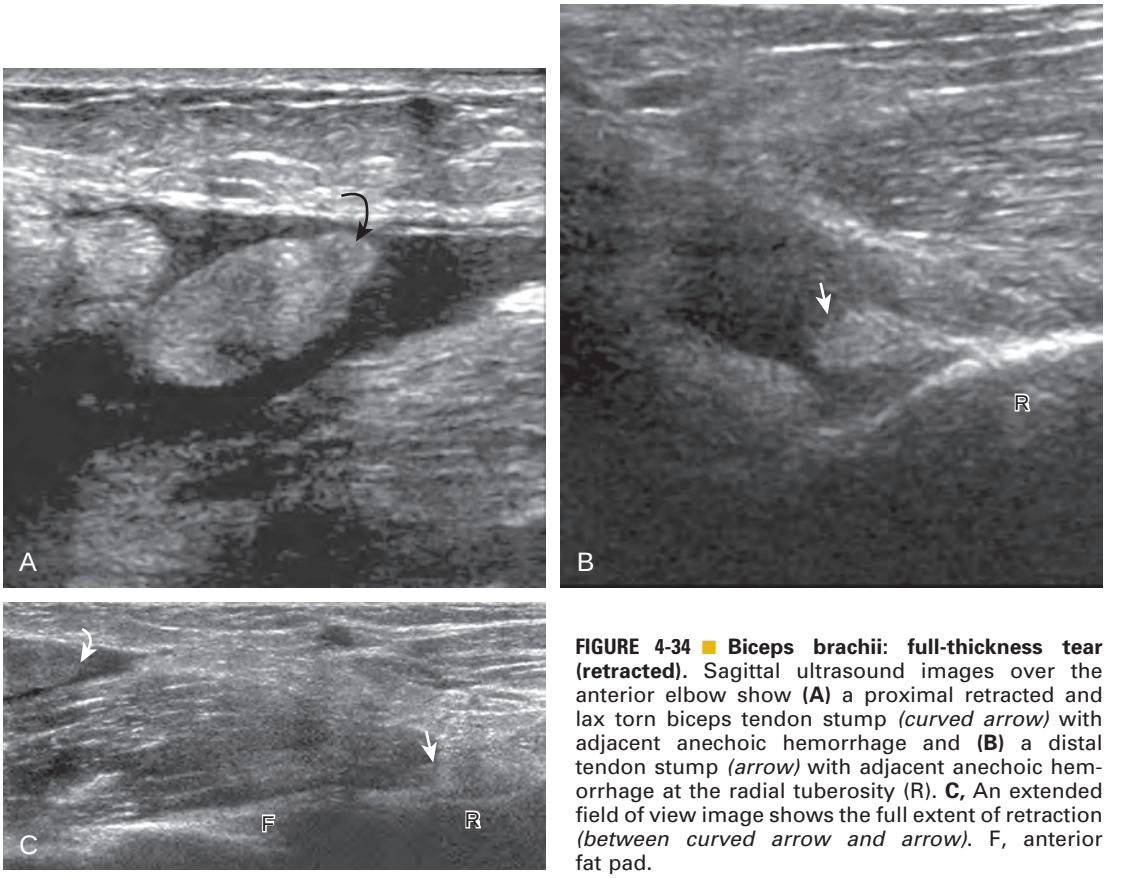

FIGURE 4-34 ■ Biceps brachii: full-thickness tear (retracted). Sagittal ultrasound images over the anterior elbow show **(A)** a proximal retracted and lax torn biceps tendon stump *(curved arrow)* with adjacent anechoic hemorrhage and **(B)** a distal tendon stump *(arrow)* with adjacent anechoic hemorrhage at the radial tuberosity (R). **C,** An extended field of view image shows the full extent of retraction *(between curved arrow and arrow)*. F, anterior fat pad.

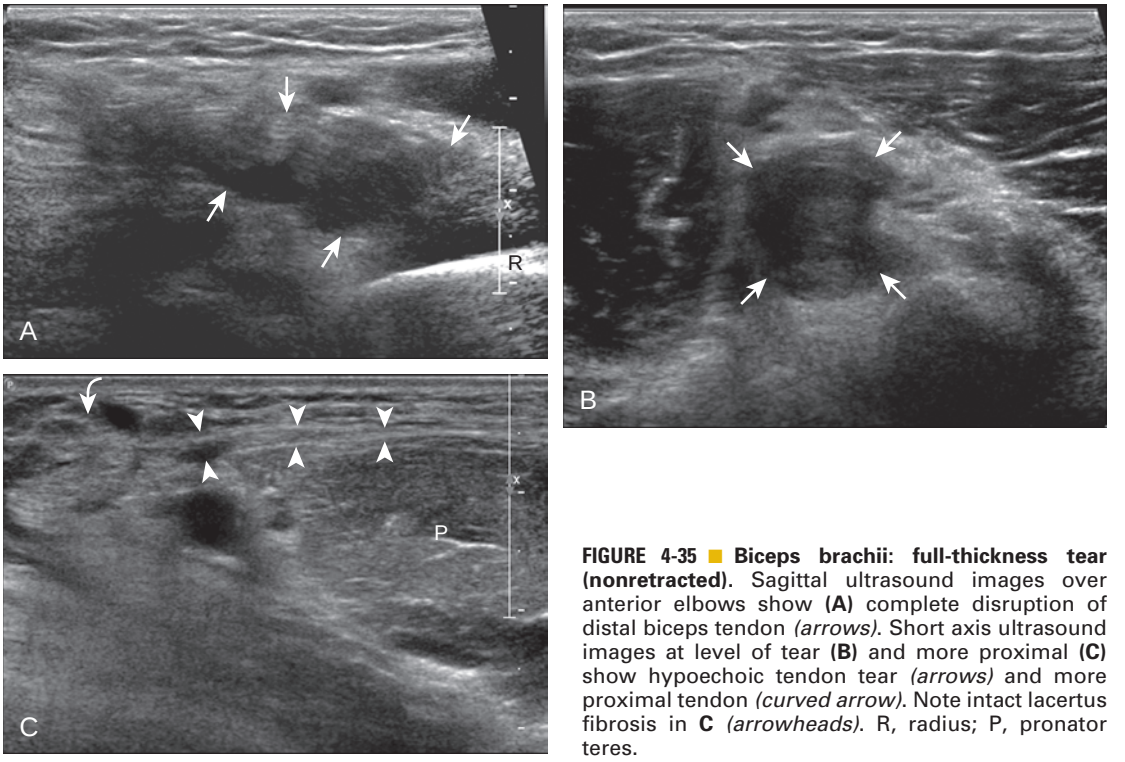

FIGURE 4-35 ■ Biceps brachii: full-thickness tear (nonretracted). Sagittal ultrasound images over anterior elbows show **(A)** complete disruption of distal biceps tendon *(arrows)*. Short axis ultrasound images at level of tear **(B)** and more proximal **(C)** show hypoechoic tendon tear *(arrows)* and more proximal tendon *(curved arrow)*. Note intact lacertus fibrosis in **C** *(arrowheads)*. R, radius; P, pronator teres.

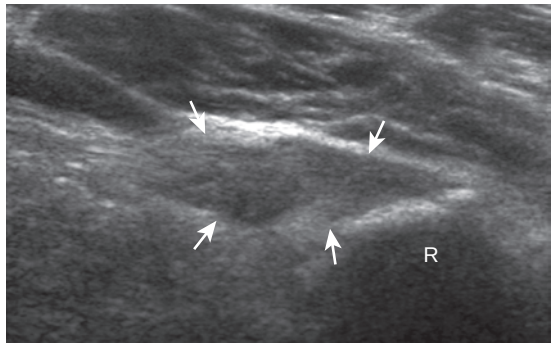

FIGURE 4-36 ■ Biceps brachii: tendinosis. Coronal-oblique ultrasound image in long axis to distal biceps tendon from a medial approach shows a hypoechoic and swollen distal biceps tendon *(arrows)* that was painful with transducer pressure. R, radial tuberosity.

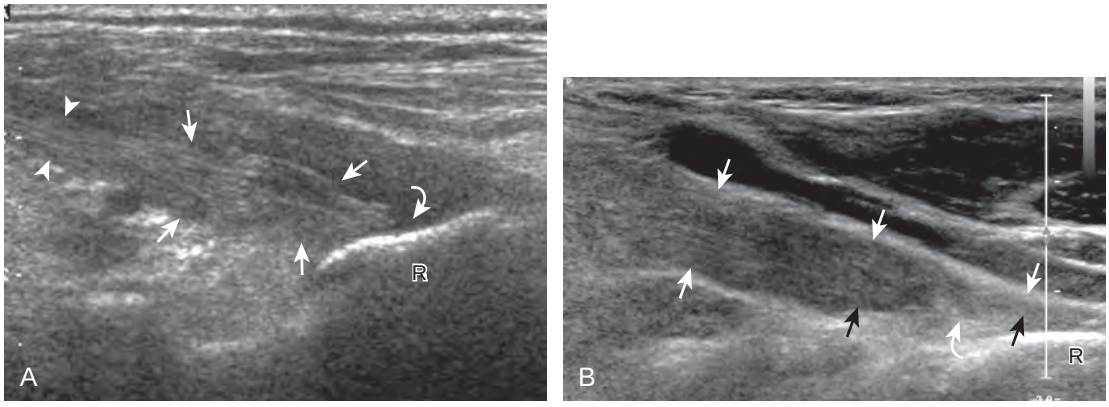

FIGURE 4-37 ■ Biceps brachii: partial-thickness tear. A and **B,** Sagittal ultrasound images in long axis to the distal biceps tendon *(arrowheads)* in two patients show hypoechoic and mildly irregular distal biceps tendon *(arrows)* with partial fiber discontinuity distally *(curved arrow)* and adjacent hypoechoic hemorrhage. Note the significant caliber change in **B** as the more superficial short head is torn while the long head remains attached. R, radial tuberosity.

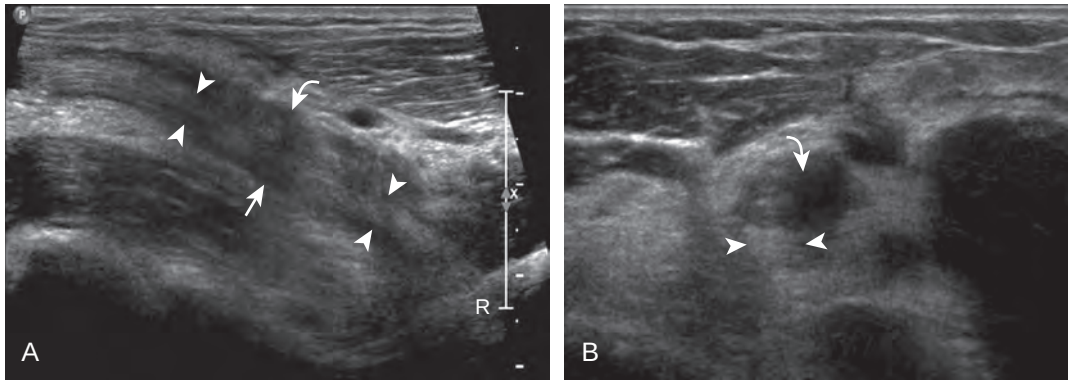

FIGURE 4-38 ■ Biceps brachii: partial-thickness tear. Long axis **(A)** and short axis **(B)** ultrasound images relative to the biceps tendon show torn and retracted superficial short head *(curved arrow)* and intact deep long head tendon *(arrowheads)* with adjacent hypoechoic hemorrhage. Note partial shadowing and sound beam attenuation deep to the short head tendon stump *(arrow)*. R, radial tuberosity.

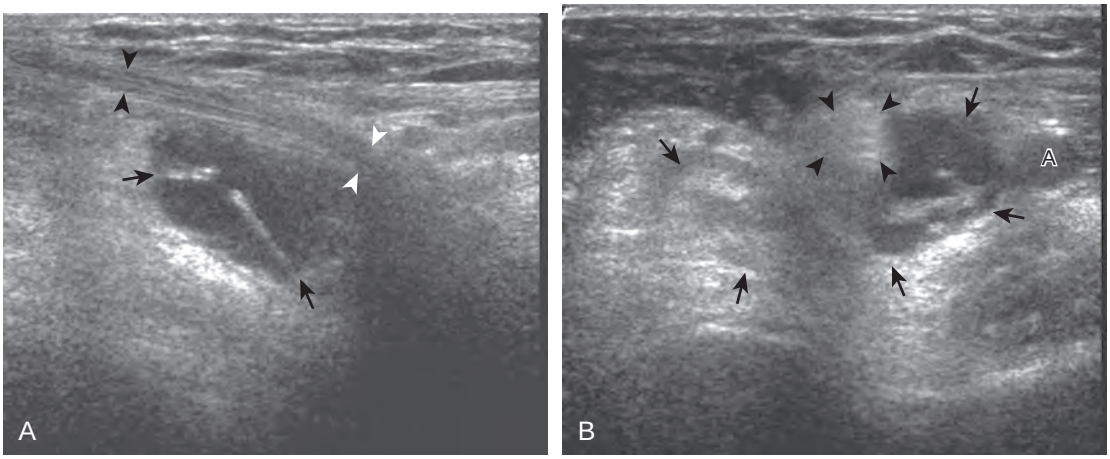

FIGURE 4-39 ■ Bicipitoradial bursitis. Ultrasound images in **(A)** long axis and **(B)** short axis to the distal biceps brachii tendon *(arrowheads)* show septated and fluid-filled bicipitoradial bursa *(arrows)* with increased through-transmission. A, brachial artery.

on color or power Doppler imaging (Fig. 4-39).[22] When symptomatic, this condition has also been called cubital bursitis and may compress the superficial branch of the radial nerve (Fig. 4-40).[21] This bursa may also be confused with a nonspecific heterogeneous mass at imaging. The key to an accurate diagnosis of bicipitoradial bursitis is identification of its horseshoe-shaped configuration as it surrounds the distal biceps brachii tendon (Video 4-8). Although any inflammatory or proliferative condition that involves a bursa may affect the bicipitoradial bursa, this condition is most commonly the result of repetitive trauma.[21] One must also be aware that a tendon sheath is not present at the distal biceps brachii tendon, so the diagnosis of tenosynovitis is not possible at this location.

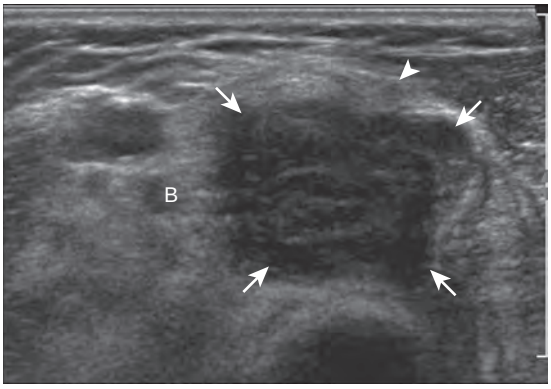

FIGURE 4-40 ■ Bicipitoradial bursitis and radial nerve compression. Transverse ultrasound image over anterolateral elbow shows distended bicipitoradial bursa *(arrows)* with adjacent compression of the superficial branch of the radial nerve *(arrowhead)*. B, biceps brachii.

Triceps Brachii

Injuries to the triceps brachii may take the form of direct impact injury or distal avulsion. As with any muscle, a direct impact can cause muscle tear and hemorrhage, most typically at the muscle belly with a heterogeneous but predominantly hypoechoic appearance (Fig. 4-41). Distally, triceps tendon tears and avulsions at the olecranon process are possible. A full-thickness tear appears as complete anechoic or hypoechoic tendon disruption with retraction. Tendinosis appears as hypoechoic swelling of intact fibers, whereas a partial-thickness tendon tear appears as incomplete hypoechoic or anechoic tendon fibers disruption. Partial-thickness tears most commonly involve the superficial layer of the tendon, which is the combined lateral and long head attachments, typically associated with a fractured and displaced enthesophyte (Figs. 4-42 and 4-43) (Video 4-9).[23] It is important to identify the intact deeper medial head, which is

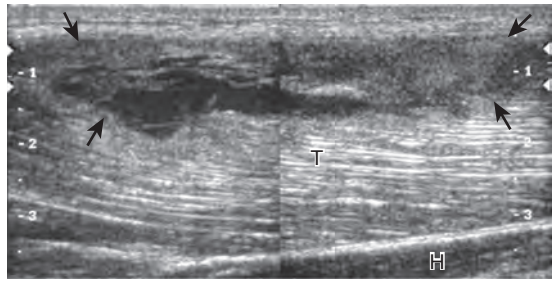

FIGURE 4-41 ■ Triceps brachii: direct impact injury. Ultrasound image in long axis to the triceps (T) shows partial muscle fiber disruption with anechoic, isoechoic, and hyperechoic hemorrhage *(arrows)*. H, humerus.

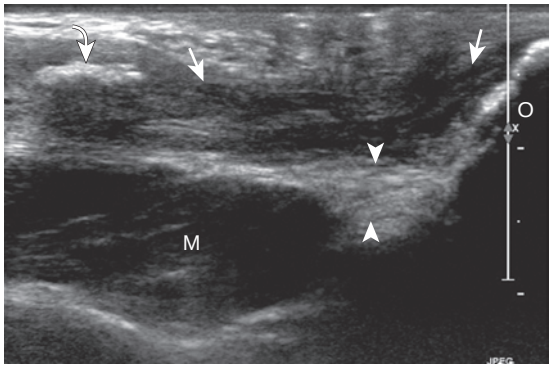

FIGURE 4-42 ■ Triceps brachii tear (partial-thickness). Ultrasound image in long axis to the triceps shows tear of the combined lateral and long head attachment *(between arrows)* with retracted enthesophyte bone fragment *(curved arrow)*. Note intact deep medial head tendon *(arrowheads)*. M, medial triceps brachii head muscle; O, olecranon.

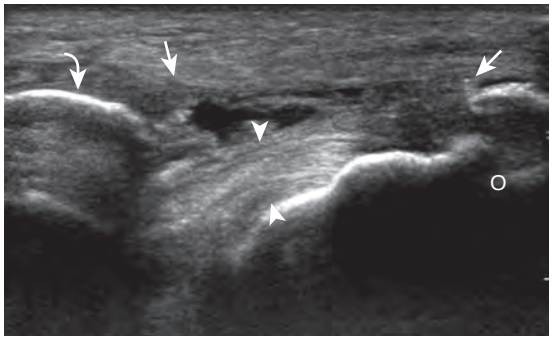

FIGURE 4-43 ■ Triceps brachii tear (partial-thickness). Ultrasound image in long axis to the triceps shows tear of the combined lateral and long head attachment *(between arrows)* with retracted enthesophyte bone fragment *(curved arrow)*. Note intact deep medial head tendon *(arrowheads)*. O, olecranon. (From Downie R, Jacobson JA, Fessell, DP, et al: Sonography of partial-thickness tears of the distal triceps brachii tendon. *J Ultrasound Med* 30:1351–1356, 2011. Reproduced with permission from the American Institute of Ultrasound in Medicine.).

predominantly muscle with a very short tendon attachment, to exclude full-thickness tear. Another abnormality of the triceps muscle, called *snapping triceps syndrome*, is described later, under the discussion of the ulnar nerve and cubital tunnel. Lastly, although a well-defined enthesophyte commonly involves the distal triceps brachii tendon from degeneration, the presence of an ill-defined enthesophyte with adjacent abnormal tendon and hyperemia could indicate an inflammatory enthesopathy, as seen with seronegative spondyloarthropathies such as psoriatic arthritis (Fig. 4-44).

Common Flexor and Extensor Tendons

Abnormalities of the common flexor tendon origin at the medial epicondyle (Fig. 4-45) and the common extensor tendon origin at the lateral epicondyle (Figs. 4-46 and 4-47) are commonly referred to as epicondylitis, or golfer's and tennis elbow, respectively.[24] The term epicondylitis is a misnomer in that the tendon is primarily involved and not the epicondyle, and the abnormality consists of degeneration, tendinosis, and possible tendon tear rather than true active inflammation.[25] This process is most often from trauma or overuse conditions, and with regard to lateral epicondylitis, the extensor carpi radialis brevis component of the common extensor tendon (seen most anterior) is most commonly affected.[26] At sonography, tendinosis appears as hypoechoic swelling of the involved tendon (>4.2 mm if common extensor tendon), with possible hyperechoic calcification and adjacent bone irregularity.[25,27,28] Hyperemia on color or power Doppler imaging is variable. A superimposed partial-thickness tear appears as anechoic clefts and

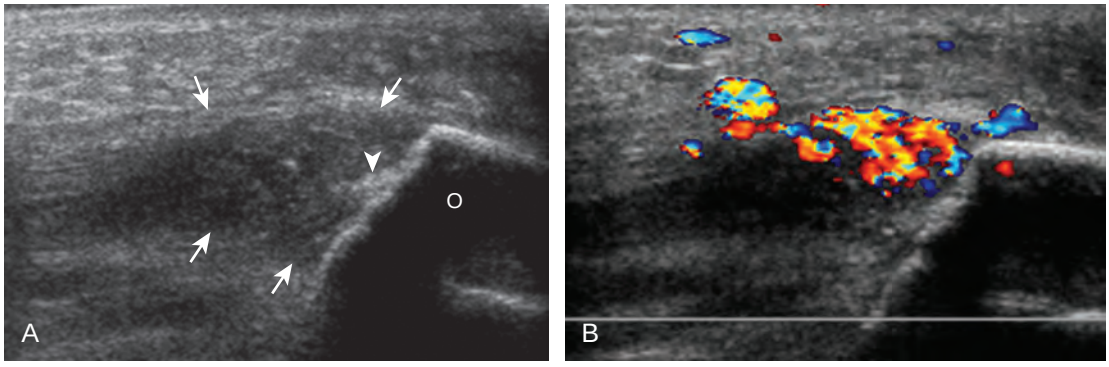

FIGURE 4-44 ■ Inflammatory enthesopathy: psoriatic arthritis. A and **B,** Ultrasound images in long axis to distal triceps brachii tendon show hypoechoic swelling of the distal tendon with hyperemia *(arrows)* and cortical irregularity of the olecranon from bone proliferation *(arrowhead)*. O, olecranon.

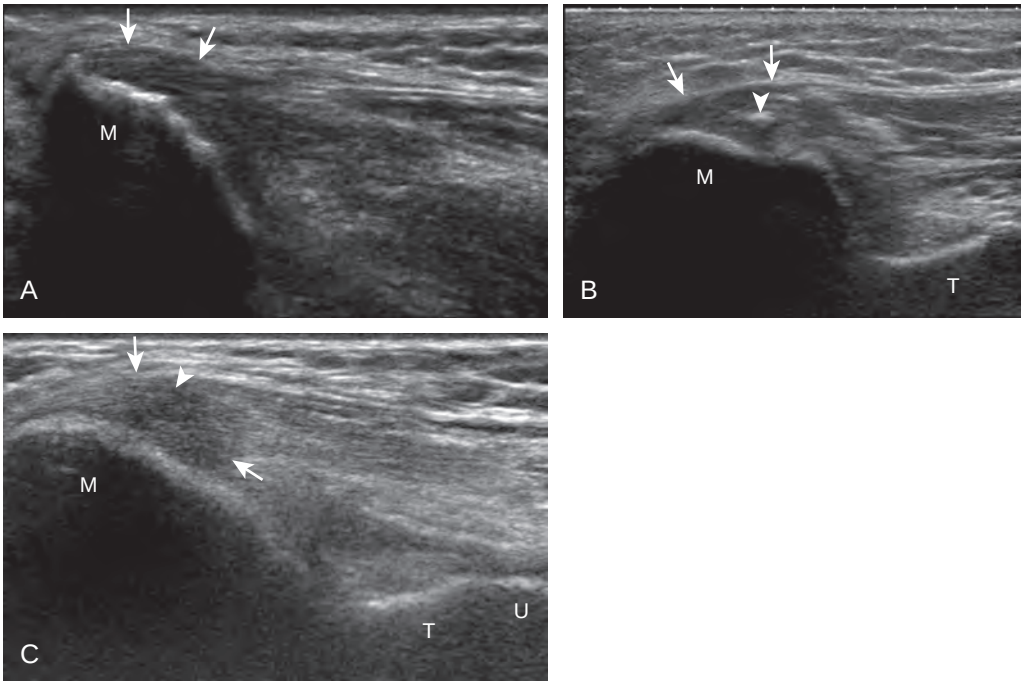

FIGURE 4-45 ■ **Medial epicondylitis.** Ultrasound images from three different patients **(A, B,** and **C)** in long axis to the common flexor tendon show hypoechoic tendinosis in all cases *(arrows)*, with additional calcification *(arrowhead)* in **B** and early superimposed interstitial tear *(arrowhead)* in **C**. M, medial epicondyle; T, trochlea; U, ulna.

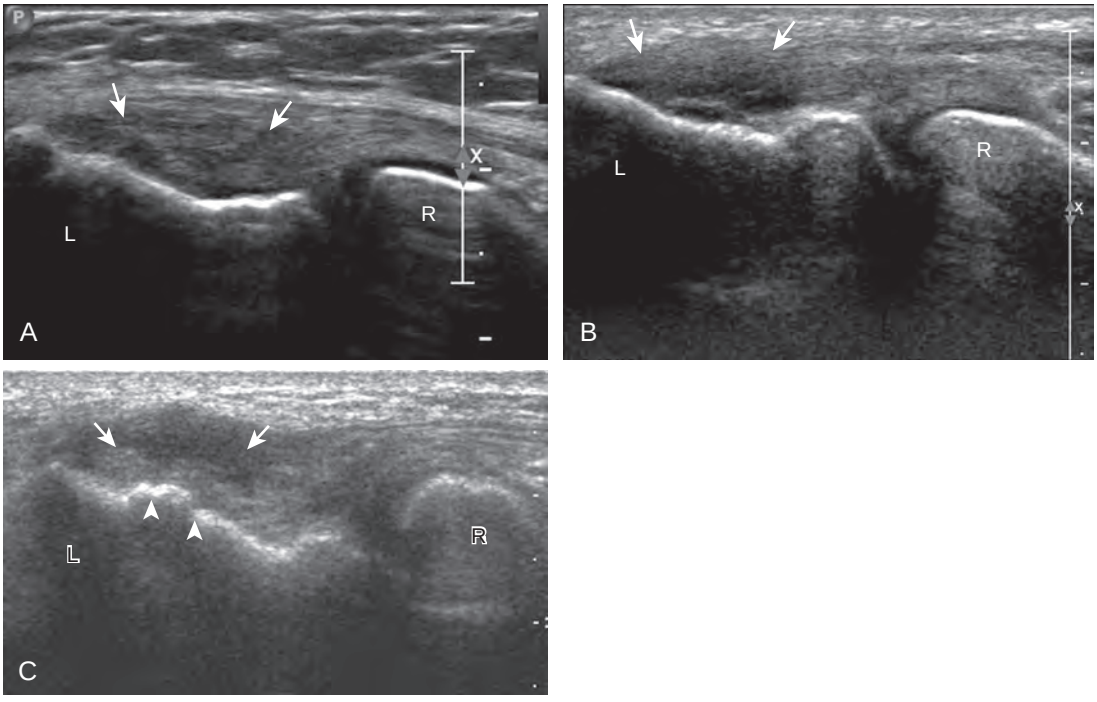

FIGURE 4-46 ■ **Lateral epicondylitis.** Ultrasound images from three different patients **(A, B,** and **C)** in long axis to the common extensor tendon show abnormal hypoechoic tendinosis in all examples *(arrows)*, with superimposed anechoic interstitial tear in **B** and **C**. Note cortical irregularity in **C** *(arrowheads)*. L, lateral epicondyle; R, radial head.

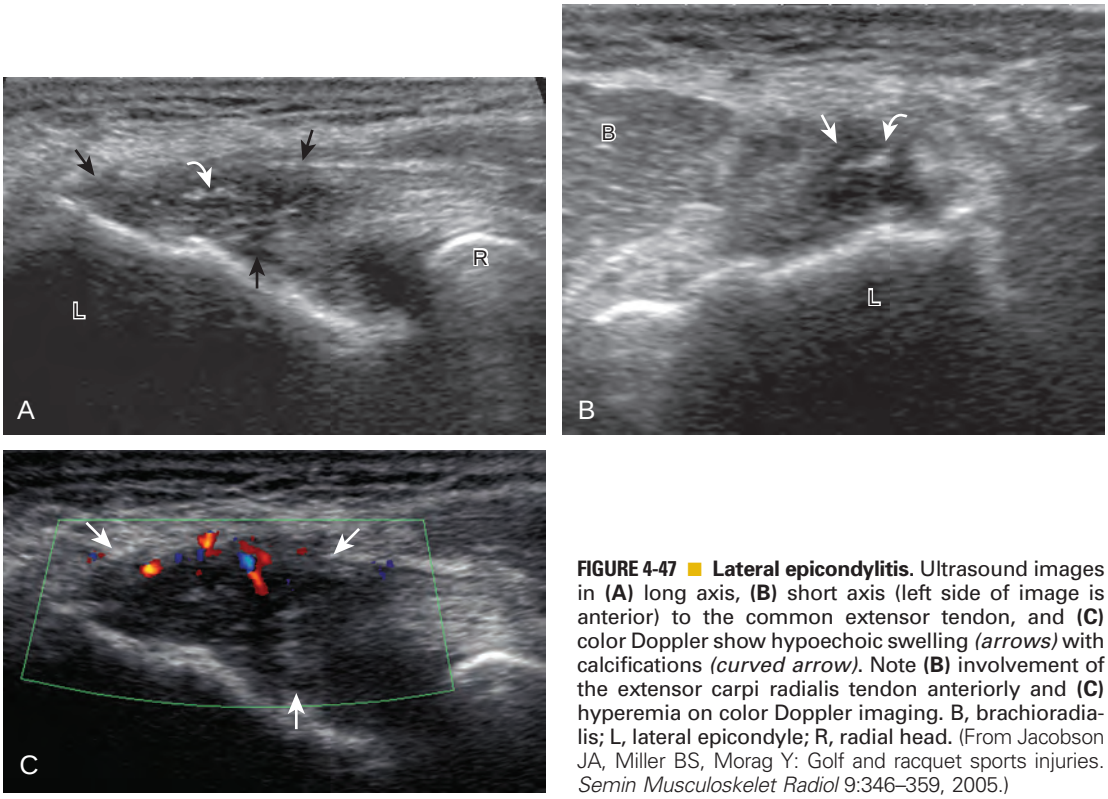

FIGURE 4-47 ■ Lateral epicondylitis. Ultrasound images in **(A)** long axis, **(B)** short axis (left side of image is anterior) to the common extensor tendon, and **(C)** color Doppler show hypoechoic swelling *(arrows)* with calcifications *(curved arrow)*. Note **(B)** involvement of the extensor carpi radialis tendon anteriorly and **(C)** hyperemia on color Doppler imaging. B, brachioradialis; L, lateral epicondyle; R, radial head. (From Jacobson JA, Miller BS, Morag Y: Golf and racquet sports injuries. *Semin Musculoskelet Radiol* 9:346–359, 2005.)

incomplete fiber discontinuity.[25,29] Ultrasound-guided tendon fenestration has been used to treat this condition with success (see Chapter 9).[30,31] Uncommonly, a full-thickness tear of the common extensor tendon can be seen with complete discontinuity and retraction (Fig. 4-48). Given the close proximity of the radial collateral ligament to the common extensor tendon, it is important to distinguish which structure is involved and in fact both may be abnormal.[12,32] The size of an intrasubstance common extensor tendon tear and the presence of a radial collateral ligament tear indicate poor outcome.[29]

LIGAMENT ABNORMALITIES

The medial elbow joint is stabilized by the ulnar collateral ligament, which consists of a strong anterior band, a posterior band, and a weaker oblique band. Evaluation primarily focuses on the anterior band, normally hyperechoic with compact fibers that extend from the undersurface of the medial epicondyle to the sublime tubercle of the proximal ulna, although its appearance may be hypoechoic from anisotropy.[6,7] A partial tear or sprain of the ulnar collateral ligament appears as hypoechoic swelling and heterogeneity of the ligament, but without complete ligament fiber disruption (Fig. 4-49). A remote injury may result in an intact but lax ligament (Fig. 4-50). A full-thickness tear appears as complete fiber discontinuity, with variable anechoic, hypoechoic, and

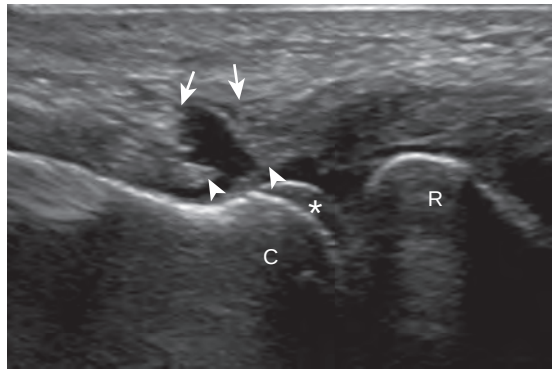

FIGURE 4-48 ■ Common extensor tendon and radial collateral ligament (full-thickness tear). Ultrasound image in long axis to the common extensor tendon shows full-thickness anechoic disruption of the tendon *(between arrows)*. Note adjacent tear of the deeper radial collateral ligament *(between arrowheads)* (*asterisk,* capitellum hyaline cartilage). C, capitellum; R, radial head.

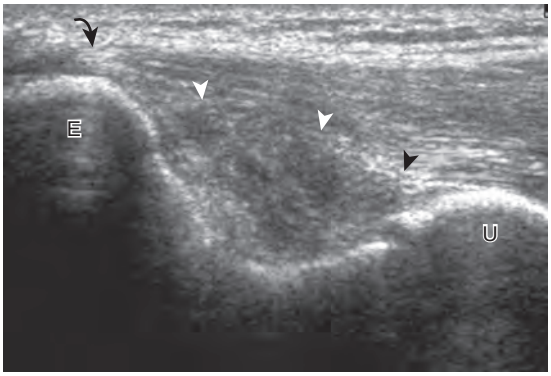

FIGURE 4-49 ■ Ulnar collateral ligament: partial-thickness tear. Ultrasound image in long axis to the anterior band of the ulnar collateral ligament shows abnormal hypoechoic swelling *(arrowheads)*. With valgus stress, the joint space did not widen, and intact ligament fibers were seen (*curved arrow*, common flexor tendon). E, medial epicondyle; U, ulna.

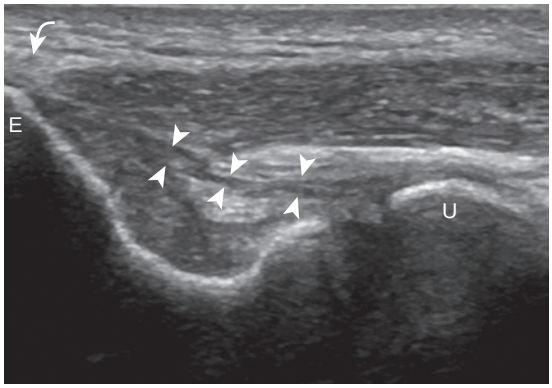

FIGURE 4-50 ■ Ulnar collateral ligament: remote injury. Ultrasound image in long axis to the anterior band of the ulnar collateral ligament shows attenuated ligament *(arrowheads)*. During valgus stress, the ligament was intact, although there was asymmetrical joint space widening (*curved arrow*, common flexor tendon). E, medial epicondyle; U, ulna.

isoechoic fluid and hemorrhage (Fig. 4-51).[33] Distinguishing between a partial-thickness and full-thickness tear may be difficult, especially if the tear is subacute and hemorrhage is present. To assist with the differentiation, dynamic imaging is employed (Videos 4-10 and 4-11). Under sonographic observation, the minimally flexed elbow (about 30 degrees) is placed into valgus stress with the hand supinated. This can be accomplished if the patient is lying down by manually applying valgus pressure with the arm extending off of the bed, or with the assistance of another person if the patient is seated.[8] In addition to visible separation of the torn ligament ends, abnormal widening of the joint immediately beneath the ligament "asymmetric to the contralateral elbow can indicate ligament injury."[9] It is important to compare this with the asymptomatic contralateral side because asymmetry supports the pathologic findings, although some asymmetry may be normal in asymptomatic baseball pitchers.[9]

At the lateral aspect of the elbow, the radial collateral ligament, the annular ligament, and the lateral ulnar collateral ligament can be identified.[12,13] As in the ulnar collateral ligament, partial tears appear as partial hypoechoic tendon disruption, whereas full-thickness tears appear as complete ligament fiber discontinuity (Fig. 4-52). Joint instability may also be demonstrated with varus stress in the setting of a full-thickness tear (Video 4-12). The proximal aspect of the radial

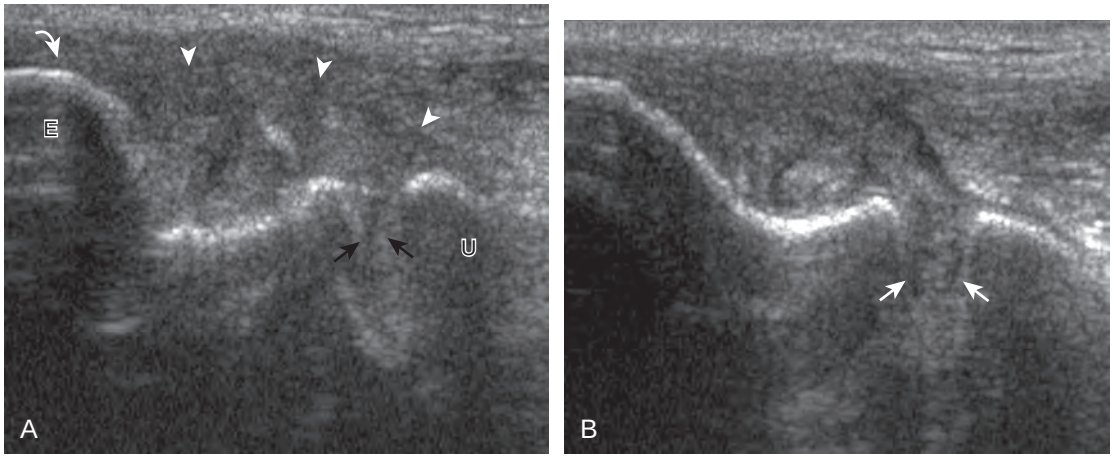

FIGURE 4-51 ■ Ulnar collateral ligament: full-thickness tear. Ultrasound image in long axis to the anterior band of the ulnar collateral ligament shows **(A)** abnormal hypoechoic swelling with no discernible fibers *(arrowheads)*. Note the widened medial joint space *(arrows)*, which increased with valgus stress in **B** (*curved arrow*, common flexor tendon). E, medial epicondyle; U, ulna.

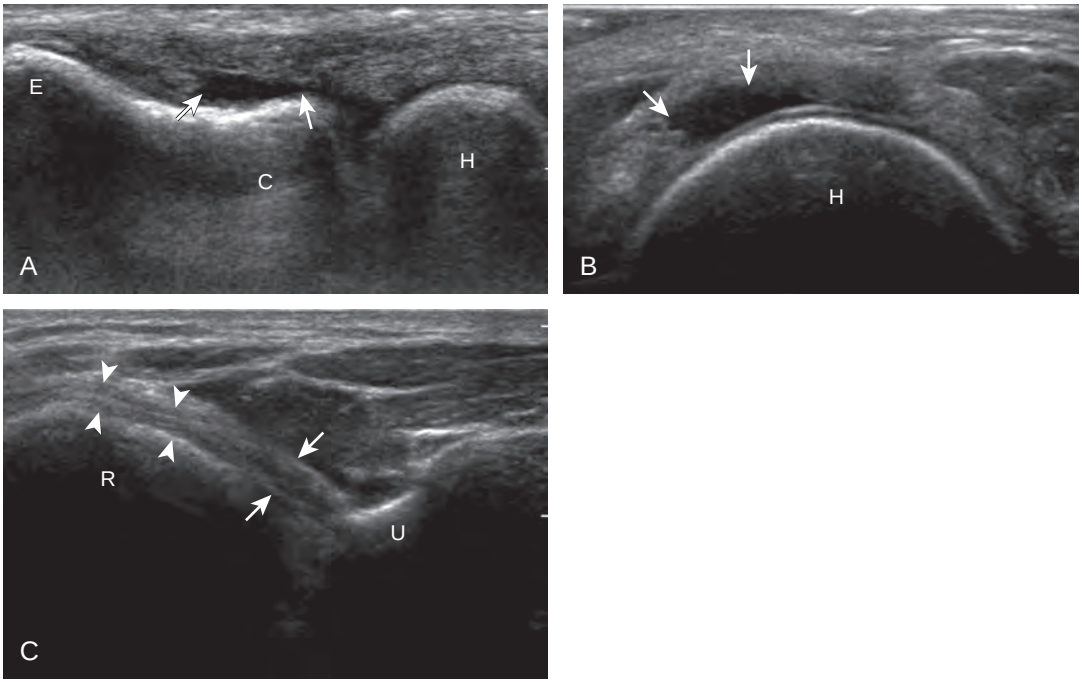

FIGURE 4-52 ■ Radial collateral ligament abnormalities. Ultrasound image **(A)** in long axis to the radial collateral ligament shows anechoic fluid *(arrows)* within radial collateral ligament tear. Ultrasound image **(B)** transverse to radial head and long axis to annular ligament shows anechoic fluid *(arrows)* within annular ligament tear. Ultrasound image **(C)** in long axis to lateral ulnar collateral ligament *(arrowheads)* shows hypoechoic thickening *(arrows)*. C, capitellum; E, lateral epicondyle; H, radial head; R, radius; U, ulna.

collateral ligament is in close proximity to the common extensor tendon, and both may be abnormal (see Fig. 4-48). It is important to evaluate the lateral elbow during hand supination and pronation for abnormal radial head movement (Fig. 4-53) (Video 4-13) or abnormal snapping of the annular ligament (Video 4-14).

PERIPHERAL NERVE ABNORMALITIES

Ulnar Nerve

The elbow has several sites where the ulnar nerve is prone to injury or entrapment.[34] Between the medial epicondyle and the olecranon process, as the ulnar nerve passes beneath the cubital tunnel retinaculum or Osborne fascia, the ulnar nerve may be affected by acute trauma, chronic repetitive injury with elbow flexion, and ulnar nerve subluxation and dislocation. More distally, the ulnar nerve may be compressed where it enters the true cubital tunnel, formed by the humeral and ulnar origins of the flexor carpi ulnaris bridged by the arcuate ligament.[3] The ultrasound

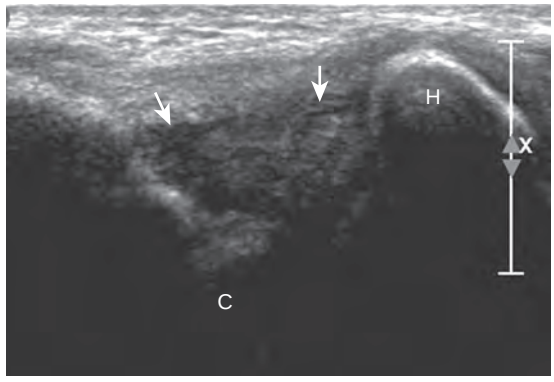

FIGURE 4-53 ■ Radial head subluxation. Ultrasound image in long axis to radial collateral ligament shows abnormal lateral displacement of radial head (H) and abnormal mixed echogenicity hypoechoic tissue *(arrows)* in region of radial collateral ligament. C, capitellum.

diagnosis of ulnar nerve entrapment at this site or cubital tunnel syndrome relies on the visualization of hypoechoic swelling of the ulnar nerve just proximal to the cubital tunnel, usually with a transition to normal size within the cubital tunnel. A cross-sectional area of the ulnar nerve greater

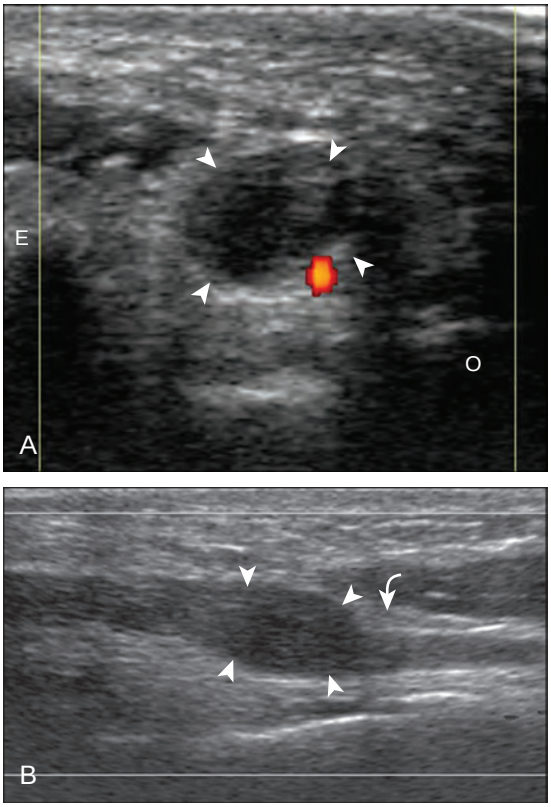

FIGURE 4-54 ■ Cubital tunnel syndrome. Ultrasound images in **(A)** short axis and **(B)** long axis to the ulnar nerve show hypoechoic swelling of the ulnar nerve *(arrowheads)* deep to the cubital tunnel retinaculum, proximal to its entrance into the cubital tunnel (*curved arrow*, arcuate ligament). E, medial epicondyle; O, olecranon.

than 9 mm^2 at the site of maximal enlargement is considered abnormal (Fig. 4-54).[35]

Although nerve entrapment may be idiopathic or from overuse, other causes of ulnar neuritis must be considered when an abnormally swollen ulnar nerve is visualized. One such cause is transient dislocation of the ulnar nerve, which may occur with absence of a cubital tunnel retinaculum.[36] In this condition, the ulnar nerve dislocates medially and anteriorly over the medial epicondyle with elbow flexion, which causes direct nerve irritation and makes it prone to direct injury (Fig. 4-55) (Video 4-15).[37] With elbow extension, the ulnar nerve relocates to normal position within the cubital tunnel. Up to 20% of individuals with ulnar nerve dislocation may be asymptomatic, so it is important to correlate with the presence of abnormal ulnar nerve swelling and symptoms that suggest neuritis. Another similar pathologic process associated with ulnar nerve dislocation is snapping triceps syndrome (Fig. 4-56) (Videos 4-16 and 4-17).[10] Described in weight lifters, this condition is characterized by abnormal dislocation of the ulnar nerve and subluxation of the medial head of the triceps muscle with elbow flexion and reduction in elbow extension, which may result in the palpation of two snaps rather than one with isolated ulnar nerve dislocation. One treatment for ulnar neuritis and dislocation is surgical transposition of the ulnar nerve, which may then be subcutaneous over the pronator teres (Fig. 4-57A) or submuscular in location (see Fig. 4-57B).

Another potential cause of ulnar nerve compression is an anconeus epitrochlearis muscle, which is a normal variant that occurs in up to 23% of the population (Fig. 4-58).[38] The anconeus epitrochlearis muscle has a variable size but characteristically is hypoechoic with hyperechoic fibroadipose tissue similar to other muscles and extends from the triceps brachii toward the medial epicondyle in place of Osborne fascia. The diagnosis of anconeus epitrochlearis is easiest when the elbow is in extension, where no muscle tissue should be present between the olecranon and medial epicondyle, which is in contrast to elbow flexion, where the triceps brachii is normally located adjacent to the medial epicondyle. Dynamic imaging with elbow flexion may also show crowding deep to Osborne fascia from an anconeus epitrochlearis as well as abnormal snapping (Fig. 4-59) (Video 4-18). Lastly, the ulnar nerve may also be compressed by adjacent elbow joint abnormalities, such as synovial hypertrophy (see Fig. 4-24), intra-articular bodies, and intra-articular hemorrhage after trauma (Fig. 4-60).

Median Nerve

The median nerve courses along the anteromedial aspect of the elbow and may be entrapped at several locations, although less commonly than nerve entrapment at the wrist as part of carpal tunnel syndrome.[34] One site of potential entrapment is at the level of the distal humerus, where the ligament of Struthers may extend from a normal variant bone excrescence of the anterior humerus (called the *supracondylar process*) to the medial epicondyle with compression of the median nerve (Fig. 4-61).[39] In the antecubital region, the median nerve may be entrapped between the humeral and ulnar heads of the pronator teres and may cause pronator teres syndrome. More distally, a branch of the median nerve, the anterior interosseous nerve, may also

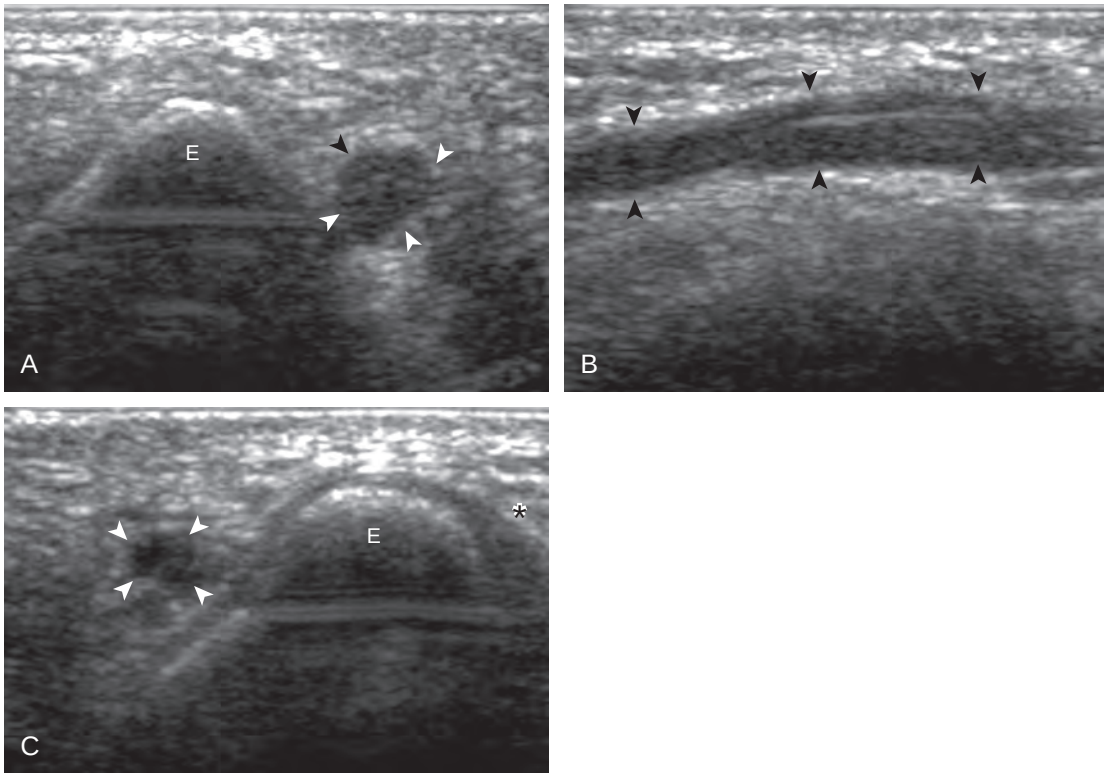

FIGURE 4-55 ■ Cubital tunnel syndrome from transient ulnar nerve dislocation. Ultrasound images in **(A)** short axis and **(B)** long axis to the ulnar nerve in elbow extension show hypoechoic swelling of the ulnar nerve *(arrowheads)*. Ultrasound image **(C)** in short axis to the ulnar nerve in elbow flexion shows dislocation of the ulnar nerve anteriorly over the medial epicondyle (E) from its normal location (*asterisk*), which reduced with elbow extension.

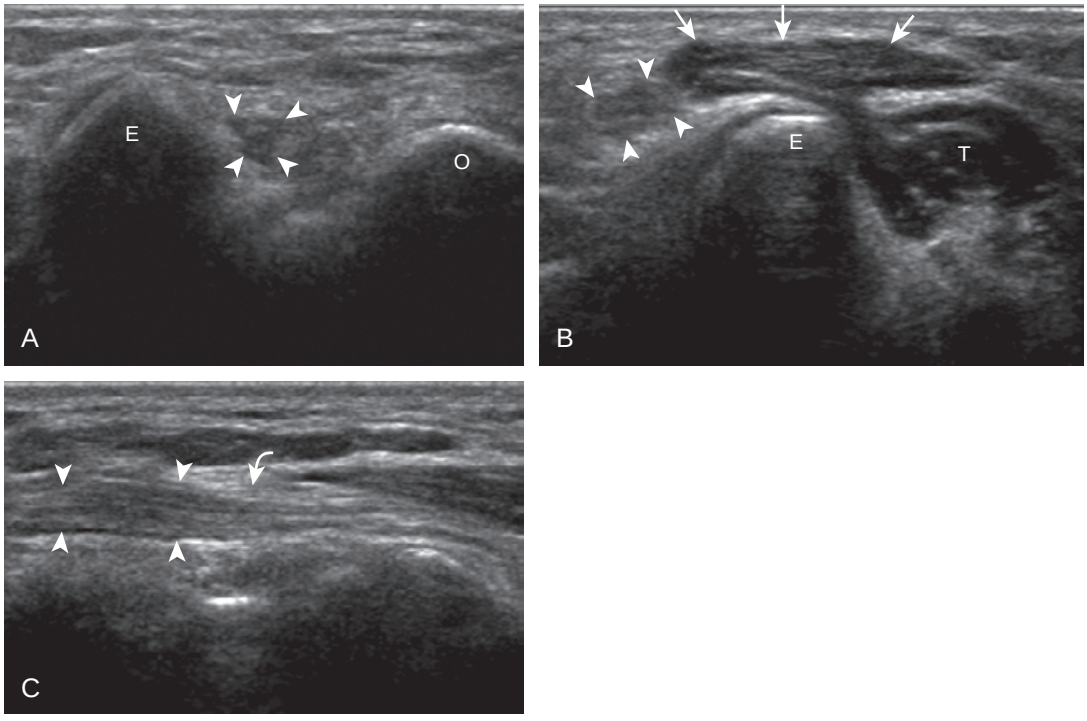

FIGURE 4-56 ■ Snapping triceps syndrome. Ultrasound images in short axis to the ulnar nerve in **(A)** elbow extension and **(B)** elbow flexion show hypoechoic swelling of the ulnar nerve *(arrowheads)*. Note the anterior dislocation of the ulnar nerve anterior to the apex of the medial epicondyle (E) with elbow flexion in **B,** accompanied by the medial head *(arrows)* of the triceps muscle (T). Ultrasound image **(C)** in long axis to ulnar nerve shows hypoechoic swelling *(arrowheads)* (*curved arrow*, arcuate ligament). O, olecranon.

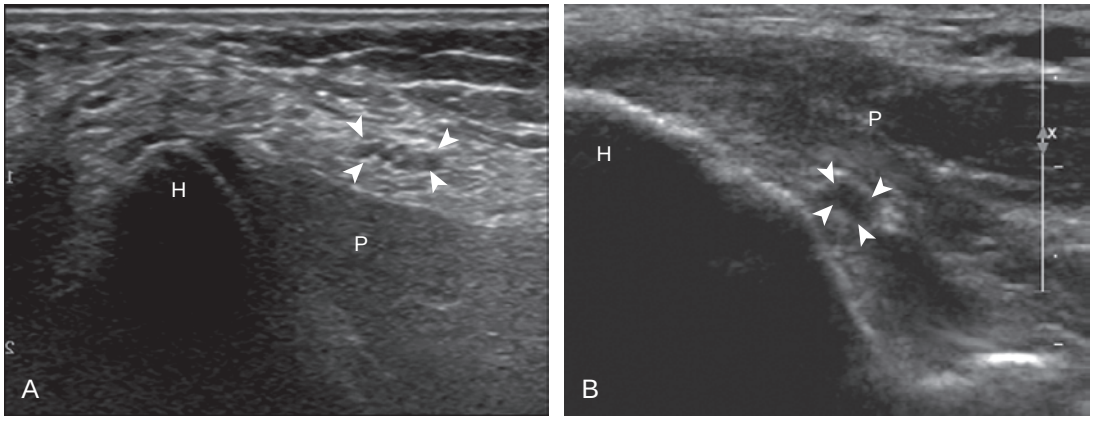

FIGURE 4-57 ■ Ulnar nerve transposition. Ultrasound image **(A)** in short axis to the ulnar nerve shows the location of the ulnar nerve *(arrowheads)* over the pronator teres muscle (P). Ultrasound image **(B)** of a different patient shows the ulnar nerve *(arrowheads)* deep to the pronator teres muscle (P). Note normal size and appearance of the ulnar nerve. H, humerus.

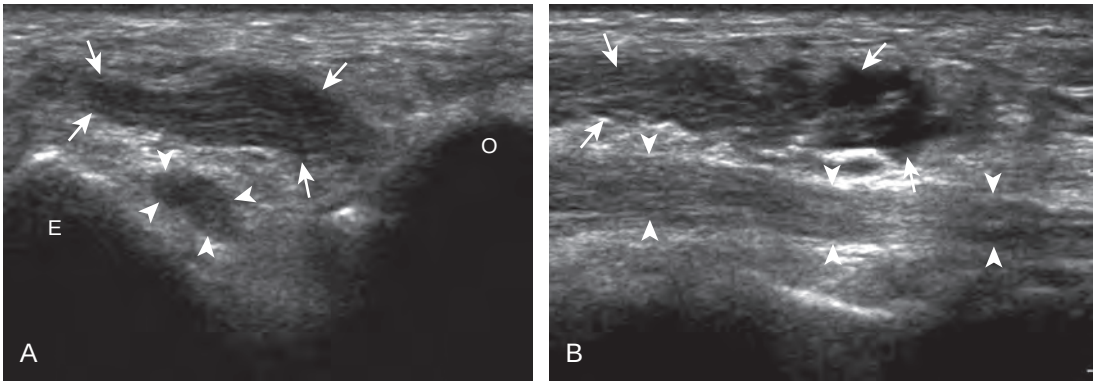

FIGURE 4-58 ■ Anconeus epitrochlearis muscle. Ultrasound image in **(A)** short axis and **(B)** long axis to the ulnar nerve *(arrowheads)* shows the anconeus epitrochlearis muscle *(arrows)* between the olecranon (O) and medial epicondyle of the humerus (E). (From Jacobson JA, Fessell DP, Lobo Lda G, et al: Entrapment neuropathies I: upper limb (carpal tunnel excluded). *Semin Musculoskelet Radiol* 14:473–486, 2010.)

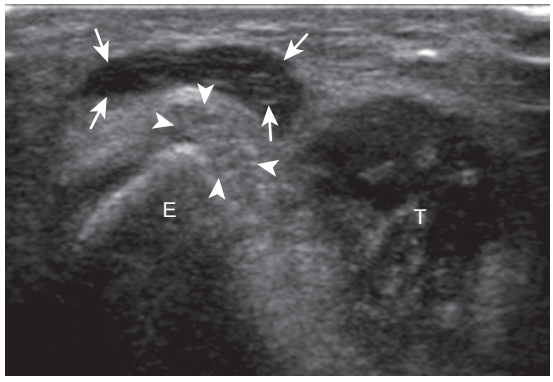

FIGURE 4-59 ■ Anconeus epitrochlearis: subluxation. Ultrasound image in short axis to the ulnar nerve *(arrowheads)* with the elbow in flexion shows abnormal subluxation of the anconeus epitrochlearis muscle *(arrows)* over the medial epicondyle (E). T, triceps brachii muscle.

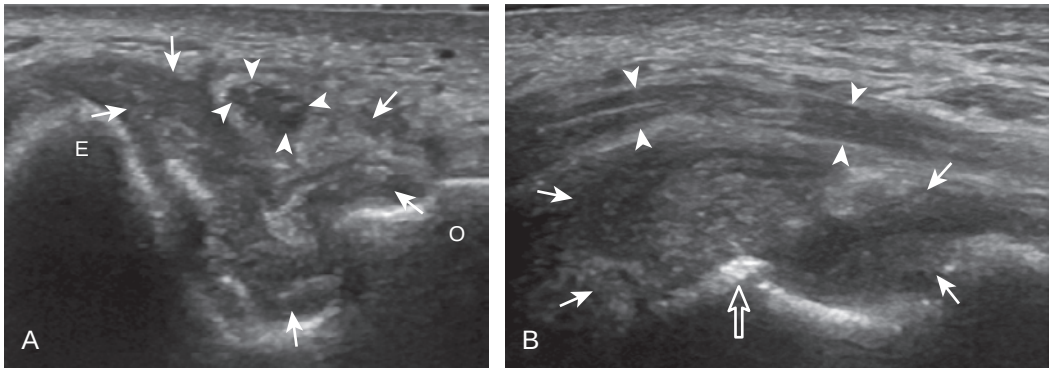

FIGURE 4-60 ■ Ulnar nerve compression: intra-articular hemorrhage. Ultrasound images in **(A)** short axis and **(B)** long axis to the ulnar nerve show displacement of the ulnar nerve *(arrowheads)* by intra-articular hemorrhage and synovial hypertrophy *(arrows)* from intra-articular humerus fracture *(open arrow)*. E, medial epicondyle; O, olecranon.

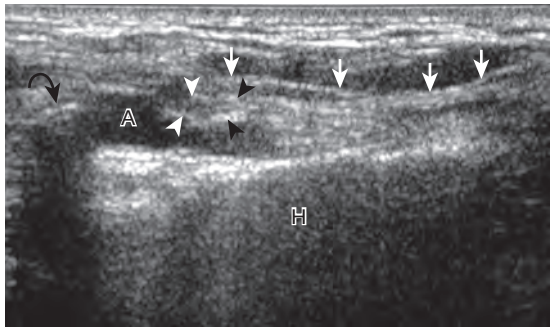

FIGURE 4-61 ■ Median nerve entrapment. Ultrasound image in long axis to the ligament of Struthers over the anteromedial distal humerus shows the median nerve *(arrowheads)* beneath the ligament of Struthers *(arrows)*. Note the supracondylar process *(curved arrow)* at the humeral attachment of the ligament of Struthers and the brachial artery (A). H, humerus.

be a site of compression from fibrous bands or an anomalous muscle. It is important to include evaluation of the distal musculature innervated by the nerve in question because increased echogenicity from atrophy may be a clue to the nerve entrapment (Fig. 4-62).[40]

Radial Nerve

Pathologic processes of the radial nerve include nerve injury associated with the spiral groove of the humerus, termed *spiral groove syndrome*, characterized by wrist drop and sensory findings but with spared triceps brachii function.[3,34] One

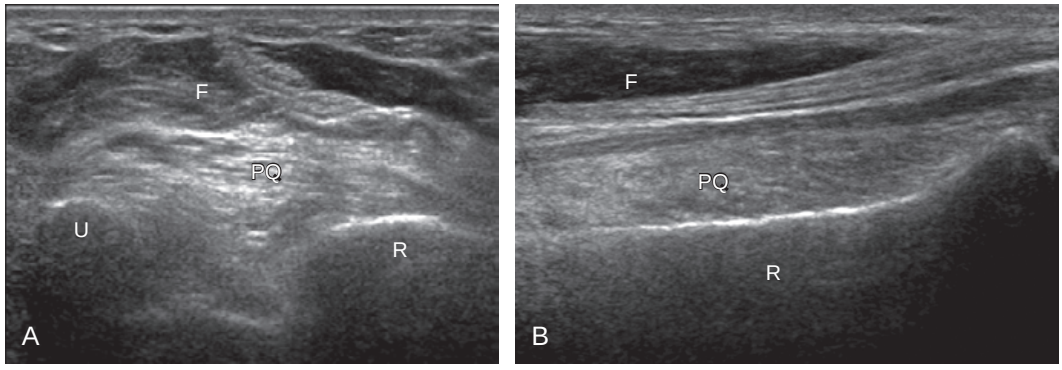

FIGURE 4-62 ■ Anterior interosseous nerve syndrome. Ultrasound images in **(A)** long axis and **(B)** short axis to the pronator quadratus (PQ) show abnormal increased echogenicity of the pronator quadratus relative to the more superficial flexor muscles (F) from denervation. R, radius; U, ulna.

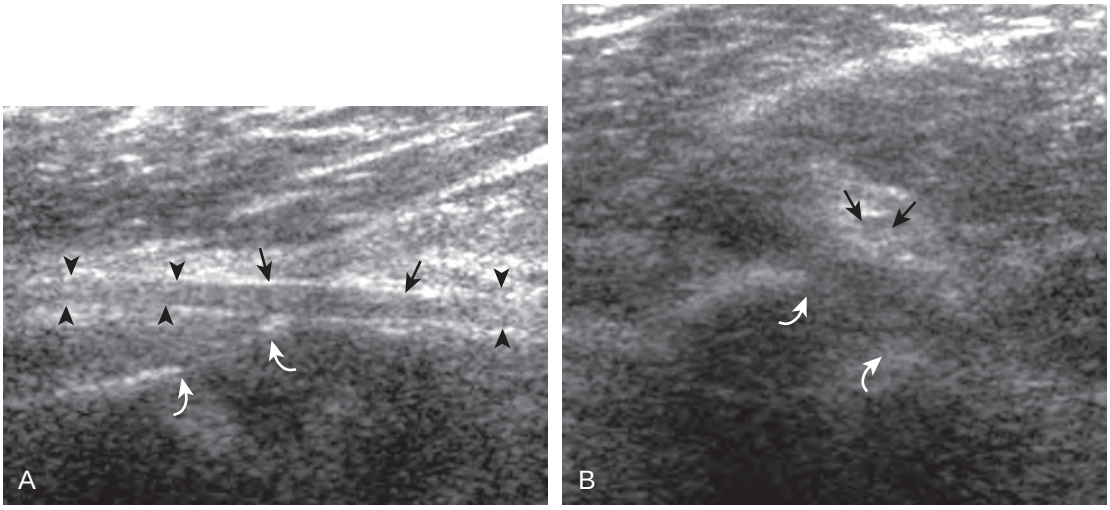

FIGURE 4-63 ■ Radial nerve injury after humeral fracture. Ultrasound images in **(A)** long axis and **(B)** short axis to the radial nerve *(arrowheads)* at the radial groove show minimal hypoechoic swelling of the intact radial nerve *(arrows)* at the site of the humerus fracture *(curved arrows)*.

cause of radial nerve injury at this site is fracture of the humeral shaft, where the injured radial nerve can range from a swollen nerve segment (Fig. 4-63) to complete nerve transection and retraction (Fig. 4-64).[41] In this latter condition, the transected nerve ends appear hypoechoic and swollen. Direct transducer pressure over the nerve end can elicit referred symptoms. The radial nerve may also be injured and swollen at the level of the spiral groove from external compression (termed *Saturday night palsy*). A swollen radial nerve may also show constriction by

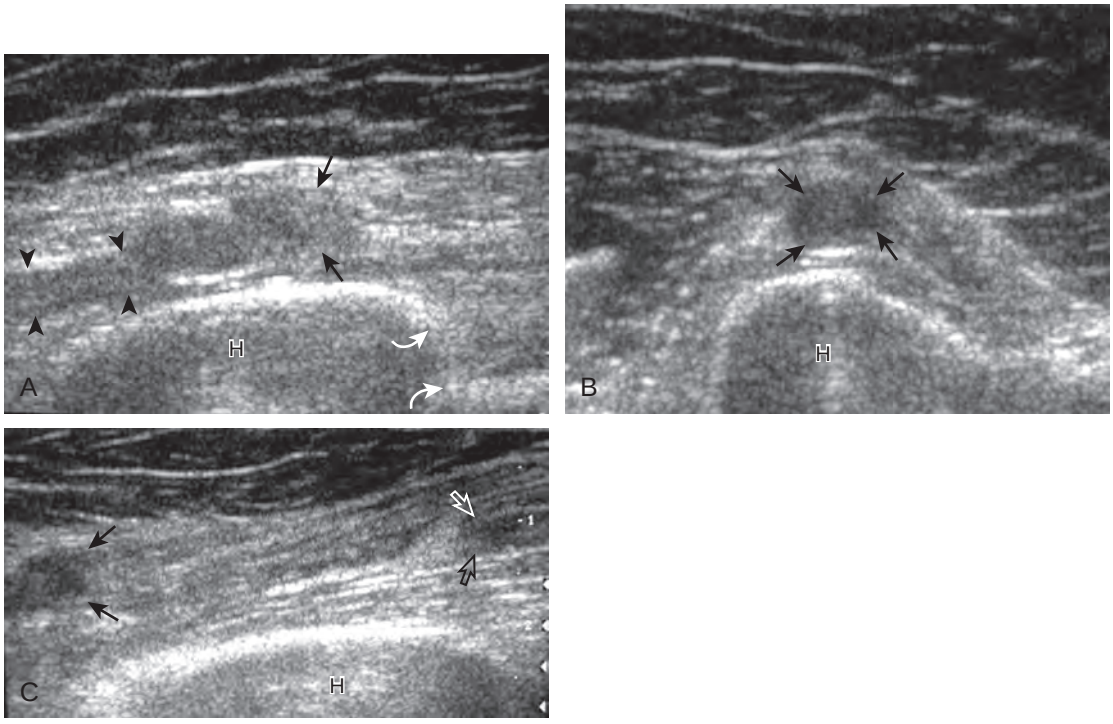

FIGURE 4-64 ■ Radial nerve transection after humeral fracture. Ultrasound images in **(A)** long axis and **(B)** short axis to the radial nerve show the retracted nerve stump *(arrows)* in continuity with the swollen and hypoechoic radial nerve *(arrowheads)* (*curved arrows*, humerus fracture). **C,** Ultrasound image in long axis more distally shows the retraction between the proximal stump *(arrows)* and the distal nerve stump *(open arrows)*. H, humerus.

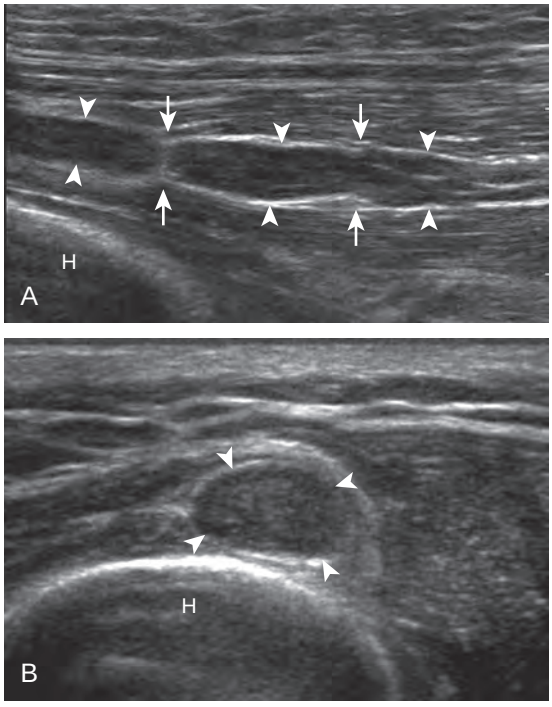

FIGURE 4-65 ■ Radial groove syndrome. Ultrasound images in **(A)** long axis and **(B)** short axis to the radial nerve show diffuse nerve swelling *(arrowheads)* and two focal constrictions *(arrows)*. H, humerus.

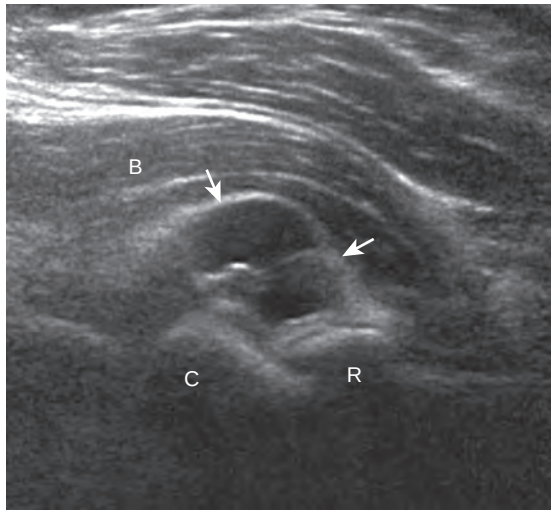

FIGURE 4-67 ■ Ganglion cyst. Sagittal ultrasound image of the anterior elbow shows hypoechoic and septated ganglion cyst *(arrows)*. B, brachialis; C, capitellum; R, radial head.

the intermuscular septum and fibrous bands (Fig. 4-65).

Another site of radial nerve entrapment involves the deep branch of the radial nerve as it courses distally and posteriorly between the two heads of the supinator (called *supinator syndrome* or *radial tunnel syndrome*).[42] Just proximal to this location, abnormal hypoechoic swelling of the involved nerve can be seen at the entry site of the arcade of Frohse (Fig. 4-66). Causes of such compression may be due to a fibrous band or prior trauma, or less commonly abnormal recurrent blood vessels (termed the *leash of Henry*).[34] Because the deep branch of the radial nerve normally flattens as it enters the supinator, it is important to assess for changes in nerve area in short axis to the nerve so as not to mistake the normal change in shape of the nerve entering the supinator as fusiform thickening in long axis.[16] A mass, cyst (Fig. 4-67), bicipitoradial bursa (see Fig. 4-40), or adjacent elbow joint process (see Fig. 4-25) may cause secondary nerve compression.

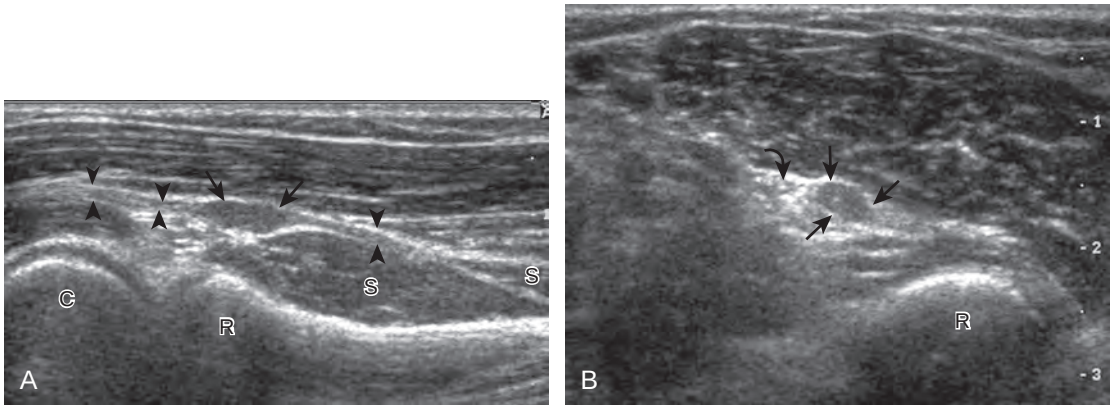

FIGURE 4-66 ■ Supinator syndrome. Ultrasound images in **(A)** long axis and **(B)** short axis to the deep branch of the radial nerve *(arrowheads)* show hypoechoic swelling *(arrows)* as the deep branch of the radial nerve enters between the two heads of the supinator muscle (S). Note the normal superficial branch of the radial nerve *(curved arrow)*. C, capitellum; R, radial head.

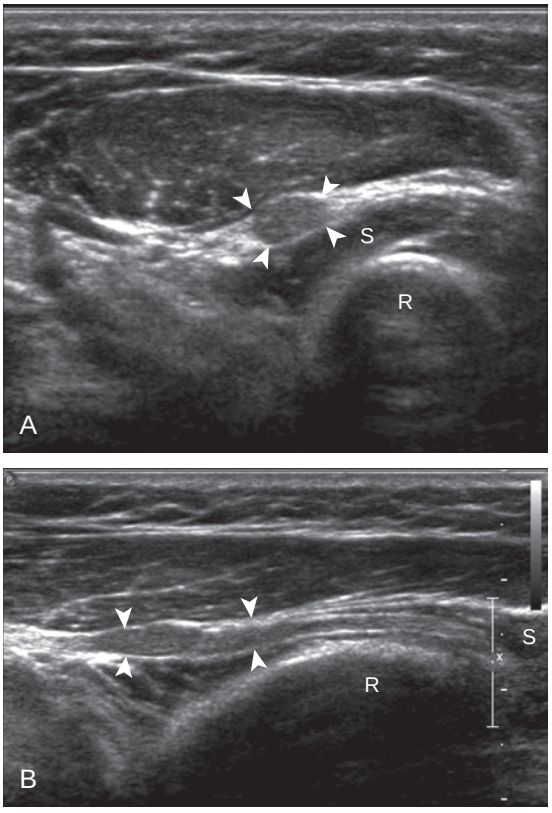

FIGURE 4-68 ■ Neurofibroma. Ultrasound images in **(A)** short axis and **(B)** long axis to the deep branch of the radial nerve *(arrowheads)* show diffuse involvement and enlargement. R, radius; S, supinator.

Peripheral Nerve Sheath Tumors

Other possible peripheral nerve conditions that are not specific to the peripheral nerves around the elbow include peripheral nerve sheath tumors. Benign forms include schwannoma and neurofibroma and appear as a defined hypoechoic mass with low-level internal echoes.[43] Plexiform neurofibromas involve peripheral nerves more extensively (Fig. 4-68) (Video 4-19). Peripheral nerve sheath tumors may be associated with increased through-transmission and can simulate a complex cyst; however, the presence of increased flow on color or power Doppler imaging indicates a solid mass. The presence of peripheral nerve continuity with the mass indicates a peripheral nerve sheath tumor. Malignant counterparts may also contain anechoic cystic or necrotic areas.

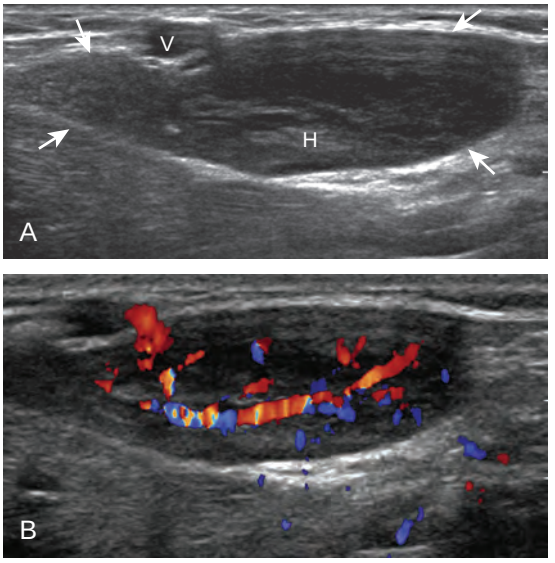

FIGURE 4-69 ■ Epitrochlear lymph node: cat-scratch disease. Ultrasound image over the distal medial humeral metaphysis shows hypoechoic enlargement of the epitrochlear lymph node *(arrows)* with narrowing of the echogenic hilum (H). Note the hilar pattern of vascularity. V, vein.

EPITROCHLEAR LYMPH NODE

Most solid masses around the elbow that are not related to the joint are not specific for a single diagnosis. However, one must be aware of an enlarged epitrochlear lymph node, which, if correctly identified, can suggest a specific diagnosis. An epitrochlear lymph node is located at the medial aspect of the elbow just proximal to the medial epicondyle of the distal humerus between muscle and the subcutaneous tissues. A normal lymph node is oval, with an echogenic central hilum and a hypoechoic rim. The echogenic center results from interfaces between the fatty tissue and sinusoids, rather than from the fat itself, because pure fat is hypoechoic or anechoic at ultrasound. When a lymph node is enlarged but maintains an oval shape, normal echogenic hilum, and hilar vascular pattern, then hyperplasia from inflammation is suggested. One such example is cat-scratch disease (Fig. 4-69), in which the scratch of an animal such as a cat around the hand characteristically produces epitrochlear lymph node enlargement. Inflammation adjacent to the enlarged epitrochlear lymph

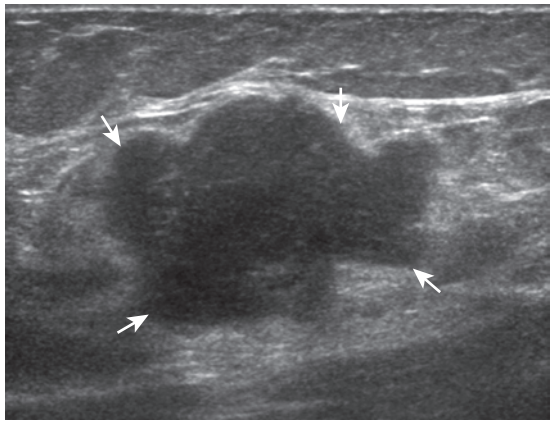

FIGURE 4-70 ■ Epitrochlear lymph node: lymphoma. Ultrasound image over medial elbow shows hypoechoic enlargement of an epitrochlear lymph node *(arrows)* with lobular margins and absence of the echogenic hilum.

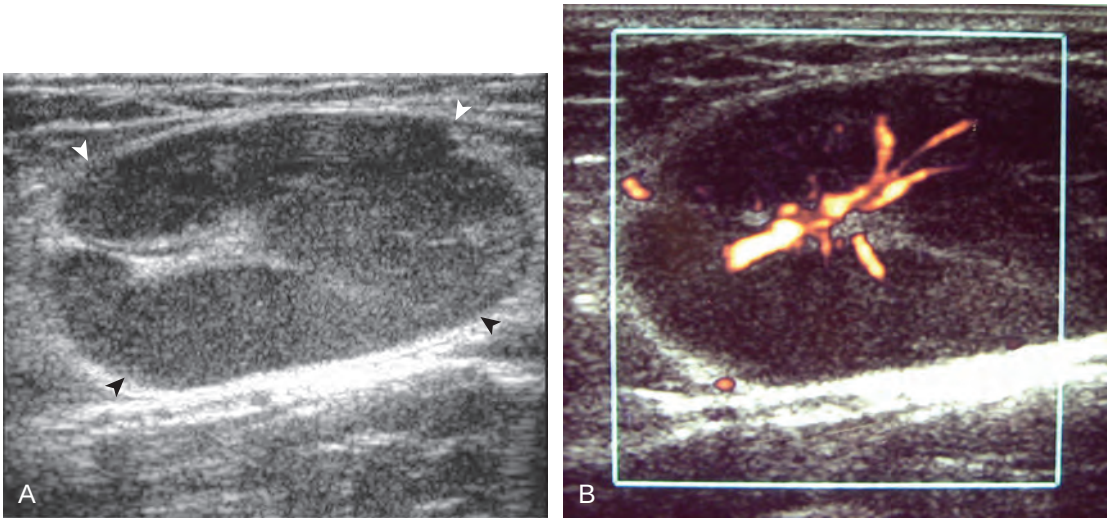

FIGURE 4-71 ■ Epitrochlear lymph node: sarcoidosis. Ultrasound image over the distal medial humeral metaphysis **(A)** shows hypoechoic enlargement of an epitrochlear lymph node *(arrowheads)* with nearly complete obliteration of the echogenic hilum. Note **(B)** the maintained hilar pattern of blood flow on the power Doppler image.

node can create a heterogeneous appearance to the soft tissues, which can make identification of the involved lymph node difficult. If an enlarged lymph node is round with absence of the echogenic hilum, thickening of the hypoechoic cortex, and a peripheral or mixed pattern of vascularity on color and power Doppler imaging, then malignancy is suspected, although biopsy is required to provide a diagnosis. Other examples of epitrochlear lymph node enlargement include lymphoma (Fig. 4-70), metastasis, and sarcoidosis (Fig. 4-71).

Online references available at www.expertconsult.com.

REFERENCES

1. Tagliafico A, Michaud J, Capaccio E, et al: Ultrasound demonstration of distal biceps tendon bifurcation: normal and abnormal findings. *Eur Radiol* 20:202–208, 2010.
2. Madsen M, Marx RG, Millett PJ, et al: Surgical anatomy of the triceps brachii tendon: anatomical study and clinical correlation. *Am J Sports Med* 34:1839–1843, 2006.
3. Martinoli C, Bianchi S, Pugliese F, et al: Sonography of entrapment neuropathies in the upper limb (wrist excluded). *J Clin Ultrasound* 32:438–450, 2004.
4. Smith J, Finnoff JT, O'Driscoll SW, et al: Sonographic evaluation of the distal biceps tendon using a medial approach: the pronator window. *J Ultrasound Med* 29:861–865, 2010.
5. Kalume Brigido M, De Maeseneer M, Jacobson JA, et al: Improved visualization of the radial insertion of the biceps tendon at ultrasound with a lateral approach. *Eur Radiol* 19:1817–1821, 2009.
6. Ward SI, Teefey SA, Paletta GA, Jr, et al: Sonography of the medial collateral ligament of the elbow: a study of cadavers and healthy adult male volunteers. *AJR Am J Roentgenol* 180:389–394, 2003.
7. Jacobson JA, Propeck T, Jamadar DA, et al: US of the anterior bundle of the ulnar collateral ligament: findings in five cadaver elbows with MR arthrographic and anatomic comparison—initial observations. *Radiology* 227:561–566, 2003.
8. De Smet AA, Winter TC, Best TM, et al: Dynamic sonography with valgus stress to assess elbow ulnar collateral ligament injury in baseball pitchers. *Skeletal Radiol* 31:671–676, 2002.
9. Nazarian LN, McShane JM, Ciccotti MG, et al: Dynamic US of the anterior band of the ulnar collateral ligament of the elbow in asymptomatic major league baseball pitchers. *Radiology* 227:149–154, 2003.
10. Jacobson JA, Jebson PJ, Jeffers AW, et al: Ulnar nerve dislocation and snapping triceps syndrome: diagnosis with dynamic sonography—report of three cases. *Radiology* 220:601–605, 2001.
11. Okamoto M, Abe M, Shirai H, et al: Morphology and dynamics of the ulnar nerve in the cubital tunnel: observation by ultrasonography. *J Hand Surg [Br]* 25:85–89, 2000.
12. Teixeira PA, Omoumi P, Trudell DJ, et al: Ultrasound assessment of the lateral collateral ligamentous complex of the elbow: imaging aspects in cadavers and normal volunteers. *Eur Radiol* 21:1492–1498, 2011.
13. Stewart B, Harish S, Oomen G, et al: Sonography of the lateral ulnar collateral ligament of the elbow: study of cadavers and healthy volunteers. *AJR Am J Roentgenol* 193:1615–1619, 2009.
14. Cotten A, Jacobson J, Brossmann J, et al: MR arthrography of the elbow: normal anatomy and diagnostic pitfalls. *J Comput Assist Tomogr* 21:516–522, 1997.
15. Husarik DB, Saupe N, Pfirrmann CW, et al: Ligaments and plicae of the elbow: normal MR imaging variability in 60 asymptomatic subjects. *Radiology* 257:185–194, 2010.
16. Dong Q, Jamadar DA, Robertson BL, et al: Posterior interosseous nerve of the elbow: normal appearances simulating entrapment. *J Ultrasound Med* 29:691–696, 2010.
17. De Maeseneer M, Jacobson JA, Jaovisidha S, et al: Elbow effusions: distribution of joint fluid with flexion and extension and imaging implications. *Invest Radiol* 33:117–125, 1998.
18. Ebrahim FS, Jacobson JA, Lin J, et al: Intraarticular osteoid osteoma: sonographic findings in three patients with radiographic, CT, and MR imaging correlation. *AJR Am J Roentgenol* 177:1391–1395, 2001.
19. Chew ML, Giuffre BM: Disorders of the distal biceps brachii tendon. *Radiographics* 25:1227–1237, 2005.
20. Miller TT, Adler RS: Sonography of tears of the distal biceps tendon. *AJR Am J Roentgenol* 175:1081–1086, 2000.
21. Skaf AY, Boutin RD, Dantas RW, et al: Bicipitoradial bursitis: MR imaging findings in eight patients and anatomic data from contrast material opacification of bursae followed by routine radiography and MR imaging in cadavers. *Radiology* 212:111–116, 1999.
22. Sofka CM, Adler RS: Sonography of cubital bursitis. *AJR Am J Roentgenol* 183:51–53, 2004.
23. Downey R, Jacobson JA, Fessell DP, et al: Sonography of partial-thickness tears of the distal triceps brachii tendon. *J Ultrasound Med* 30:1351–1356, 2011.
24. Jacobson JA, Miller BS, Morag Y: Golf and racquet sports injuries. *Semin Musculoskelet Radiol* 9:346–359, 2005.
25. Levin D, Nazarian LN, Miller TT, et al: Lateral epicondylitis of the elbow: US findings. *Radiology* 237:230–234, 2005.
26. Walz DM, Newman JS, Konin GP, et al: Epicondylitis: pathogenesis, imaging, and treatment. *Radiographics* 30:167–184, 2010.
27. Lee MH, Cha JG, Jin W, et al: Utility of sonographic measurement of the common tensor tendon in patients with lateral epicondylitis. *AJR Am J Roentgenol* 196:1363–1367, 2011.
28. Miller TT, Shapiro MA, Schultz E, et al: Comparison of sonography and MRI for diagnosing epicondylitis. *J Clin Ultrasound* 30:193–202, 2002.
29. Clarke AW, Ahmad M, Curtis M, et al: Lateral elbow tendinopathy: correlation of ultrasound findings with pain and functional disability. *Am J Sports Med* 38:1209–1214, 2010.
30. McShane JM, Nazarian LN, Harwood MI: Sonographically guided percutaneous needle tenotomy for treatment of common extensor tendinosis in the elbow. *J Ultrasound Med* 25:1281–1289, 2006.
31. McShane JM, Shah VN, Nazarian LN: Sonographically guided percutaneous needle tenotomy for treatment of common extensor tendinosis in the elbow: is a corticosteroid necessary? *J Ultrasound Med* 27:1137–1144, 2008.
32. Connell D, Burke F, Coombes P, et al: Sonographic examination of lateral epicondylitis. *AJR Am J Roentgenol* 176:777–782, 2001.
33. Miller TT, Adler RS, Friedman L: Sonography of injury of the ulnar collateral ligament of the elbow—initial experience. *Skeletal Radiol* 33:386–391, 2004.
34. Jacobson JA, Fessell DP, Lobo Lda G, et al: Entrapment neuropathies I: upper limb (carpal tunnel excluded). *Semin Musculoskelet Radiol* 14:473–486, 2010.
35. Thoirs K, Williams MA, Phillips M: Ultrasonographic measurements of the ulnar nerve at the elbow: role of confounders. *J Ultrasound Med* 27:737–743, 2008.
36. O'Driscoll SW, Horii E, Carmichael SW, et al: The cubital tunnel and ulnar neuropathy. *J Bone Joint Surg Br* 73:613–617, 1991.
37. Okamoto M, Abe M, Shirai H, et al: Diagnostic ultrasonography of the ulnar nerve in cubital tunnel syndrome. *J Hand Surg [Br]* 25:499–502, 2000.
38. Husarik DB, Saupe N, Pfirrmann CW, et al: Elbow nerves: MR findings in 60 asymptomatic subjects—normal anatomy, variants, and pitfalls. *Radiology* 252:148–156, 2009.
39. Camerlinck M, Vanhoenacker FM, Kiekens G: Ultrasound demonstration of Struthers' ligament. *J Clin Ultrasound* 38:499–502, 2010.

40. Hide IG, Grainger AJ, Naisby GP, et al: Sonographic findings in the anterior interosseous nerve syndrome. *J Clin Ultrasound* 27:459–464, 1999.
41. Bodner G, Buchberger W, Schocke M, et al: Radial nerve palsy associated with humeral shaft fracture: evaluation with US—initial experience. *Radiology* 219:811–816, 2001.
42. Chien AJ, Jamadar DA, Jacobson JA, et al: Sonography and MR imaging of posterior interosseous nerve syndrome with surgical correlation. *AJR Am J Roentgenol* 181:219–221, 2003.
43. Reynolds DL, Jr, Jacobson JA, Inampudi P, et al: Sonographic characteristics of peripheral nerve sheath tumors. *AJR Am J Roentgenol* 182:741–744, 2004.

eBOX 4-1 Sample Diagnostic Elbow Ultrasound Report:

NORMAL, COMPLETE

Examination: Ultrasound of the Elbow
Date of Study: March 11, 2011
Patient Name: Jack White
Registration Number: 8675309
History: Elbow pain, evaluate for tendon abnormality
Findings: No evidence of joint effusion or synovial process. The biceps brachii and brachialis are normal. The common flexor and extensor tendons are also normal. No significant triceps brachii abnormality. The anterior band of the ulnar collateral ligament and radial collateral ligament complex are normal. The ulnar nerve, radial nerve, and median nerve at the elbow are unremarkable. No abnormality in the cubital tunnel region with dynamic imaging. Additional focused evaluation at site of maximal symptoms was unrevealing.
Impression: Unremarkable ultrasound examination of the elbow.

eBOX 4-2 Sample Diagnostic Elbow Ultrasound Report:

ABNORMAL, COMPLETE

Examination: Ultrasound of the Elbow
Date of Study: March 11, 2011
Patient Name: Jack White
Registration Number: 8675309
History: Elbow pain, evaluate for tendon abnormality
Findings: There is a partial-thickness tear of the distal biceps brachii tendon involving the superficial short head tendon with approximately 2 cm of retraction but with intact long head. Dynamic evaluation shows continuity of the long head excluding full-thickness tear. No joint effusion. The triceps brachii, common extensor, and common flexor tendons are normal. The ulnar, radial, and median nerves are unremarkable, including dynamic evaluation of the ulnar nerve. Unremarkable ulnar and radial collateral ligaments. No bursal distention.
Impression: Partial-thickness tear of the distal biceps brachii tendon.

CHAPTER 5

Wrist and Hand Ultrasound

CHAPTER OUTLINE

WRIST AND HAND ANATOMY

ULTRASOUND EXAMINATION TECHNIQUE
- General Comments
- Wrist: Volar Evaluation
  - Median Nerve, Flexor Digitorum Tendons, and Volar Joint Recesses
  - Scaphoid, Flexor Carpi Radialis Tendon, Radial Artery, and Volar Ganglion Cysts
  - Ulnar Artery, Vein, and Nerve (Guyon Canal)
- Wrist: Dorsal Evaluation
  - Dorsal Wrist Tendons and Dorsal Joint Recesses
  - Scapholunate Ligament (Dorsal Component) and Dorsal Ganglion Cysts
  - Triangular Fibrocartilage Complex
- Finger Evaluation
  - Volar
  - Dorsal
  - Ligaments

JOINT ABNORMALITIES

TENDON AND MUSCLE ABNORMALITIES

PERIPHERAL NERVE ABNORMALITIES
- Carpal Tunnel Syndrome
- Ulnar Tunnel Syndrome
- Radial Nerve Compression
- Transection Neuromas

GANGLION CYST

LIGAMENT AND OSSEOUS ABNORMALITIES
- Scapholunate Ligament Injury
- Ulnar Collateral Ligament Injury (Thumb)
- Other Ligament Injuries
- Osseous Injury

OTHER MASSES
- Giant Cell Tumor of the Tendon Sheath and Similar Masses
- Dupuytren Contracture
- Glomus Tumor
- Miscellaneous Masses

Additional videos for this topic are available online at www.expertconsult.com.

WRIST AND HAND ANATOMY

The wrist consists of several synovial articulations between the distal radius, the distal ulna, the proximal carpal row (scaphoid, lunate, triquetrum, pisiform), and the distal carpal row (trapezium, trapezoid, capitate, and hamate). The radiocarpal joint between the distal radius and the proximal carpal row and the distal radioulnar joint between the radius and the ulna are separated by fibrocartilage, called the *triangular fibrocartilage*, which extends from the ulnar aspect of the distal radius to the base of the ulnar styloid. The midcarpal joint is located between the carpal bones and is separated from the radiocarpal joint by two intrinsic ligaments, the scapholunate and lunotriquetral ligaments. The scapholunate ligament is U shaped in the sagittal plane, with the open end of the U distal, and it consists of a volar portion, a thin proximal or central portion, and a thick and mechanically important dorsal portion.[1]

Structures enter the wrist through several fibro-osseous tunnels. In the volar wrist, the carpal tunnel contains the median nerve and the flexor digitorum profundus, flexor digitorum superficialis, and flexor pollicis longus tendons (Fig. 5-1A-E). The fibrous flexor retinaculum extends from the pisiform and hamate to the scaphoid and trapezium, to form the roof of the carpal tunnel. The Guyon or ulnar canal is also volar adjacent to the pisiform, which contains the ulnar nerve and ulnar artery and veins. Other tendons, the flexor carpi radialis and the palmaris longus tendons, are located outside the carpal tunnel, although the flexor carpi radialis is within its own fibro-osseous canal and distally is associated with the trapezium.

The tendons of the dorsal wrist are also separated into six fibro-osseous compartments

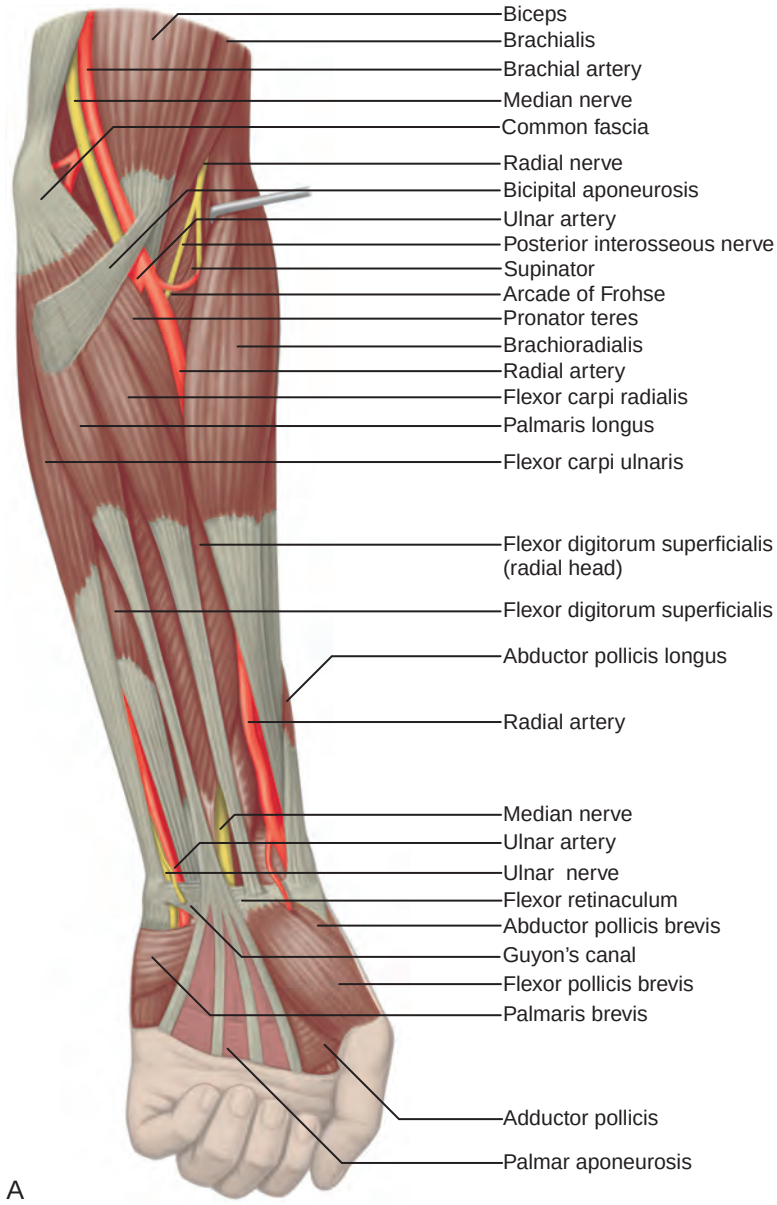

FIGURE 5-1 ■ **Forearm, wrist, and hand anatomy. A,** Superficial flexors muscles of the left forearm.

Continued

(see Fig. 5-1C). From radial to ulnar, they include the (1) abductor pollicis longus and extensor pollicis brevis, (2) extensor carpi radialis longus and brevis, (3) extensor pollicis longus, (4) extensor digitorum and extensor indicis, (5) extensor digiti minimi, and (6) extensor carpi ulnaris. A helpful bone landmark for orientation is the dorsal tubercle of the radius or Lister tubercle, which is located between the extensor carpi radialis tendons in the second compartment and the extensor pollicis longus tendon in the third compartment. The extensor carpi ulnaris is also found within a characteristic groove in the ulna.

The anatomy of the volar aspect of the fingers includes the flexor digitorum superficialis and profundus tendons. Each flexor superficialis tendon splits at the proximal interphalangeal joint, with each limb coursing to each side of the flexor digitorum profundus tendon to insert on the middle phalanx (see Fig. 5-1F-H). The flexor digitorum profundus terminates at the distal phalanx. The flexor tendons are tethered or

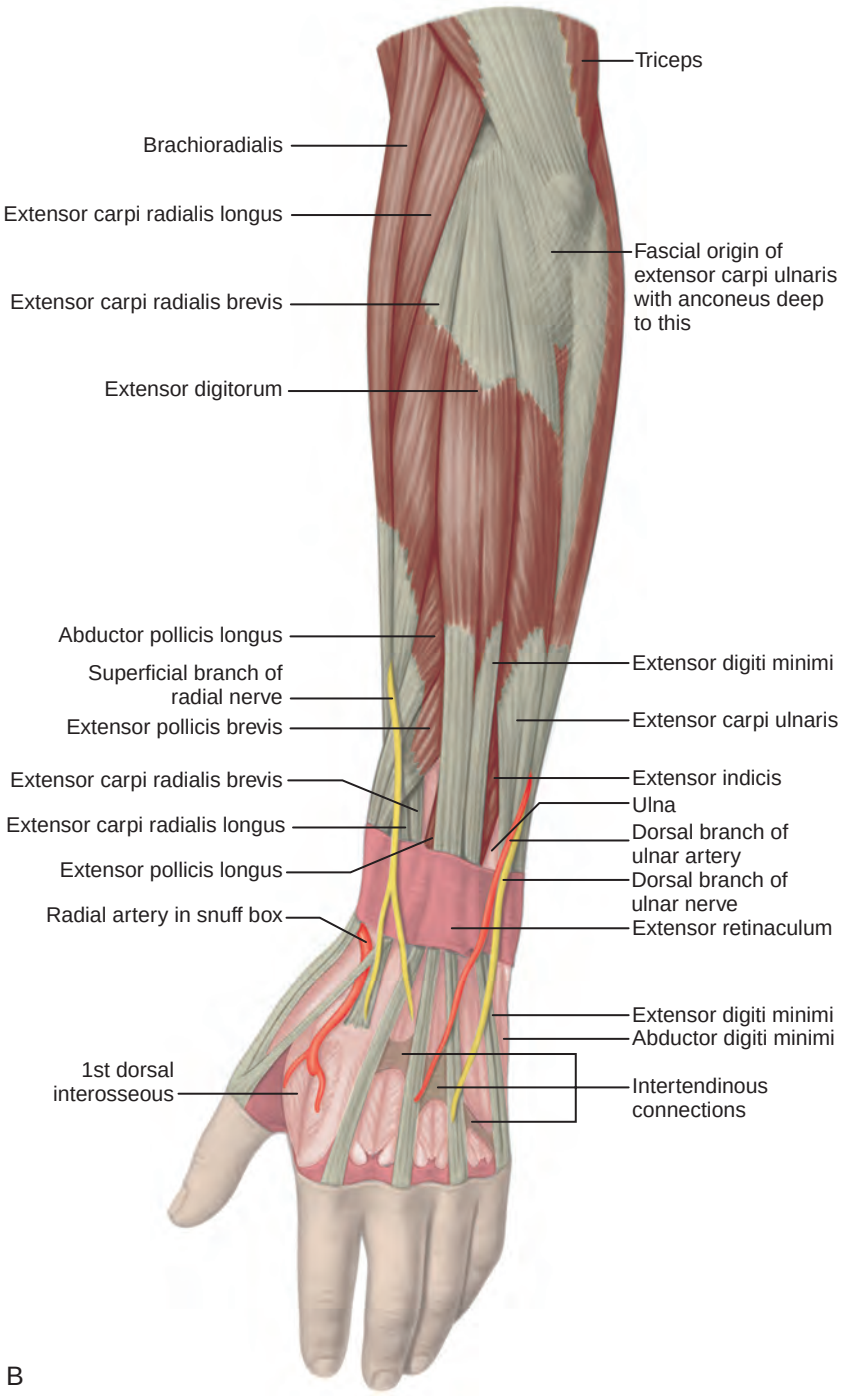

FIGURE 5-1, cont'd ■ **B,** Superficial extensor muscles of the left forearm.

secured to the adjacent phalanges through a series of fibrous pulleys to prevent bowstringing of the tendons with flexion (see Fig. 5-1F). The annular pulleys consist of the A1 pulley located at the metacarpophalangeal joint, the longer A2 pulley at the level of the proximal phalanx, the A3 pulley at the proximal interphalangeal joint, the A4 pulley at the level of the middle phalanx, and the A5 pulley at the distal interphalangeal joint.[2] Smaller cruciform pulleys are located between these pulleys along the course of the flexor tendons. At the volar aspect of each metacarpophalangeal and interphalangeal joint is a fibrous structure called the *volar* or *palmar plate*.

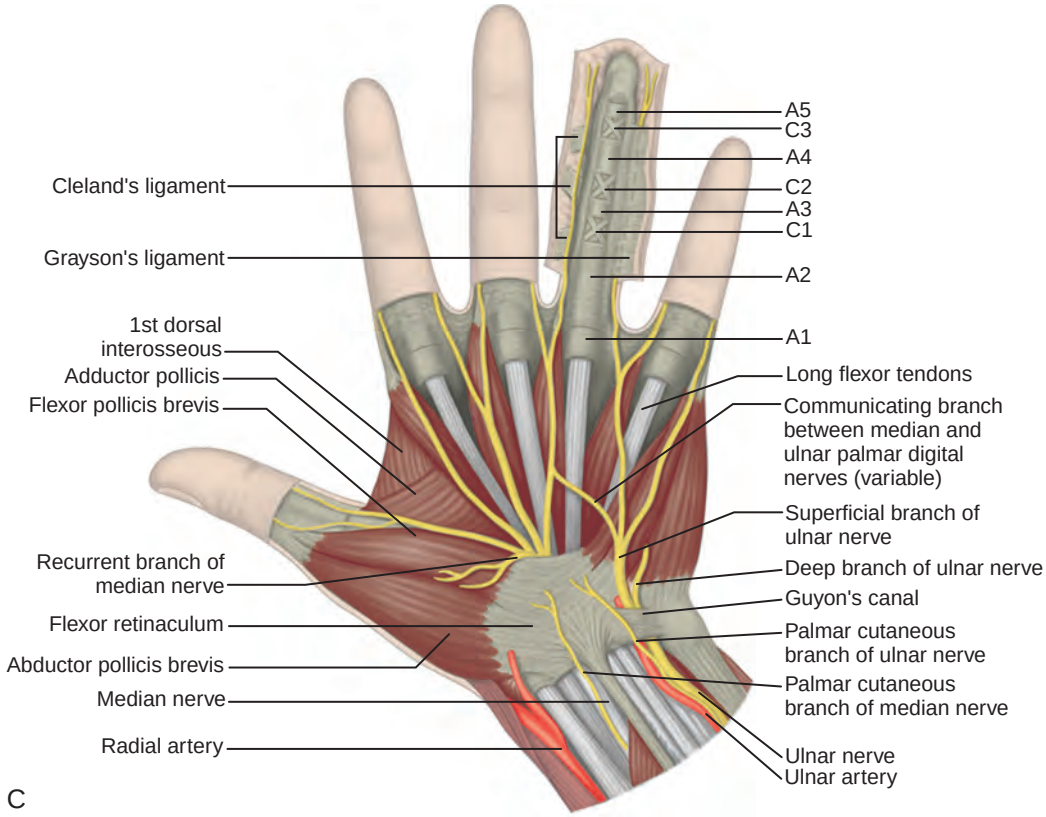

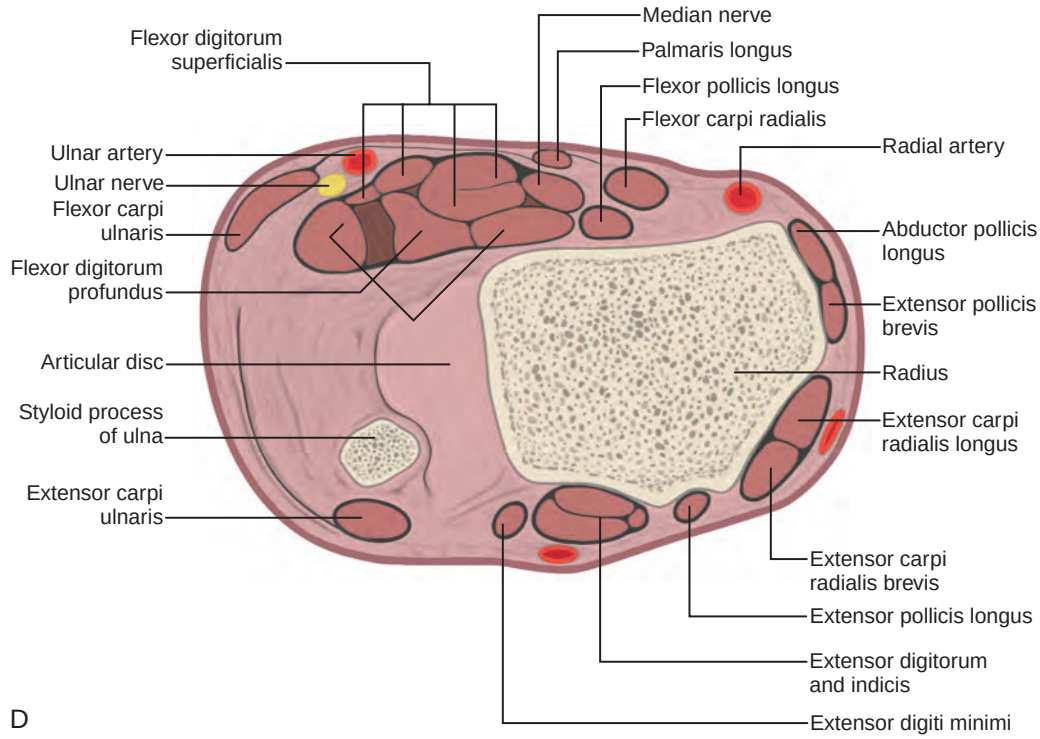

FIGURE 5-1, cont'd ■ **C,** Palmar aspect of hand including annular (A) and cruciate (C) pulleys of the digit. **D,** Transverse section through the distal left forearm at the level of the ulnar styloid.

Continued

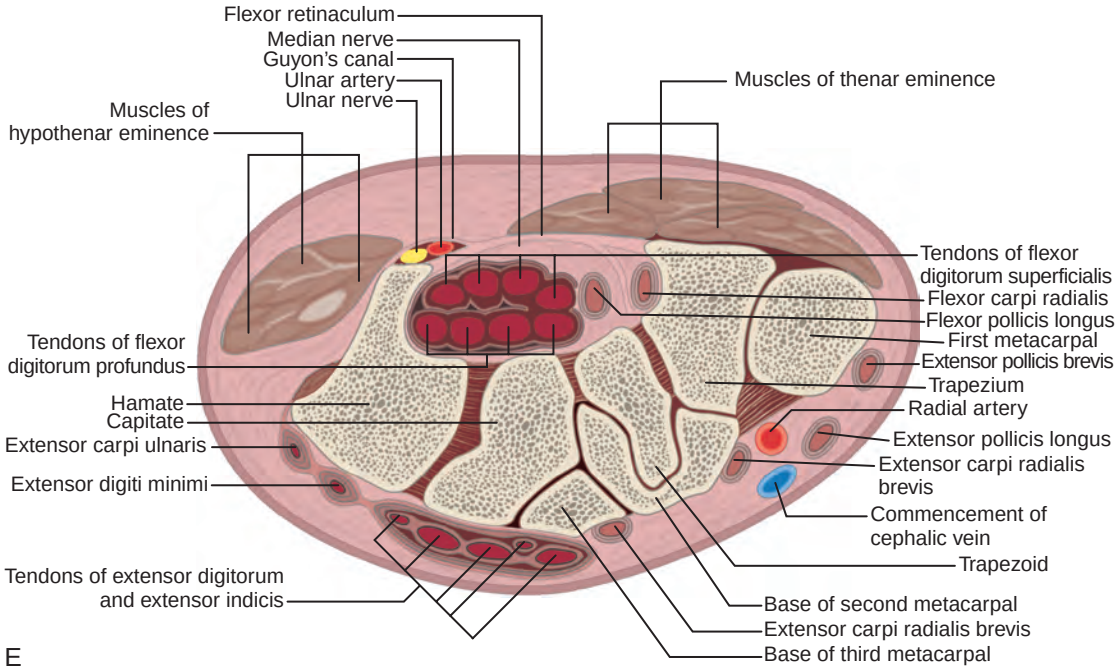

E

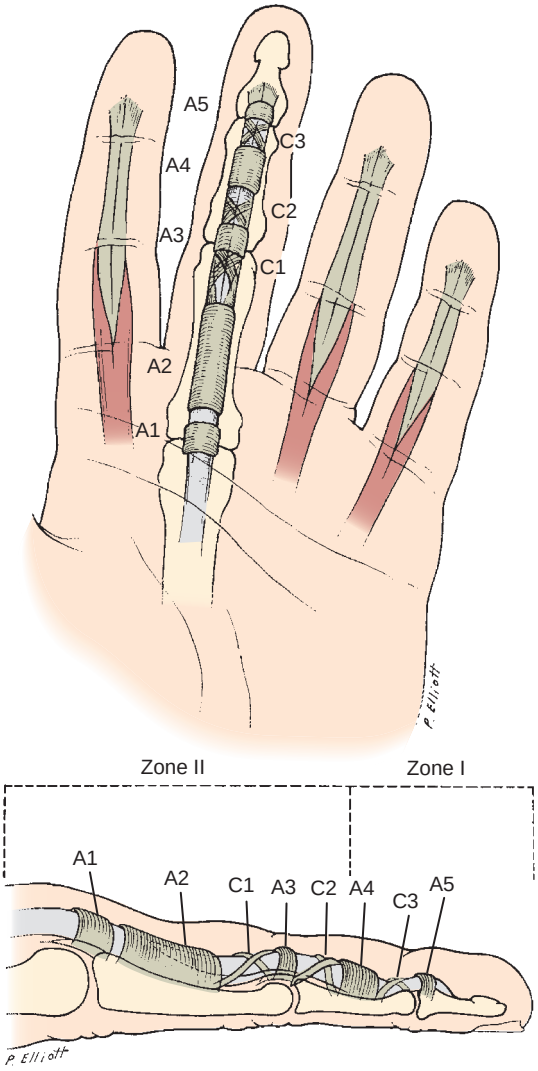

F

FIGURE 5-1, cont'd ■ **E,** Transverse section through the left wrist at the level of the hamate bone. **F,** Palmar and lateral views showing the annular (A) and cruciate (C) pulleys of the flexor tendon sheath.

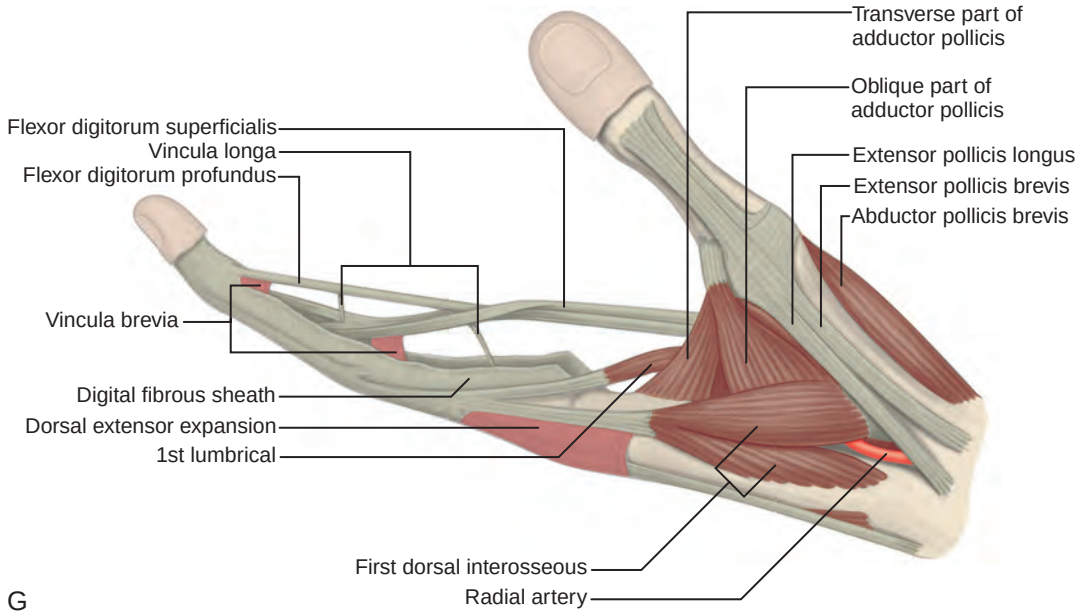

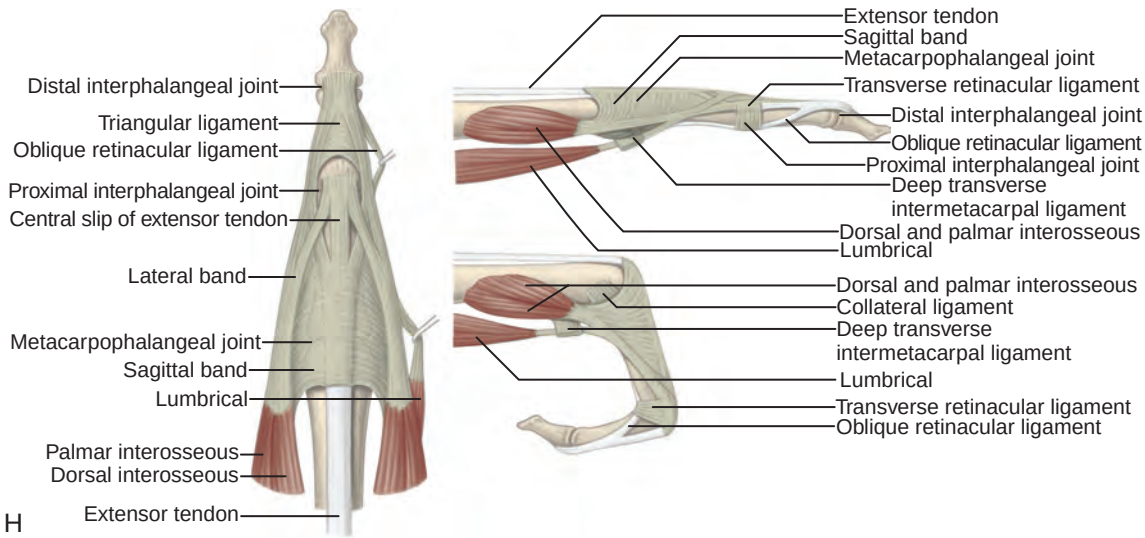

FIGURE 5-1, cont'd ■ **G,** Lateral part of the left hand showing the flexor tendons of the finger. **H,** Dorsal view, lateral view, and lateral view in flexion show the extensor mechanism of the finger. (From Standring S: *Gray's anatomy: the anatomical basis of clinical practice*, ed 39, Edinburgh, 2005, Churchill Livingstone.)

At the dorsal aspect of each finger, the extensor digitorum tendon attaches to the middle phalanx as a central band, whereas slips of the extensor tendon that contribute to the lateral bands attach to the distal phalanx. The metacarpophalangeal joints have an overlying aponeurotic sheet or extensor hood, which consists of transverse-oriented sagittal bands that stabilize the extensor tendons.[3] The metacarpophalangeal and interphalangeal joints are synovial articulations with prominent dorsal joint recesses. Each joint is stabilized with ulnar and radial collateral ligaments. The soft tissue distally at the volar aspect of distal phalanx is called the *pulp*.

ULTRASOUND EXAMINATION TECHNIQUE

Tables 5-1 and 5-2 are ultrasound examination checklists. Examples of diagnostic wrist and hand ultrasound reports are available online at www.expertconsult.com (see eBox 5-1 and 5-2).

TABLE 5-1 **Wrist and Hand Ultrasound Examination Checklist**

Location	Structures of Interest/Pathologic Features
Volar (no. 1)	Median nerve Flexor tendons Volar joint recesses
Volar (no. 2)	Scaphoid Flexor carpi radialis Radial artery Volar ganglion cyst
Volar (no. 3)	Ulnar nerve and artery
Dorsal (no. 1)	Extensor tendons Dorsal joint recesses
Dorsal (no. 2)	Scapholunate ligament Dorsal ganglion cyst
Dorsal (no. 3)	Triangular fibrocartilage complex

General Comments

Ultrasound examination of the wrist and hand is typically completed with the patient sitting and the hand resting on the examination table. This position allows easy comparison between each side if needed. A high-frequency transducer of at least 10 MHz is typically used because most of the structures are superficial, and a transducer with a small footprint is often helpful to maintain contact with the soft tissues under examination. I favor thick transmission gel over a stand-off pad. Evaluation of the wrist and hand may be focused over the area that is clinically symptomatic or relevant to the patient's history. Regardless, a complete examination of all areas should always be considered for one to become familiar with normal anatomy and normal variants and to develop a quick and efficient sonographic technique.

Wrist: Volar Evaluation

Median Nerve, Flexor Digitorum Tendons, and Volar Joint Recesses

The primary structures evaluated from the volar aspect at midline are the median nerve, the flexor tendons, and the volar aspects of the wrist joints.

TABLE 5-2 **Finger Ultrasound Examination Checklist**

Location	Structures of Interest
Volar	Flexor tendons Pulleys Volar plate Joint recesses
Dorsal	Extensor tendon Joint recesses
Other	Collateral ligaments

Examination begins short axis to the tendons and median nerve because this allows proper orientation and accurate identification of the structures. For evaluation of the median nerve, the transducer is placed in the transverse plane at the level of the wrist crease, which is at the proximal aspect of the carpal tunnel (Fig. 5-2). Normal peripheral nerves have a honeycomb appearance when they are imaged in short axis from hypoechoic nerve fascicles and surrounding hyperechoic connective tissue (see Fig. 5-2B).[4] Toggling the transducer to angle the sound beam along the long axis of the median nerve will help to show the characteristic appearance of the nerve when the sound beam is perpendicular (Video 5-1). Because peripheral nerve trunks are composed of both hypoechoic and hyperechoic elements, the median nerve appears relatively hypoechoic when surrounded by hyperechoic tissue (e.g., in the carpal tunnel) and relatively hyperechoic when surrounded by hypoechoic muscle (e.g., in the forearm). At the wrist crease, the round or oval median nerve is identified by its hypoechoic nerve fascicles, which are most conspicuous surrounded by the adjacent hyperechoic tendons (see Fig. 5-2C). If differentiation between the median nerve and adjacent tendons is difficult, median nerve identification is easily accomplished with movement of the transducer proximally in the transverse plane. During this maneuver, the normal median nerve courses radial to the flexor tendons and then moves ulnar and deep between the flexor digitorum superficialis and profundus (Fig. 5-3) (Video 5-2).[4] In addition, the median nerve now appears relatively hyperechoic as a result of the connective tissue and fat because it is surrounded by hypoechoic muscle. The characteristic course, location, and echogenicity assist in identification of the median nerve. An additional method to differentiate the median nerve from the adjacent flexor tendons at the wrist crease in the transverse plane is angulation of or toggling the transducer along the long axis of the tendons. This maneuver causes the hyperechoic tendons to become hypoechoic as a result of anisotropy, whereas the hypoechoic median nerve fascicles remain unchanged (see Video 5-1). Evaluation of the median nerve is then continued distally into the carpal tunnel, where the thin and hyperechoic flexor retinaculum can be visualized (see Fig. 5-2D). A small branch of the median nerve, the palmar cutaneous branch, originates proximal to the carpal tunnel and courses superficial to the flexor retinaculum and ulnar to flexor carpi radialis tendon (see Fig. 5-2E).[5] The transducer is turned 90 degrees to visualize the median nerve in long axis (Fig. 5-4) (Video 5-3). The variable appearance of peripheral nerve echogenicity relative to the

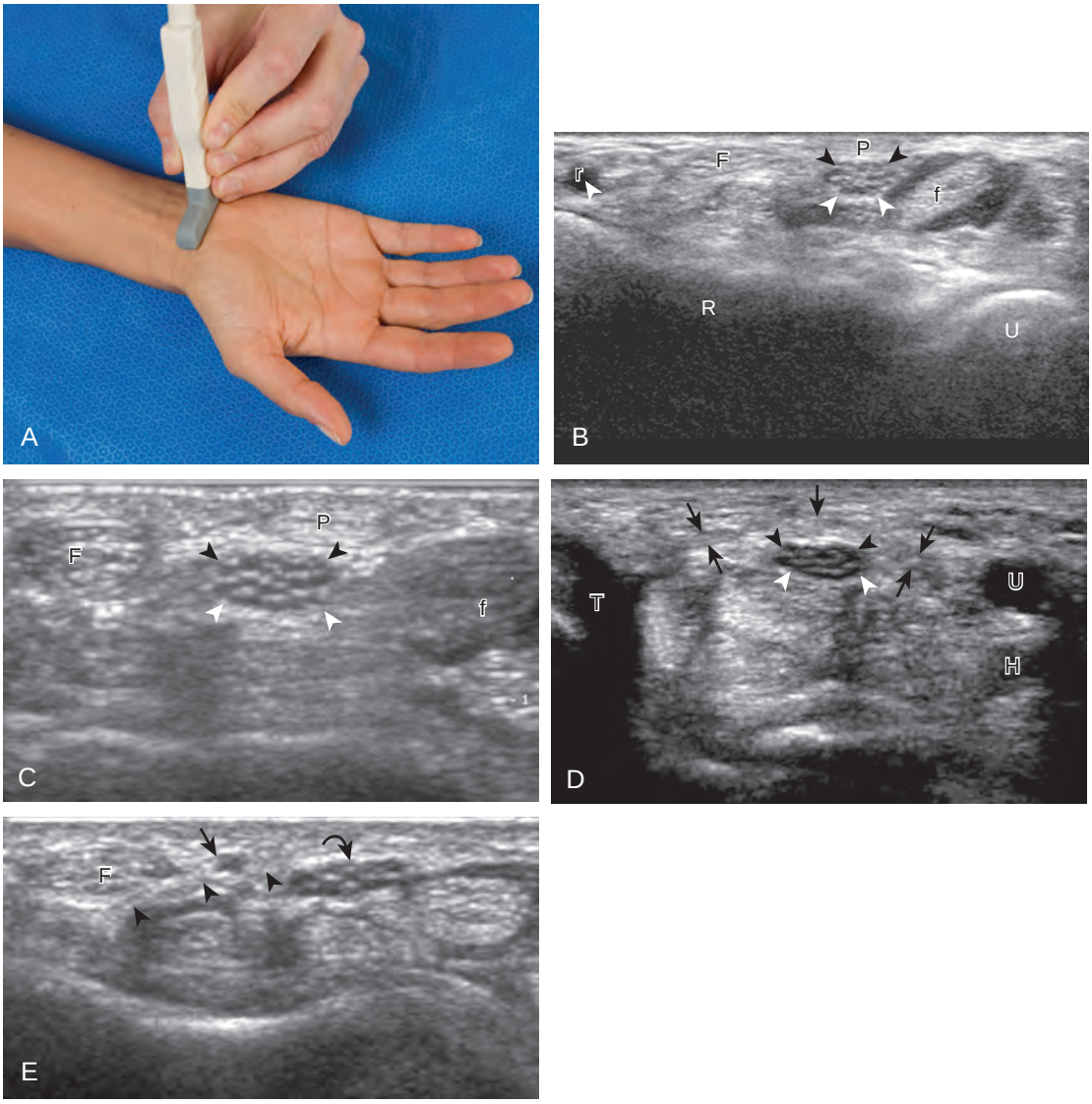

FIGURE 5-2 ■ Carpal tunnel and volar wrist evaluation (transverse). A, Transverse imaging over the volar wrist crease shows **(B** and **C)** the median nerve *(arrowheads)*, flexor carpi radialis (F), palmaris longus (P), radial artery (r), flexor digitorum tendons (f), radius (R), and ulna (U). Transverse imaging distal to the volar wrist crease shows **(D)** the flexor retinaculum *(arrows)* and median nerve *(arrowheads)* within the carpal tunnel (H, hook of hamate; T, trapezium; U, ulnar artery). Transverse imaging proximal at wrist crease **(E)** shows the palmar cutaneous branch *(arrow)* of the median nerve *(curved arrow)* superficial to the flexor retinaculum *(arrowheads)*.

surrounding tissue echogenicity is well demonstrated when imaging the median nerve in long axis in the distal forearm (see Fig. 5-4D). Proximal to the wrist joint in the transverse plane, the pronator quadratus can be identified extending between the distal radius and ulna (see Fig. 5-3A).

Attention is then turned back to the flexor tendons, with each tendon evaluated in both short axis and long axis. The flexor digitorum superficialis and profundus are identified around the median nerve as described earlier, proximally as hypoechoic muscle and distally as fibrillar and hyperechoic tendons (see Figs. 5-2 and 5-3). Just beyond the wrist crease, the thin hyperechoic flexor retinaculum is seen as it extends from the proximal scaphoid pole to the pisiform and from the trapezium to the hook of the hamate, which represents the roof the carpal tunnel (see Fig. 5-2D). If the retinaculum is not imaged perpendicular to the ultrasound beam, it will appear hypoechoic as a result of anisotropy. The flexor

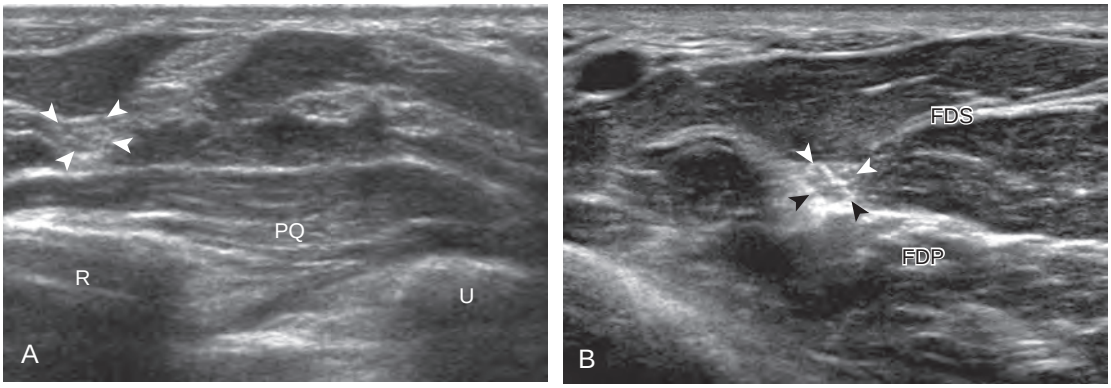

FIGURE 5-3 ■ Volar forearm evaluation (distal, transverse). Sequential transverse ultrasound images **(A** and **B)** proximal to the volar wrist crease show that the median nerve *(arrowheads)* moves deep between the flexor digitorum profundus (FDP) and flexor digitorum superficialis (FDS). PQ, pronator quadratus; R, radius, U, ulna.

digitorum tendons travel through the carpal tunnel to the digits, whereas the palmaris longus tendon, typically directly superficial to the median nerve, remains outside of the carpal tunnel. In the sagittal plane and long axis to the flexor tendons, the volar radiocarpal and midcarpal joint recesses are identified by the adjacent bone contours; the volar lip of the distal radius, the lunate bone, and the capitate bone have characteristic shapes (see Fig. 5-4B and C). Between the distal radius and the lunate is the volar recess of the radiocarpal joint, and between the lunate and capitate bones is the volar recess of the midcarpal joint. The distal radioulnar joint is identified with placement of the transducer in the transverse plane between the distal radius and ulna. This joint and

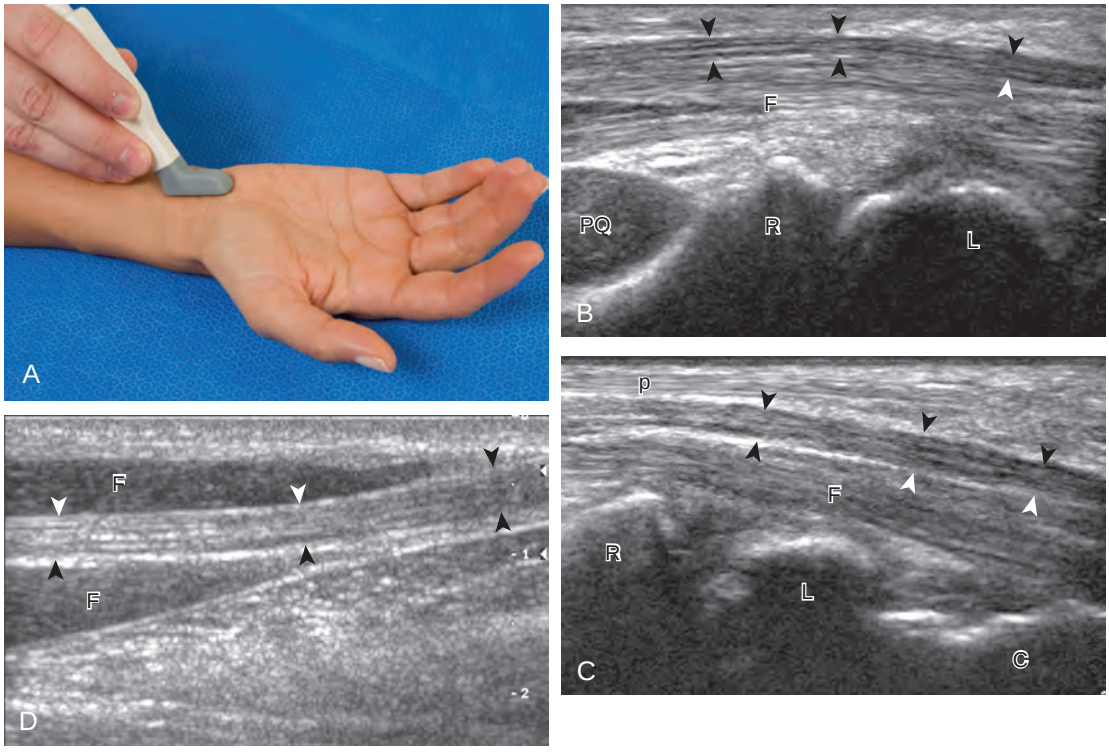

FIGURE 5-4 ■ Carpal tunnel and volar wrist evaluation (longitudinal). A, Sagittal imaging over the volar wrist crease shows **(B** to **D)** the median nerve *(arrowheads)*, flexor digitorum (F), palmaris longus (p), pronator quadratus (PQ), radius (R), lunate (L), and capitate (C). Note the median nerve in **D,** which appears relatively hyperechoic proximally and hypoechoic distally (left side of image is proximal).

the volar recesses are evaluated for anechoic fluid or variable-echogenicity synovial hypertrophy and other joint disorders.

Scaphoid, Flexor Carpi Radialis Tendon, Radial Artery, and Volar Ganglion Cysts

Evaluation of the radial aspect of the volar wrist begins in the transverse plane at the wrist crease. In this position, the various tendons of the volar wrist are identified. Just radial to the median nerve and somewhat similar in size is the flexor carpi radialis tendon, located outside the carpal tunnel in its own fibro-osseous canal (see Fig. 5-2B). Ultrasound evaluation is completed in both long and short axis from proximal to the distal insertion of the flexor carpi radialis tendon on the second and third metacarpals, although some fibers insert onto the trapezium tuberosity.[6] With placement of the transducer over the distal aspect of the flexor carpi radialis tendon in long axis (Fig. 5-5), the characteristic bilobed or peanut-shaped bone contours of the scaphoid bone are identified deep to this tendon (see Fig. 5-5C). The normal smooth and hyperechoic bone surface of the scaphoid bone is evaluated for cortical step-off fracture. Returning to the wrist crease in the transverse plane (Fig. 5-6A), the radial artery and veins are identified immediately radial to the flexor carpi radialis tendon (see Fig. 5-6B). With the flexor carpi radialis tendon and radial artery in view, the transducer is moved both proximally and distally from the radiocarpal joint to evaluate for ganglion cysts. Placement of the transducer in the transverse plane between the scaphoid and lunate will show the normal hyperechoic and fibrillar volar component of the scapholunate ligament (see Fig. 5-6C).

Ulnar Artery, Vein, and Nerve (Guyon Canal)

Evaluation of the ulnar aspect of the volar wrist begins in the transverse plane at the wrist crease (see Fig. 5-2A). Moving the transducer ulnar to the carpal tunnel (Fig. 5-7A), the bone landmark of the pisiform is identified (see Fig. 5-7B). Between the pisiform and the ulnar artery, the ulnar nerve is identified as hypoechoic nerve fascicles and surrounding hyperechoic connective tissue. The ulnar veins are usually not visible because they are easily compressed by pressure of the ultrasound transducer. As the transducer is moved distally, the hyperechoic and shadowing surface of the hook of the hamate is seen deep to

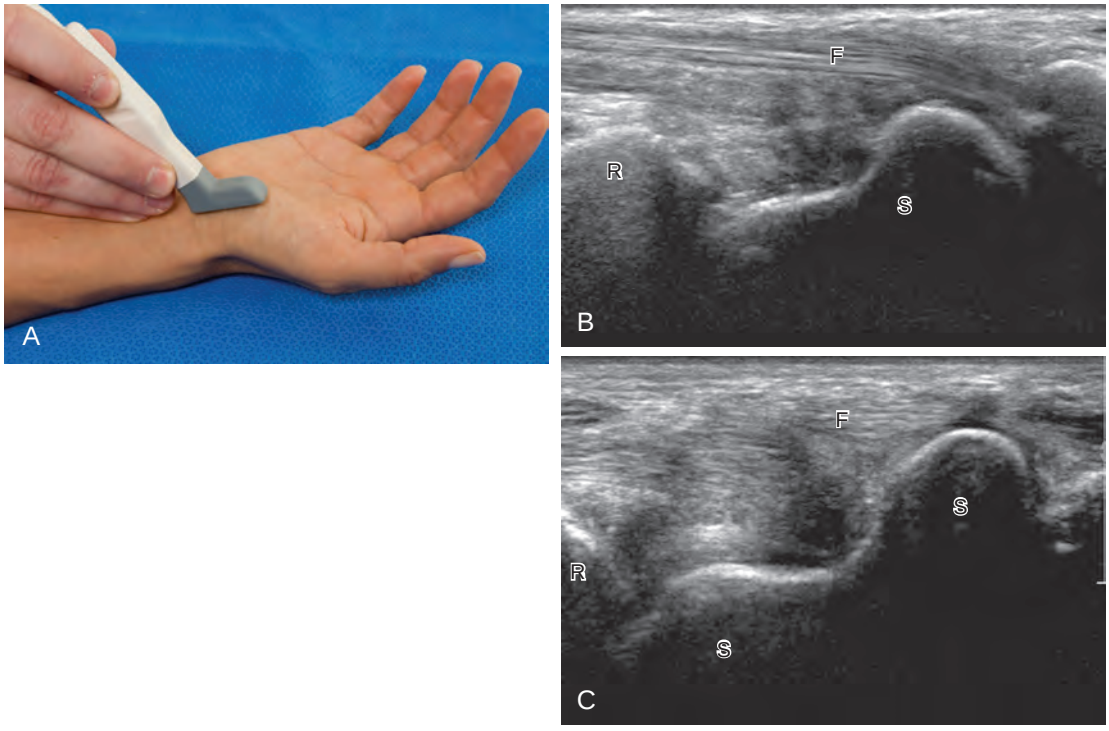

FIGURE 5-5 ■ Volar radial wrist evaluation (longitudinal). A, Sagittal-oblique imaging over the thumb base shows **(B** and **C)** the flexor carpi radialis tendon (F) and scaphoid (S). R, radius.

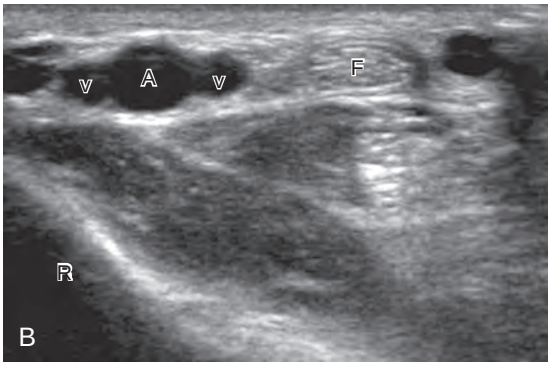

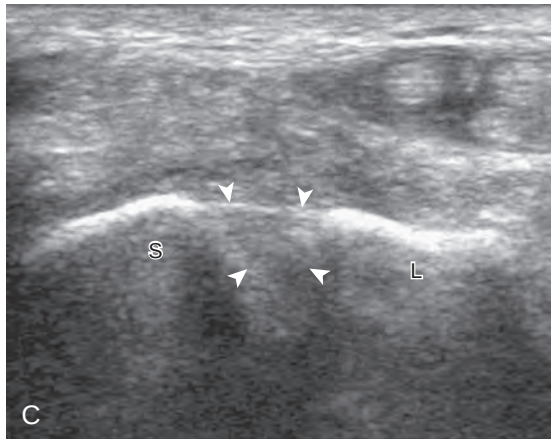

FIGURE 5-6 ■ Volar radial wrist evaluation (transverse). A, Transverse imaging shows **(B)** the flexor carpi radialis tendon (F), radial artery (A), and veins (v). Transverse imaging between scaphoid (S) and lunate (L) shows **(C)** volar portion of the scapholunate ligament *(arrowheads)*. R, radius.

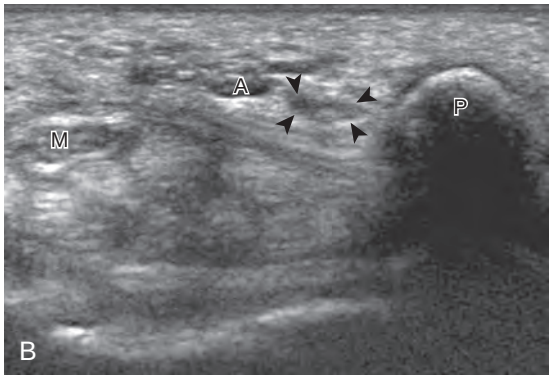

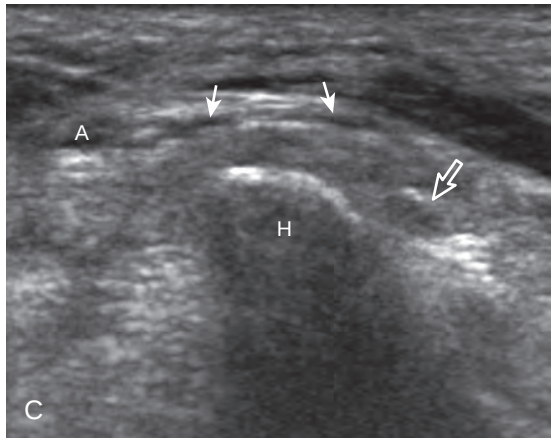

FIGURE 5-7 ■ Guyon canal evaluation (transverse). A, Transverse imaging over Guyon canal shows **(B)** the ulnar nerve *(arrowheads)* radial to the pisiform (P). Imaging distal to **B** over the hook of the hamate (H) shows **(C)** the superficial *(arrows)* and deep *(open arrow)* branches of the ulnar nerve. A, ulnar artery; M, median nerve.

the ulnar nerve and artery. The ulnar nerve branches, with a deep motor branch coursing along the ulnar side of the hamate hook and one to two predominantly sensory branches superficial to the hamate hook (see Fig. 5-7C). It is important to evaluate this area because ulnar nerve and artery abnormalities occur in this location as a result of compression by the adjacent hook of the hamate during trauma. Evaluation of the ulnar artery and nerve is also completed in long axis (Fig. 5-8). Another ulnar-sided tendon, the flexor carpi ulnaris, can also be identified by scanning proximal to the pisiform bone.

Wrist: Dorsal Evaluation

Dorsal Wrist Tendons and Dorsal Joint Recesses

The primary structures of the dorsal wrist are the various extensor and abductor tendons of the six wrist compartments and the dorsal radiocarpal, midcarpal, and distal radioulnar joint recesses. Evaluation of the dorsal tendons begins in the transverse plane over the Lister tubercle of the dorsal radius (Fig. 5-9A and B). This structure serves as an important starting point for dorsal wrist evaluation and assists in accurate identification of the wrist tendons. The Lister tubercle is seen as a pronounced bony prominence. If one has difficulty finding this structure with ultrasound, it can easily be palpated at physical examination. Once the Lister tubercle is identified, the tendon immediately ulnar to it is the extensor pollicis longus of the third wrist compartment (see Fig. 5-9B). Often there is an additional smaller dorsal radial protuberance at the ulnar aspect of the extensor pollicis longus as well. With movement of the transducer in the radial direction (see Fig. 5-9C), the extensor carpi radialis brevis and then the extensor carpi radialis longus tendons are seen in the second wrist compartment (Fig. 5-9D). On further radial movement of the transducer, the extensor pollicis brevis and abductor pollicis longus tendons are seen in the first wrist compartment (see Fig. 5-9D). It may be helpful to remember that the names of the tendons alternate from longus to brevis, beginning at the extensor pollicis longus and moving in a radial direction. The extensor pollicis longus tendon courses toward the first digit superficial to the extensor carpi radialis and ulnaris tendons in an oblique fashion proximally to distally. Therefore, when short axis to the extensor carpi radialis brevis and longus tendons and moving distally, the extensor pollicis longus is seen moving in an ulnar to radial direction over the extensor carpi radialis brevis and longus tendons (see Fig. 5-9E) (Video 5-4). In the region of the first extensor wrist compartment, the superficial branch of the radial nerve can be seen as it courses from the volar to the dorsal aspect of the distal forearm superficial to the first extensor wrist compartment tendons and extensor retinaculum, near branches of the cephalic vein (see Fig. 5-9F).

Beginning again in the transverse plane at the Lister tubercle, transducer movement ulnar from the extensor pollicis longus tendon (Fig. 5-10A) shows the extensor indicis and multiple tendons of the extensor digitorum in the fourth wrist compartment, and the extensor digiti minimi in the fifth wrist compartment near the distal radioulnar joint (see Fig. 5-10B). The posterior

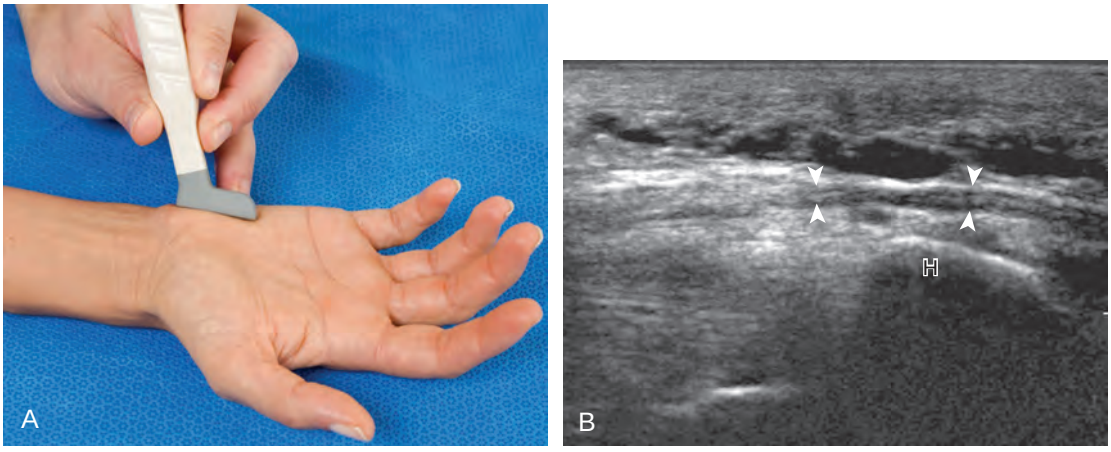

FIGURE 5-8 ■ Guyon canal evaluation (longitudinal). A, Sagittal imaging shows **(B)** the ulnar nerve *(arrowheads)* and hook of the hamate (H) (left side of image is proximal).

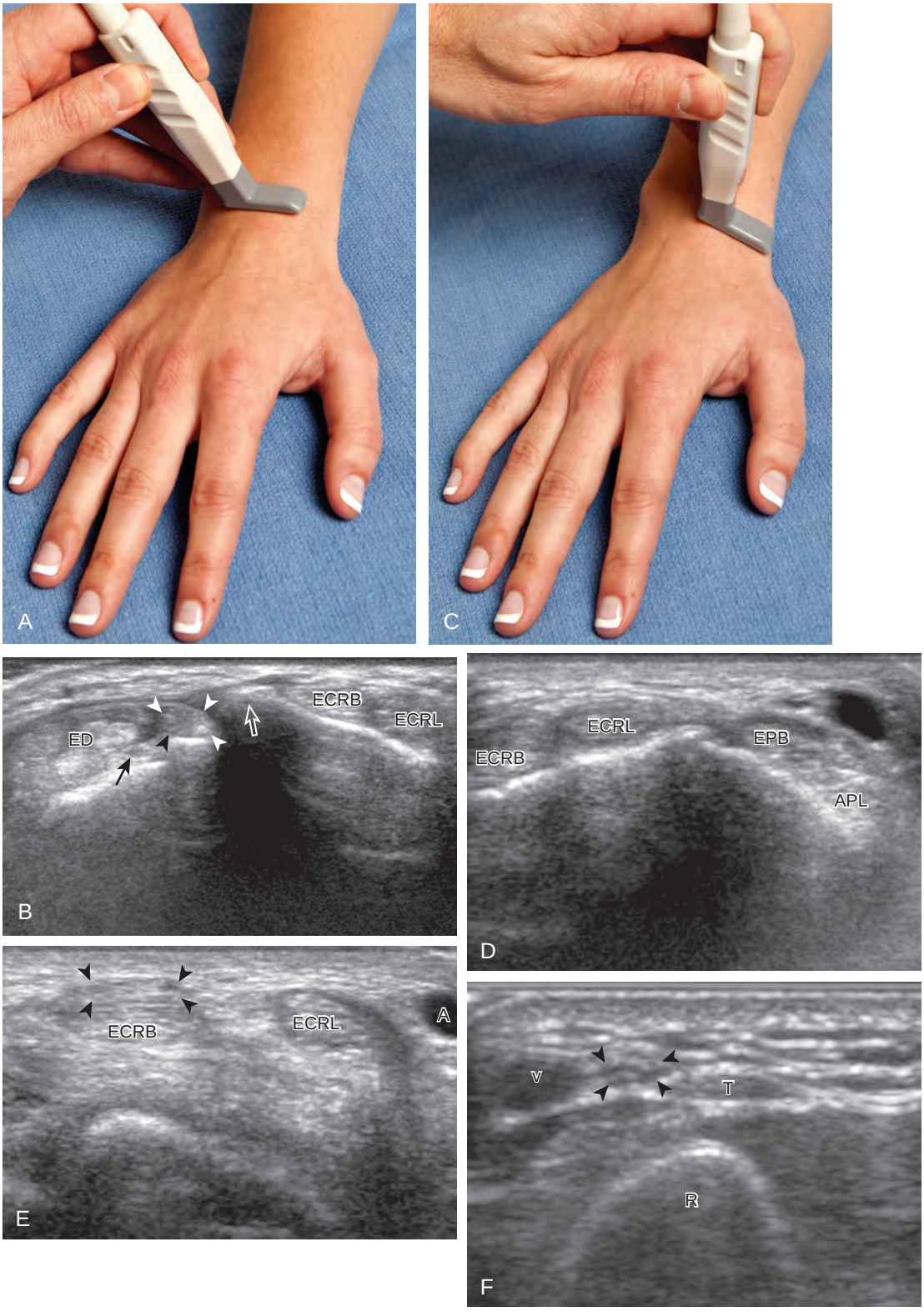

FIGURE 5-9 ■ Dorsal wrist evaluation (extensor compartments 1 to 3). A, Transverse imaging over the Lister tubercle of the radius shows **(B)** the extensor pollicis longus tendon *(arrowheads)* radial to the Lister tubercle *(open arrow)*. **C,** Transverse imaging radial to **A** shows **(D)** the second and first extensor compartment. Distal imaging over the second wrist compartment shows **(E)** the extensor pollicis longus *(arrowheads)* moving superficial to the extensor carpi radialis tendons. **F,** The superficial branch of the radial nerve *(arrowheads)* can be identified superficial to the first extensor wrist compartment (T) and near a branch of the cephalic vein (v) (*arrow,* posterior interosseous nerve). A, radial artery; APL, abductor pollicis longus; ECRB/L, extensor carpi radialis brevis and longus; ED, extensor digitorum; EPB, extensor pollicis brevis; R, radius.

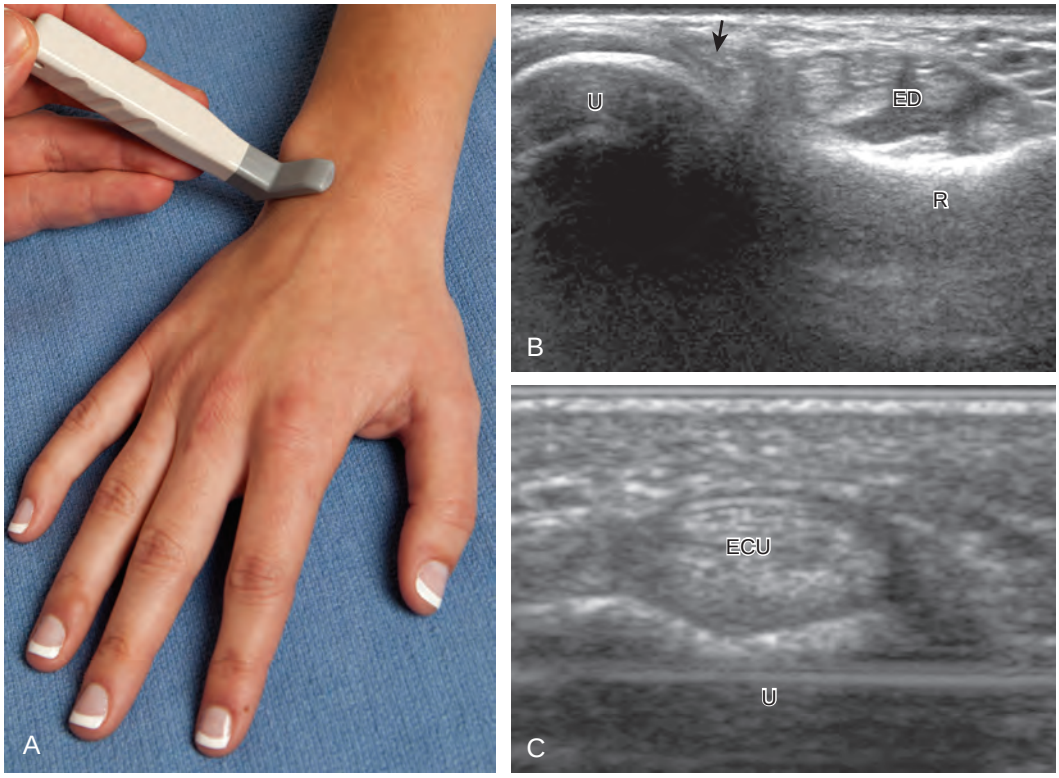

FIGURE 5-10 ■ **Dorsal wrist evaluation (extensor compartments 4 to 6). A,** Transverse imaging ulnar to that shown in Figure 5-9A shows **(B)** the extensor digitorum and extensor indicis (ED), the extensor digiti minimi *(arrow)*, and the distal radioulnar joint between the radius (R) and ulna (U). Transverse imaging over the lateral ulna shows **(C)** the extensor carpi ulnaris (ECU).

interosseous nerve is identified deep within the radial aspect of the fourth dorsal extensor compartment (see Fig. 5-9B).[7] Finally, over the most ulnar aspect of the ulna, the extensor carpi ulnar tendon is identified in a concave groove of the ulna in the sixth wrist compartment (see Fig. 5-10C). The extensor carpi ulnaris tendon often has a thin hypoechoic longitudinal cleft that should not be interpreted as a tendon tear. In addition, up to 50% of the extensor carpi ulnar tendon can be located outside of the groove and still be considered within normal.[8]

Each of the extensor tendons is also imaged in long axis throughout the wrist (Fig. 5-11). The extensor retinaculum courses transversely but slightly obliquely over the extensor tendons and appears hyperechoic, measuring up to 1.7 mm thick and 23 mm wide in cross section (see Fig. 5-11B).[9] If imaged oblique to the ultrasound beam, the extensor retinaculum can appear artifactually hypoechoic as a result of anisotropy, which should not be misinterpreted as tenosynovitis. Similar to the volar wrist, the dorsal recesses of the radiocarpal joint (between the radius and proximal carpal row), the midcarpal joint, and the distal radioulnar joint are identified with recognition of the characteristic bone contours for orientation. The radiocarpal and midcarpal joint recesses are optimally evaluated in the sagittal plane, whereas the distal radioulnar joint is evaluated in the transverse plane (see Fig. 5-10B).

Scapholunate Ligament (Dorsal Component) and Dorsal Ganglion Cysts

Similar to the dorsal tendons, evaluation of the scapholunate ligament begins in the transverse plane over the Lister tubercle (see Fig. 5-9A). The transducer is then moved distally. The bone contours of the radius are interrupted by the radiocarpal joint, so the next osseous structure in view is the scaphoid bone. With movement of the transducer in the ulnar direction, the adjacent lunate bone is brought into view. Between the dorsal aspects of the scaphoid and the lunate is a triangular area where one sees the dorsal aspect of the scapholunate ligament, which has a compact hyperechoic fibrillar echotexture (Fig. 5-12).[10] Directly superficial to the dorsal aspect of the scapholunate ligament, the dorsal radiocarpal ligament (or dorsal radiotriquetral ligament) is identified.[11,12] This area is also a common site for dorsal wrist ganglion cysts.

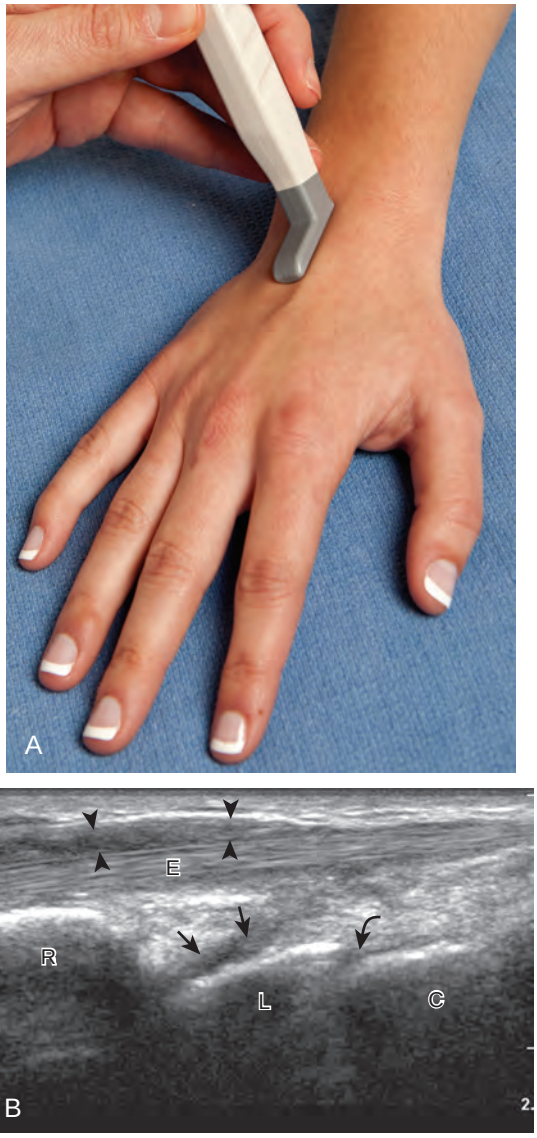

FIGURE 5-11 ■ Dorsal wrist evaluation (longitudinal). A, Sagittal imaging shows **(B)** the extensor retinaculum *(arrowheads)*, extensor tendons (E), and dorsal recesses of radiocarpal *(arrows)* and midcarpal *(curved arrow)* joints. C, capitate; L, lunate; R, radius.

Triangular Fibrocartilage Complex

The triangular fibrocartilage complex consists of the triangular fibrocartilage, the meniscus homologue, the extensor carpi ulnaris tendon sheath, and the volar and dorsal radiocarpal ligaments. For evaluation of the triangular fibrocartilage, the transducer is placed in the sagittal plane over the dorsal lateral wrist to identify the bone contours of the distal ulna and then moved toward the coronal plane with the wrist in slight radial deviation (Fig. 5-13A). A hyperechoic slab of tissue is identified as it extends from the ulnar

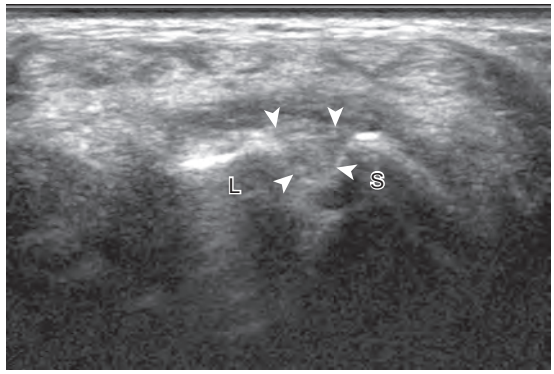

FIGURE 5-12 ■ Scapholunate ligament evaluation (dorsal component). Transverse imaging over the proximal carpal row shows the dorsal aspect of the scapholunate ligament *(arrowheads)*. L, lunate; S, scaphoid.

styloid base to the radius, which represents the triangular fibrocartilage (see Fig. 5-13B).[11] It is important to ensure complete evaluation of the triangular fibrocartilage to the radial attachment because this may be a site of traumatic tears. Evaluation of the triangular fibrocartilage can be difficult given its orientation in the transverse plane extending away from the transducer, and often a lower frequency is helpful. The meniscus homologue is seen as a hyperechoic triangular structure with its base adjacent to the extensor carpi ulnar tendon and in contact with the triquetrum, and this should not be mistaken for the triangular fibrocartilage, which is thinner and directly over the ulnar head.

Finger Evaluation

Volar

At the volar aspect of the finger in long axis (Fig. 5-14A), both the hyperechoic and fibrillar flexor digitorum superficialis and profundus tendons can be seen at the level of the metacarpophalangeal joint with the overlying A1 pulley (see Fig. 5-14B). The pulleys often have a trilaminar appearance at ultrasound. At close inspection, a pulley itself is fibrous, fibrillar, and therefore hyperechoic when imaged perpendicular to the sound beam; however, a normal pulley often appears hypoechoic relative to the adjacent superficial hyperechoic fat and connective tissue and from anisotropy. The trilaminar appearance consists of the superficial reflective surface of the pulley, the relatively hypoechoic pulley, and the deeper hyper-reflective surface of the adjacent flexor tendon sheath. With regard to imaging the flexor tendons in long axis, the individual tendons can be distinguished from each

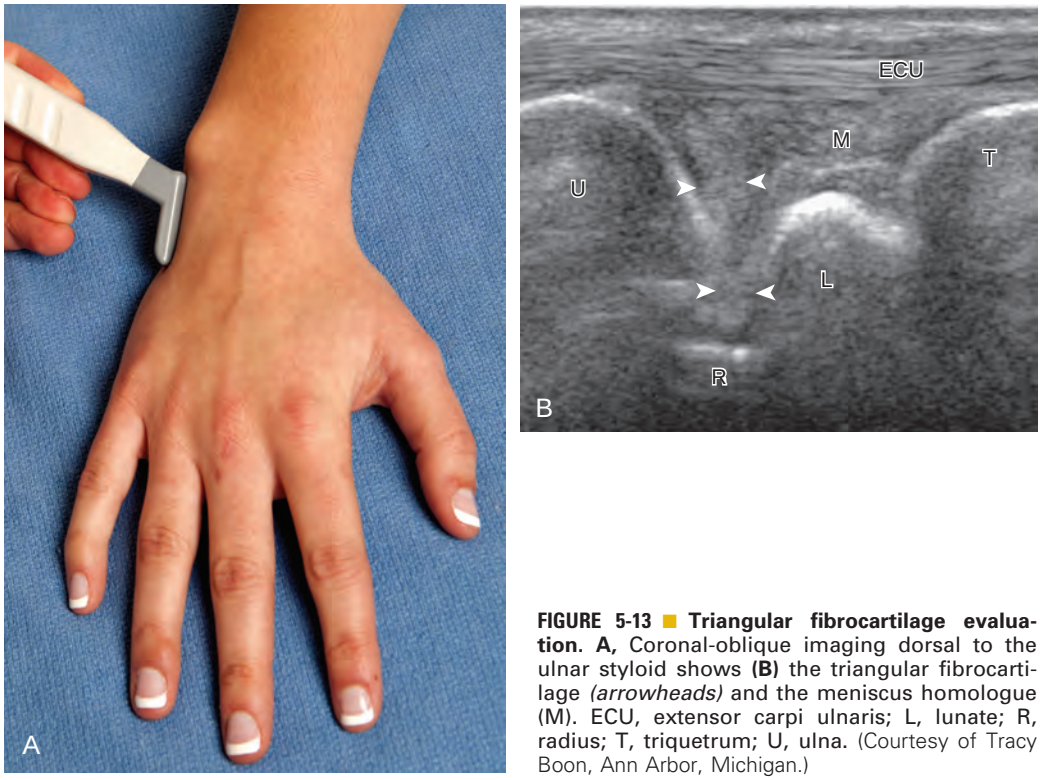

FIGURE 5-13 ■ Triangular fibrocartilage evaluation. A, Coronal-oblique imaging dorsal to the ulnar styloid shows **(B)** the triangular fibrocartilage *(arrowheads)* and the meniscus homologue (M). ECU, extensor carpi ulnaris; L, lunate; R, radius; T, triquetrum; U, ulna. (Courtesy of Tracy Boon, Ann Arbor, Michigan.)

other with isolated passive movement of the distal phalanx because this will cause movement of the flexor digitorum profundus. At the level of the proximal phalanx, the A2 pulley can be identified; slight obliquity of the transducer may make the pulley appear hypoechoic from anisotropy and can aid in its identification (see Fig. 5-14C). At the level of the proximal interphalangeal joint, the hyperechoic volar plate is identified (see Fig. 5-14D and E). The A3 and A4 pulleys are also identified superficial to the flexor tendons, at the level of the proximal interphalangeal joint and middle phalanx, respectively (see Fig. 5-14D).[2] Just distal to the proximal interphalangeal joint, the flexor digitorum superficialis inserts on the middle phalanx, whereas the flexor digitorum profundus extends distally over the volar plate of the distal interphalangeal joint to insert on the distal phalanx (see Fig. 5-14E). The flexor digitorum superficialis inserts on the middle phalanx by dividing into two bundles, with each segment moving around the flexor digitorum profundus tendon. This is best appreciated by imaging in short axis (Fig. 5-15A and B). More proximally over the palm of the hand (Fig. 5-16), the lumbrical and interosseous muscles can be identified, as can the common and proper palmar digital arteries and nerves. The volar metacarpophalangeal and interphalangeal joints are also evaluated in the sagittal plane for volar plate abnormality and joint recess distention from fluid or synovial disorders.

Dorsal

At the dorsal aspect of each digit, the thin, hyperechoic, and fibrillar extensor digitorum tendon extends over the metacarpophalangeal joint in the sagittal plane (Fig. 5-17A and B). At the level of the proximal interphalangeal joint, the central band of the extensor tendon inserts on the middle phalanx (see Fig. 5-17C and D). With movement of the transducer just off midline of the phalanx, the slips of the extensor tendon to the lateral bands can be seen (see Fig. 5-17E), which insert distally on the distal phalanx (see Fig. 5-17F). The ultrasound beam penetrates through the nail and allows visualization of the underlying hypoechoic nail bed, subungual space, and the surface of the distal phalanx (see Fig. 5-17F). At the level of the metacarpophalangeal joint, the transducer is positioned short axis to the extensor tendon, and the finger is flexed to evaluate for subluxation of the tendon, which would indicate extensor hood injury. The joints of each digit are also evaluated for distention from fluid or

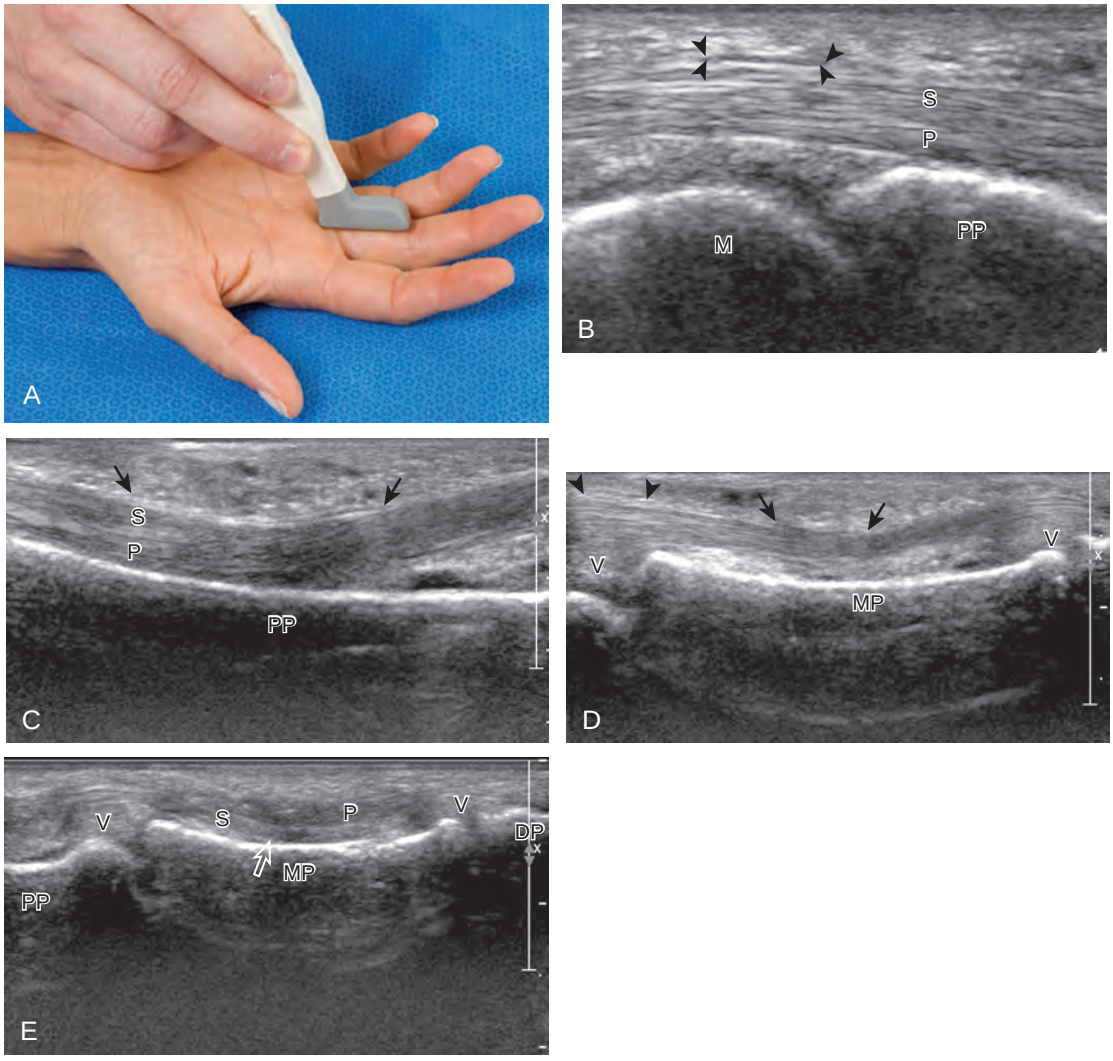

FIGURE 5-14 ■ Volar finger evaluation (longitudinal). A, Sagittal imaging of the volar finger **(B)** at the level of the metacarpophalangeal joint, **(C)** the proximal phalanx, and **(D** and **E)** the middle phalanx shows the flexor digitorum profundus (P) and superficialis (S) tendons and volar plates (V). Note **(B)** the A1 pulley *(arrowheads)*, **(C)** A2 pulley *(arrows)*, **(D)** A3 pulley *(arrowheads)*, and A4 pulley *(arrows)*. Note the attachment of the flexor digitorum superficialis *(open arrow)*. DP, distal phalanx; M, metacarpal; MP, middle phalanx; PP, proximal phalanx.

synovial hypertrophy, where often the dorsal joint recess is pronounced as it extends proximally beneath the extensor tendon. In addition, the hypoechoic hyaline articular cartilage of each joint can be visualized (see Fig. 5-17B), which is accessible with flexion of the digits (see Fig. 5-17G to I). A triangular region of connective tissue is normally found superficial to the metacarpophalangeal joint articulation (see Fig. 5-17H).[13]

Ligaments

The collateral ligaments of the digits can also be assessed with ultrasound in the coronal plane around each individual joint. To specifically evaluate the ulnar collateral ligament of the first metacarpophalangeal joint, the hand is placed around a rolled up towel, and the transducer is placed in the coronal plane relative to the first metacarpophalangeal joint (Fig. 5-18A). The ulnar collateral ligament will appear in long axis as hyperechoic with a compact fibrillar echotexture, extending from a broad concavity in the metacarpal to the proximal phalanx (see Fig. 5-18B). Because the subcutaneous fat directly overlying the ulnar collateral ligament is quite hyperechoic, the ligament may appear relatively hypoechoic but should be of relatively uniform thickness. Additionally, the ligament may appear

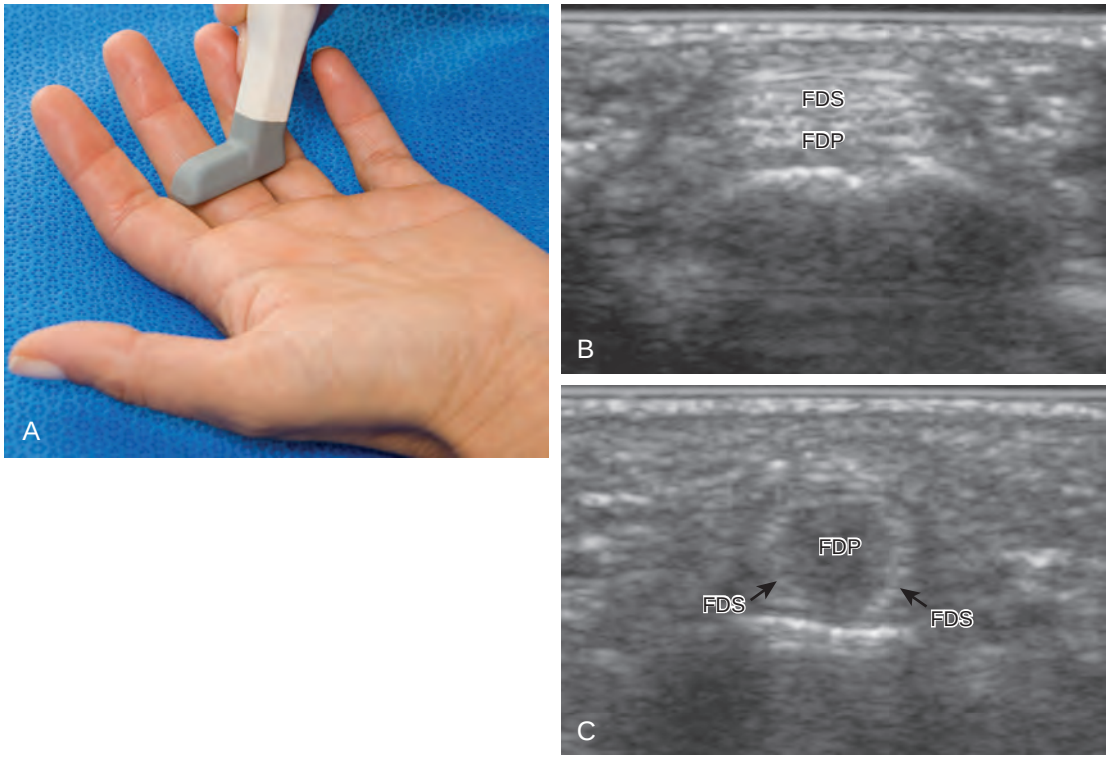

FIGURE 5-15 ■ Volar finger evaluation (transverse). A, Transverse imaging over the proximal phalanx **(B)** and middle phalanx **(C)** shows the flexor digitorum profundus (FDP) and superficialis (FDS) tendons.

artifactually hypoechoic where it is oblique to the sound beam from anisotropy. The overlying adductor pollicis aponeurosis, which is specific to the ulnar collateral ligament of the first metacarpophalangeal joint, is seen as a thin structure over the ulnar collateral ligament. Passive flexion of the interphalangeal joint will produce isolated movement of the adductor pollicis aponeurosis, which assists in its identification (Video 5-5). An additional dynamic maneuver in assessment of any collateral ligament is stressing the joint (valgus for ulnar ligaments, varus for radial ligaments). This is accomplished with minimal stress and is helpful because joint fluid will often move into the ligament tear under ultrasound visualization. Other ulnar and radial collateral ligaments

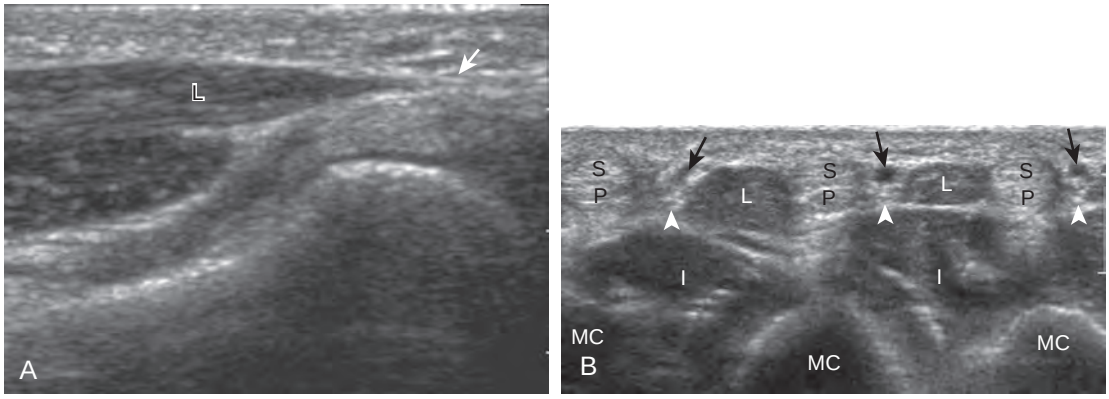

FIGURE 5-16 ■ Palmar hand evaluation (longitudinal). Parasagittal imaging **(A)** shows the distal aspect *(arrow)* of a lumbrical muscle (L). Transverse imaging **(B)** shows the flexor digitorum superficialis (S) and profundus (P) tendons, the common digital arteries *(arrows)* and nerves *(arrowheads)*, and interosseous muscles (I). MC, metacarpal.

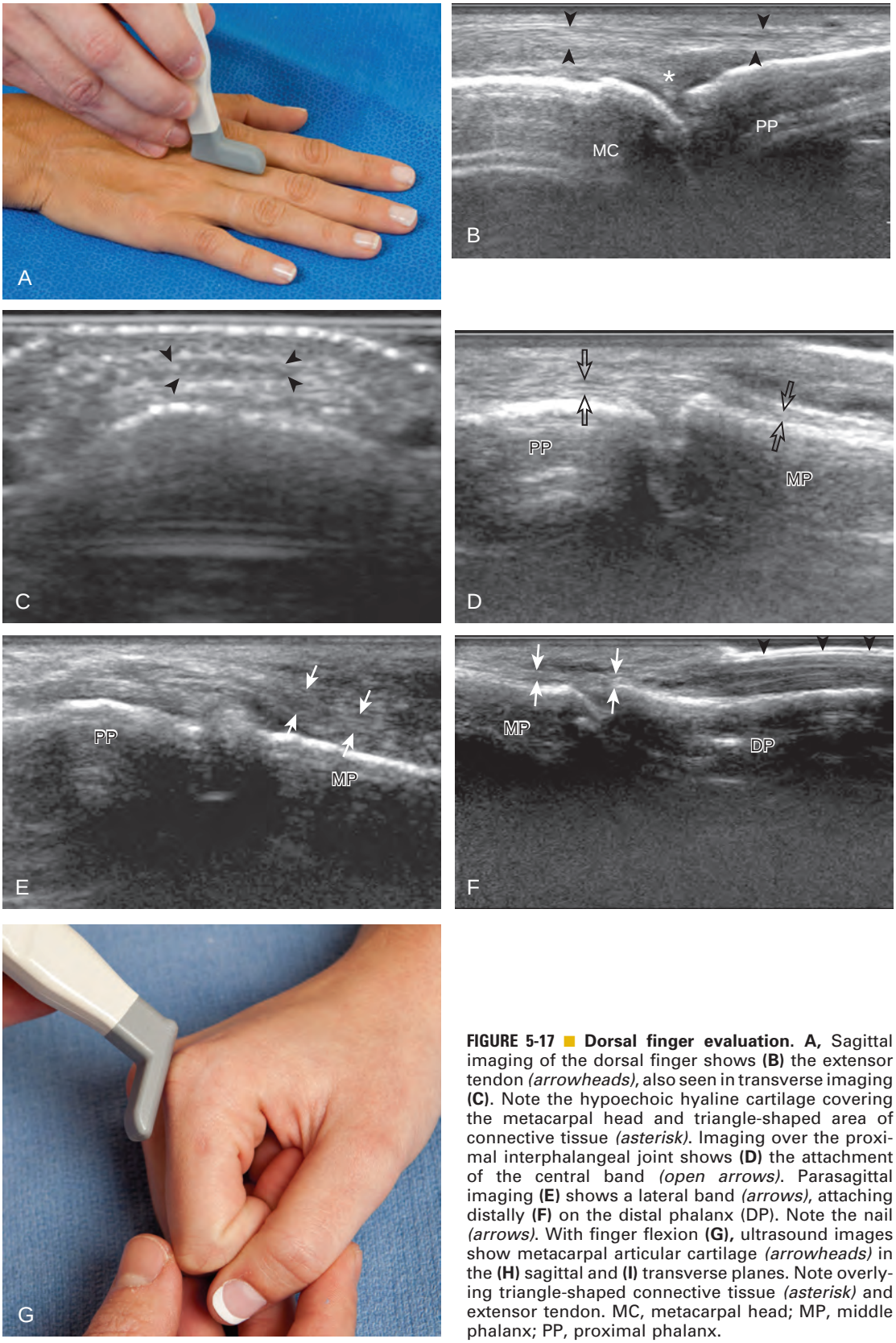

FIGURE 5-17 ■ Dorsal finger evaluation. A, Sagittal imaging of the dorsal finger shows **(B)** the extensor tendon *(arrowheads)*, also seen in transverse imaging **(C)**. Note the hypoechoic hyaline cartilage covering the metacarpal head and triangle-shaped area of connective tissue *(asterisk)*. Imaging over the proximal interphalangeal joint shows **(D)** the attachment of the central band *(open arrows)*. Parasagittal imaging **(E)** shows a lateral band *(arrows)*, attaching distally **(F)** on the distal phalanx (DP). Note the nail *(arrows)*. With finger flexion **(G),** ultrasound images show metacarpal articular cartilage *(arrowheads)* in the **(H)** sagittal and **(I)** transverse planes. Note overlying triangle-shaped connective tissue *(asterisk)* and extensor tendon. MC, metacarpal head; MP, middle phalanx; PP, proximal phalanx.

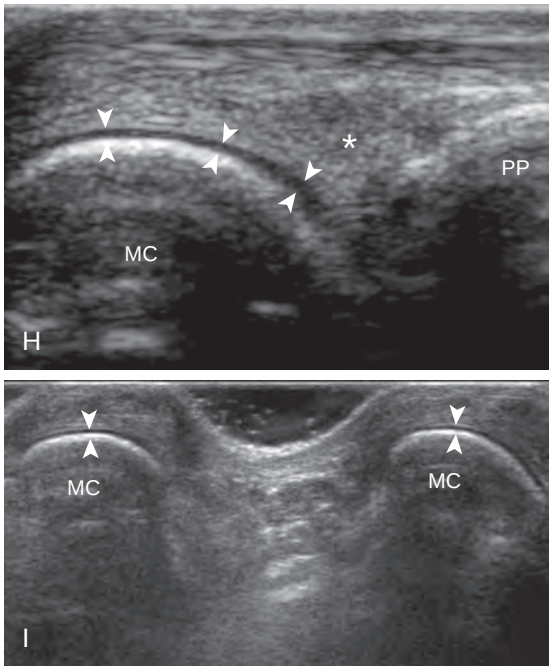

FIGURE 5-17, cont'd

of the digits similarly appear as compact and hyperechoic fibrillar structures, which extend across each joint. Any suspected ligament tear can be assessed using dynamic imaging with valgus and varus joint angulation under ultrasound visualization.

JOINT ABNORMALITIES

Because there are multiple synovial articulations of the hand and wrist, it is important to evaluate each individual site for joint abnormalities. In the sagittal plane, the volar and dorsal recesses of the radiocarpal and midcarpal joints are assessed for abnormal distention (Fig. 5-19A and B). The distal radioulnar joint is assessed from both dorsal and volar aspects in the transverse plane (see Fig. 5-19C). The digits are assessed in the sagittal plane over each joint, including the dorsal and volar joint recesses (see Fig. 5-19D and E) (Video 5-6). Anechoic distention of a joint recess typically represents simple fluid, although possible etiologies include degenerative, reactive, traumatic, and inflammatory causes; if there is concern for infection, ultrasound-guided aspiration should be considered. In the setting of trauma, one must evaluate the osseous structures at any focal area of symptoms for step-off deformity, which would indicate fracture.

If a joint recess distention is not anechoic, considerations include complex fluid versus synovial hypertrophy (Figs. 5-20 and 5-21). Differentiation between these two etiologies may be difficult because both may appear hypoechoic or isoechoic compared with the overlying subcutaneous tissues. If joint recess distention collapses with transducer pressure or joint movement (see Video 5-6), or if swirling of echoes within the recess is identified, and if there is no internal flow on color or power Doppler imaging, then complex fluid is suspected. In contrast, if there is no displacement, little compressibility of the joint recess, and flow on color or power Doppler imaging, then synovial hypertrophy is likely (see Fig. 5-21) (Video 5-7).[14] Ultrasound-guided aspiration may be needed to make this determination. Because dorsal wrist

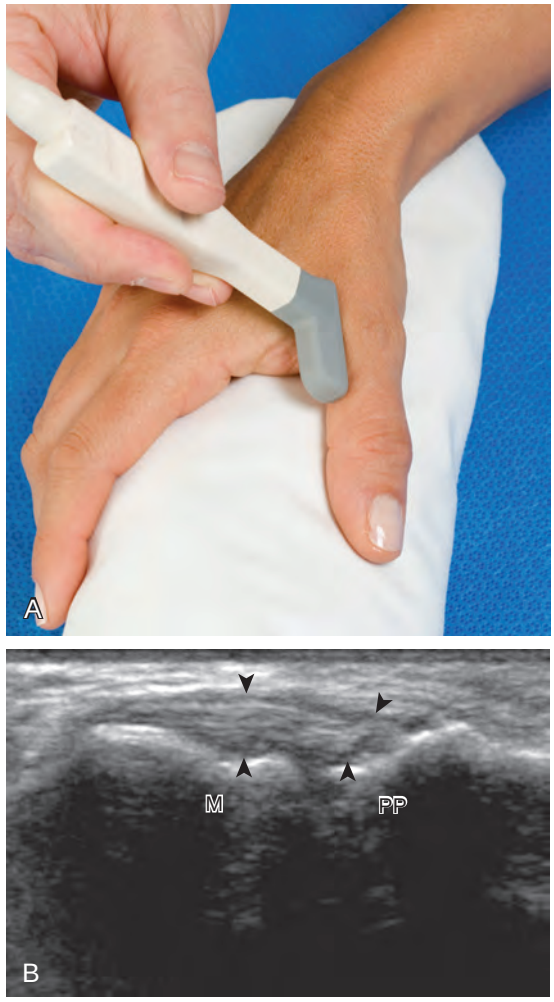

FIGURE 5-18 ■ Ulnar collateral ligament of thumb. A, Coronal imaging over the ulnar collateral ligament of the first metacarpophalangeal joint shows **(B)** the fibrillar appearance of the ulnar collateral ligament *(arrowheads)*. Note the characteristic contours of the metacarpal at the ulnar collateral ligament attachment. M, metacarpal; PP, proximal phalanx.

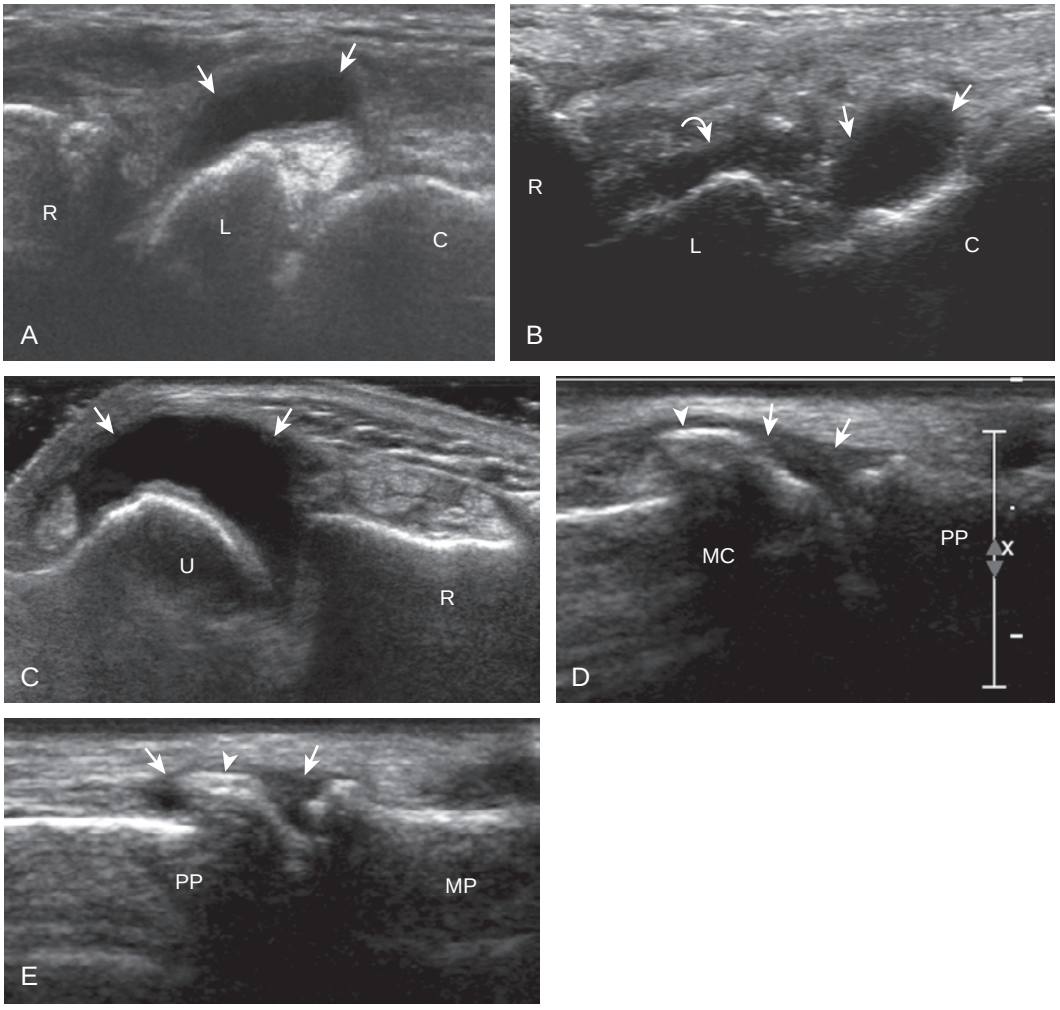

FIGURE 5-19 ■ Joint effusion. Sagittal ultrasound images over the dorsal wrist in two different patients show **(A)** anechoic distention *(arrows)* of the radiocarpal joint dorsal recess, and **(B)** anechoic distention *(arrows)* of the midcarpal joint dorsal recess. Note collapsed radiocarpal joint recess *(curved arrow)* in **B.** Ultrasound image in the transverse plane shows **(C)** anechoic distention *(arrows)* of the distal radioulnar joint dorsal recess. Sagittal ultrasound images of the **(D)** metacarpophalangeal and **(E)** proximal interphalangeal joints show dorsal recess distention *(arrows)*. Note dorsal osteophytes from osteoarthritis *(arrowheads)*. C, capitate; L, lunate; MC, metacarpal; MP, middle phalanx; PP, proximal phalanx; R, radius; U, ulna.

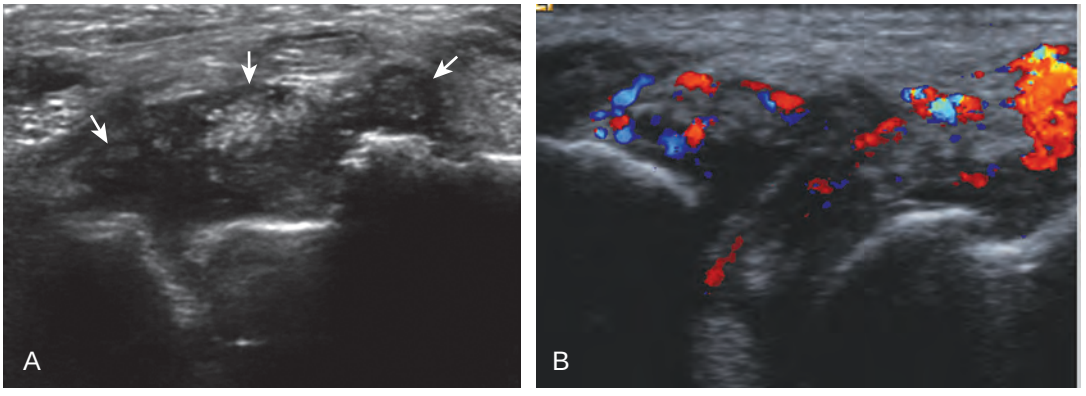

FIGURE 5-20 ■ Complex joint effusion: pseudogout. Transverse gray-scale **(A)** and color Doppler **(B)** ultrasound images over dorsal radiocarpal joint recess show mixed echogenicity but predominantly hypoechoic distention *(arrows)* and hyperemia.

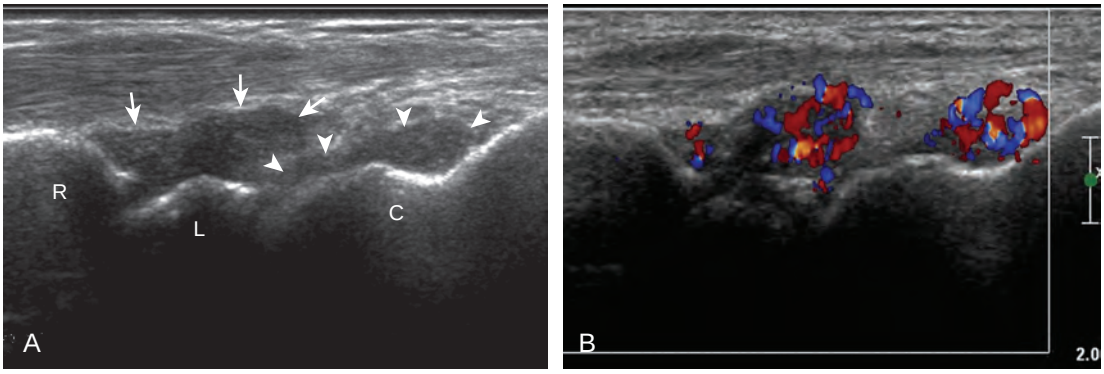

FIGURE 5-21 ■ Synovial hypertrophy: rheumatoid arthritis. Sagittal gray-scale **(A)** and color Doppler **(B)** ultrasound images over the dorsal wrist show hypoechoic distention of the radiocarpal *(arrows)* and midcarpal *(arrowheads)* dorsal joint recesses with hyperemia. C, capitate; L, lunate; R, radius.

ganglion cysts occur at the site of the dorsal radiocarpal joint recess and may appear similar, dynamic imaging with compression and joint movement also helps in their differentiation because a ganglion cyst is multilocular and noncompressible, whereas a fluid-filled joint recess is compressible (see Fig. 5-87) (see Video 5-6).[15] Possible etiologies for both complex fluid and synovial hypertrophy include hemorrhage and inflammation, which includes infection (Fig. 5-22), rheumatoid arthritis (Fig. 5-23), and gout (Fig. 5-24).

Synovial hypertrophy appears as nondisplaceable and poorly or noncompressible distention of a joint recess that is hypoechoic or less frequently isoechoic or hyperechoic compared with the adjacent subdermal fat (Fig. 5-25) (Video 5-8).[16] Active inflammatory synovitis is usually hypoechoic with hyperemia on color or power Doppler imaging. When evaluating

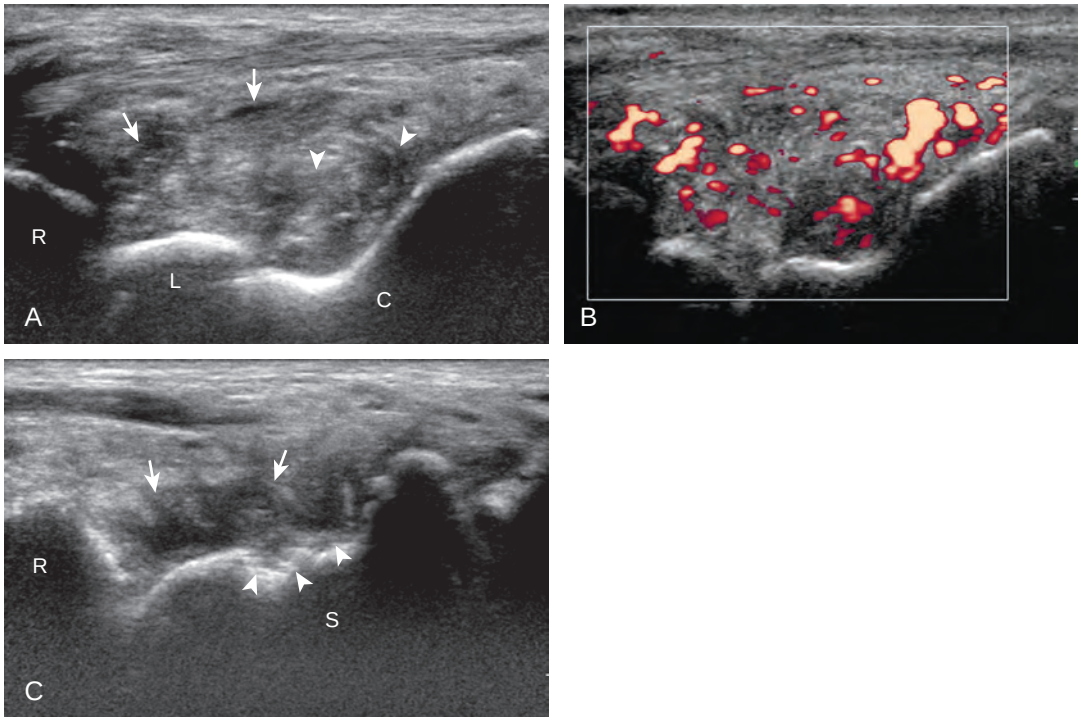

FIGURE 5-22 ■ Synovial hypertrophy: fungal infection. Sagittal gray-scale **(A)** and color Doppler **(B)** ultrasound images over the dorsal wrist show mixed echogenicity distention of the radiocarpal *(arrows)* and midcarpal *(arrowheads)* dorsal joint recesses with hyperemia. Sagittal-oblique ultrasound image shows **(C)** radiocarpal joint dorsal joint recess distention with scaphoid (S) erosions *(arrowheads)*. C, capitate; L, lunate; R, radius.

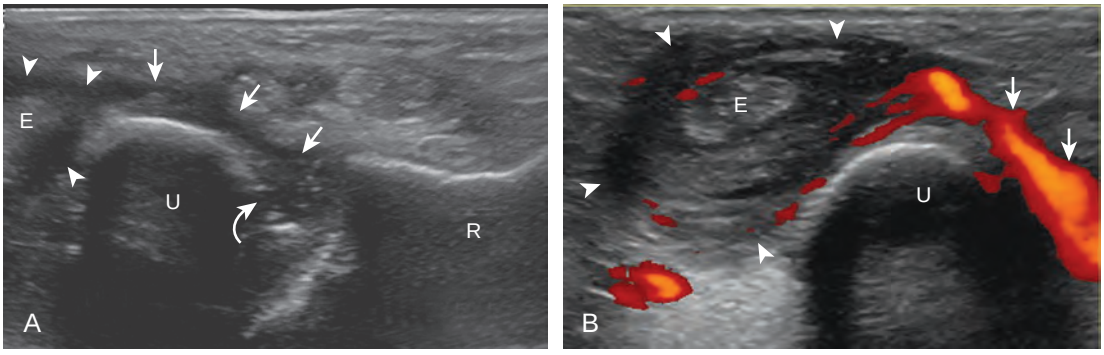

FIGURE 5-23 ■ Synovial hypertrophy: rheumatoid arthritis. A, Transverse ultrasound images show hypoechoic synovial hypertrophy distending the dorsal recess of the distal radioulnar joint *(arrows)* with hyperemia **(B)** and erosion *(curved arrow)*. Note adjacent tenosynovitis *(arrowheads)* of extensor carpi ulnaris tendon (E). R, radius; U, ulna.

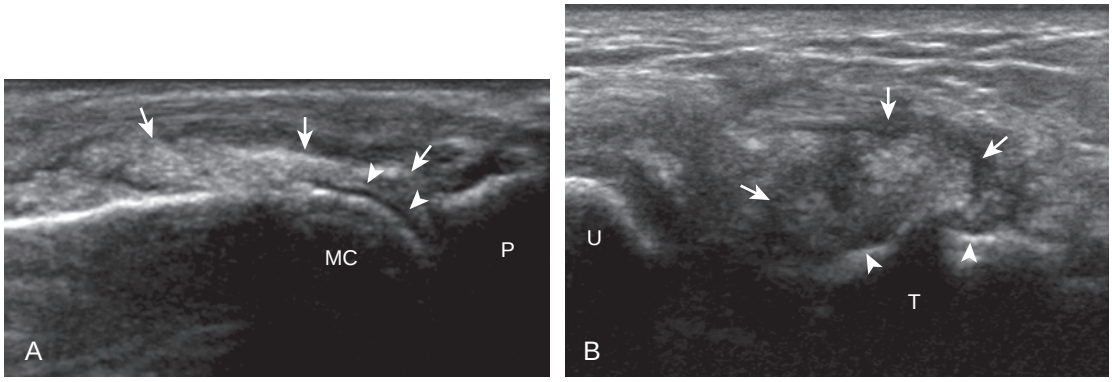

FIGURE 5-24 ■ Complex joint fluid and tophus: gout. A, Sagittal ultrasound image of the metacarpophalangeal joint shows echogenic effusion *(arrows)* and hyaline cartilage icing *(arrowheads)* from urate crystals. **B,** Coronal ultrasound image shows echogenic tophus with hypoechoic halo *(arrows)* with adjacent carpal erosions *(arrowheads)*. MC, metacarpal head; P, proximal phalanx; T, triquetrum; U, ulna.

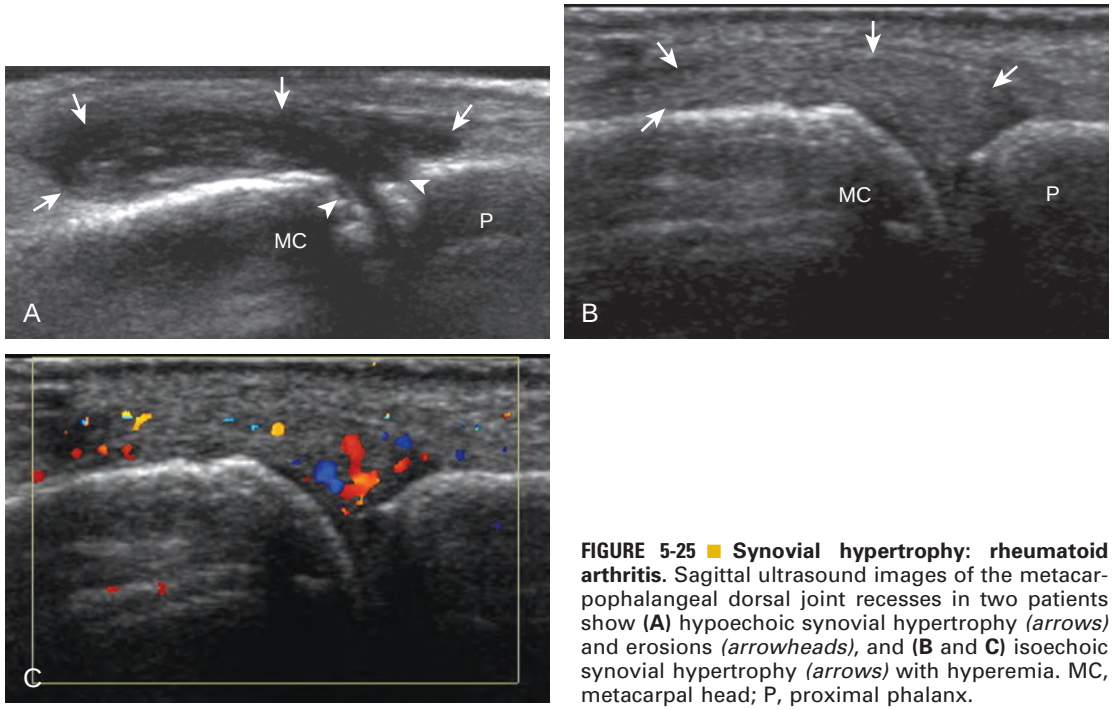

FIGURE 5-25 ■ Synovial hypertrophy: rheumatoid arthritis. Sagittal ultrasound images of the metacarpophalangeal dorsal joint recesses in two patients show **(A)** hypoechoic synovial hypertrophy *(arrows)* and erosions *(arrowheads)*, and **(B** and **C)** isoechoic synovial hypertrophy *(arrows)* with hyperemia. MC, metacarpal head; P, proximal phalanx.

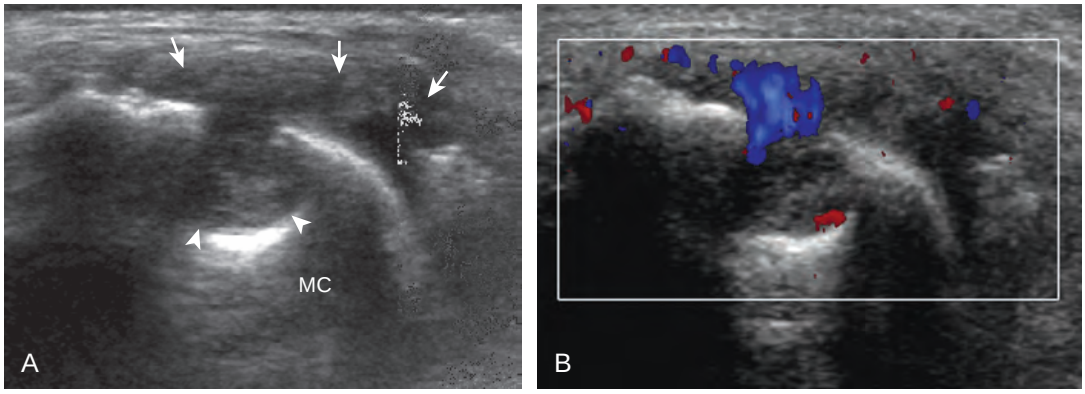

FIGURE 5-26 ■ Erosions: rheumatoid arthritis. Coronal ultrasound image of the second metacarpal head shows hypoechoic and isoechoic synovial hypertrophy *(arrows)* that extends into the metacarpal (MC) erosion *(arrowheads)* with hyperemia in **B.**

superficial structures, it is important to float the transducer on a thick layer of gel so as to not compress the vascularity (see Fig. 2-29 in Chapter 2) (Video 5-9). Minimal synovial thickening without hyperemia is not specific for one diagnosis and may be seen with osteoarthritis. Assessing multiple joints and review of history, laboratory values, and radiographic findings are important for the synthesis of a concise diagnosis of arthritis. Synovial proliferative disorders such as pigmented villonodular synovitis and synovial osteochondromatosis are other considerations. In the latter condition, superimposed hyperechoic calcifications may be seen in the synovial tissue.

If inflammatory synovitis is suspected, it is important to evaluate the hypoechoic hyaline articular cartilage and the subjacent bone cortex for erosions (Figs. 5-26 to 5-29). Thinning or

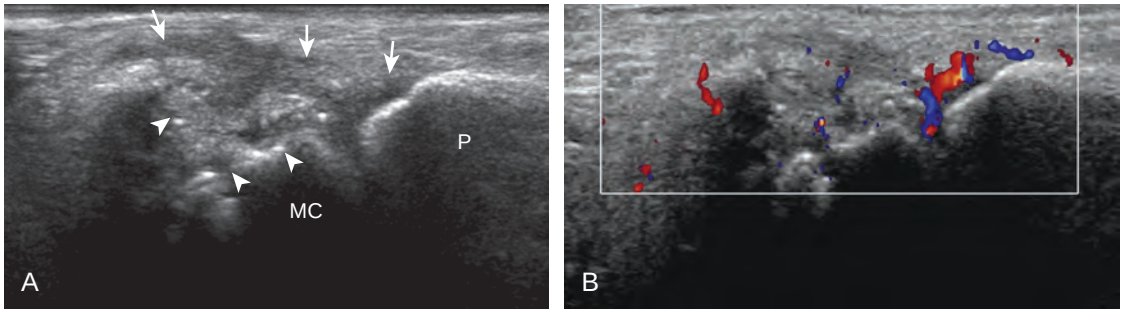

FIGURE 5-27 ■ Erosions: rheumatoid arthritis. Sagittal ultrasound image of the second metacarpal head shows synovial hypertrophy that ranges from hypoechoic to hyperechoic *(arrows)* that extends into the metacarpal (MC) erosion *(arrowheads)* with hyperemia in **B.** P, proximal phalanx.

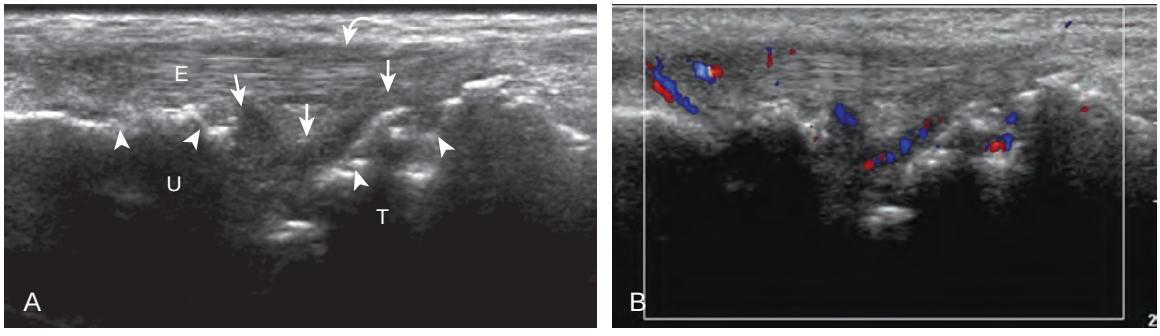

FIGURE 5-28 ■ Erosions: rheumatoid arthritis. Coronal ultrasound image over lateral wrist shows predominantly hypoechoic synovial hypertrophy *(arrows)* with erosions *(arrowheads)* of the ulna (U) and triquetrum (T) with hyperemia in **B.** Note tenosynovitis *(curved arrow)* of the extensor carpi ulnaris tendon (E).

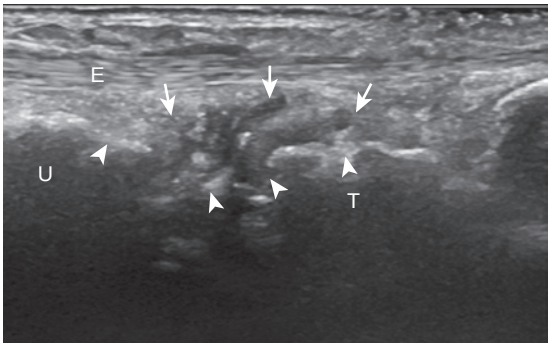

FIGURE 5-29 ■ Erosions: rheumatoid arthritis. Coronal ultrasound image over lateral wrist shows mixed echogenicity synovial hypertrophy *(arrows)* with diffuse erosions *(arrowheads)* of the ulna (U) and triquetrum (T) with hyperemia. E, extensor carpi ulnaris tendon.

defects of the hyaline cartilage may be identified. An erosion appears as discontinuity or irregularity of the normally smooth and hyperechoic bone visible in two planes.[16,17] When a bone erosion is suspected, the presence of adjacent synovitis increases the likelihood of a true erosion. Compared with radiography, ultrasound is more sensitive in detection of hand and wrist erosions and has the benefit of evaluating synovial thickness and hyperemia.[18] When a potential erosion is seen at ultrasound, correlation with history, radiography, and other joints is essential because a false-positive rate of 29% has been reported; prominent concavities of the distal metacarpals and irregular osteophytes may simulate erosions.[19] A small depression in the dorsal metacarpal at the edge of the hyaline cartilage can be a normal variation, especially at the second metacarpal (Fig. 5-30); unlike an erosion, this depression is smooth and shallow without cortical disruption or adjacent synovial hypertrophy.[13] The finding of a true erosion with overlying synovitis is not specific for one diagnosis because many inflammatory conditions can produce these findings.

Because ultrasound is very sensitive in the identification of bone cortex surface abnormalities and irregularity, it is important to consider the various causes of such findings. In addition to an erosion, bone proliferation from a seronegative spondyloarthropathy or an osteophyte from osteoarthritis may also appear as cortical irregularity, and correlation with history, distribution of findings, and radiographs is essential. Bone irregularity from degenerative change can be differentiated from seronegative spondyloarthropathy in several ways. With degenerative change, bone proliferation is at the margins of a synovial articulation (osteophytes) (Fig. 5-31; see Fig. 5-19D and E), whereas bone proliferation with spondyloarthropathy can occur anywhere along the surface of a bone and particularly occurs at tendon or ligament attachments with possible hyperemia (Fig. 5-32). Inflammatory enthesopathy is also characterized by an abnormal hypoechoic tendon or ligament at their attachment site, with possible hyperemia, in association with bone proliferation or erosion at the tendon or ligament attachment.[20]

There are various protocols for inflammatory arthritis screening of the wrist and hand. With regard to rheumatoid arthritis, the second metacarpal is an important target to assess because it is a frequent site of involvement; assessment in the coronal plane at the radial aspect should complement dorsal assessment (see Fig. 5-26). Evaluation of the dorsal recess of the three wrist joints (radioulnar, radiocarpal, midcarpal), as well as the third metacarpophalangeal, is also essential.[14] It has been shown that proximal interphalangeal

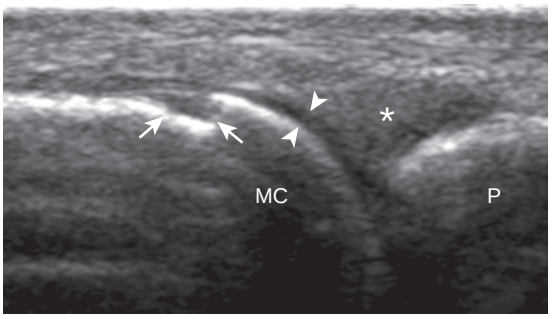

FIGURE 5-30 ■ Metacarpal head pseudoerosion. Sagittal ultrasound image over the dorsum of the second metacarpal shows shallow pseudoerosion *(arrows)*. Note hyaline cartilage *(arrowheads)* of metacarpal head (MC), proximal phalanx (P), and triangle-shaped connective tissue *(asterisk)*.

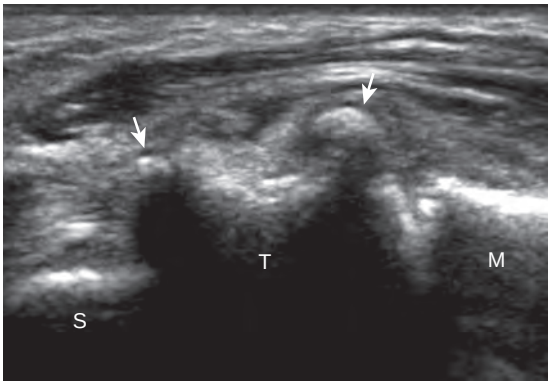

FIGURE 5-31 ■ Osteophytes: osteoarthritis. Ultrasound image over thumb base shows trapezium (T) osteophytes *(arrows)* at articulations with scaphoid (S) and first metacarpal (M).

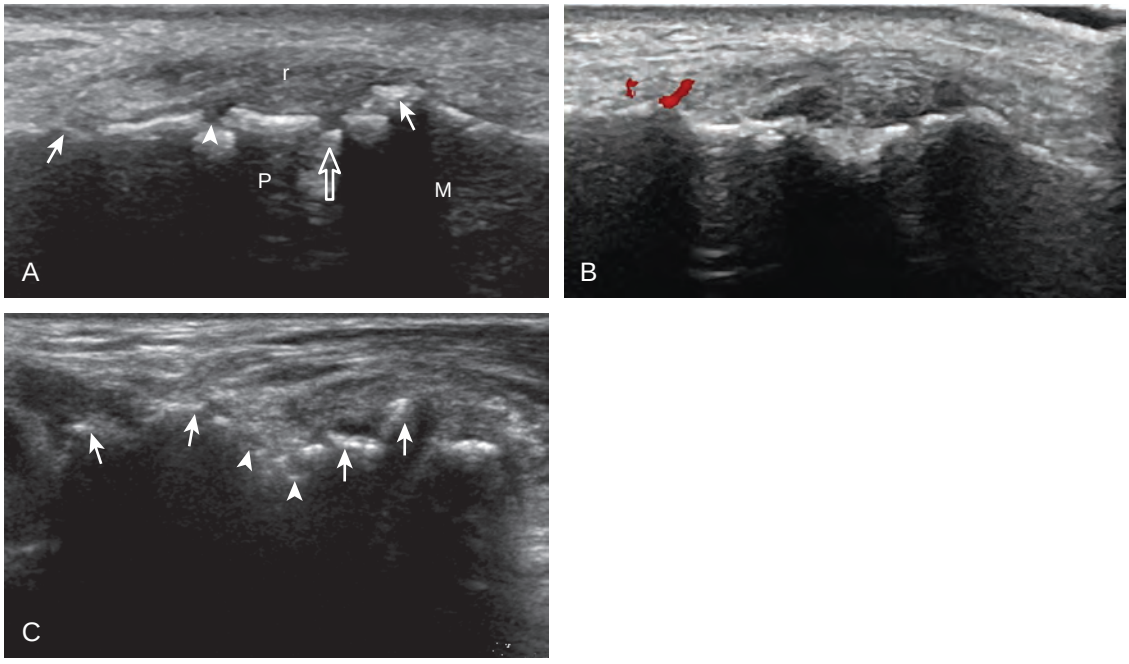

FIGURE 5-32 ■ Enthesopathy: psoriatic arthritis. A and **B,** Ultrasound images long axis to the radial collateral ligament (r) of a proximal interphalangeal joint *(open arrow)* show areas of bone proliferation at the ligament attachments *(arrows)* and an erosion *(arrowhead)* with adjacent hypoechoic soft tissue swelling and **(B)** hyperemia. **C,** Transverse ultrasound image over the dorsal wrist shows diffuse areas of bone proliferation *(arrows)* and erosions *(arrowheads)* with overlying hypoechoic soft tissue swelling. M, middle phalanx; P, proximal phalanx.

joint assessment should include both dorsal and volar imaging.[21,22] Focused assessment at any symptomatic site should also be completed, with consideration for the fifth metatarsophalangeal joint of the foot, another common site of rheumatoid arthritis involvement.[23] A limited examination of the hand and wrist for assessment of rheumatoid arthritis has been proposed, which includes the joints of the wrist, the index and long fingers (metacarpophalangeal and proximal interphalangeal joints), and second and fifth metatarsophalangeal joints.[24] However, a global or comprehensive examination of all key and symptomatic joint recesses of the wrist and hand for synovial hypertrophy can easily be accomplished with ultrasound. With regard to other inflammatory arthritis conditions, ultrasound assessment may be directed by symptoms or radiographic findings. For example, bone proliferation of psoriatic arthritis may occur anywhere, including the carpus or a single digit at ligament attachments (see Fig. 5-32). A gouty tophus may also occur at variable sites (Fig. 5-33) (Video 5-10), and one may also see monosodium urate crystals as complex fluid (see Fig. 5-24A) or layering over the hyaline cartilage (the double contour sign) (Fig. 5-34).

TENDON AND MUSCLE ABNORMALITIES

Possible tendon abnormalities of the wrist and hand include tenosynovitis (and paratendinitis if inflammation surrounds a tendon that has no tendon sheath), tendinosis, and tendon tear. Tenosynovitis is characterized by distention of

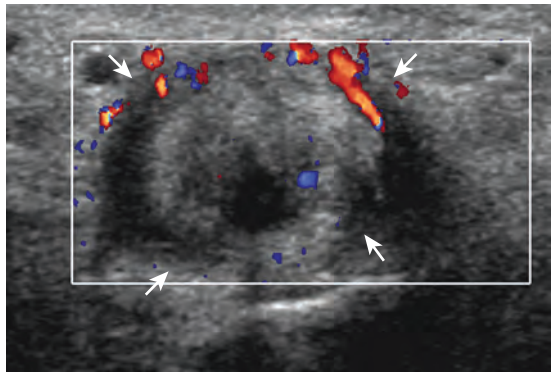

FIGURE 5-33 ■ Tophus: gout. Ultrasound image shows hyperechoic tophus with hypoechoic halo *(arrows)* and surrounding hyperemia.

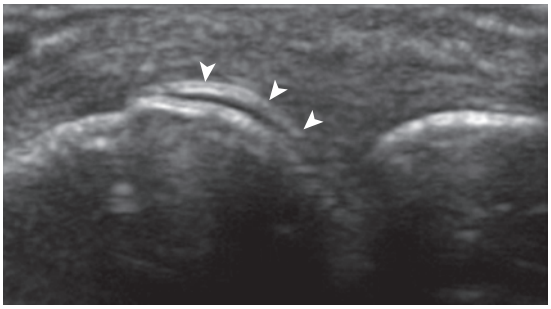

FIGURE 5-34 ■ Cartilage icing: gout. Ultrasound image over the metacarpophalangeal joint shows a hyperechoic outer margin of the articular cartilage *(arrowheads)* from urate icing, termed the *double contour sign*.

the synovial sheath around the tendon. Similar to a joint recess, distention of a tendon sheath may be predominantly anechoic (Figs. 5-35 and 5-36) (Video 5-11). If tendon sheath distention is not anechoic, possibilities include complex fluid versus synovial hypertrophy (Fig. 5-37). Compressibility, movement of internal echoes with transducer pressure, and lack of flow on color and power Doppler imaging suggest complex fluid rather than synovial hypertrophy, whereas noncompressibility and flow on color Doppler imaging suggest synovial hypertrophy (Video 5-12).[25] Synovial hypertrophy may appear hypoechoic, isoechoic, or hyperechoic compared with subdermal fat (Fig. 5-38). Tenosynovitis may cause erosion of an adjacent bone, such as the ulnar styloid with rheumatoid arthritis (Fig. 5-39). Regardless of appearance, possible etiologies of tenosynovitis include degenerative, traumatic, proliferative, and inflammatory, including crystal deposition (Figs. 5-40 and 5-41) (Video 5-13) and infection (Fig. 5-42).[26] It is important not to mistake the normal appearance of the extensor retinaculum at the level of the radiocarpal joint dorsally for tenosynovitis; the normal hyperechoic retinaculum may appear artifactually hypoechoic due to anisotropy, which adds to the potential confusion (see Fig. 5-11B).[9]

A specific stenosing tenosynovitis involves the extensor pollicis brevis and abductor pollicis longus tendons in the first dorsal wrist compartment, which is called *de Quervain disease*.[26] This condition is characterized by thickening of the tissues around the involved tendons, with

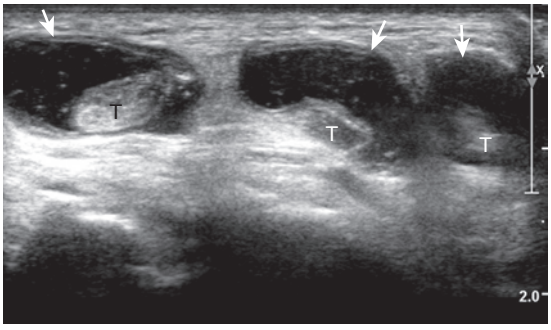

FIGURE 5-35 ■ Tenosynovitis: rheumatoid arthritis. Ultrasound over the dorsal wrist in short axis to the extensor tendons (T) shows predominantly anechoic fluid distention of the tendon sheath *(arrows)*.

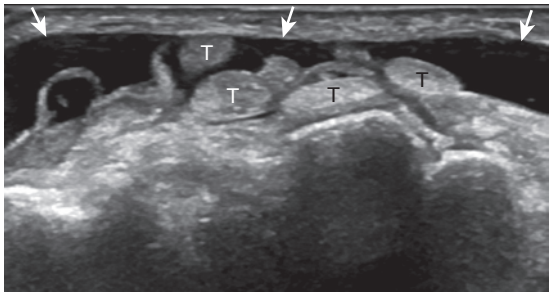

FIGURE 5-36 ■ Tenosynovitis: pseudogout. Ultrasound over the dorsal wrist in short axis to the extensor tendons (T) shows anechoic fluid distention of the tendon sheath *(arrows)*.

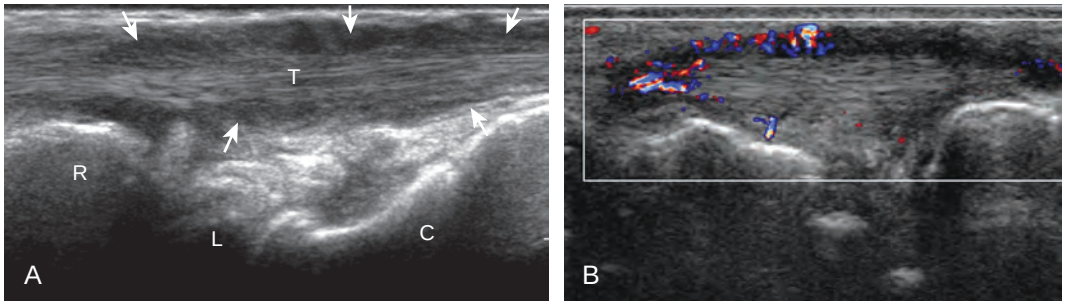

FIGURE 5-37 ■ Tenosynovitis: rheumatoid arthritis. A, Gray-scale and **(B)** color Doppler ultrasound images in long axis to the extensor tendons of the wrist (T) show hypoechoic synovial hypertrophy *(arrows)* with increased flow on color Doppler imaging. C, capitate; L, lunate; R, radius.

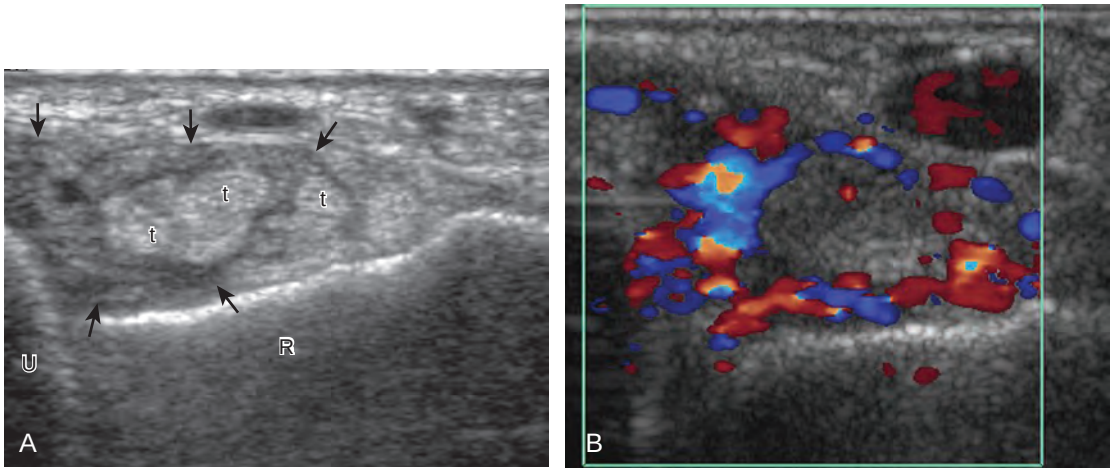

FIGURE 5-38 ■ Tenosynovitis: systemic lupus erythematosus. A, Gray-scale and **(B)** color Doppler ultrasound images in short axis to the extensor tendons of the wrist (t) show hypoechoic to isoechoic synovial hypertrophy *(arrows)* with increased flow on color Doppler imaging. R, radius; U, ulna.

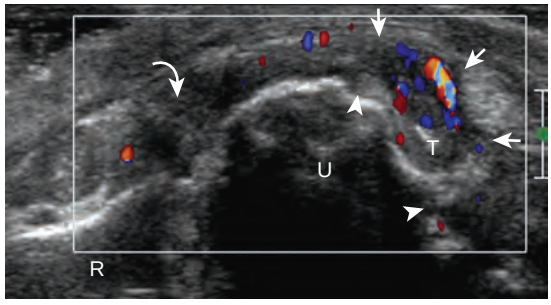

FIGURE 5-39 ■ Tenosynovitis: rheumatoid arthritis. Color Doppler ultrasound image in short axis to the extensor carpi ulnaris tendon (T) shows hypoechoic tenosynovitis with increased blood flow *(arrows)* and ulna (U) erosions *(arrowheads)*. Note synovial hypertrophy from the distal radioulnar joint *(curved arrow)* as well as increased blood flow and abnormal hypoechogenicity of the extensor carpi ulnaris. R, radius.

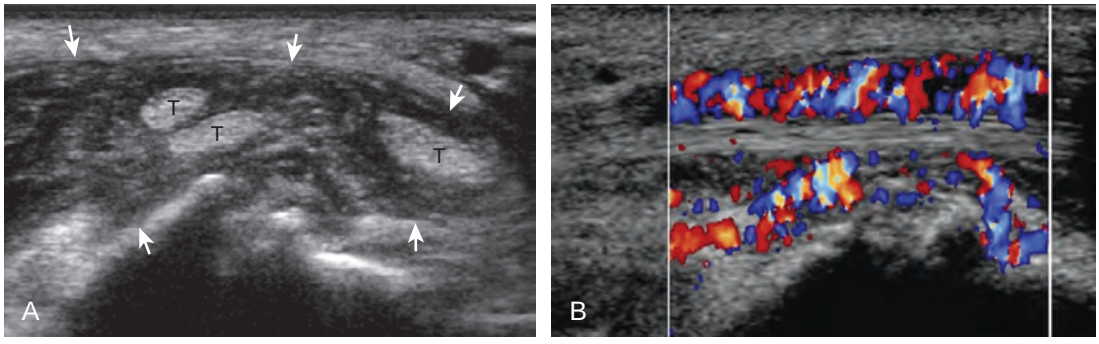

FIGURE 5-40 ■ Tenosynovitis: gout. A, Gray-scale short axis and **(B)** color Doppler long axis ultrasound images of the wrist extensor tendons (T) at the level of the radiocarpal joint show hypoechoic synovial hypertrophy with increased flow on color Doppler imaging *(arrows)*.

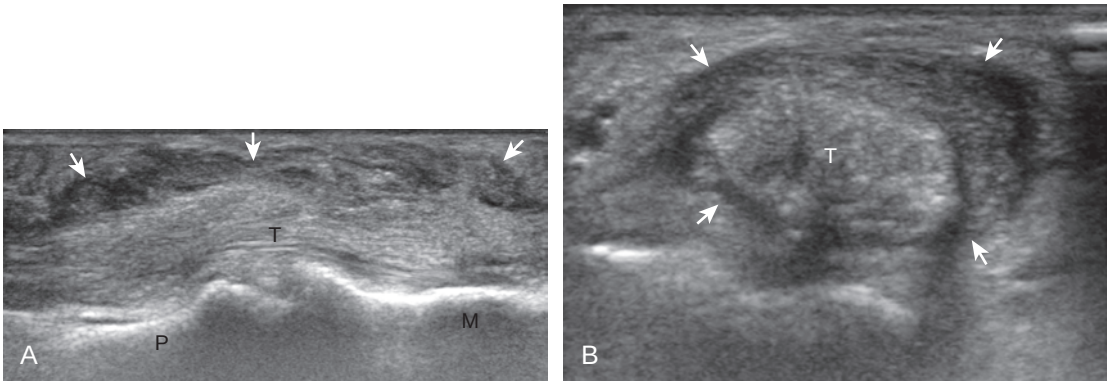

FIGURE 5-41 ■ Tenosynovitis: gout. Ultrasound images in **(A)** long axis and **(B)** short axis to the flexor tendons of the finger (T) show hypoechoic to isoechoic synovial hypertrophy *(arrows)*. M, middle phalanx; P, proximal phalanx.

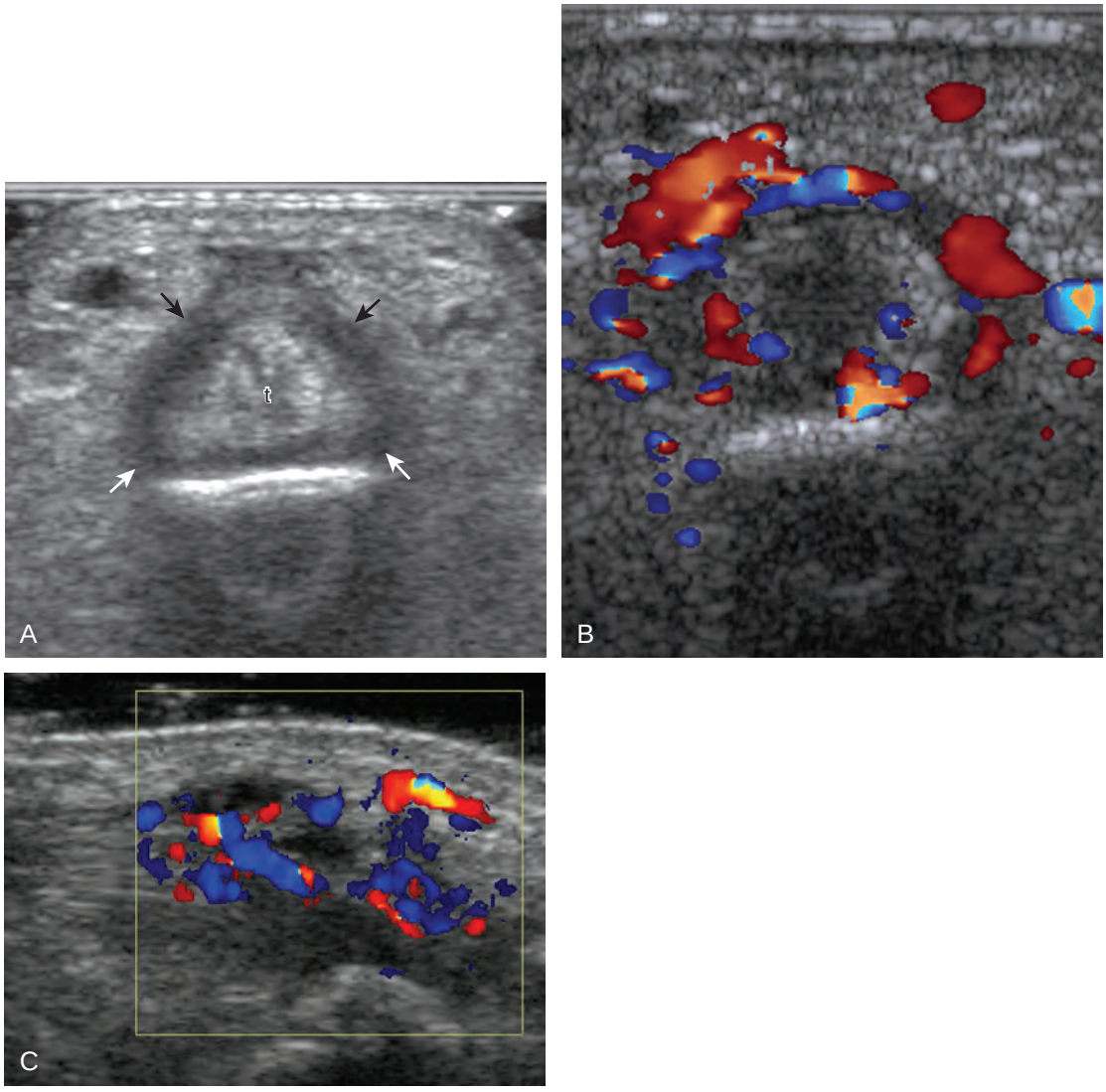

FIGURE 5-42 ■ Tenosynovitis: infection. Ultrasound images in **(A** and **B)** short axis to the flexor tendons of the finger and **(C)** long axis to the flexor tendons of the finger show hypoechoic synovial hypertrophy *(arrows)* with hyperemia. t, tendon.

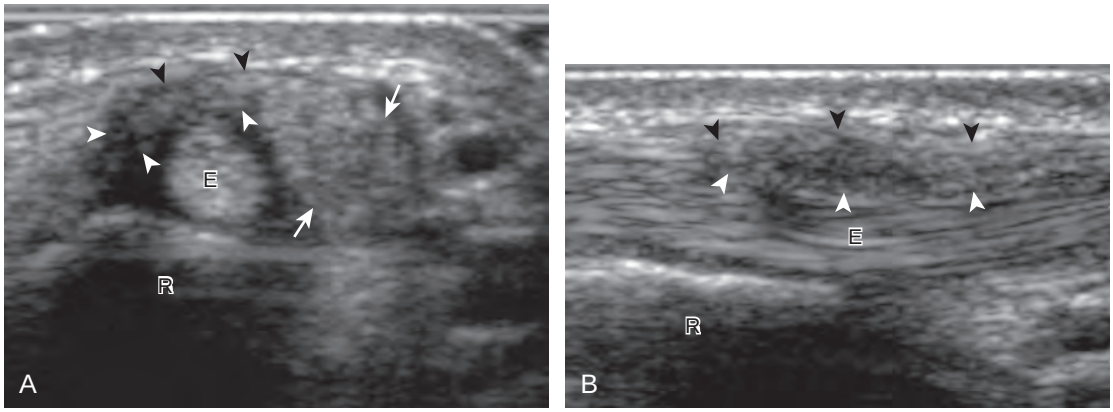

FIGURE 5-43 ■ De Quervain disease. Ultrasound images in **(A)** short axis and **(B)** long axis to the first extensor wrist tendons show hypoechoic thickening of the tendon sheath *(arrowheads)* with hypoechoic swelling of the abductor pollicis longus tendon *(arrows)*. E, extensor pollicis brevis tendon; R, radius. (From Jacobson JA, Miller BS, Morag Y: Golf and racquet sports injuries. *Semin Musculoskelet Radiol* 9:346–359, 2005.)

possible hyperemia, tendinosis, and cortical irregularity of the radius, associated with pain (Figs. 5-43 and 5-44) (Videos 5-14 and 5-15).[27] The tendon sheath is thickened at the level of the radius, typically dorsally adjacent to the extensor pollicis brevis tendon, and associated tenosynovial fluid may only be seen proximal or distal to the retinaculum. A hypoechoic septum-like structure is often present that causes subcompartmentalization of the first extensor compartment, possibly with an osseous ridge, which is important when injection of the tendon

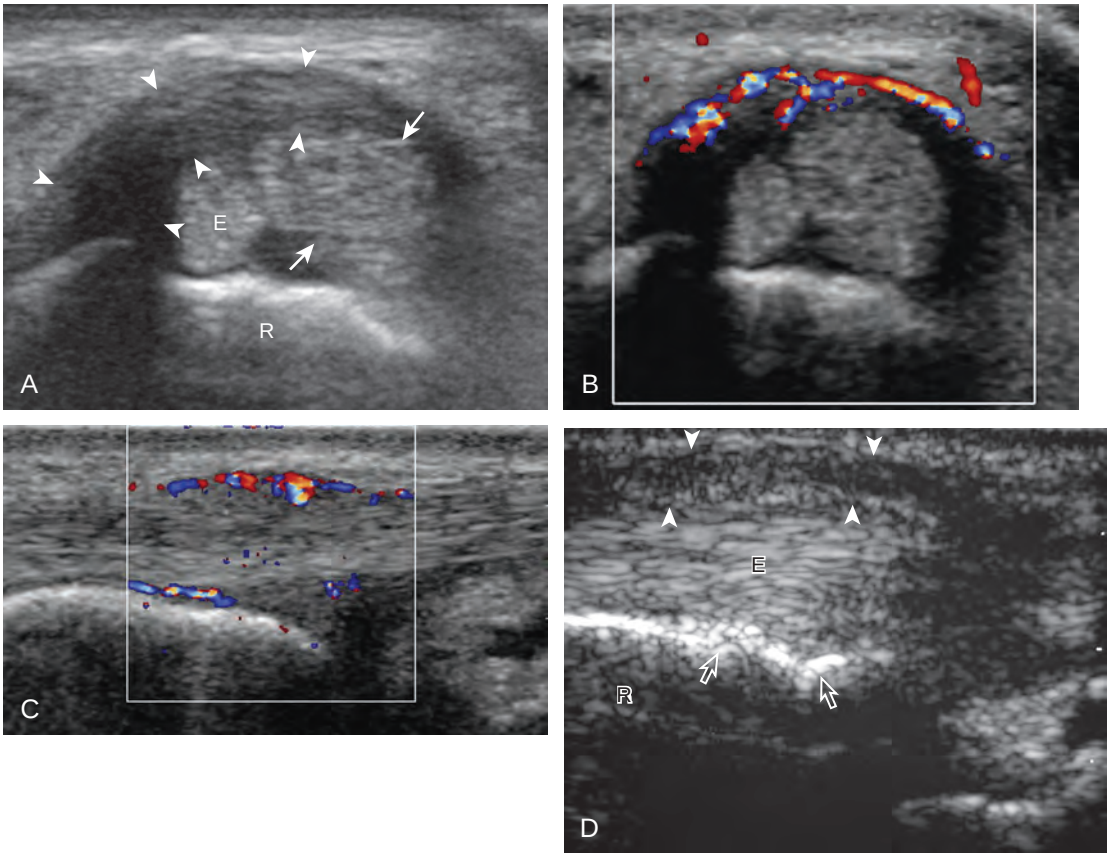

FIGURE 5-44 ■ De Quervain disease. Ultrasound images in **(A)** short axis and color Doppler **(B)** short axis and **(C)** long axis to first extensor wrist tendons show hypoechoic tendon sheath thickening *(arrowheads)* and increased flow on power Doppler imaging. Ultrasound image in **(D)** long axis in a second patient shows hypoechoic tendon sheath thickening *(arrowheads)* and cortical irregularity *(arrows)* of the radius (R). E, extensor pollicis brevis tendon.

sheath is considered.[28,29] The abductor pollicis longus tendon may also have multiple tendon slips, which should not be mistaken for longitudinal tendon tears.[28,29]

Other tendon abnormalities include tendinosis and tendon tear. Tendinosis represents tendon degeneration, typically from overuse, and is characterized by hypoechoic swelling without disruption of tendon fibers (Fig. 5-45). Involvement from psoriatic arthritis may also cause hypoechoic thickening of a tendon and adjacent soft tissues, often with adjacent enthesopathy (Fig. 5-46).[30] In the setting of inflammatory arthritis, abnormal tendon hypoechogenicity and increased flow on color or power Doppler imaging can indicate true tendinitis (see Figs. 5-39 and 5-46) (see Video 5-13). Calcium hydroxyapatite deposition appears hyperechoic with variable shadowing and may cause calcific tendinosis (Fig. 5-47). Partial tendon fiber disruption indicates partial-thickness tendon tear (Fig. 5-48). Involvement of the flexor carpi radialis tendon near the trapezium may be associated with osteoarthrosis (see Fig. 5-45B).[6] The finding of complete fiber disruption indicates a full-thickness tendon tear (Figs. 5-49 and 5-50).[31] Tendon injuries in the digits may also include bone avulsions, which will appear as a hyperechoic fragment (Fig. 5-51). This finding is best confirmed on radiography. In this setting, tendon retraction typically occurs, which is a helpful finding that indicates a full-thickness tear. If there is a question of partial versus full-thickness tendon tear, dynamic imaging with passive and active tendon movement can show either continuous fiber movement excluding a full-thickness tear (Video 5-16) or lack of tendon translation across the abnormal site, which would indicate a full-thickness tear. Dynamic evaluation is also important for a diagnosis of tendon subluxation. The extensor carpi ulnaris subluxation is considered abnormal if greater than 50% of the tendon moves beyond the osseous groove in the ulna (Fig. 5-52) (Video 5-17).[8] Extensor tendon subluxation can be seen during finger flexion with extensor hood injuries, termed *boxer knuckle* (Fig. 5-53).[32] If the patient has symptoms of intermittent snapping, clicking, or popping, the patient is asked to reproduce the symptom while evaluating the area with ultrasound.

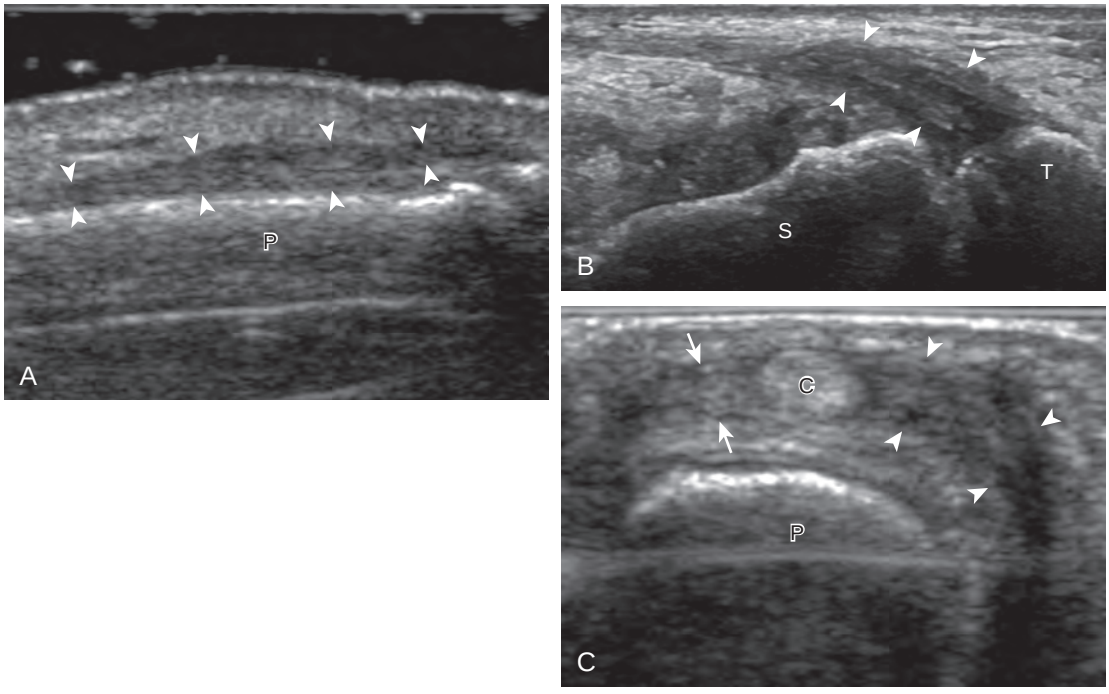

FIGURE 5-45 ■ **Tendinosis.** Ultrasound images in **(A)** long axis to the extensor tendon over the proximal phalanx, **(B)** long axis to the flexor carpi radialis tendon, and **(C)** short axis to the extensor tendon in three different patients show hypoechoic thickening of the tendon *(arrowheads)* in **A** and **B** and hypoechoic thickening of the extensor tendon sagittal band in **C** (*arrows*, normal sagittal band). C, central band of extensor tendon; P, phalanx; S, scaphoid; T, trapezium.

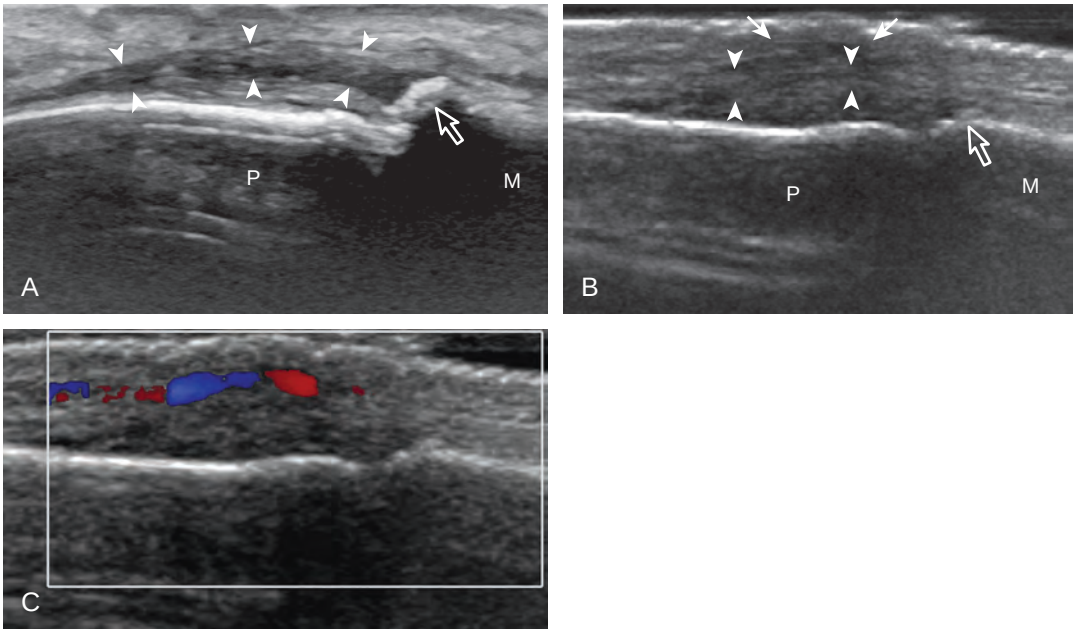

FIGURE 5-46 ■ Tendinitis: psoriatic arthritis. Ultrasound images in long axis to the extensor tendon at the proximal interphalangeal joint show **(A)** hypoechoic tendon thickening *(arrowheads)* and enthesopathy *(open arrow)*, and in another patient **(B)** hypoechoic tendon thickening *(arrowheads)*, enthesopathy *(open arrow)*, and adjacent hypoechoic swelling *(arrows)* with increased blood flow in **(C)**. M, middle phalanx; P, proximal phalanx.

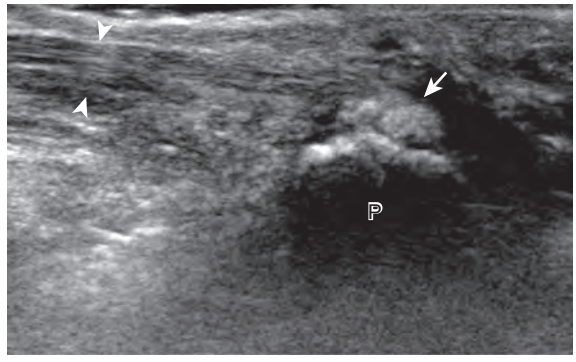

FIGURE 5-47 ■ Calcific tendinosis: flexor carpi ulnaris. Ultrasound image in long axis to the flexor carpi ulnaris tendon *(arrowheads)* shows a calcium hydroxyapatite deposit *(arrow)* adjacent to the pisiform (P). Note cortical irregularity.

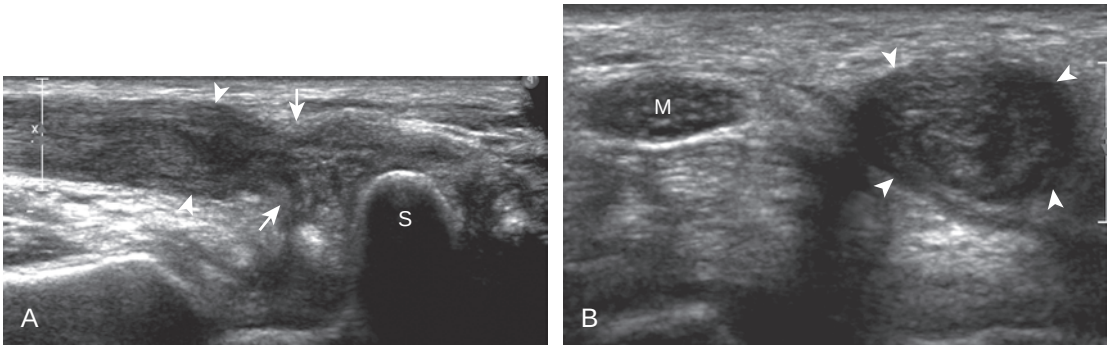

FIGURE 5-48 ■ Partial-thickness tear: flexor carpi radialis tendon. Ultrasound images in **(A)** long axis and **(B)** short axis to the flexor carpi radialis show hypoechoic thickening of the flexor carpi radialis *(arrowheads)* with partial anechoic tendon fiber disruption *(arrows)*. M, median nerve; S, scaphoid.

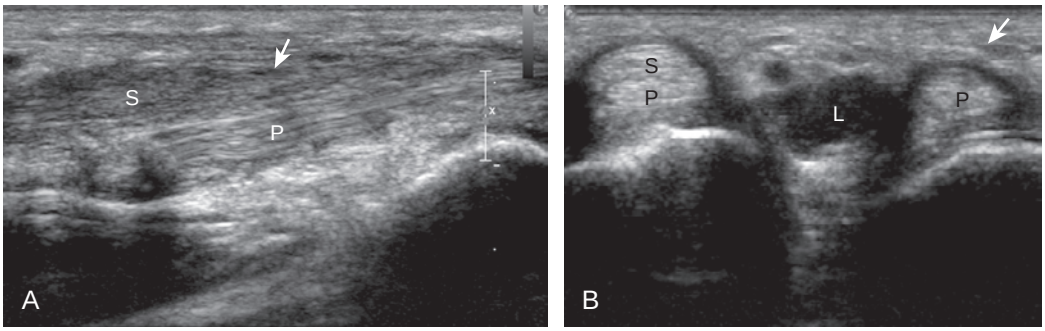

FIGURE 5-49 ■ Full-thickness tear: flexor digitorum superficialis. Ultrasound images in **(A)** long axis and **(B)** short axis to the flexor digitorum profundus (P) and superficialis (S) show a torn and retracted flexor digitorum superficialis *(arrow)*. L, lumbrical muscle.

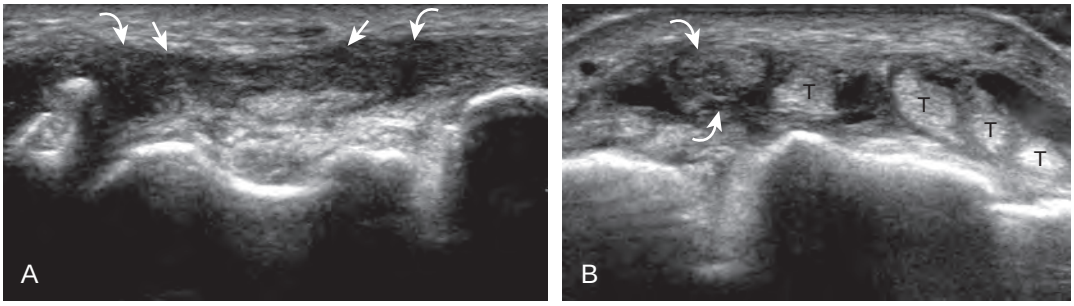

FIGURE 5-50 ■ Full-thickness tear: extensor indicis. Ultrasound images in **(A)** long axis and **(B)** short axis to the extensor indicis show a tendon tear *(between arrows)* with retracted tendon stumps *(curved arrows)*. T, extensor digitorum tendons.

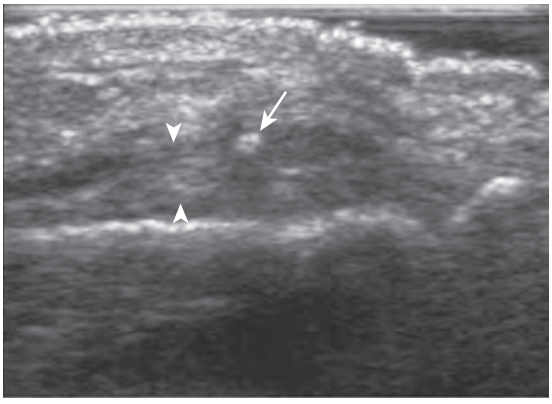

FIGURE 5-51 ■ Avulsion fracture. Sagittal ultrasound image of the volar digit shows the hyperechoic avulsion fracture fragment *(arrow)* (*arrowheads*, flexor tendon).

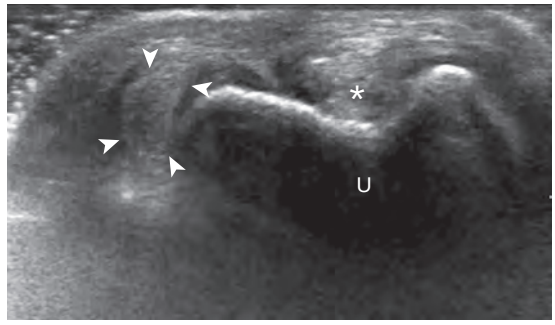

FIGURE 5-52 ■ Dislocation: extensor carpi ulnaris tendon. Ultrasound image in short axis to the extensor carpi ulnaris tendon *(arrowheads)* shows dislocation of the tendon from its normal position *(asterisk)*. U, ulna.

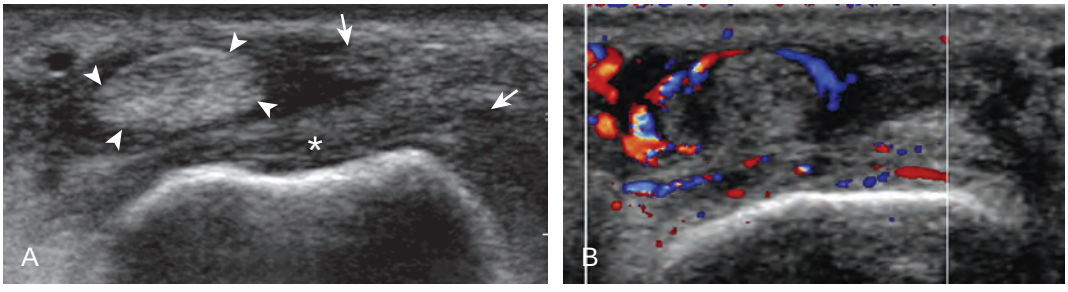

FIGURE 5-53 ■ Subluxation: extensor tendon (Boxer knuckle). Ultrasound images in **(A** and **B)** short axis to the extensor digitorum tendon *(arrowheads)* show subluxation of the tendon from its normal position *(asterisk)* and discontinuity of the sagittal band of the extensor hood *(arrows)* and increased flow on color Doppler imaging **(B)**.

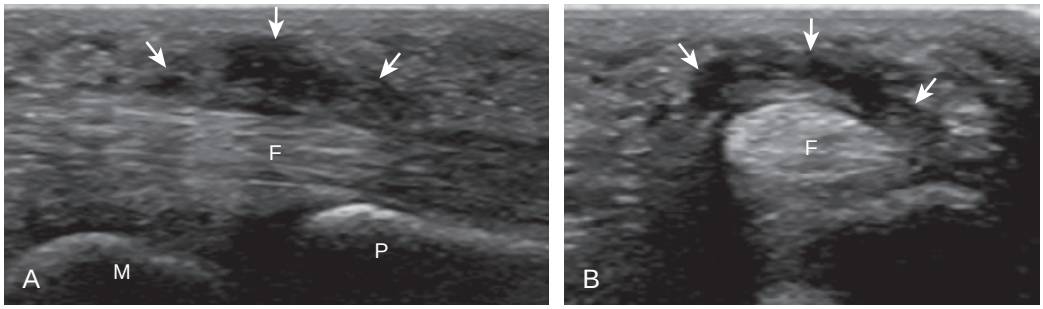

FIGURE 5-54 ■ Pulley injury: A1. Ultrasound images in **(A)** long axis and **(B)** short axis to the flexor tendons (F) of the finger show marked hypoechoic thickening of the A1 pulley *(arrows)*. M, metacarpal head; P, proximal phalanx.

Ultrasound can be effective in the evaluation of pulley injuries of the digits.[2] A pulley tear will appear as abnormal hypoechogenicity or absence of the pulley (Figs. 5-54 and 5-55). An important indirect sign of a pulley tear is abnormal volar displacement of the flexor tendons, called *bowstringing*, evaluated dynamically during active forced finger flexion (Fig. 5-56).[33-35] Injury to the A2 pulley is common, often with adjacent pulley involvement. Less commonly, a pulley injury to the thumb may also be seen (Fig. 5-57). Another digit abnormality around the hand and digits is trigger finger, whereby impaired flexor tendon gliding is caused by tendon constriction due to thickening of the A1 pulley or tendon sheath (Fig. 5-58; see Fig. 5-57) (Video 5-18), with possible cyst formation (see Ganglion Cyst), pulley hyperemia, tendinosis, and tenosynovitis.[36,37]

There are various other muscle and tendon abnormalities of the forearm, wrist, and hand, which are either uncommon or have nonspecific

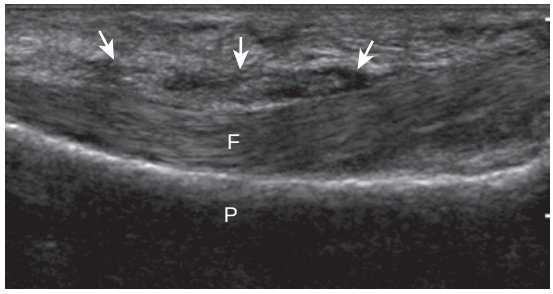

FIGURE 5-55 ■ Pulley injury: A2. Ultrasound image in long axis to the flexor tendons (F) of the finger show marked hypoechoic thickening of the A2 pulley *(arrows)*. P, proximal phalanx.

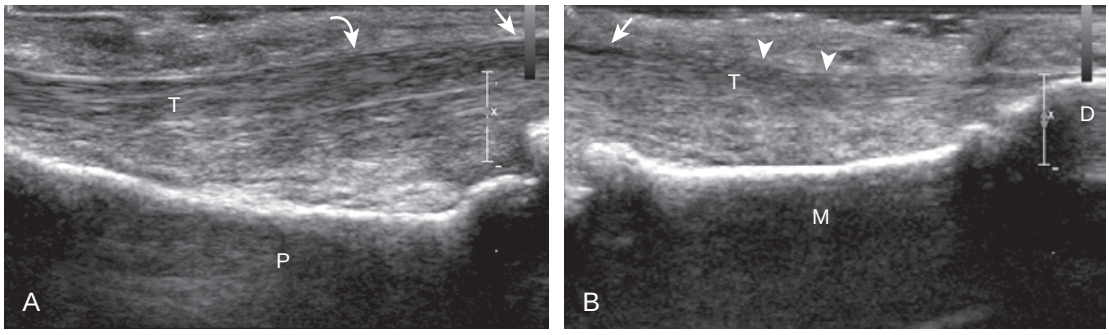

FIGURE 5-56 ■ Pulley injury: A2 to A4. Ultrasound images in **(A** and **B)** long axis to the flexor tendons (T) of the finger show disruption of the distal A2 pulley *(curved arrow)* and absence of the A3 *(arrows)* and A4 *(arrowheads)* pulleys with volar displacement of the flexor tendons (termed *bowstringing*). D, distal phalanx; M, middle phalanx; P, proximal phalanx.

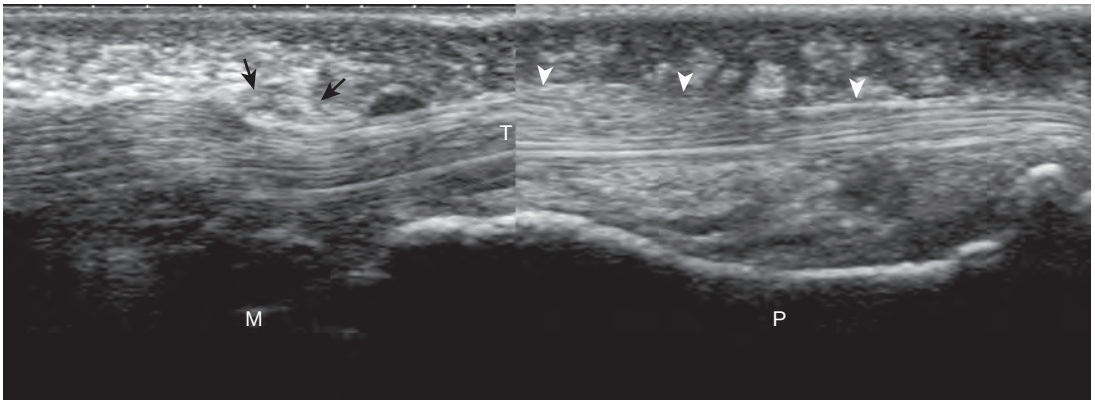

FIGURE 5-57 ■ Pulley injury: thumb. Ultrasound image in long axis to the flexor tendons (T) of the thumb show disruption of the pulleys (A2 and oblique) *(arrowheads)* with volar displacement of the flexor tendons (termed *bowstringing*). Note deviation of flexor tendon beneath a thickened A1 pulley *(arrows)*. M, metacarpal head; P, proximal phalanx.

imaging features. However, there is a specific abnormality called *intersection syndrome*, in which a patient has pain where the muscles of the first and second wrist compartments cross in the distal forearm.[27] At imaging, pain is produced with transducer pressure and hypoechoic swelling or adjacent fluid may be seen (Fig. 5-59). A more distal intersection syndrome may occur where the extensor pollicis longus tendon crosses over the extensor carpi radialis longus and brevis tendons. There exist a number of normal variations in the hand and wrist, including multiple tendon slips and the presence of accessory tendons and muscles, such as the extensor digitorum brevis manus, which may simulate a soft tissue mass at physical examination (Fig. 5-60) (Video 5-19).[38,39] Masses of the tendons are discussed later with other hand and wrist masses.

PERIPHERAL NERVE ABNORMALITIES

Carpal Tunnel Syndrome

The most common upper extremity entrapment neuropathy is carpal tunnel syndrome, which involves the median nerve at the level of the wrist.[40] Because the median nerve traverses the fibro-osseous carpal tunnel, any situation that decreases the size of the carpal tunnel or increases the volume of its contents can cause median nerve compression, such as trauma, mass, or tenosynovitis. At sonography, carpal tunnel syndrome is characterized by hypoechoic swelling of the median nerve as it enters into the carpal tunnel, although distal nerve swelling is also possible (Fig. 5-61) (Video 5-20). With regard to

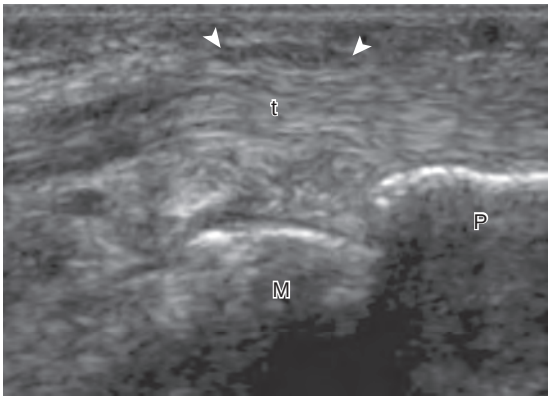

FIGURE 5-58 ■ Trigger finger. Ultrasound image in long axis to the second digit flexor tendons at the level of the metacarpophalangeal joint shows hypoechoic thickening of the A1 pulley *(arrowheads)* and mild deviation of the flexor tendons (t) as they course beneath the A1 pulley. M, metacarpal head; P, proximal phalanx.

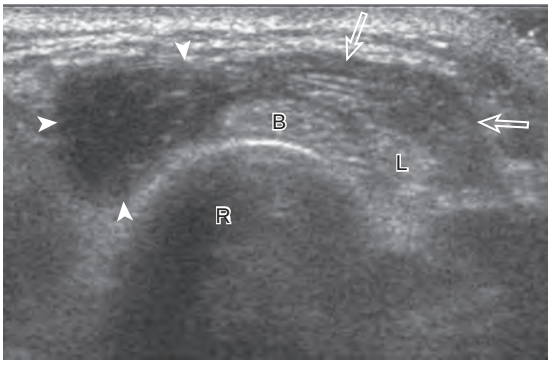

FIGURE 5-59 ■ Intersection syndrome. Ultrasound image in the axial plane at the distal forearm shows an abnormally hypoechoic extensor pollicis brevis muscle *(arrowheads)* where it crosses over the extensor carpi radialis brevis (B) and longus (L) with the abductor pollicis longus *(open arrows)*. R, radius.

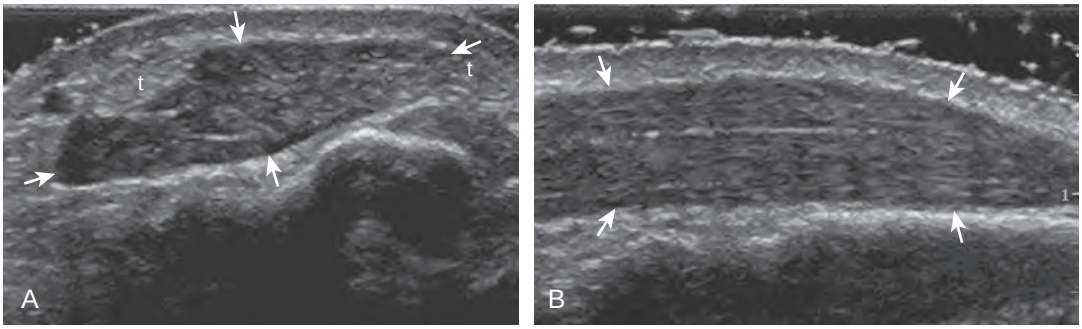

FIGURE 5-60 ■ Extensor digitorum brevis magnus. Ultrasound images **(A)** transverse and **(B)** sagittal over the dorsal wrist shows a hypoechoic accessory muscle *(arrows)*, which often is seen between the extensor tendons (t) of the second and third digits.

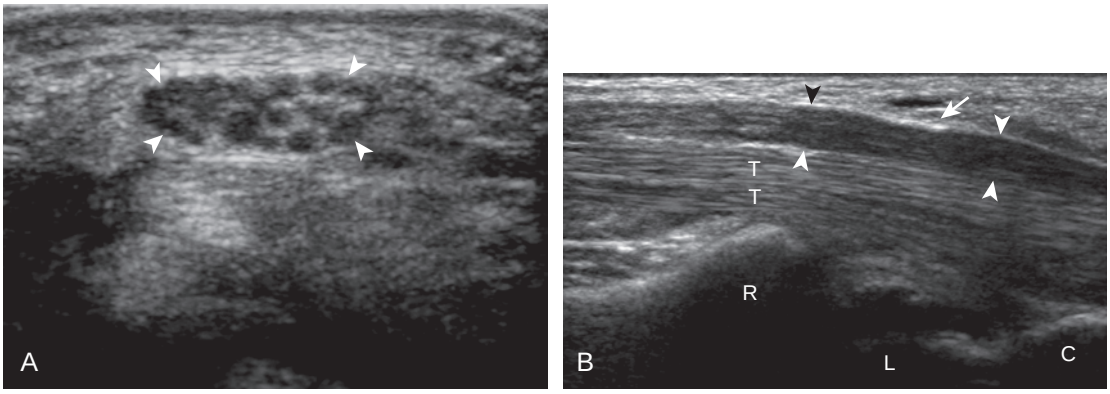

FIGURE 5-61 ■ Carpal tunnel syndrome. Ultrasound images in **(A)** short axis and **(B)** long axis to the median nerve show hypoechoic nerve swelling *(arrowheads)*. Note hyperechoic flexor retinaculum immediately superficial to the median nerve in **(A),** and mild deviation of the median nerve *(arrow)* as it courses beneath the flexor retinaculum in **(B)**. C, capitate; L, lunate; R, radius; T, flexor tendons.

quantitative assessment for carpal tunnel syndrome, there have been many studies that recommend different size criteria and depend on how one balances sensitivity and specificity. Most studies conclude a cutoff of 9 to 12 mm^2 as an indicator for carpal tunnel syndrome.[40] However, another study has shown that a difference in median nerve area of 2 mm^2 or more comparing proximal (at proximal pronator quadratus) and distal (at carpal tunnel) can diagnose carpal tunnel syndrome with 99% accuracy (Fig. 5-62). Of note, the circumferential trace method of

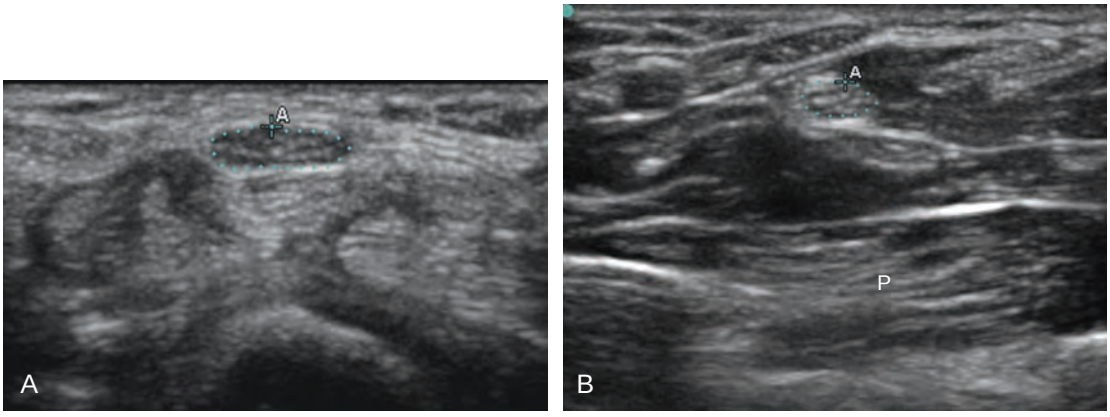

FIGURE 5-62 ■ Carpal tunnel syndrome: measurement technique. Ultrasound images in short axis to the median nerve at the level of **(A)** carpal tunnel and **(B)** pronator quadratus (P) show the circumferential trace method of calculating median nerve area (see caliper markings), which was greater than 2 mm^2 difference comparing proximal to distal.

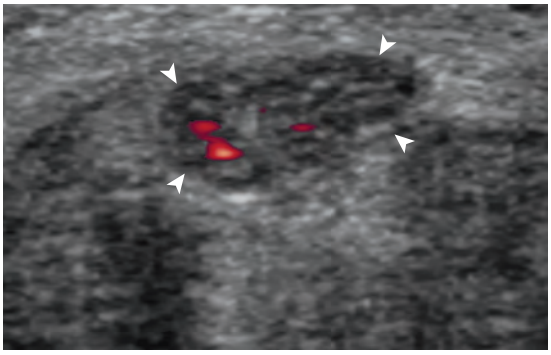

FIGURE 5-63 ■ Carpal tunnel syndrome: hyperemia. Power Doppler ultrasound image in short axis to the median nerve shows internal blood flow within the swollen and hypoechoic median nerve *(arrowheads)*.

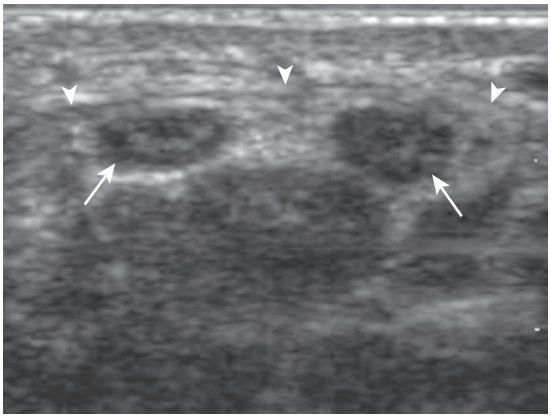

FIGURE 5-64 ■ Bifid median nerve and carpal tunnel syndrome. Ultrasound image in short axis to the median nerve shows hypoechoic swelling of each nerve trunk *(arrows)*. Note flexor retinaculum *(arrowheads)*.

measuring area is preferred, given variations in the shape of the median nerve. Other findings with carpal tunnel syndrome include bowing of the retinaculum in the transverse plane and flattening of the median nerve best seen in long axis, where the abrupt transition in size has been termed the *notch sign*. Also, imaging of the carpal tunnel during movement of the digits has shown decreased transverse sliding of the median nerve in carpal tunnel syndrome.[41] Demonstration of blood flow on color Doppler imaging has also been shown to be an accurate indicator of carpal tunnel syndrome (Fig. 5-63).[42,43] A bifid or high division of the median nerve, usually associated with a persistent median artery between the two nerve trunks, is a normal variant seen in 15% of the asymptomatic population that is often incomplete but not typically bilateral.[44,45] Carpal tunnel syndrome may exist in this situation as well, where the hypoechoic and swollen two median nerve trunk areas combined show a difference of 4 mm^2 or more comparing proximal (at pronator quadratus) and distal (at carpal tunnel) (Fig. 5-64) (Video 5-21).[46] After surgical carpal tunnel release for treatment of carpal tunnel syndrome, the retinaculum may be thickened or disrupted, whereas the median nerve may return to normal size although displaced in a volar direction (Fig. 5-65).[47] After steroid injection into the carpal tunnel, the median nerve may show a decrease in size as early as 7 days after injection.[48] Uncommonly, median nerve compression in the carpal tunnel may be secondary to extrinsic compression by a mass, ganglion cyst (Fig. 5-66), or tenosynovitis (Fig. 5-67). A rare cause of enlargement of the median nerve is fibrolipomatous hamartoma, in which there is diffuse fatty infiltration of the nerve separating the normal-appearing nerve fascicles (Fig. 5-68).[49]

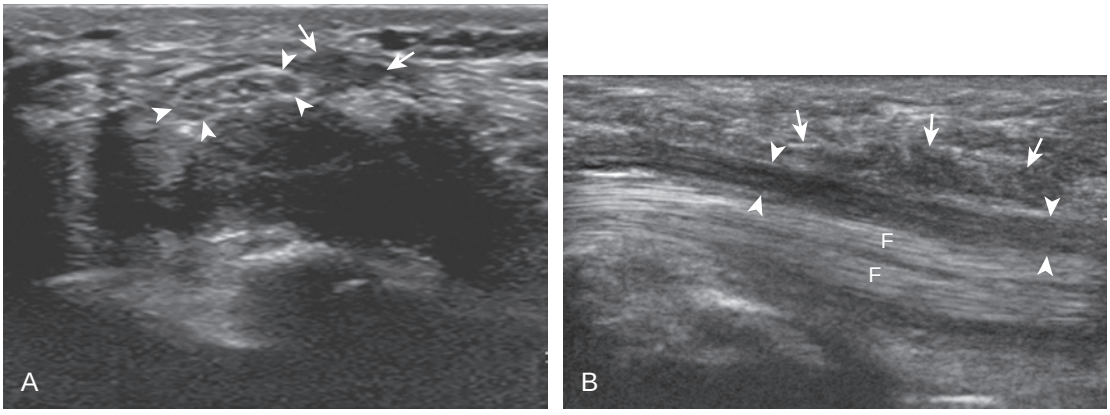

FIGURE 5-65 ■ Carpal tunnel syndrome: post-release. Ultrasound images in **(A)** short axis and **(B)** long axis to the median nerve *(arrowheads)* in two different patients after surgical carpal tunnel release show hypoechoic thickening of the flexor retinaculum *(arrows)*. F, flexor tendons.

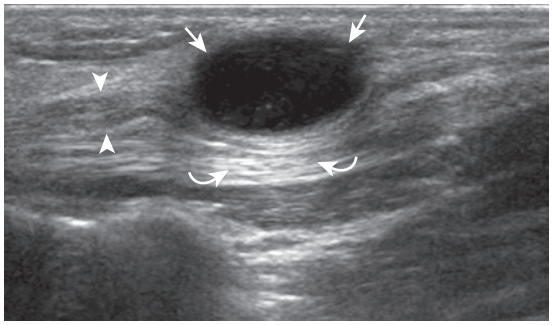

FIGURE 5-66 ■ Carpal tunnel syndrome: ganglion cyst. Ultrasound image in long axis to the median nerve *(arrowheads)* shows an anechoic ganglion cyst *(arrows)* with increased through-transmission *(curved arrows)*.

Ulnar Tunnel Syndrome

Another less common entrapment syndrome involves the ulnar nerve in Guyon canal, called *ulnar tunnel syndrome*.[50] The cause of this syndrome is most commonly trauma. Because the hook of the hamate bone is directly deep to the ulnar nerve and artery, direct impact on the ulnar aspect of the hand can cause peripheral nerve or vascular injury. This may take the form of ulnar nerve contusion, ulnar nerve compression from an ulnar artery aneurysm (Fig. 5-69, online), or swelling within the ulnar tunnel, possibly associated with ulnar artery thrombosis (Fig. 5-70, online). At sonography, an abnormal ulnar nerve will appear hypoechoic with symptoms reproduced with transducer pressure when the ulnar nerve is compressed between the transducer and the hook of the hamate bone. To find the hook of the hamate bone, place the transducer in the sagittal plane just radial and distal to the pisiform bone, which is easily identified at sonography and physical examination. Ulnar artery aneurysm will appear as a heterogeneous mass in continuity with the ulnar artery, which demonstrates to-and-fro (yin-yang) flow on color or power Doppler imaging. No flow may be present with thrombosis. There exists a related entity called hypothenar hammer syndrome, in which direct trauma results in ulnar artery thrombosis or aneurysm and distal emboli to the digits, causing vascular insufficiency.[51] Other causes of ulnar tunnel syndrome include vascular abnormalities and ganglion cyst. The ulnar nerve may also

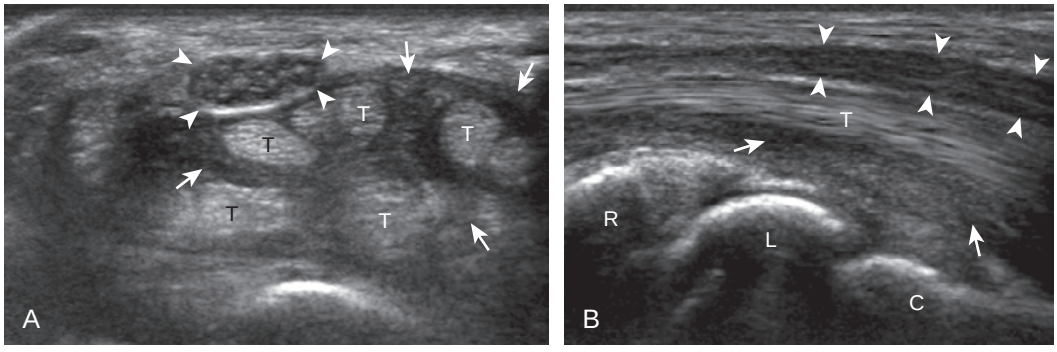

FIGURE 5-67 ■ Carpal tunnel syndrome: tenosynovitis. Ultrasound images in **(A)** short axis and **(B)** long axis to the median nerve show hypoechoic nerve swelling *(arrowheads)*. Note hypoechoic synovial hypertrophy *(arrows)* surrounding the flexor tendons (T). C, capitate; L, lunate; R, radius.

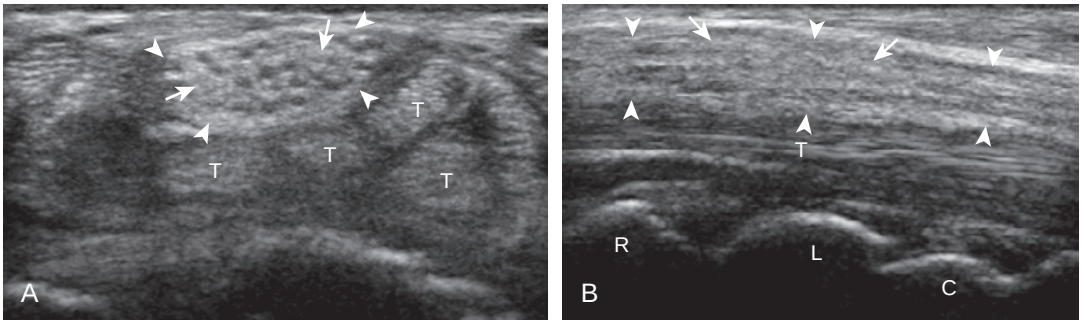

FIGURE 5-68 ■ **Fibrolipomatous hamartoma of the median nerve.** Ultrasound images in **(A)** short axis and **(B)** long axis to the median nerve *(arrowheads)* show hyperechoic fat *(arrows)* interspersed between the hypoechoic nerve fascicles. C, capitate; L, lunate; R, radius; T, flexor tendons.

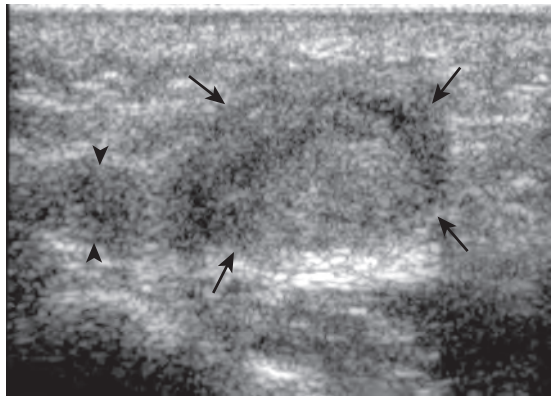

FIGURE 5-69 ■ Aneurysm: ulnar artery. Ultrasound image in long axis to the ulnar artery shows hypoechoic aneurysmal enlargement *(arrows)* continuous with the ulnar artery *(arrowheads)*.

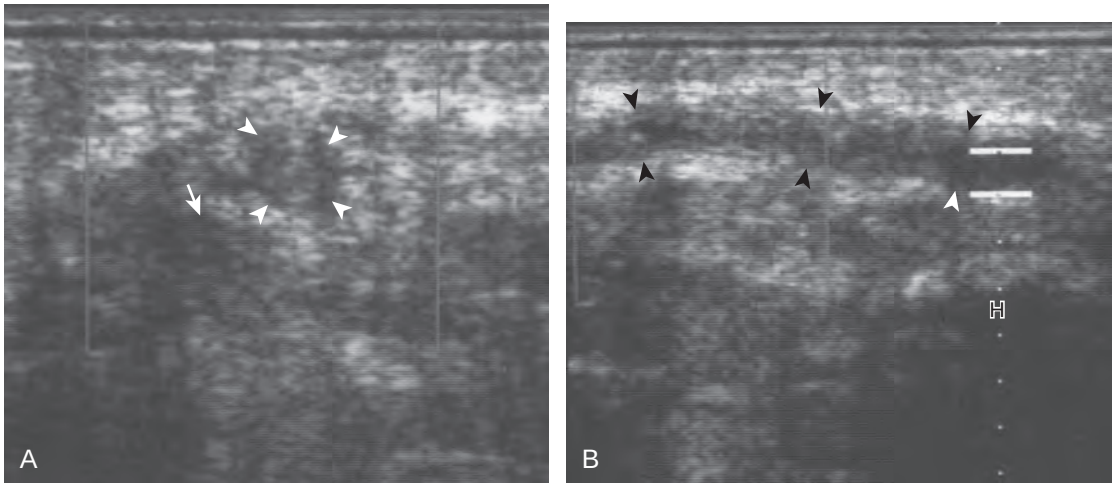

FIGURE 5-70 ■ Hypothenar hammer syndrome. Ultrasound images in **(A)** short axis and **(B)** long axis to the ulnar artery show a hypoechoic clot within the ulnar artery *(arrowheads)* (*arrow*, ulnar nerve). H, hook of hamate.

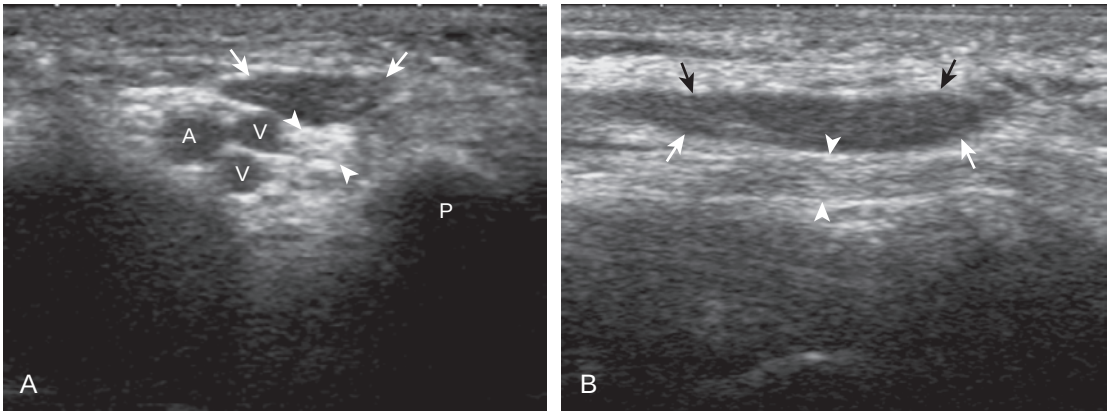

FIGURE 5-71 ■ Accessory abductor digiti minimi. Ultrasound images in **(A)** short axis and **(B)** long axis to the ulnar nerve *(arrowheads)* show the hypoechoic muscle *(arrows)* of the accessory abductor digiti minimi. A, ulnar artery; P, pisiform; V, ulnar veins.

be compressed by an accessory abductor digiti minimi muscle, a normal variant seen in up to 24% of the population (Fig. 5-71).[39]

Radial Nerve Compression

The superficial branch of the radial nerve is located in the superficial and radial aspect of the mid-forearm. As the nerve continues distally, it crosses over the radial aspect of the forearm and the extensor pollicis brevis and abductor pollicis longus muscles. More distally, the superficial branch of the radial nerve continues into the dorsal wrist superficial to the extensor retinaculum. Compression of the superficial branch of the radial nerve may occur in the distal forearm, called *Wartenberg syndrome*, and can be caused by hematoma at an intravenous catheter site. Involvement from a mass or scar tissue is also possible (Fig. 5-72) (Video 5-22) .[27,50]

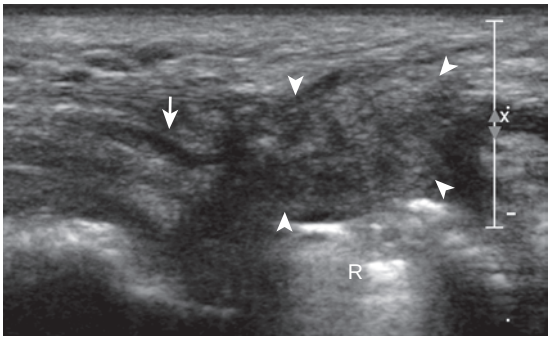

FIGURE 5-72 ■ Radial nerve, superficial branch: scar tissue. Ultrasound image shows the superficial branch of the radial nerve in long axis *(arrow)* entering into hypoechoic scar tissue and hematoma *(arrowheads)* after surgical repair of distal radius (R) fracture.

Transection Neuromas

Injury to a peripheral nerve may have a variable appearance, depending on the type and degree of injury.[52] After complete nerve transection, a neuroma may develop as the normal response of a transected nerve attempting to regenerate, which results in a tangled area of nerve fibers and scar tissue.[53] At sonography, a neuroma will appear as a heterogeneous but predominantly hypoechoic mass (Fig. 5-73, online). Its appearance is not specific until continuity between the mass and the peripheral nerve is recognized. The segment of peripheral nerve that enters into the neuroma is often abnormally hypoechoic, which aids in its identification.

LIGAMENT AND OSSEOUS ABNORMALITIES

Scapholunate Ligament Injury

Acute trauma and repetitive overuse conditions may cause abnormalities to the wrist ligaments, cartilage, and adjacent osseous structures. With regard to the intrinsic wrist ligaments, the scapholunate ligament is one of many important stabilizing structures. Normally, a ligament has a hyperechoic and fibrillar echotexture, more compact than that of tendon, which connects bone to bone. An abnormal ligament may appear hypoechoic and thickened if partially torn, or it may not be visible, possibly replaced with anechoic fluid or hypoechoic synovitis when completely torn (Fig. 5-74).[10,54] The space between the lunate and scaphoid bones may also be increased, which may further increase with clenched-fist maneuver or ulnar and radial deviation. The volar aspect of the scapholunate

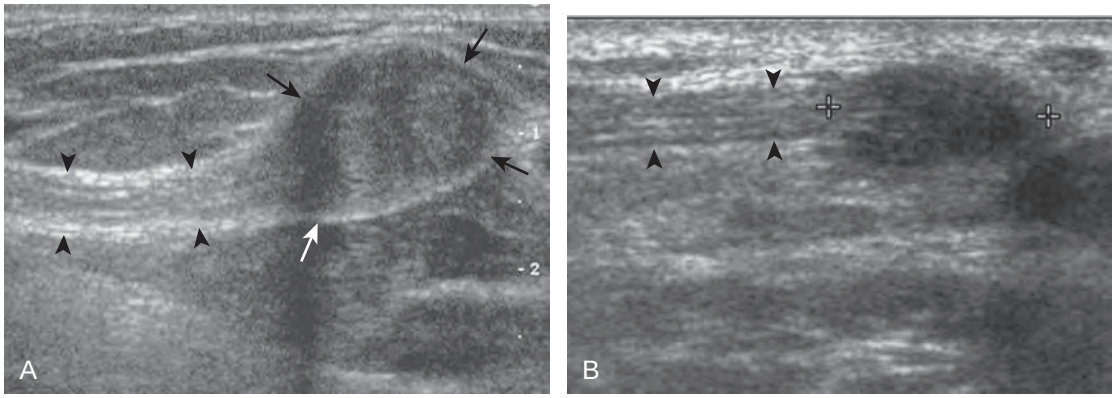

FIGURE 5-73 ■ Transection neuromas. Ultrasound images long axis to the **(A)** ulnar nerve and the **(B)** median nerve in two patients show heterogeneous but predominantly hypoechoic neuroma formation (*arrows* in **A;** between cursors in **B**). Note continuity with the respective nerve *(arrowheads)*.

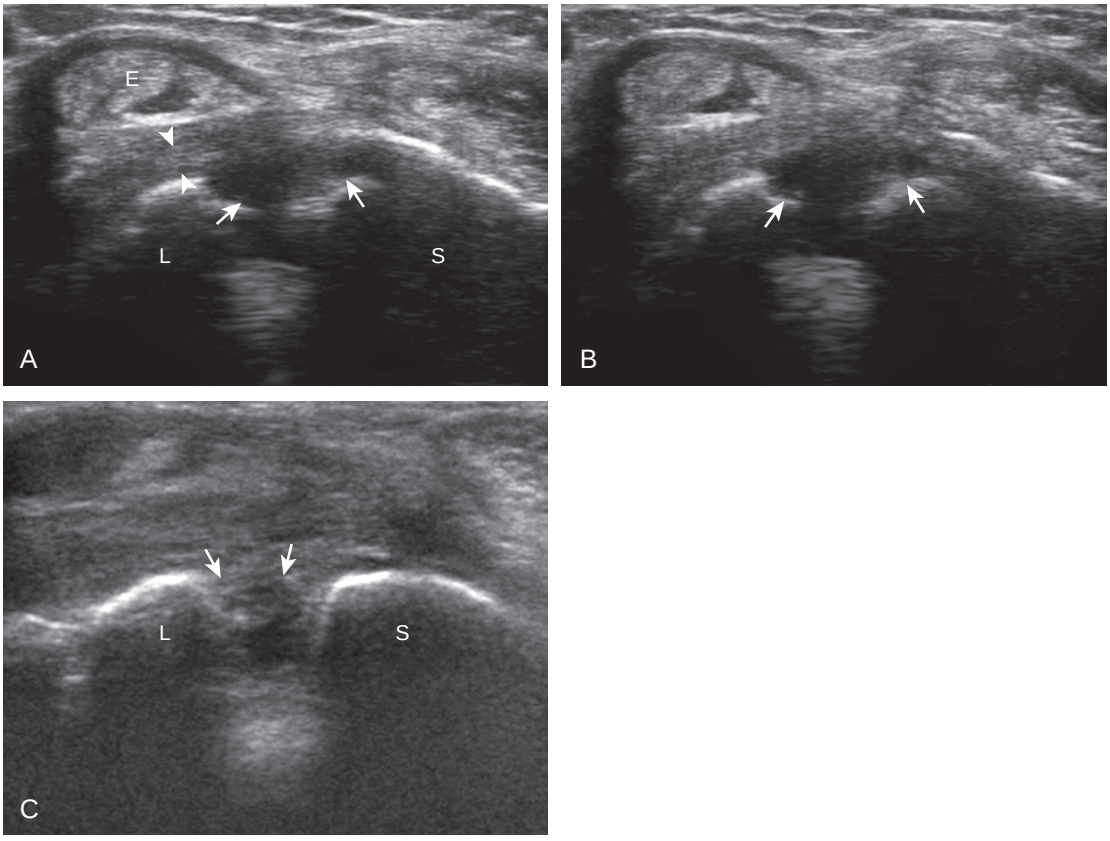

FIGURE 5-74 ■ Scapholunate ligament tear. Ultrasound images transverse over the dorsal wrist at the level of the proximal carpal row **(A)** without and **(B)** with the clench fist maneuver show abnormal hypoechogenicity *(arrows)* at the expected site of the scapholunate ligament (*arrowheads*, dorsal radiocarpal ligament). Note widening of the scapholunate distance between **(A)** and **(B)**. An ultrasound image over the volar wrist **(C)** shows similar hypoechoic scapholunate ligament disruption. E, extensor digitorum; L, lunate; S, scaphoid.

ligament, as well as the volar and dorsal aspects of the lunotriquetral ligaments, may also be evaluated.[55] In addition to the intrinsic ligaments of the wrist, the various extrinsic wrist ligaments may also be evaluated for injury or abnormality, such as the dorsal radiocarpal ligament, which lies dorsal and superficial to the scapholunate ligament (Fig. 5-75).

Ulnar Collateral Ligament Injury (Thumb)

In addition to the wrist ligaments, the collateral ligaments of the digits may also be evaluated for tear. One specific ligament, the ulnar collateral ligament of the first metacarpophalangeal joint, deserves emphasis because of important surgical

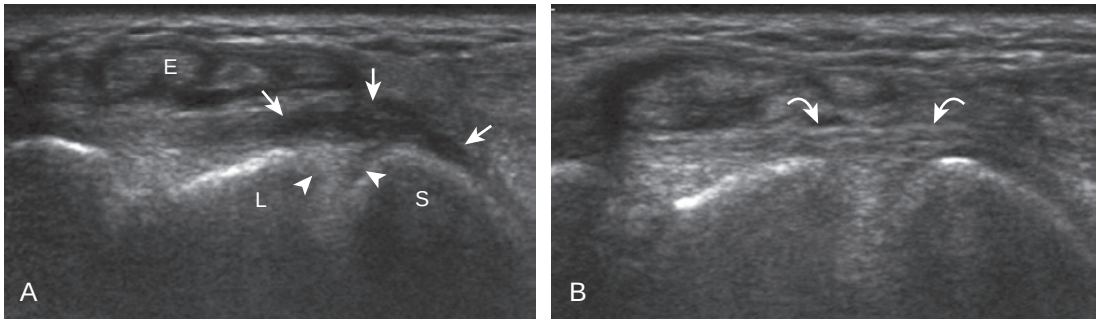

FIGURE 5-75 ■ Dorsal radiocarpal ligament: tear. Transverse ultrasound image **(A)** over the dorsal wrist shows hypoechoic disruption of the dorsal radiocarpal (or radiotriquetral) ligament *(arrows)* seen in long axis. Note the normal scapholunate ligament *(arrowheads)* and **(B)** normal contralateral side *(curved arrows)*. E, extensor digitorum; L, lunate; S, scaphoid.

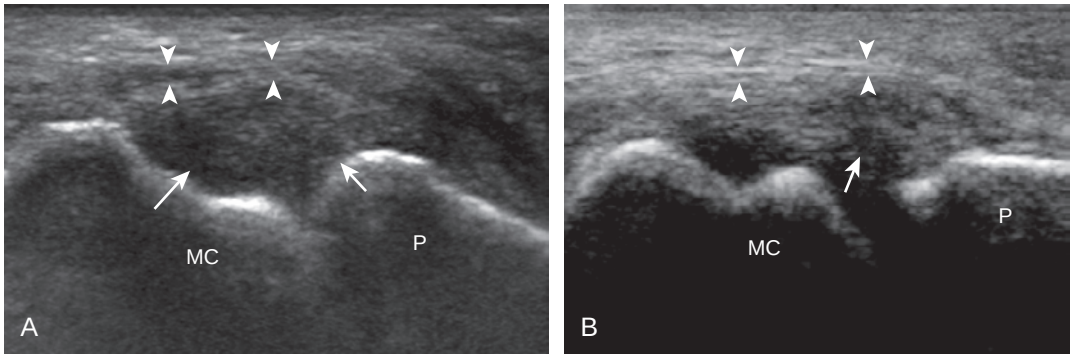

FIGURE 5-76 ■ Ulnar collateral ligament of the thumb: sprain and partial tear. Ultrasound images in long axis to the ulnar collateral ligament in two different patients show **(A)** diffuse hypoechoic swelling with intact fibers *(arrows)* and **(B)** a focal anechoic partial-thickness tear *(arrow)*. Note the intact adductor pollicis aponeurosis *(arrowheads)*. MC, metacarpal; P, proximal phalanx.

implications.[56] This injury has been historically termed *gamekeeper's thumb* because the injury occurs in hunters who strangle rabbits. More currently, this injury is called *skier's thumb*. Similar to other ligament injuries, an injured ulnar collateral ligament may appear hypoechoic and swollen (Fig. 5-76A).[57] Partial-thickness tear is characterized by partial disruption of the ligament fibers (see Fig. 5-76B), whereas complete fiber disruption will show complete fiber discontinuity (Fig. 5-77). Differentiation between a partial tear and nondisplaced full-thickness tear is extremely difficult; however, the primary goal is to identify a displaced full-thickness ulnar collateral ligament tear (or Stener lesion). Visualization of an echogenic avulsion fracture fragment may be a clue to full-thickness tear. Gentle valgus stress of the first metacarpophalangeal joint under ultrasound observation may help demonstrate a full-thickness ligament tear and retraction if fluid is identified entering into the torn ligament gap (Video 5-23A).

A Stener lesion represents a distal full-thickness ulnar collateral ligament tear of the first metacarpophalangeal joint, which is displaced proximal to the adductor pollicis aponeurosis (Fig. 5-78).[56] In this situation, the ligament will not heal spontaneously, and therefore surgery is indicated to avoid chronic instability. At ultrasound, the Stener lesion will appear as a hypoechoic but heterogeneous, round, mass-like structure located proximal to the metacarpophalangeal joint in the plane of the normal ulnar collateral ligament (Fig. 5-79) (see Videos 5-23 and 5-24). Shadowing is often present deep to the Stener lesion related to sound beam refraction at the torn

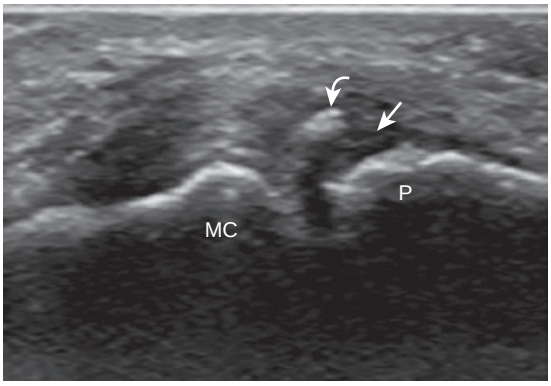

FIGURE 5-77 ■ Ulnar collateral ligament of the thumb: full-thickness tear avulsion. Ultrasound image in long axis to the ulnar collateral ligament shows distal retraction of avulsion fracture fragment *(curved arrow)* at the site of a full-thickness tear *(arrow)*. MC, metacarpal; P, proximal phalanx.

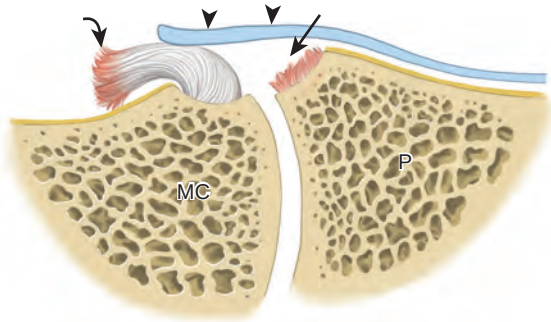

FIGURE 5-78 ■ Stener lesion. Illustration shows a distal full-thickness tear of the ulnar collateral ligament *(arrow)* with displacement *(curved arrow)* proximal to the metacarpophalangeal joint and adductor pollicis aponeurosis *(arrowheads)*. MC, metacarpal; P, proximal phalanx. (Modified from an illustration by Carolyn Nowak, Ann Arbor, Michigan; http://www.carolyncnowak.com/MedTech.html.)

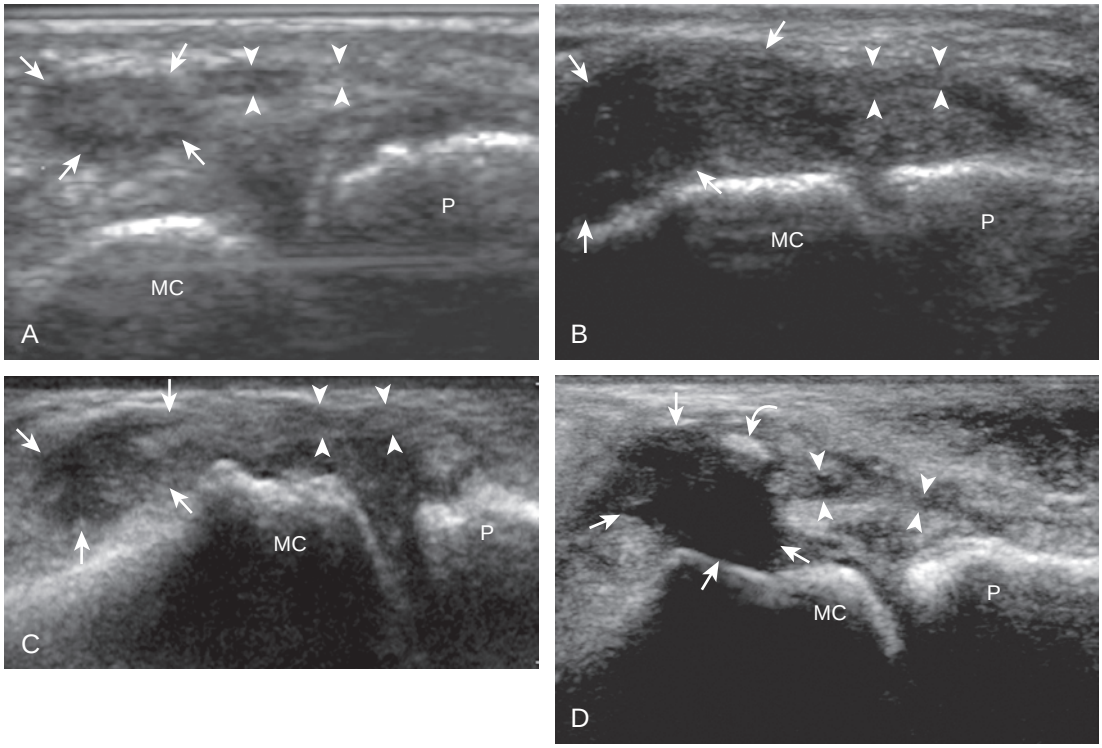

FIGURE 5-79 ■ Stener lesion. Ultrasound images in long axis to the ulnar collateral ligament of the first metacarpophalangeal joint in four different patients **(A** to **D)** show full-thickness tear of the ulnar collateral ligament with proximal displacement (Stener lesion) *(arrows)*. Note the adductor pollicis aponeurosis *(arrowheads)* (abnormally hypoechoic from injury) creating a yo-yo on a string appearance. Also note **(D)** hyperechoic avulsion fracture fragment *(curved arrow)*. MC, metacarpal; P, proximal phalanx.

ligament end. In addition, normal ligament fibers are absent in their expected location crossing the first metacarpophalangeal joint. A hyperechoic and possibly shadowing focus attached to the retracted ligament distally is characteristic of a bone avulsion (see Fig. 5-79C). The ultrasound appearance of a Stener lesion has been likened to a yo-yo on a string, similar to findings on magnetic resonance imaging.[58] The string of the yo-yo represents the adductor pollicis aponeurosis, and the yo-yo represents the balled-up and displaced proximal portion of the ulnar collateral ligament. Although the shape of the Stener lesion can be round, oval, or elongated (see Fig. 5-79C), the position of the displaced ligament is proximal to the leading edge of or uncommonly superficial to the adductor pollicis aponeurosis. Passive flexion of the interphalangeal joint will cause the adductor pollicis aponeurosis to slide over the ulnar collateral ligament, which assists in its identification and differentiation from the adjacent Stener lesion (see Videos 5-23 and 5-24). The adductor pollicis aponeurosis may be hypoechoic and thickened from injury as well (Fig. 5-80) (Video 5-25).

Other Ligament Injuries

Other collateral ligaments may be evaluated for tear, such as the radial collateral ligament of the thumb (Fig. 5-81). A hyperechoic bone fragment at a joint but not at the attachment of a ligament

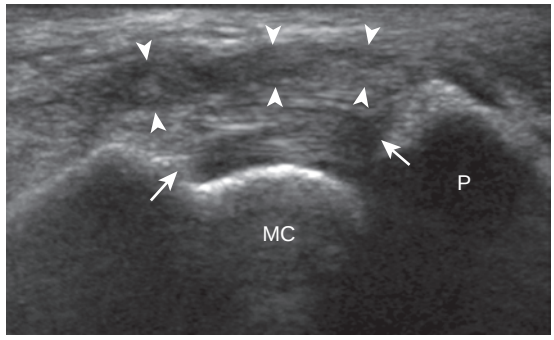

FIGURE 5-80 ■ Adductor pollicis aponeurosis: tear. Ultrasound image in long axis to the ulnar collateral ligament of the first metacarpophalangeal joint shows markedly hypoechoic and thickened adductor aponeurosis *(arrowheads)* with normal ulnar collateral ligament *(arrows)*. MC, metacarpal; P, proximal phalanx.

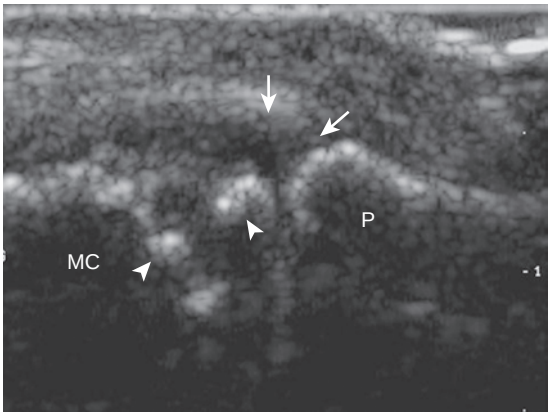

FIGURE 5-81 ■ Radial collateral ligament: tear. Ultrasound image in long axis to the radial collateral ligament shows hypoechoic discontinuity *(arrows)* and significant bone irregularity *(arrowheads)*. MC, metacarpal; P, proximal phalanx.

could relate to capsular (Fig. 5-82A) or volar plate avulsion fracture (see Fig. 5-82B). Cortical irregularity at a ligament attachment is not always due to trauma, and in the correct clinical setting, a seronegative spondyloarthropathy should be considered. Ultrasound findings in this scenario, such as psoriatic arthritis, include cortical irregularity or erosions and bone proliferation at a ligament attachment site (termed *enthesopathy*) with flow on color or power Doppler imaging and hypoechoic swelling of the adjacent ligament (Fig. 5-83) (Video 5-26). The overlying soft tissues may also be swollen and hypoechoic.

Ligament abnormalities of the wrist may be associated with triangular fibrocartilage abnormalities, often associated with ulnar-sided wrist pain. Although often difficult to evaluate comprehensively with ultrasound, abnormalities of the triangular fibrocartilage will appear as abnormal hypoechogenicity, thinning, or absence (Fig. 5-84).[11,59] It is important to identify the radius attachment of the triangular fibrocartilage to ensure complete evaluation.

An additional ligamentous-like abnormality involves the interosseous membrane between the radius and ulna of the forearm. This complex structure is comprised of a large main fiber bundle, a proximal dorsal oblique bundle, several accessory bundles, and a distal membranous portion.[60] Sonographic evaluation of the interosseous membrane begins in the transverse plane of the dorsal mid-forearm. The transducer is angled

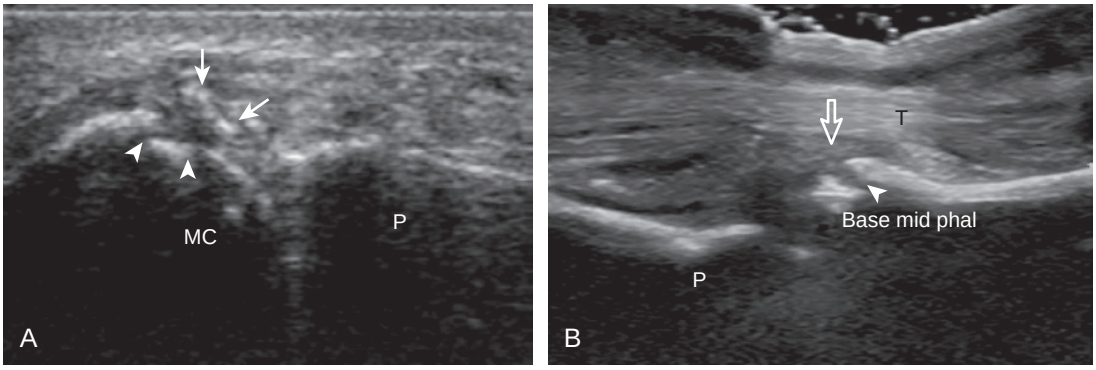

FIGURE 5-82 ■ Cortical avulsion fractures. Ultrasound images from two different patients show **(A)** fracture fragment *(arrows)* at volar capsule attachment with donor site *(arrowheads)* from metacarpal (MC), and **(B)** fracture fragment *(open arrow)* at volar plate attachment from base of middle phalanx *(arrowhead)*. P, proximal phalanx; T, flexor tendons.

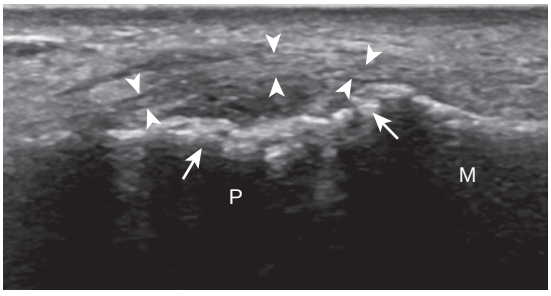

FIGURE 5-83 ■ Enthesopathy: psoriatic arthritis. Ultrasound image in long axis to the radial collateral ligament *(arrowheads)* of the proximal interphalangeal joint shows diffuse cortical irregularity from erosions and bone proliferation *(arrows)* and adjacent hypoechogenicity. M, middle phalanx; P, proximal phalanx.

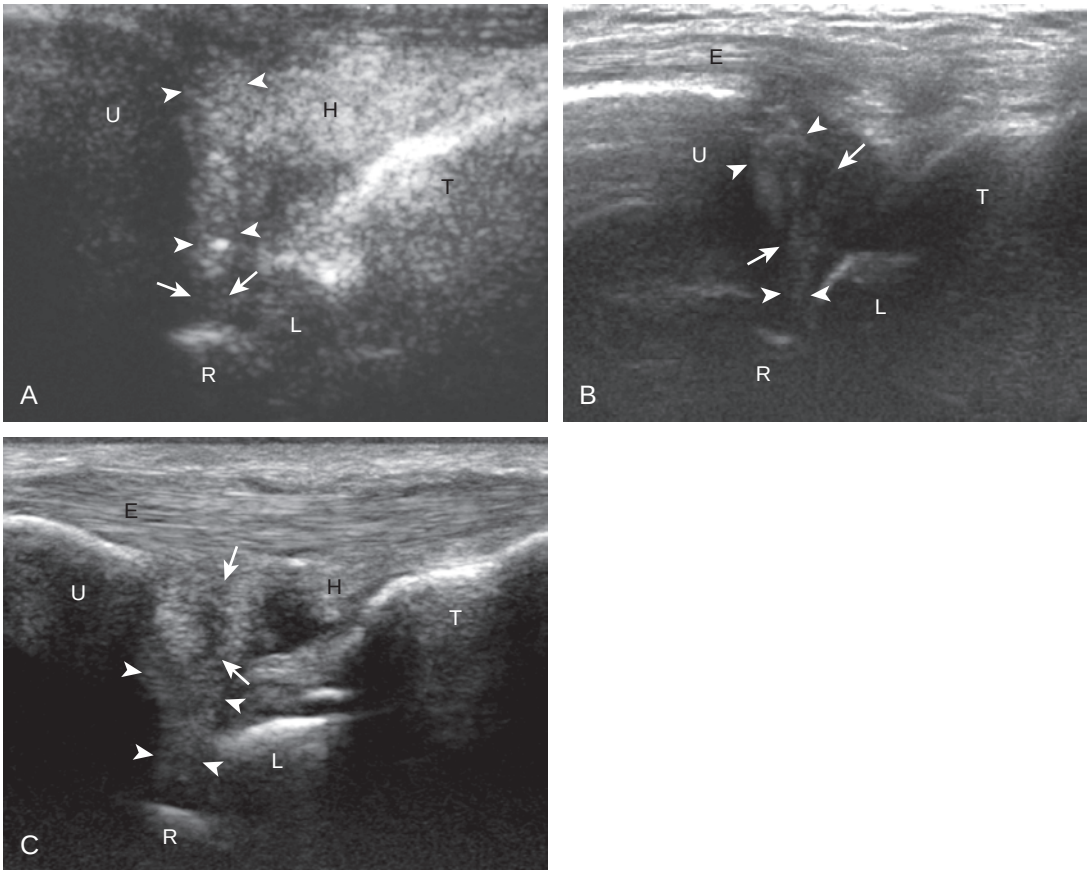

FIGURE 5-84 ■ Triangular fibrocartilage tears. Ultrasound images in coronal plane at the ulnar aspect of the wrist from three different patients show abnormal hypoechogenicity *(arrows)* involving the **(A)** radial, **(B)** central, and **(C)** ulnar peripheral aspects of the triangular fibrocartilage *(arrowheads)* and meniscus homologue (H). E, extensor carpi ulnaris tendon; L, lunate; R, radius; T, triquetrum; U, ulna.

slightly distally toward the ulna to elongate the interosseous membrane fibers. With injury of the interosseous membrane, the normally thin and hyperechoic appearance is replaced with hypoechoic thickening or disruption and nonvisualization (Fig. 5-85).[61] Interosseous membrane injury is an important component of the Essex-Lopresti injury, in which a comminuted radial head fracture at the elbow is associated with interosseous membrane injury and distal radioulnar joint disruption.[62]

Osseous Injury

Injury to bone can be visible at sonography if a fracture extends to the visible portion of the bone cortex, commonly creating cortical disruption and a step-off deformity or an avulsion fracture fragment (see Fig. 5-82). The finding of the focal cortical step-off deformity is fairly specific for fracture, which is unlike the cortical irregularity at the margin of a joint with osteoarthritis from an osteophyte, although correlation with radiography is essential (see Figs. 5-19D and E and 5-31). Hyperemia, adjacent hypoechoic soft tissue swelling, and point tenderness with transducer pressure are other important associated findings of fracture. Although fractures may occur anywhere in the hand and wrist, it is the scaphoid fracture that receives much attention because a nontreated scaphoid fracture may result in nonunion and osteonecrosis of the proximal scaphoid pole. At sonography, it is important to evaluate the scaphoid bone for a cortical step-off deformity and adjacent soft tissue hematoma when there is history of trauma and snuffbox tenderness (Fig. 5-86).[63] Small avulsion fractures of the hand and wrist are seen at tendon and ligament insertions and appear as focal hyperechoic, possibly shadowing foci.

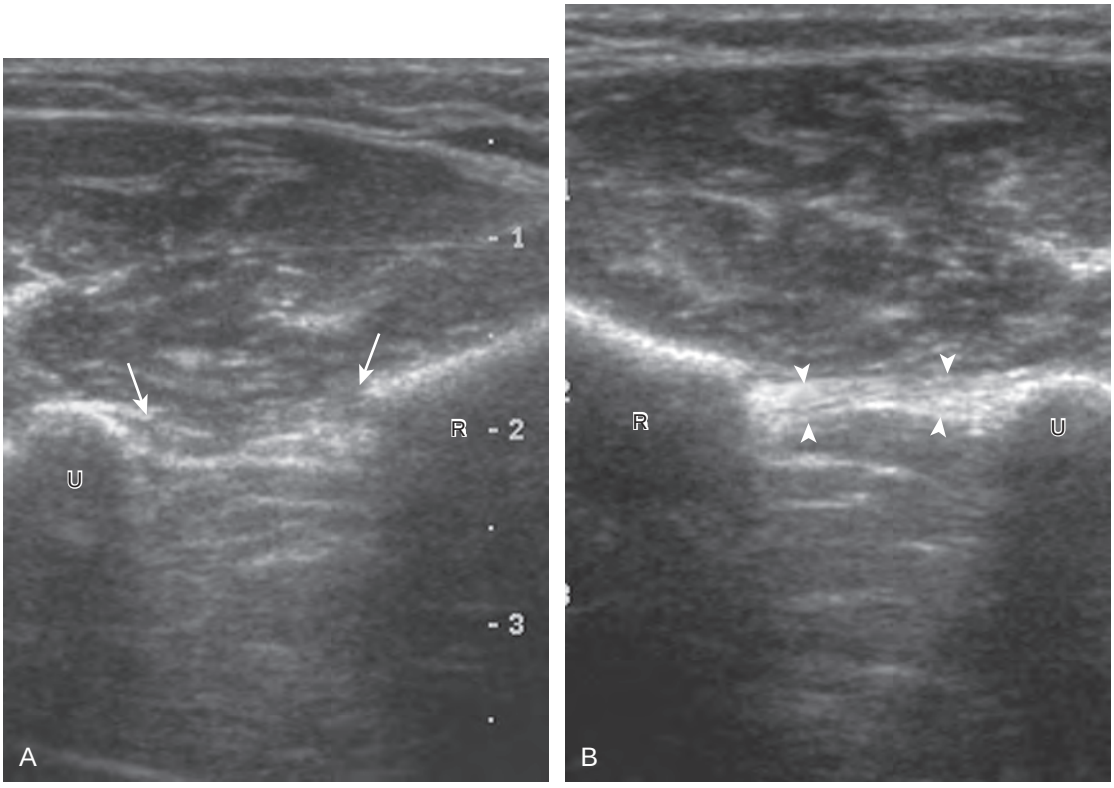

FIGURE 5-85 ■ Interosseous membrane tear: Essex-Lopresti injury. A, Oblique-transverse ultrasound image over the dorsal midforearm shows no identifiable interosseous membrane *(between arrows)*. **B,** Note the normal appearance in the contralateral asymptomatic forearm *(arrowheads)*. R, radius; U, ulna.

GANGLION CYST

Most wrist masses are benign, and are most commonly ganglion cysts. Although the cause of ganglion cysts is uncertain, they may be degenerative, related to prior injury, or idiopathic. At sonography, a ganglion cyst may appear as an anechoic simple cyst with an imperceptible wall, no nodularity, and increased through-transmission (Fig. 5-87A).[15,64,65] However, many ganglion cysts have a more variable appearance, possibly appearing multilocular (see Fig. 5-87B), irregular (see Fig. 5-87C), nodular, hypoechoic (see Fig. 5-87D), and mixed hypoechoic-isoechoic (see Fig.

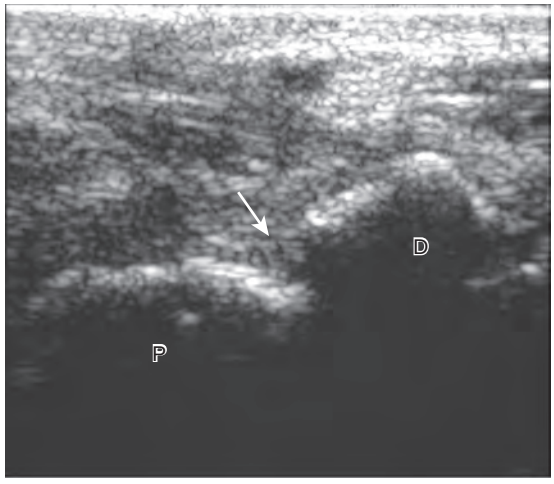

FIGURE 5-86 ■ Scaphoid fracture. Ultrasound image over the volar wrist in long axis to the scaphoid shows a cortical step-off deformity *(arrow)* and discontinuity. D, distal pole of scaphoid; P, proximal pole of scaphoid.

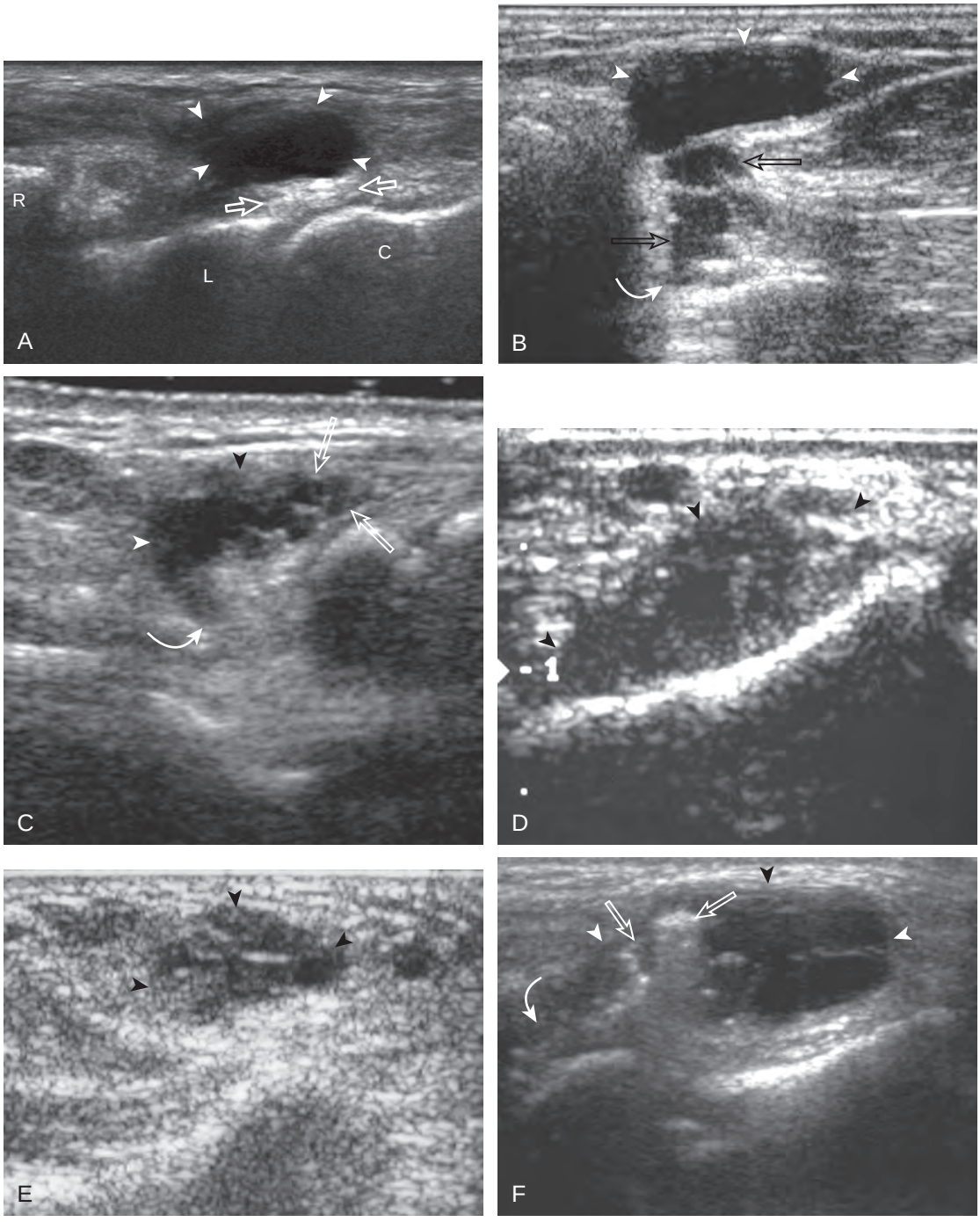

FIGURE 5-87 ■ **Ganglion cysts.** Ultrasound images from different patients show ganglion cysts *(arrowheads)* that appear **(A)** anechoic with increased through-transmission *(open arrows)*, **(B)** anechoic and multilobular *(open arrow)*, **(C)** of mixed echogenicity and irregular *(open arrows)*, **(D)** hypoechoic, **(E)** mixed hypoechoic and isoechoic, **(F)** of mixed echogenicity with hyperechoic gas *(open arrows)*, and **(G)** hyperechoic from hemorrhage *(open arrow)*. Note ganglion cyst connection to the adjacent joint *(curved arrows)*. A, radial artery; C, capitate; L, lunate; R, radius.

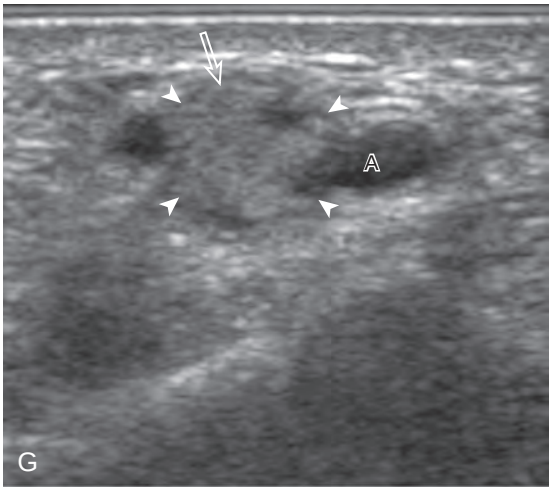

FIGURE 5-87, cont'd

5-87E).[65,66] Hyperechoic foci from communicating intra-articular vacuum joint gas (see Fig. 5-87F) and hyperechoic hemorrhage (see Fig. 5-87G) are also possible. Increased through-transmission is typically present but may be absent when ganglion cysts are small.[65] Given this somewhat variable appearance of wrist ganglion cysts, it is the location of the presumed ganglion that becomes very important in consideration of the correct diagnosis. Many ganglion cysts are located dorsal, adjacent to the scapholunate ligament (Fig. 5-88).[15] It is important to differentiate a dorsal ganglion cyst from a distended dorsal wrist joint recess; with wrist movement or transducer pressure, a joint recess typically collapses, whereas a ganglion cyst is noncompressible (Fig. 5-19) (Videos 5-27 and 5-28).[15] Another very common and often underreported site for ganglion cysts is volar, between the radial artery and the flexor carpi radialis tendon, with communication to the radiocarpal joint between the radius and scaphoid (Fig. 5-89) (Video 5-29). In this location, a ganglion cyst may appear pulsatile from the adjacent radial artery that may clinically simulate a radial artery aneurysm (Fig. 5-90). Pulsation from the adjacent radial artery may cause artifactual flow within the ganglion cyst (Fig. 5-91). Volar ganglion cysts may be small and nonpalpable, but symptomatic regardless; therefore, imaging between the radial artery and flexor

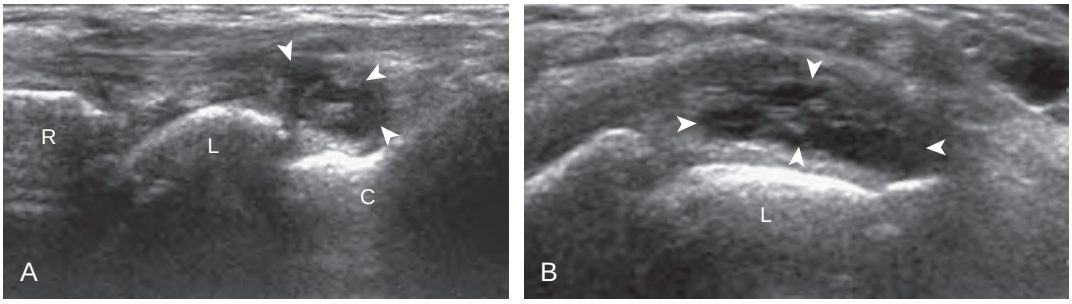

FIGURE 5-88 ■ Ganglion cyst: dorsal. Ultrasound images in **(A)** sagittal and **(B)** transverse over the lunate (L) show a anechoic to hypoechoic multilocular ganglion cyst *(arrowheads)*. C, capitate; R, radius.

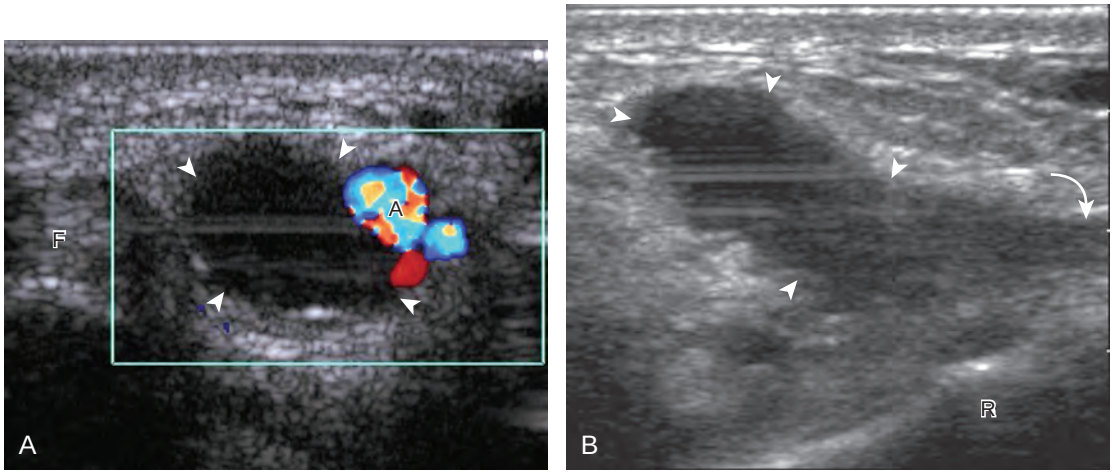

FIGURE 5-89 ■ Ganglion cyst: volar. Ultrasound images **(A)** transverse between the radial artery (A) and flexor carpi radialis tendon (F) and **(B)** sagittal over the distal radius (R) show an anechoic ganglion cyst *(arrowheads)*, which communicates with the radiocarpal joint *(curved arrow)* (horizontal linear echoes within the cyst are artifactual).

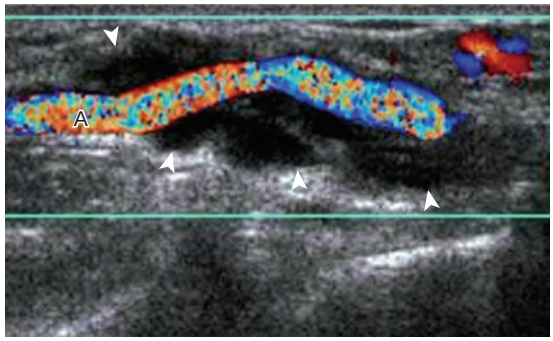

FIGURE 5-90 ■ Ganglion cyst: volar. Ultrasound color Doppler image in long axis to the radial artery (A) shows an anechoic septated ganglion cyst *(arrowheads)* that encompasses the radial artery.

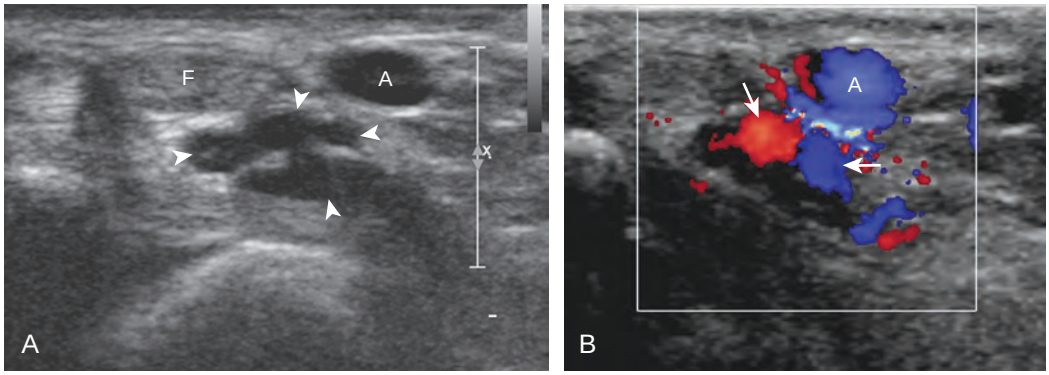

FIGURE 5-91 ■ Ganglion cyst: artifactual flow. Ultrasound **(A)** gray-scale and **(B)** color Doppler images in short axis to the radial artery show an anechoic septated ganglion cyst *(arrowheads)*. Note the artifactual flow in the ganglion cyst *(arrows)* in **(B)** from pulsation of the adjacent radial artery (A). F, flexor carpi radialis tendon.

carpi radialis tendons in addition to over the scapholunate ligament should be part of a scanning routine for wrist pain. A ganglion cyst may occur elsewhere in the wrist and hand and may cause carpal tunnel syndrome (see Fig. 5-66) and trigger finger (Fig. 5-92). It is also important to identify and describe any connection between a ganglion cyst and joint or tendon sheath because this becomes important with surgical removal. Percutaneous ultrasound-guided aspiration and steroid injection have been shown to be effective in the treatment of wrist ganglion cysts.[67]

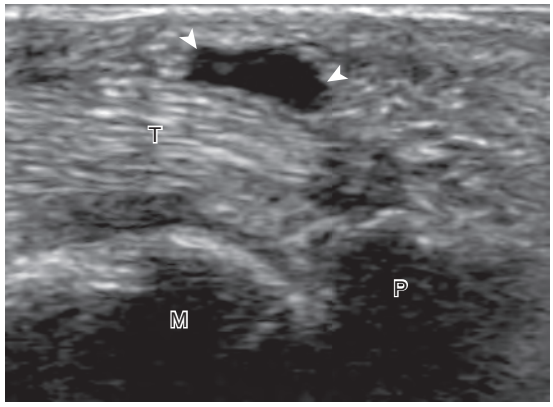

FIGURE 5-92 ■ Ganglion cyst: digit. Ultrasound image in long axis to the flexor tendons (T) at the level of the third metacarpophalangeal joint A1 pulley shows an anechoic ganglion cyst *(arrowheads)*. M, metacarpal; P, proximal phalanx.

OTHER MASSES

Giant Cell Tumor of the Tendon Sheath and Similar Masses

The differential diagnosis of a palpable abnormality of a digit near a tendon includes a cyst, such as a ganglion cyst or mucous cyst associated with osteoarthritis, or a solid mass. If in contact with a tendon, a giant cell tumor of the tendon sheath (also called *localized pigmented villonodular tenosynovitis*) should be strongly considered (Video 5-30).[68-70] This hypoechoic solid mass is in contact with the tendon sheath but does not move with tendon translation (Fig. 5-93). Increased through-transmission may be present, as with other solid masses, and may initially be misinterpreted as a hypoechoic complex cyst; however, internal flow on color or power Doppler imaging indicates a solid mass. Another solid mass of the digit that may appear similar is a fibroma or, less commonly, an angioleiomyoma (Fig. 5-94). Because solid masses are not specific for one diagnosis, pathologic confirmation is necessary.

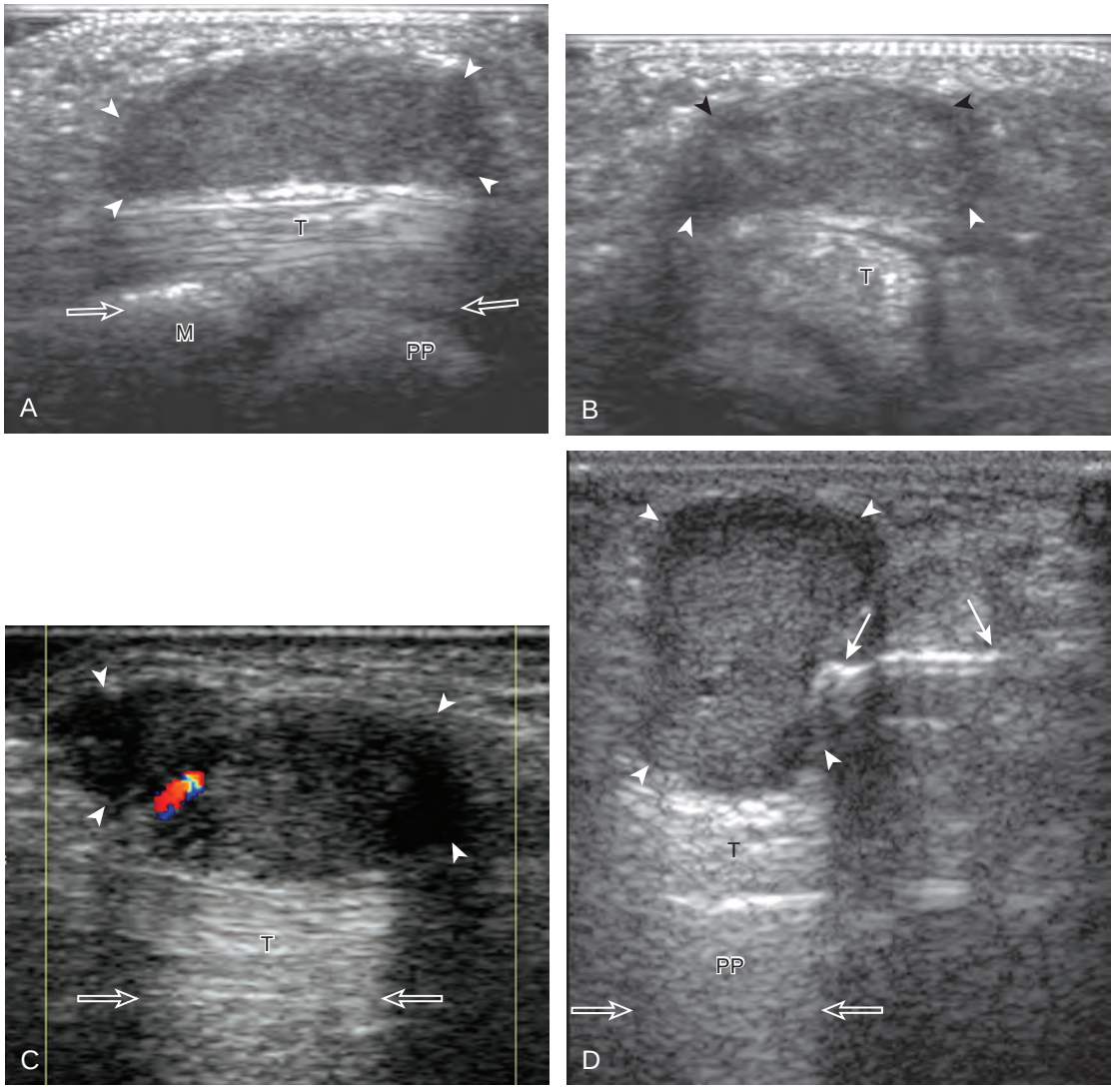

FIGURE 5-93 ■ Giant cell tumor of the tendon sheath. Long axis and short axis ultrasound images from five different patients **(A** and **B, C** and **D, E** and **F,** and **G** and **H)** show uniformly heterogeneous but predominantly hypoechoic soft tissue masses *(arrowheads)*, which represent a giant cell tumor of the tendon sheath. Note increased through-transmission in each example *(open arrows)*, variable hyperemia, and the percutaneous biopsy needle *(arrows)* in **D.** DP, distal phalanx; M, metacarpal; MP, middle phalanx; PP, proximal phalanx; T, flexor tendons.

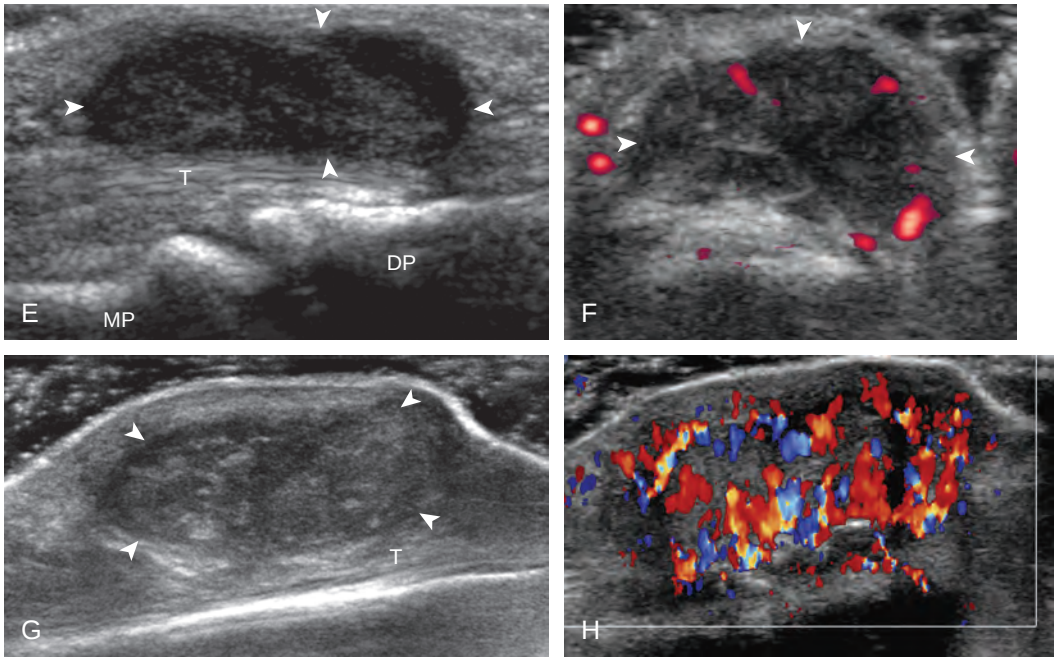

FIGURE 5-93, cont'd

Dupuytren Contracture

Patients with this fibrosing condition present with a palpable mass or nodularity superficial to the flexor tendons of the hand caused by thickening of the palmar aponeurosis, which can result in contracture.[71] At ultrasound, an elongated plaque-like hypoechoic area is identified, typically superficial to one or more of the flexor tendons without flow on color or power Doppler imaging (Fig. 5-95). Uncommonly, a ruptured epidermal inclusion cyst may create a similar appearance. Although a typical epidermal inclusion cyst has a characteristic appearance at ultrasound (round or oval, hypoechoic to mildly echogenic with a possible hypoechoic halo), a ruptured epidermal inclusion cyst may have an irregular shape (Fig. 5-96).[72,73]

Glomus Tumor

A glomus tumor arises from a neuromyoarterial glomus body, most commonly beneath the nail or about the distal aspect of the digit.

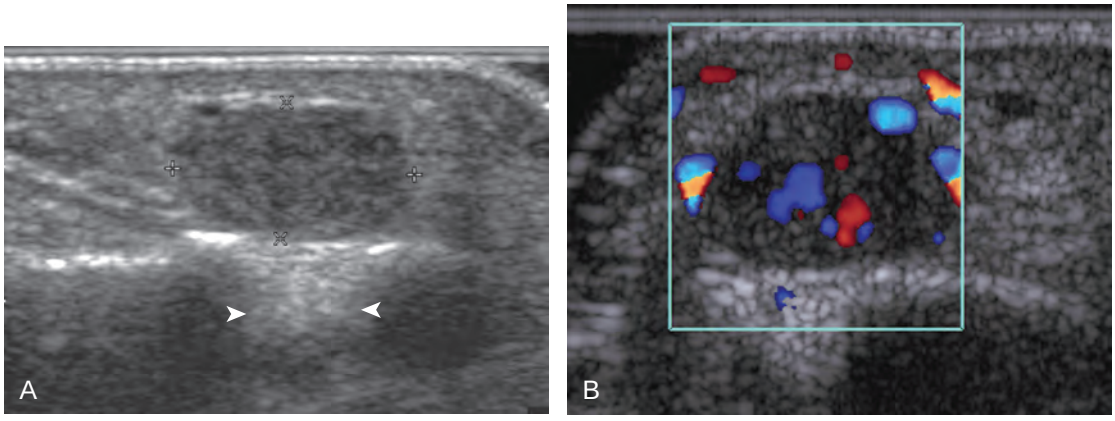

FIGURE 5-94 ■ **Angioleiomyoma.** Ultrasound images **(A)** sagittal over the volar thumb and **(B)** transverse with color Doppler imaging show a hypoechoic mass (between cursors in **A**) with increased through-transmission *(arrowheads)* and hyperemia.

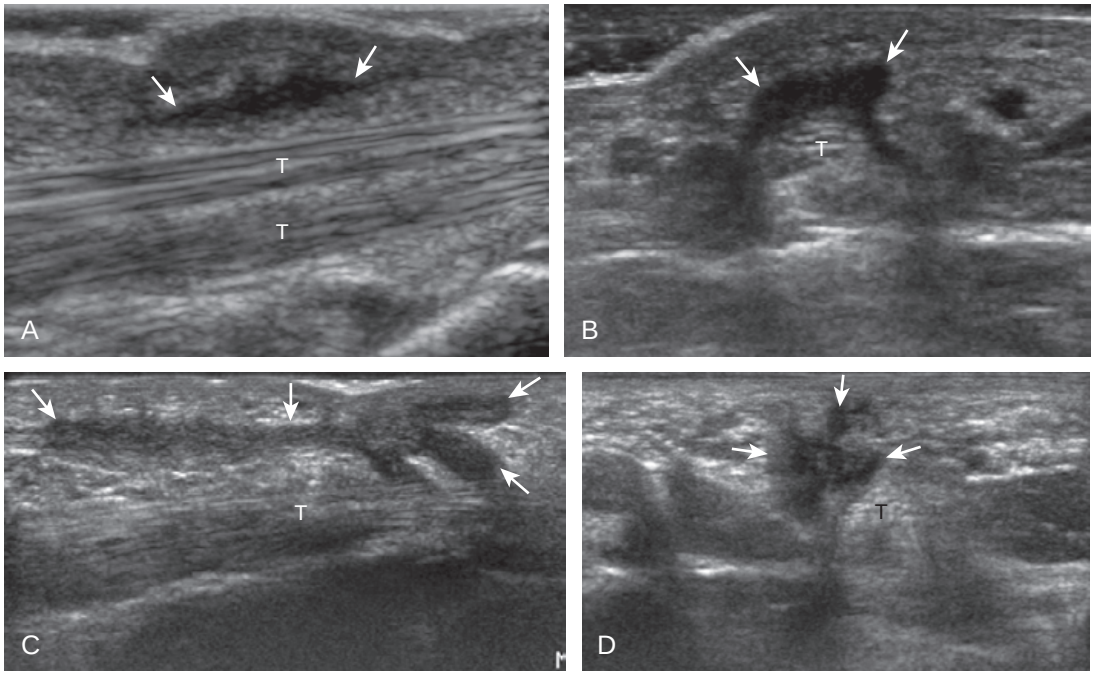

FIGURE 5-95 ■ Dupuytren contracture (palmar fibromatosis). Ultrasound images in two different patients **(A** and **B,** and **C** and **D)** in long axis and short axis to the flexor tendons (T) show hypoechoic mass-like thickening of the palmar fascia *(arrows)*.

Clinically, this tumor may present with pain, point tenderness, and sensitivity to cold exposure. At ultrasound, a glomus tumor will appear as a focal hypoechoic mass with hyperemia, increased through-transmission, and possible cortical bone remodeling (Fig. 5-97) (Video 5-31).[74] Because the imaging appearance is not specific for one diagnosis, it is the location of the abnormality that is important in suggesting the correct diagnosis.

Miscellaneous Masses

Although most solid masses are not specific for one diagnosis at ultrasound, associated imaging features may allow a precise diagnosis is some cases. For example, continuity between a mass and peripheral nerve is consistent with a peripheral nerve sheath tumor or a nerve transection neuroma (see Chapter 2). If a heterogeneous mass shows typical to-and-fro yin-yang flow

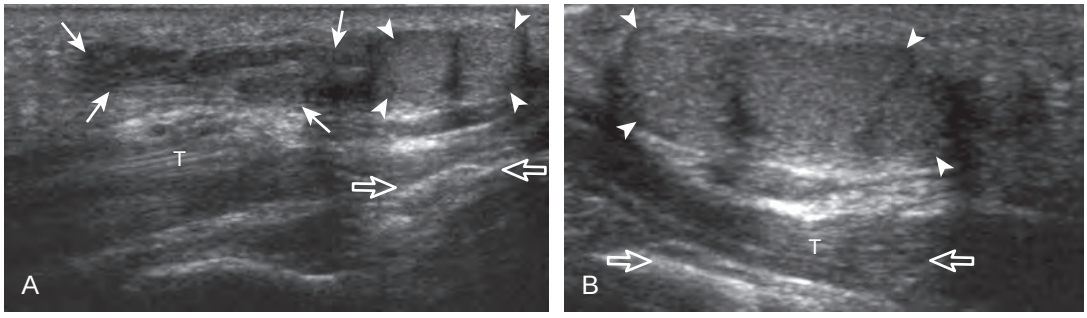

FIGURE 5-96 ■ Epidermal inclusion cyst: rupture. Ultrasound images **(A** and **B)** over the palmar aspect of the hand show an epidermal inclusion cyst *(arrowheads)* as a low-level homogeneous echo and posterior through-transmission *(open arrows)* with adjacent hypoechogenicity *(arrows)* from rupture. T, flexor tendon.

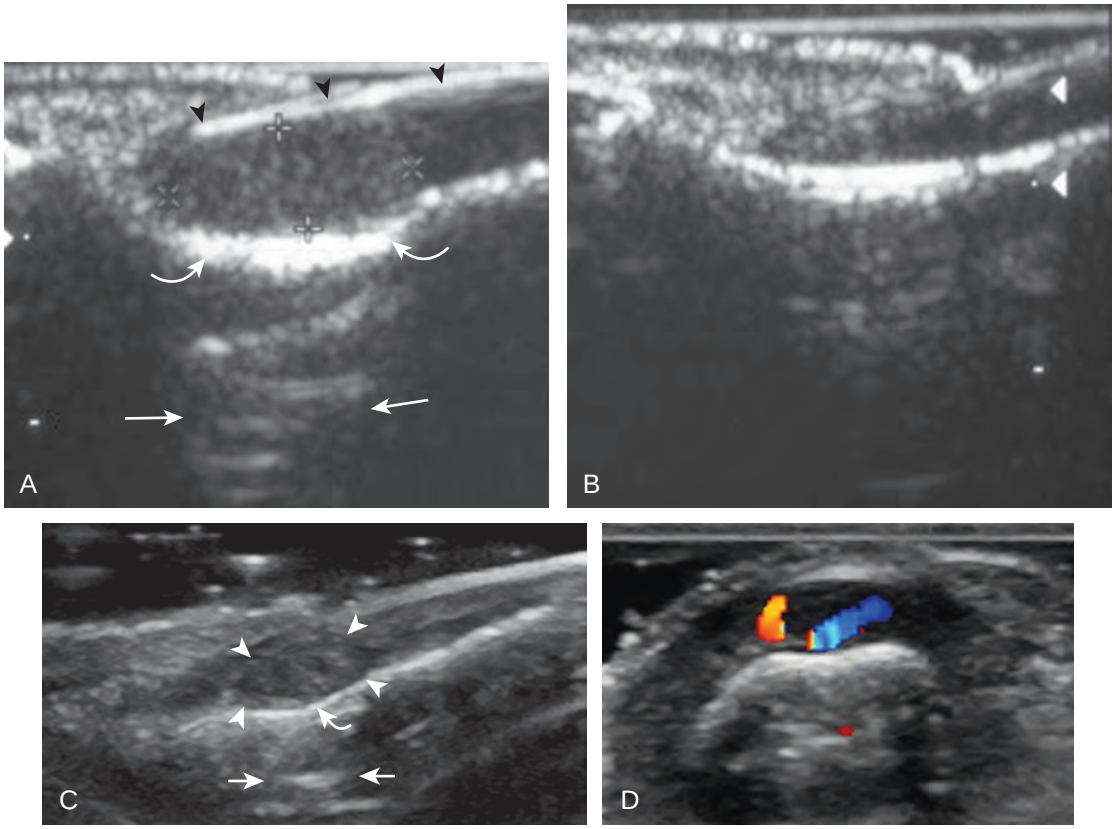

FIGURE 5-97 ■ **Glomus tumor.** Ultrasound images **(A)** sagittal over the symptomatic nail bed and **(B)** sagittal over the contralateral asymptomatic nail bed show the hypoechoic glomus tumor (between cursors in **A**). Note the nail *(arrowheads)* and the contralateral normal side **(B)**. Ultrasound images from a different patient **(C)** sagittal over the nail bed and **(D)** transverse with color Doppler show a hypoechoic glomus tumor *(arrowheads)* with increased blood flow. Note bone remodeling of the distal phalanx *(curved arrows)* and increased through-transmission *(arrows)* in both examples.

on color or power Doppler imaging and there is continuity with a vascular structure, then pseudoaneurysm is the likely diagnosis. Other tumors may involve the hand and the wrist, including benign tumors such as soft tissue chondromas and malignant tumors such as malignant fibrous histiocytoma. Retained soft tissue foreign bodies may produce a mass-like appearance (see Chapter 2).

Online references available at www.expertconsult.com.

REFERENCES

1. Linkous MD, Pierce SD, Gilula LA: Scapholunate ligamentous communicating defects in symptomatic and asymptomatic wrists: characteristics. *Radiology* 216:846–850, 2000.
2. Boutry N, Titecat M, Demondion X, et al: High-frequency ultrasonographic examination of the finger pulley system. *J Ultrasound Med* 24:1333–1339, 2005.
3. Theumann NH, Pfirrmann CW, Drape JL, et al: MR imaging of the metacarpophalangeal joints of the fingers: part I. Conventional MR imaging and MR arthrographic findings in cadavers. *Radiology* 222:437–445, 2002.
4. Jamadar DA, Jacobson JA, Hayes CW: Sonographic evaluation of the median nerve at the wrist. *J Ultrasound Med* 20:1011–1014, 2001.
5. Tagliafico A, Pugliese F, Bianchi S, et al: High-resolution sonography of the palmar cutaneous branch of the median nerve. *AJR Am J Roentgenol* 191:107–114, 2008.
6. Parellada AJ, Morrison WB, Reiter SB, et al: Flexor carpi radialis tendinopathy: spectrum of imaging findings and association with triscaphe arthritis. *Skeletal Radiol* 35:572–578, 2006.
7. Smith J, Rizzo M, Finnoff JT, et al: Sonographic appearance of the posterior interosseous nerve at the wrist. *J Ultrasound Med* 30:1233–1239, 2011.
8. Lee KS, Ablove RH, Singh S, et al: Ultrasound imaging of normal displacement of the extensor carpi ulnaris tendon within the ulnar groove in 12 forearm-wrist positions. *AJR Am J Roentgenol* 193:651–655, 2009.
9. Robertson BL, Jamadar DA, Jacobson JA, et al: Extensor retinaculum of the wrist: sonographic characterization and pseudotenosynovitis appearance. *AJR Am J Roentgenol* 188:198–202, 2007.
10. Jacobson JA, Oh E, Propeck T, et al: Sonography of the scapholunate ligament in four cadaveric wrists: correlation with MR arthrography and anatomy. *AJR Am J Roentgenol* 179:523–527, 2002.
11. Taljanovic MS, Goldberg MR, Sheppard JE, et al: US of the intrinsic and extrinsic wrist ligaments and triangular fibrocartilage complex: normal anatomy and imaging technique. *Radiographics* 31:e44, 2011.
12. Theumann NH, Pfirrmann CW, Antonio GE, et al: Extrinsic carpal ligaments: normal MR arthrographic appearance in cadavers. *Radiology* 226:171–179, 2003.
13. Boutry N, Larde A, Demondion X, et al: Metacarpophalangeal joints at US in asymptomatic volunteers and cadaveric specimens. *Radiology* 232:716–724, 2004.
14. McNally EG: Ultrasound of the small joints of the hands and feet: current status. *Skeletal Radiol* 37:99–113, 2008.
15. Cardinal E, Buckwalter KA, Braunstein EM, et al: Occult dorsal carpal ganglion: comparison of US and MR imaging. *Radiology* 193:259–262, 1994.
16. Wakefield RJ, Balint PV, Szkudlarek M, et al: Musculoskeletal ultrasound including definitions for ultrasonographic pathology. *J Rheumatol* 32:2485–2487, 2005.
17. Lund PJ, Heikal A, Maricic MJ, et al: Ultrasonographic imaging of the hand and wrist in rheumatoid arthritis. *Skeletal Radiol* 24:591–596, 1995.
18. Lopez-Ben R, Bernreuter WK, Moreland LW, et al: Ultrasound detection of bone erosions in rheumatoid arthritis: a comparison to routine radiographs of the hands and feet. *Skeletal Radiol* 33:80–84, 2004.
19. Finzel S, Ohrndorf S, Englbrecht M, et al: A detailed comparative study of high-resolution ultrasound and micro-computed tomography for detection of arthritic bone erosions. *Arthritis Rheum* 63:1231–1236, 2011.
20. Gutierrez M, Filippucci E, De Angelis R, et al: A sonographic spectrum of psoriatic arthritis: "the five targets." *Clin Rheumatol* 29:133–142, 2010.
21. Backhaus M, Burmester GR, Gerber T, et al: Guidelines for musculoskeletal ultrasound in rheumatology. *Ann Rheum Dis* 60:641–649, 2001.
22. Vlad V, Berghea F, Libianu S, et al: Ultrasound in rheumatoid arthritis: volar versus dorsal synovitis evaluation and scoring. *BMC Musculoskelet Disord* 12:124, 2011.
23. Sheane BJ, Beddy P, O'Connor M, et al: Targeted ultrasound of the fifth metatarsophalangeal joint in an early inflammatory arthritis cohort. *Arthritis Rheum* 61:1004–1008, 2009.
24. Backhaus M, Ohrndorf S, Kellner H, et al: Evaluation of a novel 7-joint ultrasound score in daily rheumatologic practice: a pilot project. *Arthritis Rheum* 61:1194–1201, 2009.
25. Breidahl WH, Stafford Johnson DB, Newman JS, et al: Power Doppler sonography in tenosynovitis: significance of the peritendinous hypoechoic rim. *J Ultrasound Med* 17:103–107, 1998.
26. Daenen B, Houben G, Bauduin E, et al: Sonography in wrist tendon pathology. *J Clin Ultrasound* 32:462–469, 2004.
27. De Maeseneer M, Marcelis S, Jager T, et al: Spectrum of normal and pathologic findings in the region of the first extensor compartment of the wrist: sonographic findings and correlations with dissections. *J Ultrasound Med* 28:779–786, 2009.
28. Choi SJ, Ahn JH, Lee YJ, et al: de Quervain disease: US identification of anatomic variations in the first extensor compartment with an emphasis on subcompartmentalization. *Radiology* 260:480–486, 2011.
29. Rousset P, Vuillemin-Bodaghi V, Laredo JD, et al: Anatomic variations in the first extensor compartment of the wrist: accuracy of US. *Radiology* 257:427–433, 2010.
30. Gutierrez M, Filippucci E, Salaffi F, et al: Differential diagnosis between rheumatoid arthritis and psoriatic arthritis: the value of ultrasound findings at metacarpophalangeal joints level. *Ann Rheum Dis* 70:1111–1114, 2011.
31. De Maeseneer M, Marcelis S, Osteaux M, et al: Sonography of a rupture of the tendon of the extensor pollicis longus muscle: initial clinical experience and correlation with findings at cadaveric dissection. *AJR Am J Roentgenol* 184:175–179, 2005.
32. Lopez-Ben R, Lee DH, Nicolodi DJ: Boxer knuckle (injury of the extensor hood with extensor tendon subluxation): diagnosis with dynamic US: report of three cases. *Radiology* 228:642–646, 2003.
33. Hauger O, Chung CB, Lektrakul N, et al: Pulley system in the fingers: normal anatomy and simulated lesions in cadavers at MR imaging, CT, and US with and without contrast material distention of the tendon sheath. *Radiology* 217:201–212, 2000.
34. Klauser A, Frauscher F, Bodner G, et al: Finger pulley injuries in extreme rock climbers: depiction with dynamic US. *Radiology* 222:755–761, 2002.
35. Martinoli C, Bianchi S, Nebiolo M, et al: Sonographic evaluation of digital annular pulley tears. *Skeletal Radiol* 29:387–391, 2000.
36. Guerini H, Pessis E, Theumann N, et al: Sonographic appearance of trigger fingers. *J Ultrasound Med* 27:1407–1413, 2008.
37. Serafini G, Derchi LE, Quadri P, et al: High resolution sonography of the flexor tendons in trigger fingers. *J Ultrasound Med* 15:213–219, 1996.
38. Ouellette H, Thomas BJ, Torriani M: Using dynamic sonography to diagnose extensor digitorum brevis manus. *AJR Am J Roentgenol* 181:1224–1226, 2003.
39. Timins ME: Muscular anatomic variants of the wrist and hand: findings on MR imaging. *AJR Am J Roentgenol* 172:1397–1401, 1999.

40. Klauser AS, Faschingbauer R, Bauer T, et al: Entrapment neuropathies II: carpal tunnel syndrome. *Semin Musculoskelet Radiol* 14:487–500, 2010.
41. Nakamichi K, Tachibana S: Restricted motion of the median nerve in carpal tunnel syndrome. *J Hand Surg [Br]* 20:460–464, 1995.
42. Ghasemi-Esfe AR, Khalilzadeh O, Vaziri-Bozorg SM, et al: Color and power Doppler US for diagnosing carpal tunnel syndrome and determining its severity: a quantitative image processing method. *Radiology* 261:499–506, 2011.
43. Mallouhi A, Pultzl P, Trieb T, et al: Predictors of carpal tunnel syndrome: accuracy of gray-scale and color Doppler sonography. *AJR Am J Roentgenol* 186:1240–1245, 2006.
44. Granata G, Caliandro P, Pazzaglia C, et al: Prevalence of bifid median nerve at wrist assessed through ultrasound. *Neurol Sci* 32:615–618, 2011.
45. Propeck T, Quinn TJ, Jacobson JA, et al: Sonography and MR imaging of bifid median nerve with anatomic and histologic correlation. *AJR Am J Roentgenol* 175:1721–1725, 2000.
46. Klauser AS, Halpern EJ, Faschingbauer R, et al: Bifid median nerve in carpal tunnel syndrome: assessment with US cross-sectional area measurement. *Radiology* 259:808–815, 2011.
47. Abicalaf CA, de Barros N, Sernik RA, et al: Ultrasound evaluation of patients with carpal tunnel syndrome before and after endoscopic release of the transverse carpal ligament. *Clin Radiol* 62:891–894; discussion 5–6, 2007.
48. Cartwright MS, White DL, Demar S, et al: Median nerve changes following steroid injection for carpal tunnel syndrome. *Muscle Nerve* 44:25–29, 2011.
49. De Maeseneer M, Jaovisidha S, Lenchik L, et al: Fibrolipomatous hamartoma: MR imaging findings. *Skeletal Radiol* 26:155–160, 1997.
50. Jacobson JA, Fessell DP, Lobo Lda G, et al: Entrapment neuropathies I: upper limb (carpal tunnel excluded). *Semin Musculoskelet Radiol* 14:473–486, 2010.
51. Velling TE, Brennan FJ, Hall LD, et al: Sonographic diagnosis of ulnar artery aneurysm in hypothenar hammer syndrome: report of 2 cases. *J Ultrasound Med* 20:921–924, 2011.
52. Tagliafico A, Altafini L, Garello I, et al: Traumatic neuropathies: spectrum of imaging findings and postoperative assessment. *Semin Musculoskelet Radiol* 14:512–522, 2010.
53. Thomas AJ, Bull MJ, Howard AC, et al: Perioperative ultrasound guided needle localisation of amputation stump neuroma. *Injury* 30:689–691, 1999.
54. Renoux J, Zeitoun-Eiss D, Brasseur JL: Ultrasonographic study of wrist ligaments: review and new perspectives. *Semin Musculoskelet Radiol* 13:55–65, 2009.
55. Boutry N, Lapegue F, Masi L, et al: Ultrasonographic evaluation of normal extrinsic and intrinsic carpal ligaments: preliminary experience. *Skeletal Radiol* 34:513–521, 2005.
56. Hergan K, Mittler C, Oser W: Ulnar collateral ligament: differentiation of displaced and nondisplaced tears with US and MR imaging. *Radiology* 194:65–71, 1995.
57. Ebrahim FS, De Maeseneer M, Jager T, et al: US diagnosis of UCL tears of the thumb and Stener lesions: technique, pattern-based approach, and differential diagnosis. *Radiographics* 26:1007–1020, 2006.
58. Spaeth HJ, Abrams RA, Bock GW, et al: Gamekeeper thumb: differentiation of nondisplaced and displaced tears of the ulnar collateral ligament with MR imaging. Work in progress. *Radiology* 188:553–556, 1993.
59. Chiou HJ, Chang CY, Chou YH, et al: Triangular fibrocartilage of wrist: presentation on high resolution ultrasonography. *J Ultrasound Med* 17:41–48, 1998.
60. McGinley JC, Roach N, Gaughan JP, et al: Forearm interosseous membrane imaging and anatomy. *Skeletal Radiol* 33:561–568, 2004.
61. Rodriguez-Martin J, Pretell-Mazzini J: The role of ultrasound and magnetic resonance imaging in the evaluation of the forearm interosseous membrane: a review. *Skeletal Radiol* 40:1515–1522, 2011.
62. Failla JM, Jacobson J, van Holsbeeck M: Ultrasound diagnosis and surgical pathology of the torn interosseous membrane in forearm fractures/dislocations. *J Hand Surg [Am]* 24:257–266, 1999.
63. Platon A, Poletti PA, Van Aaken J, et al: Occult fractures of the scaphoid: the role of ultrasonography in the emergency department. *Skeletal Radiol* 40:869–875, 2011.
64. Bianchi S, Abdelwahab IF, Zwass A, et al: Ultrasonographic evaluation of wrist ganglia. *Skeletal Radiol* 23:201–203, 1994.
65. Wang G, Jacobson JA, Feng FY, et al: Sonography of wrist ganglion cysts: variable and noncystic appearances. *J Ultrasound Med* 26:1323–1328; quiz 30–31, 2007.
66. Teefey SA, Dahiya N, Middleton WD, et al: Ganglia of the hand and wrist: a sonographic analysis. *AJR Am J Roentgenol* 191:716–720, 2008.
67. Breidahl WH, Adler RS: Ultrasound-guided injection of ganglia with corticosteroids. *Skeletal Radiol* 25:635–638, 1996.
68. Middleton WD, Patel V, Teefey SA, et al: Giant cell tumors of the tendon sheath: analysis of sonographic findings. *AJR Am J Roentgenol* 183:337–339, 2004.
69. Murphey MD, Rhee JH, Lewis RB, et al: Pigmented villonodular synovitis: radiologic-pathologic correlation. *Radiographics* 28:1493–1518, 2008.
70. Wang Y, Tang J, Luo Y: The value of sonography in diagnosing giant cell tumors of the tendon sheath. *J Ultrasound Med* 26:1333–1340, 2007.
71. Yacoe ME, Bergman AG, Ladd AL, et al: Dupuytren's contracture: MR imaging findings and correlation between MR signal intensity and cellularity of lesions. *AJR Am J Roentgenol* 160:813–817, 1993.
72. Jin W, Ryu KN, Kim GY, et al: Sonographic findings of ruptured epidermal inclusion cysts in superficial soft tissue: emphasis on shapes, pericystic changes, and pericystic vascularity. *J Ultrasound Med* 27:171–176; quiz 7–8, 2008.
73. Kim HK, Kim SM, Lee SH, et al: Subcutaneous epidermal inclusion cysts: ultrasound (US) and MR imaging findings. *Skeletal Radiol* 40:1415–1419, 2011.
74. Glazebrook KN, Laundre BJ, Schiefer TK, et al: Imaging features of glomus tumors. *Skeletal Radiol* 40:855–862, 2011.

eBOX 5-1 Sample Diagnostic Wrist Ultrasound Report

NORMAL

Examination: Ultrasound of the Wrist
Date of Study: March 11, 2011
Patient Name: Jack White
Registration Number: 8675309
History: Numbness, evaluate for carpal tunnel syndrome
Findings: The median nerve is unremarkable in appearance, measuring 8 mm^2 at the wrist crease and 7 mm^2 at the pronator quadratus. No evidence of tenosynovitis. The radiocarpal, midcarpal, and distal radioulnar joints are normal without effusion or synovial hypertrophy. The wrist tendons are normal without tear or tenosynovitis. Normal dorsal component of the scapholunate ligament. No dorsal or volar ganglion cyst. Unremarkable Guyon canal. Additional focused evaluation at site of maximal symptoms was unrevealing.
Impression: Unremarkable ultrasound examination of the wrist.

eBOX 5-2 Sample Diagnostic Wrist Ultrasound Report

ABNORMAL

Examination: Ultrasound of the Wrist
Date of Study: March 11, 2011
Patient Name: Jack White
Registration Number: 8675309
History: Numbness, evaluate for carpal tunnel syndrome
Findings: The median nerve is hypoechoic and enlarged, measuring 15 mm^2 at the wrist crease and 7 mm^2 at the pronator quadratus. No evidence for tenosynovitis. The radiocarpal, midcarpal, and distal radioulnar joints are normal without effusion or synovial hypertrophy. The wrist tendons are normal without tear or tenosynovitis. Normal dorsal component of the scapholunate ligament. No dorsal ganglion cyst. A 7-mm volar ganglion cyst is noted between the radial artery and flexor carpi radialis tendon. Unremarkable Guyon canal. Additional focused evaluation at site of maximal symptoms was unrevealing.
Impression:
1. Ultrasound findings compatible with carpal tunnel syndrome.
2. A 7-mm volar ganglion cyst.

CHAPTER 6

Hip and Thigh Ultrasound

CHAPTER OUTLINE

HIP AND THIGH ANATOMY

ULTRASOUND EXAMINATION TECHNIQUE
General Comments
Hip Evaluation: Anterior
Hip Evaluation: Lateral
Hip Evaluation: Posterior
Inguinal Region Evaluation
Thigh Evaluation: Anterior
Thigh Evaluation: Medial
Thigh Evaluation: Posterior
Hip Evaluation for Dysplasia in a Child

JOINT AND BURSAL ABNORMALITIES
Joint Effusion and Synovial Hypertrophy
Labrum and Proximal Femur Abnormalities
Bursal Abnormalities
Postsurgical Hip

TENDON AND MUSCLE ABNORMALITIES
Tendon and Muscle Injury
Snapping Hip Syndrome
Calcific Tendinosis
Diabetic Muscle Infarction
Pseudohypertrophy of the Tensor Fasciae Latae

PERIPHERAL NERVE ABNORMALITIES

MISCELLANEOUS CONDITIONS
Morel-Lavallée Lesion
Inguinal Lymph Node
Other Soft Tissue Masses
Hernias
Developmental Dysplasia of the Hip

Additional videos for this topic are available online at www.expertconsult.com.

HIP AND THIGH ANATOMY

The hip joint is a synovial articulation between the acetabulum of the pelvis and the proximal femur. The joint recess extends from the acetabulum over the femur to the level of the intertrochanteric line, just beyond the femoral neck. The joint capsule becomes thickened from the iliofemoral, ischiofemoral, and pubofemoral ligaments (Fig. 6-1A) and a reflection of the joint capsule extends proximally along the femoral neck.[1] The femoral head is covered by hyaline cartilage, whereas the acetabulum is lined by hyaline cartilage in an inverted U shape with a fibrocartilage labrum attached to the acetabular rim.

Several muscles originate from the pelvis and extend across the hip joint, and others originate from the femur itself (see Fig. 6-1B and C). Muscles that originate from the posterior surface of the ilium are the gluteus minimus (which inserts on the anterior facet of the greater trochanter), the gluteus medius (which inserts on the lateral and superoposterior facets of the greater trochanter), and the gluteus maximus (which inserts on the posterior femur gluteal tuberosity below the trochanters and iliotibial tract).[2] Posteriorly, the piriformis originates from the sacrum and extends inferior and lateral to insert onto the greater trochanter. Other muscles inferior to the piriformis that extend from the ischium to the proximal femur include the superior gemellus, obturator internus, inferior gemellus, and quadratus femoris.

At the anterior aspect of the hip joint, the iliopsoas can be seen as a continuation of the iliacus and psoas muscles, which inserts on

the lesser trochanter. Other anterior muscles include the sartorius (which originates from the anterior superior iliac spine of the pelvis and inserts on the medial aspect of the proximal tibia) and the tensor fasciae latae (which originates from the posterolateral aspect of the ilium and inserts on the iliotibial tract, which, in turn, inserts on the proximal tibia). The rectus femoris has two origins: a direct or straight head, which originates from the anterior inferior iliac spine; and an indirect or reflected head, which originates inferior and posterior to the anterior inferior iliac spine from the superior acetabular ridge.[3] Distally, the direct tendon forms an anterior superficial tendon with unipennate architecture, whereas the indirect tendon forms the central tendon with bipennate architecture.[4] The rectus femoris distally combines with the vastus medialis, vastus lateralis, and vastus intermedius musculature (which all originate from the femur) to form the quadriceps tendon, which inserts on the patella and, to a lesser extent, the tibial tuberosity by way of the patellar tendon.

Medially, the adductor musculature includes the adductor longus, the adductor brevis, and the adductor magnus, which originate from the ischium and pubis of the pelvis and insert on the femur at the linea aspera and, in the case of the adductor magnus, the adductor tubercle as well. Superficial and medial to the adductors, the gracilis muscle extends from the inferior pubic ramus to the proximal tibia as part of the pes anserinus. From medially to laterally, the posterior thigh consists of the semimembranosus, the semitendinosus (both of which originate from the ischial tuberosity and insert on the proximal tibia, with the semitendinosus being part of the pes anserinus), and the biceps femoris (with long head origin from the ischial tuberosity and short head origin from the femur; the biceps femoris inserts on the fibula and lateral tibial condyle). Proximally, the semimembranosus tendon is located anterior to the conjoint tendon of the biceps femoris long head and semitendinosus and the semitendinosus muscle belly; the semimembranosus origin on the ischium is anterolateral to the conjoint tendon origin.[5]

Other important structures of the anterior thigh include (medial to lateral) the femoral nerve, artery, and vein (use the mnemonic NAVEL for *n*erve, *a*rtery, *v*ein, *e*mpty space, *l*ymphatic). The sciatic nerve is seen posteriorly adjacent to the biceps femoris muscle, where it bifurcates as the tibial nerve and the common peroneal nerve laterally. Several bursae are located around the hip joint. The iliopsoas bursa is located anteriorly along the medial aspect of the iliopsoas tendon, has a convex lateral shape, and normally communicates with the hip joint in up to 15% of the population.[6] The trochanteric

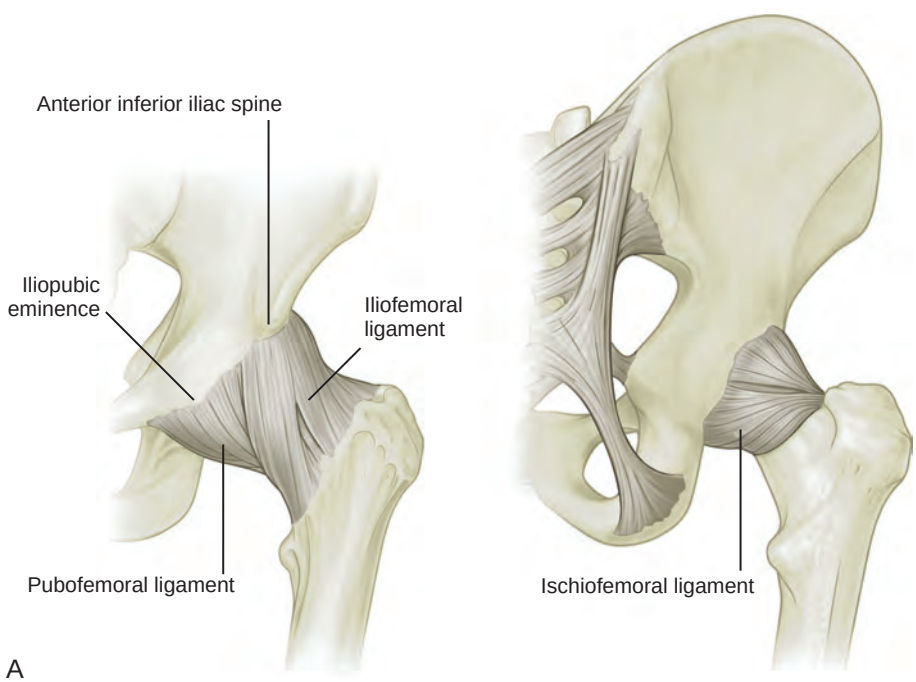

FIGURE 6-1 ■ Hip and thigh anatomy. A, Anterior and posterior views show the hip joint ligaments.

Continued

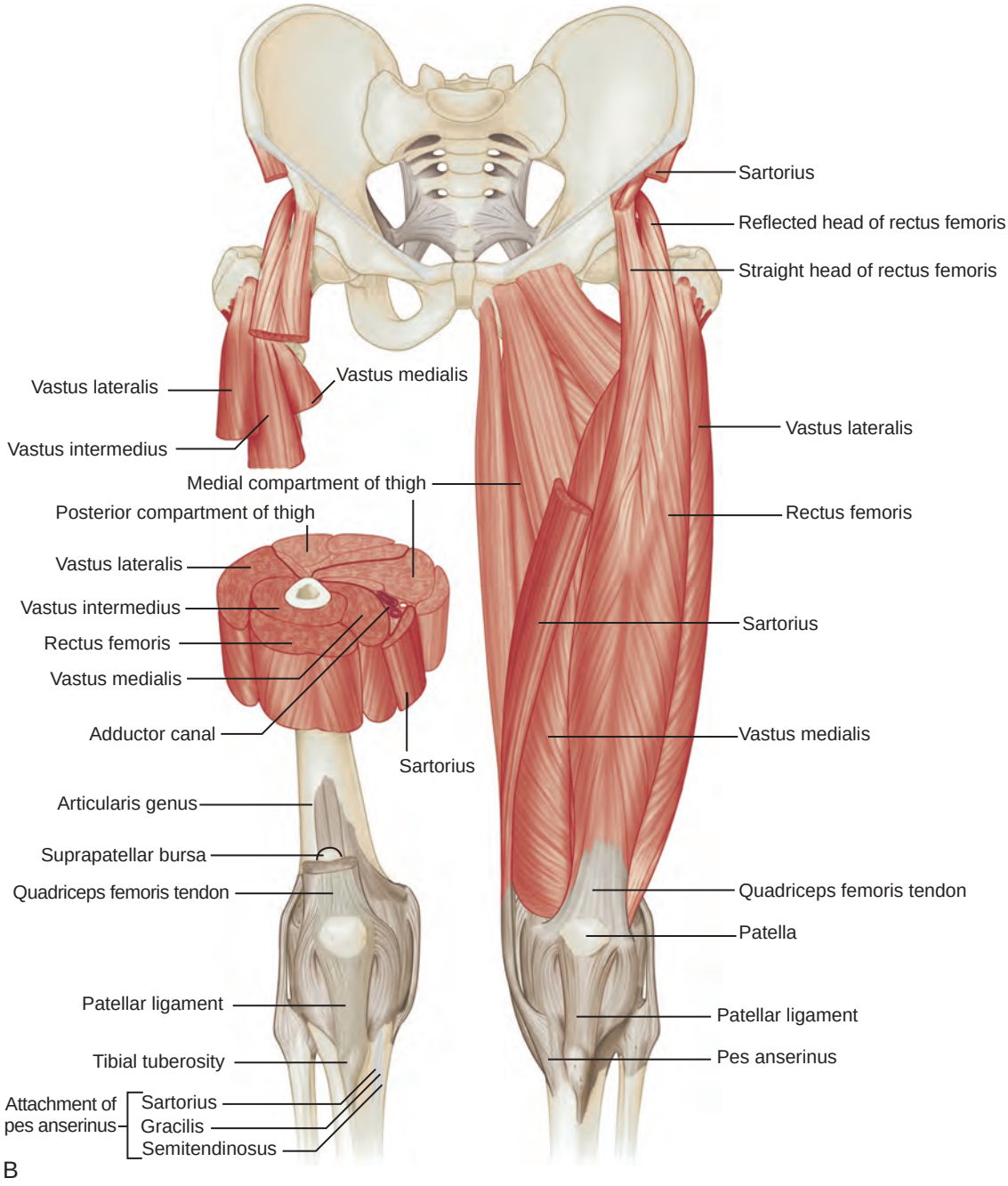

FIGURE 6-1, cont'd ■ **B,** Muscles of the anterior thigh compartment.

(or subgluteus maximus) bursa is located posterolateral over the posterior and lateral facets of the greater trochanter deep to the gluteus maximus and iliotibial tract, whereas smaller subgluteus medius and subgluteus minimus bursae are located between the lateral facet and gluteus medius and the anterior facet and gluteus minimus, respectively.[2] Other possible bursae include the obturator externus bursa, located medially and inferior to the femoral neck, which may communicate with the posteroinferior hip joint.[7]

In the inguinal region, the inguinal canal represents a triangular, elongated passage in the lower abdominal wall located just superior to the inguinal ligament (see Fig. 6-1D). The inguinal canal's posterior opening, the deep inguinal ring, is located laterally, whereas the anterior opening,

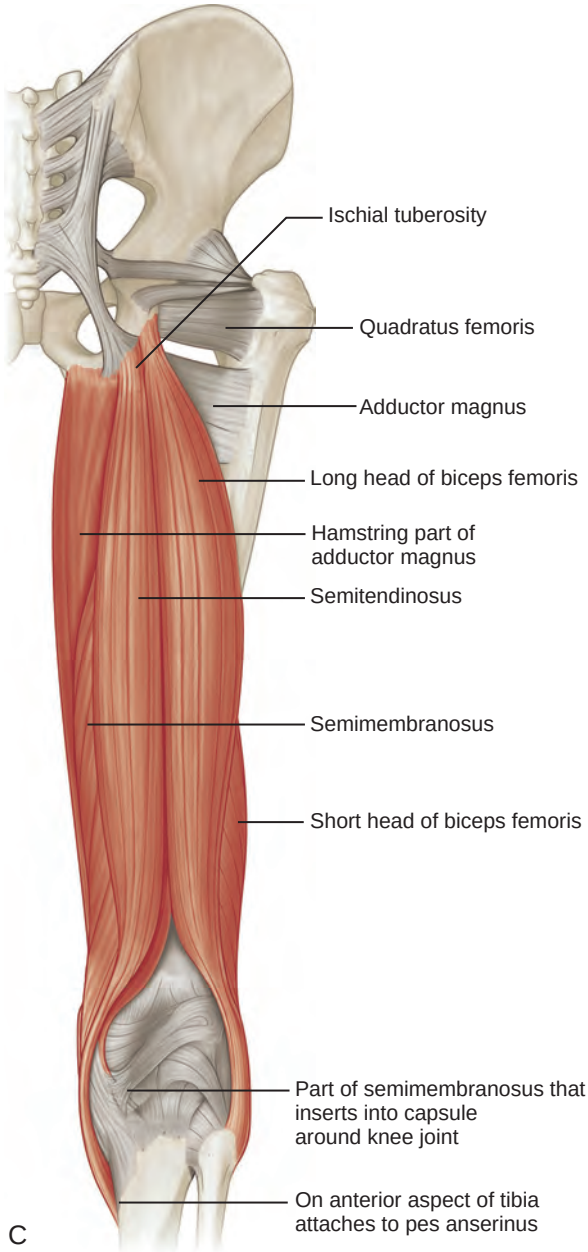

FIGURE 6-1, cont'd ■ **C,** Muscles of the posterior thigh compartment.

Continued

called the *superficial inguinal ring*, is located medially near the pubis. The contents of the inguinal canal include the ilioinguinal nerve and the spermatic cord in males and the round ligament in females. The deep inguinal ring is located just lateral to the origin of the inferior epigastric artery from the external iliac artery. The inguinal (or Hesselbach) triangle is demarcated by the lateral margin of the rectus abdominis medially, the inguinal ligament inferiorly, and the superior epigastric artery laterally.[8] Another structure near the inguinal ligament is the lateral femoral cutaneous nerve. This peripheral nerve exits the pelvis to extend over the lateral thigh in a somewhat variable manner—it may course across the iliac crest, within the sartorius tendon, within the inguinal ligament, or under the inguinal ligament.[9] The lateral femoral cutaneous nerve may also branch proximal to the inguinal ligament.

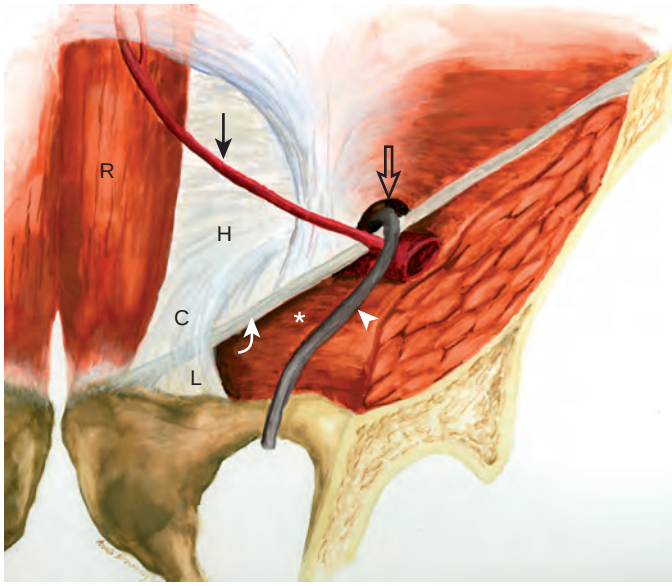

D

FIGURE 6-1, cont'd ■ **D,** Illustration of the male right inguinal region as viewed from within the abdomen shows the inferior epigastric artery *(arrow)*, deep inguinal ring *(open arrow)*, vas deferens *(arrowhead)*, inguinal ligament *(curved arrow)*, Hesselbach triangle (H), conjoint tendon (C), lacunar ligament (L), rectus abdominis (R), and location of femoral hernia *(asterisk)*. (**A** to **C,** From Drake R, Vogl W, Mitchell A: *Gray's anatomy for students,* Philadelphia, 2005, Churchill Livingstone; **D,** from Jamadar DA, Jacobson JA, Morag Y, et al: Sonography of inguinal region hernias. *AJR Am J Roentgenol* 187:185–190, 2006.)

ULTRASOUND EXAMINATION TECHNIQUE

Table 6-1 is a checklist for hip and thigh ultrasound examination. Examples of diagnostic hip ultrasound reports are available online at www.expertconsult.com (see eBox 6-1 and 6-2).

TABLE 6-1 **Hip and Thigh Ultrasound Examination Checklist**

Location	Structures of Interest
Hip: anterior	Hip joint, iliopsoas, rectus femoris, sartorius, pubic symphysis
Hip: lateral	Greater trochanter, bursae
Hip: posterior	Sacroiliac joints, piriformis, hip abductors
Inguinal region	Deep inguinal ring, Hesselbach triangle, femoral artery region
Thigh: anterior	Rectus femoris, vastus medialis, vastus intermedius, vastus lateralis
Thigh: medial	Femoral artery and nerve, sartorius, gracilis, adductors
Thigh: posterior	Semimembranosus, semitendinosus, biceps femoris, sciatic nerve

General Comments

Ultrasound examination of the hip and anterior thigh is completed with the patient supine; the patient is prone for evaluation of the posterior thigh. For evaluation of the greater trochanteric region, the patient rolls on the contralateral side. Evaluation of the hip and thigh may be considered as two separate examinations in most circumstances. Hip pain in an athlete may be caused from hip joint disease, tendon or muscle pathology, or adjacent hernia, and therefore all etiologies should be considered. The choice of transducer frequency depends on the patient's body habitus, although many times the anterior hip can be evaluated with a transducer greater than 10 MHz With large amounts of soft tissue, a transducer of less than 10 MHz may be needed to penetrate the soft tissues adequately. It is important to consider these lower frequencies initially regardless of body habitus because one should examine the entire depth of the soft tissues before focusing on the more superficial structures. This approach ensures a complete and global evaluation and also serves to orient the examiner to the various muscles, an important consideration because the bone landmarks are few and deep. One may also consider a curvilinear transducer or a virtual convex function with a linear transducer (if present) to accomplish this. Evaluation of the hip and thigh may be focused over the area that is clinically symptomatic or relevant to the patient's history. Regardless, a

complete examination of all areas should always be considered for one to become familiar with normal anatomy and normal variants and to develop a quick and efficient sonographic technique.

Hip Evaluation: Anterior

The primary structures evaluated include the hip joint and recess, iliopsoas tendon and bursa, proximal thigh musculature origin in the hip region (rectus femoris and sartorius), and pubic symphysis region. Depending on patient history and symptoms, all of these structures should be considered in the evaluation because symptoms may be referred and etiology multifactorial. Evaluation begins with the anterior hip with the transducer long axis to the femoral neck, which is in the oblique-sagittal plane (Fig. 6-2A). To find the femoral neck, one may initially image transversely over the femoral shaft to locate the curved and echogenic surface of the femur and then move the transducer proximally; once the bony protuberances of the greater and lesser trochanter are identified, the transducer is turned to the sagittal-oblique plane parallel to the femoral neck. The hip joint may also be located lateral to the femoral vasculature. The hip joint is identified long axis to the femoral neck by the characteristic bone contours of the femoral head, acetabulum, and femoral neck (see Fig. 6-2B to D). It is at this location superficial to the femoral neck where the anterior joint recess is evaluated for fluid or synovial abnormalities.[1]

The anterior recess of the hip joint over the femoral neck is normally about 4 to 6 mm thick,

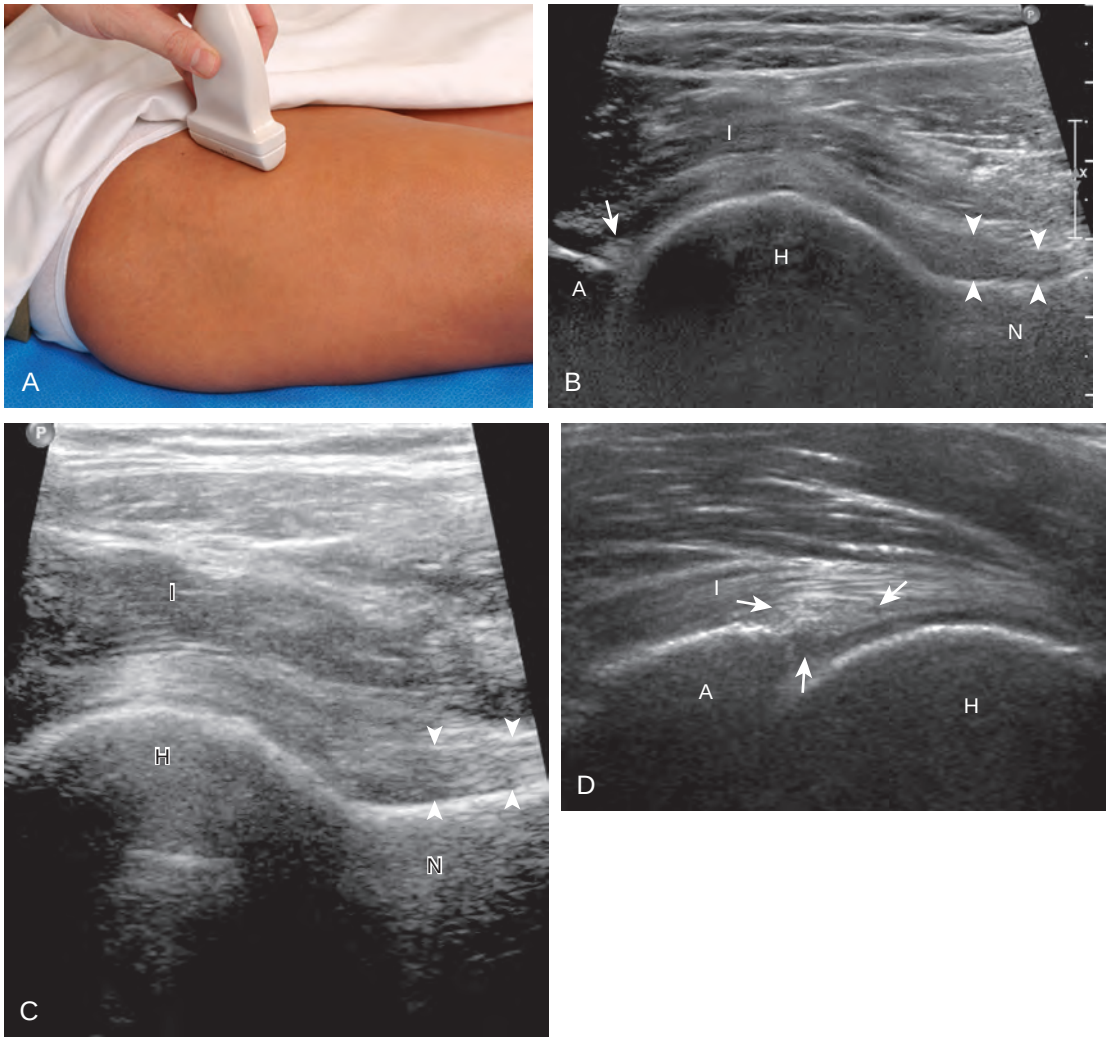

FIGURE 6-2 ■ Hip joint evaluation (long axis). A, Sagittal-oblique imaging over the proximal femur shows **(B** to **D)** the femoral head (H), femoral neck (N), and collapsed anterior joint recess *(arrowheads)*. Note the acetabulum (A) and fibrocartilage labrum *(arrows)*. I, iliopsoas.

and this can be explained anatomically.[1] The anterior joint capsule extends inferiorly from the labrum and inserts at the intertrochanteric line; however, some fibers are reflected superiorly along the femoral neck to attach at the femoral head-neck junction (Fig. 6-3). Both the anterior and posterior layers measure 2 to 3 mm each in thickness; physiologic fluid between these layers should measure less than 2 mm, and typically no fluid is identified in the normal situation.[1] The anterior capsule layer may be slightly thicker than the posterior layer as a result of capsular thickening from ligaments and the zona orbicularis, which encircles the capsule at the femoral head-neck junction. The posterior layer may demonstrate focal thickening at its attachment at the femoral head-neck junction. The normal anterior joint recess is usually concave or flat anteriorly, rather than convex. The true hyperechoic and fibrillar appearance of the joint capsule and its reflection is best appreciated when the femoral neck is perpendicular to the sound beam (see Fig. 6-2C); if imaged obliquely, the joint capsule may artifactually appear hypoechoic and may simulate fluid in echogenicity, especially in a patient with a large body habitus (see Fig. 6-2B). The femoral head and neck should be smooth, and the visualized portion of the hypoechoic hyaline cartilage that covers the femoral head should be uniform. The fibrocartilage labrum is hyperechoic and triangular and extends from the margins of the acetabulum (see Fig. 6-2D). The femoral head and neck are also evaluated in short axis to the femoral neck (Fig. 6-4).

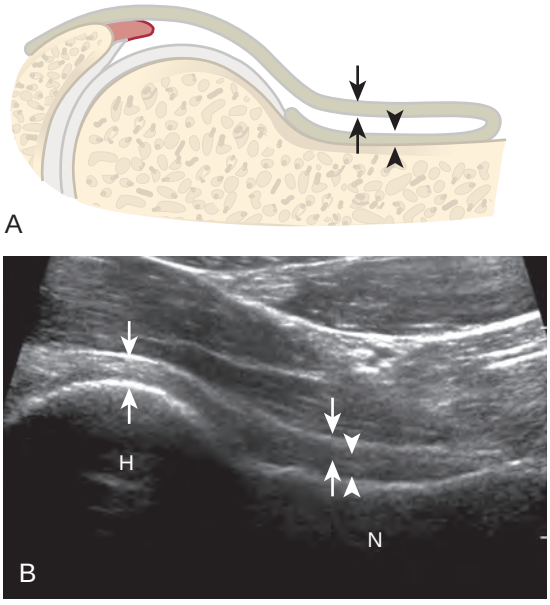

FIGURE 6-3 ■ Anterior hip joint recess. A, A sagittal-oblique illustration through the femoral head and neck and **(B)** an ultrasound image show the anterior layer of the joint capsule *(arrows)* and the posterior layer *(arrowheads)*. H, femoral head; N, femoral neck). (Modified from an illustration by Carolyn Nowak, Ann Arbor, Mich. http://www.carolyncnowak.com/MedTech.html.)

To evaluate the iliopsoas region, the transducer is first placed in the transverse plane over the femoral head because this bone landmark is easy to identify (see Fig. 6-4B). The transducer is then moved superiorly and angled parallel to the inguinal ligament (Fig. 6-5). The characteristic bone contours are seen along with the iliopsoas muscle and tendon, the rectus femoris origin at the anterior inferior iliac spine, and the external iliac vessels. As with imaging any tendon in short axis, toggling the transducer is often helpful to visualize the tendon as hyperechoic, especially because the iliopsoas normally courses deep toward the lesser trochanter and is oblique to the sound beam. The iliopsoas should be evaluated dynamically for tendon snapping (see Snapping Hip Syndrome later in the chapter). The anterior hip is also evaluated for iliopsoas bursa, which originates at the level of the femoral head and typically extends medial and possibly deep to the iliopsoas tendon. The transducer is also rotated 90 degrees to evaluate the iliopsoas tendon in long axis (see Fig. 6-2).

To further evaluate the rectus femoris origin, the transducer is positioned over the anterior inferior iliac spine in the transverse plane. The direct head is seen directly superficial to the anterior inferior iliac spine, whereas the indirect head is at the lateral aspect of the acetabulum (Fig. 6-6). When evaluating the direct head in long axis (see Fig. 6-6B), moving the transducer slightly laterally will show the indirect head coursing proximal and deep, appearing hypoechoic from anisotropy, and producing a characteristic refraction shadow (see Fig. 6-6C) (Video 6-1). The transducer can be rotated in plane with the indirect head and moved over the lateral hip to identify the origin of the indirect head without artifact (see Fig. 6-6D) (Video 6-2). The transducer is then returned to short axis relative to the rectus femoris direct head and moved proximally and laterally to visualize the sartorius and its origin on the anterior superior iliac spine (Fig. 6-7).

Evaluation for the lateral femoral cutaneous nerve begins with the transducer in the transverse plane over the proximal sartorius near the anterior superior iliac spine.[10] As the transducer is moved distally, the lateral femoral cutaneous nerve can be seen as several nerve fascicles coursing over the sartorius from medial to lateral (Fig. 6-8A). More distally, the lateral femoral cutaneous nerve is identified in a triangular hypoechoic fatty space at the lateral aspect of the sartorius (see Fig. 6-8B) (Video 6-3).[11] The transducer is

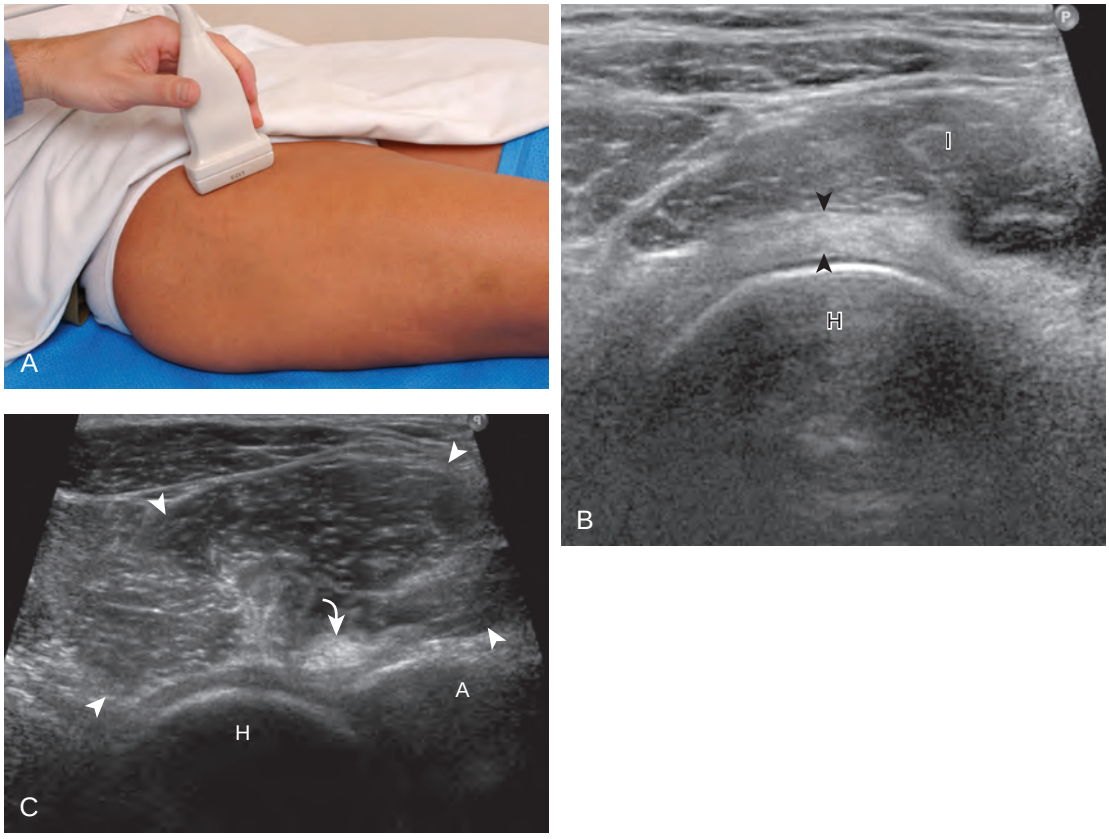

FIGURE 6-4 ■ Hip joint evaluation (short axis). A, Transverse-oblique imaging shows **(B)** the anterior layer of the joint capsule and iliofemoral ligament *(arrowheads)* with hypoechoic hyaline cartilage over the femoral head (H). **C,** Ultrasound image at the proximal aspect of the femoral head (H) shows the iliopsoas muscle *(arrowheads)* and tendon *(curved arrow)*. A, acetabulum; I, iliopsoas.

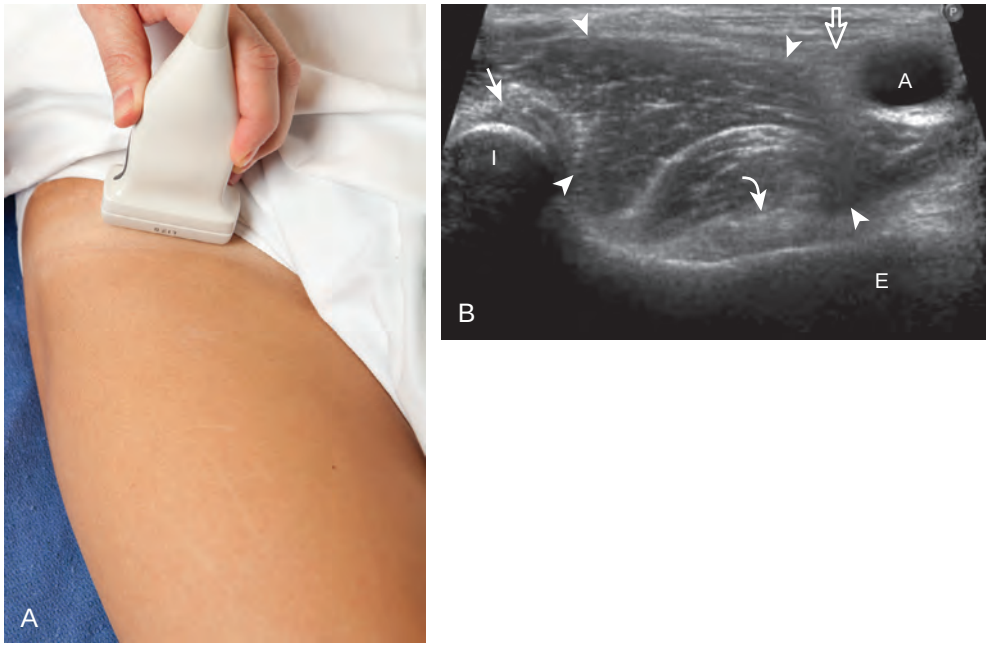

FIGURE 6-5 ■ Iliopsoas evaluation (short axis). A, Transverse-oblique imaging shows **(B)** the iliopsoas tendon *(curved arrow)* and muscle *(arrowheads)*, rectus femoris direct head *(arrow)*, femoral artery (A), and femoral nerve *(open arrow)*. E, iliopectineal eminence; I, anterior inferior iliac spine.

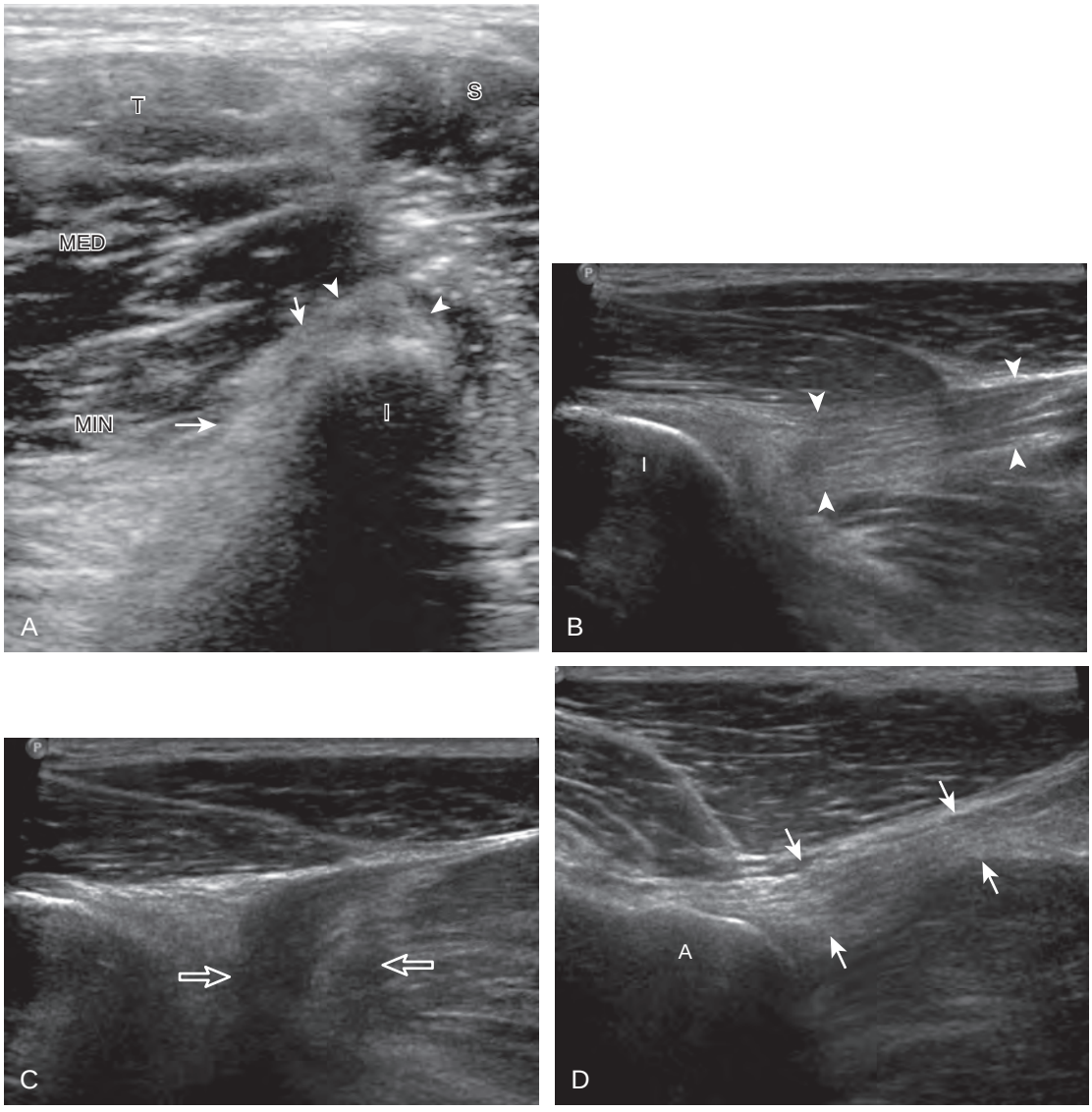

FIGURE 6-6 ■ **Rectus femoris origin evaluation. A,** Transverse imaging over the anterior inferior iliac spine (I) shows the direct head *(arrowheads)* and indirect head *(arrows)* (left side of image is lateral). **B,** Ultrasound image in sagittal plane shows the direct head of the rectus femoris in long axis *(arrowheads)*. **C,** Ultrasound image moving lateral to **(B)** shows refraction shadow *(open arrows)* from the indirect head of the rectus femoris and anisotropy. **D,** Ultrasound image in the coronal-oblique plane over the lateral acetabulum (A) shows the indirect head of the rectus femoris in long axis *(arrows)*. MED, gluteus medius; MIN, gluteus minimus; S, sartorius; T, tensor fasciae latae.

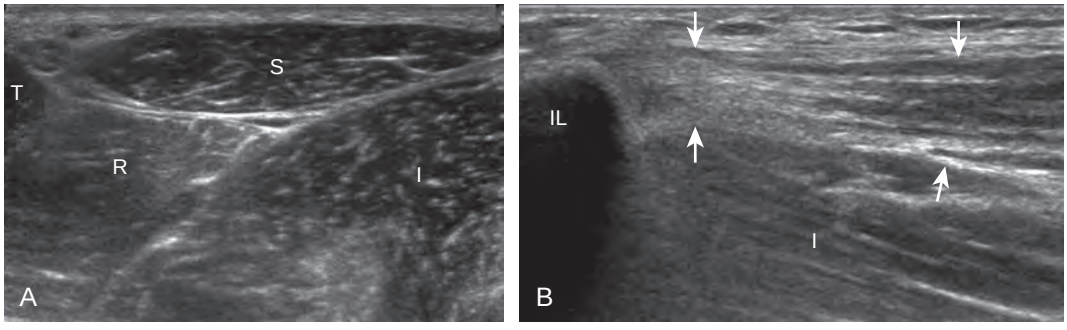

FIGURE 6-7 ■ **Sartorius evaluation.** Ultrasound images show the **(A)** short axis and **(B)** long axis of the sartorius (S and *arrows*). I, iliopsoas; IL, ilium; R, rectus femoris; T, tensor fascia latae.

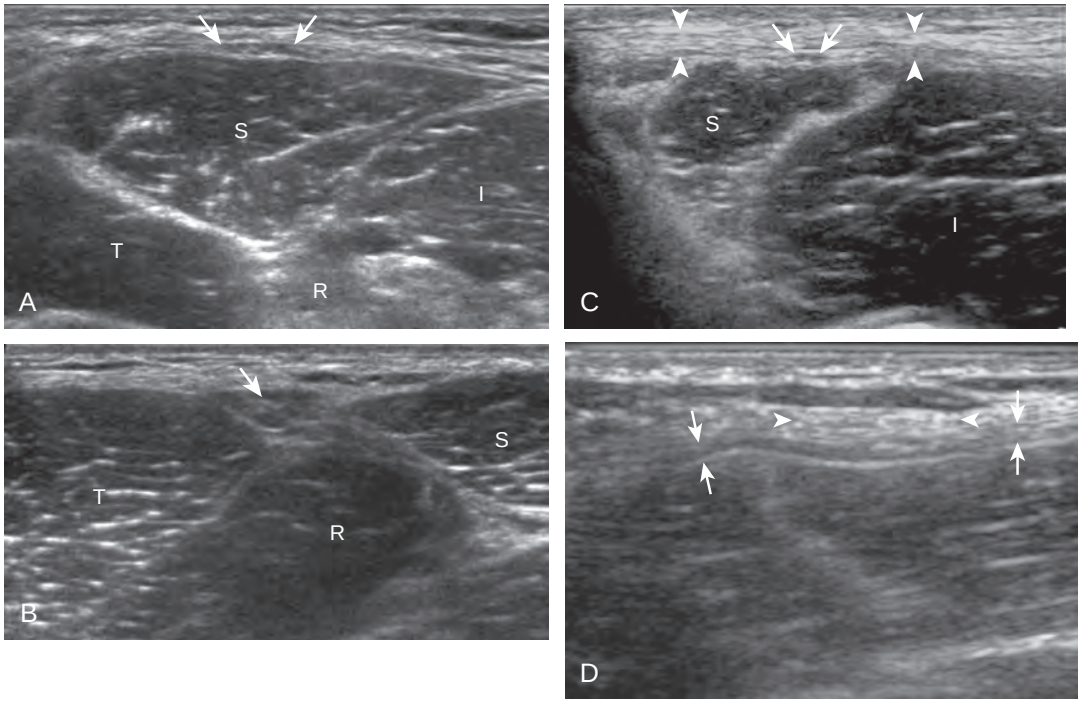

FIGURE 6-8 ■ Lateral femoral cutaneous nerve evaluation. A, Ultrasound image in short axis to the sartorius (S) shows nerve fascicles *(arrows)*. **B,** More distally, one nerve fascicle *(arrow)* is within hypoechoic fat. **C,** Proximal view at the level of the inguinal ligament *(arrowheads)* shows nerve fascicles *(arrows)* in short axis and **(D)**) long axis. I, iliacus; R, rectus femoris; T, tensor fascia latae.

then moved proximally to evaluate for potential nerve entrapment at the inguinal ligament (see Fig. 6-8C and D).[12] The lateral femoral cutaneous nerve may branch proximal to the inguinal ligament and has a variable course; it may cross over the iliac crest, through the sartorius tendon, through the inguinal ligament, or under the inguinal ligament.[9]

Although thigh evaluation is considered separately, patients with hip pain (especially sports-related pain) may have abnormalities at the adductor tendon origin and the rectus abdominis insertion, with possible abnormalities directly associated with the pubic symphysis.[13] The transducer is placed in midline over the pubic symphysis, identified by its characteristic bone contours (Fig. 6-9A). The transducer is turned 90 degrees to evaluate the rectus abdominis in long axis and then rotated toward the adductors to evaluate the common aponeurosis and adductor tendon origin (see Fig. 6-9B).

Hip Evaluation: Lateral

To evaluate the soft tissues over the greater trochanter, bone landmarks are essential (Fig. 6-10). The patient rolls toward the opposite hip to access the posterolateral region of the hip and the transducer is placed over the lateral hip (Fig. 6-11A). To locate the greater trochanter, one

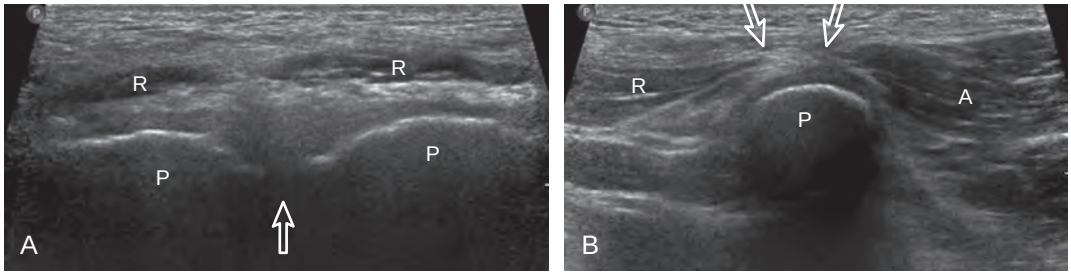

FIGURE 6-9 ■ Pubic symphysis and common aponeurosis. A, Ultrasound image transverse in midline shows distal rectus abdominis muscles (R) and pubic symphysis *(open arrow)*. **B,** Ultrasound image in the sagittal-oblique plane shows common aponeurosis *(open arrows)* over the pubis (P) between the rectus abdominis (R) and adductor musculature (A).

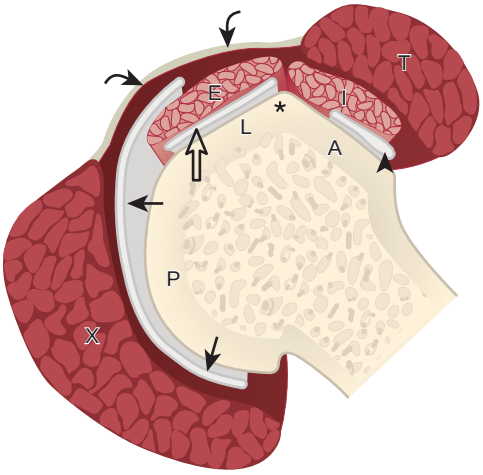

FIGURE 6-10 ■ Greater trochanter anatomy. Illustration in short axis to the proximal femur (anterior is right side of image, lateral is top of image) shows gluteus minimus (I) attachment to the anterior facet (A) with interposed subgluteus minimus bursa *(arrowhead)*, gluteus medius (E) attachment to the lateral facet (L) with interposed subgluteus medius bursa *(open arrow)*, and gluteus maximus (X) passing over the posterior facet (P) with interposed trochanteric (or subgluteus maximus) bursa *(arrows)*. Note the bone apex *(asterisk)* between the anterior and lateral facets and iliotibial tract *(curved arrows)*. T, tensor fascia latae. (Modified from an illustration by Carolyn Nowak, Ann Arbor, Mich. http://www.carolyncnowak.com/MedTech.html.)

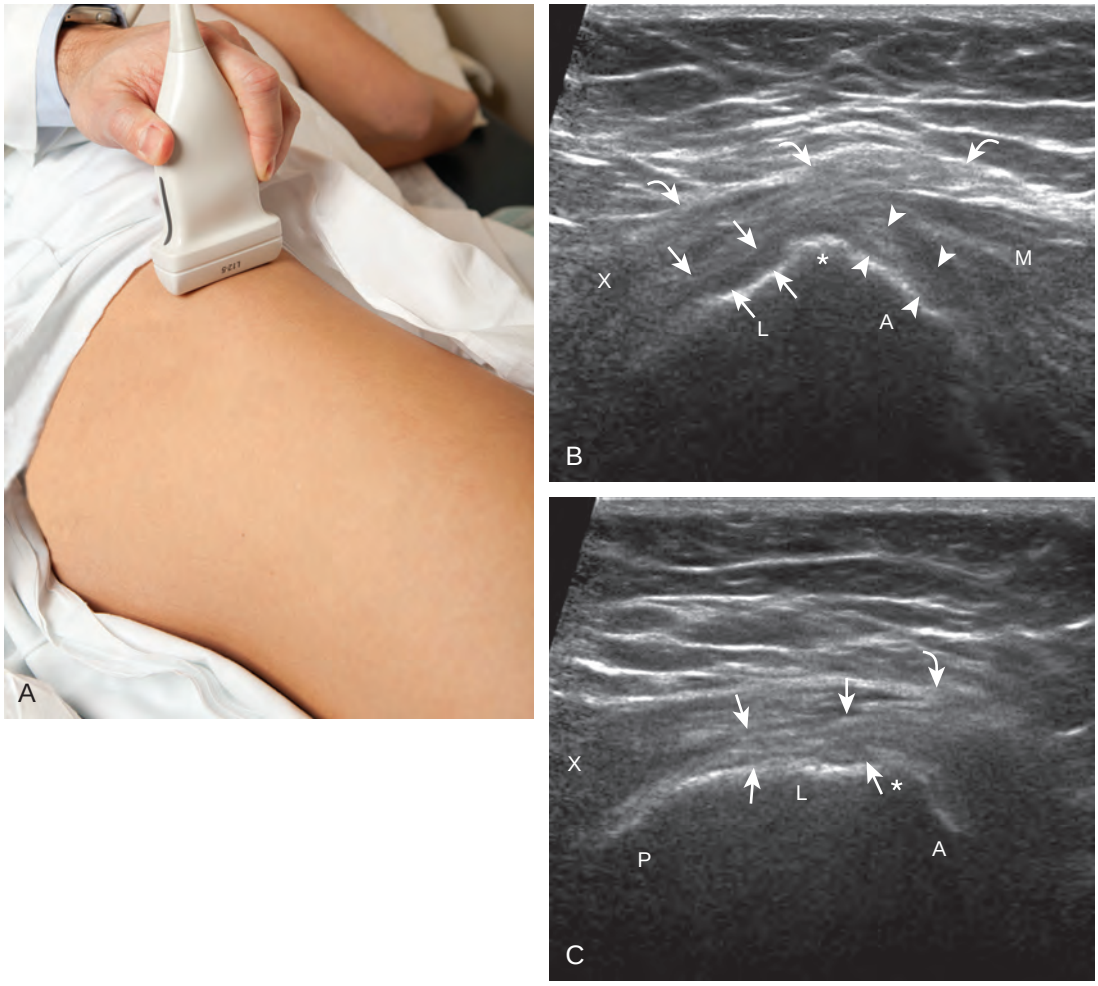

FIGURE 6-11 ■ Greater trochanter evaluation (short axis). A, Transverse imaging over the greater trochanter with the patient in the decubitus position shows **(B)** bone apex *(asterisk)* between gluteus minimus *(arrowheads)* attachment on the anterior facet and gluteus medius *(arrows)* insertion on the lateral facet. The hypoechoic appearance of the gluteus medius in **(B)** from anisotropy is corrected in **(C)** when the transducer sound beam is directed perpendicular to the lateral facet. Note the iliotibial tract *(curved arrows)* and gluteus maximus (X). A, anterior facet; L, lateral facet; M, gluteus medius muscle; P, posterior facet of the greater trochanter.

begins in short axis to the femur as described earlier. With movement of the transducer cephalad, the bony protuberance of the greater trochanter is identified laterally. The key landmark is the apex of the greater trochanter between the anterior and lateral facets (see Fig. 6-11B).[2] Posterior to the lateral facet is the rounded posterior facet of the greater trochanter. The gluteus minimus tendon is identified over the anterior facet, the distal gluteus medius over the lateral facet, and the gluteus maximus over the posterior facet. To confirm that the apex between the lateral and anterior facets is correctly identified, the soft tissues superficial to the gluteus medius and minimus should be evaluated. Superficial to the gluteus medius tendon over the lateral facet one should identify the iliotibial tract, a hyperechoic band of tissue, which is a continuation of the fascial layers that envelop the gluteus maximus posteriorly and the tensor fascia latae anteriorly (see Fig. 6-10). Superficial to the gluteus minimus tendon over the anterior facet is seen the hypoechoic muscle of the gluteus medius and iliotibial tract. Each greater trochanter facet should be evaluated separately in short (see Fig. 6-11) and long axis (Fig. 6-12); the transducer should be positioned so that the cortex of each individual facet is perpendicular to the sound beam to eliminate anisotropy of each overlying tendon (see Fig. 6-11B and C). Evaluation includes assessment for the subgluteus minimus bursa, subgluteus medius bursa, and trochanteric (subgluteus maximus) bursa, which are located between each tendon and their respective greater trochanter facet.[2] Because the trochanteric bursa is located between the gluteus maximus and posterior facet, it is essential to position the transducer posteriorly so as not to overlook bursal distention. When distended, the trochanteric bursa may extend laterally between the gluteus medius tendon and overlying iliotibial tract. For evaluation of the gluteus minimus tendon in long

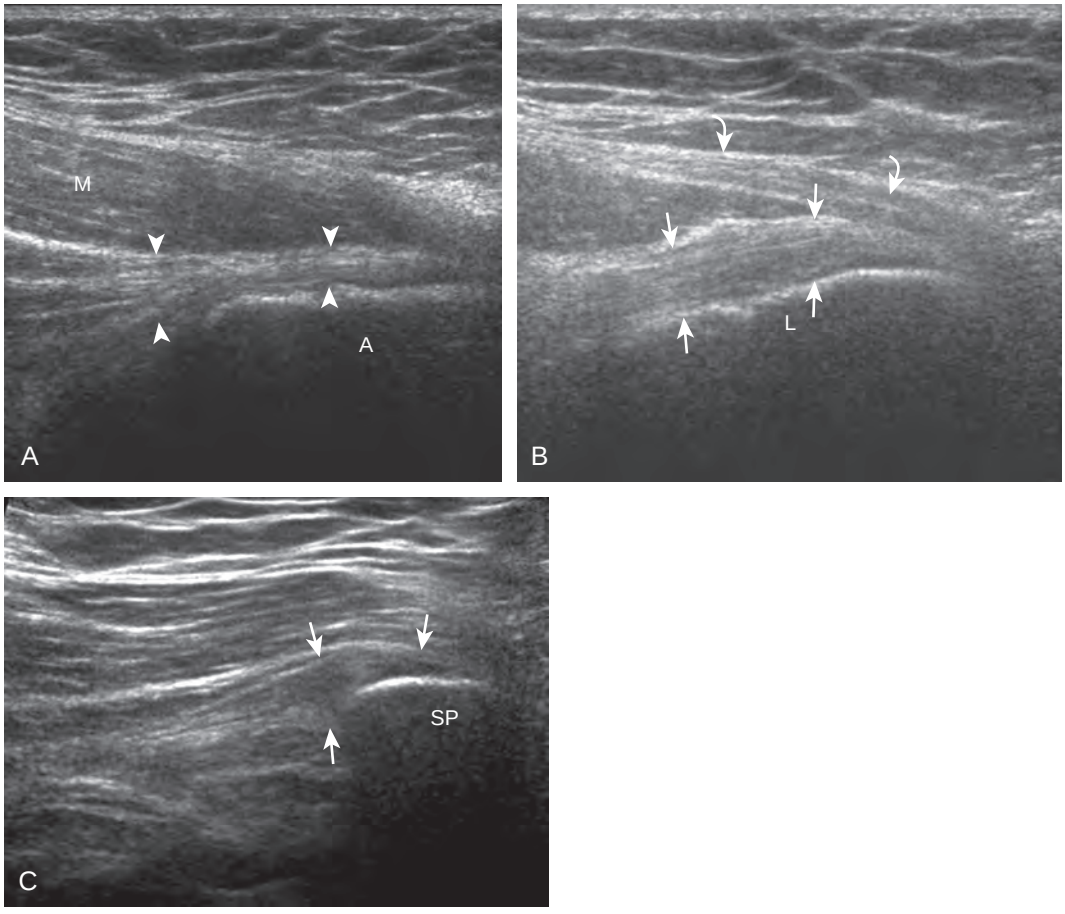

FIGURE 6-12 ■ Greater trochanter evaluation (long axis). Ultrasound images in long axis to the femur show **(A)** the gluteus minimus *(arrowheads)* and **(B)** gluteus medius *(arrows)* tendons. Note the iliotibial tract *(curved arrows)*, gluteus medius muscle (M), and greater trochanter. The transducer more posterior over the superoposterior facet (SP) of the greater trochanter shows **(C)** an additional insertion site of the gluteus medius *(arrows)*. A, anterior facet, L, lateral facet of the greater trochanter.

axis, the transducer is first positioned over the anterior facet in short axis as described previously and turned 90 degrees (see Fig. 6-12A). The same technique is used over the lateral facet to evaluate the gluteus medius tendon in long axis (see Fig. 6-12B). Because the gluteus medius tendon is attached to two facets (lateral and superoposterior), the transducer should be moved cephalad and posterior to visualize the full extent of the gluteus medius tendon attachment (see Fig. 6-12C).

Hip Evaluation: Posterior

Evaluation of the posterior hip and pelvis is not typically considered part of a routine hip evaluation but rather is guided by patient history and symptoms. Structures of interest include the sacroiliac joints, piriformis, superior gemellus, obturator internus, inferior gemellus, and quadriceps femoris. Evaluation can begin with the sacroiliac joint by first positioning the transducer in midline over the sacrum (Fig. 6-13) and then moving the transducer laterally to visualize the posterior sacral foramina and more laterally to view the sacroiliac joint (Video 6-4).[14] The posterior sacral foramina are differentiated from the sacroiliac joint by their more medial location as well as the characteristic focal disruptions in the cortex when scanning superior to inferior, which is in contrast to the more lateral and linear disruption of the sacroiliac joint. The superior aspect of the sacroiliac joint is widened at the fibrocartilage or ligamentous articulation (see Fig. 6-13A), whereas the more inferior true synovial articulation is narrow (see Fig. 6-13B).

To identify the piriformis, a curvilinear transducer with a frequency of less than 10 MHz is essential given the required depth of penetration. The transducer is first positioned in the transverse plane over the sacroiliac joint, as described previously, and then moved inferior into the greater sciatic foramen and angled inferiorly and laterally toward the greater trochanter to identify

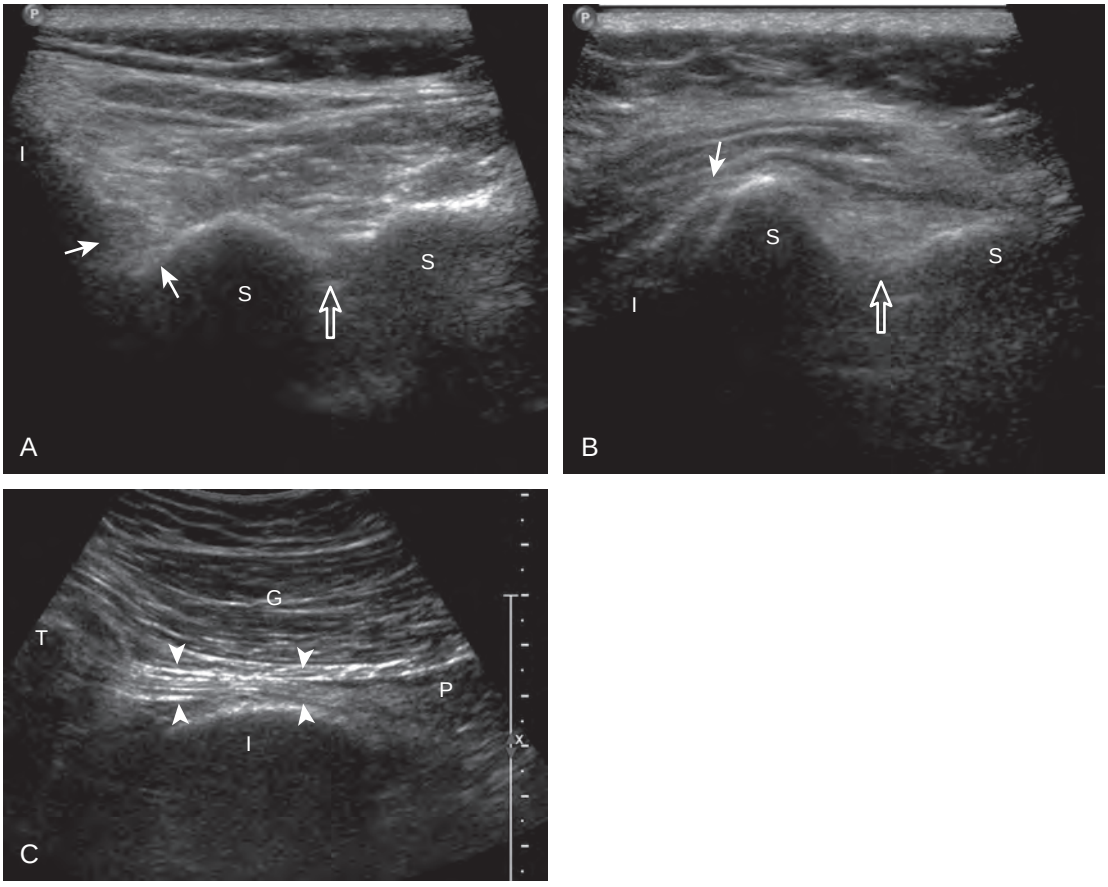

FIGURE 6-13 ■ Sacroiliac joint and piriformis evaluation. Ultrasound images in the transverse plane over **(A)** the upper and **(B)** lower sacrum (S) show the left sacroiliac joint *(arrows)*, posterior sacral foramen *(open arrow)*, and posterior ilium (I) (right side of image is at midline and left side is lateral). Oblique axial ultrasound image **(C)** shows the piriformis tendon *(arrowheads)* and muscle (P). G, gluteus maximus; I, ilium T, greater trochanter.

the piriformis in long axis (see Fig. 6-13C).[15,16] The muscle belly will be located medial to the ilium, while the tendon will be seen directly over the ilium extending to the greater trochanter. Passive hip rotation will assist in its identification because of its movement (Videos 6-5 and 6-6).

To identify the quadratus femoris, obturators, and gemelli, examination can begin in the transverse plane at the level of the hamstring origin (Fig. 6-14A). Deep to the sciatic nerve between the ischium and proximal femur is located the quadratus femoris and obturator externus. More cephalad (see Fig. 6-14B), the inferior gemellus muscle is seen, which has a slightly different course compared with the quadratus femoris as it extends deep to its lateral insertion on the medial aspect of the greater trochanter. In their short axis, from cephalad to caudal, the superior gemellus, obturator internus, inferior gemellus, and quadratus femoris are identified deep to the sciatic nerve (see Fig. 6-14C).

Inguinal Region Evaluation

Sonographic evaluation of the inguinal region for hernias may incorporate evaluation of the anterior abdominal wall for abnormalities.[8] Evaluation is begun in the transverse plane over the mid-abdomen below the umbilicus with the patient supine. At this location, the linea alba is seen as a hyperechoic fascial layer between the rectus abdominis muscles. The transducer is then moved to the lateral margin of a rectus abdominis muscle. As the transducer is moved inferior in the transverse plane, the inferior epigastric artery can be identified beneath the rectus abdominis (Fig. 6-15A, online). It is here at the lateral margin of the rectus abdominis that spigelian hernias are seen, between the rectus abdominis muscle and

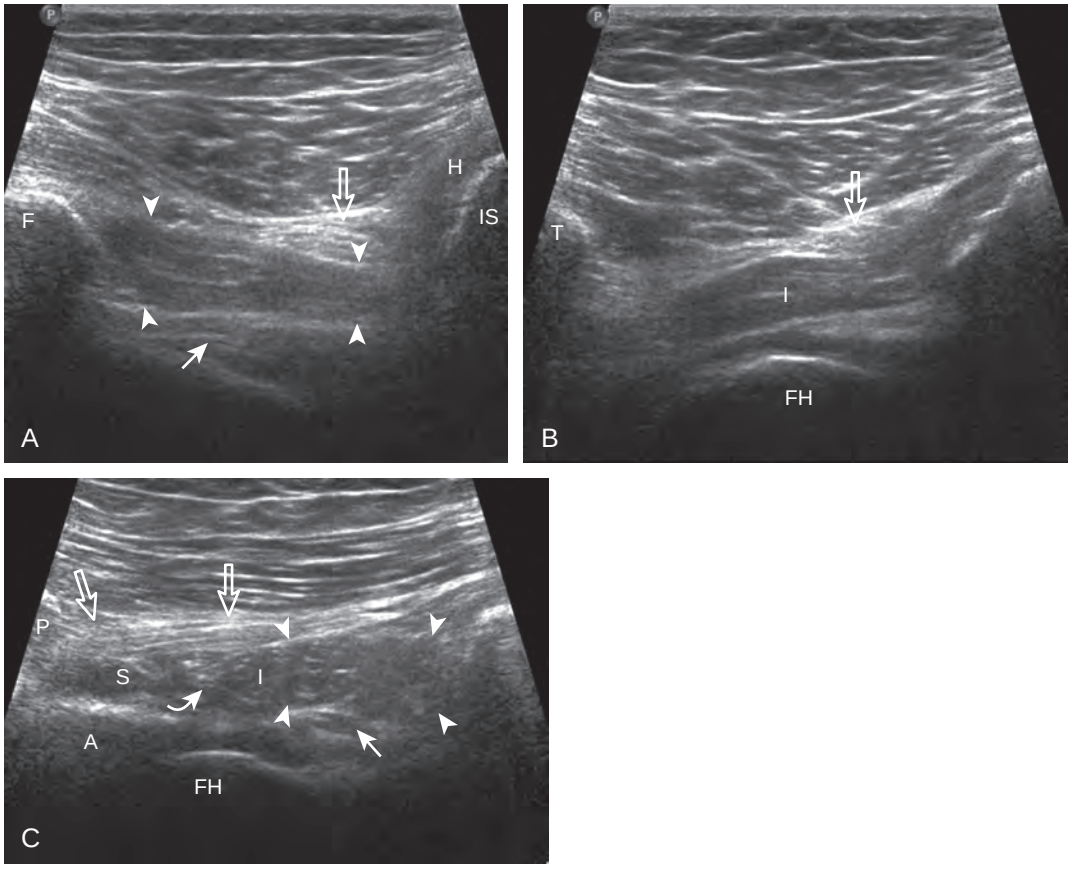

FIGURE 6-14 ■ Quadratus femoris, obturator, and gemelli evaluation. Ultrasound image in transverse plane at the level of the hamstring tendon origin shows **(A)** the quadratus femoris muscle *(arrowheads)*, obturator externus *(arrow)*, and sciatic nerve *(open arrow)*. The transducer is moved cephalad to show **(B)** the inferior gemellus (I) and sciatic nerve *(open arrow)*. In short axis **(C),** from superior to inferior is identified the superior gemellus (S), obturator internus *(curved arrow)*, inferior gemellus (I), quadratus femoris *(arrowheads)* and obturator externus *(arrow)*. Note the sciatic nerve *(open arrows)* and piriformis (P). A, acetabulum; F, femur; FH, femoral head; H, hamstring tendon origin; IS, ischium; T, greater trochanter.

lateral abdominal musculature. More inferiorly, the site where the inferior epigastric artery joins the external iliac artery is a very important landmark; just lateral and superior to this location is the deep inguinal ring (see Fig. 6-15B, online). Hernias that originate lateral to the inferior epigastric artery at the deep inguinal ring and extend superficially and medially within the inguinal canal are indirect inguinal hernias. Hernias that originate medial to the inferior epigastric origin in the Hesselbach triangle and move in an anterior direction are direct hernias.[8] At the deep inguinal ring, the transducer is then angled toward the pubis, parallel and just superior to the inguinal ligament, and long axis to the inguinal canal (see Fig. 6-15C, online). In male patients, the serpiginous and mixed-echogenicity spermatic cord can be identified (see Fig. 6-15D and E, online). In this location, the patient is asked to tighten the stomach or perform the Valsalva maneuver (forced expiration against a closed airway) to evaluate for transient herniation of intra-abdominal structures or tissue; the patient can be asked to blow against the back of the hand and puff the cheeks outward. This maneuver is also repeated with the transducer more medial, at the pubis, to evaluate for direct hernias. It is also important to image the Hesselbach triangle at its medial and superior aspects both in long and short axis to the inguinal canal for complete evaluation because the cephalocaudal extent of this triangle is greatest medially. Evaluation for inguinal hernias should also be completed in the sagittal plane. For example, when imaging the inguinal canal and spermatic cord (in males) in short axis, an indirect inguinal hernia will be seen moving in and out of the ultrasound plane displacing the spermatic cord. Similar to the transverse plane, a direct hernia will appear as focal abnormal anterior movement. After returning the transducer long axis to the inguinal ligament, the transducer is moved distally over the common femoral artery just beyond the inguinal ligament to evaluate for femoral hernias. Although the causes of "sports hernia" are debated, evaluation for hip or groin pain in the athlete should include the pubis symphyseal region, the hip joint, and the labrum (see earlier), in addition to evaluation for inguinal region hernias.[17]

Thigh Evaluation: Anterior

Structures of interest anteriorly in the thigh include the four muscles that make up the quadriceps femoris. Examination is begun in the transverse plane over the mid-anterior thigh, where the four individual muscles can be identified (Fig. 6-16A) (Videos 6-7 and 6-8). Directly below the transducer and most superficial is the rectus femoris muscle (see Fig. 6-16B). Deep to this and immediately adjacent to the femur is the vastus intermedius. Lateral to these two structures is the vastus lateralis (see Fig. 6-16C and D), and medial is the vastus medialis (see Fig. 6-16E and F). Muscle at ultrasound is predominantly hypoechoic, although interspersed hyperechoic septa are identified. The quadriceps femoris is then evaluated in long axis (Fig. 6-17). As one moves the transducer distally, the rectus femoris tapers to a tendon, followed by the vastus musculature, which forms the trilaminar quadriceps tendon that inserts on the superior pole of the patella. The superficial layer of the distal quadriceps tendon is made up of the rectus femoris, the middle layer is composed of both the vastus medialis and lateralis tendons, and the deep layer is made up of the vastus intermedius tendon. Some quadriceps tendon fibers continue over the patella (termed the *prepatellar quadriceps continuation*) to attach to the tibial tuberosity by means of the patellar tendon.[18] The distal tapering appearance of the rectus femoris is best appreciated in long axis in the sagittal plane. The individual muscles of the quadriceps can then be evaluated more proximally. As described earlier, the rectus femoris tendon proximally originates at the ilium (see Fig. 6-6), where its direct head originates from the anterior inferior iliac spine and the indirect or reflected head originates at the lateral aspect. In the thigh, the direct head flattens superficially, the indirect head continues within the central region of the rectus femoris, and more distally a posterior aponeurosis forms.[4] The adjacent tensor fasciae latae is seen lateral to the rectus femoris muscle (Fig. 6-18); the fascia of the tensor fascia latae continues laterally as the iliotibial tract (see Fig. 6-10).

Thigh Evaluation: Medial

Structures of interest in the medial thigh include the femoral nerve, artery, and vein and the sartorius, gracilis, and adductor musculature. Ultrasound examination is begun similar to the anterior thigh for orientation, with initial identification of the rectus femoris muscle. The transducer is then moved cephalad into the medial upper thigh (see Fig. 6-16E). The femoral artery is identified at the medial aspect of the rectus femoris and vastus medialis muscles and is a very helpful landmark (Fig. 6-19A). Directly superficial to the femoral artery is the sartorius muscle. Medial and posterior to these structures are the adductor muscles (see Fig. 6-19B). The most anterior is the adductor longus muscle, next posterior is the adductor brevis muscle, and most posterior and largest is

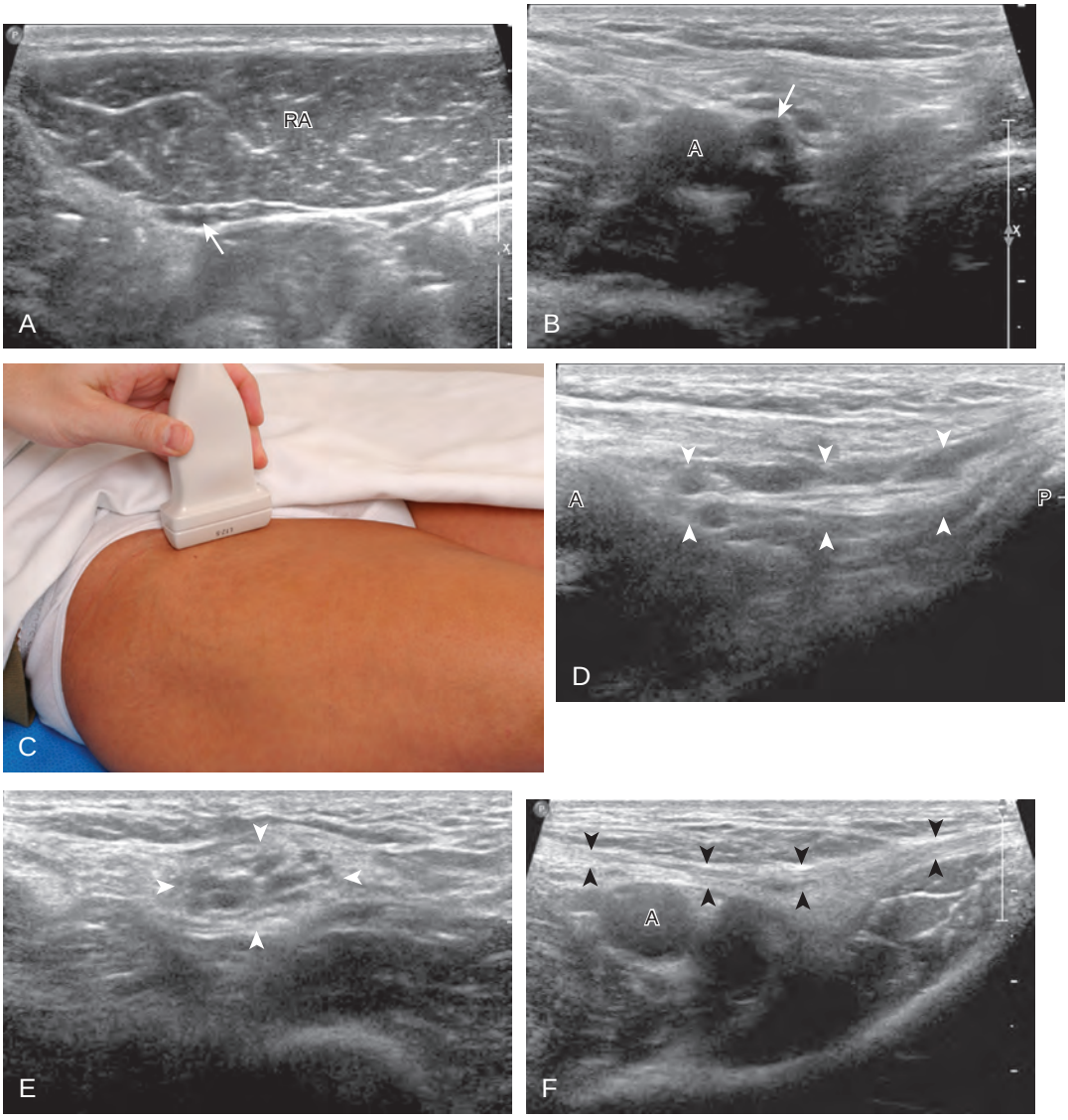

FIGURE 6-15 ■ Inguinal region evaluation. Transverse imaging over the lower abdomen shows **(A)** the rectus abdominis muscle (RA) and the inferior epigastric artery *(arrow)* (right side of image is midline). Transverse imaging inferior to **A** shows **(B)** the origin of the inferior epigastric artery *(arrow)* from the external iliac artery (A). **C,** Imaging in long axis to the inguinal canal shows **(D)** the spermatic cord *(arrowheads)*, also visible in short axis to the inguinal canal **(E)**. Imaging in long axis at the inferior extent of the inguinal canal shows **(F)** the inguinal ligament *(arrowheads)*. A, external iliac artery; P, pubis.

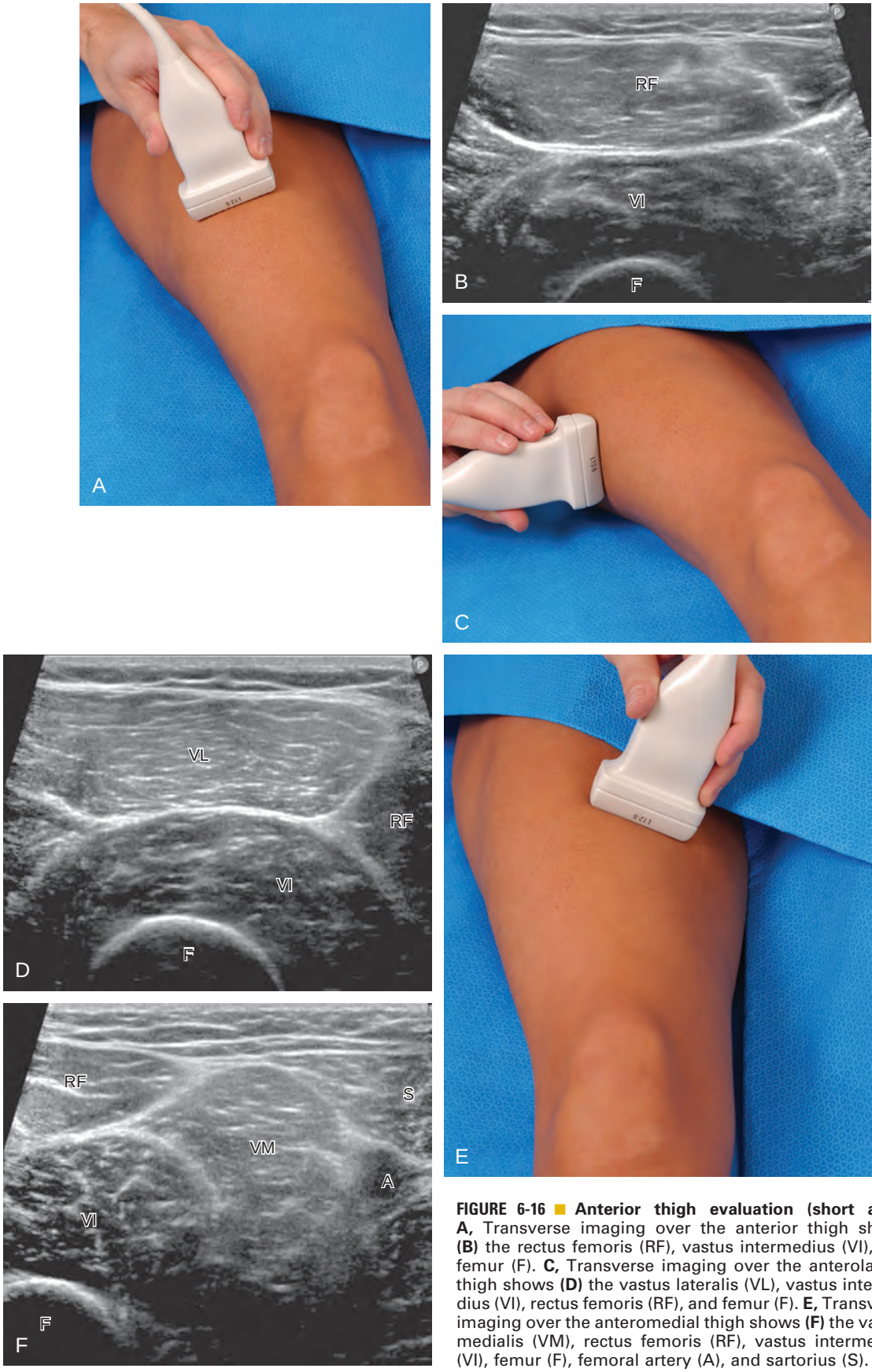

FIGURE 6-16 ■ Anterior thigh evaluation (short axis). A, Transverse imaging over the anterior thigh shows **(B)** the rectus femoris (RF), vastus intermedius (VI), and femur (F). **C,** Transverse imaging over the anterolateral thigh shows **(D)** the vastus lateralis (VL), vastus intermedius (VI), rectus femoris (RF), and femur (F). **E,** Transverse imaging over the anteromedial thigh shows **(F)** the vastus medialis (VM), rectus femoris (RF), vastus intermedius (VI), femur (F), femoral artery (A), and sartorius (S).

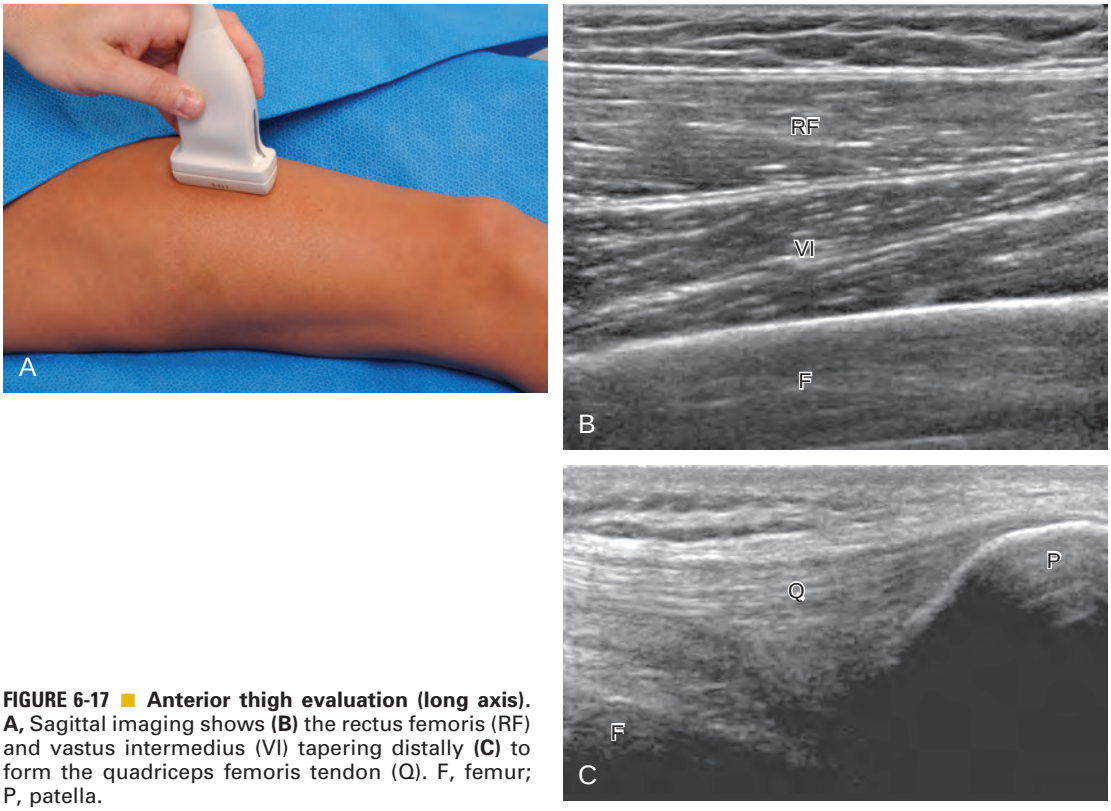

FIGURE 6-17 ■ Anterior thigh evaluation (long axis). A, Sagittal imaging shows **(B)** the rectus femoris (RF) and vastus intermedius (VI) tapering distally **(C)** to form the quadriceps femoris tendon (Q). F, femur; P, patella.

the adductor magnus muscle. Between these respective muscles are located the anterior and posterior branches of the obturator nerve. Superficial and medial to the adductor muscles is the gracilis muscle, just below the subcutaneous tissues (see Fig. 6-19C). For each of these medial thigh muscles, the proximal to distal extents can be visualized in short axis. The transducer can also be turned in long axis over each muscle to visualize the proximal origins and distal attachments (see Fig. 6-19D).

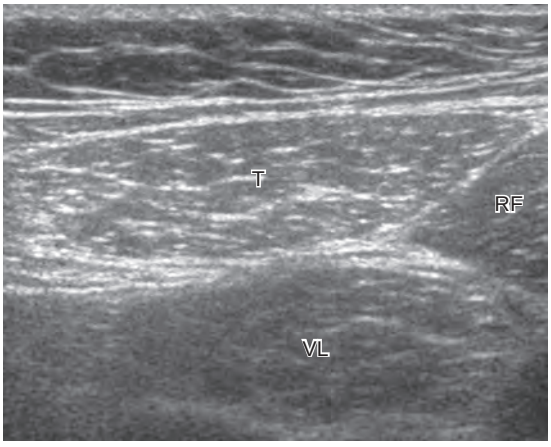

FIGURE 6-18 ■ Tensor fasciae latae evaluation. Transverse imaging over the upper thigh shows the tensor fasciae latae (T), vastus lateralis (VL), and rectus femoris (RF) (left side of image is lateral).

Thigh Evaluation: Posterior

Structures of interest in the posterior thigh include the semimembranosus, the semitendinosus, the biceps femoris, and the sciatic nerve. Ultrasound evaluation can begin in the transverse plane at the level of the mid-thigh, or more proximally at the horizontal gluteal crease or ischial tuberosity. At the level of the mid-posterior thigh (Fig. 6-20A), three distinct muscles can be identified medial to lateral, which are the semimembranosus, semitendinosus, and biceps femoris muscles (see Fig. 6-20B). The short head of the biceps femoris can be identified deep to the long head at the femoral cortex at the level of the mid-femur. When the transducer is moved in the transverse plane distally toward the knee, the semitendinosus becomes a thin tendon and moves directly superficial to the semimembranosus muscle (see Fig. 6-20B to D). This is an additional finding that aids the identification of the posterior thigh muscles. In the mid-thigh, the honeycomb appearance of the sciatic nerve can

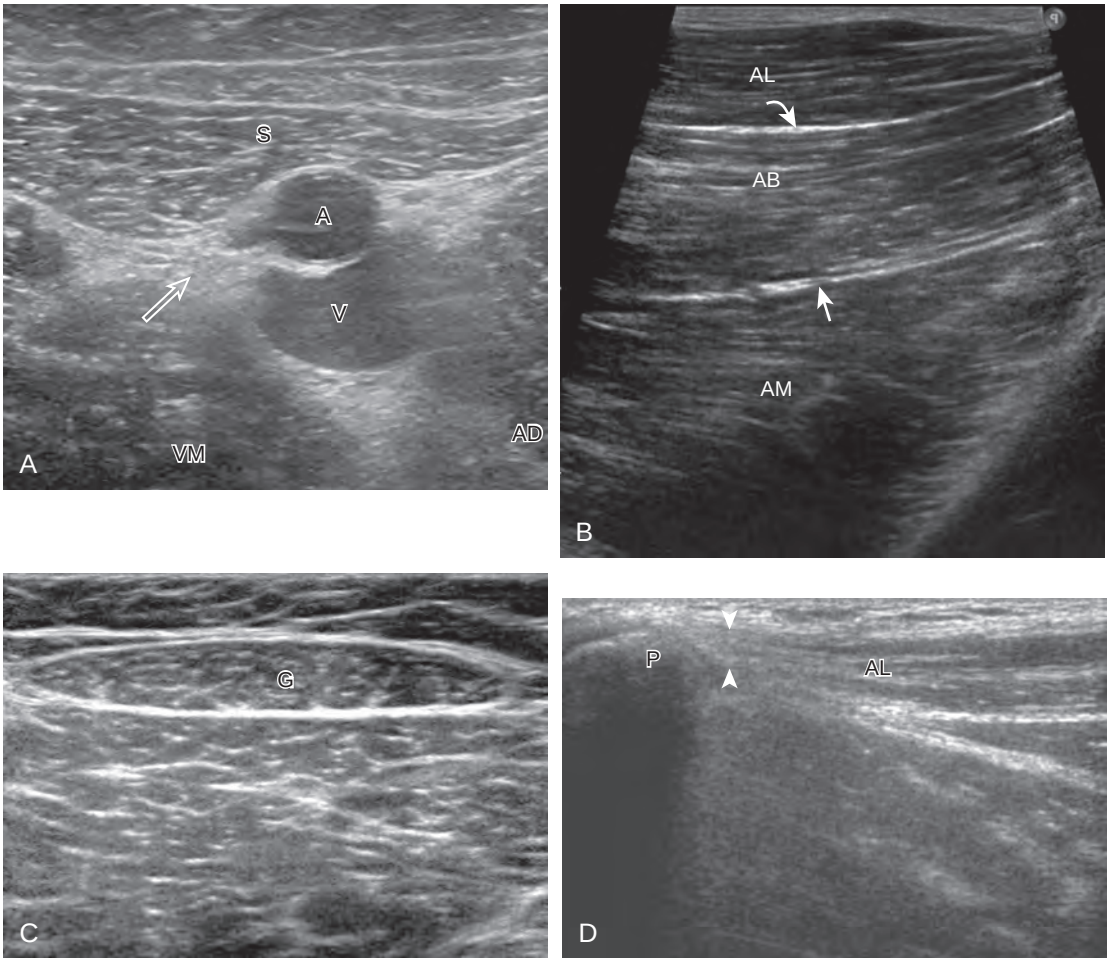

FIGURE 6-19 ■ Medial thigh evaluation. Transverse imaging over the anteromedial thigh shows **(A)** the sartorius (S) immediately superficial to the femoral artery (A) and vein (V) (*open arrow*, femoral nerve). Transverse imaging over the medial thigh shows **(B)** the adductor longus (AL), adductor brevis (AB), and adductor magnus (AM). Note the anterior *(curved arrow)* and posterior *(arrow)* divisions of the obturator nerve. Transverse imaging over the medial thigh shows **(C)**) the gracilis (G) superficial to the adductor musculature. Coronal imaging long axis to the adductor musculature shows **(D)** the adductor longus (AL), which originates *(arrowheads)* from the pubis (P). AD, adductor musculature; VM, vastus medialis.

be identified between the biceps femoris muscle and the semitendinosus muscle (see Fig. 6-20B).

As the transducer is moved cephalad in the transverse plane toward the ischium, the semimembranosus tendon and aponeurosis move anterior or deep to the conjoined biceps femoris long head and semitendinosus tendons (or conjoint tendon) and semitendinosus muscle belly (Fig. 6-21A). At this location, the conjoint tendon, the semimembranosus tendon, and the sciatic nerve are in the arrangement of a triangle, with the semimembranosus and sciatic nerve forming the base of the triangle and the conjoint tendon the more superficial apex. Toggling the transducer to eliminate anisotropy is helpful to visualize the tendons as hyperechoic (see Fig. 6-21B). As the transducer is moved in short axis more cephalad toward the ischial tuberosity, the semimembranosus tendon moves lateral and crosses under or deep to the conjoint tendon (see Fig. 6-21C). At the ischial tuberosity, the conjoint tendon originates superficially, whereas the semimembranosus origin is relatively lateral and deep (see Fig. 6-21C). In long axis (Fig. 6-22A), the conjoint tendon is visualized directly superficial to the semimembranosus tendon (see Fig. 6-22B). At the ischial tuberosity, the conjoint tendon originates in a superficial location (see Fig. 6-22C). To visualize the semimembranosus tendon, the transducer is moved slightly lateral to the conjoint tendon and angled toward midline (see Fig. 6-22D). The sciatic nerve is also

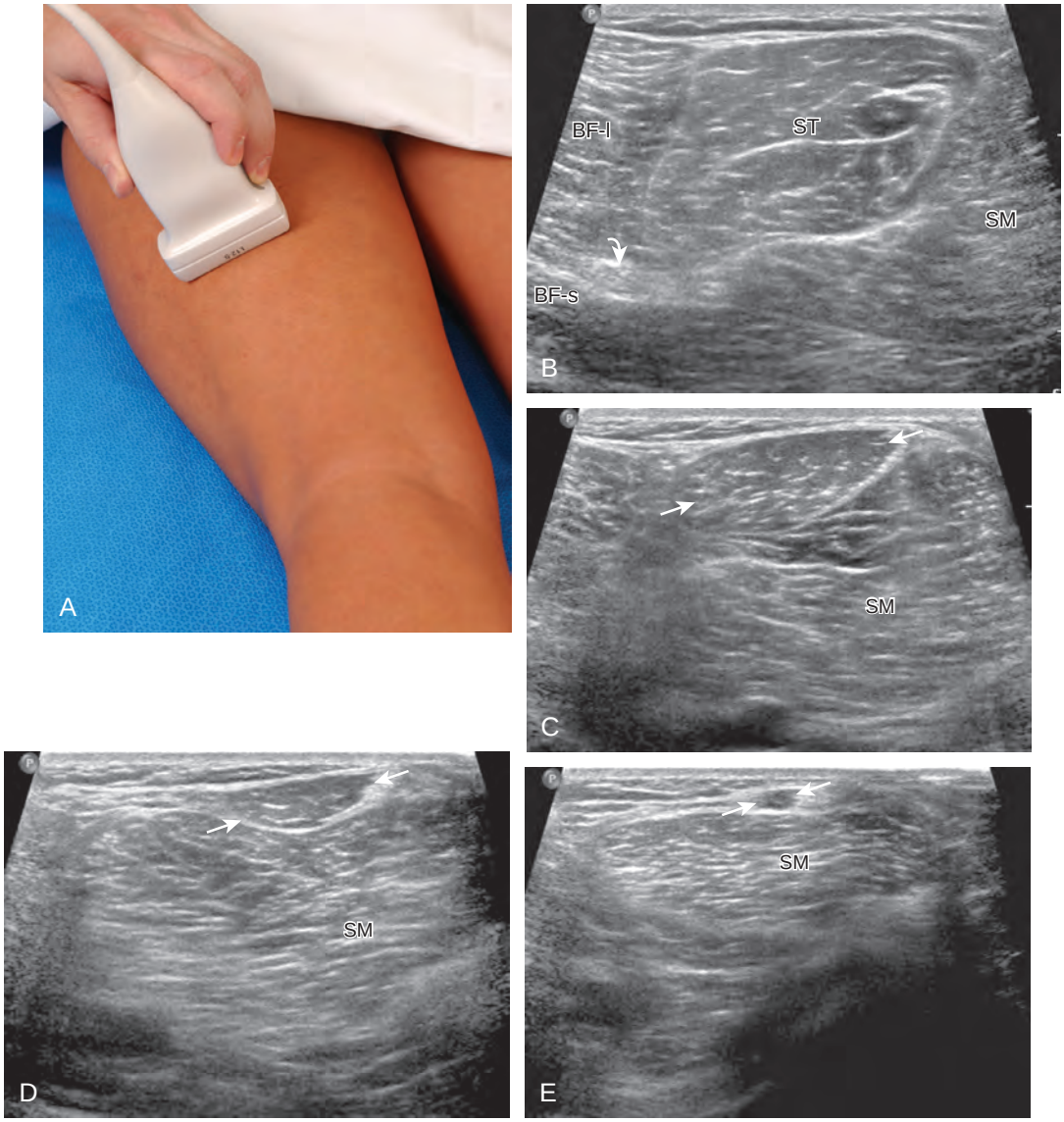

FIGURE 6-20 ■ Posterior thigh evaluation (short axis). A, Transverse imaging over the posterior thigh shows **(B)** the semitendinosus (ST), semimembranosus (SM), and biceps femoris long head (BF-l) and short head (BF-s) (*curved arrow*, sciatic nerve). Note **(C** to **E)** the distal tapering of the semitendinosus *(arrows)* over the semimembranosus (SM) (right side of image is medial).

identified and should not be mistaken for tendon (see Fig. 6-22E).

Hip Evaluation for Dysplasia in a Child

There are several opinions with regard to the ultrasound technique for hip dysplasia. Whereas one method favors the position of the femoral head and measurements, another emphasizes dynamic evaluation of position and stability using the Ortolani and Barlow maneuvers. Regardless, a minimal examination should include coronal neutral or coronal flexion positions (with optional stress and measurements) and a transverse flexion position with and without stress.[19] An ultrasound protocol for hip dysplasia may be divided into several steps. The first is a coronal view with the hip in neutral position, slightly flexed (Fig. 6-23A, online). The resulting image is likened to an egg on a spoon, in which a line drawn from the flat ilium covers at least 50% of the head and an acetabular α angle is greater than 60 degrees (see

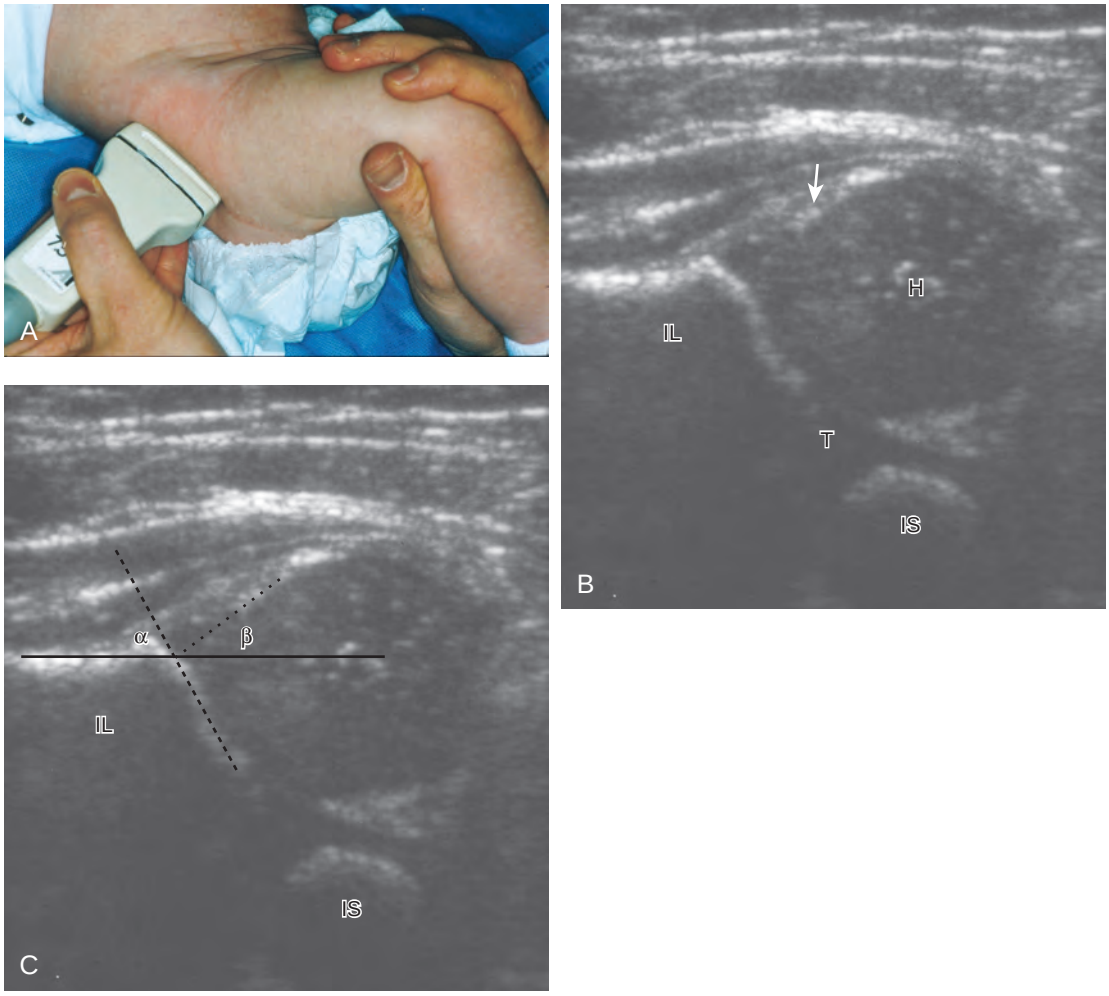

FIGURE 6-23 ■ Hip dysplasia evaluation (coronal). A, Coronal imaging over the lateral hip in extension shows **(B)** the femoral head (H), ilium (IL), ischium (IS), triradiate cartilage (T), and tip of labrum *(arrow)*. **C,** α and β angle measurements are indicated.

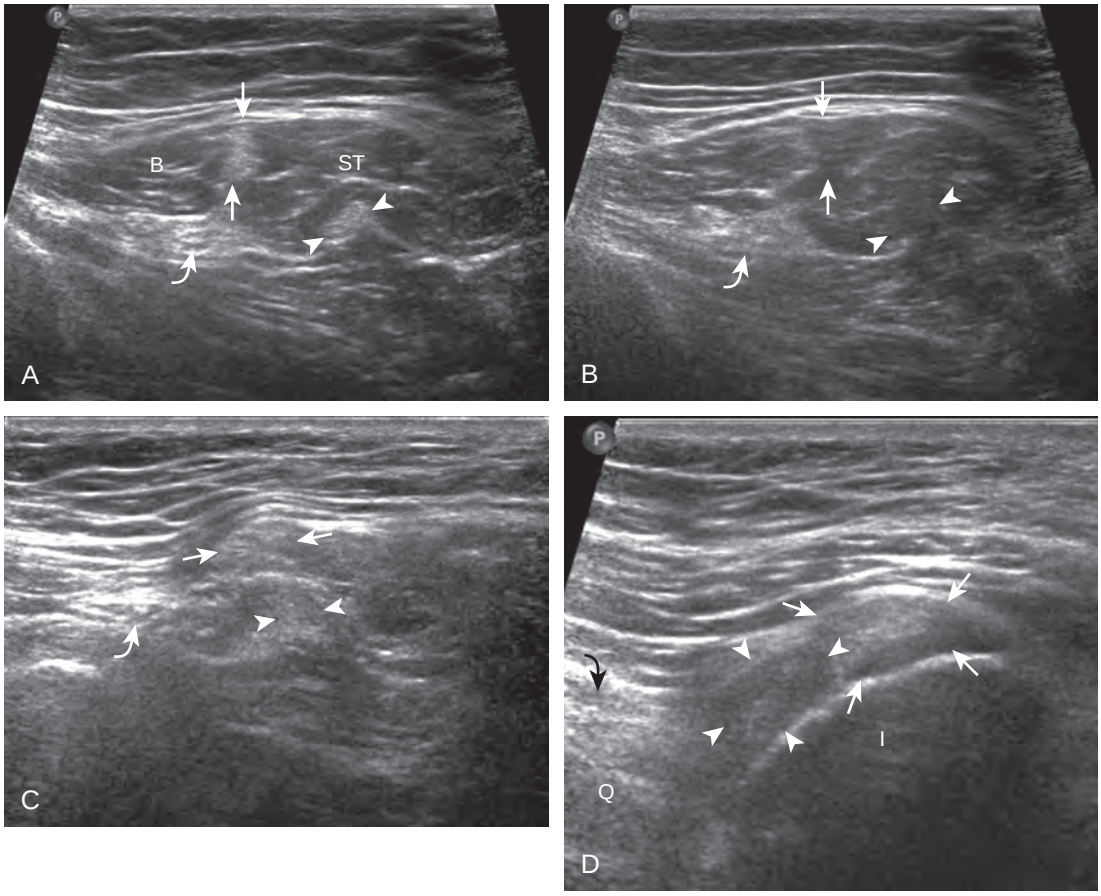

FIGURE 6-21 ■ Posterior thigh evaluation—proximal (short axis). A, Transverse imaging over the proximal hamstrings shows the semimembranosus tendon *(arrowheads)* anterior or deep to the conjoint semitendinosus and the biceps femoris long head tendon *(arrows)* and semitendinosus muscle (ST) (*curved arrow*, sciatic nerve). Toggling the transducer **(B)** shows anisotropy of the tendons. More proximal imaging **(C)** shows the conjoint tendon *(arrows)* superficial to the semimembranosus tendon *(arrowheads)*. **D,** At the ischial tuberosity (I), the conjoint tendon *(arrows)* is superficial and the semimembranosus *(arrowheads)* is deep and lateral (left side of image is lateral). B, biceps femoris long head; Q, quadratus femoris.

Fig. 6-23B and C, online). The α angle measures the angle between the lateral ilium (baseline) and the acetabular roof line, whereas the β angle measures the angle between the lateral ilium baseline and a line drawn through the hyperechoic labral tip from the lateral acetabulum (inclination line).[20] The ossified acetabulum and proximal femur are hyperechoic with shadowing, and the unossified femoral head and triradiate cartilage of the acetabulum appear speckled and hypoechoic. The second position is in the coronal plane with the hip flexed (Fig. 6-24A, online). In this position, in addition to assessment of the femoral head position, the transducer is moved posteriorly over the triradiate cartilage, and posteriorly directed stress is applied to evaluate for posterior subluxation of the femoral head (see Fig. 6-24B, online). In the third position, the hip remains flexed, and the transducer is turned to the transverse plane (Fig. 6-25A, online). In this position, dynamic hip adduction with posteriorly directed stress (the Barlow test) (see Fig. 6-25B, online) evaluates for hip subluxation, and hip abduction with anteriorly directed stress (the Ortolani test) evaluates for relocation if there is subluxation or dislocation of the hip.

JOINT AND BURSAL ABNORMALITIES

Joint Effusion and Synovial Hypertrophy

The diagnosis of a hip joint effusion relies on distention of the anterior joint recess when imaged long axis to the femoral neck (Fig. 6-26).

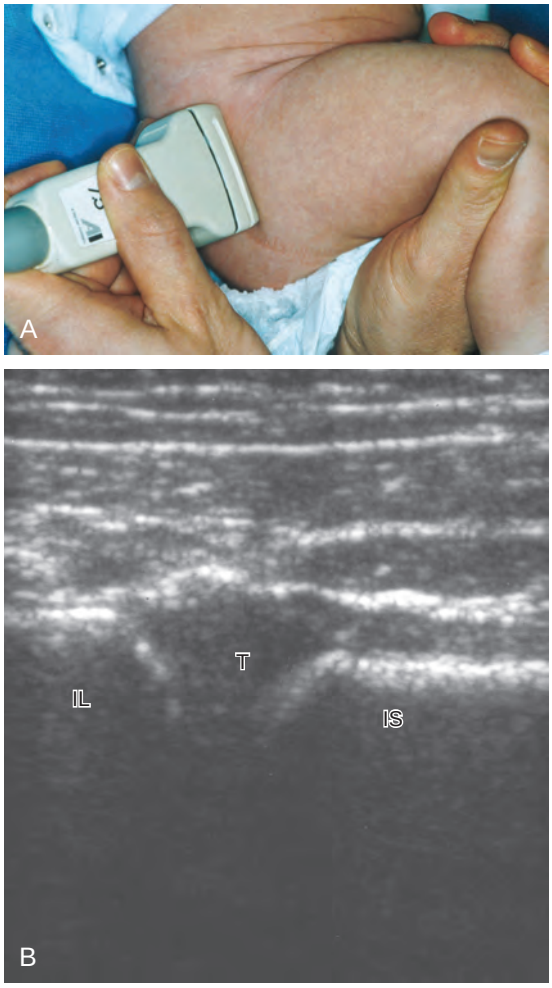

FIGURE 6-24 ■ Hip dysplasia evaluation (coronal). A, Coronal imaging with the hip in flexion and posteriorly directed stress shows **(B)** the normal triradiate cartilage (T) between the ilium (IL) and ischium (IS) without posterior displacement of the femoral head.

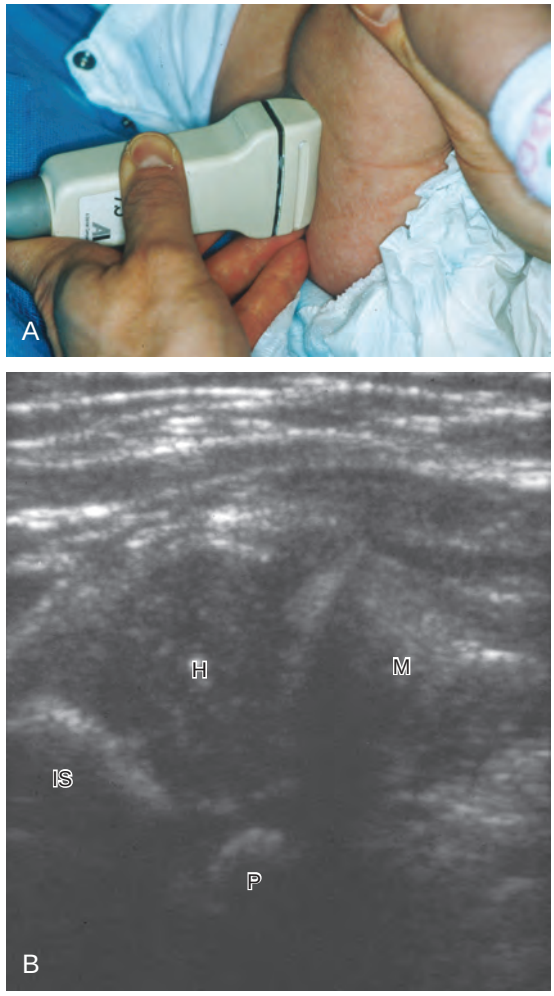

FIGURE 6-25 ■ Hip dysplasia evaluation (transverse). A, Transverse imaging with the hip in flexion and adduction with posteriorly directed stress shows **(B)** the normal location of the femoral head (H) relative to the ischium (IS) without subluxation or dislocation. M, femoral metaphysis; P, pubis.

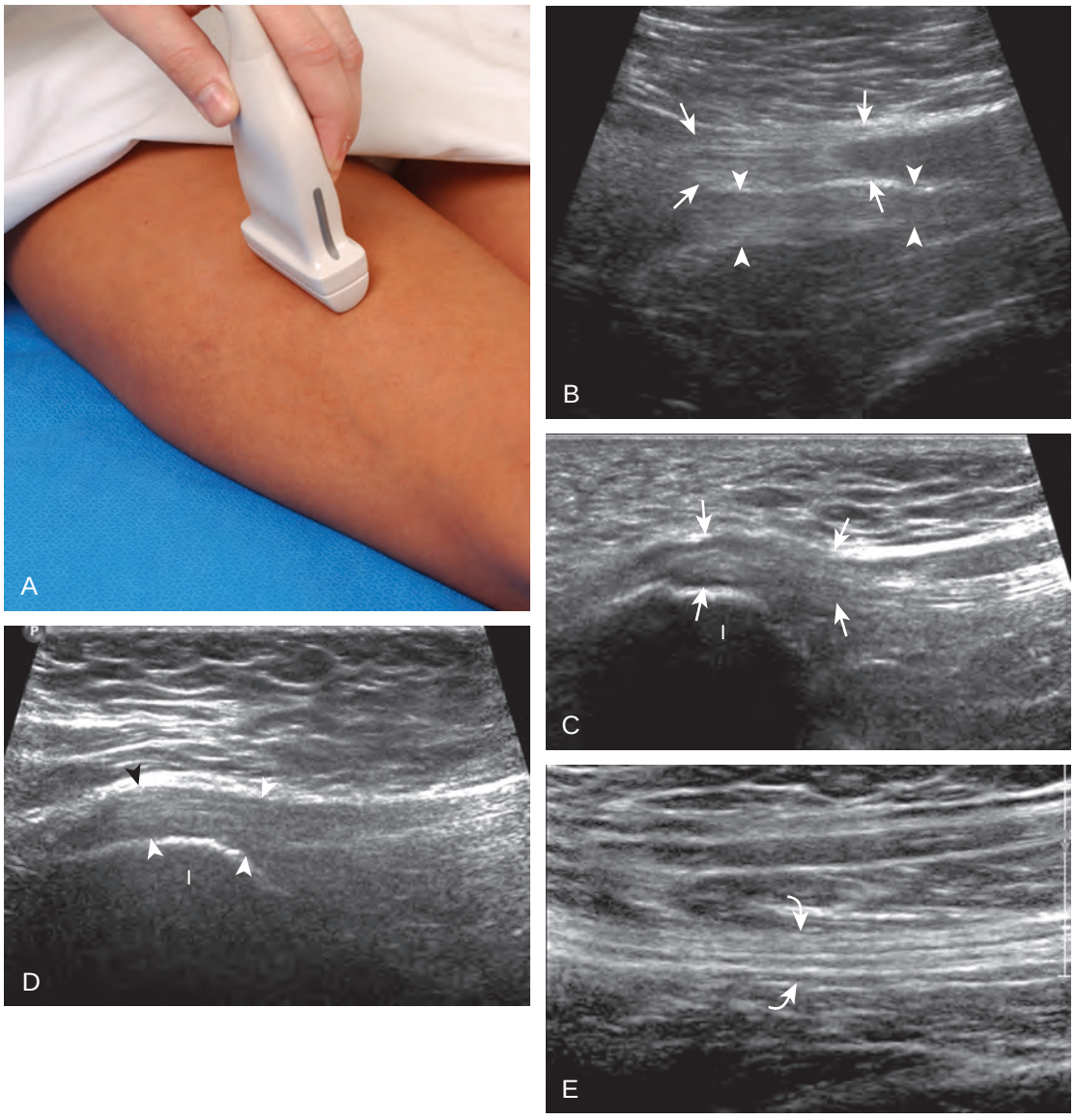

FIGURE 6-22 ■ Posterior thigh evaluation (long axis). A, Sagittal imaging shows **(B)** the conjoint tendon *(arrows)* in long axis superficial to the semimembranosus tendon *(arrowheads)* just distal to the ischial tuberosity. **C,** At the ischial tuberosity (I), the conjoint tendon *(arrows)* is identified. The transducer is moved lateral and angled toward midline **(D)** to visualize the semimembranosus tendon *(arrowheads)*. The sciatic nerve **(E)** is also visualized *(curved arrows)*.

The criterion for abnormal joint distention in a child is 2 mm of separation of the anterior and posterior capsule layers (Fig. 6-27).[1] In the adult, total capsular distention of 7 mm (measured from the femoral neck surface to the outer margin of the capsule, to include both anterior and posterior layers) or 1 mm of asymmetry compared with the contralateral asymptomatic hip has been shown to indicate joint distention,[21] although a 5-mm threshold has also been used (Fig. 6-28) (Video 6-9).[22] Regardless, when the femoral neck and anterior capsule are imaged perpendicular to the sound beam, even small amounts of joint fluid can be seen separating the anterior capsule layers. Leg extension and abduction may also improve visualization of a hip joint effusion. In addition, a convex or bulging surface of the anterior joint recess suggests abnormal distention.[1] Internal rotation of the leg may cause bulging of the normal joint capsule, which should not be misinterpreted as effusion (Fig. 6-29) (Video 6-10).[1] Uncommonly, joint effusion may extend

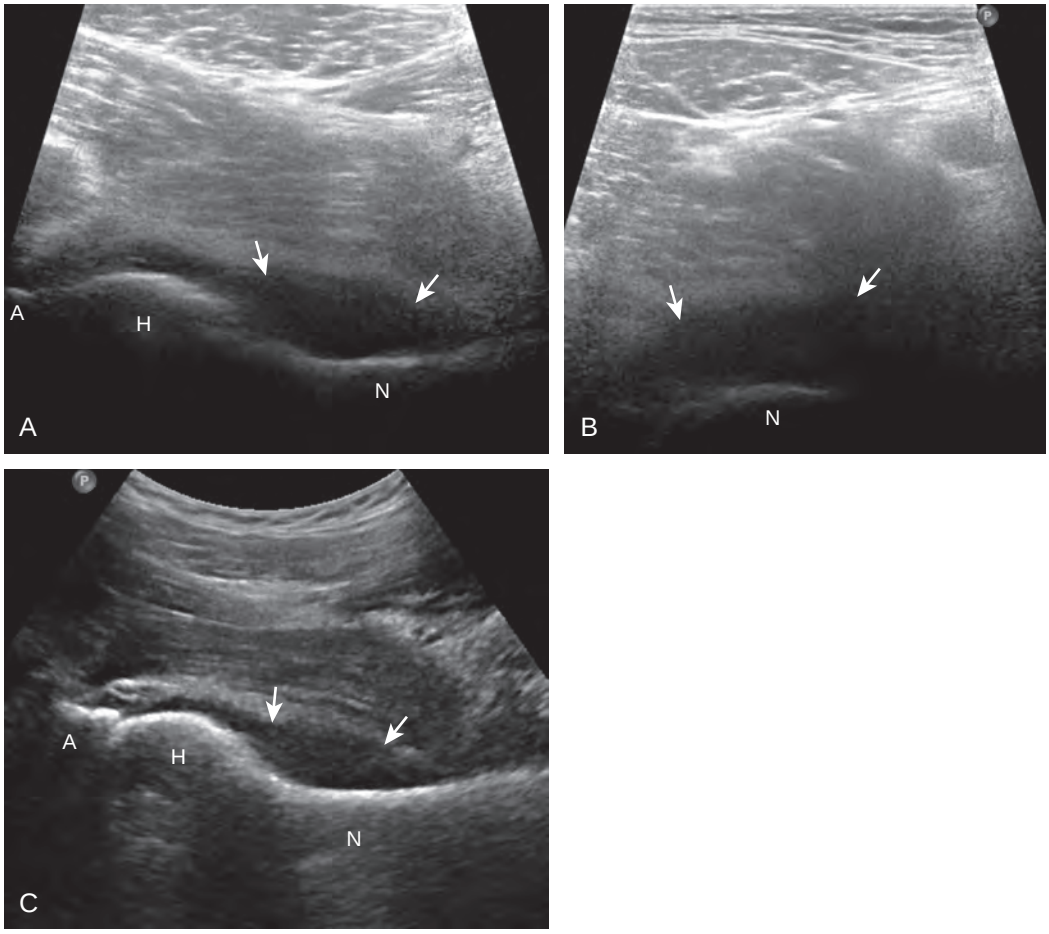

FIGURE 6-26 ■ **Septic effusion.** Ultrasound images in **(A)** long axis and **(B)** short axis to the femoral neck show anechoic anterior joint recess distention *(arrows)*. Similar findings are seen **(C)** using a lower frequency (7 MHz) curvilinear transducer. Note the difficulty in discerning the anterior and posterior capsule layers given the depth and resulting lower resolution. A, acetabulum; H, femoral head; N, femoral neck.

superficially through a defect in the hip joint capsule within a pseudodiverticulum of the synovial membrane (Fig. 6-30).[1]

It is important to be familiar with the appearance of the normal anterior hip joint recess, which may appear hyperechoic (if imaged perpendicular) or hypoechoic (if imaged obliquely or in large patients) with a thickness of less than 4 to 6 mm, owing to the normal capsular reflection (see Figs. 6-2 and 6-3). This appearance should not be misinterpreted as joint effusion or synovial hypertrophy. In fact, it has been shown that in children with toxic hip synovitis, synovial thickening is not visible at ultrasound (see Fig. 6-27).[1] Joint recess distention from an effusion may range from anechoic (if simple fluid) to hyperechoic (if synovial hypertrophy or complex fluid from hemorrhage or infection). Neither joint recess echogenicity nor flow on color or power Doppler imaging can distinguish between aseptic and septic effusion; diagnostic ultrasound-guided percutaneous aspiration should be considered if there is concern for infection.[23] In addition, it may be difficult to appreciate a small joint effusion in patients with increased soft tissues superficial to the hip and in those with a large body habitus.[24] In this situation, percutaneous aspiration should be considered regardless of ultrasound findings if there is clinical concern for infection. A large body habitus may cause anechoic fluid to appear artifactually hypoechoic or isoechoic, even with lower-frequency transducers and tissue harmonic imaging.

Causes of hip effusion include reactive fluid, trauma, infection, and hemorrhage. Hypoechoic, isoechoic, or hyperechoic distention of the hip joint recess can be caused by either complex fluid (see Fig. 6-30) or synovial hypertrophy (Fig. 6-31). In the latter condition, lack of compressibility or redistribution and positive flow on color or power Doppler imaging suggests synovial hypertrophy. Causes of synovitis include infection and inflammatory arthritis (Fig. 6-32). Other synovial proliferative disorders such as pigmented

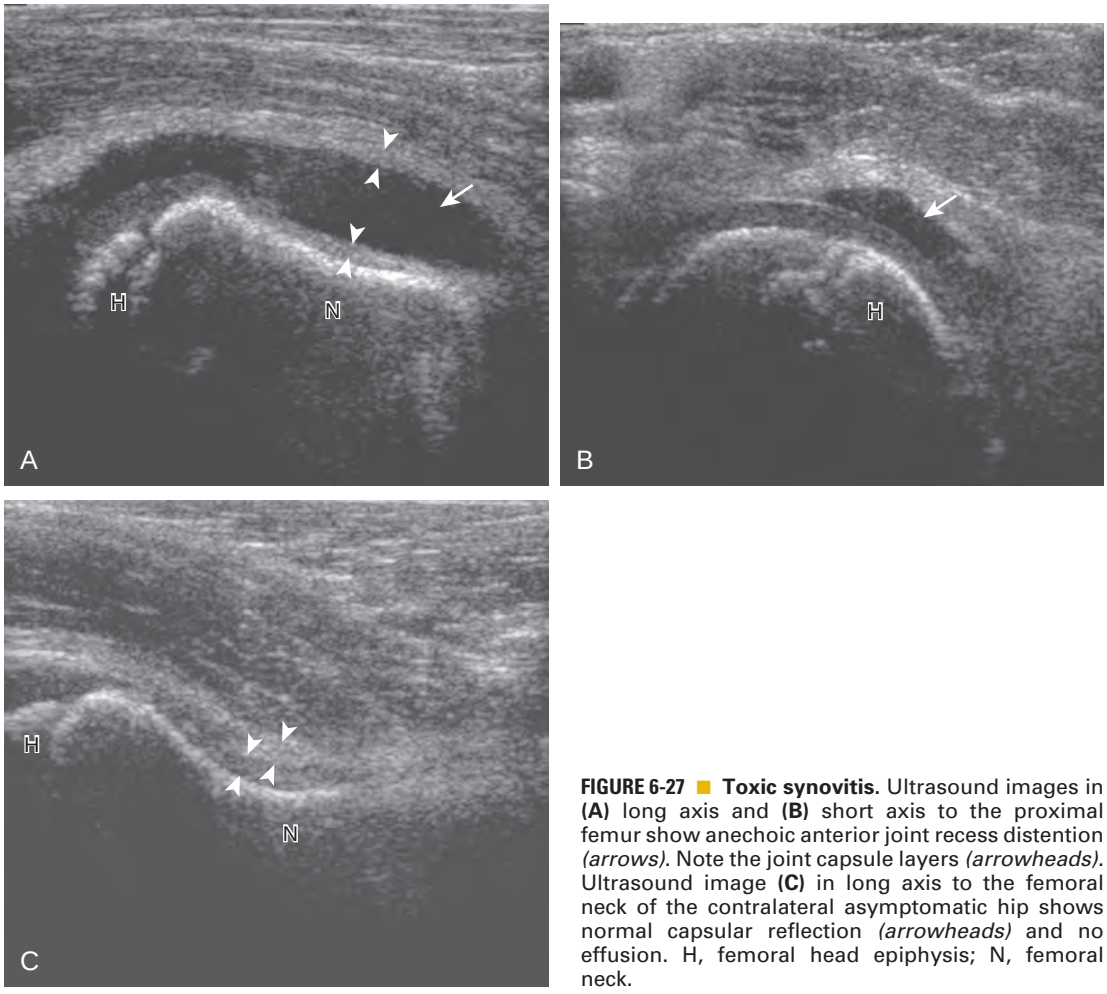

FIGURE 6-27 ■ Toxic synovitis. Ultrasound images in **(A)** long axis and **(B)** short axis to the proximal femur show anechoic anterior joint recess distention *(arrows)*. Note the joint capsule layers *(arrowheads)*. Ultrasound image **(C)** in long axis to the femoral neck of the contralateral asymptomatic hip shows normal capsular reflection *(arrowheads)* and no effusion. H, femoral head epiphysis; N, femoral neck.

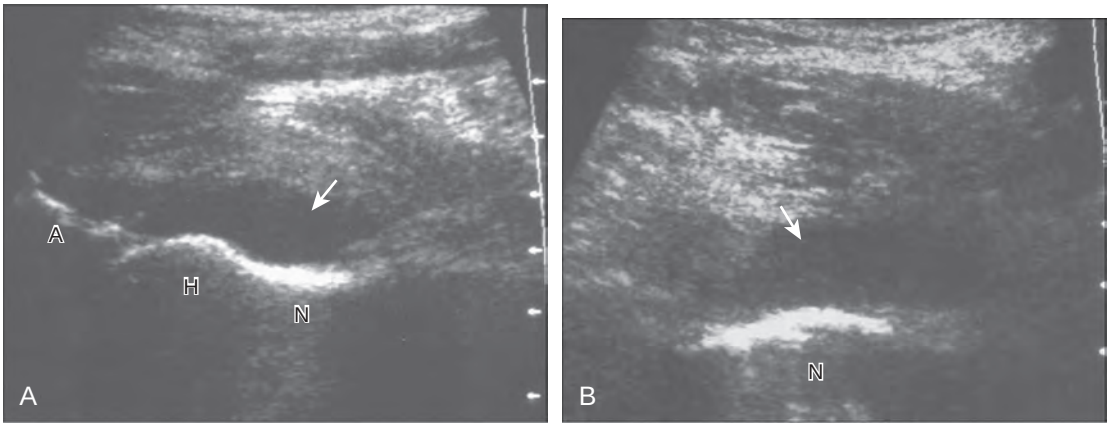

FIGURE 6-28 ■ Aseptic effusion. Ultrasound image in **(A)** long axis and **(B)** short axis to the femoral neck show anechoic anterior joint recess distention *(arrows)*. A, acetabulum; H, femoral head; N, femoral neck.

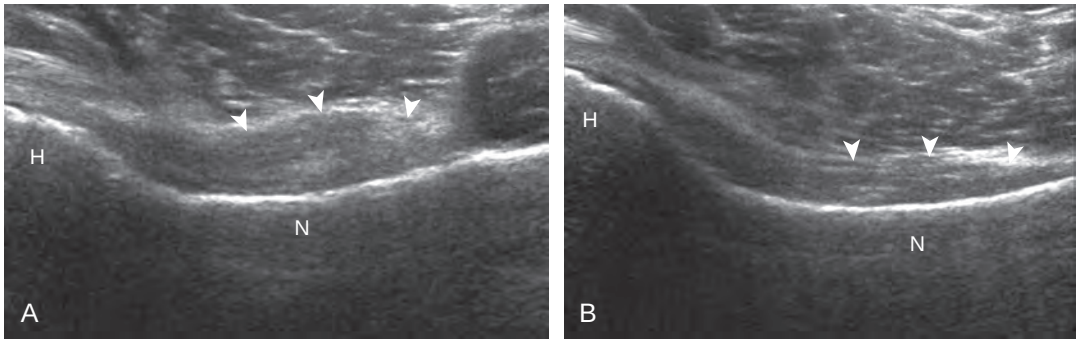

FIGURE 6-29 ■ Effects of leg position on joint capsule. Ultrasound images in long axis to the femoral with the leg in **(A)** internal rotation and **(B)** external rotation show convex bulging of the joint capsule *(arrowheads)* with internal rotation. H, femoral head; N, femoral neck.

villonodular synovitis can appear similar, as can synovial osteochondromatosis (although the latter may show hyperechoic calcific foci). Intra-articular bodies appear as hyperechoic foci with possible posterior acoustic shadowing within the joint recess.

Labrum and Proximal Femur Abnormalities

Other intra-articular structures visible by ultrasound include the hypoechoic hyaline cartilage that covers the femoral head and the hyperechoic triangle-shaped fibrocartilage acetabular labrum. A labrum tear may appear as a defined hypoechoic or anechoic cleft, which is more conspicuous when there is adjacent joint fluid (Fig. 6-33). The presence of a hypoechoic or anechoic paralabral

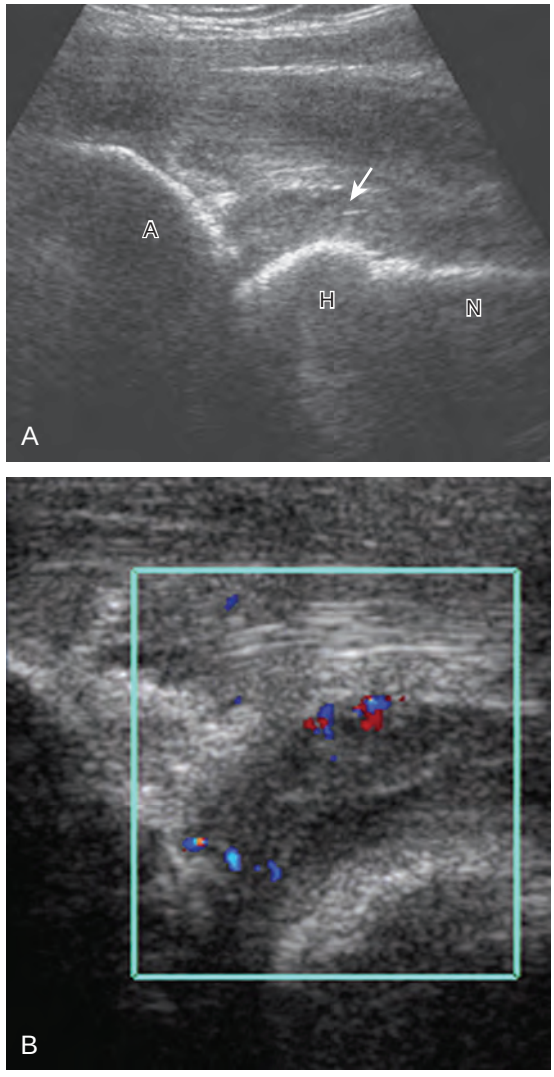

FIGURE 6-31 ■ Synovial hypertrophy: infection. Ultrasound image **(A)** in long axis to the femoral neck shows isoechoic anterior joint recess distention *(arrow)*. **B,** Note hyperemia with color Doppler imaging. A, acetabulum; H, femoral head; N, femoral neck.

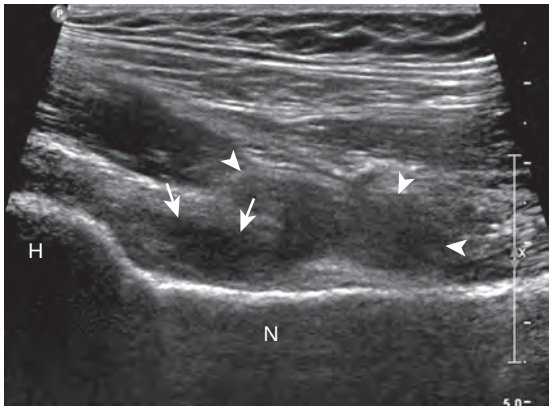

FIGURE 6-30 ■ Complex joint fluid. Ultrasound image in long axis to the femoral neck shows hypoechoic anterior joint recess distention with internal echoes *(arrows)*. Note the distention of the pseudodiverticulum *(arrowheads)*. H, femoral head; N, femoral neck.

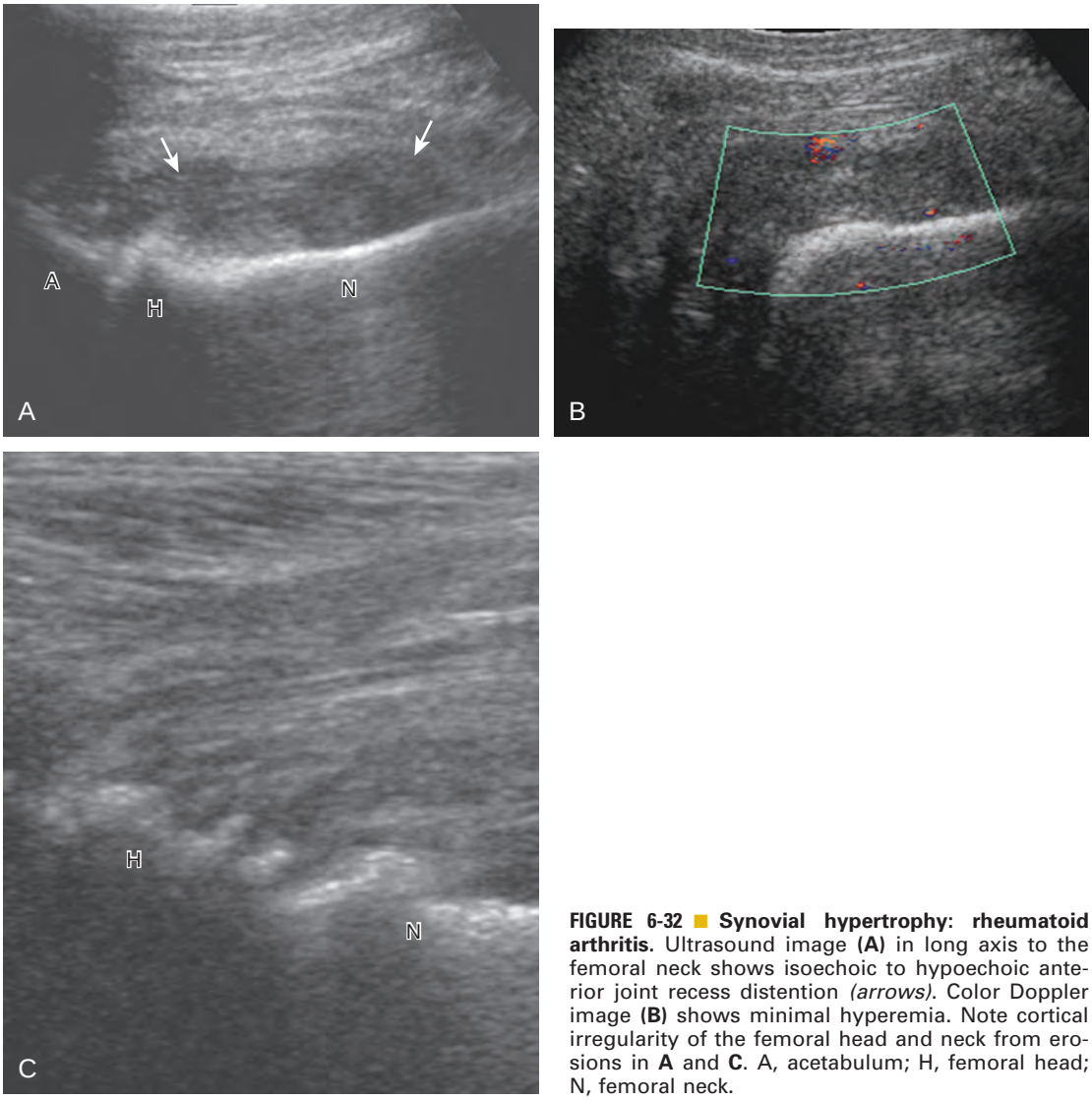

FIGURE 6-32 ■ Synovial hypertrophy: rheumatoid arthritis. Ultrasound image **(A)** in long axis to the femoral neck shows isoechoic to hypoechoic anterior joint recess distention *(arrows)*. Color Doppler image **(B)** shows minimal hyperemia. Note cortical irregularity of the femoral head and neck from erosions in **A** and **C**. A, acetabulum; H, femoral head; N, femoral neck.

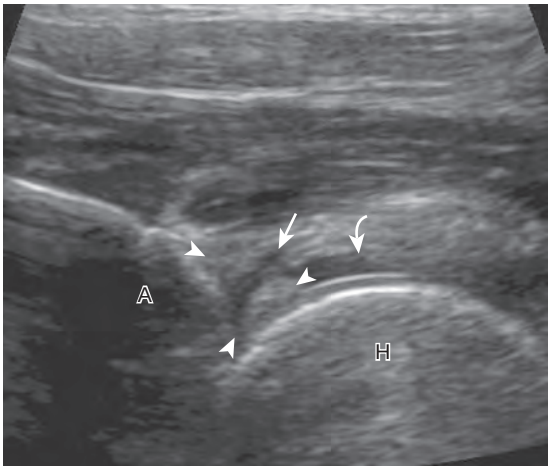

FIGURE 6-33 ■ Labral tear. Ultrasound image in long axis to the femoral neck shows an anechoic cleft *(arrow)* and irregularity of the hyperechoic fibrocartilage labrum *(arrowheads)*. Note joint effusion *(curved arrow)* adjacent to the femoral head hypoechoic hyaline cartilage. A, acetabulum; H, femoral head.

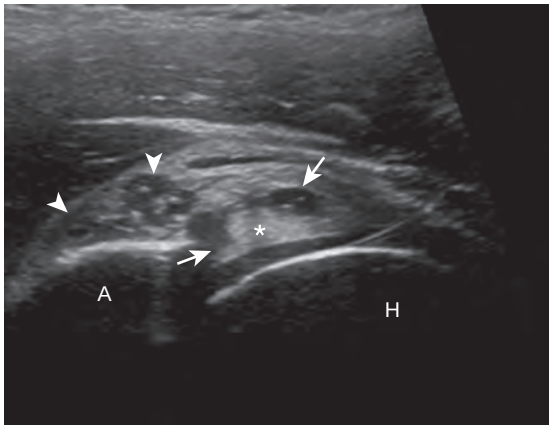

FIGURE 6-34 ■ Labral tear and paralabral cyst. Ultrasound image in long axis to the femoral neck shows an anechoic cleft *(arrows)* extending through the labrum *(asterisk)* with a hypoechoic paralabral cyst *(arrowheads)*. A, acetabulum; H, femoral head.

cyst is also an indicator of underlying hip labrum tear (Fig. 6-34). The accuracy of ultrasound in the diagnosis of hip labrum tear is variable because limitations exist given the depth of and limited access to the labrum.[25,26] Chondrocalcinosis, which may be seen with pseudogout, will create punctate reflective echoes within the labrum (Fig. 6-35).

Ultrasound is very sensitive to cortical irregularity, and correlation with radiography is essential. A step-off deformity of the femoral neck can indicate a fracture.[27] An osteophyte at the femoral neck indicates osteoarthritis (Fig. 6-36). Cortical irregularity or bone protuberance of the anterosuperior femoral head-neck junction can be seen in cam-type femoroacetabular impingement.[28-30] Dynamic imaging with hip flexion and internal rotation may show direct contact between the labral tear and femoral cortical irregularity, which supports the diagnosis

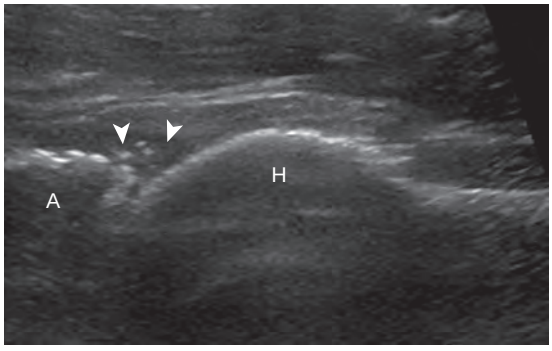

FIGURE 6-35 ■ Chondrocalcinosis. Ultrasound image in long axis to the femoral neck shows hyperechoic foci within the labrum *(arrowheads)* representing chondrocalcinosis. A, acetabulum; H, femoral head.

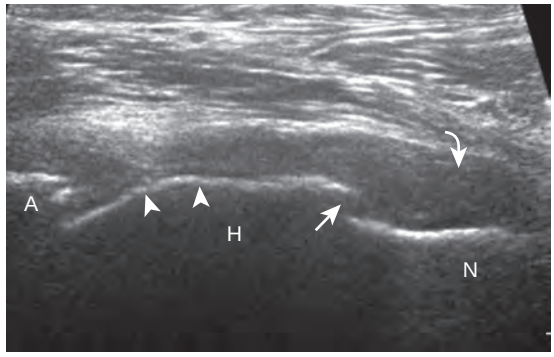

FIGURE 6-36 ■ Osteoarthritis. Ultrasound image in long axis to the femoral neck shows a marginal osteophyte at the head-neck junction *(arrow)* and irregular contour of the femoral head *(arrowheads)*. Note the hypoechoic distention of the joint capsule *(curved arrow)*. A, acetabulum; H, femoral head; N, femoral neck.

(Fig. 6-37) (Videos 6-11 and 6-12). Treatment of femoroacetabular impingement includes osteoplasty, which will appear as a cortical defect at the femoral head-neck junction (Fig. 6-38).

Bursal Abnormalities

There are several bursae that can be found about the hip. The iliopsoas bursa is located anterior to the hip joint.[31] When distended, it is seen medial to the iliopsoas tendon but may extend anterior and wrap anterolateral to the tendon, or extend lateral between the iliopsoas tendon and the acetabulum.[32] The iliopsoas bursa communicates with the hip joint in up to 15% of the population, and its distention is often related to hip joint pathology.[6] Possible communication between the iliopsoas bursa and the hip joint can be visualized in the transverse plane at the level of the femoral head immediately medial to the iliopsoas tendon (Fig. 6-39A). The iliopsoas bursa may be distended with simple fluid, complex fluid (see Fig. 6-39B and C), or synovial hypertrophy, which may range from anechoic to hyperechoic. Similar to joint recess distention, lack of compressibility and the presence of flow on color or power Doppler imaging suggest synovial hypertrophy. An abnormally distended bursa may extend into the abdomen and should not be confused for an intra-abdominal or psoas abscess.[33] In addition, distention of the bursa does not imply inflammation or true bursitis; the presence of pain with transducer pressure, increased flow on color or power Doppler imaging, and distention out of proportion to hip joint recess distention suggest true inflammation and bursitis.

The greater trochanteric region is also evaluated for abnormal bursal distention.[2] The trochanteric (or subgluteus maximus) bursa

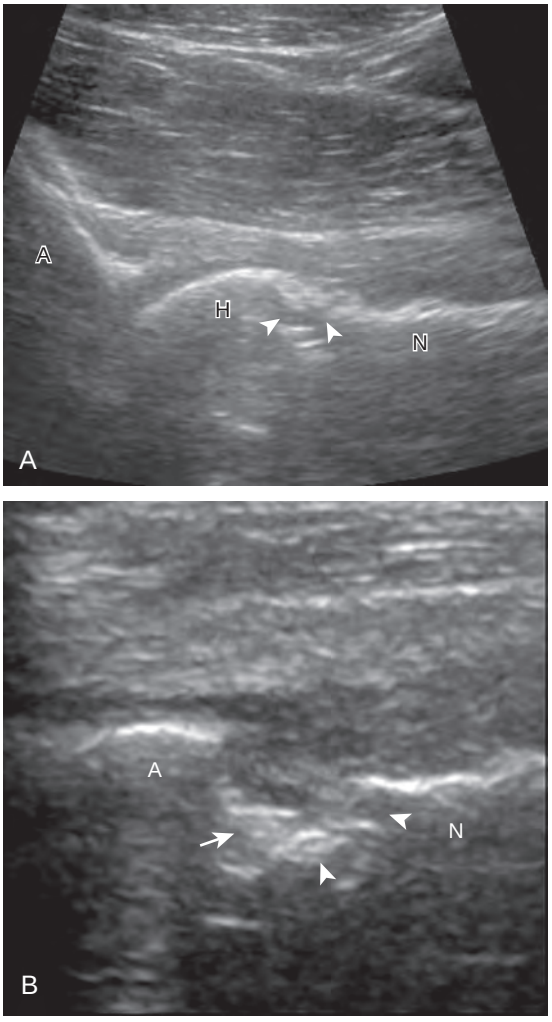

FIGURE 6-37 ■ Femoroacetabular impingement. Ultrasound image **(A)** in long axis to the femoral neck shows cortical irregularity *(arrowheads)* of the anterior femoral head (H) and neck (N). Ultrasound image **(B)** in long axis to the femoral neck with hip flexion and internal rotation shows direct contact between the femoral head-neck irregularity *(arrowheads)* and the irregular fibrocartilage labrum *(arrow)*. A, acetabulum.

originates between the gluteus maximus and posterior facet of the greater trochanter but may extend laterally between the gluteus medius tendon and overlying iliotibial tract (Fig. 6-40). It is important to completely evaluate the posterior facet of the greater trochanter so as not to overlook bursal distention. Similar to other bursae, distention of the trochanteric bursa can be from simple fluid, complex fluid, or synovial hypertrophy (Fig. 6-41) (Video 6-13). As described earlier, the subgluteus minimus bursa (Fig. 6-42) and subgluteus medius bursa are located between the greater trochanter and their respective tendons. In the setting of greater trochanteric pain syndrome, identification of a distended and inflamed bursa is not common.[34] Gluteus minimus and medius tendon abnormalities are found more often and may be associated with bursal abnormalities.[35] Uncommonly, an obturator externus bursa may be seen at the medial aspect of the lesser trochanter of the femur[7] or an ischial (ischiogluteal) bursa (Fig. 6-43) superficial to the ischial tuberosity.[36]

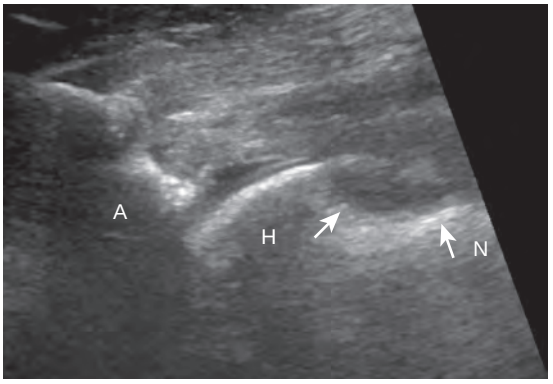

FIGURE 6-38 ■ Osteoplasty. Ultrasound image in long axis to the femoral neck shows concavity at the femoral head-neck junction *(arrows)* from prior surgical osteoplasty. A, acetabulum; H, femoral head; N, femoral neck.

Postsurgical Hip

In evaluation of the postsurgical hip, it is important first to understand the normal sonographic appearances. With regard to hip replacement, the femoral head and proximal femur are typically replaced with material composed of metal or ceramic, with a plastic, metal, or ceramic acetabular cup. At sonography, these components demonstrate a hyperechoic surface and possible posterior reverberation (with a metal surface) (Fig. 6-44).[37] When imaging the proximal femur in long axis to the femoral neck, one will see the echogenic and shadowing proximal femur disrupted by the echogenic surface contours of the arthroplasty. The posterior reverberation artifact of the arthroplasty is contrasted by the posterior acoustic shadowing of the native femur. The echogenic edge of the acetabular cup is also seen; the adjacent native acetabulum more proximally produces posterior acoustic shadowing. Hypoechogenicity superficial to the neck of the prosthesis and up to 6 mm superficial to the native femur at the prosthesis-bone junction has been described in asymptomatic patients after total hip arthroplasty.[38]

A hip joint effusion appears as a hypoechoic or anechoic layer over the femoral neck of the

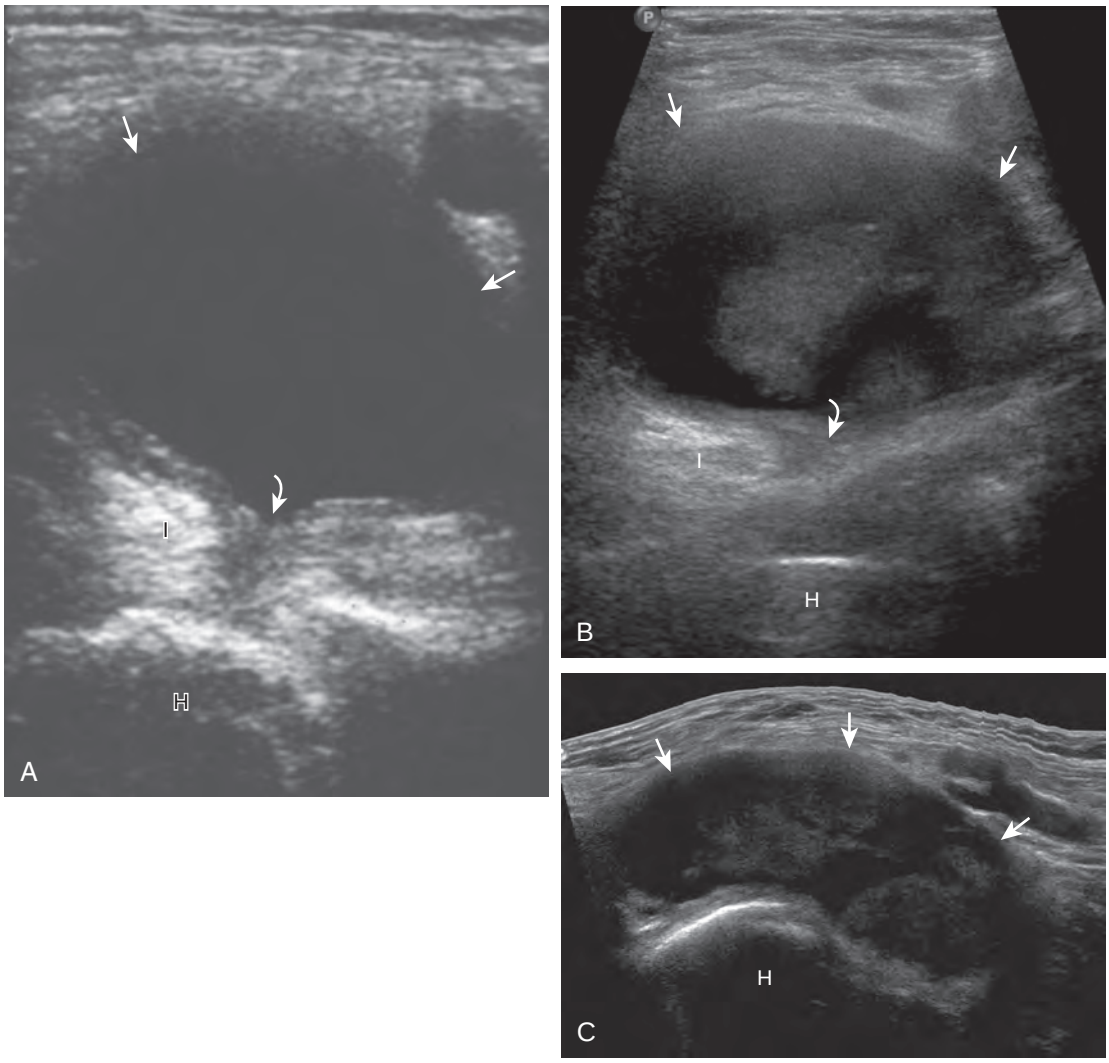

FIGURE 6-39 ■ Iliopsoas bursal distention. Ultrasound image **(A)** transverse to the femoral head (H) shows anechoic distention of the iliopsoas bursa *(arrows)*. Note the communication with the hip joint *(curved arrow)* medial to the iliopsoas tendon (I). Ultrasound images **(B)** transverse and **(C)** sagittal (with extended field of view) over the femoral head (H) in a different patient show complex fluid distention of iliopsoas bursa *(arrows)* with hip joint communication *(curved arrow)* medial to iliopsoas tendon (I).

prosthesis (Fig. 6-45).[24] The margins of the effusion may be ill defined if the hip joint capsule has been resected because the fluid will then be outlined by a pseudocapsule. Identification of a small joint effusion may be difficult because of a patient's large body habitus, an issue compounded by the possible hypoechoic postsurgical changes.[24] One should consider percutaneous aspiration when there is high clinical concern for infection, regardless of the sonographic findings. A large joint effusion can become quite prominent, especially in infection, in which complex fluid commonly extends beyond the joint into the surrounding soft tissues (Fig. 6-46).[37] Pseudocapsule distention greater than 3.2 mm over the native femur immediately adjacent to the neck of the prosthesis suggests a septic joint.[37] It is also important to evaluate the soft tissues anterior to the femoral neck before attempting percutaneous aspiration using fluoroscopy. The latter is recommended to avoid the potential contamination of a sterile joint by passing a needle through an overlying soft tissue infection. In addition, if no fluid is present at joint aspiration attempt, lavage and re-aspiration are recommended to exclude infection.

Other causes of joint effusion after arthroplasty include prosthesis loosening and particle

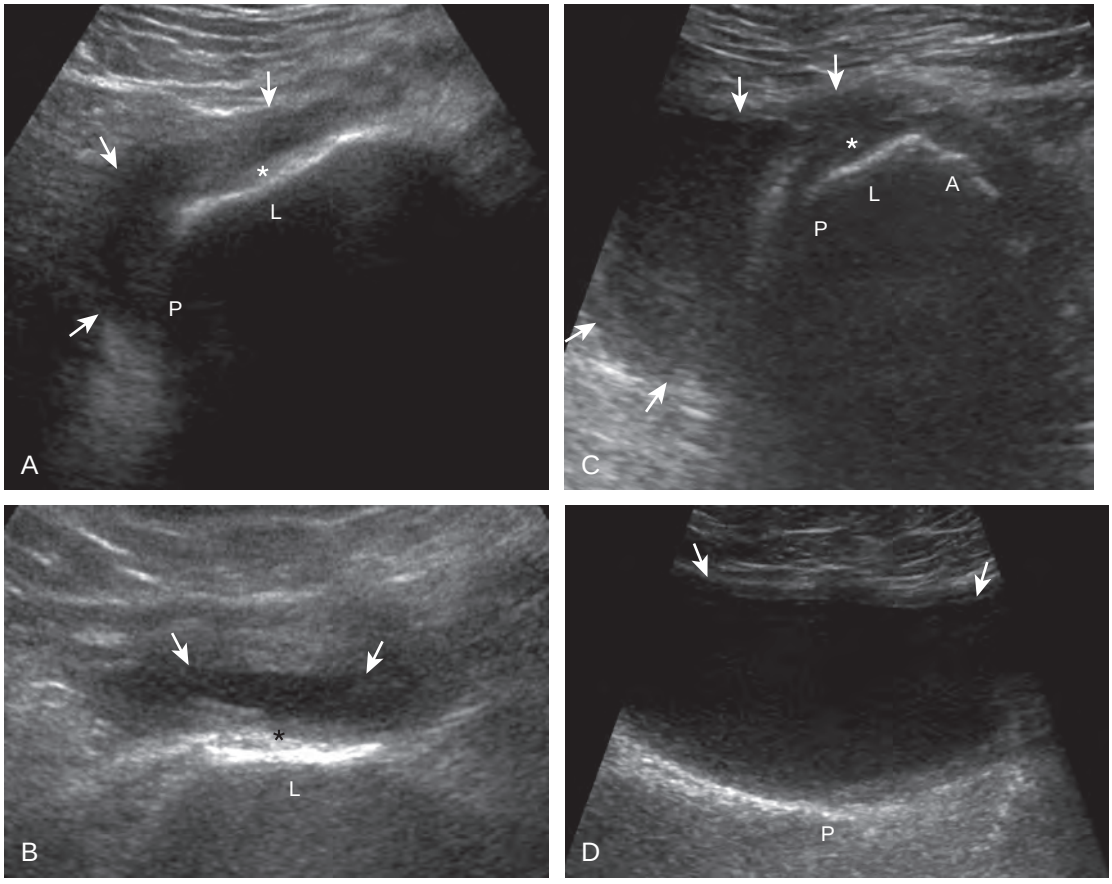

FIGURE 6-40 ■ Trochanteric (subgluteus maximus) bursal distention. Ultrasound images in **(A)** short axis and **(B)** long axis to the femur show hypoechoic distention of the trochanteric bursa *(arrows)*. Ultrasound images in **(C)** short axis and **(D)** long axis to the femur in a different patient show marked distention of the trochanteric bursa *(arrows)* (*asterisk*, gluteus medius tendon). Note posterior location of trochanteric bursa. A, anterior facet of the greater trochanter; L, lateral facet; P, posterior facet.

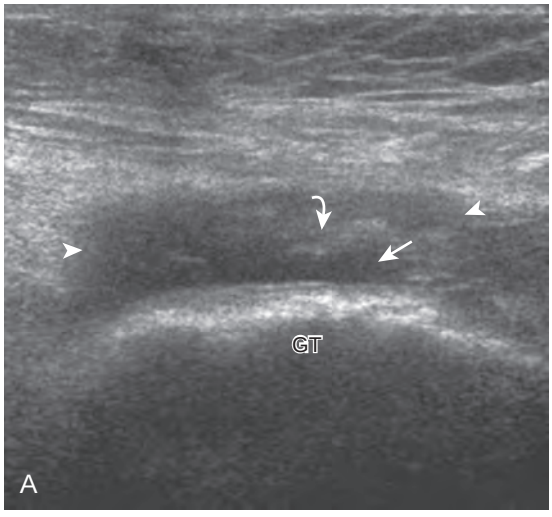

FIGURE 6-41 ■ Trochanteric (subgluteus maximus) bursal distention: lupus. Coronal ultrasound image, over the greater trochanter (GT) shows anechoic fluid *(arrow)* and hypoechoic synovial hypertrophy *(curved arrow)*, which distends the trochanteric bursa *(arrowheads)*.

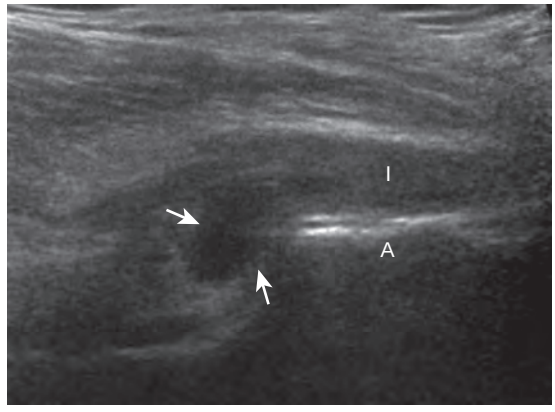

FIGURE 6-42 ■ Subgluteus minimus bursal distention. Ultrasound in long axis to the gluteus minimus tendon (I) shows hypoechoic distention *(arrows)* of the subgluteus minimus bursa. Note severe tendinosis of the gluteus minimus tendon. A, anterior facet of the greater trochanter.

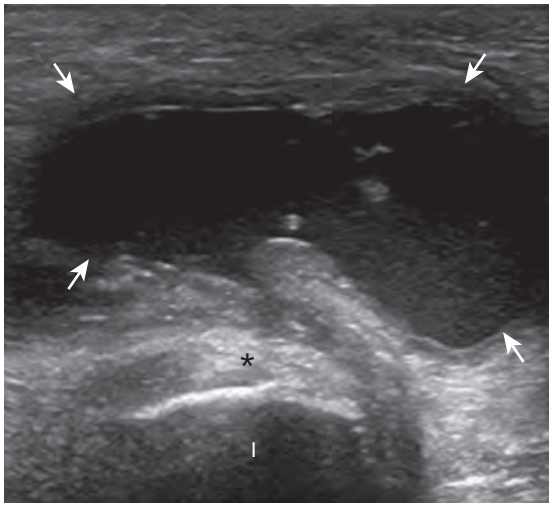

FIGURE 6-43 ■ Ischial bursal distention. Ultrasound image in the transverse plane over the ischium (I) shows heterogeneous but predominantly hypoechoic complex bursa distention *(arrows)* (*asterisk*, conjoint tendon of hamstring).

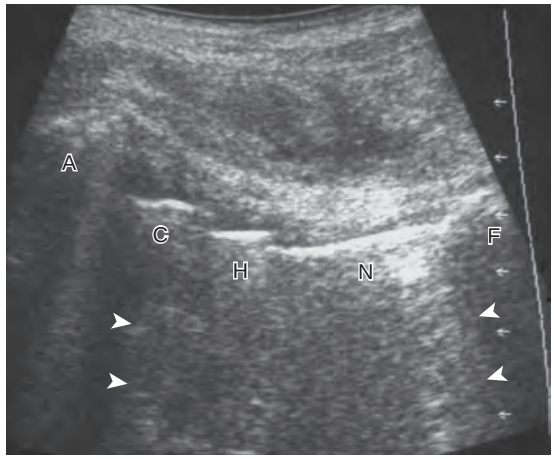

FIGURE 6-44 ■ Normal total hip arthroplasty. Ultrasound image in long axis to the femoral neck of hip arthroplasty shows the reflective surfaces of the acetabular cup (C), femoral head (H), and femoral neck (N) components with posterior reverberation artifact *(arrowheads)*. Note the native acetabulum (A) and femur (F) with posterior acoustic shadowing.

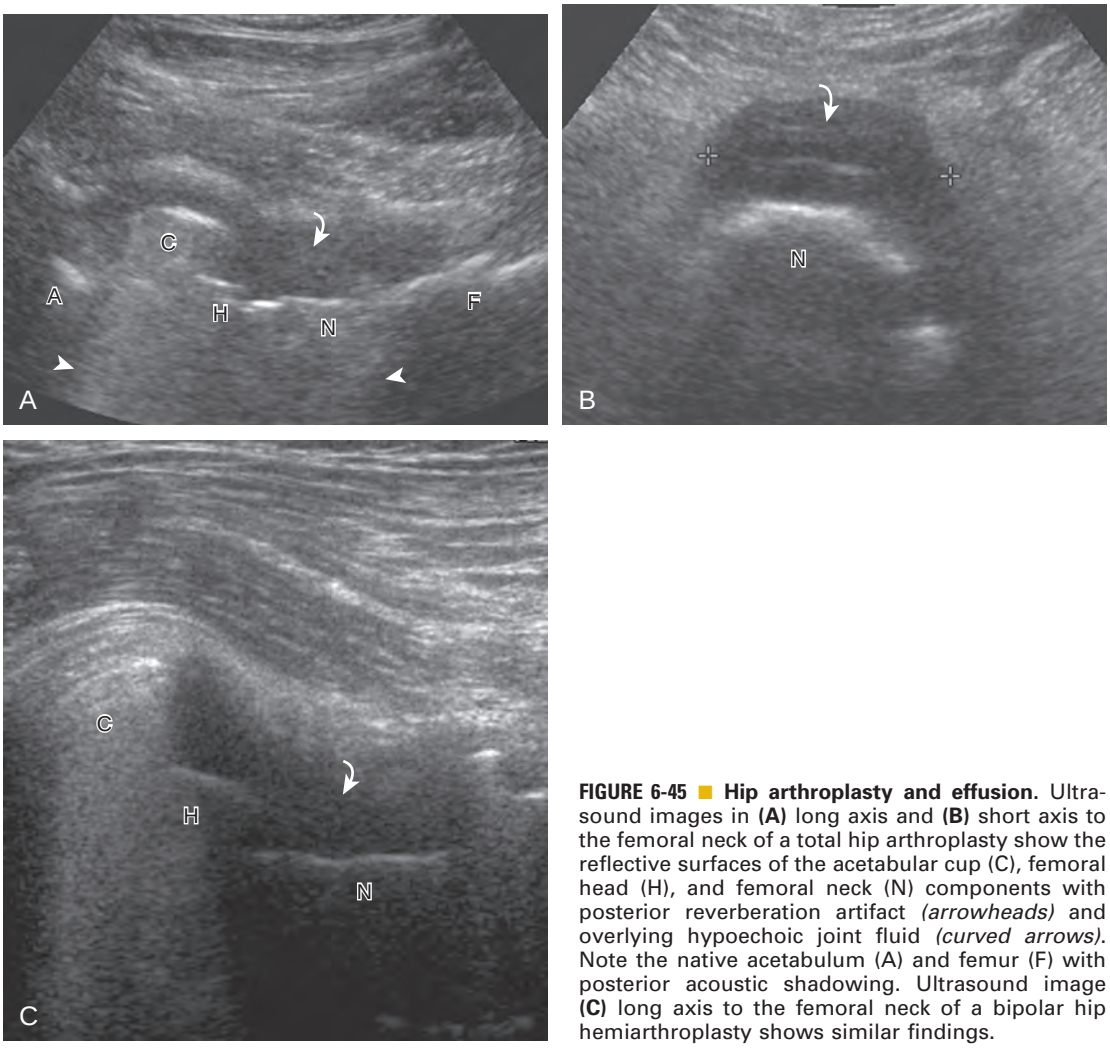

FIGURE 6-45 ■ Hip arthroplasty and effusion. Ultrasound images in **(A)** long axis and **(B)** short axis to the femoral neck of a total hip arthroplasty show the reflective surfaces of the acetabular cup (C), femoral head (H), and femoral neck (N) components with posterior reverberation artifact *(arrowheads)* and overlying hypoechoic joint fluid *(curved arrows)*. Note the native acetabulum (A) and femur (F) with posterior acoustic shadowing. Ultrasound image **(C)** long axis to the femoral neck of a bipolar hip hemiarthroplasty shows similar findings.

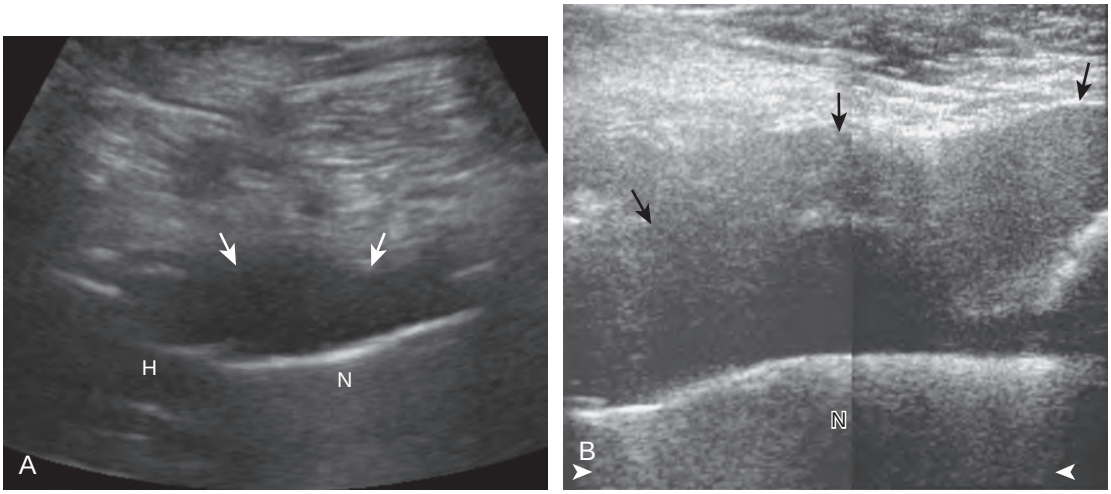

FIGURE 6-46 ■ Infected total hip arthroplasty. Ultrasound image **(A)** in long axis to the femoral neck of a hip arthroplasty shows hypoechoic fluid *(arrows)* over the femoral neck (N) and head (H) of the prosthesis. Ultrasound image **(B)** in long axis to the femoral neck of a hip arthroplasty in a different patient shows reflective surfaces of the femoral neck (N) component with posterior reverberation artifact *(arrowheads)*. Note the anechoic and hypoechoic complex fluid *(arrows)* extending from the joint into the adjacent soft tissues.

disease, the latter representing inflammatory reaction to breakdown of the prosthesis components that may cause osteolysis and joint distention. An adverse periprosthetic soft tissue reaction associated with metal-on-metal hip arthroplasties has been termed *pseudotumor* and can appear solid or cystic with ultrasound (Fig. 6-47).[39] After hip replacement, it is also important to image any symptomatic area, which may reveal bursal abnormality[40] (Fig. 6-48) and infection (Fig. 6-49) (Video 6-14). The gluteus tendons should also be evaluated for abnormality after arthroplasty, especially if an arthroplasty is placed using a direct lateral or modified anterolateral approach.[41] Another cause of symptoms includes iliopsoas impingement from the anterior aspect of the femoral component[42] or acetabular cup[43] (Fig. 6-50) of a hip arthroplasty. Acetabular liner displacement may also be detected.[44]

Regardless of the type of surgery, an incision site is a common location for pathology such as infection, hematoma (Fig. 6-51A), and seroma (see Fig. 6-51B). Heterotopic ossification may also be seen (see Fig. 6-51C). Another surgical procedure of the hip involves complete femoral head and neck resection after infection (Girdlestone procedure) (Fig. 6-52, online). Post-surgical changes can be seen at the femoral head-neck junction after osteoplasty for treatment of femoroacetabular impingement (see Fig. 6-38).

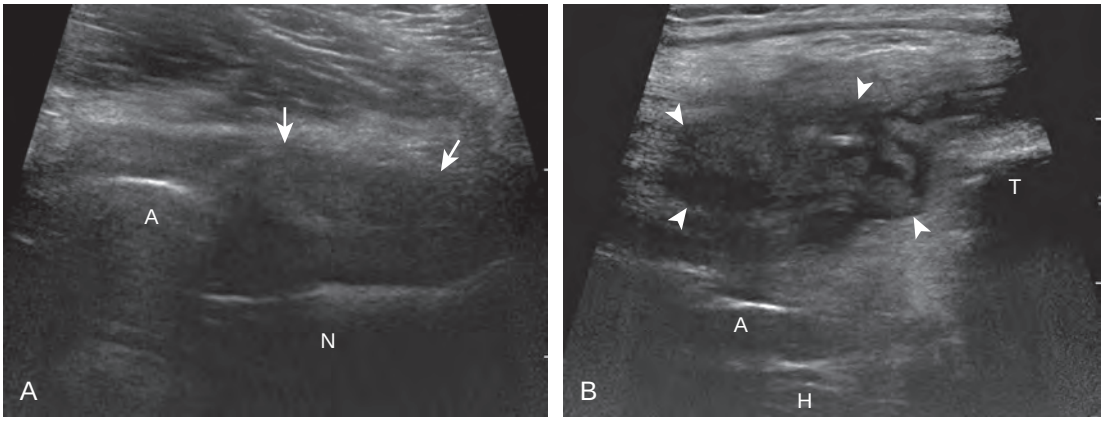

FIGURE 6-47 ■ Pseudotumor. Ultrasound images in long axis to the femoral neck of a metal-on-metal total hip arthroplasty in the **(A)** sagittal and **(B)** coronal planes show abnormal hypoechoic distention of the pseudocapsule *(arrows)* with an adjacent lateral hypoechoic and heterogeneous mass-like area of inflammation *(arrowheads)*. A, acetabular component; H, femoral head component; N, femoral neck; T, greater trochanter.

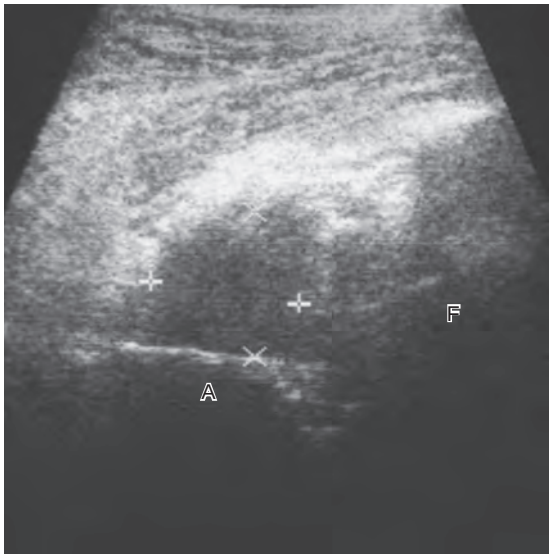

FIGURE 6-52 ■ Proximal femur resection (Girdlestone procedure). Ultrasound image coronal to the hip joint shows hypoechoic fluid *(between cursors)*. A, acetabulum; F, femoral neck at the resection site.

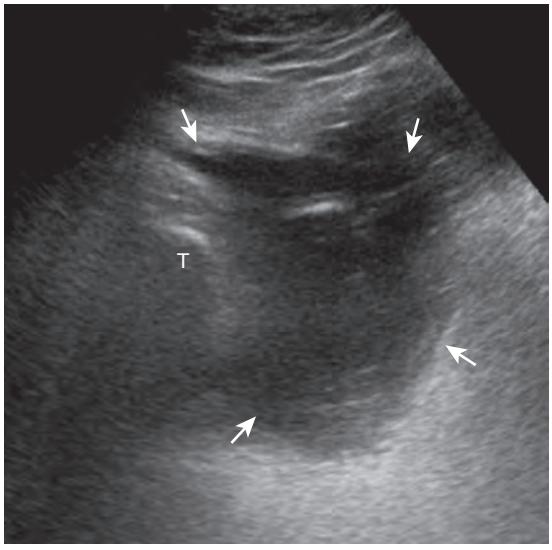

FIGURE 6-48 ■ Infected trochanteric bursa. Coronal ultrasound image over the greater trochanter (T) shows heterogeneous hypoechoic complex fluid *(arrows)*.

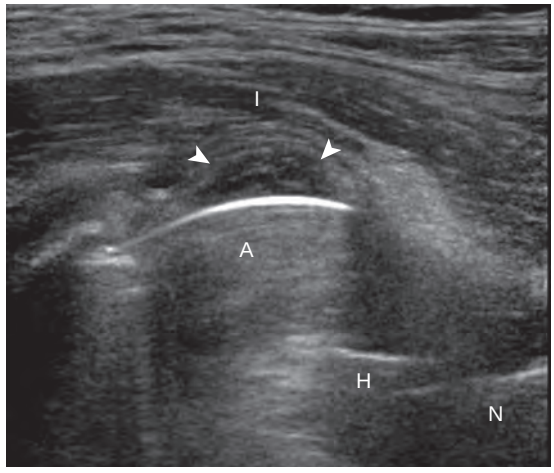

FIGURE 6-50 ■ Iliopsoas impingement. Ultrasound image in long axis to the femoral neck component of a total hip arthroplasty shows abnormal hypoechoic tissue *(arrowheads)* between the iliopsoas (I) and acetabular cup (A) of the arthroplasty. H, femoral head component; N, femoral neck component.

TENDON AND MUSCLE ABNORMALITIES

Tendon and Muscle Injury

Similar to other tendons in the body, a degenerative condition of tendons called *tendinosis* or *tendinopathy* is characterized by hypoechoic swelling of the affected tendon.[5,45,46] These terms are used instead of tendinitis because there are no significant acute inflammatory cells in this situation but rather mucoid degeneration and possible interstitial tearing. Chronic tendinopathy at a tendon attachment may produce marked cortical irregularity of the adjacent bone. Partial-thickness tendon tears are characterized by more defined hypoechoic or anechoic clefts within the involved tendon, but without the complete tendon disruption and retraction that are characteristic of full-thickness tears. In this latter condition, the tendon is torn and retracted with interposed heterogeneous but predominantly hypoechoic hemorrhage. Muscles that cross two joints are prone to tears at the musculotendinous junction; chronic injuries occur at the entheses, and direct impact injuries involve the muscle belly.

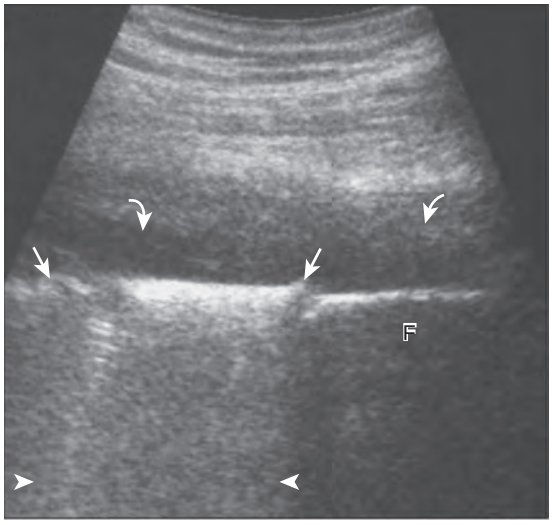

FIGURE 6-49 ■ Infected hip arthroplasty endoprosthesis. Ultrasound image in long axis to the femoral shaft at the junction of the metal endoprosthesis *(arrows)* and native femur (F) shows hypoechoic complex fluid (*curved arrows*). Note the posterior reverberation artifact from the prosthesis *(arrowheads)*.

With regard to the adductor musculature and the pubic symphyseal region, tendinosis and partial-thickness tears commonly involve the adductor longus origin at the pubis. This finding may be associated with abnormality of the common aponeurosis between the rectus abdominis and the adductor longus tendons superficial to the pubis, a finding described with sports-related hernia (Fig. 6-53).[13,47] Full-thickness tears are characterized by tendon retraction and interposed hemorrhage (Fig. 6-54). Distal to the adductor origin, a muscle strain from a stretch injury (Fig. 6-55) or a hematoma from direct impact injury may be found (Fig. 6-56). At the adductor insertion onto the posteromedial femur, chronic repetitive stress injury has been termed *thigh splints* or *adductor insertion avulsion syndrome*.[48] In this condition, an irregular bone

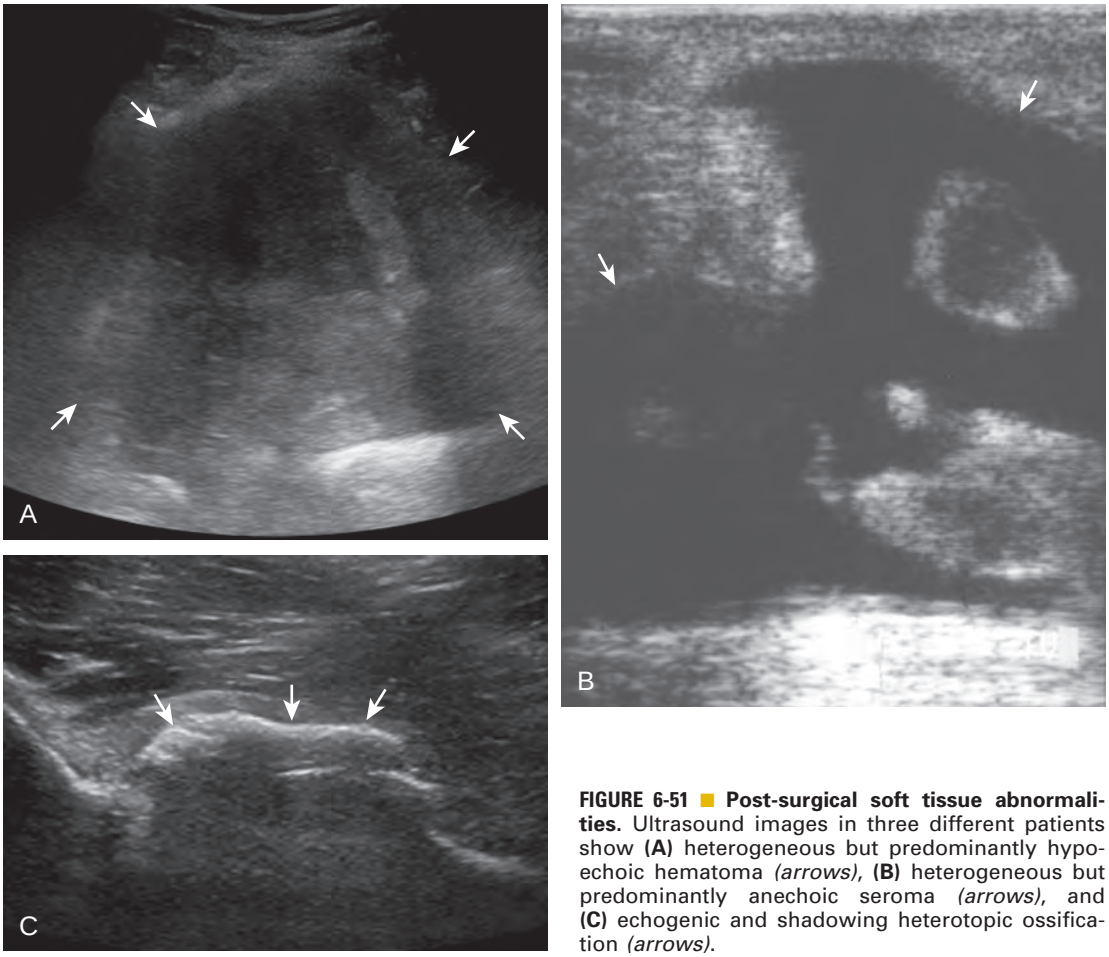

FIGURE 6-51 ■ Post-surgical soft tissue abnormalities. Ultrasound images in three different patients show **(A)** heterogeneous but predominantly hypoechoic hematoma *(arrows)*, **(B)** heterogeneous but predominantly anechoic seroma *(arrows)*, and **(C)** echogenic and shadowing heterotopic ossification *(arrows)*.

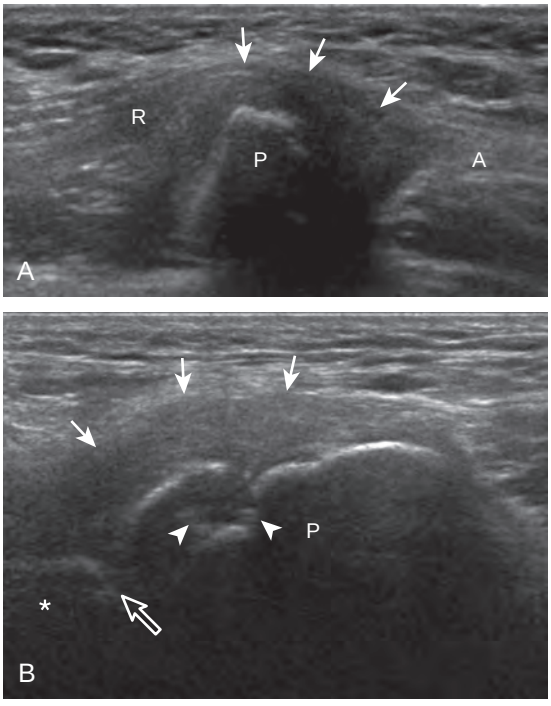

FIGURE 6-53 ■ Common aponeurosis injury (chronic). Ultrasound images in the **(A)** sagittal-oblique and **(B)** transverse planes over the pubis (P) show hypoechoic thickening of the common aponeurosis *(arrows)* between the rectus abdominis (R) and adductor longus (A) with cortical irregularity *(arrowheads)*. Note the pubic symphysis *(open arrow)* in **(B)** and contralateral pubis *(asterisk)*.

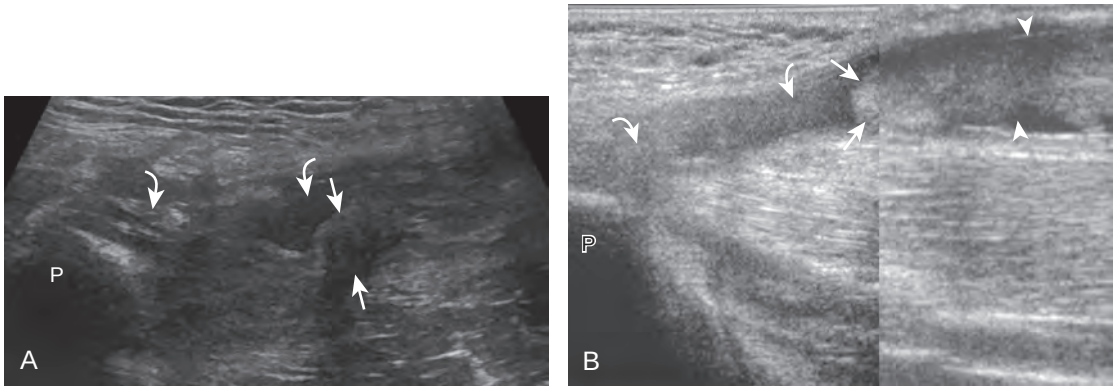

FIGURE 6-54 ■ Adductor longus tear: acute. Ultrasound images in long axis to the adductor longus tendon in two different patients **(A** and **B)** show retracted full-thickness tear *(arrows)* with intervening hemorrhage (*curved arrows)*. Note the distal tendon in **(A)** *(arrowheads)*. P, pubis.

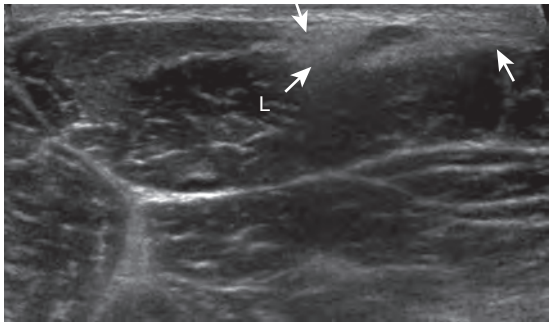

FIGURE 6-55 ■ Adductor muscle injury. Ultrasound image shows acute hyperechoic hemorrhage *(arrows)* at the superficial aspect of the adductor longus (L).

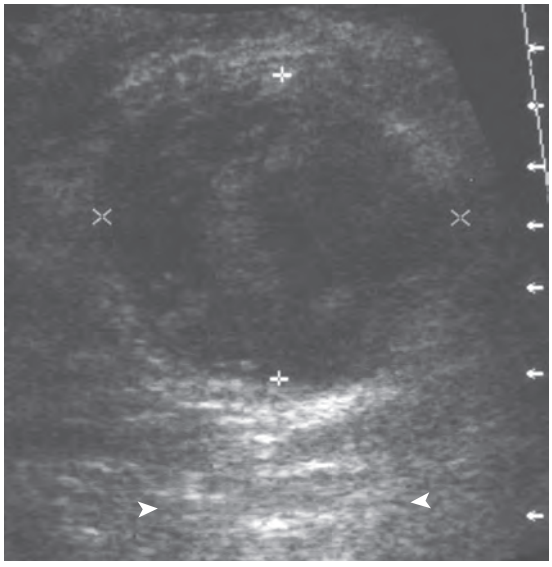

FIGURE 6-56 ■ Adductor muscle injury. Ultrasound image shows a heterogeneous hypoechoic hematoma *(between cursors)* with increased through-transmission *(arrowheads)*.

surface can indicate periostitis and possible stress fracture and is typically the site of point tenderness with transducer pressure (Fig. 6-57).

With regard to the rectus femoris, injuries may involve its origin at the anterior inferior iliac spine, where complete tears of the direct and indirect heads result in a full-thickness tear and retraction (Fig. 6-58). Injury can also occur at the central myotendinous aponeurosis, which will appear as abnormal hypoechogenicity surrounding the indirect head within the muscle belly (Fig. 6-59).[4] Partial tear can appear as hypoechoic fiber disruption (Fig. 6-60).[46] More distally, the posterior aponeurosis may be injured with resulting hematoma (Fig. 6-61A and B), which may later appear as hyperechoic scar (see Fig. 6-61C). A complete tear of the distal rectus femoris is characterized by muscle retraction and may be associated with anechoic fluid (Fig. 6-62). It is not uncommon for patients to present later with a palpable pseudomass, which represents the retracted muscle and tendon. A direct impact injury may cause an intramuscular hematoma (Fig. 6-63). Distal quadriceps tendon tears are discussed in Chapter 7.

The gluteus minimus and medius tendons may also be abnormal at their greater trochanter insertion, ranging from tendinosis (Fig. 6-64) to tendon tear (Fig. 6-65).[49] As described earlier, patients with greater trochanteric pain syndrome are much more likely to have gluteal tendon abnormalities rather than an isolated true bursitis as the cause of symptoms.[34] The reported sensitivity of ultrasound in the diagnosis of gluteal tendons tears ranges from 79% to 100%.[50] Gluteus medius tendon tears are more common than gluteus minimus tendon tears, and often a bursal abnormality is associated with the tendon tear.[35] Identification of the characteristic bone

Text continued on p. 200

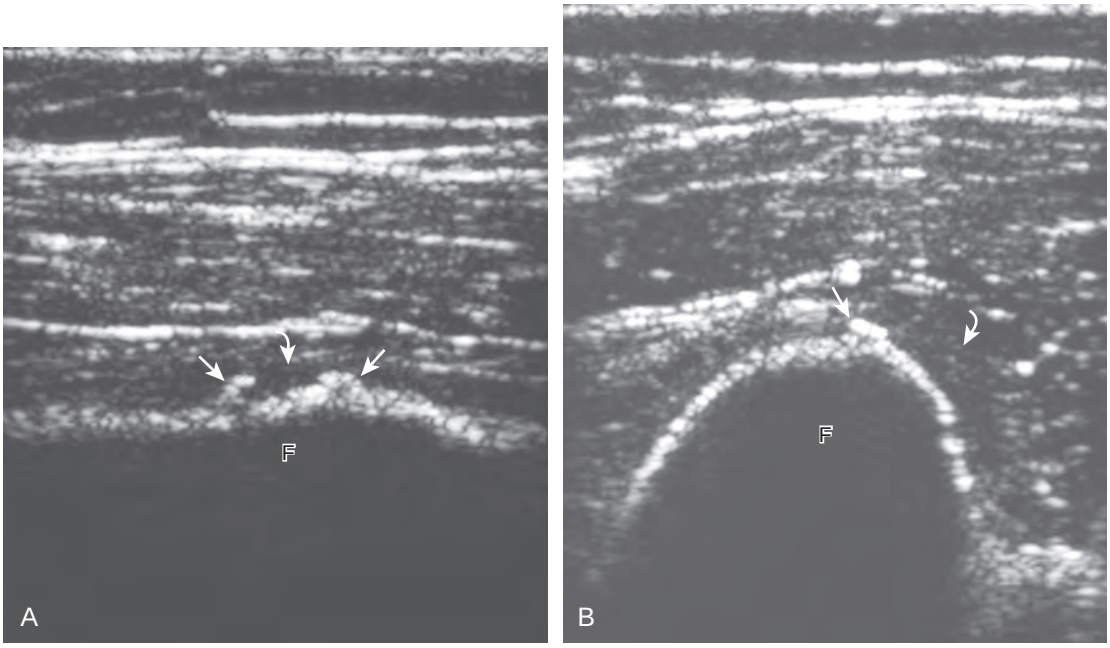

FIGURE 6-57 ■ Thigh splints (adductor insertion avulsion syndrome). Ultrasound images in **(A)** long axis and **(B)** short axis to the femoral diaphysis show a cortical irregularity *(arrows)* and adjacent hypoechoic hemorrhage or periostitis *(curved arrows)* at the adductor tendon insertion. **F, femur.** (From Weaver JS, Jacobson JA, Jamadar DA, et al: Sonographic findings of adductor insertion avulsion syndrome with magnetic resonance imaging correlation. *J Ultrasound Med* 22:403–407, 2003. Reproduced with permission from the American Institute of Ultrasound in Medicine.)

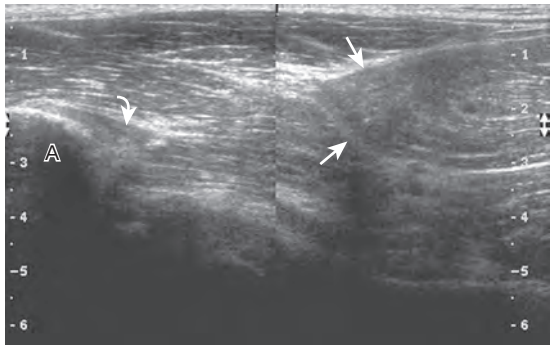

FIGURE 6-58 ■ Rectus femoris tear (proximal): full-thickness. Ultrasound image in long axis to the proximal rectus femoris shows a full-thickness tear *(arrows)* retracted distally from its origin *(curved arrow)* on the anterior inferior iliac spine (A).

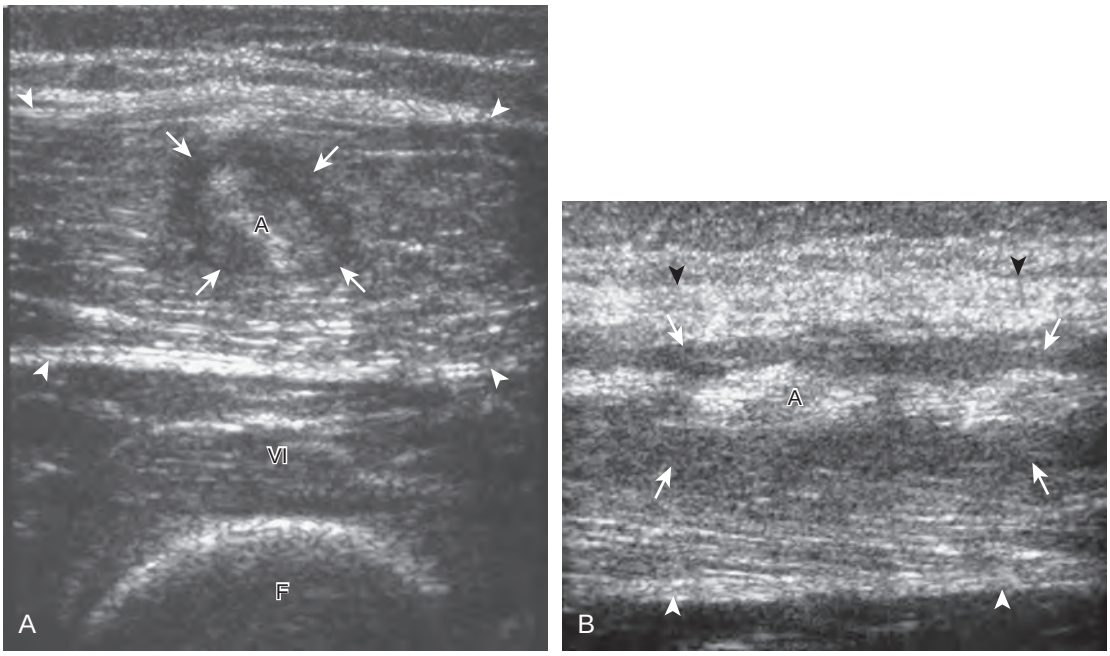

FIGURE 6-59 ■ Rectus femoris tear: central aponeurosis. Ultrasound images in **(A)** short axis and **(B)** long axis to the rectus femoris show hypoechoic hemorrhage *(arrows)* that surrounds the central aponeurosis (A) within the center of the rectus femoris muscle *(arrowheads)*. F, femur; VI, vastus intermedius.

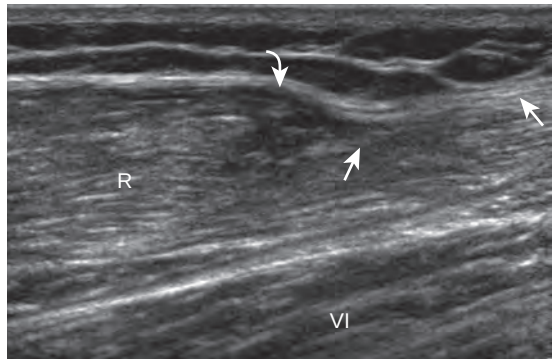

FIGURE 6-60 ■ Rectus femoris tear: partial-thickness. Ultrasound image in long axis to the rectus femoris (R) shows a partial tear of the superficial muscle fibers with volume loss *(arrows)*. Note the retracted muscle *(curved arrow)*. VI, vastus intermedius.

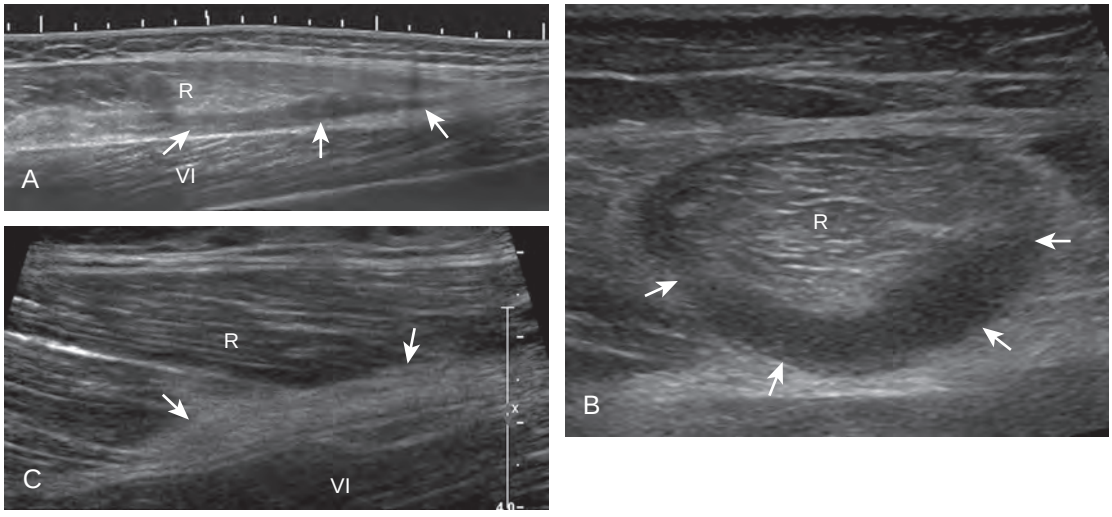

FIGURE 6-61 ■ Rectus femoris tear: posterior aponeurosis. Ultrasound images in **(A)** long axis (with extended field of view) and **(B)** short axis to the rectus femoris (R) show hypoechoic hemorrhage *(arrows)* along the posterior aponeurosis. Ultrasound image **(C)** in long axis to the rectus femoris (R) in a different patient shows hyperechoic scar *(arrows)* from remote injury. VI, vastus intermedius.

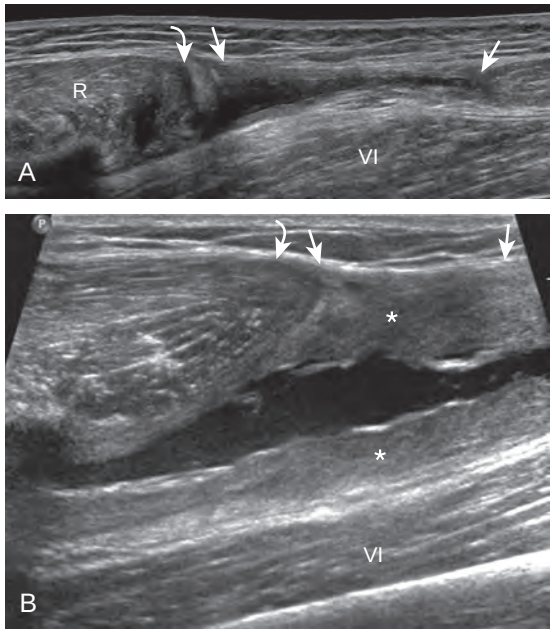

FIGURE 6-62 ■ Rectus femoris tear (distal): full-thickness. Ultrasound images in two different patients in long axis to the rectus femoris (R) show full-thickness disruption *(between arrows)* and tendon retraction *(curved arrow)* producing a palpable mass. Note hypoechoic *(asterisks)* and anechoic organizing hematoma at the site of the tear *(between arrows)*. VI, vastus intermedius.

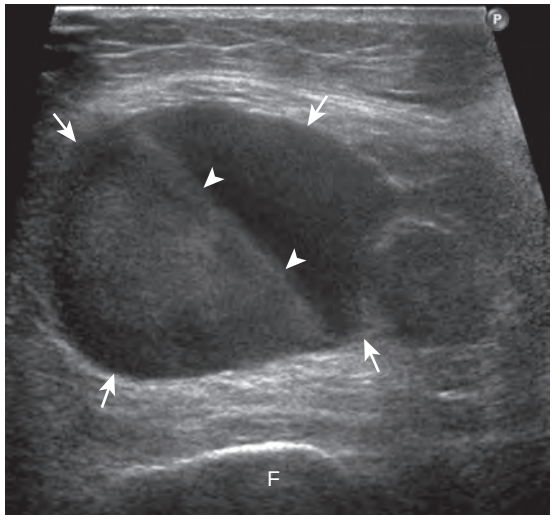

FIGURE 6-63 ■ Quadriceps hematoma. Ultrasound image in short axis to the quadriceps musculature shows acute hematoma *(arrows)* with dependent serum hematocrit level *(arrowheads)*. F, femur.

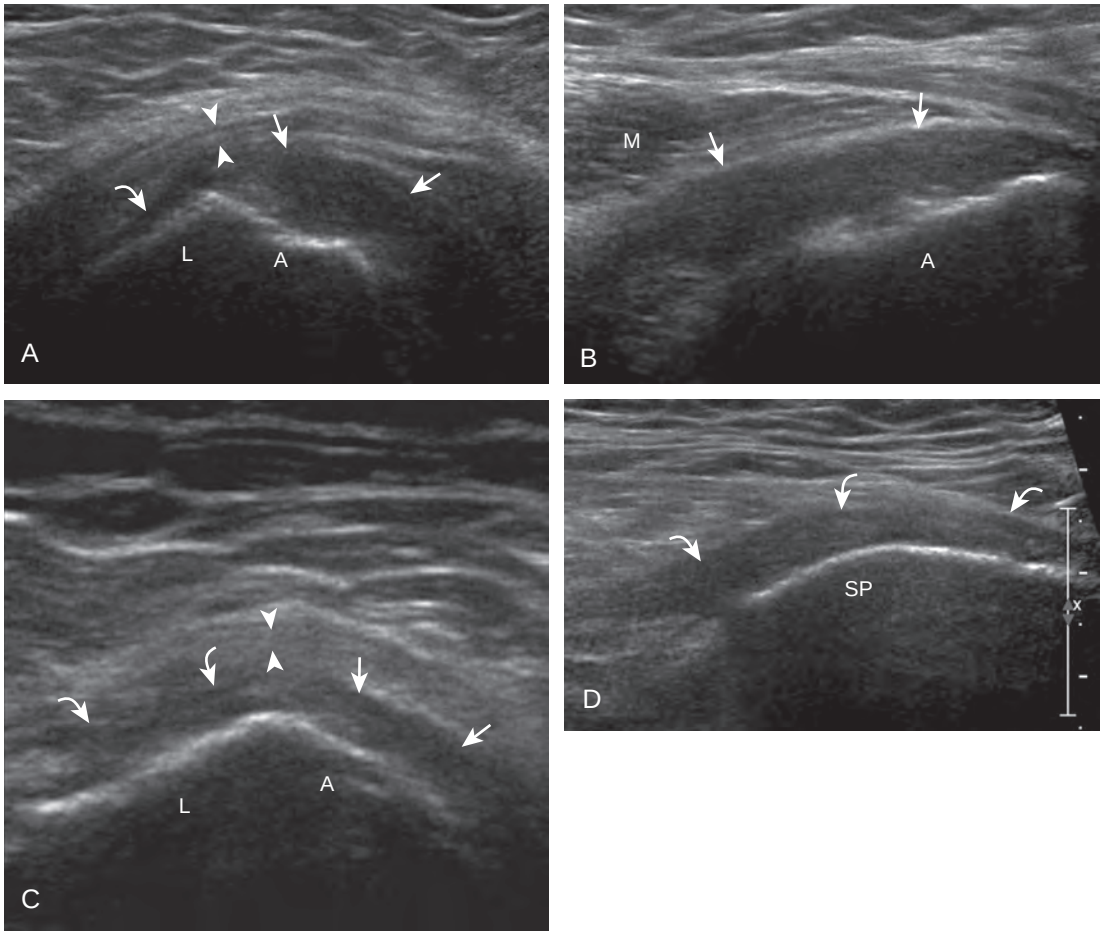

FIGURE 6-64 ■ Gluteus medius and minimus: tendinosis. Ultrasound images **(A)** short axis and **(B)** long axis to the gluteus tendons show hypoechoic thickening of the gluteus minimus *(arrows)* (*curved arrow*, gluteus medius tendon; *arrowheads*, iliotibial tract). Ultrasound images **(C)** short axis and **(D)** long axis to the gluteus tendons in a different patient show hypoechoic thickening of the gluteus medius *(curved arrows)* and minimus *(arrows)*. Note involvement of gluteus medius at the superoposterior facet (SP) in **(D)**. A, anterior facet; L, lateral facet of greater trochanter; M, gluteus medius muscle (*arrowheads*, iliotibial tract).

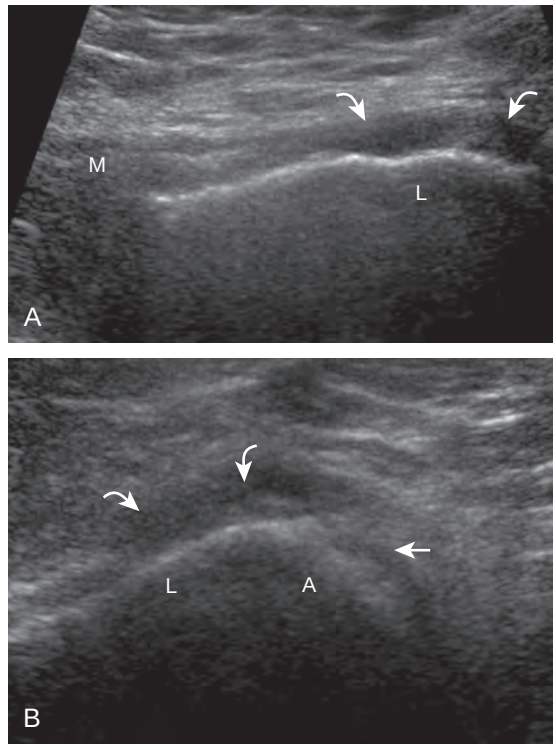

FIGURE 6-65 ■ Gluteus medius: tear. Ultrasound images in **(A)** long axis and **(B)** short axis to the gluteus tendons show hypoechoic absence of the gluteus medius tendon *(curved arrows)* (*arrows*, gluteus minimus tendon). A, anterior facet and L, lateral facet of greater trochanter; M, proximal gluteus medius tendon.

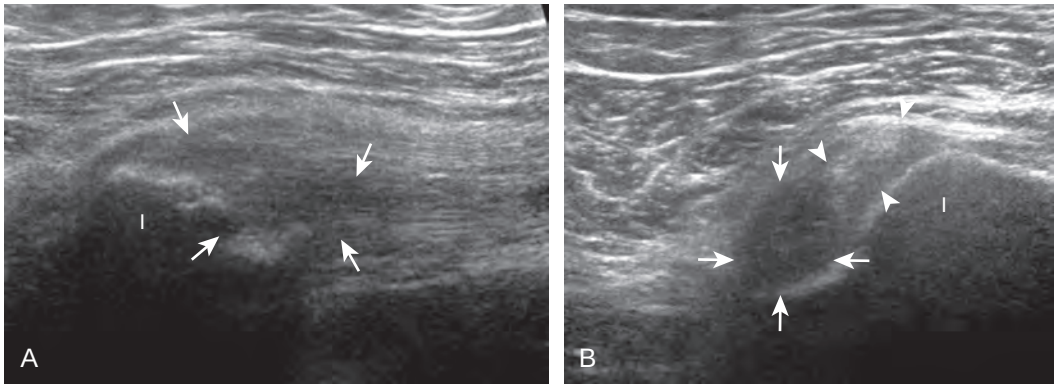

FIGURE 6-66 ■ Semimembranosus: tendinosis. Ultrasound images in **(A)** long axis and **(B)** short axis to the proximal hamstring tendons show hypoechoic swelling *(arrows)* of the semimembranosus tendon with adjacent cortical irregularity of the ischium (I) and normal conjoint tendon *(arrowheads)*. Left side of image is lateral in **(B)**.

contours of the greater trochanter is essential for orientation and accurate localization of tendon and soft tissue abnormalities (see Fig. 6-10).[2]

With regard to the hamstrings, chronic injury produces tendinosis, possible partial-thickness tear, and bone irregularity of the ischium.[5,51] Injury may selectively involve the semimembranosus tendon origin at the lateral surface of the ischial tuberosity (Fig. 6-66) or the conjoint tendon of the biceps femoris long head and semitendinosus at the superficial surface (Fig. 6-67). Isolated tear of one of the two tendons may also be possible (Fig. 6-68). Complete tear of the hamstring tendon origin is characterized by absence of tendon fibers and retraction (Fig. 6-69). Chronic injuries may be associated with hyperechoic scar formation and possible pseudotumor appearance at physical examination as a result of muscle retraction (Fig. 6-70).

Other muscle and tendon injuries can also involve the sartorius (Fig. 6-71) and proximal tensor fascia latae (Fig. 6-72). Spontaneous muscle hemorrhage has been described with the iliopsoas in the setting of hemophilia and in patients who are anticoagulated (Fig. 6-73). One must be aware of this condition because the often mixed-echogenicity mass-like swelling of the iliopsoas may simulate soft tissue tumor (Video 6-15).

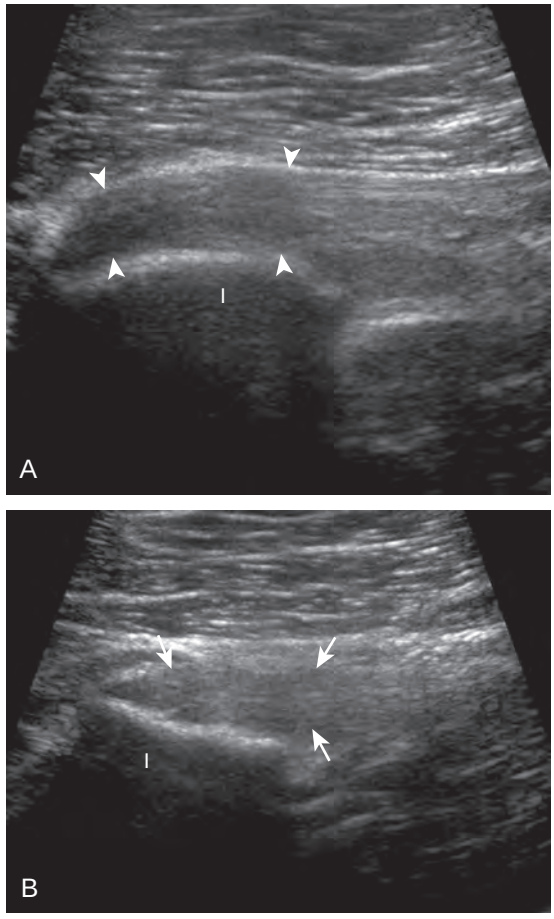

FIGURE 6-67 ■ Conjoint tendon: tendinosis. Ultrasound images in **(A)** long axis to the conjoint tendon and **(B)** long axis to the semimembranosus tendon show hypoechoic swelling *(arrowheads)* of the conjoint tendon and normal semimembranosus tendon *(arrows)*. I, ischium.

Snapping Hip Syndrome

An abnormal snapping with hip movement has been termed *snapping hip syndrome*, which can be divided into intra-articular and extra-articular causes. Intra-articular causes relate to joint processes, such as intra-articular bodies or prior trauma. Extra-articular causes can occur medially and laterally.[52] The medial variety is the result of

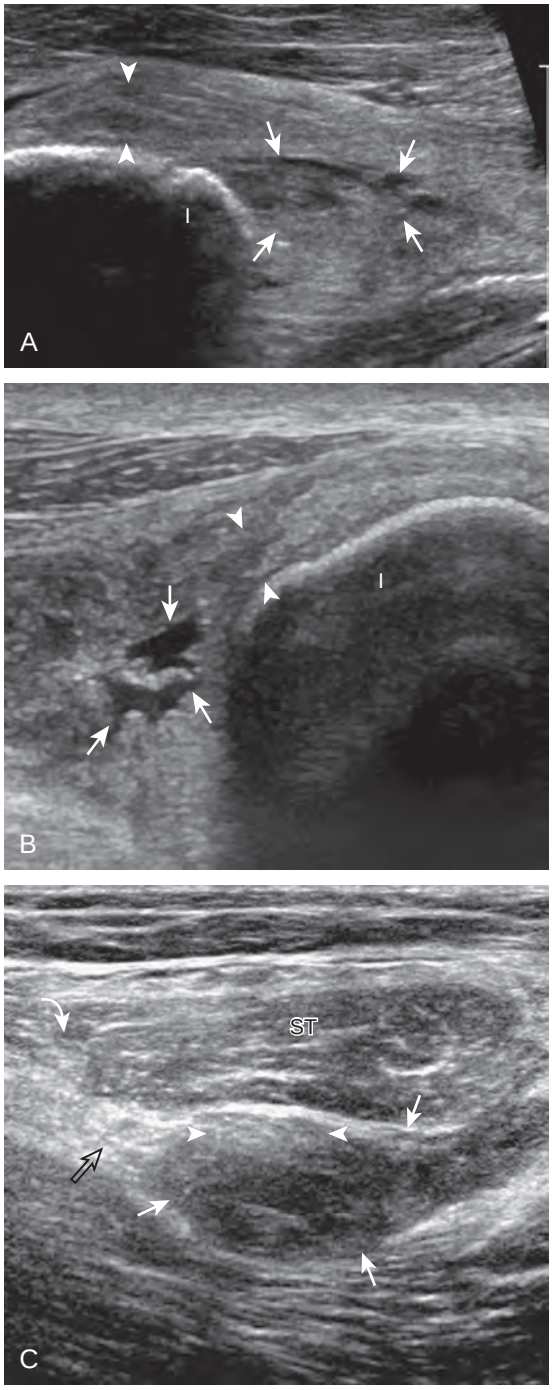

FIGURE 6-68 ■ Semimembranosus: tear. Ultrasound images in **(A)** long axis and **(B)** short axis to the proximal hamstring tendons show anechoic partial tendon disruption *(arrows)* of the semimembranosus tendon with adjacent cortical irregularity of the ischium (I). Note the tendinosis of the conjoint tendon *(arrowheads)*. Left side of image is lateral in **(B)**. Ultrasound image in short axis to the proximal hamstring tendons shows **(C)** tear of semimembranosus aponeurosis *(arrows)* (*arrowheads*, semimembranosus tendon; *curved arrow*, conjoint tendon; *open arrow*, sciatic nerve). ST, semitendinosus muscle.

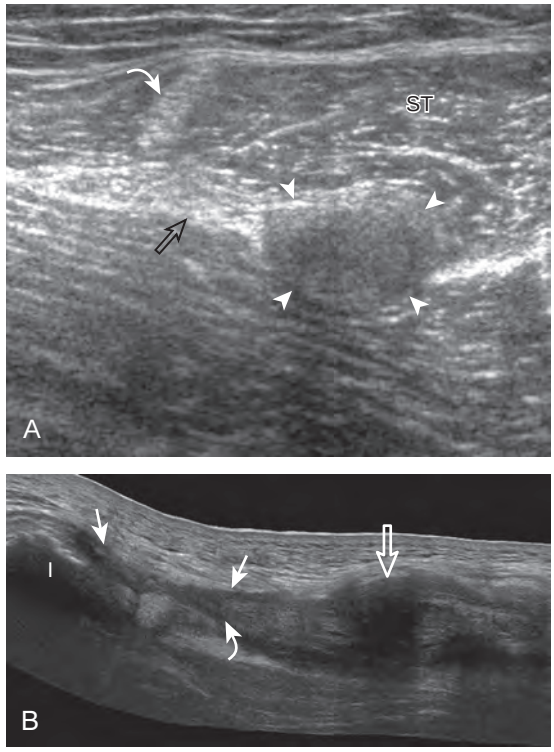

FIGURE 6-69 ■ Hamstring tendons: complete tear. Ultrasound image in **(A)** short axis to the hamstring tendons shows the absence of the semimembranosus tendon *(arrowheads)*. Note the normal conjoint tendon *(curved arrow)* and sciatic nerve *(open arrow)*. Ultrasound image **(B)** in long axis (with extended field of view) to the hamstrings in a different patient shows the absence of the proximal hamstring tendons *(between arrows)* with distal retraction *(curved arrow)* and avulsion fracture fragment *(open arrow)*. I, ischium; ST, semitendinosus.

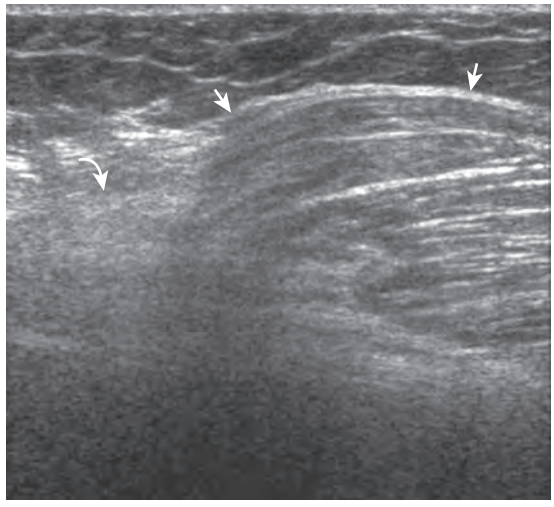

FIGURE 6-70 ■ Semimembranosus tear: chronic. Ultrasound image in long axis to the semimembranosus shows chronic tear with pseudomass appearance at the muscle contraction *(arrows)* and adjacent hyperechoic scar tissue *(curved arrow)*.

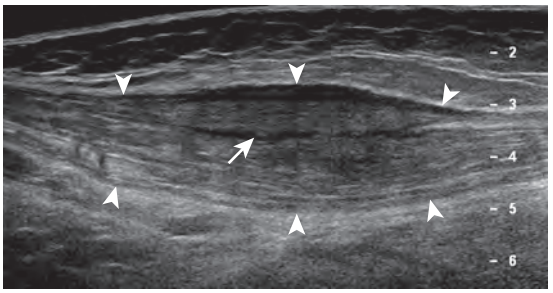

FIGURE 6-71 ■ Sartorius: partial tear. Ultrasound image in long axis to the sartorius muscle shows hypoechoic thickening *(arrowheads)* and anechoic clefts *(arrow)* representing a partial-thickness tear.

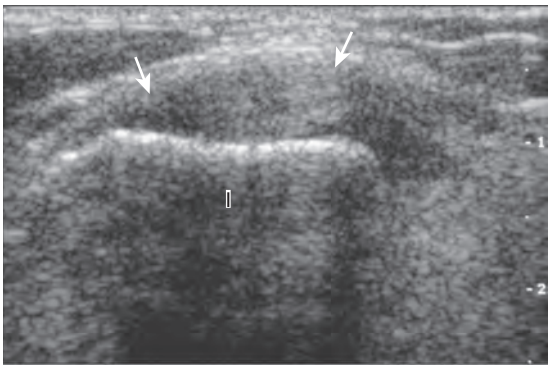

FIGURE 6-72 ■ Tensor fascia latae: tendinosis. Ultrasound image in long axis to the proximal tensor fascia latae shows hypoechoic thickening *(arrows)*. I, ilium.

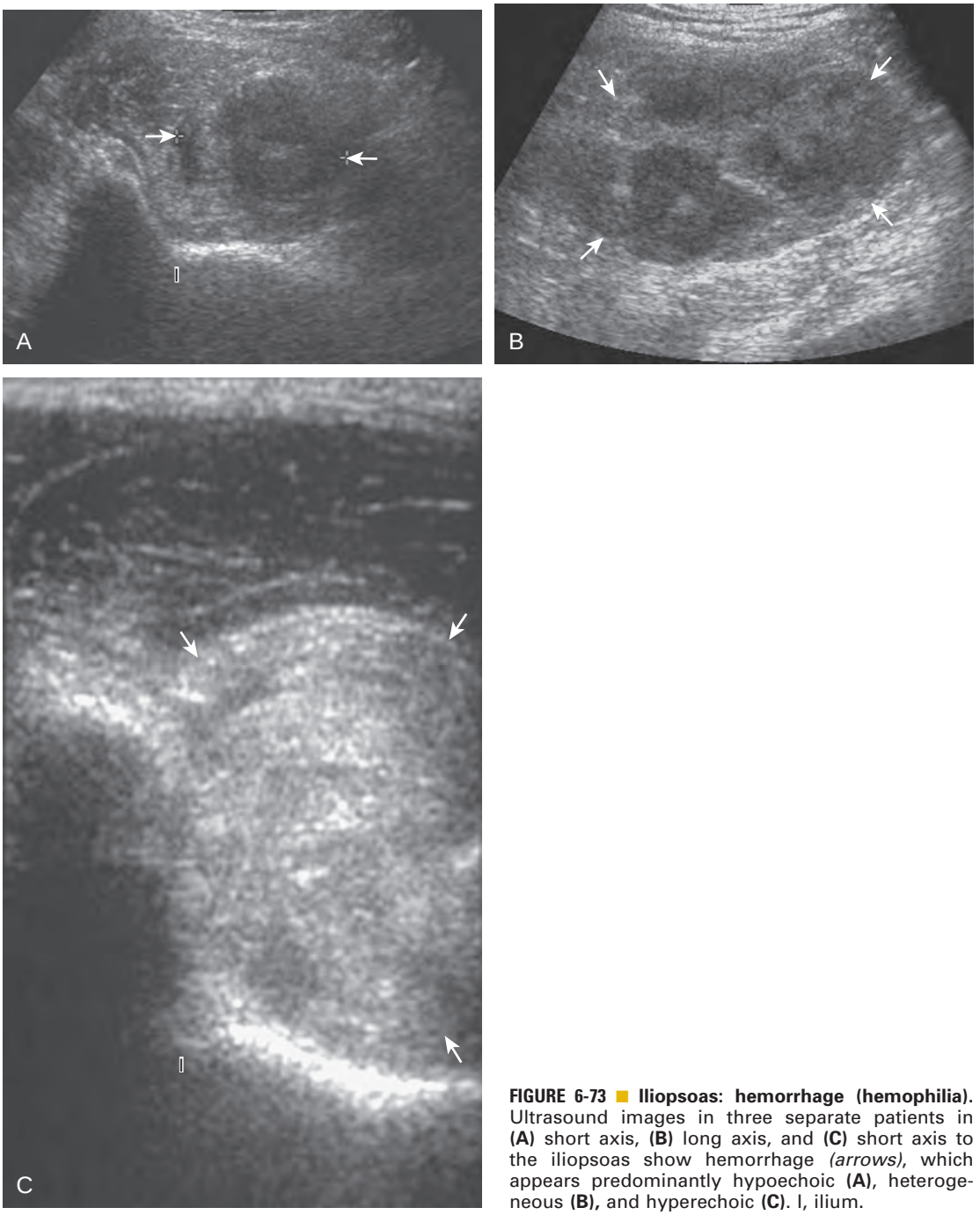

FIGURE 6-73 ■ Iliopsoas: hemorrhage (hemophilia). Ultrasound images in three separate patients in **(A)** short axis, **(B)** long axis, and **(C)** short axis to the iliopsoas show hemorrhage *(arrows)*, which appears predominantly hypoechoic **(A)**, heterogeneous **(B),** and hyperechoic **(C)**. I, ilium.

snapping of the iliopsoas tendon at the level of the anterior aspect of the acetabulum near a bony protuberance called the *iliopectineal eminence* (Fig. 6-74) (Videos 6-16 and 6-17). To diagnose this specific condition, the patient is asked to reproduce the snapping sensation, or a flexed, abducted, and externally rotated hip (frog-leg position) is straightened during sonographic visualization. Normally, the psoas major tendon moves laterally, and the iliacus muscle fibers move as well, in a smooth clockwise rotation (for the right hip; counterclockwise for the left).[53] In the abnormal condition (although asymptomatic in up to 40%), there is abrupt movement and snapping of the psoas major tendon against the superior pubic ramus, which is felt through the transducer.[53] The actual cause of the snap is temporary entrapment of the medial muscle fibers of the iliacus between the psoas major tendon and the superior pubic ramus.[53] A bifid iliopsoas tendon has also been described as a cause of snapping.[54] The lateral variety of external snapping hip syndrome can result from snapping the gluteus maximus tendon (Video 6-18) or iliotibial tract over the greater trochanter (Fig. 6-75) (Video 6-19).[55,56] Again, the patient is asked to reproduce the symptom, and many times the patient has to stand and shift weight on the affected limb, or the patient may lie on the contralateral hip to allow hip flexion and extension. Ultrasound transverse over the greater trochanter shows abnormal abrupt snapping of the involved tendon or muscle, which is often thickened, over the greater trochanter.[55]

Calcific Tendinosis

Although more common in the rotator cuff, calcium hydroxyapatite deposition may occur in a number of tendons around the hip, including the gluteus maximus, gluteus medius (Fig. 6-76), and rectus femoris (Fig. 6-77) tendons. In this situation, the hyperechoic focus may show posterior acoustic shadowing, and the involved tendon may be abnormally hypoechoic with increased flow on color or power Doppler imaging.

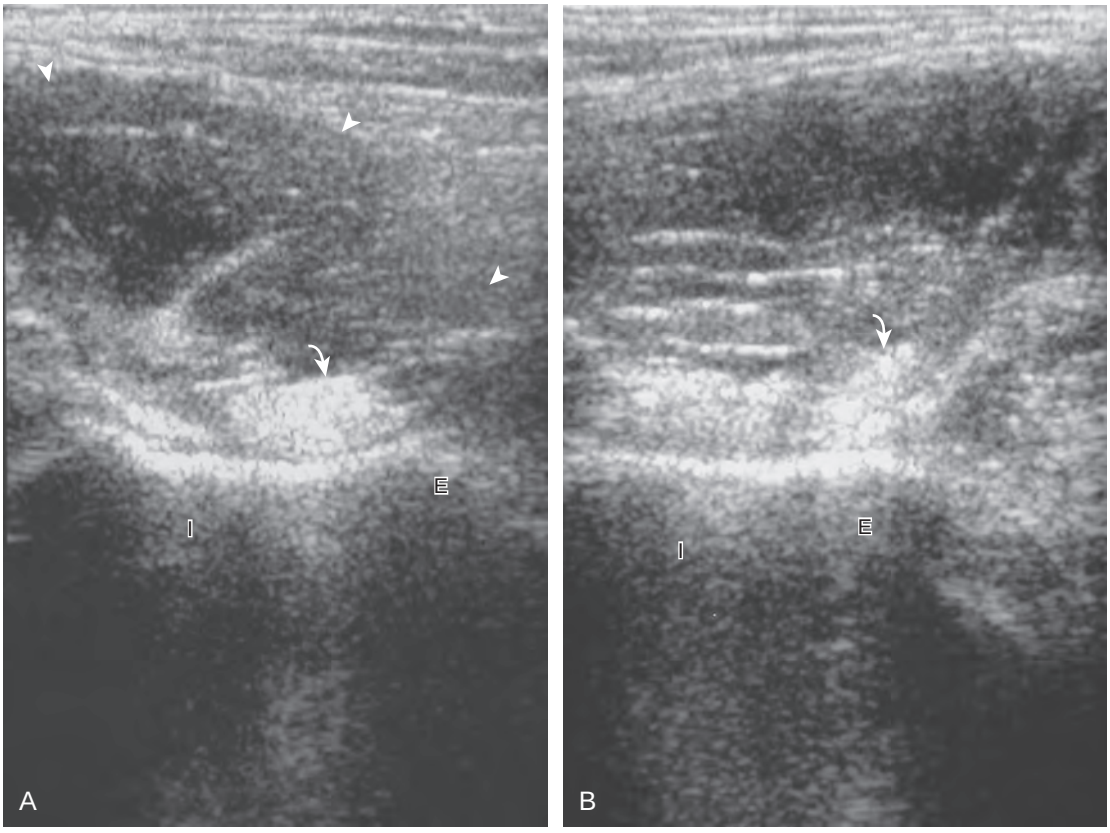

FIGURE 6-74 ■ Snapping hip syndrome: iliopsoas tendon. Ultrasound images in short axis to the iliopsoas tendon at the level of the iliopectineal eminence (E) show abrupt motion of the iliopsoas tendon *(curved arrows)* between **(A)** hip flexion/abduction and **(B)** extension (*arrowheads*, iliopsoas muscle) (left side of image is lateral). I, ilium.

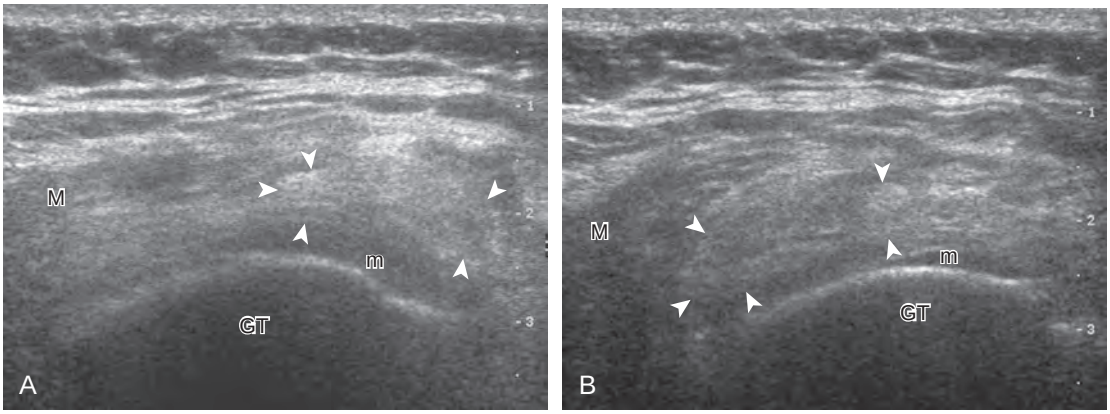

FIGURE 6-75 ■ Snapping hip syndrome: iliotibial tract. Ultrasound images in the transverse over the greater trochanter (GT) show abrupt motion of the iliotibial tract *(arrowheads)* between **(A)** active hip extension and **(B)** flexion. M, gluteus maximus; m, gluteus medius.

Ultrasound-guided percutaneous lavage and aspiration may be used for treatment.

Diabetic Muscle Infarction

In evaluation of a painful or swollen thigh, it is important to consider a condition called *diabetic muscle infarction*. Common to the thigh and calf, diabetic muscle infarction occurs in patients with longstanding diabetes, and it may be bilateral. The cause is not completely known, but a possible consideration is vascular occlusive disease. At ultrasound, the involved musculature is hypoechoic and swollen, although muscle fibers are still identified (Fig. 6-78).[57] This is an important finding to help exclude a soft tissue abscess. Subfascial fluid may also be another finding in diabetic muscle infarction. Because the differential diagnosis includes early infection, correlation with laboratory values and the patient's signs and symptoms is important; follow-up ultrasound examination may be considered.

Pseudohypertrophy of the Tensor Fasciae Latae

The most common effects of chronic denervation are muscle atrophy and fatty replacement. Uncommonly, fatty infiltration of the involved muscle may cause muscle enlargement or pseudohypertrophy. This situation may involve the tensor fasciae latae muscle in the upper thigh, although involvement of other muscles of the lower extremity have been described.[58] At ultrasound, the muscle is enlarged, with increased echogenicity and sound beam attenuation resulting from the fatty infiltration (Fig. 6-79). The finding is usually asymmetrical, and it has been described in older individuals in the setting of

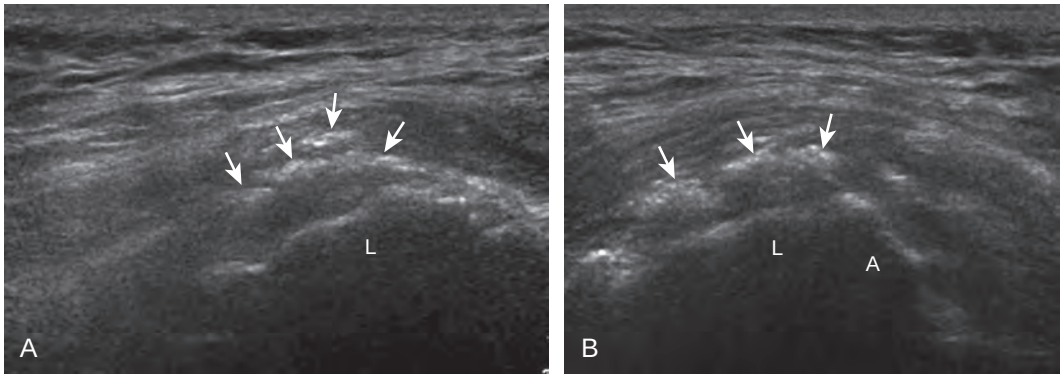

FIGURE 6-76 ■ Calcific tendinosis: gluteus medius. Ultrasound images in **(A)** long axis and **(B)** short axis to the gluteus medius tendon show hyperechoic and shadowing calcifications *(arrows)*. A, anterior facet of the greater trochanter; L, lateral facet.

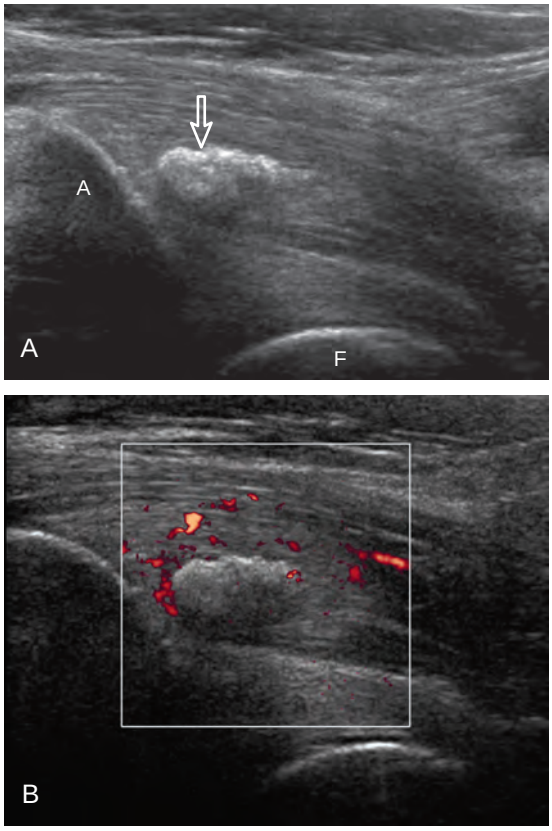

FIGURE 6-77 ■ Calcific tendinosis: rectus femoris, direct head. Ultrasound **(A)** gray-scale and **(B)** power Doppler images in long axis to the rectus femoris tendon show hyperechoic calcification *(open arrow)* with increased blood flow. A, anterior inferior iliac spine; F, femoral head.

chronic nerve impingement and partial denervation related to lumbar spine degenerative disease. Chronic peripheral neuropathy may also be a cause, and pseudohypertrophy has been described with muscular dystrophies.[58] It is important to be familiar with this entity because it may present clinically as a soft tissue mass.

PERIPHERAL NERVE ABNORMALITIES

Several peripheral nerve abnormalities are specific to the hip and thigh. One nerve entrapment condition specific to the hip involves the lateral femoral cutaneous nerve. As in other entrapment conditions, the involved nerve may demonstrate hypoechoic swelling at the site of entrapment or injury and is symptomatic with transducer pressure. The lateral femoral cutaneous nerve is susceptible to injury because of its course and variations in its location as it exits the pelvis at the inguinal ligament, sartorius, or iliac crest.[9,12]

Another peripheral nerve abnormality is nerve transection, which is characterized by nerve discontinuity, a swollen and hypoechoic terminal neuroma at the transection site, and possible retraction if completely disrupted (Fig. 6-80) (Video 6-20).[59] Neuroma formation is an expected finding after nerve transection as part of attempted nerve regeneration. After knee amputation, sonographic evaluation for neuromas is very useful.

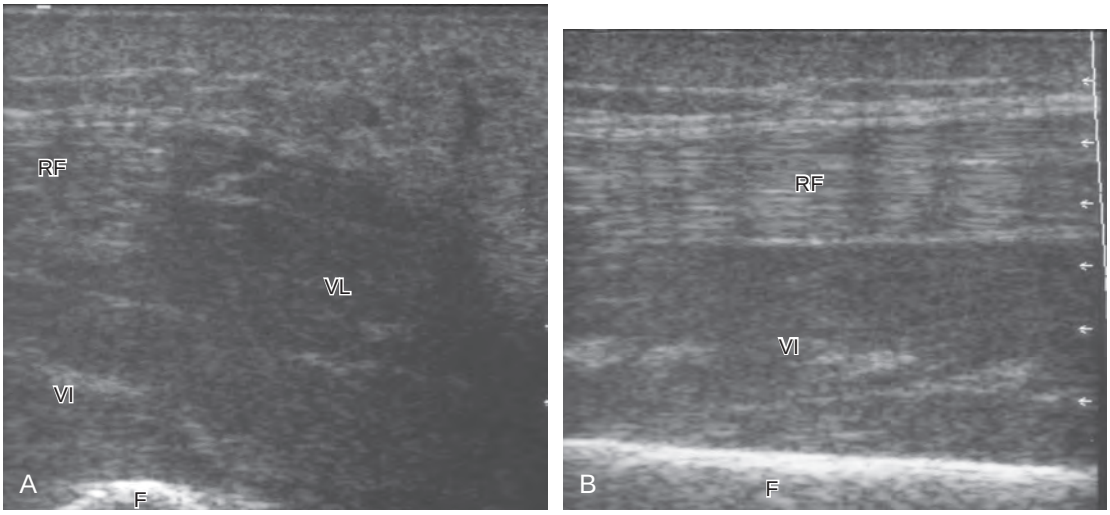

FIGURE 6-78 ■ Diabetic muscle infarction. Ultrasound images in **(A)** short axis and **(B)** long axis to the anterior thigh musculature show hypoechoic vastus lateralis (VL) and vastus intermedius (VI) with sparing of the rectus femoris (RF). Note the continuity of muscle fibers within the involved muscles. F, femur. (**A,** From Delaney-Sathy LO, Fessell DP, Jacobson JA, et al: Sonography of diabetic muscle infarction with MR imaging, CT, and pathologic correlation. *AJR Am J Roentgenol* 174:165–169, 2000.)

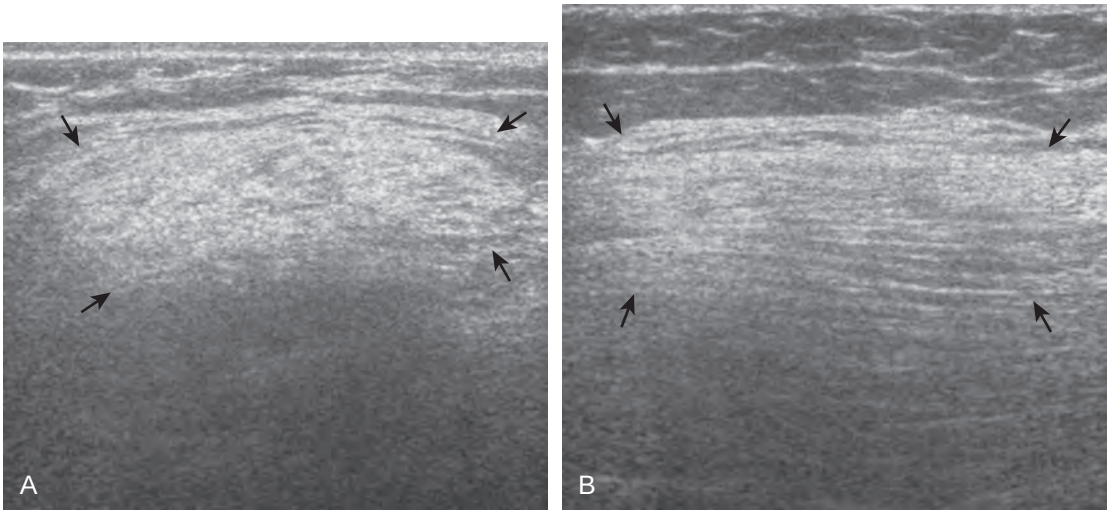

FIGURE 6-79 ■ Tensor fasciae latae pseudohypertrophy. Ultrasound images in **(A)** short axis and **(B)** long axis to the tensor fasciae latae show abnormal enlargement and with increased echogenicity *(arrows)* from fatty infiltration.

Ultrasound can diagnose the neuromas and can also identify which neuroma is the cause of patients' symptoms through application of transducer pressure over each neuroma.

MISCELLANEOUS CONDITIONS

Morel-Lavallée Lesion

This post-traumatic condition or Morel-Lavallée lesion is described at the thigh and proximal hip and is characterized by a fluid collection between the subcutaneous fat and the adjacent fascia as a result of a closed degloving injury. At ultrasound, the resulting fluid collection, usually anechoic or hypoechoic, can be heterogeneous when acute but becomes more homogeneous and flat in shape when chronic, and it is located at the interface between the superficial fat and the underlying fascial tissues (Fig. 6-81).[60]

Inguinal Lymph Node

With regard to inguinal lymph nodes, normally, a hyperechoic hilum with uniform hypoechoic

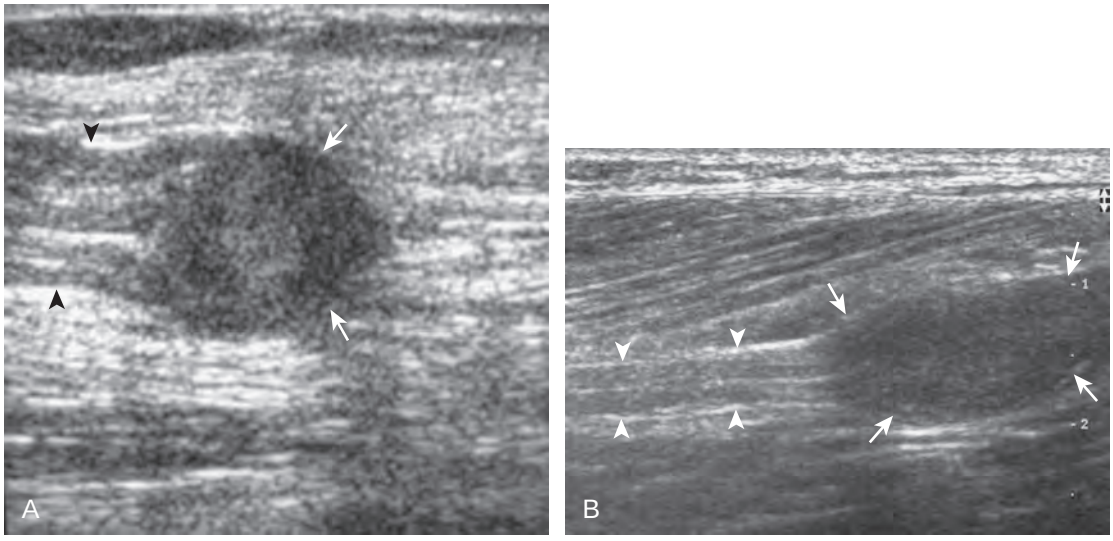

FIGURE 6-80 ■ Peripheral nerve transection neuroma. Ultrasound images from two different patients in **(A)** long axis to the sciatic nerve and **(B)** long axis to the common peroneal nerve show hypoechoic neuroma formation *(arrows)* in continuity with the transected nerve *(arrowheads)*.

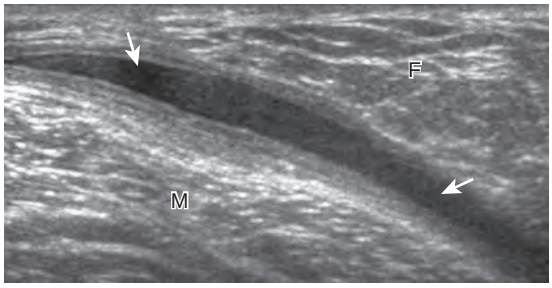

FIGURE 6-81 ■ Morel-Lavallée lesion. Ultrasound image over the lateral thigh shows anechoic fluid *(arrows)* between the subcutaneous fat (F) and thigh musculature (M).

cortex and hilar pattern of blood flow (if present) are demonstrated (Fig. 6-82). An inguinal lymph node is considered abnormal if its short axis is greater than 1.5 cm[61] or if there is eccentric thickening of the hypoechoic cortex.[62] An enlarged lymph node may be benign or malignant, although lymph node size is not a reliable criterion in this differentiation. Benign enlargement may be inflammatory or reactive, and typically the hyperechoic hilum remains present (Fig. 6-83) (Video 6-21). In contrast, a malignant lymph node is characterized by a round shape, absence or narrowing of the echogenic hilum, thickening of the cortex, and a mixed or peripheral blood flow pattern (Fig. 6-84).[62-64] Many times, percutaneous biopsy is required to determine the cause of lymph node enlargement.

Other Soft Tissue Masses

Most soft tissue masses are nonspecific in the thigh and hip region; however, some soft tissue tumors commonly involve the thigh. One benign soft tissue tumor, an intramuscular myxoma, which has a uniformly heterogeneous but overall hypoechoic appearance (Fig. 6-85), may simulate a complex cyst because it is well defined and oval, often with increased through-transmission.[65] A hyperechoic rim and hyperechoic cap have been described with intramuscular myxomas related to adjacent fatty atrophy and fatty infiltration.[65]

With regard to malignancy, the thigh is a common site for malignant sarcomas (Fig. 6-86), although other primary malignant tumors (Fig. 6-87) and soft tissue metastases (Fig. 6-88) may occur. Such tumors are generally hypoechoic relative to the adjacent tissues; however, heterogeneity is common with larger and more aggressive tumors, especially when they are associated

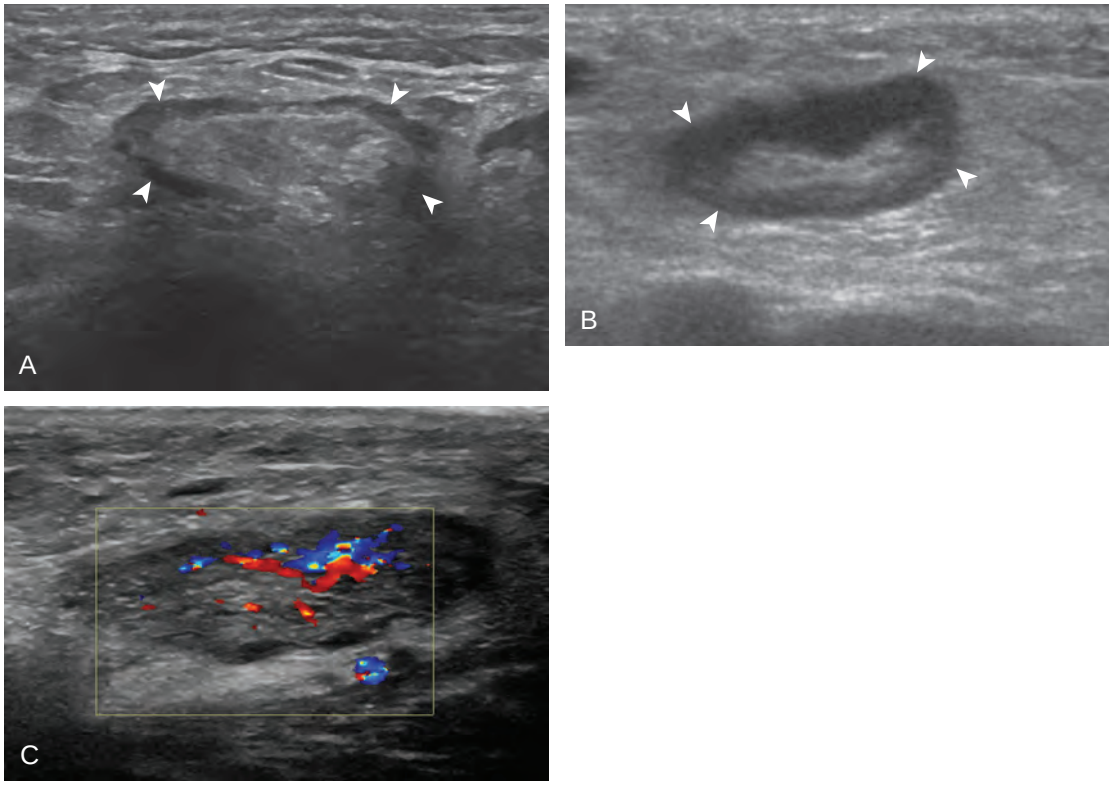

FIGURE 6-82 ■ Lymph nodes: normal. Ultrasound images **(A** to **C)** show normal oval groin lymph nodes *(arrowheads)* with echogenic hilum and hypoechoic cortex and a hilar blood flow pattern in **(C)**.

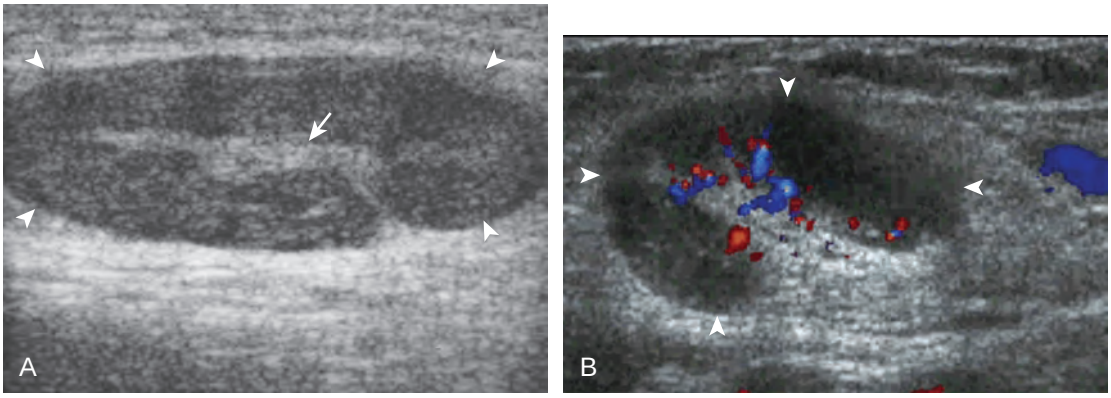

FIGURE 6-83 ■ Lymph node: hyperplastic. Ultrasound images in **(A)** long axis and **(B)** short axis with color Doppler show enlargement of a groin lymph node *(arrowheads)*, although with uniform cortical thickening, oval shape, and hilar pattern of vascularity (*arrow*, hyperechoic hilum).

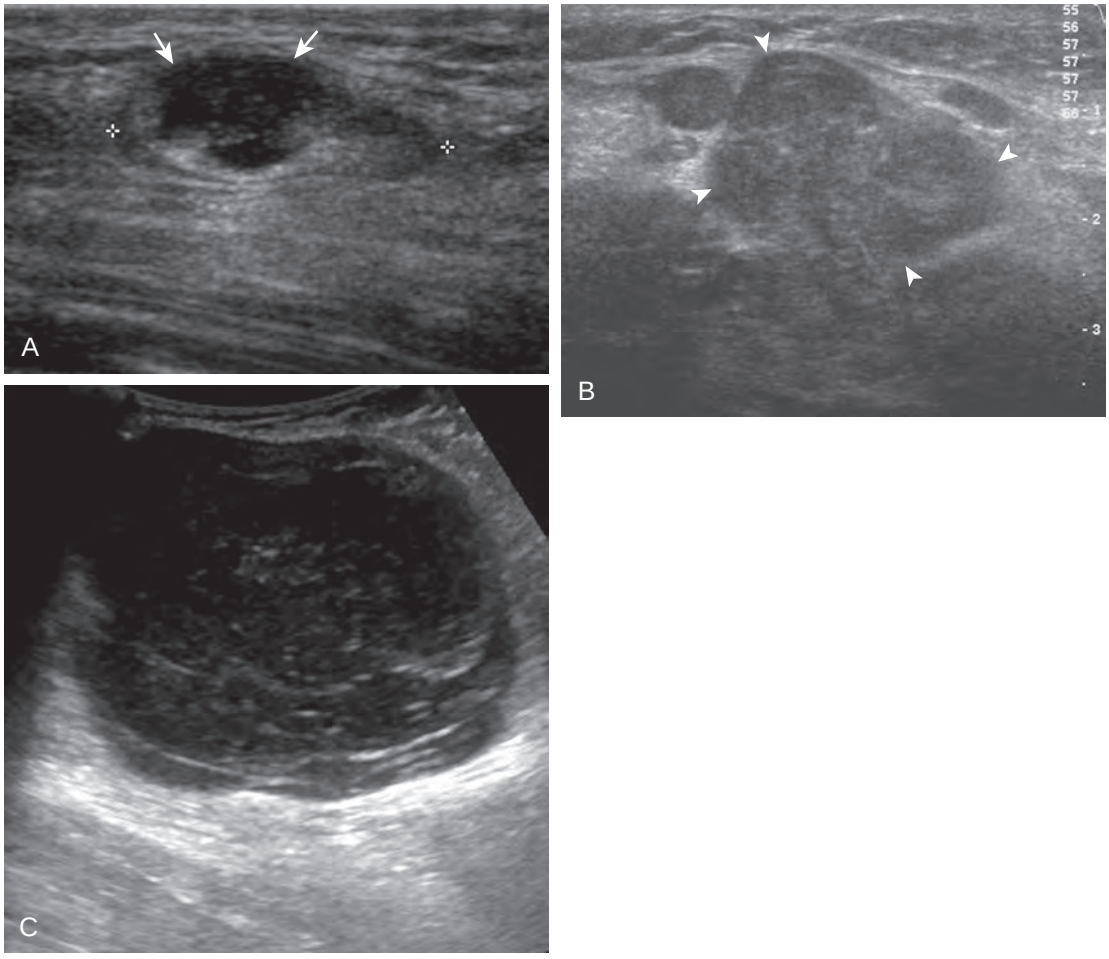

FIGURE 6-84 ■ Lymph nodes: malignant. Ultrasound images from three separate patients show **(A)** focal hypoechoic cortical enlargement *(arrows)* from angiosarcoma metastasis (lymph node length between cursors), **(B)** diffuse lobular hypoechoic enlargement *(arrowheads)* from Ewing sarcoma metastasis; and **(C)** marked hypoechoic enlargement from lymphoma with posterior through-transmission.

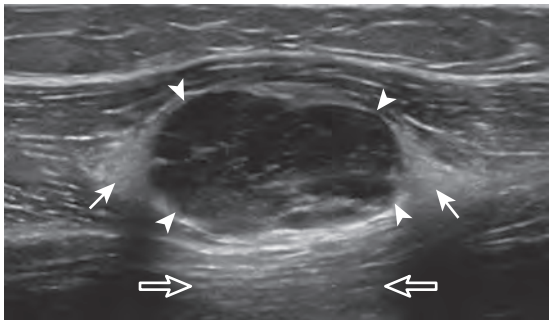

FIGURE 6-85 ■ Intramuscular myxoma. Ultrasound image shows heterogeneous but predominantly hypoechoic myxoma *(arrowheads)*. Note increased through-transmission *(open arrows)* and hyperechoic fat caps *(arrows)*.

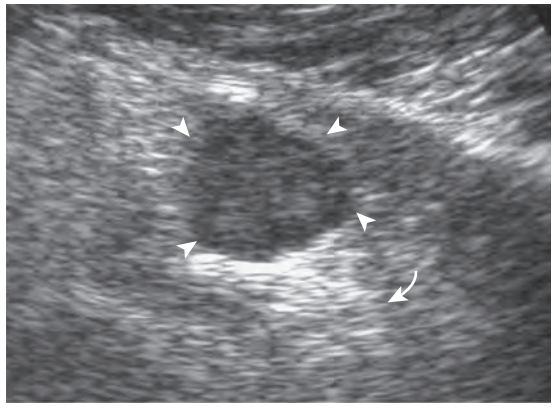

FIGURE 6-88 ■ Metastasis: lung cancer. Ultrasound image shows a well-defined hypoechoic mass *(arrowheads)* with increased through-transmission *(curved arrow)*.

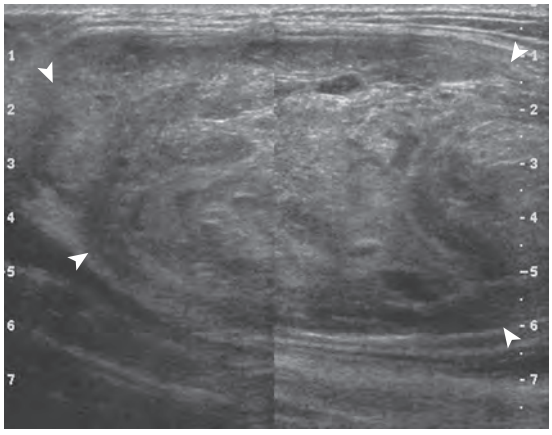

FIGURE 6-86 ■ High-grade pleomorphic sarcoma. Ultrasound image shows a heterogeneous mass *(arrowheads)*.

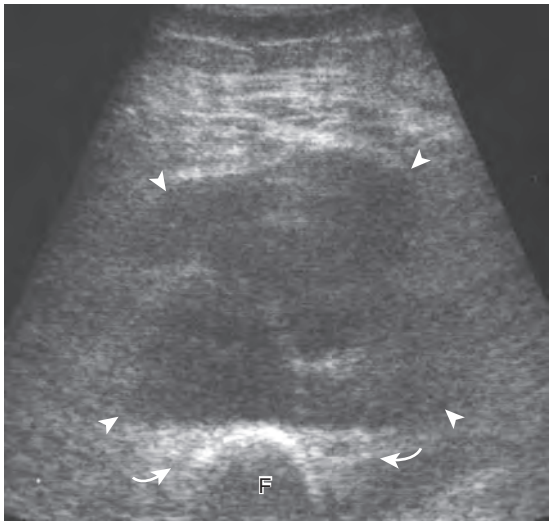

FIGURE 6-87 ■ Lymphoma. Ultrasound image shows a lobular hypoechoic mass *(arrowheads)* with increased through-transmission (*curved arrows*). F, femur.

with necrosis and hemorrhage. In addition, many solid soft tissue tumors demonstrate increased through-transmission. Although increased flow on color or power Doppler imaging is more common with malignant tumors, such findings may also be seen with benign conditions. After surgery, ultrasound is effective in evaluating for soft tissue sarcoma recurrence (Fig. 6-89).[66,67] In evaluation of a palpable soft tissue mass, it is important to exclude disorders that may produce a pseudomass appearance, such as pseudohypertrophy of the tensor fasciae latae and chronic retracted tendon or muscle tears, as described earlier.

Hernias

The key to successful evaluation for inguinal region hernias lies in sonographic technique, knowledge of anatomy, and identification of key sonographic landmarks.[8] With the Valsalva maneuver (forced expiration against a closed airway) and possibly scanning with the patient upright, one looks for abnormal movement of intra-abdominal contents from one space to another at a key anatomic location. For example, a spigelian hernia occurs at the lateral margin of the rectus abdominis (Fig. 6-90, online) (Video 6-22). Most commonly, hyperechoic fat is visualized in the hernia and, less commonly, the bowel. It is important to ascertain whether hernias are transient, reducible, or incarcerated.

An indirect inguinal hernia begins at the deep inguinal ring, at the lateral aspect of the external iliac artery just proximal to the origin of the inferior epigastric artery. Intra-abdominal contents

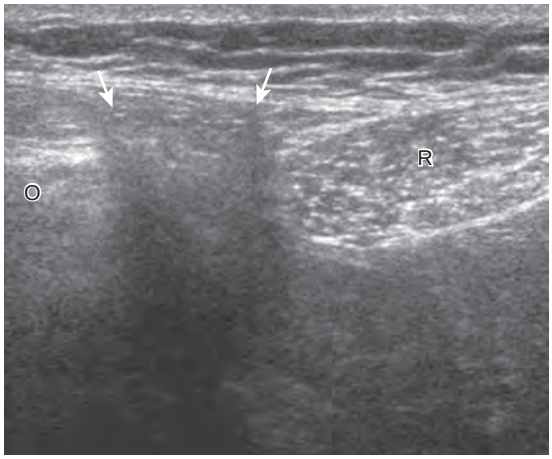

FIGURE 6-90 ■ Spigelian hernia. Ultrasound image over the lateral aspect of the right rectus abdominis muscle during the Valsalva maneuver shows movement of intra-abdominal contents *(arrows)* anteriorly between the rectus abdominis (R) and oblique musculature (O) (left side of image is lateral; right side is toward the midline).

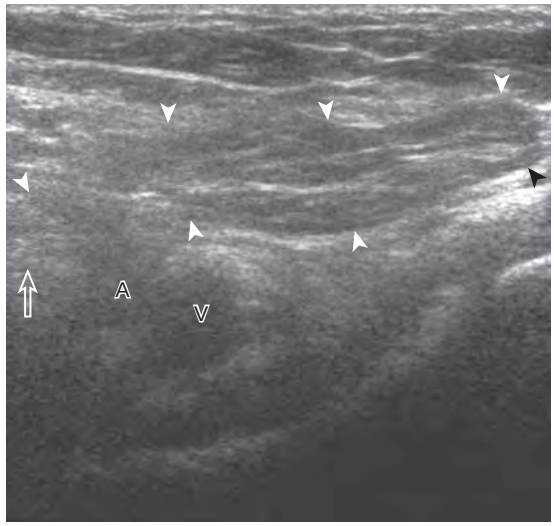

FIGURE 6-91 ■ Indirect inguinal hernia. Ultrasound image parallel to the right inguinal canal during the Valsalva maneuver shows abnormal intra-abdominal contents *(arrowheads)* that extend through the deep inguinal ring *(open arrow)*, located lateral to the external iliac vasculature (A and V), and then medial parallel to the skin surface (left side of image is lateral).

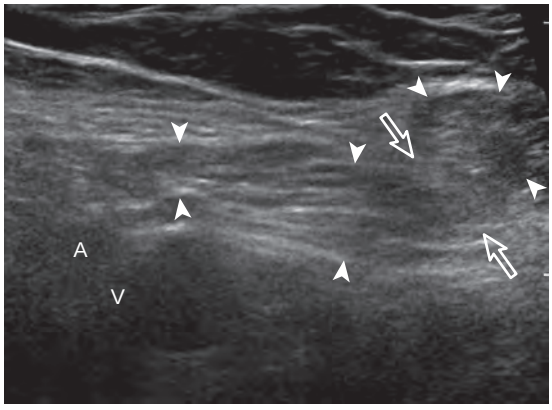

FIGURE 6-92 ■ Indirect inguinal hernia. Ultrasound image parallel to the right inguinal canal during the Valsalva maneuver shows abnormal intra-abdominal contents *(arrowheads)* that extend through the superficial inguinal ring *(open arrows)* (left side of image is lateral).

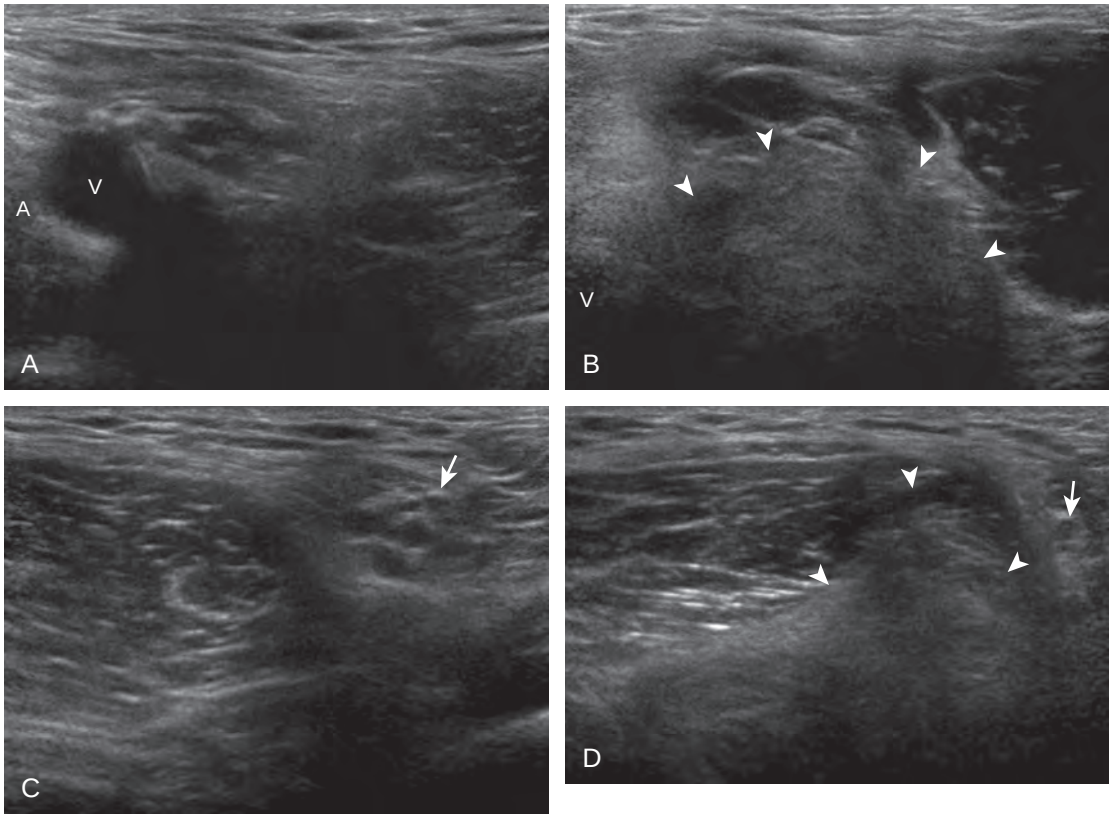

FIGURE 6-93 ■ **Direct inguinal hernia.** Ultrasound images parallel to the right inguinal canal **(A)** before and **(B)** during the Valsalva maneuver show abnormal echogenic intra-abdominal contents *(arrowheads)*, which protrude anteriorly, medial to the external iliac vasculature (A and V) (left side of image is lateral). Ultrasound images in short axis to the right inguinal canal **(C)** before and **(D)** during the Valsalva maneuver show abnormal echogenic intra-abdominal contents *(arrowheads)*, which protrude anteriorly and displace the spermatic cord *(arrow).*

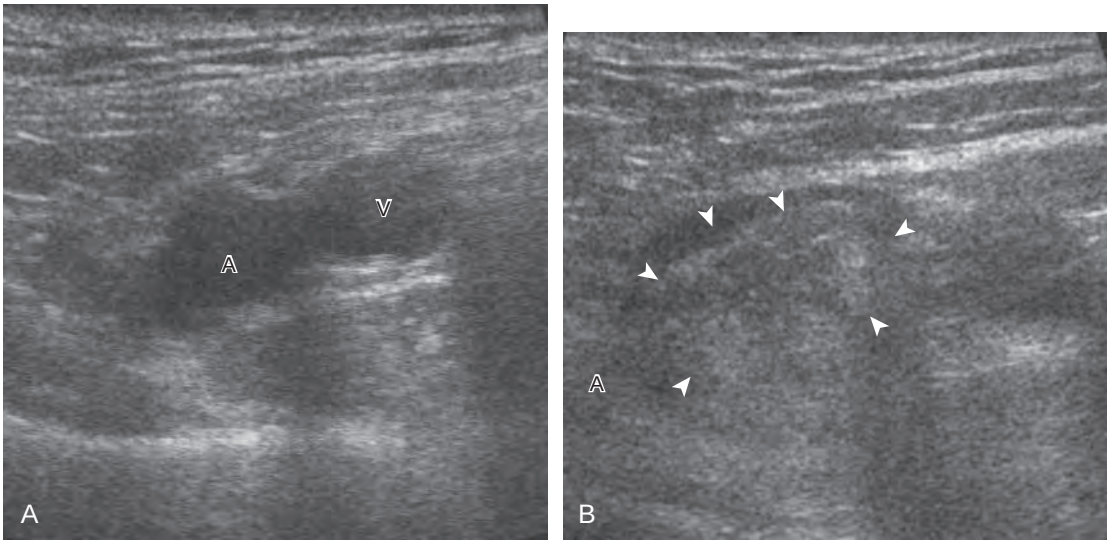

FIGURE 6-94 ■ **Femoral hernia.** Ultrasound images parallel and inferior to the right inguinal ligament **(A)** before and **(B)** during the Valsalva maneuver show abnormal intra-abdominal contents *(arrowheads)*, which protrude inferiorly, medially, and adjacent to the femoral vasculature (A and V) (left side of image is lateral).

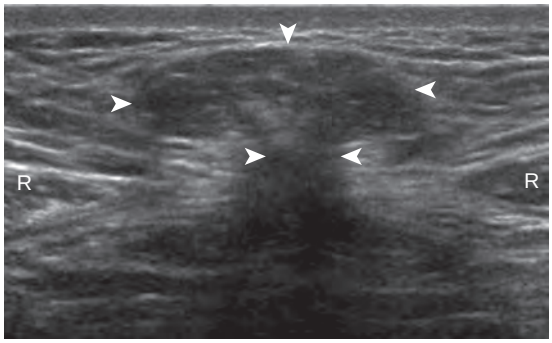

FIGURE 6-95 ■ Ventral hernia. Ultrasound image transverse over the anterior abdominal wall shows diastasis of the rectus abdominis and resulting ventral hernia *(arrowheads)*. R, rectus abdominis.

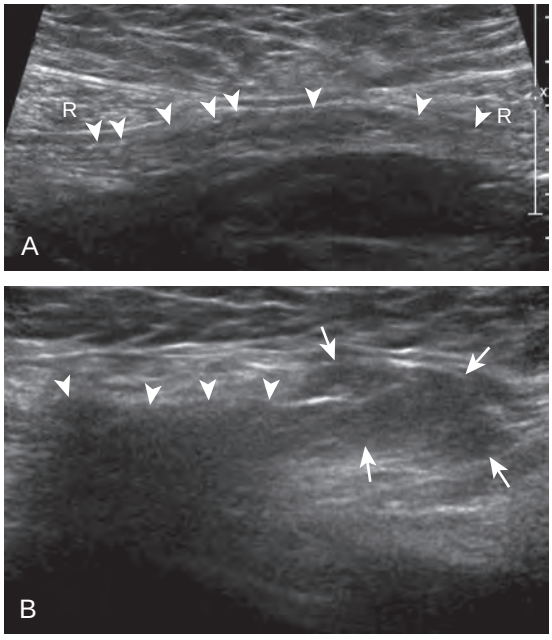

FIGURE 6-96 ■ Mesh hernia repair. Ultrasound images from two separate patients show **(A)** mesh material *(arrowheads)* beneath the anterior abdominal wall (R, rectus abdominis), and **(B)** echogenic and shadowing mesh material *(arrowheads)* with recurrent indirect right inguinal hernia *(arrows)*.

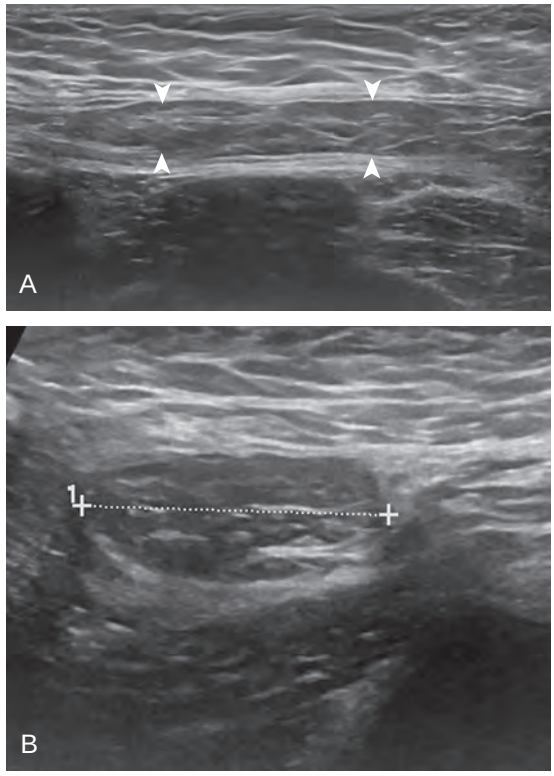

FIGURE 6-97 ■ Lipoma of the spermatic cord. Ultrasound images in **(A)** long axis and **(B)** short axis to the spermatic cord show a predominantly hypoechoic lipoma (between *arrowheads* in **A** and *cursors* in **B**).

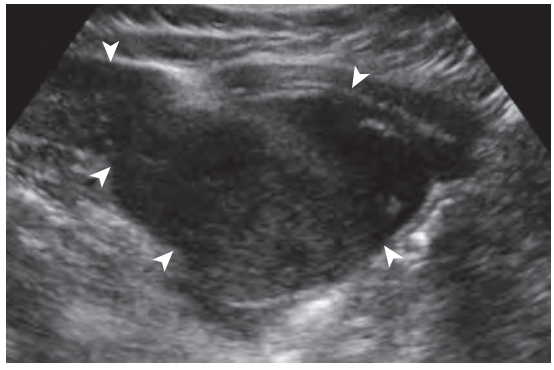

FIGURE 6-98 ■ Ewing sarcoma of the abdominal wall. Ultrasound image shows a hypoechoic mass of the abdominal wall *(arrowheads)*.

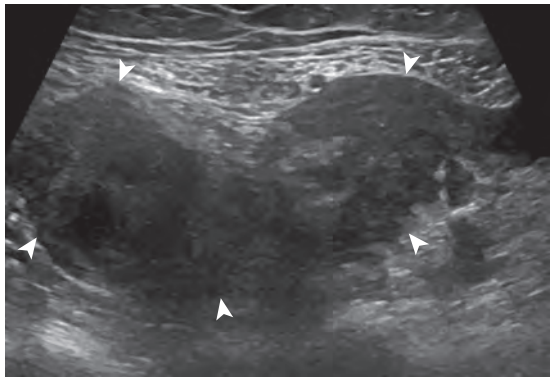

FIGURE 6-99 ■ Ovarian carcinoma with omental involvement. Ultrasound image shows a hypoechoic mass within the abdomen *(arrowheads)*.

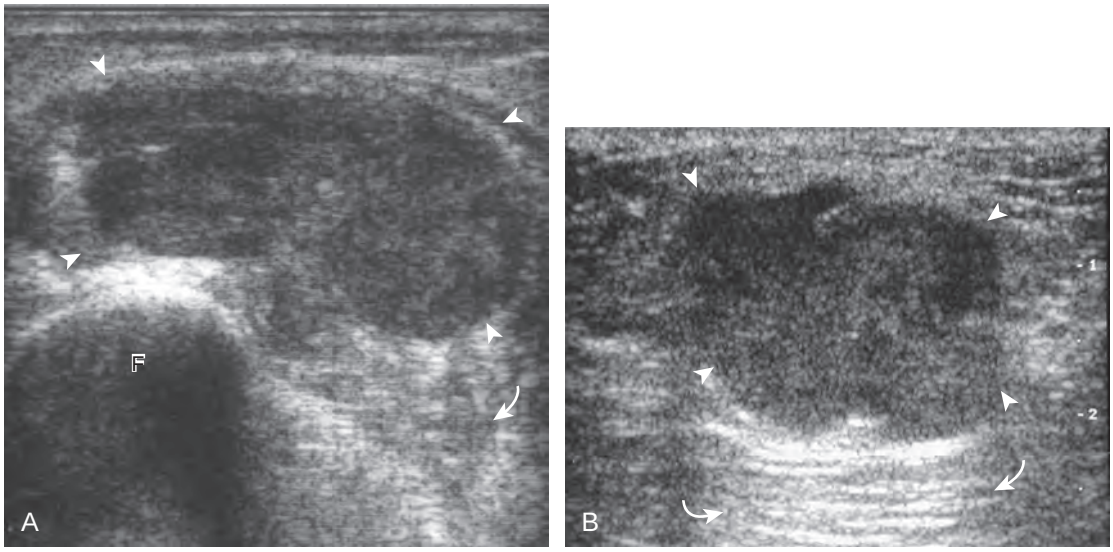

FIGURE 6-89 ■ Recurrent soft tissue malignancy. Ultrasound images from two separate patients show a lobular hypoechoic mass *(arrowheads)* from **(A)** malignant fibrous histiocytoma and **(B)** high-grade pleomorphic sarcoma recurrence. Note increased through-transmission *(curved arrows)*. F, femur.

enter into the inguinal canal, beginning at the deep inguinal ring, and move superficially and then medially toward the pubic symphysis parallel to the skin surface (Fig. 6-91, online) (Videos 6-23 through 6-25). It is important to evaluate for indirect hernia both long axis and short axis to the inguinal canal; limiting evaluation to long axis may cause one to overlook a hernia that is not included in the imaging plane. This pitfall is avoided with short axis imaging, in which the hernia can be visualized within the inguinal canal adjacent to the spermatic cord or round ligament. An indirect hernia may extend to the external inguinal ring (Fig. 6-92, online) (Video 6-26) and into the scrotum in males.

In contrast to the location of an indirect inguinal hernia, a direct inguinal hernia originates medial to the external iliac vessels and moves toward the transducer with the Valsalva maneuver (Fig. 6-93, online) (Videos 6-27 and 6-28). It is essential to evaluate for direct hernia both in the sagittal and transverse planes over the Hesselbach triangle. If one limits evaluation to the transverse plane, it is possible to misinterpret the normal abdominal contents moving from a superior to inferior direction into the imaging plane, which can simulate a direct hernia. Sagittal imaging will differentiate normal movement of abdominal contents inferiorly from a true direct hernia, in which abdominal contents move in a direct anterior direction (see Fig. 6-93C and D, online). Posterior deficiency of the posterior wall of the inguinal canal, described as a potential finding with a sports-related hernia, appears as anterior convex bulging of the inguinal canal posterior wall near the superficial inguinal ring during straining or the Valsalva maneuver.[17]

Another type of hernia seen below the level of the inguinal ligament is a femoral hernia, in which intra-abdominal contents appear adjacent to the femoral vein with the Valsalva maneuver (Fig. 6-94, online) (Videos 6-29 and 6-30). A ventral hernia occurs in midline through diastasis of the rectus abdominis (Fig. 6-95, online) or through an incision. After surgical repair of a hernia, mesh may be seen either as a linear area of speckled echoes (Fig. 6-96A, online) (Video 6-31) or a continuous echogenic area with posterior shadowing (see Fig. 6-96B, online).[68] A recurrent indirect hernia will show abnormal movement of abdominal contents into the inguinal canal (see Fig. 6-96B, online) (Video 6-32). It is also important to consider other causes of a clinically suspected hernia, such as lipoma of the spermatic cord (Fig. 6-97, online) (Video 6-33), abdominal wall mass (Fig. 6-98, online), and intra-abdominal malignancy (Fig. 6-99, online).

Developmental Dysplasia of the Hip

One screening protocol using ultrasound to detect hip dysplasia depends on the clinical examination.[19] With abnormal clinical examination findings during the Barlow and Ortolani maneuvers, ultrasound is performed in patients younger

than 2 weeks of age if the hip is unstable or at 4 to 6 weeks of age if there is a stable click. Minor physiologic laxity may disappear during the first month of life without treatment. With a normal clinical examination, ultrasound examination is performed at 4 to 6 weeks if there are risk factors for dysplasia, such as family history, breech presentation, and postural deformity, to name a few. With normal clinical examination and no risk factors present, no ultrasound examination is performed.

As described in the earlier section on ultrasound examination technique, diagnostic criteria for hip dysplasia rely on dynamic evaluation with optional measurements. Findings of hip dysplasia include subluxation or dislocation of the femoral head during the dynamic maneuvers with applied stress (Fig. 6-100, online). On the coronal image with the hip neutral or slightly flexed, an α angle is normally greater than 60 degrees. When the α angle is less than 50 degrees, the β angle becomes important and is greater than 77 degrees with femoral head subluxation and dislocation.[20] The presence of interposed echogenic fibroadipose tissue between the femoral head and the acetabulum is also noted because this is associated with hip dysplasia. Ultrasound also enables one to evaluate for proximal femoral focal deficiency and to assess for variable degrees of femoral aplasia, including the unossified femoral head cartilage.

Online references available at www.expertconsult.com.

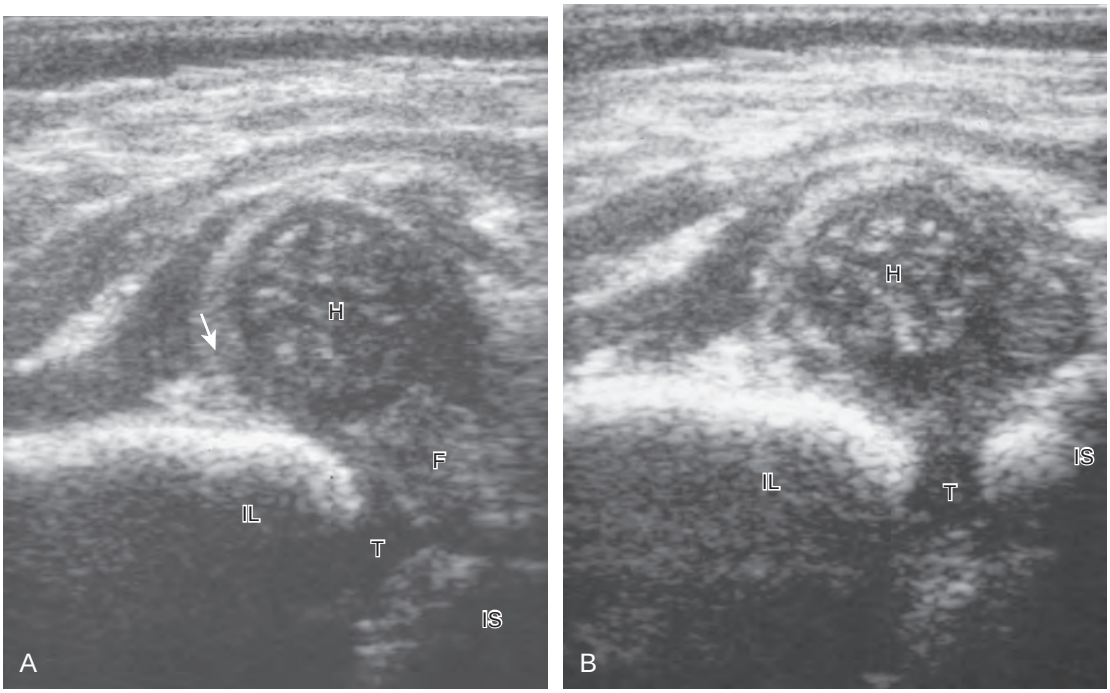

FIGURE 6-100 ■ Developmental dysplasia of the hip. A, Ultrasound image coronal to the hip joint in a 1neutral position shows dislocation of the femoral head (H), dysplasia of the acetabulum (IL, ilium), and increased echogenicity of the deformed labrum *(arrow)*. Note the fibrofatty tissue (F) in the acetabulum. **B,** Ultrasound image coronal and posterior to the hip joint with hip flexion and posteriorly directed stress shows posterior dislocation of the femoral head (H). IL, ilium; IS, ischium; T, triradiate cartilage.

REFERENCES

1. Robben SG, Lequin MH, Diepstraten AF, et al: Anterior joint capsule of the normal hip and in children with transient synovitis: US study with anatomic and histologic correlation. *Radiology* 210:499–507, 1999.
2. Pfirrmann CW, Chung CB, Theumann NH, et al: Greater trochanter of the hip: attachment of the abductor mechanism and a complex of three bursae—MR imaging and MR bursography in cadavers and MR imaging in asymptomatic volunteers. *Radiology* 221:469–477, 2001.
3. Hasselman CT, Best TM, Hughes CT, et al: An explanation for various rectus femoris strain injuries using previously undescribed muscle architecture. *Am J Sports Med* 23:493–499, 1995.
4. Bianchi S, Martinoli C, Waser NP, et al: Central aponeurosis tears of the rectus femoris: sonographic findings. *Skeletal Radiol* 31:581–586, 2002.
5. Linklater JM, Hamilton B, Carmichael J, et al: Hamstring injuries: anatomy, imaging, and intervention. *Semin Musculoskelet Radiol* 14:131–161, 2010.
6. Blankenbaker DG, Tuite MJ: Iliopsoas musculotendinous unit. *Semin Musculoskelet Radiol* 12:13–27, 2008.
7. Robinson P, White LM, Agur A, et al: Obturator externus bursa: anatomic origin and MR imaging features of pathologic involvement. *Radiology* 228:230–234, 2003.
8. Jamadar DA, Jacobson JA, Morag Y, et al: Sonography of inguinal region hernias. *AJR Am J Roentgenol* 187:185–190, 2006.
9. Aszmann OC, Dellon ES, Dellon AL: Anatomical course of the lateral femoral cutaneous nerve and its susceptibility to compression and injury. *Plast Reconstr Surg* 100:600–604, 1997.
10. Damarey B, Demondion X, Boutry N, et al: Sonographic assessment of the lateral femoral cutaneous nerve. *J Clin Ultrasound* 37:89–95, 2009.
11. Bodner G, Bernathova M, Galiano K, et al: Ultrasound of the lateral femoral cutaneous nerve: normal findings in a cadaver and in volunteers. *Reg Anesth Pain Med* 34:265–268, 2009.
12. Tagliafico A, Serafini G, Lacelli F, et al: Ultrasound-guided treatment of meralgia paresthetica (lateral femoral cutaneous neuropathy): technical description and results of treatment in 20 consecutive patients. *J Ultrasound Med* 30:1341–1346, 2011.
13. Zoga AC, Kavanagh EC, Omar IM, et al: Athletic pubalgia and the "sports hernia": MR imaging findings. *Radiology* 247:797–807, 2008.
14. Klauser A, De Zordo T, Feuchtner G, et al: Feasibility of ultrasound-guided sacroiliac joint injection considering sonoanatomic landmarks at two different levels in cadavers and patients. *Arthritis Rheum* 59:1618–1624, 2008.
15. Finnoff JT, Hurdle MF, Smith J: Accuracy of ultrasound-guided versus fluoroscopically guided contrast-controlled piriformis injections: a cadaveric study. *J Ultrasound Med* 27:1157–1163, 2008.
16. Smith J, Hurdle MF, Locketz AJ, et al: Ultrasound-guided piriformis injection: technique description and verification. *Arch Phys Med Rehabil* 87:1664–1667, 2006.
17. Garvey JF, Read JW, Turner A: Sportsman hernia: what can we do? *Hernia* 14:17–25, 2010.
18. Wangwinyuvirat M, Dirim B, Pastore D, et al: Prepatellar quadriceps continuation: MRI of cadavers with gross anatomic and histologic correlation. *AJR Am J Roentgenol* 192:W111–W116, 2009.
19. Harcke HT: Screening newborns for developmental dysplasia of the hip: the role of sonography. *AJR Am J Roentgenol* 162:395–397, 1994.
20. Graf R: Fundamentals of sonographic diagnosis of infant hip dysplasia. *J Pediatr Orthop* 4:735–740, 1984.
21. Koski JM, Anttila PJ, Isomaki HA: Ultrasonography of the adult hip joint. *Scand J Rheumatol* 18:113–117, 1989.
22. Moss SG, Schweitzer ME, Jacobson JA, et al: Hip joint fluid: detection and distribution at MR imaging and US with cadaveric correlation. *Radiology* 208:43–48, 1998.
23. Strouse PJ, DiPietro MA, Adler RS: Pediatric hip effusions: evaluation with power Doppler sonography. *Radiology* 206:731–735, 1998.
24. Weybright PN, Jacobson JA, Murry KH, et al: Limited effectiveness of sonography in revealing hip joint effusion: preliminary results in 21 adult patients with native and postoperative hips. *AJR Am J Roentgenol* 181:215–218, 2003.
25. Troelsen A, Jacobsen S, Bolvig L, et al: Ultrasound versus magnetic resonance arthrography in acetabular labral tear diagnostics: a prospective comparison in 20 dysplastic hips. *Acta Radiol* 48:1004–1010, 2007.
26. Troelsen A, Mechlenburg I, Gelineck J, et al: What is the role of clinical tests and ultrasound in acetabular labral tear diagnostics? *Acta Orthop* 80:314–318, 2009.
27. Safran O, Goldman V, Applbaum Y, et al: Posttraumatic painful hip: sonography as a screening test for occult hip fractures. *J Ultrasound Med* 28:1447–1452, 2009.
28. Buck FM, Hodler J, Zanetti M, et al: Ultrasound for the evaluation of femoroacetabular impingement of the cam type: diagnostic performance of qualitative criteria and alpha angle measurements. *Eur Radiol* 21:167–175, 2011.
29. Leunig M, Beck M, Kalhor M, et al: Fibrocystic changes at anterosuperior femoral neck: prevalence in hips with femoroacetabular impingement. *Radiology* 236:237–246, 2005.
30. Pfirrmann CW, Mengiardi B, Dora C, et al: Cam and pincer femoroacetabular impingement: characteristic MR arthrographic findings in 50 patients. *Radiology* 240:778–785, 2006.
31. Wunderbaldinger P, Bremer C, Schellenberger E, et al: Imaging features of iliopsoas bursitis. *Eur Radiol* 12:409–415, 2002.
32. Bianchi S, Martinoli C, Keller A, et al: Giant iliopsoas bursitis: sonographic findings with magnetic resonance correlations. *J Clin Ultrasound* 30:437–441, 2002.
33. Pritchard RS, Shah HR, Nelson CL, et al: MR and CT appearance of iliopsoas bursal distention secondary to diseased hips. *J Comput Assist Tomogr* 14:797–800, 1990.
34. Silva F, Adams T, Feinstein J, et al: Trochanteric bursitis: refuting the myth of inflammation. *J Clin Rheumatol* 14:82–86, 2008.
35. Fearon AM, Scarvell JM, Cook JL, et al: Does ultrasound correlate with surgical or histologic findings in greater trochanteric pain syndrome? A pilot study. *Clin Orthop Relat Res* 468:1838–1844, 2010.
36. Kim SM, Shin MJ, Kim KS, et al: Imaging features of ischial bursitis with an emphasis on ultrasonography. *Skeletal Radiol* 31:631–636, 2002.
37. van Holsbeeck MT, Eyler WR, Sherman LS, et al: Detection of infection in loosened hip prostheses: efficacy of sonography. *AJR Am J Roentgenol* 163:381–384, 1994.
38. Hoefnagels EM, Obradov M, Reijnierse M, et al: Sonography after total hip replacement: reproducibility and normal values in 47 clinically uncomplicated cases. *Acta Orthop* 78:81–85, 2007.
39. Ostlere S: How to image metal-on-metal prostheses and their complications. *AJR Am J Roentgenol* 197:558–567, 2011.
40. Steinbach LS, Schneider R, Goldman AB, et al: Bursae and abscess cavities communicating with the hip: diagnosis using arthrography and CT. *Radiology* 156:303–307, 1985.
41. Garcia FL, Picado CH, Nogueira-Barbosa MH: Sonographic evaluation of the abductor mechanism after total hip arthroplasty. *J Ultrasound Med* 29:465–471, 2010.

42. Brew CJ, Stockley I, Grainger AJ, et al: Iliopsoas tendonitis caused by overhang of a collared femoral prosthesis. *J Arthroplasty* 26:504, e17–19, 2011.
43. Wank R, Miller TT, Shapiro JF: Sonographically guided injection of anesthetic for iliopsoas tendinopathy after total hip arthroplasty. *J Clin Ultrasound* 32:354–357, 2004.
44. Jin W, Chun YS, Park SY, et al: Sonographic detection of acetabular polyethylene liner dissociation in total hip arthroplasty. *J Ultrasound Med* 28:1597–1600, 2009.
45. Davis KW: Imaging of the hamstrings. *Semin Musculoskelet Radiol* 12:28–41, 2008.
46. Douis H, Gillett M, James SL: Imaging in the diagnosis, prognostication, and management of lower limb muscle injury. *Semin Musculoskelet Radiol* 15:27–41, 2011.
47. Robinson P, Bhat V, English B: Imaging in the assessment and management of athletic pubalgia. *Semin Musculoskelet Radiol* 15:14–26, 2011.
48. Weaver JS, Jacobson JA, Jamadar DA, et al: Sonographic findings of adductor insertion avulsion syndrome with magnetic resonance imaging correlation. *J Ultrasound Med* 22:403–407, 2003.
49. Kong A, Van der Vliet A, Zadow S: MRI and US of gluteal tendinopathy in greater trochanteric pain syndrome. *Eur Radiol* 17:1772–1783, 2007.
50. Westacott DJ, Minns JI, Foguet P: The diagnostic accuracy of magnetic resonance imaging and ultrasonography in gluteal tendon tears: a systematic review. *Hip Int* 21:637–645, 2011.
51. Koulouris G, Connell D: Hamstring muscle complex: an imaging review. *Radiographics* 25:571–586, 2005.
52. Pelsser V, Cardinal E, Hobden R, et al: Extraarticular snapping hip: sonographic findings. *AJR Am J Roentgenol* 176:67–73, 2001.
53. Guillin R, Cardinal E, Bureau NJ: Sonographic anatomy and dynamic study of the normal iliopsoas musculotendinous junction. *Eur Radiol* 19:995–1001, 2009.
54. Deslandes M, Guillin R, Cardinal E, et al: The snapping iliopsoas tendon: new mechanisms using dynamic sonography. *AJR Am J Roentgenol* 190:576–581, 2008.
55. Choi YS, Lee SM, Song BY, et al: Dynamic sonography of external snapping hip syndrome. *J Ultrasound Med* 21:753–758, 2002.
56. Parker L, Nazarian LN, Carrino JA, et al: Musculoskeletal imaging: Medicare use, costs, and potential for cost substitution. *J Am Coll Radiol* 5:182–188, 2008.
57. Delaney-Sathy LO, Fessell DP, Jacobson JA, et al: Sonography of diabetic muscle infarction with MR imaging, CT, and pathologic correlation. *AJR Am J Roentgenol* 174:165–169, 2000.
58. Petersilge CA, Pathria MN, Gentili A, et al: Denervation hypertrophy of muscle: MR features. *J Comput Assist Tomogr* 19:596–600, 1995.
59. Stuart RM, Koh ES, Breidahl WH: Sonography of peripheral nerve pathology. *AJR Am J Roentgenol* 182:123–129, 2004.
60. Neal C, Jacobson JA, Brandon C, et al: Sonography of Morel-Lavallee lesions. *J Ultrasound Med* 27:1077–1081, 2008.
61. Grey AC, Carrington BM, Hulse PA, et al: Magnetic resonance appearance of normal inguinal nodes. *Clin Radiol* 55:124–130, 2000.
62. Vassallo P, Wernecke K, Roos N, et al: Differentiation of benign from malignant superficial lymphadenopathy: the role of high-resolution US. *Radiology* 183:215–220, 1992.
63. Krishna RP, Sistla SC, Smile R, et al: Sonography: an underutilized diagnostic tool in the assessment of metastatic groin nodes. *J Clin Ultrasound* 36:212–217, 2008.
64. Wu CH, Shih JC, Chang YL, et al: Two-dimensional and three-dimensional power Doppler sonographic classification of vascular patterns in cervical lymphadenopathies. *J Ultrasound Med* 17:459–464, 1998.
65. Girish G, Jamadar DA, Landry D, et al: Sonography of intramuscular myxomas: the bright rim and bright cap signs. *J Ultrasound Med* 25:865–869, 2006.
66. Arya S, Nagarkatti DG, Dudhat SB, et al: Soft tissue sarcomas: ultrasonographic evaluation of local recurrences. *Clin Radiol* 55:193–197, 2000.
67. Choi H, Varma DG, Fornage BD, et al: Soft-tissue sarcoma: MR imaging vs sonography for detection of local recurrence after surgery. *AJR Am J Roentgenol* 157:353–358, 1991.
68. Jamadar DA, Jacobson JA, Girish G, et al: Abdominal wall hernia mesh repair: sonography of mesh and common complications. *J Ultrasound Med* 27:907–917, 2008.

eBOX 6-1 Sample Diagnostic Hip Ultrasound Report

NORMAL

Examination: Ultrasound of the Right Hip
Date of Study: March 11, 2011
Patient Name: Jack White
Registration Number: 8675309
History: Hip pain, evaluate for bursitis
Findings: The hip joint is normal without effusion or synovial hypertrophy. Limited evaluation of the anterior labrum is unremarkable. No evidence of iliopsoas bursal distention or snapping iliopsoas tendon with dynamic imaging. The remaining anterior tendons, including the rectus femoris and sartorius, as well as the adductors, are normal.

Evaluation of the lateral hip is normal. No evidence of abnormal bursal distention around the greater trochanter. The gluteus minimus and medius tendons are normal. No abnormal snapping with dynamic evaluation.

Impression: Unremarkable ultrasound examination of the hip.

eBOX 6-2 Sample Diagnostic Hip Ultrasound Report

ABNORMAL

Examination: Ultrasound of the Right Hip
Date of Study: March 11, 2011
Patient Name: Jack White
Registration Number: 8675309
History: Hip pain, evaluate for tendon tear
Findings: There is a partial tear of the adductor longus origin at the pubis. No evidence of full-thickness tear or tendon retraction. The common aponeurosis and rectus abdominis tendon are normal, as is the pubic symphysis.

The hip joint is normal without effusion or synovial hypertrophy. There is a possible tear of the anterior labrum. No paralabral cyst. No evidence of iliopsoas bursal distention or snapping iliopsoas tendon with dynamic imaging.

Evaluation of the lateral hip is normal. No evidence of abnormal bursal distention around the greater trochanter. The gluteus minimus and medius tendons are normal. No abnormal snapping with dynamic evaluation.

Impression:

1. Partial-thickness tear of the proximal adductor longus.
2. Possible anterior labral tear. Consider MR arthrography if indicated.

CHAPTER 7

Knee Ultrasound

CHAPTER OUTLINE

KNEE ANATOMY

ULTRASOUND EXAMINATION TECHNIQUE
General Comments
Anterior Evaluation
Medial Evaluation
Lateral Evaluation
Posterior Evaluation

JOINT ABNORMALITIES
Joint Effusion and Synovial Hypertrophy
Cartilage Abnormalities

TENDON AND MUSCLE ABNORMALITIES
Quadriceps Femoris Injury
Patellar Tendon Injury
Other Knee Tendon Injuries
Gout

LIGAMENT AND BONE ABNORMALITIES
Medial Collateral Ligament
Lateral Collateral Ligament
Cruciate Ligaments
Osseous Injury

BURSAE AND CYSTS
Baker Cyst
Other Bursae
Ganglion Cysts

PERIPHERAL NERVE ABNORMALITIES

VASCULAR ABNORMALITIES

Additional videos for this topic are available online at www.expertconsult.com.

KNEE ANATOMY

The knee joint is a synovial joint that consists of hyaline cartilage articulations between the femur, the tibia, and the patella (Fig. 7-1). The fibrocartilage menisci are C-shaped structures between the femur and the tibia. A prominent joint recess, the suprapatellar recess, extends superiorly from the knee joint between the patella and the femur and communicates with the medial and lateral joint recesses, which extend over the medial and lateral aspects of the femoral condyles beneath the patellar retinaculum.[1] In the sagittal plane, the quadriceps fat pad is located anteriorly between the suprapatellar recess and quadriceps tendon, and the prefemoral fat pad is located between the suprapatellar recess and the femur. The infrapatellar fat pad of Hoffa is an intracapsular but extrasynovial fat pad between the anterior knee joint and the patellar tendon. Various bursae exist around the anterior knee joint, including the prepatellar bursa anterior to the patella, the superficial infrapatellar bursa anterior to the distal patellar tendon, and the deep infrapatellar bursa between the patellar tendon and proximal tibia. Additional bursae are present around the medial knee, including the pes anserinus bursa deep to the pes anserinus tendons and the semimembranosus-tibial collateral ligament bursa, which has an inverted U shape located at the joint line between the medial collateral ligament and the semimembranosus tendon.[2,3] These latter two bursae do not communicate with the knee joint. A more common bursa is the semimembranosus-medial gastrocnemius bursa, which, when distended, is called a *Baker cyst*. This bursa communicates to the knee joint in 50% of adults who are older than 50 years and becomes a common recess for joint fluid and intra-articular bodies.[4]

The knee joint is stabilized by a number of ligaments. Medially, the medial collateral ligament extends from the medial femoral condyle to the tibia in the coronal plane. Thin, deep layers of the medial collateral ligament (meniscofemoral and meniscotibial ligaments) extend from the

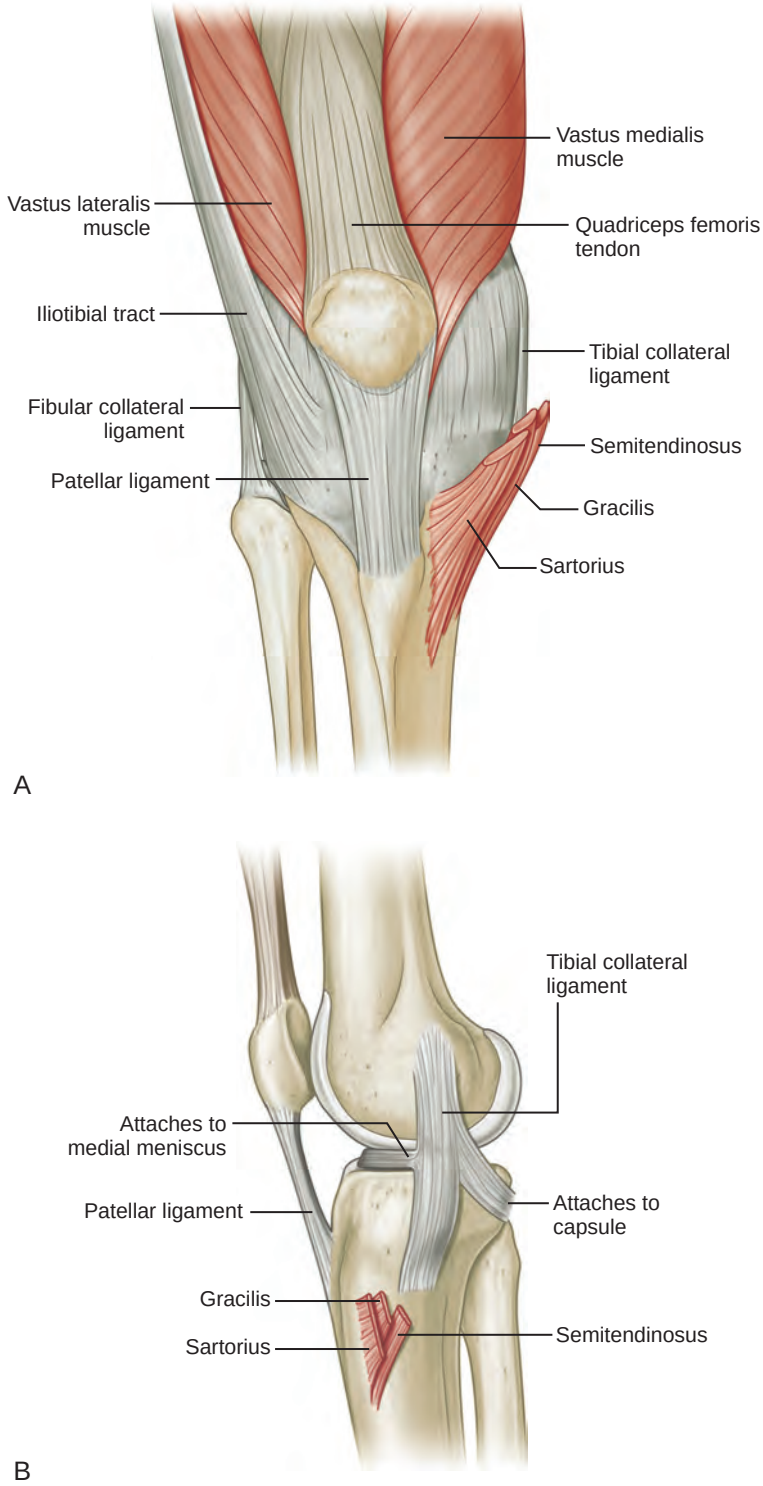

FIGURE 7-1 ■ **Knee anatomy. A,** Anterior view of the knee. **B,** Medial view of knee.

Continued

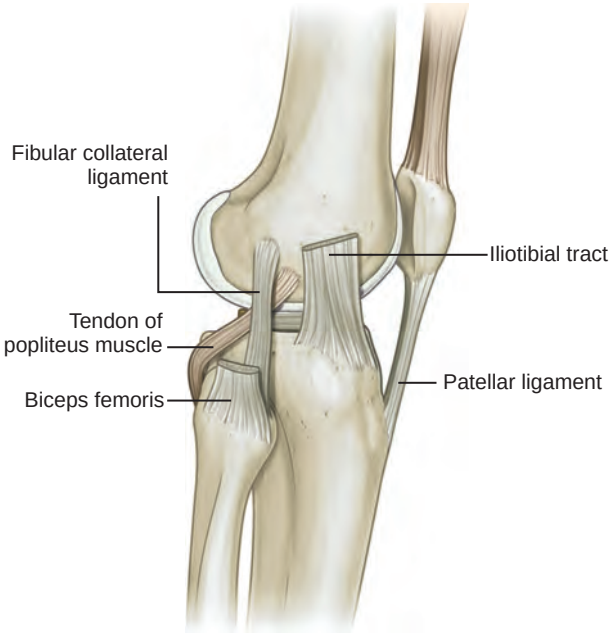

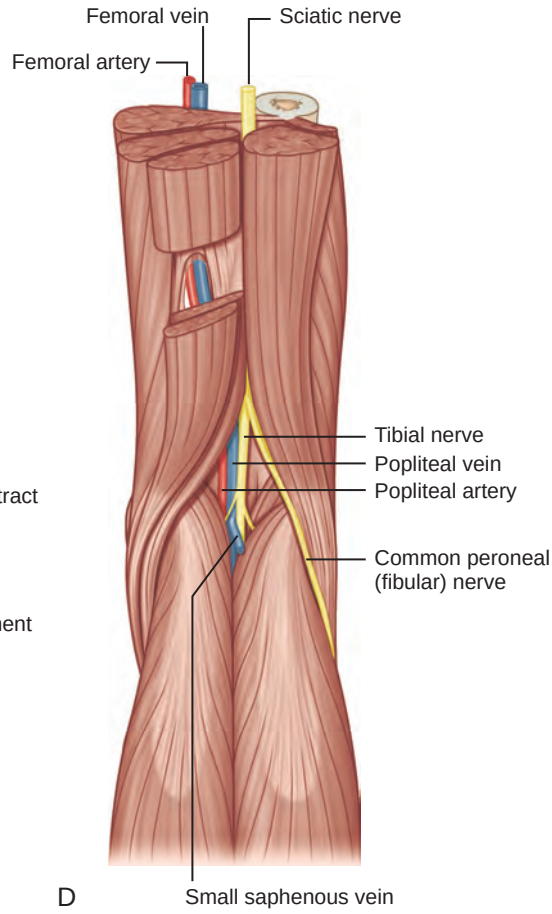

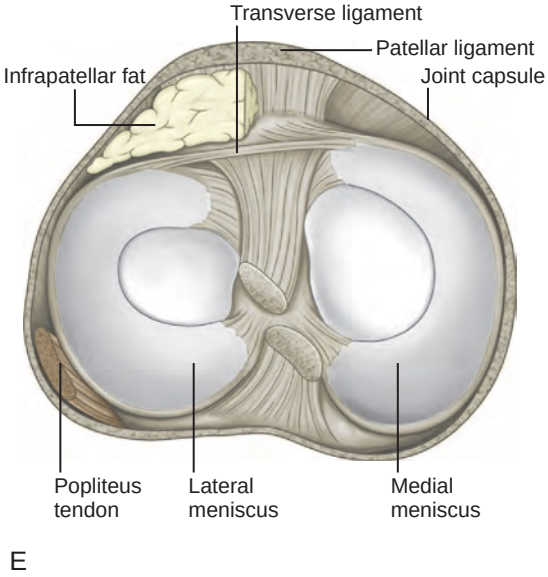

FIGURE 7-1, cont'd ■ **C,** Lateral view of knee. **D,** Posterior view of knee. **E,** Superior view of knee menisci. (From Drake R, Vogl W, Mitchell A: *Gray's anatomy for students.* Philadelphia, 2005, Churchill Livingstone.)

meniscus to the femur and tibia, whereas a thicker, more superficial layer (tibial collateral ligament) extends from the femur to insert distally on the tibia deep to the pes anserinus.[5] Superficial to the medial collateral ligament is found the deep crural fascia.[5] The lateral or fibular collateral ligament originates from the lateral femur and extends over the popliteus tendon to insert on the lateral aspect of the fibula with the biceps femoris tendon.[6] Other supporting structures of the posterolateral knee include the popliteofibular ligament and the arcuate ligament. The popliteofibular ligament extends from the popliteus tendon to the styloid process of the proximal fibula, whereas the arcuate ligament extends from the femur and joint capsule to the fibula tip as well. When a fabella is present, another posterolateral structure is the fabellofibular ligament. The anterior and posterior cruciate ligaments within the intercondylar notch extend from the femur to the proximal tibia as intracapsular but extrasynovial structures.

With regard to tendons around the knee, anteriorly the quadriceps femoris tendon inserts on the superior patellar pole, although superficial fibers extend over the patella (termed the *prepatellar quadriceps continuation*) to insert on the tibial tuberosity as part of the patellar tendon.[7] The medial and lateral patellar retinaculum extends from each side of the patella to the femur; the medial aspect is reinforced by the medial patellofemoral ligament, which extends from the medial patella to the adductor tubercle region of the medial femoral condyle.[8] The distal aspect of the vastus tibial, often termed the *vastus medialis obliquus*, blends with the medial patellar retinaculum to insert onto the medial patella.[8-10] Medially and anteriorly, the sartorius, gracilis, and semitendinosus tendons insert on the tibia near the tibial collateral ligament as the pes anserinus (a helpful mnemonic is "Say Grace before Tea" where S, Sartorius; G, Gracilis; and T, semiTendinosis). Posterior and proximal to the pes anserinus, the semimembranosus primarily inserts on the tibia just beyond the tibia articular surface, although the distal anatomy is quite complex.[11] Posteriorly, the medial and lateral heads of the gastrocnemius originate from the posterior aspect of the femoral condyles. Laterally, the biceps femoris tendon and lateral collateral ligament attach to the lateral margin of the fibular head.[12] The direct arm of the long head of the biceps femoris tendon inserts on the lateral aspect of the fibula with the lateral collateral ligament, whereas the anterior arm of the long head biceps femoris inserts more anterior on the fibula. The short head of the biceps femoris also has two insertions: the direct arm insertion on the proximal fibula medial to the long head and the anterior arm insertion on the proximal tibia.[6] The popliteus tendon originates at the lateral aspect of the femur, lies within a groove or sulcus of the femur, and courses obliquely with its muscle belly located between the posterior aspect of the tibia and the tibial artery and vein. Anterolaterally, the iliotibial tract or band inserts on the Gerdy tubercle of the proximal tibia.

With regard to the peripheral nerves, the sciatic nerve bifurcates as the tibial nerve, which extends distally posterior to the popliteal artery and vein, and the common peroneal nerve, which courses laterally parallel and posterior to the biceps femoris tendon. The common peroneal or fibular nerve curves anteriorly around the fibular neck deep to the peroneus longus origin and bifurcates as the superficial peroneal nerve, which courses along the peroneal musculature, and the deep peroneal nerve, which continues to the interosseous membrane and follows the anterior tibial artery between the tibia and fibula.

ULTRASOUND EXAMINATION TECHNIQUE

Table 7-1 is a checklist for a knee ultrasound examination. Examples of diagnostic knee ultrasound reports are available online at www.expertconsult.com (see eBox 7-1 and 7-2).

TABLE 7-1 **Knee Ultrasound Examination Checklist**

Structures/ Pathologic Features	Location of Interest
Anterior	Quadriceps tendon
	Patella
	Patellar tendon
	Patellar retinaculum
	Suprapatellar recess
	Medial and lateral recesses
	Anterior knee bursae
	Femoral articular cartilage
Medial	Medial collateral ligament
	Medial meniscus: body and anterior horn
	Pes anserinus
Lateral	Iliotibial tract
	Lateral collateral ligament
	Biceps femoris
	Common peroneal nerve
	Popliteus
	Lateral meniscus: body and anterior horn
Posterior	Baker cyst
	Menisci: posterior horns
	Posterior cruciate ligament
	Anterior cruciate ligament
	Neurovascular structures

General Comments

Ultrasound examination of the majority of the knee structures is completed with the patient supine; the posterior structures are best evaluated with the patient prone. A high-frequency transducer of at least 10 MHz is typically used, with the exception of the posterior knee, for which a transducer of 7 MHz or perhaps 5 MHz may be needed to penetrate the deep soft tissues. Evaluation of the knee may be focused over the area that is clinically symptomatic or that is relevant to the patient's history. Regardless, a complete examination of all areas should always be considered and is recommended for one to become familiar with normal anatomy and normal variants and to develop a quick and efficient sonographic technique.

Anterior Evaluation

The primary structures evaluated from the anterior approach are the quadriceps tendon, the patella, the patellar tendon, the patellar retinaculum, the suprapatellar recess, the medial and lateral recesses, and the bursa around the anterior knee. Examination is begun in the sagittal plane proximal to the patella (Fig. 7-2A). This plane demonstrates the normal hyperechoic and fibrillar appearance of the quadriceps tendon (see Fig. 7-2B). Slight flexion of the knee with a pad or roll behind the knee is often helpful because this position straightens and tenses the extensor mechanism to reduce tendon anisotropy. Often, the trilaminar appearance of the quadriceps tendon can be appreciated, with the rectus femoris as the anterior layer, the combined vastus medialis and intermedius as the middle layer, and the vastus intermedius as the deepest layer (see Quadriceps Femoris Injury). The quadriceps tendon is also evaluated in short axis (Fig. 7-3A and B). Returning to the quadriceps tendon in long axis, the suprapatellar recess is identified deep to the quadriceps tendon and evaluated for anechoic or hypoechoic joint fluid, which would separate the quadriceps fat pad (located superficial) from the prefemoral fat pad (located deep) (see Fig. 7-2). Slight knee flexion also shifts fluid from other parts of the knee joint into the suprapatellar recess. The transducer is then moved inferiorly below the patella in the sagittal plane to visualize the hyperechoic, fibrillar, and uniform patellar tendon (Fig. 7-4A and B). The Hoffa infrapatellar fat pad appears minimally hyperechoic or

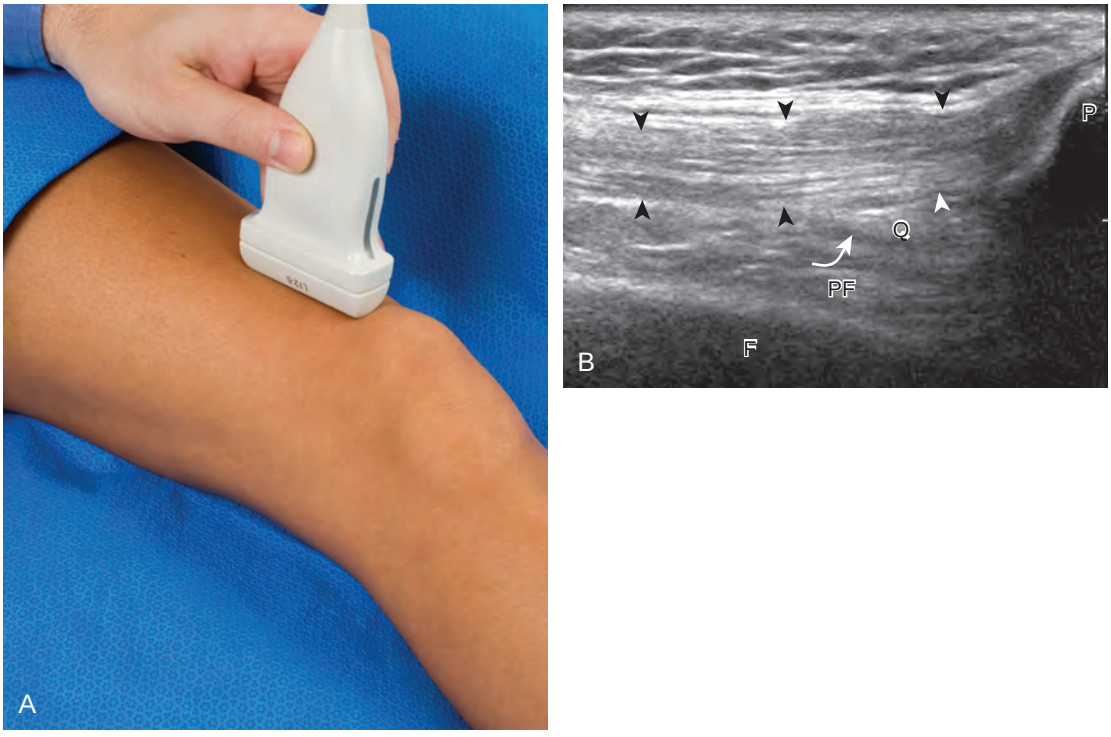

FIGURE 7-2 ■ **Quadriceps femoris: long axis. A,** Sagittal imaging over anterior knee proximal to the patella shows **(B)** the quadriceps tendon *(arrowheads)*, quadriceps fat pad (Q), prefemoral fat pad (PF), and collapsed joint recess *(curved arrow)*. F, femur; P, patella.

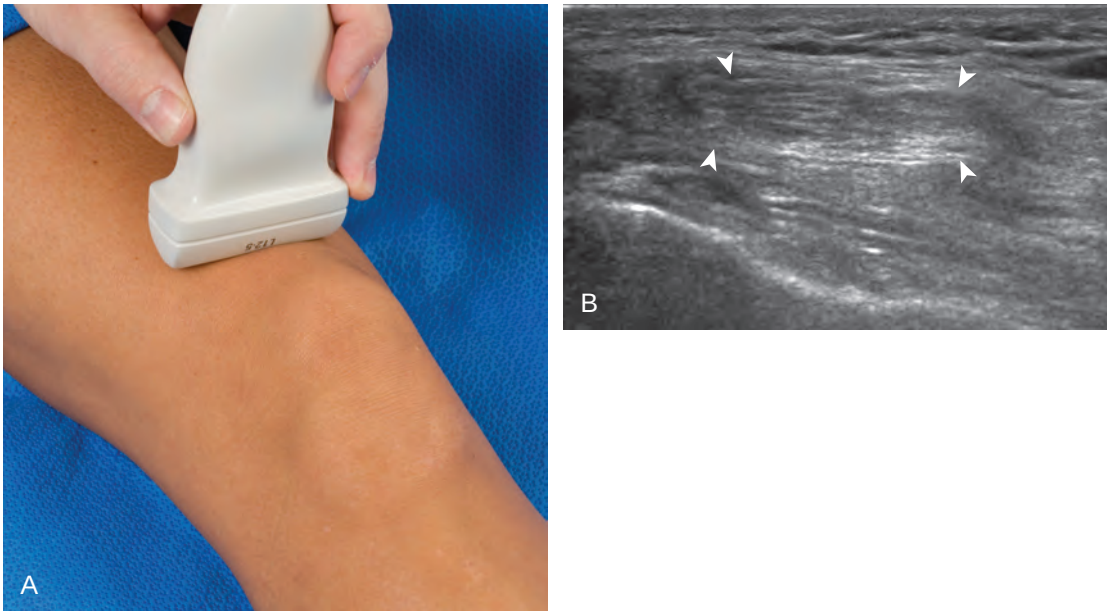

FIGURE 7-3 ■ Quadriceps femoris: short axis. A, Transverse imaging over anterior knee proximal to patella shows **(B)** the quadriceps tendon *(arrowheads)*.

isoechoic to muscle deep to the patellar tendon. The transducer should also be floated on a layer of gel over the proximal patellar tendon and patella to evaluate for patellar fracture, as well as prepatellar bursal fluid, because the latter may be easily redistributed out of view with the slightest transducer pressure. The region around the distal patellar tendon is also evaluated for superficial and deep infrapatellar bursal fluid; minimal fluid in the latter is considered physiologic (see Other Bursae). Although long axis is most important in evaluation of extensor mechanism abnormalities, imaging should also be completed in short axis to ensure a thorough evaluation, especially with the patellar tendon, where a focal abnormality may not be located in midline (Fig. 7-5A and B).

The transducer is then moved to both the medial and lateral margins of the patella in the transverse plane to visualize the thin hyperechoic patellar retinaculum as well as distention of the medial and lateral recesses that are continuous with the suprapatellar recess, which is more apparent when the knee is completely extended (Fig. 7-6A and B). One must be careful not to displace joint fluid from view with transducer pressure (see Joint Effusion and Synovial Hypertrophy). The patellar retinaculum may demonstrate three defined layers.[8] Within the medial

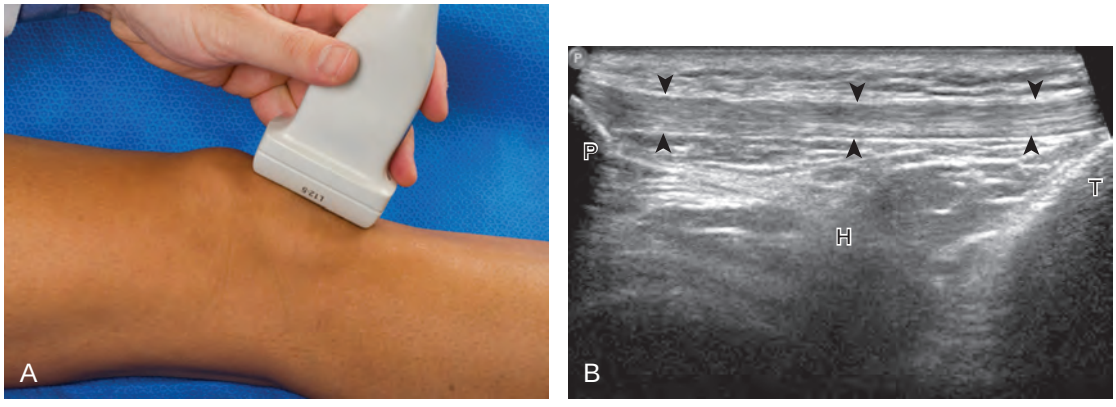

FIGURE 7-4 ■ Patellar tendon: long axis. A, Sagittal imaging over anterior knee distal to the patella shows **(B)** the patellar tendon *(arrowheads)* and Hoffa fat pad (H). P, patella; T, tibia.

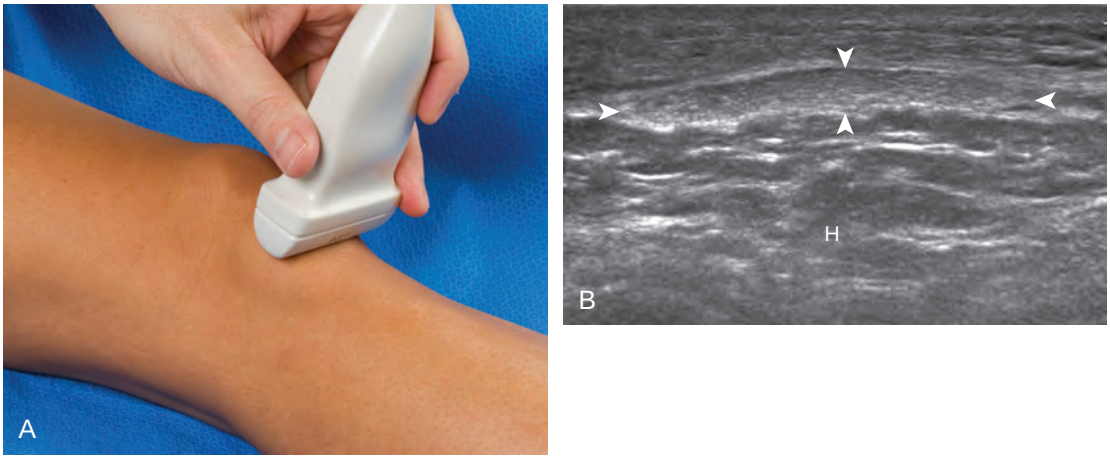

FIGURE 7-5 ■ Patellar tendon: short axis. A, Transverse imaging over anterior knee distal to patella shows **(B)** the patellar tendon *(arrowheads)* and Hoffa fat pad (H).

patellar retinaculum, the medial patellofemoral ligament may be identified as hyperechoic with a compact fibrillar echotexture, which extends from the adductor tubercle of the femur to the patella. Finally, with the knee in flexion, the hypoechoic hyaline cartilage that covers the trochlea of the anterior femur can be visualized in the transverse plane superior to the patella (Fig. 7-7A and B), and the hypoechoic hyaline cartilage covering the anterior and central aspects of the femoral condyles can be seen in the parasagittal plane (see Fig. 7-7C).[13]

Medial Evaluation

For medial knee evaluation, the patient remains supine and rotates the hip externally to gain access to the medial structures. The structures of interest include the medial collateral ligament (composed of several layers), the body and anterior horn of the medial meniscus, and the pes anserinus.[5] To begin, the transducer is placed in the coronal plane along the medial joint line, which is identified by the bone contours of the femoral condyle and the proximal tibia (Fig. 7-8A).[14] The thick hyperechoic and fibrillar superficial layer of the medial collateral ligament (or tibial collateral ligament) is easily identified in long axis (see Fig. 7-8B); it extends proximally from the medial femoral condyle and extends distally and slightly anterior to the proximal tibial metaphysis. With rotation of the transducer short axis to the tibial collateral ligament, the anteroposterior extent of this structure can be appreciated (Fig. 7-9A and B). By toggling the transducer along the long axis of the tibial collateral ligament, the borders of the ligament can be better appreciated because the ligament fibers become hypoechoic as a result of anisotropy and the adjacent soft tissues remain hyperechoic (see Fig. 7-9C). Returning to the coronal plane or long axis to the tibial collateral ligament, the thinner

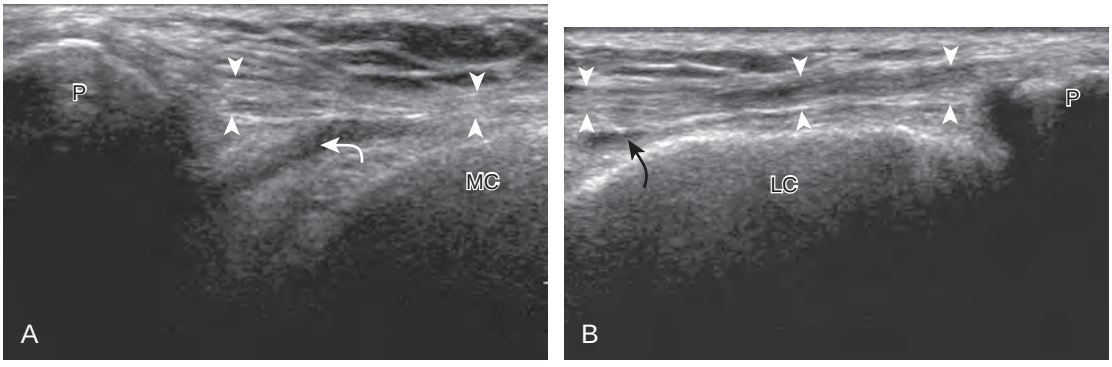

FIGURE 7-6 ■ Medial and lateral knee joint recesses. Transverse imaging on each side of the patella shows **(A)** the medial patellar retinaculum, which contains the medial patellofemoral ligament *(arrowheads)*, and **(B)** the lateral patellar retinaculum *(arrowheads)* (*curved arrows*, collapsed joint recess). LC, lateral femoral condyle; MC, medial femoral condyle; P, patella.

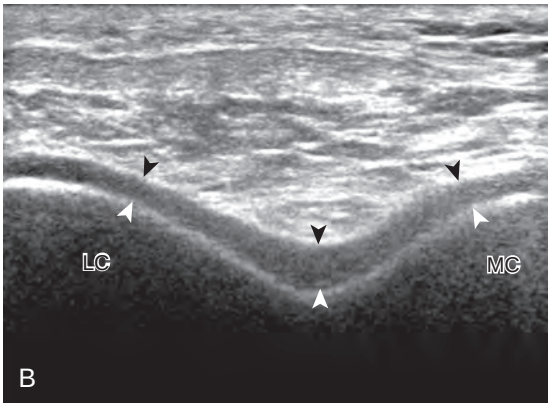

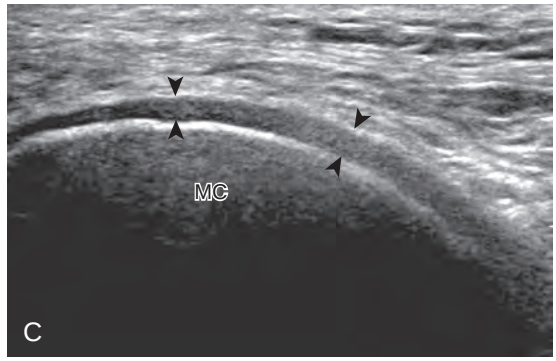

FIGURE 7-7 ■ Trochlear and femoral condyle cartilage. A, With knee flexion, **(B)** transverse imaging and **(C)** parasagittal imaging show hypoechoic hyaline cartilage *(arrowheads)*. LC, lateral femoral condyle; MC, medial femoral condyle.

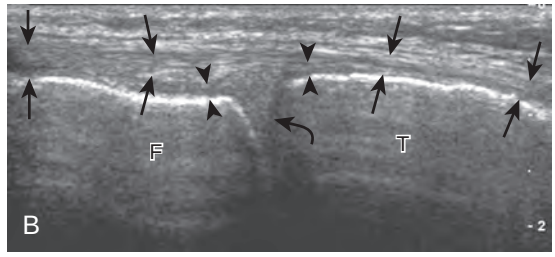

FIGURE 7-8 ■ Medial knee evaluation: coronal plane. A, Coronal imaging at the medial joint line shows **(B)** the superficial *(arrows)* and deep *(arrowheads)* layers of the medial collateral ligament (*curved arrow*, body of medial meniscus). F, femur; T, tibia.

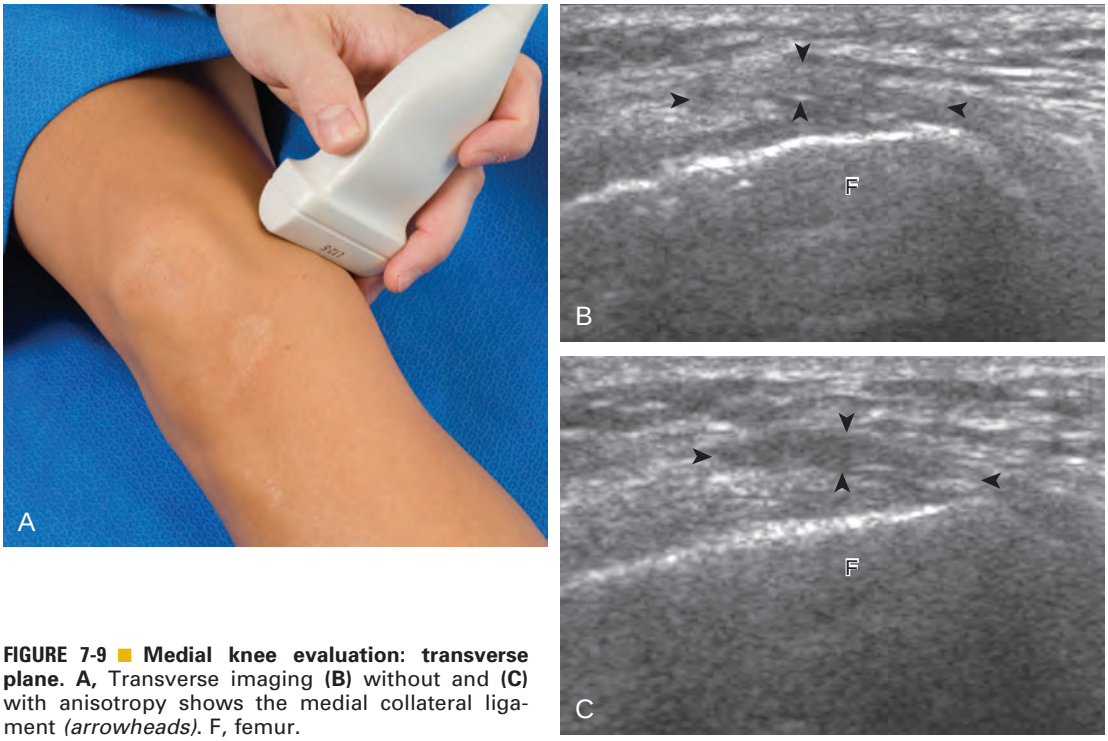

FIGURE 7-9 ■ Medial knee evaluation: transverse plane. A, Transverse imaging **(B)** without and **(C)** with anisotropy shows the medial collateral ligament *(arrowheads)*. F, femur.

hyperechoic deep layers of the medial collateral ligament, also called the *meniscofemoral* and *meniscotibial ligaments*, are identified from the meniscus to the femur and tibia, respectively (see Fig. 7-8B). The fibrocartilage meniscus is identified as a triangular hyperechoic structure between the femur and the tibia. The transducer is then moved anteriorly from the coronal plane to the oblique-sagittal plane to visualize the anterior horn of the medial meniscus.

Returning back to the coronal plane long axis to the tibial collateral ligament, the transducer is moved distally beyond the joint line along the tibial collateral ligament and slightly anterior to its attachment on the tibia, about 4 to 5 cm beyond the joint line (Fig. 7-10A). Here, the pes anserinus can be seen as three hyperechoic tendons superficial to the tibial collateral ligament that converge onto the tibia. Toggling the transducer is often helpful because this will cause the tendons of the pes anserinus superficial to the tibial collateral ligament to appear hypoechoic from anisotropy and be more conspicuous. By turning the transducer to the oblique-axial plane along the long axis of each pes anserinus tendon, the individual sartorius, gracilis, and semitendinosus tendons can be seen; they extend to their tibial attachment as the pes anserinus (see Fig. 7-10B). The more proximal aspects of the pes anserinus tendons can also be visualized when the

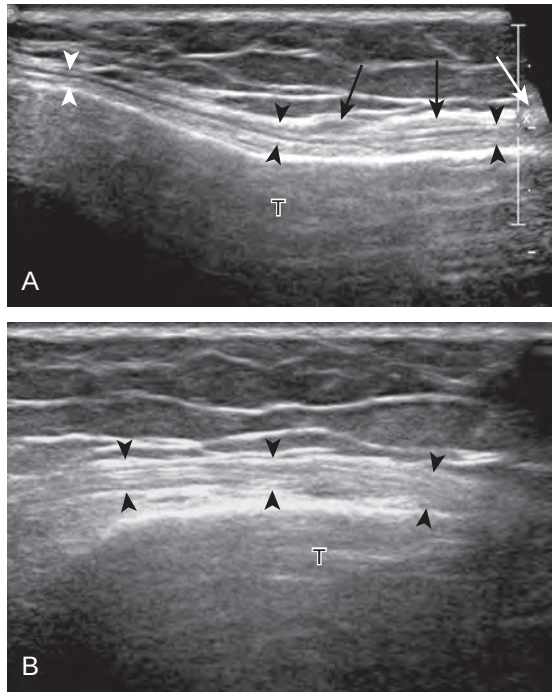

FIGURE 7-10 ■ Distal medial collateral ligament and pes anserinus. Coronal imaging distal to knee joint shows **(A)** the superficial layer of the medial collateral ligament *(arrowheads)* and the tendons of the pes anserinus *(arrows)* (T, tibial metaphysis). **B,** Imaging in long axis to semitendinosus proximal to pes anserinus shows normal tendon *(arrowheads)*.

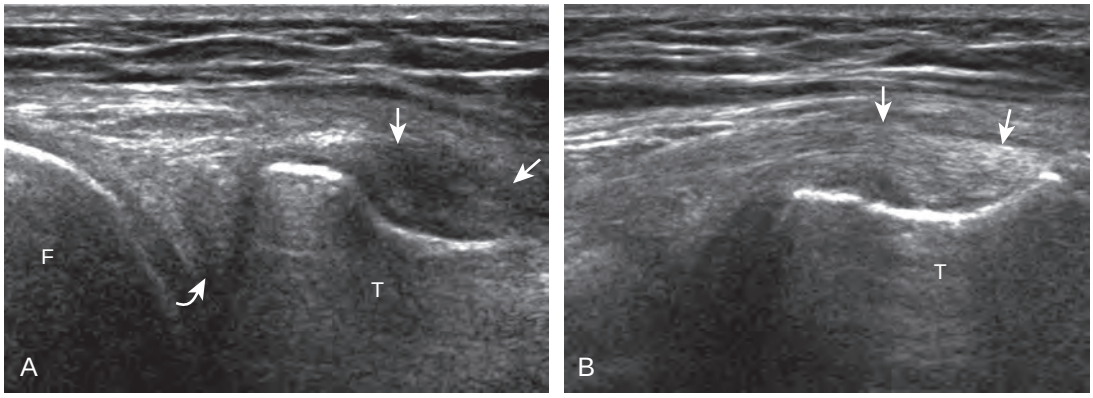

FIGURE 7-11 ■ Semimembranosus: pseudocyst appearance. Coronal-oblique imaging at the posteromedial joint line shows **(A)** a hypoechoic round area *(arrows)*, which represents anisotropy of the distal semimembranosus tendon at its tibial attachment. **B,** This area *(arrows)* becomes hyperechoic and fibrillar with repositioning of the transducer. Note characteristic bone contour of tibia (T) at semimembranosus tendon attachment (*curved arrow*, medial meniscus with intrameniscal abnormality). F, femur.

posterior knee is evaluated. One potential pitfall in evaluation of the posterior aspect of the medial meniscus body is misinterpretation of the adjacent semimembranosus tendon anisotropy as a meniscal cyst. Identification of a hypoechoic round structure just distal to the meniscus with an associated groove in the tibial cortex represents anisotropy of the semimembranosus tendon at its tibial insertion (Fig. 7-11). The normal semimembranosus tendon may be confirmed with the transducer repositioned long axis and perpendicular to the tendon to demonstrate the normal hyperechoic and fibrillar echotexture.

Lateral Evaluation

For evaluation of the lateral knee structures, the leg is internally rotated, or the patient rolls partly onto the contralateral side. Structures of interest laterally include the iliotibial tract, the lateral (or fibular) collateral ligament, the biceps femoris tendon, the supporting structures of the posterolateral corner of the knee, and the common peroneal nerve. To begin, the transducer may be initially placed over the anterior knee long axis to the patellar tendon. The transducer is then moved laterally (Fig. 7-12A). As one leaves the patellar

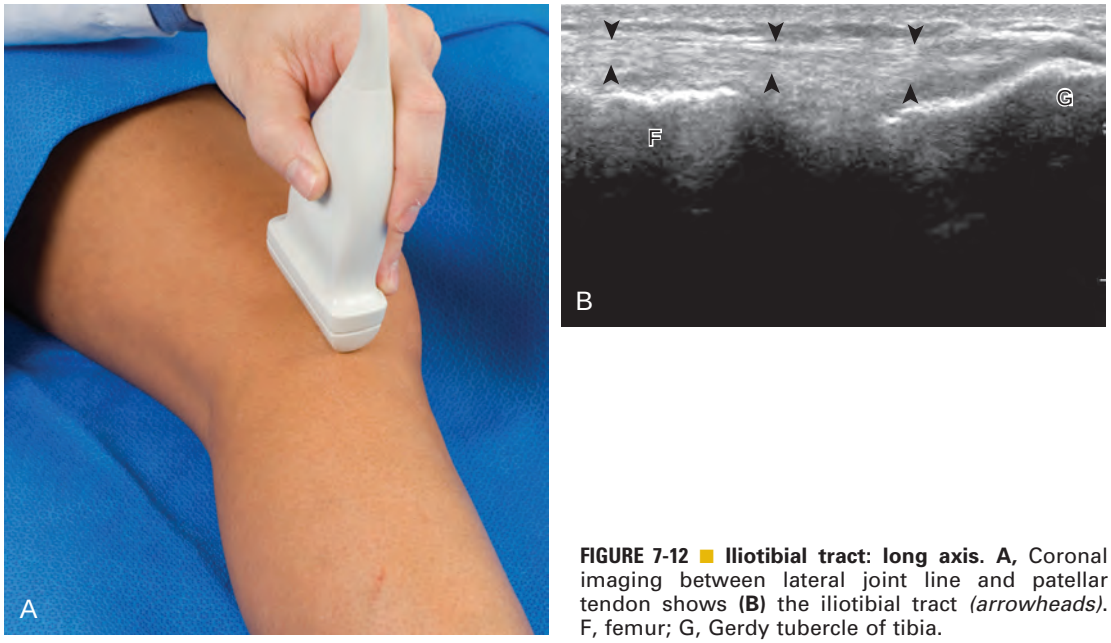

FIGURE 7-12 ■ Iliotibial tract: long axis. A, Coronal imaging between lateral joint line and patellar tendon shows **(B)** the iliotibial tract *(arrowheads)*. F, femur; G, Gerdy tubercle of tibia.

tendon, the next fibrillar structure identified is the iliotibial tract or band, which inserts on the Gerdy tubercle of the proximal tibia (see Fig. 7-12B). It is important to evaluate the tissues between the iliotibial tract and the distal femur more proximally for disorders related to iliotibial band friction syndrome. Next, the transducer is moved laterally to the coronal plane over the lateral femoral condyle. At this location, an important bony landmark is identified: the groove or sulcus for the popliteus tendon.[14] After this groove is identified, the proximal aspect of the transducer is fixed to the femur while the distal aspect is rotated posteriorly toward the fibular head (Fig. 7-13A). In this position, the hyperechoic and fibrillar echotexture of the lateral collateral ligament is seen, which extends from the lateral femoral condyle to the lateral aspect of the fibular head (see Fig. 7-13B and C). The proximal aspect of the lateral collateral ligament extends over the popliteus tendon located within the femoral groove. The distal insertion on the fibula may appear thickened and heterogeneous owing to the bifurcating distal biceps femoris tendon seen both superficial and deep to the lateral collateral ligament (see Fig. 7-13C).[15] One must be aware that slight valgus angulation of the knee joint may cause a wavy appearance to the lateral collateral ligament and possible anisotropy. This can be minimized with the patient positioned so that the opposite knee is flexed under the knee being examined; this position places the knee in slight varus angulation.

After the transducer is moved along the lateral collateral ligament to its fibular attachment, the distal aspect of the transducer is fixed to the fibular head while the proximal aspect is rotated posteriorly to the coronal plane (Fig. 7-14A) to bring the biceps femoris tendon into view; this tendon is differentiated from ligament by the less compact fibrillar echotexture and the associated hypoechoic muscle more proximally (see Fig. 7-14B). Both the lateral collateral ligament and the biceps femoris tendon insert onto the lateral aspect of the proximal fibula. The distal biceps femoris may appear heterogeneous as fibers bifurcate both superficial and deep to the lateral collateral ligament at the fibula, which should not be mistaken for tendinosis (see Fig. 7-13C).[15] As the transducer is then moved posteriorly from the biceps femoris in the coronal plane, the relatively hypoechoic appearance of the common peroneal nerve can be seen in long axis (Fig. 7-15A), although the more proximal aspect is best evaluated from a posterior approach with the patient prone in short axis. Evaluation of the posterolateral aspect of the knee proximal to the fibula demonstrates the relative locations of the lateral

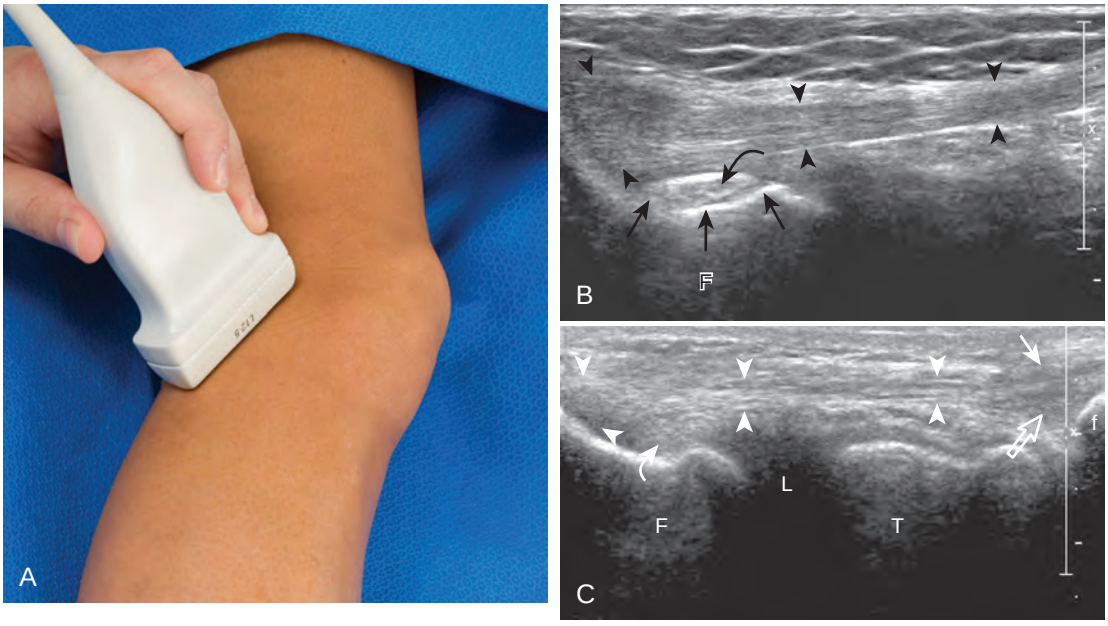

FIGURE 7-13 ■ Lateral collateral ligament. A, Coronal-oblique imaging shows **(B** and **C)** characteristic contours *(arrows)* of the femur (F) adjacent to the popliteus tendon *(curved arrow)* and proximal lateral collateral ligament *(arrowheads)*. Note superficial *(arrow)* and deep *(open arrow)* heads of bifurcating biceps femoris tendon in **C.** f, fibula; L, lateral meniscus; T, tibia.

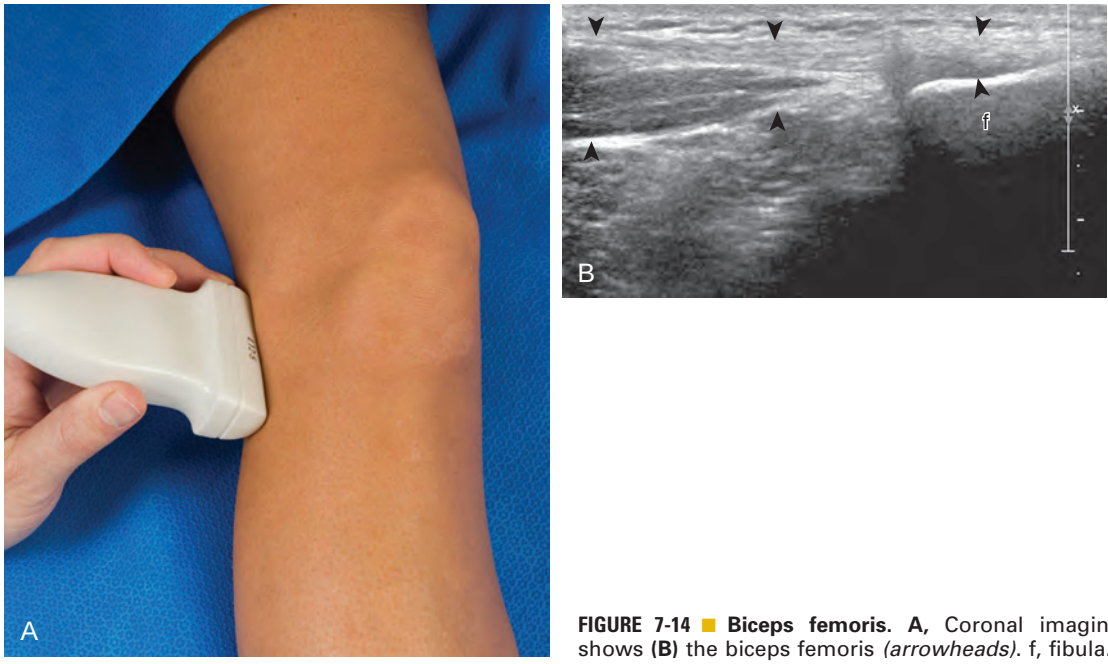

FIGURE 7-14 ■ Biceps femoris. A, Coronal imaging shows **(B)** the biceps femoris *(arrowheads)*. f, fibula.

collateral ligament, the biceps femoris, and the common peroneal nerve (see Fig. 7-15B).

Returning to the popliteus groove in the lateral femoral condyle in the coronal plane, the popliteus tendon may be followed as it curves posteriorly around the joint. The adjacent hyperechoic fibrocartilage body and anterior horn of the lateral meniscus may also be evaluated. Because of the curved course of the popliteus tendon, this tendon is assessed in segments to avoid misinterpretation of hypoechoic anisotropy as tendon abnormality (Fig. 7-16A). The popliteus muscle is best evaluated from a posterior approach, in which the muscle belly is located between the tibia and the tibial vessels (see Posterior Evaluation). Finally, a hyperechoic extension from the popliteus tendon at the joint line may be seen, which attaches to the fibular styloid, called the *popliteofibular ligament* (see Fig. 7-16B).[16] Other supporting structures of the posterolateral corner, such as the arcuate ligament and the possible fabellofibular ligament, are difficult to identify.

Posterior Evaluation

To evaluate the posterior structures of the knee, the patient is turned prone. The structures and pathology of interest include a Baker cyst, the posterior horns of the menisci, the cruciate

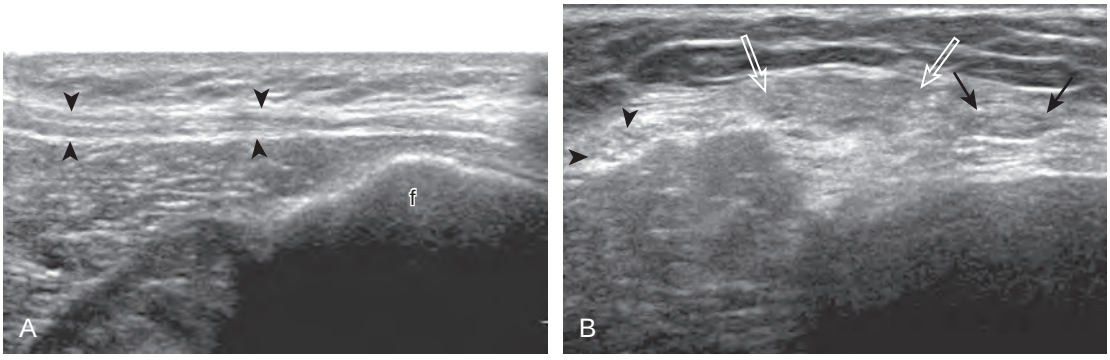

FIGURE 7-15 ■ Common peroneal nerve. Coronal imaging posterior to biceps femoris shows **(A)** the common peroneal nerve *(arrowheads)* (f, fibula). Transverse imaging proximal to the fibula shows **(B)** the lateral collateral ligament *(arrows)*, biceps femoris *(open arrows)*, and common peroneal nerve *(arrowheads)* in short axis (left side of image is posterior).

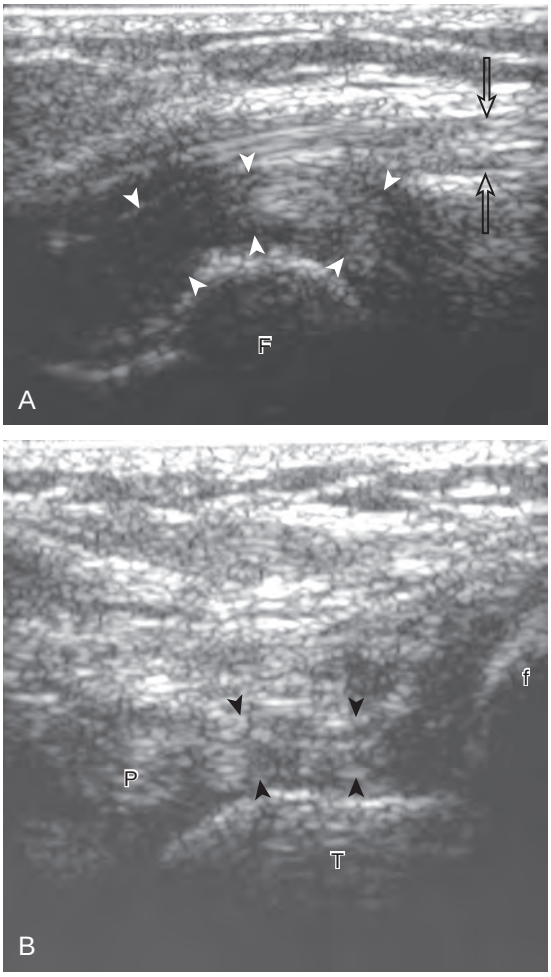

FIGURE 7-16 ■ Popliteus and popliteofibular ligament. Imaging long axis to the proximal popliteus tendon shows **(A)** the popliteus tendon *(arrowheads)* and lateral collateral ligament *(open arrows)* (F, femur). Coronal imaging shows **(B)** the popliteofibular ligament *(arrowheads)* between the popliteus tendon (P) and the fibula (f). T, tibia. (**B,** From Sekiya JK, Jacobson JA, Wojtys EM: Sonographic imaging of the posterolateral structures of the knee: findings in human cadavers. *Arthroscopy* 18:872–881, 2002.)

ligaments, and the neurovascular structures of the posterior knee. Examination begins with evaluation for a Baker cyst. One technique is to initially place the transducer in the transverse plane over the mid-calf (Fig. 7-17A).[4] At this location, three distinct muscles are identified: the soleus anteriorly and the medial and lateral heads of the gastrocnemius muscle superficially (see Fig. 7-17B). The transducer is then moved superiorly along the medial aspect of the medial head of the gastrocnemius muscle (see Fig. 7-17C). As the transducer approaches the knee joint, the distinct hyperechoic semimembranosus tendon is identified just medial to the medial head of the gastrocnemius tendon and muscle over the medial femoral condyle (see Fig. 7-17D). This is the location where distention of a semimembranosus-medial gastrocnemius bursa or Baker cyst is seen. The smaller round and hyperechoic tendon of the semitendinosus is also seen in short axis directly superficial to the semimembranosus tendon. The course of the medial head of the gastrocnemius tendon is not parallel to that of the semimembranosus tendon; therefore, it may be difficult to have both tendons appear hyperechoic in the same plane. One pitfall is incorrect interpretation of the semimembranosus tendon or the medial head of gastrocnemius tendon anisotropy as a small Baker cyst (Fig. 7-18A and B).[4] Toggling the transducer while imaging the tendons in short axis can create anisotropy (helping to identify the tendons) and eliminate anisotropy (avoiding the pitfall interpreting anisotropy as a Baker cyst) (Video 7-1). If a Baker cyst is identified, the transducer is then turned in the sagittal plane to evaluate the extent of the Baker cyst and to assess for rupture (see Fig. 7-17E). The semitendinosus can also be imaged from this point distally to its insertion at the pes anserinus.

The transducer is then moved over the medial aspect of the posterior knee in the sagittal plane (Fig. 7-19A). At this location, the posterior horn of the medial meniscus is evaluated; this structure normally appears hyperechoic and triangular (see Fig. 7-19B). It may be important to use a lower-frequency transducer (5 or 7 MHz) to assess the posterior horns of the menisci and cruciate ligaments adequately. Toward the medial aspect of the medial meniscus posterior horn, the semimembranosus can be seen as it inserts on the posteromedial tibial cortex, just beyond the meniscus at a prominent concavity or sulcus in the bone. With anisotropy, the normal semimembranosus tendon may appear hypoechoic and may potentially simulate a meniscal cyst (see Fig. 7-11). The transducer is then moved toward the midline in the sagittal plane, and the posterior cruciate ligament is seen with its attachment to the posterior tibia, identified by characteristic bone contours (see Fig. 7-19C). The normal posterior cruciate ligament may appear artifactually hypoechoic as a result of anisotropy, but its thickness should be uniform and less than 1 cm.[17] Anisotropy of the posterior cruciate ligament may be reduced with the heel-toe maneuver or the use of beam steering (available on some ultrasound machines). The transducer is then moved laterally to assess the posterior horn of the lateral meniscus, although accurate identification of pathology is difficult in this location because

FIGURE 7-17 ■ **Posterior knee evaluation: Baker cyst. A,** Transverse imaging over the mid calf shows **(B)** the soleus (S), medial head of gastrocnemius (MG), and lateral head of gastrocnemius (LG) muscles. **C,** Transverse imaging over the knee joint shows **(D)** the medial head of gastrocnemius muscle *(arrowheads)* and tendon *(curved arrow)* as well as the semimembranosus tendon *(open arrow)* and semitendinosus tendon *(arrow)* (left side of image is medial). Parasagittal imaging over the posteromedial knee shows **(E)** the semimembranosus (SM), medial head of gastrocnemius (MG) and semitendinosus (ST). F, femur.

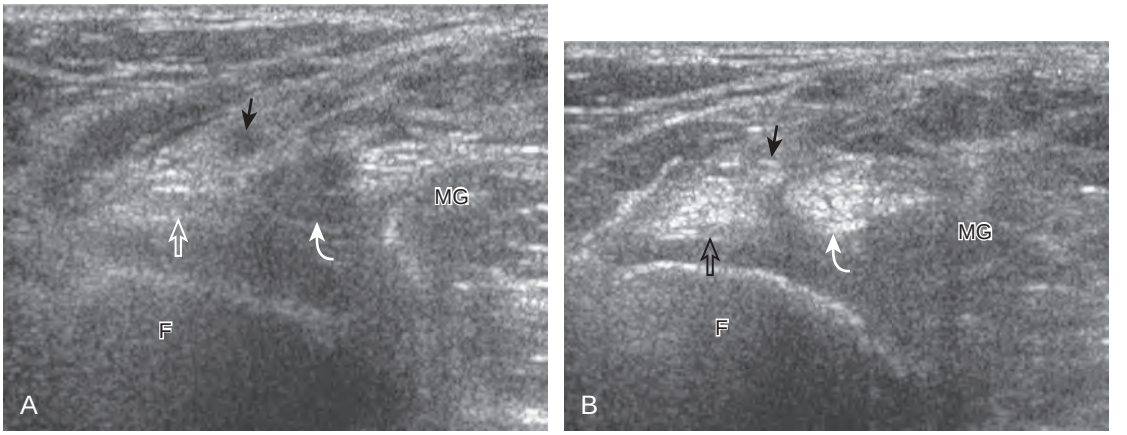

FIGURE 7-18 ■ Semimembranosus anisotropy: pseudo-Baker cyst. Transverse imaging **(A** and **B)** shows anisotropy of the medial head of gastrocnemius tendon *(curved arrows)*, which may simulate a small Baker cyst (*arrows*, semitendinosus tendon; *open arrows*, semimembranosus tendon). F, femur; MG, medial head of gastrocnemius muscle.

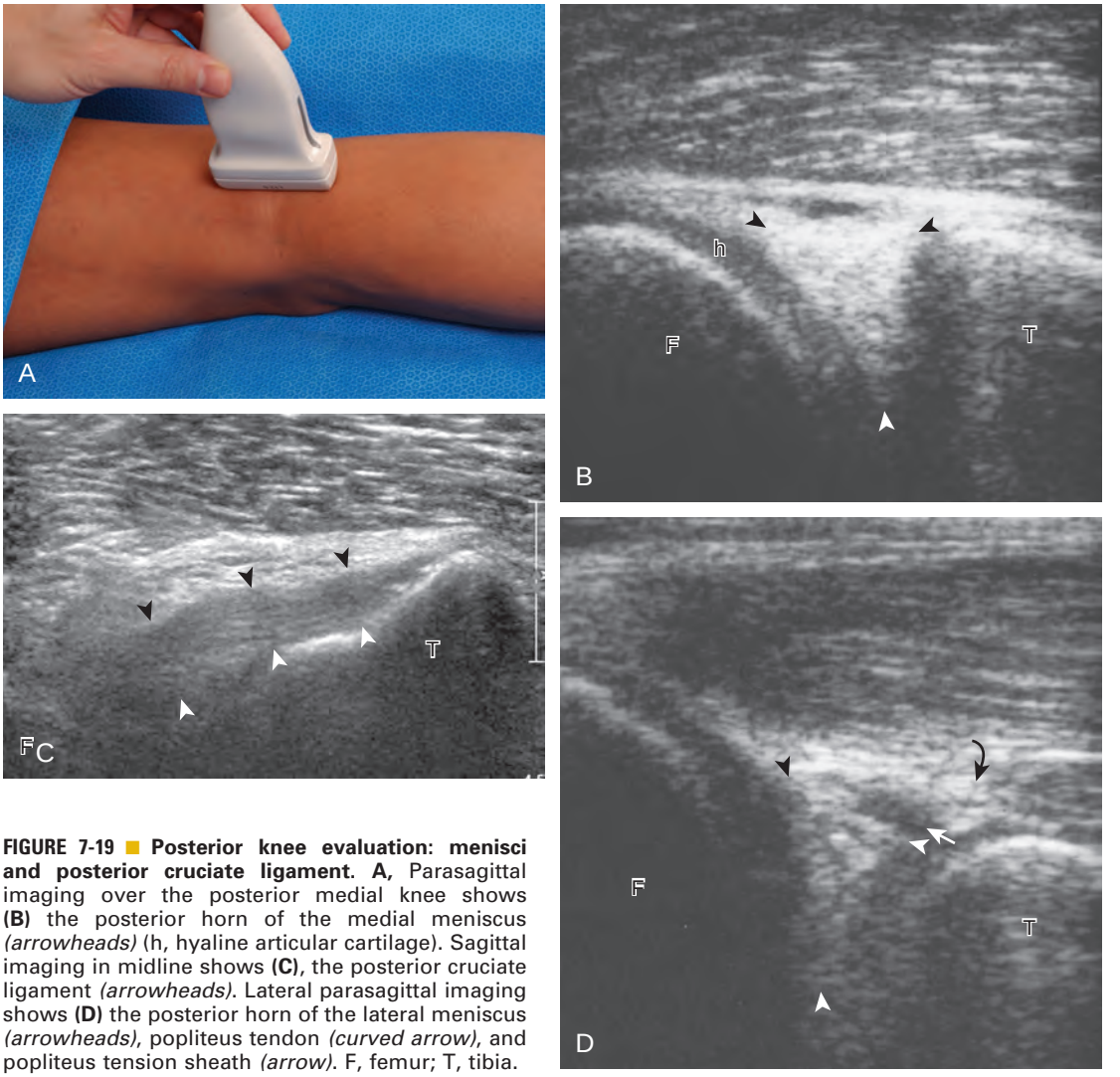

FIGURE 7-19 ■ Posterior knee evaluation: menisci and posterior cruciate ligament. A, Parasagittal imaging over the posterior medial knee shows **(B)** the posterior horn of the medial meniscus *(arrowheads)* (h, hyaline articular cartilage). Sagittal imaging in midline shows **(C)**, the posterior cruciate ligament *(arrowheads)*. Lateral parasagittal imaging shows **(D)** the posterior horn of the lateral meniscus *(arrowheads)*, popliteus tendon *(curved arrow)*, and popliteus tension sheath *(arrow)*. F, femur; T, tibia.

the popliteus tendon and sheath cross at the peripheral aspect of the lateral meniscus (see Fig. 7-19D).

The transducer is then turned to the transverse plane and is positioned over the intercondylar notch (Fig. 7-20A). Normally, this space should be hyperechoic, which contains the anterior cruciate ligament along the lateral aspect and the adjacent hyperechoic fat (see Fig. 7-20B).[18] Identification of the anterior cruciate ligament may be improved by toggling the transducer because the normal ligament becomes hypoechoic relative to the adjacent hyperechoic fat as a result of anisotropy. Finally, the popliteal artery and vein are evaluated in short axis and long axis. The muscle belly of the popliteus is located between these vessels and the tibia (Fig. 7-20C). The tibial nerve can be followed proximally to its junction with the common peroneal nerve at the sciatic nerve, which is evaluated with the posterior thigh. Although the sciatic nerve demonstrates a honeycomb appearance from hypoechoic nerve fascicles and surrounding hyperechoic connective tissue, the smaller peripheral nerve branches may consist of only a few hypoechoic fascicles.

JOINT ABNORMALITIES

Joint Effusion and Synovial Hypertrophy

Increased joint fluid in the knee is characterized by anechoic or hypoechoic distention of the suprapatellar recess. With slight knee flexion, joint recess distention preferentially occurs deep to the quadriceps tendon (Fig. 7-21), where fluid extends superiorly from between the patella and the femur. In the setting of a small joint effusion, often joint fluid is only identified superolateral to the patella with the knee in flexion, so this area should always be assessed. In knee extension, joint distention may be seen only medial or more likely lateral to the patella in the transverse plane (Fig. 7-22).[19] When imaging these areas, it is important not to apply too much pressure with the transducer because this can collapse the joint recess and displace the joint fluid out of view (Video 7-2). Joint fluid may also collect in the popliteus tendon sheath or in a Baker cyst when there is a communication with the posterior knee joint. A superior patellar plica, which typically is

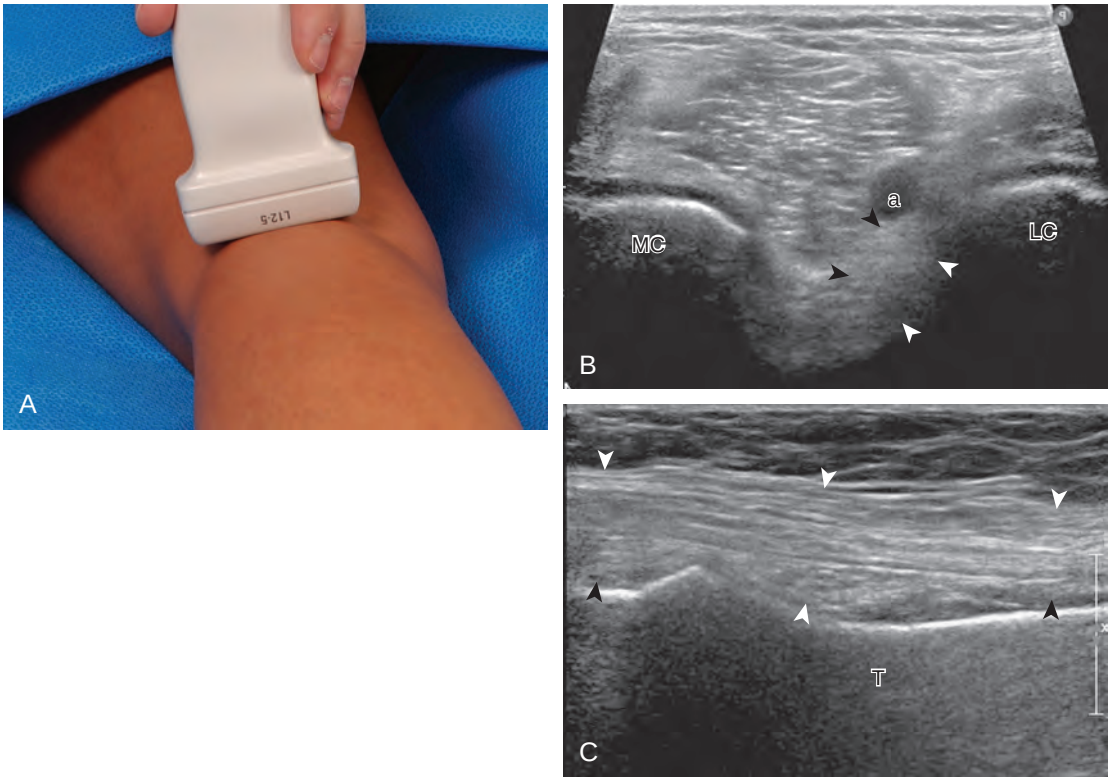

FIGURE 7-20 ■ Posterior knee evaluation: anterior cruciate ligament and popliteus. A, Transverse imaging over the posterior distal femur shows **(B)** anterior cruciate ligament in short axis *(arrowheads)* in the lateral aspect of the intercondylar notch and popliteal artery (a). Transverse-oblique ultrasound shows **(C)** a long axis view of the popliteus tendon and muscle *(arrowheads)*. LC, lateral femoral condyle; MC, medial femoral condyle; T, tibia.

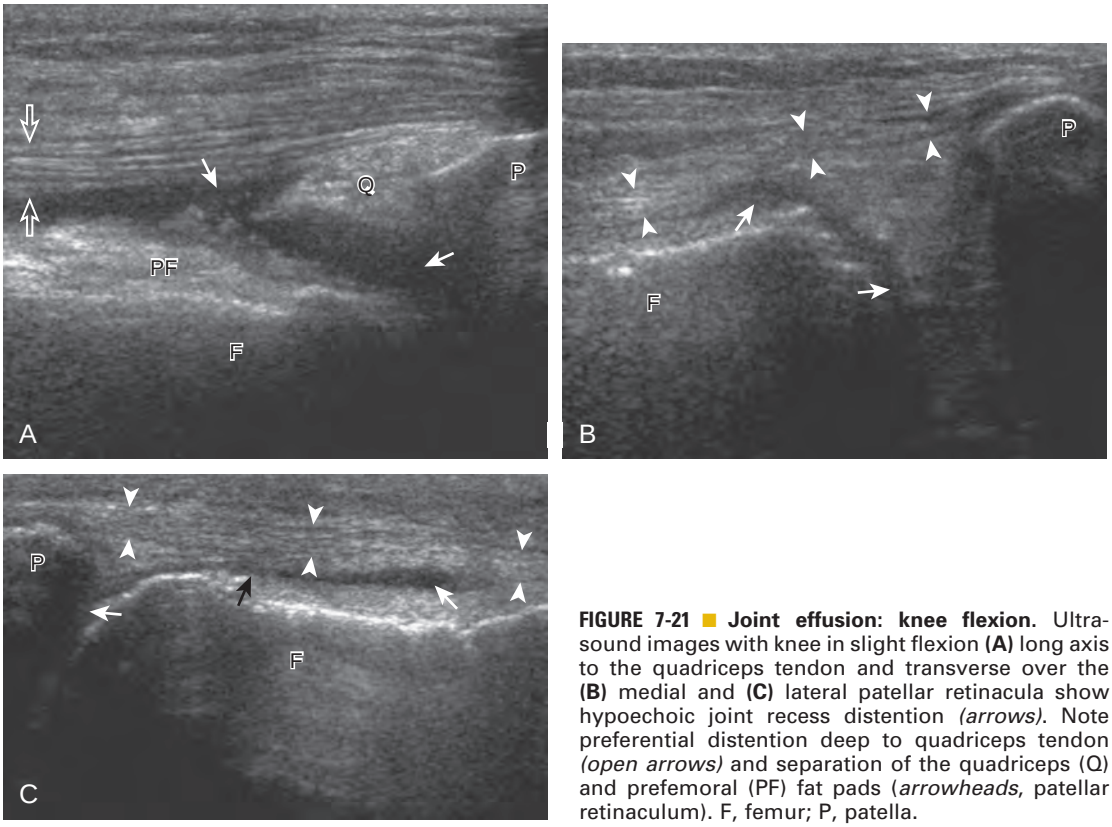

FIGURE 7-21 ■ Joint effusion: knee flexion. Ultrasound images with knee in slight flexion **(A)** long axis to the quadriceps tendon and transverse over the **(B)** medial and **(C)** lateral patellar retinacula show hypoechoic joint recess distention *(arrows)*. Note preferential distention deep to quadriceps tendon *(open arrows)* and separation of the quadriceps (Q) and prefemoral (PF) fat pads (*arrowheads*, patellar retinaculum). F, femur; P, patella.

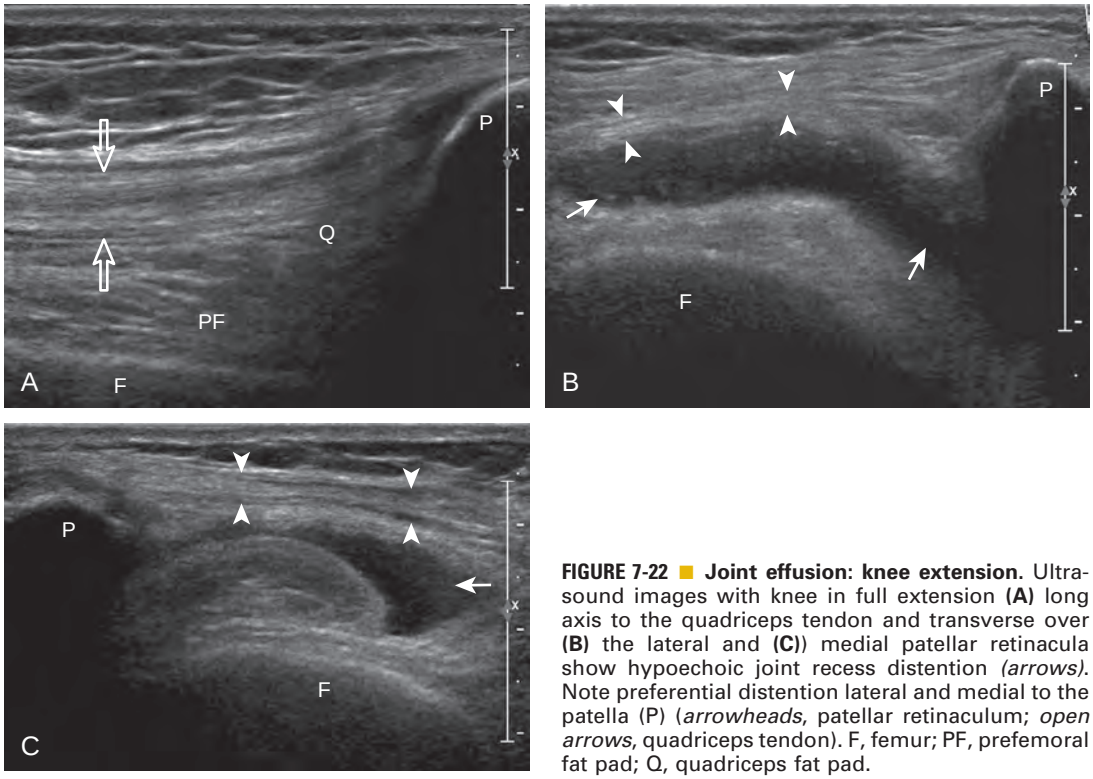

FIGURE 7-22 ■ Joint effusion: knee extension. Ultrasound images with knee in full extension **(A)** long axis to the quadriceps tendon and transverse over **(B)** the lateral and **(C)**) medial patellar retinacula show hypoechoic joint recess distention *(arrows)*. Note preferential distention lateral and medial to the patella (P) (*arrowheads*, patellar retinaculum; *open arrows*, quadriceps tendon). F, femur; PF, prefemoral fat pad; Q, quadriceps fat pad.

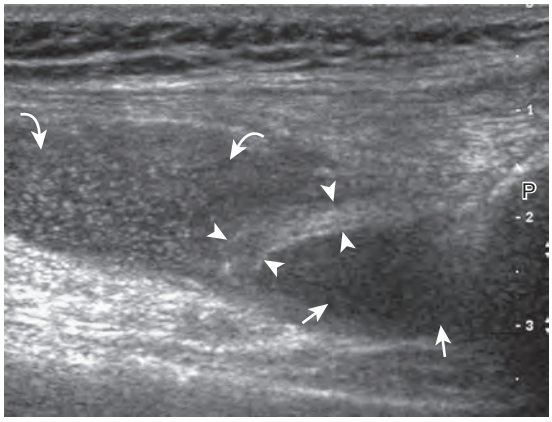

FIGURE 7-23 ■ Superior patellar plica. Ultrasound image long axis to the quadriceps tendon shows the superior plica *(arrowheads)* that separates the superior aspect of the suprapatellar recess (*curved arrow*, distended with hypoechoic complex fluid) from the knee joint (*arrows*, distended with anechoic simple fluid). P, patella.

located in the transverse plane through the suprapatellar recess superior to the patella, may uncommonly completely separate the suprapatellar recess into two compartments (Fig. 7-23). In the setting of an intra-articular fracture, several layers of varying echogenicity within the joint may be visible as a lipohemarthrosis (Fig. 7-24).[20]

The causes of joint effusion are many; however, ultrasound including color or power Doppler imaging cannot distinguish between aseptic and septic effusion (Figs. 7-25 and 7-26). If joint recess distention is not anechoic but rather

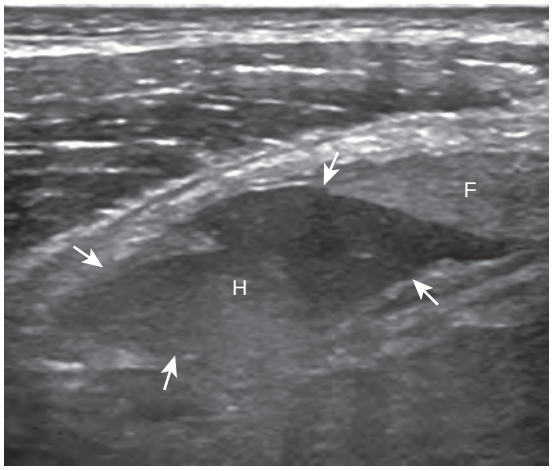

FIGURE 7-24 ■ Lipohemarthrosis. Ultrasound image over lateral aspect of suprapatellar recess shows layering of echogenic fat (F) superficial to intra-articular hemorrhage *(arrows)* and more dependent hematocrit level separating serum from blood cells (H).

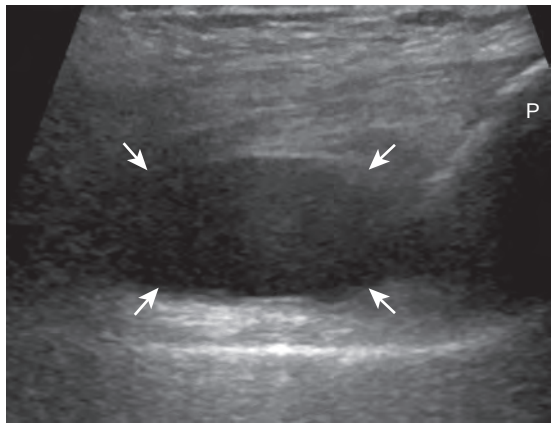

FIGURE 7-25 ■ Joint effusion: infection. Ultrasound image long axis to quadriceps tendon shows hypoechoic distention of the suprapatellar recess *(arrows)*. Note increased through-transmission. P, patella.

hypoechoic, isoechoic, or hyperechoic to muscle, then considerations include complex fluid versus synovial hypertrophy. Compressibility of the joint recess, redistribution of recess contents or swirling of the contents with compression or joint movement, and lack of internal flow on color or power Doppler imaging all suggest complex fluid rather than synovial hypertrophy.[21] The differential diagnosis for complex fluid includes inflammation (including infection) (see Fig. 7-26) and hemorrhage (Fig. 7-27; see Fig. 7-24). If there is concern for infection, percutaneous aspiration should be considered. Inflammatory synovial hypertrophy may be associated with cortical erosions, characterized by cortical irregularity and discontinuity, often associated with increased blood flow on color or power Doppler imaging. Although synovial hypertrophy may also result from inflammation, such as rheumatoid arthritis and crystal deposition (Fig. 7-28), synovial proliferative disorders such as pigmented villonodular synovitis[22] (Fig. 7-29), lipoma arborescens,[23] and synovial osteochondromatosis[24] are other considerations, with possible hyperechoic foci seen in the last condition. The differential diagnosis for mixed hyperechoic and hypoechoic tissue associated with the suprapatellar recess with compressible vascular channels is synovial hemangioma (see Vascular Abnormalities).[25] Localized nodular synovitis may also occur in the knee joint recesses, and it typically appears hypoechoic and noncompressible with possible increased through-transmission (Fig. 7-30).[26] Dynamic imaging may demonstrate snapping of synovial hypertrophy. In the setting of a total knee arthroplasty, abnormal synovial hypertrophy may cause snapping, termed *patellar clunk*

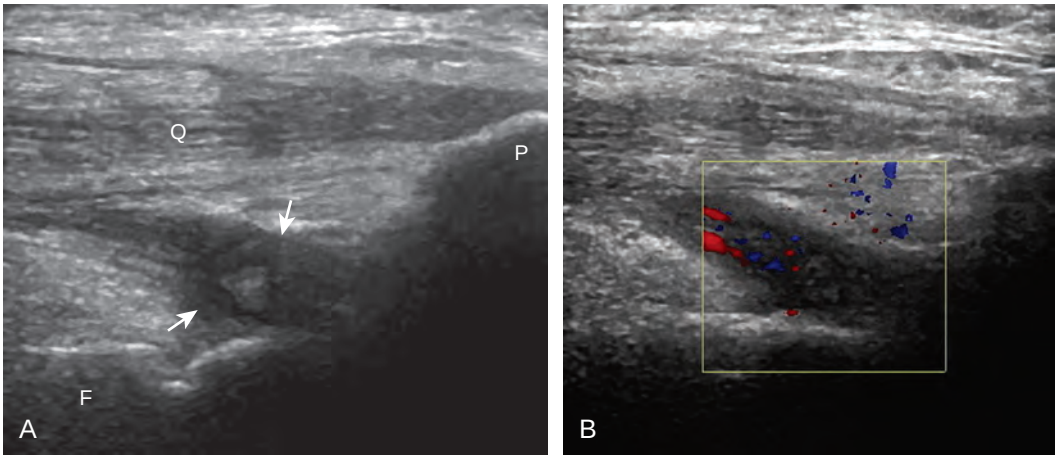

FIGURE 7-26 ■ Joint effusion: infection *(Pseudomonas)*. Ultrasound images **(A** and **B)** long axis to quadriceps tendon show heterogeneous distention of the suprapatellar recess *(arrows)* from complex fluid and synovial hypertrophy with increased flow on color Doppler imaging **(B)**. F, femur; P, patella; Q, quadriceps femoris tendon.

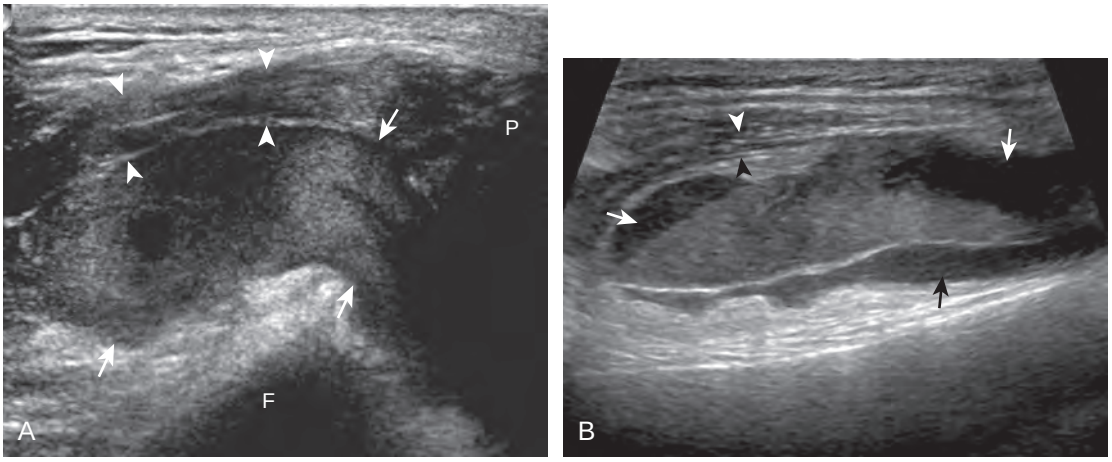

FIGURE 7-27 ■ Intra-articular hemorrhage. Ultrasound images **(A** and **B)** in the transverse plane over the lateral patellar retinaculum in two different patients show mixed-echogenicity hemorrhagic joint fluid *(arrows)* (*arrowheads*, patellar retinaculum, which is abnormally thickened in **A**). Note increased through-transmission. F, femur; P, patella.

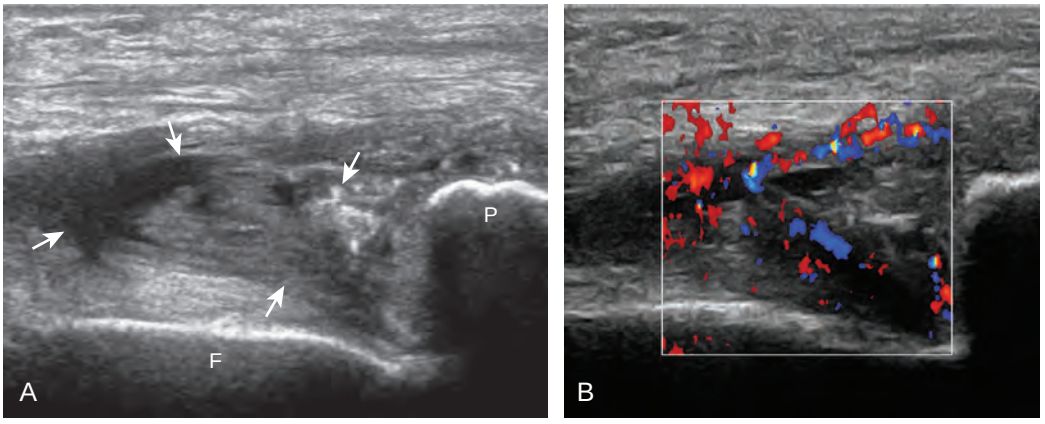

FIGURE 7-28 ■ Pseudogout (calcium pyrophosphate dihydrate deposition disease). Ultrasound images **(A** and **B)** long axis to quadriceps tendon show heterogeneous distention of the suprapatellar recess *(arrows)* from synovial hypertrophy and complex fluid with increased flow on color Doppler imaging. F, femur; P, patella.

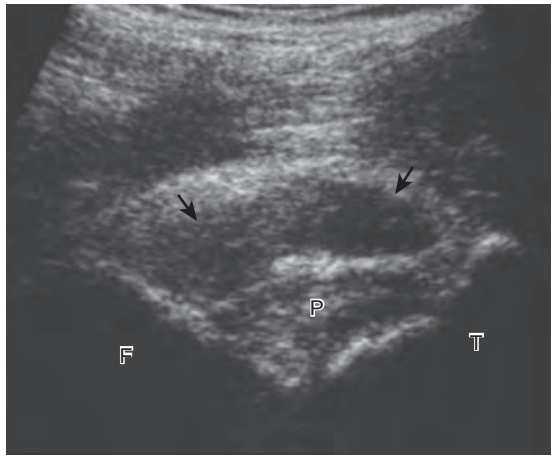

FIGURE 7-29 ■ Pigmented villonodular synovitis. Ultrasound image in the sagittal plane over the posterior knee shows hypoechoic synovial hypertrophy *(arrows)* adjacent to posterior cruciate ligament (P). F, femur; T, tibia.

syndrome (Fig. 7-31) (Video 7-3).[27] Within joint fluid, hyperechoic and shadowing intra-articular bodies may be identified, commonly in a Baker cyst (see Baker Cyst) or suprapatellar recess (Fig. 7-32). When an intra-articular body is identified, the hyaline articular cartilage should be evaluated for a donor site (Fig. 7-33).

Cartilage Abnormalities

One common cause of joint effusion is a cartilage abnormality. Meniscal degeneration may appear as heterogeneous or internal hypoechogenicity, whereas meniscal tear appears as a well-defined anechoic or hypoechoic cleft that extends to the articular surface, or possibly meniscal irregularity and truncation (Fig. 7-34). Sensitivity and specificity for diagnosis of meniscal tears using ultrasound have been described as 85% and 86%, respectively.[28] Because ultrasound is limited with respect to evaluation of the knee menisci as a result of incomplete or poor visualization, magnetic resonance imaging (MRI) remains the imaging method of choice for evaluation of the menisci.[29] However, evaluation of the menisci can be accomplished in minutes, and pathologic features are often seen. The posterior horn of the medial meniscus is the most common site for tears, so evaluation should be at least considered here. Meniscal tears often are associated with

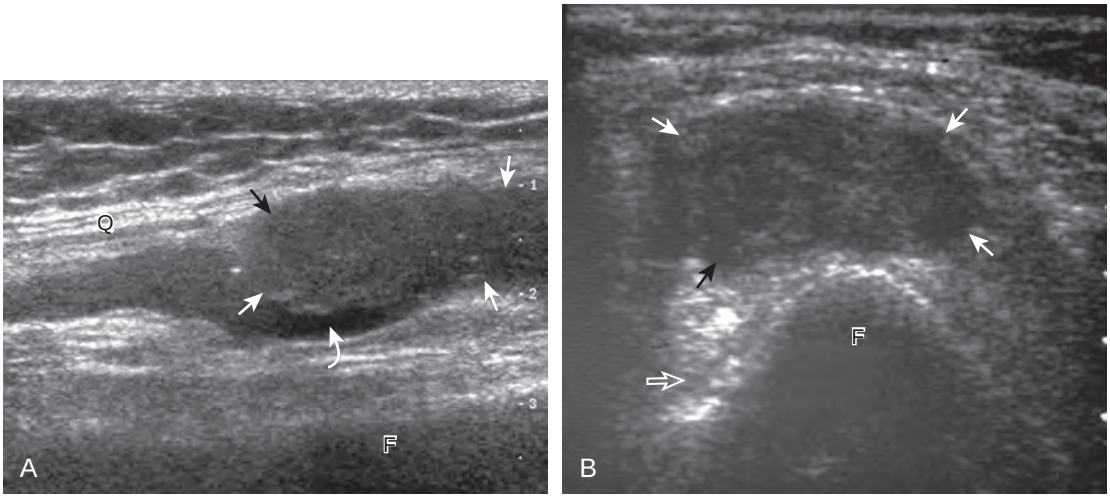

FIGURE 7-30 ■ Localized nodular synovitis. Ultrasound images from two different patients (**A** and **B**) show hypoechoic synovial hypertrophy within the suprapatellar recess *(arrows)*. Note joint effusion (*curved arrow* in **A**) and increased through-transmission (*open arrow* in **B**). F, femur; Q, quadriceps tendon.

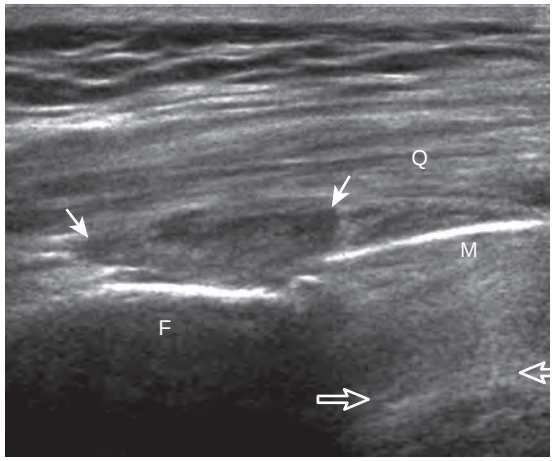

FIGURE 7-31 ■ Patellar clunk syndrome. Ultrasound image long axis to quadriceps tendon (Q) shows hypoechoic synovial hypertrophy *(arrows)*, which moved and produced a snapping sensation with knee flexion and extension. Note hyperechoic metal component of total knee arthroplasty (M) with hyperechoic posterior reverberation *(open arrows)*, and native femur (F) with shadowing (right side of image is distal).

FIGURE 7-32 ■ Intra-articular body. Ultrasound image long axis to quadriceps tendon shows hyperechoic and shadowing ossified intra-articular body *(arrows)* within the suprapatellar recess. Note anechoic joint fluid *(curved arrow)*. P, patella.

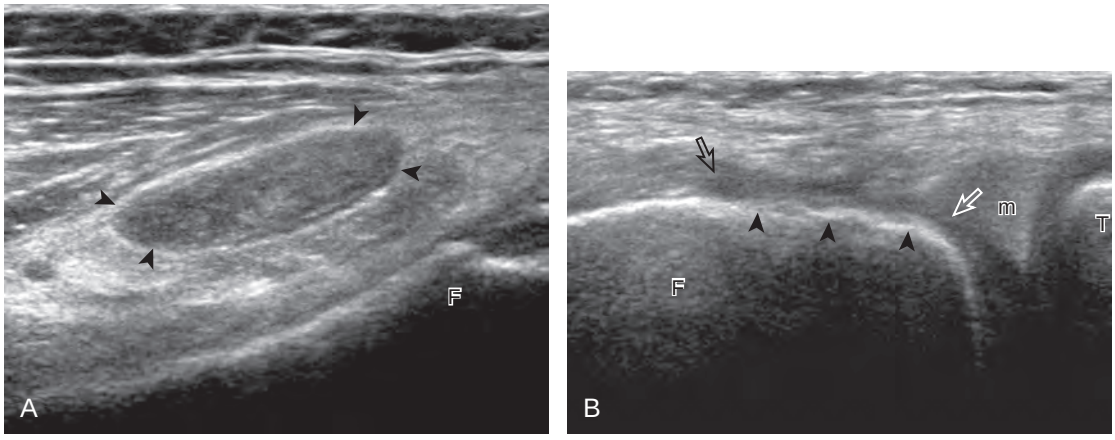

FIGURE 7-33 ■ Intra-articular body. Ultrasound image over the lateral aspect of the suprapatellar recess shows **(A)** a well-defined hypoechoic noncalcified intra-articular body *(arrowheads)*. Ultrasound image over the anterior aspect of the medial femoral condyle shows **(B)** cortical irregularity *(arrowheads)* and a cartilage defect (*between open arrows*). F, femur; m, medial meniscus; T, tibia.

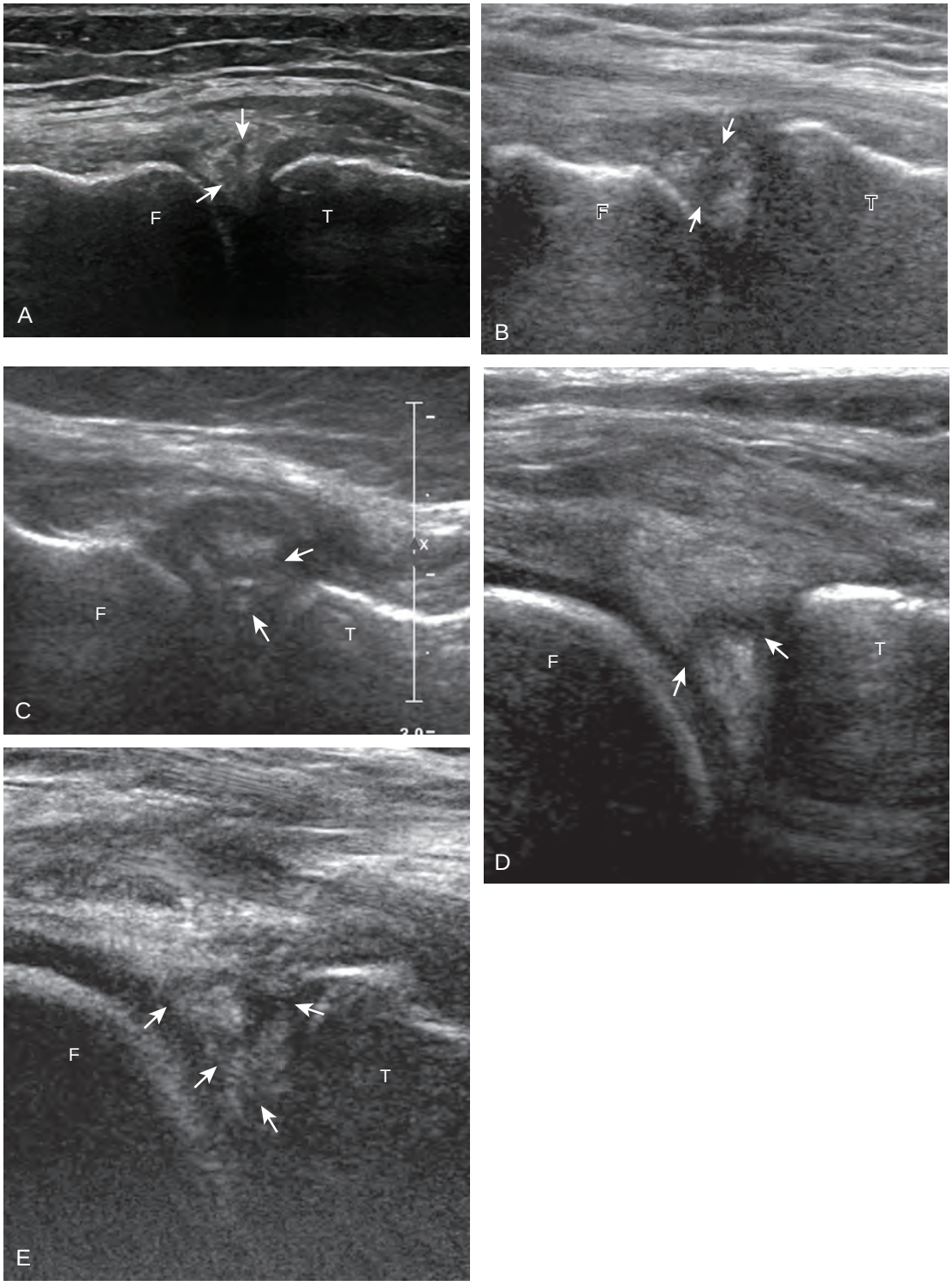

FIGURE 7-34 ■ Meniscal abnormalities. A, Coronal ultrasound image of medial meniscus body shows intrameniscal abnormality. Ultrasound images from four different patients of the **(B)** medial meniscus body, **(C)** lateral meniscus body,**(D** and **E)** posterior horns of medial meniscus show meniscal tears as hypoechoic or anechoic clefts *(arrows)* that extend to the meniscal articular surface. Note macerated or degenerative appearance of the meniscus in **E**. F, femur; T, tibia.

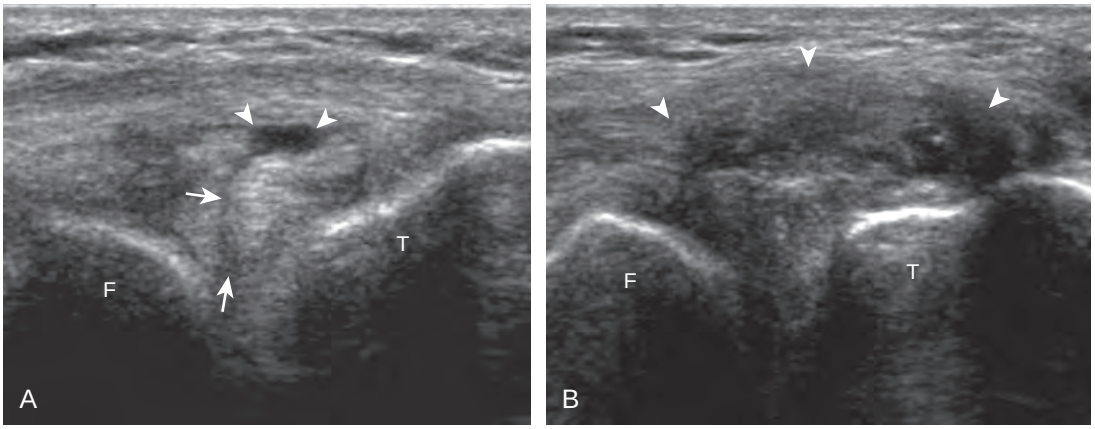

FIGURE 7-35 ■ Parameniscal cyst: lateral. Coronal ultrasound image over body of lateral meniscus shows **(A)** hypoechoic meniscal tear *(arrows)* in connection with anechoic parameniscal cyst *(arrowheads)*. Ultrasound image posterior to **(A)** shows **(B)** hypoechoic heterogeneous appearance of parameniscal cyst *(arrowheads)*. F, femur; T, tibia.

pain with transducer pressure directly over the abnormality.

Parameniscal cysts can be diagnosed at ultrasound with a reported accuracy of 88%.[30] They are typically associated with an adjacent meniscal tear, although parameniscal cysts adjacent to the anterior horn of the lateral meniscus are less likely to have an associated meniscal tear.[31] Parameniscal cysts are usually multilocular and characteristically are located at the joint line at the base of the meniscus (Fig. 7-35).[30] Whereas some parameniscal cysts are anechoic with increased through-transmission, others are complex cysts and are hypoechoic (Fig. 7-36).[32] Small meniscal cysts may be located within the meniscus; larger parameniscal cysts can be quite extensive and typically are associated with a meniscal tear. A medial parameniscal cyst may extend some distance from the meniscal tear, so the possible diagnosis of parameniscal cyst should be considered with any multilocular cyst around the knee, and possible meniscal extension should always be sought. It is important not to misinterpret the normal semimembranosus tendon insertion on the adjacent tibia as a parameniscal cyst; this tendon often appears oval and hypoechoic in evaluation of the posterior horn medial meniscus as a result of anisotropy given the oblique course of the tendon (see Fig. 7-11).

In addition to meniscal tear and degeneration, other meniscal pathology includes meniscal extrusion in the setting of osteoarthritis

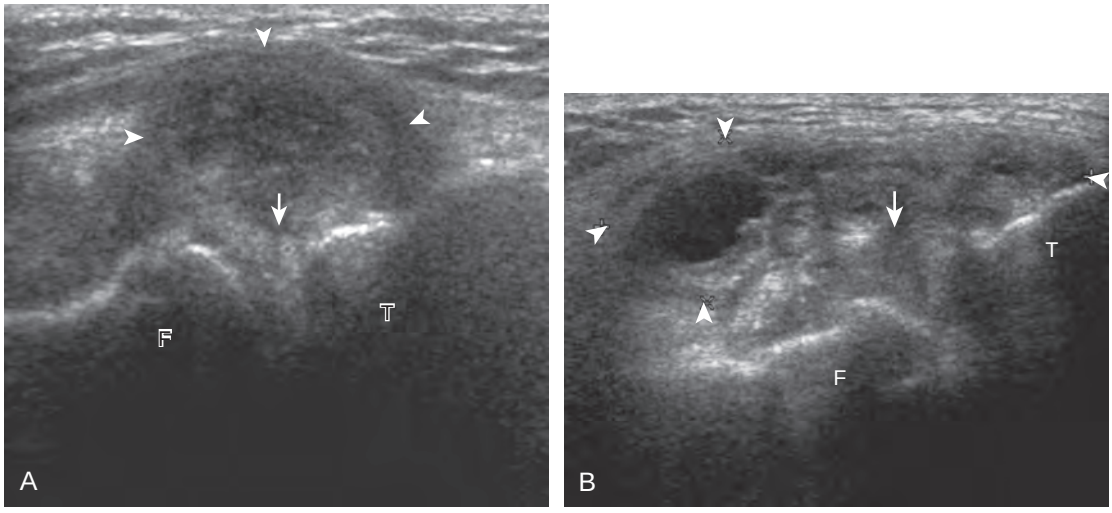

FIGURE 7-36 ■ Parameniscal cyst. Ultrasound images over the **(A)** anterior horn medial meniscus and **(B)** anterior horn lateral meniscus show hypoechoic parameniscal cyst *(arrowheads)*, which is in contact with the base of the meniscus and meniscal tear *(arrow)*. F, femur; T, tibia.

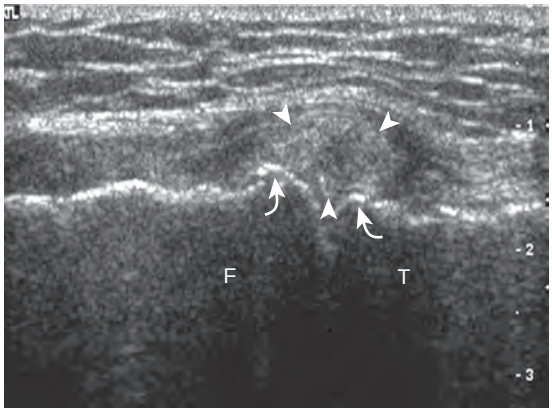

FIGURE 7-37 ■ Meniscal extrusion. Coronal ultrasound image over the medial joint shows abnormal hypoechoic meniscus *(arrowheads)* with joint space narrowing and meniscal extrusion medial to the tibia (T) (*curved arrows*, osteophyte). F, femur.

(Fig. 7-37).[33] Abnormal displacement of the meniscus relative to the tibia is often appreciated in the coronal plane deep to the tibial collateral ligament, where associated edema of the tibial collateral ligament is possible.[34] In contrast to medial meniscal extrusion, extrusion of the anterior horn and body of the lateral meniscus may be a variation of normal.[35] Abnormal symptomatic meniscal displacement may occur with knee flexion and extension and be visualized dynamically (Video 7-4).[36] One hallmark of osteoarthritis is the osteophyte, which can be reliably assessed at the knee with ultrasound.[37]

Other cartilage abnormalities may involve the hyaline articular cartilage, such as cartilage thinning or defect (Fig. 7-38; see Fig. 7-33B).[37-39] In the setting of osteoarthritis, femoral articular cartilage thickness is best assessed in knee flexion in the parasagittal plane and correlates with MRI to a better degree than imaging of the trochlear cartilage in the transverse plane.[13] If an intra-articular body is identified, the hyaline cartilage should be evaluated for a defect as a potential donor site.[40] Another cartilage abnormality relates to deposition of calcification, which can involve both the fibrocartilage meniscus (Fig. 7-39) and the hyaline articular cartilage (Fig. 7-40). Calcification deposition within cartilage is seen as hyperechoic foci and occurs in pseudogout (calcium pyrophosphate dihydrate crystal deposition disease), among other conditions.[41,42] Unlike

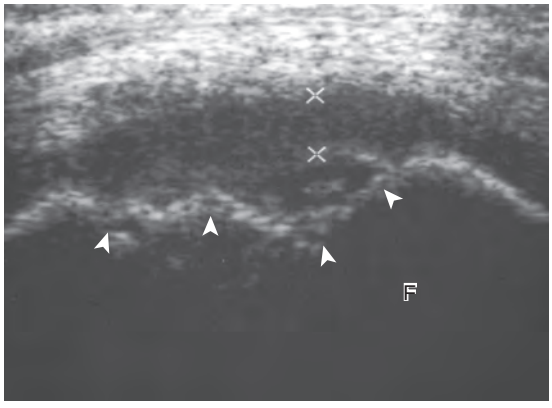

FIGURE 7-38 ■ Osteochondral abnormality. Ultrasound image over the anterior femoral condyle shows subchondral bone plate irregularity *(arrowheads)* and thickened hyaline articular cartilage *(between cursors)*. F, femur.

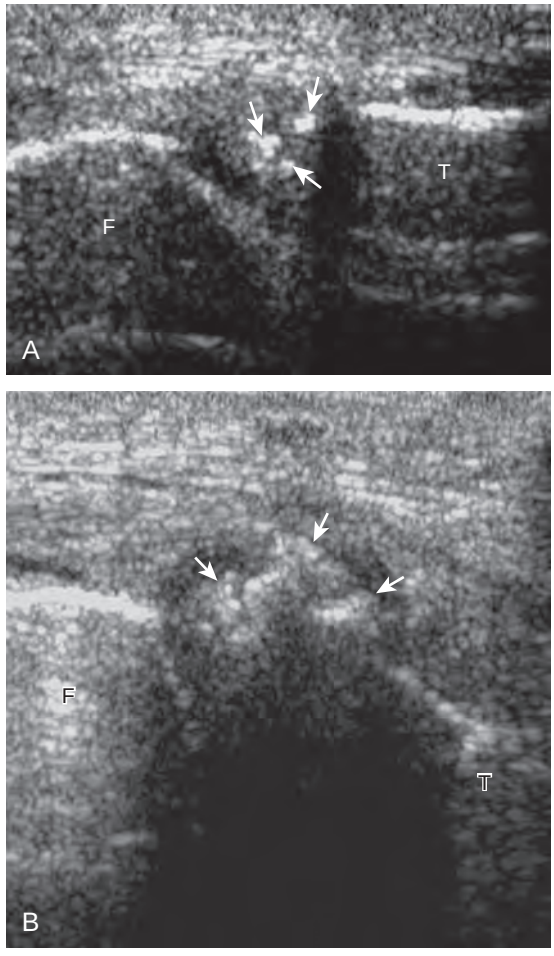

FIGURE 7-39 ■ Chondrocalcinosis: pseudogout. A and **B,** Ultrasound images of the medial meniscus in two different patients show hyperechoic and shadowing chondrocalcinosis *(arrows)* within the meniscus. F, femur; T, tibia.

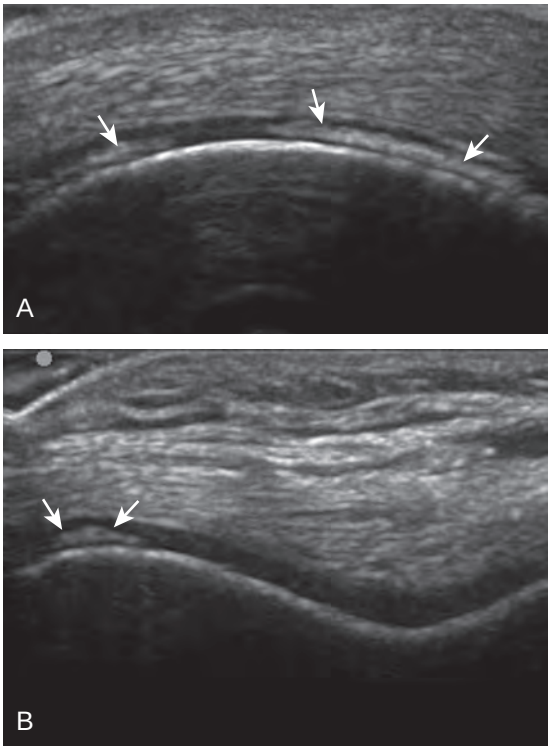

FIGURE 7-40 ■ Chondrocalcinosis: pseudogout. Ultrasound images of the **(A)** anterior femoral condyle and **(B)** trochlea show hyperechoic calcification *(arrows)* within the hypoechoic hyaline cartilage. (Courtesy of R. Thiele, MD, Rochester, NY.)

pseudogout, the deposition of monosodium urate crystals with gout is on the surface of the cartilage (Fig. 7-41), which can be seen on the meniscus (Video 7-5) and hyaline cartilage; the latter, termed the *double contour sign*, disappears when serum urate levels are below 6 mg/dL.[42-44]

TENDON AND MUSCLE ABNORMALITIES

Quadriceps Femoris Injury

Ultrasound is well suited to evaluate the extensor mechanism of the knee because the tendons are superficial and relatively large.[45] With regard to the quadriceps tendon, tendinosis will appear hypoechoic and swollen, with continuous tendon fibers visible and possible calcification and increased flow on color or power Doppler imaging, which often correlates with patient symptoms (Fig. 7-42).[46] The term *tendinosis* is used rather than *tendinitis* because this condition primarily represents a degenerative process without acute inflammatory cells. Partial-thickness tears appear as superimposed, well-defined hypoechoic or anechoic clefts or incomplete disruption of tendon fibers.[47] Partial-thickness tears of the quadriceps tendon may involve only one or two of the three layers while sparing other layers of the quadriceps tendon (Fig. 7-43). Full-thickness tears are characterized by complete tendon disruption, tendon retraction, joint fluid that tracks from the suprapatellar recess through the tendon defect, and secondary wavy appearance of the patellar tendon resulting from a low-lying patella (Fig. 7-44).[48] A retracted tendon stump may show posterior refraction shadowing, or it may be associated with a hyperechoic bone avulsion fragment. A displaced avulsion fracture fragment from the superior patellar pole may be seen in both partial-thickness and full-thickness quadriceps tendon tears.[47] Dynamic imaging during evaluation of the quadriceps tendon is often helpful in the diagnosis of a full-thickness tear because lack of tendon movement

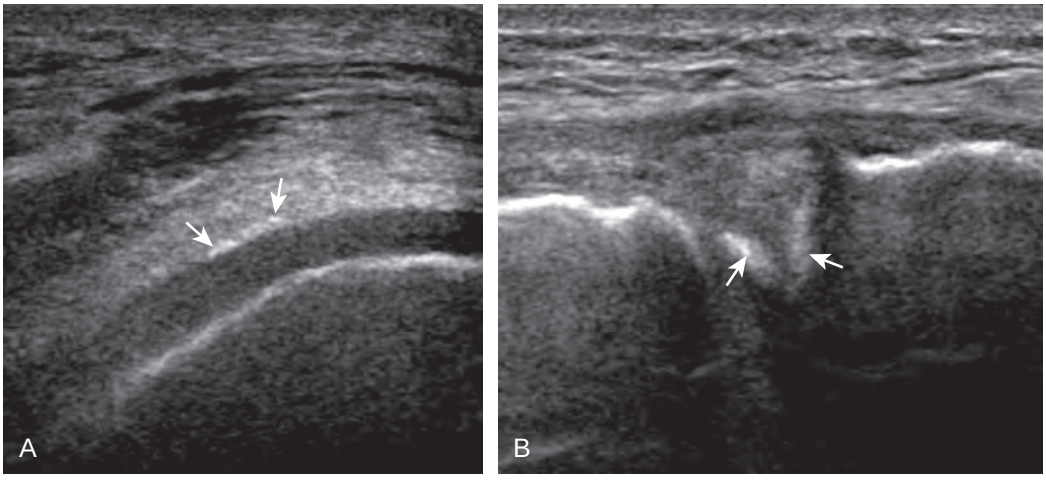

FIGURE 7-41 ■ Gout. Ultrasound images show hyperechoic monosodium urate crystals *(arrows)* on surface of **(A)** anterior femoral condyle hyaline cartilage, and **(B)** medial meniscus body.

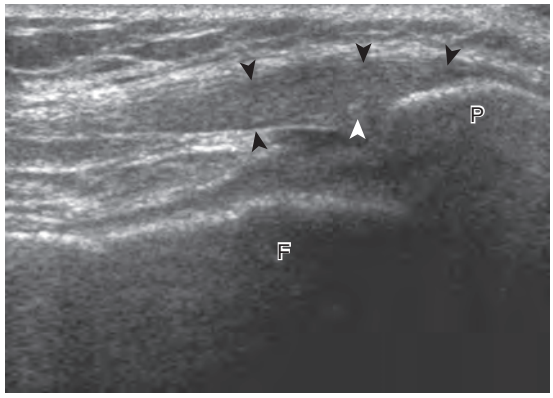

FIGURE 7-42 ■ Quadriceps tendinosis. Ultrasound image long axis to the quadriceps tendon shows hypoechoic thickening of the distal quadriceps tendon *(arrowheads)* without disruption of tendon fibers. F, femur; P, patella.

or translation across the abnormal segment or movement of the tendon stump or avulsion fragment away from the patella indicates complete tear (Video 7-6). Dynamic imaging can be accomplished by squeezing the patient's thigh, slightly flexing the knee, or manually pressing inferiorly on the patella. This method is helpful with a subacute tear, when hemorrhage may fill the torn tendon gap with echogenic material, and also with a chronic tear, in which a complete tear may demonstrate partial healing.

Patellar Tendon Injury

Tendinosis and partial-thickness tears may also involve the proximal patellar tendon, also termed *jumper's knee* (Figs. 7-45 and 7-46). At ultrasound, tendinosis appears as hypoechoic swelling with continuous tendon fibers.[49] The presence of more clearly defined hypoechoic or anechoic clefts suggests a superimposed interstitial tear. Marked hyperemia from neovascularity may be seen with color and power Doppler imaging, which is

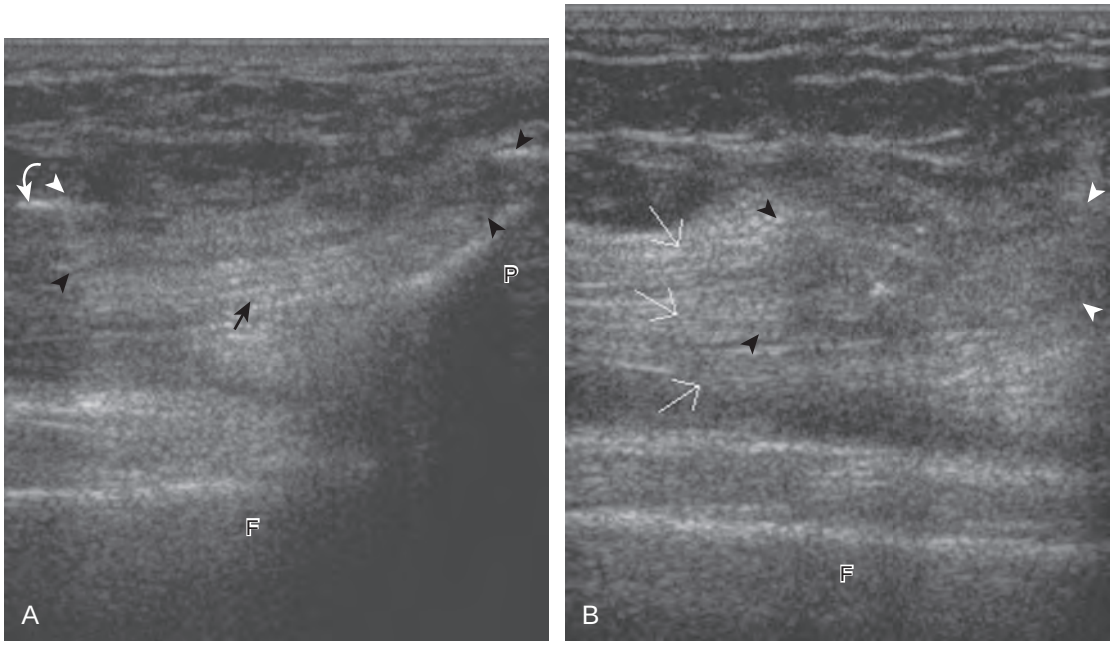

FIGURE 7-43 ■ Quadriceps partial-thickness tear. Ultrasound image long axis to the quadriceps tendon shows **(A)** absence of the superficial aspect of the quadriceps tendon *(arrowheads)* with an intact deep layer *(arrow)*. Note echogenic avulsion bone fragment *(curved arrow)*. Ultrasound image proximal to **A** shows **(B)** full-thickness tears of the superficial layer (rectus femoris) and middle layer (vastus medialis and intermedius) *(arrowheads)* with an intact deep layer (vastus intermedius) (*white arrows* indicate three layers of quadriceps tendon). F, femur; P, patella.

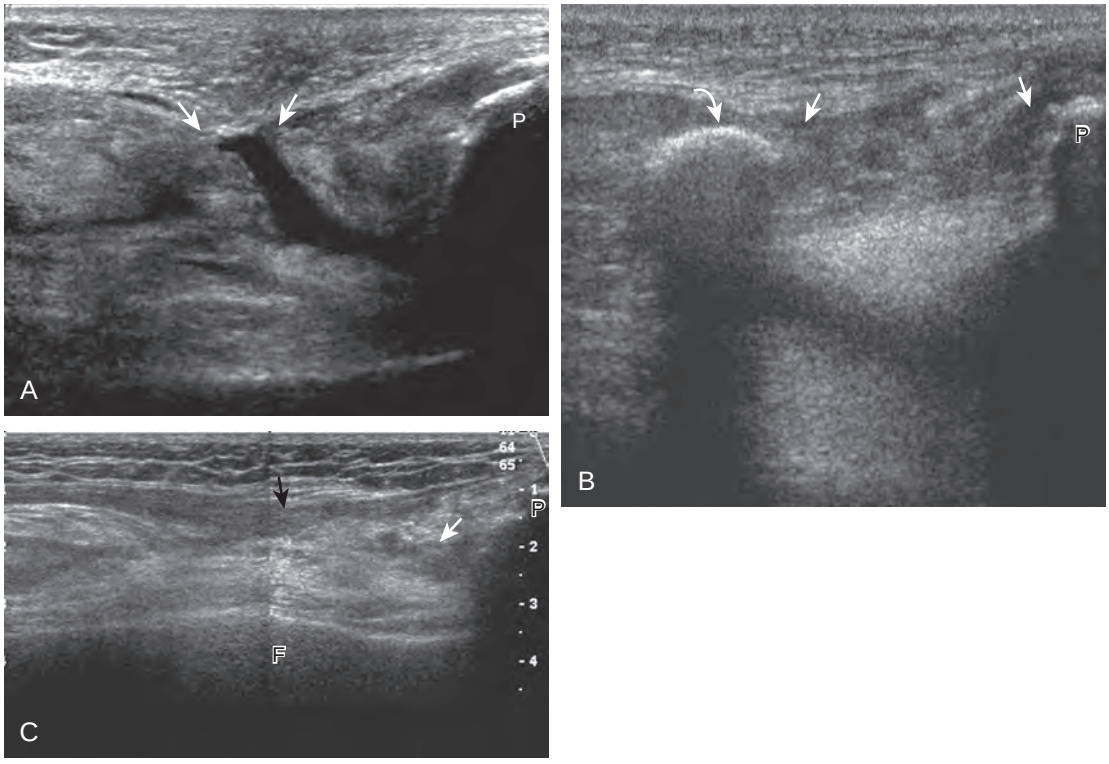

FIGURE 7-44 ■ Quadriceps full-thickness tears. Ultrasound images **(A** to **C)** long axis to the quadriceps tendon from three patients show complete disruption of the quadriceps tendon *(arrows)*. Note superior patellar pole bone avulsion *(curved arrow)* in **B**. F, femur; P, patella.

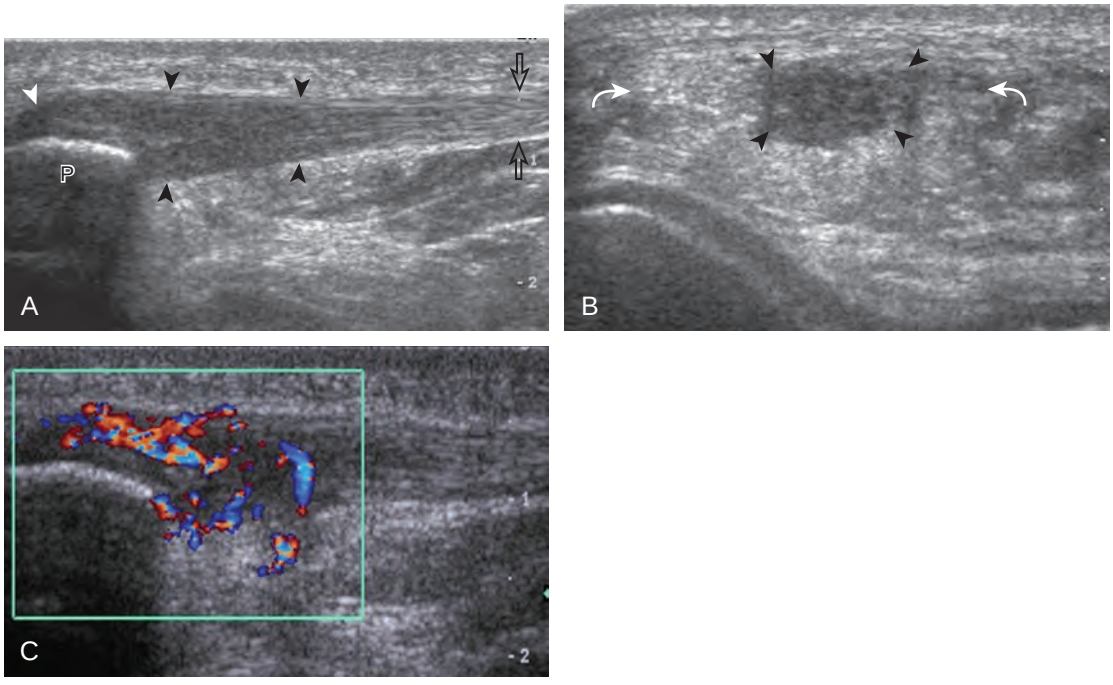

FIGURE 7-45 ■ Patellar tendon tendinosis. Ultrasound images **(A)** long axis and **(B)** short axis to proximal patellar tendon show hypoechoic tendon swelling with intact fibers *(arrowheads)*. Note the normal distal patellar tendon thickness *(open arrows)* in **A** and width of the patellar tendon *(curved arrows)* in **B**. Corresponding long axis color Doppler image is shown in **(C)**. P, patella.

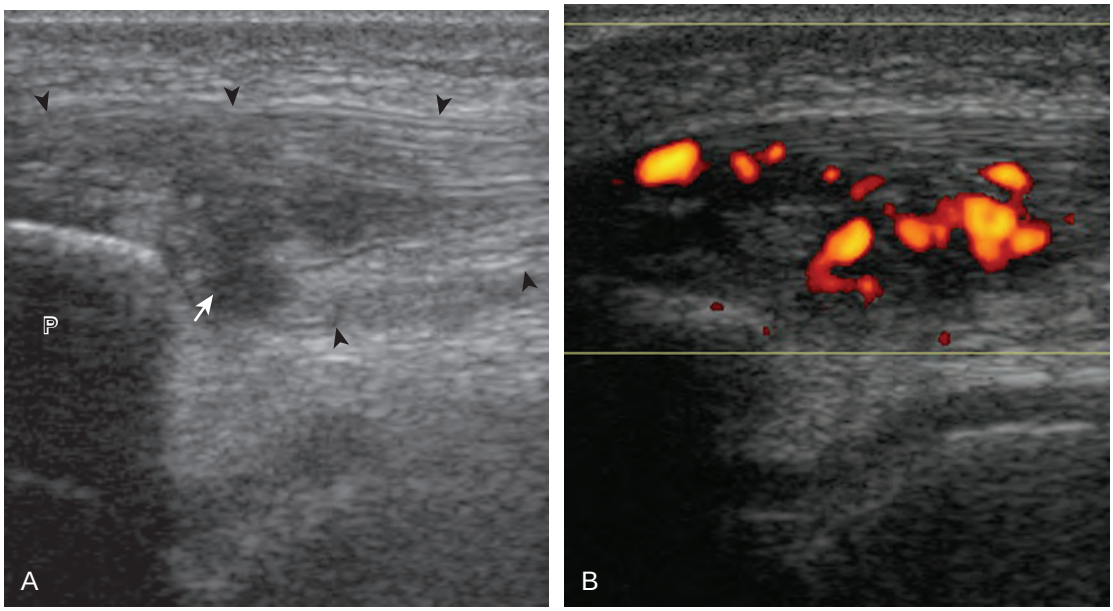

FIGURE 7-46 ■ **Patellar tendon tendinosis. A,** Gray-scale and **(B)** power Doppler ultrasound images long axis to proximal patellar tendon show well-defined hypoechoic areas *(arrow)* within the thickened and hypoechoic tendon *(arrowheads)* consistent with tendinosis. P, patella.

associated with a higher level of pain.[50] In the setting of a penetrating injury or laceration, it is important to assess the abnormal tendon in both long and short axis because spared and intact tendon fibers exclude a full-thickness tear (Fig. 7-47, online). With a full-thickness patellar tendon tear, there is complete tendon fiber discontinuity (Fig. 7-48). Similar to quadriceps tendon tears, tendon retraction, refraction shadowing at the torn tendon stump, and a wavy patellar tendon may be present; however, the patella may be high-riding in contrast to quadriceps tear, in which the tendon may be positioned low. Dynamic imaging may also be used to confirm tendon discontinuity and to identify tendon retraction in the setting of a full-thickness tendon tear by minimally flexing the knee or by manually pressing superiorly on the patella. Hypoechoic swelling of the distal patellar tendon, swelling of the nonossified cartilage, and possible fragmentation of the tibial tuberosity are consistent with Osgood-Schlatter disease, a painful condition that affects the distal patellar tendon insertion from repetitive trauma in an adolescent (Fig. 7-49).[51] Similar changes may involve the proximal patellar tendon at the inferior

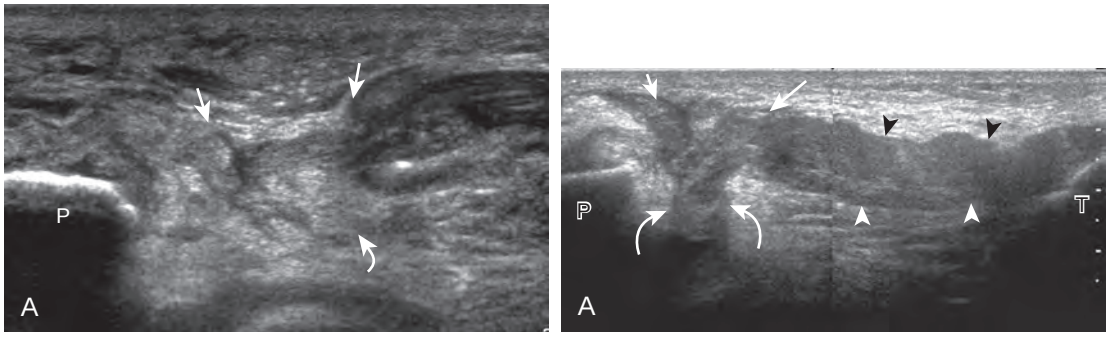

FIGURE 7-48 ■ **Patellar tendon full-thickness tears.** Ultrasound images **(A** and **B)** long axis to the patellar tendon from two patients show complete disruption of the patellar tendon *(arrows)* with refraction shadowing *(curved arrows)* deep to the torn tendon stumps. Note tendon retraction, heterogeneous hemorrhage, and diffuse thickening of the distal patellar tendon *(arrowheads)* in **B**. P, patella; T, tibia.

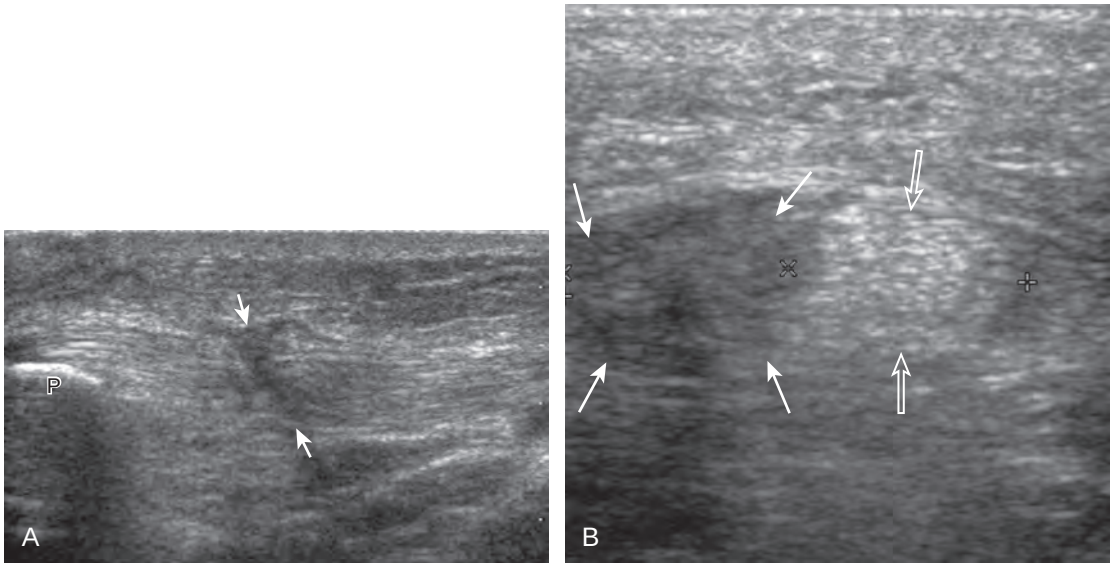

FIGURE 7-47 ■ Patellar tendon partial-thickness tear: laceration. Long axis **(A)** and short axis **(B)** ultrasound images show hypoechoic disruption of the lateral aspect of the patellar tendon *(arrows)* with intact medial fibers *(open arrows)*. P, patella.

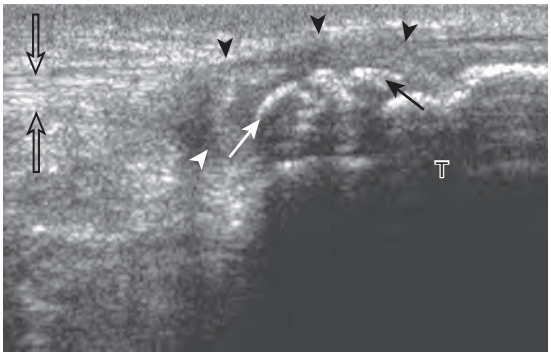

FIGURE 7-49 ■ Osgood-Schlatter disease. Ultrasound image long axis to the distal patellar tendon shows hypoechoic thickening *(arrowheads)* with tibial tuberosity bone fragmentation *(arrows)*. Pain was present with transducer pressure. Note the normal proximal patellar tendon *(open arrows)*. T, tibia.

pole of the patella, termed *Sinding-Larsen-Johansson disease*.[51] A central defect or persistent hypoechoic area in the central patellar tendon may be seen when this segment of the tendon is used for anterior cruciate ligament reconstruction (Fig. 7-50).[52] After total knee arthroplasty, the patellar tendon may be swollen as an expected finding.[53]

Other Knee Tendon Injuries

Other tendon abnormalities around the knee are less common. However, tendinosis may involve the semimembranosus (Fig. 7-51) or biceps femoris. Normal bifurcation of the distal biceps femoris tendon around the lateral collateral ligament should not be confused with tendinosis (see Fig. 7-13C).[15] One other disorder that deserves mention is iliotibial friction band syndrome.[54,55] In this condition, chronic and repetitive contact between the iliotibial tract and the lateral femoral condyle may produce hypoechoic edema, inflammation, and possibly adventitious bursa formation deep to the iliotibial tract, with a possible thickened iliotibial tract (Fig. 7-52). Acute trauma may also cause injury to the iliotibial tract (Fig. 7-53).

Gout

In the setting of gout, the patellar tendon (Fig. 7-54) (Video 7-7) and popliteus tendon (Fig. 7-55) (Video 7-8) are prone to involvement; therefore, these sites should be included when evaluating for inflammatory arthritis. Even with asymptomatic hyperuricemia, involvement of the

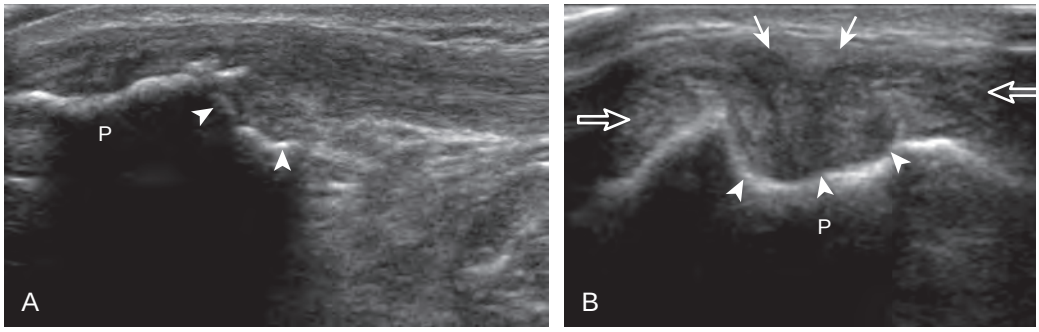

FIGURE 7-50 ■ Postoperative patellar tendon: anterior cruciate ligament (ACL) reconstruction. Ultrasound images **(A)** long axis and **(B)** short axis to patellar tendon show post-surgical defect in the inferior patella *(arrowheads)* and absence of the central third of the patellar tendon *(arrows)* for ACL reconstruction. Note full width of patellar tendon *(open arrows)* in **B**. P, patella.

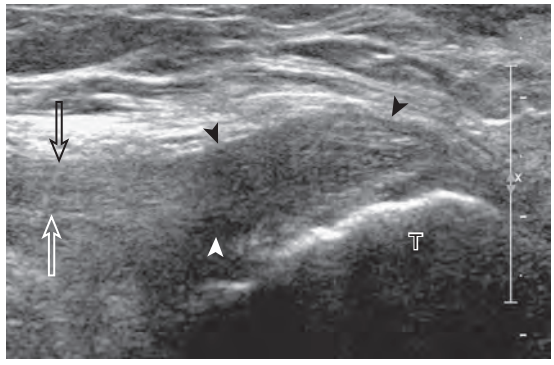

FIGURE 7-51 ■ Tendinosis: semimembranosus. Ultrasound image long axis to the distal semimembranosus tendon shows hypoechoic thickening *(arrowheads)* (*open arrows*, normal proximal semimembranosus tendon). T, tibia.

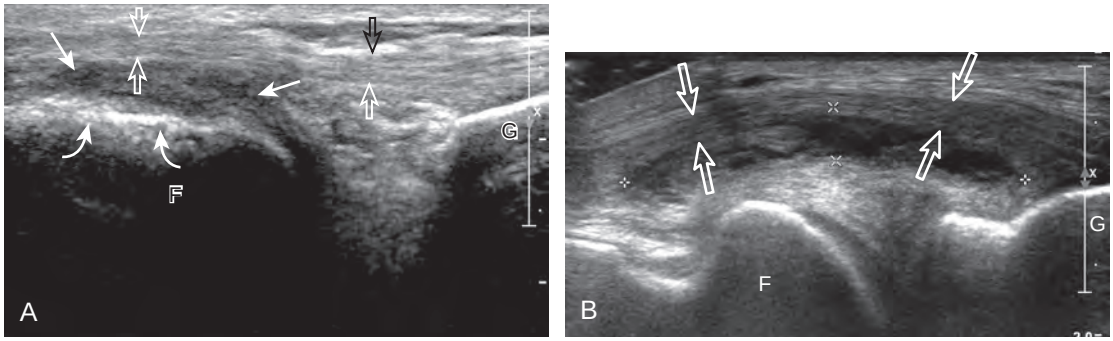

FIGURE 7-52 ■ Iliotibial band friction syndrome. Ultrasound images long axis to the iliotibial tract in two different patients show **(A)** hypoechoic soft tissue thickening *(arrows)* and **(B)** heterogeneous but hypoechoic bursa *(between cursors)* deep to the iliotibial tract *(open arrows)*. Note bone irregularity of the femur in **A** *(curved arrows)*. F, femur; G, Gerdy tubercle of tibia.

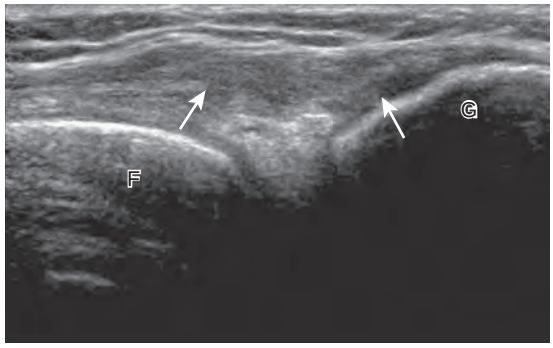

FIGURE 7-53 ■ Iliotibial tract tear. Ultrasound image long axis to iliotibial tract shows tear *(arrows)* with heterogeneous hemorrhage. F, femur; G, Gerdy tubercle of tibia.

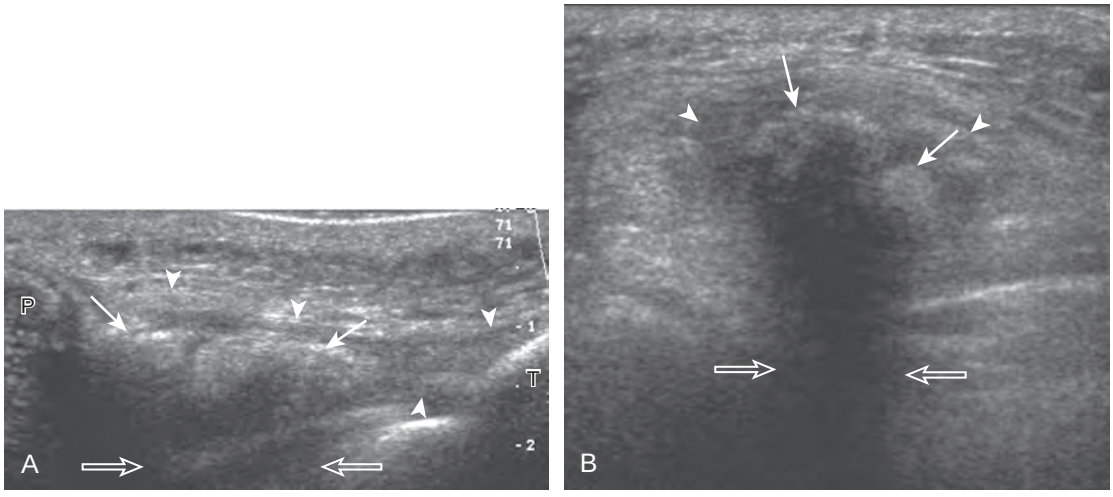

FIGURE 7-54 ■ Gout: patellar tendon tophus. Ultrasound images **(A)** long axis and **(B)** short axis to the patellar tendon show hyperechoic tophi *(arrows)* with posterior acoustic shadowing *(open arrows)* within the patellar tendon *(arrowheads)*. Shadowing was from sound beam attenuation as tophus was not calcified. P, patella; T, tibia.

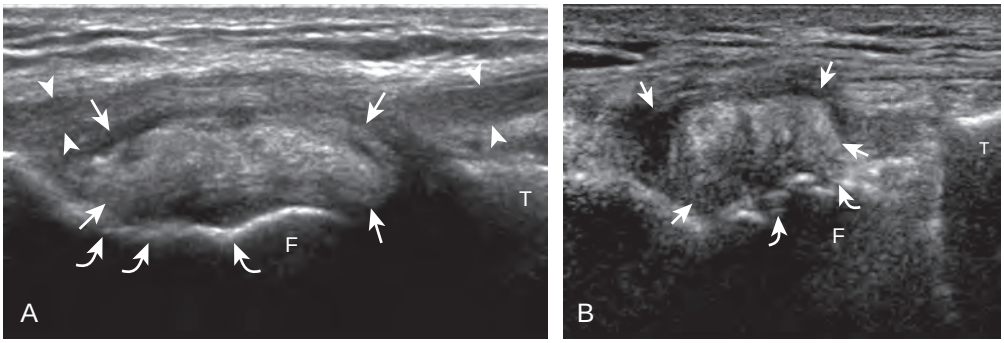

FIGURE 7-55 ■ Gout: popliteus tendon tophus. Ultrasound images **(A** and **B)** long axis to the proximal popliteus tendon in two different patients show hyperechoic tophi with hypoechoic halo *(arrows)*. Note erosions of lateral femur *(curved arrows)* (*arrowheads*, lateral collateral ligament). F, femur; T, tibia.

distal patellar tendon is not uncommon.[56] At ultrasound, a gouty tophus appears hyperechoic and amorphous, often with an anechoic or hypoechoic halo.[57,58] A tophus is often more difficult to delineate in a tendon given that both are hyperechoic; however, real-time imaging shows lack of fibrillar echotexture within the tophus. Shadowing may also be seen deep to the tophus, which is more often due to refraction rather than true shadowing from calcification of the tophus (see Fig. 7-54B). Hyperemia may also be present, as may adjacent cortical erosion (see Fig. 7-55B) and soft tissue extension of the tophus.

LIGAMENT AND BONE ABNORMALITIES

Medial Collateral Ligament

Sonographic evaluation of the ligaments around the knee is most effective for the superficially located ligaments, such as the medial collateral and lateral collateral ligaments. Transducer position long axis to a ligament is the most important plane, although any abnormality is also assessed short axis to the ligament as well. With regard to the tibial collateral ligament, a grade 1 sprain is characterized by adjacent hypoechoic or anechoic fluid but an intact ligament (Fig. 7-56A). Edema around the tibial collateral ligament may not be traumatic because it may be secondary to meniscal extrusion and osteoarthritis (see Fig. 7-37).[34] With a grade 2 injury or partial-thickness tear, the normally hyperechoic and compact fibrillar echotexture is replaced by abnormal hypoechogenicity and possible adjacent hypoechoic or anechoic fluid. With a grade 3 injury or full-thickness tear, there is complete disruption of the ligamentous fibers with heterogeneous hemorrhage and fluid (see Fig. 7-56B). Overall, a tibial collateral ligament injury is suggested when greater than 6 mm thick at the femoral attachment or greater than 3.6 mm thick at the tibial attachment.[59] Dynamic imaging may also be used to assess the integrity of the medial collateral ligament because medial joint space widening with valgus stress less than 5 mm represents a grade 1 injury, 5 to 10 mm represents a grade 2 injury, and greater than 10 mm indicates a grade 3 injury.[59] A segment of the tibial collateral ligament that is thickened with intact fibers yet no symptoms is compatible with a remote injury (see Fig. 7-56C) or prior total knee arthroplasty.[53] Because the tibial collateral ligament is a relatively flat structure, it is important to assess the entire anterior to posterior extent in short axis. It is not uncommon to have complete fiber discontinuity involving the anterior fibers, but with intact fibers posteriorly. A bursa may also be found between the superficial and deep layers of the medial collateral ligament.[60]

Lateral Collateral Ligament

The lateral collateral ligament is an important structure that is a part of the posterolateral ligamentous complex.[16] Injuries may create a swollen, hypoechoic appearance or complete discontinuity (Fig. 7-57).[61] Distal ligamentous avulsions may be associated with a hyperechoic fibular fracture fragment. In this situation, the ligament is structurally intact but functionally completely torn. Other supporting structures of the posterolateral corner include the popliteofibular ligament. Because this ligament may be difficult to visualize, it is often helpful to use other signs of posterolateral corner injury, such as lateral collateral ligament tear and abnormal widening of the lateral joint space with varus stress, where

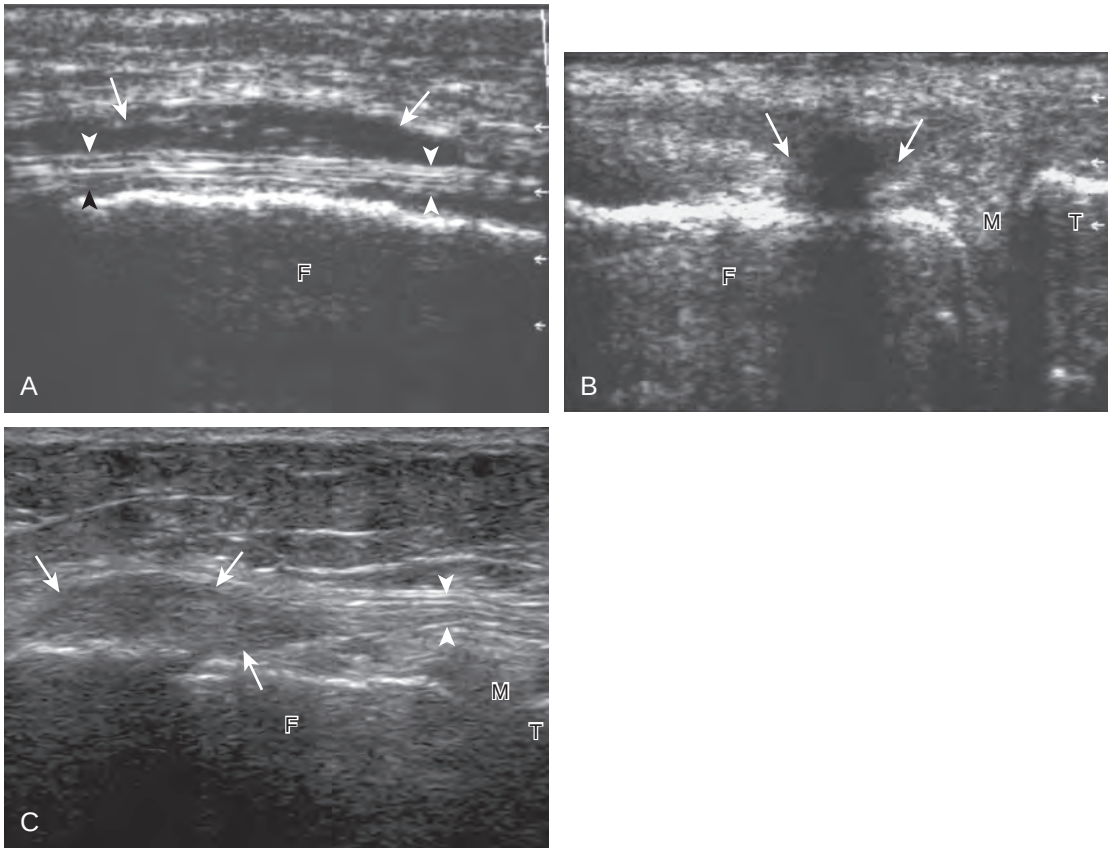

FIGURE 7-56 ■ Medial collateral ligament injury. Ultrasound images long axis to the medial collateral ligament in three different patients show **(A)** anechoic fluid *(arrows)* superficial to the intact tibial collateral ligament *(arrowheads)* (grade 1 injury), **(B)** full-thickness tear *(arrows)* (grade 3 injury), and **(C)** hypoechoic thickening of the proximal tibial collateral ligament *(arrows)* from remote injury with normal distal ligament *(arrowheads)*. F, femur; M, medial meniscus body; T, tibia.

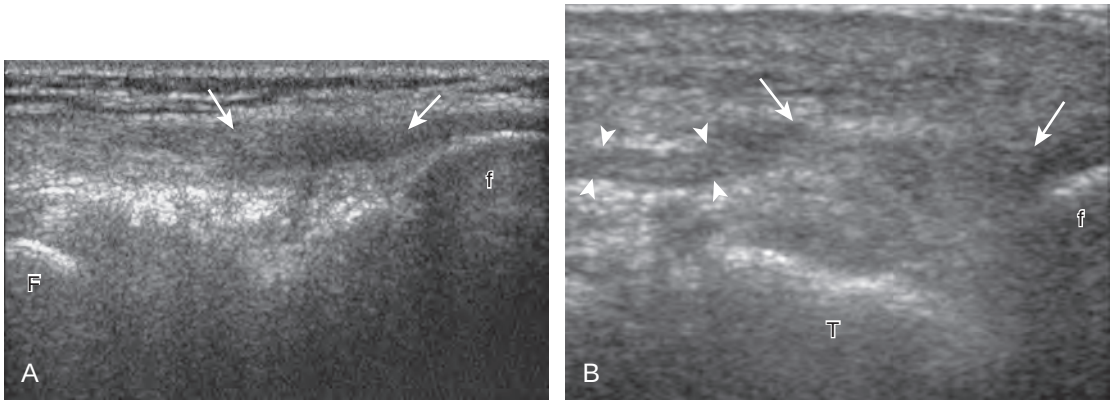

FIGURE 7-57 ■ Lateral collateral ligament tears. Ultrasound images long axis to the lateral collateral ligament in two different patients show **(A)** hypoechoic thickening *(arrows)* at the fibula (f) consistent with high-grade partial-thickness tear and **(B)** full-thickness tear *(arrows)* with proximal ligament edema and laxity *(arrowheads)*. F, femur; T, tibia.

lateral joint space of more than 10.5 mm can predict those who will require posterolateral corner repair or reconstruction.[61]

Cruciate Ligaments

With regard to the anterior cruciate and posterior cruciate ligaments, each can be partially visualized at sonography, but MRI is considered the imaging test of choice in their evaluation. At sonography, the posterior cruciate ligament is considered abnormal if it is hypoechoic or anechoic and swollen more than 1 cm thick (Fig. 7-58).[17] A torn posterior cruciate ligament may be focally disrupted or diffusely enlarged.[62] Hyperechoic bone avulsions from the posterior aspect of the tibia are also possible.[63] An anterior cruciate ligament tear is diagnosed at ultrasound when the normally hyperechoic ligament in the lateral aspect of the intercondylar notch, when imaged transversely, is abnormally hypoechoic or anechoic (Fig. 7-59).[18,64] Dynamic stress views have also been used in conjunction with ultrasound to identify abnormal anterior tibial translation as an indirect sign of anterior cruciate ligament tear.[65] Although evaluation for anterior and posterior cruciate ligament tears is limited with ultrasound, ganglion cysts associated with the cruciate ligaments (discussed later) may extend posteriorly and can be visible at sonography.[66]

Osseous Injury

With regard to ultrasound of bone, the osseous surfaces have a characteristic contour that is important for orientation, especially when evaluating ligaments. The normal bone cortex is smooth and continuous. Any focal step-off deformity, especially if point tenderness with transducer pressure, should raise concern for fracture (Fig. 7-60).[67,68] With regard to the patella, it is important not to misinterpret a bipartite or tripartite patella, which is a normal variation, as a fracture.[69] Unlike a fracture, this normal variation is isolated to the upper outer quadrant of the patella, has more irregular osseous margins, and is often asymptomatic; correlation with radiography is also important (Fig. 7-61).

BURSAE AND CYSTS

Baker Cyst

Besides parameniscal cysts described in the preceding section, other cystic abnormalities are

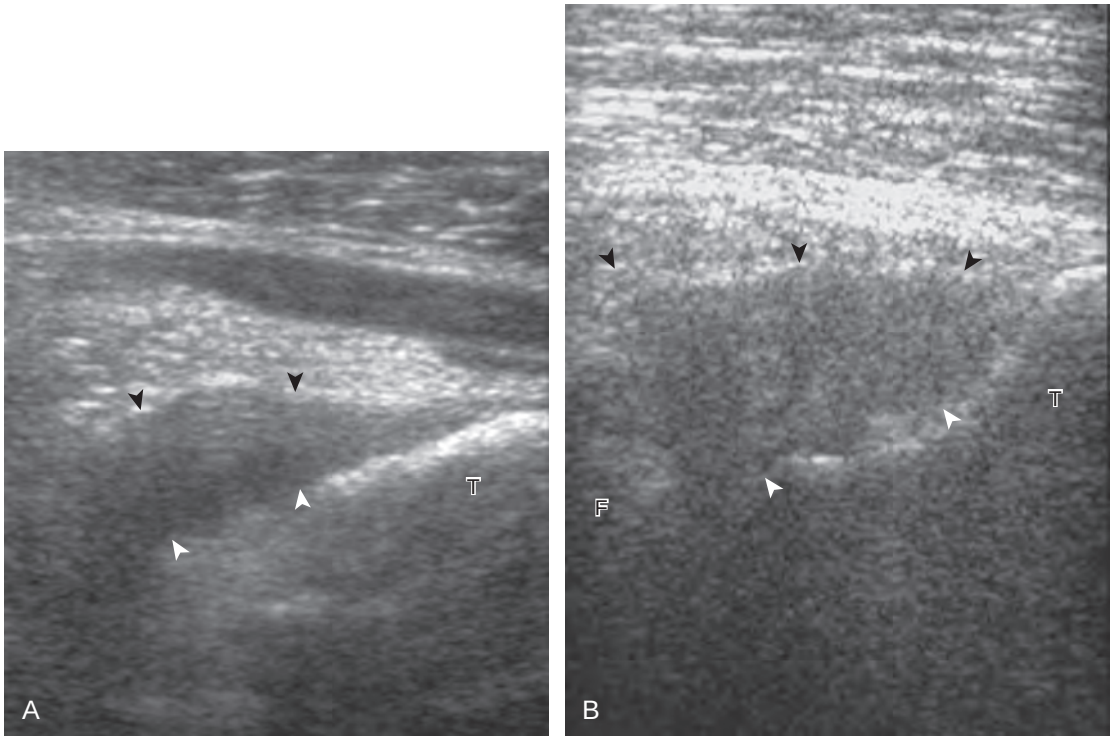

FIGURE 7-58 ■ Posterior cruciate ligament tears. Ultrasound images long axis to the posterior cruciate ligament in two different patients show hypoechoic thickening of the posterior cruciate ligament *(arrowheads)*. F, femur; T, tibia.

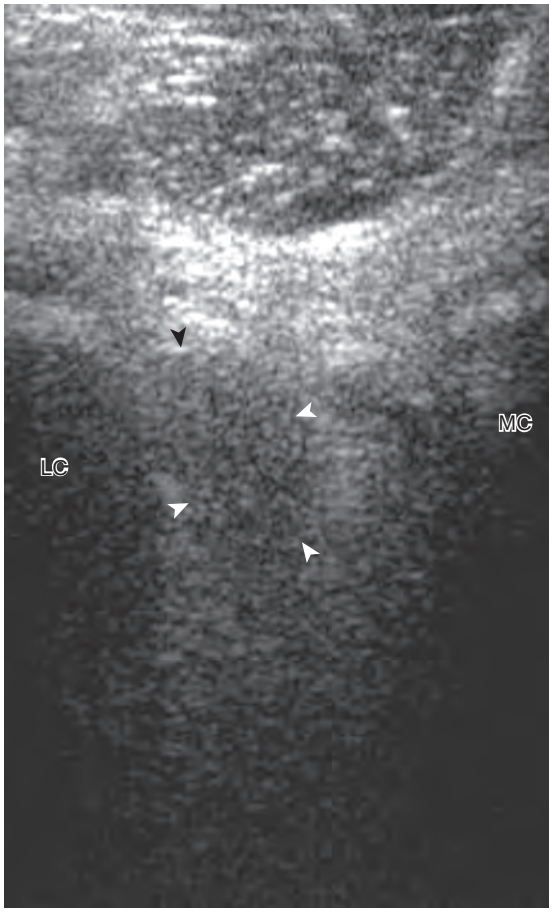

FIGURE 7-59 ■ Anterior cruciate ligament tear. Ultrasound image short axis to the anterior cruciate ligament shows hypoechoic thickening of the anterior cruciate ligament *(arrowheads)*. LC, lateral femoral condyle; MC, medial femoral condyle.

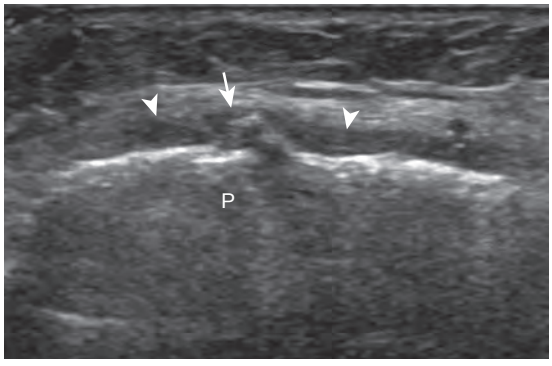

FIGURE 7-60 ■ Fracture: patella. Ultrasound image transverse over patella shows cortical discontinuity *(arrow)* and adjacent edema or hemorrhage *(arrowheads)*. P, patella.

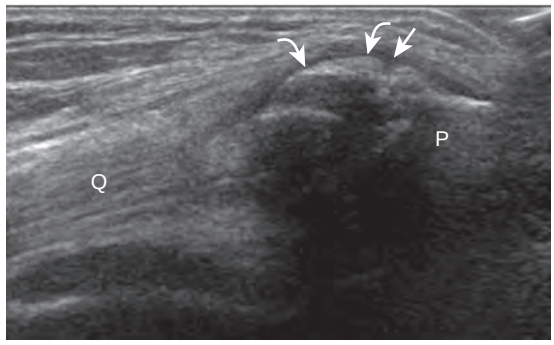

FIGURE 7-61 ■ Bipartite patella. Ultrasound image in the sagittal plane over the lateral patella shows the separate patellar bone segment *(curved arrows)* and synchondrosis *(arrow)* with native patella (P). Q, quadriceps tendon.

often seen around the knee. One of the most common is distention of the semimembranosus-medial gastrocnemius bursa, which results in Baker (or popliteal) cyst.[4] Although distention of this bursa may occur from local irritation or inflammation, more commonly it becomes distended with joint fluid through communication with the knee joint. Present in 50% of adults who are older than 50 years, this communication is acquired by a combination of degenerative weakening of the intervening capsule and increased intra-articular pressure and joint fluid from internal derangement.[4] In the pediatric population, Baker cyst may be associated with underlying arthritis or joint hypermobility.[70] Accurate diagnosis of Baker cyst relies on identification of the characteristic channel or neck between the semimembranosus and the medial head of the gastrocnemius tendon, which connects the bursa to the knee joint via the subgastrocnemius bursa. The result is a C-shaped fluid collection, concave lateral, which wraps around the medial head of the gastrocnemius tendon and muscle (Fig. 7-62).

A Baker cyst may be distended with anechoic or hypoechoic fluid. The presence of isoechoic or hyperechoic material within a Baker cyst may represent complex fluid, hemorrhage, or synovial hypertrophy (inflammatory or the result of proliferative synovial conditions such as pigmented villonodular synovitis) (Fig. 7-63). Hyperechoic and shadowing intra-articular bodies are also commonly present within a Baker cyst (see Fig. 7-63E). It is important to evaluate the inferior margin of the Baker cyst in the sagittal plane, which is normally well defined and smooth. The presence of hypoechoic fluid beyond the confines of the Baker cyst suggests rupture, which can produce diffuse edema or reactive cellulitis that typically is located superficial to the medial head

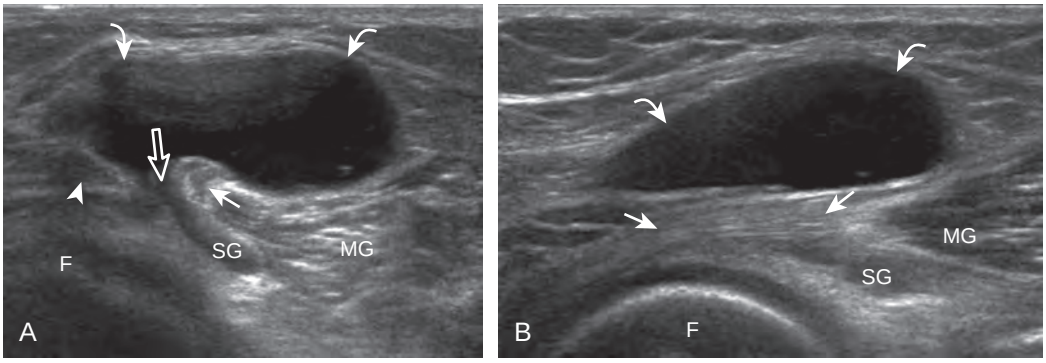

FIGURE 7-62 ■ Baker cyst. Ultrasound images transverse **(A)** and sagittal **(B)** over the posterior medial knee show predominantly anechoic distention of the semimembranosus-medial gastrocnemius bursa *(curved arrows)*. Note the communication to the knee joint *(open arrow)* between the semimembranosus tendon *(arrowhead)* and the medial head of the gastrocnemius tendon *(arrows)* and muscle (MG) via the subgastrocnemius bursa (SG). F, medial femoral condyle.

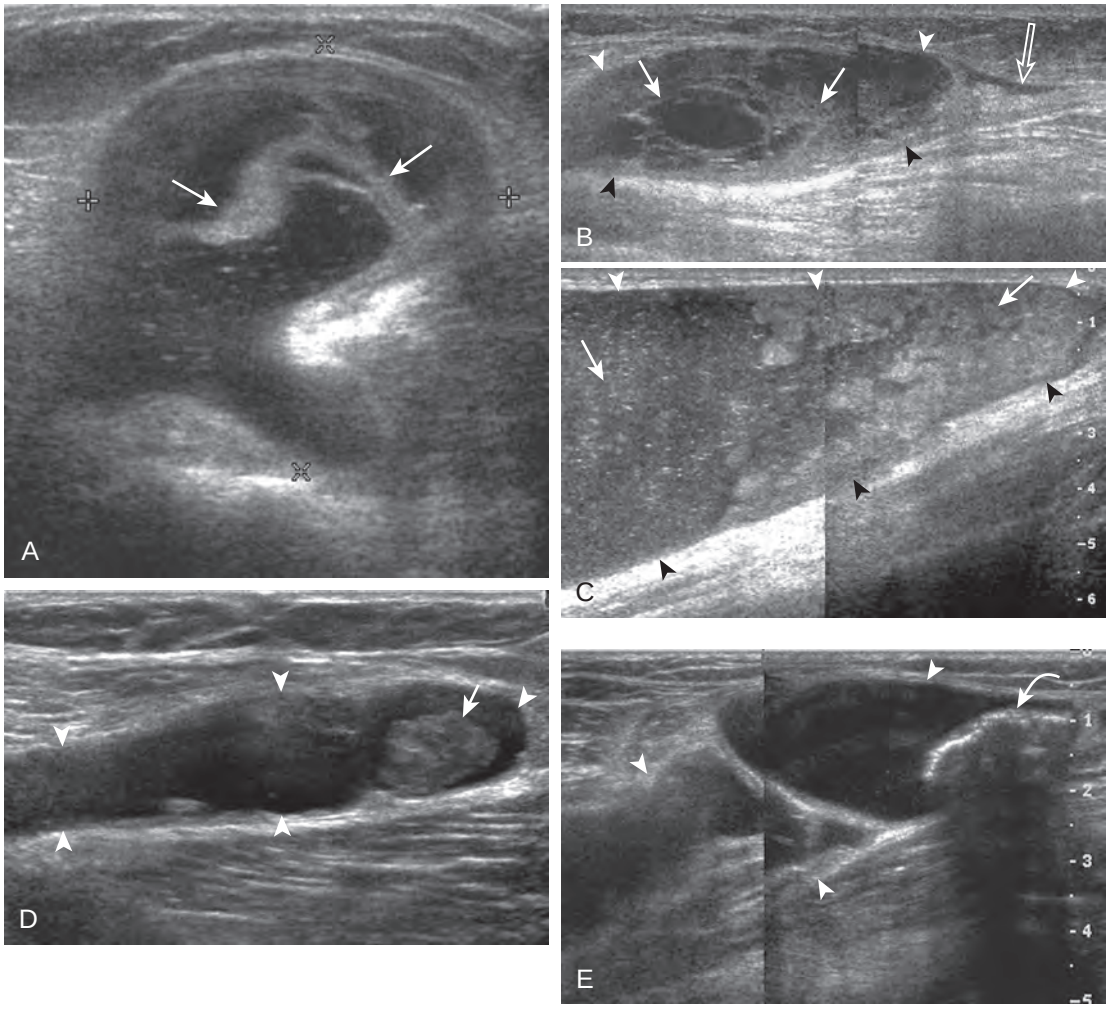

FIGURE 7-63 ■ Complex Baker cysts. Ultrasound images transverse **(A)** and sagittal **(B** to **E)** over the posterior medial knee from five different patients show heterogeneous and variable echogenicity *(arrows)* within Baker cysts (*cursors or arrowheads*) from complex fluid, hemorrhage, and synovitis. Note Baker cyst rupture *(open arrow)* in **B** and an ossified intra-articular body with posterior acoustic shadowing *(curved arrow)* in **E** that was mobile with transducer pressure.

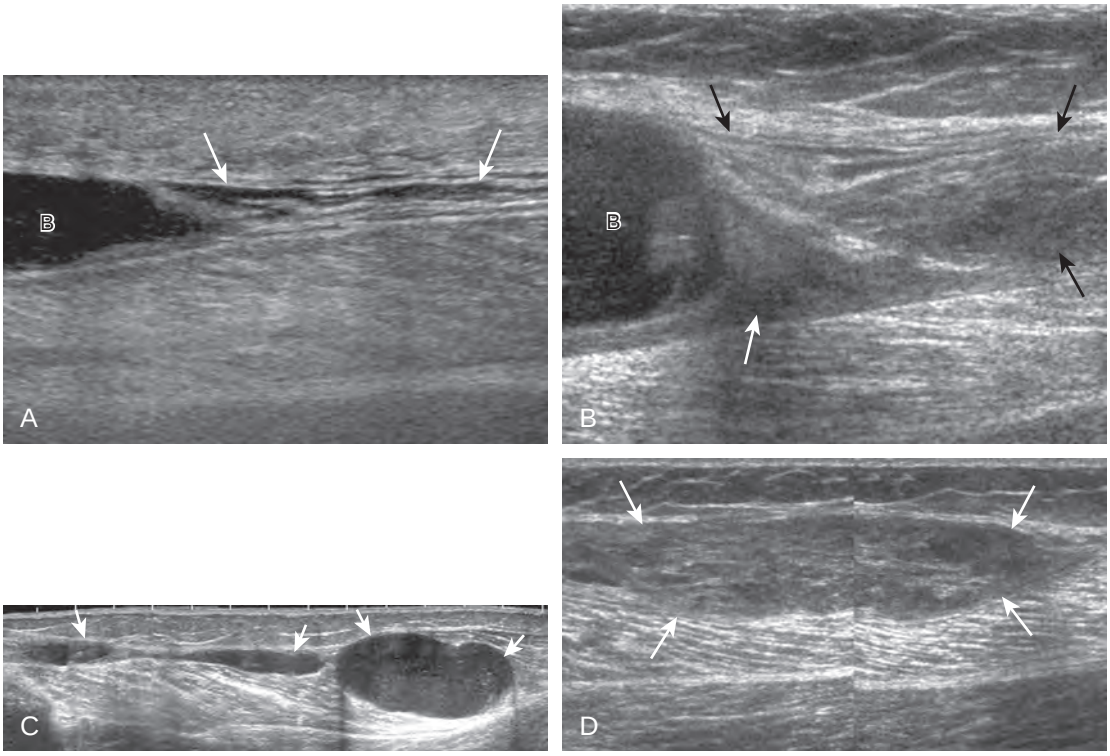

FIGURE 7-64 ■ **Ruptured Baker cysts.** Ultrasound images sagittal over the posterior medial knee from two patients show **(A)** anechoic fluid *(arrows)* and **(B)** heterogeneous hypoechoic fluid and hemorrhage *(arrows)*, which extend distal to the Baker cyst **(B)** with an irregular inferior margin. Sagittal ultrasound images in two different patients show **(C)** loculated hypoechoic fluid *(arrows)* and **(D)** hypoechoic to isoechoic hematoma (*arrows*) superficial to the medial head of the gastrocnemius. In each case, proximal communication to the posterior knee joint was demonstrated.

of the gastrocnemius muscle and may extend to the ankle (Fig. 7-64). A more chronically ruptured Baker cyst may result in a heterogeneous mass-like area in the calf, usually superficial to the medial head of the gastrocnemius muscle (see Fig. 7-64C and D). In this situation, it is important to differentiate a ruptured Baker cyst from a soft tissue neoplasm; identification of the Baker cyst communication to the knee joint between the medial head of the gastrocnemius and semimembranosus tendons is critical in this differentiation. Extension of a Baker cyst deep to the calf musculature is uncommon, and extension within the muscle is rare, so such findings should raise concern for another etiology, such as sarcoma. Ultrasound-guided aspiration and steroid injection of Baker cyst may be considered, although re-accumulation of fluid from the knee joint is possible (see Chapter 9).

Other Bursae

Several other bursae around the knee in addition to Baker cysts may become distended. Medially and anteriorly, the pes anserinus bursa is located deep to the pes anserinus adjacent to the medial tibia, but it may be extensive (Fig. 7-65).[2] Symptoms referable to the pes anserinus rarely correspond to a tendon or bursal abnormality but rather are associated with knee osteoarthritis.[71] Posterior and superior to the pes anserinus and at the joint line, the semimembranosus-tibial collateral ligament bursa takes the form of an inverted U shape as it wraps around the semimembranosus tendon (Figs. 7-66 and 7-67).[3] The prepatellar bursa is located anterior to the patella (Fig. 7-68).[72] The superficial infrapatellar bursa (Fig. 7-69) and deep infrapatellar bursa (Fig. 7-70) are located around the distal patellar tendon, the latter of which normally contains minimal fluid (see Fig. 7-70A).[73] A bursa may be distended with anechoic or hypoechoic fluid, although complex fluid, hemorrhage, or synovial hypertrophy may range from hypoechoic to hyperechoic, with possible increased flow on color or power Doppler imaging. Causes of bursal distention include trauma; inflammation, such as infection, rheumatoid arthritis, and gout;

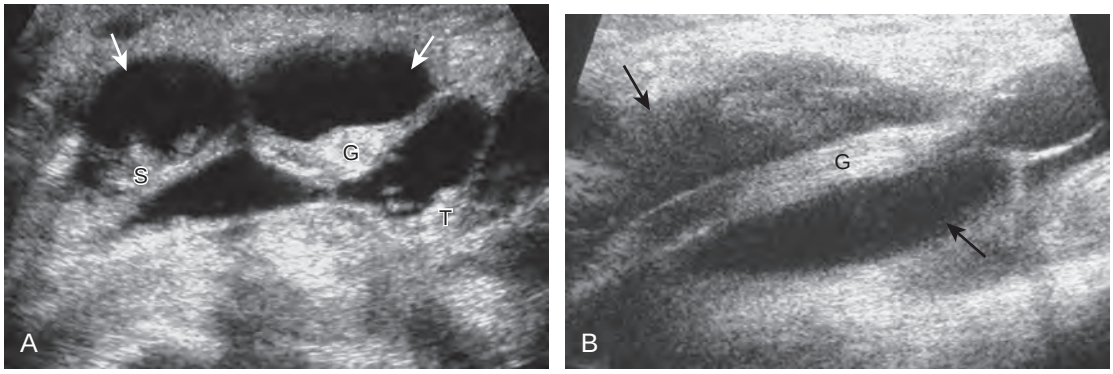

FIGURE 7-65 ■ Pes anserinus bursa. Ultrasound images **(A)** short axis and **(B)** long axis to the gracilis tendon (G) show anechoic distention of the pes anserinus bursa (*arrows*). S, sartorius; T, semitendinosus.

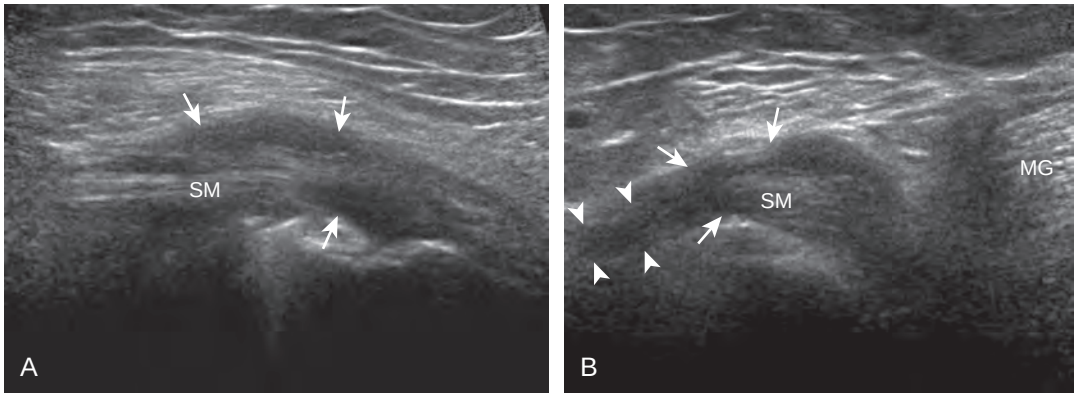

FIGURE 7-66 ■ Semimembranosus-tibial collateral ligament bursa. Ultrasound images **(A)** long axis and **(B)** short axis to the semimembranosus tendon (SM) show hypoechoic fluid *(arrows)*, which distends the semimembranosus-tibial collateral ligament bursa. Note location between the semimembranosus and tibial collateral ligament (hypoechoic from anisotropy) *(arrowheads)*. MG, medial head of gastrocnemius.

and other synovial proliferative disorders. The presence of pain with transducer pressure and hyperemia on color or power Doppler imaging suggest true inflammation or bursitis rather than mechanical or reactive bursal fluid. Knowledge of these common bursae allows one to distinguish an abnormal bursa from a nonspecific fluid collection or abscess. At points of abnormal mechanical friction or contact, an adventitious bursa may form, such as after knee amputation (Fig. 7-71).[74] Unlike a Baker cyst, the previously described bursae do not normally communicate to the knee

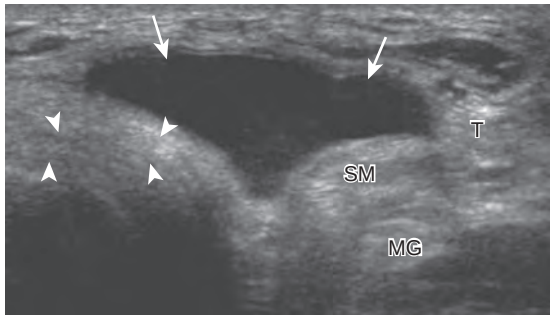

FIGURE 7-67 ■ Semimembranosus-tibial collateral ligament bursal fluid. Ultrasound image short axis to the semimembranosus tendon (SM) shows anechoic fluid *(arrows)*, which distends the semimembranosus-tibial collateral ligament bursa. Note location between the semimembranosus and tibial collateral ligament *(arrowheads)*, which is unlike the location of a Baker cyst between the semimembranosus and medial head of gastrocnemius (MG). T, semitendinosus.

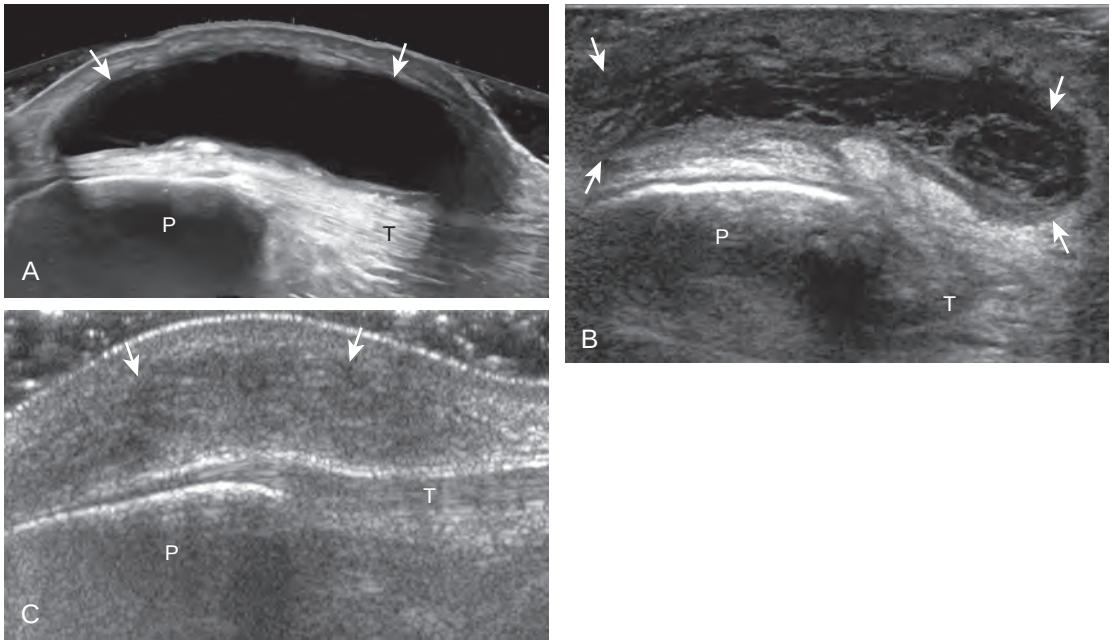

FIGURE 7-68 ■ **Prepatellar bursa.** Ultrasound images long axis to the proximal patellar tendon over distal patella in three different patients show prepatellar bursal distention *(arrows)* from **(A)** anechoic fluid (aseptic), **(B)** hypoechoic heterogeneous synovial hypertrophy and complex fluid (infection), and **(C)** isoechoic hemorrhage. P, patella; T, patellar tendon. Note that the transducer is floated on a thick layer of gel in **A** and **C**.

joint; therefore, ultrasound-guided percutaneous aspiration and injection may be warranted.

Ganglion Cysts

Ganglion cysts have a propensity to be located at several areas around the knee.[75] The exact cause of ganglion cysts is not known, but synovial herniation, tissue degeneration, and tissue response to trauma are several possibilities.[75] One common site is around the cruciate ligaments, where a ganglion cyst may extend into the soft tissue and bone (Fig. 7-72).[66] Ganglion cysts may also occur posteriorly at the gastrocnemius tendon origins (Fig. 7-73) and anteriorly in the Hoffa infrapatellar fat pad (Fig. 7-74). Most ganglion cysts demonstrate lobular margins and internal septations with a multilocular appearance. Ganglion cysts may be anechoic, with increased through-transmission, or hypoechoic, without increased through-transmission when small. Percutaneous aspiration reveals thick and clear gelatinous fluid. The differential diagnosis of a soft tissue multilocular cyst is a parameniscal cyst, with the latter located around the joint line, which extends from the meniscus. If a large cyst is identified at ultrasound that is not multilocular (such as a ganglion cyst) and not in the expected location of a bursa, then a hypoechoic solid neoplasm must be considered. Intraneural ganglion cysts of the peroneal nerve are discussed later.

PERIPHERAL NERVE ABNORMALITIES

Ultrasound evaluation of the knee includes imaging of peripheral nerves. The common peroneal nerve near the fibula is predisposed to pathology, which includes direct injury or entrapment between the peroneus longus muscle and fibula (Fig. 7-75) (Video 7-9). The findings of peripheral nerve entrapment include hypoechoic swelling of the involved nerve at and just proximal to the site of entrapment, with transition to normal-appearing nerve distally. Transducer pressure over the abnormal nerve often elicits symptoms.

An intraneural ganglion cyst characteristically involves the peroneal nerve (Fig. 7-76). More common in patients with a high body mass index, joint fluid from the proximal tibiofibular joint may extend to the peroneal nerve via the articular

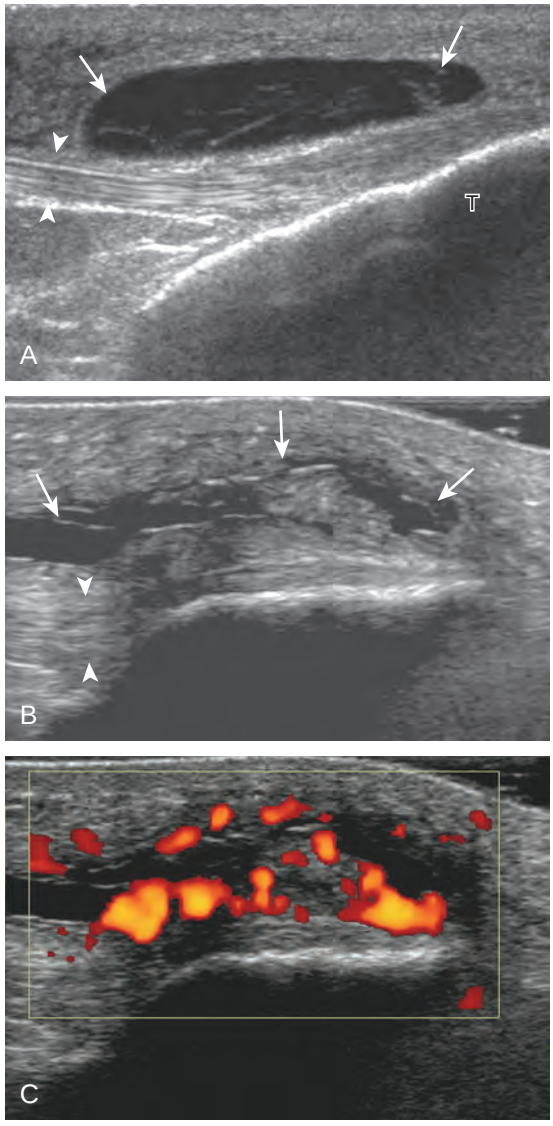

FIGURE 7-69 ■ Superficial infrapatellar bursa. Ultrasound image **(A)** long axis to the distal patellar tendon *(arrowheads)* show predominantly hypoechoic distention of the superficial infrapatellar bursa *(arrows)* with internal linear echoes resulting from sterile complex fluid and hemorrhage. **B,** Long axis ultrasound image in a different patient shows complex fluid and variable echogenicity synovitis *(arrows)* with increased blood flow on **(C)** power Doppler imaging (*arrowheads*, patellar tendon). T, tibia.

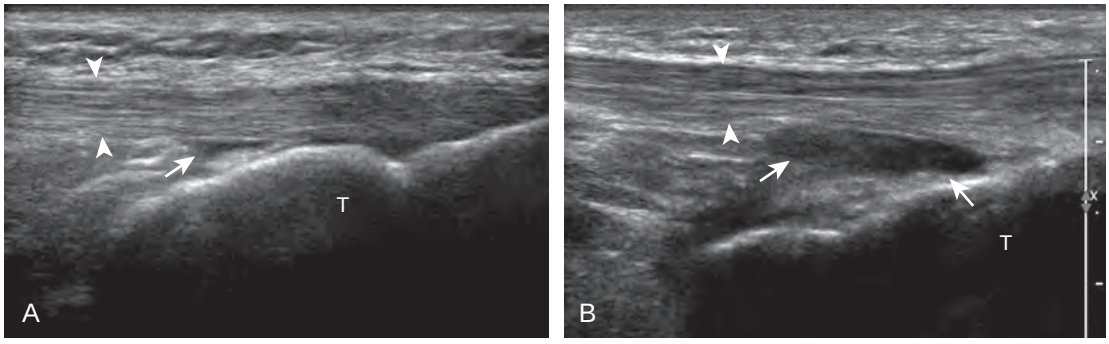

FIGURE 7-70 ■ Deep infrapatellar bursa. Ultrasound images long axis to the distal patellar tendon *(arrowheads)* in two different patients show **(A)** physiologic distention and **(B)** abnormal fluid distention of the deep infrapatellar bursa *(arrows)*. T, tibia.

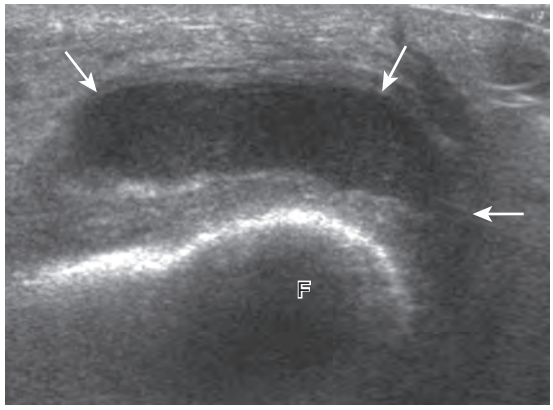

FIGURE 7-71 ■ Adventitious bursa. Sagittal ultrasound image over the distal femur (F) amputation site shows hypoechoic adventitious bursa formation *(arrows)*.

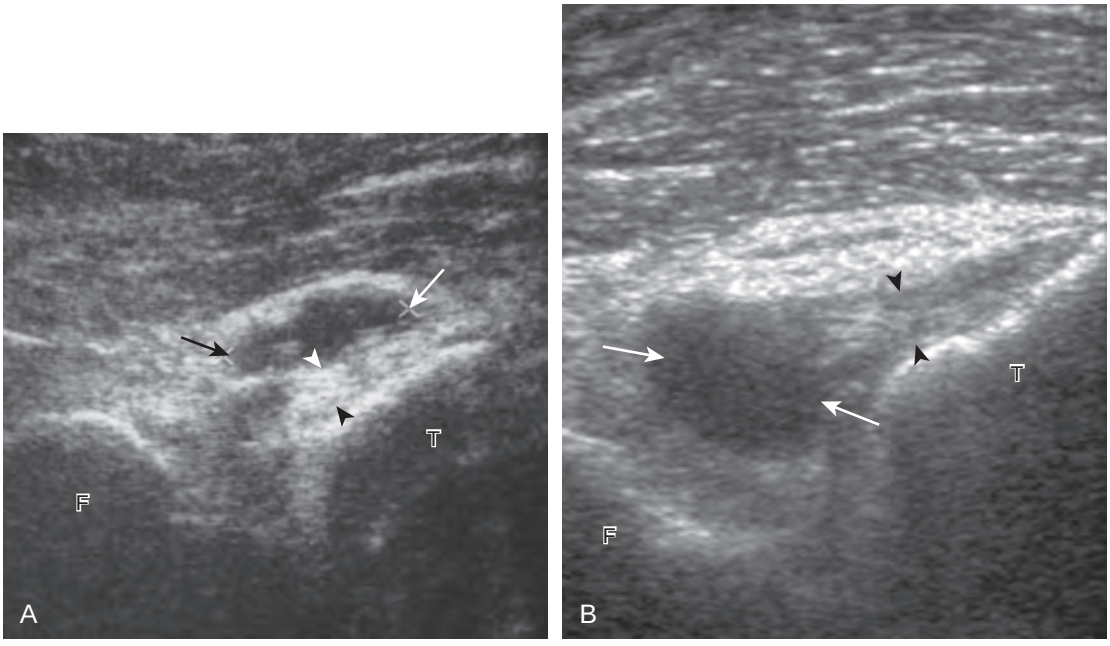

FIGURE 7-72 ■ Ganglion cysts: cruciate ligaments. Sagittal ultrasound images over posterior knee long axis to posterior cruciate ligament (PCL) in two different patients show hypoechoic ganglion cysts *(arrows)* (*arrowheads*, PCL). F, femur; T, tibia.

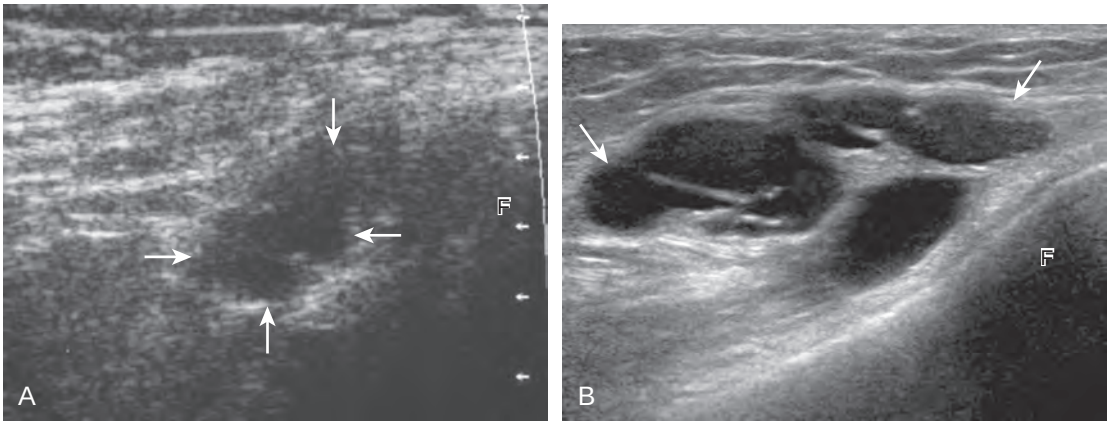

FIGURE 7-73 ■ Ganglion cysts: gastrocnemius tendon. Sagittal ultrasound images over posterior knee long axis to gastrocnemius tendons in two different patients show **(A)** hypoechoic and **(B)** anechoic multilobular gastrocnemius origin ganglion cysts *(arrows)*. Note posterior through-transmission in **B**. F, femur.

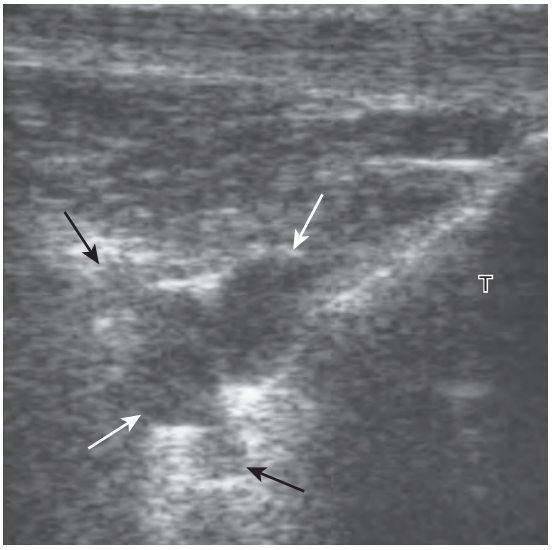

FIGURE 7-74 ■ Ganglion cyst: Hoffa fat pad. Ultrasound image long axis to patellar tendon shows hypoechoic multilobular cyst *(arrows)* in Hoffa fat pad (T, tibia) with increased through-transmission.

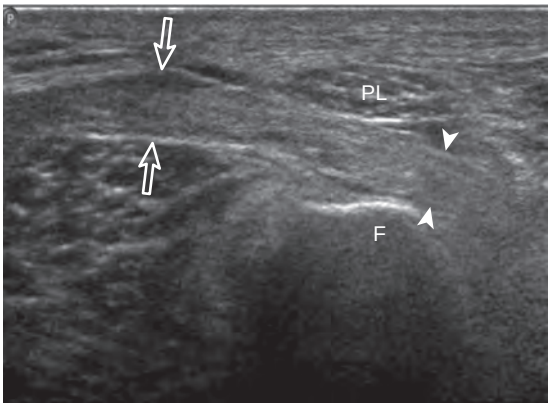

FIGURE 7-75 ■ Common peroneal nerve entrapment. Ultrasound image long axis to the common peroneal nerve shows proximal hypoechoic enlargement *(open arrows)* with transition to normal appearance distally *(arrowheads)* at compression site between peroneus longus (PL) and fibula (F).

branch to create the peroneal nerve ganglion cyst.[76] Such cysts originate near the fibular neck but can extend proximally to the level of the sciatic nerve and beyond, both proximal in the sciatic nerve and distal in the tibial nerve.[77] At ultrasound, intraneural peroneal nerve ganglion cysts are hypoechoic and often multilobular and track along the course of the involved nerves.[76] As with any peripheral nerve disorder, it is important to evaluate the distal musculature for signs of denervation (increased echogenicity) and possible atrophy (Fig. 7-77). Intraneural ganglion

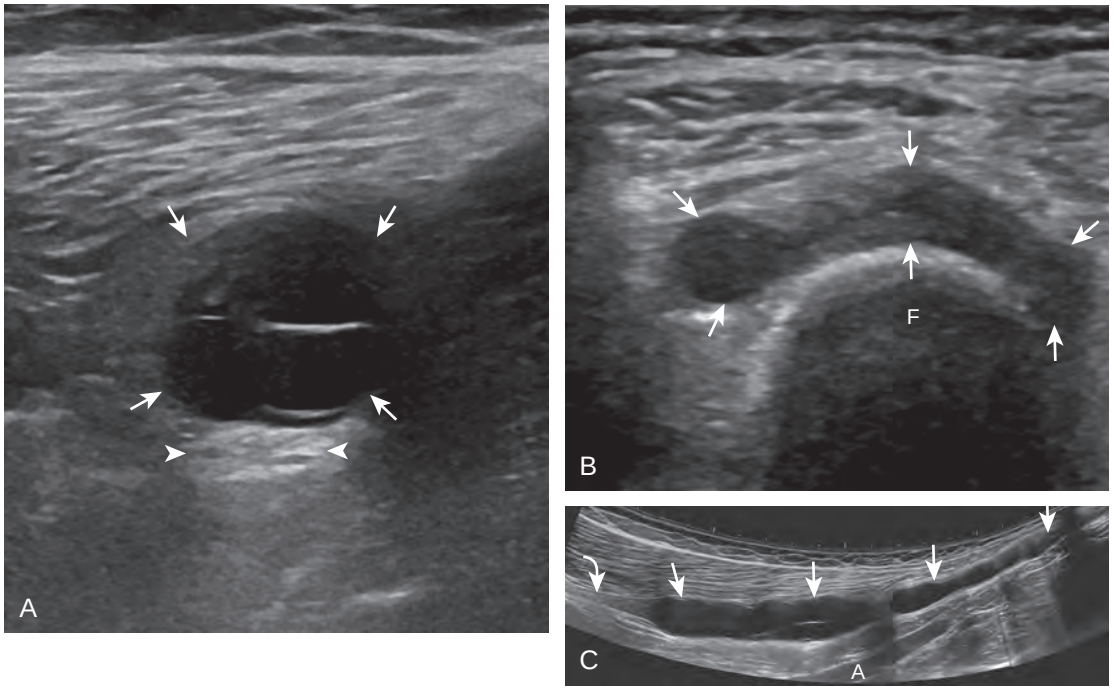

FIGURE 7-76 ■ Intraneural ganglion cyst: common peroneal nerve. Ultrasound image **(A)** short axis to common peroneal nerve *(arrowheads)* shows lobulated anechoic intraneural ganglion cyst *(arrows)*. Ultrasound image **(B)** transverse to fibula shows hypoechoic cyst *(arrows)* coursing around fibular neck (F). Extended field of view ultrasound image **(C)** shows full extent (16 cm) of ganglion cyst *(arrows)* to involve the sciatic nerve *(curved arrow)*. A, popliteal artery.

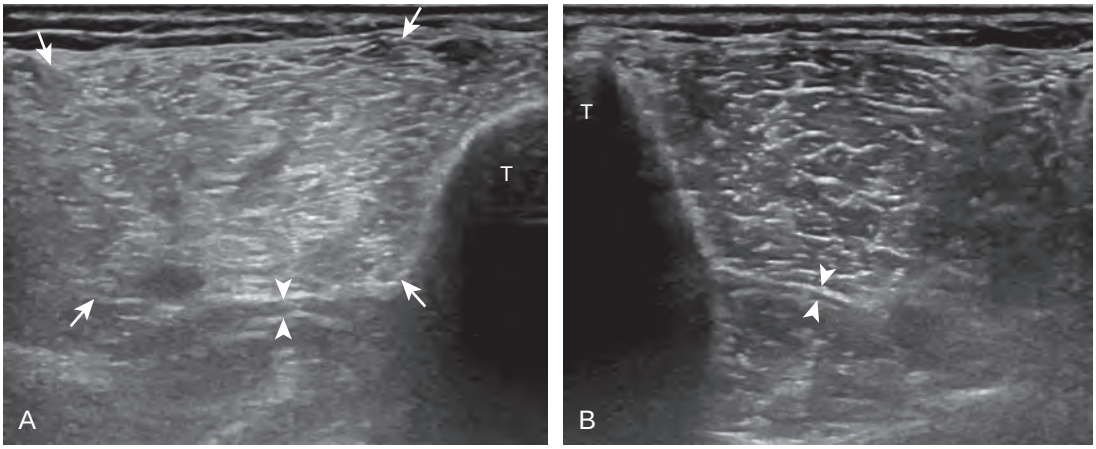

FIGURE 7-77 ■ Muscle denervation: anterior compartment of leg. Ultrasound image **(A)** shows increased echogenicity of the anterior compartment musculature *(arrows)* compared with contralateral asymptomatic side **(B)** (*arrowheads*, interosseous membrane). T, tibia.

cysts have been described in 18% of patients with isolated peroneal mononeuropathy.[78]

One additional application for peripheral nerve evaluation is in the setting of a knee amputation patient who presents with symptoms of a neuroma. After nerve transection, a neuroma is an expected finding as the nerve attempts to regenerate.[79] Ultrasound can locate each neuroma and importantly determine which neuroma is responsible for symptoms through transducer palpation. Neuromas will appear hypoechoic in continuity with the involved peripheral nerve (Fig. 7-78).[80] Deeper neuromas may be difficult to identify in the presence of surrounding muscle atrophy, which attenuates the ultrasound beam. Peripheral nerve sheath tumors are discussed in Chapter 2.

VASCULAR ABNORMALITIES

Evaluation of the posterior knee should always include assessment of the popliteal vasculature. The differential diagnosis for a cyst in the popliteal region includes aneurysm and pseudoaneurysm. Ultrasound can show the characteristic to-and-fro appearance of blood flow from the adjacent vessel into a pseudoaneurysm with color and power Doppler imaging (Fig. 7-79).[81] A soft tissue hematoma may also manifest as a soft

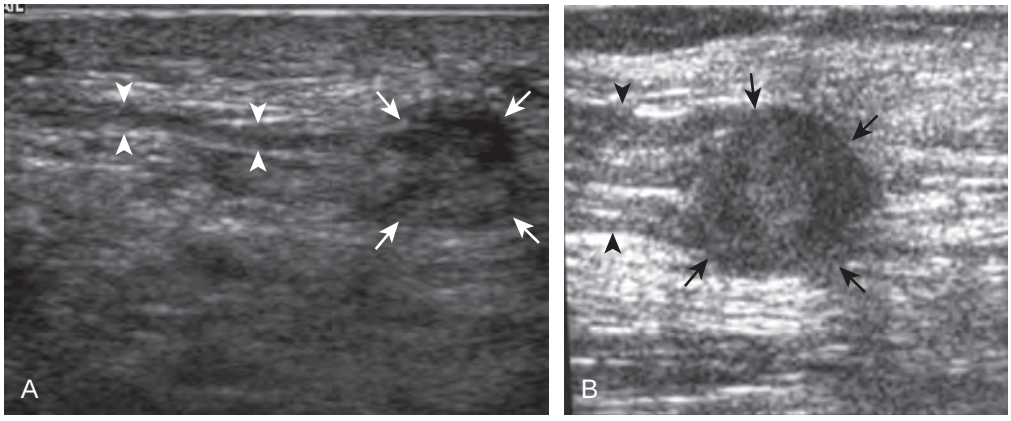

FIGURE 7-78 ■ Amputation neuromas. Ultrasound images in two different patients long axis to **(A)** a peripheral nerve branch and **(B)** sciatic nerve after knee amputation shows hypoechoic neuromas *(arrows)* in continuity with the associated nerves *(arrowheads)*.

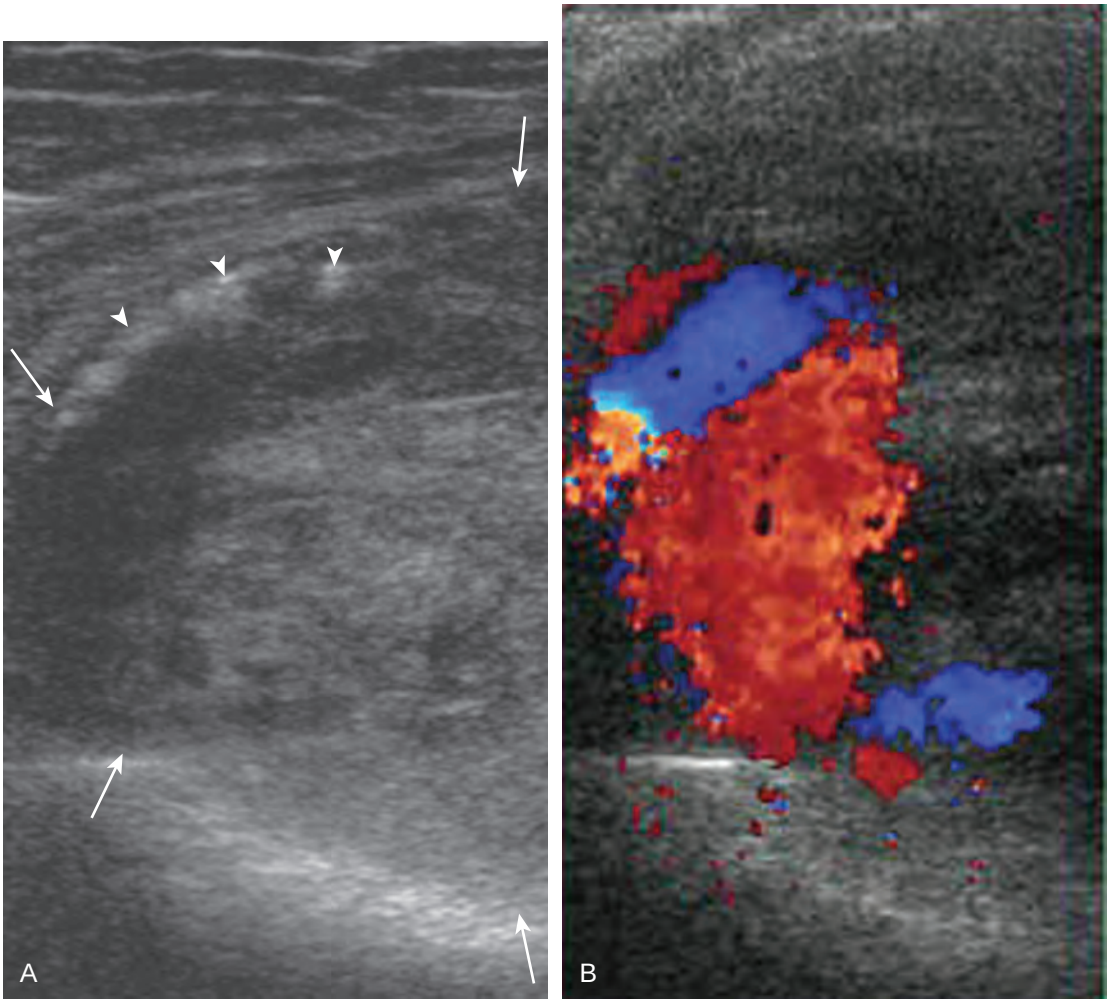

FIGURE 7-79 ■ Popliteal artery pseudoaneurysm. Sagittal ultrasound images over the posterior knee show **(A)** a heterogeneous mass-like area *(arrows)* with vascular calcifications *(arrowheads)*. Color Doppler image shows **(B)** pulsatile blood flow into the pseudoaneurysm.

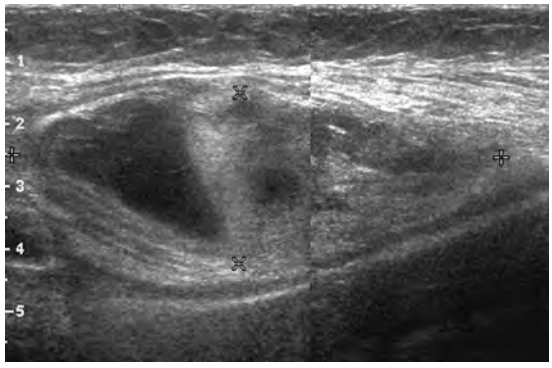

FIGURE 7-80 ■ Soft tissue hematoma. Ultrasound image shows a heterogeneous mixed-echogenicity mass-like area (*cursors*) from soft tissue hemorrhage.

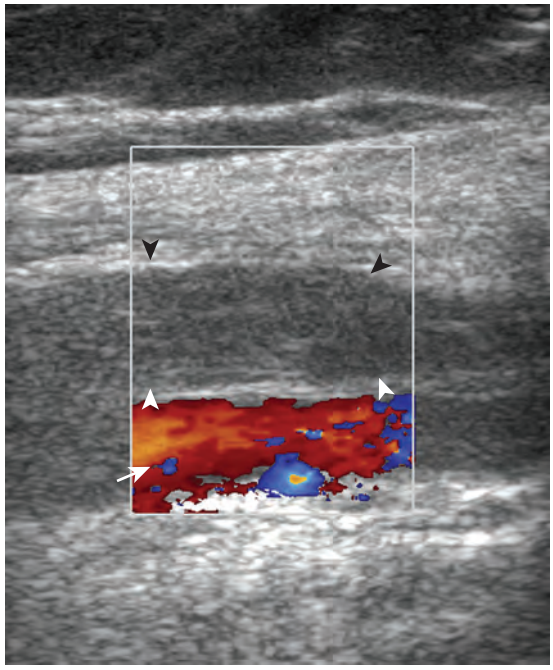

FIGURE 7-81 ■ Deep venous thrombosis: popliteal vein. Ultrasound image long axis to popliteal vein *(arrowheads)* shows abnormal hypoechogenicity from thrombus, which was noncompressible with no flow on color Doppler imaging (*arrow*, normal popliteal artery).

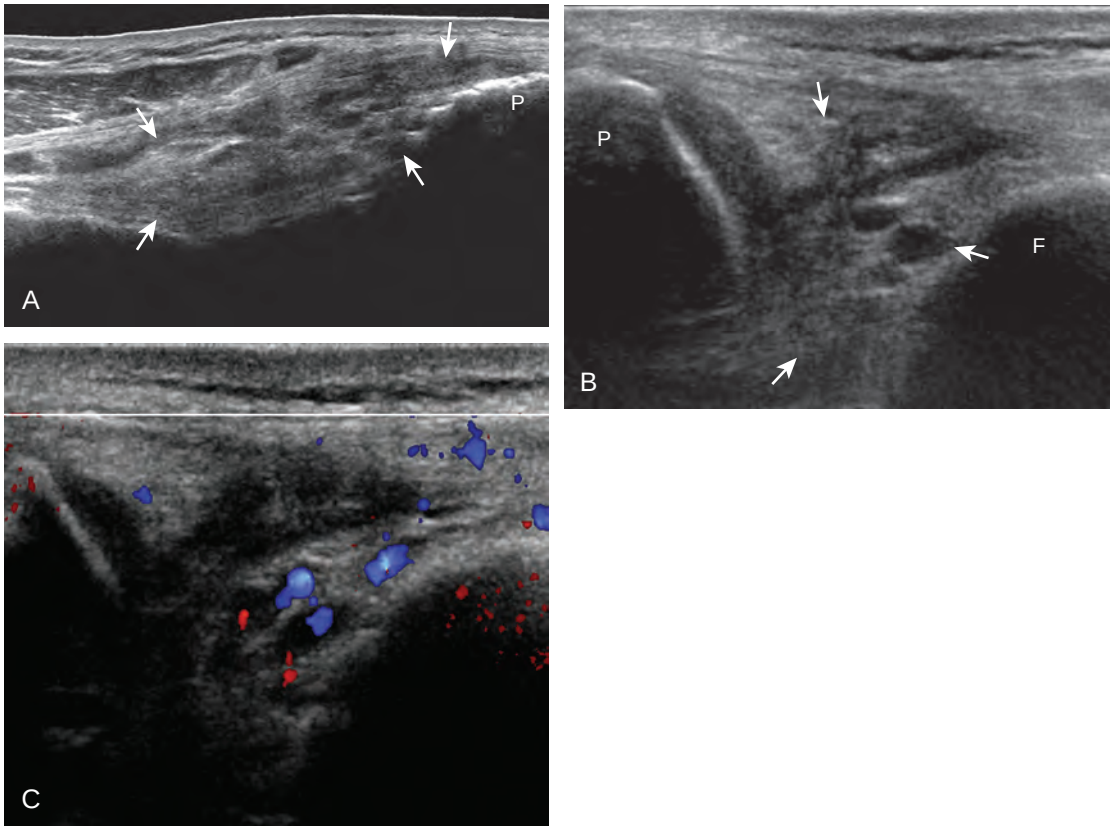

FIGURE 7-82 ■ Synovial hemangioma. Ultrasound images **(A)** in the sagittal plane over the suprapatellar recess and **(B)** transverse plane over medial patella and medial joint recess with **(C)** color Doppler imaging show mixed hyperechoic and hypoechoic hemangioma *(arrows)* with compressible vascular channels. F, femur; P, patella.

tissue mass (Fig. 7-80). The popliteal vein also should be assessed for thrombosis, which causes the popliteal vein to be noncompressible without flow (Fig. 7-81) (Video 7-10).[82] The differential diagnosis for a cyst adjacent to the popliteal artery also includes adventitial cystic disease of the popliteal artery.[83] Although hemangiomas and vascular malformations are discussed in Chapter 2, synovial hemangioma deserves mention here in that it most commonly involves the suprapatellar recess of the knee, appearing as mixed hyperechoic and hypoechoic tissue with compressible vascular channels (Fig. 7-82).[25]

Online references available at www.expertconsult.com.

REFERENCES

1. Fenn S, Datir A, Saifuddin A: Synovial recesses of the knee: MR imaging review of anatomical and pathological features. *Skeletal Radiol* 38:317–328, 2009.
2. Forbes JR, Helms CA, Janzen DL: Acute pes anserine bursitis: MR imaging. *Radiology* 194:525–527, 1995.
3. Rothstein CP, Laorr A, Helms CA, et al: Semimembranosus-tibial collateral ligament bursitis: MR imaging findings. *AJR Am J Roentgenol* 166:875–877, 1996.
4. Ward EE, Jacobson JA, Fessell DP, et al: Sonographic detection of Baker's cysts: comparison with MR imaging. *AJR Am J Roentgenol* 176:373–380, 2001.
5. De Maeseneer M, Van Roy F, Lenchik L, et al: Three layers of the medial capsular and supporting structures of the knee: MR imaging-anatomic correlation. *Radiographics* 20:S83–S89, 2000.
6. Munshi M, Pretterklieber ML, Kwak S, et al: MR imaging, MR arthrography, and specimen correlation of the posterolateral corner of the knee: an anatomic study. *AJR Am J Roentgenol* 180:1095–1101, 2003.
7. Wangwinyuvirat M, Dirim B, Pastore D, et al: Prepatellar quadriceps continuation: MRI of cadavers with gross anatomic and histologic correlation. *AJR Am J Roentgenol* 192:W111–116, 2009.
8. Phornphutkul C, Sekiya JK, Wojtys EM, et al: Sonographic imaging of the patellofemoral medial joint stabilizing structures: findings in human cadavers. *Orthopedics* 30:472–478, 2007.
9. Hubbard JK, Sampson HW, Elledge JR: Prevalence and morphology of the vastus medialis oblique muscle in human cadavers. *Anat Rec* 249:135–142, 1997.
10. Jan MH, Lin DH, Lin JJ, et al: Differences in sonographic characteristics of the vastus medialis obliquus between patients with patellofemoral pain syndrome and healthy adults. *Am J Sports Med* 37:1743–1749, 2009.
11. Beltran J, Matityahu A, Hwang K, et al: The distal semimembranosus complex: normal MR anatomy, variants, biomechanics and pathology. *Skeletal Radiol* 32:435–445, 2003.
12. Huang GS, Yu JS, Munshi M, et al: Avulsion fracture of the head of the fibula (the "arcuate" sign): MR imaging findings predictive of injuries to the posterolateral ligaments and posterior cruciate ligament. *AJR Am J Roentgenol*, 180:381–387, 2003.
13. Yoon CH, Kim HS, Ju JH, et al: Validity of the sonographic longitudinal sagittal image for assessment of the cartilage thickness in the knee osteoarthritis. *Clin Rheumatol* 27:1507–1516, 2008.
14. De Maeseneer M, Vanderdood K, Marcelis S, et al: Sonography of the medial and lateral tendons and ligaments of the knee: the use of bony landmarks as an easy method for identification. *AJR Am J Roentgenol* 178: 1437–1444, 2002.
15. Smith J, Sayeed YA, Finnoff JT, et al: The bifurcating distal biceps femoris tendon: potential pitfall in musculoskeletal sonography. *J Ultrasound Med* 30:1162–1166, 2011.
16. Sekiya JK, Jacobson JA, Wojtys EM: Sonographic imaging of the posterolateral structures of the knee: findings in human cadavers. *Arthroscopy* 18:872–881, 2002.
17. Cho KH, Lee DC, Chhem RK, et al: Normal and acutely torn posterior cruciate ligament of the knee at US evaluation: preliminary experience. *Radiology* 219:375–380, 2001.
18. Ptasznik R, Feller J, Bartlett J, et al: The value of sonography in the diagnosis of traumatic rupture of the anterior cruciate ligament of the knee. *AJR Am J Roentgenol* 164:1461–1463, 1995.
19. Hong BY, Lim SH, Cho YR, et al: Detection of knee effusion by ultrasonography. *Am J Phys Med Rehabil* 89:715–721, 2010.
20. Bianchi S, Zwass A, Abdelwahab IF, et al: Sonographic evaluation of lipohemarthrosis: clinical and in vitro study. *J Ultrasound Med* 14:279–282, 1995.
21. Wakefield RJ, Balint PV, Szkudlarek M, et al: Musculoskeletal ultrasound including definitions for ultrasonographic pathology. *J Rheumatol* 32:2485–2487, 2005.
22. Lin J, Jacobson JA, Jamadar DA, et al: Pigmented villonodular synovitis and related lesions: the spectrum of imaging findings. *AJR Am J Roentgenol* 172:191–197, 1999.
23. Learch TJ, Braaton M: Lipoma arborescence: high-resolution ultrasonographic findings. *J Ultrasound Med* 19:385–389, 2000.
24. Roberts D, Miller TT, Erlanger SM: Sonographic appearance of primary synovial chondromatosis of the knee. *J Ultrasound Med* 23:707–709, 2004.
25. Greenspan A, Azouz EM, Matthews J 2nd, et al: Synovial hemangioma: imaging features in eight histologically proven cases, review of the literature, and differential diagnosis. *Skeletal Radiol* 24:583–590, 1995.
26. Huang GS, Lee CH, Chan WP, et al: Localized nodular synovitis of the knee: MR imaging appearance and clinical correlates in 21 patients. *AJR Am J Roentgenol* 181:539–543, 2003.
27. Koh YG, Kim SJ, Chun YM, et al: Arthroscopic treatment of patellofemoral soft tissue impingement after posterior stabilized total knee arthroplasty. *Knee* 15:36–39, 2008.
28. Wareluk P, Szopinski KT: Value of modern sonography in the assessment of meniscal lesions. *Eur J Radiol* 2011, Oct 5 [Epub ahead of print].
29. Azzoni R, Cabitza P: Is there a role for sonography in the diagnosis of tears of the knee menisci? *J Clin Ultrasound* 30:472–476, 2002.
30. Rutten MJ, Collins JM, van Kampen A, et al: Meniscal cysts: detection with high-resolution sonography. *AJR Am J Roentgenol* 171:491–496, 1998.
31. De Smet AA, Graf BK, del Rio AM: Association of parameniscal cysts with underlying meniscal tears as identified on MRI and arthroscopy. *AJR Am J Roentgenol* 196:W180–186, 2011.
32. Seymour R, Lloyd DC: Sonographic appearances of meniscal cysts. *J Clin Ultrasound* 26:15–20, 1998.
33. Naredo E, Cabero F, Palop MJ, et al: Ultrasonographic findings in knee osteoarthritis: a comparative study with clinical and radiographic assessment. *Osteoarthritis Cartilage* 13:568–574, 2005.
34. Blankenbaker DG, De Smet AA, Fine JP: Is intra-articular pathology associated with MCL edema on MR imaging of the non-traumatic knee? *Skeletal Radiol* 34:462–467, 2005.
35. Miller TT, Staron RB, Feldman F, et al: Meniscal position on routine MR imaging of the knee. *Skeletal Radiol* 26:424–427, 1997.
36. Chan SK, Robb CA, Singh T, et al: Medial dislocation of the medial meniscus. *J Bone Joint Surg Br* 92:155–157, 2010.
37. Abraham AM, Goff I, Pearce MS, et al: Reliability and validity of ultrasound imaging of features of knee osteoarthritis in the community. *BMC Musculoskelet Disord* 12:70, 2011.
38. Kazam JK, Nazarian LN, Miller TT, et al: Sonographic evaluation of femoral trochlear cartilage in patients with knee pain. *J Ultrasound Med* 30:797–802, 2011.
39. Sureda D, Quiroga S, Arnal C, et al: Juvenile rheumatoid arthritis of the knee: evaluation with US. *Radiology* 190:403–406, 1994.
40. Felus J, Kowalczyk B, Lejman T: Sonographic evaluation of the injuries after traumatic patellar dislocation in adolescents. *J Pediatr Orthop* 28:397–402, 2008.

41. Ciapetti A, Filippucci E, Gutierrez M, et al: Calcium pyrophosphate dihydrate crystal deposition disease: sonographic findings. *Clin Rheumatol* 28:271–276, 2009.
42. Filippucci E, Riveros MG, Georgescu D, et al: Hyaline cartilage involvement in patients with gout and calcium pyrophosphate deposition disease: an ultrasound study. *Osteoarthritis Cartilage* 17:178–181, 2009.
43. Thiele RG, Schlesinger N: Diagnosis of gout by ultrasound. *Rheumatology (Oxford)* 46:1116–1121, 2007.
44. Thiele RG, Schlesinger N: Ultrasonography shows disappearance of monosodium urate crystal deposition on hyaline cartilage after sustained normouricemia is achieved. *Rheumatol Int* 30:495–503, 2010.
45. Friedman L, Finlay K, Popovich T, et al: Sonographic findings in patients with anterior knee pain. *J Clin Ultrasound* 31:85–97, 2003.
46. Pfirrmann CW, Jost B, Pirkl C, et al: Quadriceps tendinosis and patellar tendinosis in professional beach volleyball players: sonographic findings in correlation with clinical symptoms. *Eur Radiol* 18:1703–1709, 2008.
47. La S, Fessell DP, Femino JE, et al: Sonography of partial-thickness quadriceps tendon tears with surgical correlation. *J Ultrasound Med* 22:1323–1329; quiz 30–31, 2003.
48. Bianchi S, Zwass A, Abdelwahab IF, et al: Diagnosis of tears of the quadriceps tendon of the knee: value of sonography. *AJR Am J Roentgenol* 162:1137–1140, 1994.
49. Khan KM, Bonar F, Desmond PM, et al: Patellar tendinosis (jumper's knee): findings at histopathologic examination, US, and MR imaging. Victorian Institute of Sport Tendon Study Group. *Radiology* 200:821–827, 1996.
50. Hoksrud A, Ohberg L, Alfredson H, et al: Color Doppler ultrasound findings in patellar tendinopathy (jumper's knee). *Am J Sports Med* 36:1813–1820, 2008.
51. De Flaviis L, Nessi R, Scaglione P, et al: Ultrasonic diagnosis of Osgood-Schlatter and Sinding-Larsen-Johansson diseases of the knee. *Skeletal Radiol* 18:193–197, 1989.
52. Jarvela T, Paakkala T, Kannus P, et al: Ultrasonographic and power Doppler evaluation of the patellar tendon ten years after harvesting its central third for reconstruction of the anterior cruciate ligament: comparison of patients without or with anterior knee pain. *Am J Sports Med* 32:39–46, 2004.
53. Lee J, Robinson G, Finlay K, et al: Evaluation of the quadriceps tendon, patellar tendon, and collateral ligaments after total knee arthroplasty: appearances in the early postoperative period. *Can Assoc Radiol J* 57:291–298, 2006.
54. Bonaldi VM, Chhem RK, Drolet R, et al: Iliotibial band friction syndrome: sonographic findings. *J Ultrasound Med* 17:257–260, 1998.
55. Muhle C, Ahn JM, Yeh L, et al: Iliotibial band friction syndrome: MR imaging findings in 16 patients and MR arthrographic study of six cadaveric knees. *Radiology* 212:103–110, 1999.
56. Puig JG, de Miguel E, Castillo MC, et al: Asymptomatic hyperuricemia: impact of ultrasonography. *Nucleosides Nucleotides Nucleic Acids* 27:592–595, 2008.
57. Thiele RG: Role of ultrasound and other advanced imaging in the diagnosis and management of gout. *Curr Rheumatol Rep* 13:146–153, 2011.
58. de Avila Fernandes E, Kubota ES, Sandim GB, et al: Ultrasound features of tophi in chronic tophaceous gout. *Skeletal Radiol* 40:309–315, 2011.
59. Lee JI, Song IS, Jung YB, et al: Medial collateral ligament injuries of the knee: ultrasonographic findings. *J Ultrasound Med* 15:621–625, 1996.
60. Jose J, Schallert E, Lesniak B: Sonographically guided therapeutic injection for primary medial (tibial) collateral bursitis. *J Ultrasound Med* 30:257–261, 2011.
61. Sekiya JK, Swaringen JC, Wojtys EM, et al: Diagnostic ultrasound evaluation of posterolateral corner knee injuries. *Arthroscopy* 26:494–499, 2010.
62. Miller TT: Sonography of injury of the posterior cruciate ligament of the knee. *Skeletal Radiol* 31:149–154, 2002.
63. Hsu CC, Tsai WC, Chen CP, et al: Ultrasonographic examination of the normal and injured posterior cruciate ligament. *J Clin Ultrasound* 33:277–282, 2005.
64. Skovgaard Larsen LP, Rasmussen OS: Diagnosis of acute rupture of the anterior cruciate ligament of the knee by sonography. *Eur J Ultrasound* 12:163–167, 2000.
65. Palm HG, Bergenthal G, Ehry P, et al: Functional ultrasonography in the diagnosis of acute anterior cruciate ligament injuries: a field study. *Knee* 16:441–446, 2009.
66. DeFriend DE, Schranz PJ, Silver DA: Ultrasound-guided aspiration of posterior cruciate ligament ganglion cysts. *Skeletal Radiol* 30:411–414, 2001.
67. Boutry N, Dupont S, Glaude E, et al: Segond fracture revealed by ultrasonography. *J Ultrasound Med* 24:1431–1435, 2005.
68. Pearce T, Cobby M: Radiographically occult fracture of the tibial epiphysis: sonographic findings with CT correlation. *J Clin Ultrasound* 39:425–426, 2011.
69. Blankstein A, Cohen I, Salai M, et al: Ultrasonography: an imaging modality enabling the diagnosis of bipartite patella. *Knee Surg Sports Traumatol Arthrosc* 9:221–224, 2001.
70. Neubauer H, Morbach H, Schwarz T, et al: Popliteal cysts in paediatric patients: clinical characteristics and imaging features on ultrasound and MRI. *Arthritis* 2011:751593, 2011.
71. Uson J, Aguado P, Bernad M, et al: Pes anserinus tendinobursitis: what are we talking about? *Scand J Rheumatol* 29:184–186, 2000.
72. Aguiar RO, Viegas FC, Fernandez RY, et al: The prepatellar bursa: cadaveric investigation of regional anatomy with MRI after sonographically guided bursography. *AJR Am J Roentgenol* 188:W355–358, 2007.
73. Viegas FC, Aguiar RO, Gasparetto E, et al: Deep and superficial infrapatellar bursae: cadaveric investigation of regional anatomy using magnetic resonance after ultrasound-guided bursography. *Skeletal Radiol* 36:41–46, 2007.
74. Ahmed A, Bayol MG, Ha SB: Adventitious bursae in below knee amputees: case reports and a review of the literature. *Am J Phys Med Rehabil* 73:124–129, 1994.
75. Bui-Mansfield LT, Youngberg RA: Intraarticular ganglia of the knee: prevalence, presentation, etiology, and management. *AJR Am J Roentgenol* 168:123–127, 1997.
76. Young NP, Sorenson EJ, Spinner RJ, et al: Clinical and electrodiagnostic correlates of peroneal intraneural ganglia. *Neurology* 72:447–452, 2009.
77. Spinner RJ, Desy NM, Amrami KK: Sequential tibial and peroneal intraneural ganglia arising from the superior tibiofibular joint. *Skeletal Radiol* 37:79–84, 2008.
78. Visser LH: High-resolution sonography of the common peroneal nerve: detection of intraneural ganglia. *Neurology* 67:1473–1475, 2006.
79. Thomas AJ, Bull MJ, Howard AC, et al: Peri operative ultrasound guided needle localisation of amputation stump neuroma. *Injury* 30:689–691, 1999.
80. Tagliafico A, Altafini L, Garello I, et al: Traumatic neuropathies: spectrum of imaging findings and postoperative assessment. *Semin Musculoskelet Radiol* 14:512–522, 2010.
81. Kapoor BS, Haddad HL, Saddekni S, et al: Diagnosis and management of pseudoaneurysms: an update. *Curr Probl Diagn Radiol* 38:170–188, 2009.
82. Hamper UM, DeJong MR, Scoutt LM: Ultrasound evaluation of the lower extremity veins. *Radiol Clin North Am* 45:525–547, ix, 2007.
83. Franca M, Pinto J, Machado R, et al: Case 157: bilateral adventitial cystic disease of the popliteal artery. *Radiology* 255:655–660, 2010.

eBOX 7-1 Sample Diagnostic Knee Ultrasound Report

NORMAL

Examination: Ultrasound of the Right Knee
Date of Study: March 11, 2011
Patient Name: Jack White
Registration Number: 8675309
History: Trauma
Findings: The extensor mechanism, including the quadriceps tendon, patella, and patellar tendon, is normal without bursal abnormalities. No significant joint effusion or synovial hypertrophy. The medial collateral and lateral collateral ligaments are normal. Unremarkable iliotibial tract, biceps femoris, popliteus tendon, and common peroneal nerve. No Baker cyst. Limited evaluation of the menisci is unremarkable.
Impression: Unremarkable ultrasound examination of the right knee.

eBOX 7-2 Sample Diagnostic Knee Ultrasound Report

ABNORMAL

Examination: Ultrasound of the Right Knee
Date of Study: March 11, 2011
Patient Name: Jack White
Registration Number: 8675309
History: Pain, evaluate for cyst
Findings: The extensor mechanism, including the quadriceps tendon, patella, and patellar tendon, is normal. There is a moderate-sized joint effusion and no synovial hypertrophy or intra-articular body. The medial and lateral collateral ligaments are normal, as is the iliotibial tract, biceps femoris, popliteus tendon, and common peroneal nerve. There is medial compartment joint space narrowing and osteophyte formation with mild extrusion of the body of the medial meniscus, which is abnormally hypoechoic. No parameniscal cyst. There is a Baker cyst measuring 2 × 2 × 6 cm. Abnormal hypoechogenicity is noted at the inferior margin of the Baker cyst. There is also a hypoechoic cleft involving the posterior horn of the medial meniscus, which extends to the articular surface.
Impression:
1. Baker cyst with evidence for rupture.
2. Medial compartment osteoarthritis with moderate joint effusion.
3. Suspect posterior horn medial meniscal tear. Consider magnetic resonance imaging for confirmation if indicated.

CHAPTER 8

Ankle, Foot, and Lower Leg Ultrasound

CHAPTER OUTLINE

ANKLE AND FOOT ANATOMY
Osseous Anatomy
Muscle and Tendon Anatomy
Ligamentous Anatomy

ULTRASOUND EXAMINATION TECHNIQUE
General Comments
Anterior Ankle Evaluation
Medial Ankle Evaluation
Lateral Ankle Evaluation
Posterior Ankle and Heel Evaluation
Evaluation of the Calf
Evaluation of the Forefoot

JOINT AND BURSAL ABNORMALITIES
Joint Effusion and Synovial Hypertrophy
Inflammatory Arthritis
Bursal Abnormalities

TENDON AND MUSCLE ABNORMALITIES
Medial Ankle
Lateral Ankle
Anterior Ankle and Anterior Lower Leg
Posterior Ankle
Calf
Plantar Foot

LIGAMENT ABNORMALITIES

FRACTURE

PERIPHERAL NERVE ABNORMALITIES

MASSES AND CYSTS

Additional videos for this topic are available online at www.expertconsult.com.

ANKLE AND FOOT ANATOMY

Osseous Anatomy

The ankle joint is a hinged synovial articulation between the talus and the distal tibia and the fibula (Fig. 8-1). Inferiorly, the talus articulates with the calcaneus through three facets, joined by the cervical and interosseous talocalcaneal ligaments located in a cone-shaped region termed the *sinus tarsi*, which opens laterally.[1] The Chopart joint represents the articulations between the talus and navicular and the calcaneus and cuboid bones. The navicular, in turn, articulates with the medial, middle, and lateral cuneiforms, which then articulate with the first through third metatarsals. The fourth and fifth metatarsals articulate directly with the cuboid bone, and the tarsometatarsal articulations collectively are called the *Lisfranc joint*. Phalangeal bones extend beyond the metatarsals.

Muscle and Tendon Anatomy

Anteriorly, from medial to lateral, are the tibialis anterior (origin: proximal tibia and interosseous membrane; insertion: base of first metatarsal and medial cuneiform), the extensor hallucis longus (origin: fibula and interosseous membrane; insertion: distal phalanx of the first digit), and the extensor digitorum longus tendons (origin: tibia, fibula, and interosseous membrane; insertion: phalanges of the second through fifth digits) (see Fig. 8-1A to C). The peroneus tertius extends from the fibula and interosseous membrane to the base of the fifth metatarsal. The anterior tendons are held in place by the superior and inferior extensor retinacula. The anterior tibial artery courses beneath the superior extensor retinaculum and becomes the dorsalis pedis artery, located between the extensor hallucis and

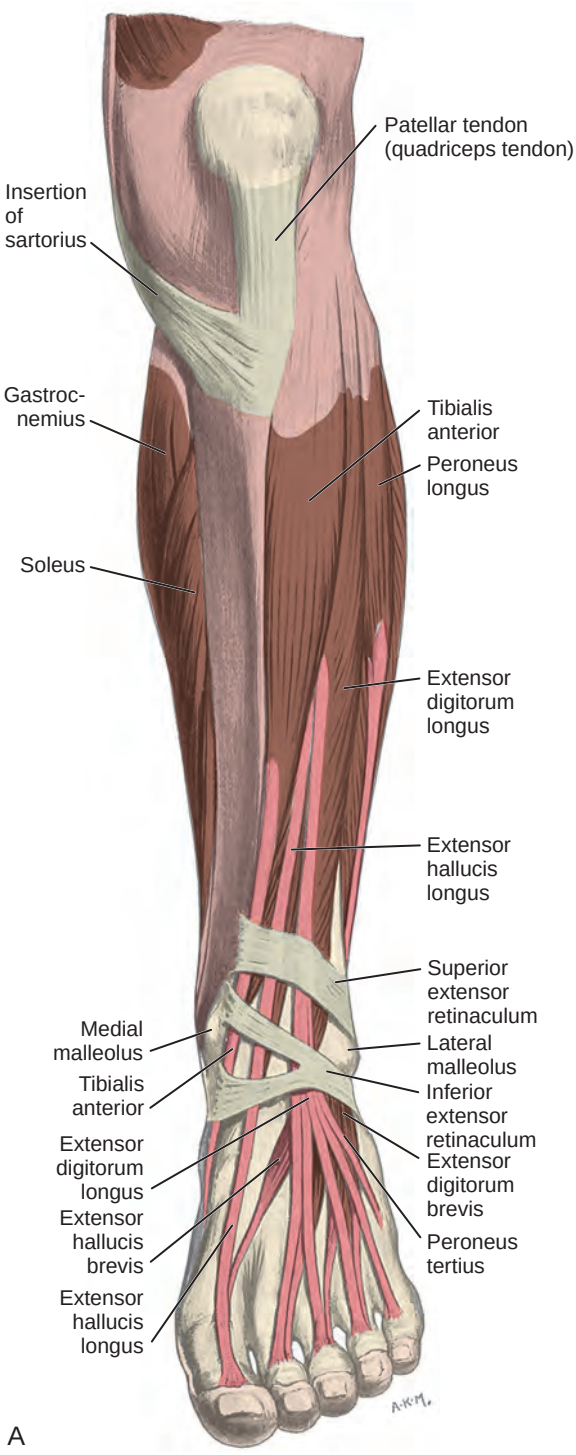

FIGURE 8-1 ■ **Leg, ankle, and foot anatomy. A,** Anterior view of left leg.

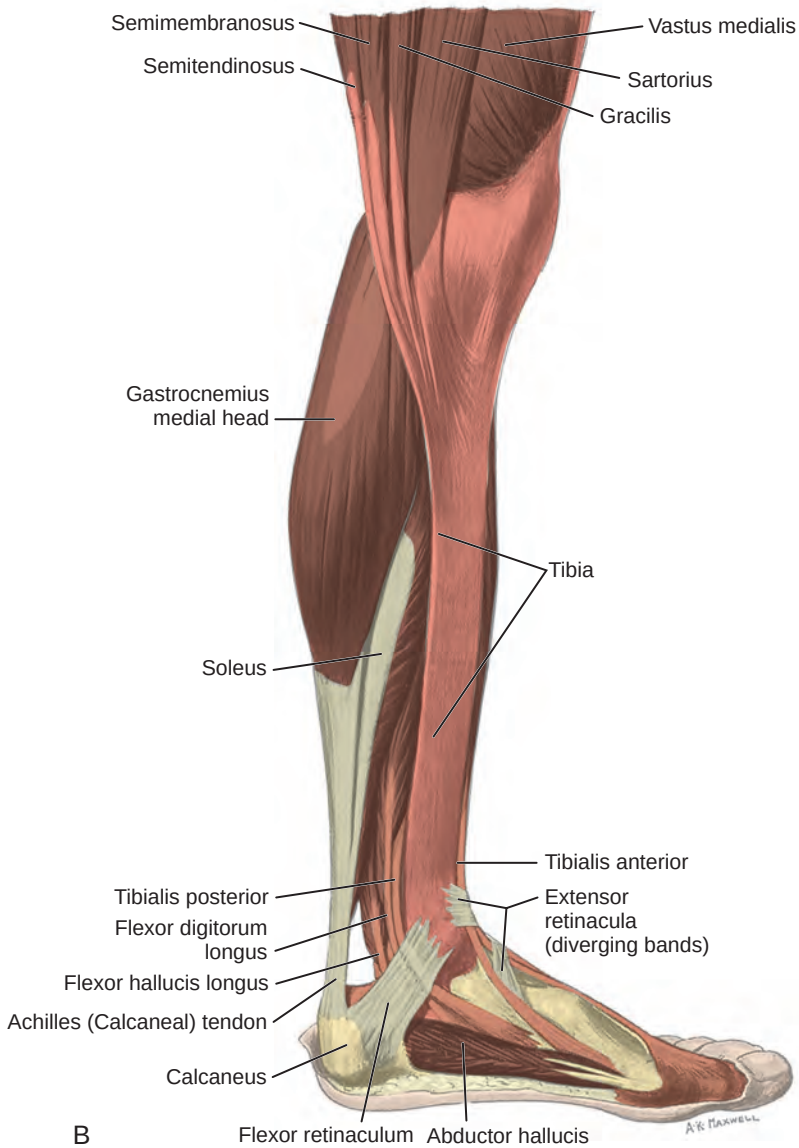

FIGURE 8-1, cont'd ■ **B,** Medial view of left leg.

Continued

extensor digitorum longus tendons. The deep peroneal nerve follows the anterior tibial artery and dorsal pedis and bifurcates as medial and lateral branches anterior to the ankle.

Medially, from anterior to posterior, are the tibialis posterior (origin: tibia, fibula, and interosseous membrane; insertion: navicular, cuneiforms, and second through fourth metatarsals), the flexor digitorum longus (origin: tibia; insertion: distal phalanges of second through fifth digits), and the flexor hallucis longus tendons (origin: fibula; insertion: base of distal phalanx of first digit) (see Fig. 8-1A to D). Between the flexor digitorum and flexor hallucis longus tendons at the posterior ankle are the tibial nerve and posterior tibial artery and veins. The order of structures from anterior to posterior from the medial malleolus can be remembered with the phrase "Tom, Dick, And Very Nervous Harry" (T, Tibialis posterior tendon; D, flexor Digitorum longus tendon; A, tibial Artery; V, tibial Veins; N, tibial Nerve; and H, flexor Hallucis longus tendon). The flexor retinaculum extends from the medial malleolus to the calcaneus superficial to the medial tendons and tibial nerve, which forms the roof of the tarsal tunnel. The tibial nerve divides into medial and lateral plantar nerves and a smaller medial calcaneal nerve.[2] The inferior

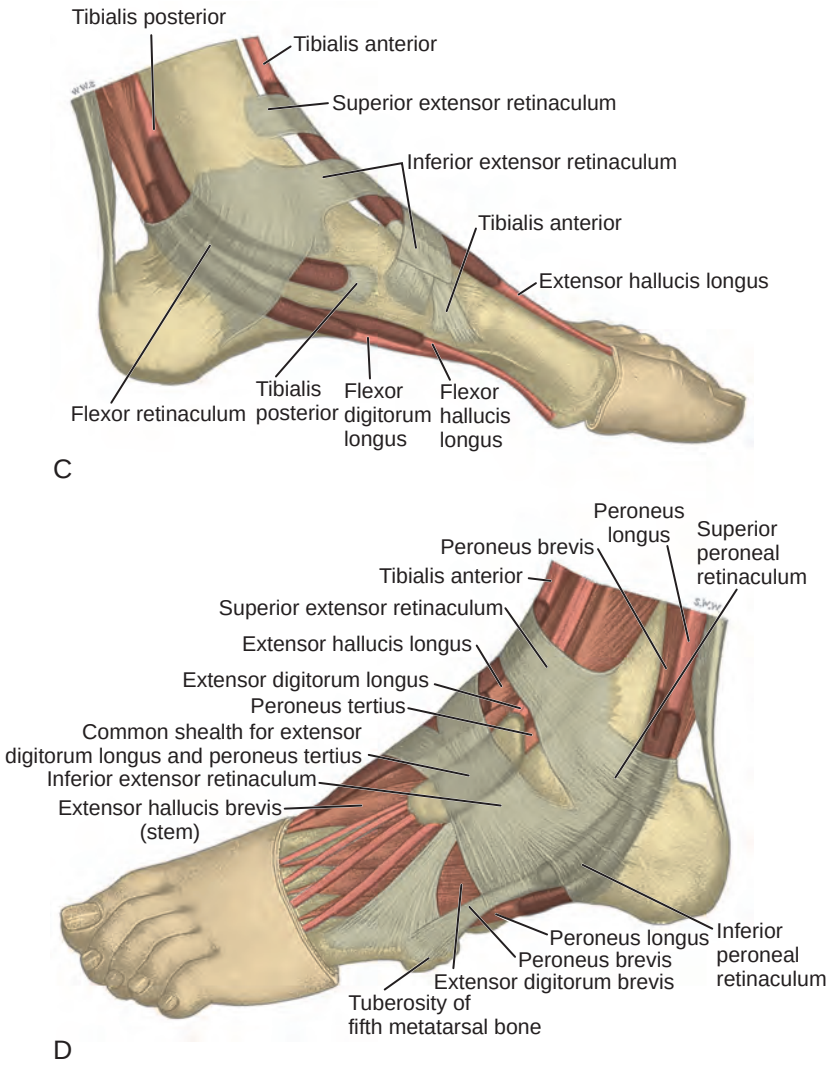

FIGURE 8-1, cont'd ■ **C,** Medial view of left ankle. **D,** Lateral view of left ankle.

calcaneal nerve usually originates from the lateral plantar branch and courses between the abductor hallucis and quadratus plantae muscles and then adjacent to the calcaneus.[3] The medial and lateral plantar nerves continue toward the digits as the common plantar digital nerves and then as the proper plantar digital nerves. More distally under the mid-foot, the flexor digitorum and flexor hallucis longus tendons cross each other, a configuration termed the *knot of Henry*. The flexor digitorum and flexor hallucis brevis muscles are located in the plantar aspect of the foot.

Laterally, the peroneus brevis (origin: distal fibula; insertion: fifth metatarsal base) and peroneus longus tendons (origin: proximal fibula and tibial condyle; insertion: first metatarsal base and medial cuneiform) are found posterior to the fibula (see Fig. 8-1A, B, D, and E). The musculotendinous junction of the peroneus longus is more superior to that of the peroneus brevis; at the level of the distal fibula, the peroneus brevis muscle and tendon are found medial and anterior to the tendon of the peroneus longus. More distally, the peroneus brevis tendon is typically in contact with the posterior fibular or retromalleolar groove. The normal peroneus muscle belly should taper so that only tendon is present at the fibula tip.[4] The peroneal tendons are held in place by the superior and inferior peroneal retinacula.[5] The peroneal tendons then course anteriorly on each side of the peroneal tubercle of the calcaneus and extend to their insertions. As a normal variant, an accessory tendon called the *peroneus quartus* may be found posterior to the fibula; this

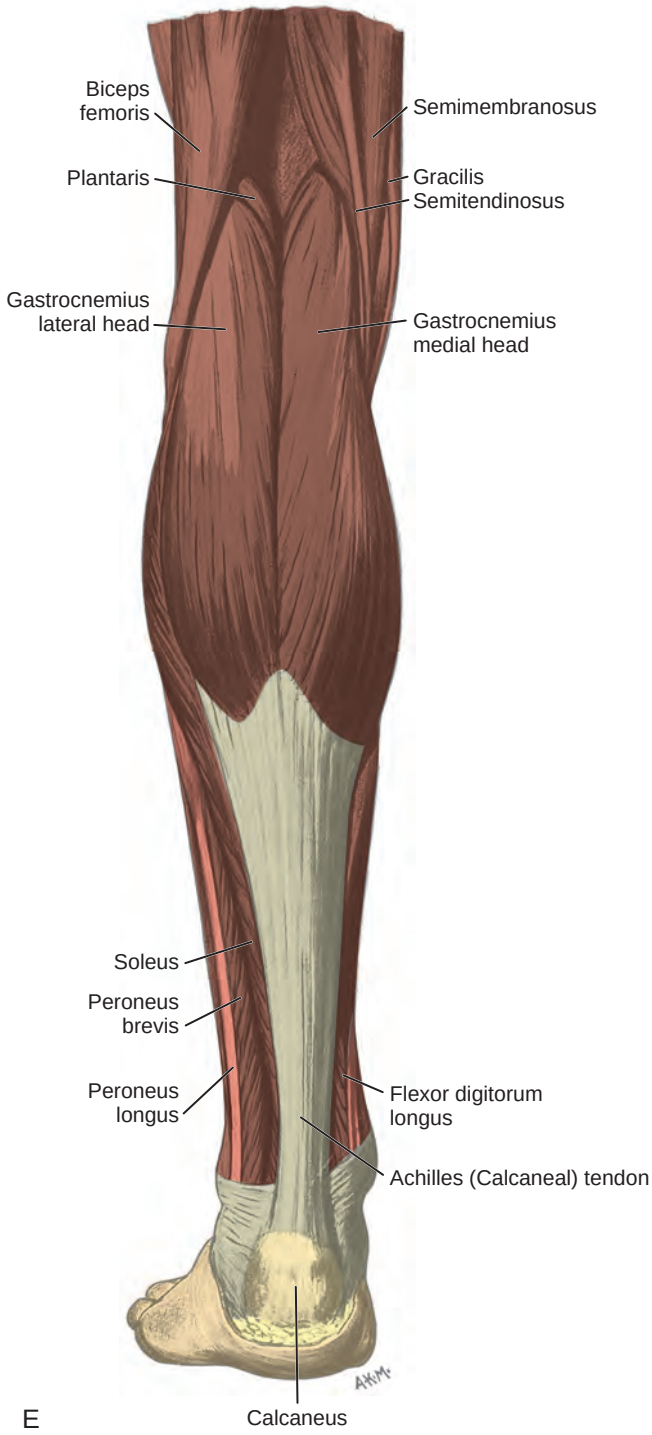

FIGURE 8-1, cont'd ■ **E,** Posterior view of calf.

Continued

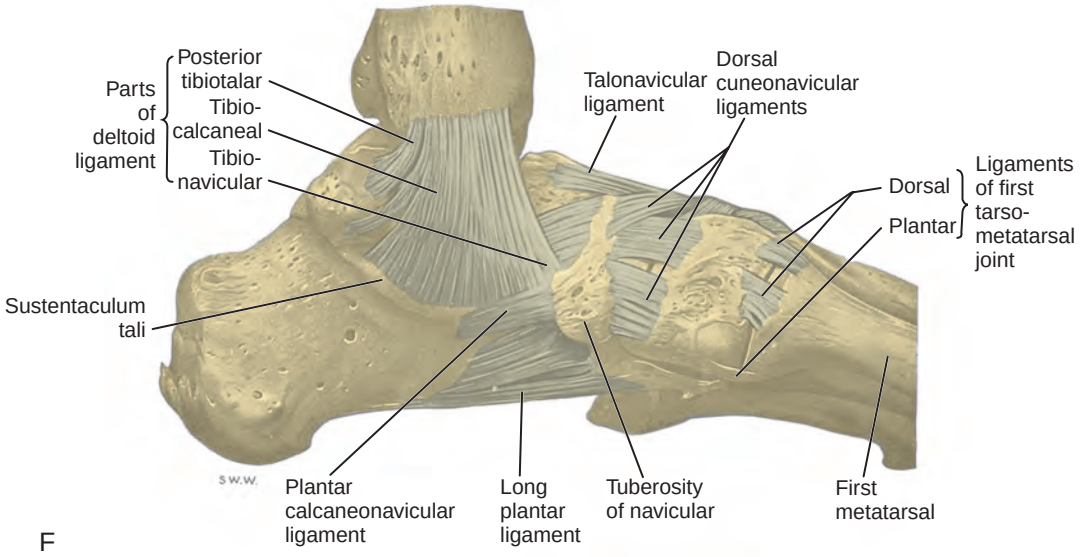

F

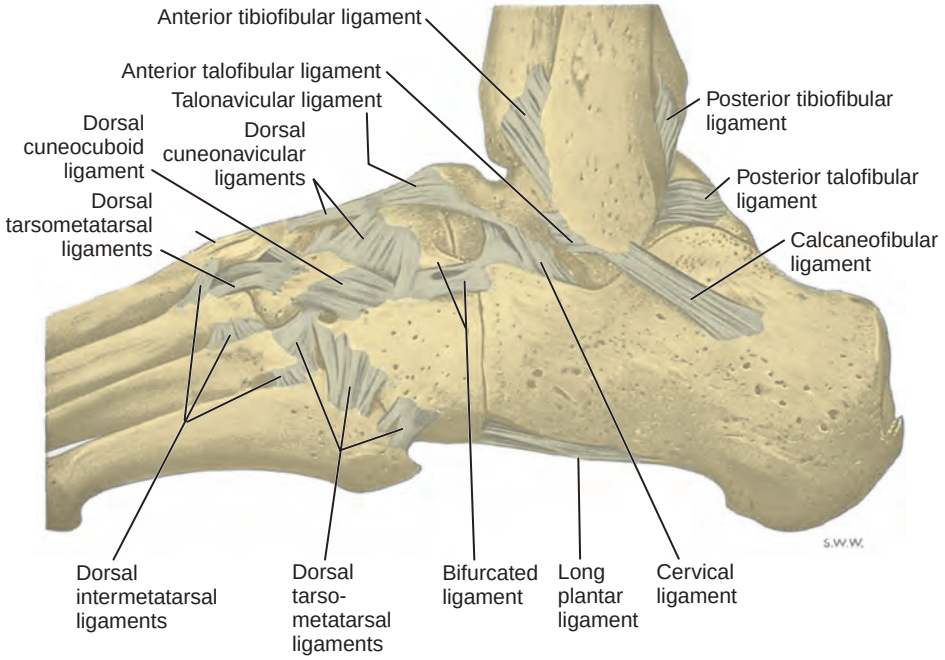

G

FIGURE 8-1, cont'd ■ **F,** Medial ankle and midfoot ligaments. **G,** Lateral ankle and midfoot ligaments.

tendon most commonly originates from the peroneus brevis and inserts on the lateral aspect of the calcaneus at the retrotrochlear eminence.[6] Over the lateral aspect of the calcaneus, the extensor digitorum brevis muscle originates from the calcaneus and extensor retinaculum and inserts distally on the second through fourth phalanges.

Posteriorly in the calf, the medial and lateral heads of the gastrocnemius muscle converge with the soleus to form the Achilles tendon (termed the *triceps surae*), which inserts onto the calcaneus (see Fig. 8-1B and E).[7] The plantaris muscle originates from the lateral femur, courses obliquely through the popliteal region, continues as a thin tendon between the muscle bellies of the medial head of the gastrocnemius and soleus muscles, courses distally at the medial aspect of the Achilles tendon, and then inserts onto the calcaneus. At the plantar aspect of the calcaneus, the plantar

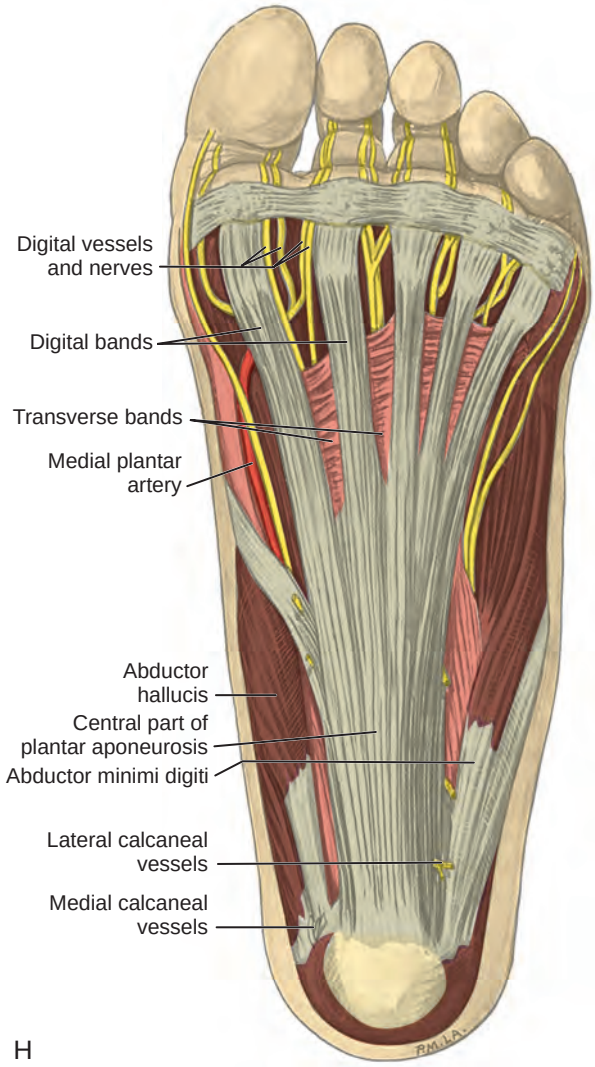

FIGURE 8-1, cont'd ■ **H,** Plantar aspect of left foot. (**A** and **E,** From Schaefer, EA, Symington J, Bryce TH [eds]: *Quain's anatomy,* 11th ed, London, 1915, Longmans, Green, with permission from Pearson Education; **B, C, D,** and **H,** from Standring S: *Gray's anatomy: the anatomical basis of clinical practice,* 39th ed, Edinburgh, 2005, Churchill Livingstone; **F** and **G,** drawn from a specimen in the Museum of the Royal College of Surgeons of England, with permission from the Council.)

aponeurosis originates from the medial calcaneus and extends distally as medial, central, and lateral cords (see Fig. 8-1H). The central cord envelops the flexor digitorum brevis muscle.

Ligamentous Anatomy

The stabilizing structures of the lateral ankle include the anterior talofibular ligament, which extends from the fibular to the talus in the transverse plane; the calcaneofibular ligament, which extends from the fibula inferiorly and posteriorly to the calcaneus deep to the peroneal tendons; and the posterior talofibular ligament, which extends from the fibula to the posterior aspect of the tibia in the transverse plane (see Fig. 8-1G).[8] In addition, the anterior and posterior tibiofibular ligaments extend laterally and inferiorly in an oblique fashion from the tibia to the fibula. An accessory anterior tibiofibular ligament may be present, also called *Bassett ligament*.[9] At the medial aspect of the ankle, the deltoid ligament is found, consisting of deep (anterior tibiotalar and posterior tibiotalar) and superficial (tibiocalcaneal and tibionavicular) components (see Fig. 8-1F).[8] The spring ligament complex consists of

superomedial, medioplantar, and inferoplantar calcaneonavicular ligaments.[10] In addition to other small ligaments that connect the various tarsal bones and are named by their osseous attachments, the Lisfranc ligament proper is a strong ligament that connects obliquely from the medial cuneiform to the base of the second metatarsal bone.[11] The bifurcate ligament extends from the calcaneus to the navicular and cuboid bones at the lateral aspect of the mid-foot.

ULTRASOUND EXAMINATION TECHNIQUE

Table 8-1 is a checklist for ankle, calf, and forefoot ultrasound examination. Examples of diagnostic ankle ultrasound reports are available online at www.expertconsult.com (see eBox 8-1 and 8-2).

General Comments

Ultrasound examination of the ankle and foot is comfortably completed with the patient supine and the foot and ankle on the examination table. Although limited examination of the distal Achilles and plantar aponeurosis may be completed in supine position with external rotation of the leg to gain access to these structures, a more thorough examination is best accomplished with the patient prone. This is essential when the clinical indication is to assess for Achilles tendon or calf abnormalities. A high-frequency transducer of at least 10 MHz is typically used because most of the structures are superficial. In general, the ankle tendons are first evaluated in short axis (with Achilles being the exception) to identify each structure and for orientation. Following this, evaluation of each tendon in long axis is completed for diagnosis of tendon tear or tendinosis. Evaluation of the calf, ankle, and foot may be initially focused over the area that is clinically symptomatic or that is relevant to the patient's history. Regardless, a complete examination of all areas should always be considered and is suggested for one to become familiar with normal anatomy and normal variants, to develop a quick and efficient sonographic technique, and to appreciate subtle or early pathologic changes. In addition to use of an ultrasound imaging protocol, it is essential that evaluation include any area of focal symptoms as directed by the patient. This is often a clue to locate pathologic processes and may include areas and structures not routinely assessed. This approach is quite important in the foot, where there are many structures closely associated that may produce symptoms. One example is identification of an osseous stress fracture.

TABLE 8-1 Ankle, Calf, and Forefoot Ultrasound Examination Checklist

Location	Structures of Interest
Ankle: anterior	Anterior tibiotalar joint recess Tibialis anterior Extensor hallucis longus Dorsal pedis artery Superficial peroneal nerve Extensor digitorum longus
Ankle: medial	Tibialis posterior Flexor digitorum longus Tibial nerve Flexor hallucis longus Deltoid ligament
Ankle: lateral	Peroneus longus and brevis Anterior talofibular ligament Calcaneofibular ligament Anterior tibiofibular ligament
Ankle: posterior	Achilles tendon Posterior bursae Plantar fascia
Calf	Soleus Medial and lateral heads of gastrocnemius Plantaris Achilles tendon
Forefoot	Dorsal joint recesses Morton neuroma

Anterior Ankle Evaluation

The primary structures evaluated from the anterior approach are the anterior ankle joint recess, the tibialis anterior, the extensor hallucis longus, the dorsalis pedis artery and superficial peroneal nerve, and the extensor digitorum longus. The transducer is first placed in the sagittal plane at the level of the tibiotalar joint with the foot in mild plantar flexion (Fig. 8-2A). The hyperechoic bone landmarks of the distal tibia and proximal talus are used for orientation, and the anterior ankle joint region is evaluated for joint abnormality (see Fig. 8-2B). It is important to evaluate not only the anterior joint recess in the sagittal plane but also the parasagittal plane laterally near the anterior talofibular ligament because small amounts of joint fluid may be present only at this site. Next, to evaluate the anterior tendons, the transducer is placed transversely at the level of the ankle joint (Fig. 8-3A). It is important to begin in the transverse plane, short axis to the tendons so that each of the tendons can be accounted for and differentiated from each other as they may appear similar in long axis. The tibialis anterior tendon is the largest, located most medially, with the typical hyperechoic and fibrillar echotexture (see Fig. 8-3B). One may toggle

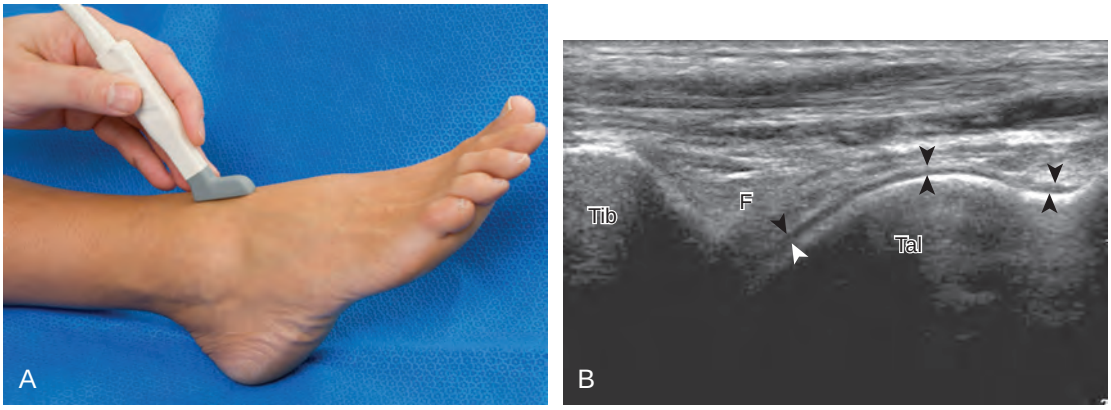

FIGURE 8-2 ■ Anterior ankle: joint recess. A, Sagittal imaging over the ankle joint shows **(B)** the normal hyperechoic anterior fat pad (F) between the tibia (Tib) and talus (Tal). Note hypoechoic hyaline articular cartilage *(arrowheads)*, which shows the full anterior extent of the anterior ankle joint recess. Bone contours appear hyperechoic when imaged perpendicular to sound beam, which is improved by toggling the transducer.

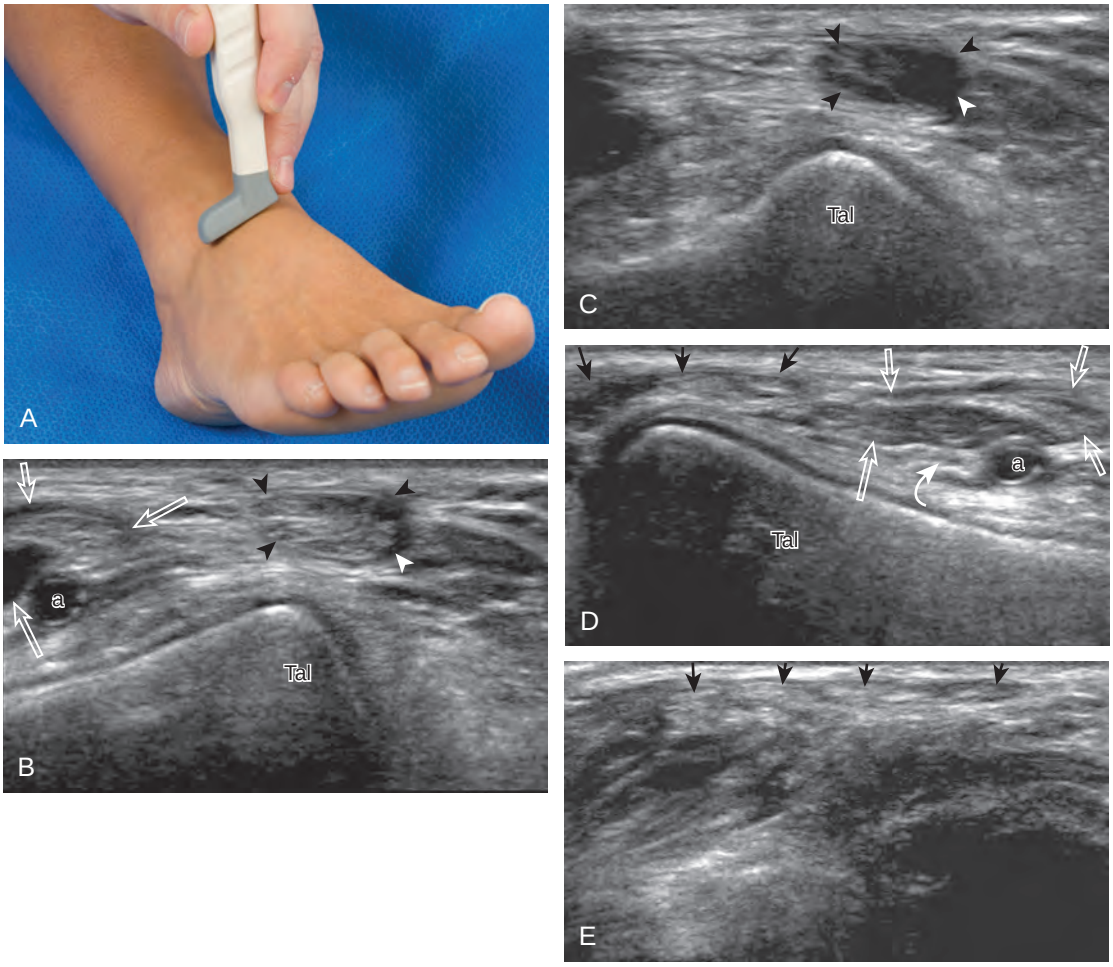

FIGURE 8-3 ■ Anterior ankle: tendons, short axis. A, Transverse imaging over the ankle shows **(B)** the tibialis anterior *(arrowheads)* and the extensor hallucis longus *(open arrows)* (right side of image is medial). Toggling the transducer shows **(C)** improved conspicuity of the tibialis anterior tendon *(arrowheads)* owing to anisotropy. Transverse imaging lateral to **B** shows **(D** and **E)** the extensor hallucis longus muscle and tendon *(open arrows)* and the extensor digitorum longus *(arrows)* (*curved arrow,* deep peroneal nerve; left side of images are lateral). a, Dorsalis pedis artery; Tal, talus.

the transducer (see Fig. 1-5B) to assist in identification of the tendons in short axis. This maneuver causes the normally hyperechoic tendon to appear artifactually hypoechoic from anisotropy, which will make the tendon more conspicuous surrounded by the hyperechoic fat (see Fig. 8-3C). Lateral to the tibialis anterior is the extensor hallucis longus (see Fig. 8-3D). The muscle belly of this structure extends more inferiorly compared with the other anterior tendons, and this hypoechoic muscle tissue should not be mistaken for tenosynovitis. The adjacent anterior tibial artery is seen as it crosses from medial to lateral deep to the extensor hallucis longus, which continues as the dorsal pedis artery once beyond the superior extensor retinaculum. The next lateral structure is the extensor digitorum longus with its multiple tendons that extend distally to the digits (see Fig. 8-3D and E). Lateral to this, the peroneus tertius extends to the fifth metatarsal base. Each of these structures should then be evaluated in long axis from proximal to the ankle joint to at least the mid-foot region, the extent of which can be guided by physical examination findings or patient history (Fig. 8-4). For identification of the deep peroneal nerve, the anterior tibial artery is an ideal landmark (Fig. 8-5); when moving the transducer from proximal to distal over the anterior tibial artery in short axis, the deep peroneal nerve is identified as it crosses from medial to lateral over the anterior tibial artery.

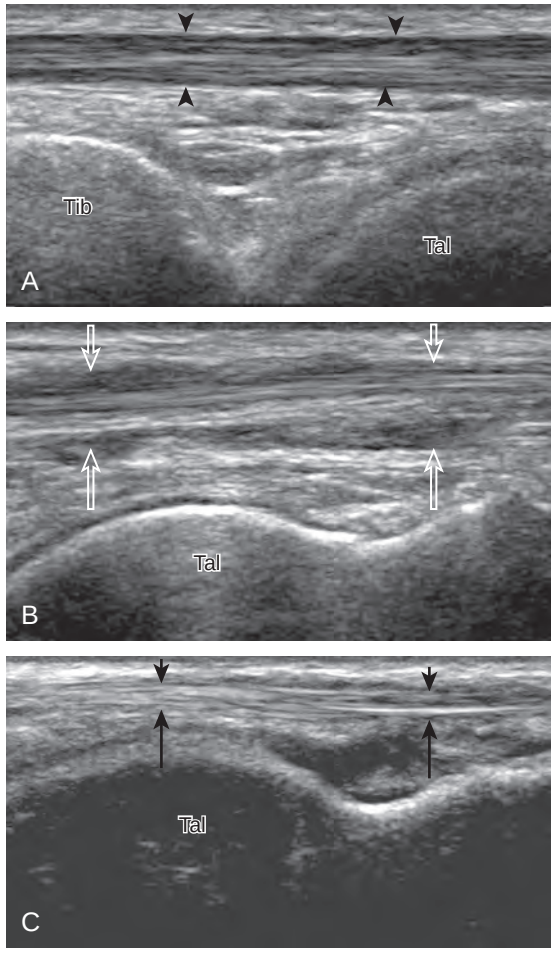

FIGURE 8-4 ■ Anterior ankle: tendons, long axis. Sagittal imaging shows **(A)** the tibialis anterior tendon *(arrowheads)*, **(B)** the extensor hallucis longus muscle and tendon *(open arrows)*, and **(C)** one of the extensor digitorum longus tendons *(arrows)* (right side of image is distal). Tal, talus; Tib, tibia.

Medial Ankle Evaluation

For medial evaluation, the supine patient externally rotates at the hip or rolls partially onto the ipsilateral side to gain access to the medial aspect of the ankle. Ultrasound examination begins in the transverse plane superior to the medial malleolus (Fig. 8-6A). The hyperechoic and shadowing surface of the tibia is seen, and the transducer is moved posteriorly. The first tendon identified is the tibialis posterior tendon in short axis (see Fig. 8-6B). One may toggle the transducer (see Fig. 1-3B) to assist in identification of the tendons in short axis, which causes the tendon to appear hypoechoic from anisotropy and improves conspicuity compared with the adjacent hyperechoic fat (see Fig. 8-6C). The transducer is then moved posteriorly to identify the flexor digitorum longus tendon, the posterior tibial artery and veins, the tibial nerve, and then the flexor hallucis longus tendon in order from anterior to posterior (see Fig. 8-6D). The tibialis posterior tendon is typically twice the size of the adjacent flexor digitorum longus tendon. The thin and hyperechoic flexor retinaculum can also be identified superficial to the tendons, and it attaches to the tibia.

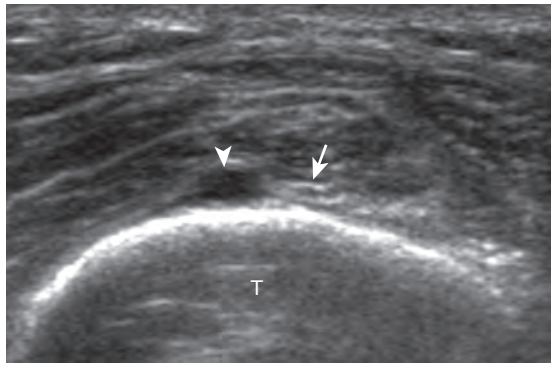

FIGURE 8-5 ■ Anterior ankle: deep peroneal nerve. Ultrasound image in the axial plane at level of distal tibia (T) shows deep peroneal nerve *(arrow)* medial to anterior tibial artery *(arrowhead)*. The anterior tibial veins are compressed and not visible.

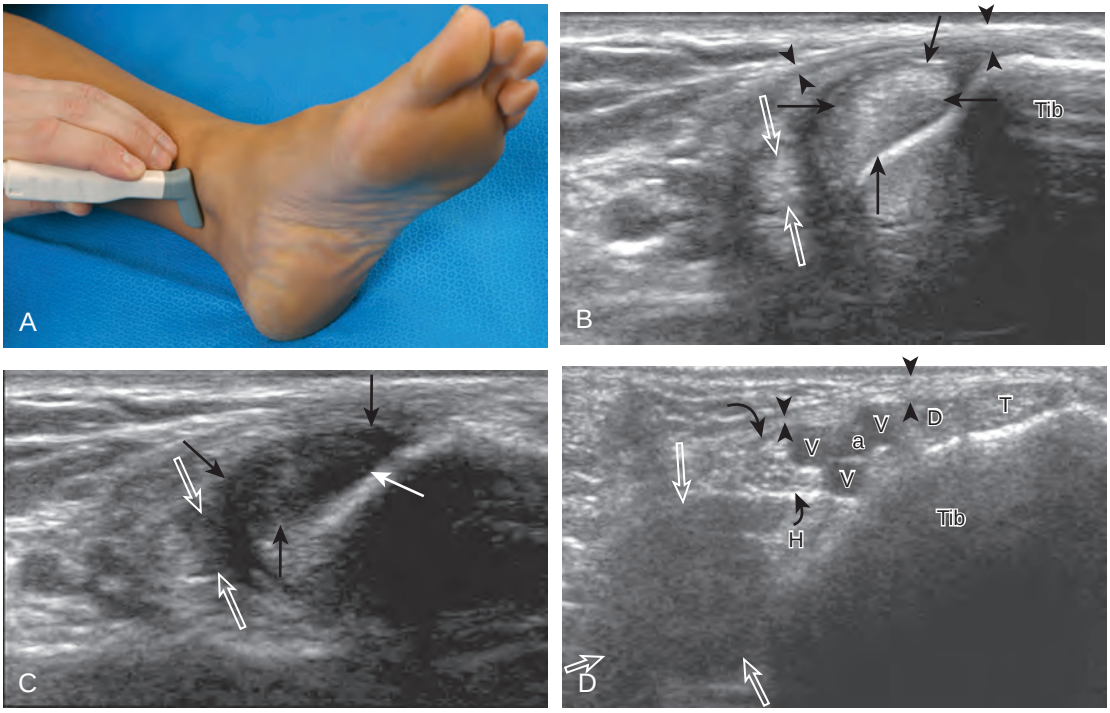

FIGURE 8-6 ■ Medial ankle: tendons, short axis, proximal. A, Transverse imaging superior and posterior to the medial malleolus shows **(B)** the tibialis posterior *(arrows)* and the flexor digitorum longus *(open arrows)* tendons (*arrowheads*, flexor retinaculum; right side of image is anterior). Toggling the transducer shows **(C)** improved conspicuity of the tibialis posterior *(arrows)* and flexor digitorum longus *(open arrows)* tendons owing to anisotropy. Transverse imaging posterior to **B** shows **(D)** the tibialis posterior tendon (T), flexor digitorum longus tendon (D), tibial artery (a) and veins (V), tibial nerve *(curved arrows)*, and flexor hallucis longus tendon (H) and muscle *(open arrows)* (*arrowheads*, flexor retinaculum). Tib, tibia.

Evaluation is continued distally with the transducer short axis to each tendon; the transducer is rotated to the coronal plane as each tendon is followed distally (Fig. 8-7A). Anisotropy is again used to help delineate each tendon in short axis (see Fig. 8-7B and C). At the medial aspect of the calcaneus, a bony protuberance called the *sustentaculum tali* protrudes medially to articulate with the talus as the middle facet of the anterior subtalar joint. The medial tendons have characteristic locations relative to the sustentaculum tali (see Fig. 8-7B). The tibialis posterior tendon is dorsal and superficial, the flexor digitorum longus lies immediately superficial, and the flexor hallucis longus tendon lies plantar to the sustentaculum tali in a bony groove of the calcaneus.

In the supramalleolar region, the tibial nerve is located between the flexor digitorum longus and flexor hallucis longus tendons. In cross section, the individual hypoechoic nerve fascicles surrounded by hyperechoic connective tissue take on a honeycomb appearance (see Fig. 8-6D), whereas in long axis a fascicular pattern is appreciated that, in contrast to adjacent tendons, is coarser in echotexture. In the supramalleolar region, a small medial calcaneal nerve arising from the tibial nerve can be identified; this branch courses directly inferior, medial to the calcaneus (Fig. 8-8). The tibial nerve then divides into medial and lateral plantar branches, which continue under the mid-foot to give off the common plantar digital nerves and then the proper plantar digital branches.

To assess for medial tendon abnormality in long axis, the transducer is then moved back to the level of the distal tibia over the tibialis posterior tendon and is turned 90 degrees (Fig. 8-9A and B). As the transducer follows the course of the tibialis posterior tendon in long axis, the transducer moves from a coronal plane relative to the body to the axial plane (see Fig. 8-9C to F). At the navicular bone, it is common to visualize mild thickening and decreased echogenicity of the distal tibialis posterior tendon, related to its insertion on the navicular and anisotropy from several of the tibialis posterior tendon fibers that course plantar to the navicular to insert at the cuneiforms and the second through fourth metatarsals

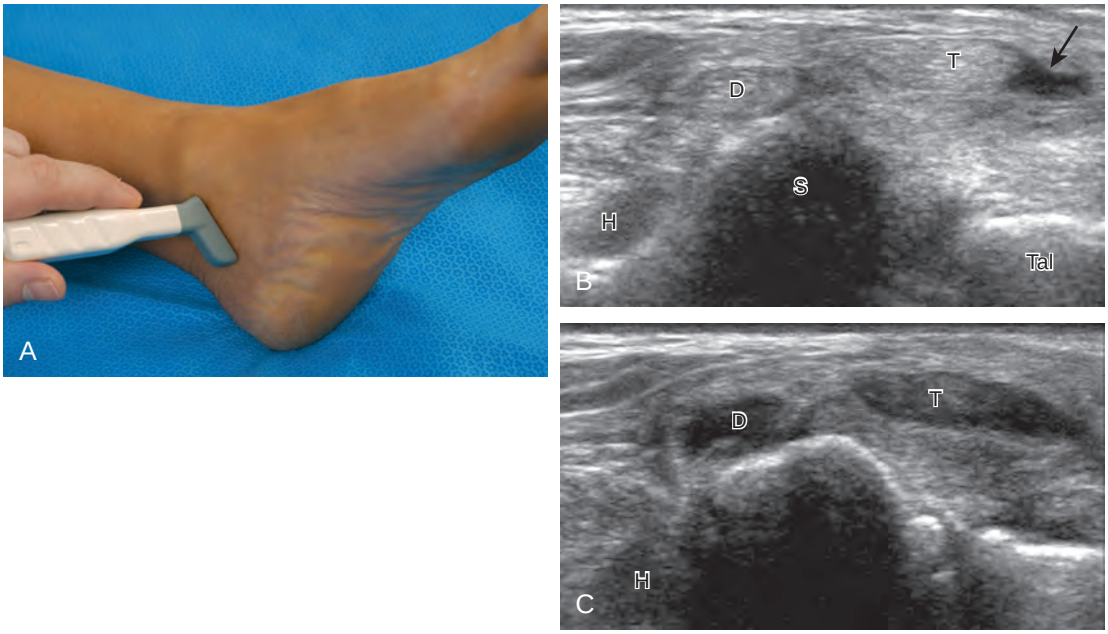

FIGURE 8-7 ■ Medial ankle: tendons, short axis, distal. A, Coronal imaging inferior to medial malleolus shows **(B)** the tibialis posterior tendon (T) with physiologic fluid *(arrow)*, the flexor digitorum longus (D), and flexor hallucis longus (H) tendons, which become more conspicuous with anisotropy **(C)** (left side of images are plantar). S, sustentaculum tali of the calcaneus; Tal, talus.

(see Fig. 8-9F). It is also common to see a small amount of fluid within the tendon sheath of the tibialis posterior tendon just beyond the medial malleolus, usually seen only along one side of the tendon; asymptomatic fluid should not be present at the navicular where a tendon sheath is absent.[12]

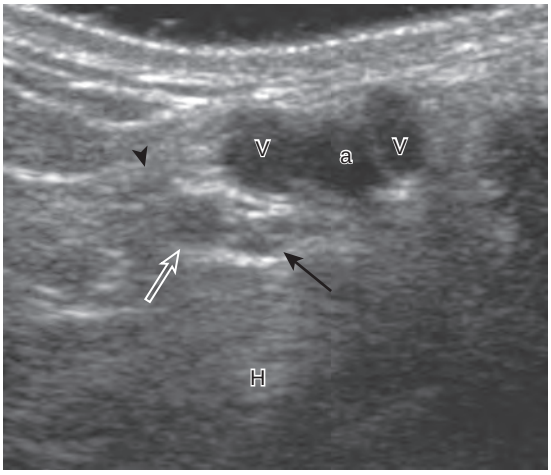

FIGURE 8-8 ■ Medial ankle: tibial nerve. Transverse imaging over the distal tibial nerve shows medial *(arrow)* and lateral *(open arrow)* plantar branches of the tibial nerve and medial calcaneal branch *(arrowhead)*. a, Tibial artery; H, flexor hallucis longus tendon; V, tibial veins.

An accessory navicular bone may be seen within the distal tibialis posterior tendon near the navicular bone (see Fig. 8-79). To assess the flexor digitorum longus tendon, examination again begins transversely superior and posterior to the medial malleolus, followed by assessment in long axis and distally (Fig. 8-10A). Similarly, the flexor hallucis longus tendon can be assessed first in short axis and then in long axis (see Fig. 8-10B). As the flexor digitorum longus and flexor hallucis longus tendons are followed distally beneath the mid-foot, the two tendons cross, called the *knot of Henry* (see Fig. 8-10C).

After assessment of the medial tendons, the components of the deltoid ligament are evaluated. The transducer is initially placed in the coronal plane at the medial malleolus (Fig. 8-11A). At this location, a superficial hyperechoic and fibrillar tibiocalcaneal component of the deltoid ligament is identified, extending from the tibia to the calcaneus (see Fig. 8-11B). With rotation of the distal aspect of the transducer anteriorly with the proximal aspect fixed to the medial malleolus, the more superficial tibionavicular and deeper anterior tibiotalar components are identified (see Fig. 8-11C). The distal aspect of the transducer is then rotated posteriorly while the proximal aspect remains fixed to the medial malleolus with the foot in dorsiflexion. In this

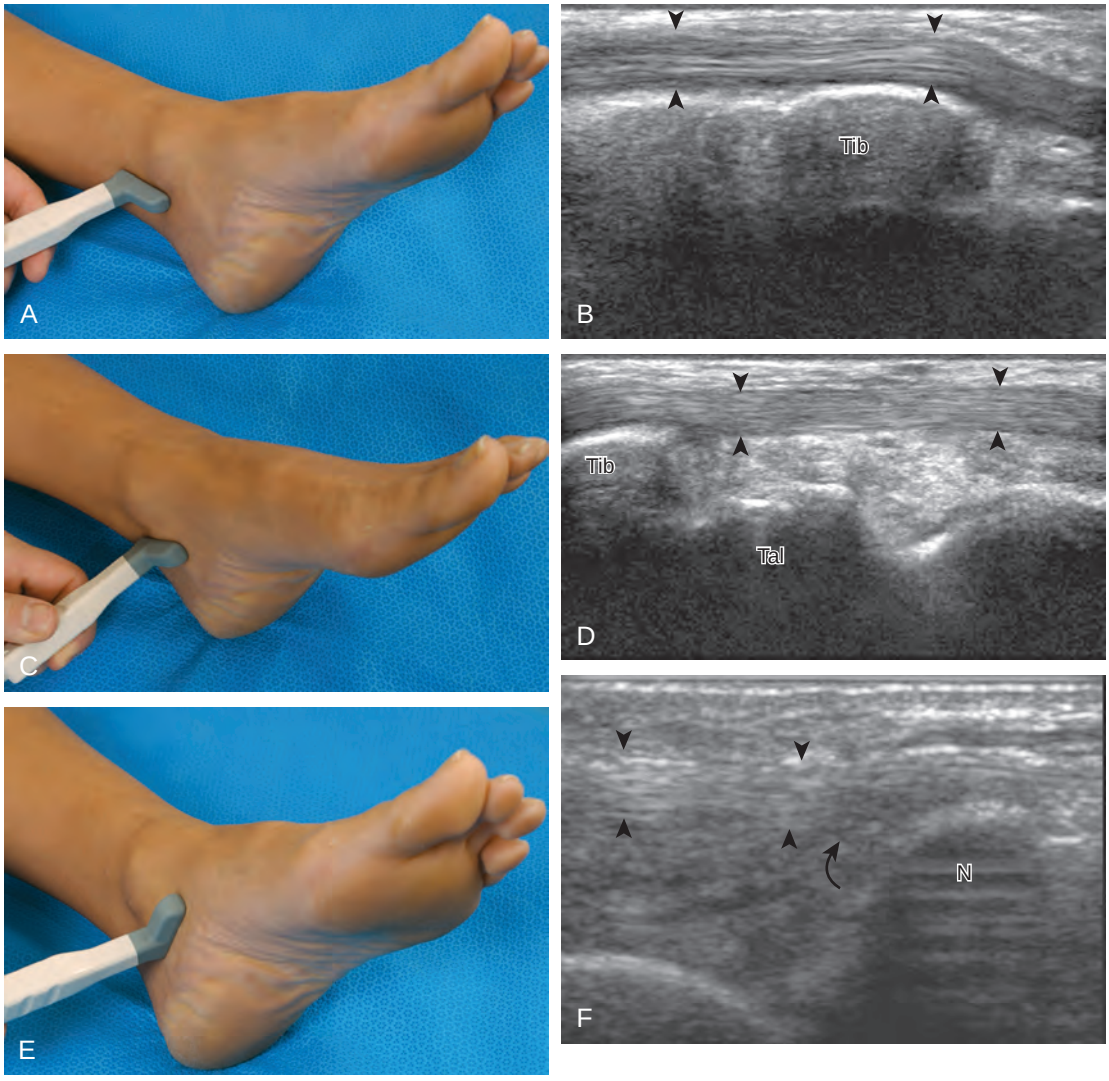

FIGURE 8-9 ■ Medial ankle: tibialis posterior tendon, long axis. Imaging long axis to tibialis posterior tendon *(arrowheads)* **(A** and **B)** proximally, **(C** and **D)** at the level of the medial malleolus, and **(E** and **F)** distally (right side of image is distal). Note hypoechoic appearance *(curved arrow)* of distal tibialis posterior tendon at navicular in **F**. N, navicular; Tal, talus; Tib, tibia.

position, the thick hyperechoic and fibrillar posterior tibiotalar component of the deltoid ligament is identified deep to the tibialis posterior tendon (see Fig. 8-11D).

The spring ligament complex consists of superomedial, medioplantar, and inferoplantar calcaneonavicular ligaments.[10] To visualize each component, the transducer is initially placed in the transverse plane inferior to the medial malleolus and over the sustentaculum tali. By moving the transducer anteriorly and angling superior toward the talar head, the superomedial calcaneonavicular ligament is identified in long axis between the tibialis posterior tendon and the talus (Fig. 8-12).[13]

Lateral Ankle Evaluation

Structures of interest include the peroneal tendons and the lateral ligamentous structures of the ankle. Examination begins in the supramalleolar region in the transverse plane, directly posterior to the fibula in the retromalleolar groove or sulcus (Fig. 8-13A). At this location, the muscle belly and tendon of the peroneus brevis are identified in short axis (see Fig. 8-13B). An adjacent tendon, the peroneus longus is also seen, characterized by lack of a muscle belly at this level. With movement of the transducer from superior to inferior, the normal peroneus brevis muscle belly will taper; only the peroneus brevis and longus tendons should be visible at the extreme fibula tip

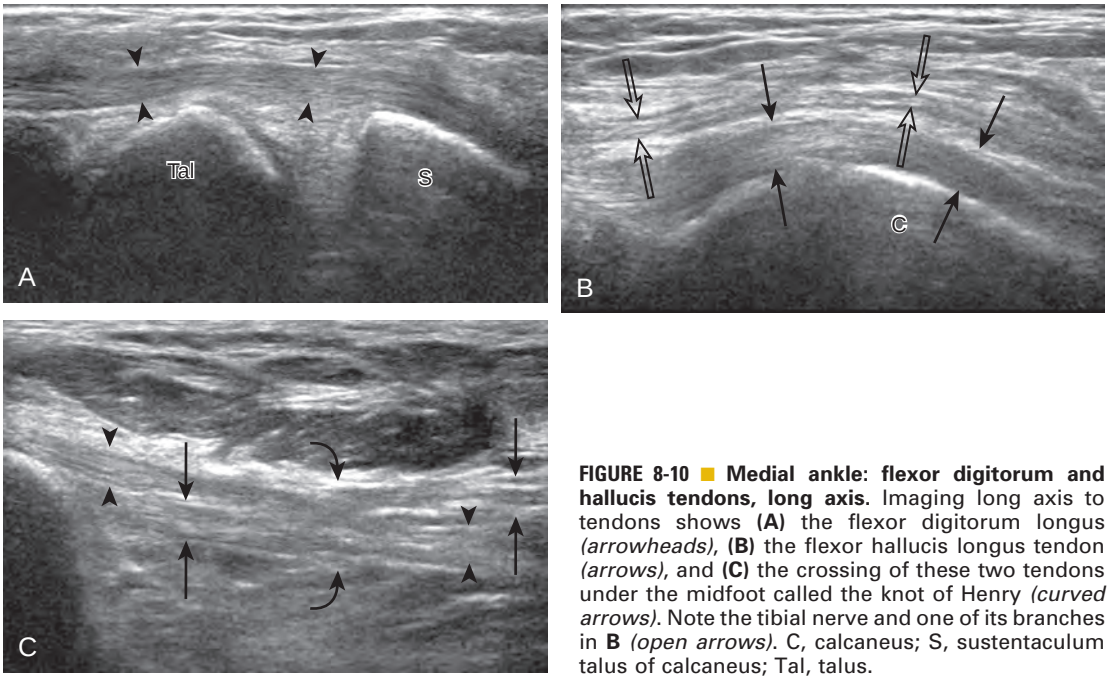

FIGURE 8-10 ■ Medial ankle: flexor digitorum and hallucis tendons, long axis. Imaging long axis to tendons shows **(A)** the flexor digitorum longus *(arrowheads)*, **(B)** the flexor hallucis longus tendon *(arrows)*, and **(C)** the crossing of these two tendons under the midfoot called the knot of Henry *(curved arrows)*. Note the tibial nerve and one of its branches in **B** *(open arrows)*. C, calcaneus; S, sustentaculum talus of calcaneus; Tal, talus.

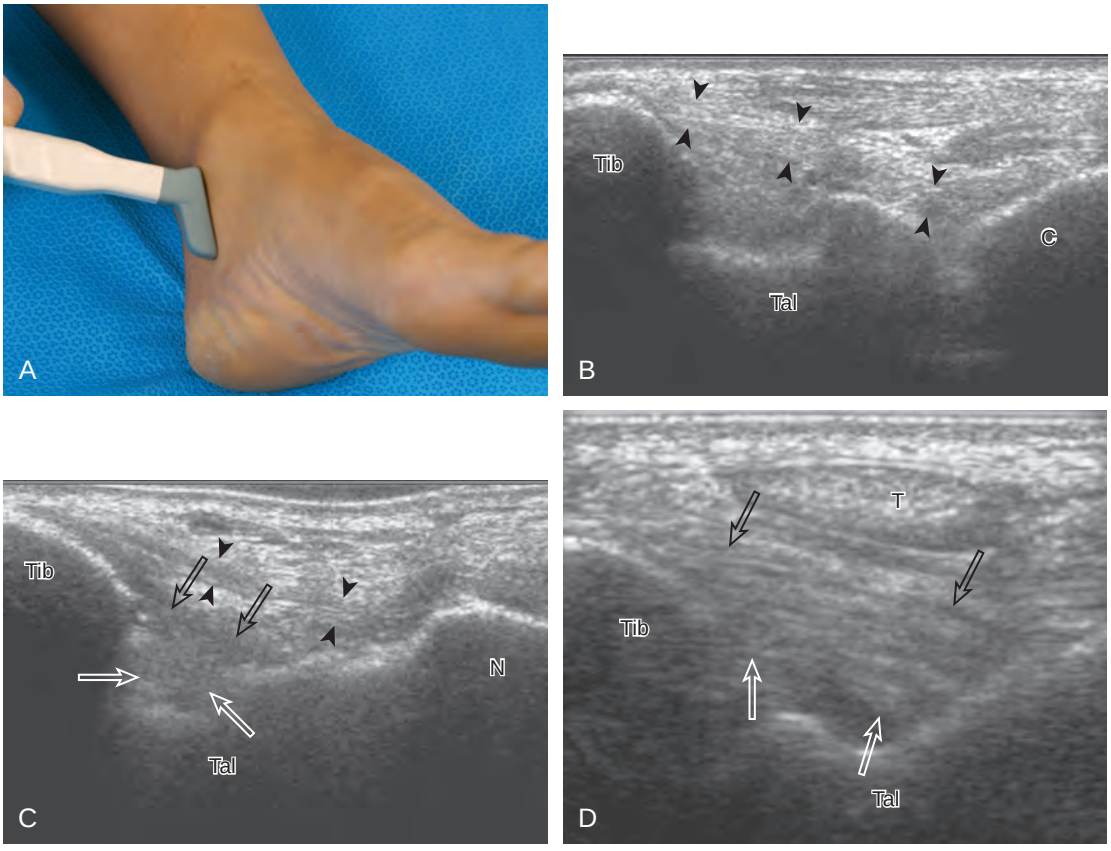

FIGURE 8-11 ■ Medial ankle: deltoid ligament. A, Coronal imaging at and distal to the medial malleolus shows **(B)** the tibiocalcaneal component *(arrowheads)* of the deltoid ligament. **C,** With rotation of the distal aspect of the transducer anteriorly, the tibionavicular *(arrowheads)* and anterior tibiotalar *(open arrows)* components are identified. **D,** With rotation of the distal aspect of the transducer posteriorly, the posterior tibiotalar component *(open arrows)* is seen deep to the tibialis posterior tendon (T). C, calcaneus; N, navicular; Tal, talus; Tib, tibia.

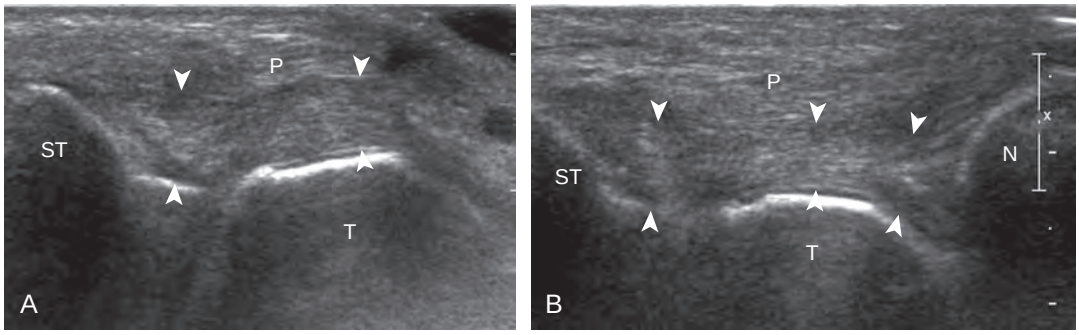

FIGURE 8-12 ■ Medial ankle: spring ligament. Ultrasound image **(A)** in the axial oblique plane angled superior from sustentaculum tali shows superomedial calcaneonavicular ligament *(arrowheads)* in long axis between the talus (T) and tibialis posterior tendon (P), and its sustentaculum tali (ST) attachment. Slight angulation of transducer shows **(B)** the navicular (N) attachment of the superomedial calcaneonavicular ligament *(arrowheads)*.

(see Fig. 8-13C). If the peroneus brevis muscle is present beyond the fibular tip, this normal variation is termed a *low-lying* muscle belly of the peroneus brevis and may be associated with tendon tear (see Fig. 8-92).[4] Although variable, the peroneus brevis is usually directly against the posterior cortex of the fibula, with the adjacent peroneus longus tendon more posterior. The thin and hyperechoic superior peroneal retinaculum can be seen extending over the tendons to insert on the posterolateral margin of the fibula.

Assessment is continued short axis to the peroneal tendons. Toggling the transducer is a helpful maneuver to identify the tendons in short axis,

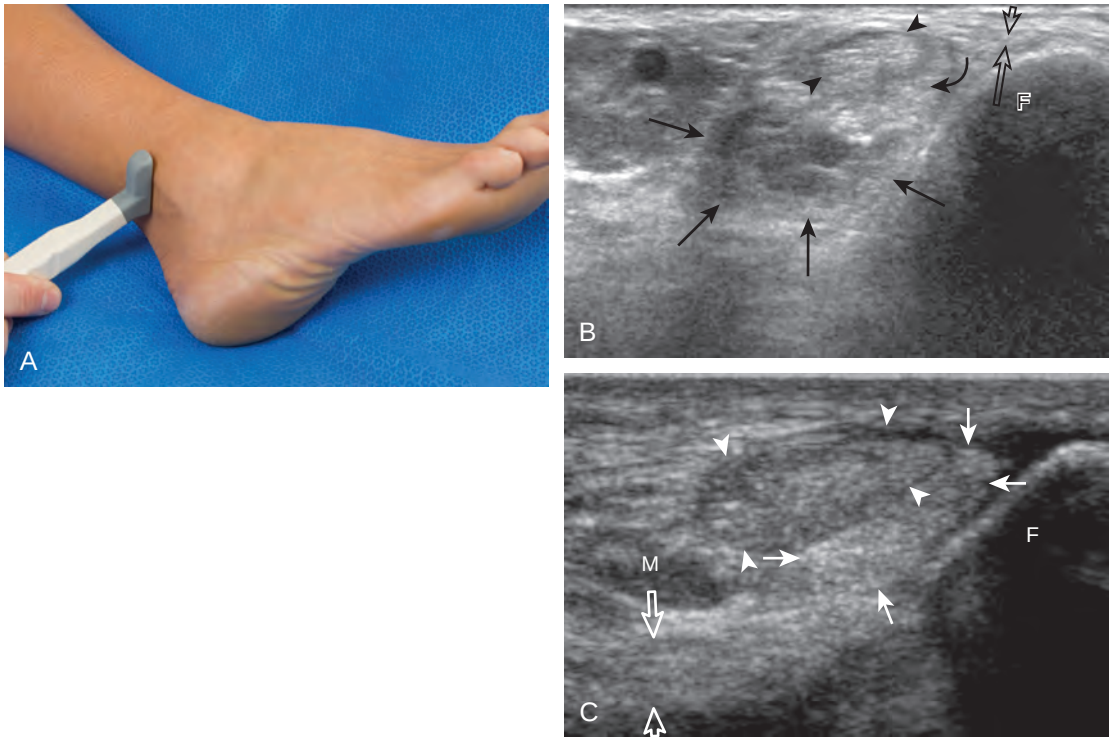

FIGURE 8-13 ■ Lateral ankle: peroneal tendons, short axis, proximal. A, Transverse imaging superior and posterior to the lateral malleolus shows **(B)** the peroneus longus tendon *(arrowheads)*, and the peroneus brevis muscle *(arrows)* and tendon *(curved arrow)* (*open arrows*, superior peroneal retinaculum; right side of image is anterior). Transverse imaging near the fibular tip shows **(C),** the peroneus longus tendon *(arrowheads)*, and the peroneus brevis tendon *(arrows)* and muscle (M) (*open arrows*, posterior talofibular ligament). F, fibula.

which causes the tendon to appear hypoechoic from anisotropy and improves conspicuity compared with the adjacent hyperechoic fat (see Fig. 1-12). As the transducer crosses the oblique plane between the tip of the fibula and the posterior aspect of the heel, the normal calcaneofibular ligament can be seen deep to the peroneal tendons (Fig. 8-14). As the peroneal tendons are followed in short axis, the transducer becomes positioned in the coronal plane (Fig. 8-15A). At the lateral aspect of the calcaneus, a bony prominence of variable size called the *peroneal tubercle* is present (see Fig. 8-15B). At this site, the peroneus brevis and longus tendons diverge into different directions. Because of their different respective orientations at the peroneal tubercle, it is difficult to image both tendons in short axis without one tendon appearing artifactually hypoechoic from anisotropy (see Fig. 8-15B). With minimal clockwise and counterclockwise transducer rotation and toggling, anisotropy of each tendon can be eliminated (see Fig. 8-15C). The peroneus brevis can be followed distally to its insertion on the fifth metatarsal base, and the peroneus longus similarly can be imaged under the mid-foot and forefoot to its insertion on the medial cuneiform and first metatarsal base.

Imaging in short axis is important in evaluation of the peroneal tendons because this is the optimal plane to visualize the common longitudinal split tears. It is also important to use dynamic maneuvers in evaluation of the peroneal tendons, to assess for subluxation or dislocation lateral and anterior to the fibula. This is accomplished with placement of the transducer in the transverse plane posterior to the distal fibula, and the patient is asked either to reproduce symptoms or to actively move the ankle into dorsiflexion and eversion. It is important to place only minimal transducer pressure throughout the dynamic examination so as not to inhibit abnormal movement of a peroneal tendon. The peroneal tendons

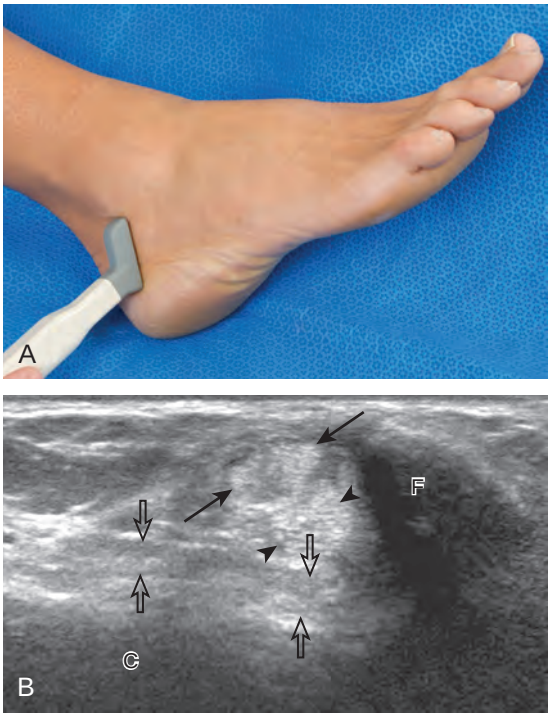

FIGURE 8-14 ■ Lateral ankle: peroneal tendons, short axis, at calcaneofibular ligament. A, Coronal-oblique imaging shows **(B)** the peroneus longus *(arrows)* and peroneus brevis *(arrowheads)* tendons, and calcaneofibular ligament *(open arrows)*. C, calcaneus; F, fibula.

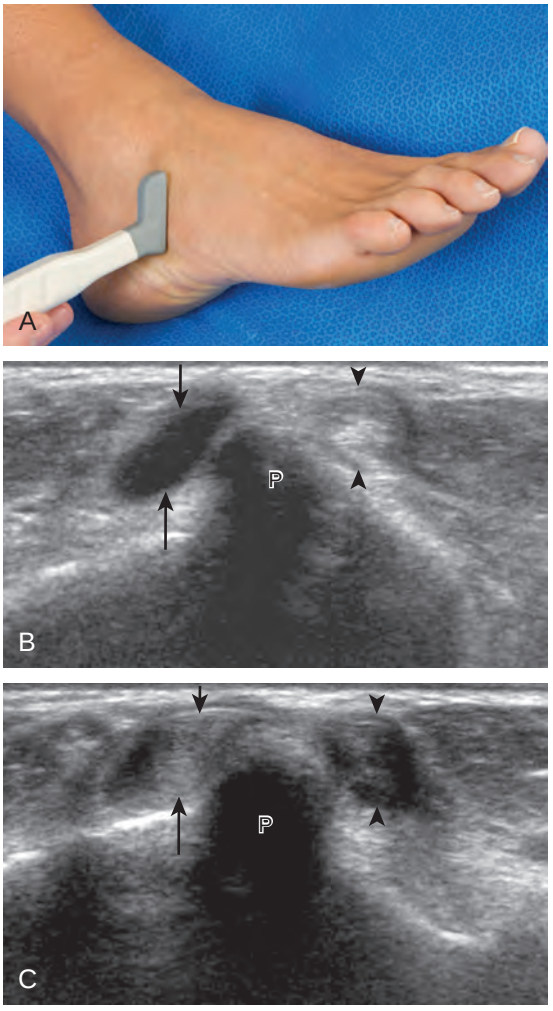

FIGURE 8-15 ■ Lateral ankle: peroneal tendons, short axis, distal. A, Coronal imaging shows **(B** and **C)** the peroneus longus *(arrows)* and peroneus brevis *(arrowheads)* tendons with anisotropy. P, peroneal tubercle.

should remain posterior to the fibula with an intact superior peroneal retinaculum.

For assessment of the peroneal tendons in long axis, one again returns to the supramalleolar region and places the transducer over the retromalleolar groove with the transducer in the oblique-sagittal plane toward the posterior aspect of the fibula (Fig. 8-16A). This approach allows visualization of the peroneus brevis and longus tendons in one imaging plane (see Fig. 8-16B). As the transducer is moved distally, the tendons begin to diverge distal to the fibula (see Fig. 8-16C and D). At this point, the peroneus longus and brevis are followed individually (see Fig. 8-16E). The peroneus longus courses deep toward the cuboid, where it commonly demonstrates anisotropy (see Fig. 8-16F). An echogenic os peroneum may be seen within the peroneus

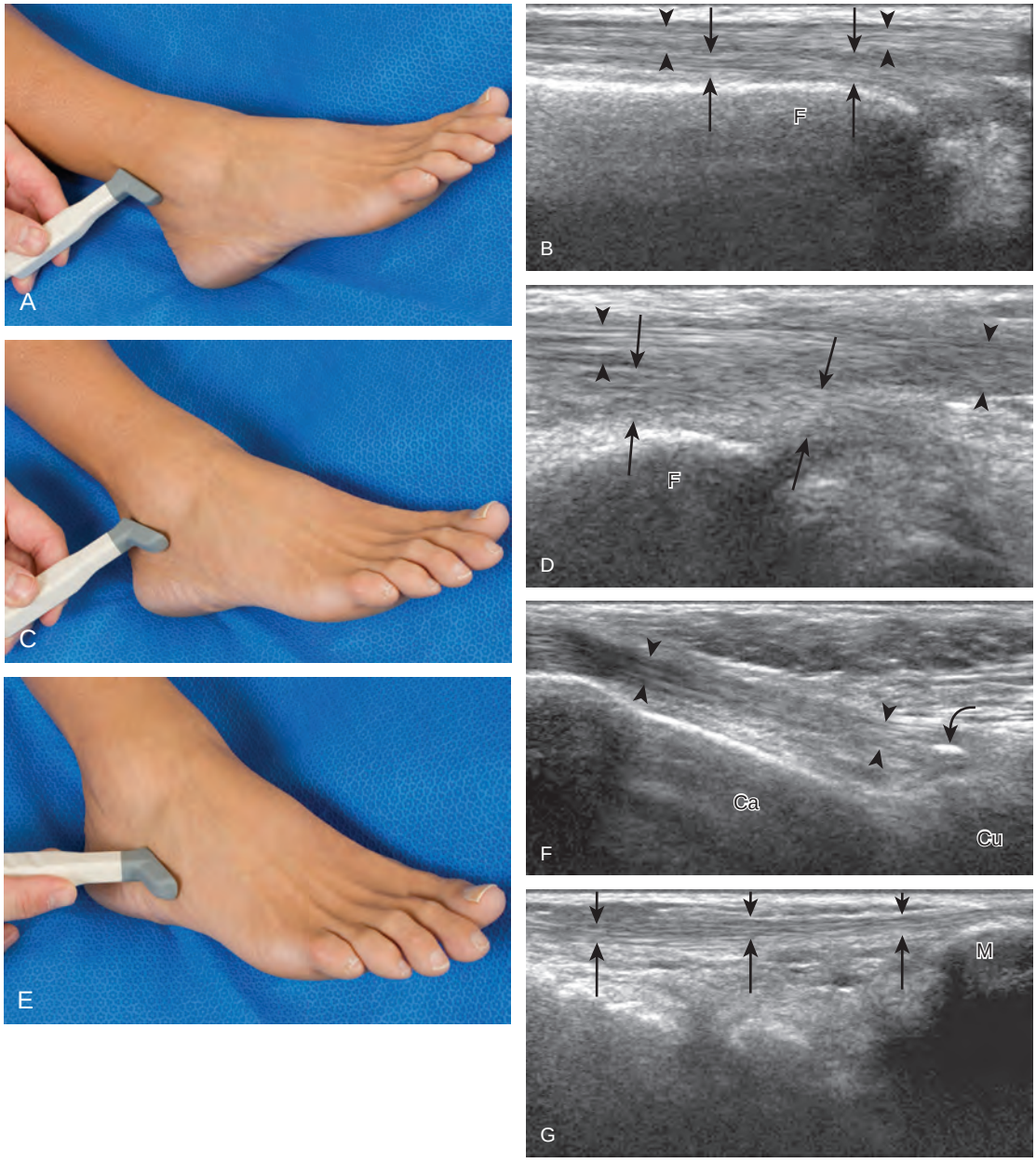

FIGURE 8-16 ■ Lateral ankle: peroneal tendons, long axis. Imaging of peroneal tendons in long axis **(A** and **B)** proximal, **(C** and **D)** at the level of the lateral malleolus, and **(E** to **G)** distal shows the peroneus longus *(arrowheads)* and peroneus brevis *(arrows)* tendons (right side of image is distal). Note the os peroneum *(curved arrow)* within the peroneus longus tendon *(arrowheads)* in **F**. Ca, calcaneus; Cu, cuboid; F, fibula; M, fifth metatarsal.

longus tendon.[14] More distal assessment of the peroneus longus may be completed if symptoms warrant. The peroneus brevis tendon can be followed distally from the fibula to its insertion on the base of the fifth metatarsal (see Fig. 8-16G).

The first lateral ankle ligament to be assessed is the anterior talofibular ligament. For localization, the transducer is first placed directly over the lateral aspect of the distal fibula. The transducer is then moved inferiorly. Once the extreme distal fibula tip is reached, the transducer is moved slightly superiorly and anteriorly to visualize the talus (Fig. 8-17A). In this position, the anterior talofibular ligament appears as a homogeneously hypoechoic structure from anisotropy resulting from the oblique course of the ligament toward the talus (see Fig. 8-17B). The transducer is then angled (heel-toe maneuver) so that the ligament fibers are perpendicular to the sound beam, to eliminate anisotropy, and the normal anterior talofibular ligament is seen as a continuous compact fibrillar structure that extends from the fibula to the talus in long axis (see Fig. 8-17C) (Video 8-1). Anisotropy is used to one's advantage in this application because initial identification of the anterior talofibular ligament is enhanced; the hypoechoic ligament is more conspicuous adjacent to the hyperechoic fat. Once the ligament is identified, it is important to eliminate anisotropy to exclude ligament abnormality.

To evaluate the calcaneofibular ligament in long axis, the transducer is placed in an oblique-coronal plane between the fibular tip and the posterior aspect of the heel where the calcaneofibular ligament is identified between the peroneal tendons and calcaneus (Figs. 8-18A and B). The calcaneofibular ligament is often incidentally seen during evaluation of the peroneal tendons in (see Fig. 8-14B). In short axis, the normal calcaneofibular ligament may appear hypoechoic from anisotropy and simulate a complex ganglion cyst associated with the peroneal tendons (see Fig. 8-18C and D).

To evaluate the anterior inferior tibiofibular ligament, the transducer is initially placed in the axial plane over the distal tibia and fibula. As the transducer is moved inferiorly, the cortex of the tibia disappears from view, and the talus appears, a finding that indicates the level of the

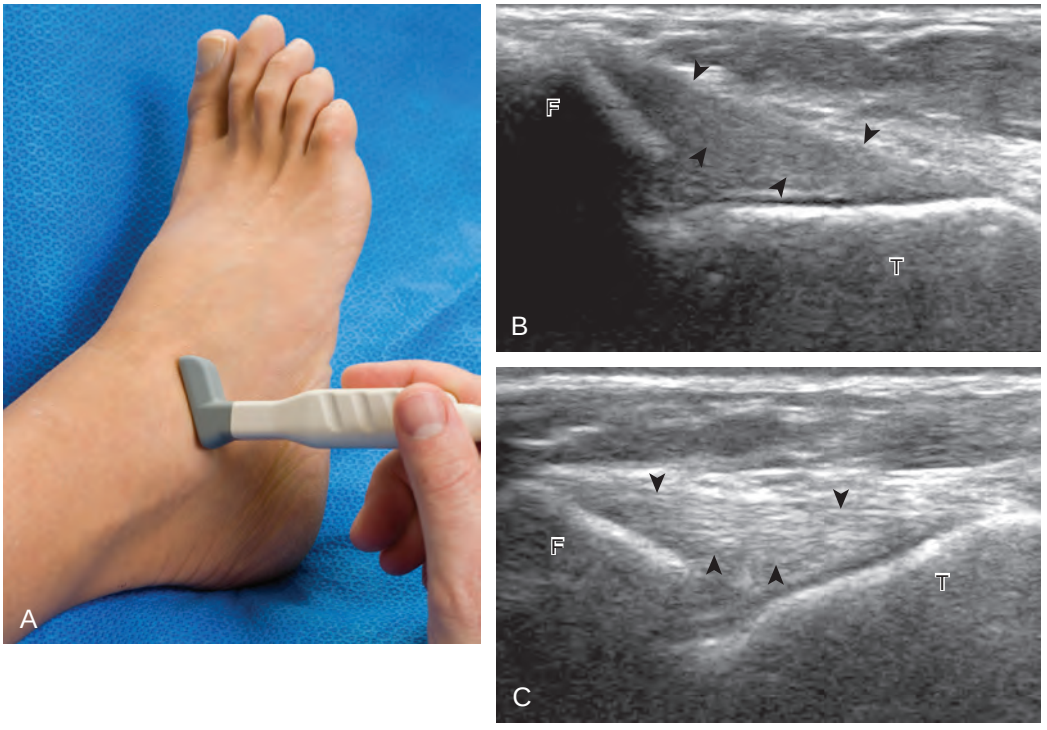

FIGURE 8-17 ■ Lateral ankle: anterior talofibular ligament. A, Axial imaging anterior to the tip of the fibula shows **(B)** the anterior talofibular ligament in long axis *(arrowheads)*, which appears hypoechoic from anisotropy. Note that the outer border of the hypoechoic ligament is made conspicuous adjacent to the hyperechoic fat. Heel-to-toe maneuver shows **(C)** the normal compact and fibrillar echotexture of the anterior talofibular ligament *(arrowheads)*. F, fibula; T, talus.

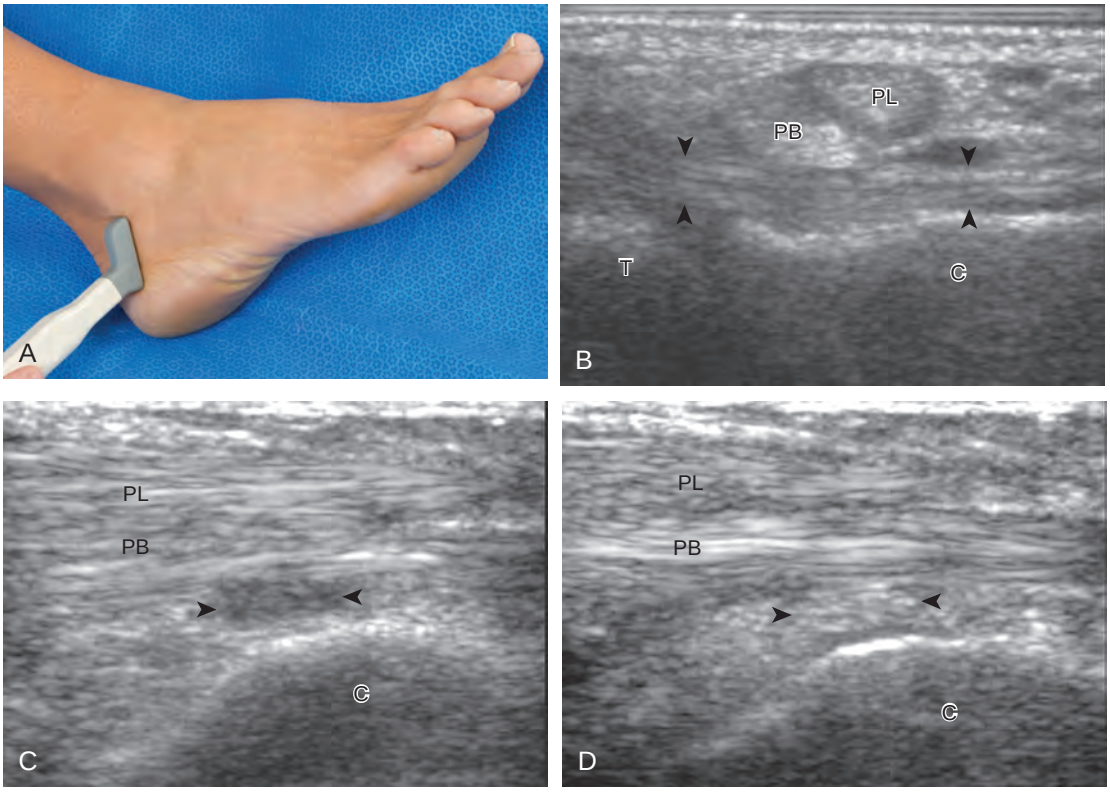

FIGURE 8-18 ■ Lateral ankle: calcaneofibular ligament. A, Coronal-oblique imaging between the fibular tip and the heel shows **(B)** the calcaneofibular ligament in long axis *(arrowheads)*. **C** and **D,** The transducer is turned 90 degrees to visualize the calcaneofibular ligament in short axis *(arrowheads)*, which demonstrates anisotropy by toggling the transducer. C, calcaneus; PB, peroneus brevis tendon; PL, peroneus longus tendon; T, talus.

ankle joint. The transducer is moved superiorly again to identify the most distal aspect of the tibia, and then the lateral aspect of the transducer is rotated inferiorly to visualize the hyperechoic and compact fibrillar anterior inferior tibiofibular ligament, which courses inferiorly from the tibia to the fibula (Fig. 8-19A and B). Another manner in identifying the anterior inferior tibiofibular ligament is to begin at the anterior talofibular ligament; fix the transducer over the fibula, and rotate the transducer so that the medial aspect moves superiorly from the talus to the tibia in an oblique plane. An accessory anterior inferior tibiofibular ligament (Bassett ligament) may also be identified as a discrete ligament bundle inferior to the anterior inferior tibiofibular ligament, slightly more horizontal and spanning a greater distance between tibia and fibula (see Fig. 8-19C).[9] Variability exists in the number of bundles or fascicles in the anterior inferior tibiofibular ligament (see Fig. 8-19D).[15,16]

It is very important to evaluate the interosseous membrane between the tibia and the fibula in the setting of an anterior tibiofibular ligament tear. At ultrasound, the interosseous membrane appears as a thin and hyperechoic often bilaminar structure extending from the tibia to the fibula and best evaluated in the transverse plane perpendicular to the sound beam (Fig. 8-20).[17] The interosseous membrane extends inferiorly and becomes thickened as the interosseous ligament superior to the tibiotalar joint. The combination of the interosseous ligament, the anterior and posterior inferior tibiofibular ligaments, and the posteriorly located inferior transverse ligament stabilizes the ankle syndesmosis or articulation.[15] Although visible, the posterior talofibular is not routinely evaluated (Fig. 8-21; see Fig. 8-13C). The posterior inferior tibiofibular ligament may also be assessed; however, the posterior ligamentous structures are more difficult to evaluate, given their depth.

Posterior Ankle and Heel Evaluation

If the patient has no symptoms posteriorly and one wants simply to screen the distal Achilles tendon and plantar aponeurosis for abnormalities, the patient can externally rotate the leg while supine to gain limited access to the posterior

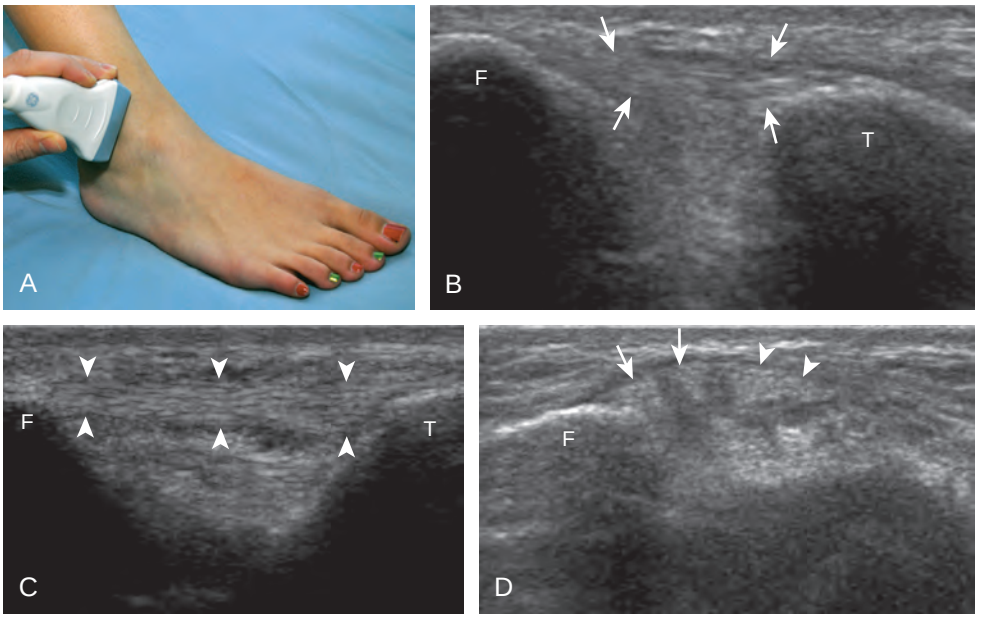

FIGURE 8-19 ■ Lateral ankle: anterior inferior tibiofibular ligament. A, Oblique imaging between the distal tibia and fibula shows **(B)** the anterior tibiofibular ligament *(arrows)*. Imaging parallel and just inferior to **(B)** shows **(C)** accessory anterior inferior tibiofibular ligament *(arrowheads)*. **D,** imaging of ligaments in short axis shows multiple fascicles of anterior inferior tibiofibular ligament *(arrows)* and accessory anterior inferior tibiofibular ligament *(arrowheads)*. F, fibula; T, tibia.

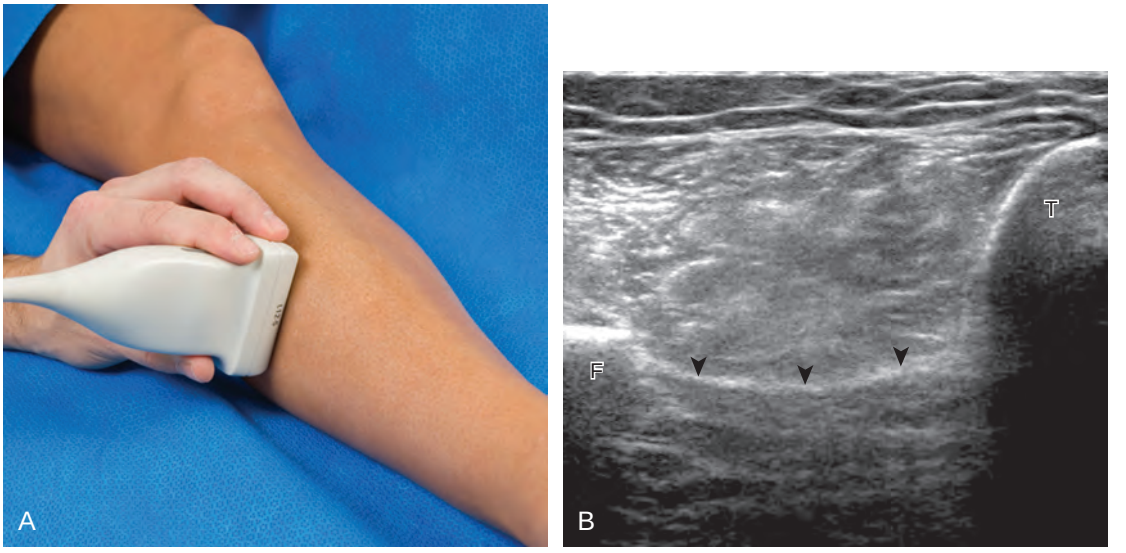

FIGURE 8-20 ■ Lower leg: interosseous membrane. A, Transverse imaging between the tibia and fibula shows **(B)** the interosseous membrane *(arrowheads)*. F, fibula; T, tibia.

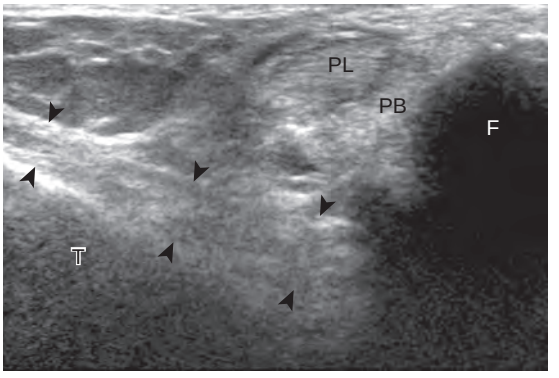

FIGURE 8-21 ■ Lateral ankle: posterior. Transverse imaging between posterior aspects of the talus (T) and fibula (F) shows the posterior talofibular ligament *(arrowheads)*. PB, peroneus brevis; PL, peroneus longus.

ankle. However, for a thorough examination, the patient should lie prone for complete access to the calf and posterior ankle. Dorsiflexion of the ankle elongates the Achilles tendon and reduces anisotropy. The Achilles tendon is easily evaluated because the transducer is placed in the sagittal plane long axis to the tendon fibers from a posterior approach (Fig. 8-22A). In long axis, the Achilles tendon should be fairly uniform in thickness (see Fig. 8-22B and C). The transducer is moved superiorly from the distal calf to the calcaneus, and the transducer is turned 90 degrees for evaluation in short axis; in this plane, the anterior margin of the Achilles tendon is predominantly flat or concave and should not be diffusely convex posterior (see Fig. 8-22D). When imaged from superior to inferior in short axis, the Achilles tendon fibers rotate 90 degrees, with the gastrocnemius component lateral and the soleus medial. A thin tendon, the plantaris, can be seen directly medial to the Achilles tendon (see Fig. 8-22D) but is often best appreciated in the setting of an Achilles tendon tear. The plantaris tendon may be absent in up to 20% of individuals.[7] Anterior to the Achilles tendon is a somewhat heterogeneous fat pad called *Kager fat pad*. Distally, a small amount of anechoic fluid (up to 2.5 mm anteroposterior) can be seen in the retrocalcaneal bursa.[12] In evaluation of the retro-Achilles bursa, located superficial to the distal Achilles tendon, it is important to float the transducer on a layer of thick gel so as not to efface the bursa and displace fluid out of the field of view.

The transducer is then moved over the plantar aspect of the heel to evaluate the plantar aponeurosis (Fig. 8-23A). The transducer is placed in the sagittal plane over the plantar and medial aspect of the heel long axis to the plantar aponeurosis, which appears hyperechoic, uniform, and 4 mm

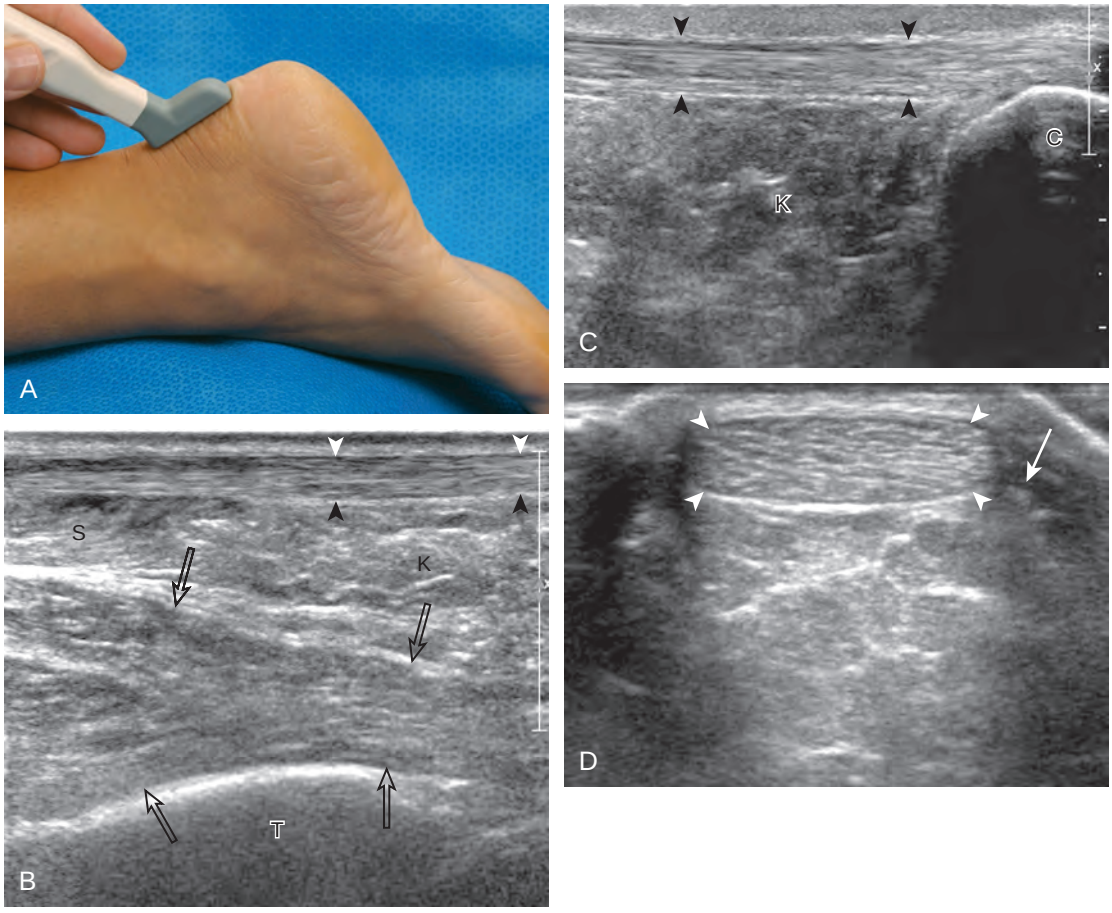

FIGURE 8-22 ■ Posterior ankle/heel: Achilles tendon. A, Sagittal imaging over the posterior ankle shows **(B** and **C)** the Achilles tendon in long axis *(arrowheads)* (*open arrows*, flexor hallucis longus muscle). Transverse imaging shows **(D)** the Achilles tendon *(arrowheads)* and plantaris tendon *(arrow)* in short axis (right side of image is medial). C, calcaneus; K, Kager fat pad; S, distal soleus muscle; T, tibia.

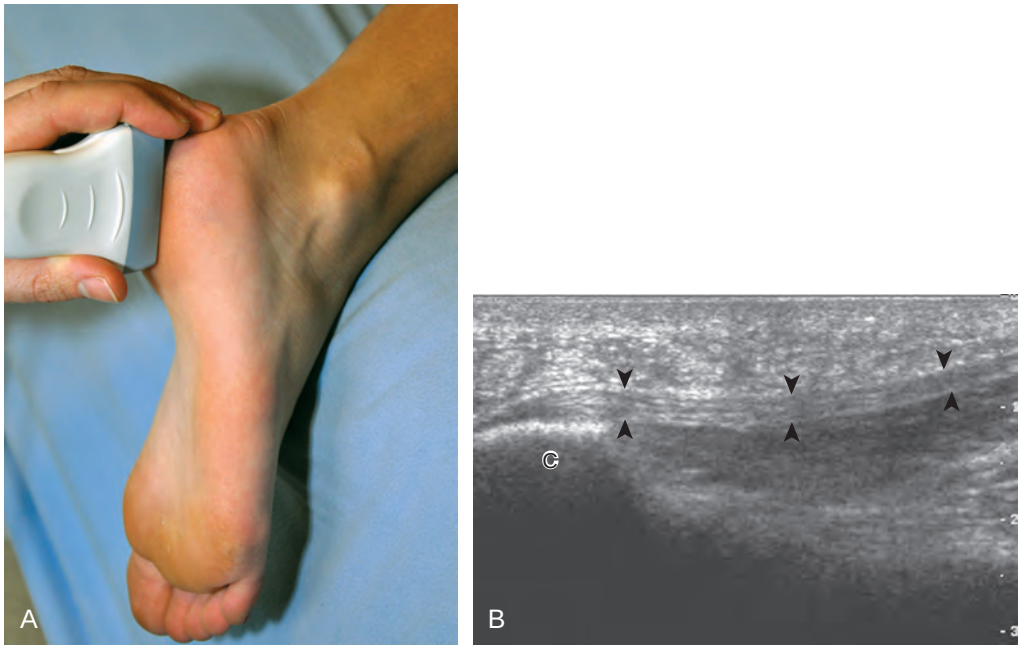

FIGURE 8-23 ■ Posterior ankle/heel: plantar aponeurosis. A, Sagittal imaging of the plantar heel shows **(B)** hyperechoic and fibrillar plantar aponeurosis *(arrowheads)* (right side of image is distal). C, calcaneus.

or less in thickness at the calcaneal attachment (see Fig. 8-23B).[18] Any identified disorder is also assessed in short axis. More distal assessment of the plantar aponeurosis can be carried out if symptoms or history warrants such evaluation.

Evaluation of the Calf

Structures of interest in the posterior calf include the soleus, the medial and lateral heads of the gastrocnemius, and the plantaris. Evaluation begins in the transverse plane over the posterior mid-calf (Fig. 8-24A). At this location, the medial and lateral heads of the gastrocnemius muscle are identified superficial to the larger soleus muscle (see Fig. 8-24B). At this point, the transducer is centered over the medial head of the gastrocnemius and then is moved distally until the muscle tapers. The transducer is then turned 90 degrees to visualize the normal tapering appearance of the medial gastrocnemius head over the soleus in long axis, a very common site of injury (see Fig. 8-24C and D). The lateral head of the gastrocnemius can be evaluated in a similar manner. It is also important to evaluate the entire calf for pathologic processes, although the patient often indicates a site of symptoms to focus evaluation. The thin, hyperechoic plantaris tendon, when present, can be seen in the posterior calf deep to the gastrocnemius muscle.[7] Initially, the plantaris crosses midline posterior to the knee joint and then moves medial directly between the muscle bellies of the medial head of the gastrocnemius and soleus muscles. Distally, the medial and lateral heads of the gastrocnemius combine with the soleus to form the Achilles tendon. The plantaris tendon courses along the medial aspect of the Achilles tendon to insert on the calcaneus.

Evaluation of the Forefoot

Evaluation of the distal aspect of the foot is largely guided by the patient's symptoms or history. Tendons around the digits, joint processes, soft tissue fluid collections, and masses can be assessed with ultrasound. If indicated, the forefoot can be assessed for Morton neuroma.[19] This is accomplished by placement of the transducer in the coronal plane on the body or short axis to the metatarsals, over the metatarsal heads from a plantar approach (Fig. 8-25A). The examiner's finger from the other hand is placed at the dorsal aspect of the forefoot over the web space to be evaluated (see Fig. 8-25B). This maneuver assists evaluation because the distal metatarsals are separated and the intermetatarsal space is widened, and it also reproduces the patient's symptoms when a neuroma is present. Evaluation for Morton neuroma also continues in long axis in the sagittal plane (see Fig. 8-25C).

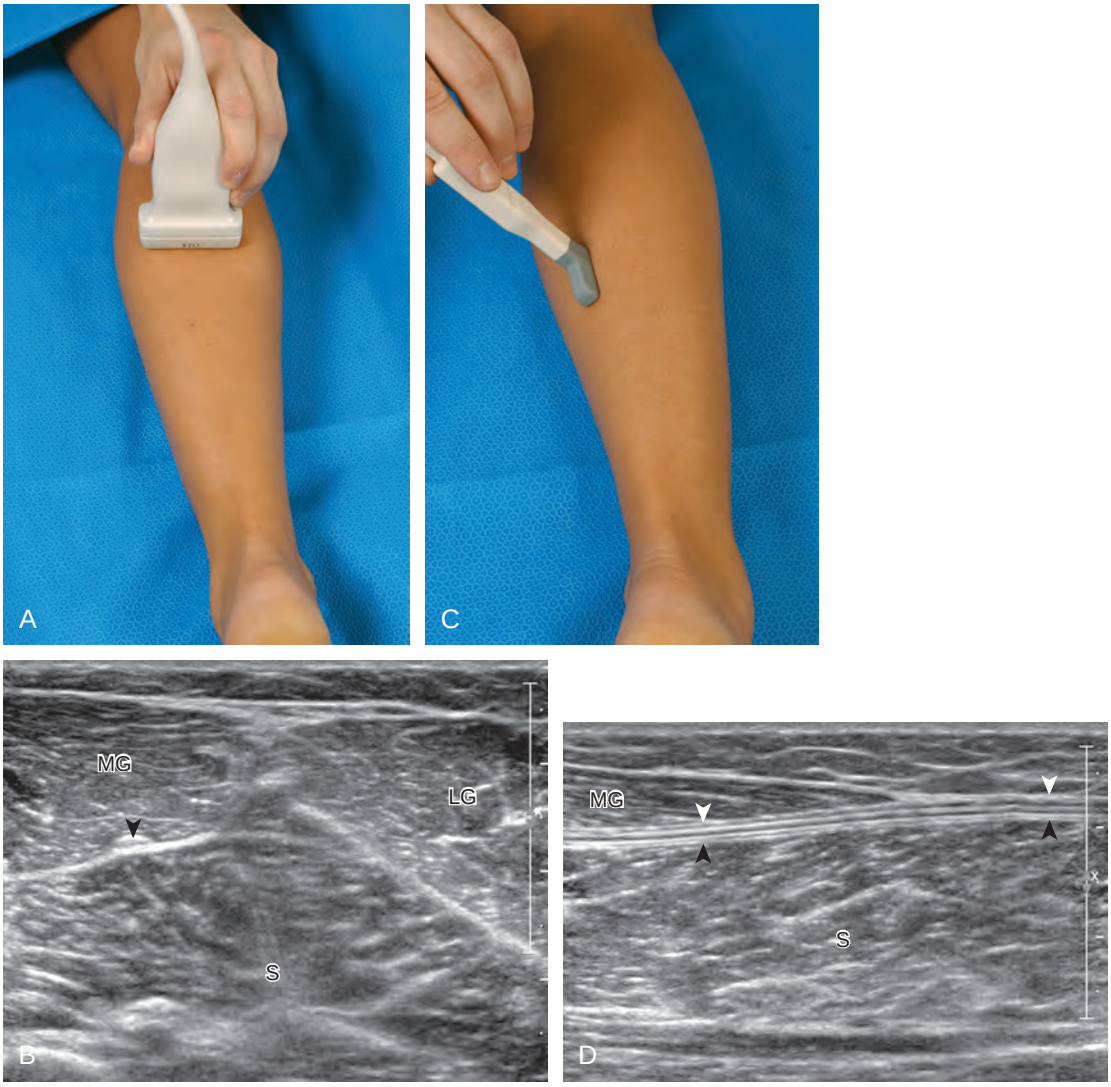

FIGURE 8-24 ■ **Calf. A,** Transverse imaging over the proximal calf shows **(B)** the medial head (MG) and the lateral head (LG) of the gastrocnemius and soleus (S) muscles in short axis. **C,** Parasagittal imaging medially shows **(D)** the medial head of the gastrocnemius (MG) in long axis, which tapers distally over the soleus (S). Note the plantaris *(arrowheads)*.

A similar long axis image can be obtained with the transducer over the dorsal foot and manual palpation over the plantar aspect. Resolution is often improved given the thinner dorsal soft tissues compared with the plantar aspect. Returning to the plantar short axis approach, dynamic assessment for Morton neuroma can be completed by manually squeezing the metatarsals together from side to side and imaging from a plantar approach. This maneuver (called the *sonographic Mulder sign*) will cause plantar displacement of a neuroma also producing symptoms.[20] When screening for inflammatory arthritis, in addition to evaluation of a symptomatic region, the fifth metatarsal head and medial first metatarsal head should be routinely imaged to assess for rheumatoid arthritis and gout, respectively.

JOINT AND BURSAL ABNORMALITIES

Joint Effusion and Synovial Hypertrophy

Evaluation for joint pathology should focus on key joint recesses for effusion and synovial hypertrophy. For the ankle or tibiotalar joint, the

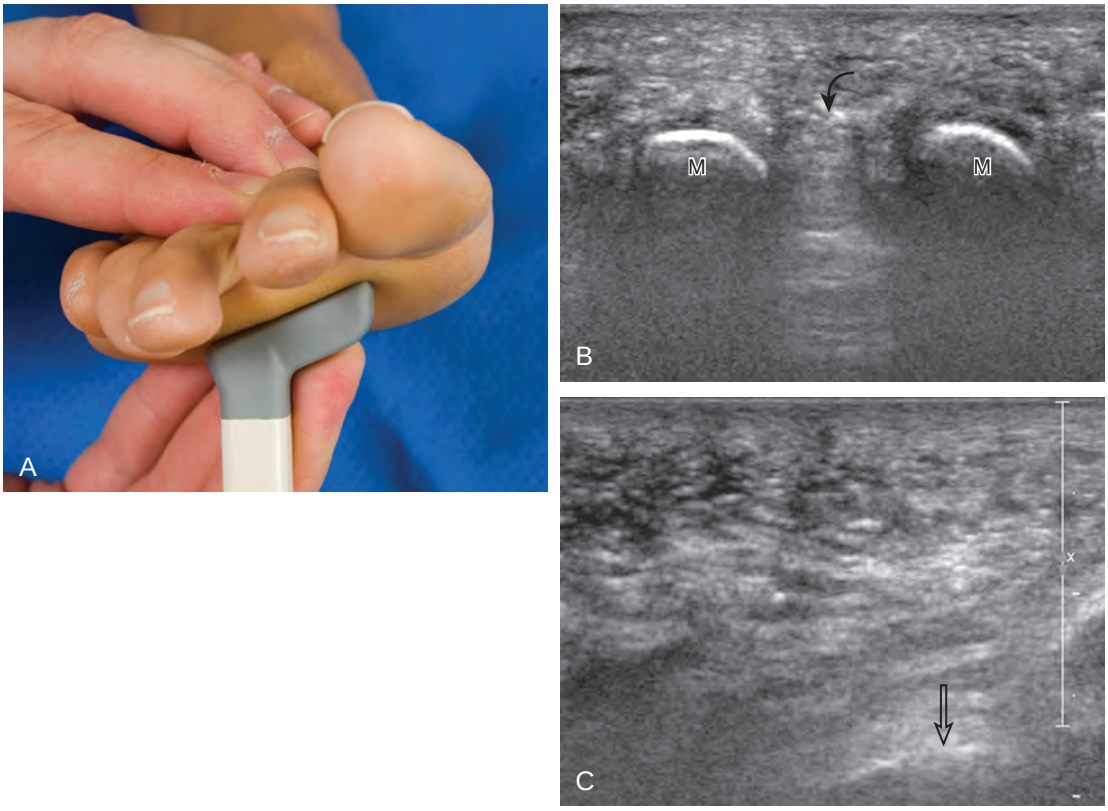

FIGURE 8-25 ■ Forefoot: Morton neuroma evaluation. A, Coronal imaging plantar over the metatarsal heads shows **(B)** hyperechoic and mildly heterogeneous tissues *(curved arrow)* between the metatarsal heads (M). Sagittal imaging between metatarsal heads shows **(C)** similar finding (*open arrow,* dorsal skin surface and examiner's finger).

anterior recess with the foot in slight plantar flexion is the most sensitive position and location to identify joint effusion.[21] Simple fluid distention of a joint is typically anechoic. Joint distention is seen in the sagittal plane or in the lateral aspect of the anterior joint recess (Fig. 8-26). A small amount of fluid may be found in the anterior ankle joint recess in normal volunteers; this fluid may measure up to 1.8 mm anteroposterior.[12] It is important not to mistake the 1 to 2 mm of hypoechoic hyaline cartilage that covers the talar dome to the talar neck for joint effusion (see Fig. 8-2B). For the foot, dorsal recesses of the tarsal, metatarsophalangeal, and interphalangeal joints are targeted. With regard to the metatarsophalangeal joints, each dorsal joint recess distends proximally over the metatarsal (Fig. 8-27A) as well as over the proximal phalanx when large (see Fig. 8-27B). Causes for anechoic joint effusion are many and include infection (Fig. 8-28), trauma, osteoarthritis (Fig. 8-29), and other arthritides (discussed later). Although commonly seen and asymptomatic, joint fluid within the first metatarsophalangeal joint often relates to early degenerative joint disease because this joint is a common site for osteoarthritis. Intra-articular bodies from degenerative arthritis and trauma appear hyperechoic with possible shadowing within a joint recess (Fig. 8-30). Intra-articular bodies may also migrate to the medial ankle tendon sheaths (see Fig. 8-68B) because communication with the ankle joint is common.

Increased echogenicity of joint fluid can be the result of complex fluid, as seen in infection (Figs. 8-31 and 8-32) and hemorrhage (Fig. 8-33). Echogenic joint fluid may resemble synovial hypertrophy (Figs. 8-34). To assist in this differentiation, compressibility and internal echo movement with transducer pressure, redistribution with joint movement, and lack of flow on color and power Doppler imaging suggest complex fluid rather than synovitis (Videos 8-2 and 8-3). Echogenicity and vascularity do not predict infection, and ultrasound-guided aspiration should be considered if there is concern for infection. In the setting of synovial hypertrophy,

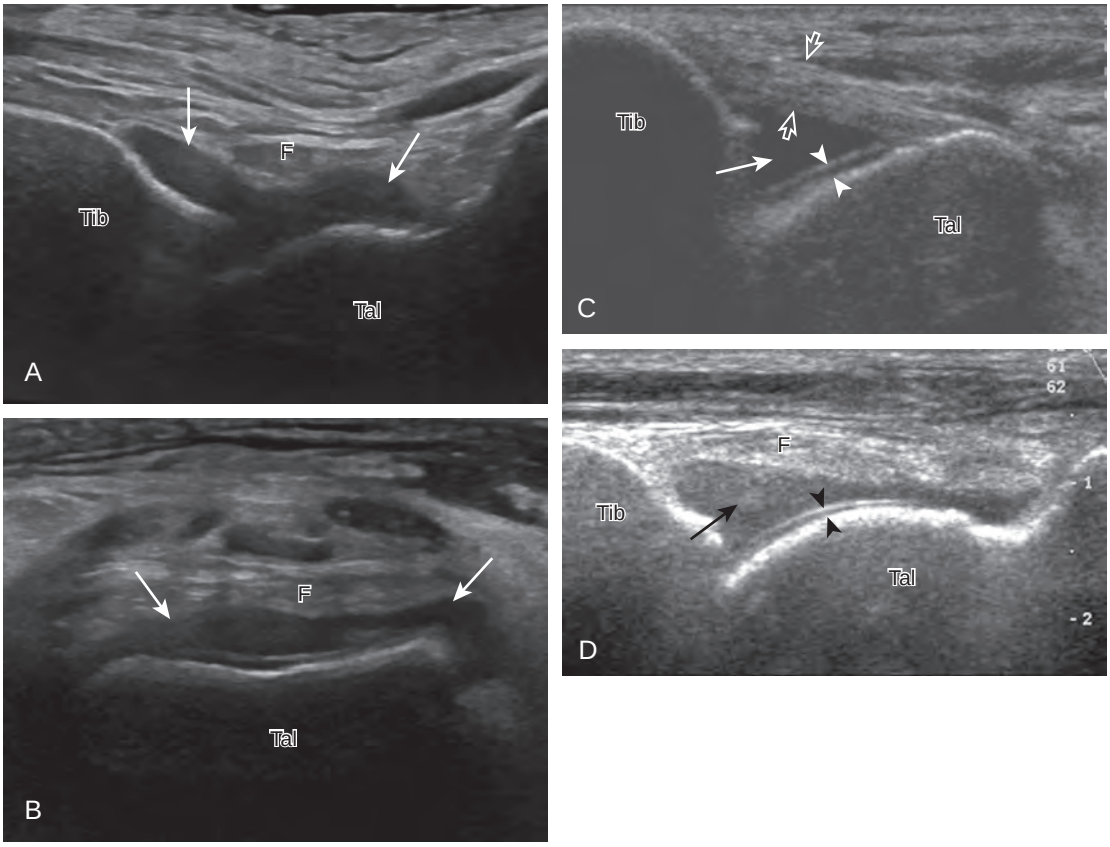

FIGURE 8-26 ■ **Joint effusion: tibiotalar joint.** Ultrasound images over the anterior ankle in three patients show **(A),** sagittal plane and **B,** transverse plane hypoechoic distention of the anterior ankle joint recess *(arrows)*, **(C)** anechoic distention *(arrow)* anterolateral deep to the anterior talofibular ligament *(open arrows)*, and **(D)** hypoechoic anterior ankle joint recess distention *(arrow)*. Note displacement of anterior fat pad (F) and the interface with hyaline articular cartilage *(arrowheads)*. Tal, talus; Tib, tibia.

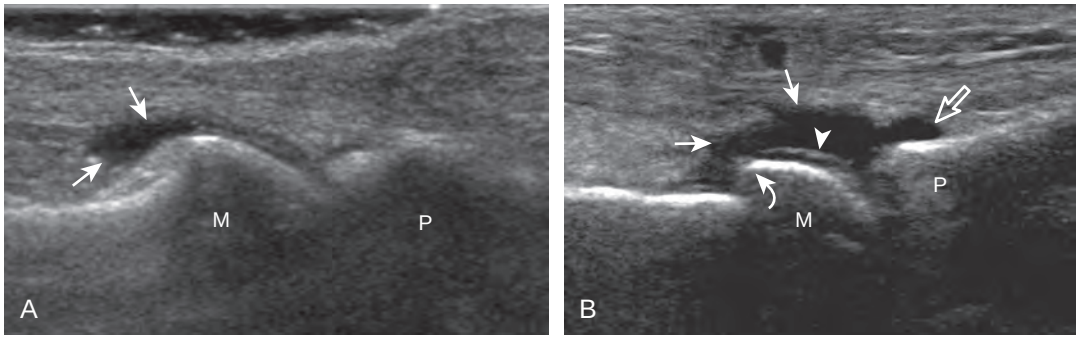

FIGURE 8-27 ■ **Joint effusion: metatarsophalangeal joint.** Ultrasound images dorsal to metatarsophalangeal joints in two patients **(A** and **B)** show anechoic distention of the dorsal joint recess, which extends proximal *(arrows)* over metatarsal (M). Note in **B,** distention *(open arrow)* over proximal phalanx (P) with larger effusion and cartilage interface *(arrowhead)* (*curved arrow*, osteophyte).

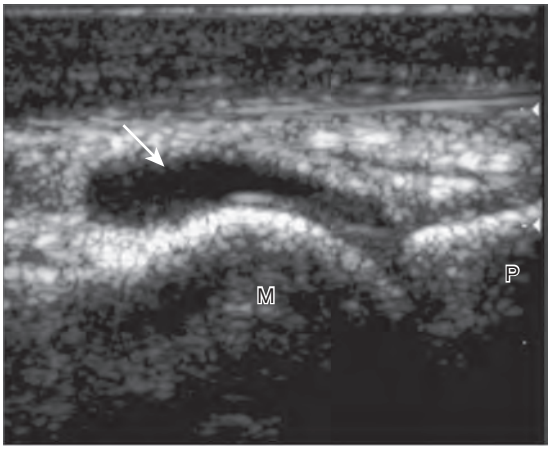

FIGURE 8-28 ■ Septic arthritis: metatarsophalangeal joint. Ultrasound image shows anechoic distention *(arrow)* of the dorsal recess of the first metatarsophalangeal joint from infection. M, metatarsal head; P, proximal phalanx.

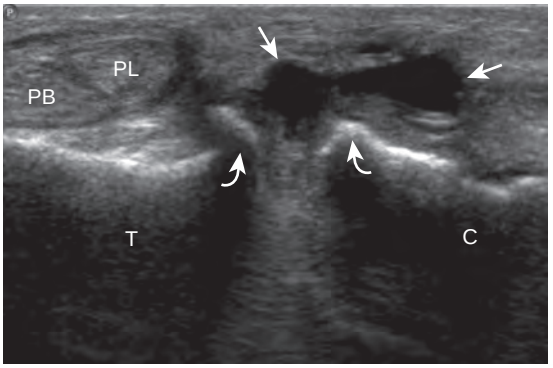

FIGURE 8-29 ■ Osteoarthritis: posterior subtalar joint. Ultrasound image in coronal plane over lateral hindfoot shows anechoic distention *(arrows)* of joint recess with adjacent osteophytes *(curved arrows)*. C, calcaneus; PL, peroneus longus tendon; PB, peroneus brevis tendon; T, talus.

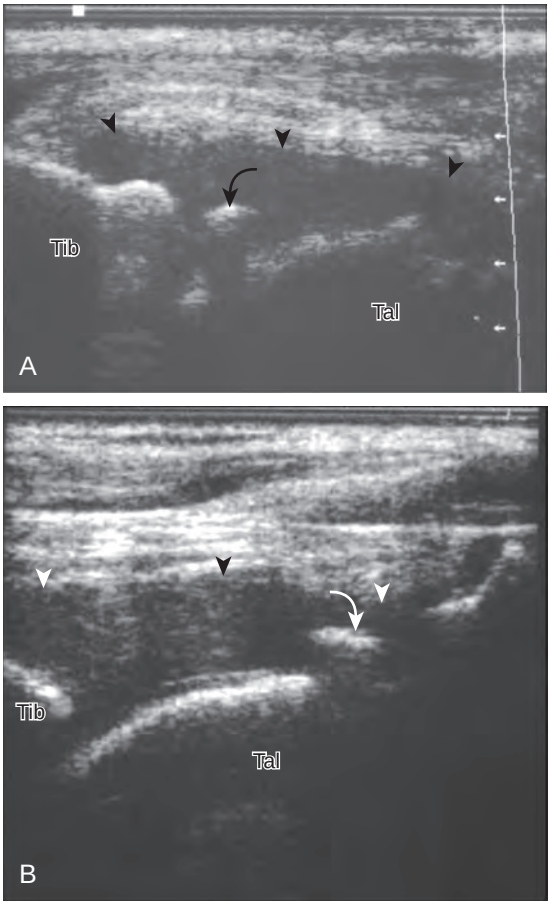

FIGURE 8-30 ■ Intra-articular body: tibiotalar joint. Ultrasound images over the anterior ankle joint recess show hyperechoic and shadowing intra-articular body *(curved arrow)* surrounded by anechoic joint fluid *(arrowheads)*. Note movement of the intra-articular body distally within the anterior ankle joint recess between **A** and **B.** Tal, talus; Tib, tibia.

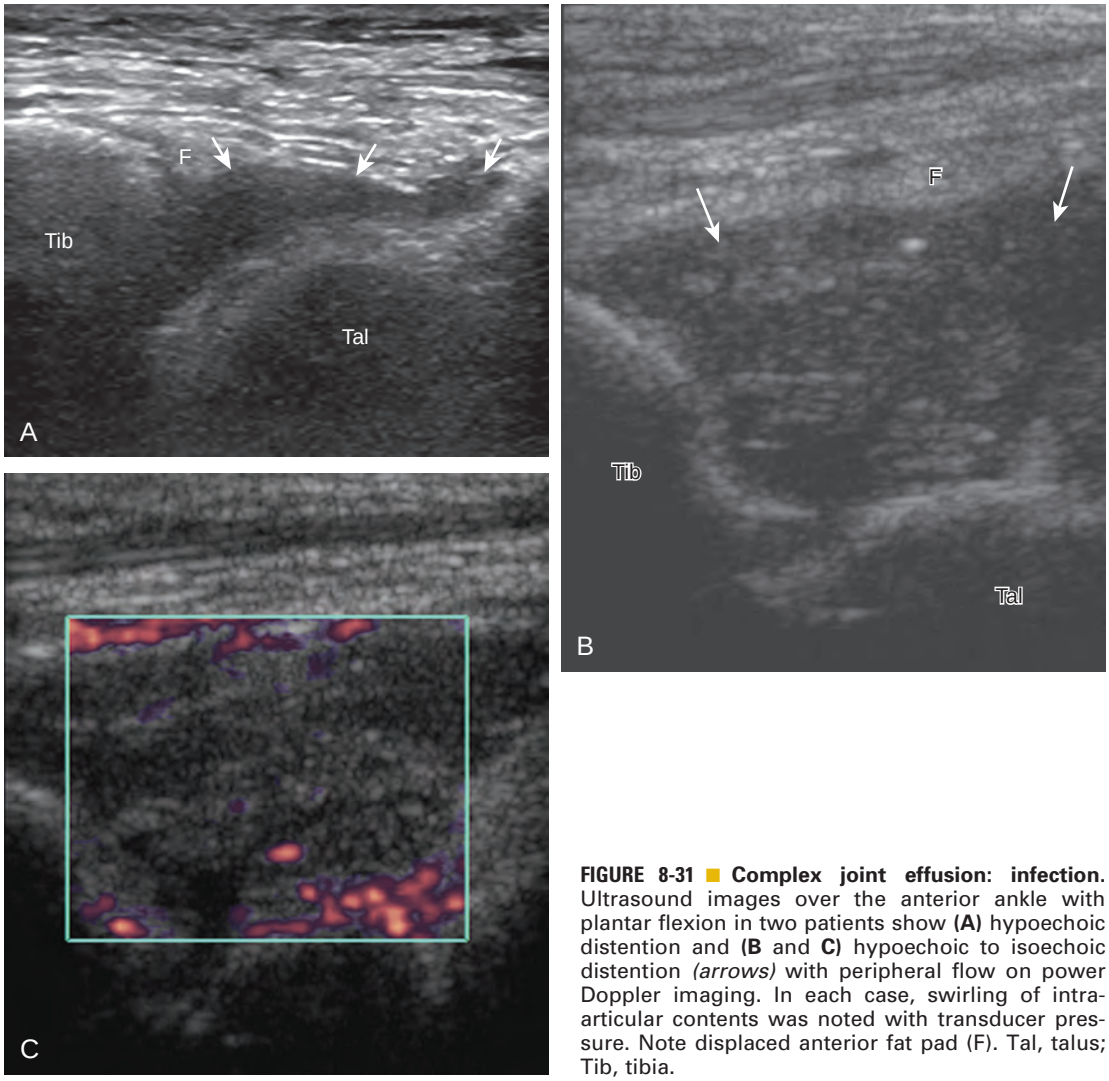

FIGURE 8-31 ■ Complex joint effusion: infection. Ultrasound images over the anterior ankle with plantar flexion in two patients show **(A)** hypoechoic distention and **(B** and **C)** hypoechoic to isoechoic distention *(arrows)* with peripheral flow on power Doppler imaging. In each case, swirling of intra-articular contents was noted with transducer pressure. Note displaced anterior fat pad (F). Tal, talus; Tib, tibia.

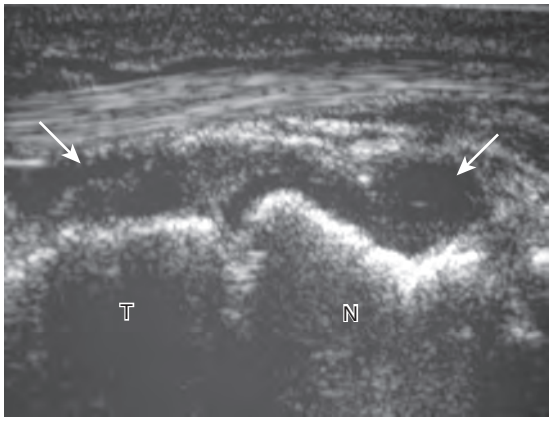

FIGURE 8-32 ■ Complex joint effusion: infection. Ultrasound image in sagittal plane over dorsal midfoot shows hypoechoic distention *(arrows)* of the talonavicular joint. N, navicular; T, talus.

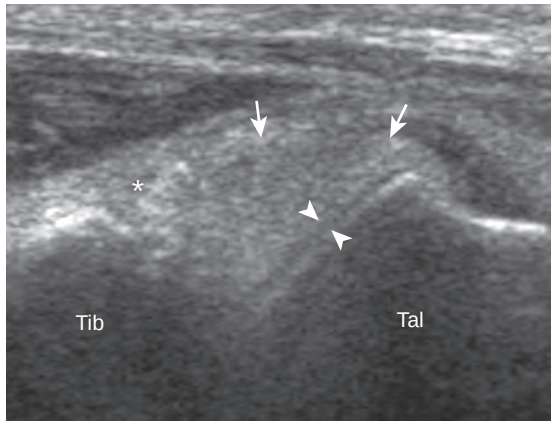

FIGURE 8-33 ■ Complex joint effusion: hemorrhage. Ultrasound image over the anterior ankle with plantar flexion shows hyperechoic distention *(arrows)* from hemorrhage after ankle trauma. Note displacement of anterior fat pad *(asterisk)* and interface with hyaline articular cartilage *(arrowheads)*. Tal, talus; Tib, tibia.

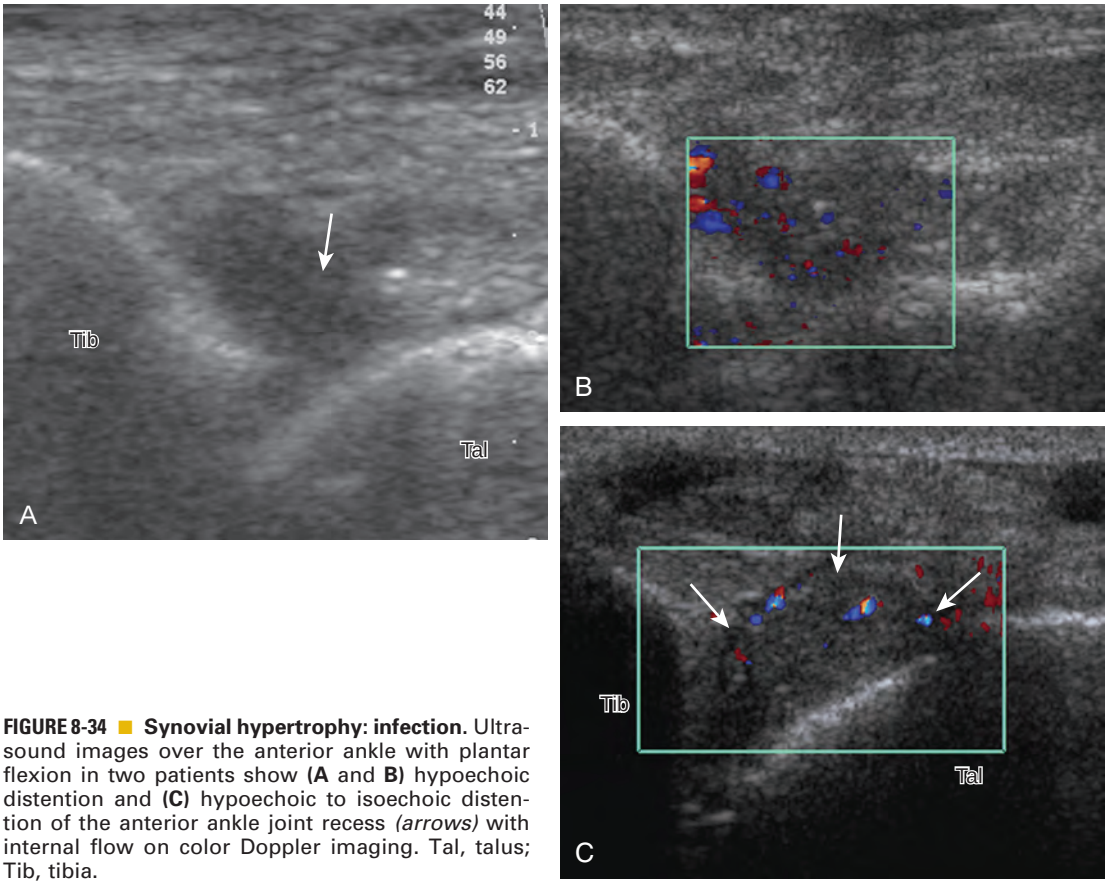

FIGURE 8-34 ■ Synovial hypertrophy: infection. Ultrasound images over the anterior ankle with plantar flexion in two patients show **(A** and **B)** hypoechoic distention and **(C)** hypoechoic to isoechoic distention of the anterior ankle joint recess *(arrows)* with internal flow on color Doppler imaging. Tal, talus; Tib, tibia.

adjacent cortical irregularity may be from erosions, which can be seen in inflammatory (see below for inflammatory arthritis and Chapter 2 for infection) and noninflammatory conditions, which include pigmented villonodular synovitis[22] (Fig. 8-35) and synovial (osteo)chondromatosis (Fig. 8-36). In the latter condition, hyperechoic and possibly shadowing foci may be identified.[23] Synovial hypertrophy may also be found in the ankle joint deep to the anterior talofibular ligament in anterolateral impingement syndrome (Fig. 8-37), where echogenic synovial hypertrophy greater than 10 mm is associated with symptoms and adjacent ligament

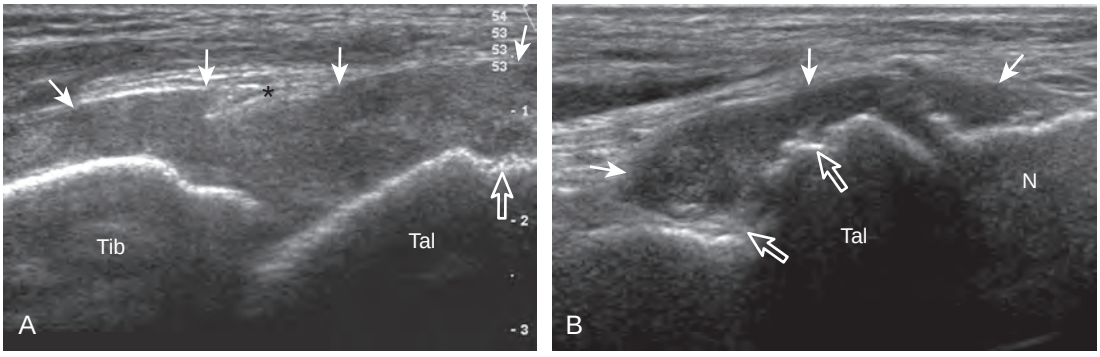

FIGURE 8-35 ■ Pigmented villonodular synovitis. Ultrasound images from two patients show hypoechoic to isoechoic distention *(arrows)* of the **(A)** anterior ankle recess and **(B)** talonavicular joint recess. Note bone erosions *(open arrows)* (*asterisk*, fat pad). N, navicular; Tal, talus; Tib, tibia.

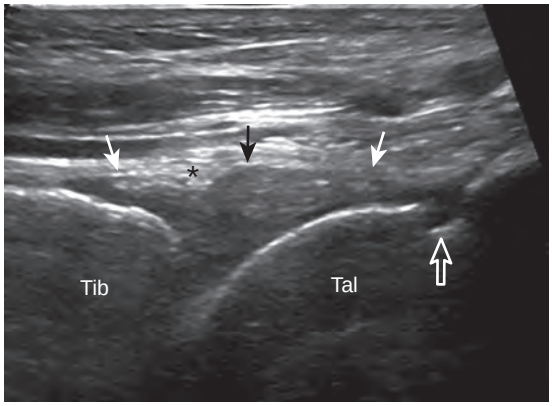

FIGURE 8-36 ■ Synovial chondromatosis. Ultrasound image over anterior ankle shows hypoechoic to isoechoic distention *(arrows)* of the anterior ankle recess with bone erosions *(open arrow)* (*asterisk*, fat pad). Tal, talus; Tib, tibia.

abnormality.[24] Nonspecific mild synovial thickening, usually with little or no flow on color or power Doppler imaging, can be seen with osteoarthritis and may not correlate with patient symptoms (Fig. 8-38).[25,26]

Inflammatory Arthritis

Important target sites for arthritis evaluation in addition to any focal symptomatic area include the distal fifth and first metatarsal heads because these are common sites for involvement from rheumatoid arthritis and gout, respectively. With regard to rheumatoid arthritis, ultrasound findings include joint effusion (Fig. 8-39) and synovial hypertrophy, which is usually hypoechoic (Figs. 8-40 and 8-41) (see Video 8-2), but is

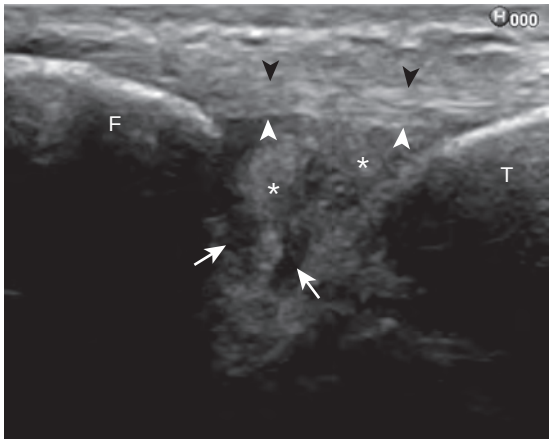

FIGURE 8-37 ■ Anterolateral impingement syndrome. Ultrasound image long axis to normal anterior talofibular ligament *(arrowheads)* shows anechoic fluid *(arrows)* and echogenic synovial hypertrophy *(asterisks)*. F, fibula; T, talus.

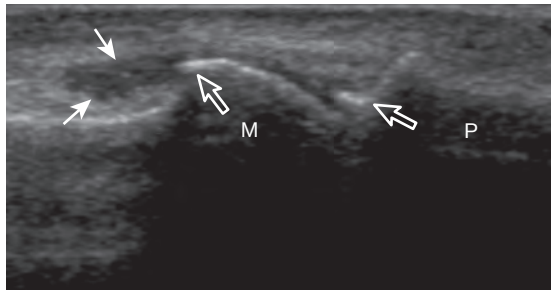

FIGURE 8-38 ■ Osteoarthritis: metatarsophalangeal joint. Ultrasound image over first metatarsophalangeal joint shows nonspecific mild synovial thickening *(arrows)* and osteophytes *(open arrows)*. M, metacarpal; P, proximal phalanx.

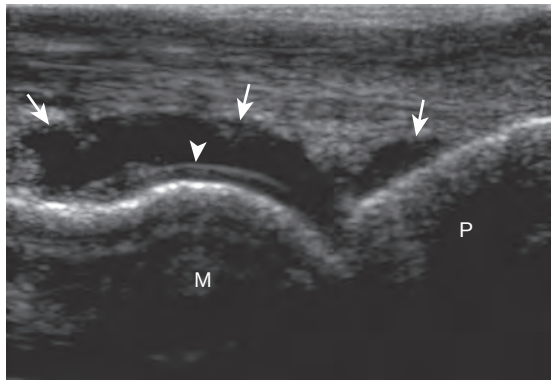

FIGURE 8-39 ■ Rheumatoid arthritis: joint effusion. Ultrasound image over dorsal metatarsophalangeal joint shows anechoic dorsal joint recess distention *(arrows)* (*arrowhead*, cartilage interface). M, metacarpal; P, proximal phalanx.

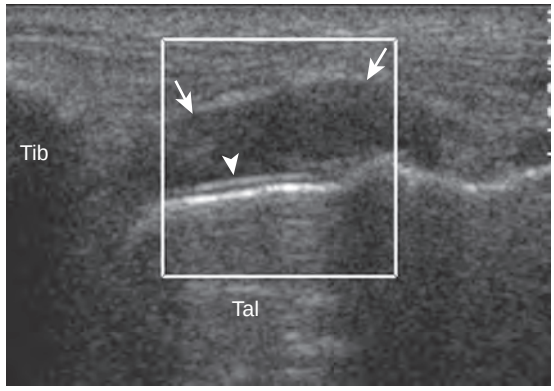

FIGURE 8-40 ■ Rheumatoid arthritis: synovial hypertrophy. Ultrasound image over the anterior ankle with plantar flexion shows hypoechoic distention *(arrows)* that was noncompressible with no flow on color Doppler imaging and no joint fluid at joint aspiration (*arrowhead*, cartilage interface). Tal, talus; Tib, tibia.

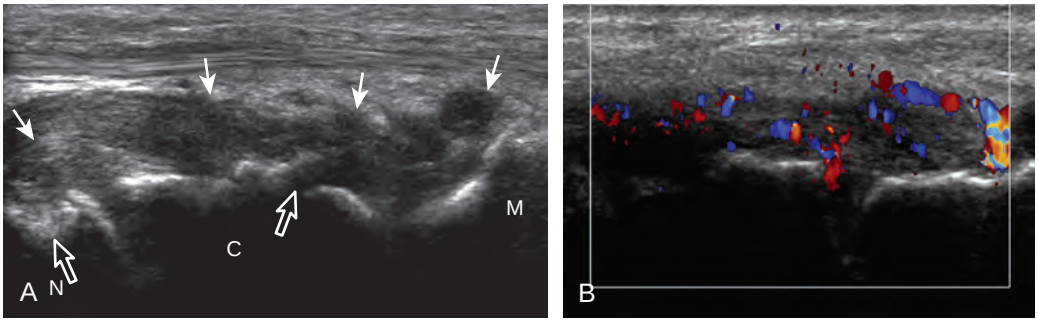

FIGURE 8-41 ■ Rheumatoid arthritis: synovial hypertrophy. Ultrasound images **(A** and **B)** over dorsal recesses of mid-foot show hypoechoic synovial hypertrophy *(arrows)*, erosions *(open arrows)*, and increased flow on color Doppler imaging. C, cuneiform; M, metatarsal; N, navicular.

possibly isoechoic (Figs. 8-42 and 8-43) (see Video 8-3), compared with subcutaneous fat, with possible increased flow on color or power Doppler imaging.[27] In the presence of synovial hypertrophy, disruption of the normally smooth bone cortex in two planes indicates erosions. Because the ultrasound findings of rheumatoid arthritis are not specific and resemble other inflammatory conditions, including other systemic arthritides and infection, the distribution of the findings is very helpful along with radiographic and serologic correlation. The fifth metatarsal head is the most common site of erosions in rheumatoid arthritis (Fig. 8-44) (Video 8-4), with less common involvement of the other metatarsophalangeal joints and first interphalangeal joint.[28-30] It is important not to misinterpret the numerous concavities of the distal metatarsal cortex as an erosion.[31] Other manifestations of rheumatoid

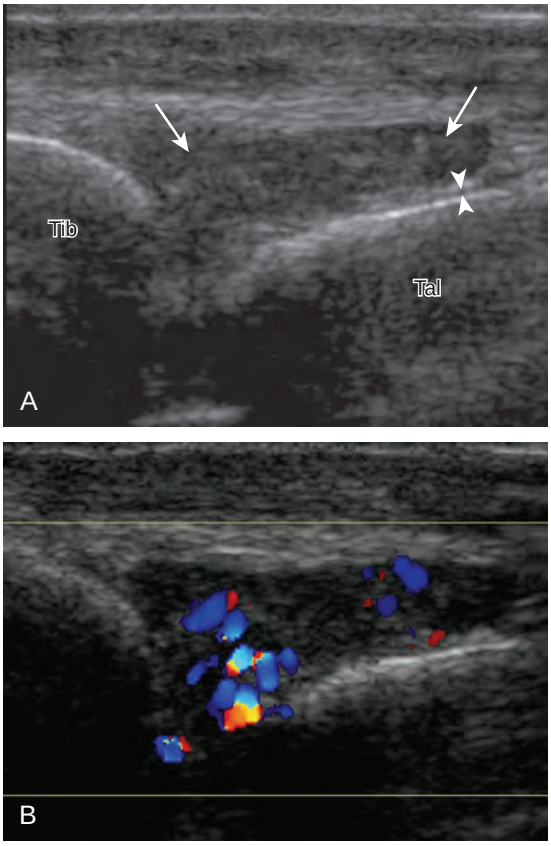

FIGURE 8-42 ■ Rheumatoid arthritis: synovial hypertrophy. Ultrasound images **(A** and **B)** over the anterior ankle with plantar flexion show hypoechoic to isoechoic distention of the anterior ankle joint recess *(arrows)* with internal flow on color Doppler imaging (*arrowheads*, hyaline articular cartilage). Tal, talus; Tib, tibia.

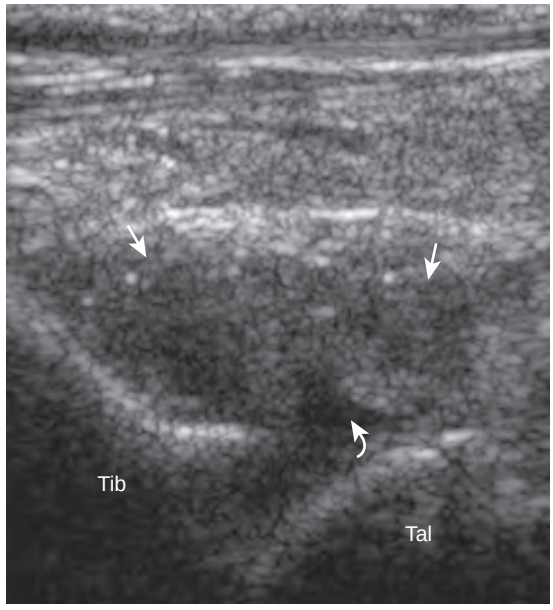

FIGURE 8-43 ■ Rheumatoid arthritis: synovial hypertrophy. Ultrasound image over the anterior ankle with plantar flexion shows isoechoic distention of the anterior ankle joint recess *(arrows)*, which had no flow power Doppler imaging. Note small collection of anechoic joint fluid *(curved arrow)*, which was aspirated revealing infection. Tal, talus; Tib, tibia.

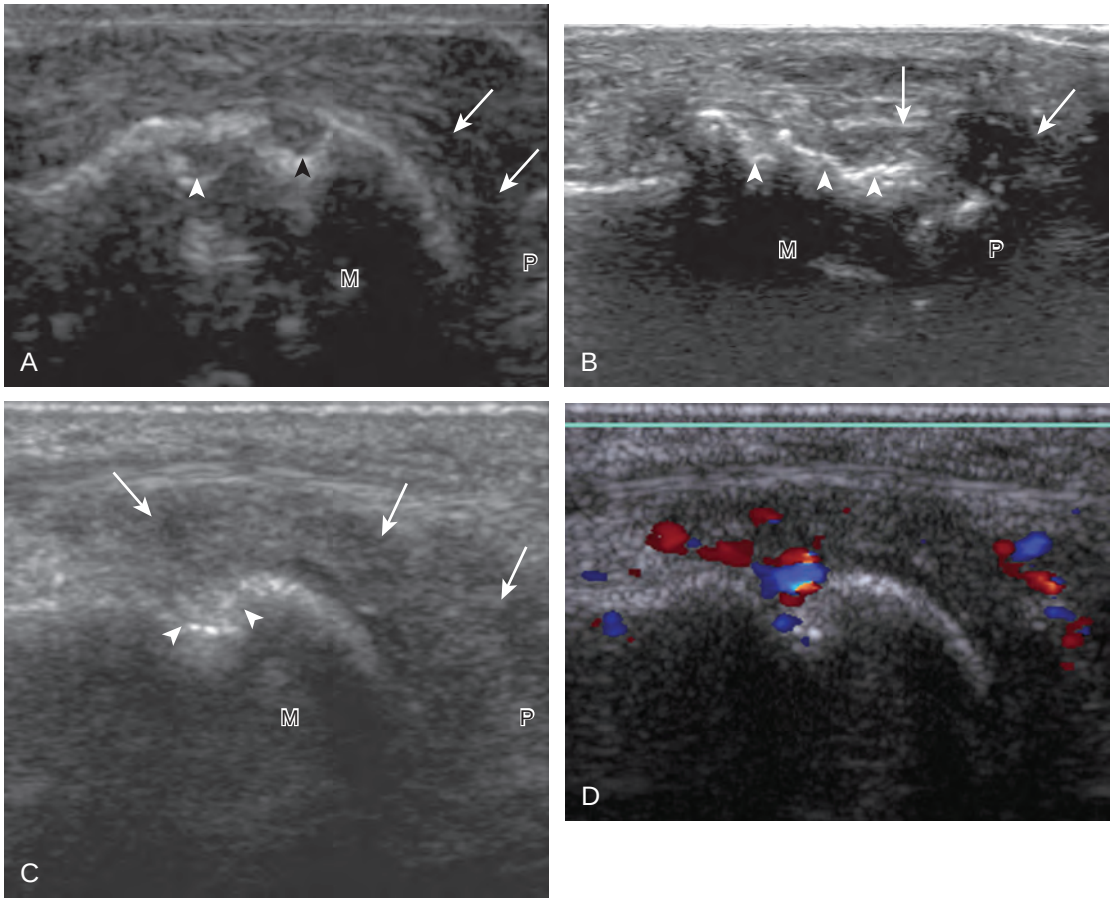

FIGURE 8-44 ■ Rheumatoid arthritis: erosions. Ultrasound images over the dorsal joint recess of the fifth metatarsophalangeal joint in three patients **(A), (B),** and **(C** and **D)** show hypoechoic synovial hypertrophy *(arrows)* and cortical erosions *(arrowheads)* and hyperemia on color Doppler imaging. M, fifth metatarsal head; P, proximal phalanx.

arthritis in the foot and ankle include the retrocalcaneal bursitis (Fig. 8-45), adventitious bursae (see Fig. 8-61A and Video 8-4), hypoechoic rheumatoid nodules (Fig. 8-46),[32] and abnormalities of the tendons and tendon sheath (see Tendon and Muscle Abnormalities).

With regard to gout, the most common site of involvement is the first metatarsophalangeal joint. Within a joint, one may see effusion (Fig. 8-47), synovial hypertrophy (Fig. 8-48), hyperechoic foci (representing microtophi) (Fig. 8-49), echogenic fluid (representing diffuse crystals)

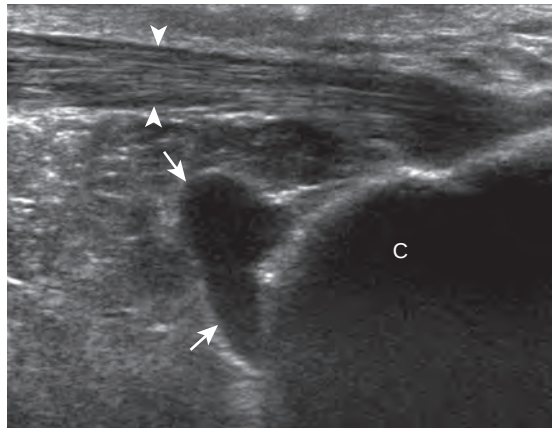

FIGURE 8-45 ■ Rheumatoid arthritis: retrocalcaneal bursitis. Ultrasound image long axis to distal Achilles tendon *(arrowheads)* shows hypoechoic distention of the retrocalcaneal bursa *(arrows)*. C, calcaneus.

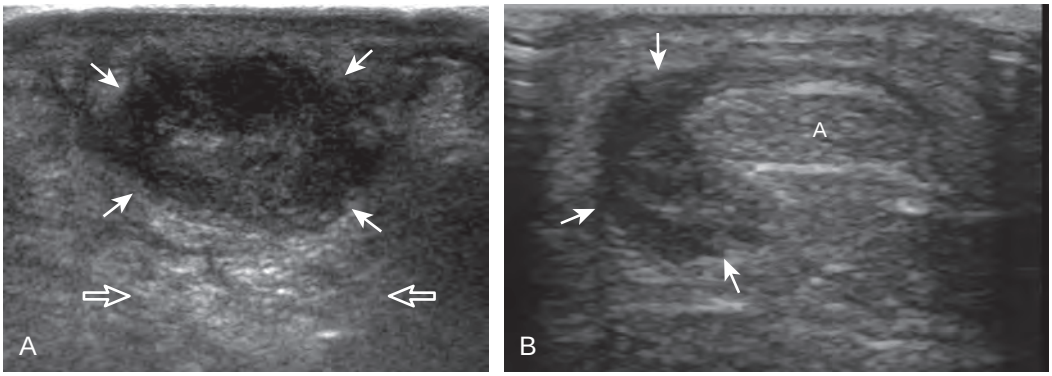

FIGURE 8-46 ■ Rheumatoid arthritis: rheumatoid nodule. Ultrasound images **(A)** over lateral foot and **(B)** short axis to Achilles tendon (A) show predominantly hypoechoic nodule *(arrows)* with increased through-transmission in **A** *(open arrows)*. (**B,** Courtesy of Brian Robertson, Ann Arbor, Mich.)

(Fig. 8-50), and coating of the hyaline cartilage with monosodium urate crystals (called the *double contour sign*) (Fig. 8-51).[33] The latter finding has been shown to disappear when the serum urate level decreases below 6 mg/dL.[34] Imaging at the medial aspect long axis to the distal first metatarsal will show amorphous hyperechoic tophus with anechoic inflammatory halo, with possible direct extension into a cortical erosion

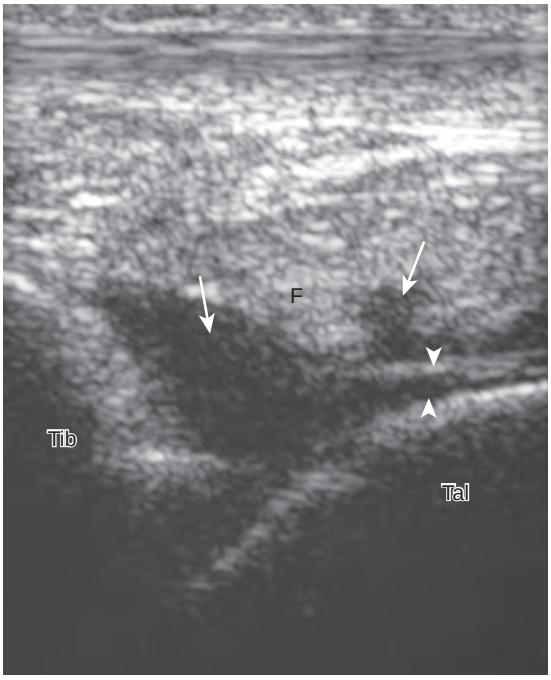

FIGURE 8-47 ■ Gout: effusion. Ultrasound image over dorsal ankle shows hypoechoic distention *(arrows)* of anterior ankle joint recess. Note hyaline cartilage *(arrowheads)* and displacement of anterior fat pad (F). Tal, talus; Tib, tibia.

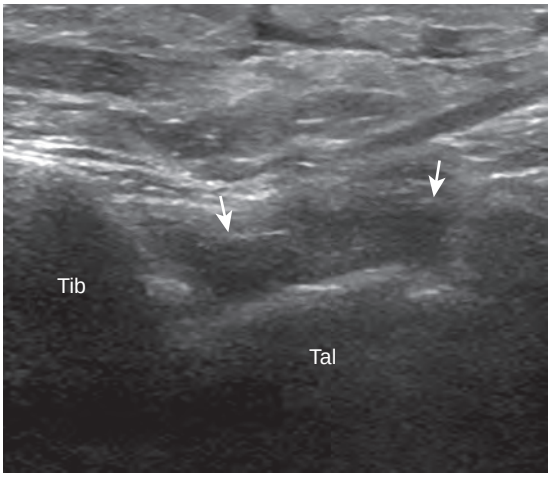

FIGURE 8-48 ■ Gout: synovial hypertrophy. Ultrasound image over dorsal ankle shows hypoechoic synovial hypertrophy *(arrows)*, which was noncompressible. Tal, talus; Tib, tibia.

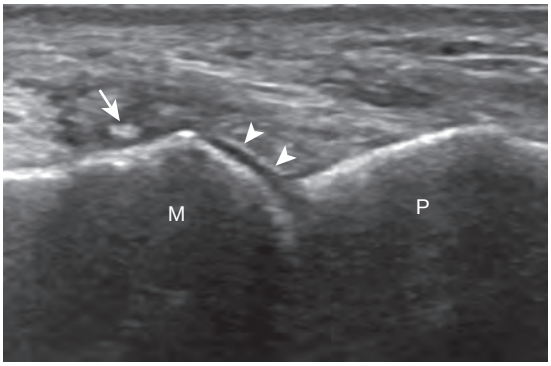

FIGURE 8-49 ■ Gout: microtophus and urate icing. Ultrasound image over first metatarsophalangeal joint shows echogenic microtophus *(arrow)* and urate icing *(arrowheads)*. M, metatarsal; P, proximal phalanx.

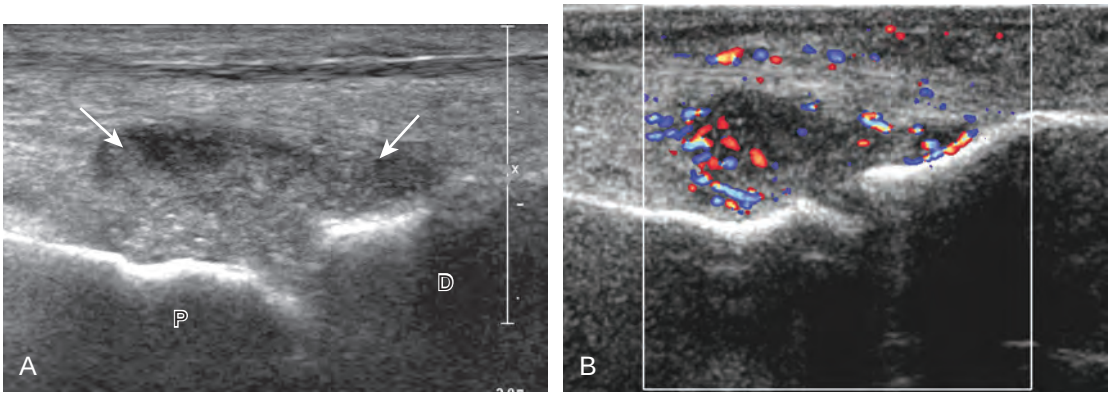

FIGURE 8-50 ■ Gout: complex joint effusion. Ultrasound images **(A** and **B)** over first interphalangeal joint show diffuse hypoechoic to isoechoic effusion *(arrows)* from unaggregated monosodium urate crystals. D, distal phalanx; P, proximal phalanx.

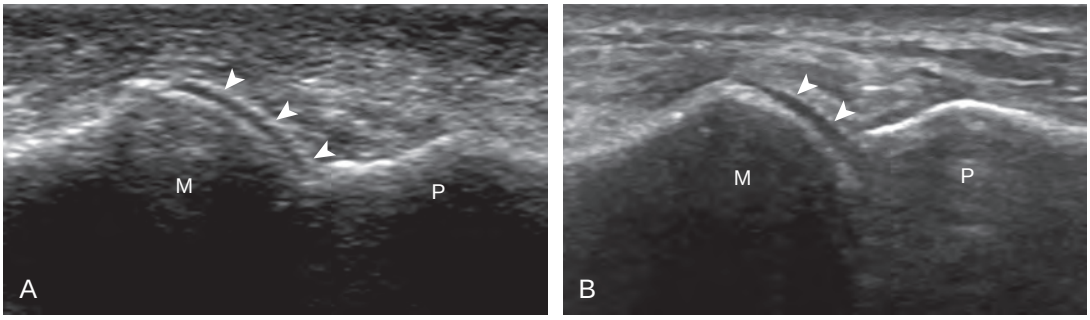

FIGURE 8-51 ■ Gout: urate icing (double contour sign). Ultrasound images **(A** and **B)** over dorsal first metacarpophalangeal joints in two patients show urate icing of hyaline articular cartilage *(arrowheads)*. M, metatarsal; P, proximal phalanx. (**A,** Courtesy of Ralf Thiele, MD, Rochester, NY.)

(Figs. 8-52 and 8-53) (Video 8-5).[35] Tophi may also involve tendon (Fig. 8-54) and tendon sheaths (Fig. 8-55) (Video 8-6) , bursae, and other joints.

Other inflammatory arthritides include seronegative spondyloarthropathies, such as reactive arthritis and psoriatic arthritis. The ultrasound findings of this category of inflammatory arthritis include nonspecific intra-articular findings of joint fluid, synovial hypertrophy, and possible erosions; however, the finding of bone proliferation in the form of inflammatory enthesopathy at tendon and ligament attachments is characteristic of seronegative spondyloarthropathy (Fig. 8-56).[36] Because degenerative enthesopathy is common at several sites in the foot and ankle, such as at the

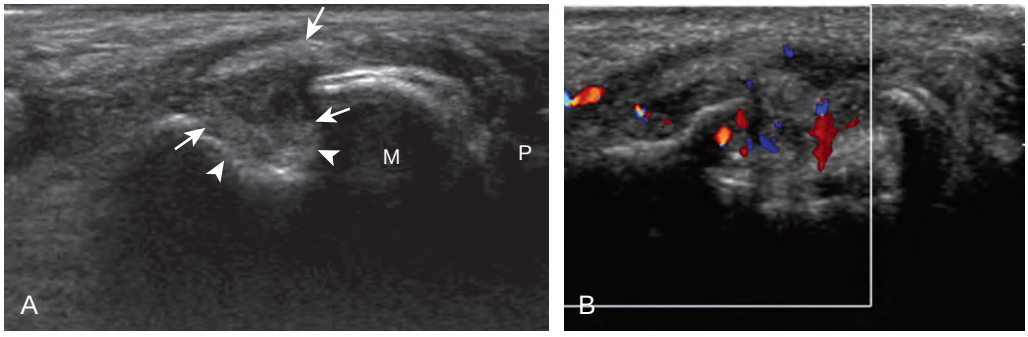

FIGURE 8-52 ■ Gout: tophus and erosion. Ultrasound images **(A** and **B)** in axial plane over medial distal first metatarsal shows cortical erosion *(arrowheads)* and adjacent echogenic tophus *(arrows)* with increased flow on color Doppler imaging. M, metatarsal; P, proximal phalanx.

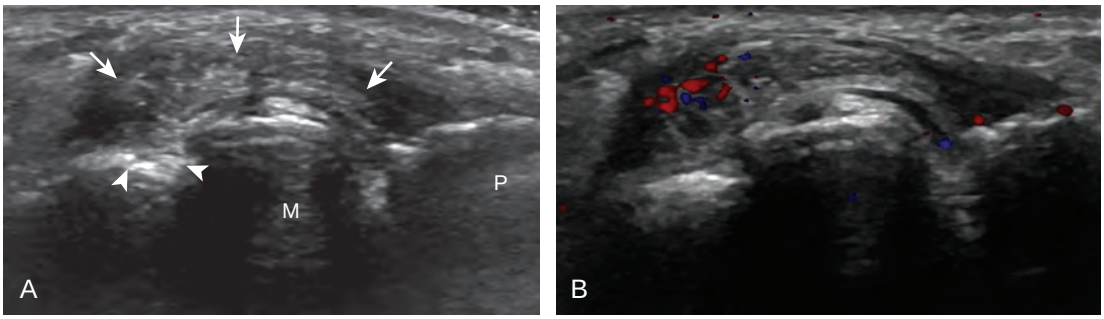

FIGURE 8-53 ■ Gout: tophus and erosion. A, Ultrasound in axial plane over medial distal first metatarsal shows cortical erosion *(arrowheads)* and adjacent echogenic tophus *(arrows)* with increased flow on color Doppler imaging **(B)**. M, metatarsal; P, proximal phalanx.

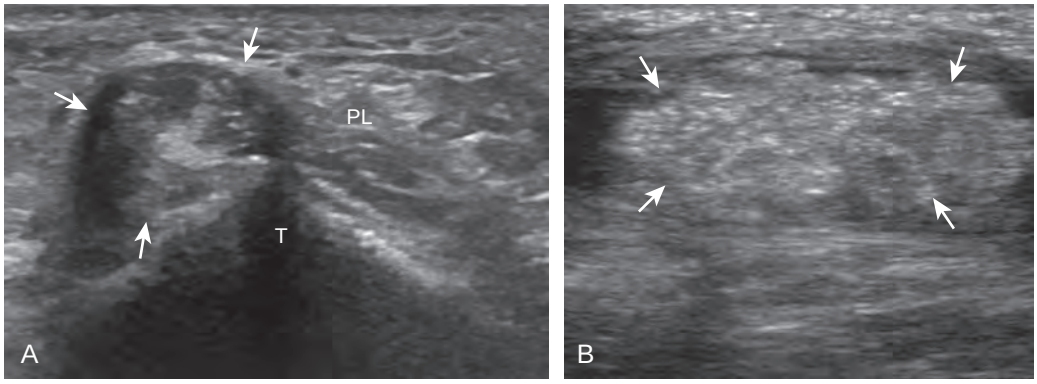

FIGURE 8-54 ■ Gout: tophus. Ultrasound images short axis to **(A)** peroneus brevis and **(B)** tibialis anterior tendons show hyperechoic tophi with hypoechoic halo *(arrows)*. PL, peroneus longus tendon; T, peroneal tubercle of calcaneus.

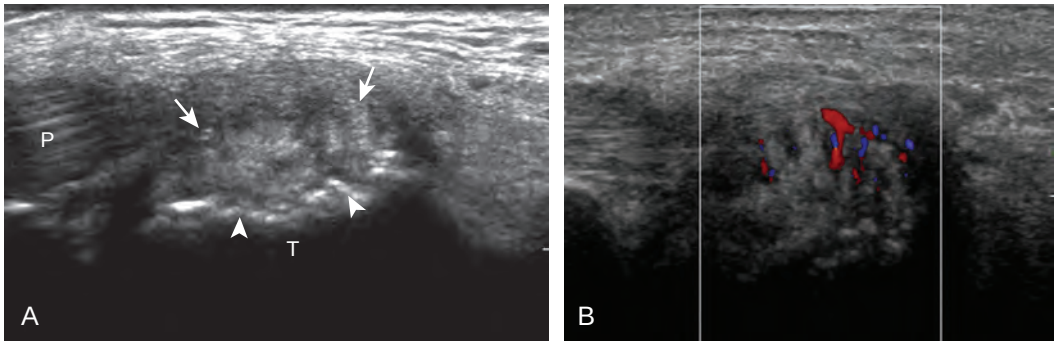

FIGURE 8-55 ■ Gout: tophus, erosion. Ultrasound image **(A)** over medial ankle shows *(arrows)* hyperechoic tophus associated with tibialis posterior tendon (P). Note erosions *(arrowheads)* of medial talus (T) and increased flow on color Doppler **(B)**.

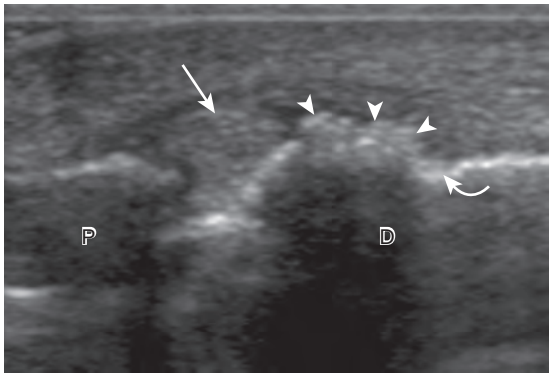

FIGURE 8-56 ■ Psoriatic arthritis. Ultrasound image over the interphalangeal joint of the first toe shows bone proliferation *(arrowheads)*, erosion *(curved arrow)*, and isoechoic to hyperechoic synovial hypertrophy *(arrow)*. D, distal phalanx; P, proximal phalanx.

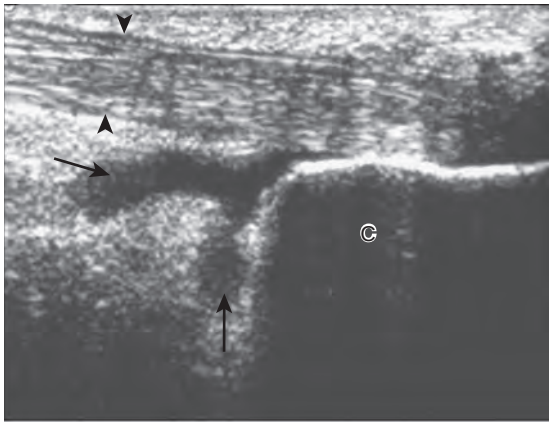

FIGURE 8-57 ■ Retrocalcaneal bursal distention. Ultrasound image in the sagittal plane shows anechoic distention of the retrocalcaneal bursa *(arrows)* (*arrowheads*, Achilles tendon). C, calcaneus.

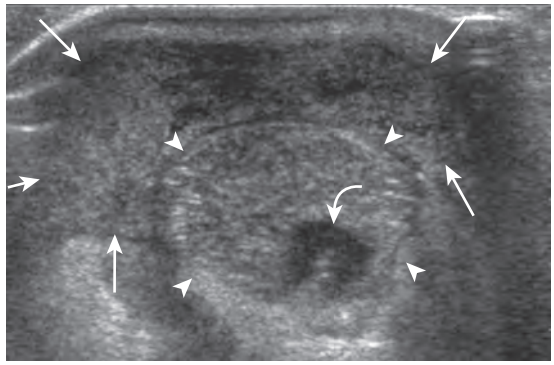

FIGURE 8-59 ■ Retro-Achilles bursal infection. Ultrasound image short axis to the Achilles tendon shows hypoechoic to isoechoic distention of the retro-Achilles bursa *(arrows)*. Note incidental tendinosis *(curved arrow)* of the Achilles tendon *(arrowheads)*.

Achilles tendon attachment, correlation with radiography and identifying true inflammatory findings at ultrasound are critical.

Bursal Abnormalities

There are two bursae around the distal Achilles tendon: the retrocalcaneal and retro-Achilles bursae. The retrocalcaneal bursa, located between the calcaneus and distal Achilles tendon, may normally contain fluid with anteroposterior distention up to 2.5 mm.[12] Abnormal distention of the retrocalcaneal bursa may be mechanical (Fig. 8-57), from adjacent tendon tear (Fig. 8-58), from primary inflammation as in rheumatoid arthritis (see Fig. 8-45), or related to adjacent Achilles enthesopathy. The retro-Achilles bursa, located superficial to the distal Achilles tendon, is not normally visualized and is considered an adventitious bursa. Distention of the retro-Achilles bursa may also be mechanical or inflammatory (Fig. 8-59). The presence of an abnormally distended retrocalcaneal bursa and retro-Achilles bursa with adjacent abnormalities of the Achilles tendon and a prominent posterior superior aspect of the calcaneus is described in patients with Haglund syndrome (Fig. 8-60).[37]

Bursae may also form around the foot and ankle at sites of abnormal pressure, termed *adventitious bursae* (Fig. 8-61) (Video 8-4).[38] Another site of an adventitious bursa is superficial to the medial malleolus (Fig. 8-62).[39] Normal bursae are located between the metatarsal heads, called *intermetatarsal bursae*, and are often distended in associated with Morton neuromas (see Fig. 8-151).[40] Another bursa at the anterior ankle

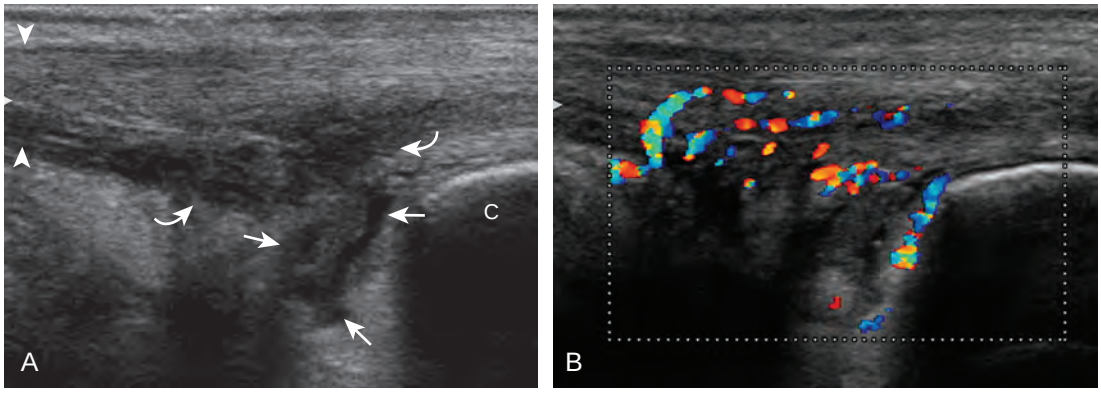

FIGURE 8-58 ■ Retrocalcaneal bursal distention and Achilles tendon tear. Ultrasound images (**A** and **B**) in the sagittal plane show heterogeneous distention of the retrocalcaneal bursa *(arrows)* with adjacent Achilles tendon partial tear and tendinosis *(curved arrows)* (*arrowheads*, Achilles tendon). C, calcaneus.

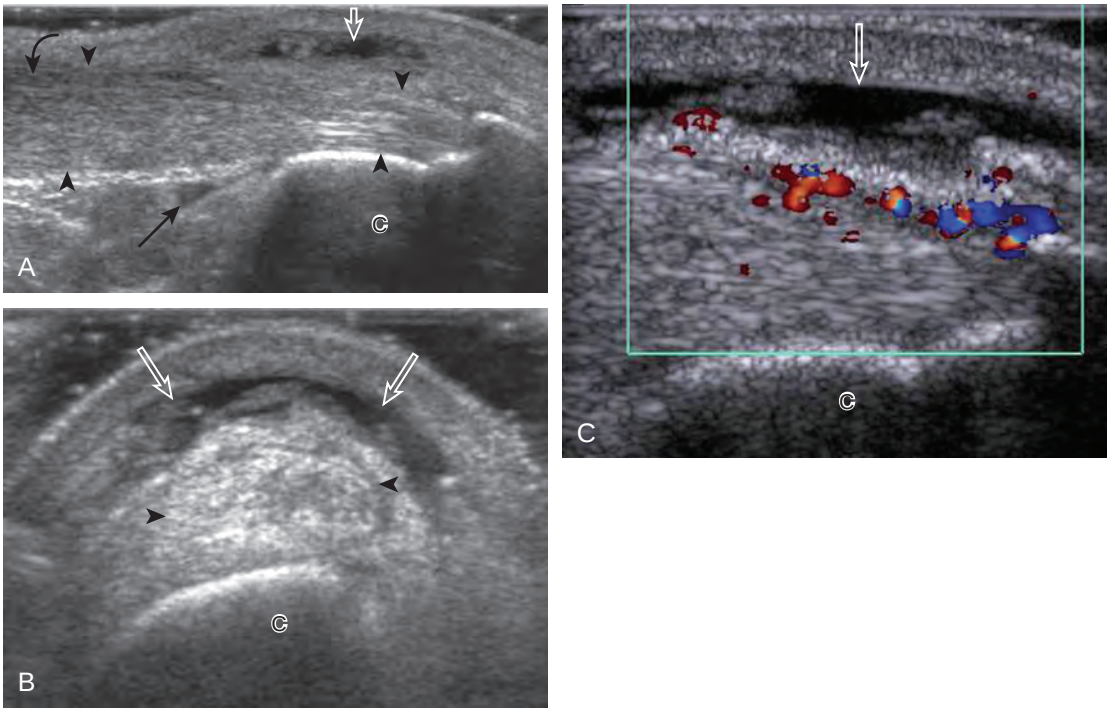

FIGURE 8-60 ■ Haglund syndrome. Ultrasound images **(A)** long axis and **(B)** short axis to the distal Achilles tendon show anechoic fluid in the retrocalcaneal bursa *(arrow)*, the retro-Achilles bursa *(open arrows)*, and tendinosis *(curved arrow)* of the Achilles tendon *(arrowheads)*. **C,** Note increased flow on color Doppler imaging (*open arrow*, retro-Achilles bursa). C, calcaneus.

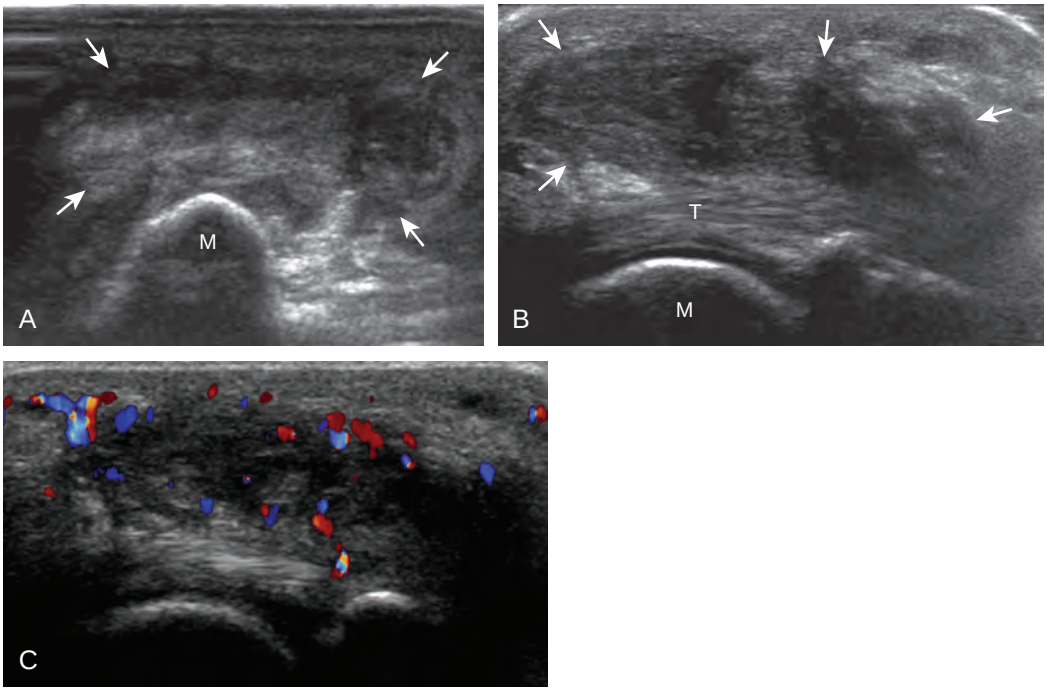

FIGURE 8-61 ■ Adventitious bursa. Ultrasound images over the plantar aspect of the foot in two patients (**A,** with rheumatoid arthritis, and **B** and **C**) show heterogeneous but predominantly hypoechoic adventitious bursa formation *(arrows)*, which was collapsible with transducer pressure. M, metatarsal; T, flexor tendon.

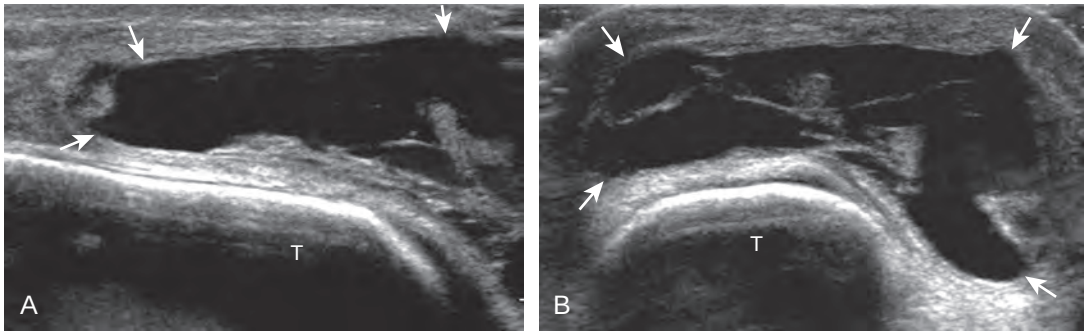

FIGURE 8-62 ■ **Medial malleolus bursa.** Ultrasound images in the **(A)** coronal and **(B)** axial planes over the distal tibia (T) show predominantly anechoic distention *(arrows)* with internal septations.

that commonly contains minimal fluid is the "bursa sinus tarsi" or "bursa mucosa Gruberi" located between the extensor digitorum longus tendons and the talus (Fig. 8-63).[41] Unlike a ganglion cyst, this bursa is easily compressed with transducer pressure and in a characteristic location deep to the extensor digitorum longus (Video 8-7).

TENDON AND MUSCLE ABNORMALITIES

Medial Ankle

Of the medial tendons, the tibialis posterior tendon is most frequently abnormal, usually at the level of the medial malleolus. Tenosynovitis is characterized by distention of the tendon sheath and may be anechoic if it consists of simple fluid (Fig. 8-64A).[42] Tendon sheath distention that is of increased echogenicity may be from complex fluid or synovial hypertrophy; when distention is not anechoic, displacement and internal movement of echoes with transducer pressure as well as absence of internal color flow suggest complex fluid (see Fig. 8-64B).[43] Up to 4 mm of fluid may normally distend the posterior tibial tendon sheath just beyond the medial malleolus.[12] This normal fluid may be asymmetrical, but a helpful feature is the lack of symptoms with transducer pressure and lack of flow on color Doppler imaging. In addition, the ankle joint can normally communicate with the medial tendon sheaths, especially the flexor hallucis longus tendon. Distention of the posterior tibial tendon sheath greater than 5.8 mm indicates early posterior tibial tendon dysfunction (see Fig. 8-64C).[44]

Tenosynovitis is commonly mechanical or traumatic, potentially associated with an underlying tendon abnormality. Inflammation related to systemic arthritis, such as seronegative spondyloarthropathy (Fig. 8-65) and rheumatoid arthritis (Fig. 8-66), is another cause. Uncommonly, infection can involve the tendon sheath as an extension from adjacent soft tissue or bone infection (see Fig. 8-64B). Regardless of origin, a peripheral rim of increased flow may be demonstrated on color or power Doppler imaging (see Fig. 8-64A). While more commonly hypoechoic, synovial tissue surrounding a tendon may be isoechoic or hyperechoic to tendon; toggling the transducer

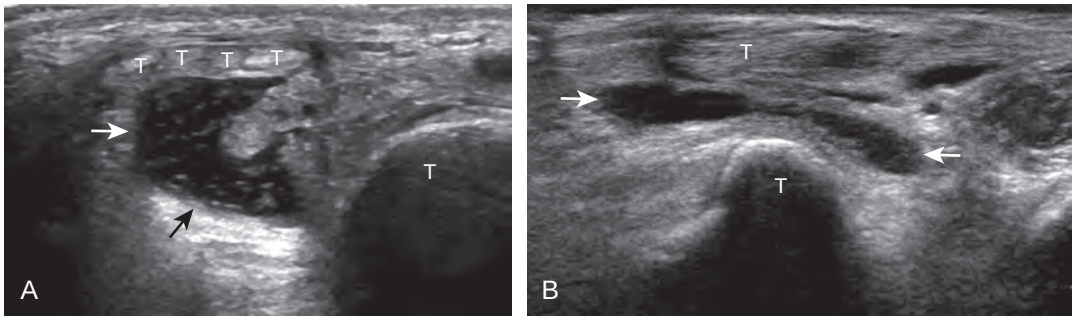

FIGURE 8-63 ■ **Gruberi bursa.** Ultrasound images **(A)** short axis and **(B)** long axis to extensor digitorum longus tendons (T) in two patients show distention of the Gruberi bursa *(arrows)*, which was easily compressible. Note increased through-transmission. T, talus.

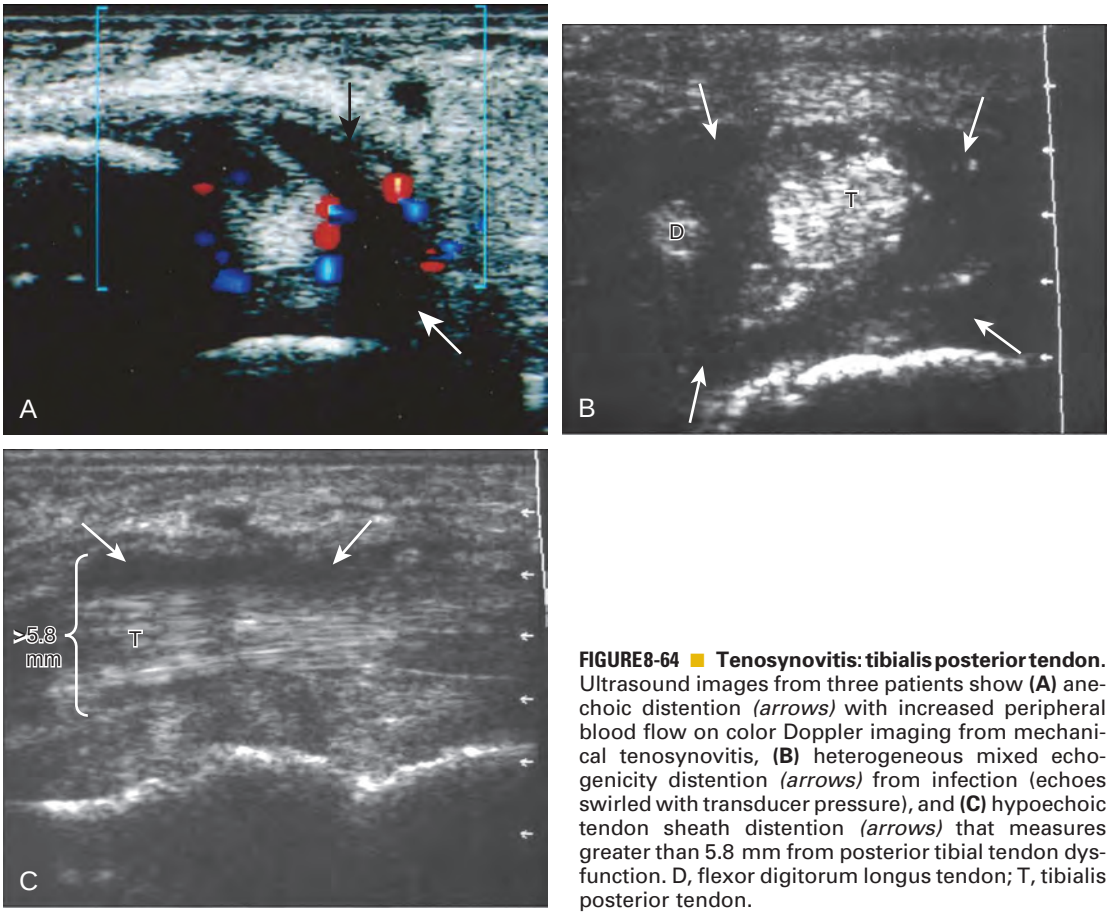

FIGURE 8-64 ■ Tenosynovitis: tibialis posterior tendon. Ultrasound images from three patients show **(A)** anechoic distention *(arrows)* with increased peripheral blood flow on color Doppler imaging from mechanical tenosynovitis, **(B)** heterogeneous mixed echogenicity distention *(arrows)* from infection (echoes swirled with transducer pressure), and **(C)** hypoechoic tendon sheath distention *(arrows)* that measures greater than 5.8 mm from posterior tibial tendon dysfunction. D, flexor digitorum longus tendon; T, tibialis posterior tendon.

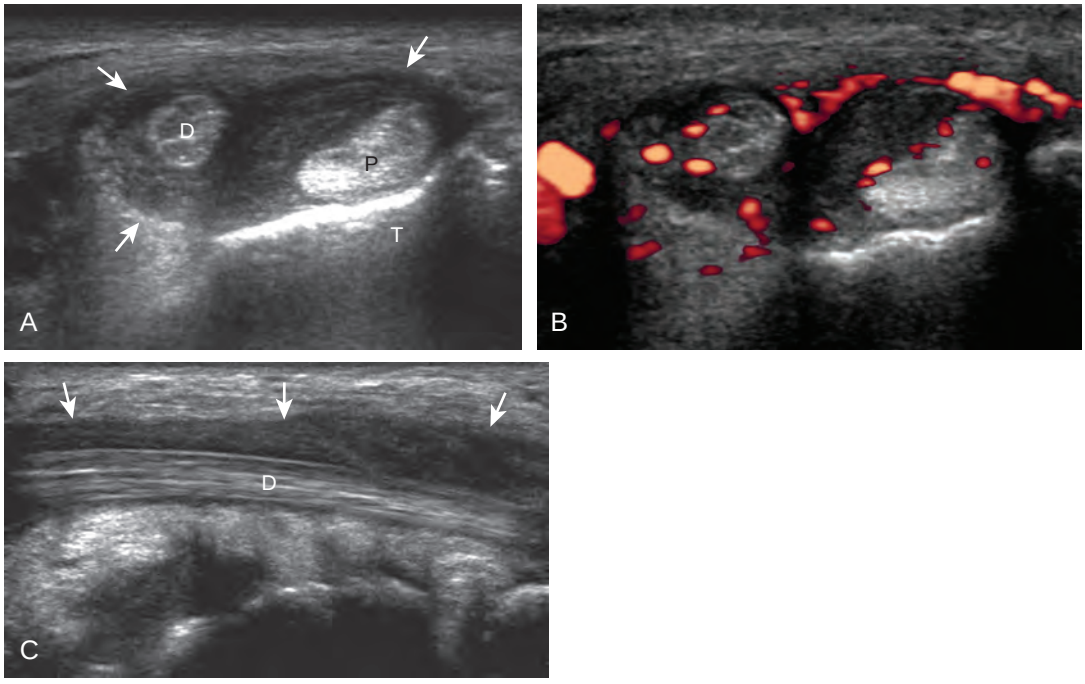

FIGURE 8-65 ■ Tenosynovitis: ankylosing spondylitis. Ultrasound images **(A** to **C)** short axis to the tibialis posterior (P) and flexor digitorum longus (D) tendons show surrounding mixed hypoechoic and isoechoic synovial hypertrophy *(arrows)* with increased flow on color Doppler imaging. T, tibia.

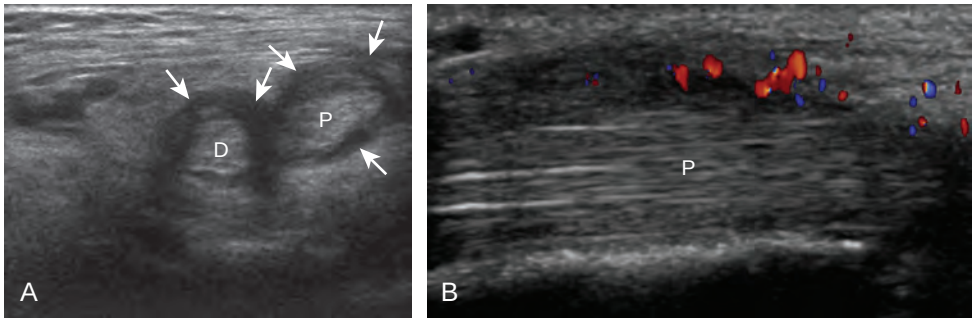

FIGURE 8-66 ■ Tenosynovitis: rheumatoid arthritis. Ultrasound images **(A)** short axis and **(B)** long axis to the tibialis posterior (P) and flexor digitorum longus (D) tendons show surrounding mixed hypoechoic and isoechoic synovial hypertrophy *(arrows)* with increased flow on color Doppler imaging.

when imaging the tendon in short axis will differentiate tendon from echogenic synovial hypertrophy in that the latter does not demonstrate anisotropy and will remain hyperechoic adjacent to the hypoechoic tendon (Fig. 8-67). Tendon sheath distention may also focally involve the flexor hallucis longus tendon at the level of the os trigonum, posterior to the talus in the setting of os trigonum syndrome. More distally, tendon sheath distention may also occur where the flexor hallucis longus and flexor digitorum longus tendons cross (the knot of Henry) under the midfoot (Fig. 8-68A). Because of the normal communication between the medial tendon sheaths and the ankle joint, intra-articular bodies may migrate into a medial tendon sheath (see Fig. 8-68B). Marked focal distention of a single tendon sheath in the absence of anterior ankle joint recess distention suggests tenosynovitis, rather than communicating ankle joint fluid (Fig. 8-69).

Tendinosis is characterized by hypoechoic enlargement of the involved tendon, without disruption of tendon fibers (Fig. 8-70).[45] The involved tendon appears hypoechoic and swollen. The term *tendinosis* is used rather than *tendinitis* because this condition typically represents a degenerative process and not an inflammatory process. Tendinosis commonly involves a segment of tendon that courses around an osseous structure, such as at the medial malleolus.

Partial-thickness tears may initially occur as well-defined intrasubstance anechoic or hypoechoic areas or clefts that partially disrupt the tendon fibers, often in the setting of underlying tendinosis (Fig. 8-71).[46] It is difficult to differentiate between severe intrasubstance tendinosis and interstitial tear in the continuum of a diseased tendon, although the latter is more likely if the abnormality is well defined and anechoic. One type of tear is a longitudinal split, which may extend to one (Fig. 8-72) or two (Fig. 8-73) tendon surfaces.[47] This latter type of tear is best visualized with the tendon in short axis, where the normal tendon is split into two bundles separated

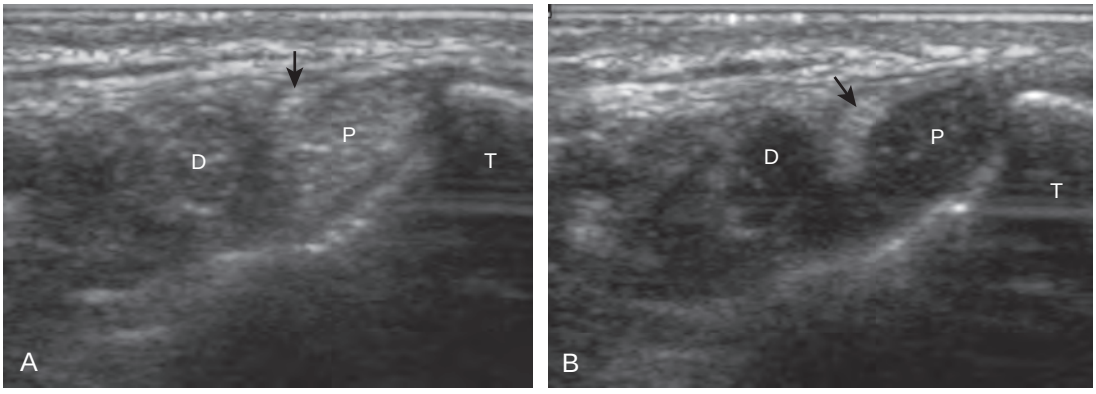

FIGURE 8-67 ■ Synovial hypertrophy: pitfall. Ultrasound images short axis to the tibialis posterior (P) and flexor digitorum (D) longus tendons show hyperechoic synovial hypertrophy *(arrow)* without **(A)** and with **(B)** tendon anisotropy by toggling the transducer. T, tibia.

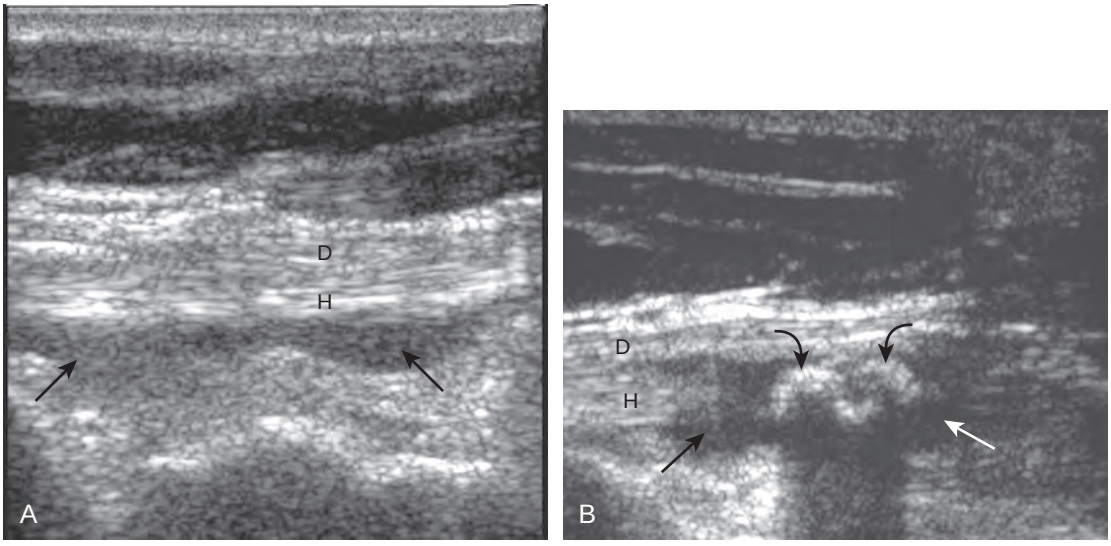

FIGURE 8-68 ■ Intra-articular bodies: flexor hallucis longus. Ultrasound images **(A** and **B)** long axis to the flexor hallucis longus (H) and flexor digitorum longus (D) tendons show anechoic joint fluid *(arrows)* and ossified intra-articular bodies *(curved arrows)* at the knot of Henry from the ankle joint.

by anechoic or hypoechoic fluid, hemorrhage, or synovial hypertrophy. A longitudinal split of the tibialis posterior tendon may be associated with abnormal tendon dislocation or subluxation, which may be apparent only during ankle movement (Fig. 8-74).[48] Direct visualization with ultrasound is important during a dynamic maneuver because tendon subluxation may be transient. An avulsed bone fragment from the medial margin of the medial malleolus at the attachment of the flexor retinaculum increases the risk for tibialis posterior dislocation (see Fig. 8-74). Partial-thickness tendon tears may also occur from abnormal contact between a tendon

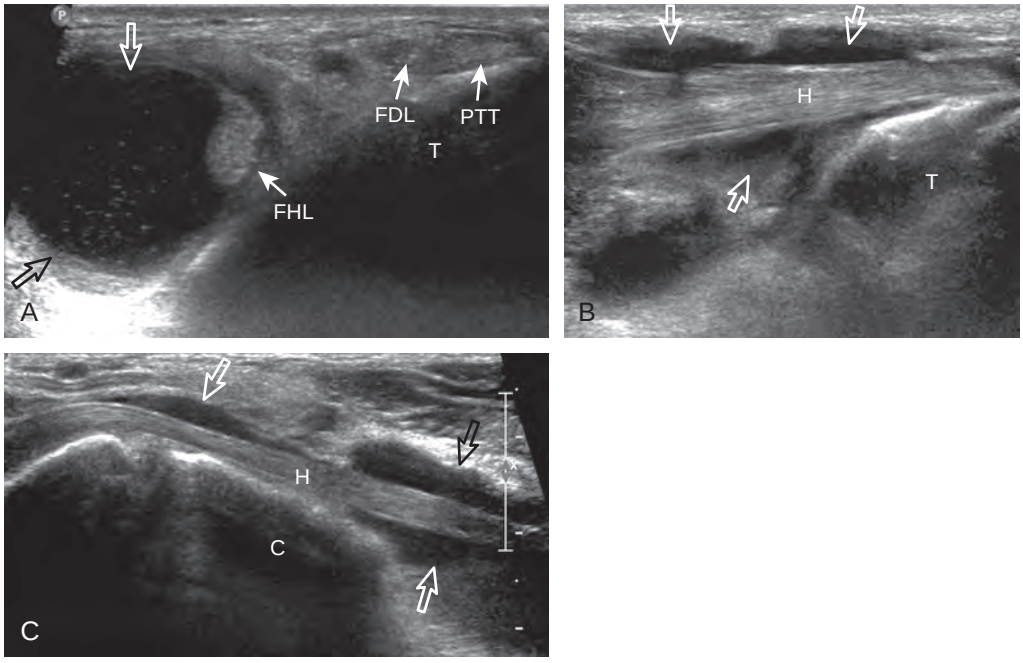

FIGURE 8-69 ■ Tenosynovitis: flexor hallucis longus. Ultrasound images **(A)** short axis and **(B** and **C)** long axis to flexor hallucis longus tendon (H) show isolated hypoechoic distention of the tendon sheath *(open arrows)*. C, calcaneus; FDL, flexor digitorum longus; FHL, flexor hallucis longus; PTT, tibialis posterior; T, tibia.

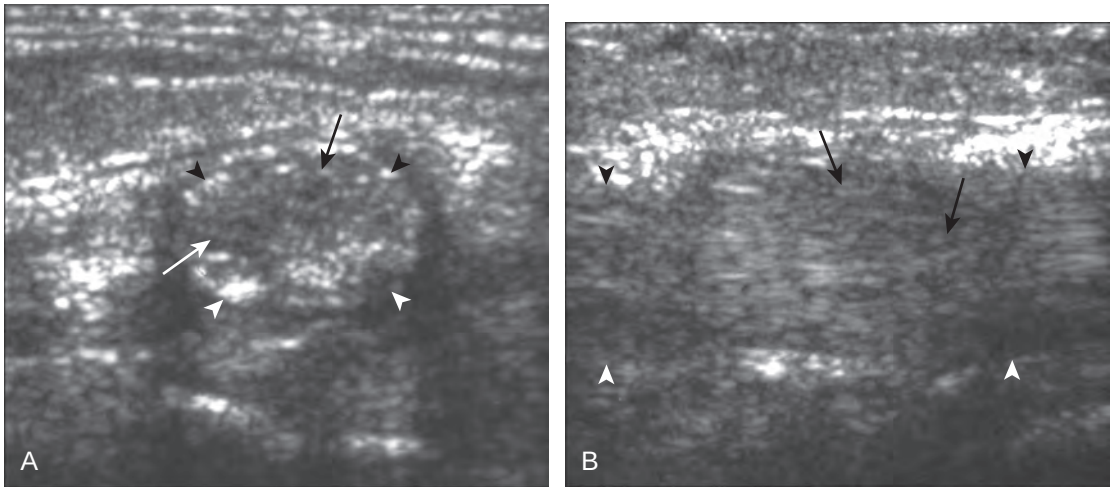

FIGURE 8-70 ■ Tendinosis: tibialis posterior tendon. Ultrasound images **(A)** short axis and **(B)** long axis to the tibialis posterior tendon *(arrowheads)* show hypoechoic swelling *(arrows)* from tendinosis without disruption of tendon fibers.

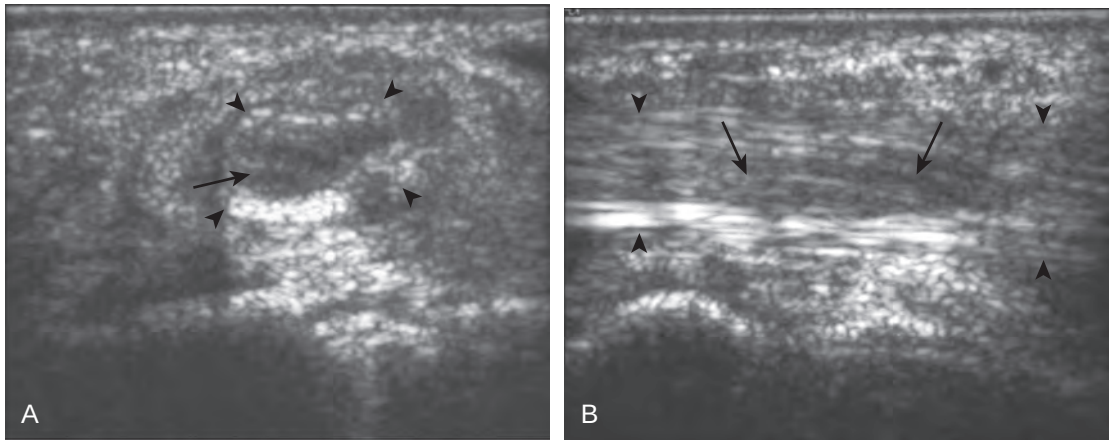

FIGURE 8-71 ■ Intrasubstance tear: tibialis posterior tendon. Ultrasound images **(A)** short axis and **(B)** long axis to the posterior tibial tendon *(arrowheads)* show well-defined hypoechoic areas *(arrows)* with disruption of tendon fibers.

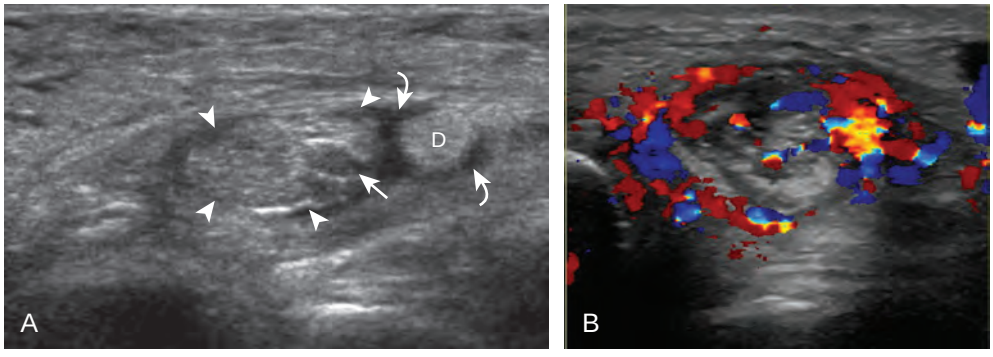

FIGURE 8-72 ■ Longitudinal split tear: tibialis posterior tendon. Ultrasound images **(A** and **B)** short axis to the tibialis posterior tendon *(arrowheads)* show a longitudinal cleft *(arrow)* that involves one surface of the tendon and represents a partial-thickness tear. Note surrounding hypoechoic tenosynovitis *(curved arrows)* with **(B)** increased flow on color Doppler imaging. D, flexor digitorum longus tendon.

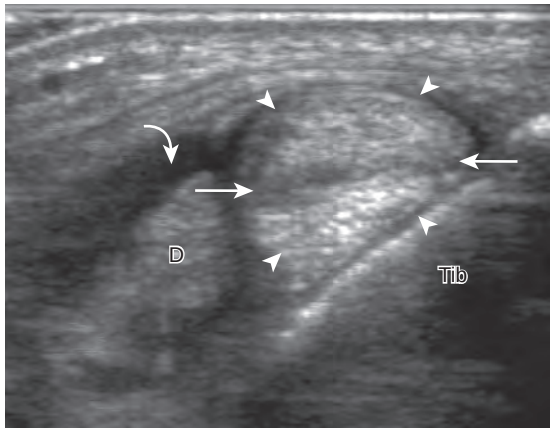

FIGURE 8-73 ■ Longitudinal split tear: tibialis posterior tendon. Ultrasound image short axis to the tibialis posterior tendon *(arrowheads)* shows a longitudinal cleft *(arrows)* that involves two surfaces of the tendon (*curved arrow*, anechoic fluid in tendon sheath). D, flexor digitorum longus tendon; Tib, tibia.

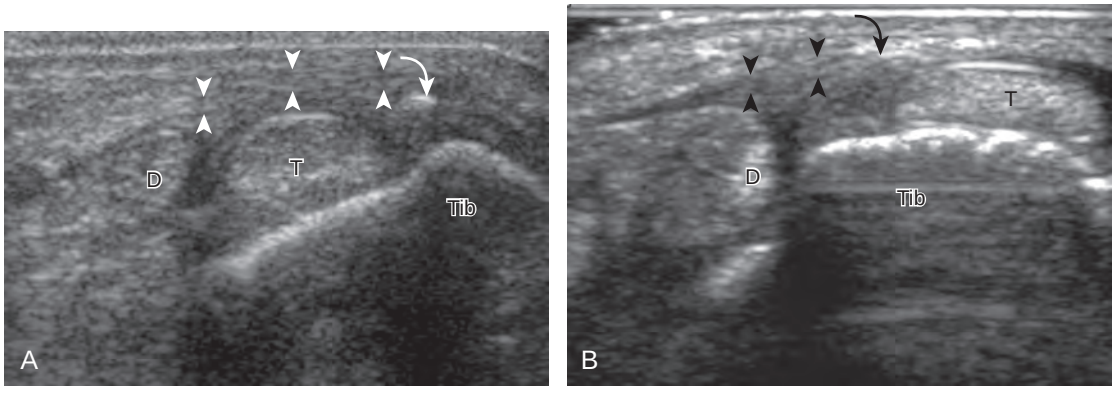

FIGURE 8-74 ■ Flexor retinaculum tear and tendon dislocation. Ultrasound images from two patients show **(A)** tibial bone fragment *(curved arrow)* from flexor retinaculum *(arrowheads)* avulsion (Tib, tibia) and **(B)** anterior dislocation of the tibialis posterior tendon (T) with tibial detachment *(curved arrow)* of the flexor retinaculum *(arrowheads)*. D, flexor digitorum longus tendon.

and fixation hardware (Fig. 8-75), between a tendon and a fracture fragment (Fig. 8-76), or when entrapped within a fracture (Fig. 8-77).[49]

Full-thickness complete tears are characterized by full-width fiber disruption, tendon stump retraction, and interposed fluid, hemorrhage, or synovial hypertrophy that fills the torn tendon gap (Fig. 8-78).[47] Tear of the tibialis posterior tendon may occur at the level of the medial malleolus. In short axis, it is important not to mistake the intact flexor digitorum longus tendon for the tibialis posterior tendon when the latter is torn and retracted from view. The tibialis posterior tendon may also tear distally or avulse a fragment of the navicular bone, especially in diabetic patients, associated with tendon retraction. More commonly, a bone in the distal tibialis posterior tendon represents an accessory navicular, which is a normal variant that may become symptomatic

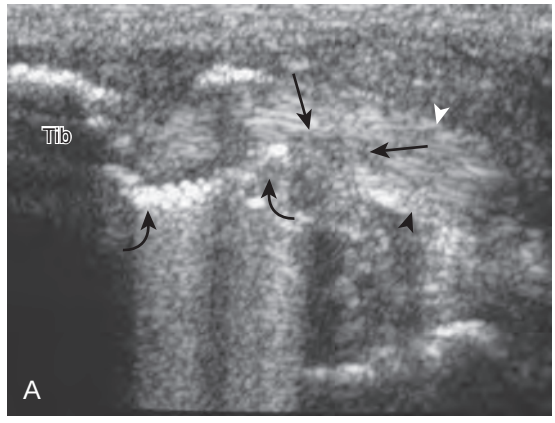

FIGURE 8-75 ■ Partial-thickness tear: tibialis posterior tendon, hardware. Ultrasound image shows partial tendon disruption *(arrows)* of the tibialis posterior tendon *(arrowheads)* from a protruding metal screw *(curved arrows)*. Note reverberation artifact deep to screw. Tib, tibia.

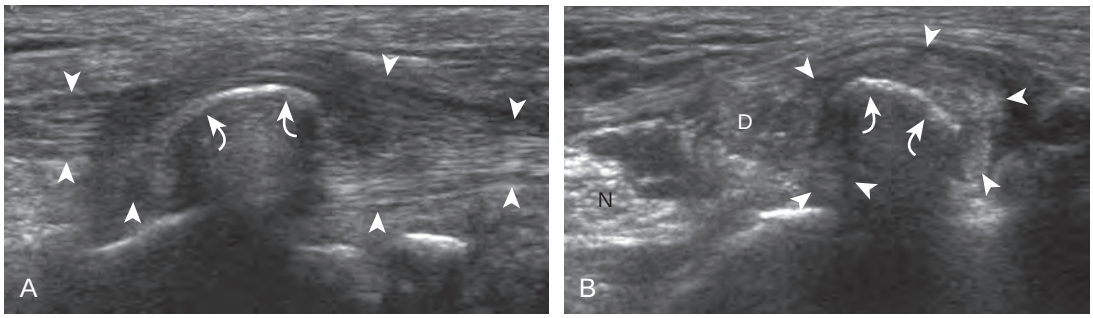

FIGURE 8-76 ■ Partial-thickness tear: tibialis posterior tendon, bone fragment. Ultrasound images **(A)** short axis and **(B)** long axis to tibialis posterior tendon *(arrowheads)* show partial tendon disruption as cortical bone fragment *(curved arrows)* protrudes within tendon. D, flexor digitorum longus tendon; N, tibial nerve.

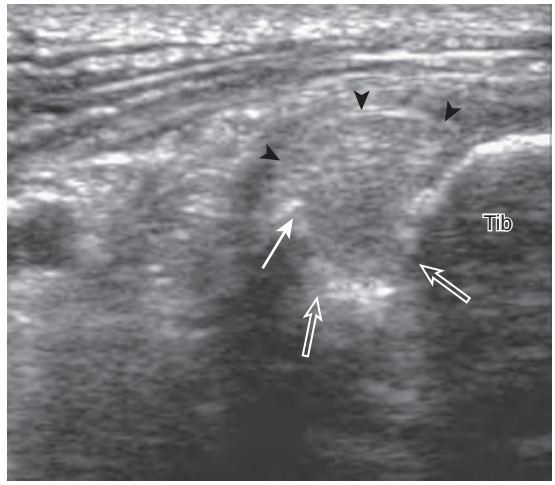

FIGURE 8-77 ■ Tendon entrapment: tibialis posterior. Ultrasound image short axis to tibialis posterior tendon *(arrowheads)* shows tendon entrapment within a tibial fracture *(open arrows)*, where bone partially enters the tendon *(arrow)*. Tib, tibia.

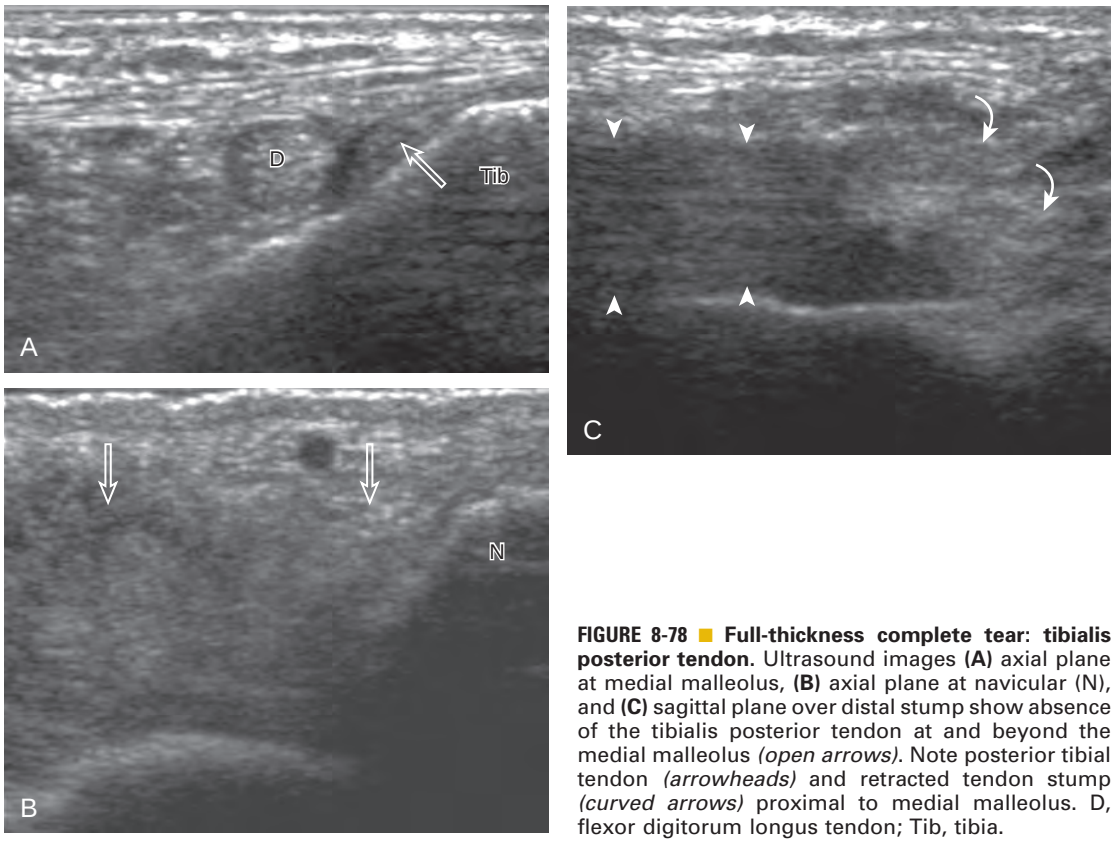

FIGURE 8-78 ■ Full-thickness complete tear: tibialis posterior tendon. Ultrasound images **(A)** axial plane at medial malleolus, **(B)** axial plane at navicular (N), and **(C)** sagittal plane over distal stump show absence of the tibialis posterior tendon at and beyond the medial malleolus *(open arrows)*. Note posterior tibial tendon *(arrowheads)* and retracted tendon stump *(curved arrows)* proximal to medial malleolus. D, flexor digitorum longus tendon; Tib, tibia.

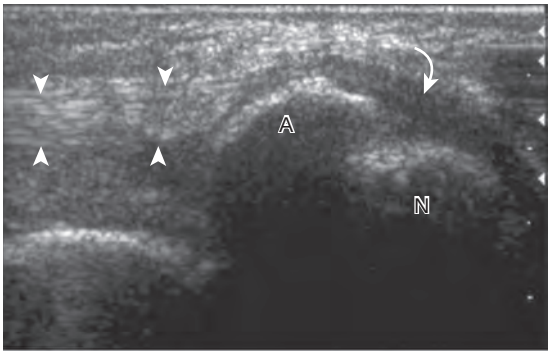

FIGURE 8-79 ■ Symptomatic accessory navicular. Ultrasound image long axis to the distal tibialis posterior tendon *(arrowheads)* shows the accessory navicular (A), adjacent navicular (N), and soft tissue edema *(curved arrow)*. Pain was present at this site with transducer pressure.

in some individuals when the synchondrosis between the accessory navicular and the native navicular is injured (Fig. 8-79). Pain induced by focal pressure from the transducer over the bone fragment is a helpful finding. The flexor digitorum longus tendon may be rerouted to the navicular for treatment of a complete tibialis posterior tendon tear. Ultrasound can evaluate for associated complications, such as flexor digitorum longus tendon avulsion from the implantation site on the navicular (Fig. 8-80).

Disorders of the other medial tendons are less common. Nonetheless, it is important to evaluate the flexor digitorum longus and flexor hallucis longus tendons, at least at locations where pathology may occur, such as at the medial malleolus and posterior malleolus, respectively. This approach ensures a thorough evaluation, which is important when patient symptoms are referred from adjacent structures or locations. Patient history and symptoms may be used to guide evaluation to ensure that pathologic features are not overlooked. Evaluation for tibialis posterior tendon dysfunction should also include the adjacent spring ligament for abnormalities.[46] It is also important always to consider dynamic imaging of tendons. In addition to posterior tibial tendon dislocation (see Fig. 8-74B), another example of this application is dynamic evaluation of the flexor hallucis longus tendon to diagnose impingement (Fig. 8-81) (Video 8-8).

Lateral Ankle

As in the medial tendons, tenosynovitis of the peroneal tendons may occur at the level of the lateral malleolus, which appears anechoic from simple fluid, or hypoechoic, isoechoic, or hyperechoic from complex fluid or synovial hypertrophy (Fig. 8-82).[50] Although less common than the medial tendon sheaths, up to 3.1 mm of fluid may normally distend the peroneal tendon sheaths, usually just distal to the lateral malleolus.[12] Synovial tissue, although more commonly hypoechoic, may also appear isoechoic or hyperechoic relative to subcutaneous fat, which may simulate tendon (see later). The presence of hyperemia on color or power Doppler imaging suggests that hypoechoic distention is from synovial hypertrophy, rather than from complex fluid.[43]

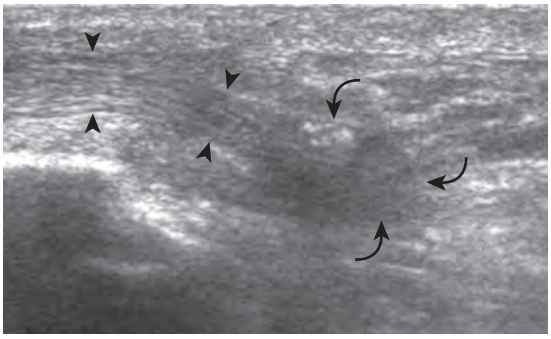

FIGURE 8-80 ■ Tear of flexor digitorum longus. Ultrasound image long axis to the distal flexor digitorum longus tendon *(arrowheads)* that was surgically attached to the navicular shows tendon tear at the navicular with retraction *(curved arrows)*. Note the echogenic suture material at the distal stump.

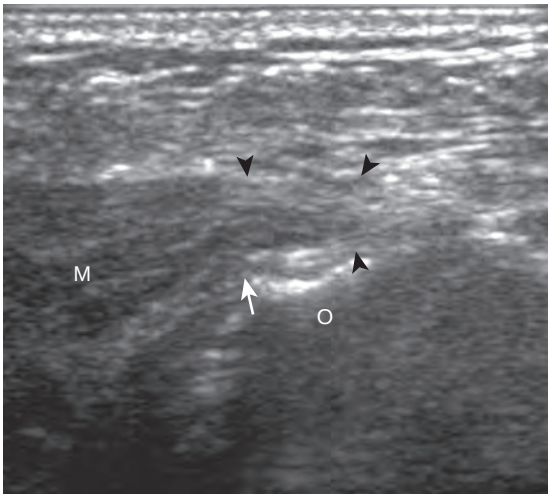

FIGURE 8-81 ■ Flexor hallucis longus impingement. Ultrasound image long axis to the flexor hallucis longus tendon *(arrowheads)* and muscle (M) shows impingement *(arrow)* at the os trigonum (O) that was present during dynamic imaging with toe flexion.

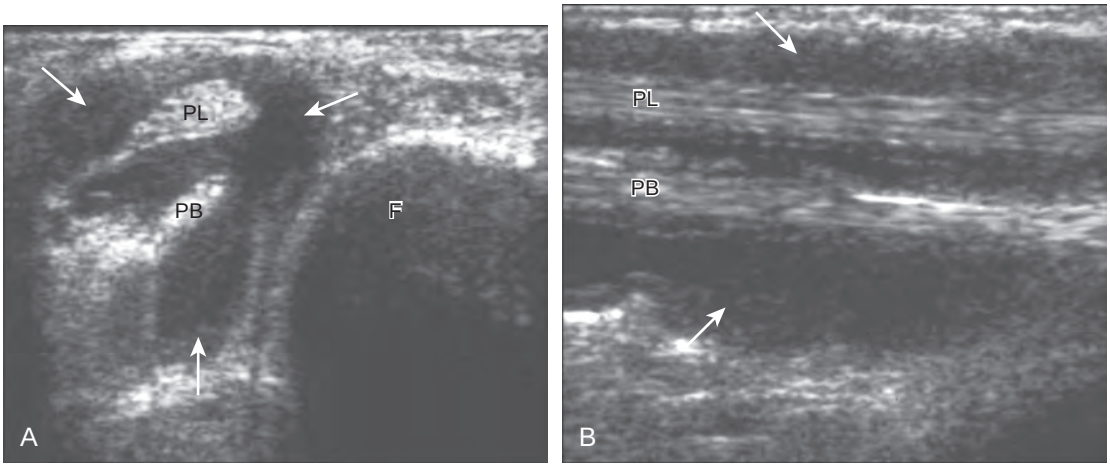

FIGURE 8-82 ■ Tenosynovitis: peroneal tendons. Ultrasound images **(A)** short axis and **(B)** long axis to the peroneus longus (PL) and peroneus brevis (PB) tendons show anechoic and hypoechoic distention *(arrows)* of the tendon sheath. F, fibula.

Tendinosis is also common at the lateral malleolus, where it appears as hypoechoic enlargement of the involved tendon without tendon fiber disruption (Fig. 8-83).[51] Well-defined abnormalities within the substance of the tendon could represent severe tendinosis (Fig. 8-84) or an intrasubstance tendon tear (Fig. 8-85). An abnormal hypoechoic or anechoic cleft that extends to the tendon surface is characteristic of a longitudinal split (Figs. 8-86 and 8-87).[52] In the diagnosis of peroneal tendon tear, ultrasound has been shown to be 100% sensitive and 90% accurate.[51]

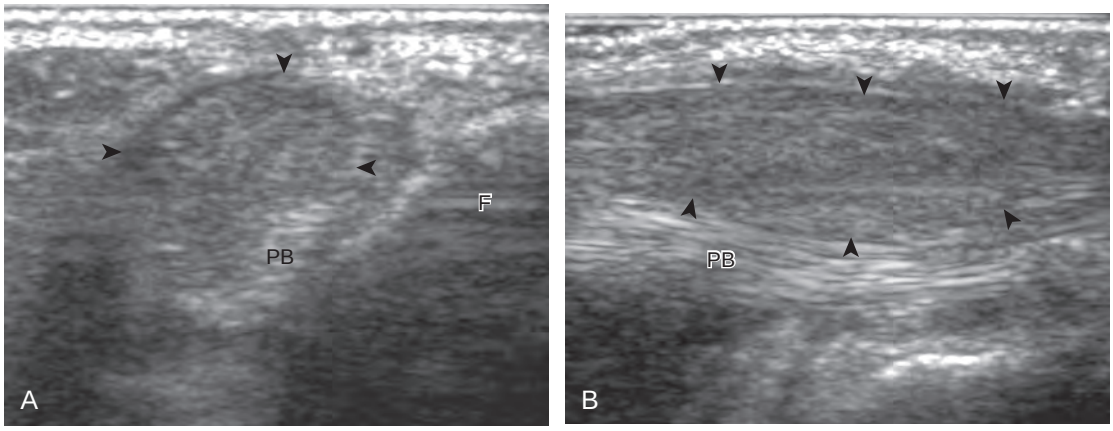

FIGURE 8-83 ■ Tendinosis: peroneal longus. Ultrasound images **(A)** short axis and **(B)** long axis to peroneal tendons show hypoechoic enlargement of the peroneus longus *(arrowheads)*. F, fibula; PB, peroneus brevis.

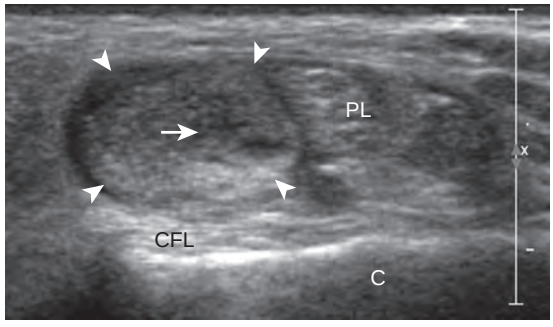

FIGURE 8-84 ■ Tendinosis: peroneus brevis tendon. Ultrasound image short axis to the enlarged peroneus brevis tendon *(arrowheads)* shows well-defined hypoechoic areas *(arrows)* with possible intrasubstance tear. C, calcaneus; CFL, calcaneofibular ligament; PL, peroneus longus.

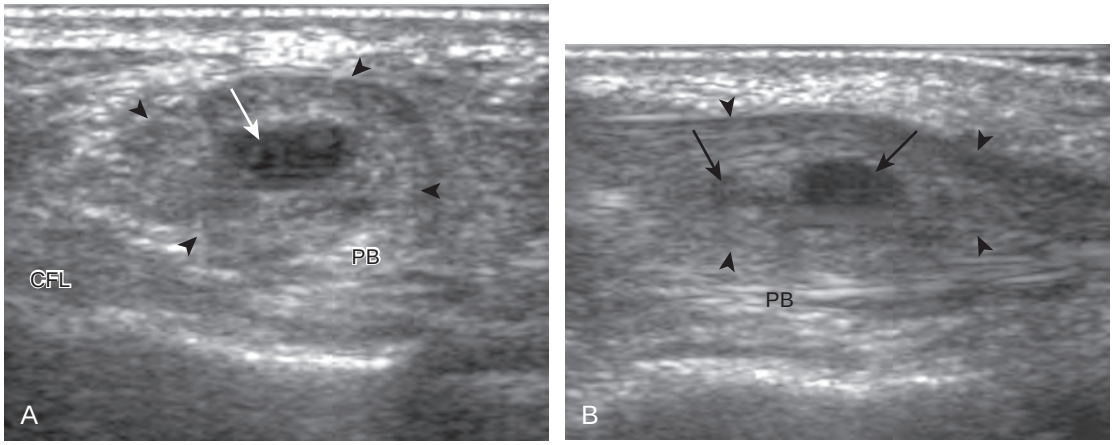

FIGURE 8-85 ■ Tendinosis and intrasubstance tear: peroneal longus. Ultrasound images **(A)** short axis and **(B)** longitudinal show a well-defined anechoic area *(arrows)* that disrupts the fibers within the peroneus longus tendon. Note coexisting hypoechoic and swollen tendinosis *(arrowheads)*. CFL, calcaneofibular ligament; PB, peroneus brevis.

Although involvement of either peroneal tendon is possible, the peroneus brevis tendon is more commonly torn, in part because of its more common location between the peroneus longus and fibula. Initially, the peroneus brevis tendon appears as a horseshoe shape that encompasses the peroneus longus tendon with a small cleft.[51] The two segments of peroneus brevis tendon may separate, best appreciated in short axis, and the peroneus longus tendon may be seen to interpose between the two peroneus brevis tendon pieces (Video 8-9).[51]

At its attachment on the fibula, the superior peroneal retinaculum may be injured, which may appear as hypoechoic thickening or complete disruption with associated cortical irregularity (Fig. 8-88).[53] With complete retinaculum discontinuity, subluxation or dislocation of the peroneal tendons may occur, predisposing to tenosynovitis and tendon tear. Because tendon displacement may only occur transiently, dynamic ankle evaluation with dorsiflexion and eversion is important in this setting for diagnosis of tendon displacement.[52,54] With peroneal tendon displacement, the superior peroneal retinaculum may be thickened and partially stripped away from the fibula, termed a *type 1 injury* (Fig. 8-89A) (Video 8-10).[5] With peroneal tendon subluxation or dislocation, the retinaculum may be detached, without (see Fig. 8-89B) (Video 8-11) or with (see Fig. 8-89C and D) (Video 8-12) a fibular avulsion bone fragment.[5] Peroneal tendon displacement may be transient, so continual observation with sonography is important throughout the dynamic maneuvers (see Fig. 8-89C and D). Intrasheath peroneal tendon subluxation may also be demonstrated dynamically,

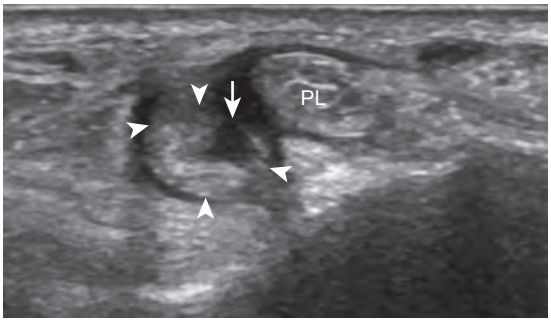

FIGURE 8-86 ■ Longitudinal split tear: peroneus brevis tendon. Ultrasound image short axis to peroneus brevis tendon *(arrowheads)* shows anechoic cleft that extends to tendon surface *(arrow)*. Note mild hypoechoic tenosynovitis. PL, peroneus brevis tendon.

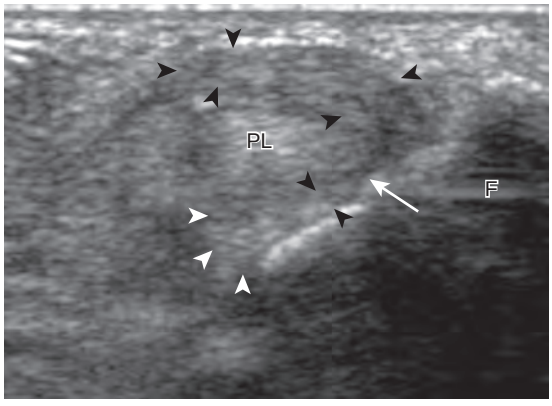

FIGURE 8-87 ■ Longitudinal split tear: peroneal brevis. Ultrasound image transverse shows a horseshoe-shaped peroneus brevis tendon *(arrowheads)* with focal discontinuity *(arrow)*. F, fibula; PL, peroneus longus tendon.

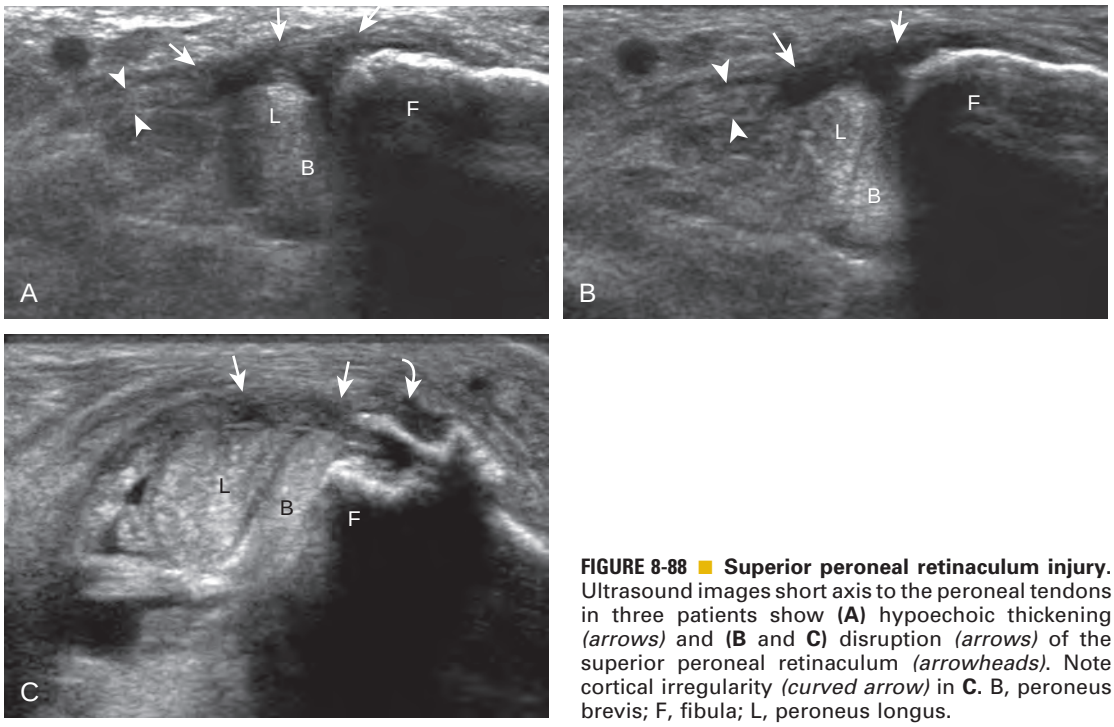

FIGURE 8-88 ■ Superior peroneal retinaculum injury. Ultrasound images short axis to the peroneal tendons in three patients show **(A)** hypoechoic thickening *(arrows)* and **(B** and **C)** disruption *(arrows)* of the superior peroneal retinaculum *(arrowheads)*. Note cortical irregularity *(curved arrow)* in **C.** B, peroneus brevis; F, fibula; L, peroneus longus.

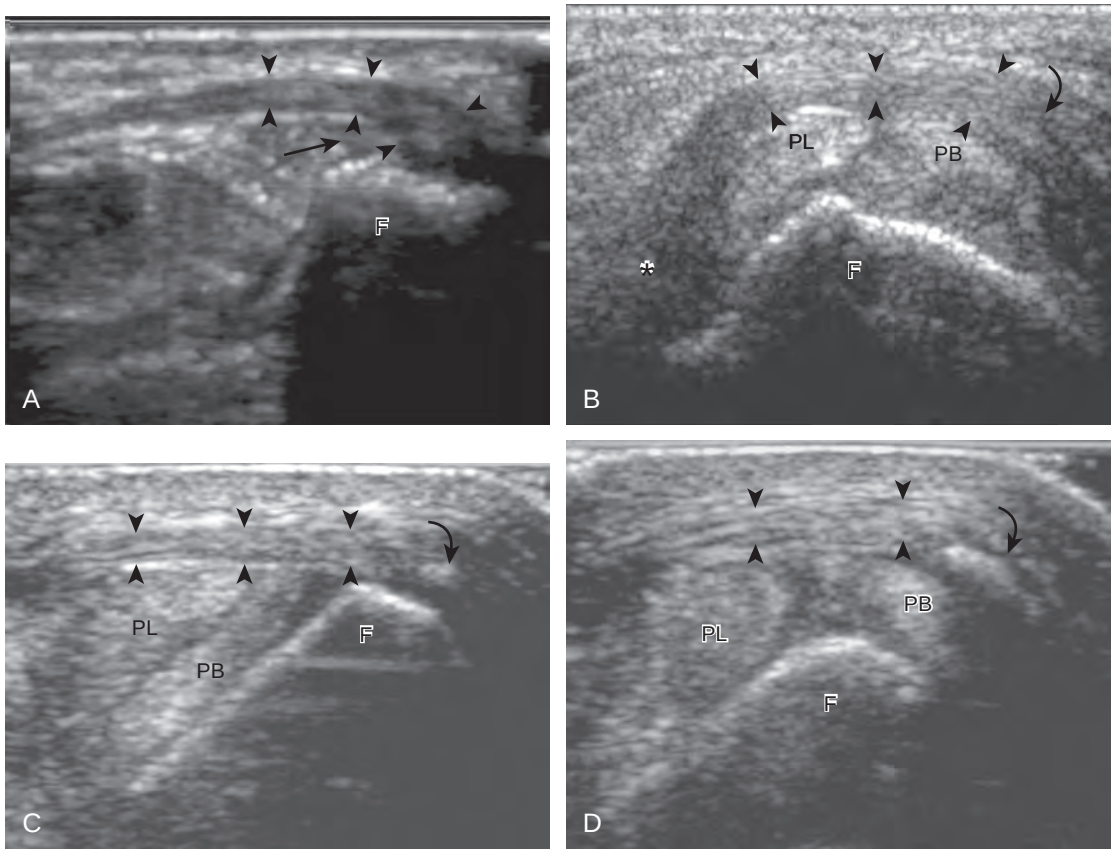

FIGURE 8-89 ■ Peroneal tendon subluxation and dislocation. Ultrasound images in three patients short axis to the peroneal tendons show **(A)** transient peroneal subluxation into a type 1 retinaculum injury pouch *(arrow)* with thickened and hypoechoic superior peroneal retinaculum *(arrowheads)* and bone irregularity of the fibula (F), **(B)** anterolateral peroneus longus (PL) subluxation and peroneus brevis (PB) dislocation from their normal position *(asterisk)* with detachment *(curved arrow)* of the superior retinaculum *(arrowheads)* from the fibula (F), and **(C** and **D)** superior peroneal retinaculum *(arrowheads)* avulsion fracture *(curved arrows)* from the fibula (F) with peroneus brevis dislocation (PB), which is present only at dorsiflexion and eversion **(D)** (right side of images is anterior). PL, peroneus longus.

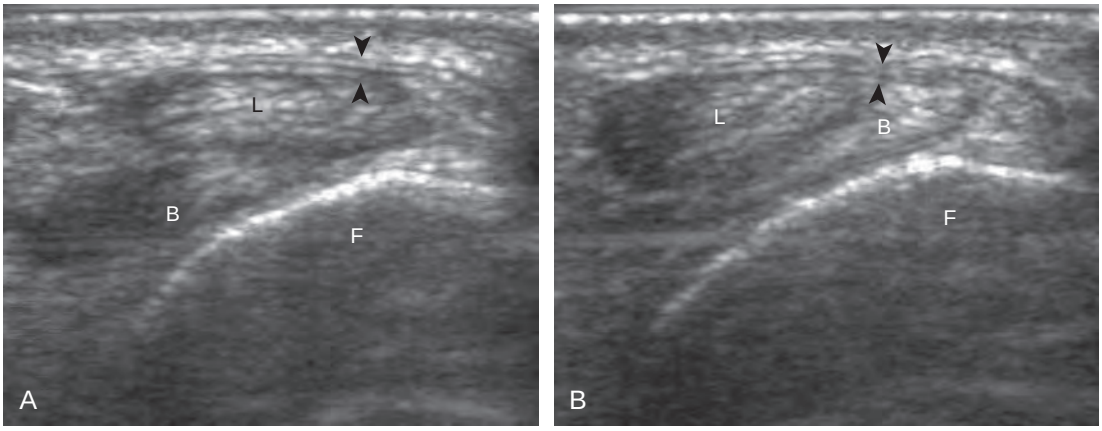

FIGURE 8-90 ■ Peroneal intrasheath subluxation. Ultrasound images short axis to peroneal tendons show abnormal movement of tendons with dynamic imaging between **A** and **B** (*arrowheads*, superior peroneal retinaculum). B, peroneus brevis; F, fibula; L, peroneus longus.

which is associated with an abnormal convex posterior contour of the posterior fibula, low-lying peroneus brevis muscle, peroneus quartus, and subsequent tendon tear (Fig. 8-90) (Videos 8-13 to 8-15).[54,55] Less commonly, tendon subluxation may occur at the level of the peroneal tubercle. Even in the absence of abnormal subluxation, an enlarged or hypertrophied peroneal tubercle may be associated with peroneal tendon pathology (Fig. 8-91).[56] The presence of a low-lying muscle belly of the peroneus brevis may predispose to peroneus tendon pathology, which is diagnosed when the peroneus brevis muscle tissue is identified beyond the fibula (Fig. 8-92).[4]

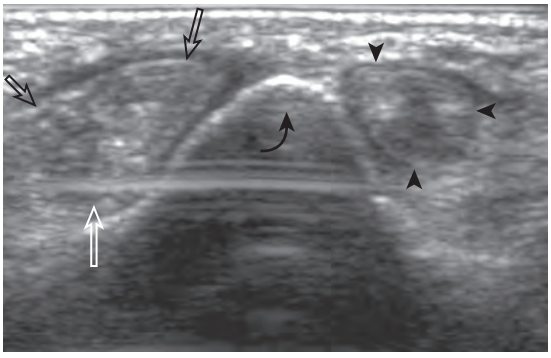

FIGURE 8-91 ■ Abnormalities at peroneal tubercle of calcaneus. Ultrasound image short axis to the peroneal tendons shows hypoechoic and swollen tendinosis of the peroneus brevis *(arrowheads)* and peroneus longus *(open arrows)* at an enlarged peroneal tubercle *(curved arrow)*.

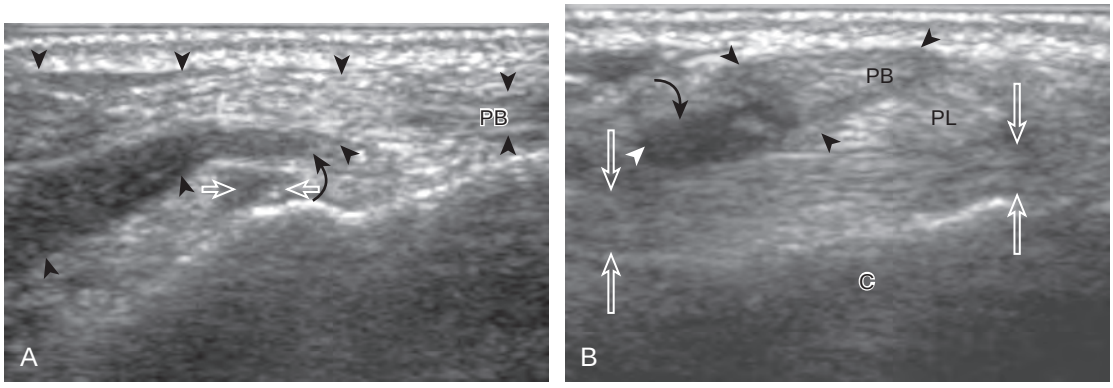

FIGURE 8-92 ■ Low-lying muscle belly of peroneus brevis. Ultrasound images **(A)** long axis and **(B)** short axis to peroneal tendons show tapering peroneus brevis *(arrowheads)* to tendon (PB) with muscle tissue that extends distally *(curved arrow)* beyond the fibula and over the calcaneofibular ligament *(open arrows)*. C, calcaneus; PL, peroneus longus.

It is also important to distinguish an accessory tendon, the peroneus quartus, from a peroneal longitudinal split (Fig. 8-93).[6] If unrecognized, the accessory tendon can be misinterpreted as one of the segments of a peroneal tendon split. To differentiate between the two conditions, distal imaging is helpful because a peroneus quartus typically inserts onto the retrotrochlear eminence of the calcaneus, whereas a true longitudinal split follows the direction of the peroneal tendons, and the two tendon pieces eventually reunite to constitute a normal peroneal tendon distally. The peroneus quartus is present in up to 22% of ankles and has a variable appearance representing hypoechoic muscle, hyperechoic tendon, or both.[6] It is also important not to misinterpret echogenic synovial tissue near a tendon as a separate segment of tendon, which would falsely indicate a longitudinal split. Toggling the transducer (see Fig. 1-3) causes the tendon tissue to become hypoechoic from anisotropy, whereas echogenic synovial tissue remains hyperechoic (Fig. 8-94).

Full-thickness complete tears are characterized by full-width tendon fiber disruption, tendon stump retraction, and interposed hemorrhage or fluid in the torn tendon gap.[51] Such tears may occur at the level of the lateral malleolus (Fig. 8-95). More distally, a peroneus longus tendon tear may be associated with fracture of the os peroneum, a normal ossicle within the peroneus longus tendon at the level of the cuboid bone (Fig. 8-96).[14] Because the normal os peroneum may be bipartite, it is important to correlate with symptoms elicited by transducer pressure and degree of retraction of the fractured bone fragments, if present. Os peroneum fragment separation of 6 mm or more suggests os peroneum fracture and a full-thickness peroneus longus tendon tear.[14] It is important to identify the distal stump of the torn peroneus longus tendon and the proximal os

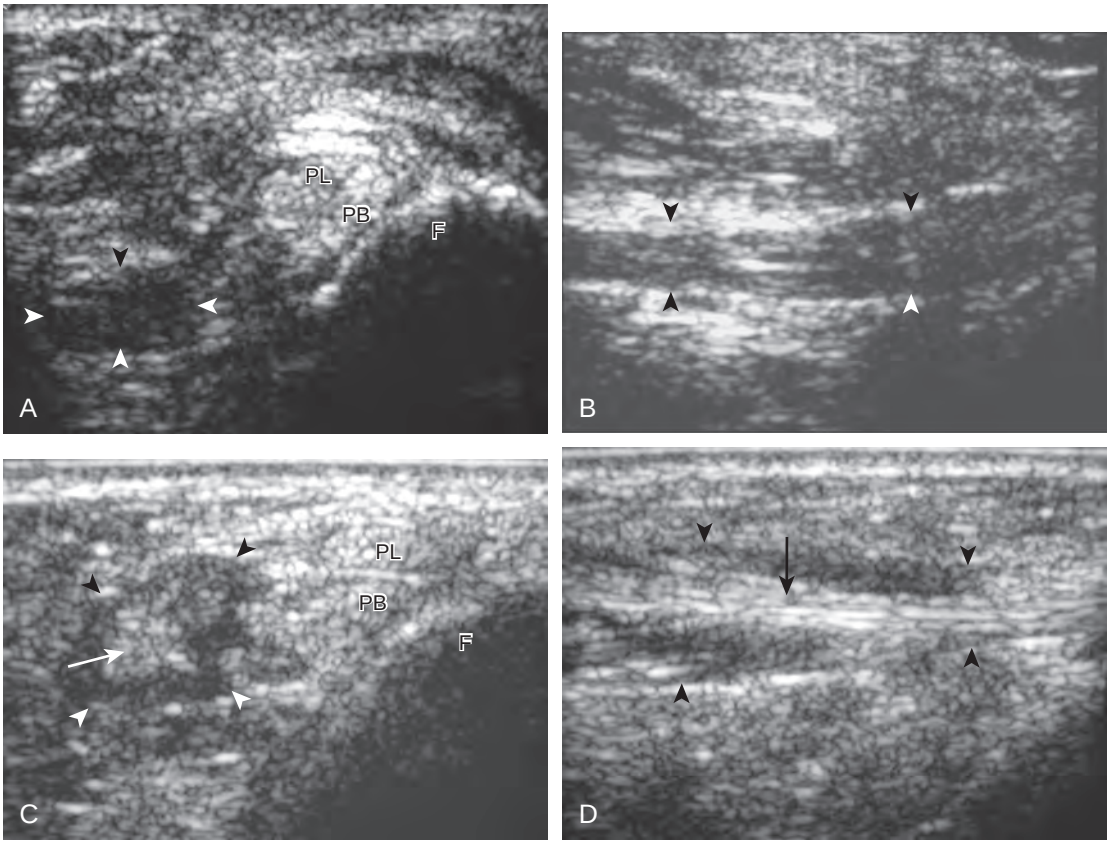

FIGURE 8-93 ■ Peroneus quartus. Ultrasound images from two patients show peroneus quartus **(A** and **B)** as hypoechoic muscle *(arrowheads)* and **(C** and **D)** hypoechoic muscle *(arrowheads)* with a central hyperechoic tendon *(arrow)*. **F, fibula; PB, peroneus brevis; PL, peroneus longus.** (From Chepuri NB, Jacobson JA, Fessell DP, Hayes CW: Sonographic appearance of the peroneus quartus muscle: correlation with MR imaging appearance in seven patients. *Radiology* 218:415-419, 2001.)

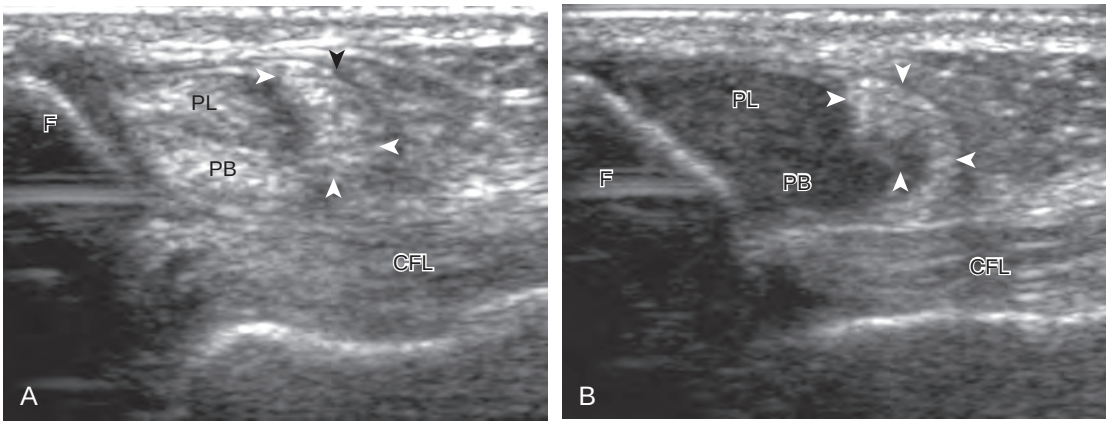

FIGURE 8-94 ■ Hyperechoic synovial hypertrophy. Ultrasound image short axis to the peroneal tendons shows **(A)** hyperechoic tissue *(arrowheads)* adjacent to the peroneus longus (PL) and peroneus brevis (PB) tendons that may simulate tendon. Toggling the transducer shows **(B)** anisotropy of the peroneus longus (PL) and peroneus brevis (PB) tendons, whereas the hyperechoic synovial tissue *(arrowheads)* does not change in echogenicity thereby excluding a tendon fragment. CFL, calcaneofibular ligament; F, fibula.

peroneum fragment because retraction to the level of the tibiotalar may be seen (see Fig. 8-96C). Avulsion fracture of the base of the fifth metatarsal may also be seen related to plantar aponeurosis and the peroneus brevis tendon (Fig. 8-97).[57]

After injury to the lateral ligaments of the ankle, the peroneal tendons may be used in lateral ligament reconstruction.[58] In general, the peroneus brevis tendon may be rerouted through a tunnel in the fibula and reattached to the fifth metatarsal, the peroneal brevis tendon may be split so that one segment is looped around the fibula and reattached to itself, or the peroneus brevis may be transected above the fibula and used through various tunnels in the fibula and calcaneus while still attached to the fifth metatarsal.[58] At ultrasound, the peroneus brevis split segment may be followed from distal to proximal as it enters into the anterior aspect of the fibula, exits the fibula posteriorly, and then is reattached to itself (Fig. 8-98). It is often helpful to evaluate the peroneus brevis from both the superior aspect and the distal attachment on the fifth metatarsal base to understand which procedure was used, although there are many modifications for each type of reconstruction.

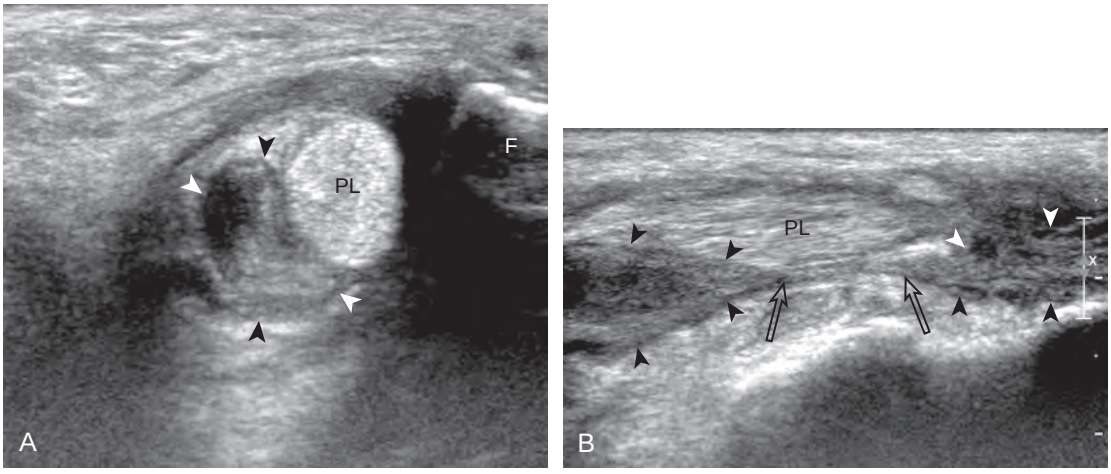

FIGURE 8-95 ■ Full-thickness complete tear: peroneal brevis. Ultrasound images **(A)** short axis and **(B)** long axis to the peroneal tendons show focal discontinuity *(open arrows)* of the peroneus brevis tendon *(arrowheads)*. F, fibula; PL, peroneus longus.

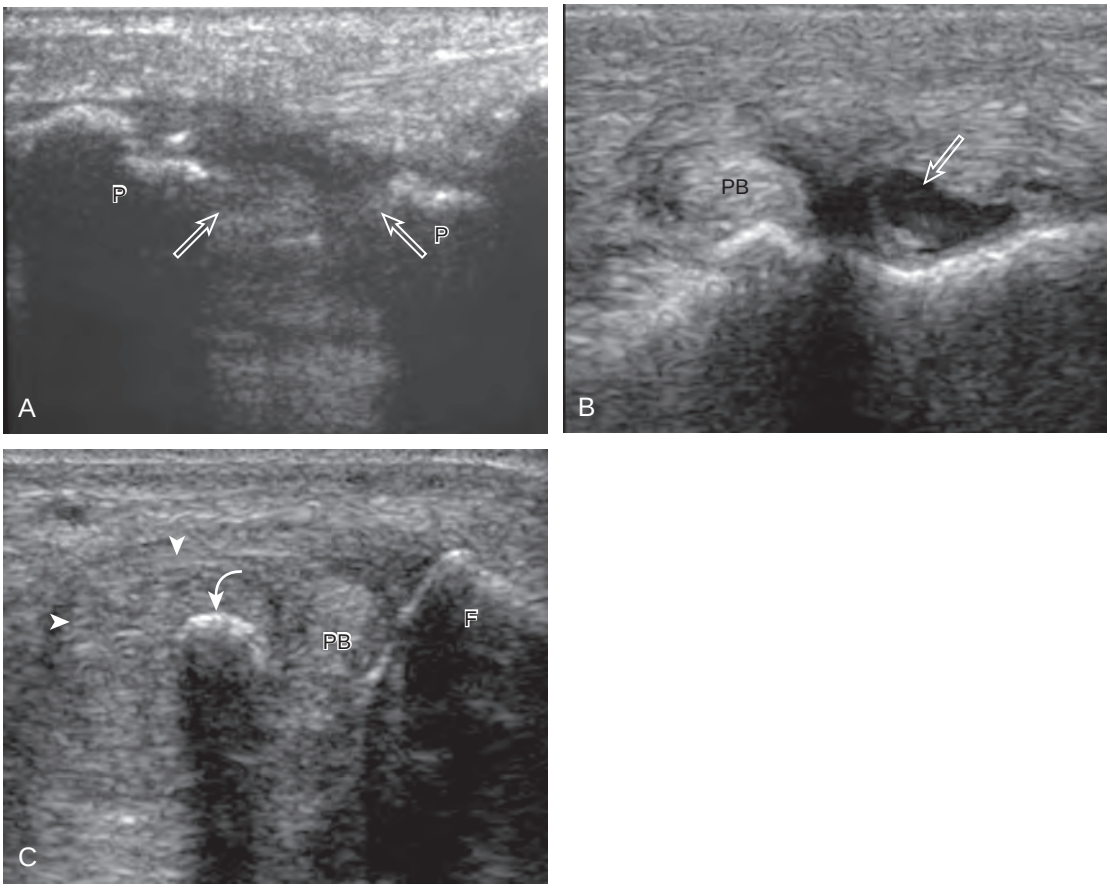

FIGURE 8-96 ■ Full-thickness tear: peroneal longus and os peroneum fracture. Ultrasound image **(A)** long axis to the distal peroneus longus shows fracture *(open arrows)* of the os peroneum (P) with distraction and full-thickness peroneus longus tear (left side of image is proximal). Ultrasound image from a different patient **(B)** short axis to the peroneal tendons over the peroneal tubercle shows absence of the peroneus longus tendon *(open arrow)*. **C,** Proximally at the level of the distal fibula (F), the retracted os peroneum fracture fragment *(curved arrow)* and peroneus longus tendon stump *(arrowheads)* are identified. PB, peroneus brevis.

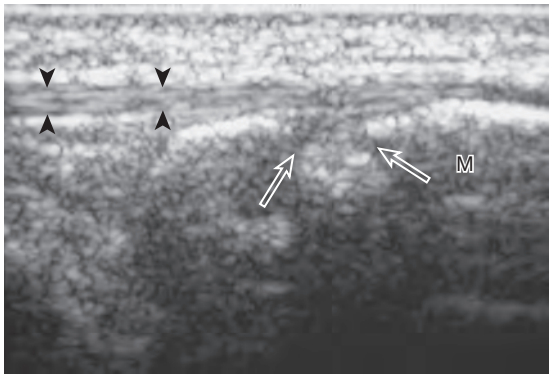

FIGURE 8-97 ■ Avulsion fracture of the fifth metatarsal base. Ultrasound image long axis to the distal peroneus brevis tendon *(arrowheads)* shows fracture *(open arrows)* at the base of the fifth metatarsal (M).

Anterior Ankle and Anterior Lower Leg

Pathology of the anterior tendons is less common than of other areas of the ankle, but similar findings of tenosynovitis (Fig. 8-99), tendinosis (Fig. 8-100), and tendon tear may occur (Fig. 8-101). As a possible variation of normal, the distal tibialis anterior tendon may have a longitudinal split near its insertion.[59] Findings that suggest a tendon tear rather than normal variation include associated symptoms, pain with transducer pressure, and associated findings such as hyperemia on color Doppler imaging. Most tibialis anterior tendon tears occur within 3.5 cm of its insertion.[59] Full-thickness tibialis anterior tendon tears may retract significantly and produce a mass-like area at the tendon stump possibly

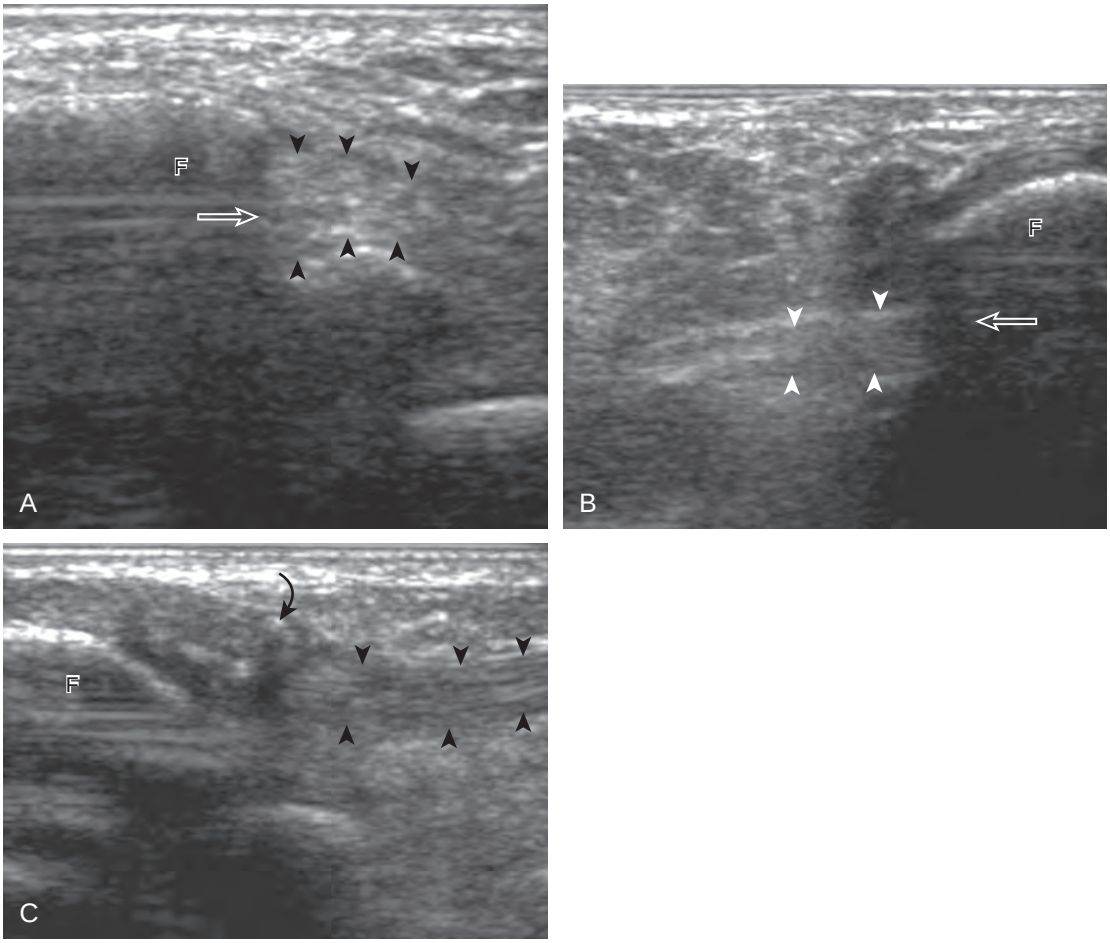

FIGURE 8-98 ■ Lateral ankle ligament reconstruction (Chrisman-Snook procedure). Ultrasound image **(A)** long axis to the peroneus brevis shows the peroneus brevis tendon *(arrowheads)*, which enters into a tunnel *(open arrow)* from the anterior aspect of the fibula (F). Ultrasound image **(B)** long axis to the peroneus brevis shows the peroneus brevis tendon *(arrowheads)*, which leaves the fibular tunnel *(open arrow)* from the posterior aspect. Ultrasound image **(C)** long axis to the peroneus brevis shows peroneus brevis tendon with suture material *(curved arrow)* reattached to the native peroneus brevis tendon *(arrowheads)*. F, fibula.

associated with an avulsion fracture fragment. Other avulsion fractures may occur, such as extensor digitorum brevis avulsion from the calcaneus (see Fig. 8-101C). Tendon abnormalities may also result from abnormal contact between a tendon and fixation hardware (Fig. 8-102) (Video 8-16).[49] An injured superior extensor retinaculum will appear hypoechoic and thickened (Fig. 8-103).[53]

Other types of anterior compartment disorders include muscle hernias, which most commonly involve the tibialis anterior, although other muscle compartments may be involved (Fig. 8-104). At ultrasound, a muscle hernia is characterized by muscle tissue that extends superficial to and beyond the enveloping fascial layer (Fig. 8-105).[60] A well-defined defect in the thin hyperechoic fascia may be seen, usually at the site of a perforating vessel. A muscle hernia may also occur at a site of intact but thinned fascia.[60] Dynamic imaging with joint movement or muscle contraction may be needed to demonstrate the muscle hernia, which may be transient and absent at rest (Videos 8-17 to 8-19).[60,61]

Posterior Ankle

Abnormalities of the Achilles tendon may involve the tendon itself or surrounding tissues. Because the Achilles tendon does not possess a true tendon sheath but rather a peritenon, abnormal hypoechoic swelling or anechoic fluid immediately adjacent to the tendon represents paratendinitis (or paratenonitis) (Figs. 8-106 and 8-107).[62]

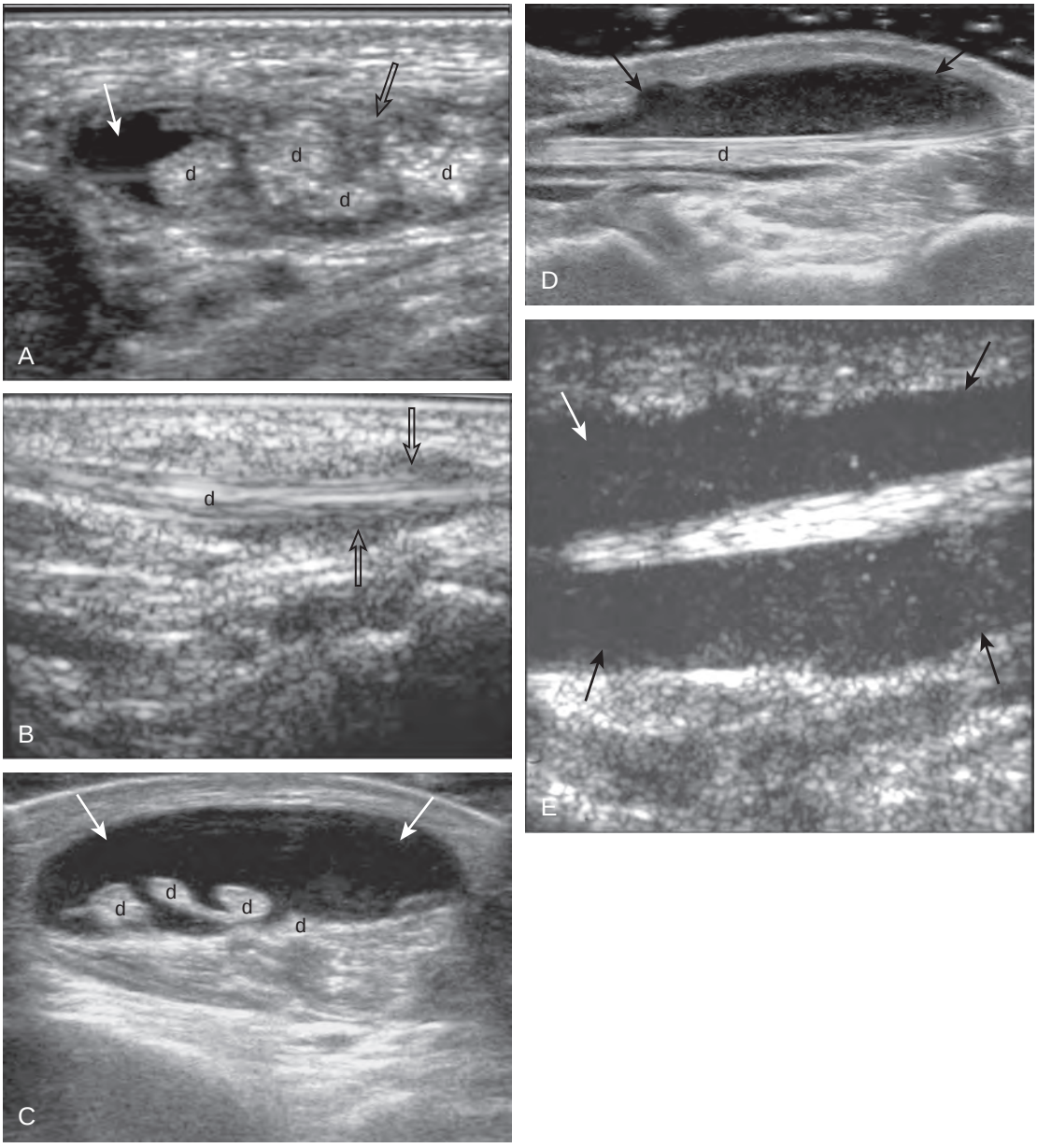

FIGURE 8-99 ■ Tenosynovitis: anterior tendons. Ultrasound images from three patients show **(A** and **B)** short and long axis images of extensor digitorum (d) with anechoic *(arrow)* and isoechoic *(open arrow)* distention of the tendon sheath, **(C** and **D)** short and long axis images of extensor digitorum (d) with hypoechoic complex fluid *(arrows)* distention of the tendon sheath, and **(E)** heterogeneous predominantly hypoechoic complex fluid distention *(arrows)* from infection.

Tendinosis, a degenerative process, appears as hypoechoic fusiform swelling of the Achilles tendon but without disruption of the tendon fibers (Figs. 8-108 to 8-111). Achilles tendon abnormalities such as tendinosis may demonstrate increased flow on color or power Doppler imaging (Video 8-20). Not present in normal Achilles tendons, increased blood flow has been shown to represent neovascularity and not inflammation, which correlates with patient symptoms.[63] Power Doppler imaging demonstrates more flow than conventional color Doppler imaging, which originates from the deep or anterior surface of the tendon.[63] It is important to float the transducer on a layer of thick gel in evaluation for flow on color or power Doppler imaging. The slightest amount of pressure from

Text continued on p. 315

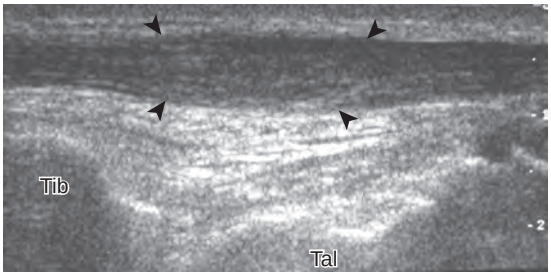

FIGURE 8-100 ■ Tendinosis: tibialis anterior. Ultrasound image long axis to the tibialis anterior tendon shows hypoechoic fusiform enlargement *(arrowheads)* without tendon fiber disruption. Tal, talus; Tib, tibia.

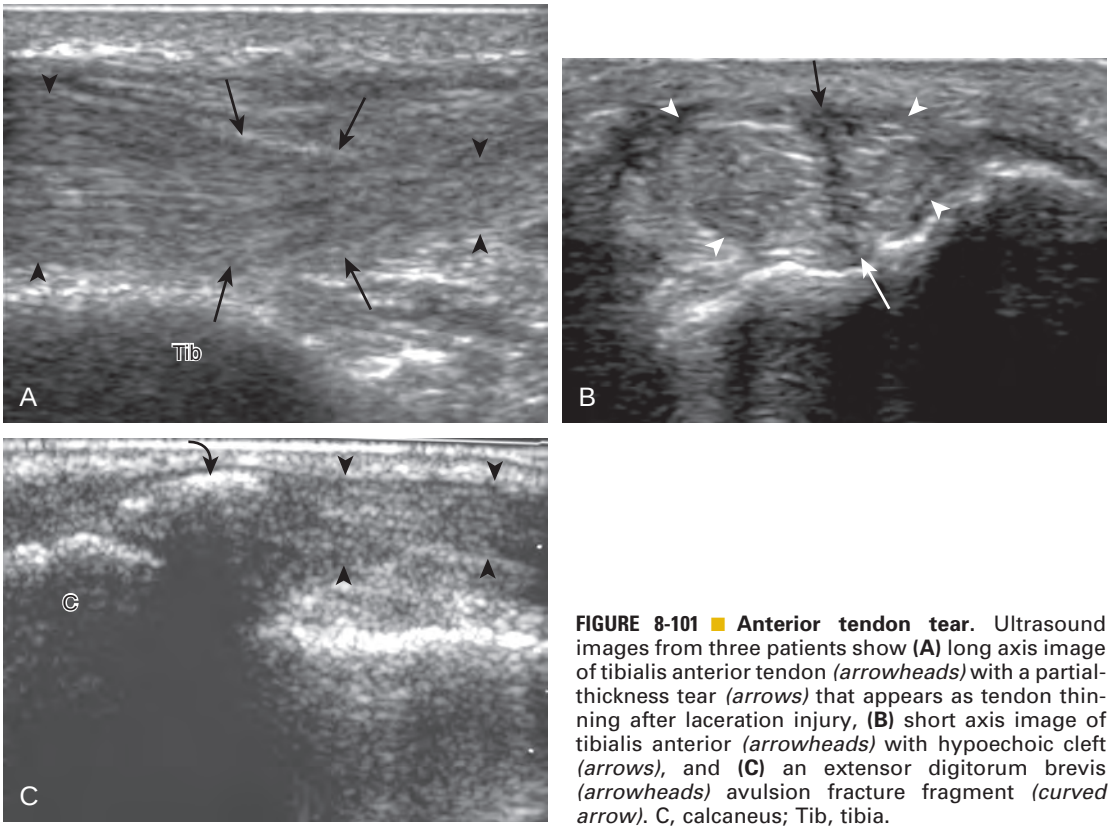

FIGURE 8-101 ■ Anterior tendon tear. Ultrasound images from three patients show **(A)** long axis image of tibialis anterior tendon *(arrowheads)* with a partial-thickness tear *(arrows)* that appears as tendon thinning after laceration injury, **(B)** short axis image of tibialis anterior *(arrowheads)* with hypoechoic cleft *(arrows)*, and **(C)** an extensor digitorum brevis *(arrowheads)* avulsion fracture fragment *(curved arrow)*. C, calcaneus; Tib, tibia.

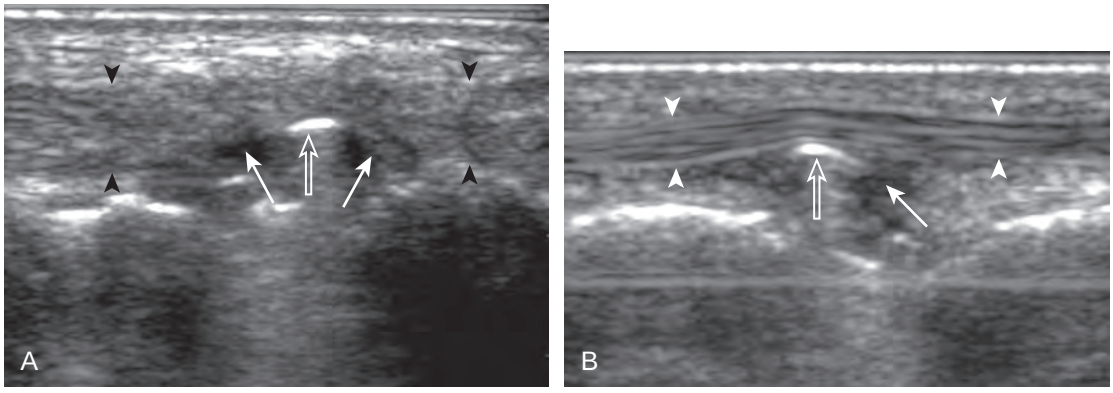

FIGURE 8-102 ■ Metal hardware and adjacent tendon abnormalities. Long axis ultrasound images from two patients show **(A)** anechoic partial tear *(arrows)* of the tibialis anterior tendon *(arrowheads)* at the site of a metal screw *(open arrow)* and **(B)** painful deviation of the extensor hallucis longus tendon *(arrowheads)* by a protruding screw *(open arrow)* with adjacent edema *(arrow)*.

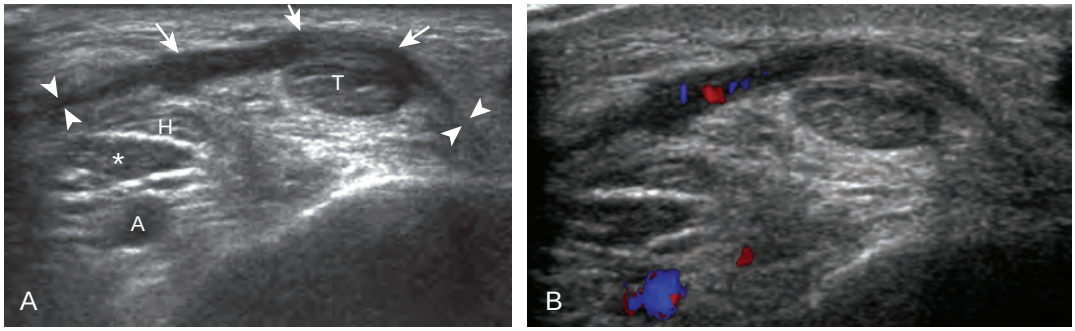

FIGURE 8-103 ■ Superior extensor retinaculum injury. Ultrasound images **(A** and **B)** short axis to tibialis anterior tendon (T) at level of distal tibia shows hypoechoic thickening *(arrows)* of the normal superior extensor retinaculum *(arrowheads)* with increased blood flow on color Doppler imaging (*asterisk*, extensor hallucis longus muscle). A, anterior tibial artery; H, extensor hallucis longus tendon.

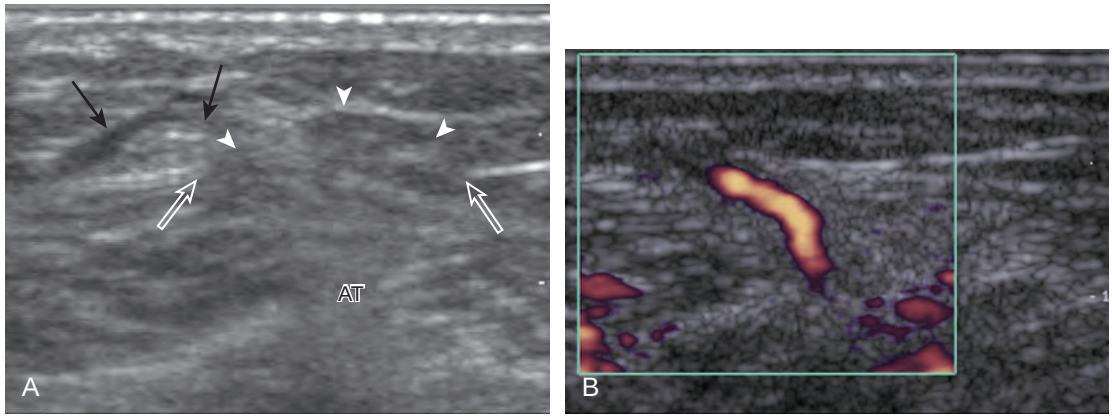

FIGURE 8-104 ■ Muscle hernia. Ultrasound images **(A** and **B)** short axis to tibialis anterior muscle (AT) show defect in the fascia *(between open arrows)* and muscle hernia *(arrowheads)* at the site of a perforating vessel *(arrows)*.

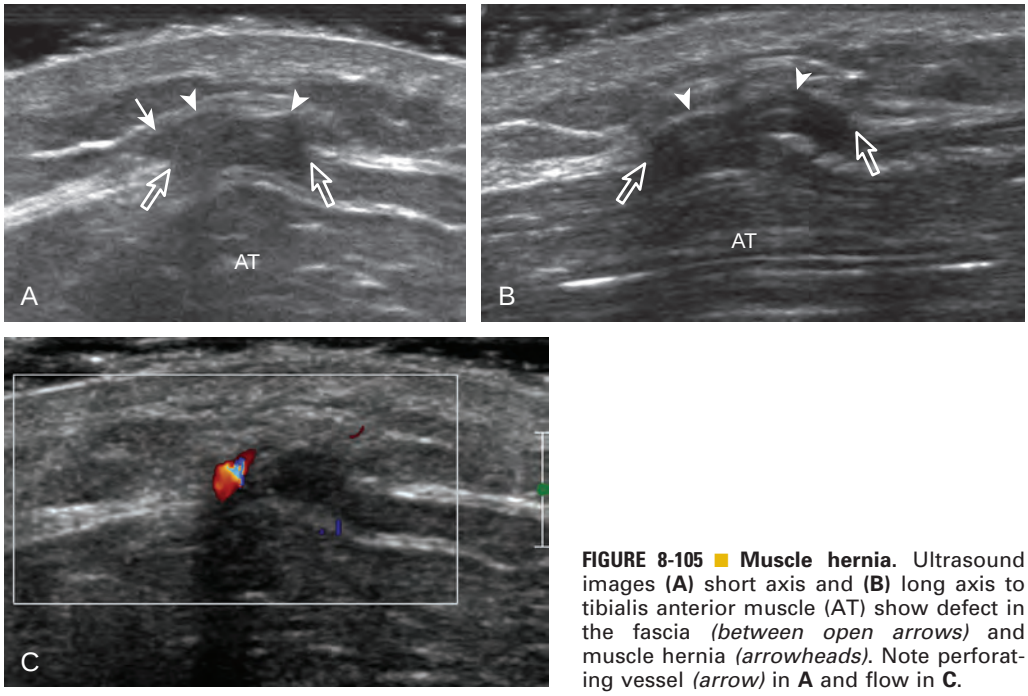

FIGURE 8-105 ■ Muscle hernia. Ultrasound images **(A)** short axis and **(B)** long axis to tibialis anterior muscle (AT) show defect in the fascia *(between open arrows)* and muscle hernia *(arrowheads)*. Note perforating vessel *(arrow)* in **A** and flow in **C**.

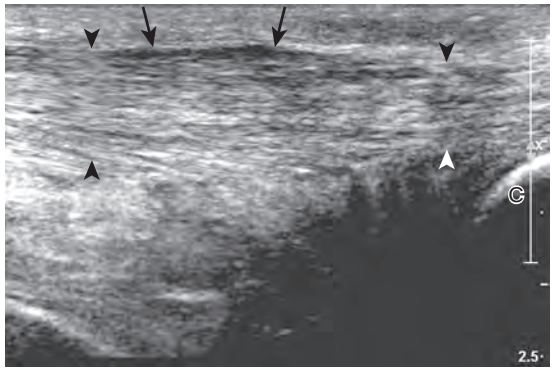

FIGURE 8-106 ■ Achilles paratendinitis. Ultrasound image long axis to the Achilles tendon *(arrowheads)* shows a superficial hypoechoic area *(arrows)* (note mild Achilles tendinosis). C, calcaneus.

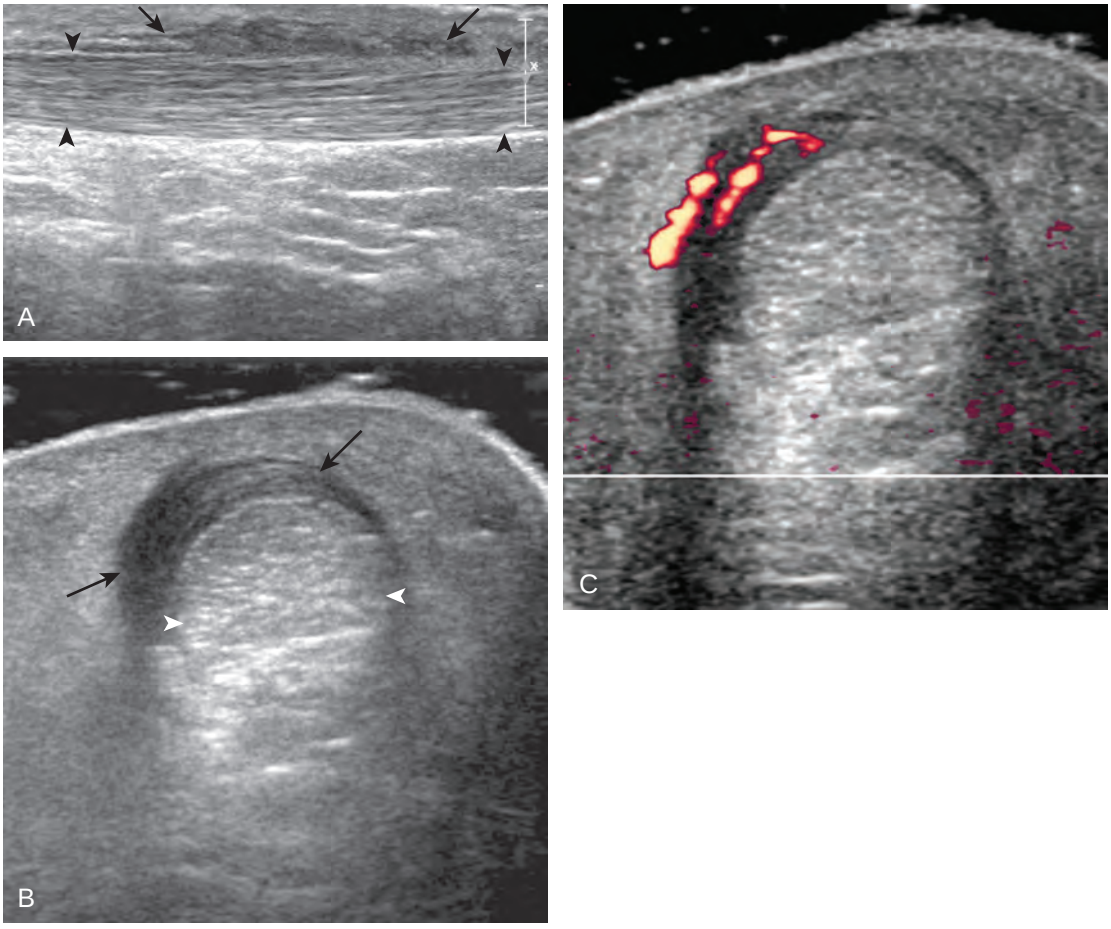

FIGURE 8-107 ■ Achilles paratendinitis. Ultrasound images **(A)** long axis and **(B** and **C)** short axis to Achilles tendon *(arrowheads)* show adjacent hypoechoic soft tissue thickening *(arrows)* with increased flow on power Doppler imaging.

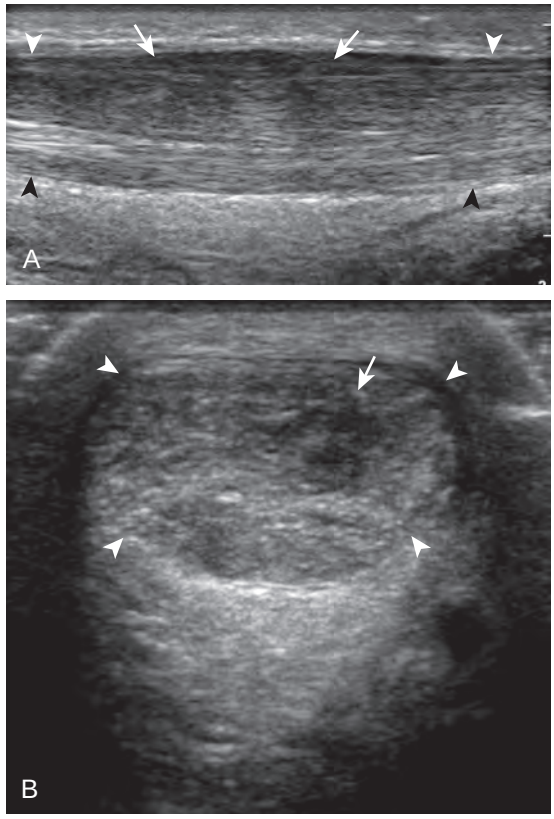

FIGURE 8-108 ■ Tendinosis: Achilles. Ultrasound images **(A)** long axis and **(B)** short axis to the Achilles tendon *(arrowheads)* show hypoechoic swelling *(arrows)* of the posterior aspect of the Achilles tendon without tendon fiber discontinuity.

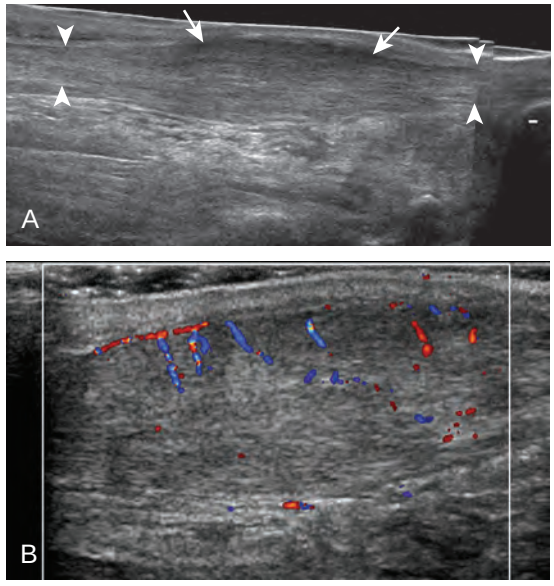

FIGURE 8-109 ■ Tendinosis: Achilles. Ultrasound **(A)** gray scale and **(B)** color Doppler images long axis to the Achilles tendon *(arrowheads)* show hypoechoic swelling *(arrows)* without tendon fiber discontinuity. Note increased blood flow representing neovascularity in **B**.

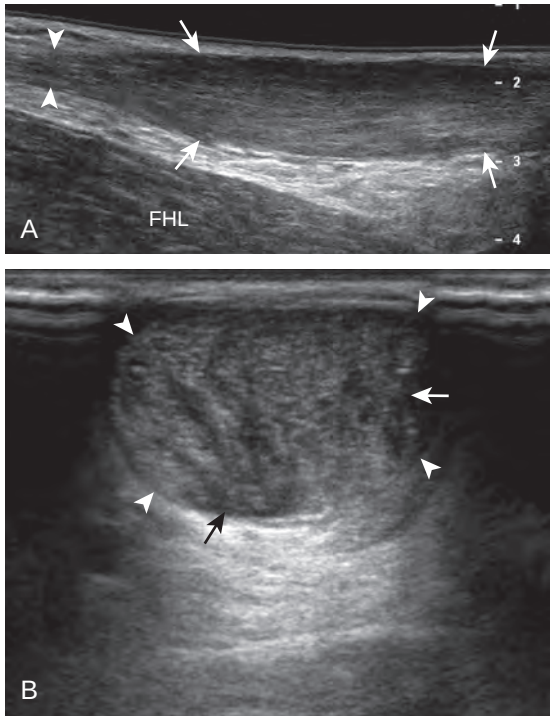

FIGURE 8-110 ■ Tendinosis: Achilles. Ultrasound images **(A)** long axis and **(B)** short axis to the Achilles tendon *(arrowheads)* show diffuse hypoechoic swelling *(arrows)* without tendon fiber discontinuity. FHL, flexor hallucis longus.

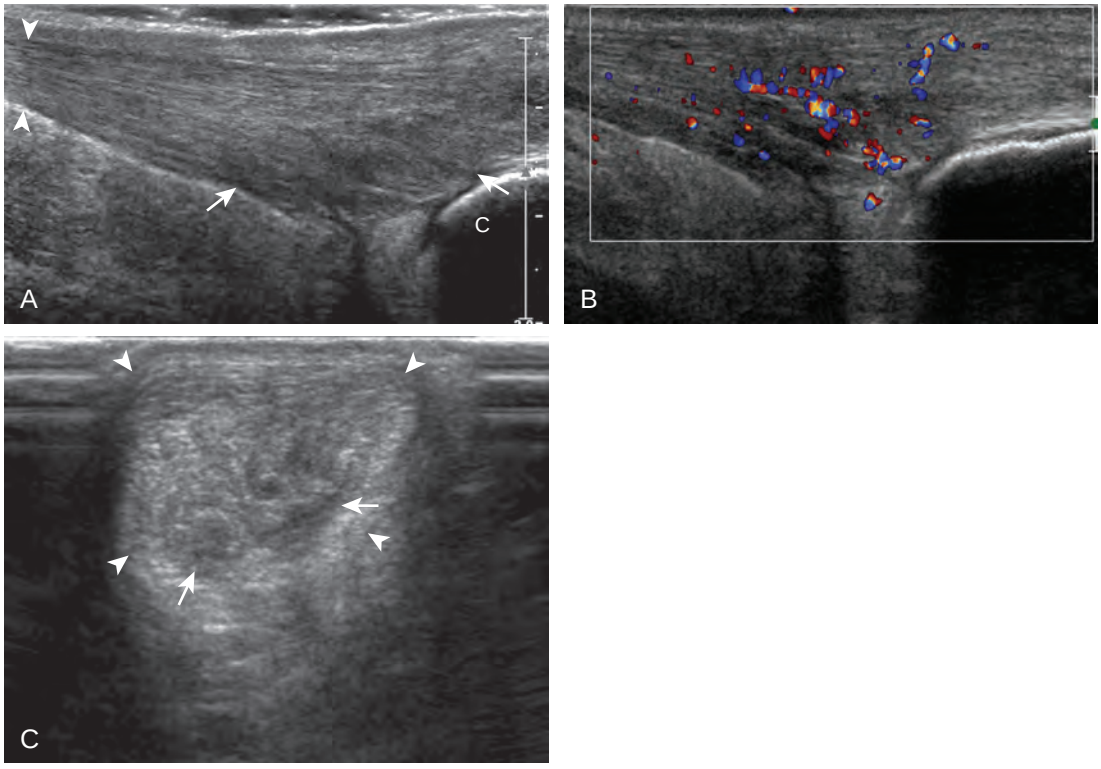

FIGURE 8-111 ■ Tendinosis: Achilles. Ultrasound **(A)** gray scale and **(B)** color Doppler images long axis and **(C)** short axis to the Achilles tendon *(arrowheads)* show hypoechoic swelling *(arrows)* and increased blood flow from neovascularity without tendon fiber discontinuity. C, calcaneus.

the transducer may obliterate visible flow in the Achilles tendon and surrounding soft tissues (Video 8-21). In addition, dorsiflexion at the foot may also obliterate visible blood flow as the Achilles tendon is stretched. When enthesophytes are identified at the distal Achilles tendon, common degenerative enthesopathy should not be confused with inflammatory enthesopathy, the latter of which will show hyperemia, adjacent tendon abnormality, possible erosions, and ill-defined enthesophyte borders at ultrasound and radiography.[64,65] The term *tendinosis* is used rather than *tendinitis* because no true inflammation is present.[66] Tendinosis may be somewhat focal within a tendon segment or may diffusely involve the tendon diameter.[66]

Partial-thickness Achilles tendon tears may initially appear as a more defined hypoechoic or anechoic area or cleft within the tendon that partially disrupts tendon fibers (Fig. 8-112); Achilles tendon enlargement greater than 1 cm and significant intrinsic tendon abnormalities indicate a partial-thickness tear.[66] Partial-thickness tears can extend to the surface of the Achilles tendon and usually are associated with tendinosis. The use of dynamic imaging by flexing the ankle is important to demonstrate tendon fiber continuity to exclude full-thickness tendon tear (Video 8-22). Achilles tendinosis and partial-thickness tears may also involve the extreme distal aspect of the Achilles tendon, often associated with cortical irregularity of the calcaneus and adjacent retrocalcaneal or retro-Achilles bursal fluid (Fig. 8-113). The combination of a distal Achilles tendon abnormality, adjacent bursal distention (retrocalcaneal and retro-Achilles), and prominence of the posterosuperior corner of the calcaneus is termed *Haglund syndrome* (see Fig. 8-60).[37]

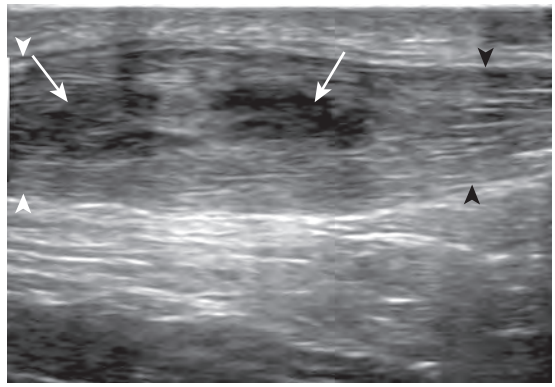

FIGURE 8-112 ■ Partial-thickness tear: Achilles. Ultrasound image long axis to Achilles tendon *(arrowheads)* shows with fusiform hypoechoic swelling and focal anechoic fiber disruption *(arrows)*.

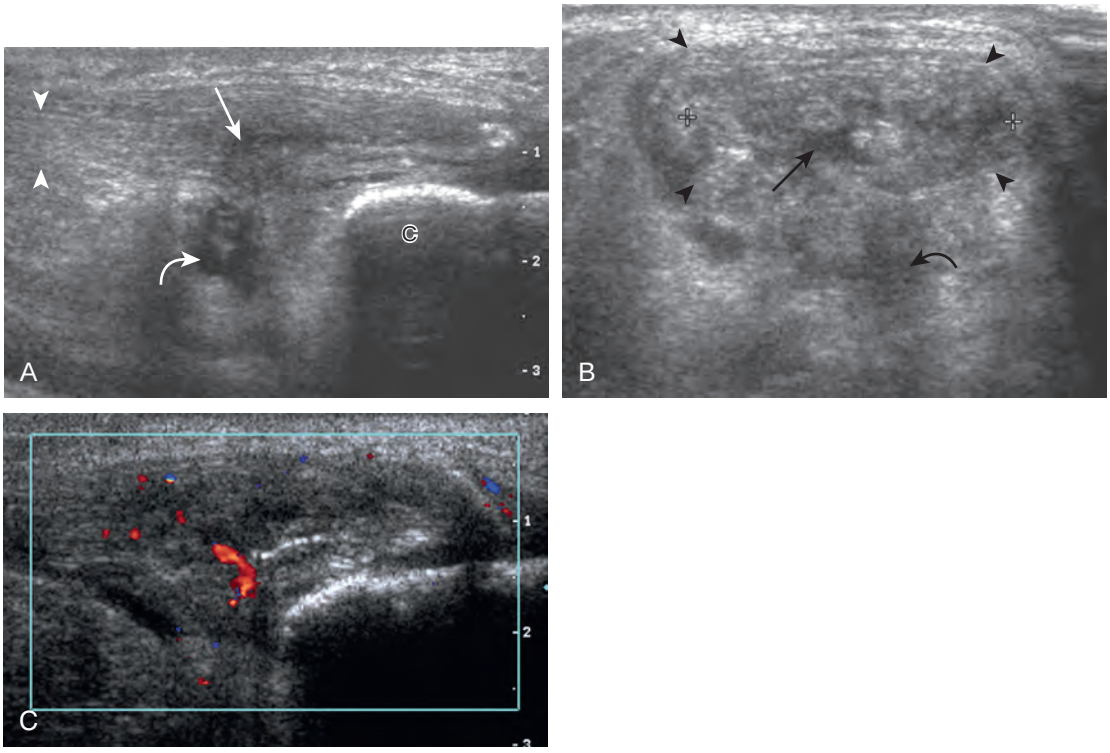

FIGURE 8-113 ■ Partial-thickness tear: Achilles. Ultrasound images **(A)** long axis and **(B)** short axis to the Achilles tendon *(arrowheads)* show diffuse fusiform hypoechoic swelling and focal tendon tear anteriorly *(arrows)* and **(C)** increased flow on color Doppler imaging (*curved arrow*, retrocalcaneal bursa). C, calcaneus.

Full-thickness tears of the Achilles tendon are characterized by complete tendon fiber disruption and tendon retraction, commonly 2 to 6 cm proximal to the calcaneal attachment (Fig. 8-114).[67] At the torn tendon ends, the Achilles tendon ends are tapered, and often there is posterior acoustic shadowing from refraction at the tendon stumps (see Fig. 8-114C).[67] It is important to increase the depth of field to appreciate the posterior acoustic shadowing, which often assists in localization of the tendon ends for accurate measurements (see Fig. 8-114D). The distal tendon stump commonly is angled anterior toward the Kager fat pad. The torn tendon gap may fill with mixed echogenicity fluid or hemorrhage, or possibly a portion of the adjacent hyperechoic fat pad.[68] One important pitfall in the setting of a full-thickness Achilles tendon tear is the presence of an intact plantaris tendon at the medial aspect of the Achilles tendon that may simulate intact Achilles tendon fibers (Fig. 8-115) (Video 8-23).[67] The plantaris tendon is often intact in the setting of a full-thickness Achilles tendon tear, which may be related to the fact that the plantaris is a stronger tendon than the Achilles.[69] With a suspected full-thickness Achilles tendon tear, it is always important to consider dynamic imaging to ensure an accurate diagnosis. With passive movement of the foot, tendon retraction at the tear becomes more obvious because one tendon stump moves without translation of movement to the other tendon stump (Fig. 8-116) (Videos 8-24 and 8-25). This becomes important in the setting of a subacute or chronic tendon tear, in which hemorrhage and scar tissue may simulate tendon fibers, and, in fact, partial healing may be present (Video 8-26). If conservative management of a full-thickness Achilles tendon is being considered, the distance of residual distraction at the tendon stumps in neutral and plantar flexion is important information that may change management decisions. After surgical repair, the intact Achilles tendon may be heterogeneous and hypoechoic with hyperechoic

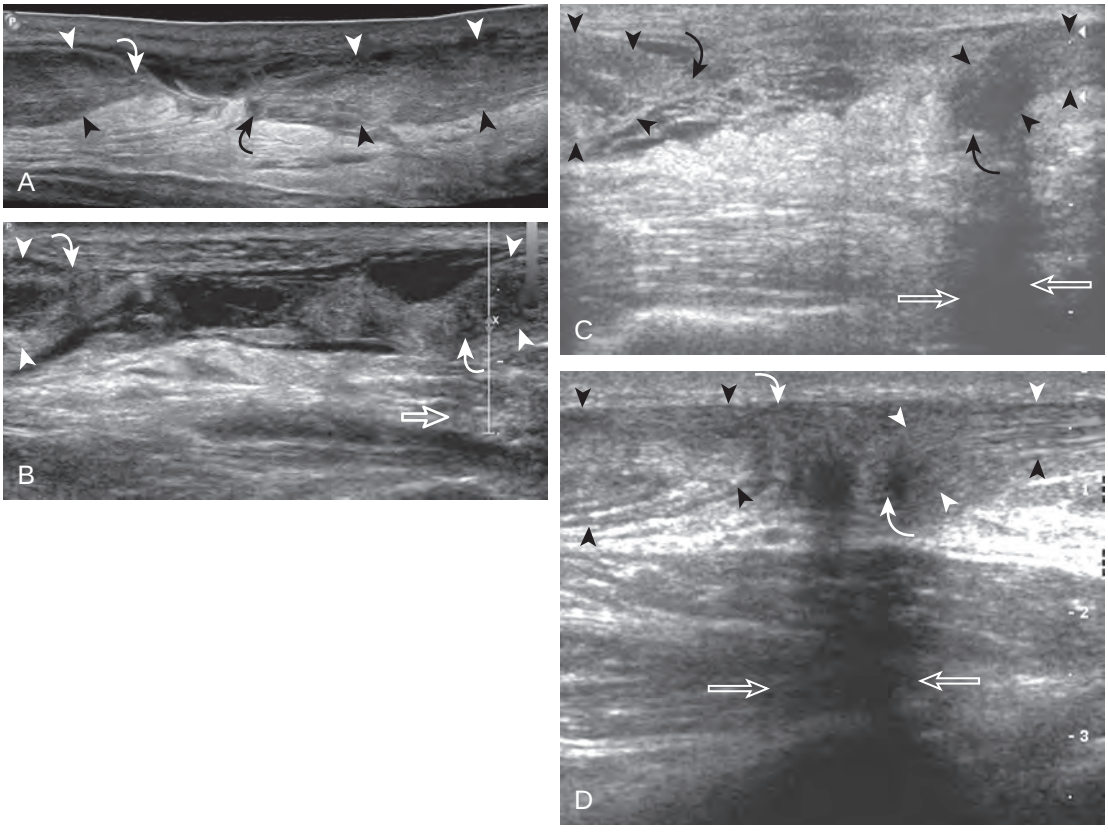

FIGURE 8-114 ■ Full-thickness tear: Achilles. Ultrasound images **(A** to **D)** long axis to the Achilles tendon *(arrowheads)* in four patients show full-thickness tear between torn tendon stumps *(curved arrows)* and interposed hemorrhage. Note posterior acoustic shadowing *(open arrows)* deep to the tendon stumps, tapered appearance of the Achilles tendon at the tear, and variable hypoechoic hemorrhage.

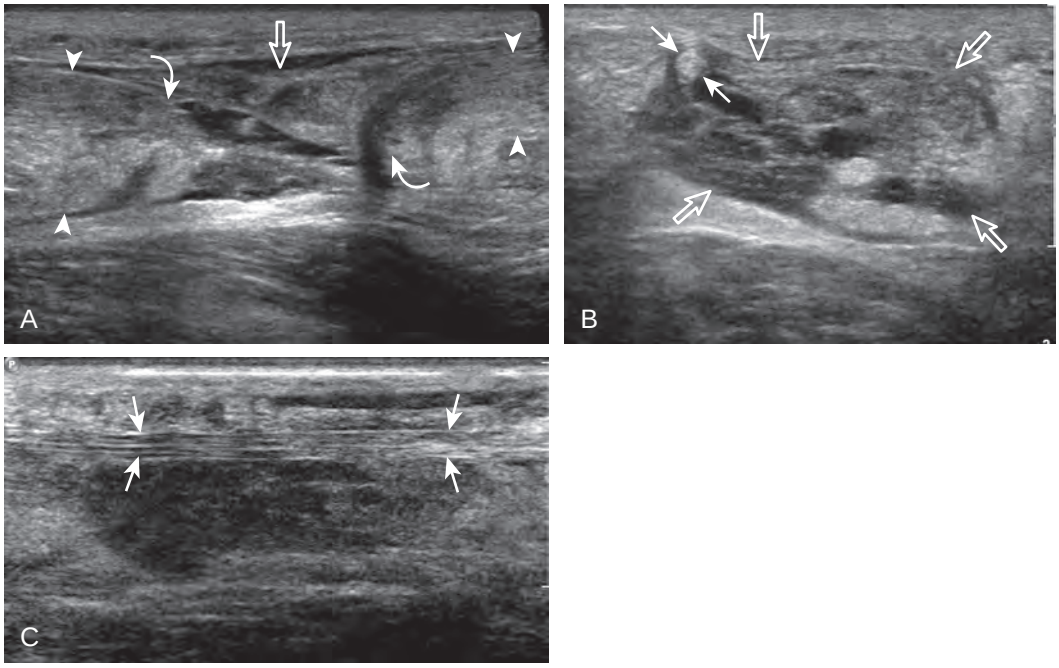

FIGURE 8-115 ■ Full-thickness tear of Achilles: intact plantaris tendon. Ultrasound images **(A)** long axis and **(B)** short axis to the Achilles tendon *(arrowheads)* shows retracted tendon stumps *(curved arrows)* at site of tear *(open arrows)*. **C,** Note intact plantaris tendon *(arrows)* in long axis located at medial aspect of tendon tear. Plantaris tendon is also shown in **(B)**.

suture material, although tendon fiber continuity should be seen (Fig. 8-117) (Video 8-27). A full-thickness recurrent tear of the Achilles tendon repair typically shows tendon retraction (Fig. 8-118). The flexor hallucis longus may also insert into the calcaneus as a treatment for Achilles tendon tear (Fig. 8-119).[70] In the diabetic patient, the distal Achilles tendon may avulse a large bone fragment from the calcaneus (Fig. 8-120, online).

Other Achilles tendon abnormalities include ossification of the Achilles tendon, associated with prior trauma, surgery, and ankle immobilization (Fig. 8-121).[71] Ultrasound can also identify xanthoma deposition in the Achilles tendon, which represents xanthoma cells, extracellular cholesterol, giant cells, and inflammatory cells, seen in heterozygous familial hypercholesterolemia.[72] Such deposits range from focal hypoechoic nodules to a heterogeneously hypoechoic swollen Achilles tendon (Fig. 8-122).[73]

Calf

Proximal to the Achilles tendon, the calf muscles and tendons may be injured. One of the most commonly injured structures is the medial head

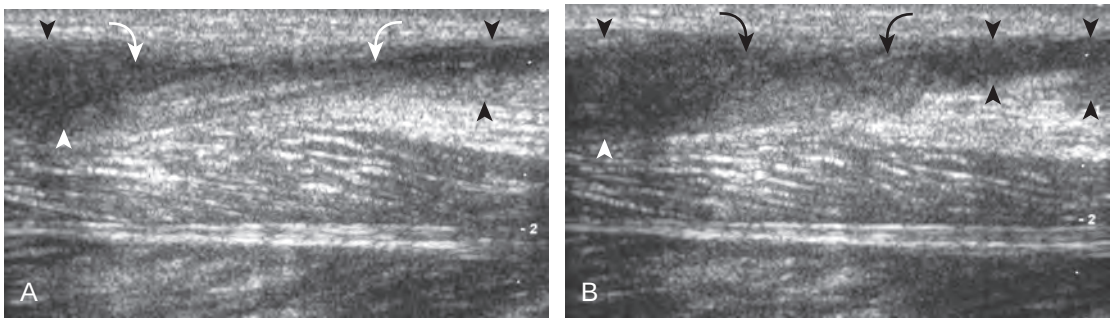

FIGURE 8-116 ■ Full-thickness tear of Achilles: dynamic imaging. Ultrasound images long axis to the Achilles tendon *(arrowheads)* with **(A)** foot in neutral position and **(B)** plantar flexion show full-thickness tear with tendon stumps *(curved arrows)* that become closer in proximity in **B** but without apposition.

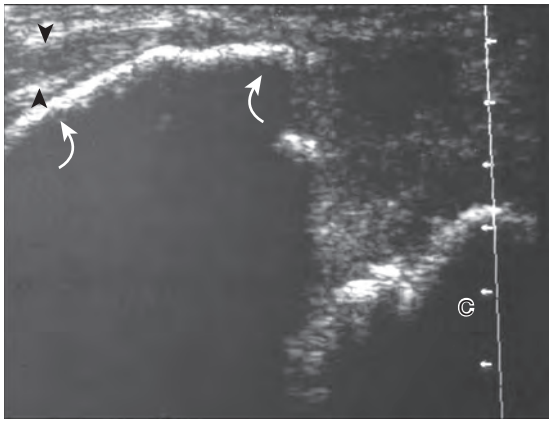

FIGURE 8-120 ■ Achilles avulsion at calcaneus. Ultrasound image long axis to the Achilles tendon *(arrowheads)* shows hyperechoic fracture fragment *(curved arrows)* proximally displaced from the calcaneus (C) (right side of image is distal).

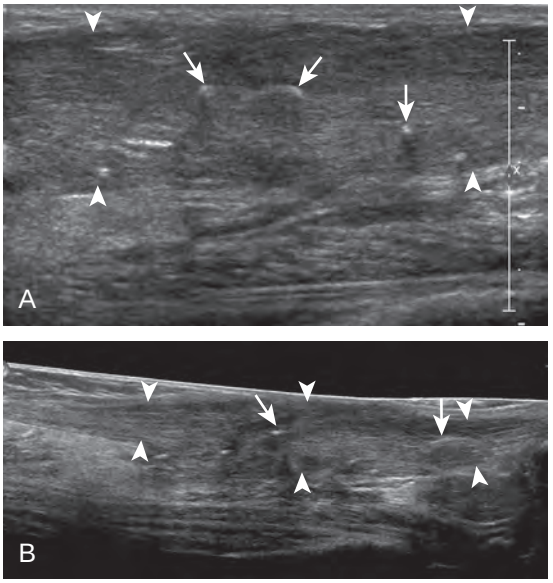

FIGURE 8-117 ■ Achilles tendon: primary repair. Ultrasound images **(A)** including extended field of view **(B)** long axis to the Achilles tendon *(arrowheads)* show hypoechoic and swollen tendon with hyperechoic suture *(arrows)* at site of repair.

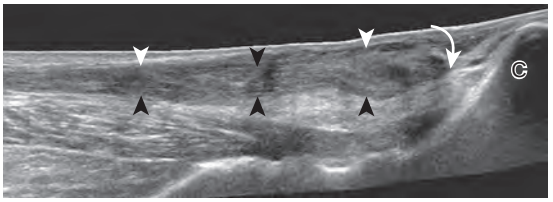

FIGURE 8-118 ■ Achilles tendon: re-tear. Ultrasound extended field of view image long axis to the Achilles tendon *(arrowheads)* shows hypoechoic and swollen tendon with distal full-thickness re-tear *(curved arrow)*. C, calcaneus.

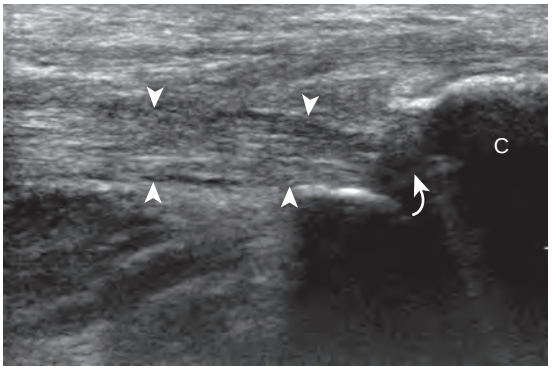

FIGURE 8-119 ■ Achilles reconstruction: flexor hallucis longus. Ultrasound image long axis to Achilles tendon at site of tear shows re-routed flexor hallucis long tendon *(arrowheads)* with calcaneal (C) insertion *(curved arrow)*.

of the gastrocnemius where it tapers distally over the soleus, also called *tennis leg* (Fig. 8-123).[7] At this site, the tendon fibers are disrupted at the aponeurosis with anechoic or hypoechoic fluid or hemorrhage with variable degrees of tendon retraction (Fig. 8-124).[74] The patient can usually indicate the site of injury based on the location of symptoms. A remote injury at this site will show increased echogenicity and distortion of the normal fiber architecture (Fig. 8-125).[75]

Another calf abnormality is a plantaris tendon injury.[76,77] A partial-thickness tear appears as a hypoechoic and irregular but intact tendon (Fig. 8-126). A complete tear will appear as a tubular anechoic or mixed-echogenicity fluid collection between the muscle bellies of the medial gastrocnemius and soleus with lack of visualization of the plantaris tendon or tendon discontinuity

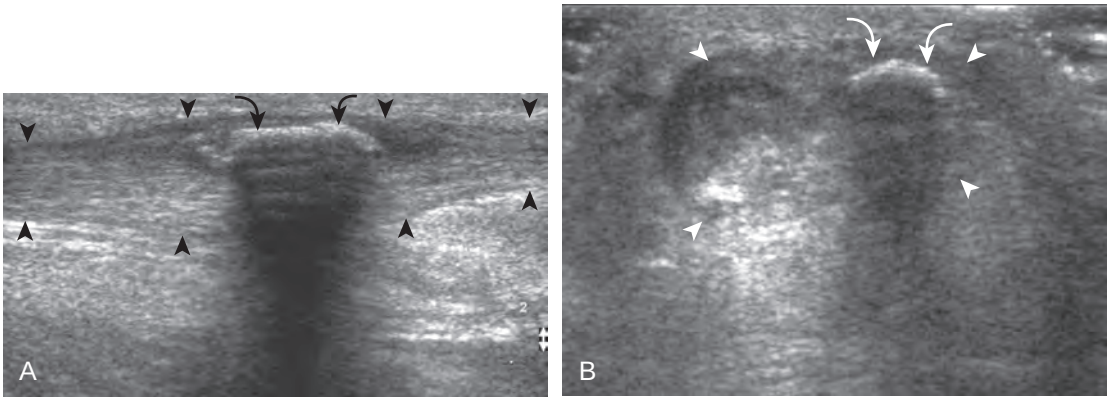

FIGURE 8-121 ■ Achilles tendon ossification. Ultrasound images **(A)** long axis and **(B)** short axis to the Achilles tendon *(arrowheads)* show hyperechoic and shadowing ossification *(curved arrows)* within the thickened Achilles tendon.

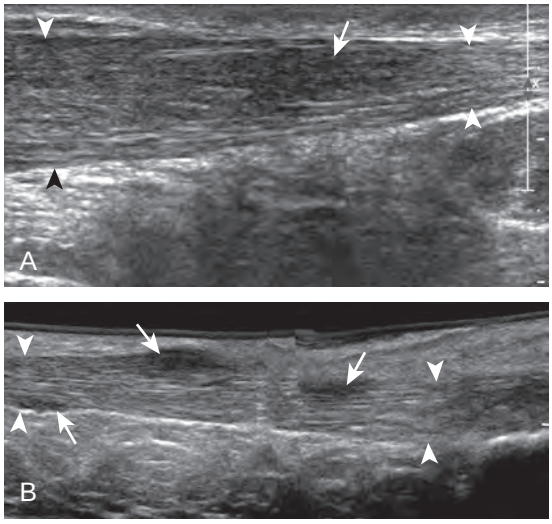

FIGURE 8-122 ■ Xanthoma deposition: Achilles tendon. Ultrasound images **(A)** long axis and **(B)** short axis to the Achilles tendon *(arrowheads)* show focal hypoechoic xanthoma deposits *(arrows)*.

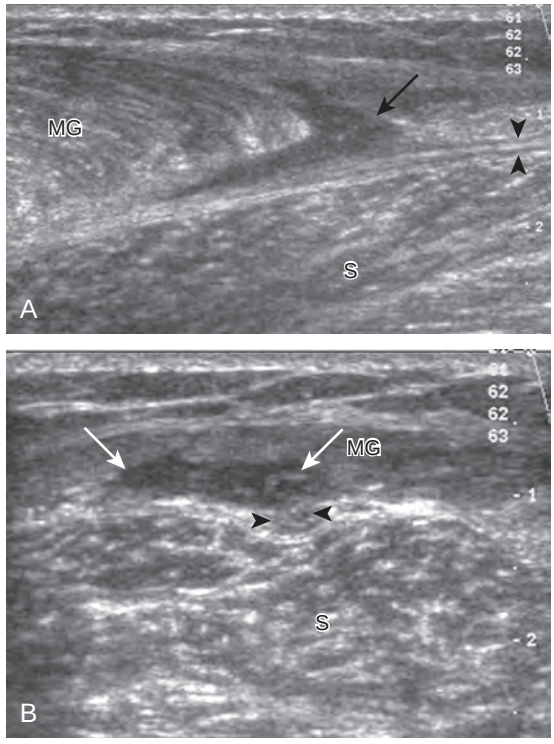

FIGURE 8-123 ■ Medial head of gastrocnemius tear. Ultrasound images **(A)** long axis and **(B)** short axis to the distal medial head of gastrocnemius (MG) show a hypoechoic tear *(arrows)* at the aponeurosis with mild retraction (*arrowheads*, plantaris). S, soleus.

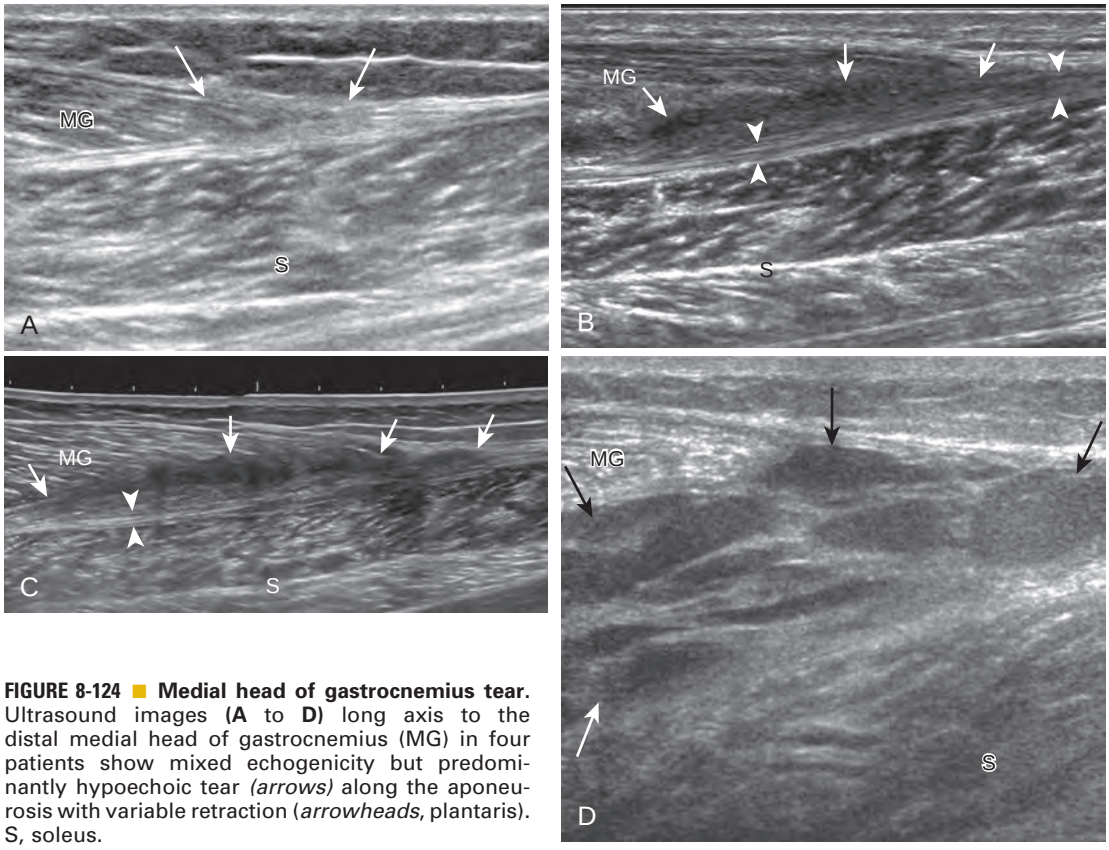

FIGURE 8-124 ■ Medial head of gastrocnemius tear. Ultrasound images **(A** to **D)** long axis to the distal medial head of gastrocnemius (MG) in four patients show mixed echogenicity but predominantly hypoechoic tear *(arrows)* along the aponeurosis with variable retraction (*arrowheads*, plantaris). S, soleus.

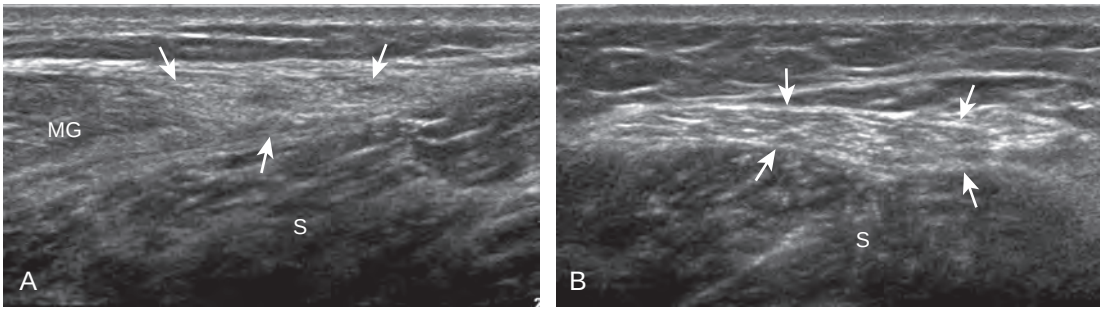

FIGURE 8-125 ■ Medial head of gastrocnemius tear: remote. Ultrasound images **(A)** long axis and **(B)** short axis to the distal medial head of gastrocnemius (MG) show a hyperechoic scar *(arrows)* at site of prior tear. S, soleus.

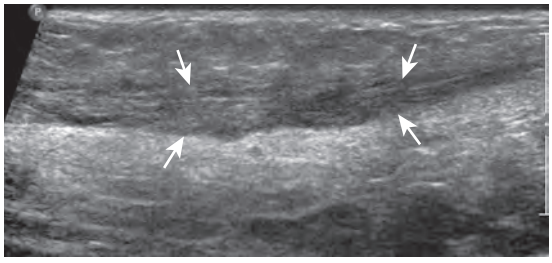

FIGURE 8-126 ■ Plantaris tear. Ultrasound image long axis and medial to Achilles tendon shows heterogeneous hypoechoic thickening of the plantaris tendon *(arrows)*.

(Fig. 8-127).[76,78] These findings are commonly located more proximally in the calf compared with a medial head of the gastrocnemius tear. Distal medial head of the gastrocnemius and plantaris tears may occur together.

Injuries to the soleus and lateral gastrocnemius muscles may occur less commonly, often the result of a direct injury (Fig. 8-128). Although a hematoma may occur in this setting or in patients predisposed to bleeding, the finding of a hematoma, especially if spontaneous, should raise concern for underlying primary malignancy or

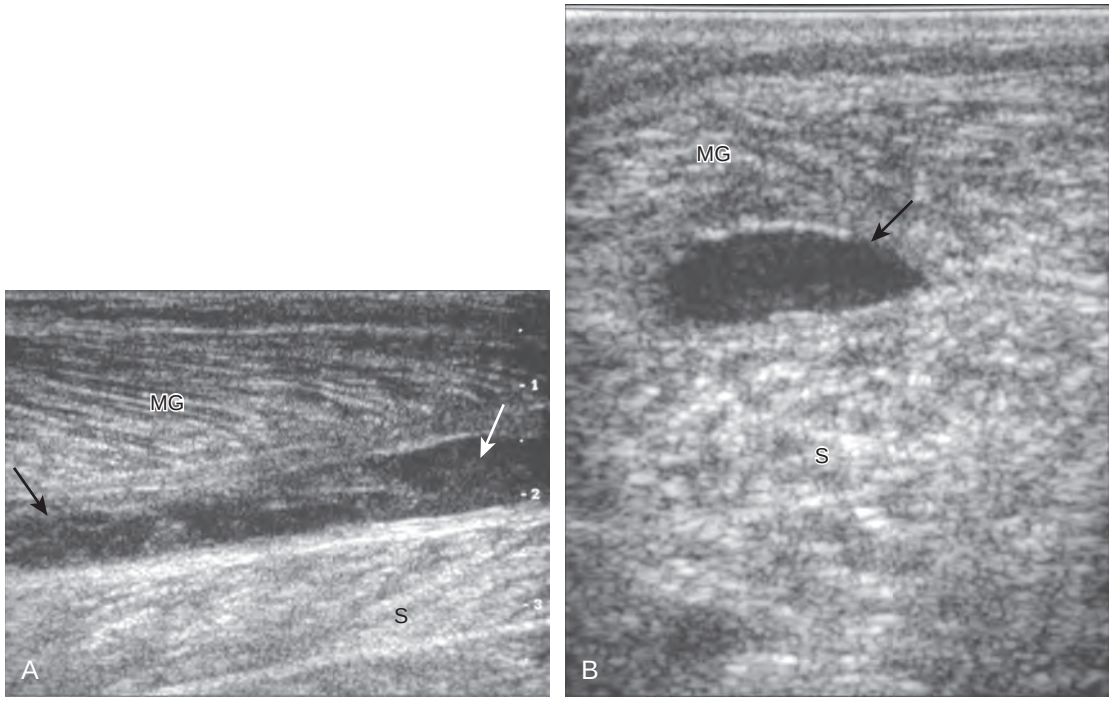

FIGURE 8-127 ■ Plantaris tear. Ultrasound images **(A)** long and **(B)** short axis to the medial head of gastrocnemius (MG) show heterogeneous hypoechoic hemorrhage *(arrows)* in the expected location of the plantaris tendon. S, soleus. (From Jamadar DA, Jacobson JA, Theisen SE, et al: Sonography of the painful calf: differential considerations. *AJR Am J Roentgenol* 179:709-716, 2002.)

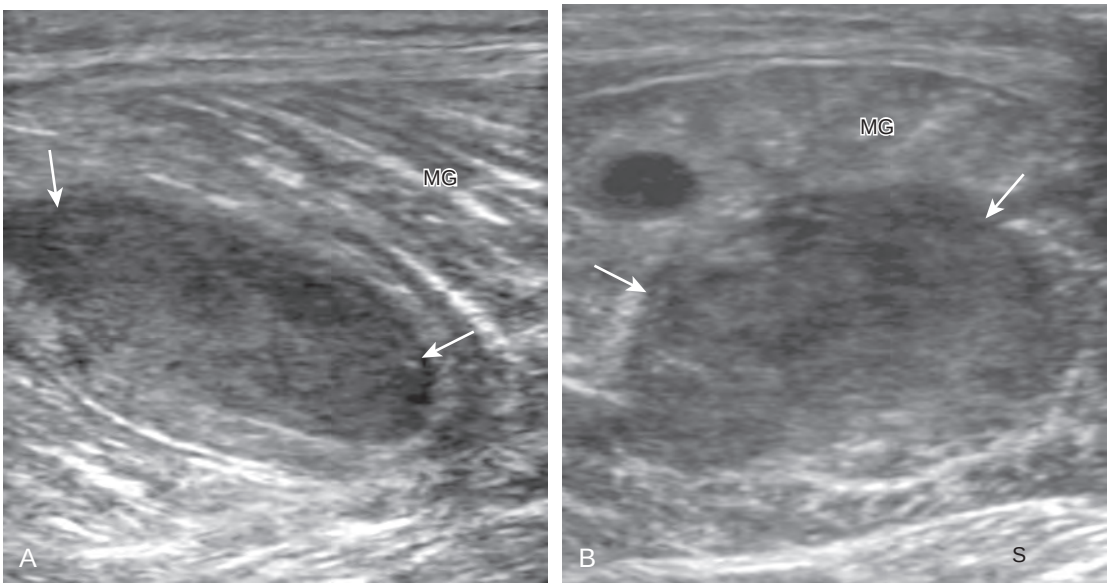

FIGURE 8-128 ■ Hematoma: medial head of gastrocnemius. Ultrasound images **(A)** long axis and **(B)** short axis to the medial head of the gastrocnemius (MG) show heterogeneous hypoechoic to isoechoic hemorrhage *(arrows)*. S, soleus.

metastasis as a cause for the hemorrhage (Fig. 8-129). As a normal variation, an accessory soleus muscle can be identified adjacent to the Achilles tendon in the Kager fat pad, which inserts either on the Achilles or onto the calcaneus (Fig. 8-130). Although this may present clinically as a mass, its normal muscle echotexture at sonography and characteristic location are diagnostic for accessory soleus muscle.[79] Injury to an accessory soleus may also occur (Fig. 8-131). The calf is a site for cosmetic surgery, where silicone implant is placed superficial to the gastrocnemius muscle for calf augmentation (Fig. 8-132).

Plantar Foot

Abnormalities of the plantar aponeurosis may take several forms.[80] A common abnormality represents hypoechoic thickening (>4 mm) of the proximal plantar fascia at the calcaneal origin, best measured in long axis (Fig. 8-133).[18,81] Although termed *plantar fasciitis*, findings may relate to repetitive microtrauma, repair of microtears, degeneration, or edema.[18] An acute injury of the plantar fascia may cause hypoechoic thickening if partially torn (Fig. 8-134) or complete disruption with heterogeneous hemorrhage if a full-thickness tear.

Another abnormality that involves the plantar fascia at the central and medial aspect of the foot arch is plantar fibromatosis.[82] This condition represents fibroblastic proliferation, commonly at

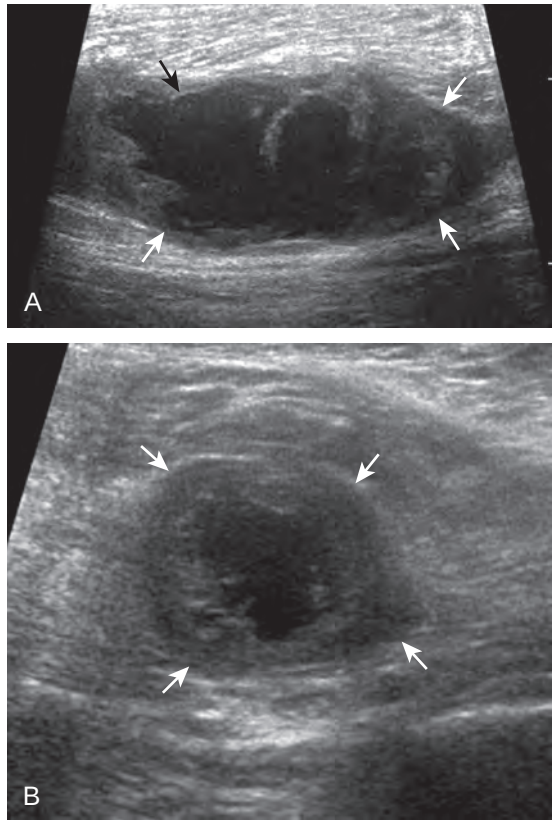

FIGURE 8-129 ■ Metastasis. Ultrasound images **(A)** long axis and **(B)** short axis to gastrocnemius show heterogeneous but predominantly hypoechoic intra-muscular metastasis *(arrows)*.

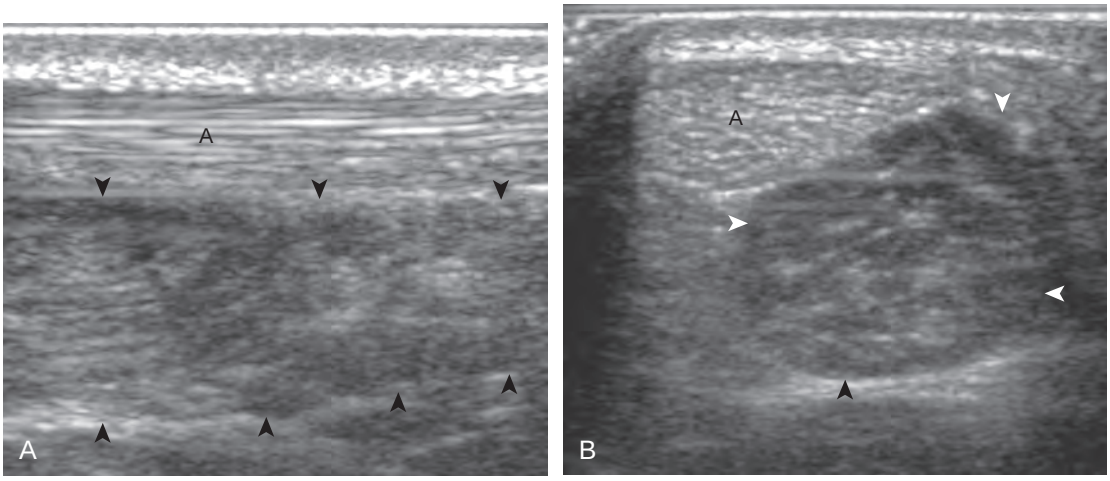

FIGURE 8-130 ■ Accessory soleus muscle. Ultrasound images **(A)** long axis and **(B)** short axis to the distal Achilles tendon (A) show accessory soleus muscle *(arrowheads)*.

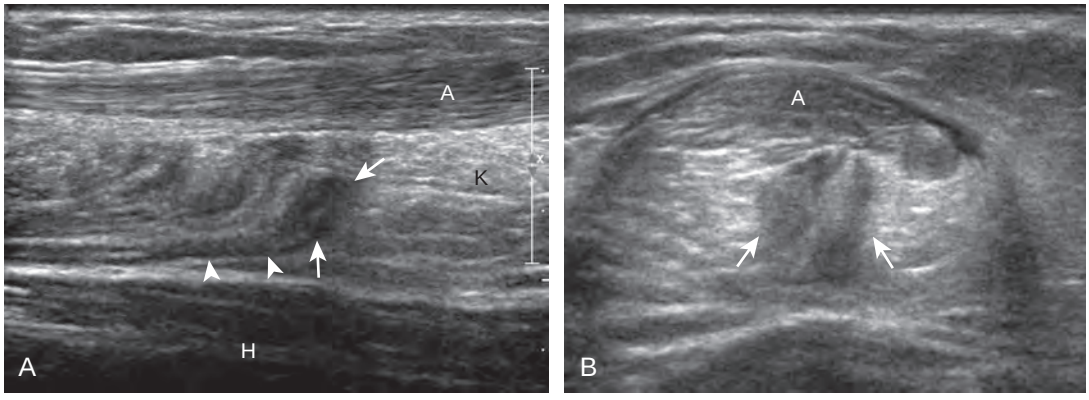

FIGURE 8-131 ■ Injury: accessory soleus muscle. Ultrasound **(A)** long axis and **(B)** short axis to the accessory soleus muscle *(arrowheads)* shows abnormal hypoechogenicity *(arrows)*. A, Achilles tendon; H, flexor hallucis longus muscle; K, Kager fat pad.

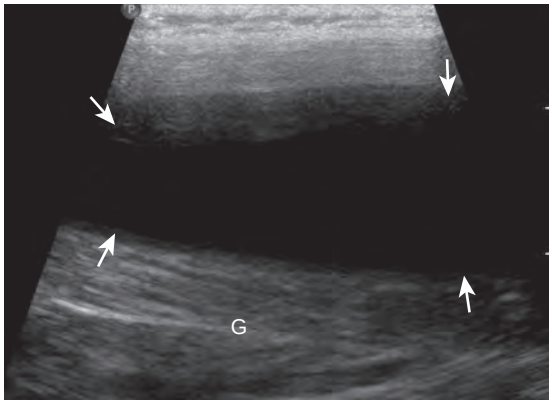

FIGURE 8-132 ■ Silicone calf implant. Ultrasound image long axis to gastrocnemius muscle shows anechoic silicone calf implant *(arrows)* superficial to gastrocnemius muscle (G).

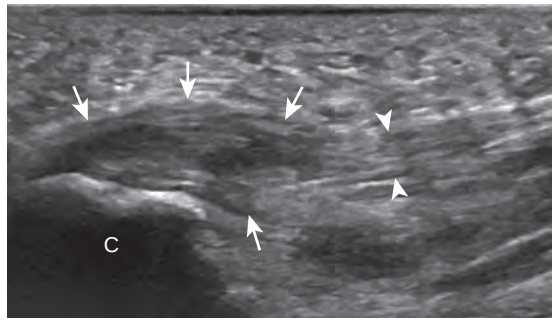

FIGURE 8-133 ■ Plantar fasciitis. Ultrasound image long axis to the proximal plantar aponeurosis *(arrowheads)* shows hypoechoic thickening *(arrows)*. C, calcaneus.

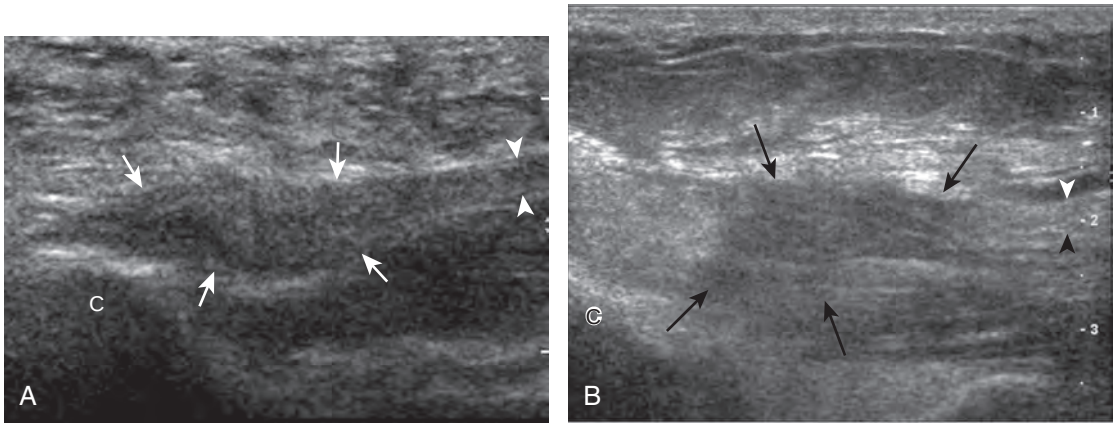

FIGURE 8-134 ■ Plantar aponeurosis injury. Ultrasound images **(A** and **B)** long axis to the plantar aponeurosis *(arrowheads)* in two patients show abnormal hypoechoic thickening *(arrows)*. C, calcaneus.

multiple sites in the plantar fascia and bilateral. At ultrasound, plantar fibromatosis appears as hypoechoic or isoechoic fusiform nodules or masses that cause thickening of the plantar fascia and may extend in a dorsal or plantar direction from the plantar fascia (Fig. 8-135) (Video 8-28).[83,84] These nodules may show significant vascularity and increased through-transmission.[82] Because the appearance of plantar fibromatosis is not specific for one diagnosis at ultrasound, the location of the abnormality and its multiplicity or bilaterality (if present) suggest the diagnosis of plantar fibromatosis.

LIGAMENT ABNORMALITIES

The lateral ankle is a common site for ligament injury. At ultrasound, partial ligament tears are characterized by hypoechoic thickening of the involved ligament, but some continuous ligament fibers are still seen.[85] An acute full-thickness ligament tear is characterized by discontinuity or nonvisualization of the ligament and replacement with hypoechoic or heterogeneous tissue that represents the torn ligament and hemorrhage.[85] Osseous avulsions appear as hyperechoic and shadowing bone fragments attached to the involved ligament. Depending on the severity of the ligament tear, remote evaluation of the ligament may show nonvisualization or a thickened ligament. Bone fragments may persist, but lack of pain with transducer pressure is a helpful indicator that the injury was remote.

Of the lateral ankle ligaments, the anterior talofibular ligament is most commonly torn, isolated or in combination with calcaneofibular ligament tear (in up to 70%).[85] Isolated tears of the calcaneofibular ligament are not common, whereas posterior talofibular ligament tears are rare.[85] Ultrasound has been shown to be effective in evaluation for anterior talofibular ligament tears (Fig. 8-136).[86] Dynamic imaging that elicits an anterior drawer sign is helpful in equivocal cases.[87] This can be accomplished with the patient lying prone, placing the transducer long axis to the anterior talofibular ligament, and then manually applying anterior directed stress over the heel and observing asymmetrical anterior translation of the talus relative to the fibula. A calcaneofibular ligament tear may appear as abnormal hypoechoic swelling deep to the peroneal tendons at the calcaneus (Fig. 8-137). Lateral ankle ligament reconstruction may involve a direct ligament repair (Fig. 8-138) or the peroneus brevis tendon (see Fig. 8-98).[58]

Another important lateral ankle ligament is the anterior inferior tibiofibular ligament. Injury to this ligament resembles other ligament injuries (Fig. 8-139).[85] Dynamic imaging with the foot in dorsiflexion and eversion will often show widening between the distal tibia and fibula at the site of the ligament tear.[88] In the setting of an anterior inferior tibiofibular ligament tear, it is important to consider a possible associated tear of the ankle syndesmosis and interosseous membrane between the tibia and fibula (Fig. 8-140).[17] Also termed a *high ankle sprain*, this injury is associated with prolonged morbidity if it is not accurately diagnosed and treated. The superiorly transmitted force of a high ankle sprain not only may propagate through the interosseous membrane but also may exit as a high fibular fracture, which is termed a *Maisonneuve fracture* (see Fig. 8-140B). The fibular fracture appears as a cortical step-off at ultrasound. This type of injury may also be associated with an isolated posterior malleolus fracture of the tibia.

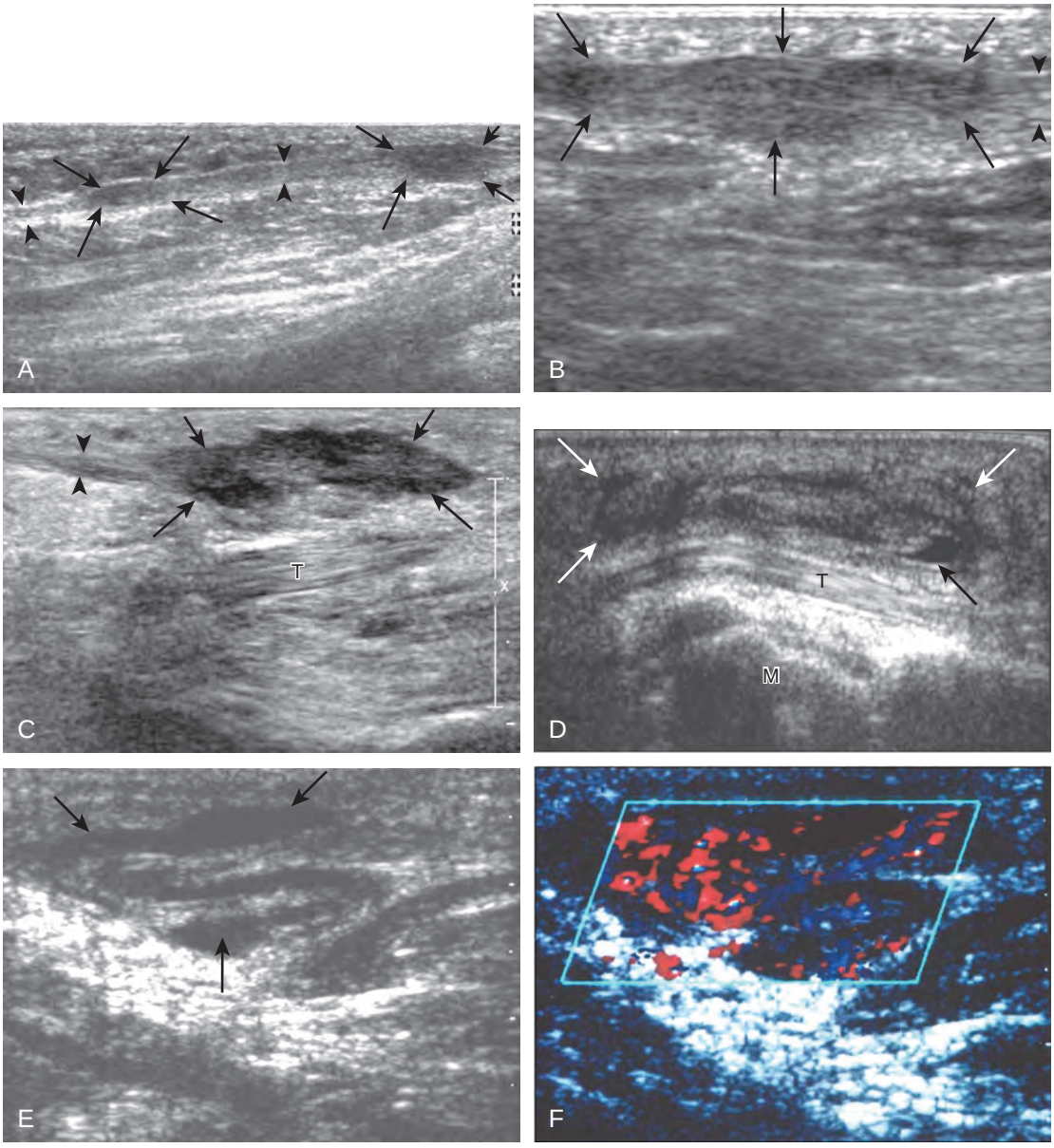

FIGURE 8-135 ■ **Plantar fibromatosis.** Ultrasound images **(A** to **F)** from five patients show hypoechoic nodules and masses *(arrows)* of plantar aponeurosis *(arrowheads)*. Note vascular channels and increased blood flow on color Doppler imaging in **E** and **F**. M, first metatarsal head; T, flexor tendons. (**D,** From Pham H, Fessell DP, Femino JE, et al: Sonography and MR imaging of selected benign masses in the ankle and foot. *AJR Am J Roentgenol* 180:99-107, 2003.)

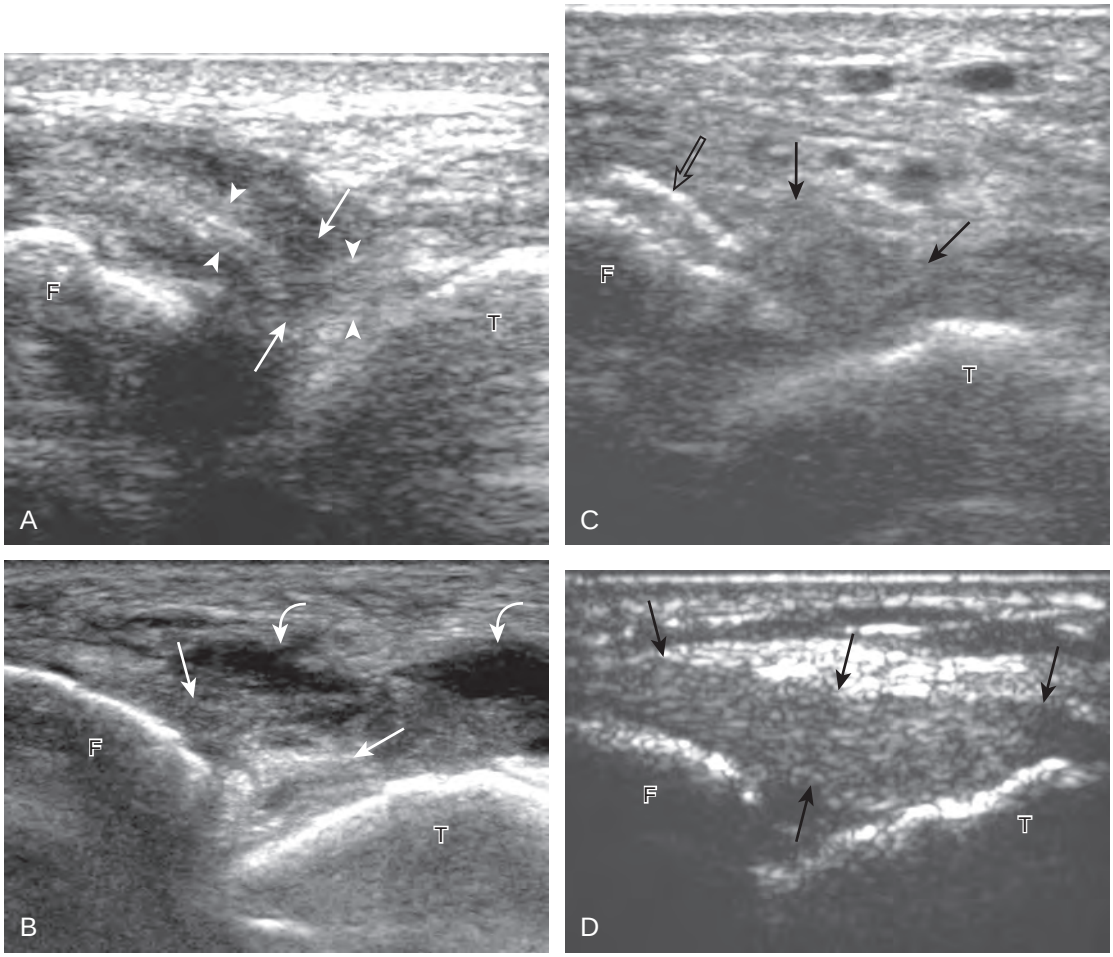

FIGURE 8-136 ■ Anterior talofibular ligament tear. Ultrasound images long axis to the anterior talofibular ligament from three patients after acute injury show **(A)** hypoechoic discontinuity *(arrows)* of the anterior talofibular ligament *(arrowheads)*, **(B)** heterogeneous mixed-echogenicity nonvisualization *(arrows)* of the anterior talofibular ligament with adjacent hemorrhage *(curved arrows)*, and **(C)** hypoechoic discontinuity *(arrows)* with a hyperechoic avulsion fracture fragment *(open arrow)*. Long axis ultrasound image in a fourth patient shows **(D)** hypoechoic thickening without ligament discontinuity *(arrows)* that represents remote injury. F, fibula; T, talus.

Deltoid ligament tears are more difficult to diagnose at ultrasound, largely because this structure represents the confluence of several ligaments, unlike the single defined ligaments laterally.[8] Although each of the individual components of the deltoid ligament can be evaluated in the normal ankle, deltoid ligament injuries typically produce hypoechoic swelling that involves several components with possible ligament disruption. At ultrasound, there is diffuse hypoechoic swelling or discontinuity of the deltoid ligament with possible hyperechoic avulsion fracture fragments (Fig. 8-141).[85,89] Pain with transducer pressure directly over the deltoid ligament is further evidence to support acute injury. The spring ligament may also be injured, which can appear as hypoechoic thickening of the superomedial calcaneonavicular ligament, often associated with adjacent tibialis posterior tendon abnormality (Fig. 8-142).[13]

Other ligament injuries around the foot and ankle are often manifested by bone avulsion fragments or malalignment of the osseous structures. Although these smaller and less commonly injured ligaments are not routinely evaluated with ultrasound, a patient may direct examination to an area of ligament injury based on symptoms. Examples include avulsion at the calcaneocuboid ligament, the talonavicular ligament, and bifurcate ligament attachment on the anterior process

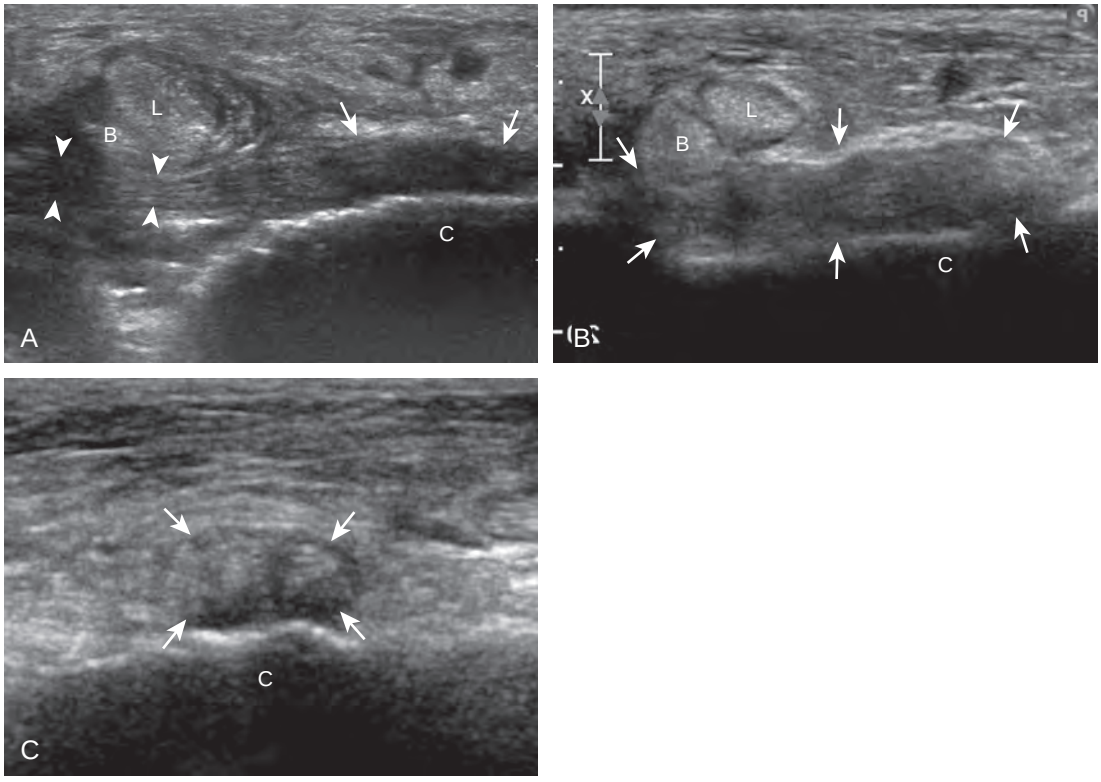

FIGURE 8-137 ■ Calcaneofibular ligament tear. Ultrasound image **(A)** long axis to the calcaneofibular ligament *(arrowheads)* shows hypoechoic thickening of distal calcaneofibular ligament *(arrows)* at calcaneus (C). Ultrasound images **(B)** long axis and **(C)** short axis to the calcaneofibular ligament in a second patient show diffuse hypoechoic thickening *(arrows)*. L, peroneus longus; B, peroneus brevis.

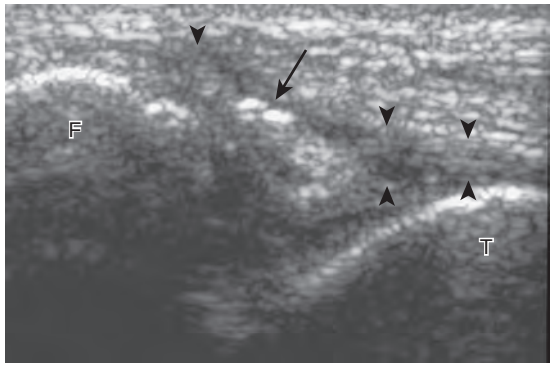

FIGURE 8-138 ■ Primary anterior talofibular ligament repair (Brostrom procedure). Ultrasound image long axis to the anterior talofibular ligament shows echogenic suture *(arrow)* and hypoechoic but continuous anterior talofibular ligament fibers *(arrowheads)*. F, fibula; T, talus.

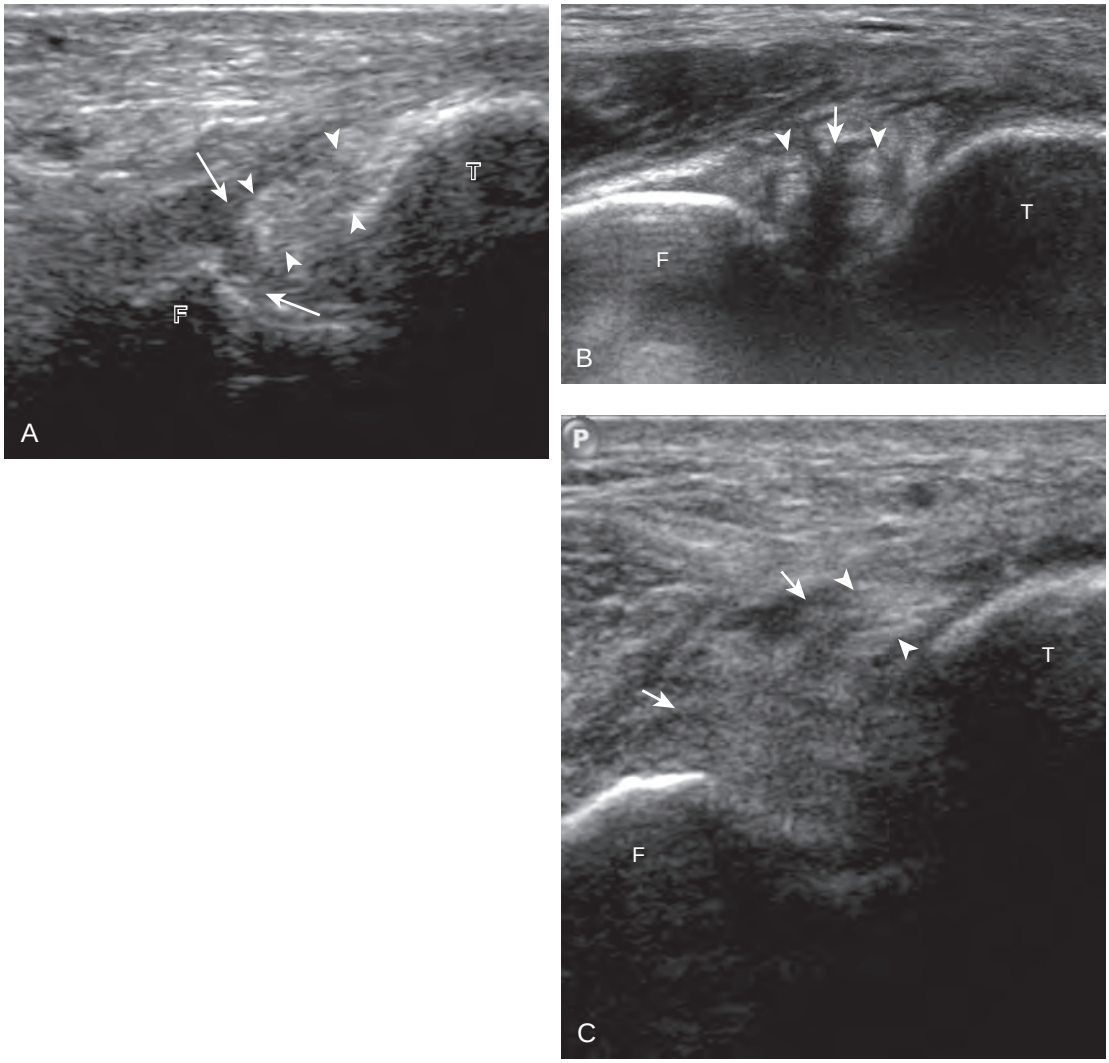

FIGURE 8-139 ■ Anterior inferior tibiofibular ligament tear. Ultrasound images long axis to the anterior inferior tibiofibular ligament from three patients after acute injury show hypoechoic discontinuity *(arrows)* of the anterior inferior tibiofibular ligament *(arrowheads)*. F, fibula; T, tibia.

of the calcaneus, which should not be confused with extensor digitorum brevis avulsion (Fig. 8-143).[90] In addition, abnormal widening and hypoechoic hemorrhage between the medial cuneiform and second metatarsal base can indirectly suggest Lisfranc ligament disruption (Fig. 8-144).[91] Tear of the dorsal tarsometatarsal ligament between the medial cuneiform and second metatarsal base, which can be identified at ultrasound, is another indirect sign of a tear of Lisfranc ligament proper. It is important to not mistake the normal variant os intermetatarsus, located between the first and second metatarsal bases, for a Lisfranc ligament injury–related fracture fragment (Fig. 8-145). Location of the os intermetatarsus distal to the middle cuneiform and normal tarsometatarsal alignment assists in this differentiation.

FRACTURE

Although it is understood that radiography should be the initial imaging method of choice to evaluate for fracture, it is not uncommon for an radiographically occult fracture to be identified at ultrasound. There are many osseous structures in the ankle and foot, and therefore it is not practical to assess each osseous structure routinely for abnormality. To identify a fracture at

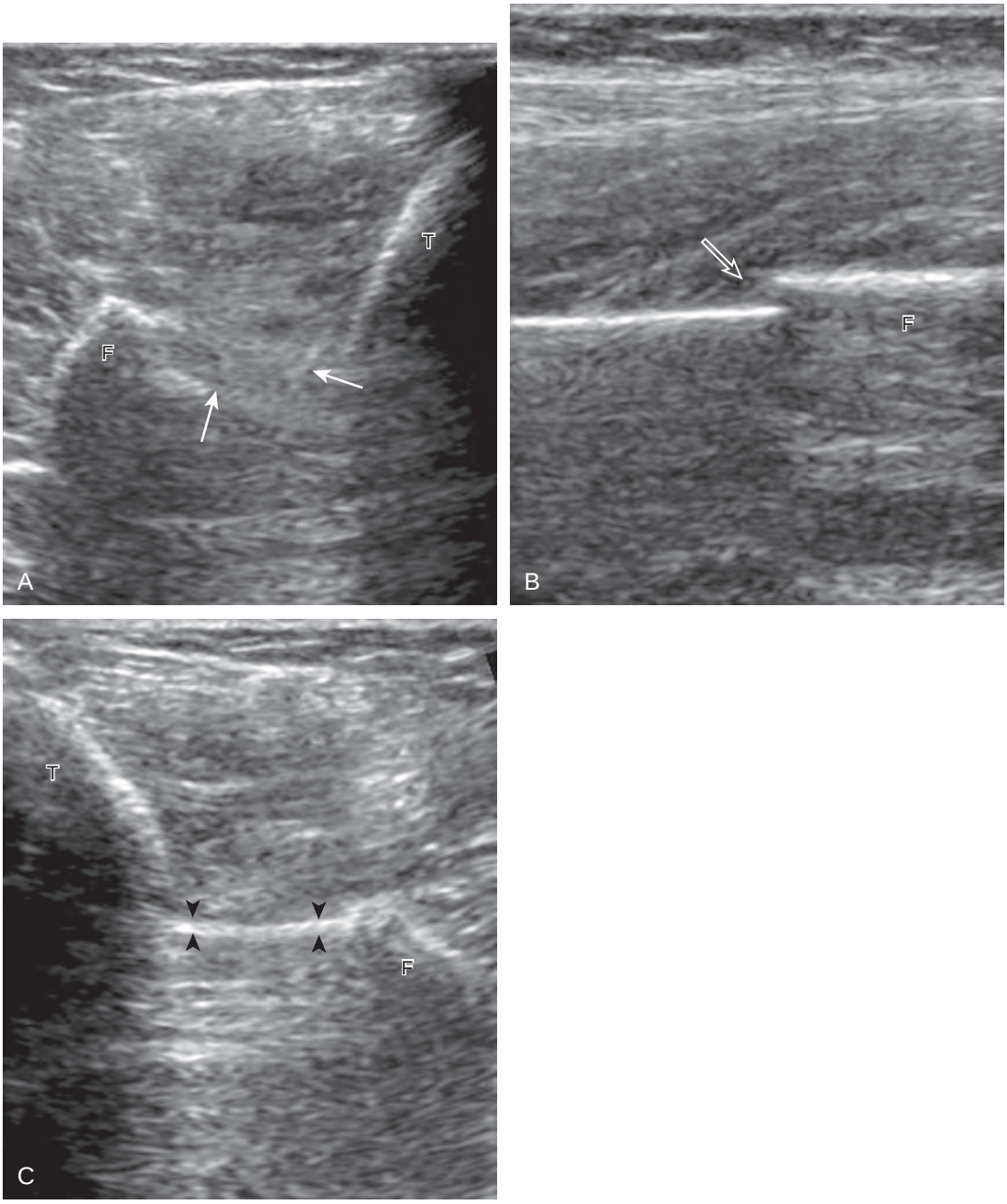

FIGURE 8-140 ■ Maisonneuve fracture. Transverse ultrasound image of anterolateral lower leg shows **(A)** nonvisualization of the interosseous membrane *(arrows)*. Coronal ultrasound of proximal lateral fibula shows **(B)** cortical step-off fracture *(open arrow)*. Transverse ultrasound image of contralateral asymptomatic leg shows **(C)** normal interosseous membrane *(arrowheads)*. F, fibula; T, tibia.

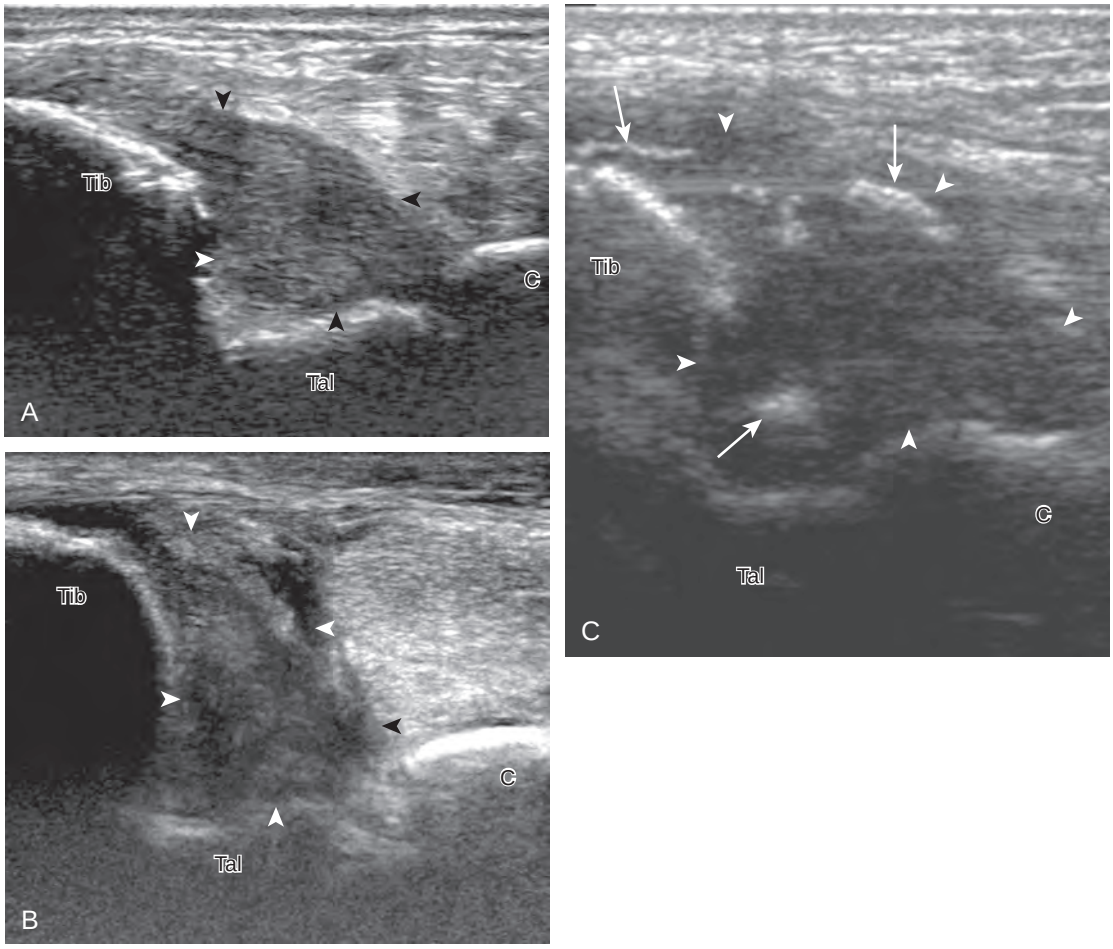

FIGURE 8-141 ■ Deltoid ligament tear. Ultrasound images at the medial malleolus in the coronal plane from three patients after acute injury show **(A)** hypoechoic thickening *(arrowheads)* of the deltoid ligament, **(B)** heterogeneous hypoechoic discontinuity *(arrowheads)* of the deltoid ligament, and **(C)** hypoechoic thickening *(arrowheads)* with fracture fragments *(arrows)* of the deltoid ligament. C, calcaneus; Tal, talus; Tib, tibia.

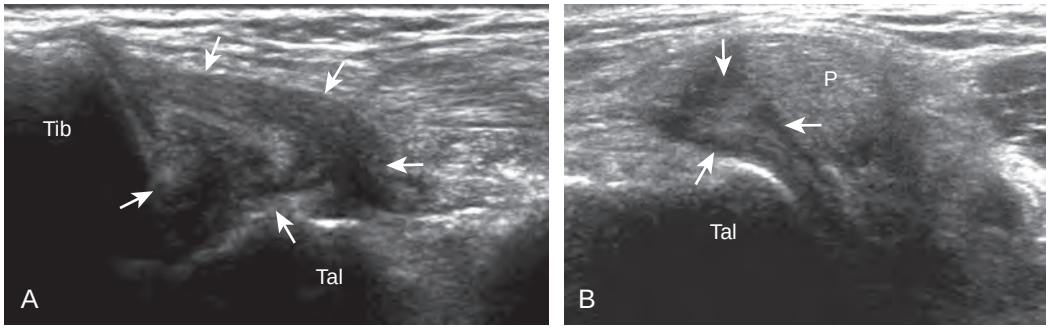

FIGURE 8-142 ■ Spring ligament injury. Ultrasound image over medial ankle shows **(A)** hypoechoic thickening of the injured deltoid ligament *(arrows)*. Ultrasound image over medial talus shows **(B)** hypoechoic thickening *(arrows)* and adjacent thinning of the superomedial calcaneonavicular ligament. P, tibialis posterior tendon; Tal, talus; Tib, tibia.

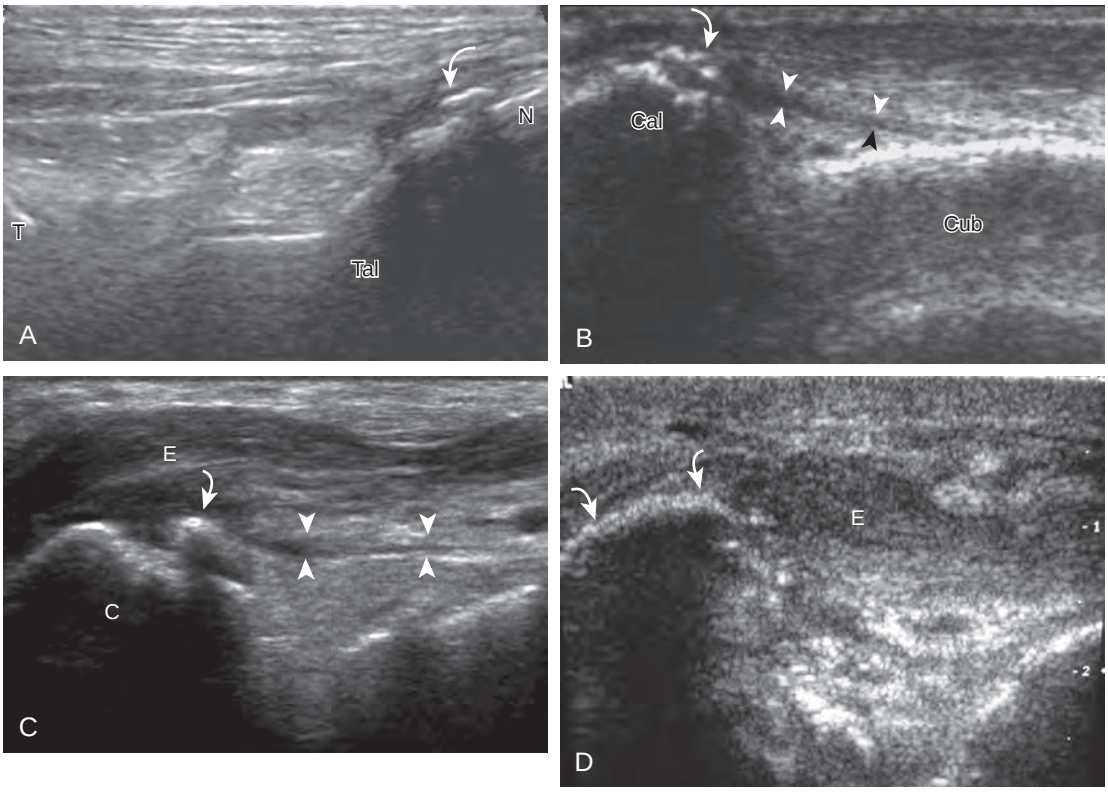

FIGURE 8-143 ■ **Other avulsion fractures.** Ultrasound sagittal image shows **(A)** avulsion fracture *(curved arrow)* at the talonavicular joint. Ultrasound image long axis to the calcaneocuboid ligament *(arrowheads)* shows **(B)** avulsion fracture *(curved arrow)* from calcaneus (Cal). Ultrasound image long axis to the bifurcate ligament *(arrowheads)* shows **(C)** avulsion fracture *(curved arrow)* from the anterior process of the calcaneus (C). Ultrasound image **(D)** long axis to the extensor digitorum brevis (E) shows avulsion fracture from calcaneus *(curved arrows)*. Cub, cuboid; E, extensor digitorum brevis muscle; N, navicular; Tal, talus; T, tibia.

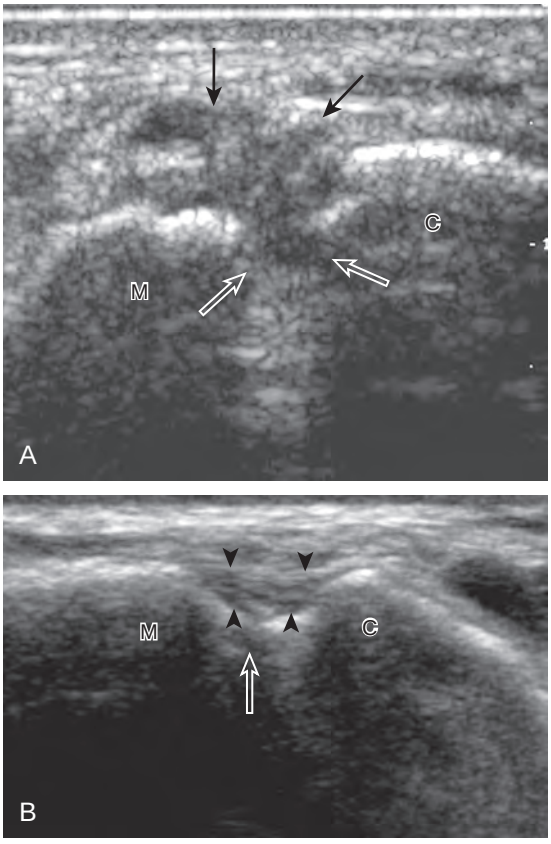

FIGURE 8-144 ■ **Lisfranc ligament tear.** Ultrasound image in the coronal plane between the medial cuneiform (C) and second metatarsal base (M) shows **(A)** abnormal widening *(open arrows)*, hypoechoic hemorrhage *(arrows)*, and nonvisualization of the dorsal tarsometatarsal ligament. Asymptomatic comparison shows **(B)** normal dorsal tarsometatarsal ligament *(arrowheads)* and normal distance and alignment *(open arrow)* between medial cuneiform (C) and second metatarsal base (M).

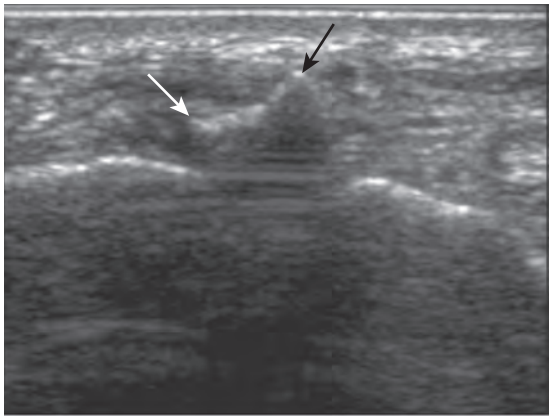

FIGURE 8-145 ■ Os intermetatarsus. Ultrasound image in the sagittal plane between the first and second metatarsals shows the hyperechoic and shadowing os intermetatarsus *(arrows)*.

ultrasound, one relies on the patient to direct examination based on point tenderness or the focal point of symptoms. It is critical, before completion of an ultrasound examination of the foot or ankle, that the patient be asked to indicate any focal site of symptoms. Identification of a cortical step-off of the normally smooth and echogenic cortical surface is diagnostic for fracture, especially if it is associated with pain from transducer pressure.[92] Knowledge of the normal osseous structures and their articulations is essential to not mistake a joint space for a displaced fracture. One may image the normal contralateral foot and ankle for comparison.

Acute fractures may occur at tendon or ligament attachments, and these were discussed earlier, in the tendon and ligament sections of this chapter. Besides these locations, acute fractures may occur essentially anywhere in the foot and ankle, related to the mechanism of injury. For example, distal fibular (Fig. 8-146A) and proximal fifth metatarsal (see Fig. 8-97) fractures are associated with inversion ankle injuries.[93] Stress fractures of bone classically involve the metatarsal shafts (Fig. 8-146B and C), the navicular bone (usually in the sagittal plane) (Fig. 8-147A), and the hallux sesamoids (see Fig. 8-147B).[94] With stress fractures, early ultrasound findings include focal hypoechogenicity along the cortex from hematoma or periostitis.[95] A step-off deformity or fracture line may also be identified. Later with bone remodeling, hyperechoic callous formation

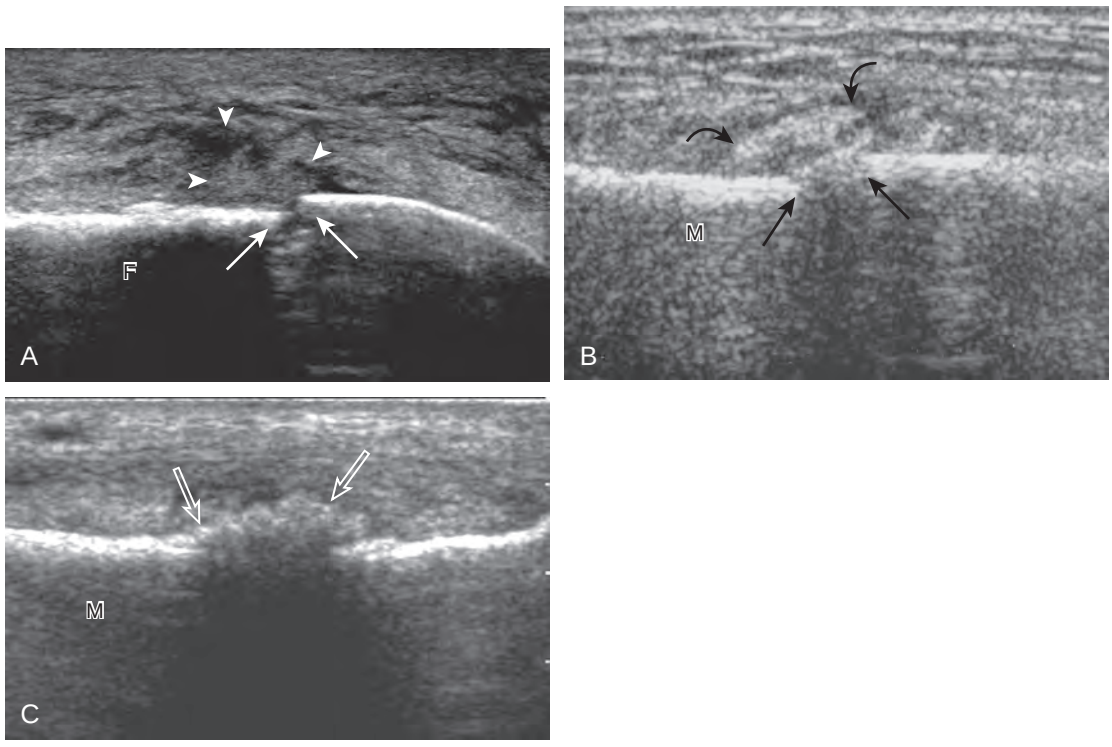

FIGURE 8-146 ■ Fractures: fibula and metatarsal. Ultrasound image of the fibula (F) shows **(A)** fracture step-off deformity *(arrows)* and adjacent hypoechoic and isoechoic hemorrhage *(arrowheads)*. Ultrasound images of the metatarsal shaft (M) in two patients show **(B)** fracture step-off *(arrows)* and hyperechoic callus *(curved arrows)* and **(C)** bone remodeling and bridging callus *(open arrows)*. (**C,** From Craig JG, Jacobson JA, Moed BR: Ultrasound of fracture and bone healing. *Radiol Clin North Am* 37:737-751, ix, 1999.)

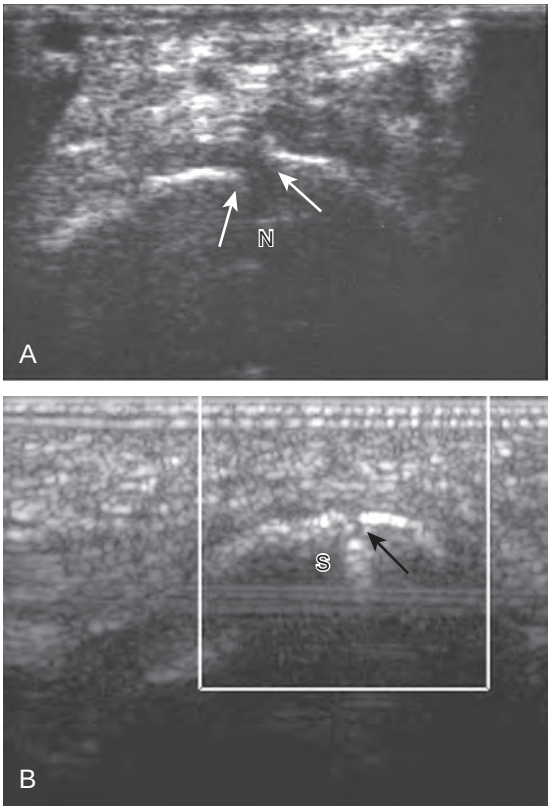

FIGURE 8-147 ■ Fractures: navicular and sesamoid. Ultrasound image in the coronal plane shows **(A)** step-off and mild displacement *(arrows)* of navicular (N) stress fracture. Ultrasound image in the sagittal plane shows **(B)** fracture *(arrow)* of a hallux sesamoid (S).

becomes evident. Ultrasound can also diagnose physeal injuries in children, which appear as adjacent hypoechoic hemorrhage or edema and possible wide or irregular physis and adjacent subperiosteal hematoma.[96] Although difficult to visualize, cortical irregularity and collapse of the metatarsal head (commonly the second) can indicate Freiberg disease or infraction, which is fracture and necrosis of the metatarsal head from

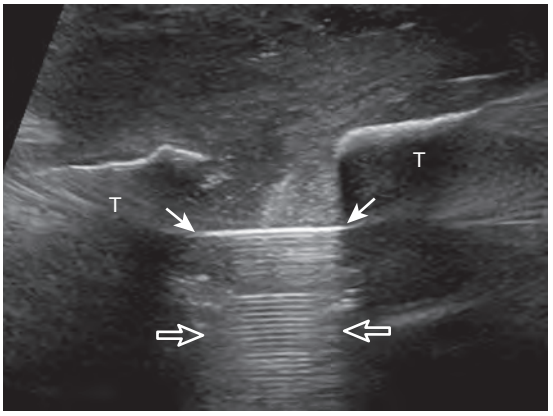

FIGURE 8-149 ■ Tibia fracture: nonunion. Ultrasound image long axis to tibial (T) shaft at site of fracture shows visualization of the hyperechoic metal intramedullary nail *(arrows)* with posterior reverberation artifact *(open arrows)* with no overlying callus.

repetitive trauma (Fig. 8-148). Ultrasound has been used to assess callous formation after static interlocked nail placement for tibia fracture (Fig. 8-149).[94]

PERIPHERAL NERVE ABNORMALITIES

Morton neuroma is a non-neoplastic enlargement of a common plantar digital nerve as a result of nerve entrapment or trauma characterized by perineural fibrosis, vascular proliferation, endoneurium edema, and axonal degeneration.[97] The most common site for Morton neuroma is the third web space, followed by the second, at the level of the metatarsal heads.[97] At ultrasound, Morton neuroma appears as a hypoechoic mass, which is more likely symptomatic when it is greater than 5 mm (Fig. 8-150).[98] In the coronal plane, the neuroma often extends in a plantar

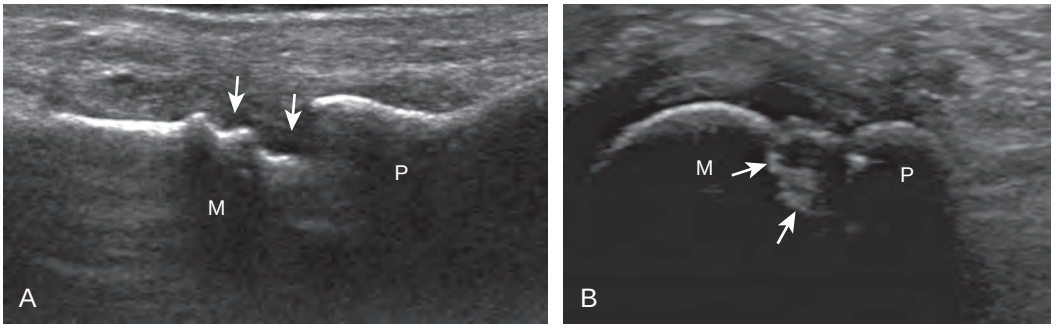

FIGURE 8-148 ■ Freiberg disease. Ultrasound images over dorsal **(A)** and plantar **(B)** aspects of the second metatarsal head in two patients shows cortical irregularity *(arrows)* of the metatarsal head (M). P, proximal phalanx.

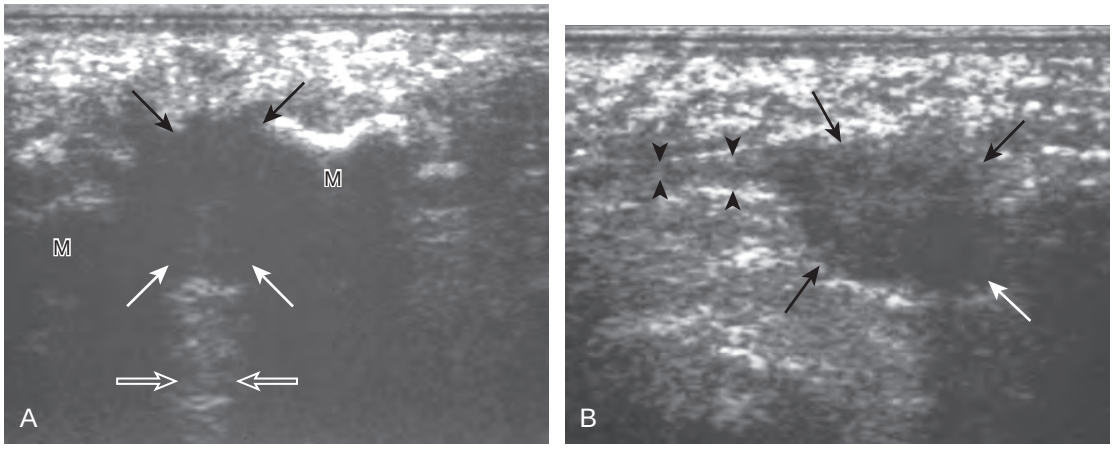

FIGURE 8-150 ■ Morton neuroma. Ultrasound images in the **(A)** coronal and **(B)** sagittal planes show hypoechoic Morton neuroma *(arrows)*. Note hypoechoic common plantar digital nerve *(arrowheads)* continuous with the neuroma and increased through-transmission *(open arrows)*. M, metatarsal heads.

direction from between the metatarsal heads with concave borders medial and lateral.[99] In the sagittal plane, identification of the hypoechoic common plantar digital nerve, which enters into the neuroma, ensures the diagnosis (Fig. 8-151).[97] This finding, along with noncompressibility of the mass, helps to exclude bursal distention as a cause for a hypoechoic mass (Videos 8-29 and 8-30). Compression of the neuroma between the transducer at the plantar aspect and the examiner's finger over the dorsal aspect of the foot should reproduce the patient's symptoms related to the neuroma. Conversely, if scanning from the dorsal aspect, compression is applied from the plantar aspect. Dynamic evaluation with application of opposed medial and lateral force to compress the metatarsal heads may displace a neuroma in a plantar direction and cause a palpable click (the sonographic Mulder sign), which can increase diagnostic confidence (Fig. 8-152) (Video 8-31).[20] This dynamic maneuver can increase sensitivity of ultrasound in diagnosis of an intermetarsal mass from 65% to 100%.[100] It is not uncommon for Morton neuromas to be associated with intermetatarsal bursal distention, which can appear as an adjacent anechoic fluid collection or possibly a large complex heterogeneous mass.

Another example is potential nerve entrapment of the tibial nerve in the tarsal tunnel, which

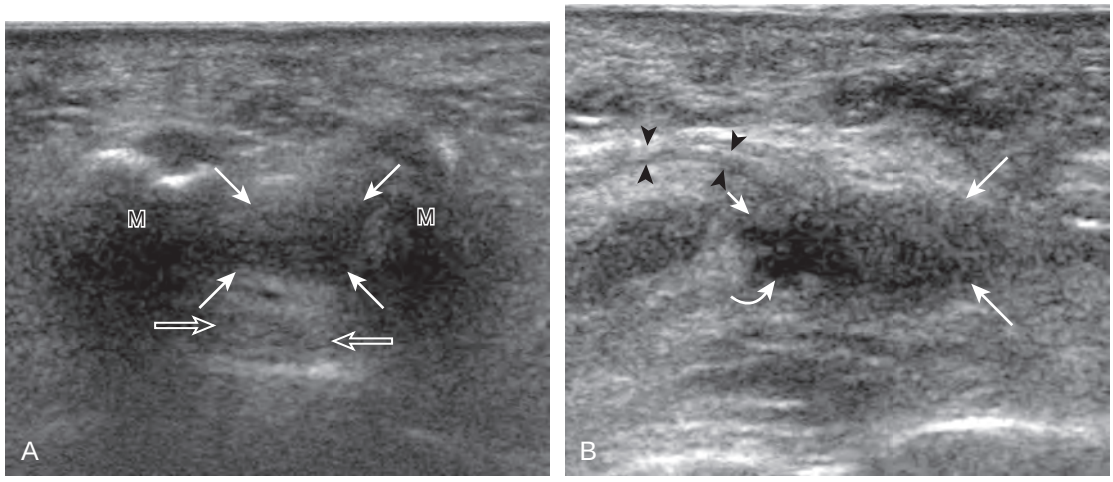

FIGURE 8-151 ■ Morton neuroma. Ultrasound images in the **(A)** coronal and **(B)** sagittal planes show hypoechoic Morton neuroma *(arrows)*. Note hypoechoic common plantar digital nerve *(arrowheads)* continuous with the neuroma and increased through-transmission *(open arrows)* and associated anechoic intermetatarsal bursa *(curved arrow)*. M, metatarsal heads.

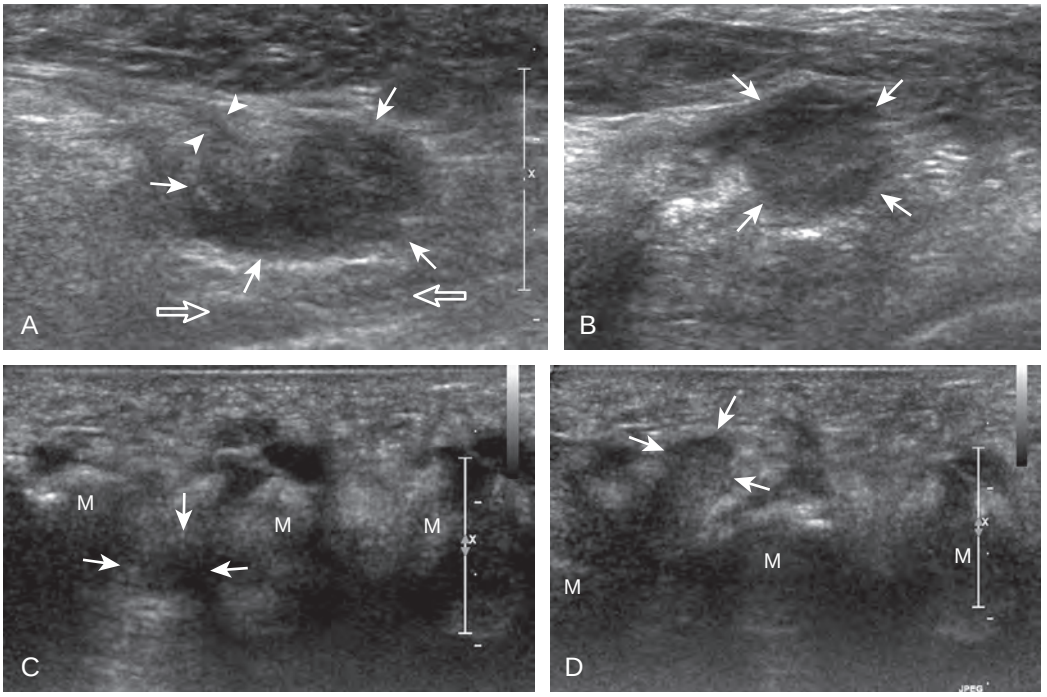

FIGURE 8-152 ■ Morton neuroma. Ultrasound images in the sagittal plane scanned from **(A)** plantar and **(B)** dorsal show hypoechoic Morton neuroma *(arrows)*. Note hypoechoic common plantar digital nerve *(arrowheads)* continuous with the neuroma and increased through-transmission *(open arrows)*. Ultrasound images in the coronal plane in neutral **(C)** and with side-to-side compression of metatarsals **(D)** show plantar displacement of the Morton neuroma *(arrows)*, which produced symptoms. M, metatarsal heads.

is an enclosed space posterior to the distal tibia bound by the flexor retinaculum that contains the medial tendons and tibial nerve. Tibial nerve entrapment at this site, called tarsal tunnel syndrome, may be secondary to a ganglion cyst (Fig. 8-153) (Video 8-32), although any space-occupying process can have the same effect.[101] Tarsal tunnel syndrome also has been associated with talocalcaneal coalition.[101] It is important not to mistake a hypoechoic peripheral nerve sheath tumor, which may be eccentric to the tibial nerve axis and demonstrate increased through-transmission, as a complex ganglion cyst compressing the tibial nerve (Fig. 8-154).[102] Another site prone to nerve compression is the superficial

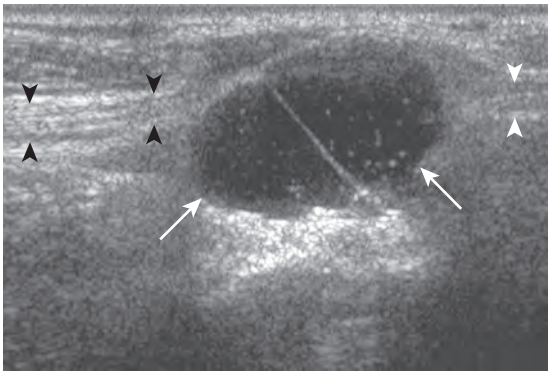

FIGURE 8-153 ■ Tarsal tunnel syndrome: ganglion cyst. Ultrasound image long axis to tibial nerve *(arrowheads)* shows ganglion cyst *(arrows)* causing nerve compression. Note internal echoes of cyst and increased through-transmission.

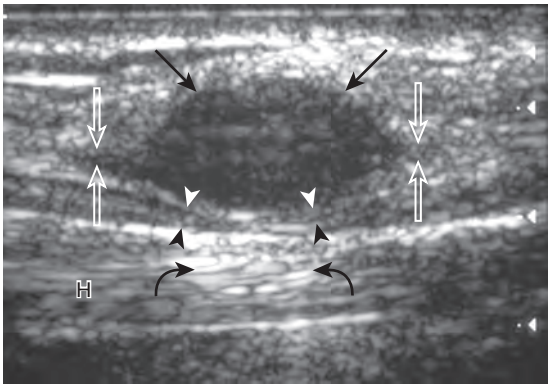

FIGURE 8-154 ■ Schwannoma: tibial nerve. Ultrasound image shows a hypoechoic schwannoma *(arrows)* that originates from a portion of the tibial nerve *(open arrows)* with compression of other tibial nerve fibers *(arrowheads)*. Note increased through-transmission *(curved arrows)*. H, flexor hallucis longus tendon. (From Reynolds DL Jr, Jacobson JA, Inampudi P, et al: Sonographic characteristics of peripheral nerve sheath tumors. *AJR Am J Roentgenol* 182:741-744, 2004.)

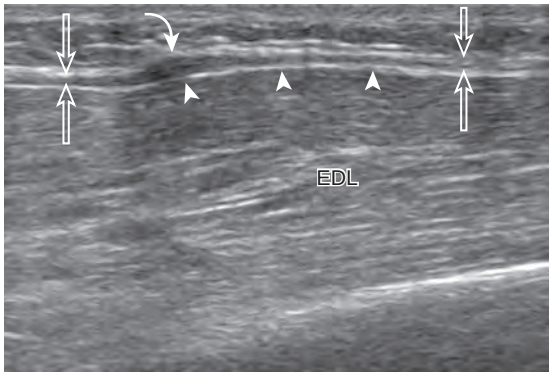

FIGURE 8-155 ■ Superficial peroneal nerve neuroma from muscle hernia. Ultrasound image long axis to superficial peroneal nerve *(open arrows)* shows hypoechoic swelling *(curved arrow)* where nerve penetrates fascia at site of a focal muscle hernia *(arrowheads)*, present only during muscle contraction. EDL, extensor digitorum longus.

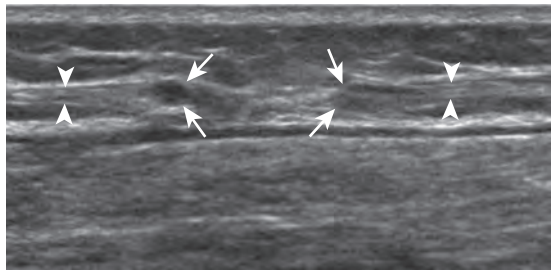

FIGURE 8-157 ■ Traumatic neuromas: sural nerve. Ultrasound image long axis to sural nerve *(arrowheads)* shows hypoechoic swelling *(arrows)* at the nerve ends at site of transection. Note degree of retraction.

peroneal nerve where it pierces the crural fascia at an average of 9 cm proximal to the fibular tip.[103] A neuroma can form at this site, appearing swollen and hypoechoic, owing to traction injury, thickened fascia, or muscle hernia (Fig. 8-155) (Video 8-33).[104]

Trauma to a peripheral nerve may cause findings at ultrasound that range from hypoechoic swelling to complete nerve discontinuity with retraction. In the setting of nerve transection, neuroma formation is an expected response as the nerve attempts to regenerate, which appears as hypoechoic swelling of the terminal nerve end (Figs. 8-156 and 8-157).[105] Peripheral nerve sheath tumors are discussed in Chapter 2.

MASSES AND CYSTS

In evaluation of a foot or ankle mass, it is important to determine whether the mass originates from a joint, from the bone, or from the soft tissues apart from a joint. Most joint processes that may manifest as a mass are synovial proliferative disorders, such as pigmented villonodular synovitis (see Fig. 8-35)[22] or synovial chondromatosis (see Fig. 8-36). Similarly, a well-defined hypoechoic mass arising from a tendon sheath commonly represents a giant cell tumor of the tendon sheath (pigmented villonodular tenosynovitis) (Fig. 8-158).[106] Masses that arise from bone are often malignant or aggressive (see Chapter 2) and are best evaluated with radiography and magnetic resonance imaging. Regarding other soft tissue masses, ultrasound may differentiate cystic and solid masses and may guide percutaneous biopsy or aspiration.

The most common benign mass in the foot and ankle is a ganglion cyst.[107] Classically, a ganglion cyst is anechoic, with increased through-transmission and no associated mass (Fig. 8-159A).[107] However, many ganglion cysts are hypoechoic, multilocular, and lobular (see Fig. 8-159B and C). In addition, the viscous nature of the fluid may create reflective echoes within the cyst. Location of a ganglion cyst within the tarsal tunnel may compress the tibial nerve

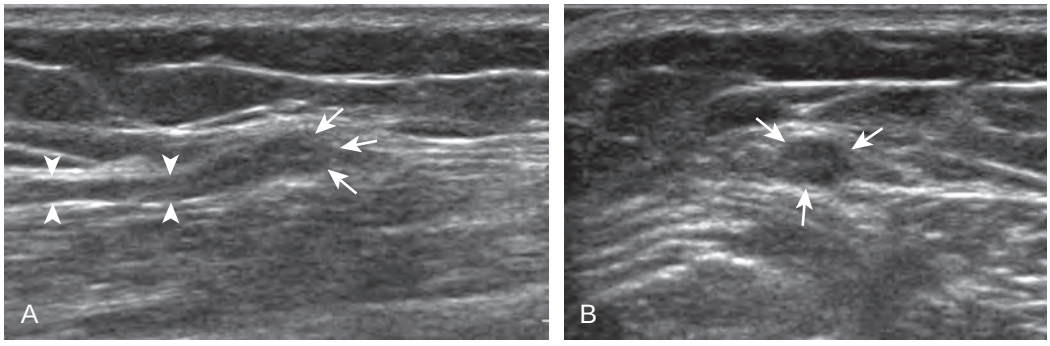

FIGURE 8-156 ■ Traumatic neuroma: superficial peroneal nerve. Ultrasound image **(A)** long and **(B)** short axis to superficial peroneal nerve *(arrowheads)* shows hypoechoic terminal nerve swelling *(arrows)* at transection site.

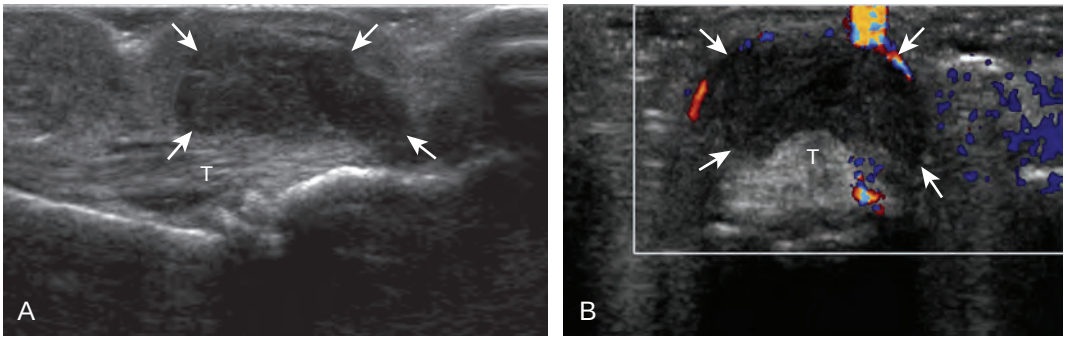

FIGURE 8-158 ■ Giant cell tumor of tendon sheath. Ultrasound images **(A)** long axis and **(B)** short axis to flexor tendons (T) of second toe show hypoechoic mass *(arrows)* in contact with tendon. Note increased through-transmission.

(see Fig. 8-153). Ganglion cysts of the foot and ankle may show communication with adjacent joints or tendon sheaths and involve the sinus tarsi (see Fig. 8-159C). It is important not to mistake a bursa, such as the sinus tarsi bursa of Gruberi, between the extensor digitorum longus tendons and talus (see Fig. 8-63) as a ganglion cyst.[41] Ultrasound can be used to guide percutaneous aspiration, in which a large-bore needle is often needed because of the high viscosity of the cyst contents. In evaluation of the lateral ankle, it is important not to mistake the normal calcaneofibular ligament in cross section, which may appear hypoechoic as a result of anisotropy, for a small ganglion cyst (see Fig. 8-18C and D).

Another type of cyst that may involve the foot is an epidermal inclusion cyst, with implantation of epidermis into the dermis or subcutis from trauma proposed as one cause.[108] At ultrasound, an epidermal inclusion cyst typically appears hypoechoic to surrounding tissues but with low-level internal echoes and a hypoechoic rim and increased through-transmission, which at times may simulate a solid mass (Fig. 8-160).[109]

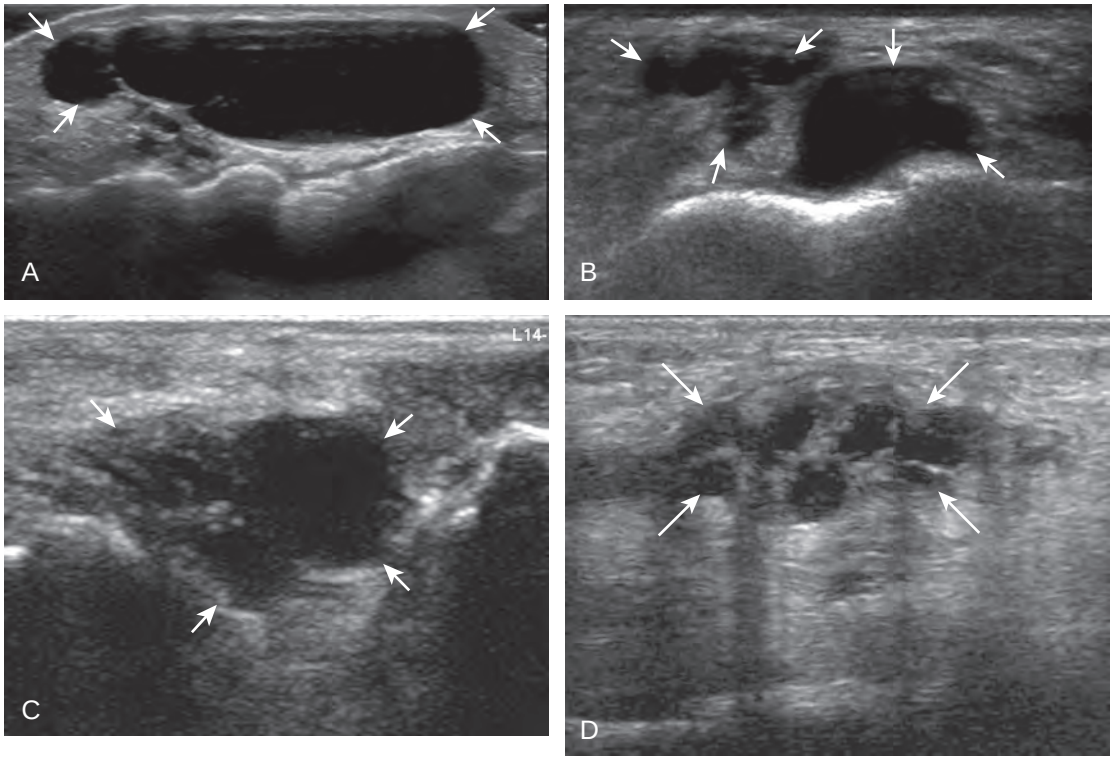

FIGURE 8-159 ■ Ganglion cysts. Ultrasound images **(A** to **D)** from four patients show anechoic to hypoechoic ganglion cysts *(arrows)*, with features of internal echoes, lobulations, multiple locules, septations, and increased through-transmission. Note **(C)** location of the ganglion cyst in the sinus tarsi.

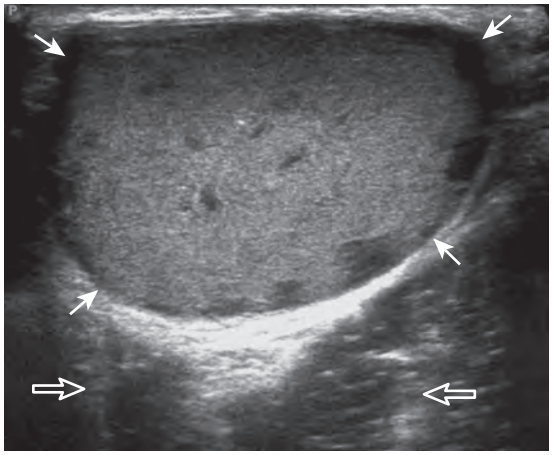

FIGURE 8-160 ■ Epidermal inclusion cyst. Ultrasound image shows heterogeneous cyst with low-level echoes *(arrows)*, vague hypoechoic halo, and increased through-transmission *(open arrows)*.

Increased blood flow on color Doppler imaging and lobulated margins are more likely after cyst rupture.[110]

Other benign and malignant masses that are not specific to the foot and ankle are discussed in Chapter 2. Plantar fibromatosis (see Fig. 8-135) was discussed earlier in this chapter. One must also consider the possibility of an inflammatory process that simulates a soft tissue mass, such as a chronic foreign body reaction (see Chapter 2). Other causes for palpable mass include muscle hernia (see Figs. 8-104 and 8-105) and accessory soleus muscle (see Fig. 8-130). Soft tissue masses associated with inflammatory arthritis include rheumatoid nodule (see Fig. 8-46), adventitious bursa (see Fig. 8-61), and gouty tophi (see Fig. 8-55).

Online references available at www.expertconsult.com.

REFERENCES

1. Lektrakul N, Chung CB, Lai Y, et al: Tarsal sinus: arthrographic, MR imaging, MR arthrographic, and pathologic findings in cadavers and retrospective study data in patients with sinus tarsi syndrome. *Radiology* 219:802–810, 2001.
2. Louisia S, Masquelet AC: The medial and inferior calcaneal nerves: an anatomic study. *Surg Radiol Anat* 21:169–173, 1999.
3. Chundru U, Liebeskind A, Seidelmann F, et al: Plantar fasciitis and calcaneal spur formation are associated with abductor digiti minimi atrophy on MRI of the foot. *Skeletal Radiol* 37:505–510, 2008.
4. Rosenberg ZS, Beltran J, Cheung YY, et al: MR features of longitudinal tears of the peroneus brevis tendon. *AJR Am J Roentgenol* 168:141–147, 1997.
5. Rosenberg ZS, Bencardino J, Astion D, et al: MRI features of chronic injuries of the superior peroneal retinaculum. *AJR Am J Roentgenol* 181:1551–1557, 2003.
6. Chepuri NB, Jacobson JA, Fessell DP, et al: Sonographic appearance of the peroneus quartus muscle: correlation with MR imaging appearance in seven patients. *Radiology* 218:415–419, 2001.
7. Delgado GJ, Chung CB, Lektrakul N, et al: Tennis leg: clinical US study of 141 patients and anatomic investigation of four cadavers with MR imaging and US. *Radiology* 224:112–119, 2002.
8. Muhle C, Frank LR, Rand T, et al: Collateral ligaments of the ankle: high-resolution MR imaging with a local gradient coil and anatomic correlation in cadavers. *Radiographics* 19:673–683, 1999.
9. Subhas N, Vinson EN, Cothran RL, et al: MRI appearance of surgically proven abnormal accessory anterior-inferior tibiofibular ligament (Bassett's ligament). *Skeletal Radiol* 37:27–33, 2008.
10. Harish S, Jan E, Finlay K, et al: Sonography of the superomedial part of the spring ligament complex of the foot: a study of cadavers and asymptomatic volunteers. *Skeletal Radiol* 36:221–228, 2007.
11. Castro M, Melao L, Canella C, et al: Lisfranc joint ligamentous complex: MRI with anatomic correlation in cadavers. *AJR Am J Roentgenol* 195:W447–455, 2010.
12. Nazarian LN, Rawool NM, Martin CE, et al: Synovial fluid in the hindfoot and ankle: detection of amount and distribution with US. *Radiology* 197:275–278, 1995.
13. Mansour R, Teh J, Sharp RJ, et al: Ultrasound assessment of the spring ligament complex. *Eur Radiol* 18:2670–2675, 2008.
14. Brigido MK, Fessell DP, Jacobson JA, et al: Radiography and US of os peroneum fractures and associated peroneal tendon injuries: initial experience. *Radiology* 237:235–241, 2005.
15. Boonthathip M, Chen L, Trudell DJ, et al: Tibiofibular syndesmotic ligaments: MR arthrography in cadavers with anatomic correlation. *Radiology* 254:827–836, 2010.
16. van den Bekerom MP, Raven EE: The distal fascicle of the anterior inferior tibiofibular ligament as a cause of tibiotalar impingement syndrome: a current concepts review. *Knee Surg Sports Traumatol Arthrosc* 15:465–471, 2007.
17. Durkee NJ, Jacobson JA, Jamadar DA, et al: Sonographic evaluation of lower extremity interosseous membrane injuries: retrospective review in 3 patients. *J Ultrasound Med* 22:1369–1375, 2003.
18. Cardinal E, Chhem RK, Beauregard CG, et al: Plantar fasciitis: sonographic evaluation. *Radiology* 201:257–259, 1996.
19. Lee KS: Musculoskeletal ultrasound: how to evaluate for Morton's neuroma. *AJR Am J Roentgenol* 193:W172, 2009.
20. Torriani M, Kattapuram SV: Technical innovation. Dynamic sonography of the forefoot: the sonographic Mulder sign. *AJR Am J Roentgenol* 180:1121–1123, 2003.
21. Jacobson JA, Andresen R, Jaovisidha S, et al: Detection of ankle effusions: comparison study in cadavers using radiography, sonography, and MR imaging. *AJR Am J Roentgenol* 170:1231–1238, 1998.
22. Yang PY, Wang CL, Wu CT, et al: Sonography of pigmented villonodular synovitis in the ankle joint. *J Clin Ultrasound* 26:166–170, 1998.
23. Roberts D, Miller TT, Erlanger SM: Sonographic appearance of primary synovial chondromatosis of the knee. *J Ultrasound Med* 23:707–709, 2004.
24. McCarthy CL, Wilson DJ, Coltman TP: Anterolateral ankle impingement: findings and diagnostic accuracy with ultrasound imaging. *Skeletal Radiol* 37:209–216, 2008.
25. Hayashi D, Roemer FW, Katur A, et al: Imaging of synovitis in osteoarthritis: current status and outlook. *Semin Arthritis Rheum* 41:116–130, 2011.
26. Keen HI, Conaghan PG. Ultrasonography in osteoarthritis. *Radiol Clin North Am* 47:581–594, 2009.
27. Wakefield RJ, Balint PV, Szkudlarek M, et al: Musculoskeletal ultrasound including definitions for ultrasonographic pathology. *J Rheumatol* 32:2485–2487, 2005.
28. Riente L, Delle Sedie A, Scire CA, et al: Ultrasound imaging for the rheumatologist. XXXI. Sonographic assessment of the foot in patients with rheumatoid arthritis. *Clin Exp Rheumatol* 29:1–5, 2011.
29. Sheane BJ, Beddy P, O'Connor M, et al: Targeted ultrasound of the fifth metatarsophalangeal joint in an early inflammatory arthritis cohort. *Arthritis Rheum* 61:1004–1008, 2009.
30. Lopez-Ben R, Bernreuter WK, Moreland LW, et al: Ultrasound detection of bone erosions in rheumatoid arthritis: a comparison to routine radiographs of the hands and feet. *Skeletal Radiol* 33:80–84, 2004.
31. Torshizy H, Hughes TH, Trudell D, et al: Anatomic features of metatarsal heads that simulate erosive disease: cadaveric study using CT, radiography, and dissection with special emphasis on cross-sectional characterization of osseous anatomy. *AJR Am J Roentgenol* 190:W175–181, 2008.
32. Nalbant S, Corominas H, Hsu B, et al: Ultrasonography for assessment of subcutaneous nodules. *J Rheumatol* 30:1191–1195, 2003.
33. Thiele RG: Role of ultrasound and other advanced imaging in the diagnosis and management of gout. *Curr Rheumatol Rep* 13:146–153, 2011.
34. Thiele RG, Schlesinger N: Ultrasonography shows disappearance of monosodium urate crystal deposition on hyaline cartilage after sustained normouricemia is achieved. *Rheumatol Int* 30:495–503, 2010.
35. de Avila Fernandes E, Kubota ES, Sandim GB, et al: Ultrasound features of tophi in chronic tophaceous gout. *Skeletal Radiol* 40:309–315, 2011.
36. Gutierrez M, Filippucci E, De Angelis R, et al: A sonographic spectrum of psoriatic arthritis: "the five targets." *Clin Rheumatol* 29:133–142, 2010.
37. Lee JC, Calder JD, Healy JC: Posterior impingement syndromes of the ankle. *Semin Musculoskelet Radiol* 12:154–169, 2008.
38. Studler U, Mengiardi B, Bode B, et al: Fibrosis and adventitious bursae in plantar fat pad of forefoot: MR imaging findings in asymptomatic volunteers and MR imaging-histologic comparison. *Radiology* 246:863–870, 2008.
39. Brown RR, Sadka Rosenberg Z, Schweitzer ME, et al: MRI of medial malleolar bursa. *AJR Am J Roentgenol* 184:979–983, 2005.

40. Zanetti M, Strehle JK, Zollinger H, et al: Morton neuroma and fluid in the intermetatarsal bursae on MR images of 70 asymptomatic volunteers. *Radiology* 203:516–520, 1997.
41. Lovell AG, Tanner HH: Synovial membranes, with special reference to those related to the tendons of the foot and ankle. *J Anat Physiol* 42:415–432, 1908.
42. Bianchi S, Poletti PA, Martinoli C, et al: Ultrasound appearance of tendon tears. Part 2: lower extremity and myotendinous tears. *Skeletal Radiol* 35:63–77, 2006.
43. Breidahl WH, Stafford Johnson DB, Newman JS, et al: Power Doppler sonography in tenosynovitis: significance of the peritendinous hypoechoic rim. *J Ultrasound Med* 17:103–107, 1998.
44. Chen YJ, Liang SC: Diagnostic efficacy of ultrasonography in stage I posterior tibial tendon dysfunction: sonographic-surgical correlation. *J Ultrasound Med* 16:417–423, 1997.
45. Premkumar A, Perry MB, Dwyer AJ, et al: Sonography and MR imaging of posterior tibial tendinopathy. *AJR Am J Roentgenol* 178:223–232, 2002.
46. Kong A, Van Der Vliet A: Imaging of tibialis posterior dysfunction. *Br J Radiol* 81:826–836, 2008.
47. Miller SD, Van Holsbeeck M, Boruta PM, et al: Ultrasound in the diagnosis of posterior tibial tendon pathology. *Foot Ankle Int* 17:555–558, 1996.
48. Prato N, Abello E, Martinoli C, et al: Sonography of posterior tibialis tendon dislocation. *J Ultrasound Med* 23:701–705, 2004.
49. Shetty M, Fessell DP, Femino JE, et al: Sonography of ankle tendon impingement with surgical correlation. *AJR Am J Roentgenol* 179:949–953, 2002.
50. Bianchi S, Delmi M, Molini L: Ultrasound of peroneal tendons. *Semin Musculoskelet Radiol* 14:292–306, 2010.
51. Grant TH, Kelikian AS, Jereb SE, et al: Ultrasound diagnosis of peroneal tendon tears: a surgical correlation. *J Bone Joint Surg Am* 87:1788–1794, 2005.
52. Diaz GC, van Holsbeeck M, Jacobson JA: Longitudinal split of the peroneus longus and peroneus brevis tendons with disruption of the superior peroneal retinaculum. *J Ultrasound Med* 17:525–529, 1998.
53. Demondion X, Canella C, Moraux A, et al: Retinacular disorders of the ankle and foot. *Semin Musculoskelet Radiol* 14:281–291, 2010.
54. Neustadter J, Raikin SM, Nazarian LN: Dynamic sonographic evaluation of peroneal tendon subluxation. *AJR Am J Roentgenol* 183:985–988, 2004.
55. Thomas JL, Lopez-Ben R, Maddox J: A preliminary report on intra-sheath peroneal tendon subluxation: a prospective review of 7 patients with ultrasound verification. *J Foot Ankle Surg* 48:323–329, 2009.
56. Khoury NJ, el-Khoury GY, Saltzman CL, et al: Peroneus longus and brevis tendon tears: MR imaging evaluation. *Radiology* 200:833–841, 1996.
57. Theodorou DJ, Theodorou SJ, Kakitsubata Y, et al: Fractures of proximal portion of fifth metatarsal bone: anatomic and imaging evidence of a pathogenesis of avulsion of the plantar aponeurosis and the short peroneal muscle tendon. *Radiology* 226:857–865, 2003.
58. Chien AJ, Jacobson JA, Jamadar DA, et al: Imaging appearances of lateral ankle ligament reconstruction. *Radiographics* 24:999–1008, 2004.
59. Mengiardi B, Pfirrmann CW, Vienne P, et al: Anterior tibial tendon abnormalities: MR imaging findings. *Radiology* 235:977–984, 2005.
60. Beggs I: Sonography of muscle hernias. *AJR Am J Roentgenol* 180:395–399, 2003.
61. Bianchi S, Abdelwahab IF, Mazzola CG, et al: Sonographic examination of muscle herniation. *J Ultrasound Med* 14:357–360, 1995.
62. Calleja M, Connell DA: The Achilles tendon. *Semin Musculoskelet Radiol* 14:307–322, 2010.
63. Richards PJ, Win T, Jones PW: The distribution of microvascular response in Achilles tendonopathy assessed by colour and power Doppler. *Skeletal Radiol* 34:336–342, 2005.
64. Kiris A, Kaya A, Ozgocmen S, et al: Assessment of enthesitis in ankylosing spondylitis by power Doppler ultrasonography. *Skeletal Radiol* 35:522–528, 2006.
65. Filippucci E, Aydin SZ, Karadag O, et al: Reliability of high-resolution ultrasonography in the assessment of Achilles tendon enthesopathy in seronegative spondyloarthropathies. *Ann Rheum Dis* 68:1850–1855, 2009.
66. Astrom M, Gentz CF, Nilsson P, et al: Imaging in chronic Achilles tendinopathy: a comparison of ultrasonography, magnetic resonance imaging and surgical findings in 27 histologically verified cases. *Skeletal Radiol* 25:615–620, 1996.
67. Hartgerink P, Fessell DP, Jacobson JA, et al: Full- versus partial-thickness Achilles tendon tears: sonographic accuracy and characterization in 26 cases with surgical correlation. *Radiology* 220:406–412, 2001.
68. Jacobson JA, Miller BS, Morag Y: Golf and racquet sports injuries. *Semin Musculoskelet Radiol* 9:346–359, 2005.
69. Alfredson H: Midportion Achilles tendinosis and the plantaris tendon. *Br J Sports Med* 45:1023–1025, 2011.
70. Mahajan RH, Dalal RB: Flexor hallucis longus tendon transfer for reconstruction of chronically ruptured Achilles tendons. *J Orthop Surg (Hong Kong)* 17:194–198, 2009.
71. Richards PJ, Braid JC, Carmont MR, et al: Achilles tendon ossification: pathology, imaging and aetiology. *Disabil Rehabil* 30:1651–1665, 2008.
72. Bude RO, Adler RS, Bassett DR, et al: Heterozygous familial hypercholesterolemia: detection of xanthomas in the Achilles tendon with US. *Radiology* 188:567–571, 1993.
73. Bureau NJ, Roederer G: Sonography of Achilles tendon xanthomas in patients with heterozygous familial hypercholesterolemia. *AJR Am J Roentgenol* 171:745–749, 1998.
74. Bianchi S, Martinoli C, Abdelwahab IF, et al: Sonographic evaluation of tears of the gastrocnemius medial head ("tennis leg"). *J Ultrasound Med* 17:157–162, 1998.
75. Kwak HS, Han YM, Lee SY, et al: Diagnosis and follow-up US evaluation of ruptures of the medial head of the gastrocnemius ("tennis leg"). *Korean J Radiol* 7:193–198, 2006.
76. Bianchi S, Sailly M, Molini L: Isolated tear of the plantaris tendon: ultrasound and MRI appearance. *Skeletal Radiol* 40:891–895, 2011.
77. Leekam RN, Agur AM, McKee NH: Using sonography to diagnose injury of plantaris muscles and tendons. *AJR Am J Roentgenol* 172:185–189, 1999.
78. Jamadar DA, Jacobson JA, Theisen SE, et al: Sonography of the painful calf: differential considerations. *AJR Am J Roentgenol* 179:709–716, 2002.
79. Yu JS, Resnick D: MR imaging of the accessory soleus muscle appearance in six patients and a review of the literature. *Skeletal Radiol* 23:525–528, 1994.
80. McNally EG, Shetty S: Plantar fascia: imaging diagnosis and guided treatment. *Semin Musculoskelet Radiol* 14:334–343, 2010.
81. Cheng JW, Tsai WC, Yu TY, et al: Reproducibility of sonographic measurement of thickness and echogenicity of the plantar fascia. *J Clin Ultrasound* 40:14–19, 2012.
82. Griffith JF, Wong TY, Wong SM, et al: Sonography of plantar fibromatosis. *AJR Am J Roentgenol* 179:1167–1172, 2002.

83. Bedi DG, Davidson DM: Plantar fibromatosis: most common sonographic appearance and variations. *J Clin Ultrasound* 29:499–505, 2001.
84. Pham H, Fessell DP, Femino JE, et al: Sonography and MR imaging of selected benign masses in the ankle and foot. *AJR Am J Roentgenol* 180:99–107, 2003.
85. Peetrons P, Creteur V, Bacq C: Sonography of ankle ligaments. *J Clin Ultrasound* 32:491–499, 2004.
86. Oae K, Takao M, Uchio Y, et al: Evaluation of anterior talofibular ligament injury with stress radiography, ultrasonography and MR imaging. *Skeletal Radiol* 39:41–47, 2010.
87. Campbell DG, Menz A, Isaacs J: Dynamic ankle ultrasonography: a new imaging technique for acute ankle ligament injuries. *Am J Sports Med* 22:855–858, 1994.
88. Mei-Dan O, Kots E, Barchilon V, et al: A dynamic ultrasound examination for the diagnosis of ankle syndesmotic injury in professional athletes: a preliminary study. *Am J Sports Med* 37:1009–1016, 2009.
89. Chen PY, Wang TG, Wang CL: Ultrasonographic examination of the deltoid ligament in bimalleolar equivalent fractures. *Foot Ankle Int* 29:883–886, 2008.
90. Boutry N, Vanderhofstadt A, Peetrons P: Ultrasonography of anterosuperior calcaneal process fracture: report of 2 cases. *J Ultrasound Med* 25:381–385, 2006.
91. Woodward S, Jacobson JA, Femino JE, et al: Sonographic evaluation of Lisfranc ligament injuries. *J Ultrasound Med* 28:351–357, 2009.
92. Wang CL, Shieh JY, Wang TG, et al: Sonographic detection of occult fractures in the foot and ankle. *J Clin Ultrasound* 27:421–425, 1999.
93. Hsu CC, Tsai WC, Chen CP, et al: Ultrasonographic examination for inversion ankle sprains associated with osseous injuries. *Am J Phys Med Rehabil* 85:785–792, 2006.
94. Craig JG, Jacobson JA, Moed BR: Ultrasound of fracture and bone healing. *Radiol Clin North Am* 37:737–751, ix, 1999.
95. Drakonaki EE, Garbi A: Metatarsal stress fracture diagnosed with high-resolution sonography. *J Ultrasound Med* 29:473–476, 2010.
96. Farley FA, Kuhns L, Jacobson JA, et al: Ultrasound examination of ankle injuries in children. *J Pediatr Orthop* 21:604–607, 2001.
97. Quinn TJ, Jacobson JA, Craig JG, et al: Sonography of Morton's neuromas. *AJR Am J Roentgenol* 174:1723–1728, 2000.
98. Redd RA, Peters VJ, Emery SF, et al: Morton neuroma: sonographic evaluation. *Radiology* 171:415–417, 1989.
99. Park HJ, Kim SS, Rho MH, et al: Sonographic appearances of Morton's neuroma: differences from other interdigital soft tissue masses. *Ultrasound Med Biol* 37:1204–1209, 2011.
100. Perini L, Del Borrello M, Cipriano R, et al: Dynamic sonography of the forefoot in Morton's syndrome: correlation with magnetic resonance and surgery. *Radiol Med* 111:897–905, 2006.
101. Nagaoka M, Matsuzaki H: Ultrasonography in tarsal tunnel syndrome. *J Ultrasound Med* 24:1035–1040, 2005.
102. Reynolds DL Jr, Jacobson JA, Inampudi P, et al: Sonographic characteristics of peripheral nerve sheath tumors. *AJR Am J Roentgenol* 182:741–744, 2004.
103. Canella C, Demondion X, Guillin R, et al: Anatomic study of the superficial peroneal nerve using sonography. *AJR Am J Roentgenol* 193:174–179, 2009.
104. Beltran LS, Bencardino J, Ghazikhanian V, et al: Entrapment neuropathies III: lower limb. *Semin Musculoskelet Radiol* 14:501–511, 2010.
105. Tagliafico A, Altafini L, Garello I, et al: Traumatic neuropathies: spectrum of imaging findings and postoperative assessment. *Semin Musculoskelet Radiol* 14:512–522, 2010.
106. Wang Y, Tang J, Luo Y: The value of sonography in diagnosing giant cell tumors of the tendon sheath. *J Ultrasound Med* 26:1333–1340, 2007.
107. Ortega R, Fessell DP, Jacobson JA, et al: Sonography of ankle ganglia with pathologic correlation in 10 pediatric and adult patients. *AJR Am J Roentgenol* 178:1445–1449, 2002.
108. Lee HS, Joo KB, Song HT, et al: Relationship between sonographic and pathologic findings in epidermal inclusion cysts. *J Clin Ultrasound* 29:374–383, 2001.
109. Kim HK, Kim SM, Lee SH, et al: Subcutaneous epidermal inclusion cysts: ultrasound (US) and MR imaging findings. *Skeletal Radiol* 40:1415–1419, 2011.
110. Jin W, Ryu KN, Kim GY, et al: Sonographic findings of ruptured epidermal inclusion cysts in superficial soft tissue: emphasis on shapes, pericystic changes, and pericystic vascularity. *J Ultrasound Med* 27:171–176; quiz 7–8, 2008.

eBOX 8-1 Sample Diagnostic Ankle Ultrasound Report

NORMAL

Examination: Ultrasound of the Right Ankle
Date of Study: March 11, 2011
Patient Name: Jack White
Registration Number: 8675309
History: Pain, evaluate for tendon tear
Findings: No evidence of ankle joint effusion. Anteriorly, the tibialis anterior, extensor hallucis longus, and extensor digitorum longus are normal. Medially, the tibialis posterior, flexor digitorum longus, flexor hallucis longus, tibial nerve, and deltoid ligament are normal. Laterally, the peroneus brevis and longus are normal, as are the anterior talofibular, calcaneofibular ligament, and anterior tibiofibular ligaments. Posteriorly, the Achilles tendon and plantar fascia are normal. Focused ultrasound examination directed by patient symptoms over the lateral ankle revealed no abnormality.
Impression: Unremarkable ultrasound examination of the right ankle. No tendon abnormality.

eBOX 8-2 Sam.ple Diagnostic Ankle Ultrasound Report

ABNORMAL

Examination: Ultrasound of the Right Ankle
Date of Study: March 11, 2011
Patient Name: Jack White
Registration Number: 8675309
History: Pain, evaluate for tendon tear
Findings: There is a small ankle joint effusion. No synovial hypertrophy. Laterally, there is abnormal anechoic fluid and hypoechoic synovial hypertrophy surrounding the peroneal tendons at the level of the distal fibula. A longitudinal tear is seen in the peroneus brevis. The superior peroneal retinaculum is torn at the fibula, and peroneal tendon dislocation occurs with dynamic evaluation in ankle dorsiflexion and eversion. No low-lying peroneus brevis muscle. Otherwise, the anterior talofibular, calcaneofibular ligament, and anterior tibiofibular ligaments.
Anteriorly, the tibialis anterior, extensor hallucis longus, and extensor digitorum longus are normal. Medially, the tibialis posterior, flexor digitorum longus, flexor hallucis longus, tibial nerve, and deltoid ligament are normal.
Posteriorly, the Achilles tendon and plantar fascia are normal. Focused ultrasound examination directed by patient symptoms over the lateral ankle corresponded to the peroneal tendon tear.
Impression:
1. Longitudinal split tear of the peroneus brevis.
2. Superior peroneal retinaculum tear and transient anterolateral dislocation of the peroneal tendons with dynamic imaging.
3. Small ankle joint effusion.

CHAPTER 9

Interventional Techniques

CHAPTER OUTLINE

TECHNICAL CONSIDERATIONS
Needle Guidance Overview
Approach, Transducer and Needle Selection, and Ergonomics
Prepping the Site
Needle Visualization

JOINT PROCEDURES
Shoulder
Elbow
Wrist and Hand
Hip and Pelvis
Knee
Ankle and Foot

BURSAL PROCEDURES
Subacromial-Subdeltoid Bursa
Iliopsoas Bursa
Greater Trochanteric Bursae
Baker Cyst
Other Bursae

TENDON SHEATH PROCEDURES
Biceps Brachii Long Head
De Quervain Tenosynovitis
Iliopsoas
Piriformis

TENDON PROCEDURES
Calcific Tendinosis Lavage and Aspiration
Tendon Fenestration (Tenotomy or Dry Needling)
Platelet-Rich Plasma and Whole Blood Injection

MISCELLANEOUS PROCEDURES
Cyst Aspiration
Peripheral Nerve Block
Biopsy

Additional videos for this topic are available online at www.expertconsult.com.
Examples of interventional ultrasound reports are available online at www.expertconsult.com (see eBox 9-1 and 9-2).

Ultrasound-guided percutaneous procedures have several advantages, including real-time assessment and guidance, in which continuous visualization of a needle is possible throughout the procedure.[1,2] With ultrasound guidance, a needle can be precisely placed in a target while avoiding important structures, such as nerves and blood vessels. This allows very high accuracy and low complication rate, especially compared with blind needle placement. Compared with other imaging-guided techniques like computed tomography (CT), ultrasound is especially effective when a target is superficial. In addition, procedure time is typically reduced compared with CT, and ultrasound is not limited to standard imaging planes. Other intrinsic advantages of ultrasound are not specifically related to intervention but include availability, portability, lack of ionizing radiation, and relatively low cost.

This chapter first reviews technical considerations when performing an ultrasound-guided procedure. This is followed by topics related to joint, bursal, tendon sheath, tendon, and miscellaneous procedures. Because the procedure that is completed using ultrasound guidance can vary widely (diagnostic or therapeutic injection versus aspiration), the ultrasound guidance aspect is emphasized here, rather than the efficacy of the specific procedure.[3,4] Regardless of the procedure, if one can identify the target and the needle with ultrasound, and understand what structures lie in the projected needle path, ultrasound can offer an accurate and safe method for needle guidance for essentially any procedure. Knowledge of anatomy and of normal and abnormal

sonographic findings is essential to accurately identify a target. Of note, the photographs in this chapter that show needle and transducer placement are for illustrative purposes only, in that sterile technique and needles were not used.

TECHNICAL CONSIDERATIONS

Needle Guidance Overview

When performing a percutaneous needle procedure using ultrasound guidance, there are several techniques that can be used. Generally speaking, ultrasound-guided procedures can be separated into indirect and direct approaches. With the indirect approach, ultrasound is used to identify a target and to determine the depth, and then the skin directly overlying the target is marked. The transducer is removed, and the needle is directed perpendicular to the skin into the target. This approach may work for large superficial targets but is significantly limited because the needle is never directly visualized in the target, and real-time assessment during the procedure is not possible. The direct approach is preferred over the indirect approach in that the needle is identified within the target, which ensures a much higher accuracy and lower complication rate.

There are several techniques that may be employed when using the direct approach, including needle guide or freehand techniques. The one option that is not routinely used for musculoskeletal procedures employs a needle guide that is physically attached to the ultrasound transducer. Because most musculoskeletal procedures are relatively superficial, and given the extra steps required when using a needle guide, a freehand approach is favored. When using the freehand direct approach, there are two methods to direct a needle relative to the transducer and sound beam: in plane and out of plane. With the in-plane approach, the needle is directed under the long axis of the transducer and sound beam in plane, and the entire needle, including its tip, is visible at all times during the procedure (Fig. 9-1) (Video 9-1). This enables real-time correction of angle and depth while the needle is advanced. The in-plane approach is the preferred method in most situations because continual visualization of the entire needle, including the needle tip and target, minimizes complications and maximizes accuracy.

With the out-of-plane approach, the needle is passed perpendicular to the transducer so that the needle passes through the plane of the sound beam (Fig. 9-2) (Video 9-2). The disadvantage with this approach is that only a short segment of the needle is seen where the needle passes through the sound beam plane. When using the out-of-plane approach, the needle entrance site is centered over the target, and the needle enters from the side of the transducer (see Fig. 9-12). When inserting the needle, there is some trial and error required as the needle passes through the sound beam, is retracted, and then repeatedly redirected, typically deeper, to eventually get to the target. Another disadvantage is that one cannot determine what segment of the needle is represented on the ultrasound image, the shaft or tip of the needle, because they look exactly the same as a single bright echo with reverberation artifact.

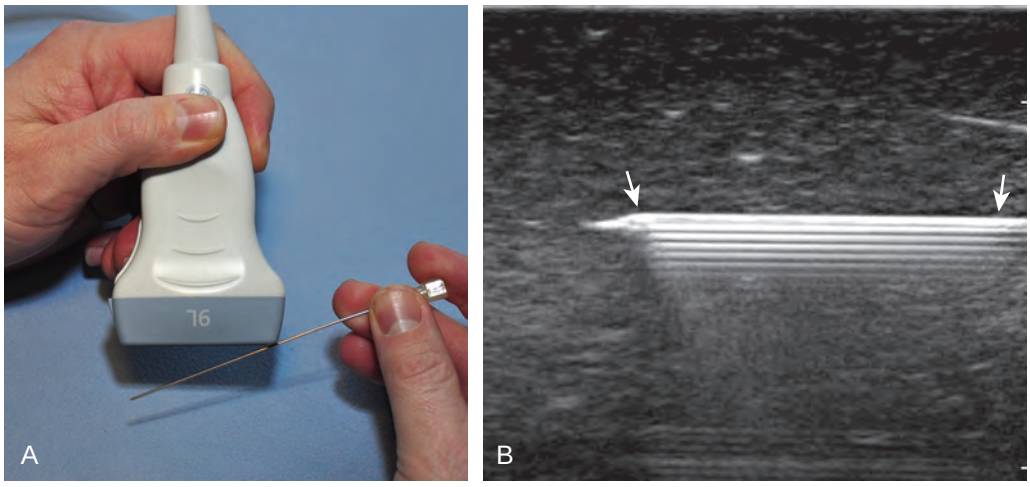

FIGURE 9-1 ■ Needle guidance: in plane. A, Image shows that needle is parallel to the transducer and in plane with sound beam. **B,** Ultrasound image shows needle *(arrows)* in plane with sound beam. Note posterior reverberation artifact when needle is perpendicular to sound beam.

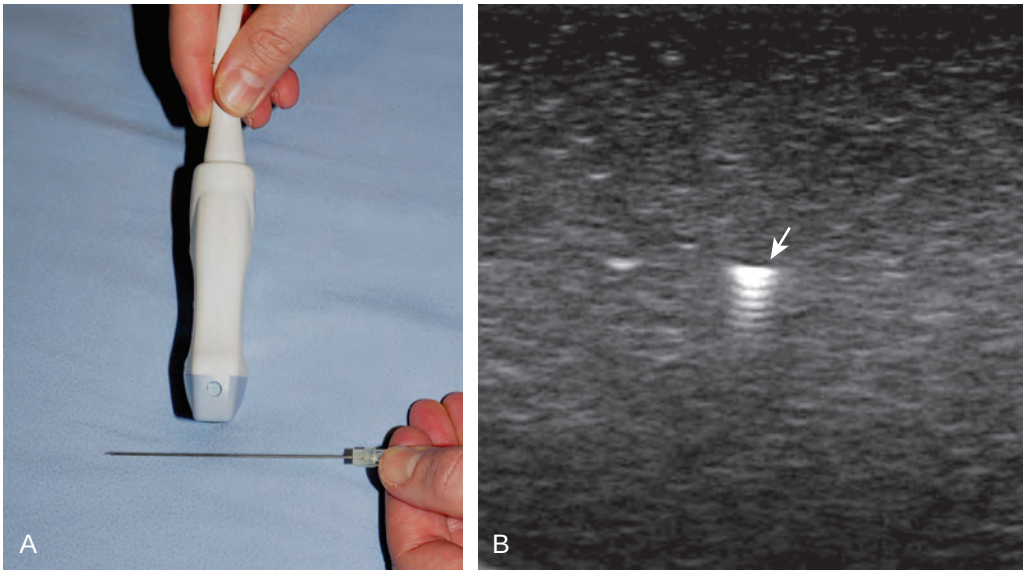

FIGURE 9-2 ■ Needle guidance: out of plane. A, Image shows that needle is 90 degrees to transducer axis or crossing the plane of the sound beam, which results in **(B)** a hyperechoic focus *(arrow)* and reverberation artifact at ultrasound. Note that it is unclear whether **B** shows the needle tip or shaft.

Although the in-plane approach is preferred in most situations, the out-of-plane approach is favored in situations in which the target is very superficial, such as guiding a needle into small joints of the hand and foot. Regardless of the in-plane or out-of-plane approach, once the needle is seen in the target, it is critical that the transducer is turned 90 degrees to confirm accurate location of the needle tip. It is wise to become comfortable with both in-plane and out-of-plane direct methods of needle guidance.

Approach, Transducer and Needle Selection, and Ergonomics

The first step in planning an ultrasound-guided procedure (after performing a limited diagnostic ultrasound) is proper positioning of the patient. I prefer to always have the patient supine when performing any procedure, to avoid the potential for a vasovagal reaction. Next, the generalized needle approach and transducer plane are planned before marking and cleansing the skin. When performing an extremity procedure, there is often a choice between having the needle enter along the flat surface of the extremity or the curved surface. There are several benefits of having the needle enter along the curved surface, including more room to work in the space next to the extremity rather than directly over the flat surface of an extremity. Another advantage is that the puncture site can be an increased distance from the transducer (Fig. 9-3). This is helpful in that the needle can be more perpendicular to the sound beam (and therefore more conspicuous), and in addition the needle is not directly touching the transducer, which comes into play depending on the level of aseptic technique (see later discussion).

Transducer choice should also be considered at this time. In procedures of the extremities involving the elbow, wrist, hand, knee, ankle, and foot, a linear transducer greater than 10 MHz is typically used because the target is usually superficial. A high-frequency transducer provides the highest resolution, and the sound beam projecting in a linear fashion parallel to the transducer face creates an echogenic appearance of the needle (see Fig. 1-1A). A small-footprint transducer is often helpful at the distal extremities; often, a larger footprint transducer does not make contact with the full surface of the skin because of the multiple curvatures of the distal extremities and decreased thickness of soft tissues compared with more proximal joints. An offset to a small-footprint probe (often referred to as a *hockey-stick design*) is not required but is helpful when performing procedures of small parts because the hand holding the transducer is then away from the puncture site, improving visualization at the puncture site (see Fig. 1-1C). When performing procedures of the shoulder and hip, a curvilinear transducer is often selected (see Fig. 1-1B). The benefits of this type of transducer include a larger field of view of deeper structures and a lower frequency, improving sound beam penetration. In addition, the sound beam is emitted in a more

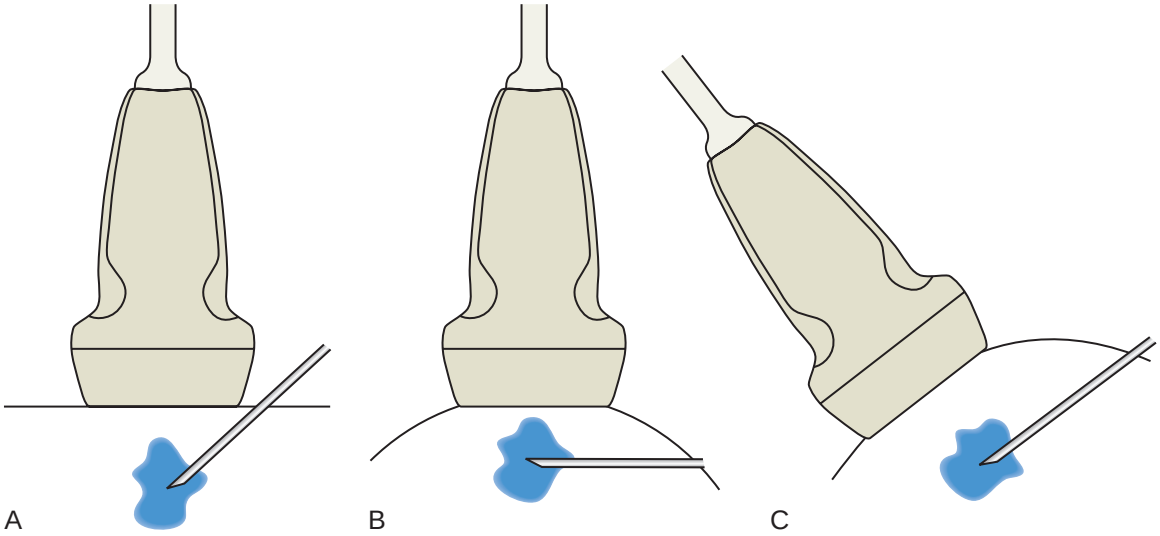

FIGURE 9-3 ■ Needle entry site: flat versus curved surface. Illustrations show **(A)** needle entry over the flat surface of an extremity, which results in oblique orientation of needle relative to sound beam. Needle entry **(B)** over the curved surface allows the puncture site to be farther from the transducer and the needle orientation perpendicular relative to sound beam. A similar arrangement can be obtained **(C)** by moving the transducer away from the puncture site using heel-toe maneuver to deform the overlying soft tissues. (Adapted from illustrations by Carolyn Nowak, Ann Arbor, Mich; http://www.carolyncnowak.com/MedTech.html.)

radial fashion, which helps to improve conspicuity of a needle that is steeply angled to reach a deep target.

With regard to needle selection, I prefer a 20-gauge spinal needle (3.5 inches long) for shoulder and knee procedures, and a 22-gauge needle (either 3.5 or 1.5 inches long) for more distal procedures. Regardless of needle gauge, a stiffer needle is preferred to avoid bending of the needle. Because the goal of the direct in-plane method is to have the needle aligned with the ultrasound beam, a bent needle would not be fully visible in the ultrasound beam. A needle with a stylet may improve conspicuity at ultrasound and will ensure that the needle does not get plugged with tissue as the needle is advanced.

With regard to ergonomics, it is essential that the operator is comfortable during a procedure. I prefer to have the ultrasound monitor directly beyond the patient so that simply looking up from the procedure field will enable full view of the ultrasound image. If this cannot be achieved, the ultrasound monitor should ideally be less than 45 degrees to either side of the patient to minimize turning of the head or spine. A wall-mounted accessory monitor with an adjustable arm is very effective. I also prefer to have a stool on wheels to minimize fatigue and maximize mobility. Typically, the operator's dominant hand should hold the needle, and the other hand should hold the transducer, although it is ideal to develop ambidextrous skills.

Prepping the Site

The first step in the procedure after finding the target, determining the approach, and choosing the transducer is marking the skin. This is completed before cleansing the skin and before sterile conditions. With a direct method of needle guidance, the transducer is placed over the target and the puncture site is determined. A mark is placed at the puncture site (such as an X), and a line is placed at the other end of the transducer to indicate the imaging plane (Fig. 9-4). The use of a surgical marker will help to ensure that the marks are not washed off during cleansing of the skin. If using the indirect method, an opened paperclip passed between the transducer face and the skin can be used to accurately mark the skin directly over a target (Video 9-3).[5]

With regard to sterile technique, the use of a probe cover and preparing a sterile field at the puncture site will minimize the risk of infection. Although sterile preparation of the site can take variable forms, the following represents the procedure used by this author. The operator wears sterile gloves and prepares the site with chlorhexidine solution. Sterile drapes or towels are placed around the puncture site covering the areas not washed with chlorhexidine solution. The puncture site is anesthetized with local anesthetic using a 25-gauge needle. A sterile probe cover kit is opened and placed on the sterile tray (Fig. 9-5A). The sterile operator opens the probe

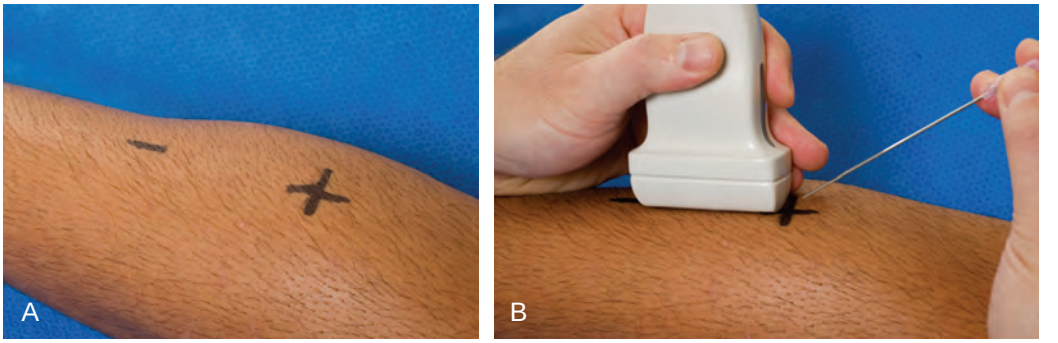

FIGURE 9-4 ■ Skin marking: freehand direct in-plane approach. A and **B,** Photographs show the transducer positioned between the X at site of needle insertion and a line defining the transducer position and imaging plane.

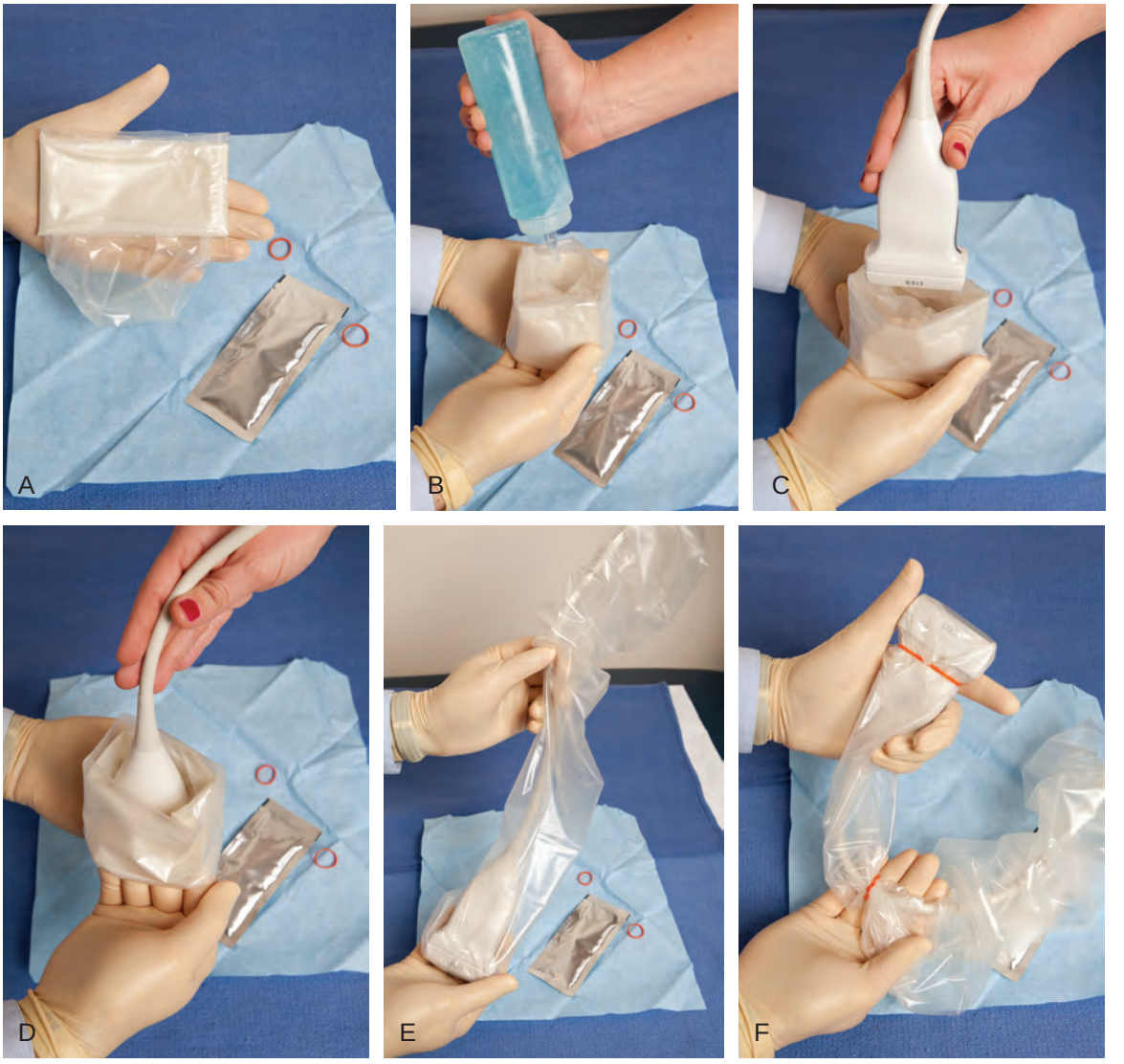

FIGURE 9-5 ■ Sterile probe cover. Photographs show **(A)** sterile probe cover kit with cover, sterile gel, and rubber bands; **(B)** assistant filling insider of cover with nonsterile gel; **(C** and **D)** assistant lowering nonsterile probe into cover; **(E)** extending probe cover over transducer cable; and **(F)** securing with sterile rubber bands.

cover, and an assistant places nonsterile gel in the inside of the probe cover, followed by the transducer (see Fig. 9-5B to D). The operator then extends the probe cover along the transducer cable (see Fig. 9-5E) and secures the cover with sterile rubber bands (included with the probe cover) (see Fig. 9-5F). Sterile gel that is also included in the sterile probe cover kit is opened and deposited on one of the sterile drapes near the puncture site. The transducer in the cover is then dipped into the sterile gel and placed between the X and the line to reconfirm the target. The probe is removed from the site, and the procedure needle enters the skin (about 1 cm) at the puncture site. The transducer is returned to the procedure site to visualize the needle. Of note, the transducer is removed from the procedure site until the needle penetrates the skin to avoid inadvertent puncture of the transducer or transducer cover. With a sterile field placed around the procedure site, the operator can easily set the transducer down on the field while exchanging syringes, minimizing contamination.

Needle Visualization

The first critical rule when performing the in-plane method of needle guidance is that the needle should not be advanced unless it is seen in its entirety; otherwise, the procedure is essentially blind and not image guided. As stated earlier, the procedure is initiated when the needle is placed through the skin at the puncture site about 1 cm. At this point, the transducer is placed over the projected needle path, and the echogenic needle is identified. This is accomplished by translating the transducer side to side over the needle. Because the sound beam is focused, it is not uncommon to have the needle directly under the transducer but not visible on the ultrasound image. Side-to-side translation of the transducer should only be 1 mm at a time so as not to move the transducer away from the needle. It is often helpful to look down at the procedure site to ensure that the needle is indeed beneath and parallel to the transducer plane. Once again, the needle should not be advanced until seen in its entirety. Another basic concept is that the needle and transducer should not be moved at the same time. The transducer is moved to identify the needle, and the needle is then advanced (see Video 9-1). If the needle is no longer visualized during the procedure, needle advancement is stopped, and the transducer is moved as it was before, until the needle is again visualized and fully in plane. The transducer is then fixed in position as the needle is advanced again.

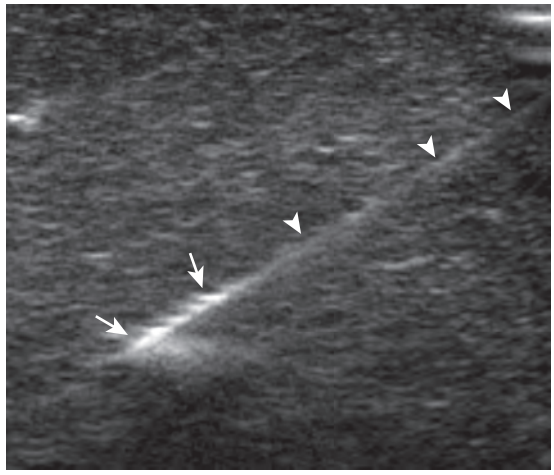

FIGURE 9-6 ■ Echogenic needle tip. Ultrasound image shows needle *(arrowheads)* with increased echogenicity at needle tip *(arrows)*.

There are several options to improve conspicuity of the needle with ultrasound. A larger needle with a stylet may help, but a larger needle is not chosen for this reason. Some manufacturers have a coated or etched needle so that the needle becomes more echogenic (Fig. 9-6).[6] This is helpful when performing a procedure that is deep where the needle angle is steep in order to get to the target. A very helpful option is to "jiggle" the needle while moving the transducer over the projected needle path (Video 9-4). With this maneuver, the needle is moved minimally forward and backward along the needle path, similar to needle movement with an intention tremor, which causes movement of the adjacent soft tissue and can help locate the needle. Of note, the needle in this maneuver is not advanced or moved side to side. Another option is to rotate the needle because the bevel of the needle may produce a more echogenic appearance. The most important technique to improve visualization of the needle is to have the needle as close to perpendicular to the sound beam as possible. Similar to anisotropy of tendons, a needle that is oblique to the sound beam will be less echogenic (Fig. 9-7A), whereas a needle that is perpendicular will be very echogenic with a strong reverberation artifact (see Fig. 9-1B) (Video 9-5). A perpendicular alignment between the sound beam and needle can be accomplished by having the puncture site farther removed from the transducer, which is possible when performing a procedure along the curvature of an extremity (see Fig. 9-3B). Another option is to move the transducer or deform the soft tissues with a heel-toe maneuver (see Fig. 9-3C). Many ultrasound

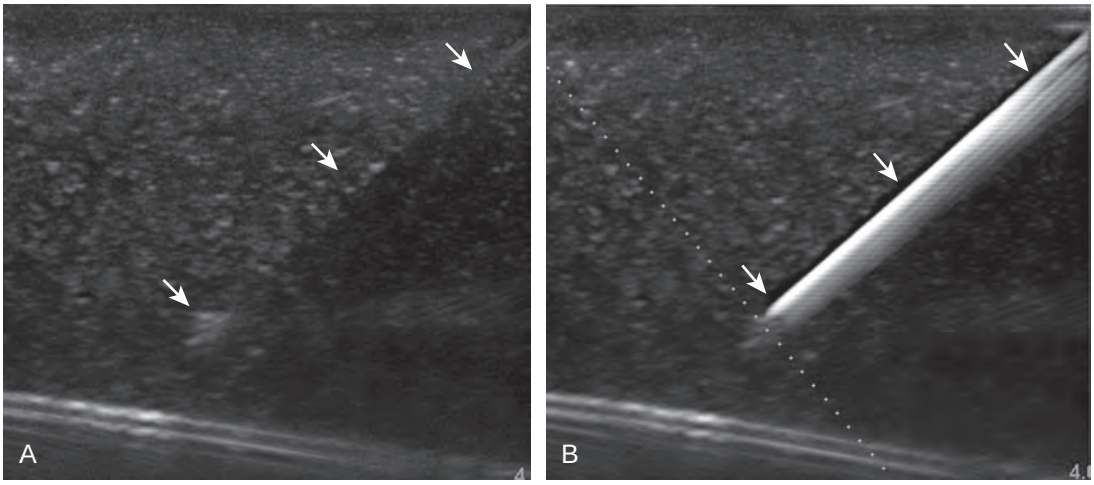

FIGURE 9-7 ■ Needle anisotropy and beam steering. Ultrasound image with needle oblique to sound beam shows **(A)** poor visualization of needle *(arrows)* due to anisotropy. The use of beam steering **(B)** will direct the sound beam perpendicular to needle, eliminating anisotropy and increasing echogenicity of needle *(arrows)*.

machines have the ability to steer the ultrasound beam so that the insonation angle between the needle and the beam is ideally perpendicular to eliminate needle anisotropy (see Fig. 9-7B).

When attempting to align the needle along the long axis of the sound beam, as in the in-plane approach, it is not uncommon to identify only a short segment of the needle. This finding indicates that the transducer alignment and needle are not parallel but instead are crossing each other (Fig. 9-8). The longer the visible segment, the more the needle and sound beam are parallel. To correct this, the transducer should be turned clockwise or counterclockwise. If the segment of needle is increasing in length, the rotation is in the correct direction because the needle and sound beam become more parallel (Video 9-6). On the contrary, if the segment of needle becomes shorter, the transducer is being turned in the wrong direction because less of the needle is in the sound beam path.

JOINT PROCEDURES

Percutaneous joint procedures can include aspiration (for infection or crystal analysis), injection (both diagnostic and therapeutic using anesthetic agents or corticosteroids, or for the purpose of injecting contrast before magnetic resonance imaging [MRI] or CT), or less commonly synovial biopsy. Accuracy of such procedures is improved compared with blind attempt if the needle tip is directly visualized with ultrasound within the target.[4] One key concept is that nearly every synovial joint in the extremity has one

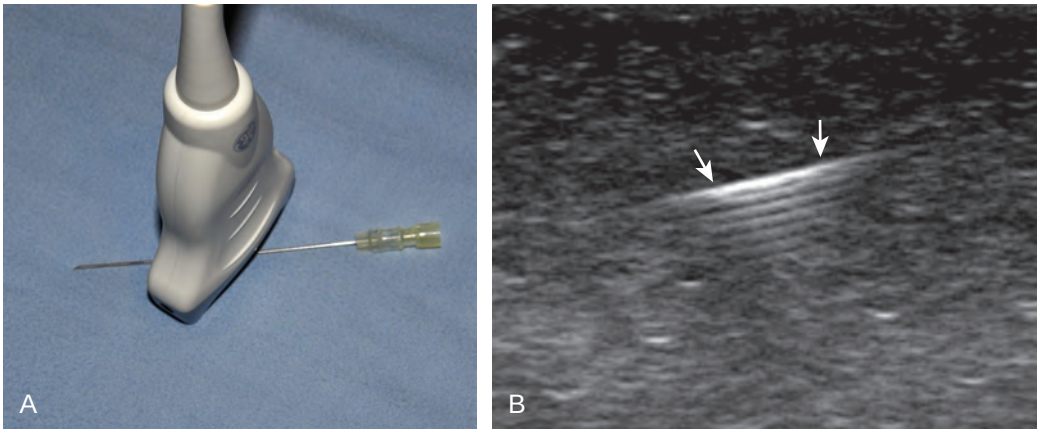

FIGURE 9-8 ■ Oblique needle orientation. Photograph **(A)** shows needle oblique to transducer sound beam producing **(B)** a short segment of the needle *(arrows)* visible at ultrasound.

recess that preferentially distends with joint fluid and is visible at imaging.[7] These recesses directly communicate with their respective joint articulations so that a joint procedure targets these sites rather than the joint articulations, which would potentially harm fibrocartilage and hyaline cartilage. These distinct joint recesses are assessed for joint fluid or synovial hypertrophy and are targeted for the joint procedure.

When accessing a joint recess for a procedure, the specific recess of a joint is assessed. If there is distention of the recess with fluid, that site would be the ideal target. If the recess is not distended, then the site is still targeted, although injection of a collapsed recess is more difficult. In this situation, it is important to confirm intra-articular needle placement before a diagnostic or therapeutic injection. This is accomplished with a test injection of local anesthetic. Uncommonly, if a joint does not have a prominent recess, a needle can be directly advanced into a joint articulation, such as accessing the sacroiliac joint or first carpometacarpal joint. Joint injection can be completed with almost any needle gauge, although I prefer a 20- or 22-gauge needle for stiffness. Joint aspiration should be at least 20 or 22 gauge, with 18—gauge considered if joint fluid is heterogeneous. Synovial biopsies may be completed with soft tissue core biopsy guns, whereas 22-gauge needles with short throw (i.e., 1 cm) are preferred given the small sizes of the various joint recesses (Video 9-7). Biopsies of synovial hypertrophy tend to be reserved to evaluate for atypical infection or synovial proliferative disorders (such as pigmented villonodular synovitis); such biopsies in the setting of a systemic inflammatory arthritis often reveal nonspecific inflammation.

Shoulder

Regarding the shoulder joint, joint effusions accumulate within the biceps brachii tendon sheath because this space openly communicates with the glenohumeral joint (in the absence of biceps brachii long head tenosynovitis). Other glenohumeral joint recesses include the axillary recess, the subscapularis recess, and the posterior glenohumeral joint recess (assessed in external rotation).[8] To access the glenohumeral joint, a posterior approach targeting the posterior glenohumeral recess is preferred (Fig. 9-9).[3,9] The transducer is placed long axis to the infraspinatus tendon, and the needle is advanced in plane from lateral to medial (or medial to lateral) until the needle tip is located at the surface of the humeral head hyaline cartilage (see Video 9-7). The joint recess is wider more medial adjacent to the hyperechoic fibrocartilage labrum, especially with external rotation of the shoulder. The biceps brachii tendon sheath is not typically targeted for glenohumeral joint access because open communication between the biceps sheath and joint may not always be present in the setting of biceps tenosynovitis.

The acromioclavicular joint can be accessed in several different ways. If the joint is distended superiorly, an in-plane needle approach can be used with the transducer in the coronal plane on the body and with the needle entering from lateral to medial (Fig. 9-10) (Video 9-8). Another method is an in-plane approach with the transducer in the sagittal plane and the needle entering from anterior to posterior (Fig. 9-11), although this technique may be difficult if the joint is narrowed. Lastly, an out-of-plane approach may be used with the transducer in the coronal plane on the body (Fig. 9-12). Similarly, the sternoclavicular joint can be approached in plane from lateral to medial or out of plane (Fig. 9-13).

Elbow

For the elbow joint, the most sensitive location to identify a joint effusion by ultrasound is the posterior olecranon recess (in the olecranon fossa) with the elbow flexed, where a joint effusion or synovial process displaces the adjacent hyperechoic fat pad posterior and superior.[10] Needle placement is transverse to the extremity, in plane with the transducer, with the needle advanced from lateral to medial (Fig. 9-14) (Video 9-9). Positioning of the elbow in slight extension prior to needle placement may redistribute the joint fluid more superficially, aiding in aspiration.

Wrist and Hand

With regard to the wrist and hand, the dorsal recesses are the typical accessible targets. There are three wrist joints: distal radioulnar, radiocarpal, and midcarpal. For all three of these joint recesses, I prefer the in-plane approach with the transducer in the axial plane on the body and the needle entering from ulnar or radial along the curvature of the extremity (Fig. 9-15) (Video 9-10). Aspiration of the small joints of the hand can be more difficult, although the dorsal recesses are usually targeted. To access the dorsal recesses, either an in-plane (Fig. 9-16) or out-of-plane approach (Fig. 9-17) is effective, with the needle entering into the actual joint space with the latter.[11] It is important to avoid the overlying tendon in the sagittal plane and the neurovascular structures at the medial and lateral aspects, so a parasagittal approach is ideal.

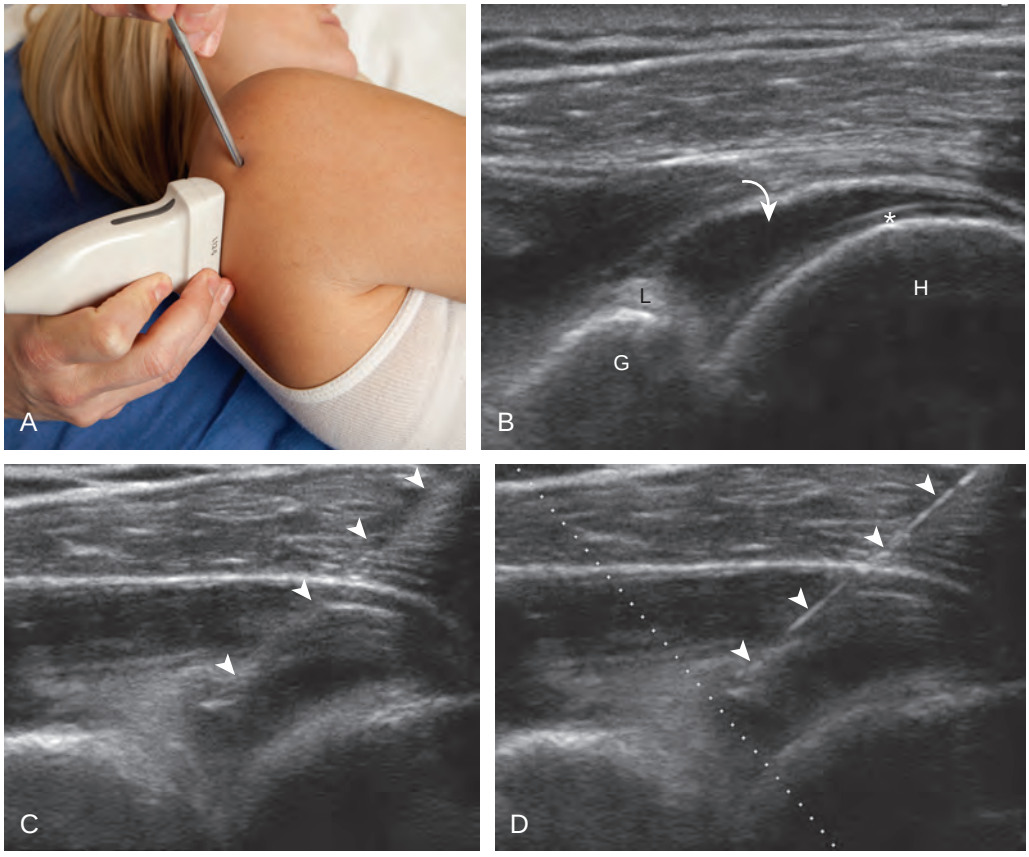

FIGURE 9-9 ■ Shoulder joint aspiration: in-plane lateral approach (Infection). Photograph **(A)** shows transducer and needle position for simulated posterior glenohumeral joint recess procedure. Ultrasound images show **(B)** anechoic distention of posterior glenohumeral joint recess *(curved arrow)* before aspiration (*asterisk*, hyaline articular cartilage), **(C)** needle placement *(arrowheads)* within joint effusion, with **(D)** improved needle visualization *(arrowheads)* using beam steering. H, humeral head; G, glenoid; L, labrum.

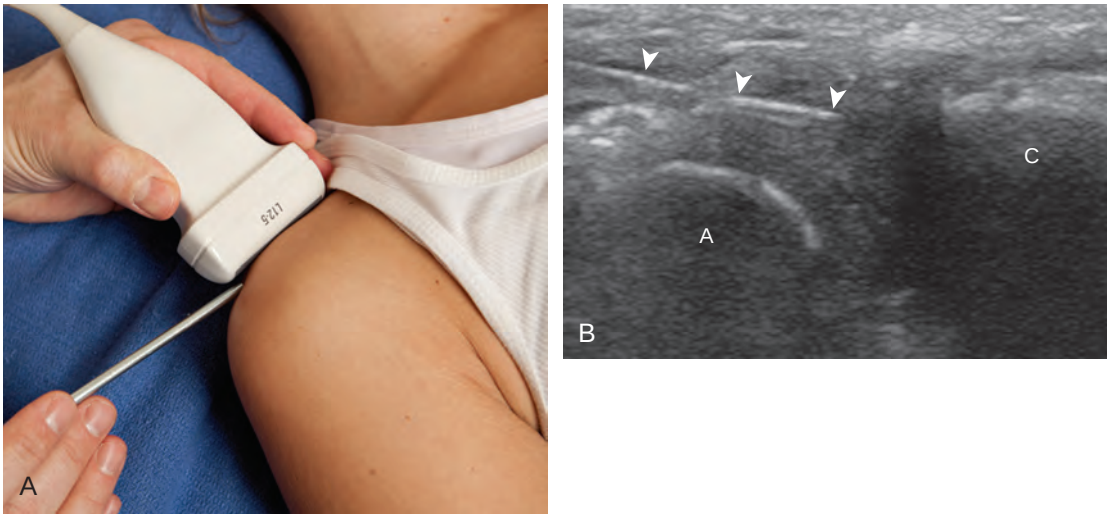

FIGURE 9-10 ■ Acromioclavicular joint: in-plane lateral approach. (A) shows transducer and needle position for simulated acromioclavicular joint procedure. Ultrasound image shows **(B)** needle *(arrowheads)* within acromioclavicular joint. A, acromion; C, clavicle.

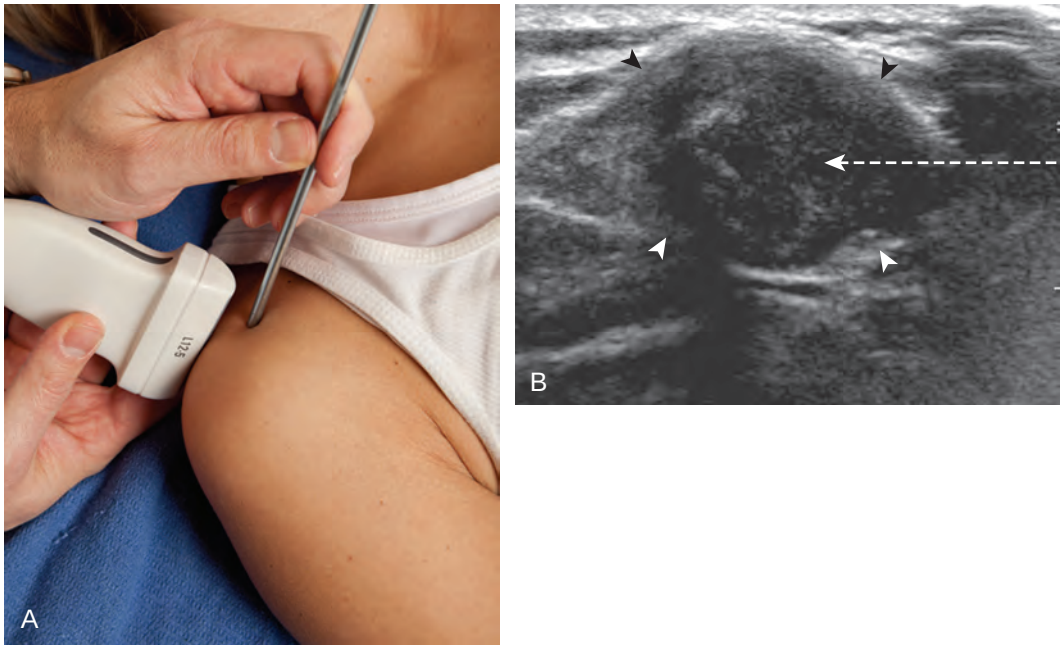

FIGURE 9-11 ■ Acromioclavicular joint: in-plane anterior approach. (A) shows transducer and needle position for simulated acromioclavicular joint procedure. Ultrasound image shows **(B)** proposed location of needle *(dashed arrow)* into acromioclavicular joint *(arrowheads)*.

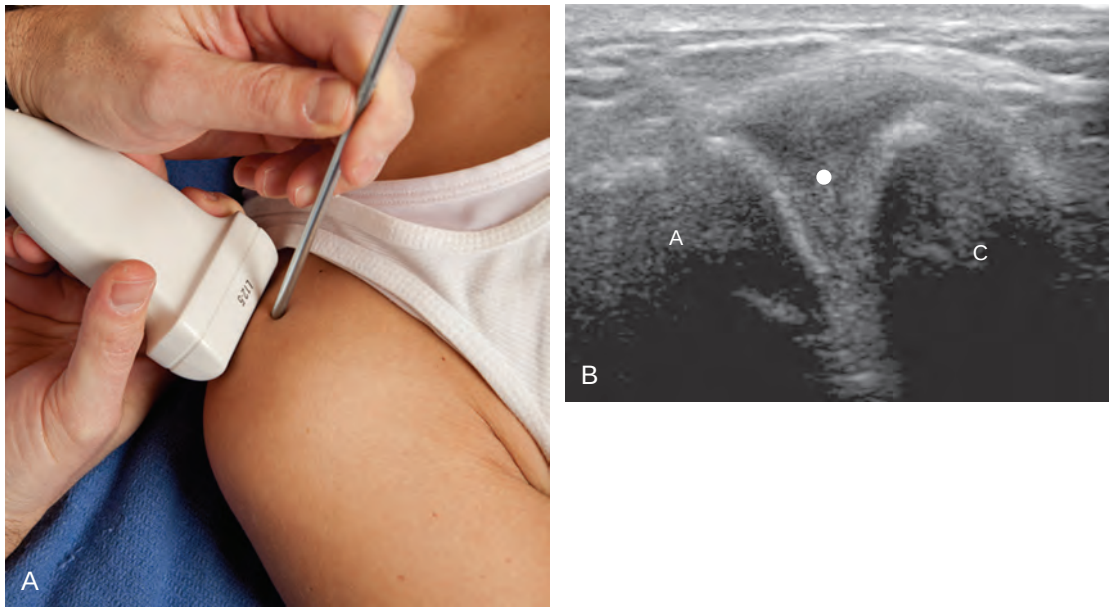

FIGURE 9-12 ■ Acromioclavicular joint: out-of-plane anterior approach. Photograph **(A)** shows transducer and needle position for simulated acromioclavicular joint procedure. Ultrasound image shows **(B)** proposed location of needle *(white circle)* between acromion (A) and clavicle (C).

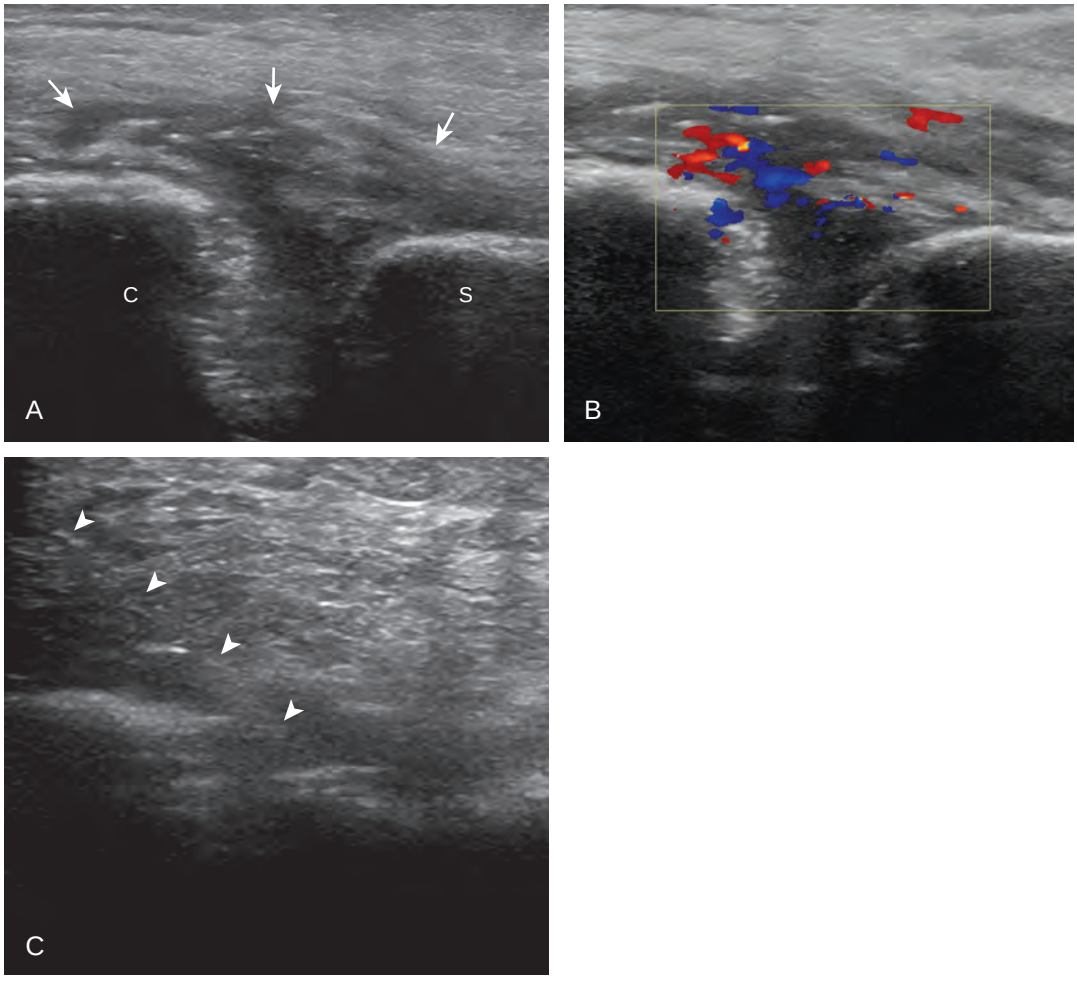

FIGURE 9-13 ■ Sternoclavicular joint aspiration: in-plane lateral approach (Infection). Ultrasound images **(A** to **C)** show hypoechoic distention of the sternoclavicular joint *(arrows)* and hyperemia, with needle aspiration *(arrowheads)*. C, clavicle; S, sternum.

Hip and Pelvis

For the hip joint, the anterior recess overlying the femoral neck is the site for aspiration or injection.[12] I prefer an in-plane approach with the needle entering from inferior to superior along the plane of the femoral neck (sagittal oblique) (Fig. 9-18) (Video 9-11), although an in-plane approach with the needle entering from lateral to medial is an additional technique.[7,13] Because of the depth of the target in many adults, the needle is often quite oblique to the sound beam, which makes the needle less conspicuous. The use of a curvilinear transducer is often helpful. As described earlier, for injecting a collapsed joint recess, it is often helpful to first test inject with local anesthetic to ensure accurate needle position before final injection.[14]

For aspiration or injection of the pubic symphysis, the transducer is placed in the transverse plane, and the needle can enter lateral to medial with an in-plane approach (Fig. 9-19), or an out-of-plane approach may be used.

Ultrasound-guided needle placement into the sacroiliac joint typically is in plane with the transducer in the axial plane on the body, with the needle entering from medial to lateral.[15,16] It is critical not to mistake the adjacent sacral neural foramina, which are just medial to the sacroiliac joints, as the sacroiliac joints (Fig. 9-20). Last, at the superior aspect of the sacroiliac joints where the space between the ilium and sacrum is widened, this is not the true synovial joint articulation, which is located more inferiorly where the joint space is relatively narrow.

Knee

Distention of the knee joint occurs around the patella, most commonly just superolateral to the

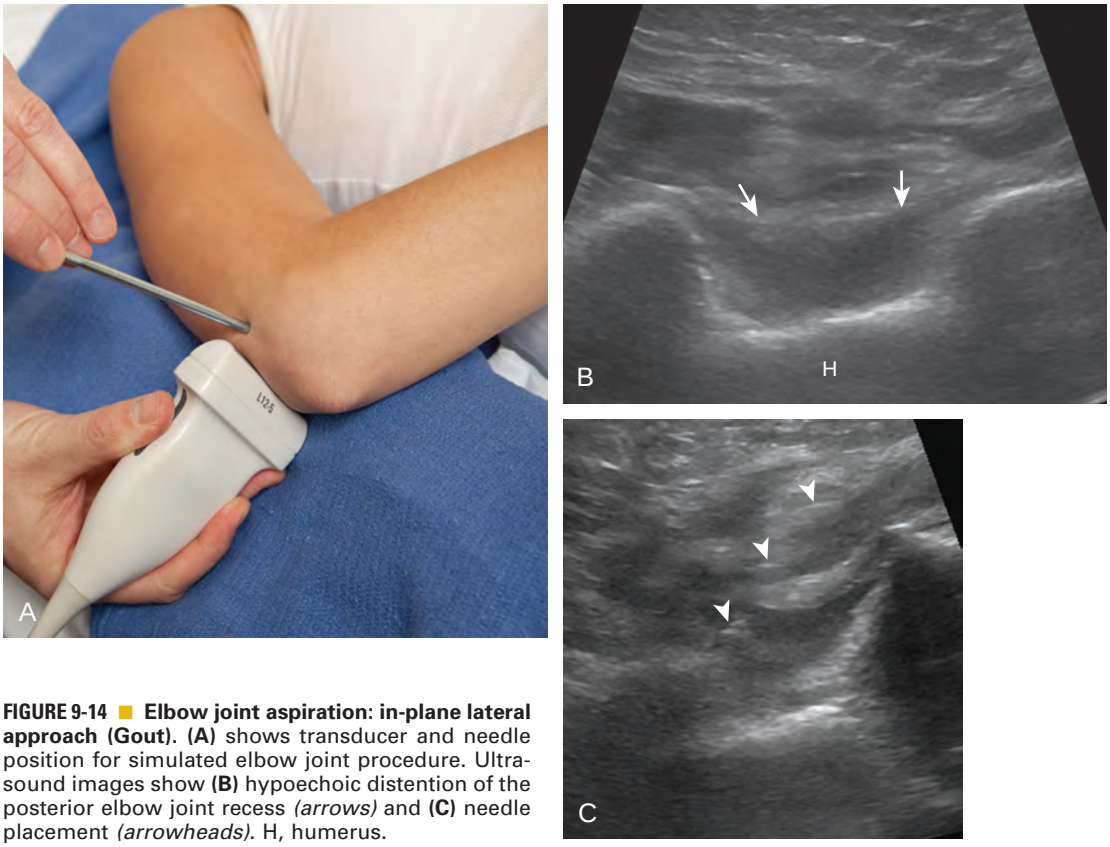

FIGURE 9-14 ■ Elbow joint aspiration: in-plane lateral approach (Gout). (A) shows transducer and needle position for simulated elbow joint procedure. Ultrasound images show **(B)** hypoechoic distention of the posterior elbow joint recess *(arrows)* and **(C)** needle placement *(arrowheads)*. H, humerus.

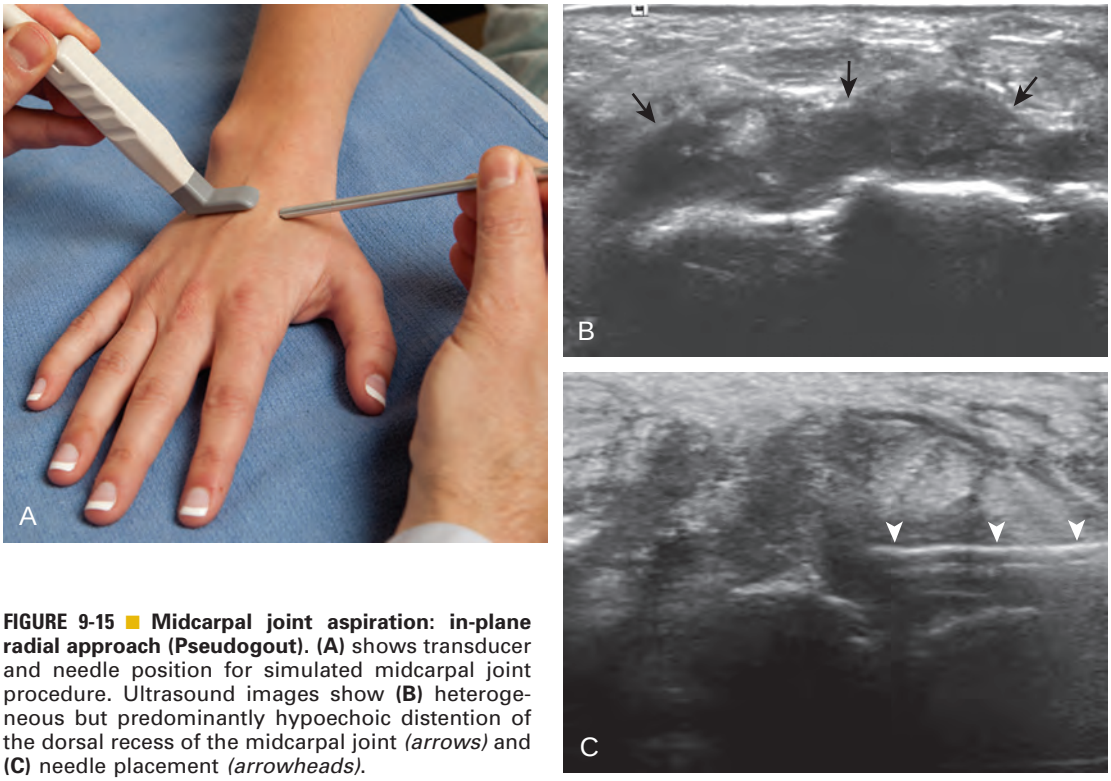

FIGURE 9-15 ■ Midcarpal joint aspiration: in-plane radial approach (Pseudogout). (A) shows transducer and needle position for simulated midcarpal joint procedure. Ultrasound images show **(B)** heterogeneous but predominantly hypoechoic distention of the dorsal recess of the midcarpal joint *(arrows)* and **(C)** needle placement *(arrowheads)*.

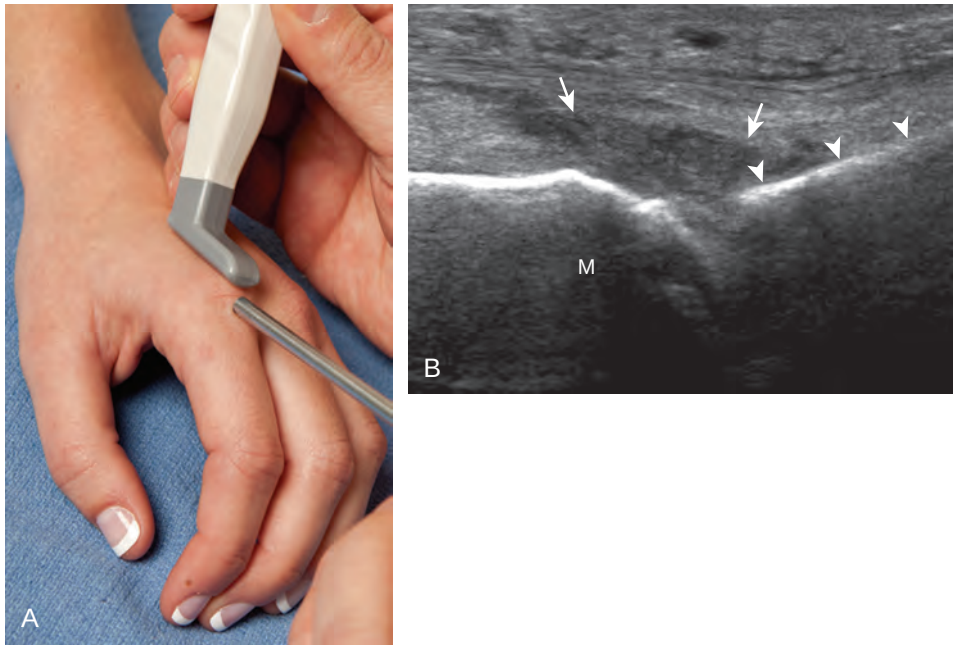

FIGURE 9-16 ■ Metacarpophalangeal joint aspiration: in-plane approach. (A) shows transducer and needle position parasagittal and adjacent to the extensor tendon for simulated metacarpophalangeal joint procedure. Ultrasound image shows **(B)** hypoechoic dorsal recess distention *(arrows)* and needle *(arrowheads)*. M, metacarpal head.

patella. Fluid collects in the suprapatellar recess under the quadriceps with the knee in slight flexion, or medial or lateral to the patella under the retinaculum when the knee is extended.[17] Given this variability, it is important to screen all areas around the patella for joint recess distention. To access the knee joint, I prefer an in-plane approach with the transducer transverse on the body and the needle entering from lateral to medial along the curvature of the extremity, usually targeting the superolateral aspect of the joint recess (Fig. 9-21) (Video 9-12) .[18] To access

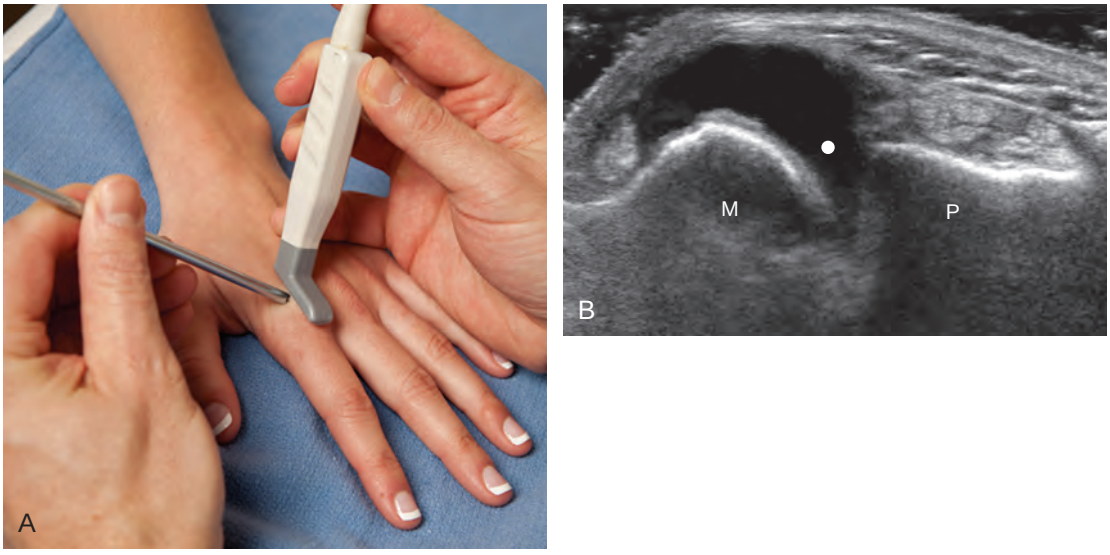

FIGURE 9-17 ■ Metacarpophalangeal joint: out-of-plane approach. (A) shows transducer and needle position for simulated metacarpophalangeal joint procedure. Ultrasound image shows **(B)** proposed location of needle *(white circle)*. M, metacarpal head; P, proximal phalanx.

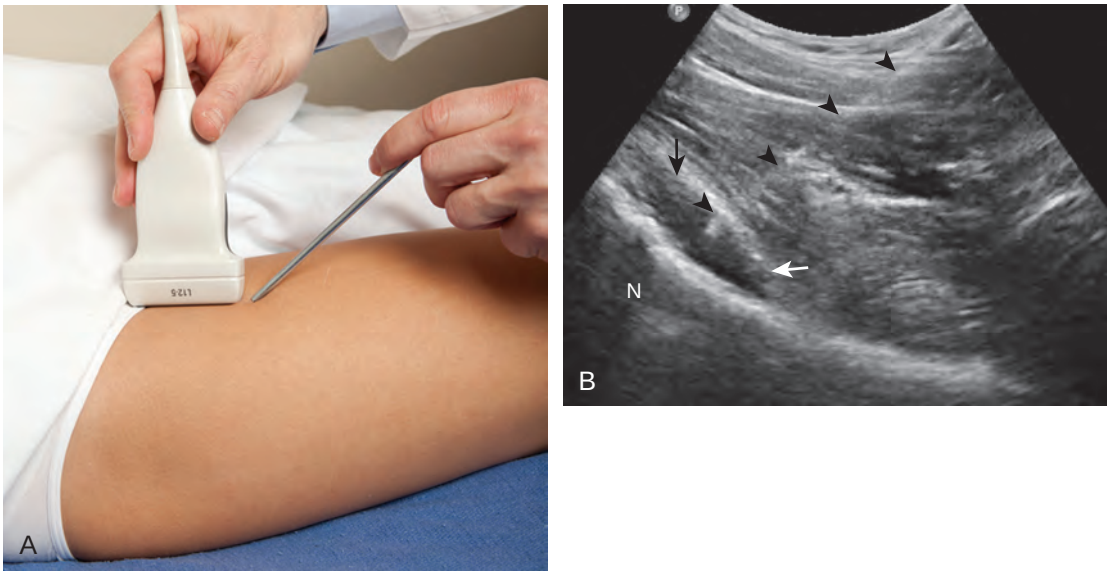

FIGURE 9-18 ■ Hip joint aspiration: in-plane inferior approach (infection). (A) shows transducer and needle position for simulated hip joint procedure. Ultrasound image shows **(B)** needle placement *(arrowheads)* within the anechoic distended anterior hip joint recess *(arrows)*. N, femoral neck.

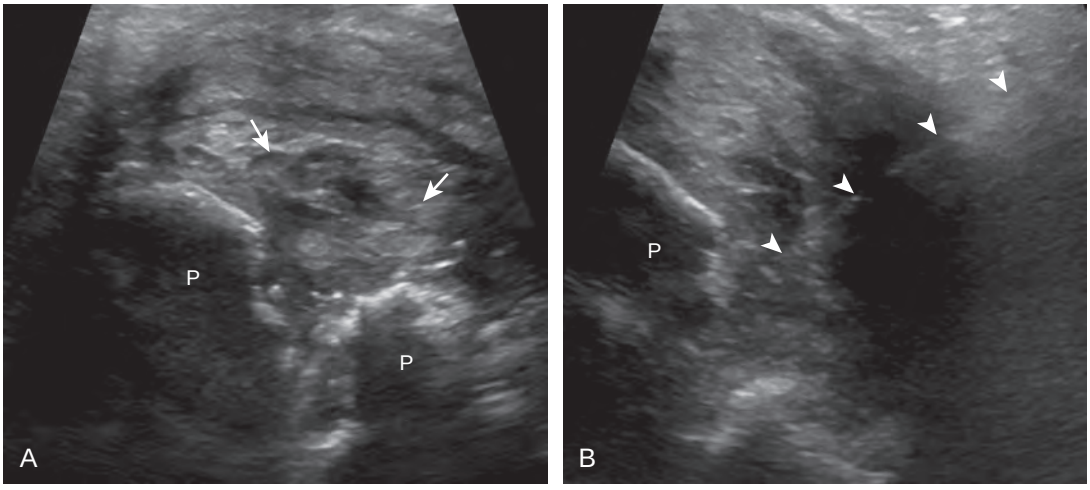

FIGURE 9-19 ■ Symphysis pubis aspiration: in-plane lateral approach (infection). Ultrasound images show **(A)** heterogeneous but predominantly hypoechoic distention of the pubic symphysis joint recess *(arrows)* and **(B)** needle placement *(arrowheads)*. Note erosions of pubis (P).

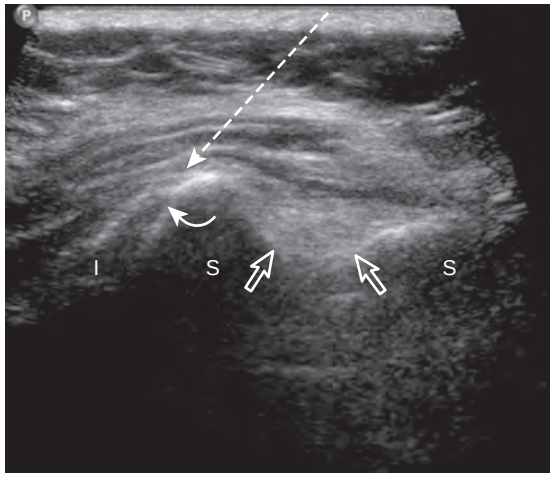

FIGURE 9-20 ■ Sacroiliac joint: in-plane midline approach. Ultrasound image shows proposed location of needle *(dashed arrow)* to sacroiliac joint *(curved arrow)* (right side of image is midline). Note sacral neural foramen *(open arrows)*. I, ilium; S, sacrum.

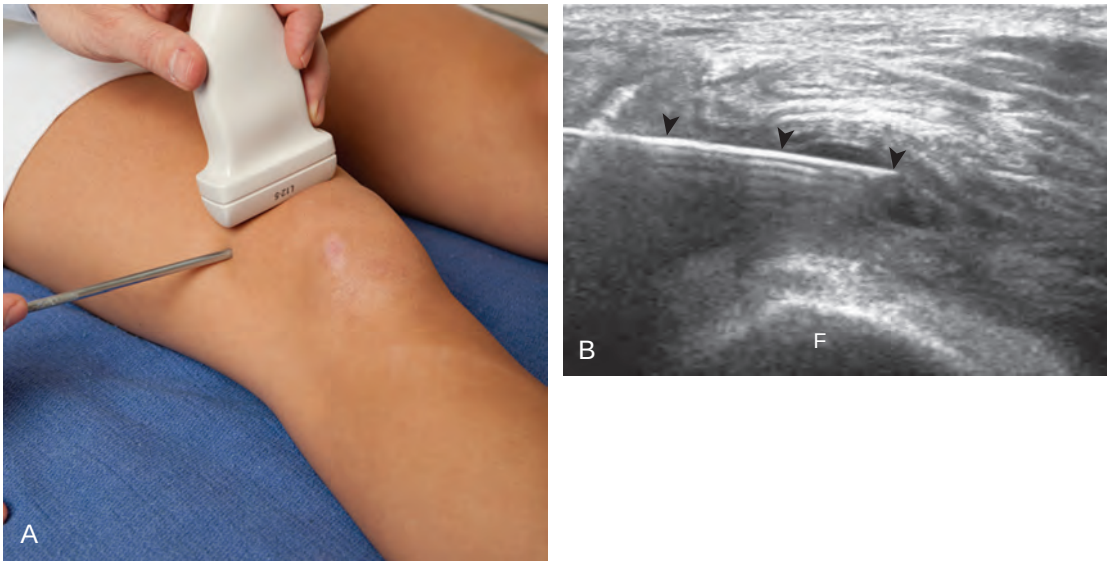

FIGURE 9-21 ■ Knee joint aspiration: in-plane lateral approach. (A) shows transducer and needle position for simulated knee joint procedure. Ultrasound image shows **(B)** needle placement *(arrowheads)* within the anechoic distended knee joint recess. F, femur.

the proximal tibiofibular joint, the transducer is placed in the transverse plane on the body over the anterior aspect of the joint, and an out-of-plane approach is used (Fig. 9-22) (Video 9-13).[19]

Ankle and Foot

For the ankle joint, the anterior recess is accessed for aspiration or injection. There are two different approaches to consider. The first is an in-plane approach with the transducer in the sagittal plane on the body and the needle entering from inferior to superior, usually between the tibialis anterior and extensor hallucis longus tendons (Fig. 9-23).[20] The other approach is an in-plane approach with the transducer transverse on the body and the needle entering from medial to lateral beneath the tibialis anterior tendon and dorsalis pedis artery (Fig. 9-24) (Video 9-14). For the subtalar joint, there are several approaches that can be considered, including anterolateral (Fig. 9-25), posterolateral, and posteromedial.[21] For the metatarsophalangeal and interphalangeal joints, an in-plane (Fig. 9-26) (Video 9-15) or out-of-plane (Fig. 9-27) approach can access the dorsal

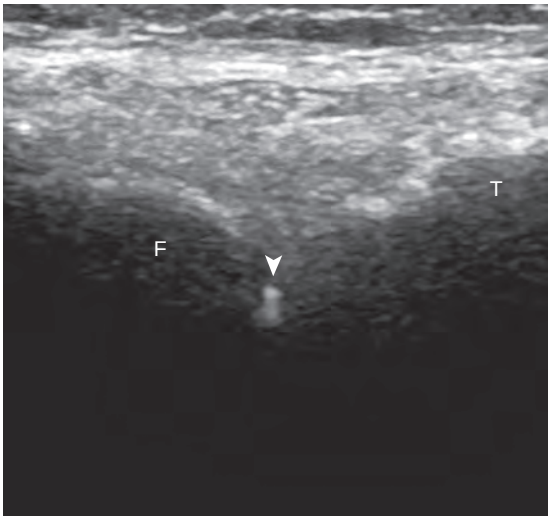

FIGURE 9-22 ■ Proximal tibiofibular joint injection: out-of-plane approach. Ultrasound image shows needle *(arrowhead)* with posterior reverberation artifact within tibiofibular joint. F, fibula; T, tibia.

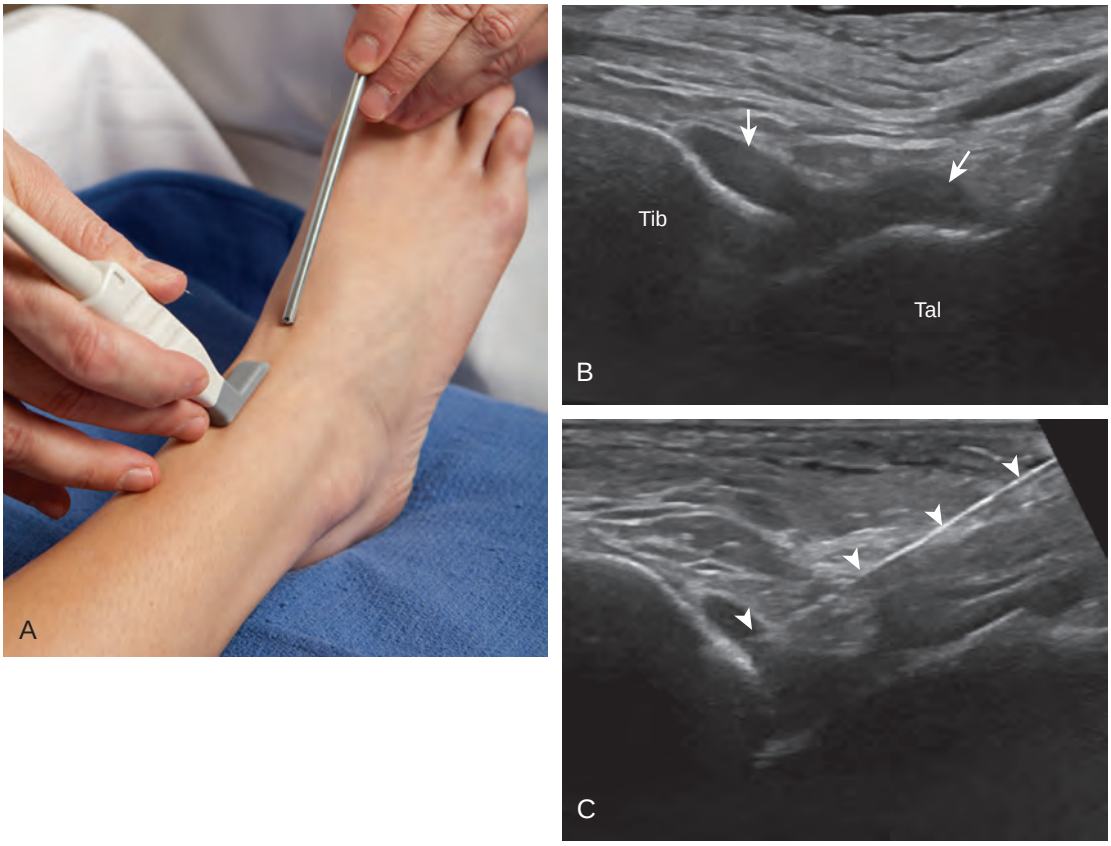

FIGURE 9-23 ■ Ankle joint aspiration: in-plane anterior approach. (A) shows transducer and needle position for simulated ankle joint procedure. Ultrasound images show **(B)** hypoechoic distention of the anterior ankle joint recess *(arrows)* and **(C)** needle placement *(arrowheads)*. Tal, talus; Tib, tibia.

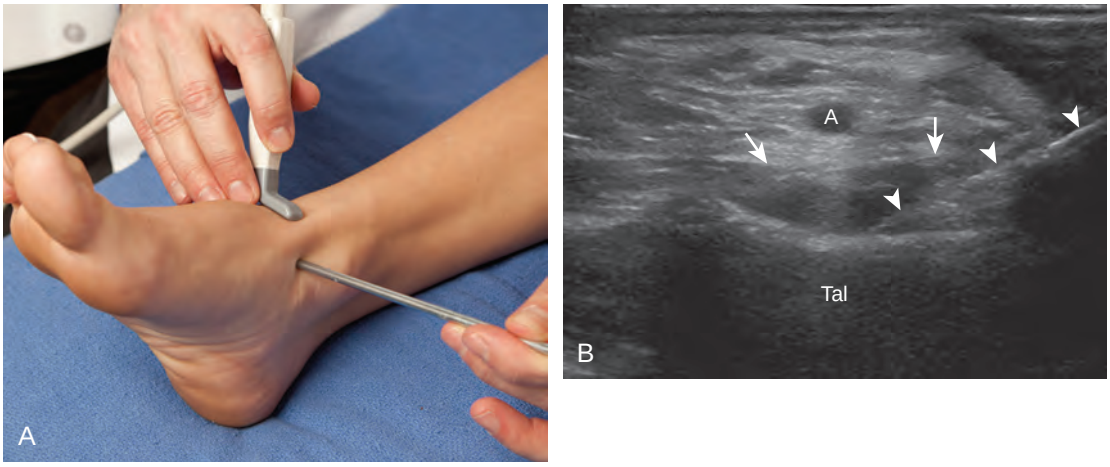

FIGURE 9-24 ■ Ankle joint aspiration: in-plane medial approach. (A) shows transducer and needle position for simulated ankle joint procedure. Ultrasound image shows **(B)** hypoechoic distention of the anterior ankle joint recess *(arrows)* and needle placement *(arrowheads)*. A, dorsalis pedis artery; Tal, talus.

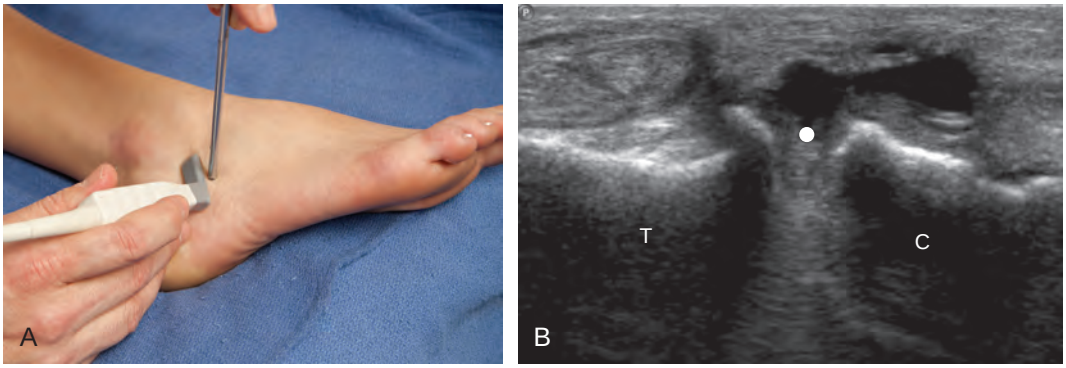

FIGURE 9-25 ■ Posterior subtalar joint: anterolateral out-of-plane approach. (A) shows transducer and needle position for simulated posterior subtalar joint procedure. Ultrasound image shows **(B)** proposed location of needle *(white circle)*. C, calcaneus; T, talus.

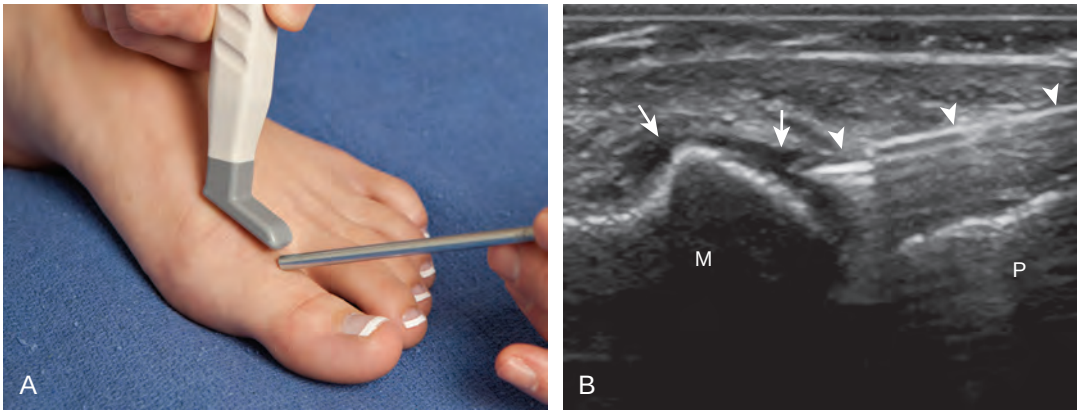

FIGURE 9-26 ■ Metatarsophalangeal joint aspiration: in plane approach. (A) shows transducer and needle position parasagittal and adjacent to the extensor tendon for simulated metatarsophalangeal joint procedure. Ultrasound image shows **(B)** hypoechoic dorsal recess distention *(arrows)* and needle *(arrowheads)*. M, metatarsal head; P, proximal phalanx.

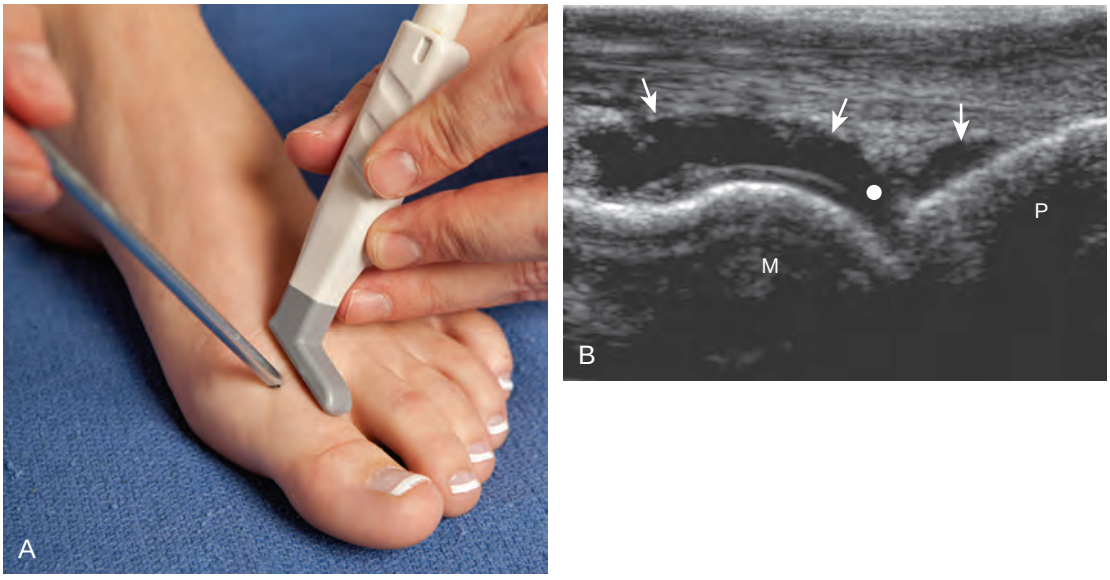

FIGURE 9-27 ■ Metatarsophalangeal joint: out-of-plane approach. (A) shows transducer and needle position for simulated metatarsophalangeal joint procedure. Ultrasound image shows **(B)** anechoic distention of dorsal joint recess *(arrows)* and proposed location of needle *(white circle)*. M, metatarsal head; P, proximal phalanx.

recesses or joint articulations, similar to what was described for the hand.

BURSAL PROCEDURES

Bursal injection or aspiration using ultrasound guidance can be more accurate than a blind attempt when the needle tip is accurately identified within the bursa.[3] Regardless, needle placement within a collapsed bursa is more difficult than within one that is distended with fluid. Before attempting injection into a collapsed bursa, it is important to test-inject with a small amount of local anesthetic to ensure accurate needle placement in the bursa, which will appear as bursal distention with the injection moving away from the needle tip and low resistance to injection. Knowledge of the various bursae around the body allows differentiation between true bursal distention and a nonspecific soft tissue fluid collection. When guiding a needle into a bursa, the bursal wall is often difficult to penetrate, and frequently the needle tents the wall, which may simulate an intrabursal location of the needle tip (see Baker Cyst). True intrabursal location is evident when the needle does not retract on its own and can be easily and freely moved within the bursa. When one anticipates complete aspiration of a bursa, an introducer rather than a standard needle should be considered. With an introducer, the inner stylet is removed after the needle is in the bursa, and the needle end is relatively blunt, which minimizes trauma and potential bleeding as the opposing wall of the bursa collapses down onto the needle tip.

Subacromial-Subdeltoid Bursa

One of the more common bursal injections involves the subacromial-subdeltoid bursa. I prefer the in-plane approach with the transducer in the coronal (Fig. 9-28) or axial plane (Fig. 9-29) on the body and the needle entering from

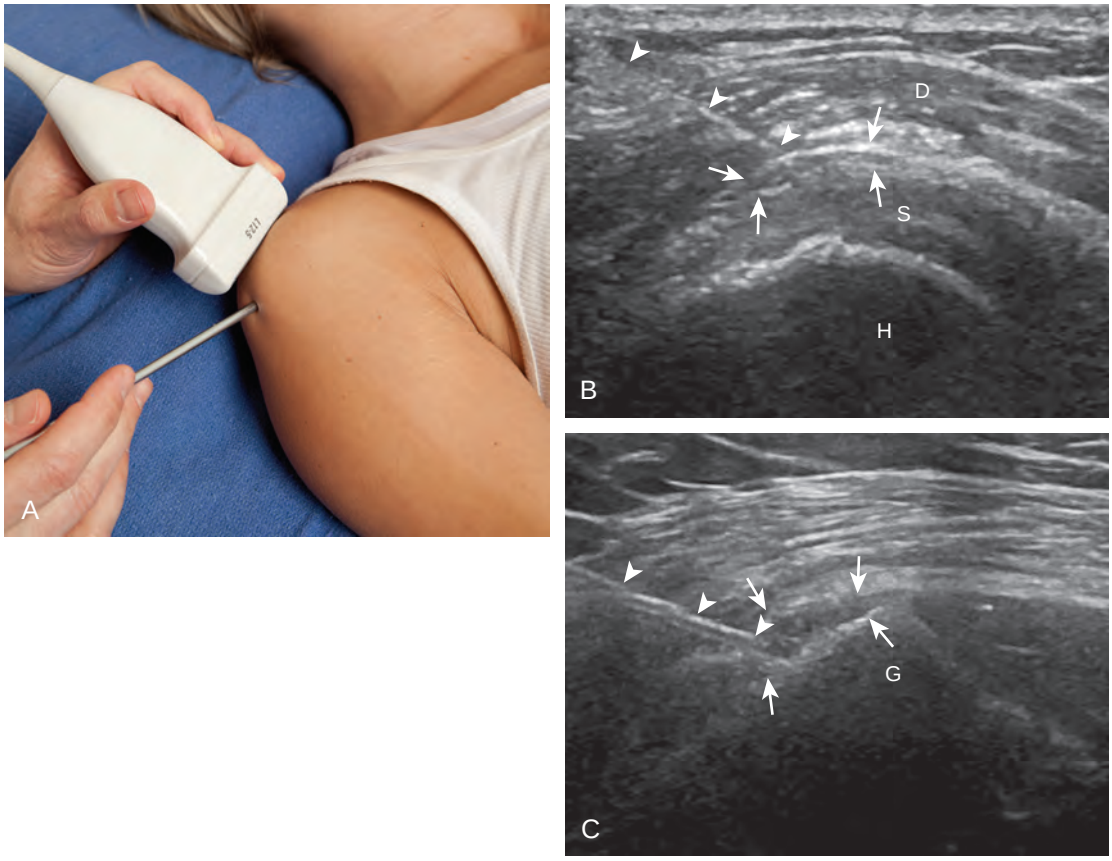

FIGURE 9-28 ■ Subacromial-subdeltoid bursa injection. (A) shows transducer and needle position for simulated subacromial-subdeltoid procedure. Ultrasound image shows **(B)** focal hypoechoic distention of the subacromial-subdeltoid bursa *(arrows)* and needle placement *(arrowheads)*. Ultrasound image from a different patient shows **(C)** needle placement in the subacromial-subdeltoid bursa, which is distended distal to the greater tuberosity (G). D, deltoid; H, humeral head; S, supraspinatus tendon.

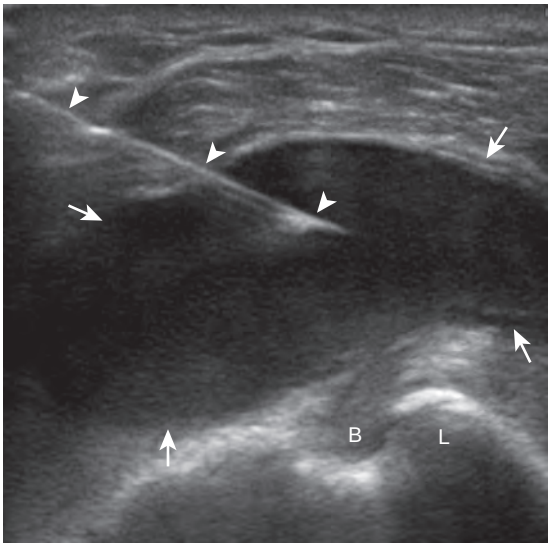

FIGURE 9-29 ■ Subacromial-subdeltoid bursa aspiration. Ultrasound image shows anechoic distention of the subacromial-subdeltoid bursa *(arrows)* and needle placement *(arrowheads)*. B, biceps brachii long head tendon; L, lesser tuberosity.

lateral to medial, targeting the area of the bursa that is distended (Videos 9-16 and 9-17). If the bursa is not distended, the needle is directed superficial to the supraspinatus tendon; a test injection with anesthetic agent is completed to confirm bursal location of the needle before corticosteroid injection (Video 9-18). If the puncture site is several centimeters away from the end of the transducer, then the needle will be more perpendicular to the transducer sound beam, making the needle more conspicuous. The subacromial-subdeltoid bursa extends from under the acromion, over the rotator cuff, and along the cortex of the proximal humerus, where any site of bursal distention can be a target for aspiration or injection (see Fig. 9-28C and Video 9-19).

Iliopsoas Bursa

Another bursa that may be targeted is the iliopsoas bursa.[22] As described in Chapter 6, the iliopsoas bursa is uncommonly distended, and if distended, it usually relates to a hip joint process because of the potential communication between the two synovial spaces. Ultrasound-guided aspiration or injection is typically completed when a distended iliopsoas bursa is identified. For needle placement into the iliopsoas bursa, the transducer is placed parallel to the inguinal ligament just at or superior to the level of the femoral head, and an in-plane approach from lateral to medial is used (Fig. 9-30).

Greater Trochanteric Bursae

There are several bursae around the greater trochanter, the largest being the trochanteric (or subgluteus maximus) bursa, located between the

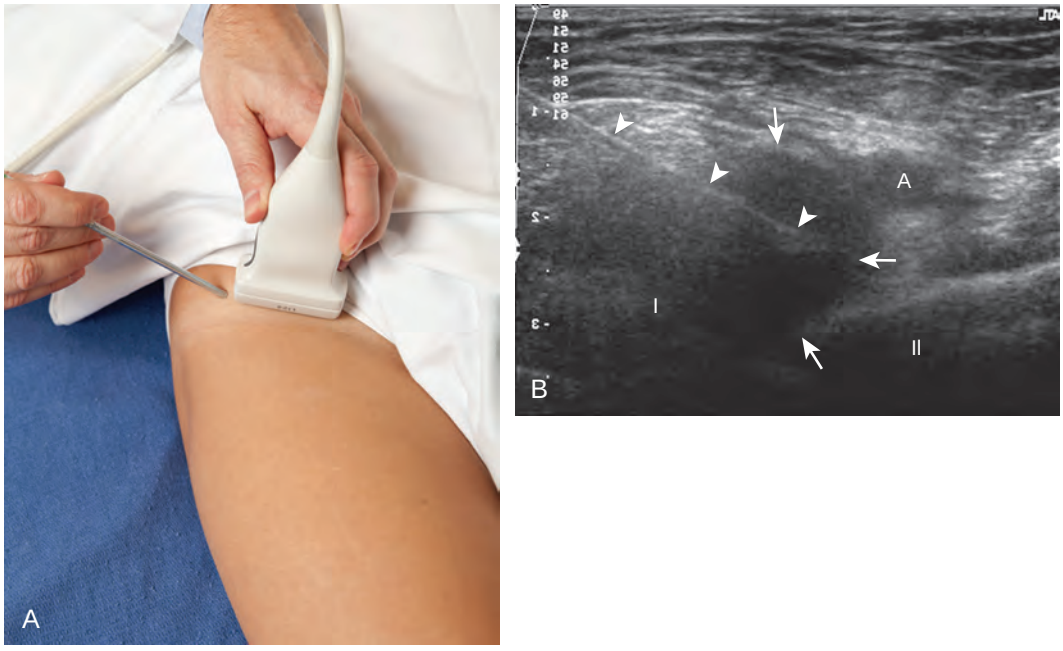

FIGURE 9-30 ■ Iliopsoas bursa aspiration and injection. (A) shows transducer and needle position for simulated iliopsoas bursa procedure. Ultrasound image shows **(B)** hypoechoic iliopsoas bursa distention *(arrows)* medial to iliopsoas (I) and needle *(arrowheads)*. A, external iliac artery; II, ilium.

posterior facet of the greater trochanter and the gluteus maximus, although a distended trochanteric bursa can extend anterior over the gluteus medius tendon.[23] Similar to the iliopsoas bursa, the trochanteric bursa is uncommonly distended and rarely inflamed as an isolated cause of symptoms, but rather is associated with adjacent gluteus tendon abnormalities in the setting of greater trochanteric pain syndrome. To aspirate or inject a distended trochanteric bursa using ultrasound guidance, the patient is rolled decubitus, the transducer is placed in the transverse plane on the body, and the needle is directed in plane with the transducer from posterior to anterior (Fig. 9-31).

Baker Cyst

Another common bursal aspiration is the semimembranosus-medial gastrocnemius bursa, when distended termed a *popliteal* or *Baker cyst.* Injection or aspiration can be completed with the needle in plane with the transducer and the needle either entering from inferior to superior (Fig. 9-32) (Videos 9-20 and 9-21) or from medial or lateral (Fig. 9-33). Because about 50% of Baker cysts communicate to the knee joint in patients older than 50 years, the knee joint should be aspirated first if distended before aspiration and injection of a Baker cyst.[24] Failure to do so can result in immediate re-accumulation of joint fluid within the Baker cyst (see Fig. 9-33C).

Other Bursae

Among the various other bursae throughout the body, those that are very superficial, including the olecranon (Fig. 9-34) and prepatellar bursae (Fig. 9-35), are often aspirated blindly, with ultrasound guidance used only when blind aspiration attempt has failed or bursal injection is required. Virtually any bursae, such as the retrocalcaneal bursa, medial collateral ligament, pes anserinus, and bicipitoradial bursae, to name a few, can be targeted with ultrasound guidance.

TENDON SHEATH PROCEDURES

Ultrasound is also an ideal method to guide tendon sheath injections or aspirations. When performing such procedures, an area of fluid distention of the tendon sheath is an optimal target and preferred over an attempt to place a needle in a collapsed tendon sheath. When attempting injection into a nondistended tendon sheath, it is important to test-inject with a small amount of local anesthetic to ensure accurate placement of

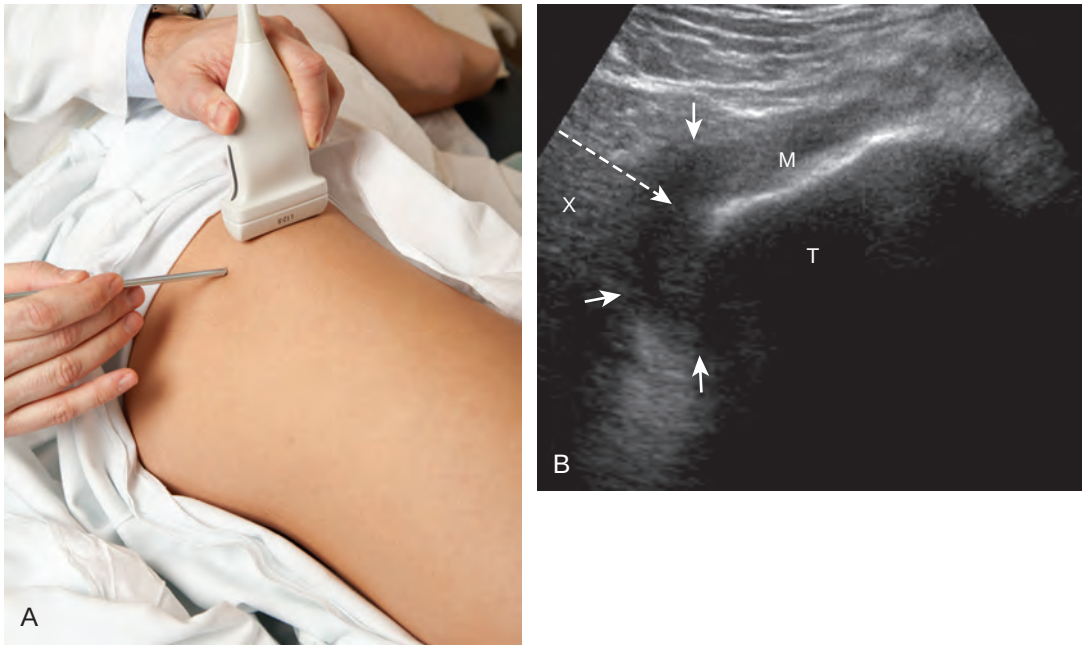

FIGURE 9-31 ■ Trochanteric bursa. (A) shows transducer and needle position for simulated trochanteric bursa procedure. Ultrasound image shows **(B)** hypoechoic distended trochanteric bursa *(arrows)* and proposed location of needle *(dashed arrow)* (left side of image is posterior). M, gluteus medius; T, greater trochanter; X, gluteus maximus.

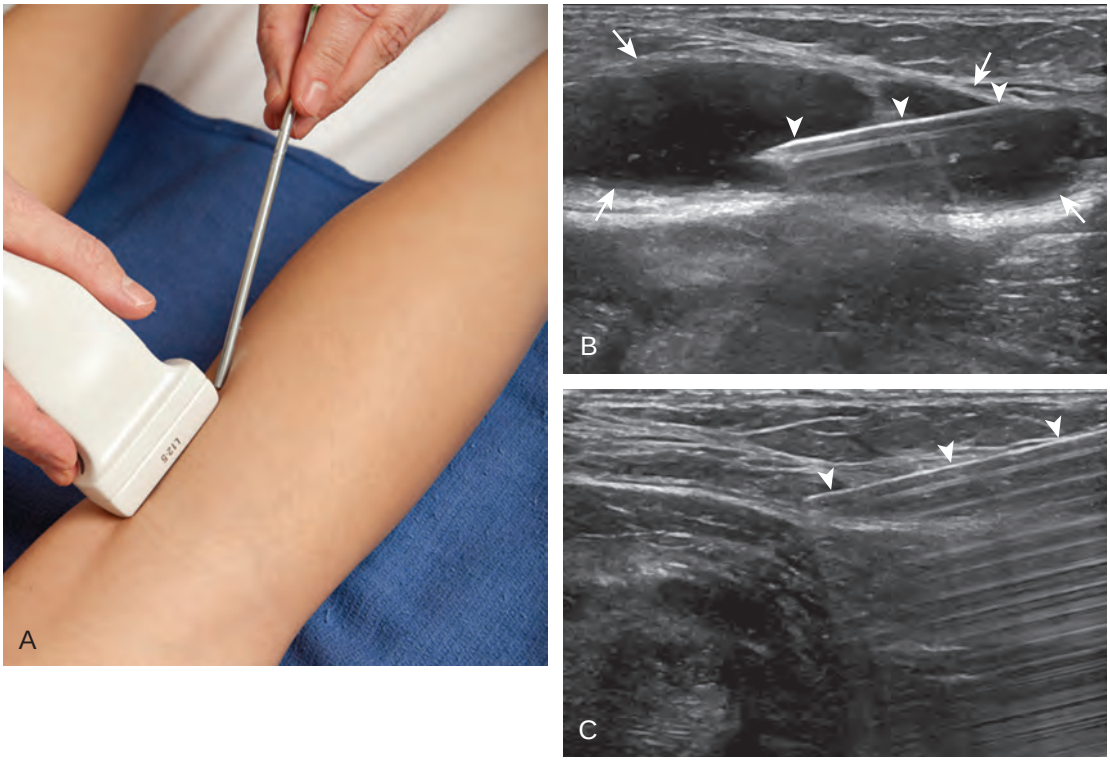

FIGURE 9-32 ■ Baker cyst aspiration: in-plane inferior approach. (A) shows transducer and needle position for simulated Baker cyst procedure (right side of image is distal). Ultrasound images show **(B)** predominantly anechoic distention of a Baker cyst *(arrows)* with needle placement *(arrowheads)* successfully aspirated in **(C)**.

the needle tip where the injection will flow freely away from the needle in the tendon sheath with low resistance.

There are two approaches to guiding a needle into a tendon sheath: short axis and long axis relative to the tendon. I prefer the short axis for several reasons. First, when approaching a tendon sheath in short axis to the tendon, the needle tip can be placed superficial to the tendon, next to the tendon, or deep to the tendon (Fig. 9-36). In long axis, the needle can only be placed superficial to the tendon. The flexibility in using the short axis method enables one to target fluid distention of the tendon sheath that may only be located deep to the tendon. In addition, when injecting corticosteroids, I prefer to inject deep to the tendon rather than superficially, adjacent to the subcutaneous fat, which increases the risk for fat atrophy. The other reason that short axis is ideal is that the needle is typically introduced from lateral to medial over the curvature of the extremity, which allows more room to work as well as a puncture site away from the transducer, decreasing the obliquity of the needle relative to the sound beam and increasing needle conspicuity. When injecting corticosteroids, the needle should be flushed with local anesthetic or saline before withdrawing it to avoid corticosteroid deposition in the subcutaneous tissues, which may cause depigmentation and atrophy.

Biceps Brachii Long Head

The biceps brachii long head tendon sheath is a common injection that is more accurate using ultrasound guidance compared with blind attempt.[25] I prefer an in-plane approach, with the transducer short axis to the tendon and the needle entering from lateral to medial (Fig. 9-37) (Video 9-22). It is important to assess the projected needle path with color Doppler because the anterior circumflex humeral artery and its branches are routinely seen and may be in the needle path (see Fig. 9-37C).

De Quervain Tenosynovitis

Another upper extremity tendon injection site is the first extensor wrist compartment for de Quervain tenosynovitis (Fig. 9-38). I prefer an in-plane

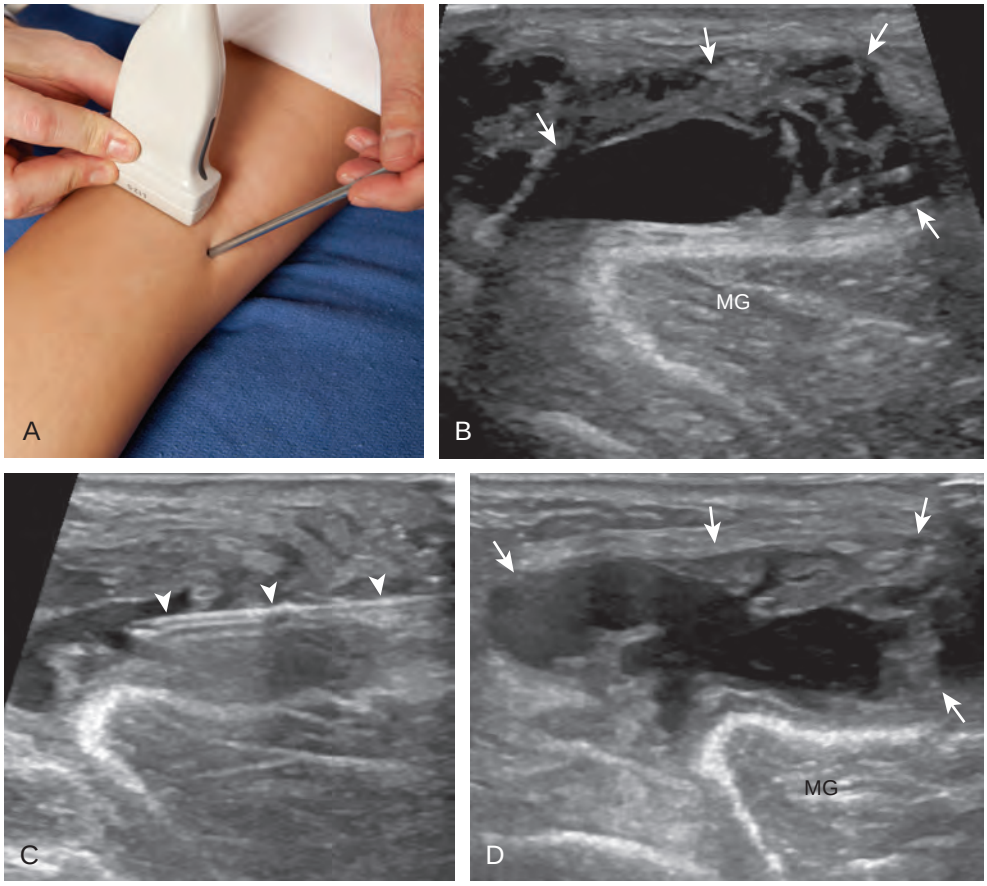

FIGURE 9-33 ■ Baker cyst aspiration: in-plane medial and lateral approach with re-accumulation. (A) shows transducer and needle position using medial approach for simulated Baker cyst procedure. Ultrasound images show **(B)** predominantly anechoic but heterogeneous distention of a Baker cyst *(arrows)* and **(C)** needle placement *(arrowheads)* using lateral approach. After successful and complete aspiration, the patient immediately returned **(D)** because joint was not aspirated first and Baker cyst fluid had re-accumulated from the knee joint. MG, medial head of gastrocnemius.

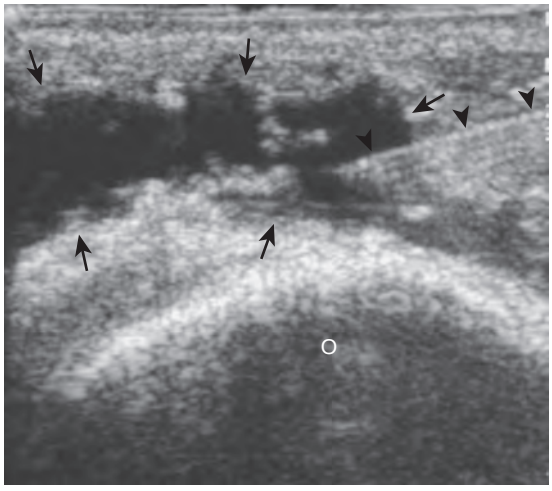

FIGURE 9-34 ■ Olecranon bursa aspiration (aseptic). Ultrasound image over olecranon process (O) shows needle placement *(arrowheads)* within the anechoic distended olecranon bursa *(arrows)*.

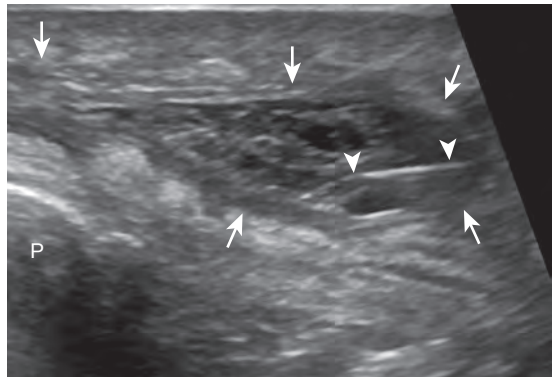

FIGURE 9-35 ■ Prepatellar bursa aspiration (infection). Ultrasound image shows needle placement *(arrowheads)* within the hypoechoic and heterogeneous distended prepatellar bursa *(arrows)*. P, patella.

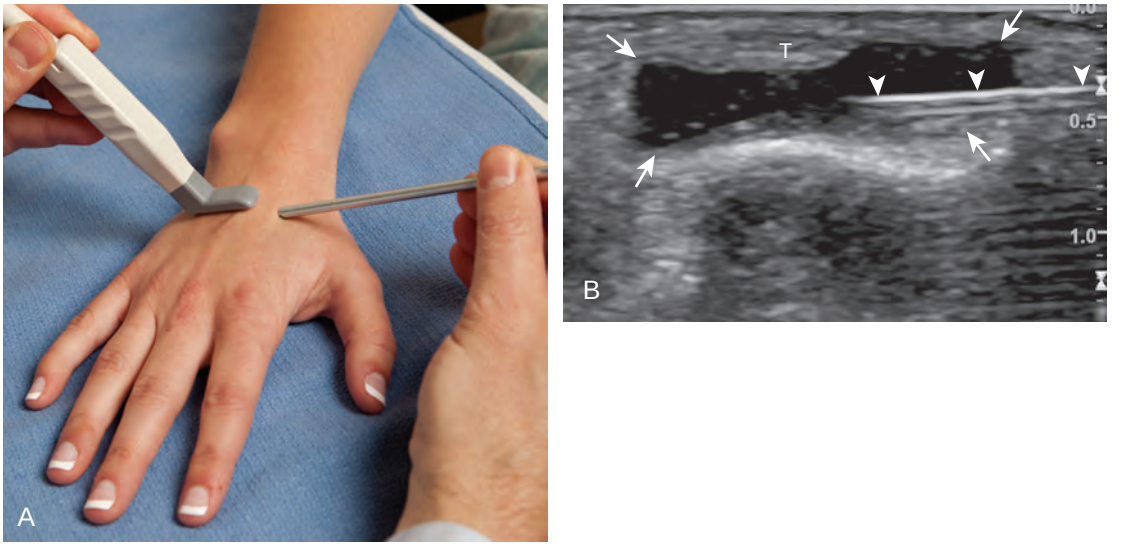

FIGURE 9-36 ■ Extensor digitorum tendon sheath aspiration. (A) shows transducer and needle position for simulated wrist tendon sheath procedure. Ultrasound image shows **(B)** anechoic distention of the tendon sheath *(arrows)*. Note needle placement *(arrowheads)* deep to tendon (T).

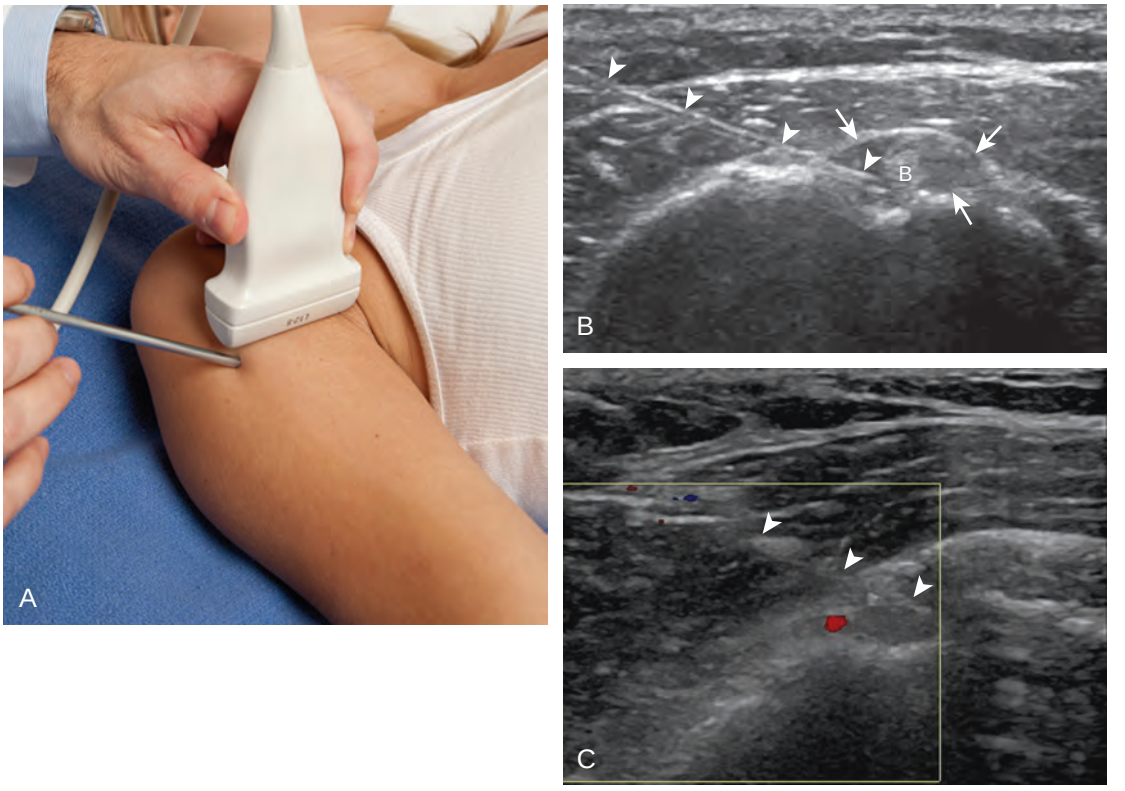

FIGURE 9-37 ■ Biceps brachii long head tendon sheath injection. (A) shows transducer and needle position for simulated biceps brachii long head tendon sheath procedure. Ultrasound images show **(B)** needle placement *(arrowheads)* with hypoechoic distention of tendon sheath *(arrows)* (left side of image is lateral). Note flow in adjacent branch of the anterior circumflex humeral artery in **(C)**. B, long head of biceps brachii tendon.

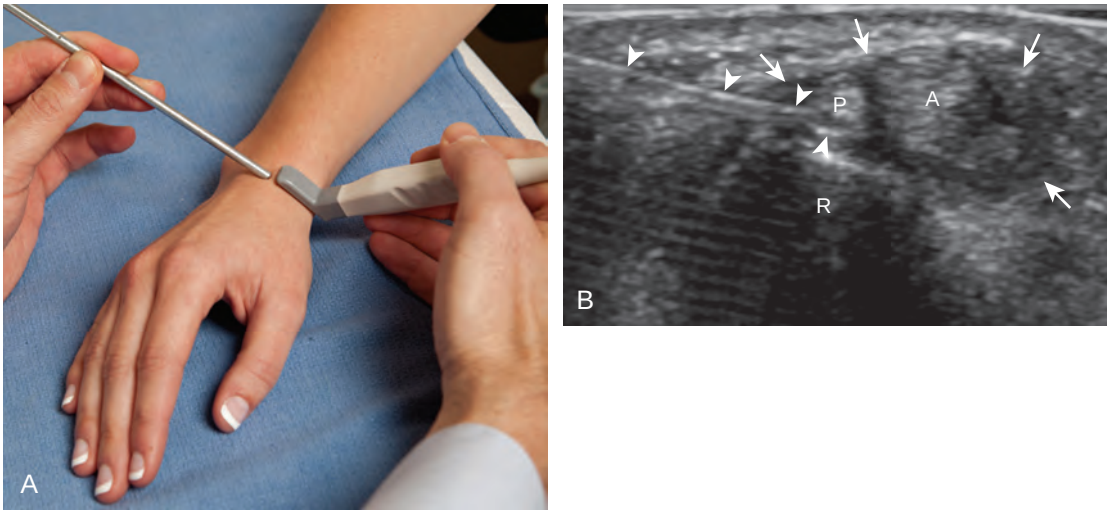

FIGURE 9-38 ■ De Quervain tenosynovitis injection. (A) shows transducer and needle position for simulated first dorsal wrist compartment procedure. Ultrasound image shows **(B)** needle *(arrowheads)* positioned between extensor pollicis brevis tendon (P) and radius (R). Note filling of both extensor pollicis brevis and abductor pollicis longus (A) tendon sheaths *(arrows)*.

approach, with the transducer in short axis to the tendons and the needle entering from ulnar to radial at the dorsal wrist (Video 9-23).[26] The needle is advanced between the extensor pollicis brevis tendon and the adjacent radius for injection. Because subcompartmentalization of the first extensor compartment is frequent, the needle can be advanced deep to the extensor pollicis brevis into the abductor pollicis longus tendon sheath if diffuse filling around each tendon is not noted at the initial injection.[27,28] This is another advantage of the short axis approach for this procedure. Positioning the needle deep to the extensor pollicis brevis also avoids contact with the superficial branch of the radial nerve overlying the tendons and minimizes fat atrophy or depigmentation if corticosteroids leak into the adjacent tissues. As a rule, the needle is typically flushed with local anesthetic after injecting corticosteroids before removing the needle to avoid deposition of corticosteroids along the exiting needle track.

Iliopsoas

Another common peritendon injection involves the iliopsoas.[29] For this procedure, an in-plane approach is used with the transducer in the oblique axial plane (parallel to the inguinal ligament and just superior to the femoral head) and the needle entering from lateral to medial (Fig. 9-39) (Video 9-24). The needle tip is positioned between the tendon and the adjacent ilium, and a test injection with local anesthetic confirms that the needle is not within muscle or tendon before corticosteroid injection. This injection should be completed superior to the femoral head to avoid inadvertent injection into the hip joint. Typically, the injection accumulates between the iliopsoas tendon and the adjacent ilium, lifting the iliopsoas anteriorly (Videos 9-25 and 9-26). Less commonly, the injection may freely flow medial to the iliopsoas tendon with low resistance, which indicates filling of the iliopsoas bursa. Ultrasound-guided injections may also target the iliopsoas as it passes over the acetabular component of a total replacement when symptomatic from impingement.[30]

Piriformis

Ultrasound can guide injection of the piriformis, where it has been reported that the use of ultrasound guidance improves accuracy over fluoroscopic guidance.[31] For this technique, the piriformis is first identified in long axis with the transducer in the oblique-axial plane on the body just inferior to the sacroiliac joint and greater sciatic notch. A curvilinear transducer of frequency lower than 10 MHz helps to ensure depth penetration and a large field of view. Passive internal and external hip rotation during imaging is also helpful in that movement of the piriformis during this maneuver makes it more conspicuous. A needle can then be guided as a peritendon injection, or intramuscular if desired, using an

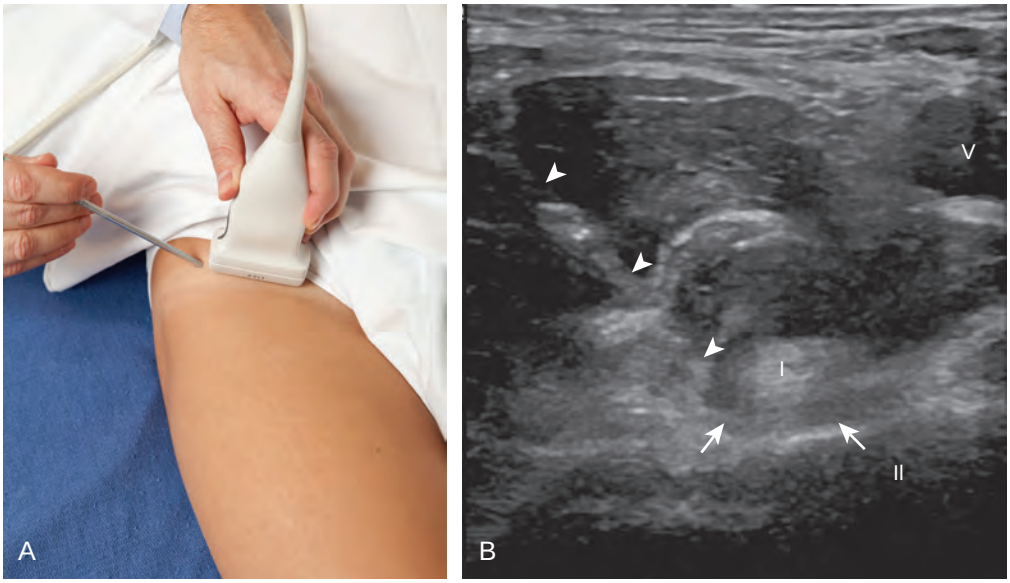

FIGURE 9-39 ■ Iliopsoas peritendon injection. (A) shows transducer and needle position for simulated iliopsoas peritendon procedure. Ultrasound image shows **(B)** needle *(arrowheads)* positioned between the iliopsoas tendon (I) and ilium (II) with hypoechoic injection *(arrows)*. V, external iliac vein.

in-plane approach in long axis to the piriformis from either a lateral or medial approach (Fig. 9-40). If the segment of piriformis over the ilium is targeted, then the ilium can be used as a backstop for safety measures if the needle visualization is difficult. Other peritendon injections around the hip include the gluteus medius tendon at the greater trochanter and the proximal hamstring tendons.[32,33]

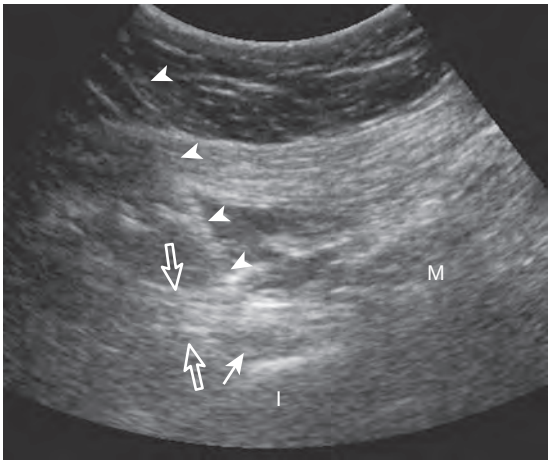

FIGURE 9-40 ■ Piriformis peritendon injection. Ultrasound image shows needle *(arrowheads)* with hypoechoic injection *(arrow)* around piriformis tendon *(open arrows)* (left side of image is lateral). I, ilium; M, piriformis muscle.

TENDON PROCEDURES

Calcific Tendinosis Lavage and Aspiration

Treatment of calcific tendinosis can be carried out with a single puncture of a 20-gauge needle with a stylet using an in-plane approach (Figs. 9-41 and 9-42) (see Video 9-26).[34] The use of a stylet helps to ensure that the needle does not get plugged with calcification while entering the calcific deposit. If the calcification is associated with shadowing, one cannot visualize the needle after it enters into the calcification, so care should be taken not to advance the needle through the other side of the calcification. When the needle is in place within the center of the calcification, the stylet is removed, and a syringe with several millimeters of anesthetic agent is connected to the needle. The procedure begins with lavage of the calcification by injecting minimal anesthetic agent. Typically, the calcification is quite thick, and there will be much resistance to injection. As the plunger is released, the backpressure from inside the calcific deposit will bring the calcifications into the needle. The maneuver of minimal injection with aspiration from spontaneous backpressure is repeated. When there is minimal shadowing, one will see swirling of the calcification and decreasing echogenicity as the calcium is diluted and aspirated (Videos 9-27 and 9-28). During the aspiration, echogenic

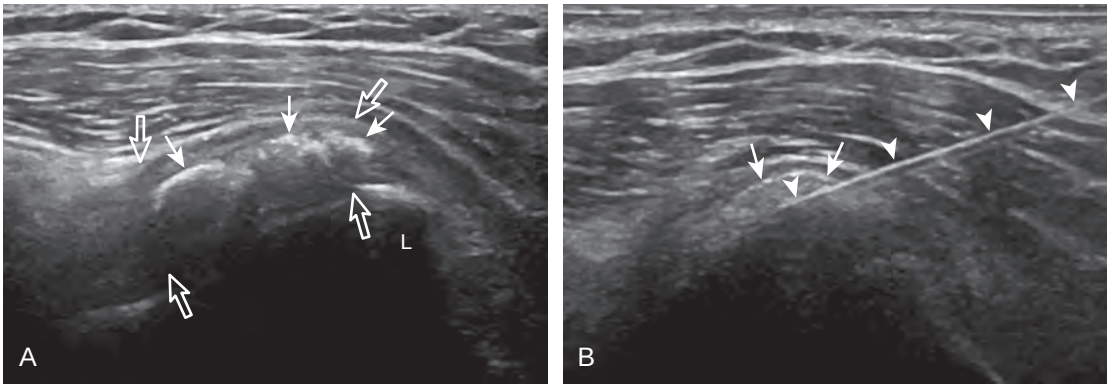

FIGURE 9-41 ■ Calcific tendinosis lavage and aspiration: subscapularis. Ultrasound images long axis to the subscapularis tendon *(open arrows)* show **(A)** echogenic and partially shadowing calcifications *(arrows)*. Note needle placement *(arrowheads)* and decreased shadowing as calcification is aspirated in **B**. L, lesser tuberosity.

calcifications are often seen moving within the needle (Video 9-29). When the syringe becomes slightly opaque from calcification, a new syringe is connected, and the process is repeated. This continues with a third syringe. Positioning of the syringe dependent relative to the targeted tendon calcification will allow the more dependent calcifications to collect in the syringe instead of being reinjected. In the situation in which the original calcification is amorphous without shadowing, the procedure is complete when the calcification decreases in amount or echogenicity and the

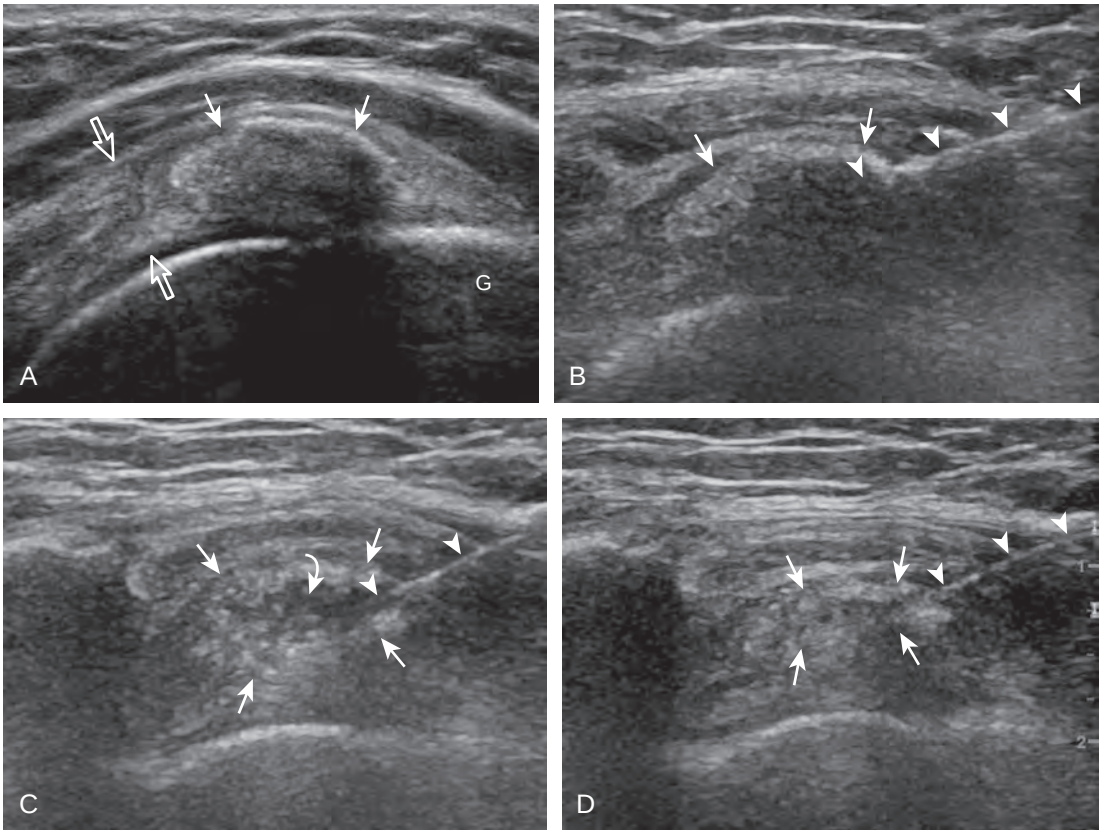

FIGURE 9-42 ■ Calcific tendinosis lavage and aspiration: supraspinatus. Ultrasound images long axis to the supraspinatus tendon *(open arrows)* show **(A)** echogenic and partially shadowing calcification *(arrows)*. Note **(B)** needle placement *(arrowheads)* within calcification. With continued lavage and aspiration, **(C)** the central aspect is more hypoechoic *(curved arrow)* with decreased shadowing and decreased size in **(D)**. G, greater tuberosity.

syringes contain calcification. When the calcification is echogenic with shadowing (usually when more chronic), progressive dilution of the calcification is not visible because of the shadowing, so one relies on visualization of the calcification within the syringes to indicate completion (Video 9-30). In this latter situation, there may be little or no change when comparing the calcification before and after the procedure; however, a dramatic interval change with resorption of calcification can still be seen (Fig. 9-43).

At the completion of the lavage and aspiration of rotator cuff calcific tendinosis, the needle is withdrawn into the adjacent subacromial-subdeltoid bursa for corticosteroid and anesthetic injection (Video 9-31). This latter procedure is essential because patients can develop a calcific bursitis after the procedure. Studies have shown that lavage and aspiration result in immediate improvement of symptoms, although transient increase in symptoms may occur about 15 weeks after the procedure.[35] Improved symptoms correlate with reduction in size of the calcification.[36] Although patients treated with lavage and aspiration had better outcomes 1 year after the procedure than those who were not treated, outcomes at 5 and 10 years were similar.[37] Lavage and aspiration of calcium may be completed in any accessible tendon and also can be considered with calcific bursitis.

Tendon Fenestration (Tenotomy or Dry Needling)

When a tendon shows tendinosis or partial tear, a needle can be guided into the affected tendon segment using ultrasound guidance. Common sites for this procedure include the common extensor tendon of the elbow (Fig. 9-44) (Video 9-32),[38-40] the gluteus minimus and medius tendons (Fig. 9-45) (Video 9-33), the patellar tendon (Fig. 9-46) (Video 9-34),[41] and the Achilles tendon (Fig. 9-47) (Video 9-35), although other tendons have been treated with success.[42] By repeatedly passing the needle into the abnormal tendon, healing can be stimulated by disruption of the degenerative area and by causing local bleeding, which releases growth factors.[42] The procedure is completed with a 20- or 22-gauge

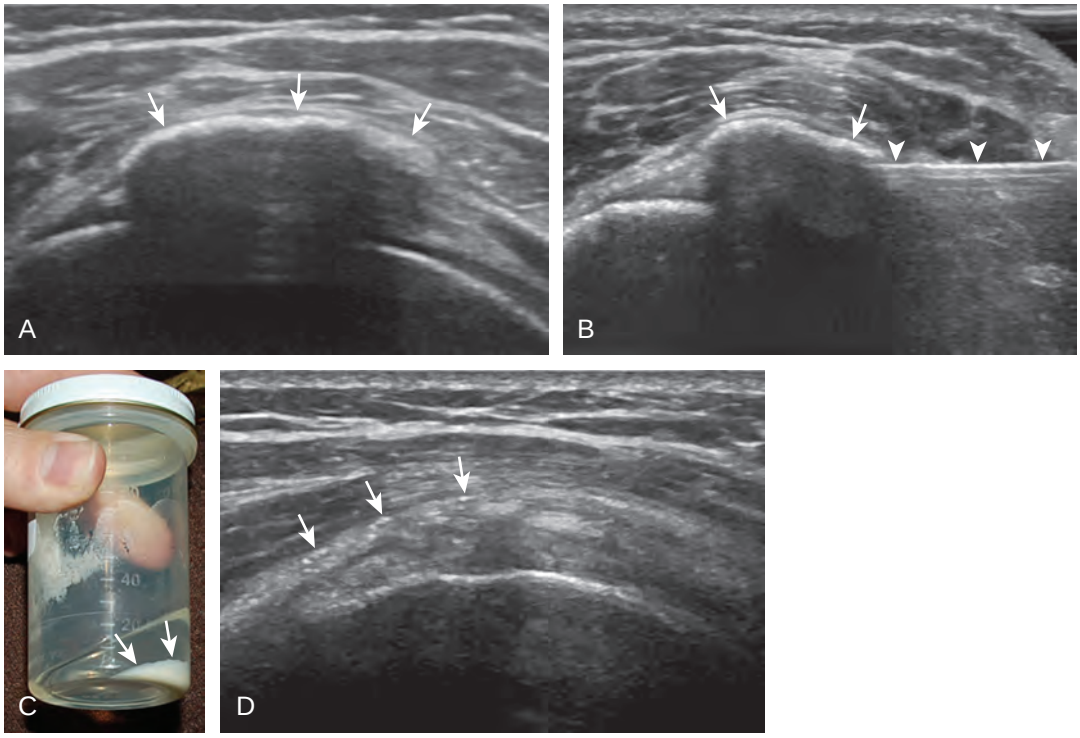

FIGURE 9-43 ■ Calcific tendinosis lavage and aspiration: supraspinatus. Ultrasound images short axis to the supraspinatus tendon show **(A)** echogenic and shadowing large calcification *(arrows)*. Note **(B)** needle placement *(arrowheads)* within calcification. After lavage and aspiration, specimen jar **(C)** shows calcification dependent within the local anesthetic *(arrows)*. Although there was no immediate change in the ultrasound appearance of the calcification at the end of the lavage and aspiration, repeat ultrasound 3 weeks after the procedure showed **(D)** nearly complete resorption of the calcifications, several of which were found in the subacromial-subdeltoid bursa *(arrows)*.

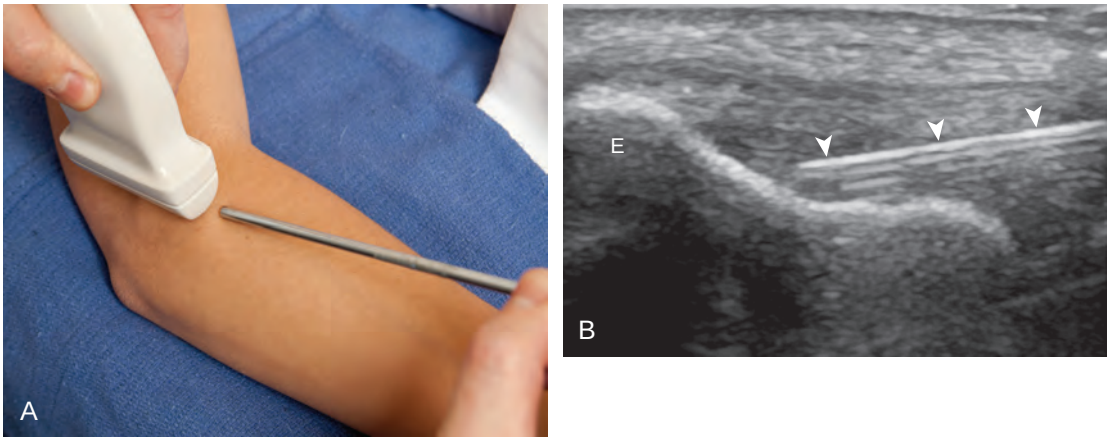

FIGURE 9-44 ■ Tendon fenestration: common extensor tendon of elbow. (A) shows transducer and needle position for simulated common extensor tendon procedure. Ultrasound image shows **(B)** needle *(arrowheads)* long axis to common extensor tendon with distal tip located within hypoechoic tendinosis. E, lateral epicondyle of humerus.

needle using an in-plane technique relative to the transducer and sound beam and the needle entering along the long axis of the tendon. The needle is placed through the skin, and a small amount of anesthetic agent is placed at the surface of the abnormal tendon (if needed). The needle is then repeatedly inserted into the abnormal segment; the needle is withdrawn just out of the tendon, redirected and advanced to an adjacent area, and repeated. The procedure continues until the entire segment of abnormal tendon is treated and softens, confirmed in both short axis and long axis dimensions. This typically involves passing the needle 20 to 30 times, but this varies depending on the size of the tendon abnormality. If the tendon abnormality is adjacent to bone at the enthesis, the needle is also directed to the bone surface. If there is hyperemia on color or power Doppler imaging in the abnormal tendon segment before the fenestration, one will see increased

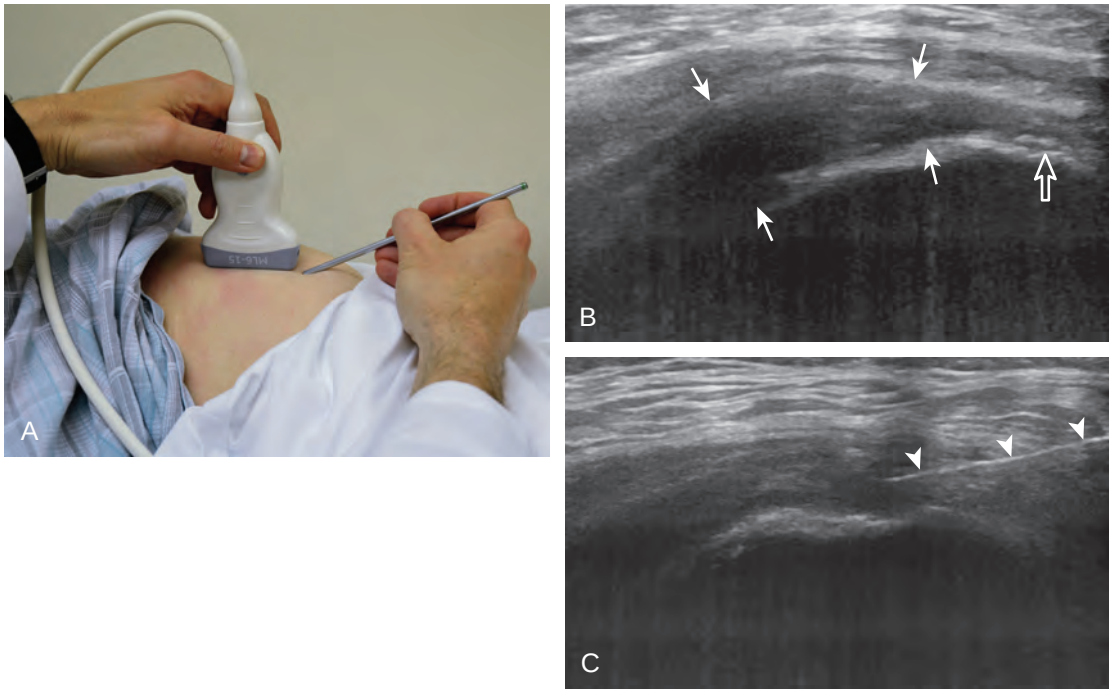

FIGURE 9-45 ■ Tendon fenestration: gluteus medius tendon. (A) shows transducer and needle entry site for simulated gluteus medius procedure. Ultrasound images **(B** and **C)** show hypoechoic tendon swelling *(arrows)* with cortical irregularity of greater trochanter *(open arrow)*. Note **(C)** needle position *(arrowheads)*.

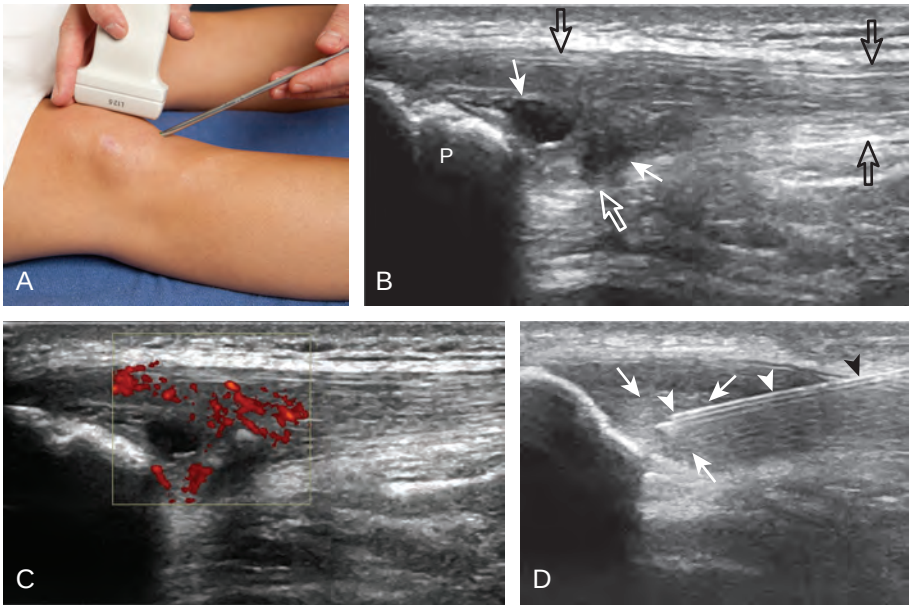

FIGURE 9-46 ■ Tendon fenestration: patellar tendon. (A) shows transducer and needle position for simulated proximal patellar tendon procedure. Ultrasound images **(B** and **C)** show abnormal hypoechogenicity *(arrows)* of the patellar tendon *(open arrows)* with increased through transmission, cortical irregularity of the patella (P), and neovascularity in **C**. During tendon fenestration procedure **(D),** no fluid could be aspirated. Note needle *(arrowheads)* and increased echogenicity at the fenestration site from hemorrhage *(arrows)*.

echogenicity from bleeding. As a precaution, a patient is immobilized, with direction from the patient's clinician if the tendon is weight bearing. Patients are also instructed not to take nonsteroidal anti-inflammatory drugs for 2 weeks before and after the procedure so that released growth factors related to bleeding will not be inhibited.

Platelet-Rich Plasma and Whole Blood Injection

Although the complexity and controversy of platelet-rich plasma injection are beyond the scope of this chapter, several topics related to ultrasound-guided injection deserve comment.

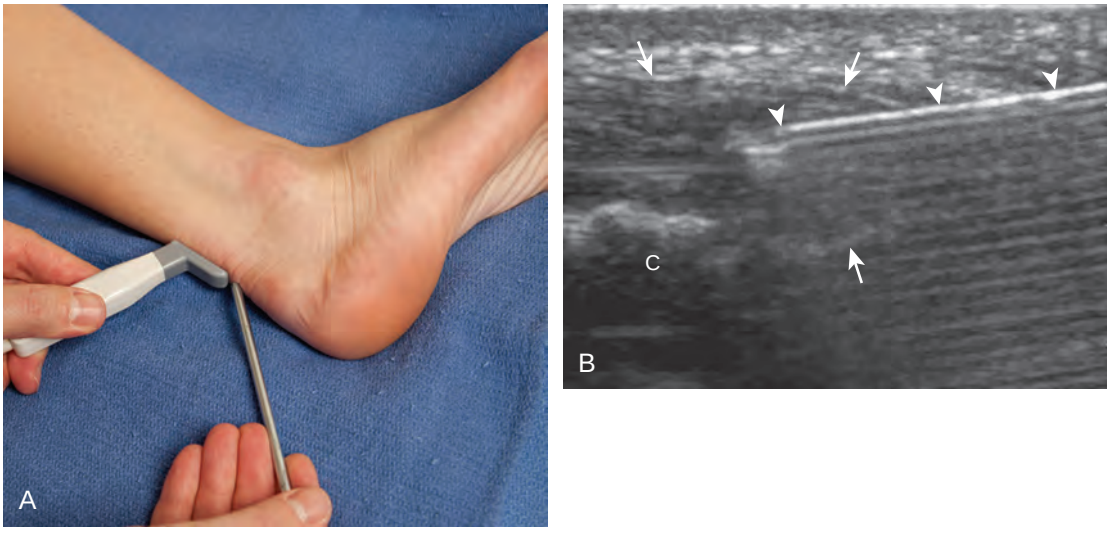

FIGURE 9-47 ■ Tendon fenestration: Achilles tendon. (A) shows transducer and needle position for simulated Achilles tendon procedure. Ultrasound image **(B)** shows needle placement *(arrowheads)* within abnormal hypoechoic swollen distal Achilles tendon *(arrows)*. C, calcaneus.

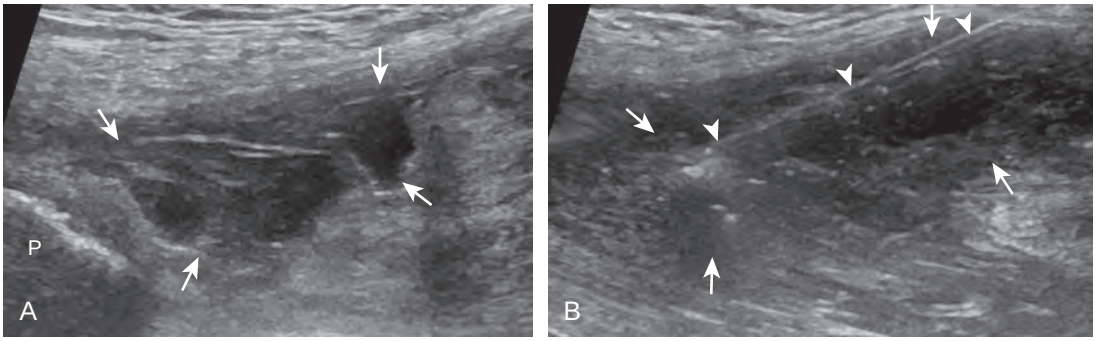

FIGURE 9-48 ■ Platelet-rich plasma injection: adductor longus tendon. Ultrasound images long axis to the adductor longus show **(A)** predominantly hypoechoic heterogeneous tear of the proximal adductor longus tendon *(arrows)* with **(B)** subsequent needle placement *(arrowheads)* and platelet-rich plasma injection *(arrows)*. P, pubis.

The use of ultrasound guidance can ensure that the platelet-rich plasma or whole blood injection is accurate while minimizing complications as for any other percutaneous ultrasound-guided procedure (Fig. 9-48) (Video 9-36). Similar to other procedures, an in-plane approach relative to the transducer is favored, although an out-of-plane approach can be considered with superficial targets. Typically, platelet-rich plasma or whole blood injection into a tendon occurs in conjunction with and immediately following tendon fenestration (Video 9-37).

MISCELLANEOUS PROCEDURES

Cyst Aspiration

Two general categories of cysts that may be aspirated using ultrasound guidance are ganglion cysts and cysts associated with fibrocartilage tears (meniscus and labrum).[43] In both settings, the fluid in the cyst is often viscous, and the cyst is often multilocular, which can limit the success of the aspiration (Fig. 9-49). Typically, a large-gauge (16-gauge) needle is used, and cyst lavage may

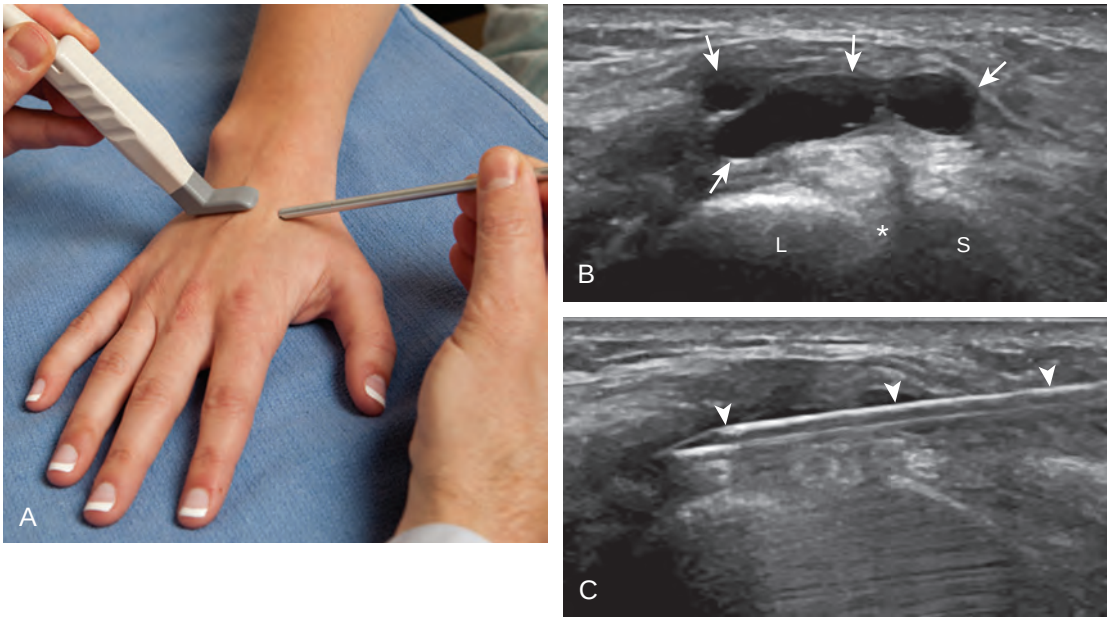

FIGURE 9-49 ■ Ganglion cyst aspiration: wrist. (A) shows transducer and needle position for simulated dorsal wrist ganglion procedure. Ultrasound images show **(B)** anechoic and lobular dorsal ganglion cyst *(arrows)* and **(C)** subsequent needle placement *(arrowheads)* for aspiration (*asterisk*, scapholunate ligament). L, lunate; S, scaphoid.

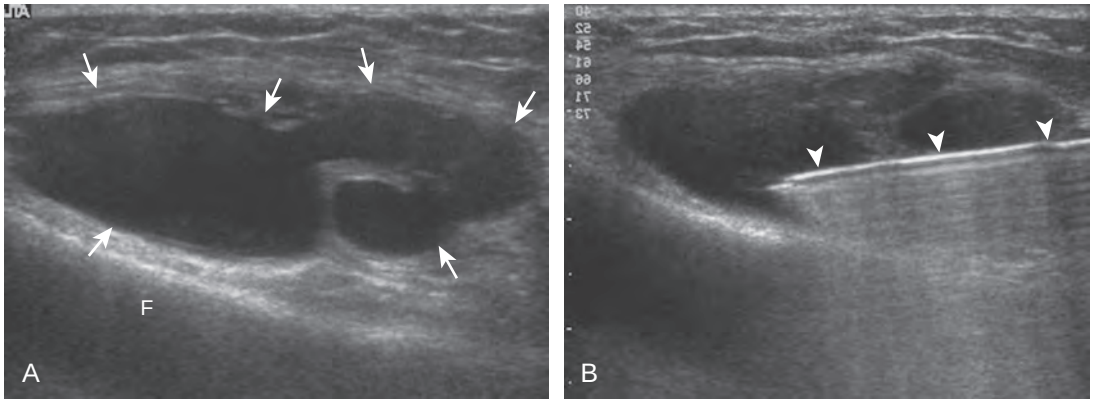

FIGURE 9-50 ■ Ganglion cyst aspiration: knee. Ultrasound images show **(A)** anechoic and lobular ganglion cyst *(arrows)* and **(B)** subsequent needle placement *(arrowheads)* for aspiration. F, femur.

improve aspiration (Fig. 9-50) (Video 9-38). Ganglion cysts may recur after aspiration and injection because a connection or neck to a joint or tendon sheath is usually present. Ganglion cyst aspiration may also be followed by corticosteroid injection.[44] Cysts associated with fibrocartilage often recur as well because the origin of the cyst is in fact the tear of the meniscus or labrum (shoulder or hip) (Fig. 9-51) (Video 9-39).

Peripheral Nerve Block

Injections adjacent to a peripheral nerve are carried out in an in-plane approach with the transducer in short axis to the peripheral nerve. The characteristic appearance of a peripheral nerve is best appreciated in short axis, and adjacent vascular are also easily seen (see earlier chapters). For injection of the carpal tunnel, the needle is in plane with the transducer and sound beam, with the transducer in short axis to the median nerve, and the needle enters from ulnar to radial over the volar aspect of the wrist.[45] With regard to the tarsal tunnel, the needle is in plane with the transducer in short axis to the tibial nerve, and the needle enters from posterior to anterior next to the Achilles tendon and over the flexor hallucis longus tendon.

Biopsy

Although a full discussion of ultrasound-guided biopsy is beyond the scope of this textbook, a few fundamentals will be mentioned.[46] The first is

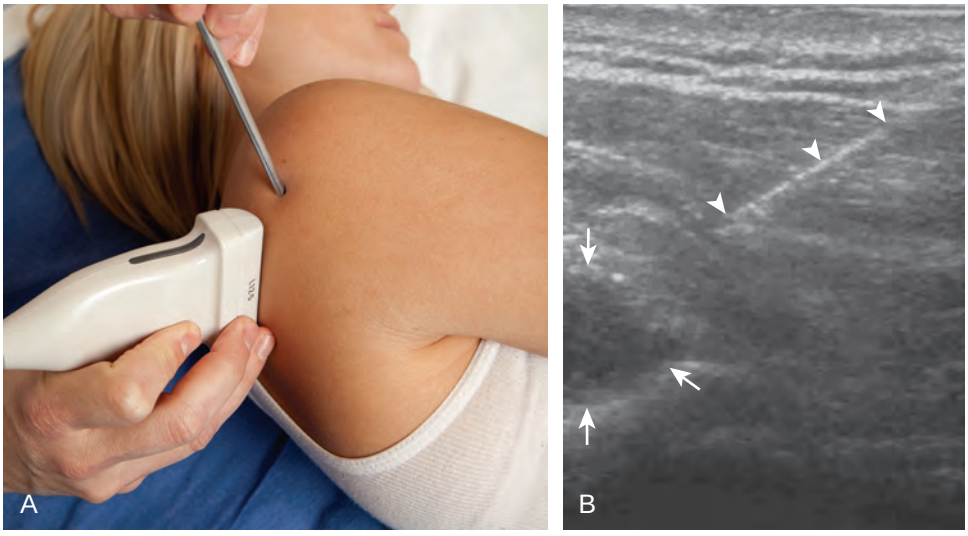

FIGURE 9-51 ■ Paralabral cyst aspiration: shoulder. (A) shows transducer and needle position for simulated posterior shoulder paralabral procedure. Ultrasound image shows **(B)** needle *(arrowheads)* approaching hypoechoic paralabral cyst *(arrows)*. Right side of ultrasound image is lateral.

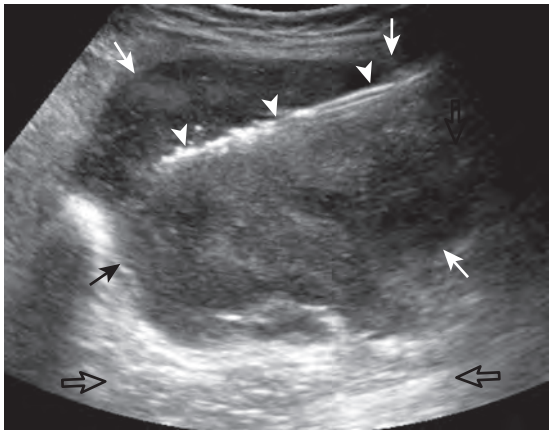

FIGURE 9-52 ■ Soft tissue mass biopsy: lymphoma. Ultrasound images shows hyperechoic biopsy needle *(arrowheads)* within hypoechoic mass *(arrows)*. Note increased through-transmission *(open arrows)*.

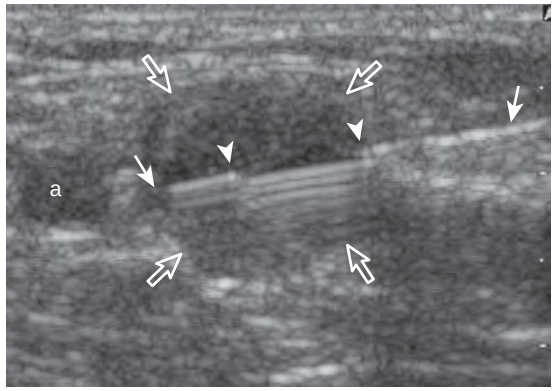

FIGURE 9-53 ■ Lymph node biopsy: lymphoma. Ultrasound image shows the entire length of the needle *(arrows)*, including the distal tip, visible in the long axis of the transducer. Note the opening in needle surface for biopsy *(arrowheads)* with reverberation artifact and needle placement within an axillary lymph node *(open arrows)*. Biopsy revealed a B-cell lymphoma. a, Artery.

that a biopsy of a suspected mass or malignancy should occur at a hospital or institution where the tumor will be treated. This allows an open communication between the physician performing the procedure and the surgical oncologist. Because the surgery resects the tumor along the biopsy needle path, this planning is critical. Using ultrasound guidance, several biopsy specimens are taken from various areas of the soft tissue tumor to ensure thorough sampling (Fig. 9-52).[47,48] Guiding the biopsy needle with an in-plane approach and using real-time observation of the biopsy ensure accurate sampling (Videos 9-40 and 9-41). In addition, seeding of adjacent compartments, such as neurovascular structures and an adjacent joint, should be avoided (Fig. 9-53).

Online references available at www.expertconsult.com.

REFERENCES

1. Joines MM, Motamedi K, Seeger LL, et al: Musculoskeletal interventional ultrasound. *Semin Musculoskelet Radiol* 11:192–198, 2007.
2. Adler RS, Sofka CM: Percutaneous ultrasound-guided injections in the musculoskeletal system. *Ultrasound Q* 19:3–12, 2003.
3. Daley EL, Bajaj S, Bisson LJ, et al: Improving injection accuracy of the elbow, knee, and shoulder: does injection site and imaging make a difference? A systematic review. *Am J Sports Med* 39:656–662, 2011.
4. Gilliland CA, Salazar LD, Borchers JR: Ultrasound versus anatomic guidance for intra-articular and periarticular injection: a systematic review. *Phys Sportsmed* 39:121–131, 2011.
5. Creel SA, Girish G, Jamadar DA, et al: Sonographic surface localization of subcutaneous foreign bodies and masses. *J Clin Ultrasound* 37:158–160, 2009.
6. Jandzinski DI, Carson N, Davis D, et al: Treated needles: do they facilitate sonographically guided biopsies? *J Ultrasound Med* 22:1233–1237, 2003.
7. Fessell DP, Jacobson JA, Craig J, et al: Using sonography to reveal and aspirate joint effusions. *AJR Am J Roentgenol* 174:1353–1362, 2000.
8. Zubler V, Mamisch-Saupe N, Pfirrmann CW, et al: Detection and quantification of glenohumeral joint effusion: reliability of ultrasound. *Eur Radiol* 21:1858–1864, 2011.
9. Gokalp G, Dusak A, Yazici Z: Efficacy of ultrasonography-guided shoulder MR arthrography using a posterior approach. *Skeletal Radiol* 39:575–579, 2010.
10. De Maeseneer M, Jacobson JA, Jaovisidha S, et al: Elbow effusions: distribution of joint fluid with flexion and extension and imaging implications. *Invest Radiol* 33:117–125, 1998.
11. Lohman M, Vasenius J, Nieminen O: Ultrasound guidance for puncture and injection in the radiocarpal joint. *Acta Radiol* 48:744–747, 2007.
12. Kantarci F, Ozbayrak M, Gulsen F, et al: Ultrasound-guided injection for MR arthrography of the hip: comparison of two different techniques. *Skeletal Radiol* 2011, Oct 14 [Epub ahead of print].
13. Rowbotham EL, Grainger AJ: Ultrasound-guided intervention around the hip joint. *AJR Am J Roentgenol* 197:W122–127, 2011.
14. Smith J, Hurdle MF, Weingarten TN: Accuracy of sonographically guided intra-articular injections in the native adult hip. *J Ultrasound Med* 28:329–335, 2009.
15. Klauser A, De Zordo T, Feuchtner G, et al: Feasibility of ultrasound-guided sacroiliac joint injection considering sonoanatomic landmarks at two different levels in cadavers and patients. *Arthritis Rheum* 59:1618–1624, 2008.
16. Pekkafahli MZ, Kiralp MZ, Basekim CC, et al: Sacroiliac joint injections performed with sonographic guidance. *J Ultrasound Med* 22:553–559, 2003.
17. Fenn S, Datir A, Saifuddin A: Synovial recesses of the knee: MR imaging review of anatomical and pathological features. *Skeletal Radiol* 38:317–328, 2009.
18. Park Y, Lee SC, Nam HS, et al: Comparison of sonographically guided intra-articular injections at 3 different sites of the knee. *J Ultrasound Med* 30:1669–1676, 2011.
19. Smith J, Finnoff JT, Levy BA, et al: Sonographically guided proximal tibiofibular joint injection: technique and accuracy. *J Ultrasound Med* 29:783–789, 2010.
20. Wisniewski SJ, Smith J, Patterson DG, et al: Ultrasound-guided versus nonguided tibiotalar joint and sinus tarsi injections: a cadaveric study. *PM R* 2:277–281, 2010.
21. Smith J, Finnoff JT, Henning PT, et al: Accuracy of sonographically guided posterior subtalar joint injections: comparison of 3 techniques. *J Ultrasound Med* 28:1549–1557, 2009.
22. Blankenbaker DG, De Smet AA, Keene JS: Sonography of the iliopsoas tendon and injection of the iliopsoas bursa for diagnosis and management of the painful snapping hip. *Skeletal Radiol* 35:565–571, 2006.
23. Pfirrmann CW, Chung CB, Theumann NH, et al: Greater trochanter of the hip: attachment of the abductor mechanism and a complex of three bursae—MR imaging and MR bursography in cadavers and MR imaging in asymptomatic volunteers. *Radiology* 221:469–477, 2001.
24. Ward EE, Jacobson JA, Fessell DP, et al: Sonographic detection of Baker's cysts: comparison with MR imaging. *AJR Am J Roentgenol* 176:373–380, 2011.
25. Hashiuchi T, Sakurai G, Morimoto M, et al: Accuracy of the biceps tendon sheath injection: ultrasound-guided or unguided injection? A randomized controlled trial. *J Shoulder Elbow Surg* 20:1069–1073, 2011.
26. Jeyapalan K, Choudhary S: Ultrasound-guided injection of triamcinolone and bupivacaine in the management of De Quervain's disease. *Skeletal Radiol* 38:1099–1103, 2009.
27. Choi SJ, Ahn JH, Lee YJ, et al: De Quervain disease: US identification of anatomic variations in the first extensor compartment with an emphasis on subcompartmentalization. *Radiology* 260:480–486, 2011.
28. Rousset P, Vuillemin-Bodaghi V, Laredo JD, et al: Anatomic variations in the first extensor compartment of the wrist: accuracy of US. *Radiology* 257:427–433, 2010.
29. Adler RS, Buly R, Ambrose R, et al: Diagnostic and therapeutic use of sonography-guided iliopsoas peritendinous injections. *AJR Am J Roentgenol* 185:940–943, 2005.
30. Wank R, Miller TT, Shapiro JF: Sonographically guided injection of anesthetic for iliopsoas tendinopathy after total hip arthroplasty. *J Clin Ultrasound* 32:354–357, 2004.
31. Finnoff JT, Hurdle MF, Smith J: Accuracy of ultrasound-guided versus fluoroscopically guided contrast-controlled piriformis injections: a cadaveric study. *J Ultrasound Med* 27:1157–1163, 2008.
32. Labrosse JM, Cardinal E, Leduc BE, et al: Effectiveness of ultrasound-guided corticosteroid injection for the treatment of gluteus medius tendinopathy. *AJR Am J Roentgenol* 194:202–206, 2010.
33. Zissen MH, Wallace G, Stevens KJ, et al: High hamstring tendinopathy: MRI and ultrasound imaging and therapeutic efficacy of percutaneous corticosteroid injection. *AJR Am J Roentgenol* 195:993–998, 2010.
34. Lee KS, Rosas HG: Musculoskeletal ultrasound: how to treat calcific tendinitis of the rotator cuff by ultrasound-guided single-needle lavage technique. *AJR Am J Roentgenol* 195:638, 2010.
35. del Cura JL, Torre I, Zabala R, et al: Sonographically guided percutaneous needle lavage in calcific tendinitis of the shoulder: short- and long-term results. *AJR Am J Roentgenol* 189:W128–134, 2007.
36. Yoo JC, Koh KH, Park WH, et al: The outcome of ultrasound-guided needle decompression and steroid injection in calcific tendinitis. *J Shoulder Elbow Surg* 19:596–600, 2010.
37. Serafini G, Sconfienza LM, Lacelli F, et al: Rotator cuff calcific tendonitis: short-term and 10-year outcomes after two-needle US guided percutaneous treatment—nonrandomized controlled trial. *Radiology* 252:157–164, 2009.
38. McCarthy CL, Wilson DJ, Coltman TP: Anterolateral ankle impingement: findings and diagnostic accuracy with ultrasound imaging. *Skeletal Radiol* 37:209–216, 2008.
39. McShane JM, Nazarian LN, Harwood MI: Sonographically guided percutaneous needle tenotomy for treatment of common extensor tendinosis in the elbow. *J Ultrasound Med* 25:1281–1289, 2006.

40. McShane JM, Shah VN, Nazarian LN: Sonographically guided percutaneous needle tenotomy for treatment of common extensor tendinosis in the elbow: is a corticosteroid necessary? *J Ultrasound Med* 27:1137–1144, 2008.
41. Housner JA, Jacobson JA, Morag Y, et al: Should ultrasound-guided needle fenestration be considered as a treatment option for recalcitrant patellar tendinopathy? A retrospective study of 47 cases. *Clin J Sport Med* 20:488–490, 2010.
42. Housner JA, Jacobson JA, Misko R: Sonographically guided percutaneous needle tenotomy for the treatment of chronic tendinosis. *J Ultrasound Med* 28:1187–1192, 2009.
43. Chiou HJ, Chou YH, Wu JJ, et al: Alternative and effective treatment of shoulder ganglion cyst: ultrasonographically guided aspiration. *J Ultrasound Med* 18:531–535, 1999.
44. Breidahl WH, Adler RS: Ultrasound-guided injection of ganglia with corticosteroids. *Skeletal Radiol* 25:635–638, 1996.
45. Smith J, Wisniewski SJ, Finnoff JT, et al: Sonographically guided carpal tunnel injections: the ulnar approach. *J Ultrasound Med* 27:1485–1490, 2008.
46. Gogna A, Peh WC, Munk PL: Image-guided musculoskeletal biopsy. *Radiol Clin North Am* 46:455–473, v, 2008.
47. Peer S, Freuis T, Loizides A, et al: Ultrasound guided core needle biopsy of soft tissue tumors: a fool proof technique? *Med Ultrason* 13:187–194, 2011.
48. Vasilevska V, Gligorievski A, Zafiroski G, et al: Radiologic-pathologic correlation of 100 consecutive biopsied soft tissue musculoskeletal lesions after multimodality imaging. *Cancer Imaging* 11:S42, 2011.

eBOX 9-1 Sample Interventional Ultrasound Report

Examination: Ultrasound-Guided Injection of Right Biceps Brachii Long Head Tendon Sheath
Date of Study: March 11, 2011
Patient Name: Jack White
Registration Number: 8675309
History: Pain
Findings: Limited ultrasound over the anterior right shoulder demonstrates minimal joint fluid distending the biceps brachii long head tendon sheath. No evidence for hyperemia or synovial hypertrophy to suggest tenosynovitis. No evidence for biceps brachii long head tendon tear. No tendon subluxation or dislocation with dynamic imaging. No abnormal subacromial-subdeltoid bursal thickening.

After obtaining both written and verbal informed consent discussing potential risks (bleeding, infection, soft tissue injury) and benefits, using sterile technique and local anesthetic injection (provide type and amount), a 20-gauge spinal needle with stylet was inserted into the long head of the biceps brachii tendon sheath. Intrasheath location of needle tip was confirmed with a small amount of anesthetic injection. This was followed by corticosteroid injection (provide type and amount).

The patient tolerated the procedure well without complications. The patient's pain level changed from 8/10 before procedure to 2/10.

Impression:
1. Limited diagnostic ultrasound of the anterior shoulder showed minimal joint fluid.
2. Successful long head biceps brachii tendon sheath corticosteroid injection with pain relief as noted above and without complications.

eBOX 9-2 Sample Interventional Ultrasound Report

Examination: Ultrasound-Guided Right Iliopsoas Peritendon Injection
Date of Study: March 11, 2011
Patient Name: Jack White
Registration Number: 8675309
History: Pain, evaluate for tendon tear
Findings: Limited ultrasound over the anterior right hip showed no hip joint effusion and unremarkable anterior hip labrum. The rectus femoris was normal. No evidence for iliopsoas bursal distention. Dynamic imaging showed no evidence for snapping iliopsoas tendon.

After obtaining both written and verbal informed consent discussing potential risks (bleeding, infection, soft tissue injury) and benefits, using sterile technique and local anesthetic injection (provide type and amount), a 20-gauge spinal needle with stylet was directed between the iliopsoas tendon and ilium superior to the femoral head. Needle tip location between the iliopsoas tendon and ilium was confirmed with a small amount of anesthetic injection. This was followed by corticosteroid injection (provide type and amount).

The patient tolerated the procedure well without complications. The patient's pain level changed from 8/10 before procedure to 2/10.

Impression:
1. Limited diagnostic ultrasound of the anterior right hip showed no abnormality.
2. Successful right iliopsoas peritendon corticosteroid injection with pain relief as noted above and without complications.

APPENDIX

Examination Checklists

Shoulder Ultrasound Examination Checklist

Step	Structures/Pathologic Features of Interest
1	Biceps brachii long head
2	Subscapularis, biceps tendon dislocation
3	Supraspinatus, infraspinatus
4	Acromioclavicular joint, subacromial-subdeltoid bursa, dynamic evaluation
5	Posterior glenohumeral joint, labrum, teres minor, infraspinatus

Wrist and Hand Ultrasound Examination Checklist

Location	Structures of Interest/Pathologic Features
Volar (no. 1)	Median nerve
	Flexor tendons
	Volar joint recesses
Volar (no. 2)	Scaphoid
	Flexor carpi radialis
	Volar ganglion cyst
Volar (no. 3)	Ulnar nerve and artery
Dorsal (no. 1)	Extensor tendons
	Dorsal joint recesses
Dorsal (no. 2)	Scapholunate ligament
	Dorsal ganglion cyst
Dorsal (no. 3)	Triangular firbrocartilage complex

Elbow Ultrasound Examination Checklist

Location	Structures of Interest
Anterior	Brachialis
	Biceps brachii
	Median nerve
	Anterior joint recess
Medial	Ulnar collateral ligament
	Common flexor tendon and pronator teres
	Ulnar nerve
Lateral	Common extensor tendon
	Radial collateral ligament complex
	Radial head and annular recess
	Capitellum
	Radial nerve
Posterior	Posterior joint recess
	Triceps brachii
	Olecranon bursa

Finger Ultrasound Examination Checklist

Location	Structures of Interest
Volar	Flexor tendons
	Pulleys
	Volar plate
	Joint recesses
Dorsal	Extensor tendon
	Joint recesses
Other	Collateral ligaments

Hip and Thigh Ultrasound Examination Checklist

Location	Structures of Interest
Hip: anterior	Hip joint, iliopsoas, rectus femoris, sartorius, pubic symphysis
Hip: lateral	Greater trochanter, bursae
Hip: posterior	Sacroiliac joints, piriformis, hip abductors
Inguinal region	Deep inguinal ring, Hesselbach triangle, femoral artery region
Thigh: anterior	Rectus femoris, vastus medialis, vastus intermedius, vastus lateralis
Thigh: medial	Femoral artery and nerve, sartorius, gracilis, adductors
Thigh: posterior	Semimembranosus, semitendinosus, biceps femoris, sciatic nerve

Knee Ultrasound Examination Checklist

Structures/ Pathologic Features	Location of Interest
Anterior	Quadriceps tendon
	Patella
	Patellar tendon
	Patellar retinaculum
	Suprapatellar recess
	Medial and lateral recesses
	Anterior knee bursae
	Femoral articular cartilage
Medial	Medial collateral ligament
	Medial meniscus: body and anterior horn
	Pes anserinus
Lateral	Iliotibial tract
	Lateral collateral ligament
	Biceps femoris
	Common peroneal nerve
	Popliteus
	Lateral meniscus: body and anterior horn
Posterior	Baker cyst
	Menisci: posterior horns
	Posterior cruciate ligament
	Anterior cruciate ligament
	Neurovascular structures

Ankle, Calf, and Forefoot Ultrasound Examination Checklist

Location	Structures of Interest
Ankle: anterior	Anterior tibiotalar joint recess
	Tibialis anterior
	Extensor hallucis longus
	Dorsal pedis artery
	Superficial peroneal nerve
	Extensor digitorum longus
Ankle: medial	Tibialis posterior
	Flexor digitorum longus
	Tibial nerve
	Flexor hallucis longus
	Deltoid ligament
Ankle: lateral	Peroneus longus and brevis
	Anterior talofibular ligament
	Calcaneofibular ligament
	Anterior tibiofibular ligament
Ankle: posterior	Achilles tendon
	Posterior bursae
	Plantar fascia
Calf	Soleus
	Medial and lateral heads of gastrocnemius
	Plantaris
	Achilles tendon
Forefoot	Dorsal joint recesses
	Morton neuroma